東京帝國大學

地震研究所彙報

第19號

昭和 16 年

BULLETIN

OF THE

EARTHQUAKE RESEARCH INSTITUTE

TOKYO IMPERIAL UNIVERSITY

Vol. XIX

1940

目　次

第 19 號

第 1 册 (昭和 16 年 3 月)

			頁
1.	地球核の熱力學的成因について(第 2 報)(英文)…………	妹澤克惟 金井清	1
2.	地震計に於ける高次の不安定について(第 2 報)(英文)…	金井清 妹澤克惟	9
3.	地球の内部に於ける粘性の分布 (第 2 報) 地震波の蔭になる地帶について(英文)……………………	妹澤克惟 金井清	14
4.	重力異常と地下構造との關係 (VI.) (英文)………………	坪井忠二 山口生知	26
5.	油壺及細島に於ける海水面變化に就て(英文)…………	山口生知	39
6.	火成岩に於ける熱殘留磁氣生成の機構に就いて (序報) (英文)……………………………………………………	永田武	49
7.	三宅島の噴火に伴つた垂直磁力の變化 (概要)(英文)……	高橋龍太郎 平能金太郎	82
8.	昭和 15 年 8 月 2 日日本海に起つた津浪 (邦文) …………	宮部直巳	104
9.	山梨縣鳳凰山・地藏ヶ岳附近の地質 (邦文)………………	大塚彌之助	115
10.	輕石流堆積物と拋出輕石堆積物との差異に就いて (英文)……………………………………………………	久野久	144

第 2 册 (昭和 16 年 6 月)

11.	演算法を應用せる任意形彈性波の傳播の問題 (第 1 報) (英文) ……………………………………	妹澤克惟 金井清	151
12.	演算法によりて解いた地震計の初動問題について (第 1 報) (英文) ……………………………………	妹澤克惟 金井清	162
13.	地震計に於ける高次の不安定に就いて (第 3 報) 新しい上下動振動臺による實驗 (英文) ………………	金井清 妹澤克惟	177
14.	等方不均一球内の一點より起る彈性彼 (第 3 報) (英文)……………………………………………………	吉山良一	185

15.	横濱港の埋立地及岸壁に於ける地震動（邦文）…………	齋田時太郎 松尾春雄	206
16.	筑波山に於ける土地傾斜變化の觀測（其の二）（英文）…………	萩原尊禮	218
17.	中國山地の隆起運動に就て（英文）…………	宮部直巳	228
18.	年平均潮位の高さの變化（英文）…………	宮部直巳	238
19.	東京市内水準改測の成果（邦文）…………	宮部直巳 福西清治	248
20.	昭和15年7月三宅島の噴火（英文）…………	津屋弘逵 高橋龍太郎 萩原尊禮 水上武 永田武 表俊一郎 平能金太郎	260
21.	昭和15年8月三原火山小活動に關する地球磁氣學的調査（英文）…………	永田武	402
22.	地震の頻度と振幅に關する石本・飯田の實驗式 $na^m=k$ に就いて（獨文）…………	松澤武雄	411

第3册（昭和16年9月）

23.	演算法を應用せる任意形彈性波の傳播の問題（第2報）（英文）…………	妹澤克惟 金井清	417
24.	演算法によりて解いた地震計の初動問題について（第2報）（英文）…………	妹澤克惟 金井清	443
25.	重價平均に關する一問題（英文）…………	坪井忠二	458
26.	最近に於ける關東地方の地震に就いて（英文）…………	那須信治 保田柱二	476
27.	昭和15年7月三宅島の噴火 三宅島噴火の地質學的觀察（II）（英文）…………	津屋弘逵	492
28.	緩慢な變化の遠隔記錄法（英文）…………	萩原尊禮	523
29.	比較觀測を目的とする水平動變位計の製作（邦文）…………	高橋龍太郎 平能金太郎	527
30.	軟弱地盤に於ける地震動（邦文）…………	高橋龍太郎 平能金太郎	534
31.	三宅島における三角再測量の結果（邦文）…………		544

第4册（昭和16年12月）

32.	固體自體が分散性なる場合に於けるレーレー波の傳播（英文）…………	妹澤克惟 金井清	549

33. 鋸齒狀小屋の耐震性（英文）……………………………… 金　井　　清 554
34. 三鷹基線菱形の變形と共の附近に於ける地震活動
（英文）………………………………………………………… 坪　井　忠　二 559
35. 岩石の帶磁率の溫度に因る變化の測定（英文）………… 永　田　　武 579
36. 三宅島産火山彈の形態及び構造に就いて（英文）………… 津　屋　弘　逵 597
37. 三宅島新熔岩流の帶磁（英文）……………………………… 水　上　　武 612
38. 三宅島新寄生火山及び新熔岩流の第3回地形測量
（英文）………………………………………………………… 表　俊　一　郞 619
39. 昭和16年7月15日長野地震の統計的調査（邦文）……… 岸上冬彥・永田武・宮村攝三 628
40. 昭和16年7月15日長野地震の家屋被害に就て
（邦文）………………………………………………………… 金　井　　清 647
41. 善光寺平に於ける民家構造の特異性と被害（邦文）……… 齋田時太郞 661
42. 秋田縣男鹿半島附近震災地三角點水準點復舊測量記事
（邦文）…………………………………………………………… 陸地測量部 671

Contents.

Vol. XIX.

Part 1.—March, 1941.

Page

1. K. SEZAWA and K. KANAI, Thermodynamical Origin of the Earth's Core. II. (in English) 1
2. K. KANAI and K. SEZAWA, On the Problem of Instabilities of Higher Orders in a Seismometer. II. (in English) 9
3. K. SEZAWA and K. KANAI, Viscosity Distribution within the Earth. II. On the Shadow Zone for Seismic Waves. (in English) 14
4. C. TSUBOI and S. YAMAGUTI, Relation between the Gravity Anomalies and the Corresponding Subterranean Mass Distribution. (VI.) (in English) 26
5. S. YAMAGUTI, On the Change in the Heights of the Monthly Mean Sea-level at Aburatubo and Hosozima. (in English) 39
6. T. NAGATA, The Mode of Causation of Thermo-Remanent Magnetism in Igneous Rocks. Preliminary Note. (in English)... 49
7. R. TAKAHASI and K. HIRANO, Changes in the Vertical Intensity of Geomagnetism that Accompanied the Eruption of Miyakezima, in 1940. (in English) 82
8. N. MIYABE, Tunami associated with the Earthquake of August 2, 1940. (in Japanese) 104
9. Y. OTUKA, Geology of Mt. Zizô and Hôô, Yamanasi Prefecture, Japan. (in Japanese) 115
10. H. KUNO, Characteristics of Deposits formed by Pumice Flows and Those by Ejected Pumice. (in English) 144

Part 2.—June. 1941.

11. K. SEZAWA and K. KANAI, Transmission of Arbitrary Elastic Waves from a Spherical Source, Solved with Operational Calculus. I. (in English) 151
12. K. SEZAWA and K. KANAI, On the Initial Movement of a Seismograph subjected to an Arbitrary Earthquake Motion, Solved with Operational Calculus. I. (in English) 162
13. K. KANAI and K. SEZAWA, On the Problem of Instabilities of Higher Orders in a Seismometer. III. Experiments with a New Vertical Vibration Table. (in English) 177
14. R. YOSIYAMA, Elastic Waves from a Point in an Isotropic Heterogeneous Sphere. Part 3. (in English) 185
15. T. SAITA and H. MATUO, Earthquake Vibrations on Quays and on Reclaimed Ground in the Harbour of Yokohama. (in Japanese) 206
16. T. HAGIWARA, Observation of Changes in the Inclination of the Earth's Surface at Mt. Tukuba (Second Report). (in English) 218
17. N. MIYABE, Upwarp Deformation of the Land in Tyūgoku. (in English) 228
18. N. MIYABE, Secular Changes in the Heights of Yearly Mean Sea-Level at Japanese Stations. (in English) 238
19. N. MIYABE and S. HUKUNISI, Results of Relevelling in Tokyo, in 1940. (in Japanese) 248
20. H. TSUYA, R. TAKAHASI, T. HAGIWARA. T. MINAKAMI, T. NAGATA, S. OMOTE and K. HIRANO, The Eruption of Miyake-sima, One of the Seven Izu Islands, in 1940. (in English) 260
21. T. NAGATA, A Geomagnetic Study of the Minor Activities of Volcano Mihara, Oosima Island, August 1940. (in English) ... 402
22. T. MATUZAWA, Über die empirische Formel von Ishimoto und

Iida $na^m = k$ zwischen der Bebenhäufigkeit n und der Amplitude a. (im Deutschen) 411

Part 3.—September, 1941.

23. K. SEZAWA and K. KANAI, Transmission of Arbitrary Elastic Waves from a Spherical Source, Solved with Operational Calculus. II. (in English) 417

24. K. SEZAWA and K. KANAI, On the Initial Movement of a Seismograph subjected to an Arbitrary Earthquake Motion, Solved with Operational Calculus. II. (in English)............ 443

25. C. TSUBOI, A Problem of Weighted Mean. (in English) 458

26. N. NASU and C. YASUDA, Recent Earthquakes of the Kwanto District. (in English) 476

27. H. TSUYA, The Eruption of Miyake-sima, One of the Seven Izu Islands, in 1940. Geological Observations of the Miyake-sime Eruption of 1940 (II). (in English)........................ 492

28. T. HAGIWARA, A New Device for Remote Mechanical Recording of Slow Movements. (in English).............................. 523

29. R. TAKAHASI and K. HIRANO, A New Horizontal-Component Seismograph for Comparison Observations. (in Japanese)... 527

30. R. TAKAHASI and K. HIRANO, Seismic Vibrations of Soft Ground. (in Japanese).. 534

31. Results of Re-triangulation in Miyake-sima. (in Japanese)...... 544

Part 4.—December, 1941.

32. K. SEZAWA and K. KANAI, On the Propagation of Rayleigh-waves in Dispersive Elastic Media. (in English)............... 549

33. K. KANAI, The Seismic Vibration of a Saw-tooth Roof Structure. (in English).. 554

34. C. TSUBOI, Secular Deformations of the Base Line Rhombus at Mitaka in Relation to Seismic Activities in its Vicinity.

(in English) 559

35. T. NAGATA, Measurement of Changes in Magnetic Susceptibility of Igneous Rocks with Temperature in a Weak Magnetic Field. (in English) 579

36. H. TSUYA, On the Form and Structure of Volcanic Bombs from Volcano Miyake-sima. (in English) 597

37. T. MINAKAMI, Magnetization of the New Lava-Flows of Miyakesima Island. (in English) 612

38. S. OMOTE, The Third Topographic Survey of the New Parasitic Cones and the New Lava Flow of Miyake-sima Island. (in English) 619

39. F. KISHINOUYE, T. Nagata and S. MIYAMURA, A Statistical Investigation of the Strong Earthquake of July 15, 1941, near Nagano. (in Japanese) 628

40. K. KANAI, On the Damage to Buildings in the Nagano Earthquake of July 13, 1941. (in Japanese) 647

41. T. SAITA, The Peculiarities of Dwelling House Construction and the Earthquake Damages in Zenkoji Plain, Nagano Prefecture. (in Japanese) 661

42. Millitary Land Survey, Results of Revisions of Triangulation and Levelling in the Neighbourhood of Ogasima. Akita Prefecture. (in Japanese) 671

1. *Thermodynamical Origin of the Earth's Core. II.*

By Katsutada SEZAWA and Kiyoshi KANAI,

Earthquake Research Institute.

(Read Oct. 16, 1940.—Received Dec. 20, 1940.)

1. *A review of the results of the last investigation.*

In the previous paper[1] we solved a problem of polytropic gas within the core. The density distribution in the rocky shell was assumed to be uniform in one case and to be that of Jeffreys in another. The polytropic conditions used in that paper were $n=1$ and 5. Although the temperature in the core became of the order of 10^3 K, it varied proportionally with the atomic weights of the gases in the core. With the theory of nuclear transformation of elements in mind, should the earth's core be gaseous, it is likely that the elements composing that gas are of relatively low atomic numbers.

In the present investigation the polytropic conditions will be extended to a range so wide as $n=5$, 3, 2, 1, 0·5, 0·3, from the result of which it will be shown that even if the earth's core be gaseous, the gases may be of metallic elements of relatively high atomic numbers, say, iron or nickel, but that the indices for the polytropy will be as low as $n=0{\cdot}3\sim0{\cdot}5$.

2. *Formulae for the polytropic gases in the core.*

Let ρ, ϕ, T, G $(=6{\cdot}66.10^{-8}$ C.G.S.), $\Re\,(=8{\cdot}26.10^{7})$ be the density, the gravitational potential, the temperature, the gravitational constant, and the universal gas constant, respectively. Let also κ, γ $(=1+1/n)$ be the constants of polytropy showing the relation $P=\kappa\rho^{\gamma}$, where P is the gas pressure. Then, using the relations

$$\rho=\left\{\frac{\phi}{(n+1)\kappa}\right\}^{n},\quad P=\frac{\rho\phi}{n+1},\quad T=\frac{\beta\mu\phi}{(n+1)\Re},\qquad (1),\ (2),\ (3)$$

and writing

1) K. SEZAWA and K. KANAI, *Bull. Earthq. Res. Inst.*, **18** (1940), 359~369.

$$a^2=\frac{4\pi G}{\{(n+1)\kappa\}^n},\quad \phi=\phi_0 u,\quad z=ar\phi_0^{\frac{1}{2}(n-1)},\qquad (4),\ (5),\ (6)$$

we get the equation

$$\frac{d^2u}{dz^2}+\frac{2}{z}\frac{du}{dz}+u^n=0. \qquad (7)$$

To solve this equation we write

$$u=1+a_1z+a_2z^2+a_3z^3+\ldots\ldots . \qquad (8)$$

From (7), (8) it is possible to determine the constants a_1, a_2,...... . The expressions of u thus determined for the different n's are

$$n=3;\quad u=1-0{\cdot}16667z^2+2{\cdot}5.10^{-2}z^4$$
$$-3{\cdot}7698.10^{-3}z^6+5{\cdot}6860.10^{-4}z^8$$
$$-8{\cdot}5763.10^{-5}z^{10}+1{\cdot}2936.10^{-5}z^{12}+\ldots\ldots,$$

$$n=2;\quad u=1-\frac{1}{6}z^2+\frac{1}{60}z^4-\frac{11}{7560}z^6$$
$$+\frac{1}{8505}z^8-\frac{97}{10692000}z^{10}+\ldots\ldots,$$

$$n=0{\cdot}5;\quad u=1-0{\cdot}16667z^2+4{\cdot}1667.10^{-3}z^4$$
$$+3{\cdot}3069.10^{-5}z^6+1{\cdot}3779.10^{-6}z^8$$
$$+7{\cdot}7662.10^{-8}z^{10}+5{\cdot}1978.10^{-9}z^{12}+\ldots\ldots,$$

$$n=0{\cdot}3;\quad u=1-0{\cdot}16667z^2+2{\cdot}5.10^{-3}z^4$$
$$+5{\cdot}1587.10^{-5}z^6+2{\cdot}3957.10^{-6}z^8$$
$$+1{\cdot}5205.10^{-7}z^{10}+1{\cdot}1477.10^{-8}z^{12}+\ldots\ldots . \qquad (9)$$

The solutions for the cases $n=1$, 5 can be obtained exactly as shown in the previous paper.

Let ρ_2, the density in the rocky shell, be uniform and let also c, a be respectively the radius of the core and that of the earth's surface. Then, since the mass within the radius r in the shell is

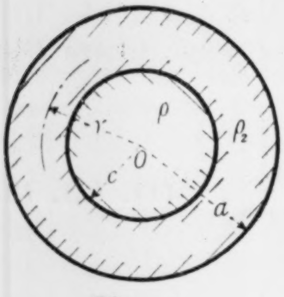

Fig. 1.

$$M_r=\frac{4\pi\rho_2}{3}(r^3-c^3)+M_c$$

$$=\frac{4\pi\rho_2}{3}(r^3-c^3)+\int_0^c 4\pi\rho_1 r^2dr, \qquad (10)$$

and since the pressure P_2 in the shell is related to M_r with the formula

$$\frac{dP_2}{dr} = -\frac{\rho_2 GM_r}{r^2} = -\frac{4\pi G}{3}\rho_2^2\left(r - \frac{c^3}{r^2}\right) - \frac{\rho_2 G}{r^2}M_c, \tag{11}$$

the same pressure is expressed by

$$P_2 = -\frac{4\pi G}{3}\rho_2^2\left(\frac{r^2}{2} + \frac{c^3}{r}\right) + \frac{\rho_2 GM_c}{r} + B. \tag{12}$$

The constant B can be determined from the condition $P=0$ at the free surface $r=a$, from which it follows that

$$P_2 = -\frac{4\pi G}{3}\rho_2^2\left\{\frac{1}{2}(r^2 - a^2) + c^3\left(\frac{1}{r} - \frac{1}{a}\right)\right\} + \rho_2 GM_c\left(\frac{1}{r} - \frac{1}{a}\right). \tag{13}$$

The conditions at the boundary $r=c$ are that $P=P_2$ and that M_c, the mass within the core, shall be given, namely, $1{\cdot}915.10^{27}$gm.mass. These conditions are expressed by

$$\frac{\rho\phi_c}{n+1} = -\frac{4\pi G}{3}\rho_2^2\left\{\frac{1}{2}(c^2 - a^2) + c^3\left(\frac{1}{c} - \frac{1}{a}\right)\right\} + \rho_2 GM_c\left(\frac{1}{c} - \frac{1}{a}\right), \tag{14}$$

$$M_c = \int_0^c 4\pi\rho r^2 dr\left[= \int_0^c 4\pi\left\{\frac{\phi}{(n+1)\kappa}\right\}^n r^2 dr\right], \tag{15}$$

where ϕ_c is the value of ϕ at $r=c$. Using the relations in (4), (5), (6), the above two conditions are replaced by

$$\frac{a^2\phi_0^{n+1}u_c^{n+1}}{n+1} = 1{\cdot}040.10^6, \quad \frac{\phi_0^{\frac{1}{2}(3-n)}}{a}\int_0^{z_c} u^n z^2 dz = 1{\cdot}275.10^{20}, \qquad (16), (17)$$

where z_c is the value of z at $r=c$. There are four unknown constants a, ϕ_0, u_c, z_c in (16), (17). Since however the relations (6), (9) can be used as auxiliary conditions, all these unknown constants can be determined.

In the actual calculation, after drawing the curve that represents the relation in (9), we take a set of u_c and z_c for trial. Using, then, the curve just mentioned, equations (16), (17) will give the values of a and ϕ_0. If all the quantities thus determined satisfy the relation in (6), namely, $z_c = ac\phi_0^{\frac{1}{2}(n-1)}$, the solutions are true, but if not, we shall again assume another set of u_c and z_c and repeat the above calculation until all the quantities satisfy relation (6). In this way the problem can be solved.

3. *Distributions of density, pressure, and wave velocity within the core.*

With the aid of the constants determined by the method shown in the preceding section, it is now possible to calculate the distributions of density, pressure, and wave velocity within the core. The formulae for the distributions of these quantities are (1), (2), and $V=\sqrt{\gamma P/\rho}=\sqrt{\phi/n}$. The results are shown in Figs. 2, 3, 4.

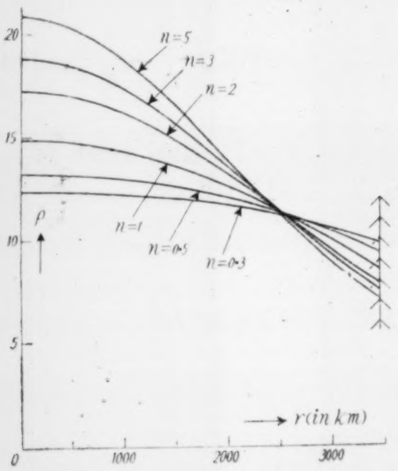

Fig. 2. Density distribution within the core for different values of n.

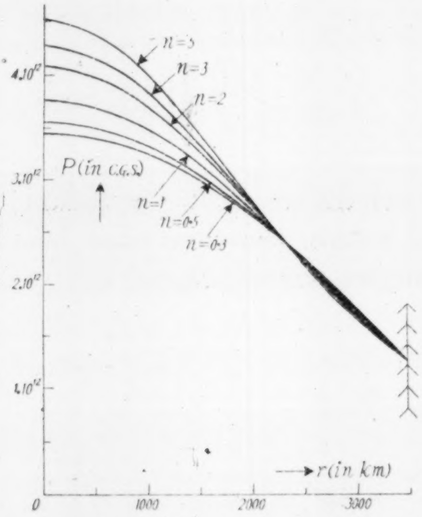

Fig. 3. Pressure distribution within the core for different values of n.

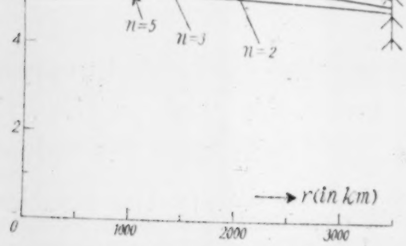

Fig. 4. Velocity distribution within the core for different values of n.

It will be seen from these figures that whereas the distributions of density and pressure within the core tend to be uniform with decrease in n, the distribution of wave velocity becomes rather uniform with increasing n. This arises from the condition that the increase in pressure with depth is not small for any n.

The distribution of velocity of longitudinal seismic waves within the core, as given by Gutenberg and others, is also plotted by broken line in Fig. 4. This shows that the polytropic gaseous state, $n=0{\cdot}3$, within the core is quite similar to that of the actual core, at least, with

respect to the distribution of the longitudinal waves. In such a case, the distribution of density is almost uniform. On the other hand, the same distribution within the liquid core that was determined by Jeffreys[2], is rather similar to the case $n=1$ in the polytropic state. But, Bullen[3] has stated quite recently that, in the usual calculation, the moment of

	$p=1$ atm.	$p=25$ atm.	$p=100$ atm.	$p=200$ atm.
$\theta=-79{\cdot}3°$C.	$n=2{\cdot}47$	$n=1{\cdot}755$	$n=0{\cdot}826$	$n=0{\cdot}752$
$\theta=0°$	$n=2{\cdot}48$	$n=2{\cdot}13$	$n=1{\cdot}52$	$n=1{\cdot}18$

inertia of the earth is likely to be so large that the assumption of uniform distribution of density within the core is still insufficient to explain that large moment of inertia. This shows that the small n of the polytropy does not seriously contradict the probable condition of density distribution. Jeans[4] showed, although in the case of air, that the value of n decreases enormously with pressure and increases very little with temperature, so that the smallness of n in the case of core gas is almost certain. Jeans's results are shown in the above table.

4. *Distribution of temperature within the core.*

In the previous paper, we introduced the idea of nuclear transmuta-

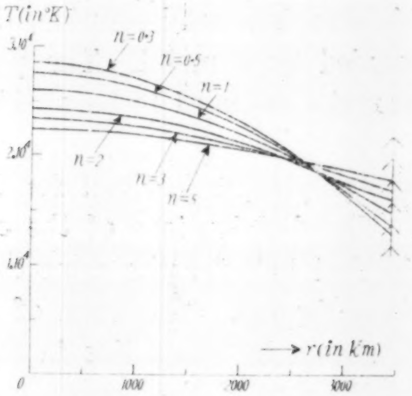

Fig. 5. Temperature distribution within the core for different values of n, it being assumed that $\mu=8{\cdot}5$.

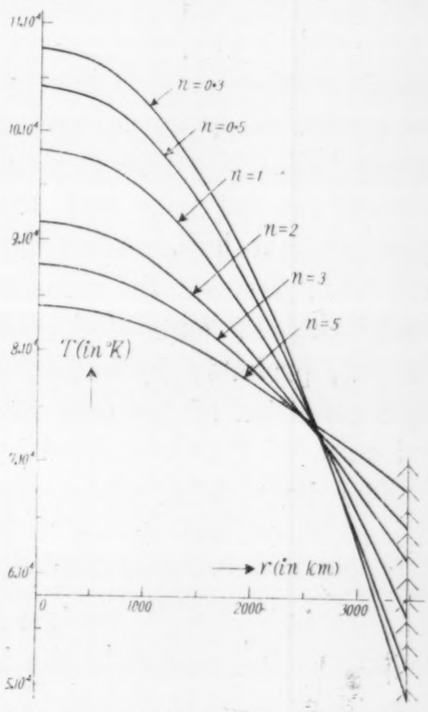

Fig. 6. Temperature distribution within the core for different values of n, it being assumed that $\mu=32$.

tion of the core gas, for which the condition of such a low atomic

2) H. JEFFREYS, *M. N. R. A. S. Geophys. Suppl.* **4** (1937), 50~61.
3) K. E. BULLEN, *Nature,* **145** (1940), 599.
4) J. H. JEANS, *The Dynamical Theory of Gases.* 4th ed. (1925), 189.

weight as $\mu=8{\cdot}5$ was considered. Although, in the present paper, we do not restrict ourselves to the condition of nuclear transmutation, we shall again take the case as $\mu=8{\cdot}5$ together with that of $\mu=32$, the latter case probably representing the mean atomic weight of all the elements in the earth. The results of calculation are shown in Figs. 5, 6. The temperature at any point, from the nature of things, is proportional to the atomic weight of the polytropic gas. The variation of temperature with depth tends to diminish with increasing values of n. At all events, the temperature within the core in the present cases is more than 10^4 °K.

5. *Condensation of a polytropic gas ball.*

The distributions of temperature and the condensing points of the elements in a polytropic gas ball corresponding to the primitive earth were investigated by Mercier[5] and also by us[6]. Since the temperature of the gas ball outside a certain radius is less than the condensing point (corresponding to partial pressure) of some element in the ball, the same element resting outside that radius ought to condense. The element thus condensed, however, cannot fall below the radius in question in the gaseous ball. If every element in the gas ball condenses, then the remaining gaseous part will tend to be sealed in the central spherical region of that ball. According to our present idea, if the core of the earth were gaseous, the same core would have been formed in this way. Lynch[7] recently suggested that the earth's core is a solid solution, that is a gas, probably hydrogen, heavily occluded by a metal. The polytropic condition of the core in our case may be assumed to be an idealized state of that suggested by Lynch.

The distribution of temperature of the polytropic gas ball for two cases $n=1$, $0{\cdot}5$ are shown in Figs. 7, 8. The distributions of the condensing points for iron and silicon within that ball for the same cases of n are indicated by broken lines in these figures. The mass of the gas within any radius in the ball is also shown by chain line in these figures, the mass corresponding to that of the core of the present earth being represented by M_c.

With increasing condensation of the various elements, the boundary

5) A. MERCIER, Archives *Sc. e. Nat.*, **20** (1938), 31~58.

6) K. SEZAWA and K. KANAI, *Bull. Earthq. Res. Inst.*, **17** (1939), 525, 675; **18** (1940), 27.

7) J. LYNCH, "What is the State of the Earth's Core?," *Bull. Seism. Soc. Amer.*, **30** (1940), 337~342.

between the condensed outer shell and the sealed inner gas tends to decrease in radial distance from the centre of the earth. This results from the increasing pressure within the shell and the core with increase in the mass of the condensed part. The temperature of the gaseous part also increases with increasing pressure. It will be seen from Figs. 7, 8 that, even if the condensed element were iron or silicon, the mass

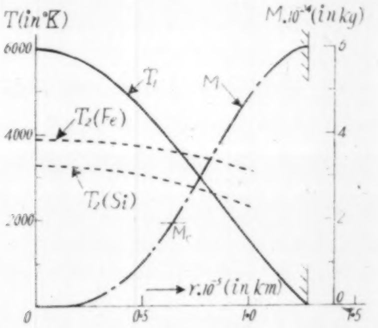

Fig. 7. The distributions of temperature T_1 and condensing point T_2 in a polytropic gas ball, and mass M of the gas within radius r in the same ball. $n=1$.

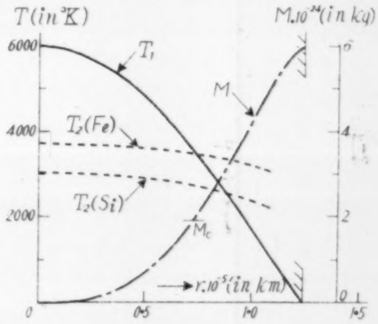

Fig. 8. The distributions of temperature T_1 and condensing point T_2 in a polytropic gas ball, and mass M of the gas within radius r in the same ball. $n=0{\cdot}5$.

of the gaseous part that cannot condense would, although incidentally, fairly resemble mass M_c of the core of the present earth, at any rate for $n=1$ or 0·5. If we specially plot the mass of the gaseous part (not condensed) on the basis of n (Fig. 9), it can be ascertained that the mass of the core in the case of iron being condensed, approaches in quantity more that of the core of the present earth. Thus, although it does not at once follow that the core of the earth is ferrous, it is possible to conclude that the shell of the earth tends to be ferrous with depth. The intersection of the line for Fe and that for M_c in Fig. 9 is near abscissa $n=0{\cdot}3$. In Section 3, it was shown that the distribution of wave velocity for the polytropic gas condition $n=0{\cdot}3$ quite resembles that of the velocity of longitudinal waves in the core of the actual earth, whence it holds that if the core of the earth were gaseous, the polytropic condition of the gas would be $n=0{\cdot}3$.

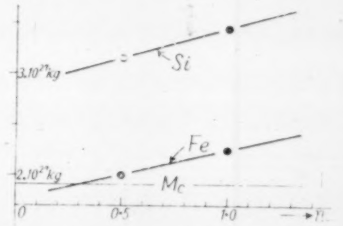

Fig. 9. The mass of gas that cannot condense for any n.

6. *General summary and concluding remarks.*

On the assumption that the earth's core is gaseous, the polytropic

condition of the same gaseous part was investigated mathematically. From the conditions of density, pressure, and longitudinal waves in the core, it is likely that the polytropic index of the gas is nearly $n=0{\cdot}3$. On the other hand, the condensation of the primitive gaseous ball of the earth was considered separately, from which it was also ascertained that the polytropic index of the ball should also be $n=0{\cdot}3$. It was concluded that in the beginning stage of the earth, the gaseous part that was not condensed was sealed near the central region of the ball and pressed from outside, the temperature of the gaseous part having increased with increasing pressure. However, this condition may be an idealized case of the state shown by Lynch, that is, the state of a gas heavily occluded by a metal.

In conclusion, we wish to express our thanks to the officials for Scientific Research in the Ministry of Education for financial aid (Funds for Scientific Research) granted us for a series of investigations, of which this study is a part.

---

1. 地球核の熱力學的成因について (第2報)

地震研究所 妹澤克惟
金井清

この前の報告でも述べたやうに，地球核が瓦斯體であると假定した場合に於ける瓦斯のポリトロープの狀態の數理的研究を續けた．密度，壓力，縱波の速度の關係からポリトロープの指數は $n=0{\cdot}3$ 位が適當してをる事がわかつた．一方に於ては，地球が瓦斯狀の母體から液化した狀態を考へるとやはりポリトロープの指數が $n=0{\cdot}3$ 位である方がよい．結論として，この母體が冷却したときに外殼に液化した部分が出來，瓦斯の部分は中央に封じ込まれながら周圍から壓力を加へられたとすればよいのである．尙，この瓦斯の部分は金屬と瓦斯との固溶體になつた狀態の理想的場合と考へてもよいのである．核瓦斯の溫度はこの壓力によつて次第に上昇した事になるのである．

2. *On the Problem of Instabilities of Higher Orders in a Seismometer. II.*

By Kiyoshi KANAI and Katsutada SEZAWA,

Earthquake Research Institute.

(Read Nov. 21, 1940.—Received Dec. 20, 1940.)

1. *Introduction.*

In our previous paper,[1] various vibrational frequencies at which a seismometer becomes unstable was ascertained both mathematically and experimentally. It was shown that if the damping of a seismometer is great, it is not likely that instability of any order can occur unless the vibration amplitude of the ground is extremely large. In the same paper, the problem was restricted to that condition in which a seismometer becomes unstable, and was not concerned with the vibrational state, whether in the stable or the unstable condition. Since the nature of the instability in any case can generally be ascertained when the whole range of the stability condition has been investigated, our present problem will also be extended to such a range, although the order of instability particularly in experiments is for such part as is near 1/2.

2. *Mathematical formulae.*

The mathematical solution for instability in the case of approximately sinusoidal ground motion was obtained in the previous paper. The damping factor σ for one complete cycle may be represented by the equation

$$\sigma^2-2\sigma e^{-2\pi\frac{\kappa}{p}}\cosh 2\pi\mu-e^{-4\pi\frac{\kappa}{p}}=0, \qquad (1)$$

where

$$\left|\cos\pi\omega_1\cos\pi\omega_2-\frac{\omega_1^2+\omega_2^2}{2\omega_1\omega_2}\sin\pi\omega_1\sin\pi\omega_2\right|=\cosh 2\pi\mu. \qquad (2)$$

In solving equation (1), the damping factor is of the type

1) K. KANAI and K. SEZAWA, *Bull. Earthq. Res. Inst.*, **18** (1940), 483~496.

$$\sigma = e^{-2\pi\frac{\kappa}{p} \pm 2\pi\mu}, \tag{3}$$

so that the damping coefficient of the seismometer in the case of ground movements at right angles to the direction of the pendulum oscillation, is

$$\kappa' = \kappa - \mu p, \tag{4}$$

the coefficient therefore depending on the frequency of the ground movements. The critical condition that $\kappa' = 0$, is shown in Fig. 1.

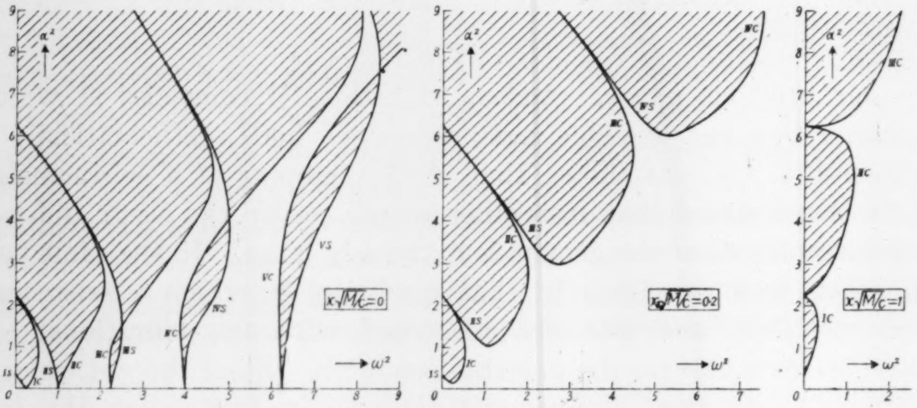

Fig. 1. Curves showing criticals of stability.

Let M, κ, c, L be the mass, logarithmic decrement in the quiescent state, vibrational stiffness (cy being the restitutive force), and the equivalent pendulum length, respectively. If

$$\frac{8A}{\pi^2 L} \ll 1 \quad (\alpha^2 \ll \omega^2), \quad \kappa^2 \frac{M}{c} \ll 1 \quad (\varepsilon^2 \ll \omega^2), \tag{5}$$

the damping coefficient κ' in the vibratory state is approximately

$$\left.\begin{aligned} \kappa' &= \kappa - \frac{32\sqrt{2}\,A}{\pi^2 L T_0} && \text{for 1/2 order stability,} \\ \kappa' &= \kappa - \frac{4}{\pi}\sqrt{2\left(1-\frac{1}{\pi}\right)}\frac{A}{LT_0} && \text{for 2/2 order stability,} \\ \kappa' &= \kappa - \frac{16\sqrt{17}\,A}{27\pi^2 L T_0} && \text{for 3/2 order stability,} \end{aligned}\right\} \tag{6}$$

and so on.

When, especially, damping in the quiescent state is critical, namely, $\kappa\sqrt{Mc} = 1$, the value of κ' near the 1/2 order instability becomes

$$\left.\begin{array}{ll}\kappa'<0 & \text{for } A/L>1{\cdot}233,\\ 0<\kappa'<\kappa & \text{for } 0{\cdot}4394<A/L<1{\cdot}233,\\ \kappa'=\kappa+ic & \text{for } A/L<0{\cdot}4394,\end{array}\right\} \quad (7)$$

the numerical values of κ' being shown in Fig. 2.

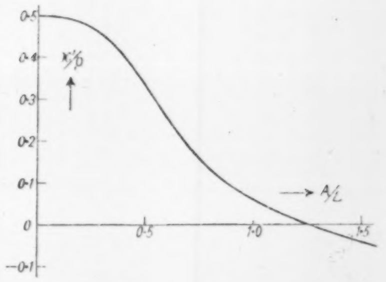

Fig. 2. The relation between κ'/p and A/L for $\kappa\sqrt{M}/c=1$.

3. *Experimental investigation, and its result compared with that of the mathematical calculation.*

The vibration table shown in the previous paper was also used in the present experiment. The vibration period T_0 was always kept at that of the 1/2 order instability. Since there were four models, the period in question was also of four kinds, the amplitude of the table, A, being also kept constant in each model. The logarithmic decrement in the quiescent state, however, varied over a wide range. The conditions of the model and the table in each case are shown in Table I. Although κ_1 shown in the same table represents the damping coefficient of the pendulum without the vibration table, for such a value of κ_1 the pendulum on the vibration table is in a state of critical stability, that is, state $\kappa'=0$.

Table I.

Case	T_0 (sec)	M (kg)	L (cm)	A (cm)	κ_1 (sec^{-1})
A	0·187	1·41	10·7	0·16	0·37
B	0·208	1·12	7·75	0·17	0·48
C	0·188	15·05	11·0	0·185	0·41
D	0·188	15·05	11·0	0·35	0·78

If, in experiments with table vibration, the condition of the seismometer is stable, the free oscillation of that pendulum decays with time, but if, on the contrary, the condition is unstable, the amplitude of the same oscillation augments, the feature of the latter oscillation being however quite regular with an envelop of the form of a diverging exponential curve. Photographic records of two cases of B, namely, case B 1 and case B 2, are shown, as examples, in Figs. 3, 4. The table movements corresponding to these two cases are shown in Figs. 5, 6. When the table is not moving, the oscillation of the seismometer is quite stable for both cases as shown in Figs. 7, 8.

The vibration experiments were conducted for a wide range in the

value of κ in each case, the results being shown in Fig. 9. The condition of the points plotted on the positive side of the ordinate is stable, whereas that of the points plotted on the negative side is unstable.

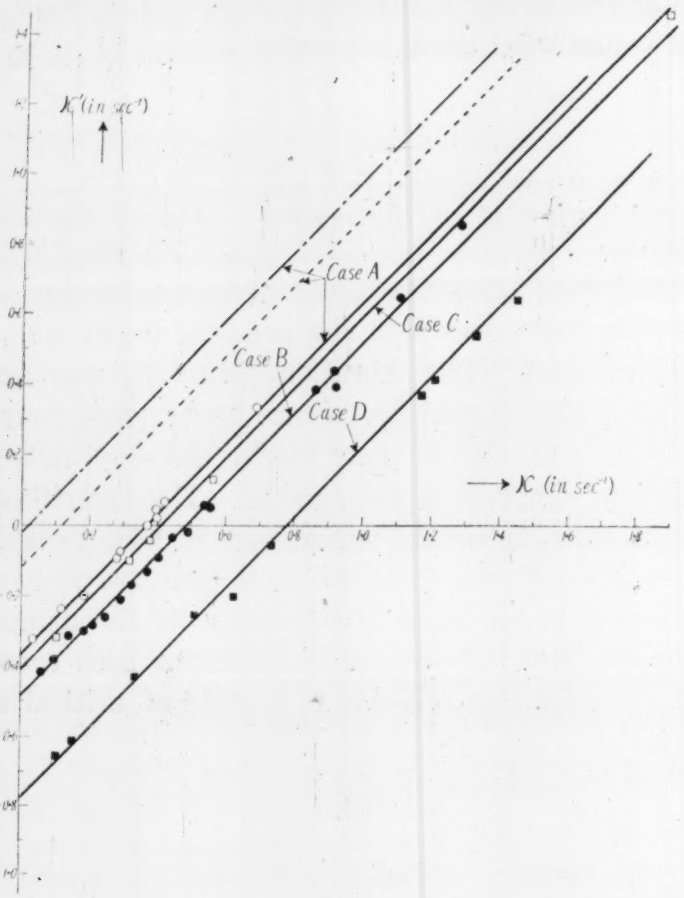

Fig. 9. Variation of κ' with κ.

On the other hand, it is also possible to get mathematically the relation between κ and κ', using the expression (6), the results of which are shown by a series of straight lines. The broken line and the chain line in the same figure correspond to the 2/2 order and the 3/2 order instabilities in case A. It will be seen from this figure that the mathematical and the experimental results agree fairly well. Although no experiment was made for the 2/2 order and the 3/2 order instabilities, we feel confident that a similar result could be obtained if the investigation were extended to such cases.

Equation (7) shows that the seismometer cannot be unstable unless the vibration amplitude of the ground is abnormally large. At all events, in view of the results in (6), (7), and also in Fig. 9, it is now possible to conclude that a seismometer of Ewing-type or a similar pendulum could be made an oscillatory stable one, provided a certain viscous damp-

Fig. 3. B 1. $\kappa' = 0{\cdot}393$.

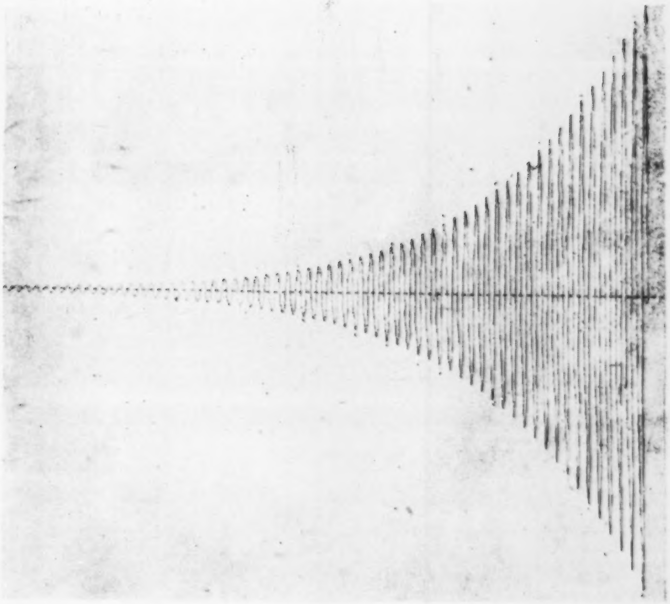

Fig. 4. Case B 2. $\kappa' = 0{\cdot}381$.

Fig. 5. Case B 1.

Fig. 6. Case B 2.

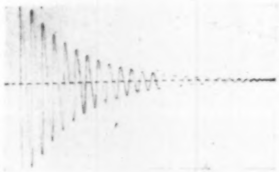

Fig. 7. Case B 1.
$\kappa = 0{\cdot}919$.

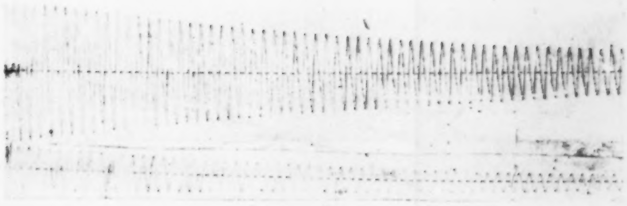

Fig. 8. B 2. $\kappa = 0{\cdot}0976$.

ing were added to that pendulum, although its sensitivity would change with difference in the vibration amplitude of the ground at right angles to the direction of the pendulum oscillation.

4. *Concluding remarks.*

The damping coefficient of a seismometer when there are ground movements at right angles to the direction of the pendulum oscillation, was investigated both for stable and unstable conditions. The results of our mathematical investigation agreed well with the experimental. It was concluded that although the instability of a seismometer can be prevented by merely changing its damper, it is impossible to keep invariably the same sensitivity if there were such ground movements as just mentioned.

In conclusion, we wish to express our thanks to Mr. Kodaira, who assisted us greatly in our work. We also wish to express our thanks to the officials of the Division of Scientific Research, in the Ministry of Education, for financial aid (Funds for Scientific Research) granted us for a series of our investigations, of which this study is a part.

---

2. 地震計に於ける高次の不安定について

地震研究所 {金井　清
妹澤克惟

地震計に於ける高次の不安定の問題の研究の續きとして，振子の振動方向に直角の向きに土地の振動がある場合の振子の振動減衰係數を安定の場合及不安定の場合につき研究した．數理的研究の結果は實驗的研究の結果とよく一致した．結論として地震計の不安定はその粘性的制振器を強くする事によつていくらでも免れる事が出來るけれども，土地のかくの如き振動がある場合にその感度を常に一定に保つのは不可能である事がわかつたのである．

---

3. *Viscosity Distribution within the Earth. II. On the Shadow Zone for Seismic Waves.*

By Katsutada SEZAWA and Kiyoshi KANAI,

Earthquake Research Institute.

(Read Dec. 19, 1940.—Received Dec. 20, 1940.)

1. *Introduction.*

In the previous paper[1], from the analysis of seismic records and from the theory of surface waves as well as bodily waves, it was ascertained that the coefficient of viscosity of the surface layer of the earth is less than 10^{10} in C.G.S. units. Another fact not very clearly made out in that paper, is that the viscosity at depth of the rocky shell may be as small as 10^{5}. This follows from the condition that if the phases for P, S, SS, ScS in seismic data were compared, the value of μ' would be of the order of unity in km.gr.sec. units. Although the viscosity in the surface crustal layer and that at depth of the shell were ascertained in this way to a certain extent, the condition of the intermediate part remains somewhat obscure. On the other hand, Gutenberg and Richter[2] recently showed that at a depth of about 70 km, there is probably a decrease in longitudinal waves of from 8·0 to 7·9 km/sec. A similar statement was also made by L. Don Leet[3] and others. In the present paper we shall mainly discuss the problem in the manner of Gutenberg and Richter, assuming that such a little discontinuous layer gives a shadow zone for seismic waves, and furthermore treat that case in which the discontinuity in question is replaced by a continuous layer, with however the restriction that the viscosity in the same layer shall differ from that outside.

2. *Calculation of wave path.*

In the present paper only the paths of waves arriving from distances

1) K. SEZAWA and K. KANAI, "Viscosity Distribution within the Earth. Prelim. Notes", *Bull. Earthq. Res. Inst.*, **18** (1940), 169～177. $\mu' \ll 1$ in line 21, p. 174 in that paper was a misprint of $\mu' \simeq 1$.

2) B. GUTENBERG and C. RICHTER, *Bull. Seism. Soc. Amer.*, **29** (1939), 531～537.

3) L. DON LEET, *Practical Seismology and Seismic Prospecting* (1938).

not greater than 20° of arc are considered, the earth's surface being assumed to be a plane, all of which greatly simplifies the problem, the numerical errors in its treatment being also minimized. Although it is likely that the velocity of bodily waves increases with depth even in the surface layers, for simplicity, we shall assume that the distribution of the velocity in two surface layers (sum of the thicknesses of these layers being 50 km.) is the same as that shown by Imamura[4] and Matuzawa[5]. Below these layers, on the other hand, the velocity of the waves increases linearly with depth, the law of increase being the same as that of Jeffreys[6]. The distributions of the velocities given above are shown by full lines in Fig. 1. As an alternative treatment of the problem, we also assume that there may be a little drop in the velocity of the longitudinal waves at a depth of 70 km from the free surface, namely, a drop from 8 km/sec to 7·9 km/sec, as shown by the broken line in Fig. 1. The drop gradually decreases until it vanishes at a depth of $H=83{\cdot}8$ km. The idea of velocity drop originated with Gutenberg, and also with Daly[7]. The results in Fig. 1 may also be written in the following formulae:

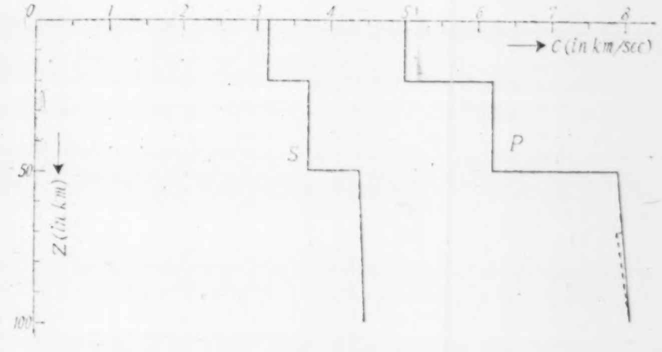

Fig. 1.

P-waves for the ordinary treatment:

$$\left.\begin{aligned} &H=\ 0\sim 20\text{ km}; && c_1=5{\cdot}0\text{ km/sec},\\ &H=20\sim 50\text{ km}; && c_2=6{\cdot}2\text{ km/sec},\\ &H=50\text{ km}; && c_3=(7{\cdot}75+0{\cdot}00588\,z)\ \text{km sec}. \end{aligned}\right\}\qquad(1)$$

P-waves for an alternative treatment:

$$\left.\begin{aligned} &H=\begin{cases}0\sim 70\text{ km};\\ 83{\cdot}8\text{ km};\end{cases} && \text{the same as for the ordinary treatment.}\\ &H=70\sim 83{\cdot}8\text{ km}; && c_4=(7{\cdot}488+0{\cdot}00588\,z)\ \text{km/sec}. \end{aligned}\right\}\qquad(2)$$

S-waves:

4) A. IMAMURA, K. KISHINOUYE, and T. KODAIRA, *Bull. Earthq. Res. Inst.*, **7** (1929), 471∼485.

5) T. MATUZAWA, K. YAMADA, and T. SUZUKI, *ibid.*, **7** (1929), 241∼485.

6) H. JEFFREYS, *M. N. R. A. S. Geophys. Suppl.*, **4** (1937), 50∼61.

7) R. A. DALY, *Bull. Seism. Soc. Amer.*, **44** (1933), 243∼264.

$$
\left.\begin{aligned}
&H=\ 0\sim 20\ \text{km};\quad c_1=3{\cdot}15\ \text{km/sec},\\
&H=20\sim 50\ \text{km};\quad c_2=3{\cdot}7\ \text{km/sec},\\
&H=50\ \text{km};\qquad\ \ c_3=(4{\cdot}3+0{\cdot}0019\,z)\ \ \text{km/sec}.
\end{aligned}\right\}\tag{3}
$$

Although the alternative treatment naturally applies also to S-waves, the formula for it will be omitted.

When the distribution of the velocities is as simple as shown in (1) ~ (3), the path of the waves and the travel time are readily determined by elementary mathematics. Let c' be the wave velocity at the lowest level $z=H$ in a wave path, and c that at any depth z. Let also x and s be the horizontal distance and the length along the wave path.

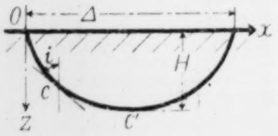

Fig. 2.

Then, since $\sin i=c/c'=dx/ds$, that is to say, $dx/dz=\tan i=(c/c')/\sqrt{1-(c/c')^2}$, the horizontal distance between levels z_1 and z_2 is

$$x=\int_{z_1}^{z_2}\frac{c/c'}{\sqrt{1-(c/c')^2}}\,dz. \tag{4}$$

If $c=A+Bz$, the horizontal distance corresponding to the wave path between z_1 and z_2 is

$$x=\frac{c'}{B}\left[\sqrt{1-\left(\frac{A+Bz}{c'}\right)^2}\,\right]_{z_2}^{z_1}. \tag{5}$$

The travel time corresponding to the wave path between levels z_1 and z_2 is

$$T=\int\frac{ds}{c}=\int_{z_1}^{z_2}\frac{dz}{c\sqrt{1-(c/c')^2}}, \tag{6}$$

so that if $c=A+Bz$, we get

$$T=\frac{1}{B}\left[\log\left(\frac{1+\sqrt{1-\left(\frac{A+Bz}{c'}\right)^2}}{(A+Bz)c'}\right)\right]_{z_2}^{z_1}, \tag{7}$$

Similarly, the length of the wave path between levels z_1 and z_2 is

$$S=\int_{z_1}^{z_2}\frac{dz}{\sqrt{1-(c/c')^2}}, \tag{8}$$

so that if $c=A+Bz$, we get

$$S=\frac{c'}{B}\left[\sin^{-1}\left(\frac{A+Bz}{c'}\right)\right]_{z_2}^{z_1}. \quad (9)$$

In the case of surface layers, constant B is zero, whereas in the case of the lower layers it is not. Even should the distribution of the velocities be of the type of a parabolic curve, the calculation is not difficult. It is however not necessary to consider such distribution at present.

3. *Existence of a shadow zone.*

Substituting the formulae (1), (2), (3) in (5), it is possible to determine the wave paths. A few paths for the case of no velocity drop at 70 km depth are shown in Fig. 3, and those for the case of velocity drop at the same depth, in Fig. 4. In the latter case, owing to the velocity decrease, the refracting angle for waves arriving at an epicentral distance of 10° becomes critical. Thus, the region between the two curves in Fig. 4, namely, the region between the epicentral distance 6·53° and that of 10°, is, as a matter of fact, a shadow zone. Although even within such a shadow zone, it is possible for diffraction waves to be transmitted, the energy of such waves would be very small.

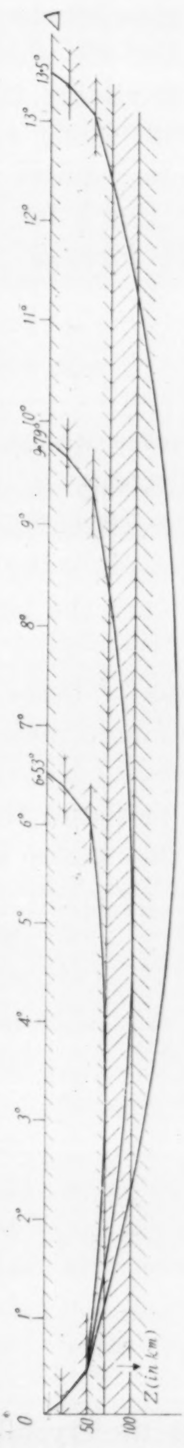

Fig. 3. Wave paths determined by ordinary treatment.

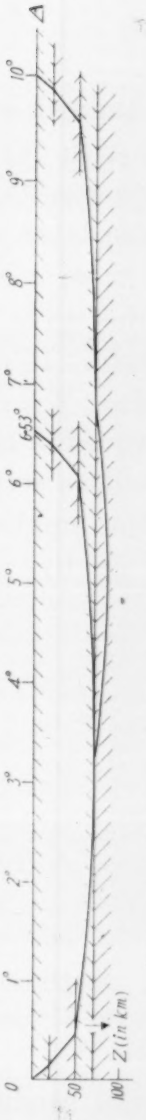

Fig. 4. Wave paths in the case of a velocity drop from 8 km/s to 7·9 km/s at a depth of 70 km, the region Δ between 6·53° and 10° is a shadow zone.

In the case of wave paths (Fig. 3) determined with the assumption that there is no velocity drop at 70 km depth, were that layer of about 30 km thickness below the 70 km depth more viscous than out-

side of it, then since the path of the waves arriving at 9·79°, that is, the epicentral distance within the shadow zone as shown in Fig. 4, is mainly involved in the same viscous layer, the waves in question would be mostly damped, the result being apparently the same as that of a shadow zone[8]. In order to confirm this effect, we calculated wave paths of the type shown in Fig. 3 for various epicentral distances, after which calculation, using the formula

$$A = A_0 e^{-ks}, \quad \left[k = \frac{a^2}{2c} \frac{\lambda' + 2\mu'}{\lambda + 2\mu}, \quad k = \frac{a^2}{2c} \frac{\mu'}{\mu} \right] \tag{10}$$

for longitudinal and transverse waves, we obtained the change in amplitude A with change in viscosity μ_2' of the special viscous layer just given, the results for $a = 2\pi/10\ \text{sec}^{-1}$, $\lambda = \mu$, $\lambda' = \mu'$, and the viscosity of the outside layer $\mu_1' = 10^{10}$C.G.S., being shown in Fig. 5. In the formula (10), s, $2\pi/a$, c, λ, μ, λ', μ' are the lengths along wave path, the wave period, the wave velocity, the elastic constants, and viscous constants, respectively. It should also be borne in mind that owing to the very slight effect, the decrease of amplitude in three-dimensional transmission of the waves is omitted.

It will be seen from this figure that with a relatively small increase in μ_2', the amplitude of the waves becomes fairly small at distance $\Delta = 10°$. In this case, too, although it is possible for wave energy to be supplied to the shadow zone by diffraction phenomena, the resulting increase in amplitude cannot amount to much.

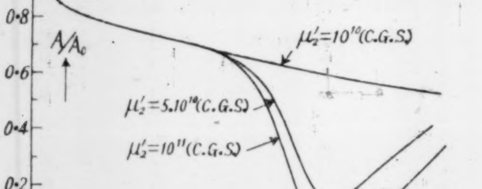

Fig. 5. Amplitude decrease near 10° owing to a viscous layer at 70 km depth.

Judging from the foregoing results, the origin of the shadow zone may either be a velocity drop at a certain depth or viscosity increase at the same depth. According to Daly[9], and also to Gutenberg[10], it is likely that at a depth of about 60 km or so there is a transition of material condition from the crystalline to the vitreous state. In the case of silica and glass, increase in viscosity far exceeds decrease in elasticity in the transition from the crystalline to the vitreous state.

8) In the present example, the most viscous layer was taken relatively too deep. If the same layer were shallower, the epicentral distance of the minimum amplitude would lie midway of the shadow zone shown in Fig. 4.

9), 10) *loc. cit.* 7), 2).

The existence of a more viscous layer at a certain depth thus becomes more probable.

4. *Travel-time curves and waves reflected more than once.*

Even should the shadow zone exist, owing either to a critical condition of refraction at a certain layer or to the special viscous state of the same layer, the waves in discussion would first be restricted to those that are never reflected on the free surface of the earth. If the waves were those that are reflected more than once at the free surface, then, since these waves are not transmitted through the special layer already mentioned, it is not possible for any shadow zone to exist. Thus, the discussion in the previous section applies only to the first phase of the seismic movements. As to the amplitudes of the second and other phases, say, *PP*, *SS*......, it is not necessary that they be subject to the condition in question. For ascertaining the lag in time of the second and other phases, we calculated travel time curves, using equation (7), the results being shown in Fig. 6. The curves in this figure will serve to identify the phases in the seismic records to be shown presently. The marks indicating the value of H represent the lowest depth through which the waves are transmitted, so that it is possible to confirm that condition that waves that have been reflected more than once can scarcely pass through the special layer mentioned.

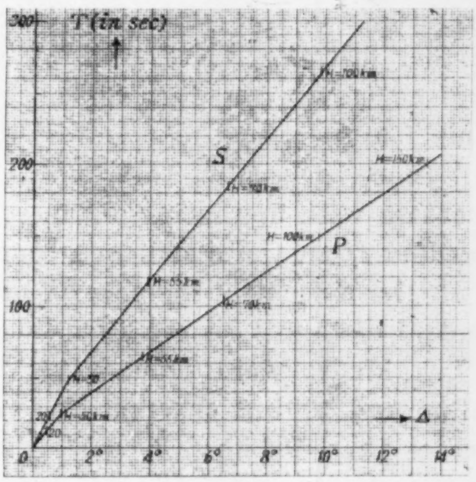

Fig. 6. Travel-time curves calculated by mathematical formula.

5. *Analysis of seismic records. Amplitudes of surface waves relative to those of bodily waves.*

With a view to confirming the theory with actual seismic data, the records of eight earthquakes observed in Tokyo will be used, the seismic origins, the dates of occurrence, and the epicentral distances, etc., being shown in Table 1.

Comparing Figs. 7～19, it will be seen that in the seismic records of near earthquakes (Nos. 1～3) of epicetral distances shorter than

Table I.

No.	Date	Epicence			Epicentral distance		Seismic record
		Vicinity	λ_E	φ_N			
1	1932 XII 2	Vicinity of Mito	140·29	36·47	$\Delta=0{\cdot}71°$	Short distance	Fig. 7
2	1938 XI 5	off Sioyamisaki	141·60	37·07	$\Delta=1{\cdot}7°$		Figs. 8, 9
3	1933 III 3	off Sanriku Coast	144·00	38·50	$\Delta=4{\cdot}3°$		Fig. 10
4	1931 XI 2	Hyûga Sea	132·1	32·4	$\Delta=7{\cdot}0°$	Medium distance	Figs. 11, 12, 13
5	1914 I 12	Sakurazima	130·39	31·34	$\Delta=8{\cdot}38°$		Fig. 14
6	1940 VIII 2	Kamoimisaki	139·1	44·3	$\Delta=8{\cdot}5°$		Fig. 15
7	1919 XII 20	Taiwan	—	—	$\Delta=20{\cdot}0°$	Long distance	Figs. 16, 17
8	1922 III 5	Kamchatka	157·5	52·5	$\Delta=21{\cdot}0°$		Figs. 18, 19

$\Delta=4{\cdot}3°$, no marked surface waves appear, whereas in those of earthquakes of medium distances (Nos. 4∼6), namely, $\Delta=7°\sim8{\cdot}5°$, the amplitudes of the surface waves are very marked. For earthquakes of farther distances (Nos. 6∼8), say, $\Delta=20°$, although the phases of the surface waves are discernible, their amplitudes are never very large. This feature seems to manifest itself in almost every earthquake.

Since, generally, the amplitudes of surface waves should tend to decrease with epicentral distance, the feature just referred to probably resulted from the anomalous change in the amplitudes of bodily waves with the epicentral distance in question. Bodily waves arriving at epicentral distances nearer than 10°, whether of the *P*, *S* or of the *PP*, *SS*......kinds, were transmitted through a layer at a depth between 50 km and 100 km, whereas those reaching $\Delta=20°$ passed through a layer deeper than 100 km. It holds then that the viscosity in the layer that is not deeper than 100 km exceeds by far that in a layer of depth greater than 100 km. Although in Section 3, it was assumed that the layer between 70 km and 100 km is only very viscous, from the present result it follows that the layer that is shallower than 70 km may also be fairly viscous. It is now possible to invoke the viscosity distribution in the crust to explain, to a great extent, the occurrence of a shadow zone in the case of seismic waves.

6. *Analysis of seismic records. Amplitudes of P, S relative to those of PP, SS.......*

It is impossible to discriminate *PP*, *SS* from *P*, *S* for earthquakes of short distances. For earthquakes of medium distance, the phases of *PP*, *SS*...... can clearly be identified. In this case, the amplitudes of *PP*, *SS* are considerably larger than those of *P*, *S*, as will be seen from

Figs. 11~15. Since, waves corresponding to P and S were mainly transmitted through that layer between 70~100 km depth and those corresponding to PP, SS through that layer which is shallower than 70 km, but mostly deeper than 50 km, it follows that the layer at 70~100 km depth is more viscous than that which is shallower than 70 km. As shown in the previous paper, the viscosity of the upper layer of the earth is of the order of 10^{10} C.G.S. (predicted from the condition of surface waves). Judging from this and the result in Fig. 5, it appears that the viscosity of the layer of depth from 70 km to 100 km would be of the order from 10^{10} to 10^{11} in C.G.S. units. The viscosity of the medium that is deeper than 100 km ought to be much less than 10^{10}, tending further to decrease with depth. The viscosity at depth, say, 1,000 km or 2,000 km, would be of the order 10^{5} C.G.S.

In Section 3, it was concluded that shadow zones for seismic waves may arise from the critical condition of the refraction of the waves. But, should the relation that the amplitudes of PP waves or SS waves are fairly small compared with those of the surface waves, invariably hold, then it would seem that the problem is more satisfactorily explained by assuming a difference in viscosity from layer to layer.

7. *General distribution of viscosity within the earth's crust near its surface.*

From the results of the present investigation and those of the preceding paper, it appears that the viscosity of a layer that is shallower than 70 km is less than 10^{10} C.G.S. and that of a layer between 70 km and 100 km is of the order of the range from 10^{10} to 10^{11} in C.G.S. At depths exceeding 100 km the viscosity becomes much smaller than 10^{10} C.G.S. The viscosity in a layer deeper than 100 km decreases with increasing depth, finally tending to 10^{5} C.G.S. at a great depth, say, 1,000 km or 2,000 km.

8. *General summary and concluding remarks.*

In investigating the origin of the shadow zone for seismic waves at an epicentral distance near 10° of arc, two conditions of the crust, were considered, one being the critical state of the refracting angle of the waves and the other the viscosity distribution within the earth. Actual seismic records of various epicentral distance were examined from both standpoints. Although the difference in amplitudes between the waves PP, SS and the waves P, S can be explained from the two

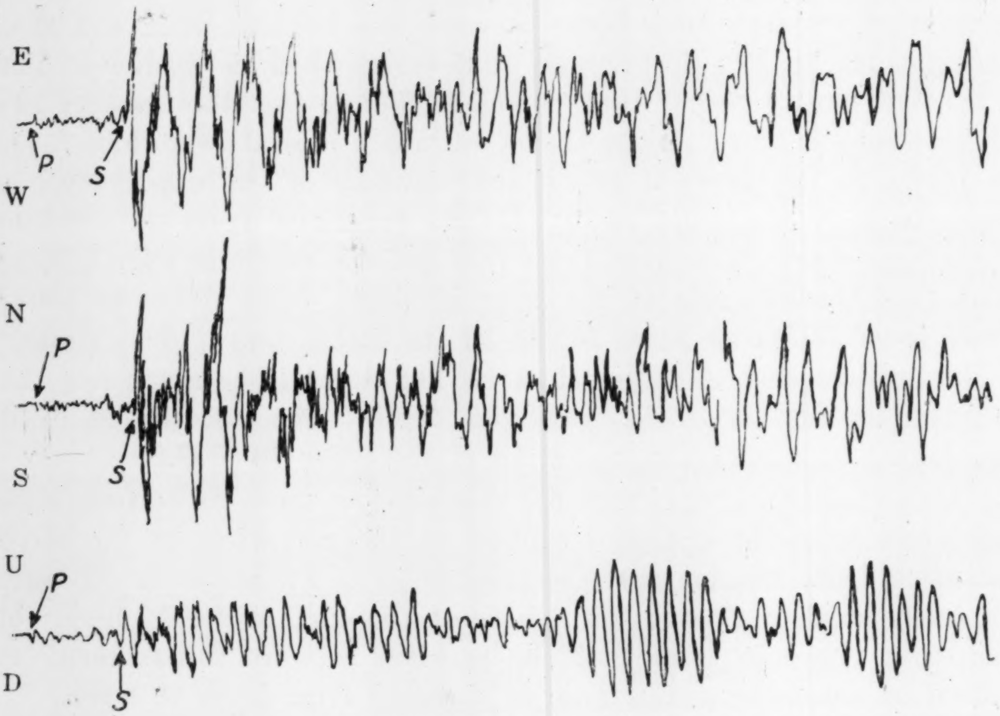

Fig. 7. No. 1. $\Delta=0{\cdot}71°$; Vicinity of Mito, 1932 XII 2; V (NE, EW) $=50$, (Vert) $=28$, $T=7$ sec, $\varepsilon=1{\cdot}5$. Actual size.

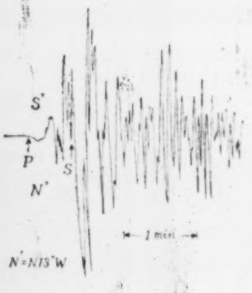

Fig. 8. No. 2. $\Delta=1{\cdot}7°$; off Sioyamisaki, 1938 XI 5; NS; $V=1{\cdot}5$, Original $\times 1/4$.

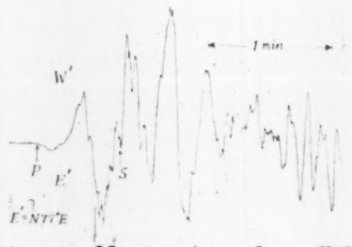

Fig. 9. No. 2. $\Delta=1{\cdot}7°$; off Sioyamisaki, 1938 XI 5; EW; $V=1{\cdot}5$, Original $\times 1/4$.

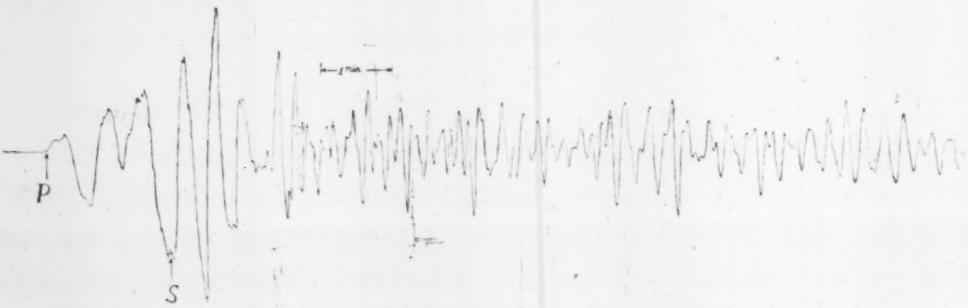

Fig. 10. No. 3. $\Delta=4{\cdot}3°$; off Sanriku Coast, 1933 III 3; EW; $V=1{\cdot}5$, $T=33$ sec, $\varepsilon=1{\cdot}5$. Original $\times 1/4$.

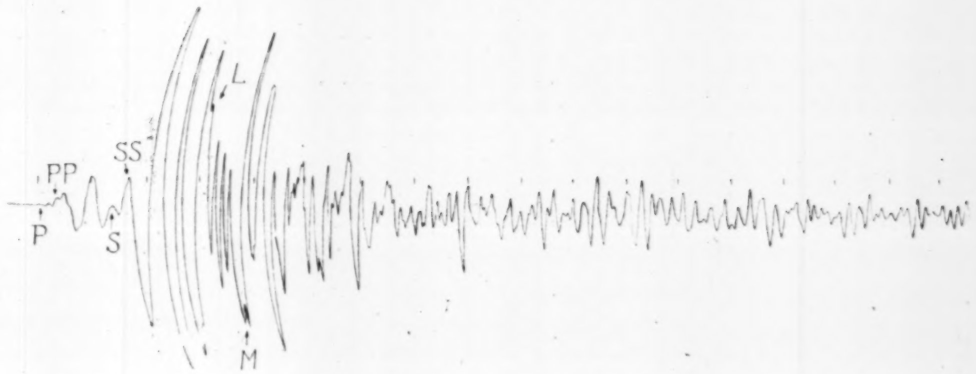

Fig. 11. No. 4. $\Delta=7°$; Hy ga Sea, 1931 XI 2; NS; $V=20$, $T=60$ sec, $\varepsilon=2{\cdot}0$. Original×1/4.

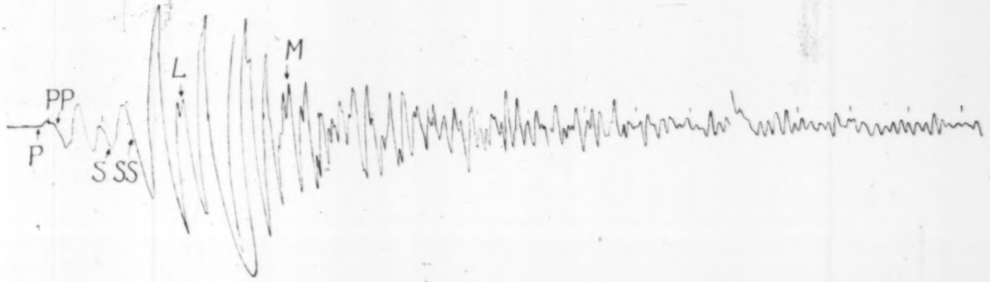

Fig. 12. No. 4. $\Delta=7°$; Hyûga Sea, 1931 XI 2; EW; $V=15$, $T=60$ sec, $\varepsilon=3{\cdot}2$. Original×1/4.

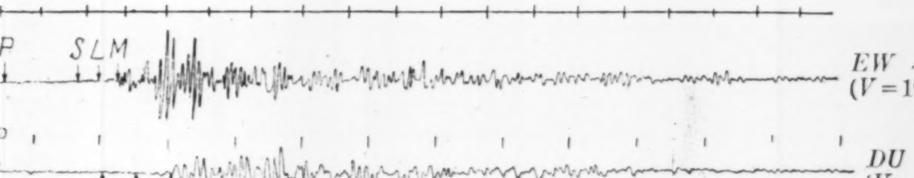

Fig. 13. No. 4. $\Delta=7°$; Hyûga Sea, 1931 XI 2; UD; $V=20$, $T=15$ sec, $\varepsilon=1{\cdot}7$. Original×1/4.

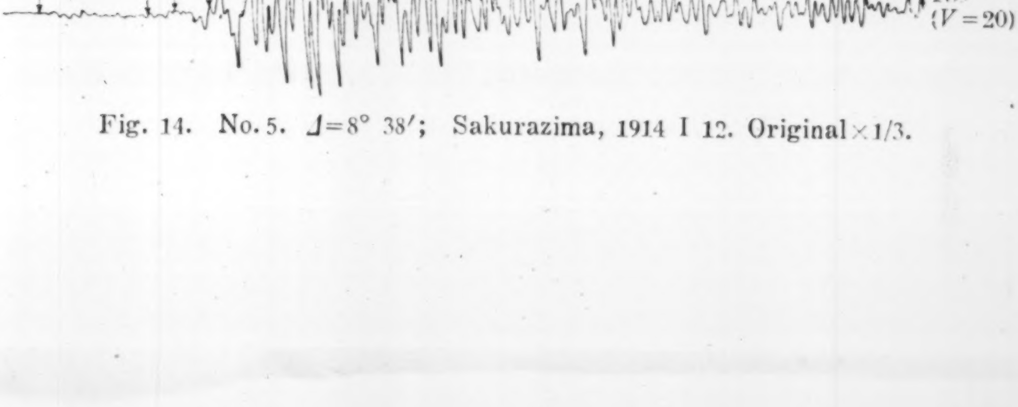

Fig. 14. No. 5. $\Delta=8°\ 38'$; Sakurazima, 1914 I 12. Original×1/3.

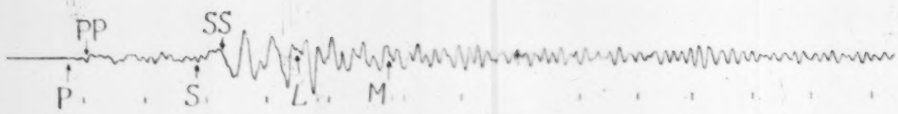

Fig. 15. No. 6. $\Delta=8{\cdot}5°$; Kamoimisaki, 1940 VIII 2; NS; $V=5{\cdot}5$, $T=50$ sec, $\varepsilon=1{\cdot}5$. Original×1/4.

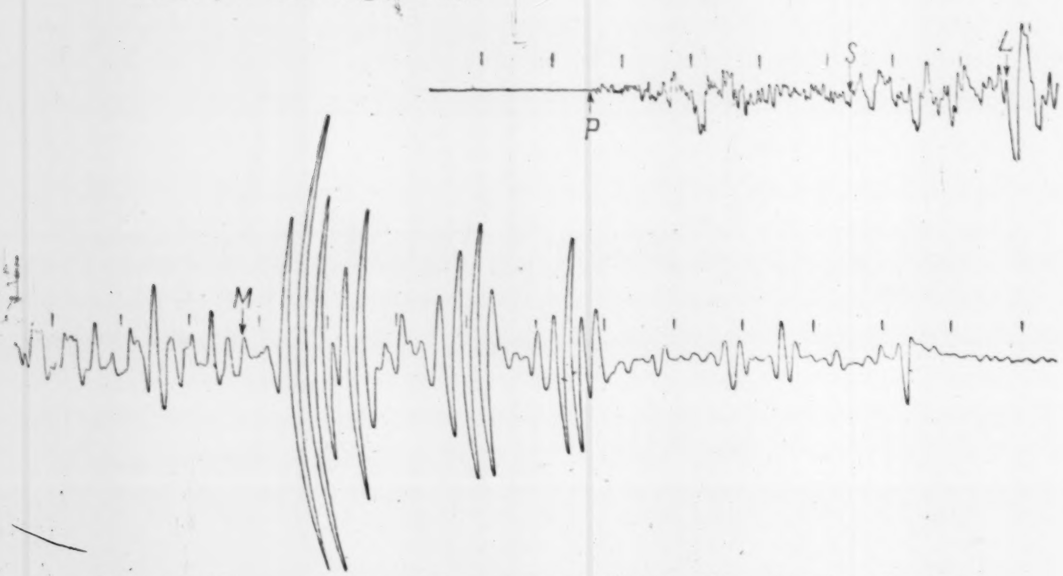

Fig. 16. No. 7. $\Delta=20°$; Taiwan, 1919 XII 20; NS; $V=120$, $T=20$ sec, $\varepsilon=2{\cdot}0$. Original×1/3.

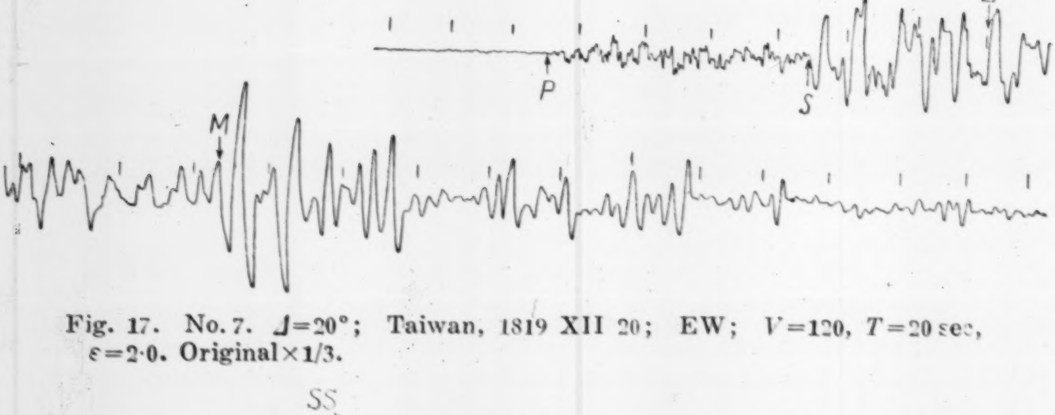

Fig. 17. No. 7. $\Delta=20°$; Taiwan, 1819 XII 20; EW; $V=120$, $T=20$ sec, $\varepsilon=2{\cdot}0$. Original×1/3.

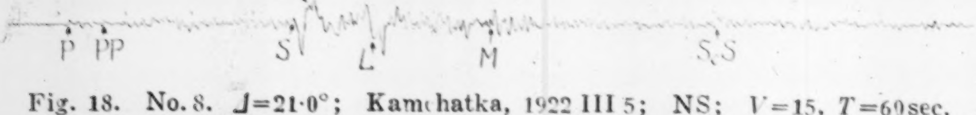

Fig. 18. No. 8. $\Delta=21{\cdot}0°$; Kamchatka, 1922 III 5; NS; $V=15$, $T=60$ sec, $\varepsilon=2{\cdot}0$. Original×1/4.

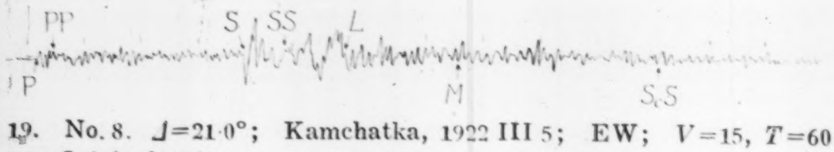

Fig. 19. No. 8. $\Delta=21{\cdot}0°$; Kamchatka, 1922 III 5; EW; $V=15$, $T=60$ sec, $\varepsilon=3{\cdot}2$. Original×1/4.

ideas just mentioned, investigation of the amplitudes of the surface waves relative to those of bodily waves leads us to believe that viscosity distribution more satisfactorily explains the problem. It appears that the viscosity in the layer shallower than 70 km is less than 10^{10} C.G.S. and that in the layer between 70 km and 100 km is of the order between 10^{10} and 10^{11} in C.G.S. The increase in viscosity is probably due to change of rock state from crystalline to vitreous. At depths greater than 100 km, the viscosity is much less than 10^{10} C.G.S. The viscosity in the layer that is deeper than 100 km decreases with increasing depth, finally tending to 10^5 C.G.S. at a great depth, say, 1,000 km or 2,000 km.

In the present investigation, Mr. Yasuda loaned us well selected valuable seismic data of different epicentral distances observed in Tokyo. To this gentleman we wish to express our hearty thanks. We also wish to express our warmest thanks to the officials of the Division of Scientific Research in the Ministry of Education for Financial Aid (Funds for Scientific Research) granted us for a series of investigations, of which this study is a part.

---

3. 地球の内部に於ける粘性の分布（第2報）地震波の陰になる地帯について

地震研究所 {妹澤克惟 / 金井清}

震央距離 10 度附近に地震固體波の陰が出來る事の説明を與へるために，ある深さの地層で波の屈折角が限界になるといふ考方と同じ深さで固體の粘性が少しく高くなるといふ考方との兩方を試みてみた．表面で一度も反射しない波と反射した波とを比較すると何れの説でもよい事がわかるが，之に表面波までも入れて考へると固體の粘性に變化があるといふ説明の方が多少有理なやうである．地表から 70 粁までの深さでは粘性が 10^{10} (C.G.S.) 以下であるとし，70 粁から 100 粁までは 10^{10} 乃至 10^{11} とすればよい樣である．又 100 粁よりも深い所では 10^{10} 以下になり，それから下は深さと共に粘性が次第に減少して 1,000 粁乃至 2,000 粁の如く深い所では 10^5 (C.G.S.) 程度になるものと考へられるのである．

---

4. Relation between the Gravity Anomalies and the Corresponding Subterranean Mass Distribution. (VI.)

By Chuji TSUBOI and Seiti YAMAGUTI,

Earthquake Research Institute.

(Read June 20, 1940.—Received Dec. 20, 1940.)

In his earlier papers[1], one of the present writers developed a direct method, with the aid of which it is possible to estimate, from the gravity anomalies that are observed in a certain region, the responsible subterranean mass distribution. In subsequent papers, the method was successfully applied for studying the geophysical structure of the earth in various localities of the world where gravity data for such studies are available. Particularly in the fourth and fifth papers of the series[2], the method was applied for studying the isostatic conditions of the earth's crust in the United States of America. The thickness of the isostatic earth's crust d, the degree of regionality of isostasy R, and the undulation of the isostatic geoid in the U.S.A. could be found directly from the Bouguer gravity anomalies observed in that country. The present paper, which is the sixth of the series, similarly deals with that part of the Dutch East Indies, bounded by latitudes 0° and 10°S and longitudes 118°E and 132°E, approximately $1000 \times 1400 \text{km}^2$ in area. Since for the purpose of the present study, the same method will be followed as in the previous ones, no detailed explanation of it will be repeated.

Being situated in the eastern part of the Dutch East Indies, most of the area to be studied belongs to the Banda Sea, including the Celebes, Flores, Timor, Ceram, and many other islands. The gravity anomalies in this area was measured by Vening Meinesz during his famous submarine expeditions. The extremely interesting facts as disclosed by these measurements concerning the geophysical structure in this area

1) C. TSUBOI and T. FUCHIDA, *Bull. Earthq. Res. Inst.*, **15** (1937), 636; **16** (1938), 273.
C. TSUBOI, *ibid.*, **15** (1937), 650; **17** (1939), 351; *Proc. Imp. Acad. Tokyo*, **14** (1938), 170.

2) C. TSUBOI and others, *Bull. Earthq. Res. Inst.*, **18** (1939), 385.
C. TSUBOI, *ibid.*, **18** (1940), 384.

have already been discussed by Vening Meinesz himself and many others. The area to be studied in the present paper is exactly where the belt of large negative gravity anomalies that was found by Vening Meinesz changes its trend acutely into a NS direction after running in an EW direction off the southern coasts of Java, Sumatra, and other islands of the East Indian Archipelago.

First of all, it is important that the earth's crust in this area is, very roughly speaking, in isostatic equilibrium. If the Bouguer gravity anomalies in this area are plotted against the depths of the sea where the anomalies were measured, Fig. 1 is obtained, in which is an unmistakable tendency of the anomaly $\Delta g_0''$ to increase with the depth $(-H')$. The least square calculations show that the relation between

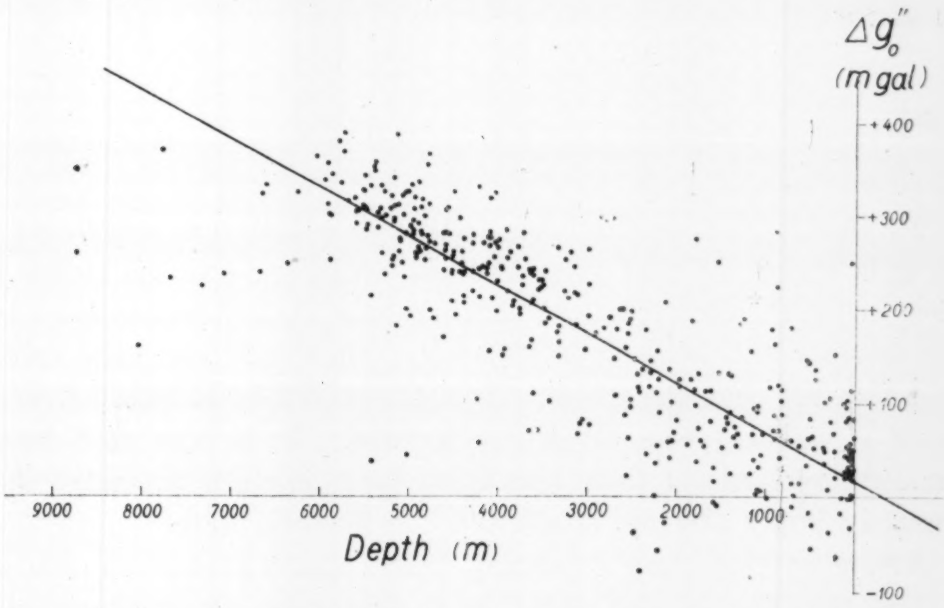

Fig. 1. Relation between the Bouguer Gravity Anomalies and Depth.

the two quantities is given by

$$\Delta g_0''(\text{mgal}) = 15 - 0{\cdot}05\, H'(\text{m}).$$

On the other hand, using the notations as shown in Fig. 2, perfect Airy isostasy implies that

$$\rho_1 H' + \rho_2 d_2 + \rho_3 d_3 = \rho_2 (H' + d_2 + d_3),$$

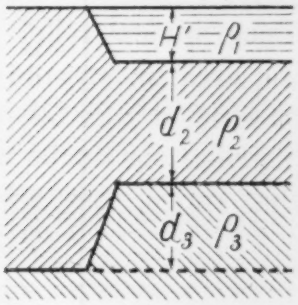

Fig. 2.

where ρ_1, ρ_2, and ρ_3 are respectively the densities of the sea-water, of the earth's crust and of the subcrustal material underlying it, whence we have

$$d_3 = \frac{\rho_2 - \rho_1}{\rho_3 - \rho_2} H'.$$

The Bouguer anomaly as observed on the surface of the sea will then be

$$\begin{aligned} \Delta g_0'' &= 2\pi k^2 (\rho_3 - \rho_2) d_3 \\ &= 2\pi k^2 (\rho_2 - \rho_1) H' \end{aligned}$$

provided isostasy is perfect. Equating $2\pi k^2(\rho_2 - \rho_1)$ with the numerical constants $0{\cdot}05 \times 10^{-5}$, which was found by the least square calculation, and putting

$$\rho_1 = 1{\cdot}0,$$

then from

$$2\pi k^2 (\rho_2 - \rho_1) = 0{\cdot}05 \times 10^{-5}$$

we get

$$\rho_2 = 2{\cdot}2$$

which value is not unreasobable, although a little too small. At any rate, it is important that even in those areas, such as the Dutch East Indies, in which intense tectonic disturbances are believed to have taken place, isostasy still holds approximately. Those who state the contrary forget the fact that the gravity anomalies would be at least a few time greater if isostasy was altogether ignored. It is true that isostatic anomalies are large in these areas, but large isostatic anomalies do not necessarily imply absolute absence of the isostatic state.

Assuming that Airy's isostasy holds approximately in this area, the first requisite in this study is to determine the thickness of the earth's crust under that asssumption. As was shown in the previous papers, this can be done by comparing the Fourier coefficients for the topographical relief and for the observed Bouguer gravity anomalies in the area under study. In the present case, the whole range of area to be studied was taken as $\pi \times \pi$, and since the symmetric images of the distributions to be analysed into the Fourier series were added beyond that range, they are expressed by a cosine series, such as

$$H(xy) = \sum\sum H_{mn} \cos mx \cos ny,$$

$$\Delta g_0''(xy) = \sum\sum B_{mn} \cos mx \cos ny.$$

In executing the Fourier analysis of the topographical relief, due reductions were made for the effect of the sea-water. Thus the actual

Table I. Fourier Coefficients H_{mn} for the Topographical Relief. (in 10 m.)

n \ m	0	1	2	3	4	5	6	7	8	9	10	11	12	13	14	15	16	17	18
0	−98·7	38·1	42·4	−12·3	−19·8	−19·5	3·2	− 6·9	− 5·1	−11·1	− 0·8	4·0	17·9	− 8·3	13·3	6·4	3·4	− 2·8	0·8
1	22·6	16·1	36·8	− 4·3	−53·0	−14·9	− 6·2	−10·7	− 5·4	− 5·0	−12·8	6·8	3·1	0·8	11·9	16·3	10·0	− 1·6	− 1·1
2	45·5	−61·3	−16·1	− 1·4	16·2	4·5	−22·4	− 2·6	1·2	21·3	− 8·5	11·1	− 3·3	8·6	− 2·7	8·7	− 6·8	− 1·8	4·8
3	−41·5	7·4	−45·1	− 4·5	17·8	16·6	12·9	7·7	1·9	11·7	5·5	− 5·2	11·8	− 7·0	− 8·1	−13·2	− 4·8	−14·2	2·6
4	− 2·3	17·0	−20·9	5·0	0·1	19·9	3·3	−18·5	− 2·3	− 0·9	− 5·5	1·3	14·7	4·9	12·8	− 1·7	6·3	−12·7	− 4·0
5	4·3	−15·5	−10·7	0·7	− 0·2	− 8·8	28·9	19·7	2·2	0·2	0·2	11·5	− 7·7	10·0	4·2	5·3	− 6·1	5·7	− 9·2
6	−25·8	− 9·3	22·6	13·5	−16·3	− 6·8	− 2·0	− 7·3	− 2·2	8·9	− 1·7	−15·2	−12·5	1·3	− 7·3	− 3·7	5·4	11·2	9·2
7	3·9	19·1	3·9	24·6	5·9	3·4	− 6·3	20·8	− 0·4	− 7·5	− 0·3	3·3	3·2	− 1·9	6·9	− 6·8	15·6	0·9	14·8
8	−16·7	−18·6	− 0·2	3·1	1·5	8·1	4·8	−12·8	− 8·4	− 1·4	− 4·3	− 7·2	− 8·3	3·0	− 0·5	− 5·4	− 0·9	3·5	− 2·8
9	− 5·5	5·4	8·8	9·4	6·6	−13·5	− 3·6	7·7	8·4	− 9·1	− 5·0	4·8	7·9	− 4·8	2·9	8·9	− 5·4	4·9	− 2·5
10	− 0·1	−11·6	−13·8	3·5	10·3	10·7	1·2	− 0·8	− 6·6	6·9	12·0	7·0	− 0·3	0·7	− 1·9	− 2·1	0·5	− 0·9	− 4·1
11	−10·5	− 8·7	−19·9	3·9	8·1	− 9·8	− 0·9	4·6	4·2	2·0	− 5·4	4·9	−12·1	−14·0	−11·3	− 5·4	6·5	4·6	3·1
12	18·1	7·9	− 1·7	3·0	− 2·5	4·0	0·5	6·1	− 3·9	15·5	10·0	2·9	− 4·1	2·4	− 5·3	− 7·6	− 0·5	− 0·6	8·7
13	− 2·0	−16·9	− 0·5	11·8	4·1	− 4·3	−12·0	8·7	4·2	− 1·7	− 3·5	−13·0	− 4·7	1·6	0·1	3·8	− 1·3	6·5	0·4
14	− 1·3	8·8	4·9	− 5·1	−12·9	2·5	1·5	− 6·6	5·8	− 6·5	2·0	− 4·8	9·0	2·5	− 3·5	4·0	− 8·7	5·9	− 5·3
15	− 7·4	6·8	10·0	− 1·3	6·0	11·4	4·4	−13·8	1·2	8·1	− 8·3	− 3·5	− 1·4	3·2	− 4·3	4·1	1·5	2·2	0·5
16	−14·2	− 1·2	0·2	− 1·1	0·4	−13·6	1·2	5·0	10·1	− 1·2	−13·1	11·6	− 1·7	0·3	3·7	0·3	− 3·3	− 5·1	1·5
17	5·1	8·4	14·4	− 4·7	− 8·3	5·9	− 9·7	− 9·7	− 6·3	− 0·5	5·0	0·7	4·1	8·4	− 0·8	0·7	− 5·5	− 2·0	− 3·2
18	5·2	− 3·8	3·4	1·3	− 6·1	− 8·4	− 8·9	10·3	− 3·2	− 6·9	8·4	7·9	4·5	− 1·7	− 0·1	3·5	− 5·0	− 1·5	− 3·8

Table II. Fourier Coefficients for the Bouguer Gravity Anomalies. (in mgal.)

m \ n	0	1	2	3	4	5	6	7	8	9	10	11	12	13	14	15	16	17	18
0	118·0	−24·0	−38·7	13·9	10·4	8·6	−20·3	7·1	−1·1	11·5	−4·5	−0·8	−0·6	1·1	−1·1	2·7	−4·4	−3·0	2·1
1	6·7	−11·4	4·4	3·9	30·5	4·3	−6·9	−16·3	6·2	4·6	−2·2	−6·8	1·0	0·4	1·5	−3·7	−2·1	−5·1	5·1
2	−53·6	59·1	40·8	−28·4	−11·6	2·3	23·8	−15·9	1·9	−5·6	2·2	−7·1	4·2	−7·5	5·7	−3·3	1·8	−2·5	1·5
3	20·6	−6·1	12·6	7·6	−36·8	−11·4	5·1	−8·1	1·6	0·5	0·7	4·7	−3·0	2·6	−4·9	2·4	3·2	4·2	−2·4
4	−16·7	−23·4	42·2	−2·2	−18·9	5·9	11·7	−5·3	5·8	−0·0	−2·9	4·7	−3·6	2·9	−7·6	5·6	−3·5	4·9	−1·4
5	−1·3	13·1	−6·6	−12·6	8·0	22·8	−14·7	−1·3	0·7	2·4	0·1	−0·5	4·9	−9·7	2·8	−1·1	1·2	−2·9	2·6
6	2·6	−3·4	−16·8	0·2	−6·7	8·5	0·0	7·7	0·3	0·6	−7·7	1·9	−2·4	0·3	2·9	−0·6	5·7	−4·0	−0·7
7	−9·2	4·0	−6·9	−2·0	−0·0	1·6	6·4	0·2	4·3	−7·2	−3·7	−7·8	3·5	1·0	−1·2	8·3	−2·9	2·9	−3·7
8	2·8	1·2	−8·0	5·7	4·8	−3·7	−5·6	3·3	1·0	−3·3	4·4	−0·2	4·4	−0·1	−4·5	−2·9	0·0	1·4	−1·4
9	4·3	−1·9	−7·1	2·3	7·6	−6·4	2·0	−3·6	0·9	7·1	−6·5	1·5	−1·3	5·1	−0·2	−5·1	1·1	−2·0	2·0
10	−1·7	−1·4	3·5	−0·6	0·9	−1·1	−9·6	0·1	2·7	−5·7	4·3	0·6	−5·1	6·9	−0·4	−1·3	0·4	1·4	2·5
11	−2·1	4·0	3·3	−9·8	−0·1	6·7	−12·3	2·4	0·1	−3·7	5·2	1·7	1·9	−3·3	2·3	0·8	−0·2	0·8	−2·0
12	1·7	2·0	7·9	−3·3	−0·6	−3·8	1·5	3·3	−1·5	0·9	−2·5	1·1	−1·1	−4·4	2·4	−1·8	−0·0	3·9	0·5
13	1·9	−1·3	0·3	−6·8	−2·3	−1·6	−1·7	−2·6	1·3	4·4	−3·2	3·4	−0·8	4·2	−0·2	0·7	−1·2	0·4	0·3
14	5·0	−1·1	−3·4	4·7	−0·2	−6·3	0·3	−1·5	1·2	2·2	0·3	−0·7	2·8	0·0	−1·6	3·3	−3·0	2·4	−1·2
15	−1·5	−1·8	−2·5	1·3	−2·3	0·0	−1·6	1·4	0·0	−0·7	3·3	1·0	2·3	−4·2	−1·3	−0·4	−1·6	3·2	0·9
16	1·2	0·1	2·6	2·0	−1·7	−6·7	−0·9	2·8	0·6	−1·0	−3·4	1·5	2·0	0·6	0·0	1·5	2·8	−5·1	4·7
17	2·8	−0·5	−6·3	2·3	1·8	−3·3	2·7	3·8	−0·2	−3·8	−0·1	0·4	−1·8	1·0	0·3	−1·4	1·8	−4·5	−1·9
18	0·9	3·0	−4·7	0·1	0·7	1·5	−2·4	−2·3	3·8	−2·0	0·1	−1·7	1·1	−4·0	1·8	1·2	−1·7	1·6	0·4

depth $(-H')$ was regarded effectively as of $-0{\cdot}62H'$, since

$$\frac{\rho_2-\rho_1}{\rho_2}H'=\frac{2{\cdot}7-1{\cdot}0}{2{\cdot}7}H'=0{\cdot}62H'.$$

The Fourier coefficients H_{mn} and B_{mn}, which were found down to the order $m=18$ and $n=18$, are given in Tables I and II.

It was already shown that if we assume Airy isostasy, B_{mn} and the corresponding H_{mn} are connected by the relation

$$B_{mn}=-2\pi k^2\rho_2 H_{mn}\exp(-\sqrt{m^2+n^2}d)$$

where d is the thickness of the isostatic earth's crust. From this relation, we get

$$d=-\frac{1}{\sqrt{m^2+n^2}}\log\left(-\frac{B_{mn}}{2\pi k^2\rho_2 H_{mn}}\right)$$

whence d can be found for each pair of B_{mn} and H_{mn}. In order that the resulting value of d shall be reasonable, the following two conditions must be satisfied; (1) B_{mn} and the corresponding H_{mn} must differ in algebraic sign, and (2) $|2\pi k^2\rho_2 H_{mn}|$ must be greater than $|B_{mn}|$. Of the 361 pairs of H_{mn} and B_{mn} $(m\times n=19\times 19=361)$, 169 pairs fulfill the above two conditions. The weighted mean of d's, as determined from these 169 pairs of B_{mn} and the corresponding H_{mn}, worked out to

$$d=0{\cdot}0722 \text{ (radian)}.$$

Since 1400 km has been taken as π, this value of d corresponds to

$$\frac{1400}{\pi}\times 0{\cdot}0722=32{\cdot}2\text{ km}.$$

In this connection, it is interesting that from the study of the dispersion of the Rayleigh seismic waves across the Pacific, K. E. Bullen[3] recently obtained the value of 26 km as the thickness of the earth's crust under that ocean. Since the average of the effective depth of the whole area under study is 1 km, the thickness of the earth's crust corresponding to zero elevation is

$$32+1\times\frac{2{\cdot}7}{3{\cdot}0-2{\cdot}7}=41\text{ km}.$$

There are various combinations of m and n that result in equal

3) K. E. Bullen, *Monthly Notices Roy. Astro. Soc. Geophys. Suppl.*, **4** (1939), 579.

Table II. Fourier Coefficients for the Bouguer Gravity Anomalies. (in mgal.)

m \ n	0	1	2	3	4	5	6	7	8	9	10	11	12	13	14	15	16	17	18
0	118·0	−24·0	−38·7	13·9	10·4	8·6	−20·3	7·1	−1·1	11·5	−4·5	−0·8	−0·6	1·1	−1·1	2·7	−4·4	−3·0	2·1
1	6·7	−11·4	4·4	3·9	30·5	4·3	−6·9	−16·3	6·2	4·6	−2·2	−6·8	1·0	0·4	1·5	−3·7	−2·1	−5·1	5·1
2	−53·6	59·1	40·8	−28·4	−11·6	2·3	23·8	−15·9	1·9	−5·6	2·2	−7·1	4·2	−7·5	5·7	−3·3	1·8	−2·5	1·5
3	20·6	−6·1	12·6	7·6	−36·8	−11·4	5·1	−8·1	1·6	0·5	0·7	4·7	−3·0	2·6	−4·9	2·4	3·2	4·2	−2·4
4	−16·7	−23·4	42·2	−2·2	−18·9	5·9	11·7	−5·3	5·8	−0·0	−2·9	4·7	−3·6	2·9	−7·6	5·6	−3·5	4·9	−1·4
5	−1·3	13·1	−6·6	−12·6	8·0	22·8	−14·7	−1·3	0·7	2·4	0·1	−0·5	4·9	−9·7	2·8	−1·1	1·2	−2·9	2·6
6	2·6	−3·4	−16·8	0·2	−6·7	8·5	0·0	7·7	0·3	0·6	−7·7	1·9	−2·4	0·3	2·9	−0·6	5·7	−4·0	−0·7
7	−9·2	4·0	−6·9	−2·0	−0·0	1·6	6·4	0·2	4·3	−7·2	−3·7	−7·8	3·5	1·0	−1·2	8·3	−2·9	2·9	−3·7
8	2·8	1·2	−8·0	5·7	4·8	−3·7	−5·6	3·3	1·0	−3·3	4·4	−0·2	4·4	−0·1	−4·5	−2·9	0·0	1·4	−1·4
9	4·3	−1·9	−7·1	2·3	7·6	−6·4	2·0	−3·6	0·9	7·1	−6·5	1·5	−1·3	5·1	−0·2	−5·1	1·1	−2·0	2·0
10	−1·7	1·4	3·5	−0·6	0·9	−1·1	−9·6	0·1	2·7	−5·7	4·3	0·6	−5·1	6·9	−0·4	−1·3	0·4	1·4	2·5
11	−2·1	4·0	3·3	−9·8	−0·1	6·7	−12·3	2·4	0·1	−3·7	5·2	1·7	1·9	−3·3	2·3	0·8	−0·2	0·8	−2·0
12	1·7	2·0	7·9	−3·3	−0·6	−3·8	1·5	3·3	−1·5	0·9	−2·5	1·1	−1·1	−4·4	2·4	−1·8	−0·0	3·9	0·5
13	1·9	−1·3	0·3	−6·8	−2·3	−1·6	−1·7	−2·6	1·3	4·4	−3·2	3·4	−0·8	4·2	−0·2	0·7	−1·2	0·4	0·3
14	5·0	−1·1	−3·4	4·7	−0·2	−6·3	0·3	−1·5	−1·2	2·2	0·3	−0·7	2·8	0·0	−1·6	3·3	−3·0	2·4	−1·2
15	−1·5	−1·8	−2·5	1·3	−2·3	0·0	−1·6	1·4	0·0	−0·7	3·3	1·0	2·3	−4·2	−1·3	−0·4	−1·6	3·2	0·9
16	1·2	0·1	2·6	2·0	−1·7	−6·7	−0·9	2·8	0·6	−1·0	−3·4	1·5	2·0	0·6	0·0	1·5	2·8	−5·1	4·7
17	2·8	−0·5	−6·3	2·3	1·8	−3·3	2·7	3·8	−0·2	−3·8	−0·1	0·4	−1·8	1·0	0·3	−1·4	1·8	−4·5	−1·9
18	0·9	3·0	−4·7	0·1	0·7	1·5	−2·4	−2·3	3·8	−2·0	0·1	−1·7	1·1	−4·0	1·8	1·2	−1·7	1·6	0·4

depth $(-H')$ was regarded effectively as of $-0{\cdot}62H'$, since

$$\frac{\rho_2-\rho_1}{\rho_2}H'=\frac{2{\cdot}7-1{\cdot}0}{2{\cdot}7}H'=0{\cdot}62H'.$$

The Fourier coefficients H_{mn} and B_{mn}, which were found down to the order $m=18$ and $n=18$, are given in Tables I and II.

It was already shown that if we assume Airy isostasy, B_{mn} and the corresponding H_{mn} are connected by the relation

$$B_{mn}=-2\pi k^2\rho_2 H_{mn}\exp(-\sqrt{m^2+n^2}d)$$

where d is the thickness of the isostatic earth's crust. From this relation, we get

$$d=-\frac{1}{\sqrt{m^2+n^2}}\log\left(-\frac{B_{mn}}{2\pi k^2\rho_2 H_{mn}}\right)$$

whence d can be found for each pair of B_{mn} and H_{mn}. In order that the resulting value of d shall be reasonable, the following two conditions must be satisfied; (1) B_{mn} and the corresponding H_{mn} must differ in algebraic sign, and (2) $|2\pi k^2\rho_2 H_{mn}|$ must be greater than $|B_{mn}|$. Of the 361 pairs of H_{mn} and B_{mn} $(m\times n=19\times 19=361)$, 169 pairs fulfill the above two conditions. The weighted mean of d's, as determined from these 169 pairs of B_{mn} and the corresponding H_{mn}, worked out to

$$d=0{\cdot}0722 \text{ (radian)}.$$

Since 1400 km has been taken as π, this value of d corresponds to

$$\frac{1400}{\pi}\times 0{\cdot}0722=32{\cdot}2\text{ km}.$$

In this connection, it is interesting that from the study of the dispersion of the Rayleigh seismic waves across the Pacific, K. E. Bullen[3] recently obtained the value of 26 km as the thickness of the earth's crust under that ocean. Since the average of the effective depth of the whole area under study is 1 km, the thickness of the earth's crust corresponding to zero elevation is

$$32+1\times\frac{2{\cdot}7}{3{\cdot}0-2{\cdot}7}=41\text{ km}.$$

There are various combinations of m and n that result in equal

3) K. E. BULLEN, *Monthly Notices Roy. Astro. Soc. Geophys. Suppl.*, **4** (1939), 579.

or nearly equal $\sqrt{m^2+n^2}$, which is the order of the Fourier coefficients. The whole 361 pairs of H_{mn} and B_{mn} may be grouped according to this order. In each of such groups, there are two kinds of pairs, (α) and (β). While in the α pairs, H_{mn} and B_{mn} differ in algebraic sign, in the β pairs, they do not. It was already shown that from the consideration of regional isostasy, the percentage $\frac{\alpha}{\alpha+\beta}$ is ex-

Table III.

$\sqrt{m^2+n^2}$	Total Number of Pairs	α Pairs	$\frac{\alpha}{\alpha+\beta}$	
0~1	1	1	100%	75
1~2	3	2	67	
2~3	4	3	75	86
3~4	3	3	100	
4~5	7	6	86	80
5~6	8	6	75	
6~7	6	5	83	60
7~8	9	4	44	
8~9	12	6	50	58
9~10	12	8	67	
10~11	11	5	45	52
11~12	14	8	57	
12~13	15	9	60	63
13~14	15	10	67	
14~15	18	9	50	58
15~16	18	12	67	
16~17	20	14	70	60
17~18	20	10	50	
18~19	23	12	52	55
19~20	17	10	59	
20~21	14	5	36	56
21~22	18	13	72	
22~23	19	9	47	50
23~24	13	7	54	
24~25	15	7	47	44
25~26	17	7	41	
26~27	9	4	44	41
27~28	8	3	38	
28~29	6	3	50	30
29~30	4	0	0	
30~31	2	2	100	
Total	361	203	56	

pected to decrease from 100 down to 50 as the order $\sqrt{m^2+n^2}$ increases. Table III and Fig. 3 show this tendency very clearly.

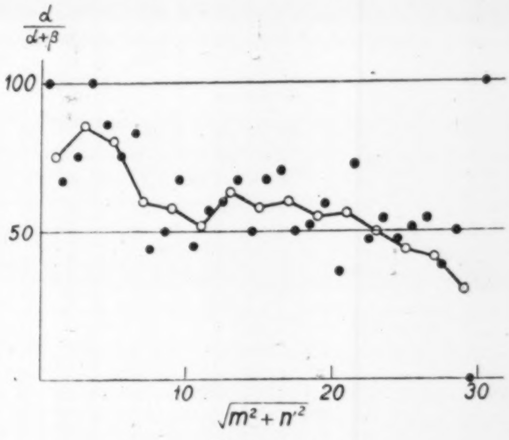

Fig. 3.

In Fig. 4, a small square defined by a combination of m and n is made black, if H_{mn} and B_{mn} corresponding to that m n are of opposite algebraic sign, while it is left blank if H_{mn} and B_{mn} are of the same sign. The abundance of the black squares for smaller m and n is noteworthy.

If, from Fig. 3, we regard that the percentage $\dfrac{\alpha}{\alpha+\beta}$ is 50 when $\sqrt{m^2+n^2}$ exceeds 25, this will correspond to

$$m=n=18.$$

Since 1400 km was taken as π in the present analysis, the wave-length of this harmonics is

$$1400\times 2\div 18=160 \text{ km}.$$

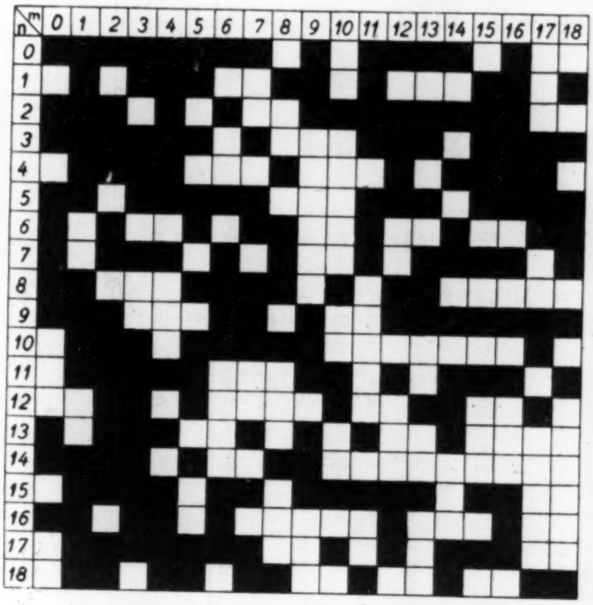

Fig. 4.

The natural conclusion to be drawn from the foregoing results is that topographical features that are smaller than half this length, 80 km across, are supported by some mechanism other than isostasy; in other words the degree of regionality R is 80 km. The ratio of this regionality to the thickness of earth's crust is, in the present case,

$$80\div 32=2.5.$$

According to perfect Airy isostasy, the mass that is expressed by

$$-\rho_2\sum\sum H_{mn}\cos mx\cos ny$$

is distributed at a depth which is 32·2 km in the present case. The gravity due to this mass that is to be observed on the earth's sur-

Table IV. Fourier Coefficients for the Isostatic Anomalies. (in mgal.)

n \ m	0	1	2	3	4	5	6	7	8	9	10	11	12	13	14	15	16	17	18
0	6·3	16·1	2·9	2·7	− 6·4	− 6·8	−17·9	2·4	− 4·3	4·9	− 4·9	1·2	7·9	− 2·6	4·4	5·2	− 3·2	− 3·9	2·3
1	29·8	4·7	39·8	0·1	−13·7	− 7·3	−11·4	−23·5	2·8	1·7	− 9·2	− 3·3	2·5	0·8	6·4	2·5	1·4	− 5·6	4·8
2	−11·5	3·1	26·6	−29·6	1·3	5·7	8·1	−17·6	2·6	6·6	− 2·3	− 1·6	2·7	− 3·8	4·6	0	− 0·6	− 3·1	3·0
3	−14·1	0	−23·9	4·1	−23·5	0·3	13·7	− 3·3	2·7	7·0	3·5	2·2	2·3	− 0·3	− 8·1	− 2·4	1·6	− 0·3	− 1·6
4	−18·4	−10·7	26·8	1·4	−18·8	19·0	13·8	−16·3	4·5	− 0·5	− 5·6	5·3	2·8	4·9	− 2·7	5·0	− 1·4	0·9	− 2·6
5	1·6	2·6	−13·8	−12·1	7·9	17·5	2·1	9·6	1·9	2·5	0·2	4·6	1·7	− 5·8	4·3	0·7	− 0·8	− 1·2	0
6	−13·3	− 9·1	− 3·1	8·2	−16·1	4·7	− 1·1	4·0	− 0·8	4·7	− 8·4	− 4·4	− 7·3	0·8	0·4	− 1·8	7·4	− 0·8	1·8
7	− 7·0	14·6	− 4·8	11·2	3·1	3·3	3·3	10·1	4·1	−10·5	− 3·8	− 6·5	4·7	0·3	1·1	6·2	1·6	3·1	0·1
8	− 5·6	− 8·2	− 8·1	7·2	5·5	0·1	− 3·4	− 2·3	− 2·5	− 3·9	2·7	− 2·8	1·6	0·9	− 4·7	− 4·5	− 0·3	2·3	− 2·1
9	1·8	0·6	− 3·1	6·5	10·5	−12·1	0·5	− 0·5	4·1	3·7	− 8·3	3·1	1·2	3·6	0·6	− 2·7	− 0·3	− 0·8	1·4
10	− 1·7	− 3·4	− 2·1	0·8	5·0	3·	− 9·1	− 0·2	0·4	− 3·3	8·2	2·8	− 5·2	7·1	− 0·9	− 1·8	0·5	1·2	− 3·4
11	− 6·0	0·8	− 4·1	− 8·4	2·8	3·3	−12·6	3·9	1·5	− 3·1	3·6	3·1	− 1·5	− 7·0	− 0·6	− 0·5	1·3	1·8	− 1·4
12	7·8	4·7	7·3	− 2·3	− 1·4	− 2·5	1·7	5·2	− 2·7	5·3	0·3	1·9	− 2·1	− 3·8	0·6	− 4·1	− 0·1	3·8	2·2
13	1·3	− 6·4	1·1	− 3·3	− 1·1	− 2·8	− 5·1	− 0·2	2·4	4·0	− 4·1	0·2	− 1·9	4·6	− 0·2	1·5	− 1·5	1·6	0·4
14	4·6	1·3	− 2·1	3·3	− 3·6	− 5·6	0·7	− 3·2	0·2	0·7	0·8	− 1·8	4·7	0·5	− 2·3	4·1	− 4·6	3·4	− 2·1
15	− 3·3	− 0·1	0	1·0	− 0·9	2·7	− 0·6	− 1·8	0·3	1·1	1·6	0·3	2·0	− 3·6	− 2·1	0·3	− 1·3	3·6	1·0
16	− 2·0	− 0·2	2·6	1·8	− 1·6	− 9·6	− 0·6	3·8	2·6	− 1·2	− 5·9	3·7	1·7	0·7	0·6	1·5	2·3	− 5·9	4·9
17	3·8	1·2	− 3·4	1·4	0·1	− 2·1	0·8	2·0	− 1·4	− 3·9	0·8	0·5	− 1·1	2·3	0·2	− 1·3	1·0	− 4·8	− 2·3
18	1·9	2·3	− 4·1	0·3	− 0·4	0	− 4·0	− 0·5	3·3	− 3·1	1·4	− 0·5	1·8	− 4·2	1·8	1·7	− 2·4	1·4	− 0·1

Table V. Fourier Coefficients for the Undulation of the Isostatic Geoid. (in 10^{-3} radian.)

n \ m	0	1	2	3	4	5	6	7	8	9	10	11	12	13	14	15	16	17	18
0		16·1	1·5	0·9	− 1·6	− 1·4	− 3·0	0·3	− 0·5	0·5	− 0·5	0·1	0·7	− 0·2	0·3	0·4	− 0·2	− 0·2	0·1
1	21·3	2·7	17·8	0	− 3·2	− 1·4	− 1·9	− 3·3	0·3	0·2	− 0·9	− 0·3	0·2	0·6	0·5	0·2	0·1	− 0·3	0·3
2	− 4·1	1·0	7·8	− 7·2	0·3	1·0	1·2	− 2·3	0·3	0·7	− 0·2	− 0·1	0·2	− 0·3	0·3	0	0	− 0·2	0·2
3	− 3·4	0	− 5·1	0·8	− 4·1	0·5	1·9	− 0·4	0·3	0·7	0·3	0·2	0·2	− 0·2	− 0·6	− 0·2	0·1	0	− 0·1
4	− 3·3	− 1·9	4·5	0·2	− 2·7	2·5	1·7	− 1·8	0·5	0	− 0·5	0·4	0·2	0·3	− 0·2	0·3	− 0·1	0·1	− 0·1
5	0·2	0·4	− 1·9	− 0·2	1·0	2·0	0·2	1·0	0·2	0·2	0	0·4	0·1	− 0·4	0·3	0	0	− 0·1	0
6	− 1·6	− 1·1	− 0·4	0·9	− 1·7	0·5	− 0·1	0·4	− 0·1	0·4	− 0·6	− 0·3	− 0·5	0·1	0	− 0·1	0·4	0	0·1
7	− 0·7	1·5	− 0·5	1·1	0·3	0·3	0·3	0·8	0·3	− 0·8	− 0·3	− 0·4	0·3	0	0·1	0·3	0·1	0·2	0
8	− 0·5	− 0·7	− 0·7	0·6	0·5	0	− 0·3	− 0·2	− 0·2	− 0·3	0·2	− 0·2	0·1	0·1	− 0·3	− 0·2	0	0·1	− 0·1
9	0·1	0	− 0·2	0·5	0·8	− 0·9	0	0	0·3	0·2	− 0·5	0·2	0·1	0·2	0	− 0·1	0	0	0·1
10	− 0·1	− 0·2	− 0·1	0·1	0·3	0·2	− 0·6	0	0	− 0·2	0·5	0·2	− 0·3	0·4	− 0·1	− 0·1	0	0·1	− 0·1
11	− 0·4	0·1	− 0·3	− 0·5	0·2	0·2	− 0·8	0·2	0·1	− 0·2	0·2	0·2	− 0·1	− 0·3	0	0	0·1	0·1	− 0·1
12	0·5	0·3	0·4	− 0·1	− 0·1	− 0·1	0·1	0·3	− 0·1	0·3	0	0·1	− 0·1	− 0·2	0	− 0·2	0	0·2	0·1
13	0·1	− 0·4	0	− 0·2	− 0·1	− 0·1	− 0·3	0	0·1	0·2	− 0·2	0	− 0·1	0·2	0	0·1	− 0·1	0·1	0
14	0·2	0·1	− 0·1	0·2	− 0·2	− 0·3	0	− 0·2	0	0	0	− 0·1	0·2	0	− 0·1	0·2	− 0·2	0·1	− 0·1
15	− 0·2	0	0	0	0	0·1	0	− 0·1	0	0	0·1	0	0·1	− 0·1	− 0·1	0	0	0·1	0
16	− 0·1	0	0·1	0	0	− 0·4	0	0·1	0	0	− 0·1	0·1	0·1	0	0	0·1	0·1	− 0·2	0·2
17	0·2	0·1	− 0·1	0·1	0	− 0·1	0	0·1	− 0·1	− 0·2	0	0	0	0·1	0	0	0	− 0·2	− 0·1
18	0·1	0·1	− 0·2	0	0	0	− 0·2	0	0·1	− 0·1	0·1	0	0·1	− 0·1	0·1	0·1	− 0·1	0	0

face is

$$-2\pi k^2\rho_2\sum\sum H_{mn}\exp(-\sqrt{m^2+n^2}\,d)\cos mx\cos ny.$$

Since, on the other hand, the gravity anomaly actually observed is expressed by

$$\sum\sum B_{mn}\cos mx\cos ny,$$

the isostatic anomaly is given by

$$\sum\sum\{B_{mn}+2\pi k^2\rho_2 H_{mn}\exp(-\sqrt{m^2+n^2}d)\}\cos mx\cos ny.$$

Table IV gives the coefficients for this last series. The values of this series at every 10° of x and y in the area under study were then calculated, utilizing the B_{mn}, H_{mn} and d that were already found. The distribution of the isostatic anomalies obtained in this way agreed very well with those obtained by Vening Meinesz on the assumption of 25 km Airy regional isostasy.

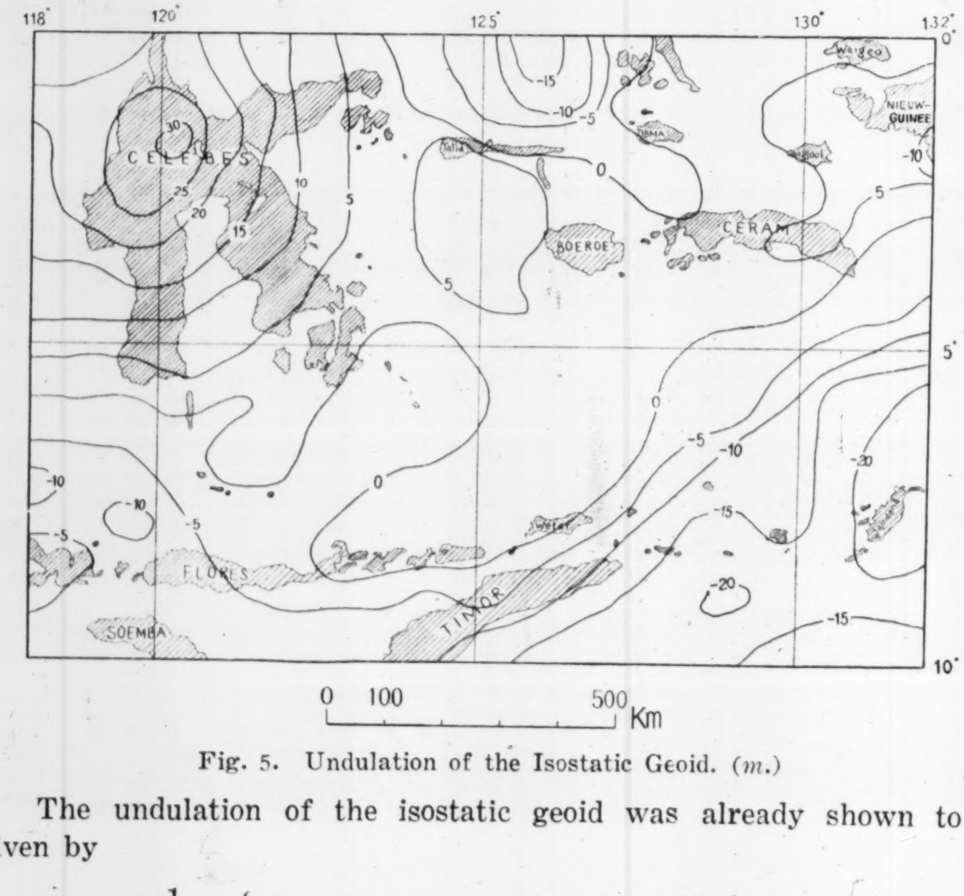

Fig. 5. Undulation of the Isostatic Geoid. (m.)

The undulation of the isostatic geoid was already shown to be given by

$$\sum\sum\frac{1}{\sqrt{m^2+n^2}}\left\{B_{mn}+2\pi k^2\rho_2 H_{mn}\exp(-\sqrt{m^2+n^2}d)\right\}\cos mx\cos ny.$$

Table V gives the value of the coefficients of this series. The value of this series at every 10° of x and y were also calculated, Fig. 5 showing the contour lines of the isostatic geoid as expressed in m.

It will be seen that along the zone of large negative gravity anomalies, the isostatic geoid is depressed by more than 20 m below the average earth's surface, which was taken as a geometrical plane in the present analysis.

Although the present study is scarcely more than a mere addition of the example of applications of Tsuboi's method, owing to the accumulation of similar studies, several interesting geophysical facts were found. For instance, it is likely that the regionality of isostasy R is always approximately from 2 to 3 times the thickness of the isostatic earth's crust d, irrespective of the thickness itself, as Table VI shows. This noteworthy behavior of the earth's crust is likely to be connected with the empirical fact that there is an upper limit to the energy of an earthquake. An hypothesis regarding this point has been proposed in another paper[4].

Table VI.

Place	d	R	R/d
Japan	50 km	85	1·9
U.S.A.	61	145	2·4
Dutch East Indies (Western Half)	36	60	1·7
Dutch East Indies (Eastern Half)	32	80	2·5

Miss T. Ayabe, to whom we express our thanks, has helped us much in the numerical computations involved in the present study. A part of the expense necessary for this study was defrayed from the Funds for Scientific Research of the Department of Education.

4) C. TSUBOI, *Proc. Amp. Acad. Tokyo*, **16** (1940), 449.

4. 重力異常と地下構造との關係 (VI.)

地震研究所 {坪井忠二
山口生知}

蘭領東インド諸島の東半分に於ける重力異常を材料とし，二重 Fourier 級數を利用して此の地域の地下構造を論じた．其の結果を要約すれば次の通りである．

1. Airy 均衡地殼の厚さは 32 km である．
2. 地方的均衡の極限は 80 km である．
3. 均衡ジオイドは最大 20 m も凹んで居る．
4. 一般に地方的均衡の極限は均衡地殼の厚さの 2～3 倍であるらしい．

5. *On the Change in the Heights of the Monthly Mean Sea-level at Aburatubo and Hosozima.*

By Seiti YAMAGUTI,

Earthquake Research Institute.

(Read Sept. 19, 1940.—Received Dec. 20, 1940.)

Introduction.

In his previous papers,[1] the writer compared curves of the monthly mean sea-levels for Aburatubo, Sagami Province, and for Hosozima, Hyûga Province, corrected for the effect of the cyclones that frequent the Pacific Coast, and also for that of the "Kurosiwo" ocean current, when it was shown that a parallelism was observed between the two curves. The present paper is a continuation of these papers. It deals with changes in monthly mean of the sea-levels at Aburatubo, at Hosozima, and also at Kusimoto, Kii Province, the object of the study being to obtain the small residual anomalies of the monthly mean sea-levels after making due corrections for the effects of the cyclone and for the ocean current, and to detect the actual deformation of the earth crust, if any, from the mareograph data.

The data of the sea-level for Aburatubo and Hosozima were taken from the "Tidal Record," published by the Military Land Survey, and that for Kusimoto from "Tidal Observation" published by the Imperial Marine Observatory, Kobe. The latter data are grouped according to the Moon's age, that is, monthly mean values were taken for the period between two successive full moons.

The data of the ocean current were taken from "Reports of Ocean Current," published by the Hydrographic Department of the Imperial Japanese Navy, and those of the barometric pressures from the Monthly Report of the Central Meteorological Observatory in Japan. The values at Yokosuka, Siwonomisaki, and Miyazaki were used instead of those of the mareograph stations of Aburatubo, Kusimoto, and Hosozima.

Method of Investigation, and Results.

The procedure was as follows.

Taking the monthly mean sea-levels for the stations mentioned

1) S. YAMAGUTI, *Bull. Earthq. Res. Inst.*, 7 (1929), 115, 8 (1930), 75.

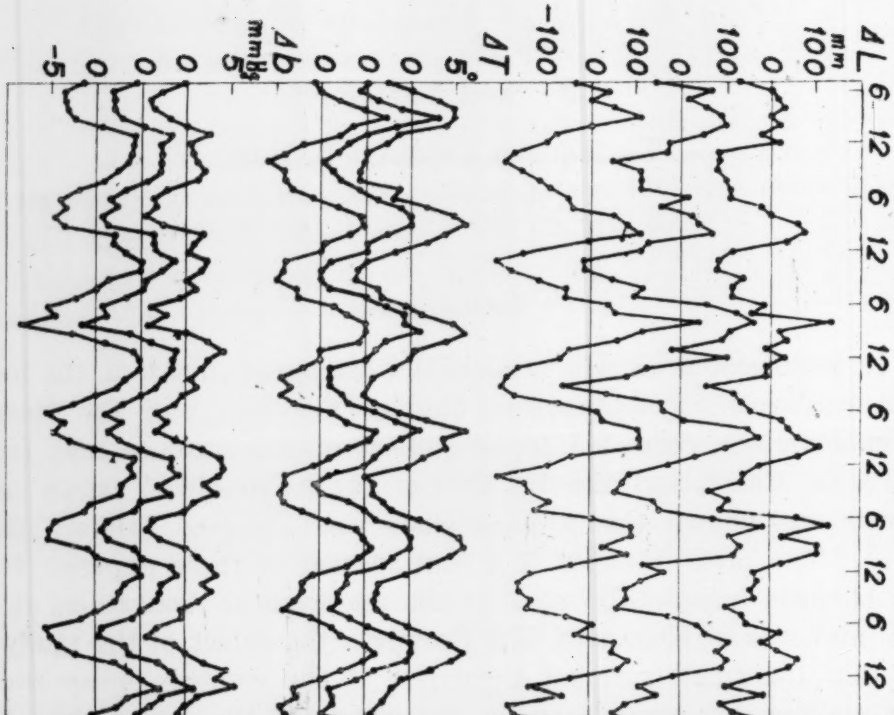

Fig. 1. a: Observed sea-levels, b: Sea water temperatures, c: Barometric pressures.
A: Aburatubo, K: Kusimoto, H: Hosozima.

during a period of 11 years and 8 months, namely, from May, 1926 to Dec., 1937, the values of the deviations $\varDelta L$ (140 in number) from the mean values for the eleven years and eight months were calculated and plotted against the month which was taken as abscissa, as shown in Fig. 1, a. It will be seen that there is a marked variation in the heights of the monthly mean sea-level with an annual period, which is minimum in March or April and maximum in September or October, and which may be due in part to variations in the sea water temperature or density, probably the effect of the ocean current and other meteorological causes, with results similar to those shown in the writer's earlier papers just cited.

The values of the sea water temperatures and the east and the north velocity components of the ocean current were taken from the values for points not far off the coasts of the respective stations on the chart, "Reports of Ocean Current." Their monthly mean values were calculated, and the values of the respective deviations $\varDelta T$, $\varDelta V_e$, $\varDelta V_n$ deduced from the mean values for 140 months, and the values of $\varDelta T$ plotted as shown in Figs. 1, b.

The monthly mean barometric pressures, which may be regarded as including the monthly mean cyclonic effect upon sea level, were also taken, and the values of the deviations $\varDelta b$ from the mean for 140 months were calculated and plotted, as shown in Fig. 1, c.

The values of the correlation coefficients r between $\varDelta L$ and $\varDelta b$, $\varDelta T$, $\varDelta V_e$, $\varDelta V_n$ for Aburatubo and Hosozima were calculated by the usual formula $r=\frac{\sum \varDelta x \varDelta y}{\sqrt{\sum(\varDelta x)^2 \sum(\varDelta y)^2}}$, the probable error in r being $\frac{1-r^2}{\sqrt{n}}$ where n is the total number, the results being shown in the annexed Table.

Table I, (a). Correlation Coefficients for Aburatubo between the two elements in the first column, top row.

	Sea level (original)	Sea level (corrected)	Sea water temperature
Barometric pressure	$-0{\cdot}294\pm0{\cdot}077$		$-0{\cdot}302\pm0{\cdot}077$
Sea water temperature	$0{\cdot}750\pm0{\cdot}037$		—
N-comp. of current velocity	$0{\cdot}165\pm0{\cdot}082$	$0{\cdot}044+0{\cdot}084$	$0{\cdot}147\pm0{\cdot}083$
E-comp. of current velocity	$0{\cdot}157\pm0{\cdot}082$	$0{\cdot}100\pm0{\cdot}084$	$0{\cdot}129\pm0{\cdot}083$

Table I, (b). Correlation Coefficients for Hosozima between the two elements in the first column, top row.

	Sea level (original)	Sea level (corrected)	Sea water temperature
Barometric pressure	$-0{\cdot}578\pm0{\cdot}056$		$-0{\cdot}547\pm0{\cdot}059$
Sea water temperature	$0{\cdot}765\pm0{\cdot}035$		
N-comp. of current velocity	$0{\cdot}076\pm0{\cdot}084$	$-0{\cdot}171\pm0{\cdot}082$	$0{\cdot}085\pm0{\cdot}084$
E-comp. of current velocity	$-0{\cdot}072\pm0{\cdot}084$	$-0{\cdot}023\pm0{\cdot}084$	$0{\cdot}009\pm0{\cdot}093$

It will be seen from these tables that although the effect of sea water temperature upon sea-level is very marked, followed by that of barometric pressure, the dynamical effect of the ocean current falls short of that expected.

In view of these results it was assumed that the height of the sea-level is affected only by the barometric pressure and by the temperature of the sea water not far off the tide gauge station, that is, $\Delta L=p\Delta b+q\Delta T$. In determining coefficients p and q by taking first the theoretical value for p, namely $p=-13{\cdot}2$, the values of $\Delta L'=\Delta L-p\Delta b$ were calculated, and the *$\Delta L'$-ΔT-diagram* was then drawn as shown in Figs. 2, a, b, c. The values of q thus obtained graphically were 20

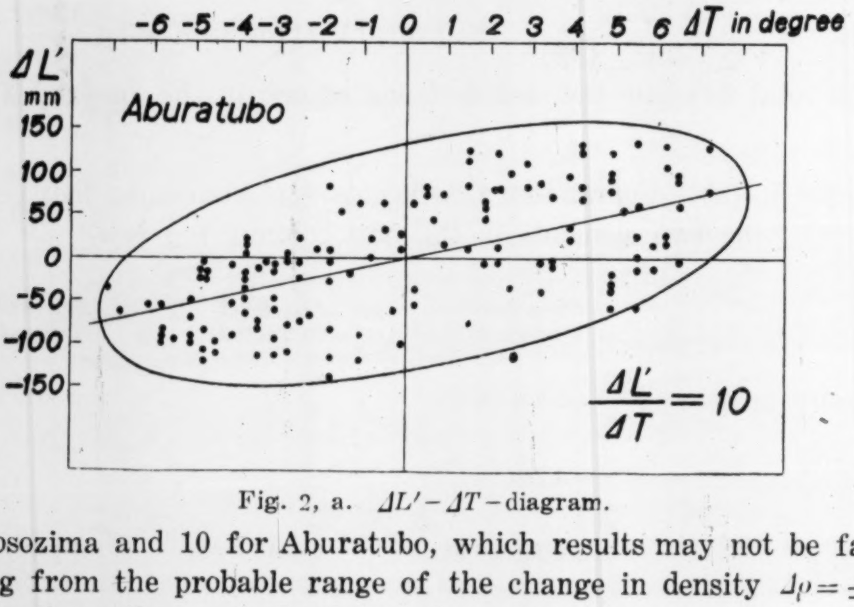

Fig. 2, a. $\Delta L'-\Delta T$-diagram.

for Hosozima and 10 for Aburatubo, which results may not be far out, judging from the probable range of the change in density $\Delta\rho=\pm10^{-3}$, and also from the mean depths of the water not far off Hosozima and Aburatubo, which are about 170 and 90 metres respectively.

With the aid of these values of q, the heights of the monthly mean sea-level were corrected, that is, $\Delta L'' = \Delta L' - q\Delta T$ were calculated and plotted

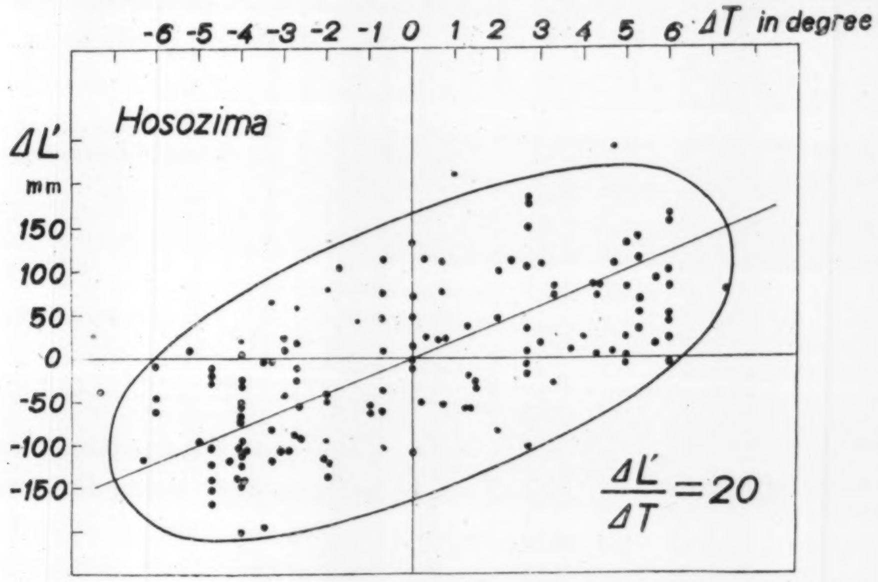

Fig. 2, b. $\Delta L' - \Delta T$ - diagram.

against the month that was taken as abscissa, as shown in Fig. 3. Even then, parallelism will be seen between the two curves that show

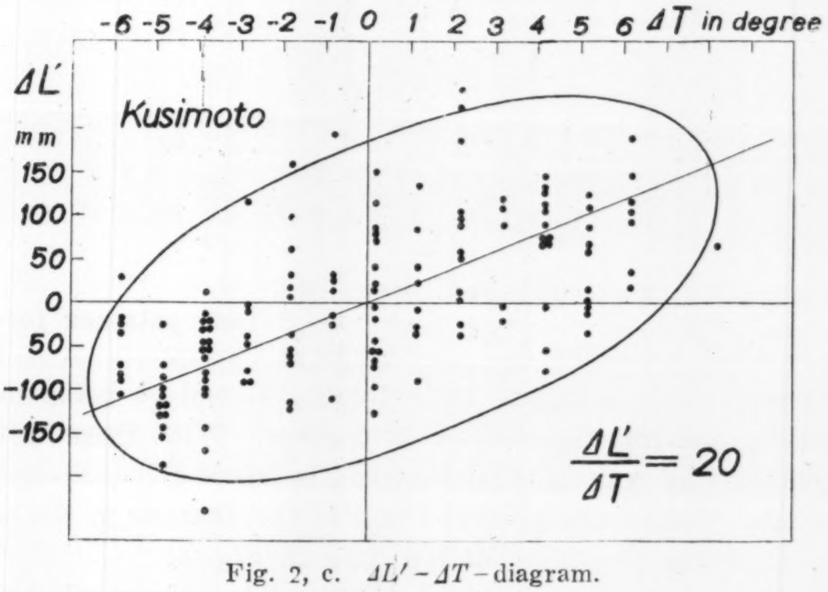

Fig. 2, c. $\Delta L' - \Delta T$ - diagram.

the corrected changes in the heights of the monthly mean sea-level at Aburatubo and Hosozima, which suggests a parallel movement of the earth's crust in that region where the two stations are situated.

To check this possible conclusion, the data for Kusimoto were also treated in the same way as in those of the above two stations. The

curves for sea-levels, both original and corrected for both the sea water temperature and the barometric pressure, the *ΔL′-ΔT-diagram* is plotted for comparison, as shown in Figs. 1, 2, 3, respectively, the value of q, obtained graphically, being 20. The correlation coefficients in this case are shown in Table 1, c.

Table I, c. Correlation Coefficients for Kusimoto between the two elements in the first column, top row.

	Sea-level (original)	Sea water temperature
Barometric pressure	−0·425±0·069	−0·596±0·054
Sea water temperature	0·741±0·038	

Next, the values of the coefficients p and q in the equation $\Delta L = p\Delta b + q\Delta T$ were determined by the method of least squares, using the formulae

$$p=\frac{\sum\Delta L\Delta b\sum(\Delta T)^2-\sum\Delta L\Delta T\sum\Delta b\Delta T}{\sum(\Delta b)^2\sum(\Delta T)^2-(\sum\Delta b\Delta T)^2},$$

$$q=\frac{\sum(\Delta b)^2\sum\Delta L\Delta T-\sum\Delta b\Delta T\sum\Delta L\Delta b}{\sum(\Delta b)^2\sum(\Delta T)^2-(\sum\Delta b\Delta T)^2},$$

or

$$p=\frac{r_{\Delta L\Delta b}-r_{\Delta L\Delta T}r_{\Delta b\Delta T}}{1-r^2_{\Delta b\Delta T}}\sqrt{\frac{\sum(\Delta L)^2}{\sum(\Delta b)^2}},$$

$$q=\frac{r_{\Delta L\Delta T}-r_{\Delta L\Delta b}r_{\Delta b\Delta T}}{1-r^2_{\Delta b\Delta T}}\sqrt{\frac{\sum(\Delta L)^2}{\sum(\Delta T)^2}},$$

when $\left.\begin{matrix}p=-1{\cdot}5\\ q=\ 13{\cdot}3\end{matrix}\right\}$, $\left.\begin{matrix}p=\ 0{\cdot}92\\ q=20{\cdot}8\end{matrix}\right\}$ and $\left.\begin{matrix}p=-7{\cdot}1\\ q=19{\cdot}5\end{matrix}\right\}$ were obtained for Aburatubo, Kusimoto, and Hosozima, respectively, ΔL and Δb being measured in millimetres and mm Hg, and ΔT in degrees. With these values of p and q, the residual values of the sea-levels $\Delta L''=\Delta L-p\Delta b-q\Delta T$ were calculated and plotted, the general trend of the changes in the corrected sea-level $\Delta L''$ being shown by dotted lines in Fig. 3.

Comparing these three curves for Aburatubo, Kusimoto, and Hosozima, it will still be seen that they are parallel for many months, and that the correlation coefficients between each two of them are very nearly 1, as shown in Table 2, which may be due to some unknown factor that may affect the heights of the sea-levels.

In order to ascertain the gradual changes in the heights of the

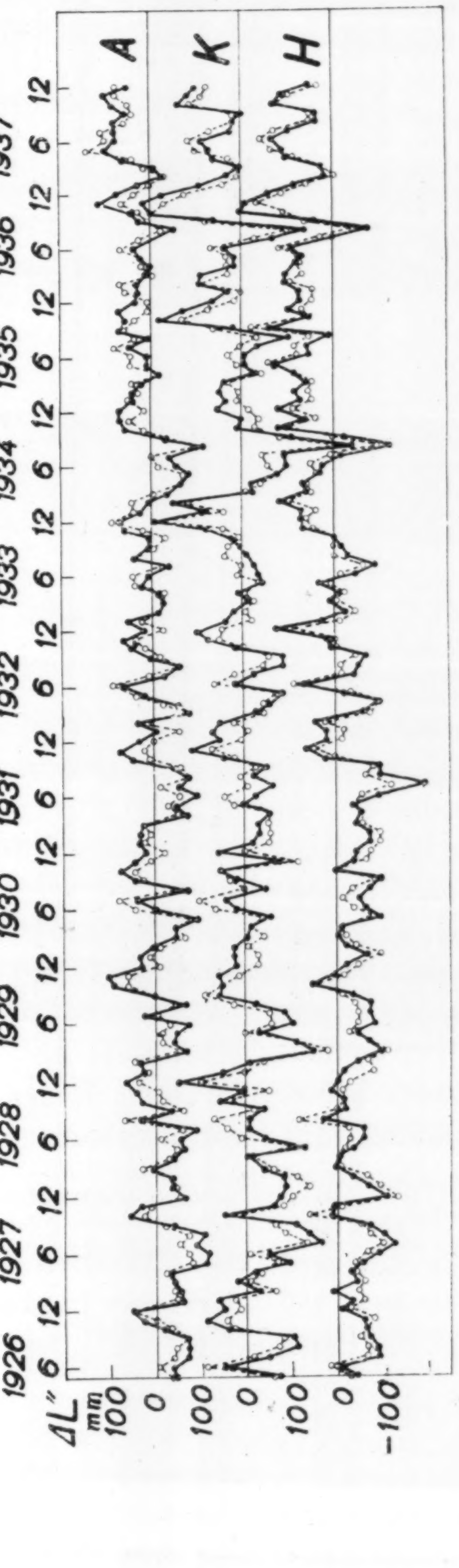

Fig. 3. Sea levels, corrected graphically and by the method of least squares.

A: Aburatubo, K; Kusimoto, H; Hosozim.

mean sea-levels, the values of the annual mean sea levels for a number of mareograph stations were calculated and plotted as ordinates against the year taken as abscissa, as shown in Fig. 4. All these graphs seem to show appreciable downward displacement of the earth's crust from 1927 to the end of 1937 at the rates of 8 mm a year for Aburatubo and Kusimoto, and 13 mm a year for Hosozima. Moreover, marked parallelism is seen between the two corrected curves of the yearly mean sea-levels for Aburatubo and Kusimoto, showing rather conspicuous minima in 1927 and 1934, with an interval of about 7 years. The conspicuous minima in 1934 for Aburatubo and Kusimoto, but not for Hosozima, may show the effect of the cold ocean current "Oyasiwo" upon the sea-levels.

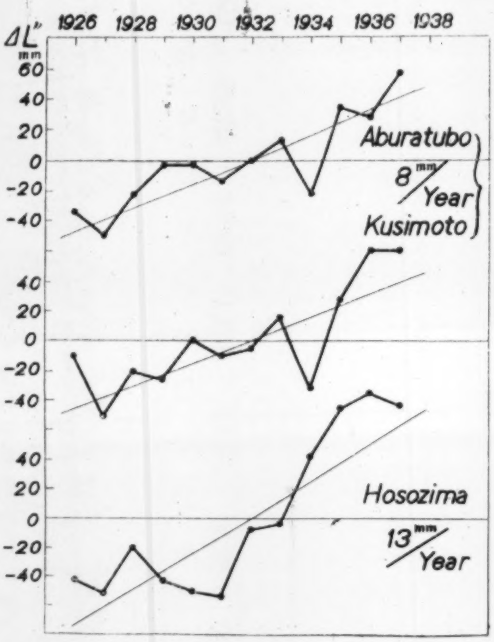

Fig. 4. Annual mean sea-levels.

From the results of the studies described in the papers already cited, and of the present study, it may be said that at Aburatubo, at any rate, a downward displacement of the earth's crust continued from the Great Earthquake of Sept. 1, 1923, until the end of 1937, showing some small vertical oscillatory motions with a period of about three or four years—a point that may be worth following up.

Next, the correlation coefficients between the monthly mean sea-levels, observed or corrected, for Aburatubo, Kusimoto, and Hosozima were calculated and tabulated, with results as shown in the annexed Table.

Table II. Correlation Coefficients between Sea-levels.

Between two stations	Sea-levels		
	Observed (or original)	Corrected graphically	Corrected by the method of least squares
Aburatubo and Hosozima	0·806±0·030	0·655±0·048	0·645±0·049
Aburatubo and Kusimoto	0·817±0·028	0·533±0·061	0·608±0·053

The correlation coefficients between two stations for the observed or original values of the sea-levels seem to have greater values than

those for the residual values, which is probably because of the parallel variation in the sea water temperatures and the barometric pressures at the stations mentioned.

Finally, the probable errors $\varepsilon = 0.6745 \sqrt{\frac{\sum \Delta^2}{n-1}}$ of the observed, as well as of the corrected deviations ΔL and $\Delta L''$ from the monthly mean sea-levels were calculated, resulting in the numerical figures of the following Table.

Table III. Probable Errors ε in millimetres.

Stations	Sea levels				
	Observed ε_0	Corrected graphically ε_1	Corrected by the method of least squares ε_2	Deviations from inclined time axis ε_3	$\frac{\varepsilon_3}{\varepsilon_0}$
Aburatubo	49	37	32	28	0·57
Kusimoto	69	56	46	43	0·62
Hosozima	75	49	46	34	0·45

By taking into account the downward motion of the earth's crust shown in Fig. 4 and deducing the deviations in the sea-levels $\Delta L'''$ from the inclined time axis with proper inclination (8 mm a year for Aburatubo and Kusimoto, and 13 mm a year for Hosozima), instead of taking the original mean for 140 months, the probable errors can be reduced from those given in the third column of Table 3. The results are shown in the fourth column of the same table. Such small values of probable errors for the residual values of the sea-levels, which are about 60 percent for Aburatubo and Kusimoto and 45 percent for Hosozima of the probable errors of the observed or original values, may show the importance of the corrections for the barometric and density effects. Consequently, by applying the corrections for atmospheric pressure and for the ocean current, or the density effects (the dynamical effect of the ocean current may be negligible here) upon the observed values of the monthly mean sea-levels, it may be possible to detect an actual deformation of the earth's crust from the mareograph data.

In conclusion, I wish to express my best thanks to Dr. N. Miyabe for the many useful suggestions made me in the course of this study.

5. 油壺及細島に於ける海水面變化に就て

地震研究所 山口生知

著者は嘗て大正十二年より昭和二年迄の五年間に於ける油壺，細島，花咲，輪島の海水面變化に及ぼす低氣壓の影響，海流の影響等を調査して之等の影響の著しいことを知つた．又之等の諸影響を取り去つた殘りの海水面變化に就て調べて見ると油壺と細島とは著しい類似變化をしてゐることを知つた．

之に關して此の兩地方の地盤が，同じ樣な動き方をするのであらうと云ふ說を出された人もあつたが，當時吾々は五年間の材料では，判然としたことが斷言出來ないから，今少し長年月の材料が集つてから決論しやうと考へてゐた．適々本年の春頃宮部直巳博士より，海流の材料が大部集つたから海水面變化を調べて見ないかといふ助言を承けたので早速，陸地測量部の「驗潮記錄」と水路部の「海流通報」それから海洋氣象臺の「潮汐觀測」及中央氣象臺の「氣象要覽」とを借用して，先づ大正十五年五月より昭和十二年十二月迄滿十一年八ケ月の間の月々の平均海水面に及ぼす氣壓の影響並に主として海流の影響を調査して見た．次で之等の影響を除去した殘りの海水面變化に就いて，比較研究を試み更に其の年平均も取つて見た．又參考の爲に串本の海水面變化に就ても同樣の調査を試みた．其の結果は次の通りである．

1. 月々の平均海水面變化に及ぼす影響の最も大なるものは，海流の靜力學的影響即ち海水密度變化の影響であり，氣壓の影響が之に次ぎ海流の動力學的影響は豫期に反して案外小である．

2. 海流の影響や氣壓の影響を除去した殘りに就いても，油壺，串本，細島に於ける月々の平均海水面は類似の變化を爲してゐる．

3. 年平均海水面に就いても，油壺と串本とは類似變化を爲してゐる．即ち關東大震災以來地盤は何れも3年乃至4年の週期を以つて小なる上下運動を繰返しながら1年に8粍の割合を以つて徐々に沈降を續けてゐることが推定される．又細島に就いても，同樣に地盤が1年に 13 粍の割合を以って沈降してゐることが推定される．油壺と串本に於ては昭和9年 (1934) に著しい海水面變化の極小を示してゐるが細島に於ては之を示さない．之は恐らく油壺と串本とは海水表面下或深さの所より寒流の影響を受けたものと推量される．

6. *The Mode of Causation of Thermo-Remanent Magnetism in Igneous Rocks. Preliminary Note.*

By Takesi NAGATA,

Earthquake Research Institute.

(Read Nov. 21, 1940.—Received Dec. 20, 1940.)

1. Introduction.

Since the discovery of the fact that the igneous rocks, especially the effusive ones, are permanently magnetized in their natural state, a number of investigators[1] have studied the characteristics of this permanent magnetism. This permanent magnetism in igneous rocks, which is usually called natural remanent magnetism, is generally much larger than the intensity of the magnetism that is induced in the same rocks by the present geomagnetic field. Since it had been experimentally proved[2] that this natural remanent magnetism is chiefly due to the magnetization that remains after the rock has cooled from the state of high temperature (in an external magnetic field), and that the direction of the residual magnetization agrees with that of the applied magnetic field, many investigators[1] have attempted to estimate the direction of the earth's magnetic force in remote times when the remanent

1) G. FOLGHERAITER, *Rend. Ac. Lincei. Roma.* **3~2** (1894), 53; **4~1** (1895), 203; **4~2** (1895), 78.

P. MERCANTON, *C. R. Acad. Sci. Paris.* **182** (1926), 859, 1231; **194** (1932), 1371; *C. R. Soc. Suisse. Geophys. Meteor. Astro.* (1926), 345.

F. POCKELS, *Phys. Z. S.*, **2** (1901), 306.

P. DAVID, *C. R. Acad. Sci. Paris.* **138** (1904), 41.

R. CHEVALLIER, *Ann. Phys. Paris.* **4** (1925), 5.

B. BRUNHES, *Journ. Phys. Paris.* **5** (1906), 705.

E. THELLIER, *C. R. Acad. Sci. Paris.* **197** (1933), 232, 1399; **203** (1636), 743; **204** (1937), 876.

A. F. HALLIMOND and E. F. HERROUN, *Rroc. Roy. Soc. London*, **A.**, **141** (1933), 302.

J. G. KÖNIGSBERGER, *Z. S. Geophys.* **6** (1930), 190; *Gerl. Beitr. Geophys.* **35** (1932), 151.

2) J. G. KÖNIGSBERGER, *Z. S. Geophys.* **6** (1930), 190; **8** (1932), 322; *Gerl. Beitr. Geophys.* **35** (1932), 204; **38** (1933), 47; *Beitr. Angew. Geophys.* **5** (19 5), 193.

G. E. ALLEN, *Phil. Mag.* **7** (1904), 45; **17** (1909), 572.

S. NAKAMURA and S. KIKUCHI, *Proc. Phys. Math. Soc. Japan.* **6** (1912), 268.

T. NAGATA, *Bull. Earthq. Res. Inst.*, **18** (1940), 281; *Zisin.* **12** (1940), 285, 544.

magnetization originally came into existence, assuming that the direction of the remanent magnization in rocks, upon cooling and solidifying, agrees with the geomagnetic direction, so long as the rock mass had not moved after completion of the cooling. Such studies were also made by M. Matuyama[3] and others[4] with certain Japanese igneous rocks. This method of presuming the geomagnetic direction in remote times, having been applied also to the remanent magnetization of certain kinds of baked earths, we have at present a number of papers[5] on this subject.

Our present knowledge of the characteristics of thermo-remanent magnetism, that is, the residual permanent magnetism that results when the igneous rock is cooled from high temperature in a weak magnetic field, however, is largely the result of the comprehensive experimental work of J. G. Königsberger.[6] According to this investigator, cooling of ferromagnetic minerals in rocks in a magnetic field from Curie-temperature may produce certain results, depending on the change in the coercive force with temperature and on the demagnetizing force at near Curie-point, the effect finally resulting in thermo-remanent magnetism. He further presumed that the effect just mentioned was due to the lattice-change in the magnetite, which might be caused by escape of the Fe_2O_3.

The main objcct of these investigators, including Königsberger, seems to have been in discovering the character of natural remanent magnetism and its relation to the geomagnetic field in remote geological times. We have, however, another interesting phenomenon of geophysics that seems to be closely related to the causation of thermo-remanent magnetism in nature. It is the local anomalous variation in geomagnetism that follows severe volcanic activity. To illustrate, in a recent expedition that we made to Miyake island,[7] we observed by means of both magnetograph records and absolute measurements that the geomagnetic dip at a point about two *km* north of a region in which severe volcanic eruptions had occurred, made a total change of about 25 minutes during

3) M. MATSUYAMA, *Proc. Imp. Acad. Japan.* **5** (1932), 113; *Proc. Fourth Pacific Sc. Congress* (Java), (1929), 567.

4) S. NAKAMURA and S. KIKUCHI, *loc. cit.*
T. NAGATA, *loc. cit.*

5) P. MERCANTON, *C. R. Acad. Sci. Paris.* **143** (1906), 138; **166** (1918), 681.
E. THELLIER, *Ann. Inst. Phys. Globe.* **10** (1932), 113; **16** (1238), 157; *C. R. Acad. Sci. Paris.* **197** (1933), 1399.

6) J. G. KÖNIGSBERGER, *loc. cit.*
The results of his studies are summarized in his paper, "Natural Residual Magnetism of Eruptive Rocks" (*Terr. Mag.* **43** (1938), 119, 299.)

7) H. TSUYA, R. TAKAHASI, T. HAGIWARA, T. MINAKAMI, T. NAGATA, and others. "Report of Volcanic Eruption of Miyakesima-Island, July 1940." *Zisin.* **12** (1940), 435~533. (In Japanese).

twenty days after the volcanic activity began. Seeing that the ejected lava flow and bombs (already cooled to ordinary temperature) showed a natural remanent magnetism of $5\times10^{-3}\sim3\times10^{-2}$ in its specific intensity, while their specific susceptibility in ordinary temperature amounted only to $0{\cdot}6\times10^{-3}\sim1{\cdot}2\times10^{-3}$, it may be concluded that much of the observed geomagnetic change might be due to the change in the thermo-remanent magnetism of the subterranean magma rather than to the temperature change in its susceptibility. Although in the cases of activities of other volcanoes, local geomagnetic changes were also observed by means of magnetographs,[8] the magnitude of the variation in these cases was smaller than that observed in Miyake island, while according to S. T. Nakamura,[9] who analysed the results of intermittent re-surveys of geomagnetic dip (with the aid of the dip-circle), secular geomagnetic variation seems to be related to volcanic activity.

Hence, our keen interest is in the causation of thermo-remanent magnetism and its disappearance, seeing that these phenomena can be presumed to occur in the earth's crust accompanying changes in temperature and sometimes accompanying changes in stress distribution. If it can be physically established that the magnetic condition of the igneous rocks is influenced by temperature, the external magnetic field, and pressure, we should then be able to form some idea of the physical conditions and their changes in the earth's crust by measuring the anomalous distribution of the geomagnetic field on the earth's surface and its changes. For this purpose, it is necessary to examine experimentally the characteristics of the thermo-remanent magnetism as well as the magnetic susceptibility of rocks due to temperature changes. The physical aspect of the causes that gave rise to thermo-remanence will especially be interesting both from the geophysical standpoint just mentioned and from the standpoint of the physics of the magnetism of such aggregate of complex solid solutions and crystals that we call rocks.

We shall however deal here only with the general phenomenological aspect of the causation of thermo-remanence as suggested by our experimental studies with a few basic volcanic rocks.

2. Thermo-Remanent Magnetism.

As mentioned in the introduction, the residual permanent magnetism

8) T. Nagata, *Zisin.*, **10** (1938); Read before the 148 th (1939) and 163 rd (1940) meetings of the *E. R. I.* (Not yet published).

T. Minakami, *Bull. Earthq. Res. Inst.*, **13** (1935), 799.

9) S. T. Nakamura, *Proc. Imp. Acad. Japan.*, **11** (1935), 102.

that remains after the sample is cooled from temperature t to zero in a uniform magnetic field of H, we shall call thermo-remanent magnetism, indicated here by J_{tH} for unit mass of sample. Since the intensities of the remanent magnetism that is produced by cooling from t°C to 0°C and that to the ordinary room temperature (about 20°C) are practically the same, the remanent magnetism produced in the latter case will frequently be taken as J_{tH}. The apparatus for measuring the thermo-remanent magnetism in the present study is, in outline, as follows. A non-inductive electric furnace, 22 cm large and 2·5 cm in its inner diameter, is set coaxially in the centre of a large Helmholtz's coil of 25 cm radius, the axes of the furnace and of the coil being, obviously, perpendicular to the geomagnetic meridian. The resistance wire in the furnace is pure nichrome wire of magnetic susceptibility smaller than 1×10^{-4}. The specimen to be measured was pulverized into small grains, 0·5∼1·0 mm in their mean diameter, and a silica tube, 11 cm long and 1·8 cm in its inner diameter, was filled with this powder. The tube containing the rock grains was placed in the centre of the furnace coaxially. In the space occupied by the tube, the magnetic field supplied by the Helmholtz's coil was thus nearly uniform, with an error of less than 0·1 percent. The temperature of the specimen was measured at its centre with Pt, Pt–Rh thermo-junction, the temperature throughout the sample being uniform, with an error of less than 5°C, provided the heating or cooling velocity did not exceed 0·05 degrees per second. The intensity of the thermo-remanent magnetism produced in the apparatus was measured by means of another instrument by a ballistic method, already described in the previous paper.[10]

In measuring the J_{tH} of various values of t successively, the J_{tH} obtained in the first experiment was purposely nullified by heating the specimen to a temperature higher than t and cooling it in a non-magnetic space, before proceeding with the next experiment. Thus in every treatment, the sample was in standard condition. In this way, the intensity of the thermo-remanent magnetism of various values of t in a constant magnetic field was measured. The direction of the thermo-remanence always agreed with the direction of the external magnetic field applied. Several typical examples of the observed data are given in Table I, as also Fig. 1, where the intensity of the applied magnetic field was 0·458 Gauss for all the examples.

As will be seen from these results, J_{tH} in a constant magnetic field H increases with increase of temperature t, and reaches maximum value

10) T. NAGATA, *Bull. Earthq. Res. Inst.*, **18** (1940), 102.

Table I. Specific Intensity of Thermo-remanent Magnetism.

t	$J_{t.H}$ ($H=0{\cdot}458$ Gauss)					
	No. 1	No. 2	No. 3	No. 4	No. 5	No. 6
20°C	$0{\cdot}00\times10^{-3}$	$0{\cdot}00\times10^{-3}$	$0{\cdot}00\times10^{-3}$	$0{\cdot}00\times10^{-3}$	$0{\cdot}00\times10^{-3}$	$0{\cdot}00\times10^{-3}$
200	0·65	0·20	0·62	2·85	0·30	0·56
300	0·96	0·75	2·36	6·50	0·45	2·17
350				9·77		
400		4·21	6·18	15·35	1·22	5·63
450	2·84	8·80	7·95	20·95	3·97	6·28
500	3·75				8·58	6·70
550	4·81	11·32	9·86	26·45	16·45	
600	5·30				21·20	6·68
650		11·60	9·87	27·25		
700	5·70				22·10	
750				27·35	21·95	
800	5·65					

No. 1. Volcano Mihara Somma lava.
No. 2. 〃 〃 Bomb.
No. 3. 〃 〃 Bomb.
No. 4. Volcano Mihara Bomb.
No. 5. Miyakesima Volcano Lava flow.
No. 6. 〃 〃 Bomb.

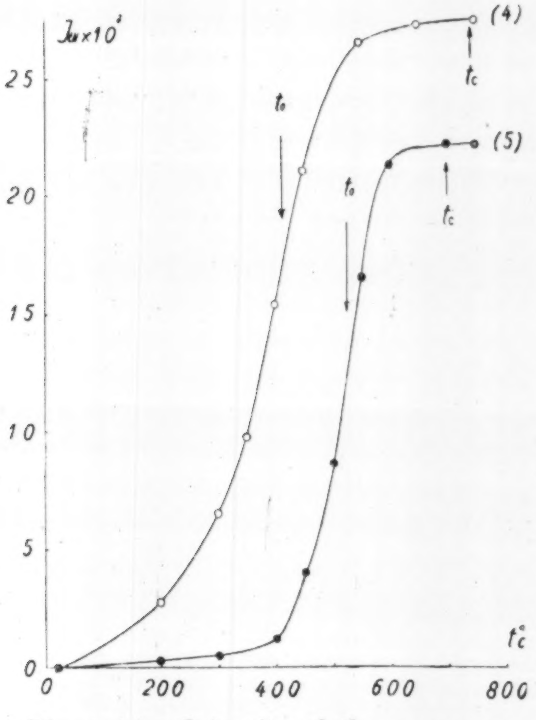

Fig. 1 (a). Intensity of thermo-remanent magnetism ($H=0{\cdot}458$ Gauss)

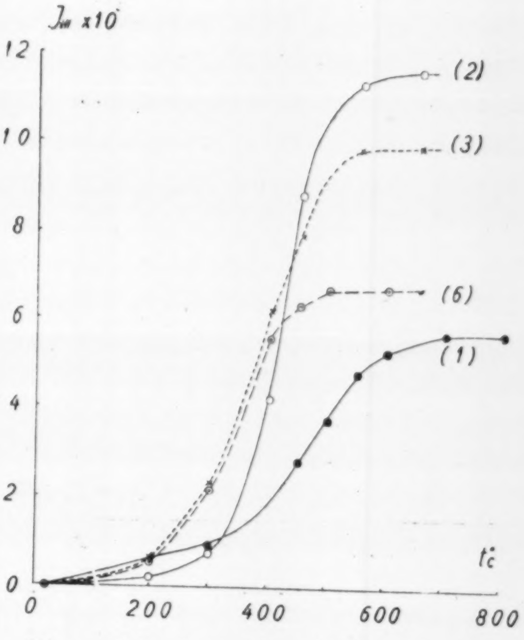

Fig. 1 (b). Intensity of thermo-remanent magnetism ($H=0{\cdot}458$ Gauss)

at t_c, a J_{tH} of higher temperature than t_c being always constant and

equal to $J_{t_c H}$. The intensity of the *saturated thermo-remanent magnetism*, of volcanic rocks is then in most cases larger than the intensity of the induced magnetism $H \cdot \chi$ at ordinary room temperature in the same magnetic field H, where χ denotes the specific magnetic susceptibility of the same specimen. It is notable that the $J_{t_c H}$ of basic rocks, basalt or basaltic andesite, is frequently much larger than its $H \cdot \chi$, the ratio of $J_{t_c H}$ to χH in them sometimes amounting to one hundred. The observed values of $J_{t_c H}$ and χ of several typical specimens are given in Table VII, where Q_t[11] denotes the ratio $J_{t_c H}/\chi H$, and is called here the *coefficient of the thermo-remanent magnetism*. Qualitatively speaking, the magnitude of Q_t seems to be given not only by the chemical composition and crystal structure of the ferromagnetic minerals in the rocks, but also by the size of those grains; that is to say, the ferromagnetic minerals that are scattered as microcrystals in the groundmass occupy a larger percentage of the total ferromagnetic component of the rock the larger the value of Q_t. In other words, the Q_t of such a rock in which the larger part of the ferromagnetic component in it consists of phenocrysts, seems to be comparatively small. This conclusion, however, is only the qualitative result of microscopic observations of thin sections of these rocks. A more quantitative solution of this problem will be discussed in a future report.

It will be seen from Fig. 1 that the differential coefficient of the curve for $J_{t,H}$ with respect to temperature is largest at t_0, and that $\partial^2 J_{tH}/\partial t^2$ is positive for the range at temperatures lower than t_0, whereas it is negative at temperatures higher than t_0, so that temperature t_0 may be taken as a transcendental point of thermo-remanence, while t_c would have another important physical meaning in its causation.

Next, the intensity of the saturated thermo-remanent magnetism in various external magnetic fields was measured, although, at present, we have only the experimental data obtained in a weak magnetic field, that is, smaller than 1·7 Gauss. A number of the observed results are given in Table II and Fig. 2.

Table II (a).

H	$J_{t_c H}$	$J_{t_c} = J_{t_c H}/H$	H	$J_{t_c H}$	$J_{t_c} = J_{t_c H}/H$
0 Gauss	$0{\cdot}00 \times 10^{-2}$	~	0·98 Gauss	$4{\cdot}07 \times 10^{-2}$	$4{\cdot}2 \times 10^{-2}$
0·27	1·21	$4{\cdot}5 \times 10^{-2}$	1·34	5·62	4·2
0·63	2·78	4·4	1·70	6·68	4·1

11) J. G. Königsberger has already proposed certain notations for the various characteristics of thermo-remanent magnetism, and used them for a long time. In this paper, we shall follow his notations as far as possible.

Table II (b).

H	$J_{t_c H}$	J_{t_c}	H	$J_{t_c H}$	J_{t_c}
0 Gauss	$0{\cdot}00\times10^{-2}$		0·82 Gauss	$5{\cdot}90\times10^{-2}$	7·2
0·14	0·96	6·9	1·00	7·20	7·2
0·28	2·10	7·5	1·36	9·22	6·8
0·46	3·53	7·6	1·72	11·33	6·6
0·64	5·07	7·9			

Since, as will be seen from these results, $J_{t_c H}$ is nearly proportional to H, if H is not large, we may write the relation in the case of a weak magnetic field

$$J_{t_c H}=F(H)\cdot J_{t_c},$$
$$F(H)\doteqdot H, \qquad (1)$$

where $F(H)$ denotes a function of H alone. On the other hand, from the relation between J_{tH} and t in two different values of H are given in Table III and Fig. 3, we get the relation

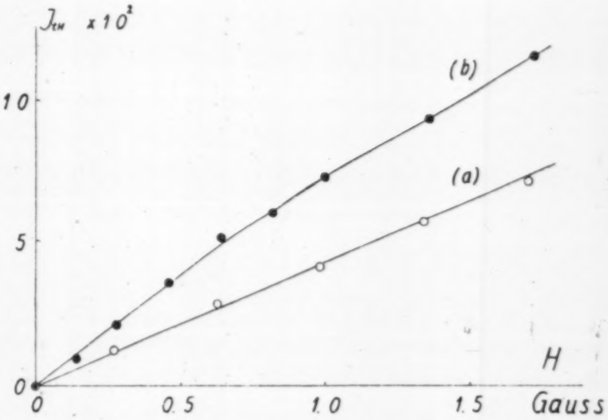

Fig. 2. Intensity of saturated thermo-remanent magnetism in various magnetic fields.

$$\frac{J_{tH_1}}{J_{tH_2}}=\frac{H_1}{H_2}. \qquad (2)$$

Extending the results obtained with eqs. (1) and (2), we may say that generally,

$$J_{tH}=H\cdot J_t, \qquad (3)$$

so long as H is not very much larger than 1 Gauss; or more generally

$$J_{tH}=F(H)\cdot J_t. \qquad (3')$$

In the above expressions, J_t is a function of temperature only, and does not include H. Thus, the effect of the external magnetic field on the rise of thermo-remanence is, apparently at any rate, separated from the temperature effect, and the intensity of the saturated thermo-remanence produced in a magnetic field of unit intensity will be taken as a parameter in order to show the character of the thermo-remanence of the materials, because J_{t_c} which is independent fo H, is a constant pe-

culiar to the rock specimen. Should relation (3) be established, the coefficient of the thermo-remanence Q_t may also be taken as a characteristic quantity of the material, because

$$Q_t = \frac{J_{t_c \cdot H}}{\chi \cdot H} = \frac{J_{t_c}}{\chi}. \qquad (4)$$

It will be presumed, however, that $F(H)$ is not always equal to H for every value of H, for the reason that the maximum intensity of the remanent magnetization is expected to be limited to a value that is smaller than its saturated magnetization (in the magnetization curve), owing to the fact that the magnetic properties of the rocks is due to the ferromagnetic minerals in them, particularly as these rocks show the characters of ferromagnetism, for example, the hysteresis phenomenon in the magnetization curve. A more definite expression for $F(H)$ must be sought by further studies. Here, we shall accept eqs. (1), (2), and (3) that were established within the limits of a weak magnetic field.

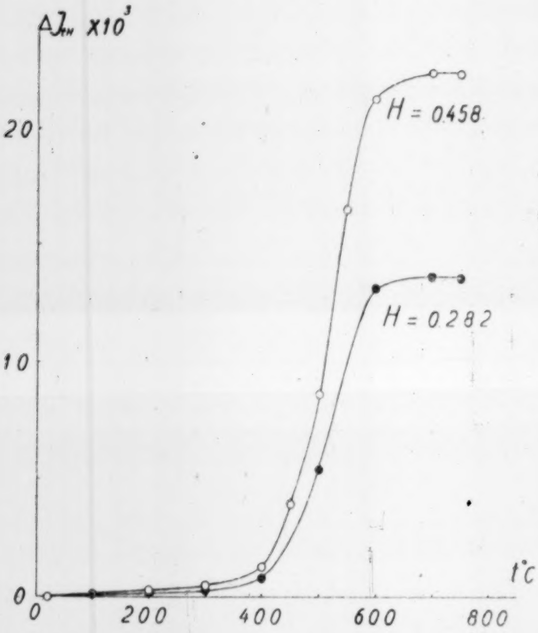

Fig. 3 (a). Intensity of thermo-remanent magnetism in different magnetic fields.

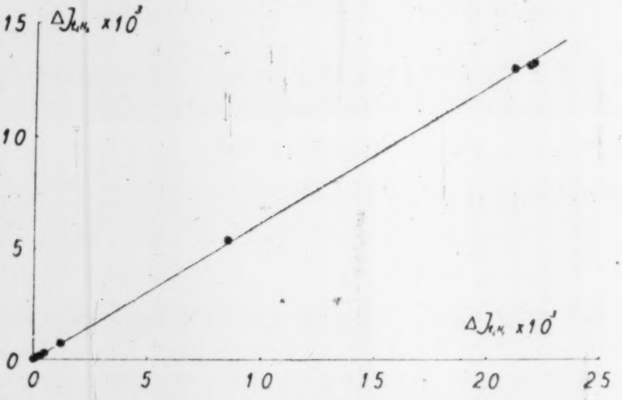

Fig. 3 (b). The relation between $\Delta J_{t_i \cdot H_1}$ and $\Delta J_{t_i \cdot H_2}$. The straight line gives $\Delta J_{t_i \cdot H_2}/\Delta J_{t_i \cdot H_1} = H_1/H_2 = 1{\cdot}62$.

Table III.

t_i	$\Delta J_{t_i \cdot H_1}$ ($H_1 = 0{\cdot}458$)	$\Delta J_{t_i \cdot H_2}$ ($H_2 = 0{\cdot}282$)	$\Delta J_{t_i \cdot H_1}/\Delta J_{t_i \cdot H_2}$
20	$0{\cdot}00 \times 10^{-3}$	$0{\cdot}00 \times 10^{-3}$	—
100	0·15	0·10	1·5

(to be continued.)

Table III. (*continued.*)

t_i	$\Delta J_{t_i H_1}$ (H_1=0·458)	$\Delta J_{t_i H_2}$ (H_2=0·282)	$\Delta J_{t_i H_1}/\Delta J_{t_i H_2}$
200°C	0·30×10⁻³	0·18×10⁻³	1·7
300	0·45	0·28	1·6
400	1·22	0·75	1·65
450	3·97	—	—
500	8·58	5·40	1·59
550	16·45	—	—
600	21·20	13·15	1·61
700	22·10	13·45	1·64
750	21·95	13·35	1·64

3. Partial Magnetization during Cooling.

The relation between J_t and t were obtained in the preceding paragraph. This characteristic of J_t seems to be common to every one of the twenty specimens of igneous rocks that the writer studied. There remains, however, the fundamental question in what manner does thermo-remanent magnetism arise in the process of cooling from a high temperature. Although the dynamical mechanism of the causation of J_t may be a difficult problem, some of the phenomenological and kinematical features could be seen in the results of the following experiment.

First, we examined the effect of *partial magnetization during cooling*. That is, in the cooling of the specimen, the magnetic field of H was applied only in the temperature range of from t_{i+1} to t_i, while in other temperature ranges, higher than t_{i+1} and lower than t_i, the external magnetic field applied was kept always at zero. The specimen which was then cooled to 0°C also showed residual permanent magnetism. We shall call this permanent magnetism the partial magnetism during cooling, and refer to it as $\Delta J_{t_i H}$, while $\Delta t = t_{i+1} - t_i$. The experiment for bringing about partial magnetism during cooling was made with the same apparatus as that for producing thermo-remanence, and its intensity was measured also by the ballistic instrument. Tests were made before each experiment in order to see that the intensity of the permanent magnetic component of the specimen was zero in its initial state.

Thus, the $\Delta J_{t_i H}$ for various successive values of t_i was measured, the temperature range $\Delta t = t_{i+1} - t_i$ being kept constant during every experiment. The values, for example, of $\Delta J_{t_i H}$ for Δt=50°C are shown in Fig. 4 and Table IV. As will be seen from Fig. 4, $\Delta J_{t_i H}$ is very

small, nearly zero, in the temperature range lower than 100°C, and also zero in the range higher than the critical temperature t'_c, while it has maximum value at temperature t'_0 below t'_c. Comparing the relation between $\Delta J_{t\,H}$ and t with that between $J_{t\,H}$ and t of the same specimen, we get

$$t'_c = t_c, \quad t'_o = t_o, \tag{5}$$

provided we neglect small quantities of the order of observational errors.

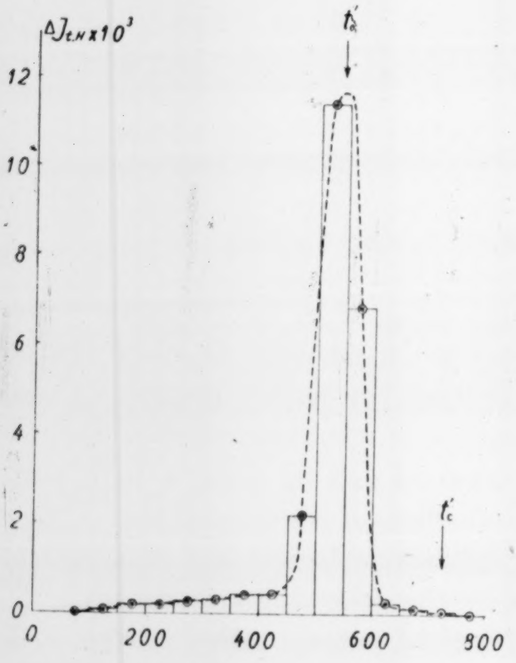

Fig. 4 (a). Partial magnetism during cooling at various temperatures. (Δt = 50°C, H=0·458 Gauss). Specimen No. 5.

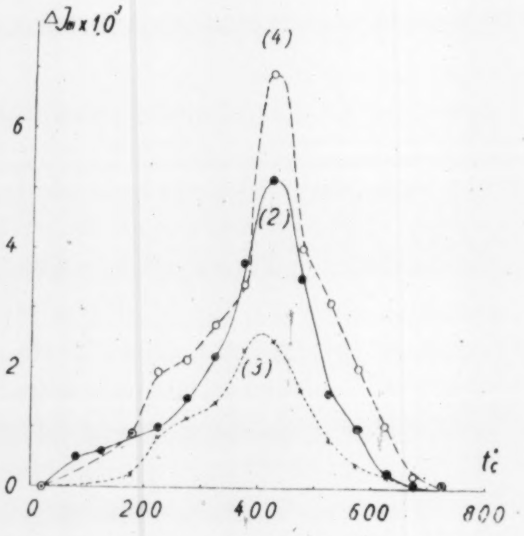

Fig. 4 (b). Partial magnetism during cooling at various temperatures. (H =0·458 Gauss).

Table IV. Specific Intensity of Partial Magnetism during Cooling.

Δt	$\Delta J_{t\,H}$ (H=0·458 Gauss)			
	No. 2	No. 3	No. 4	No. 5
150 → 100°C	0·63×10⁻³	—	—	0·07×10⁻³
200 → 150	0·90	0·22×10⁻³	0·88×10⁻³	0·21
250 → 200	0·99	0·86	1·94	0·21
300 → 250	1·51	1·15	2·15	0·26
350 → 300	2·22	1·42	2·76	0·32
400 → 350	3·78	2·32	3·38	0·43
450 → 400	5·14	2·47	6·90	0·44

(*to be continued.*)

Table IV. (*continued.*)

Δt	$\Delta J_{t\,H}$ ($H=0{\cdot}458$ Gauss)			
	No. 2	No. 3	No. 4	No. 5
500 → 450°C	3·52×10⁻³	1·64×10⁻³	3·97×10⁻³	2·20×10⁻³
550 → 500	1·58	0·79	3·12	11·40
600 → 600	0·99	0·40	2·02	6·86
650 → 600	0·24	0·20	1·03	0·25
700 → 650	0·09	0·03	0·21	0·14
750 → 700	0·01		0·04	0·08

As shown in Table V and in Fig. 5, the sum of the $\Delta J_{t\,H}$ of the whole range of 0 to t, that is, the sum of $\Delta J_{t_i\,H}$ from $t_i=0$ to $t_i=t-\Delta t$, is always nearly equal to the amount of $J_{t\,H}$, the thermo-remanence caused by cooling from t to 0 in the same magnetic field H. This rela-

Table V (a). Specimen, No. 4.

Δt	$\Delta J_{t\,H}$	$\frac{\partial}{\partial t}J_{t\,H}\times\Delta t$	$\Sigma\Delta J_{t\,H}$	$J_{t\,H}$	t
				0·00	20°C
200 → 150°C	0·88×10⁻³	1·20×10⁻³	0·88×10⁻³	2·85×10⁻³	200
250 → 200	1·94	1·60	2·82		250
300 → 250	2·15	2·05	4·97	6·50	300
350 → 300	2·76	3·27	7·73	9·77	350
400 → 350	3·38	5·20	11·11	15·35	400
450 → 400	6·90	5·98	18·01	20·95	450
500 → 450	3·97	3·40	21·98		500
550 → 500	3·12	2·10	25·10	26·45	550
600 → 550	2·02	0·60	27·12		600
650 → 600	1·03	0·20	28·15	27·25	650
700 → 650	0·21	0·10	28·36		700
750 → 700	0·04	0·00	28·40	27·35	750

Table V (b). Specimen, No. 5.

Δt	$\Delta J_{t\,H}$	$\frac{\partial}{\partial t}J_{t\,H}\times\Delta t$	$\Sigma\Delta J_{t\,H}$	$J_{t\,H}$	t
		0·10×10⁻³		0·00×10⁻³	20°C
150 → 100°C	0·07×10⁻³	0·10	0·07×10⁻³		150
200 → 150	0·21	0·10	0·28	0·30	200
250 → 200	0·21	0·10	0·49		250
300 → 250	0·26	0·20	0·75	0·45	300

(*to be continued.*)

Table V (b). (*continued.*)

Δt	$\Delta J_{t\,H}$	$\frac{\partial}{\partial t} J_{t\,H} \times \Delta t$	$\sum \Delta J_{t\,H}$	$J_{t\,H}$	t
350 → 300°C	$0{\cdot}32\times10^{-3}$	$0{\cdot}32\times10^{-3}$	$1{\cdot}07\times10^{-3}$		350
400 → 350	0·43	0·45	1·56	$1{\cdot}22\times10^{-3}$	400×10^{-3}
450 → 400	0·44	2·75	1·96	3·97	450
500 → 450	2·20	4·61	4·16	8·58	500
550 → 500	11·40	7·87	15·56	16·45	550
600 → 550	6·86	4·75	22·42	21·20	600
650 → 600	0·25	0·20	22·67		650
700 → 650	0·14	0·10	22·81	22·10	700
750 → 700	0·08	−0·15	22·89	21·95	750

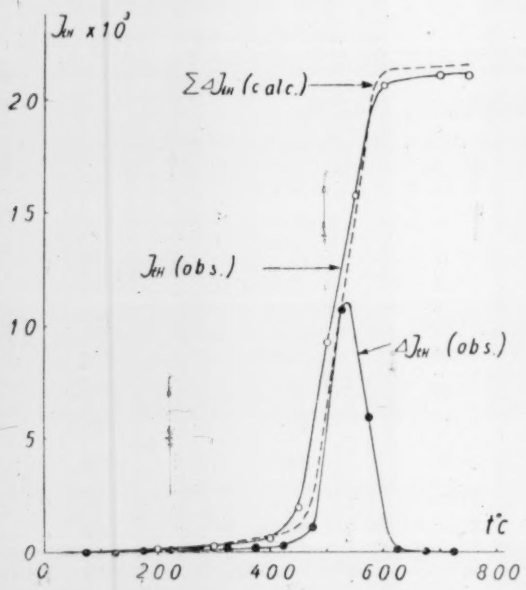

Fig. 5 (a). Comparison of $\sum \Delta J_{t\,H}$ with $J_{t\,H}$. ($H=0{\cdot}458$ Gauss).
Specimen, No. 5.

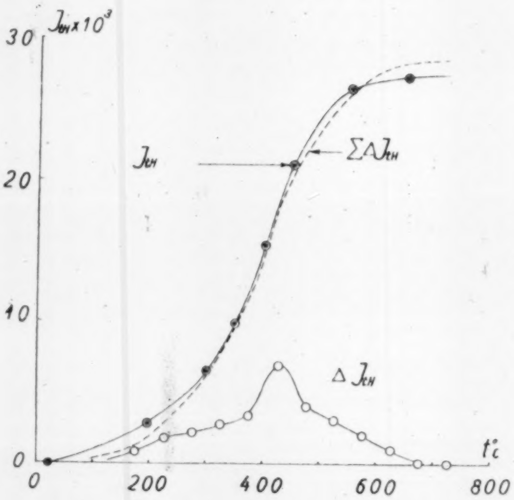

Fig. 5 (b). Comparison of $\sum \Delta J_{t\,H}$ with $J_{t\,H}$. ($H=0{\cdot}458$ Gauss).
Specimen, No. 4.

tion holds for any value of t, although there is a discrepancy of a few per cent between the intensity of $J_{t\,H}$ and the sum of $\Delta J_{t\,H}$, while the general tendency of the $J_{t\,H} \sim t$ relation and that of $\sum \Delta J_{t\,H} \sim t$ seems always to be parallel. Neglecting the small discrepancy, seeing that it may probably be the result of experimental errors, we can establish the following relation, at any rate, as a first approximation,

$$\sum_{t_i=0}^{t_i=t-\Delta t} \Delta J_{t_i\,H} = J_{t\,H}. \qquad (6)$$

Conversely, we compare $\Delta J_{t\,H}$ with the gradient of the $J_{t\,H}$ curve for

the same range. The difference of $J_{t_{i+1},H} \sim J_{t_i,H}$, where $t_{i+1} > t_i$ and the value of $\Delta J_{t_i\,H}$ of the same specimen for the temperature range $\Delta t = t_{i+1} - t_i$, are given in Fig. 6, Δt being actually taken as 50°C. Although

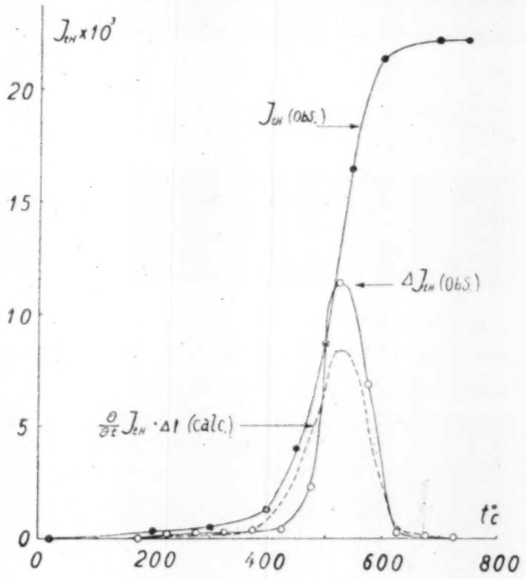

Fig. 6 (a). Comparison $\frac{\partial}{\partial t} J_{t\,H} \times \Delta t$ with $\Delta J_{t\,H}$. ($H = 0{\cdot}458$ Gauss). Specimen, No. 5.

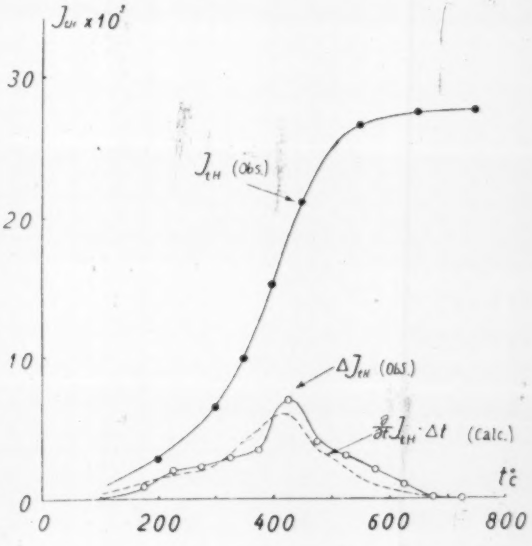

Fig. 6 (b). Comparison $\frac{\partial}{\partial t} J_{t\,H} \times \Delta t$ with $\Delta t_{t\,H}$. ($H = 0{\cdot}458$ Gauss). Specimen, No. 4.

there is also a small discrepancy in these two quantities for the same temperature range, the general tendency is identical. Hence we can write, approximately,

$$J_{t_{i+1}\,H} - J_{t_i\,H} = \frac{\partial}{\partial t} J_{t_i\,H} \cdot \Delta t = \Delta J_{t_i\,H}\,. \qquad (7)$$

The fact indicated by eqs. (6) and (7) shows that the net intensity of the partial magnetism during cooling, which arises during the cooling from t_{i+1} to t_i, remains unchanged in the process of continued cooling to zero or to ordinary room temperature in non-magnetic space. Thus the partial magnetism during cooling brought about in different ranges of Δt remains unchanged and accumulates, becoming a permanent feature. The important fact shown by these equations is that the thermo-remanent magnetism of t is the total sum of the partial magnetism during coooling in the small ranges given by dividing the whole range from 0 to t, and that the difference in the $J_{t\,H}$'s varying values of t is equal to the partial magnetism during cooling in the range of its temperature difference. In other words, this is the law of composition and decomposition of thermo-remanent magnetism.

In the foregoing results the magnitude of the partial temperature range was always taken as 50°C. In the next step, the magnitude of the partial magnetism during cooling corresponds to a 25°C range. The observed results are given in Table VI and Fig. 7.

Table VI.

Δt	$\Delta' J_{t\,H}$	$\Delta_1' J_{t\,H} + \Delta_2' J_{t\,H}$	$\Sigma \Delta' J_{t\,H}$	$\Delta J_{t\,H}$ ($\Delta t = 50$°C)	$J_{t\,H}$	t
					$0{\cdot}00 \times 10^{-3}$	20°C
75 → 50°C	$0{\cdot}23 \times 10^{-3}$	$0{\cdot}51 \times 10^{-3}$	$0{\cdot}23 \times 10^{-3}$			
100 → 75	0·28		0·51			
125 → 100	0·41	0·99	0·92			
150 → 125	0·48		1·40			
175 → 150	0·48	1·02	1·88	$0{\cdot}88 \times 10^{-3}$		
200 → 175	0·54		2·32		2·85	200
225 → 200	0·91	1·83	4·23	1·94		
250 → 225	0·92		5·15			
275 → 250	0·97	1·98	6·12	2·15		
300 → 275	1·01		7·13		6·50	300
325 → 300	1·17	2·28	8·30	2·76		
350 → 325	1·11		9·41		9·77	350
375 → 350	1·29	3·00	10·70	3·38		
400 → 375	1·71		12·41		15·35	400
425 → 400	3·25	7·26	15·56	6·90		
450 → 425	4·01		19·57		20·95	450
475 → 450	1·54	3·02	21·11	3·97		
500 → 475	1·48		22·59			
525 → 500	1·05	2·12	23·64	3·12		
550 → 525	1·07		24·71		26·45	550
575 → 550	1·05	1·62	25·76	2·02		
600 → 575	0·57		26·33			
625 → 600	0·57	1·04	26·90	1·03		
650 → 625	0·47		27·37		27·25	650
675 → 650	0·25	0·31	27·52	0·21		
700 → 675	0·06		27·58			
725 → 700	0·00	0·00	27·58	0·04		
750 → 725	0·00		27·58			

In this experiment, the 50°C temperature range for the preceding experiment was divided into two equal ranges of $\Delta_1' t = \Delta_2' t = 25$°C. The partial magnetism during cooling corresponding to $\Delta_1' t$ and $\Delta_2' t$ is denoted by $\Delta_1' J_{t_i\,H}$ and $\Delta_2' J_{t_i\,H}$ respectively, while that corresponding to Δt is $\Delta J_{t_i\,H}$, as already noted. Comparing, then, the results given in Fig. 6 with those

in Fig. 4, we get approximately for any value of t_i,

$$\Delta_1' J_{t_i H} + \Delta_2' J_{t_i H} = \Delta J_{t_i H}. \qquad (8)$$

The feasibility of this relation is graphically shown in Fig. 7. In the present case, the law of composition of thermo-remanence,

$$\sum_{0}^{t-\Delta t} \Delta' J_{t_i H} = J_{t H} \qquad (8')$$

also holds approximately, as shown in Fig. 8. Since it seems difficult under present experimental limitations to calculate the differential coefficient of the $J_{t H}$ curve with respect to temperature for an elemental range narrower than 50°C, comparison of $\Delta' J_{t H}$ for a 25°C range with the gradient of $J_{t H}$ is omitted.

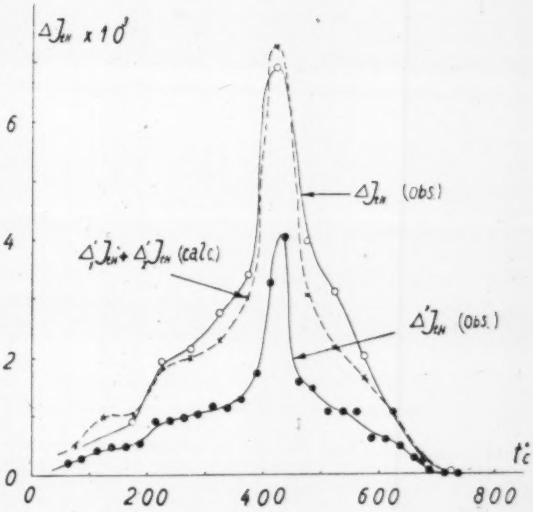

Fig. 7. Comparison of $\Delta_1' J_{t H} + \Delta_2' J_{t H}$ with $\Delta J_{t H}$. ($H = 0{\cdot}458$ Guss). Specimen, No. 4.

Thus the laws of composition and decomposition of the thermo-remanence were established as a first approximation in our quest. As it was difficult, however, to measure quantitatively the partial magnetism during cooling for the narrower elemental temperature range by means of the present apparatus, the order of intensity of the partial magnetism during cooling $\delta J_{t H}$, corresponding to a cooling down of about 2°C at various temperatures in the same magnetic field, was measured, the results being shown in Fig. 9. Comparing these results with those of $\Delta J_{t H}$ and of $\Delta' J_{t H}$, we can get the relation for any temperature,

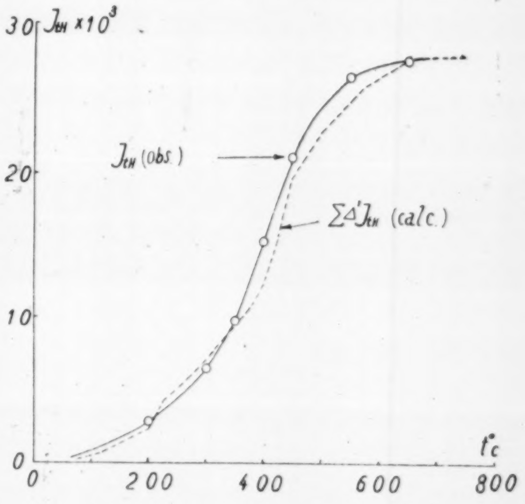

Fig. 8. Comparison of $\sum \Delta' J_{t H}$ with $J_{t H}$. ($H = 0{\cdot}458$ Gauss). Specimen, No. 4.

$$\frac{\partial}{\partial t} J_{t H} \sim \frac{\Delta J_{t H}}{\Delta t} \sim \frac{\Delta' J_{t H}}{\Delta' t} \sim \frac{\delta J_{t H}}{\delta t}, \qquad (9)$$

where Δt, $\Delta' t$, and δt denote respectively 50°, 25°, and 2°C temperature

range for cooling. Thus, we may conclude that the ratio of the intensity of partial magnetism during cooling to the corresponding temperature range at any temperature may have a finite value in the limiting case, namely, $\Delta t \rightarrow 0$, and that the ratio agrees with the differential coefficient of $J_{t_i H}$ with respect to temperature at t_i, that is, that $\lim_{\Delta t \to 0} \frac{\Delta J_{t_i H}}{\Delta t}$ exists, and that it is a function of temperature. Expressing this conclusion by formula, we get

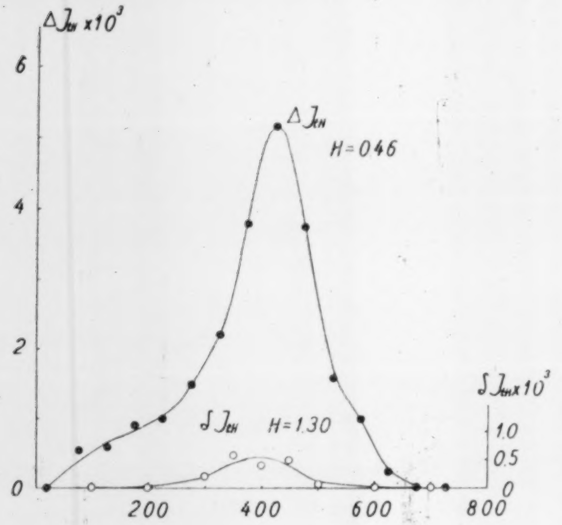

Fig. 9. Comparison of $\delta J_{t.H}$ with $\Delta J_{t \cdot H}$, where $\delta t = 2°C$ and $\Delta t = 50°C$.
Specimen, No. 2.

$$\lim_{\Delta t \to 0} \frac{\Delta J_{t_i H}}{\Delta t} = \frac{\partial}{\partial t} J_{t_i H} = P(t_i, H) \quad (10)$$

In the preceding paragraph, we found that the effects of temperature cooling and of applying an external magnetic field in order to cause thermo-remanent magnetism can be expressed by their functions separated into the function of t and that of H. Since, on the other hand, thermo-remanence is given by the sum of the partial magnetism during cooling in each temperature range, obtained by dividing the whole range, through which it must cool in order to bring about thermo-remanence, the effect of the magnetic field on partial magnetism during cooling may be regarded as being quite similar to that on thermo-remanence. Consequently we get

$$\Delta J_{t\,H} = H \cdot \Delta J_t, \quad (11)$$

$$\sum_i \Delta J_{t_i} = J_t, \quad (12)$$

$$\lim_{\Delta t \to 0} \frac{\Delta J_{t\,H}}{\Delta t} = H \cdot \frac{\partial}{\partial t} J_t = H \cdot P(t). \quad (13)$$

Summarizing the facts obtained from the foregoing experiments we can establish the relation

$$\vec{J}_{t\,H} = \vec{H}\ J_t = \vec{H} \cdot \int_t^0 P(t)\,dt, \quad (14)$$

where the arrow means a vector quantity. And, more generally, if the residual permanent magnetism at 0°C (in the process of causation of which, magnetic field H is applied during the cooling range from t to t' alone) is denoted by $J_{tH}^{(t')}$, we get

$$\vec{J}_{tH}^{(t')} = \vec{H} \cdot \int_{t}^{t'} P(t)\,dt. \qquad (t' < t) \tag{15}$$

The general character of the function $P(t)$ in eqs. (14) and (15), is given by the curve shown in Fig. 4 (a) and (b), which has two particular points on the temperature coordinate, i.e. t_o and t_c, where

$$\left.\begin{array}{l} P(t_o) = \text{Maximum}, \\ P(t \geqq t_c) = 0 \end{array}\right\}.$$

On the other hand, we must examine the dependency of the magnetism during cooling on the time required for cooling. For this purpose, the intensity of ΔJ_{tH}, corresponding to the range of cooling from 400°C to 350°C in 0·458 Gauss, was measured, the cooling velocity during the range being varied. In actual treatment, the time for cooling during a 50°C range was varied from about one minute to 80 minutes. The result of the experiment is shown in Fig. 10. As will be seen from the figure, the magnitude of ΔJ_{tH} for the various periods of cooling seems to be nearly constant, the fluctuations forming only a small percentage, with a tendency for ΔJ_{tH} to become smaller, the shorter the time of cooling. It must, however, not be overlooked that the experimental error may not be small, should the time required for cooling be shorter than ten minutes, because in that case the uniformity of temperature in the specimen would be disturbed It may therefore be concluded that, as a first approximation in our quest, the causation of magnetism during cooling, and therefore of thermo-remanent magnetism, is independent of the velocity of cooling, whence we get

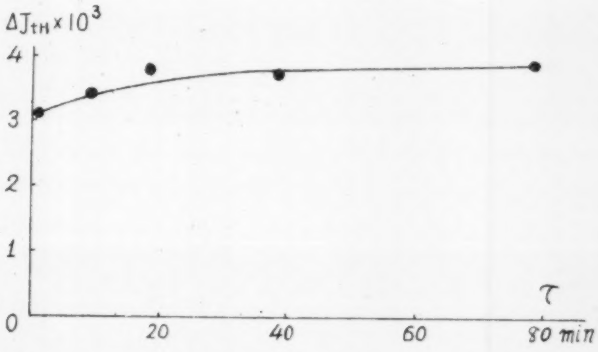

Fig. 10. Relation between ΔJ_{tH} and the cooling time (τ) through Δt.
Specimen, No. 4.

$$\frac{\partial}{\partial \tau} \Delta J_{t\,H} = 0. \tag{17}$$

$P(t)$ is then not a function of time τ, that is,

$$\frac{\partial}{\partial \tau} P(t) = 0. \tag{18}$$

Consequently, equation (14) and (15) must be established independently of the time of cooling.

4. Magnetization during Cooling.

As the next step, the intensity of magnetization at any temperature during the heating and cooling processes in an applied external magnetic field was measured, the object being to see directly the way in which thermo-remanence, which was already determined indirectly in the preceding experiments, is caused. For this study, an astatic magnetometric method was used, the apparatus being shown in Fig. 11, in which the distance between the two magnets is 28·8 cm. Coaxially with the horizontal line perpendicular to the geomagnetic meridian through the centre of the lower magnet, two circular cylindrical solenoids are set, one of which is fixed, while the other is movable with the aid of an adjusting screw. The fixed solenoid contains an electric furnace made of non-inductively wound pure nichrome wire. Between the solenoid and the furnace, a circular double tube of hard glass is set coaxially with them, water being made to flow through the double glass tube in order to absorb the heat that would flow from the furnace to the solenoid and the magnet system.

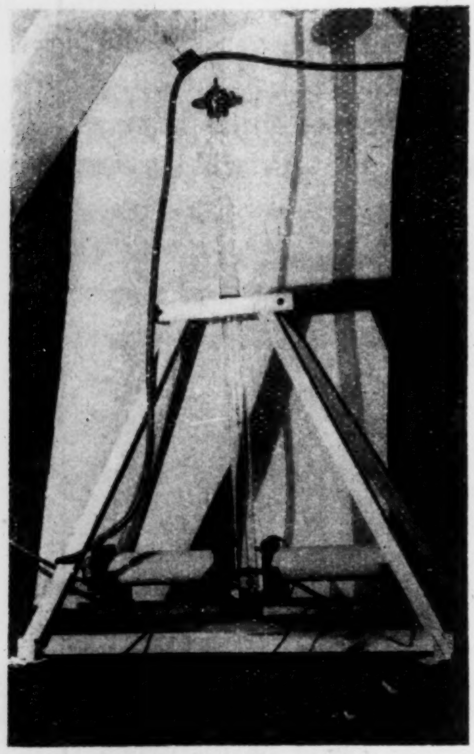

Fig. 11. Astatic magnetometer for measuring magnetism during cooling.

The specimen to be measured is set coaxially in the furnace with the axis-line of the solenoid. The movable coil is for compensating the

magnetic field at the point of the lower magnet due to the fixed solenoid. Provided the whole magnetometric apparatus is well adjusted, the magnetic susceptibility of the pure nichrome wire being sufficiently small, and the heat absorption of the water cooling device adequate, the suspended magnet system scarcely deflects during the temperature change from 0°C to 800°C in the furnace, when no rock specimen there is in the furnace, that is, when it is empty. Consequently it was possible to measure the intensity of magnetization of rock specimens in the furnace with a certain degree of accuracy, provided the specific intensity exceeded 2×10^{-4} c.g.s.e.m.u.

An example of the results obtained in this experiment is given in Fig. 12 (a), (b), (c), where the values shown in (a) give the intensity of magnetization J_h of a fresh unused specimen in its initial heating process, while those in (b) give that in the cooling process, J_c, both being in the magnetic field of H; whereas (c) gives the intensity of magnetization during the process of heating in non-magnetic space, the specimen used having already, in its initial state at 0°C, the thermo-

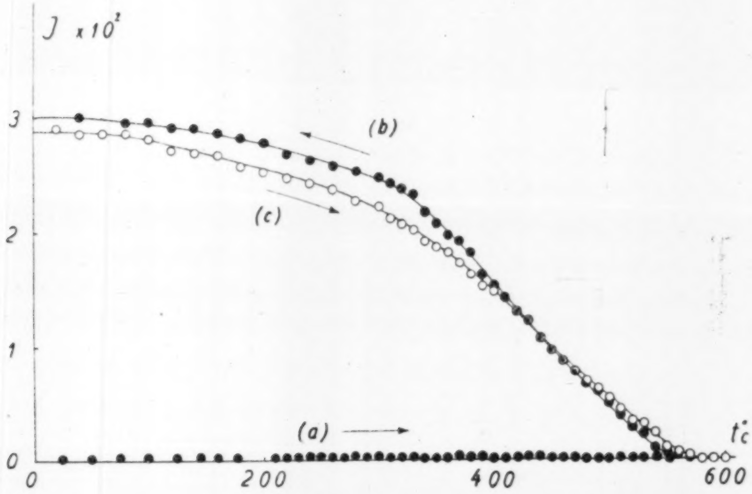

Fig. 12. Intensity of magnetization in heating and cooling processes.
(a) J_h in initial heating process. (b) J_c in cooling process.
(c) Second heating process. $H=1{\cdot}30$ Gauss.
Specimen, No. 2.

remanent magnetism caused in the process shown in (b). As is clear from (a) and (b), Fig. 12, the intensity of magnetization undergoes a marked irreversibility owing to change of temperature, that is, at temperatures below a certain value, J_c is much larger than J_h at the same temperature in the initial heating process. We shall now compare the result shown in Fig. 12 (b) with the curve showing the relation between

$J_{t\cdot H}$ and t of the same sample, where the magnitude of $J_{t\cdot H}$ has been corrected to $H=1\cdot30$ Gauss with the aid of eq. (1). Since J_c at 0°C is nearly equal to $J_{t_c\cdot H}$, as shown in Fig. 13, it may be concluded that J_c, at any temperature, gives the approximate value of the permanent magnetism that was produced during the cooling from t_c to t. The permanent magnetism at t in the cooling process from a temperature higher than t_c, that is, the magnetism caused upon cooling from t_c to t, we shall call $J_c(t,H)$. Precisely speaking, however, magnetization J_c, given in Fig. 12 is the sum of the magnetism that was caused during the cooling and the induced magnetism $H\cdot\chi(t)$, where $\chi(t)$ is the specific susceptibility at t, that is,

$$J_c=J_c(t,H)+H\cdot\chi(t). \tag{19}$$

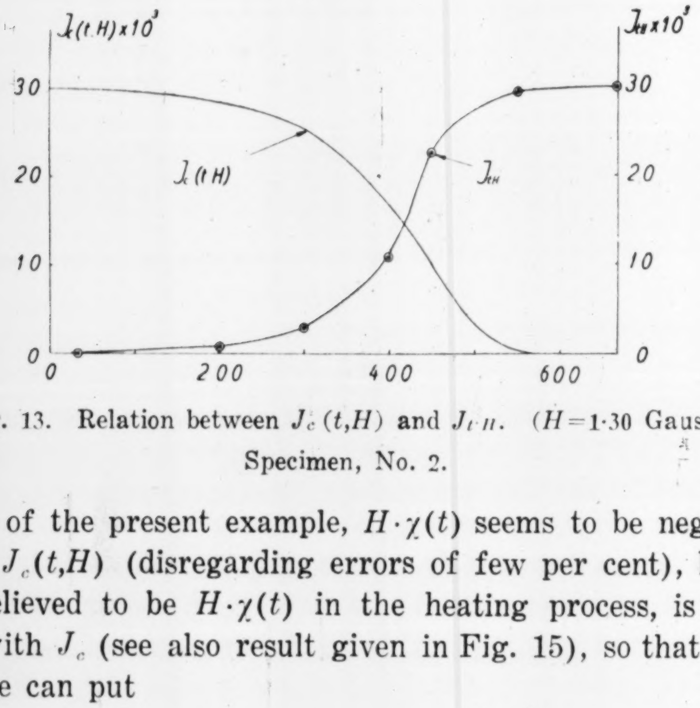

Fig. 13. Relation between $J_c(t,H)$ and $J_{t\cdot H}$. ($H=1\cdot30$ Gauss). Specimen, No. 2.

In the case of the present example, $H\cdot\chi(t)$ seems to be negligible compared with $J_c(t,H)$ (disregarding errors of few per cent), because, J_h, which is believed to be $H\cdot\chi(t)$ in the heating process, is very small compared with J_c (see also result given in Fig. 15), so that in the present case we can put

$$J_c \doteq J_c(t,H). \tag{20}$$

Assuming that eq. (20) holds in the example shown in Fig. 12, we get approximately

$$J_c(0,H)=J_{t_c\cdot H},\quad J_c(t_c\cdot H)=0, \tag{21}$$

and

$$J_{t\cdot H}=J_c(0,H)-J_c(t,H) \tag{22}$$

If, for example, eq. (22) holds, it must result, in the equation

$$J_{t_{\frac{1}{2}}\cdot H}=\frac{1}{2}J_c(0,H)=\frac{1}{2}J_{t_c\cdot H},$$

where
$$J_{t_i \cdot H} = J_c(t_i, H).$$

It will also be seen from Fig. 13 that this relation is satisfied. Fig. 14 shows that it is possible to establish the relations

$$-\frac{\partial}{\partial t} J(t_i, H)\,\Delta t \doteq \Delta J_{t_i \cdot H}, \tag{23}$$

$$\sum_{t_c - \Delta t}^{t} \Delta J_{t_i \cdot H} = J(t, H). \tag{24}$$

It may be an axiomatic conclusion, however, that relations (23) and (24) are established, provided eqs. (6), (7), and (22) have been obtained.

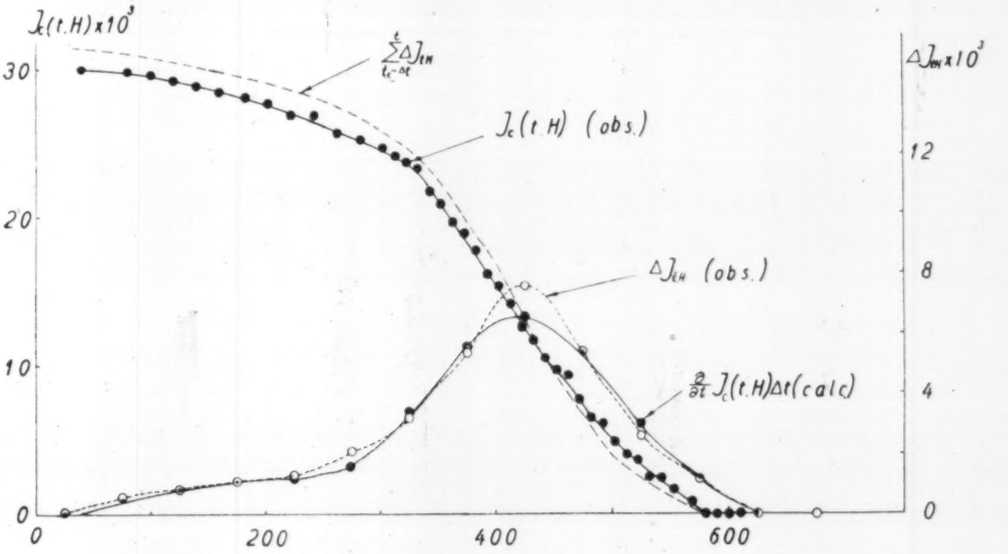

Fig. 14. Comparison of $J_c(t,H)$ with $\sum \Delta J_{t \cdot H}$, and that $\frac{\partial}{\partial t} J_c(t,\mathrm{H}) \times \Delta t$ with $\Delta J_{t_i \cdot H}$.

Thus, comparing eqs. (21), (22) with eqs. (14), (15), we finally get

$$\vec{J}_c(t,H) = \vec{H}\int_{t_c}^{0} P(t)\,dt - \vec{H}\cdot\int_{t}^{0} P(t)\,dt = \vec{H}\cdot\int_{t_c}^{t} P(t)\,dt \equiv \vec{J}^{(t)}_{t_c \cdot H}, \tag{25}$$

and

$$\vec{J}_c(t,H) = \vec{H}\cdot J_c(t). \tag{26}$$

The relation (25) may be additional proof that the almost net intensity of the magnetism produced during the cooling from t_c to t in H remains as permanent magnetism, undisturbed by the continued cooling from t to 0°C in non-magnetic space—a fact already referred to in paragraph (§ 3).

Next, we take into consideration that the curve (c) in Fig. 12, showing the disappearance of the thermo-remanent magnetization during the heating process in non-magnetic space, nearly agrees with that of $J_c(t,H)$, although the sense of temperature change in the two cases are the reverse of each other. In other words, the magnetism during cooling caused in any range of cooling in the magnetic field of H, vanishes when the sample is heated through that range in non-magnetic space. This fact was independently ascertained at the time it was found that the magnetism produced during the cooling from t to t' always vanished when the specimen was heated to t, and cooled again in non-magnetic space.

This result may suggest that the physical state which is capable of being permanently magnetized as $P(t_i)\varDelta t$ in a magnetic field of unit intensity, corresponds to the elemental cooling range $\varDelta t$ at t_i, the external magnetic field affecting the initial physical state in such a way as to cause magnetization of $\vec{H}\cdot P(t_i)\varDelta t$, whereas the said physical state vanishes when it corresponds to a heating of $\varDelta t$ at t_i, independently of $\vec{H}$, resulting in the disappearence of magnetization $\vec{H}\cdot P(t_i)\varDelta t$, regardless of the magnitude of H. Putting the foregoing fact in a formula, we get

$$\frac{\partial}{\partial t}J_o=\frac{\partial}{\partial t}J_c(t,H)=-\frac{\partial}{\partial t}J_{t\,H}=-H\cdot P(t), \tag{27}$$

where J_o denotes the permanent magnetism due to the thermo-remanence in H. As an example of the application of eq. (27) in practical treatment, the specimen with its thermo-remanence saturated was heated in non-magnetic space to t, and then cooled in a magnetic field of $-H$ to 0°C. The intensity of the residual magnetism after this treatment ought to be

$$J_{t_c H}+\int_0^t\frac{\partial}{\partial t}J_o dt-H\int_t^0 P(t)\,dt=J_{t_c H}-2J_{t\,H}. \tag{28}$$

From the experiments in which the foregoing treatments for various values of t, from 0 to t_c, were carried out, it was proved, as shown in Fig. 15, that relation (28) nearly holds. When eq. (28) is applied in measuring thermo-remanence, we may get a double value for $J_{t\,H}$ for any value of t.

Finally, in the series of experiments with the aid of the magnetometer, measurement of δJ_c, corresponding to a small cooling range δt at various temperatures t, was tried. Since quantitative measurement of the value was difficult with the present apparatus, all that can be said

here is that the intensity of δJ_c, corresponding to δt cooling, was negligible compared with the magnitude of $J_c(t,H)$. In this examination, the external magnetic field of $H=1{\cdot}30$ Gauss was applied only during the time it was being cooled at 2°C from t_i throughout the entire cooling range from t_c to 0°C; actually the time it was kept at about 1·5 minutes in every experiment. The magnitude of δJ_c for various values of t_i is given in Fig. 16, where the $J_c(t,H)$ curve is also shown for comparison. As already discussed, we must interpret the magnitude of δJ_c as being

$$\delta J_c = H\cdot\chi(t_i) + H\cdot P(t_i)\cdot\delta t.$$

Whence, we get from Fig. 15 the result that in the present example, the intensity of the induced magnetism $H\cdot\chi(t)$ in the cooling process is also negligible compared with J_c. This conclusion being already assumed in the interpretation of the result

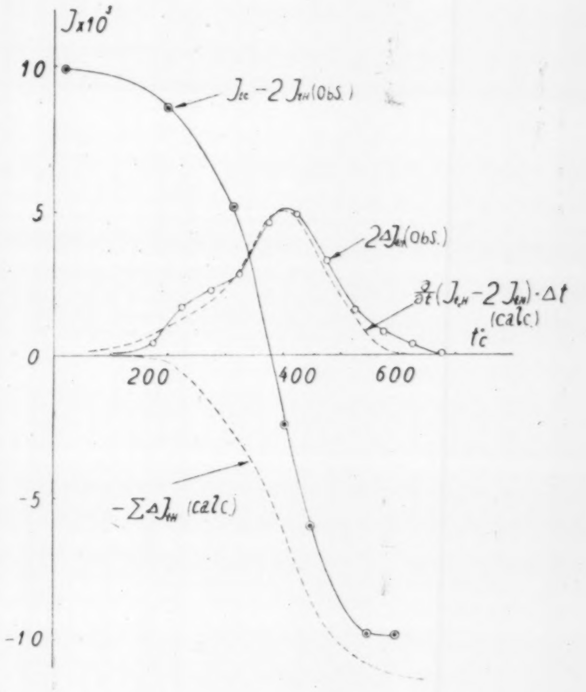

Fig. 15. Comparison of $\Delta J_{t\cdot H}$ with $\frac{\partial}{\partial t}\left(J_{t_c\cdot H}+\int_0^t \frac{\partial}{\partial t} J_{0\cdot}\,dt - H\cdot\int_t^0 P(t)\,dt\right)$

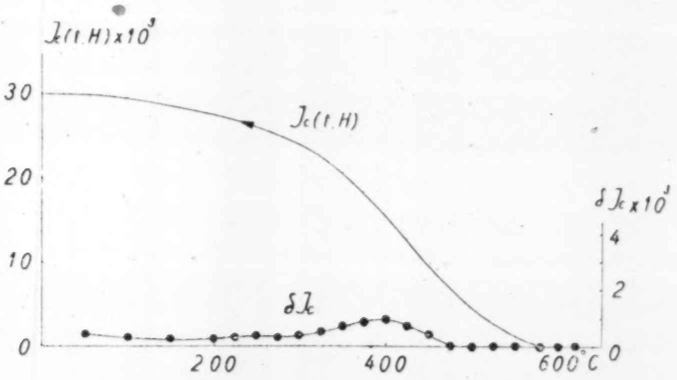

Fig. 16. Comparison of δJ_c with $J_c(t\cdot H)$.

given in Fig. 11, it is possible to confirm the conclusion that partial magnetism during cooling is smaller, the smaller the cooling range (see eq. (7)).

It must be noted here that the relation $H\cdot\chi(t)\ll J_c(t,H)$ holds only for basic rocks, which have a large Q_t value, whereas in the case of intermediate and acidic rocks, the Q_t of which is generally small, amounting to 0·5∼5·0, approximation of $J_c\simeq J_c(t,H)$ is not permissible. However, since eq. (20) is used only as an approximation to get the relation of $J_c(t,H)$ to J_{tH}, and to ΔJ_{tH}, and since the result thus obtained must be independent of this approximation, the final conclusion from eqs. (21) to (27) would also hold in the case of magnetism during cooling of intermediate and acidic rocks.

5. Examples of Actual Characteristic Values of Magnetism during Cooling, and their Application to Geophysics.

We have found in the present studies general apparent characteristics of the mode of causation of thermo-remanent magnetism, a number of the values of the characteristics being defined. They are the intensity of saturated thermo-remanent magnetism in unit magnetic field J_{t_c}, the coefficient of thermo-remanence Q_t, and two particular temperatures t_o and t_c in the characteristic function $P(t)$. As examples, the actual values of these characteristics of several basic rocks are given in Table VII. These rocks are either basalt or basaltic andesite, the chemical and normative compositions of some of them being shown in Table VIII.

As frequently mentioned, the magnitude of J_{t_c} of these basic rocks is generally very large compared with their magnetic susceptibilities, Q_t being much larger than unity. Their temperature t_o is from 300°C to 520°C, while t_c is from 580°C to 720°C, where the former is nearly equal to the Curie-temperature of pure magnetite, the latter being that of pure hematite. Whether transcendental temperature exactly agrees with the Curie-temperature of the rock is, at present, not clear. It will be presumed, however, that they are closely related to each other. Besides the quantities mentioned above, other parameters, in order to give the characteristic of the thermo-remanence, will be considered, as, for example, the magnitude of $P(t_o)$ and the sharpness of the peak of $P(t)$ around t_o. A clear example of discrepancy in the sharpness of the peak will be seen in the results shown in Fig. 4. All these characteristics of the rocks may be closely related to their petrological constitution, exactly like their susceptibilities and Curie-points. Since, in the present study, the general mode of causation of thermo-remanent magnetism has been found, although only approximately and phenomenologically, the relation of the causation of thermo-remanence to the composition of the rock wil be sought by measuring the charac-

Table VII. Numerial Values of Characteristics in Thermo-remanent Magnetism of Volcanic Rocks.

No.	Locality	Rock	J_{t_c}	χ	Q_t	t_0	t_c
1	Mihara Volcano. Somma Lava.	Hypersthene-bearing olivine-basalt.	$1{\cdot}23\times10^{-2}$	$2{\cdot}50\times10^{-3}$	5	470°C±20°C	710°C±20°C
2	Mihara Volcano. Bomb. ejec. Aug. 1940.	Basalt.	2·53	0·37	68	420 ±10	690 ±20
3	〃	Basalt.	2·16	0·85	25	405 ±10	690 ±20
4	〃	Basalt.	5·95	0·69	86	430 ±10	720 ±20
5	Miyakesima Volcano. Lava. Flow. ejec. July. 1940.	Olivine-hypersthene-augite-basaltic andesite.	4·81	1·12	43	520 ± 5	710 ±20
6	Miyakesima. Bomb. ejec. July. 1940.	Augite-olivine-basalt.	1·46	0·74	20	380 ±10	580 ±20
7	Mihara. Bomb. ejec. Aug. 1940.	Basalt.	1·81	0·34	53	400 ±10	690 ±20
8	〃	Basalt.	2·43	1·03	24	430 ±10	630 ±20
9	Mihara. An'ei Lava Flow(1778).	Hypersthene-bearing basalt.	4·19	0·56	75	420 ±10	600 ±20
10	Mihara. Meizi-Taisyo Lava (1911 ~1914).	Basalt.	3·15	0·34	93	480 ±10	700 ±20
11	Mihara. An'ei Lava Flow(1778).	Hypersthene-bearing basalt.	5·12	2·21	23	480 ±10	620 ±20
12	〃 〃	〃	2·92	0·76	38	480 ±10	—
13	Zawo Volcano. Dyke Rock.	Olivine-two-pyroxene-andesite.	0·57	0·49	12	570 ±10	605 ±10
14	Usami Volcano. Lava Flow.	Augite-hypersthene-andesite.	0·68	0·79	9	540 ±10	580 ±10
15	Usami Volcano. Lava Flow.	Hypersthene-bearing olivine-augite-andesite.	0·20	1·07	2	—	—
16	Asama Volcano. Bomb. ejec. 1940.	Andesite.	1·09	0·50	22	—	—

Table VIII. Chemical Compositions of the Specimens.

	No. 1[12]	No. 2[15]	No. 3[14]	No. 9[12]	No. 14[13]
SiO_2	51·23	50·78	53·01	52·45	51·67
Al_2O_3	15·24	17·05	14·83	13·48	19·88
Fe_2O_3	4·18	3·65	5·35	4·60	3·25
FeO	8·99	8·76	9·98	10·02	6·97
MgO	4·85	4·55	3·82	4·78	3·30
CaO	11·14	11·08	9·97	10·23	9·46
Na_2O	2·19	2·20	1·76	1·99	2·18
K_2O	0·54	0·25	0·46	0·52	0·40
H_2O+	n.d.	0·95	0·01	n.d.	1·26
H_2O-		0·01	0·01		1·00
TiO_2	0·83	0·77	0·61	1·39	0·92
P_2O_5	0·03	0·11	0·32	0·33	0·10
MnO	0·33	0·21	tr.	0·31	0·16
BaO	0·03	—	—	0·03	—
S	0·10	—	—	0·18	—
Total	99·68	100·39	100·13	100·32	100·55
Norms. Q	5·35	4·68	12·67	9·61	9·31
Or	3·34	1·67	2·78	3·34	2·23
Ab	18·35	13·35	14·68	16·78	18·35
An	30·04	35·88	31·15	26·15	43·39
Wo	10·57	7·67	6·85	9·41	1·16
En	12·01	11·34	9·54	11·95	8·23
Fs	12·01	12·13	12·79	12·80	8·83
Mt	6·02	5·32	7·87	6·71	4·63
Il	1·52	1·52	1·21	2·58	1·82
Ap	tr.	0·33	0·66	0·65	0·33

teristics of various igneous rocks. This will be the subject of the writer's further studies on thermo-remanent magnetism.

It must be mentioned here that J. G. Königsberger[16] and others have already reported the results of their studies in the relation between the magnitude of Q_t and grain-size and the chemical composition of the ferromagnetic minerals contained in the rocks, namely, FeO, Fe_2O_3, and

12) I. IWASAKI, *Analyst*. (I. IWASAKI, *Journ. Chem. Soc. Japan.*, **56** (1935), 1511.)

13) S. TANAKA, *Analyst*. (H. TSUYA, *Bull. Earthq. Res. Inst.*, **15** (1937), 215.)

14) S. NAKAZIMA, *Analyst*. (H. TSUYA, *Zisin.*, **12** (1940), 475.)

15) This rock specimen was analyzed by Mr. S. NAKAZIMA in Dr. TSUYA's laboratory in the E.R.I. at the writer's request. The writer wishes to express his sincere thanks to these two gentlemen.

16) J. G. KÖNIGSBERGER, *loc. cit.*

TiO_2, according to whom, a solid solution of magnetite and Fe_2O_3 in excess seems to give a large value of Q_t, although the microscopic mechanism of this phenomenon is not clear at present. They also assumed that the transcendental temperature in the process of causation of the thermo-remanence is the Curie-point, chiefly because the former almost agrees with the latter of pure magnetite. On the other hand, R. Chevallier[17] measured the temperature-change of magnetization of seven rocks in a rather strong magnetic field (larger than 100 Gauss) by means of the magnetometric method. According to him, the Curie-point in absolute temperature scale of the solid solution of FeO and Fe_2O_3, or more strictly speaking, of FeO and Fe_3O_4, decreases nearly proportionally to the percentage of the amount of FeO in excess, that is, the Curie-point seems to be proportional to the ratio $Fe_2O_3/(FeO+Fe_2O_3)$, so long as the ratio is smaller than 0·69, where FeO and Fe_2O_3 compose Fe_3O_4 without excess of FeO or Fe_2O_3. On this ground he proposed a phenomenological theory of the relation.

In the present study, however, the mode of causation of the thermo-remanent magnetism was more minutely observed, where the permanently magnetized component and the component reversible for applied external magnetic field, namely, the induced magnetism, are separated in the sense of a first approximation. Hence, the two temperatures t_a and t_c in $P(t)$ as well as its functional form, should be examined in their relation to the composition of the material, while the temperature change of the induced magnetization, reversible at any rate for a weak magnetic field, should be measured independently, for example, by the ballistic method.

Aside from the foregoing problem, the results of our studies thus far may furnish interesting suggestions on the physical conditions in the earth's crust, seeing that the two processes of causation and disappearence of thermo-remanent magnetism occur in the earth's crust, if its temperature either increases or decreases in a geomagnetic field. However, the temperature in the earth's crust at depths exceeding 20 km from the earth's surface is believed to be higher than 600°C, while the largest part of the causation and disapperence of thermo-remanence is accomplished during the change in temperature from 300°C to 600°C. Consequently, the change in magnetization of the earth's crust due to variation in its temperature, if any, can be expected only in its outer part, where the thickness of the crust is less than 20 km, so long as we assume that the critical temperature of the thermo-remanence is not greatly affected by increase of the hydrostatic pressure in the earth's crust.

17) R. CHEVALLIER et J. PIERRE, *Ann. Phys. Paris*, **18** (1932), 383.

On the other hand, according to J. Bartels,[18] secular variation in geomagnetism seems to be due rather to an inhomogeneous variation in the magnetic condition of the earth's crust, in view of the fact that expansion of the secular variation by means of spherical harmonic analysis failed to give such good convergency as that of the general permanent field, and because the first term $P_1(\cos\theta)$ in the expansion series was not so prominent as in the latter. The isoporic charts by H. W. Fisk[19] and by A. G. McNish[20] lead to the same conclusion. It may therefore be presumed that the change in intensity of thermo-remanent magnetism in the subterranean layer due to rise and fall of the isotherm near t_0 would be a contributory cause of the secular variation. Explanation of the secular change by changes in the induced magnetism caused by the rise and fall of the Curie-point isotherm in the earth's crust is regarded as beset with the difficulty that the magnetic susceptibility of the rocks composing the upper part of the crust is too small compared with the amount required for explaining the intense focus of distribution of the secular variation. However, adding the effect of magnetism during cooling to changes in induced magnetism, we may expect the presence of a larger amount of magnetic change in the earth's crust; the total intensity amounting to about ten times that of induced magnetism in the intermediate rocks, while in the case of basic rock, such as basalt, given in Table VII, whose chemical composition is nearly the same as the average composition of plateau basalt given by R. A. Daly,[21] the intensity amounts sometimes to more than one hundred times. In these circumstances, we may expect that the contribution of the temperature change within the earth's crust to secular variation in geomagnetism would be much larger than that estimated so far.[22]

The disturbance in the geomagnetic field as the effect of magnetism during cooling would be particularly marked in volcanic regions, where the temperature and its space gradient in the earth's crust near the surface may be much higher and larger respectively than those in other districts. A severe volcanic activity, especially, would be followed by local anomalous geomagnetic changes, at any rate, in the neighbourhood of the volcano. For example, as mentioned in the introduction to this paper, the severe volcanic eruption of Miyake-island, in July 1940, was

18) J. BARTELS, *Veröff. Preuss. Meteor. Inst. Abhandl.* 8 Nr. 2 (1935).

19) F. W. FISK, *Third Rep. Comm. Solar and Terr. Relationship.* (1931).

20) A. G. MCNISH, "*Terrestrial Magnetism and Electriary,*" 1939, New York, pp. 329~330.

21) R. A. DALY, "*Igneous Rocks and the Depth of the Earth,*" (1933) New York.

22) J. G. KÖNIGSBERGER has also proposed almost the same theory on the origin of the secular variation in geomagnetism, (*Z. S. Geophys.* 8 (1932), 322.)

accompanied with a fairly large geomagnetic change in the island. All the results of geomagnetic observations accomplished by four parties independently, namely, by R. Takahasi and K. Hirano,[23] with a vertical intensity variometer; by T. Minakami,[24] with a dip-circle, by the writer[25] with a dip-magnetograph: and by Y. Katô[26] of the Tôhoku Imperial University, with an earth inductor, gave without exception a large secular variation, more than twenty minutes in dip or a few hundred gamma in vertical intensity. The details of these results will be given in the reports by the respective observers. We shall merely say here that we have not the slightest doubt that a local anomalous variation of considerable magnitude occurred simultaneously with the volcanic activity.

Although so far, we have not obtained so precise a knowledge of the distribution of the anomalous variation as to enable us to determine the mechanism of the origin of the variation uniquely, there will be no doubt that much of the variation was due to the change in the thermo-remanent magnetization of the basaltic rocks of the island.

It is scarcely necessary to stress the fact that the effusive rocks ejected from volcanoes always retain natural remanent magnetism of fairly large magnitude, nor that permanent magnetism is the thermo-remanent magnetism produced during its cooling in the geomagnetic field, as a number of investigators have reported. Consequently, that the geomagnetic field near a large mass of newly ejected rock slowly varied owing to the change in the magnetic intensity of the mass as the result of magnetization caused during cooling, can also be readily considered, the phenomenon having been recognized by a number of investigators.[27]

6. Conclusion and Summary.

The equations of condition for causing magnetism during cooling, established in the present study, may be accepted as a first approximation to the unravelling of the phenomenon. The experiments always seem to be subject to errors of a few per cent, namely, the error in measuring the temperature of the specimen owing to its lack of homogeneity, and

23) R. TAKAHASI and K. HIRANO, *Zisin.*, **12** (1940), 510.
24) T. MINAKAMI, *ibid.* 507.
25) T. NAGATA, *ibid.* 496.
26) Y. KATO, *Proc. Imp. Acad. Japan.*, **16** (1940), 352.
27) Y. KATO, *loc. cit.*
T. MINAKAMI, Read before the 165th meeting (1940) of the E. R. I. Not yet published.

to that in measuring the magnetic intensities. The other serious cause of errors is that the exact standard condition of a rock was not attainable, not even in the initial state of the experiment at 0°C, for there is no means at present of knowing what is the normal state of a rock both from the standpoint of petrology and that of the magnetism of such a complex aggregate of matter as a rock. These obstacles are inevitable in the quest for a full understanding of the apparent magnetic properties of a rock. In order to circumvent this difficulty, it is necessary to examine the property of magnetism during cooling of each mineral composing a rock, the mutual reaction between them, and lastly the law that functions them, such as the apparent magnetic property of a rock.

In the present phenomenological description of the mode of causation of magnetism during cooling, this magnetism at whatever temperature, is regarded as a permanent component separated from the component that is reversible with respect to the applied magnetic field. Although this is done for convenience, it does not seriously differ from the truth, not at any rate within the limits of the apparent intensity of magnetization. The reliability of this separation was directly proved by the fact that the intensity of magnetization of a sample diminished slightly in magnitude of the order of the magnetization induced, the permanent component defined as $J_c(t,H)$, however, remaining unchanged when the external magnetic field was removed at any temperature during the cooling process. This fact may allow us to presume that a part or whole of the induced magnetism at t remains as permanent residual magnetism when the temperature becomes $t-dt$, when induced magnetization corresponding to $t-dt$ also appears.

Although, whether this phenomenon is due to a character of the ferromagnetic minerals in the rock alone or whether it is the result of their reaction with other minerals, is not clear at present, there is no doubt that the phenomenon is a result of the ferromagnetic property of the semi-conducting material. Moreover, the relation between $P(t)$ and $\chi(t)$, if obtained, will give a clearer aspect of the mode of causation of the magnetism during cooling. According to measurements of the temperature change in magnetic susceptibility $\chi(t)$ of a few basic rocks in a magnetic field of 2·2 Gauss, $\chi(t)$ seems to increase about 20∼50% at temperatures of from 100°C to 200°C below the Curie-point, although the increase was not so marked as that in iron in a weak magnetic field, as reported by J. Hopkinson[28] and others. After measuring $\chi(t)$ in a weaker magnetic field, a comparison of the characteristics of $\chi(t)$

28) J. HOPKINSON, *Proc. Roy. Soc. London*, A. **45** (1889), 318.

and $P(t)$ will be made. For the present, however the writer presumes that a part of $\chi(t)$ may concern $P(t)$.

Summarizing the conclusions reached in the present study, we may say that

(1). Thermo-remanent magnetism is defined as the magnetism that persists (remains) after the specimen has been cooled to 0°C or to ordinary room temperature.

(2). The magnetism $J_{t \cdot H}^{(t')}$, caused during cooling from t to t' in magnetic field H is given by

$$\vec{J}_{t \cdot H}^{(t')} = \vec{H} \cdot \int_{t}^{t'} P(t)\,dt,$$

where $P(t)$ has the functional form given in Fig. 3.

(3). The causation of magnetism during cooling is independent of the velocity of cooling.

(4). The permanent component of magnetization of a fresh specimen in the initial heating process is nearly zero, regardless of the intensity of H.

(5). Although $J_{t \cdot H}^{(t')}$ seems to be reversible with change in temperature, disappearence of magnetization due to increase in temperature does not depend on H.

(6). Although $P(t)$ seems to be in the same order as or rather smaller than $\chi(t)$, the magnitude of $\int_{t_c}^{0} P(t)\,dt$ is usually much larger than the susceptibility.

(7). The causation and disappearence of magnetism during cooling are expected to occur in the earth's crust. This phenomenon is related to secular variation in geomagnetism as well as to regional and local magnetic changes.

In conclusion, the writer wishes to express his sincere thanks to Dr. H. Tsuya, Dr. C. Tsuboi, and Dr. R. Takahasi, for their encouragement and advice in the course of the present study, and to Prof. S. Kaya for his interest in this study. His hearty thanks are also due to the Hattori Hôkô Kai, with the aid of whose grant the present experiment was carried out, and to Mr. H. Isiwara for assistance rendered.

6. 火成岩に於ける熱殘留磁氣生成の機構に就いて（序報）

地震研究所 永 田 武

火成岩の自然殘留磁氣及び熱殘留磁氣に關しては J. Königsberger, G. Folgheraiter, P. Mercanton, R. Chevallier 其の他の甚だ多くの研究があり，本邦に於いても中村清二博士，松山博士，及び筆者等の研究がある．この報告に於いては，火成岩の熱殘留磁氣生成過程に於ける諸狀態及び生成の條件等を觀測し，その生成機構の究明への準備とするものである．この研究で得られた結果を要約すれば次の如くである．

（1） 弱磁場 (H) に於いて，任意の溫度 t から常溫 (20°C) 乃至 0°C まで冷却した後の火成岩は，既に良く知られてゐる樣に熱殘留磁氣 $J_{t\cdot H}$ を持つ．

（2） $J_{t\cdot H}$ は少くとも弱磁場の範圍では，磁場の強さに比例する．(第2圖．第3圖)．

$$\vec{J}_{t\cdot H}=\vec{H}\cdot J_t. \tag{3}$$

（3） J_t (又は $J_{t\cdot H}$) は第1圖に示す如き傾向を有し，t_0 に於いて $\frac{\partial}{\partial t}J_t$ が極大，更に高溫の t_c に於いて J_t が最大値に達し，それ以上の t に對しては一定である．即ち t_c 以上の高溫から弱磁場冷却をした後の J_t は，その岩石の一特性常數である．これを J_{t_c} で表はし，飽和熱殘留磁氣と呼ぶ．

（4） 火山岩を高溫から 0°C まで冷却する場合に，ある溫度 $t_i+\varDelta t$ から t_i までの $\varDelta t$ の間のみ磁場 H を與へ，他の溫度區間では常に $H=0$ に保つ時，やはり殘留磁氣が表はれる．之を部分磁場冷却磁氣と呼び，$\varDelta J_{t_i\cdot H}$ を以て表はす．$\varDelta t$ の幅を一定に保つて，異れる t_i に於ける $\varDelta J_{t_i\cdot H}$ を測定した結果は第4圖に示す如く，t_0' に於いて極大値をとり，t_c' 以上では 0 である．又實驗誤差の範圍で t_0', t_c' はそれぞれ t_0, t_c に一致する．

（5） $J_{t\cdot H}$ と $\varDelta J_{t\cdot H}$ の間には

$$\sum_{t_i=0}^{t-\Delta t}\varDelta J_{t_i\cdot H}=J_{t\cdot H}. \tag{6}$$

$$\frac{\partial}{\partial t}J_{t_i\cdot H}\cdot\varDelta t=\varDelta J_{t_i\cdot H}. \tag{7}$$

が成立する．(第5圖．第6圖)．

（6） $\varDelta t$ を更にいくつかの溫度區間に分けて，それぞれに對應する部分磁場冷却磁氣を求めると，結局

$$\lim_{\Delta t\to 0}\frac{\varDelta J_{t_i\cdot H}}{\varDelta t}=\frac{\partial}{\partial t}J_{t_i\cdot H}=H\cdot P(t). \tag{13}$$

が成立すると考へられる．

（7） 以上の結果を綜合すると結局

$$\vec{J}_{t\cdot H}=\vec{H}\cdot\int_t^0 P(t)dt. \tag{14}$$

なる關係が得られる．更に (14) 式を擴張して，t から t' まで磁場冷却した場合に表はれる磁場冷却磁氣を $J_{t\cdot H}^{(t')}$ で表はせば

$$\vec{J}_{t\cdot H}^{(t')}=\vec{H}\cdot\int_{t}^{t'}P(t)\,dt. \qquad (15)$$

が得られる．

（8） 冷却速度か 1°C/sec 以上の範圍では，第一近似として $\Delta J_{t\cdot H}$ は冷却速度に無關係といふ結果を得た．從つて (14) (15) 兩式は冷却速度に無關係に成立する．

（9） (14) (15) 兩式の表はす性質を直接に觀測する爲に，不定位磁力計によつて，弱磁場内の任意の溫度に於ける帶磁の強さを測定した．その結果，初期狀態に於いて剛磁性を持たない試料の最初の加熱過程では，誘導磁氣 $H\cdot\chi(t)$ のみが表はれるのに對して，t_c 以上の高溫からの磁場冷却の過程に於いては，帶磁の強さが $H\cdot\chi(t)+J_c(t\cdot H)$ である．$J_c(t\cdot H)$ は剛磁性成分であつて，磁場 H を取除いてもそのまゝ殘留する．$H\cdot\chi(t)\ll J_c(t\cdot H)$ なる試料について $J_c(t\cdot H)$ の溫度變化を求めた結果，(第 13 圖)

$$J_c(0\cdot H)=J_{t_c\cdot H},\quad J_c(t_c\cdot H)=0. \qquad (21)$$

$$J_c(t\cdot H)=J_{t_c\cdot H}-J_{t\cdot H}. \qquad (22)$$

を得，更に $\Delta J_{t\cdot H}$ との間には (6) (7) 兩式と同樣の關係が成立する事を認めた．結局

$$\vec{J}_c(t\cdot H)=\vec{H}\cdot\int_{t_c}^{t}P(t)\,dt=J_{t_c\cdot H}^{(t)}. \qquad (25)$$

であつて，(15) 式を直接證明した事になる．

(10) 熱殘留磁氣 J_o を既に剛磁性として保存してゐる試料を加熱すれば，その J_o を生成する過程を表はす $J_c(t\cdot H)\sim t$ 曲線に殆んど等しい經路を逆行して，J_o は減少する．即ち

$$\frac{\partial}{\partial t}J_o=-H\cdot P(t). \qquad (27)$$

但し，(27) 式の H は J_o を生成する時に與へた H であつて，加熱の場合には無磁場の場合にも，上述の事は成立する．

(11) 以上の實驗結果は，任意の溫度に於ける微小溫度區間 Δt の間の溫度變化に對して，溫度降下に對して剛磁性を生成し，上昇に對して消失する性能を有する，溫度變化に對して可逆的なある物理的狀態 $P(t)\Delta t$ が存在し，冷却の際にはこの狀態に外部磁場 $\vec{H}$ が作用して $\vec{H}\cdot P(t)\Delta t$ の剛磁性が表はれるのに對し，加熱の場合には，その狀態の消失の故に，H の有無には無關係に $\vec{H}\cdot P(t)dt$ だけ剛磁性が消失するといふ事を暗示する．この現象の微視的機構は今後の問題である．

(12) 十數個の試料に就いて，χ, J_{t_c}, t_o, t_c, $Q_t\equiv J_{t_c}/\chi$ 等の實際値を例示したが（第 VII 表），Q_t が一般に 1 より大きく，100 近くに達する場合も存在する事を考慮すれば，地磁氣の永年變化，特に火山活動に伴ふ局部的異常變化に對して，地殼内の岩石に於ける磁場冷却磁氣の生成及び消失が，主要なる原因と考へられる事を論じた．一般に $P(t)\leqq\chi(t)$ ではあるが，ある有限範圍の溫度變化に對しては $\int P(t)dt$ が問題になり，この値が χ に比して大きいといふ事實が，地球物理學上の問題では注意されねばならないと思ふ．

この研究は服部報公會の御援助によつて遂行されたものであり，此處に同會に對して厚く感謝の意を表する．

7. *Changes in the Vertical Intensity of Geomagnetism that Accompanied the Eruption of Miyakezima, in 1940.*

By Ryûtarô TAKAHASI and Kintarô HIRANO,

Earthquake Research Institute.

(Read Nov. 20, 1940.—Received Dec. 20, 1940.)

1. *Introduction.*

Soon after the eruption of Komagatake, Hokkaido, in 1929, S. M. Nakamura[1] executed a magnetic survey around the volcano, using a dip-circle. Since then, the survey was repeated once every year until 1937, with the remarkable discovery that a conspicuous change, sometimes amounting to thirty minutes in the magnetic dip, occurs with the activity of the volcano.

Y. Kato[2] has pointed out, by means of a bold and ingenious contouring technic, that these changes in magnetic dip are closely related to the topographic changes caused by the eruption. After studying the results of six magnetic surveys made since 1882, each covering the whole of Japan, he[3] discovered also some changes in the magnetic elements that seem to have been related to the activities of Azumayasan during 1893∼96, of Adatarasan during 1899∼1900, of Zaosan during 1918∼25 and 1894∼97, of Ususan and Tarumaisan in 1893, 1909∼19, of Komagatake, Hokkaido, during 1919∼24, and of Sakurazima and Asosan in 1914.

In the recent eruption of the volcanic island, Miyakezima, on July 12, the writers executed magnetic surveys of the island, using a vertical intensity magnetometer, with the object of detecting changes in the vertical intensity of geomagnetism that usually accompany eruptions, all eventually to furnish some clue for elucidating the mechanism of volcanic eruptions.

The writers will begin with a short note on the recent eruption of Miyakezima. This island volcano, situated about 100 km south of Tokyo, belongs to the Huzi volcanic chain, and is one of the seven islands of

1) S. T. NAKAMURA, *Proc. Imp. Acad.*, **11** (1935), 102.
2) Y. KATO, *Sci. Rep. Tohoku Imp. Univ.*, Ser. 1, **27** (1938), No. 1.
3) *loc. cit.*, *Disin*, **5** (1933), 156, 573.

Idu Province. The island, which is circular, about 8 km in diameter, is a cone-shaped stratified double volcano, having a somma, and a central cone called Oyama, standing about 800 m above sea level. It is of basaltic augite andesite and olivine two-pyroxene andesite. Before the recent eruption, there were three craters on the central cone, each 300 m～500 m in diameter, lying side by side in an E—W direction. The volcano was dormant until the recent eruption.

The recent activity began on July 12, 1940, with a sort of fissure eruption on the eastern slope of the island. A number of craterlets were opened in two lines from a height of about 500 m down to the sea, where a new cinder cone, 60 m high, was formed, filling up the bay of Akabakke. This new hill, afterwards named Hyôtanyama, consists of ashes, scoriae, bombs, and lava bearing large phenocrysts of anorthite.

From the craters on the slope of the island, molten lava poured out and flowed down the valleys, forming two lava streams. They are of basaltic block lava, without any visible phenocrysts. One of the lava flows, the northern, flowed into the sea, burying the hamlet of Simasita on the northern shore of Akabakke bay, and joined Hyotanyama, a broad lava field, forming a new land, 800 m wide and 1 km long, projecting into the sea. Besides these lava flows, scoriae, ashes, and bombs were projected from the craterlets just mentioned in such quantities that the topography of the neighbourhood was completely altered.

Fig. 1. Positions of stations.

These eruptions from the eastern slope of the island ceased in the evening of July 13, the day following the outbreak, but from July 14, activity shifted to the central cone, Oyama. This eruption of the central cone, however, developed very gradually, attaining maximum violence on and after July 25, and continued till the early part of August. Filling up the old craters on the central cone, a lava flow and a cinder cone, 50m high, had formed, besides accumulations of ashes, scoriae, and bombs.

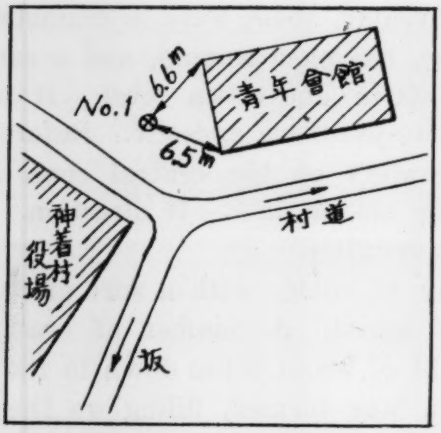

Station No. 1. Kamituki-m.
Young Men's Hall.

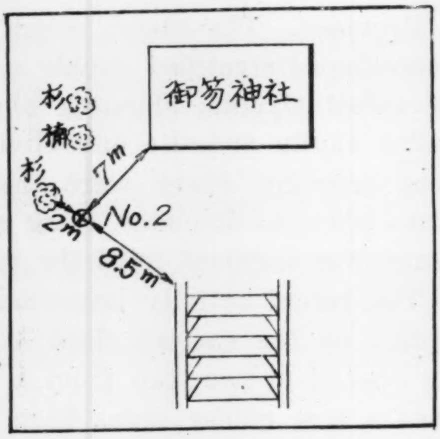

Station No. 2. Kamituki-m.
Osyaku shrine.

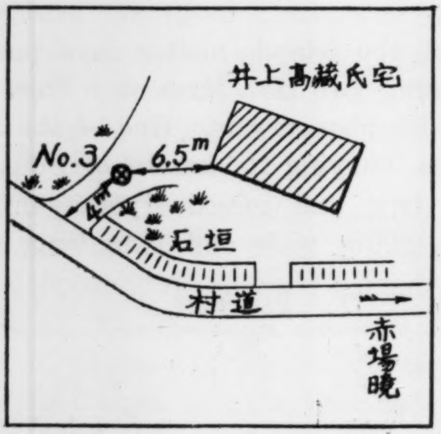

Station No. 3. Kamituki-m.
Mr. T. Inoue's garden.

Station No. 4. Kamituki-m.
Yamanokami.

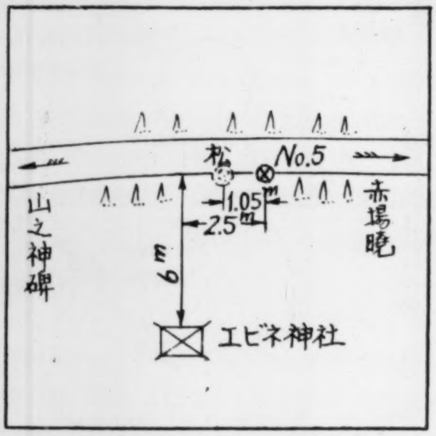

Station No. 5. Kamituki-m.
Ebine shrine.

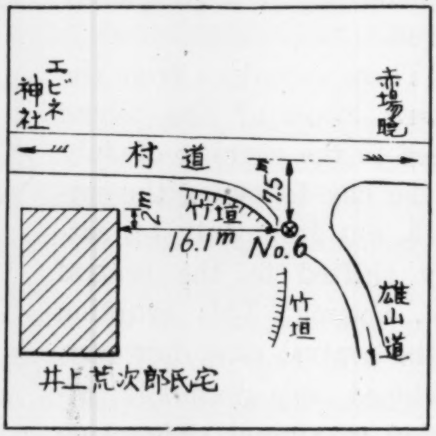

Station No. 6. Kamituki-m.
Mr. A. Inoue's garden.

Fig. 2a.

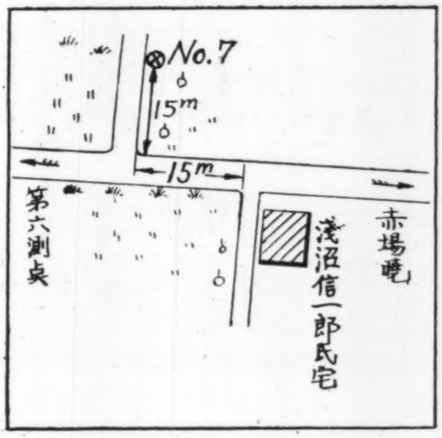

Station No. 7. Kamituki-m.
Nadaado.

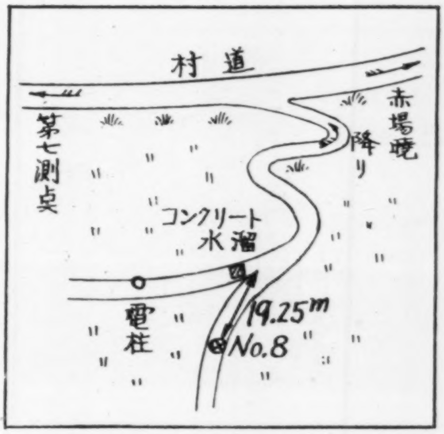

Station No. 8. Kamituki-m.
Minowa.

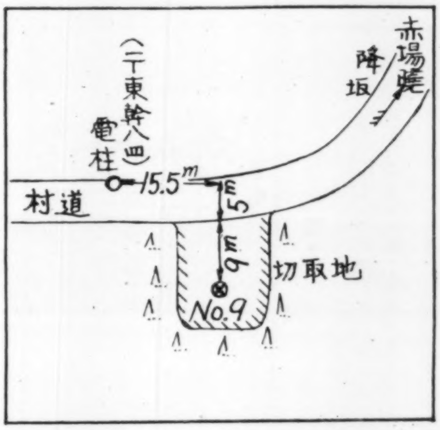

Station No. 9. Kamituki-M.
Hôdai.

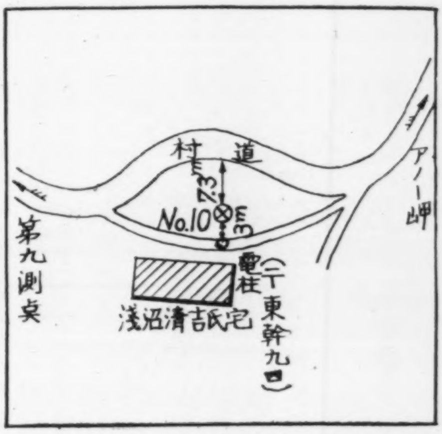

Station No. 10. Kamituki-m.
Kamanosiri.

Station No. 11. Kamituki-m.
Cape of Nisiano.

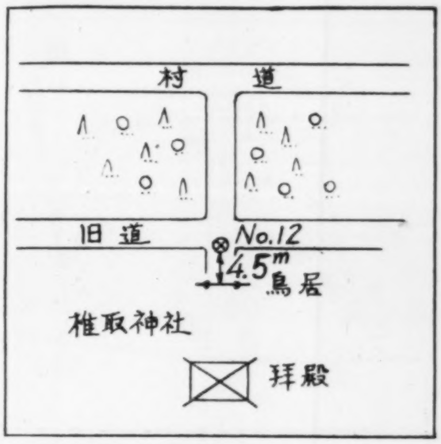

Station No. 12. Kamituki-m.
Siitori shrine.

Fig. 2b.

Station No. 13. Kamituki-m.
The new lava flow.

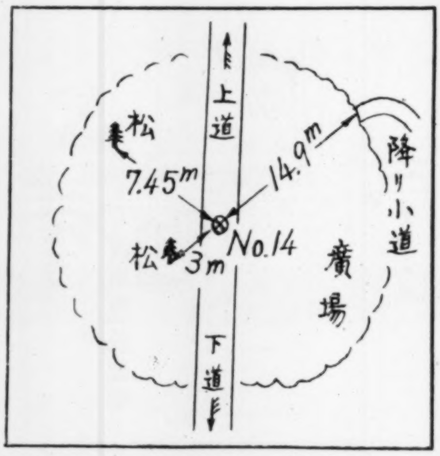

Station No. 14. Kamituki-m.
Takenoo.

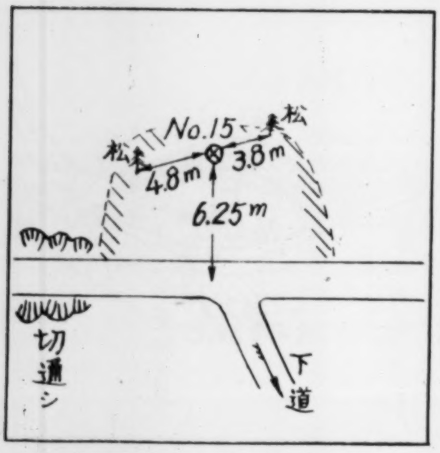

Station No. 15. Kamituki-m.
Uemiti.

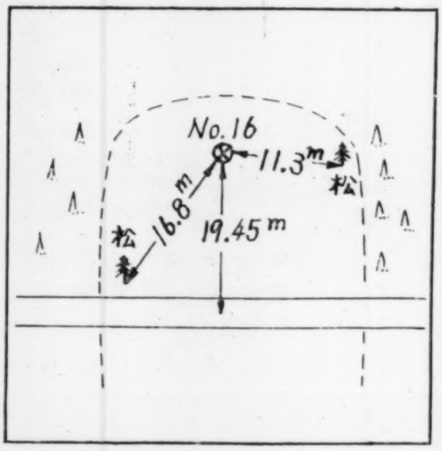

Station No. 16. Kamituki-m.
Nadaado Ue.

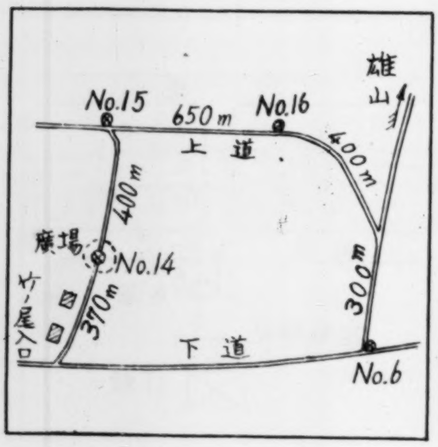

Stations Nos. 6, 14, 15, 16.

Station No. 17. Kamituki-m.
Sugiyama Hotel.

Fig. 2c.

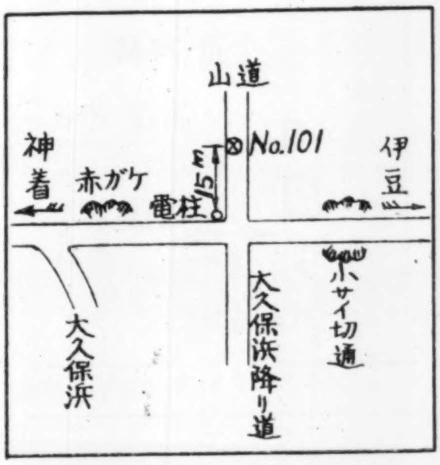

Station No. 101. Kamituki-m.
Okubohama.

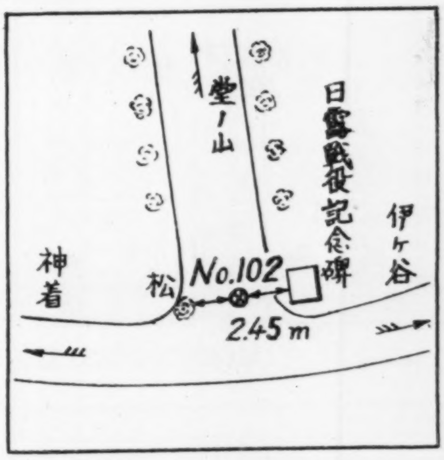

Station No. 102. Idu-m.
Monument.

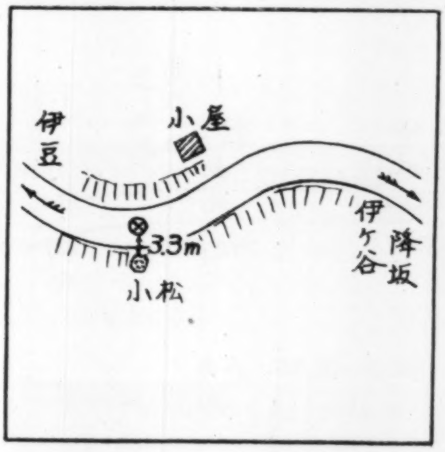

Station No. 103. Igaya-m.

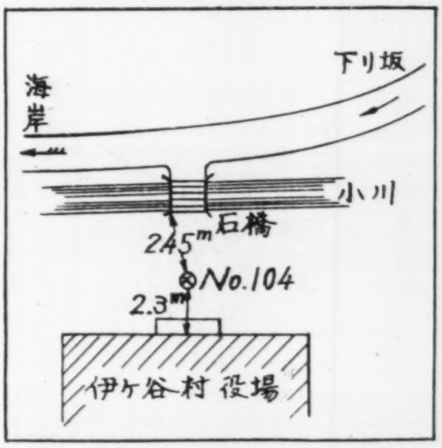

Station No. 104. Igaya-m.
Public Office.

Station No. 105. Igaya-m.

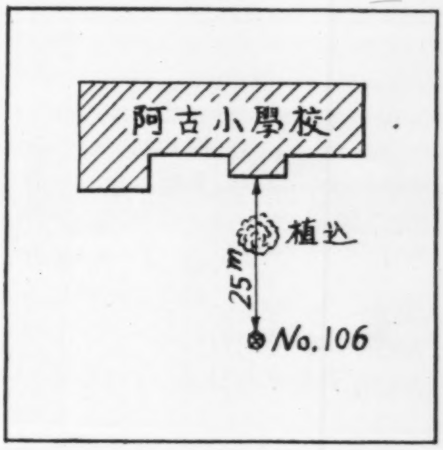

Station No. 106. Ako-m.
Primary School.

Fig. 2d.

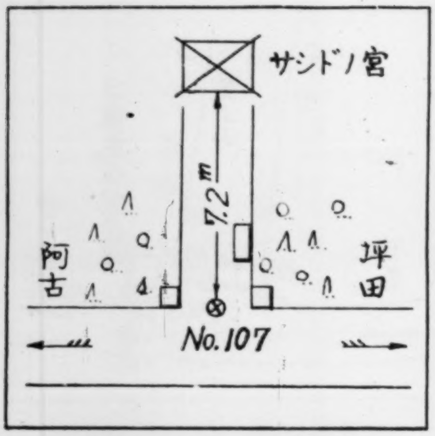

Station No. 107. Ako-m.
Sabinohama.

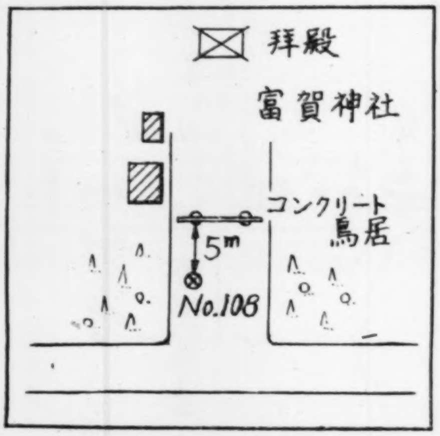

Station No. 108. Ako-m.
Toga shrine.

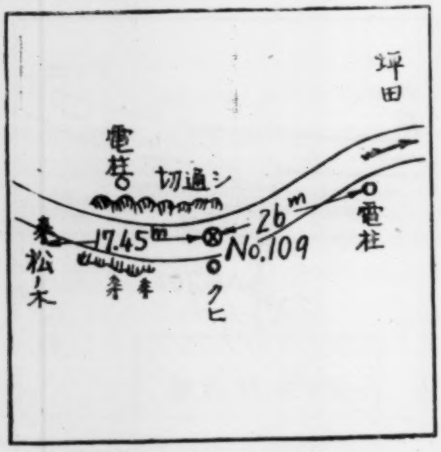

Station No. 109. Ako-m.
Upw. of Toga shrine.

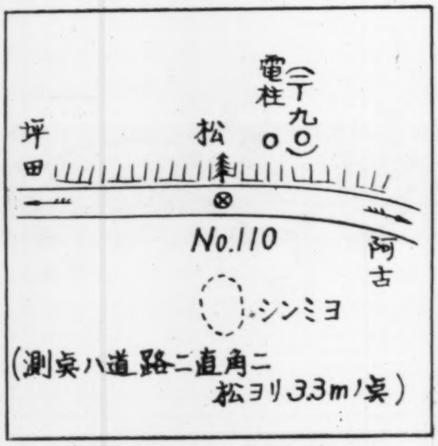

Station No. 110. Ako-m.
Sinmiyo.

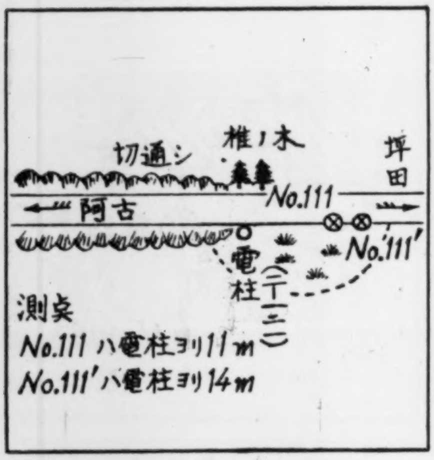

Stations Nos. 111 and 111'.
Boundary bet. Ako & Tubota.

Station No. 112. Tubota-m.
Ninomiya.

Fig. 2e.

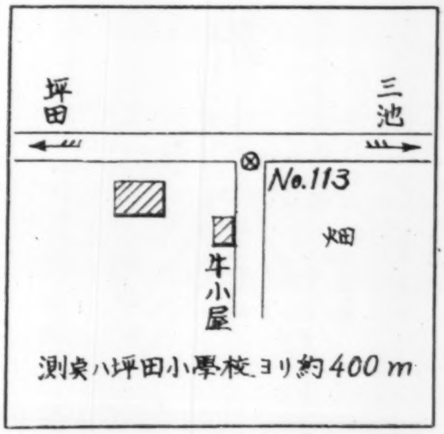

Station No. 113. Tubota-m.

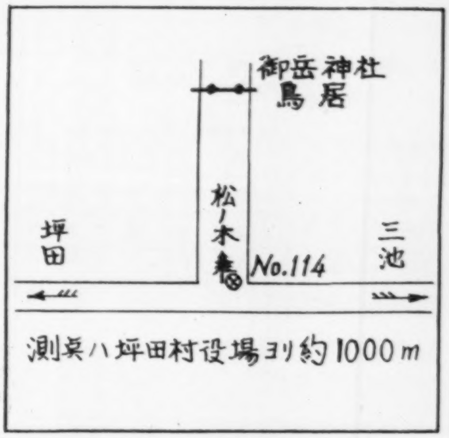

Station No. 114. Tubota-m.
Mitake shrine.

Station No. 115. Tubota-m.

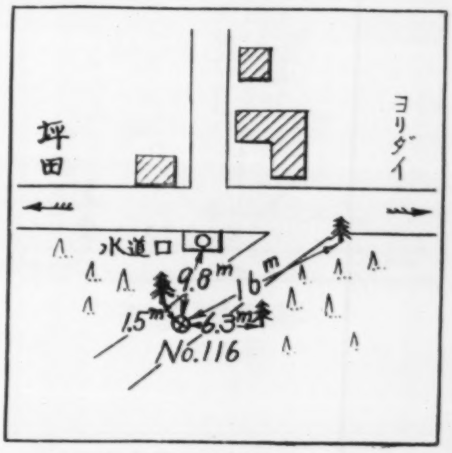

Station No. 116. Tubota-m.
Miikehama.

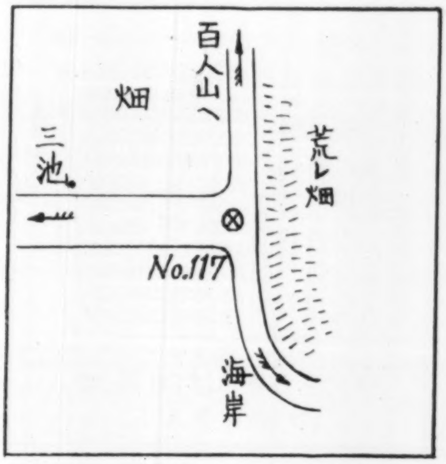

Station No. 117. Tubota-m.
Yoridaisawa.

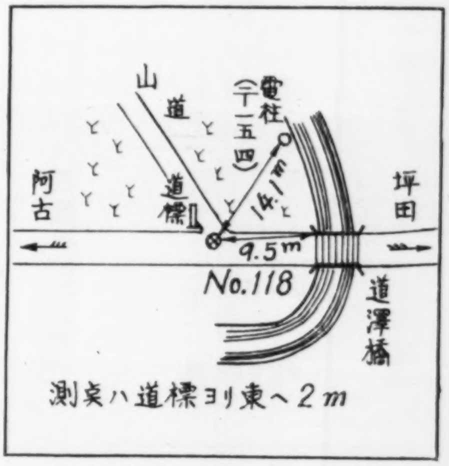

Station No. 118. Tubota-m.
Entrance to Goyômiti.

Fig. 2f.

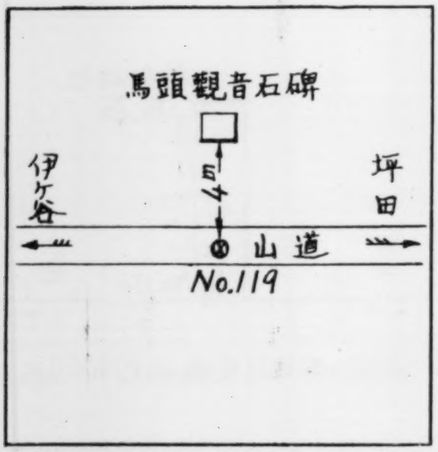

Station No. 119. Tubota-m.
Batô Kannon.

Station No. 120. Branch point of Ako and Igaya-m.

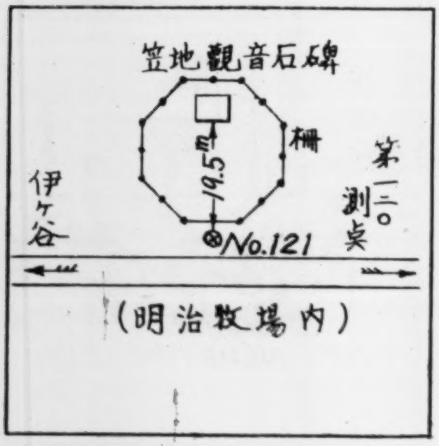

Station No. 121. Tubota-m.
Kasadidaira.

Station No. 122. Igaya-m.
Kamata.

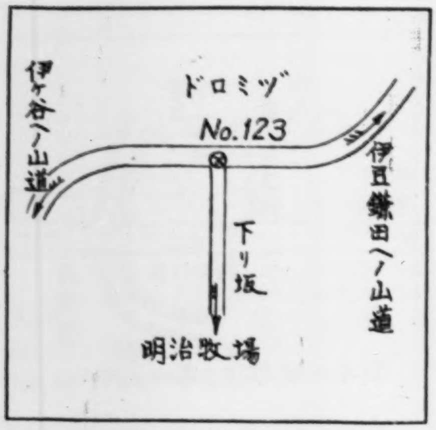

Station No. 123. Igaya-m.
Doromidu.

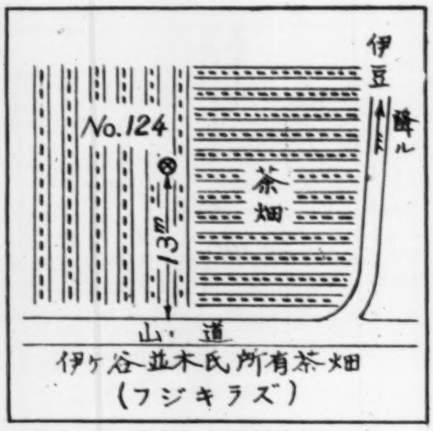

Station No. 124. Igaya-m.
Huzikirazu.

Fig. 2g.

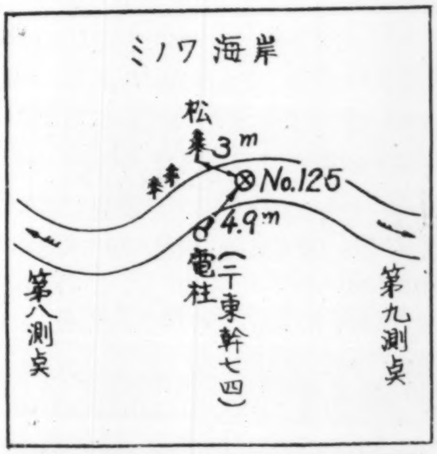

Station No. 125. Kamituki-m.
Minowa.

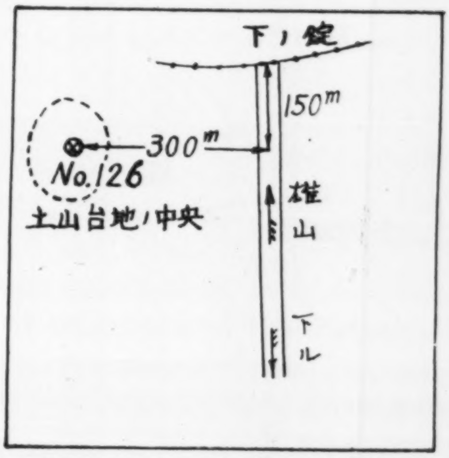

Station No. 126. Kamituki-m.
Kazahaya. (Sumiya no tairo)

Station No. 127. Kamituki-m.
Nango shrine.

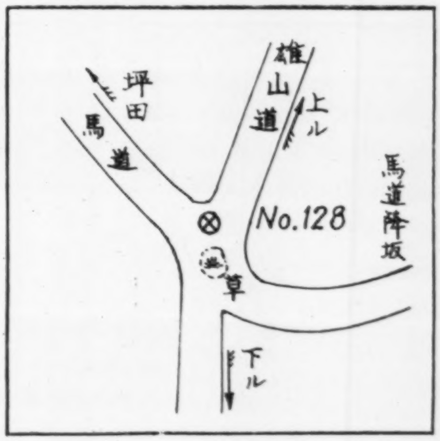

Station No. 128. Kamituki-m.
Umamiti.

Station No. 129. Boundary of
Kamituki-m. and Tubota-m.

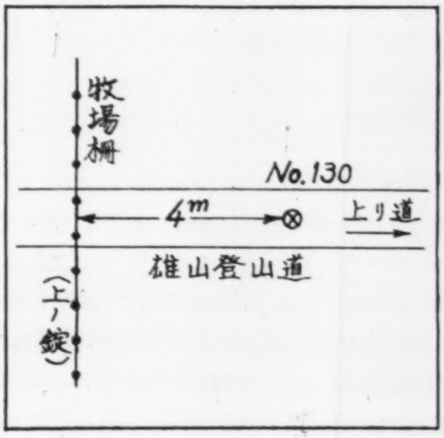

Station No. 130. Tubota-m.
Ue no Zyô.

Fig. 2h.

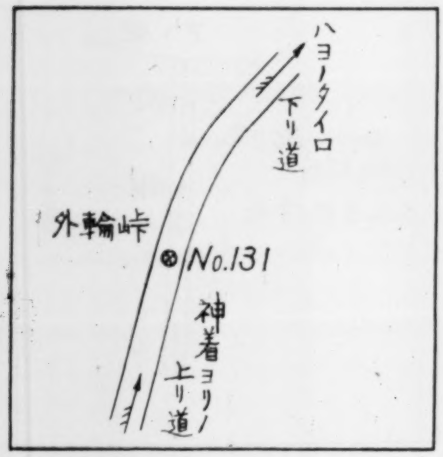

Station No. 131. A pass on the somma.

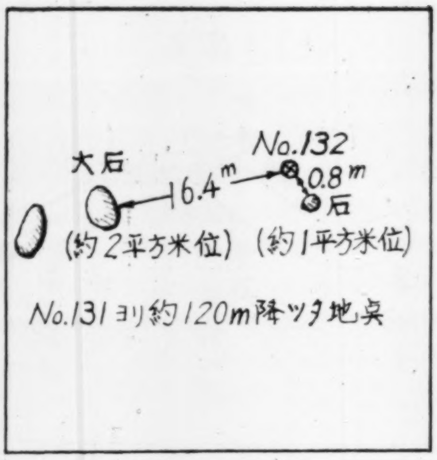

Station No. 132. Hayonotairo.

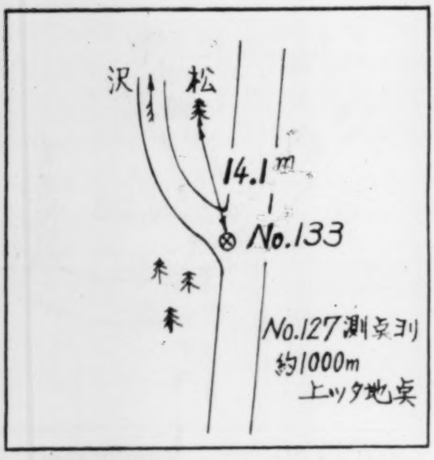

Station No. 133. Kamituki-m. Attakayama.

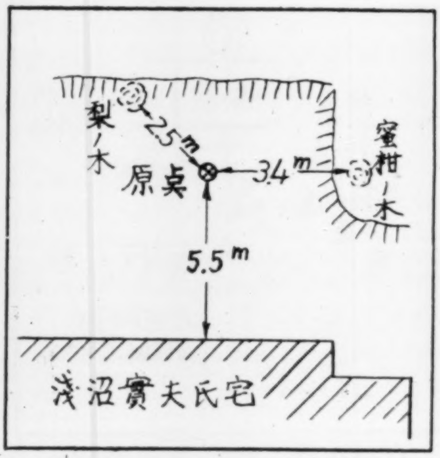

Station No. 0. Kamituki-m. Mr. Asanuma's garden.

Fig. 2i.

2. *Survey.*

The writers attempt here to describe the requisites in geomagnetic surveys that are made with the object of detecting changes in the distribution of the magnetic elements. The first requisite in such surveys is to have the observing stations distributed as close to one another, and in the most uniform distances apart, possible, because the greater the number of stations, the more minutely can the changes in the distribution be detected. In the surveys cited above, the number of stations were so few, being only 10 even in the case of Komagatake, that scarcely anything could be learned of what happened under the ground. Since, on the other hand, increase in the number of stations means

increased time and cost, there is a limit in some cases to the number of stations that can be used. The writers think that for a volcano, several scores of stations are necessary.

The second requisite is that the stations shall be occupied exactly in the same way for each survey. Not only the horizontal positions, but the height of the instrument also must be the same as that in previous surveys. In volcanic regions, it is not seldom that a difference in position of only a few decimeters will result in so large a difference in the magnetic dip as several scores of minutes. In this respect, such places must be selected for stations as represent the mean topography of its neighbourhood. Ridges, valleys, and edges of lava flows must be avoided. It is best to make measurements at three or four points, a few meters distant from one another, to certify that the magnetic gradient is not large. Station marks must, preferably, be a group of pegs, otherwise they are lost after a few years. Every possible care must be taken to keep the station marks intact, because the accuracy of the re-survey depends entirely on whether the station marks exist or not.

As to the instrument, the best is a vertical intensity variometer or an earth inductor. With a dip circle, an error of 1～2 minutes is unavoidable, even in the best of conditions. Under bad conditions, such as rain, snow, wind, or ash precipitation, unexpectedly large errors are liable to be introduced into the observed values. If the probable error of a survey is 3′, the probable error in the difference of two surveys will amount to 5′, which, in the case of a vertical intensity variometer, corresponds to an error of 50 gammas.

The effects of magnetic storms and of the daily variation must be considered, especially when the changes sought are not large. With a station instrument that records continuously the variations in the magnetic elements, the troubles just enumerated are inmaterial, so that it is adequate for ascertaining the existence of magnetic variations that accompany the eruption of a volcano. As a matter of fact, T. Minakami[4] and T. Nagata[5] observed changes in dip and declination at volcano Asama with station instruments.

3. *Stations and Instruments.*

In the present survey, there were 50 stations, the reason for this comparatively small number being that the survey could then be completed in a short time, during which period the condition of the eruption and the

4) *Bull. Earthq. Res. Inst.*, **13** (1935), 799.

5) *Disin*, **10** (1938), 221.

conditions of the phenomena underneath the volcano may be regarded as having been alike. The distribution of stations in the island is shown in Fig. 1. The numerals denote the serial numbers of the stations. For lack of roads, the stations, to our regret, are somewhat scanty on the southeastern side of the island, notwithstanding our desire for uniform distribution. In the reconaissance work, due attention was paid to the geology as well as to the topography of the sites, selected for the stations. With a view to shortening the time required for survey, the magnitude of the space gradient in the geomagnetism was not measured at all the stations, but every caution was taken to occupy exactly the same position in every measurement. The distances of the station peg from the corners of neighbouring buildings, trees, etc., were measured in anticipation of possible accidents by which the station marks may get lost. Sketch maps were made of each station, and photographs taken. These are shown in Figs. 2 a∼2 i and in Pl. I, Fig. 3.

A vertical intensity magnetometer, designed by one of the writers, was used in the present survey. The magnetometer can be modified by a simple procedure into a horizontal intensity variometer. The moving magnet system of the instrument was reconstructed just before the outburst of Miyakezima, the compensation adjustment for temperature not yet being complete. In these circumstances it was decided to determine the temperature coefficient of the instrument in the field, and to correct the reading according to the coefficient thus determined. Although our instrument is capable of being adjusted to any sensitivity, it was kept sealed during the intervals from the beginning of the first survey to the end of the second, in order that neither sensitivity nor the zero-point shall suffer the slightest change. The sensitivity of the instrument was adjusted to 82·5 gamma/division at the beginning of the first survey, under the expectation that in such a volcanic island as Miyakezima, which is built up of basaltic lava and ashes, the magnetic anomaly would sometimes be very large. The total range that can be measured without using a compensating magnet amounts thus to 8000 gammas, so that the compensating magnet, the moment of which is 210 c.g.s., was not necessary for any of the stations except No. 130. The sensitivity of the instrument was measured by means of a Helmholtz coil several times during the surveys.

4. *Corrections.*

(a) Correction for the air temperature. As just mentioned, because the temperature compensation adjustment of the moving system

of the magnetometer was incomplete, the temperature coefficient was determined in the field. The magnetometer was installed at a station, and its readings and those of the thermometer attached to the instrument were taken from time to time. The following is an example of such readings. In order to avoid the effect of diurnal variation, several series of such readings were taken at various times of the day. The most probable temperature coefficient thus determined and adopted was 47·8 gamma/1°C, or 0·58 div./1°C, converted into the sensitivity used

Table I.

July 17 Fine.

Reading (E)	Temperature	Time	Remarks
20·8	26·°0C	6^h 10^m	
22·4	27· 0	30	
22·7	27· 3	45	
22·9	27· 5	7 00	Sensitivity 13·31 gamma/div.
24·3	29· 0	16	
33·0	32· 2	45	
32·2	31· 0	8 00	
35.2	32· 5	10	

during the surveys. The compensation was excessive, that is, the reading increased with the temperature. Since the temperature variation during the survey was 6∼7°C at the most, an error of 10 gamma/div. in the determination of the temperature coefficient introduces into the observed values only an error of less than 60∼70 gammas, the same order of error as that from the diurnal variation. Since the changes in the vertical intensity detected by the present surveys reaches ten times this amount, the general situation of the change would scarcely be affected even if there were an error of this order in the adopted temperature coefficient.

(b) Changes in vertical intensity at the reference station. In such magnetic surveys as this, it is a common practice to make measurements every day at one and the same station that has been selected for the reference station, both before and after the measurements have been made at the other stations. The reason for this procedure was to ascertain whether or not changes had occurred in the zero value and sensitivity of the magnetometer during the day's journey. Since, in the present case, the vertical intensity is expected to change at the reference station as well as at other stations, it is necessary to know the extent to which the vertical intensity has changed at the reference station.

For this purpose, the mean values of the daily morning and evening readings, each corrected for temperature, were plotted against time. The result showed, as indicated in Fig. 4, in which the oridinate is arbitrary, that the vertical intensity at the reference station decreased for the period July 20∼25, and then increased. It is interesting that this tendency was also discovered in variations in the magnetic dip observed by T. Nagata[6] and T. Minakami[7] at Hôdai, 1·5 km east of our reference station. Similar variations were also observed by T. Hagiwara[8] in the earth current at Kamituki. The decrease of 55 gammas in the vertical intensity, shown in Fig. 4, corresponds to a decrease of 9′ in the dip.

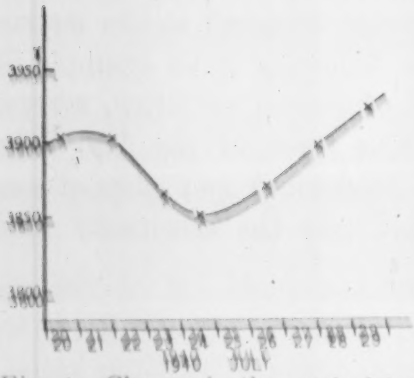

Fig. 4. Change in the vertical intensity of geomagnetism at the reference station.

Since the vertical intensity at the reference station was already subject to variations as stated above, it was decided to denote the vertical intensity at the various stations by values relative to the value of the reference station at 0^h on July 25. The difference of the morning and evening values at the reference station, which still remains after the correction is made for temperature, is mainly due to the diurnal variation in geomagnetism. This difference was accordingly distributed to the observed values of that day in proportion to the time elapsed.

(c) Geomagnetic storms. The first survey was made during the period July 20∼24, and the second during the period July 26∼29, the stations being occupied in entirely the same order as that in the first survey. During these periods of surveys there was fortunately no magnetic storm greater than 50 gammas. Since in the present surveys, the magnetometer, as mentioned above, was adjusted to a very low sensitivity, there is no need to take any account of such small magnetic storms.

5. *Results of the surveys.*

The results of the surveys are shown in Fig. 5 and in Table II. These values are already corrected for temperature and diurnal variation. In Fig. 5 are given the result of the of the first survey. In the figure,

6) *Disin*, **12** (1940), 12.
7) *Ditto*, 18.
8) *Ditto*, 44.

contour lines are drawn at intervals of 1500 gammas. The negative parts are shaded by a fine mesh, and the parts greater than 3000 gammas by thick diagonal lines.

In volcanic regions, there are usually so many intense local anomalies that the contour-lines given in Fig. 5, being based on only 50 measurements, do not necessarily show the real anomalies. Considering however that due attention was paid to selecting the positions of the stations, the writers believe that they represent to some extent the general trend of the disribution of the vertical intensity of the earth's magnetism. It is interesting that the contour-lines curve inward at the old explosion craters

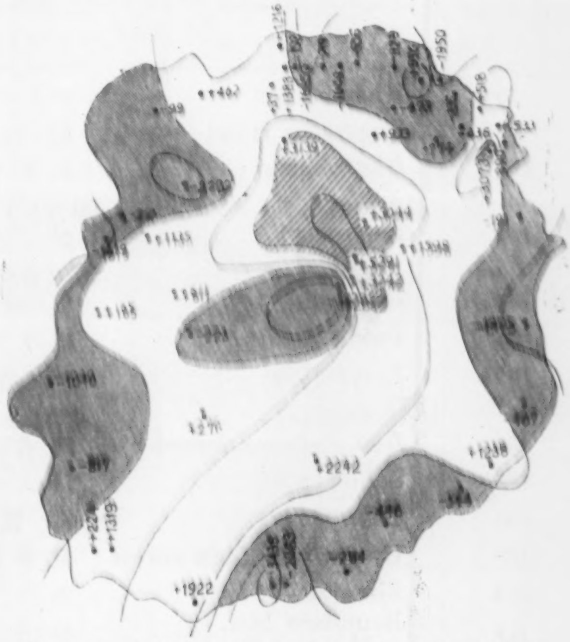

Fig. 5. Distribution of vertical intensity. Unit=γ.

Table II.

Nos. of Station	Locality		I	II	II−I
	(Kamitukimura)	(神着村)			
0	Mr. Asanuma's garden	淺沼方庭	+ 37 γ	+ 8 γ	− 29 γ
1	Young Men's Hall	青年會館	+1383	—	—
2	Osyaku shrine	御笏神社	− 198	− 188	+ 10
3	Mr. Inoue's garden	井上高藏方庭	−1685	—	—
4	Yamanokami	山神碑前	− 219	− 79	+ 140
5	Ebine shrine	エビネ神社前	−1049	—	—
6	Mr. A. Inoue's garden	井上荒次郎方前	− 636	− 570	+ 66
7	Nadaado	ナダアド	− 929	—	—
8	Minowa	三ノ輪入口	+ 950	+ 941	− 9
9	Hôdai	砲臺	− 335	− 347	− 12
10	Kamanosiri	釜ノ尻	+ 518	+ 545	+ 27
11	Cape of Nisiano	西アノー岬	+ 533	+ 512	− 21
12	Siitori shrine	椎取神社前	− 890	− 880	+ 10
13	Beside the new lava flow	新熔岩脇	+3073	—	—
14	Takenoo	竹ノ尾	− 436	− 240	+ 196
15	Uemiti	上道	− 774	− 818	− 44

(*to be continued.*)

Table II. (*Continued.*)

Nos. of Station	Locality		I	II	II−I
16	Nadaado Ue	ナダアド眞上	− 473 γ	− 434 γ	+ 39 γ
17	Sugiyama Hotel	杉山旅館	+1216	+1140	− 76
101	Okubohama	大久保濱上	+ 462	+ 454	− 8
	(Idumura)	(伊豆村)			
102	Monument	伊豆村	− 99	− 79	+ 20
	(Igayamura)	(伊ケ谷村)			
103	Igayamura	伊ケ谷へ下り口	− 810	− 777	+ 33
104	Public Office	伊ケ谷役場	−1619	—	—
105	Igayamura	伊ケ谷阿古間	+ 165	+ 152	− 13
	(Akomurna)	(阿古村)			
106	Ako Primary school	阿古小學校	−1040	− 950	+ 90
107	Sabinohama	錆ノ濱	− 817	− 835	− 18
108	Toga shrine	富賀神社	+ 224	+ 206	− 18
109	Upward of Toga shrine	富賀神社上	+1319	—	—
110	Sinmiyo	新ミヨ	+1922	+1907	− 15
111	Boundary btw. Ako and Tubota	坪田，阿古境	−3439	—	—
111′	Do.	同上	−2283	−2305	− 22
	(Tubotamura)	(坪田村)			
112	Ninomiya	二ノ宮	− 284	− 203	+ 81
113	Tubotamura	坪田村	− 544	− 529	+ 15
114	Mitake shrine	御岳神社	+1238	+1337	+ 99
115	Btw. 114 and 116	御岳，三池間	− 467	− 509	− 42
116	Miikehama	三池濱	−1975	−2033	− 58
117	Yoridaisawa	ヨリダイ澤	− 191	− 207	− 16
118	Entrance to Goyomiti	御用道入口	− 446	− 387	+ 59
119	Bato Kannon	馬頭觀音前	+2242	+1734	− 508
120	Branch pt. of Ako and Tubota	坪田阿古分岐點	+ 276	+ 214	− 62
121	Kasadidaira	笠地平	− 223	− 360	− 137
	(Igayamura)	(伊ケ谷村)			
122	Kamata	鎌田飼場	+ 611	+ 416	− 195
123	Doromidu	泥水	+1135	+1040	− 95
124	Huzikirazu	藤不切	−2202	−2293	− 91
	(Kamitukimura)	(神着村)			
125	Minowa	三ノ輪	−1950	−1751	+ 199
126	Kazahaya	風早	+ 933	−1045	+ 112
127	Nango shrine	南郷祠	+3139	+3130	− 9
128	Umamiti	雄山馬道	+3044	+2893	− 151
129	Boundary of Kamituki and Tubota	坪田，神着境界	+1598	—	—
	(Tubotamura)	(坪田村)			
130	Ue no Zyo	上ノ錠	+5291	+5061	− 230
131	Pass on Somma	外輪頂上	+3242	+3029	− 213
132	Hayonotairo	八丁平	−1528	−1741	− 213

of Miikehama, Midutamari, Hurumiyo, etc., and at the attrio of Hayonotairo, as also that the positive anomalies on the northern slope of the volcano coincides with the region of activity in 1874.

The difference in the first and second surveys is shown in Fig. 6. The parts in which the differences are less than -100 gammas, and those in which the variations exceed $+100$ gammas are shaded differently. It is remarkable that the figure shows a large negative area of oval shape, extending from the center to the southern half of the island, and also a small positive zone of elliptic shape at the northern part of the island. The maximum and minimum values of these variations are 120 and 500 gammas respectively.

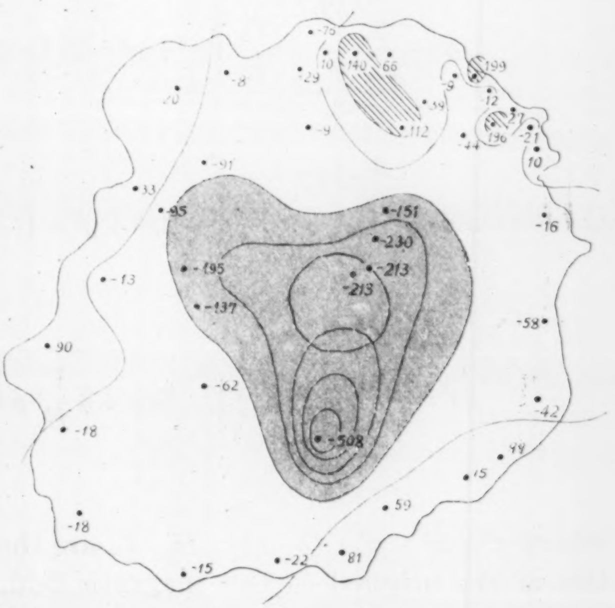

Fig. 6. Changes in the vertical intensity (II—I) Unit=γ.

6. *Interpretation of the result.*

We shall now consider the changes in the condition under the volcano that have caused these changes in the vertical intensity of geomagnetism. Miyakezima is a conical volcanic island. Since the coastline of the island is nearly circular, 8 km in diameter, and its height about 800 m above sea level, the island is aptly represented by a cone of gradient 1 in 5. We take the origin of the coordinate at the summit, the x-axis to the north, and the y-axis to the east, and the z-axis downward. We shall assume that a spherical part of radius R, of which the centre is at $x=0$, $y=0$, and $z=t$ km, has been heated and thus lost its magnetic properties. Because rocks have comparatively small susceptibility, it is obvious that the above assumption is equivalent, in the first approximation, to assuming that the susceptibility of the surrounding rocks is zero, while that of the spherical part changes from zero to $-k$. The change in the geomagnetic elements that ought to be observed at a point (x, y, $z=\frac{1}{5}\sqrt{x^2+y^2}$) on the surface of the cone is

given by

$$\left.\begin{aligned}
\Delta Z &= \frac{\frac{4}{3}\pi k R^3}{1+\frac{4}{3}\pi k}\frac{V_0}{r^5}\left[x^2+y^2-2(t-z)^2+3\frac{H_0}{V_0}x(t-z)\right], \\
\Delta X &= \frac{\frac{4}{3}\pi k R^3}{1+\frac{4}{3}\pi k}\frac{H_0}{r^5}\left[-2x^2+y^2+(t-z)^2+3\frac{V_0}{H_0}x(t-z)\right], \\
\Delta Y &= \frac{\frac{4}{3}\pi k R^3}{1+\frac{4}{3}\pi k}\frac{H_0}{r^5}\left[-3xy+3\frac{V_0}{H_0}y(t-z)\right],
\end{aligned}\right\} \quad (1)$$

where $r^2=x^2+y^2+(t-z)^2$; H_0, V_0 are the horizontal and vertical intensities of the original earth's magnetic field, ΔX, ΔY, ΔZ, the x-, y-, and z-components of the change in the geomagnetism, and $z^2=\frac{1}{25}(x^2+y^2)$.

With this formula, it is easy to calculate the variations respectively in the magnetic declination, dip, horizontal, and vertical intensities.

According to measurements made by the Hydrographic Department of the Imperial Japanese Navy,[9] the geomagnetic elements at the following stations in Miyakezima are

Locality		δ	i	H_0	Epoch
Okubohama	(大久保濱)	5° 22′	46° 11′	31408 γ	Jan. 28, 1933
Akabakke	(赤場曉)	3 52	44 01	31346	
Ako	(阿　古)	3 49	48 18	29396	
Tubota	(坪　田)	5 41	48 01	30213	

It may therefore be safely assumed that $H_0=V_0=30000\gamma$, $i=45°$, in the formula just given. The susceptibilities of all the rocks of Miyakezima, as measured by Nagata,[10] are nearly 2×10^{-3}. Adopting this value for k, and assuming $t=3$ km, $R=2{\cdot}7$ km., ΔZ, ΔH, and Δi[11] were evaluated with results as shown in Figs. 7 and 8. ΔZ, ΔH., and Δi are symmetric with respect to the x-axis.

9) *Bull. Hydr. Dep. Imp. Jap. Navy*, **8** (1936), 316

10) *Disin*, **12** (1940), 524.

11) $\Delta i=\cos^2 i_0\left(\frac{\Delta V}{H_0}-\frac{\Delta H\cdot V_0}{H_0^2}\right)=\frac{1}{2H_0}(\Delta V-\Delta H)$

Comparing Figs. 7 and Fig. 6, it is surprising that the two figures are very similar, not only in regard to the distribution of positive and

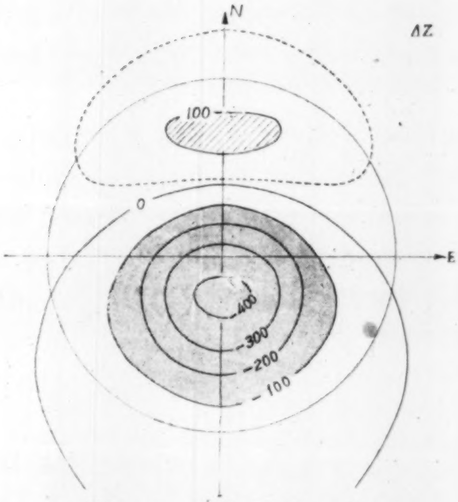

Fig. 7. ΔZ. Unit=γ.

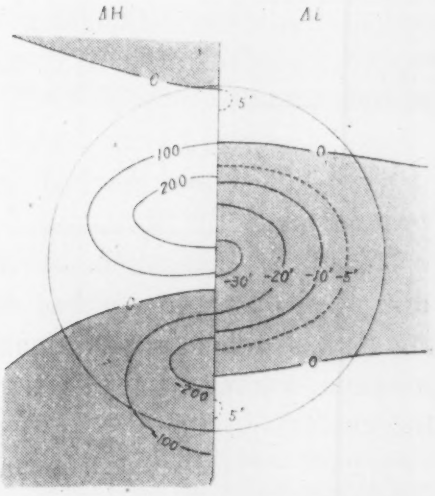

Fig. 8. ΔH and Δi. Unit=γ.

negative areas, but also in regard to their values. It may be said that the measured change in the vertical intensity is thus satisfactorily explained. The results of the surveys show therefore that a spherical part, 3 km beneath the summit of the volcano, had become heated above the Curie point about July 25, that is, between the time of our first and second surveys. We shall now compare this consideration with the development of the eruption. As already mentioned, the fissure eruption that took place on the eastern slope of the island ceased entirely in the evening of July 13, but on July 15, the activity shifted to the central cone Oyama. This central cone eruption developed, however, very slowly. On July 18, when the writers descended to the bottom of Oana, the largest of the three craters on the central cone, the eruption was still in its very in itial stage; only hot gases being seen rising with a hissing noise from a new pit opened in the NE corner of the crater bottom of Oana. Since, at this time, no solid material was being ejected, the centre of the crater bottom of Oana could be reached quite safely. This new pit however gradually enlarged, and on July 20 began to throw up lava blocks. Two more new craters then opened SW of the first crater, and, when the writers ascended the volcano on July 25, a beautiful day, they saw fountains of incandescent lava rising high into the sky from a lava pool in the westernmost crater. The central cone eruption was thus in a developing stage until July 25, after which the eruption attained maximum violence, a large cinder cone, 50 m high, having arisen later from the site of the lava fountain just mentioned.

The underground conditions may be regarded as having then been all "set" for the eruption. That is, underneath the central cone, the rocks seem to have been gradually melting, or magma had been stoping up until July 25, when the melting or stoping had completed. Our surveys were executed, fortuitously, during the most favourable time for observation imaginable.

Simultaneously with these underground changes, the seismicity of the island had shown marked changes. According to micro-seismic observations made by Minakami,[12] the volcanic earthquakes ceased after July 25, and in lieu of the earthquakes, volcanic tremors of large amplitude were observed on that day and since. This is very interesting, seeing that a volcanic earthquake is caused by the stoping or intrusion of magma, whereas volcanic tremors are caused by superficial activities in the crater.

Since in equations 1, the value of k^3R, not R, is determined from the observed changes in the vertical intensity of geomagnetism, there is something arbitary about the radius R of the spherical part stated above. According to Nagata,[13] the basalt of Miyakezima has thermo-remanent magnetism in the direction of the present geomagnetic field, the intensity of magnetisation being 10 to 20 times that due to the induced magnetism. If this is so, even in the depth of the volcano, we have to take for k the value $2\times10^{-2}\sim4\times10^{-2}$, R decreasing accordingly to 1·2 ~1·0 km.

The magnetic dip, as measured by Minakami,[14] has shown marked decrease at all of his stations in the island. Seeing that the change in magnetic dip, as calculated under the present assumption, predicts decrease in dip for almost the entire island, as shown in Fig. 8, the results of Minakami's survey seem to be in good accordance with the results of our survey.

In conclusion, the writers wish to express their cordial thanks to the Officials of the Division of Scientific Research in the Ministry of of Education for the financial aid granted them for a series of investigations, of which this study is a part.

---

12) *Disin*, **12** (1940), 492.
13) *Disin*, **12** (1940), 524.
14) *Disin*, **12** (1940), 507.

Station No. 117.

Station No. 105.

(震研彙報 第十九號 圖版 高橋・平能)

Station No. 110.

Station No. 124.

Fig. 3.

7. 三宅島の噴火に伴つた垂直磁力の變化（概要）

地震研究所 {高橋龍太郎
平能金太郎

昭和 15 年 7 月 12 日三宅島の噴火に際し，筆者等は垂直磁力計を用ひて噴火に伴つて起つた垂直磁力の變化の測定を行つた．三宅全島に分布された測點の數は 50 である．本文中第 1 圖に測點の位置及び番號を示した．第 4 圖は 7 月 20〜24 日に行つた第 1 回測定の結果であり，第 5 圖は第 1 回測定と，其れに引續いて 7 月 26〜30 日に行はれた第 2 回測定との差を示す．此等の變化は山頂下 3 km の點を中心とする半徑 1〜2.7 km の球狀部分が其の感應磁氣或は熱殘留磁氣を失つたものとすれば，變化の分布は勿論，其の量に至るまで非常にうまく說明がつく．磁氣を失つた原因は岩漿の上昇とか或は又他の原因によつて其の部分の岩石の溫度が上昇したとか考へればよい．此の考は同時に荻原，水上，永田理學士等によつて行はれた地磁氣の伏角や地震，微動等の觀測結果ともよく調和する．

本研究は文部省科學研究費によつて爲されたものである事を記し，玆に深謝の意を表す．

8. 昭和15年8月2日日本海に起つた津浪

地震研究所　宮　部　直　巳

（昭和15年9月20日發表—昭和年15 12月20日受理）

1. 昭和 15 年8月2日午前0時頃，北海道西部の各地に於いて中震程度の地震を感じ，それから 15 分乃至 30 分位を經て海岸地方は津浪の襲來を受けた．

地震そのものによる災害は極めて些少であつたが，津浪による災害はそれに比すれば稍大きかつたやうである．卽ち津浪による被害として數へられるものは，行方不明者7，磯舟の流失數千艘等である．

地震の震央は積丹半島神威岬の北西約 140 km 位の海底で，震央に於ける發震時は8月2日午前0時8分頃であると報告されてゐる．津浪の傳播に關する調査を行ふ場合には數分の誤差は之を免れ得ないから，發震時の表示は以上の程度で充分である．さうしてその程の精度の範圍內で，後に述べる樣に定められる津浪の中心は，地震の震央を含むかなり廣い區域である．

この津浪に關する調査は全く現地の踏査をすることなしに行はれた．卽ち多數の港灣における驗潮記錄を蒐集し，之を整理すること，及び之に北海道から寄せられた津浪の觀察記錄を參照することによつて，この津浪の大體の相貌を明かにしようと試みたものである．

驗潮記錄は，陸地測量部の好意と內務省土木試驗所松尾春雄技師の配慮とにより，北海道における驗潮記錄及び津浪に關する情報に就いては，北大理學部の米田勝彥氏の援助によつて蒐集し得たものである．玆に記して諸氏の御好意と御配慮とに對し深く謝意を表するものである．

2. 驗潮記錄に顯はれた津浪の記象に關する檢討に入る前に，北海道各地に於ける津浪の觀察記錄に就いて一瞥しよう．

第1圖に示した場所について北から順を逐へば

（i） 利尻島沓形港では津浪の高さは最大 2m 位に及んでゐる．此處に於ける磯舟の流失數は約300隻であると報ぜられてゐる． 津浪襲來の時刻は午前 1 時頃で地震の後約1時間である．回數は2回 20 分を隔てゝ來襲したが，その後 15 時間位の間は大體 20 分に1回の割合で異常なる海水面の昇降があつたといふことである．殆ど

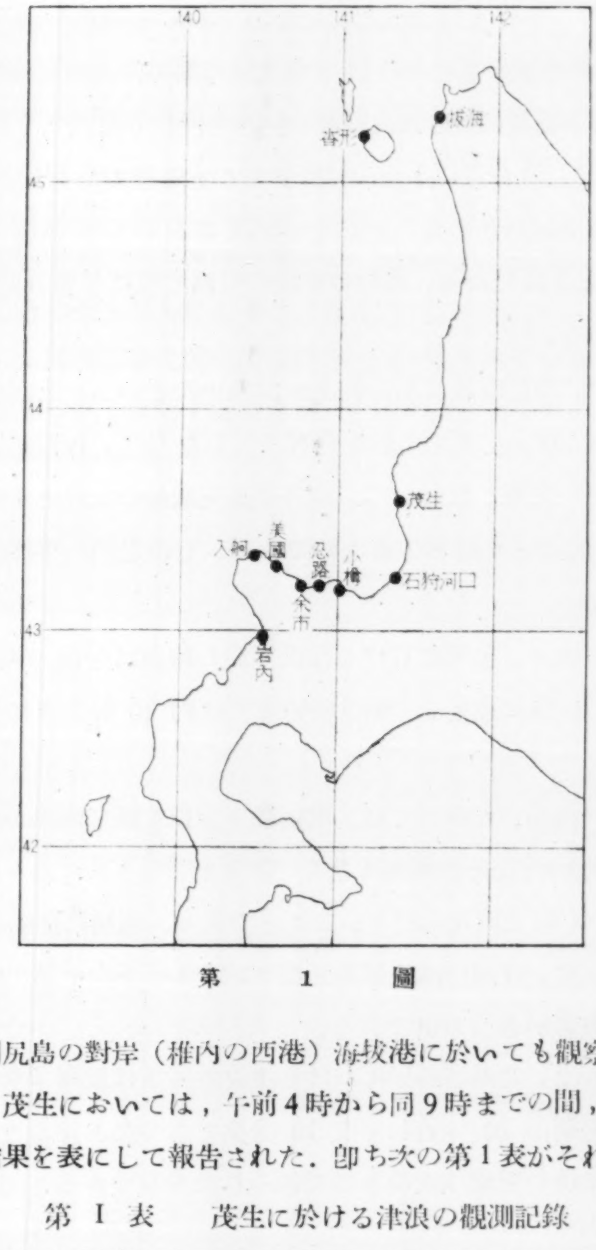

第　1　圖

同様のことは，利尻島の對岸（稚内の西港）海抜港に於いても觀察されてゐる．

（ii）濱益郡，茂生においては，午前4時から同9時までの間，時々海水面の狀態を觀察し，その結果を表にして報告された．即ち次の第1表がそれである．

第 I 表　茂生に於ける津浪の觀測記錄

時刻	高潮位	低潮位	摘要	
午前 4 時	+1·2 m	−0·9 m	津浪なし	約7分毎
4 時 30 分	+1·1	−0·5	〃	約10分毎
5 時	+0·5	−0·6	〃	〃
6 時	+1·2	−0·5	〃	〃
6 時 30 分	+0·68	−0·55	〃	〃
9 時	+0·45	−0·5	〃	〃

（iii）小樽では地震の爲め埋立地の一部に龜烈を生じ，又附近の鹽谷村字桃内村地内道路に沿うて崖の崩壞あり，3600立米の土砂が道路上に堆積した．津浪は地震の後

45分を經て襲來した．午前5時頃最高となり +1.5 m を示した．

（iv） 余市では，驗潮儀があつたけれども故障の爲め津浪の記錄を完全にとることは出來なかつた．たゞ乾地に殘された浸潤の跡から潮位の最高 +1·20 m 位と推定された．又川筋に於いて約20分毎に水面の昇降することを認めたことが報ぜられてゐる．

（v） 岩内では驗潮記錄がある．が，その記錄においては振幅が實際のものの約1/1·9になつてゐるとされてゐる．實際の津浪の最高水位は午前0時50分頃 +1·7 m 位となつたものである．

尙余市と岩内とで，地震直後に潮が約1 m 位退いたといふことが報告されてゐるがあまり確かではない．併し，若しこれが眞實であるならば，後段に記されてゐる入舸村における地震直後の退潮と綜合して，積丹半島突端部の上昇とその東方への傾斜とが地震に伴つたといふことを暗示するものである．この退潮の事實は併し乍ら，驗潮記錄には認められない．

（vi） 積丹半島の北岸，美國に於ける津浪來襲の時刻は午前0時30分頃である．さうして最高 1·55 m 位に達し，午前3時頃までは約10分おきに昇降を繰返したといふことである．

（vii） 積丹半島の西端，入舸村では，地震後3分位を經て海水が退き始め，1分を經て約 −2·0 m となつた．その後間もなく“物凄き潮鳴と共に處々に大渦卷を畫きつゝ”增水し，+2·0 m 以上に及んだといふことである．週期に類似の事項に關しては報告されてゐない．又，日司村に於ける〆切コンクリートの一部が破壞し，工事用材料が流失した等の被害があつた由である．

以上の報告によれば，北海道西岸における津浪の高さは最高 2·0 m 以上から 1·5 m 前後であり，その週期は20分若しくは10分位であつたと言ふことが出來やう．

3. 蒐集された津浪の記象は次の各地で得られたものである．

本斗（樺太）

石狩河口 I，石狩河口 II，小樽，忍路，余市，岩内（以上，北海道）

能代，土崎，酒田 I，酒田 II，新潟，伏木，七尾，輪島（以上本州）

元山，羅津（以上朝鮮）

以上の中，土崎酒田 II 及び元山の記錄には津浪の徵候が現はれてゐない．又，石狩河口 II，及び能代の記錄は，リシヤール型一週間卷の記錄筒に記錄されたものである爲，詳細の點が判然しない．尙余市の記錄には前節にも述べた樣に器械の故障の爲め，津浪の後半のみの記象が得られてゐるに過ぎない．其故，これら5個所の中能代を除いた4個所の記象及び津浪の記錄が不明瞭な伏木，七尾の2個所の記錄は之を採

錄しないことにした．土崎及び酒田 II の驗潮儀は，海岸から 1 km 乃至數を遡つた場所に設けてある．其故，川の流れその他に阻まれて津浪が充分の振幅を以てそこまで到達し得なかつたものであらうと考へることが出來る．元山に於いても，港内の水が淺くて，津浪が減衰したか，又は驗潮場の井戸への導水管が土砂の爲に閉塞した等の理由で津浪の如き波動は記錄し得なかつたのであらうと考へてもよいであらう．尙小樽，その他においても，殆ど同樣の理由で，記錄された津浪の振幅が實際のものよりも遙かに小さくなつたと見られるやうである．

本報告に輯錄した津浪記象を得た所の驗潮儀の所在地の分布は第2圖に示してある．又，津浪の記象の寫しは第3圖乃至第 12 圖に掲げてある．

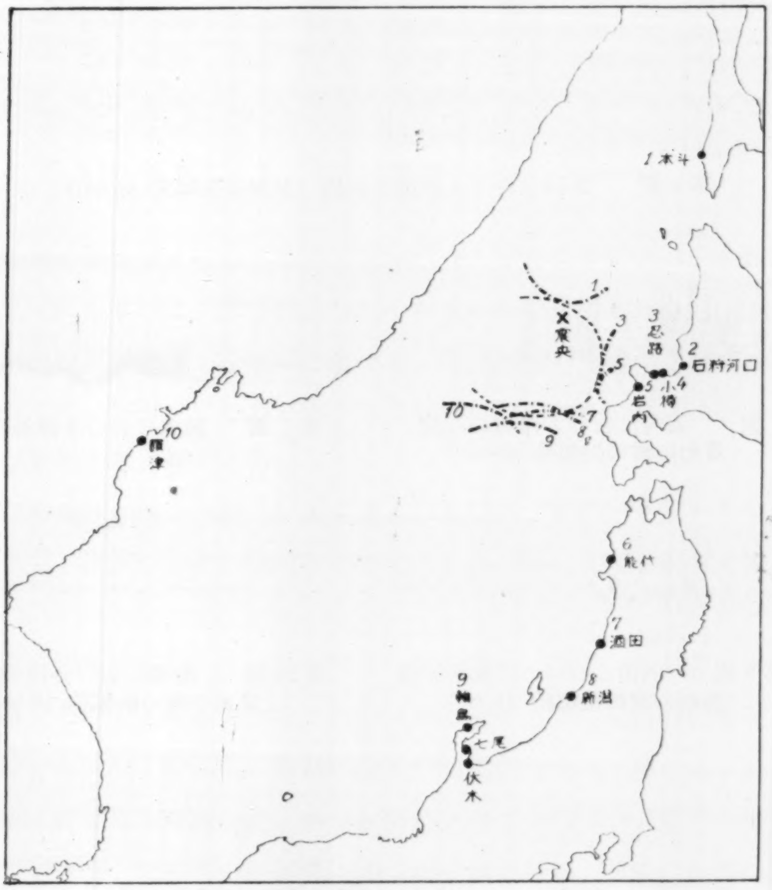

第2圖　　驗潮場の分布と津浪の中心

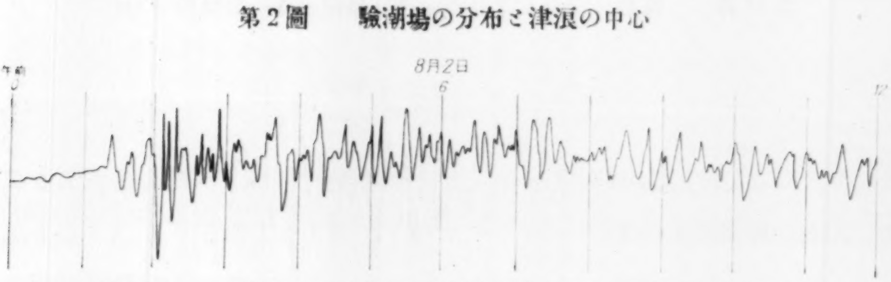

第3圖　　本斗における津浪の記錄（最初の波の振幅約 24 cm）

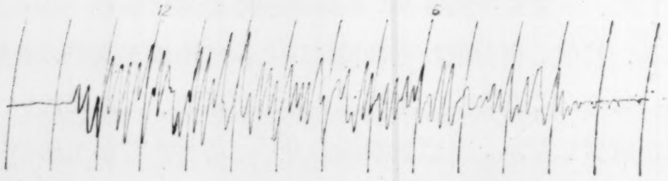

第 4 圖　石狩河口における津浪の記錄（最初の波の振幅約 14 cm）

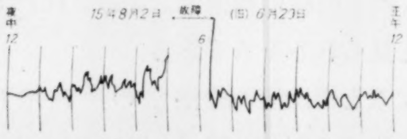

第 5 圖　小樽における津浪の記錄

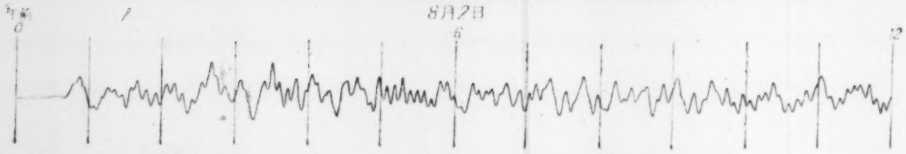

第 6 圖　忍路における津浪の記錄（最初の振幅約 16 cm）

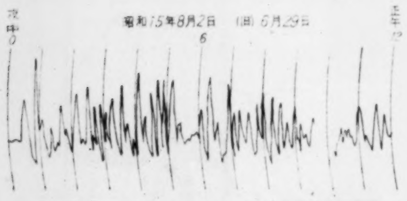

第 7 圖　岩内における津浪の記錄
（最初の波の振幅約 45 cm）

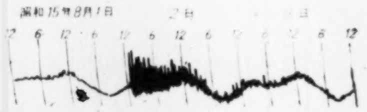

第 7 圖　能代における津浪の記錄

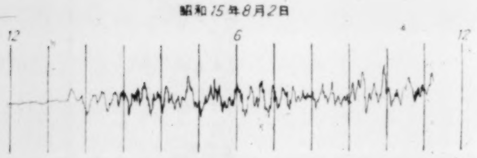

第 9 圖　酒田における津浪の記錄
（最初の波の振幅約 10 cm）

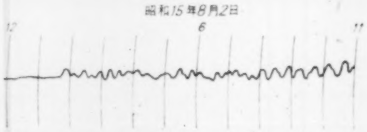

第 10 圖　新潟における津浪の記錄
（最初の波の振幅約 10 cm）

第 11 圖　輪島における津浪の記錄（最初の波の振幅約 8 cm）

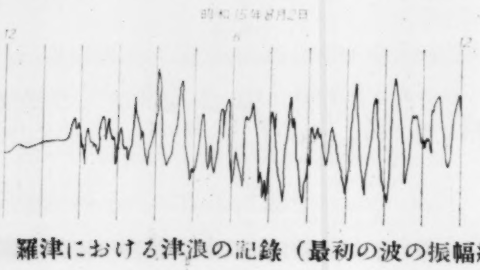

第 12 圖　羅津における津浪の記錄（最初の波の振幅約 8 cm）

是等の記錄から讀定すべき事項は差當り，(i) 津浪發顯の時刻，(ii) 第一波の向き，(iii) その週期，(iv) その振幅等である．讀定によつて得た値は次の第 2 表に示してある．

第　II　表

場　所	發顯時刻	向き	週　期	振　動	地震發生より津浪到達まで
本　斗	午前1時 17 分	上	18 分	24 cm	69 分
石狩川口 I	——	上	15 分	14 cm	—
小　樽	午前 0 時 50 分	上	10 分	?	42 分
忍　路	〃 0 時 40 分	上	23 分	16 cm	32 分
岩　内	〃 0 時 22 分	上	20 分	86 cm	14 分
酒　田 I	〃 1 時 30 分	上	17 分	10 cm	82 分
新　潟	〃 1 時 41 分	上	19 分	10 cm	93 分
輪　島	〃 1 時 50 分	上	21 分	7 cm	102 分
羅　津	〃 1 時 40 分	上	20 分 9 分	8 cm	92 分

津浪發顯時刻の讀定値にはいろいろの誤差が介入するのであるが，それらの誤差の中で主要と思はれるものは，津浪の始の點の判定が明確に出來ないといふこと，記錄紙を貼付した廻轉筒の速度が不整であること，時刻標識の位置の不整なること（リシヤール型時計では，毎日又は毎週一回の記錄取換に際してその初又は終りに記入する時刻標識の不整がある）等である．

この津浪の場合は，第 3 乃至 12 圖に見られる樣に，その始めがかなり明確であつて，記象の上で，津浪の始めの位置を何れにとるかに關して疑を起させるやうなものは殆どない．

從つて時刻の誤差は主として，回轉筒又は記錄紙の“送り”の裝置におけるその速度の不整に基くものであると考へることが出來る．そこで，忍路の記象をとり，この記象紙上に印せられた 1 時間毎の時刻標識線の間隔が幾干の不整を示すかを調べてみた．この記象における 1 時間の長さの 24 個の平均は 25·5 mm，であつて，讀定値の標準偏差は 0·28 mm，又最大の偏差は ±0·5 mm 位である．其故，時間の方の誤差は最大

$$\pm\left(\frac{0{\cdot}5}{25{\cdot}5}\times 60\right)\text{分}=\pm 1{\cdot}2\text{ 分}$$

といふことになる．併し，この時刻標識を記入する爲の時計の誤差も介入するから，實際の誤差はこれよりも稍大きくなるであらう．又，忍路の驗潮儀は，本斗，輪島などと共に陸地測量部の管理に屬しケルヴィン型である．其故，主としてリシヤール型

が使用されてゐる土木關係の驗潮記錄に比して時刻標識の精度は高いかもしれない．それらのことを顧慮して，全般的に津浪發顯時刻の誤差は平均 ±5 分位であるとすれば大差はないのではないかと思はれる．

週期や，振幅については更にいろいろと議論の余地があると思はれる．それらの讀定値は，驗潮儀場在地の水域の性質，卽ち，港灣の形や水深の分布等に影響される所が大きい．

これらの點に關しては後節に述べる．

第 2 表の中に，伏木及び七尾における觀測値が除かれてゐるのは，それらの港において觀測された津浪の最初の部分が極めて不明瞭であることによるものである．

震源に於いて地震の起つた時刻は 8 月 2 日午前 0 時 8 分頃であるが[1]，讀定時刻の偏差として ±5 分位の誤差は許容しなくてはならないからそれ以上詳しく發震時を知らなくてもよい．さういふ意味でなら上述の如く午前 0 時 8 分を地震の起つた時刻と見てよい．この時刻と，津浪の到達した時刻との差は，津浪が起つてから各驗潮場に到達するまでに要した時間であると見做すことが出來る．第 2 表の最後の行に示したものがそれである．

津浪が，地震と同時に起つたか否かについて疑を持つ見方もあるやうである．津浪は，地震が起る以前に起つたものであるといふ考もないではない．併し，その問題は，もつと時刻の精度がよくなり，且つ他の色々な事情がよく判明しなければ到底その當否を判定し得ないであらうと考へられる．

4.　前節第 2 表の最後の行の數値を資料として次の如き操作を行ふことにより，津浪の發散の中心を見出すことが出來る．

津浪は海水中を傳はる長波と見做すことが出來るから，その傳播速度は

$$v = \sqrt{gh}$$

で與へられる．h は深さ，g は重力加速度である．ある短かい距離 ΔS の間で深さ h が一樣であるならば，ΔS を進むに要する時間 Δt は

$$\Delta t = \frac{\Delta S}{\sqrt{gh}}$$

である．

そこで，一つの驗潮場を津浪の假の中心とし，地震が起ると同時にこゝから津浪が四方に傳播すると考へ，Δt を經た後の波面をつくる．更に次の ΔS の間で深さ h が一樣であるとして次の波面を作圖する．以下同樣の操作を反復して，各驗潮場を假の

1)　氣象要覽 No. 492 (1940), 954～960.

中心とする"津浪の中心から各驗潮場に到るまで要した時間"(第2表第6行)を經た後の波面を作るのである．第2圖に鎖線で記したものが斯くの如くして求められた最後の波面の切口である．この線に附した數字は，その鎖線が同番號の驗潮場のデータに關するものであることを示すものである．これらの最後の波面への包絡線を描いてみると地震發生の時に波面がこの包絡線（第2圖の點線）にあれば，觀測された時刻に各地に津浪が到達することになる．

斯くして求めた包絡線で圍まれた地域或は水域は津浪の中心水域とも稱せられるべきもので，それが震央を含むある擴がりを有するものの如く見える點に注意される．震央は×で示し，その位置は $\lambda = 139{\cdot}1\,E$, $\varphi = 4{\cdot}43\,N$ であると報ぜられてゐる．

勿論，玆に使用した資料の數値が充分正確であつて，而も斯樣な結果を得たのであるならば，正しく津浪の中心はある擴がりを有するものであると言ふことが出來る．併し既に述べた樣に，津浪發顯時刻については ±5 分位の誤差を認容しなければならないといふことの外，海の深さ h の分布を求めるのには 250 萬分の 1 の海圖によつたこと而して海圖の投影法はメルカトル式であるから海圖上で水平距離を測つた場合に南と北とで縮率が異ること，等による誤差もあるわけである．

この中，h の値は寧ろ大き過ぎる樣な採り方をしてゐることになる．即ち，もつと詳しい海圖によれば，海岸に近い淺い場所も勘定に入ることになるから，その結果として求められる津浪の中心水域の廣さは增加する傾向を持つやうになる．

投影法に基く誤差は，北の方で尺度が延びるから，これは，津浪の中心水域の廣さを縮少する樣な效果を齎らすものである．併し，その縮小率は大きくとも 1～2 割位であつて，第2圖に求められた樣な廣さの水域が全然無くなることにはならない．而も，實際には時間的に ±5 分の誤差を許容するので，投影法に基づく誤差の大部分もその中に含まれると考へられる．是等のことを考慮した上でも尙，徑 200 km 程度の"津浪の中心水域"といふものは認められるやうに思はれるのである．

一方において地震又はそれに伴つた地殼の變形によつて起される海水の動搖の初期の形が，波長に關係のある大いさを有するであらうといふことは，津浪が一點から出發するといふよりは寧ろ自然的な考へ方であると思はれる．同樣な傾向は既に昭和 8 年3月3日の三陸津浪の際にも認められたことであり[2]，更に，昭和 14 年5月1日の男鹿地震に伴つた津浪[3] についても相似た事實が認められてゐる．

5. この津浪の場合について注意される一つの事は，津浪の初動の向きが，何れも

2) N. Miyabe, *Bull. Earthq. Res. Inst, Suppl. vol.* 1 (1934), 112～126.
3) 岸上冬彥，飯田汲事，地震 11 (1939), 365～371.

上向きであるといふ點であらう．その向きに關しては，各地の記象において見られる樣に疑の餘地は殆ど無いのである．最も不明瞭である所の伏木，七尾に於ける記錄に就いてさへ，少くとも下向きではないといふことは言へるのである．この點は昭和8年の三陸津浪や，昭和14年の男鹿島地震の際の津浪とはその趣きを異にしてゐる．殊に，男鹿島地震に伴つた津浪については，初動が上向のところと下向のところとの區別が規則的であるとされて居る．然るに，この津浪では，本斗から羅津まで，中心からの方位にして180°以上の範圍に亘り盡く初動は上向きである．このことは津浪がその中心から凡ゆる方向に全く對稱的に傳播されたといふことを意味するものではないかと思はれる．

觀測された津浪の初動の週期は，小樽における10分と，石狩川口Iにおける15分とを除けば，あとは殆ど20分内外である．

又忍路の記錄を見ると，20分位の週期の波動に10分位の週期の波動が重なつてゐる事を認めることが出來る．而して，後者の波動は最初の中はその振幅が小さく殆ど認め難いが次第に增大し，再び減少し，以下數回これを反復してゐる有樣を認めることが出來る．短週期の波動は或は，その港灣の固有振動週期かもしれないが，さうすると，津浪そのものの中にもその位の週期の波動がなければ，かくの如き振動を勵起することは難かしいであらうと思はれる．

以上の如く見れば，津浪の週期として主要なものは20分であつて，これに10分又はそれよりも更に短週期の波動が重なつてゐたと見るべきであらうか．波型の不規則な點もそれがもし港灣の形の影響でないならば，短週期の波動が重つてゐたと考へることに有利な資料と言へるかもしれない．

6. 津浪の振幅に關する考究は一層困難である．その理由の一は，驗潮儀の在る港灣が夫々固有の靜振を生ずる可能性があり，又驗潮場の井戸と外海との連絡が場所によつて異なり，ある場所ではその導水管が不完全である爲，津浪元來の振幅や位相が變形されることも可能である．斯樣な事情の下に於いて津浪の本來の振幅を求めることは極めて困難なことであると言はねばならない．

例へば，岩内に於ける記錄に關しては，記錄された振幅の 1·9 倍が眞の振幅であるといふ注意書が添へてあつた．其故，第2表の振幅には 86 cm としたが，記象上の讀取の値は 45 cm である．同樣の補正は少くとも小樽や忍路等の値に對しても必要なのであらうと思はれるが，補正を加ふべき資料がないので暫らく，讀定値そのまゝを掲げておく．

併し，それらの事情もあるが，他の驗潮儀は，槪して外海に直接接して設けてある

様に見られるので，とにかく試みに，津浪の中心と思はれる地點からの距離に對する觀測された振幅の分布を圖に記入してみると，第 13 圖の様なものが得られる．

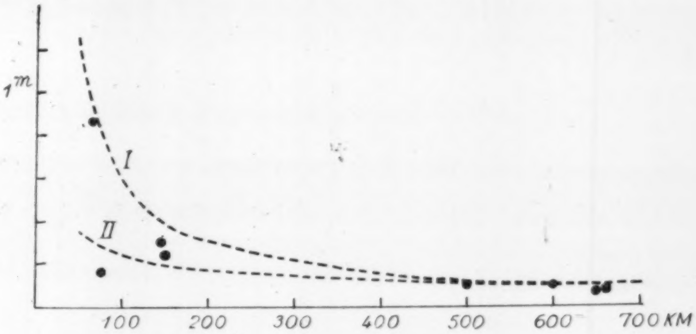

第 13 圖　振幅と距離との關係

驗潮記錄上で讀定された振幅の値の外に，目測による津浪の初動の振幅の資料もある．目測された振幅は最大振幅に潮汐の影響を加へたものである．尤も日本海沿岸では潮汐の振幅は極めて小さく，8 月 2 日に於ける各地の潮汐の干滿の差は 0·3 乃至 0·4 m であるから，目測された振幅をそのまゝ採用しても誤差は 2 割を越えない程度であつて，目測それ自體の誤差の範圍では，それで充分であらう．目測の振幅は上述の様に最大振幅であるから，津浪の記象から推察される様に初動の振幅はそれよりは小さいと見られる．又，初動の振幅は津浪本來の振幅よりは幾分か小さく記錄されてゐると見てもよいやうであり實際，岩内の場合の如き例もある．斯く津浪振幅の目測値に關しては論ずべき點もあるので第 13 圖においては單に驗潮記錄上で讀定した津浪の振幅分布を示した．そして，振幅の距離によつて變化するさまを表はす曲線として I，II を描いてみた．I，II は共に津浪の中心から 600 km のところで 10 cm の振幅を與へ，I は r^{-1} に II $r^{-1/2}$ はに比例する様な曲線である．實際の振幅と距離との關係は何れの曲線で示した方が眞に近いかは判らないが，何れにしても津浪の中心附近に於いては實際の振幅より著しく小さくなる勘定となる．而して，若し深さが一様な海の中の一點にある衝擊が與へられ，波動が，四方に一様に傳播するものとすれば，その場合の振幅と距離との關係は波長に對して遠い場所では振幅が $r^{-0.5}$ に比例する[4]．上述の結果はこれからはかなり離れた事情にあることを示すもので，その理由を數へてみると，理論の要請たる $kr \gg 1$ $\left(k=\dfrac{2\pi}{\lambda}\right.$，$\lambda$: 波長$\left.\right)$ が滿されてゐないこと，傳播機巧における理論と實際との相異，港灣における靜振の勵起狀態如何といふやうなことが關係してゐると思はれる．

7. 以上に述べた調査の結果を要約すると次の通りになる．

（イ） 津浪の中心は北海道西岸とソ聯領沿海州との間にあり，地震の震央（$\lambda_0 = 139{\cdot}1°E$，$\varphi_0 = 44{\cdot}3°N$）を含む徑 200～300 km の廣さを有する水域であると考へら

4) H. Lamb, *Hydrodynamics*. 3 rd *Ed.* (1924), 277.

れる．(震央の概略の位置は第1圖に×で示してある)．

(ロ) 各驗潮場で觀測された津浪の初動は何れも上向きである．觀測所の分布が津浪の中心からの方位で 180° 以上に亘つてゐる點から見て，凡ゆる方向に上げ波で傳播されたものと思はれる．

(ハ) 津浪の振幅は前述の2項より一層不確ではあるが中心からの距離 r について大體 r^{-1} に近い形で減小するやうである．

以上の結果は，津浪の成生に關する理論的考察をなす上に參考となり得ることであらうと思はれる．

---

8. *Tunami associated with the Earthquake of August 2, 1940.*

By Naomi MIYABE,

Earthquake Research Institute.

On August 2, 1940, a severe earthquake was felt at various places in Hokkaido, at 0 h 07 min. a. m. In less than an hour a tunami visited the Japan Sea coast of Hokkaido, as a result of which more than a thousand fishing boats were swept away and seven lives were lost. The epicentre of the earthquake was reported to be situated about a hundred kilometres off the western coast of the Syakotan peninsula.

The results of the study are summarized as follows:

(i) The central area of the tunami is believed to be of such an extent that its effective radius was several hundred kilometres, and probably of the same order of magnitude as the wave-length of the tunami wave. The epicentre of the earthquake lies within this central area.

(ii) At all the mareograph stations, the first motions of the tunami were found to be directed upwards. But since, on the other hand, the mareograph stations are distributed within a range of more than 180° in azimuth from the centre of the tunami, it is thought that the tunami waves were propagated from a common centre symmetrically in all directions.

(iii) The distribution of the amplitudes of the tunami, although they differ with the station, was affected by the shapes and depths of the bays on which the stations are situated. This is expressible as a function of r, the distance of the station from the centre of the tunami, roughly by Ar^{-1}, which deviates considerably from the expression theoretically deduced for the case in which $kr = \gg 1$, where $k = \frac{2\pi}{\lambda}$ and λ is the wave length, i. e. $Ar^{-1/2}$. This may not only be due to the modification of the wave-form caused by the shape and depth of the bay, but also to the fact that the condition $kr \gg 1$ is not fulfilled, and to the difference in mechanism of occurrence and of propagation of tunami waves from that adopted in theoretical calculation.

This disagreement between the actual phenomena and expectations from theory may be due not only to the fact that the effect of the proper oscillation of the sea water of the bay is not the same for different mareograms, but also to the fact that the condition $kr \gg 1$ is not perfectly fulfilled in actual case and that the mechanism of occurrence and of propagation of the tunami waves differs from that assumed in theoretical calculation.

(iv) In connexion with this earthquake, the earth's crust of Syakotan Peninsula seem to have tilted eastward, although the tilting might have occurred before the arrival of the tunami.

---

9. 山梨縣鳳凰山·地藏ヶ岳附近の地質

地震研究所 大 塚 彌 之 助

（昭和15年12月19日發表——昭和15年12月20日受理）

目　　次

緒　　論
1．地形上の問題
2．層序上の問題
3．地質構造上の問題
4．深成火成岩の地質構造上の問題
地　　形
地　　質
1．第 四 系
a．冲 積 統
b．段 丘 礫 層
c．中山輝石安山岩體
2．新 第 三 系
a．圓井酸性深成岩體
b．巨摩玢岩體
c．櫛 形 山 層
d．桃 ノ 木 層
3．新第三系以前（桃ノ木層堆積以前）
a．鳳凰山深成岩體，附．賽ノ河原深成岩
b．燒地藏深成岩體
c．所謂秩父古生層
地 質 構 造
a．表皮的な地層・岩石の構造
b．基盤岩石の地質構造
c．鹽尻—靜岡地質構造線
結　　語

緒　　論

筆者は數年來日本本洲島の中部を横斷すると言はれてゐる，日本の第三紀造構造帶の一つである，フォツサ・マグナのその西南縁の地質構造を闡明することに努力してゐる．今春も筆者は井尻正二理學士・岩井四郎・藤城新一君等の協力を得て，その地域に該當する山梨縣中巨摩郡・北巨摩郡の地質調査を行つたが，二三從來より新しい知識を得たので此處にそれらの概略を記して先輩の御批判を得やうと思ふ．こゝに御協力を得た三君に深く謝意を表する．

この地域は山梨縣西部の山地の一部で山梨縣中巨摩郡蘆安村・北巨摩郡清哲村・駒城村を含む地域で，海拔 2500 m 以上の高度を持つ鳳凰山・地藏ヶ岳等の花崗岩山地を含んでゐる．

この地域は地質調査所 20 萬分之一地質圖幅及び說明書に於いて鈴木敏博士[1] が極めて詳細に調査されてをられる上に，近年には田中元之進技師[2] が調査され，この附近に發達する第三系を細分されてをられる．又地形學的觀點に立つては辻村太郎先

1） 鈴木敏，1/20 萬 甲府圖幅說明書．
2） 田中元之進，小川博士還暦記念論文集地學論叢，549〜576.

生[3]・田中啓爾教授[4]・岡山俊雄氏[5] の御研究・調査もあり，筆者等の研究結果は誠に屋上屋を重ねるの嫌がないでもない．

鈴木博士に依れば本地方は古生界・所謂御坂層の火山碎屑岩を含む水成岩層と之等を貫く花崗岩・玢岩等よりなり，古生界は輝岩・チャート・含ラヂオラリアスレート・凝灰質岩・綠色珪質スレート・石灰岩・角岩・砂岩・頁岩等からなり，岩相上古生界上部層とされてゐる．

所謂御坂層は主として火山碎屑岩層であるが，外に水成岩層の部分もかなりあつたが當時は未だ化石が發見されてゐなかつた．

之等の地質系統を貫く花崗岩類は二種に分たれ，一つは小武川—御勅使川間の山麓部を占め主として正長石・斜長石・長石・石英を含む外に黑雲母を交えた黑雲母花崗岩で前述の所謂御坂層を貫くもので，一つは鳳凰山・地藏ヶ岳を作り角閃石をも混ずる閃雲花崗岩とからなつてゐるとの事である．閃雲花崗岩はその質粗狀で長石の巨晶を含むと．

玢岩は御坂層・古生界を貫き種々な特徵を持ち色彩その他も多樣である．

古生界と御坂層又は御坂層を貫く玢岩との境界は明瞭な斷層である事も指摘されてゐる．

その後田中技師の詳細な研究で所謂御坂層は中山層・櫛形山層・靜川層に分たれたが，筆者[6] は更に西八代統と曙礫層とを設け層序を下部から上部へ向けて中山層・櫛形山層・西八代統・靜川層・曙礫層となし，靜川層及び曙礫層を古生物學上の資料から鮮新統とした．

今回調査した區域には西八代統以上の新第三系は發達してゐない．

田中啓爾教授は之等の地域に斷層地形の存在を指摘され，岡山學士は所謂御坂層の西緣の地質構造上の性質に就いて地形上の觀點から得た推論を，困難な野外調査によつて確め，その西緣が斷層である事を主張された．

辻村先生もこの山地の斷層地形に就いて詳細な記載をされてをられる．

以上の樣に地學的には研究がかなり進められてゐて，殆ど記述の要もない程であるが，構造地質學的に之等の知識を檢討する時は更に興味ある諸問題の横はつてゐるのに氣付くのである．筆者等は重復の嫌はあつたが，こゝに筆者等の調査した結果を記し，之と共にこの地域の地質構造上の諸問題に就き簡單な論述をしやうと思ふ．

3) 辻村太郎，地理學評論，2，205～216.
4) 田中啓爾，地理學評論，1，925～945.
5) 岡山俊雄，地理學評論，5，949～960；6，479～499
6) 大塚彌之助，地理學評論，14，969～984.

1. 地形上の問題

岡山氏は"中央日本山地の切峯面及び區分に就いて"の題下に赤石山地の切峰面に於いて，その山地の東縁に就いて論じ，その東縁を代表する地形區分の境界である甲斐駒ヶ岳東側の急斜面が韮崎町方面へ延長するものの他に，この急斜面から分岐して地藏ヶ岳・鳳凰山下の石空川・小武川の上流より辻山・千頭星山間を經て略ぼ早川に沿ひ，次いで青薙山・大無間山・板取山等の南東を限る様に略々南 5°～10° 西へ向つて延長するものもある事を指摘してゐる．之等の大地形上の特長が地質構造と如何なる程度の調和が見られるかが一つの問題であつた．之等切峯面に現はれた急斜面が果して斷層に基く地形上の特色であるか否かはかの矢部博士の言はれた糸魚川――靜岡地質構造線の一部である韮崎――靜岡地質構造線が元來この地形上の特長に一部基いて推定されてゐるのに又他の一部は第三系御坂層の西縁の斷層に基いて推定されてゐる一地質構造線である點から見て興味ある問題である．

2. 層序上の問題

筆者は嘗て日本の第三系の層序を論じた際に，御坂層の火山碎屑岩の豐富な部分を以て淺貝・幌內時代末期の堆積物とし，*Lepidocyclina japonica* 等を含む地層を寧ろ淺貝・幌內時代の暖流系動物群とした．

今回筆者等の調査した地域には所謂御坂層が發達してゐて，田中技師によつて火山碎屑岩が殆ど稀で主として黑色の泥岩・砂岩及び礫岩からなる厚い地質系統を中山層として下部に，火山碎屑岩及びその沈積岩の豐富な部分を櫛形山層として上部に分たれた．併しながら之等からは何等時代を決定することのできる化石類が發見されず，岩相だけで富士火山の周圍に露出してゐる御坂層に對比されてゐた．そして火山碎屑岩の少い下部の地質系統は第三系より更に古いものではあるまいかの疑をさへ抱かれてゐる．若し筆者が推論した如くであるならば，この火山碎屑岩層の下の中山層は *Lepidocyclina* 類を含む幌內時代の堆積物である疑が起る．果してさうであらうか之は層序上興味ある問題である．

3. 地質構造上の問題

本地域が日本群島本州島の中央部を横ぎる一つの大きな地質構造上の境界部に該當する事は既に讀者の知らるる所であり，矢部博士の糸魚川――駿東・糸魚川――靜岡（之は今日では大町――靜岡と呼ぶべきであらう）なる夫々形成の地質時代の異つた二つの地質構造線の相重つた部分であることも何等說明を要せぬ所である．併しながら假に糸魚川――駿東地質構造線は後期の地殼變形によつて明でないとしても，糸魚川――靜岡地質構造線とは何かと言ふ問題は上に述べた地形上の問題からみても考究す

る必要のある問題である．

矢部長克博士[7]の記事に從へば糸魚川—靜岡地質構造線は糸魚川—鹽尻・鹽尻—韮崎・韮崎——靜岡の三部分に分たれてゐる．今筆者等の調査區域には後二者のみが含まれてゐるので，こゝでは北部は論ぜぬこととする．鹽尻——韮崎の線は，之は，明に地形學上の特長によられたものと考へられる．然るに韮崎より靜岡へのこの地質構造上の意義を包含する線は韮崎以南に於いて何處を通過するか全く不明であつた．

又一方矢部博士の記事をみるとこの地質構造線は第三系と西南日本の外帶をなす中生界・古生界との間の境界の斷層線であるかの如くにも思惟せられるのである．若しさうであるならば，その斷層線或は境界線は既に鈴木敏博士が調査せられたる 20 萬之1地質圖幅「甲府」に示されたる御坂層分布區域の西緣としなければならぬ．若しこの線を以て糸魚川—靜岡地質構造線の一部とするならば，それは韮崎町から遙か西方 10 km を南北に走り北は諏訪に達し，南は靜岡附近に達し韮崎は全く通過してゐない．この意味に於いて之等の鹽尻—韮崎・韮崎—靜岡兩地質構造線の性質をより明確にする事は一つの重要な問題である．

4．深成火成岩の地質構造上の問題

今上に記したやうに地質構造線の問題に言及して更に氣付いた問題は鈴木敏博士の20 萬分之1地質圖幅「甲府」に於いて，中生界・古生界と新生界との境界に沿うて鳳凰山・地藏ケ岳を構成する花崗岩が横つてゐる事である．之等の花崗岩は前記境界線の形成された後に生じたものか又は形成されぬ前に貫入したものか又は同時に貫入したものか明でない．卽ち田中技師は所謂御坂層に變質を與へてゐると述べ，岡山氏は斷層說を主張してゐる．之等を解決するために今回は多少この花崗岩塊の構造に就いても調査を試みた．

御勅使川——小武川間の山地の東麓部に發達する花崗岩と前記花崗岩類と如何なる關係にあるのか，之亦興味ある一問題である．之等の解決によつて斷層成生の時代・機巧等に何等かの手懸りを得られるのではあるまいか．

次に本地方の地質の概略を記して之等の諸問題に關して 2，3 の解釋を試みやう．

地　　　形

本地域は高度分布の上から南北に並んだ次の 4 つの地形區に分けられる．卽ち 1 甲府盆地底の西部，2 巨摩山地東麓の 750～1000 m 內外の高度の前山山地，3 巨摩山地，及び 4 赤石山地の東北端部に分たれる．

1．甲府盆地底西部は更に詳細に調べると西部山地から流下する各溪谷が多量の碎屑を盆地底に擴げてゐるために多數の扇狀地形の集合からなつてゐる．一方釜無川そ

7）矢部長克．現代之科學，6，(3)，1～4．

の他の河流がそれらの東縁部を略ぼ南北に侵蝕してゐるために現在の河原と二段以上の段丘とから形成されてゐる．之等の扇狀地形の内御勅使川のものは極めて大きいために釜無川はこの扇狀地を避けるやうその流路を東へと迂回させてゐる．

この扇狀地の集合したものからなる甲府盆地西部は略ぼ南北に近い山麓線によつて境され，第2區の巨摩山地東麓の急斜面に接してゐる．この南北の山麓線に沿つて古い扇狀地の殘部が處々に分布してゐるが，これらの古い扇狀地の殘部がその分布の東縁をこの南北の山麓線で了へてゐることは興味ある事實である．例へば大武川溪谷下流の北巨摩郡新富村の“原”段丘，黑澤段丘，新奥段丘の如きは清哲村青木・折居・圓野村入戸野・下圓井等を結ぶ山麓線の延長上に於いてその分布を限つてゐる．又御勅使川の溪谷の出口に當る源村築山・福路の古い扇狀地形の殘物である段丘にしても曲輪田・有野・上條南割等を結ぶ山麓線の西で終つてゐて，この南北の山麓線を明なものにしてゐる．この特異な地形上の特長は之等の殘された古い扇狀地形が形作られてから現在見られるやうな新しい扇狀地形が形作られる間にかなりな地殼の變位のあつた事を示してゐる．

北巨摩郡圓野村下圓井は上記山麓線に接した一部落であるが，こゝから西南へ入込む澤の出口の北側の崖（第1圖右A地點）には第1圖左のやうな露出が見られる．この露出はこの附近に發達してゐる圓井深成岩（後に述べる）と釜無川沿岸に發達する段丘粗砂礫層とからなり，この段丘粗砂礫層は傾角約20°の西へ傾く斷層面によつて前者と境されて

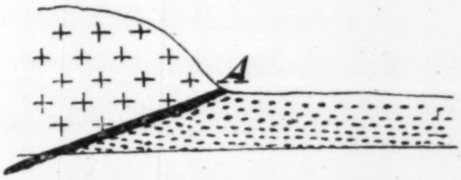

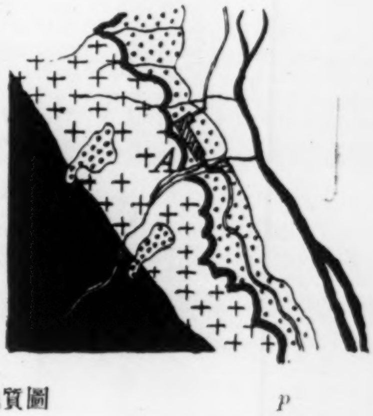

第1圖　下圓井附近地質圖

前者の下に横はつてゐる．且つこの推し被せ斷層面の延長は地形上の山麓部（第1圖p）と一致してゐる．この重要な地質學上の一事實は上記の特異な地形が斷層に基く形態であらうことを示してゐる．筆者等の觀察はこの山麓部に於ける斯の如き推し被せ構造を他の箇處に於て充分に確める迄に至つてゐないから，こゝでは地形上の特異性とその一部に推し被せ斷層構造のある點とを指摘するに止めておく．

第2區巨摩山地東麓前山山地帶は嘗て筆者が平須面と呼んだものに稍々類似する低い山地で，巨摩山地の東に前山をなし，高度は 750～1000 m 内外を示してゐる．こ

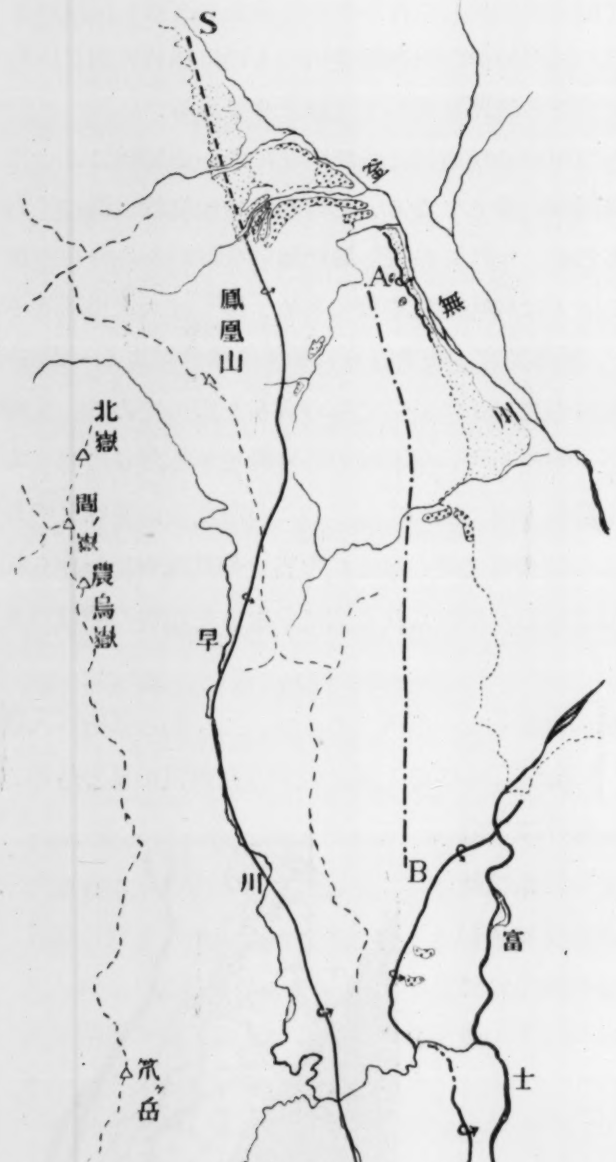

第 2 圖 鳳凰山附近の主要斷層分布圖

の東麓山地の東縁は前記境界線で代表されるが，西縁は巨摩山地との間の急斜面の麓と考へられ中山・鷹ノ田・椹池・穂見神社・向川・泊平・清水等の部落を結ぶ線がそれを代表してゐる．この西縁は第2圖 AB に示す様に略ぼ南北の直線狀の境界をなし，斷層に起因した如き地形を想起させる．この地形は既に辻村先生によつて詳しく記載されたものである．

筆者等が大柳川溪谷に於いて地質調査をした限に於いてはこの境界部に近き位置に大きな斷層を認めることができた．併しこの急斜面の地質學的意義の解決には今後更に充分な調査をなす迄未決にして置きたい．

巨摩山地は 2000 m 前後の山地からなり，御所山・千頭星山・櫛形山・高谷山・丸山・源氏山等からなり，西縁は深く野呂川（早川の上流）の溪谷で深く刻まれ 1 km² で比高約 800 m に達する部分さへある．この山地中を深く刻む大きな河流は北から大武川・小武川・御勅使川・戸川・大柳川等があり，何れも下流は地質構造上の走向を横ぎる東西の走向の横谷をなしてゐるが上流は地質構造上の特長に從ひ南北の流路をとるものが多い．

第4區赤石山地との境界部は殆ど地形圖上からは不明瞭であるが，切峯面にするとかなり明瞭に表はされる．それによるとこの境界線は甲斐駒ヶ岳の東麓から略南北に大武川の支流である石空川に沿ひ小武川の上流の溪谷へと出で，千頭星山と辻山との間の大ナジカ峠を經て大崖頭山を經て早川の溪谷に出る．この境界線は後述する樣に斷層線と一部は一致するが全くは一致しない．假に之を境界とするならば白根三山卽ち農鳥岳・間ノ岳・北岳の他に甲斐駒ヶ岳もこの地域に含まれてゐる譯である．

地　　　　質　（第 24 圖　地質圖參照）

1．第　四　系

a．冲積統　冲積統は富士川・釜無川及びそれらの支流の沿岸に廣く分布し，主として砂礫層からなつてゐる．小武川・大武川等溪谷底には巨大な花崗岩塊の河礫を多量にみるが，御勅使川では集塊岩質礫岩の大礫を多量にみる．冲積統は山地では比較的狹い面積を占めるが下流部（前記第1地形區）ではその大部がこの砂礫層堆積面からなつてゐる．

b．段丘礫層　も冲積統と同樣に釜無川沿岸に分布してゐる．この段丘礫層は高度により大きく2分することができ，高位と低位とに分たれ，低位は大武川の中流口大坊附近，韮崎町の南西方に廣く分布してゐる．主として砂泥り礫層からなり，表面は緩斜するが比較的平坦である．第2圖中にその分布を示してある．

高位段丘は大體低位段丘の分布範圍と等しい分布を示してゐるが，堆積物の粒形は大きく且つその表面には輕石を含んだ赤土が堆積してゐる．

北部の高位段丘中には河礫と安山岩角礫との互層をした部分があり，この安山岩角礫層は八ヶ岳火山に起源を持つものである．

地表のこの輕石は本地域の北部の高位段丘の地表に特に多く，中村慶三郎理學士が八ヶ岳火山よりの噴出物であるとされてゐるものである．

c．中山輝石安山岩體

本地域の北部にある中山山地の西部には輝石安山岩質集塊岩及びその熔岩流等の火山噴出物からなる一地質系統が分布してゐる．略ぼ中山峠以西の海拔 770 m 以内の高度の山體を作つてゐる．この山地の北側では板狀節理を示した熔岩流と集塊岩とが相重つてゐる樣が觀察できる．(第3圖 Loc. *221*)．この中山安山岩體は菅原村横手・西組附近で前述した低位段丘層で不整合に被はれてゐる．(第3圖 Loc. *240*)．

熔岩流は暗灰色緻密な孔隙のある含輝石・紫蘇輝石・安山岩で八ヶ岳地方のものと類似し，八ヶ岳の或る時代の裾野が嘗て當地域に迄延長してゐたことを想像し得る．

この中山安山岩體の分布の上端は海拔約 770 m であるが，釜無川の北岸八ヶ岳の

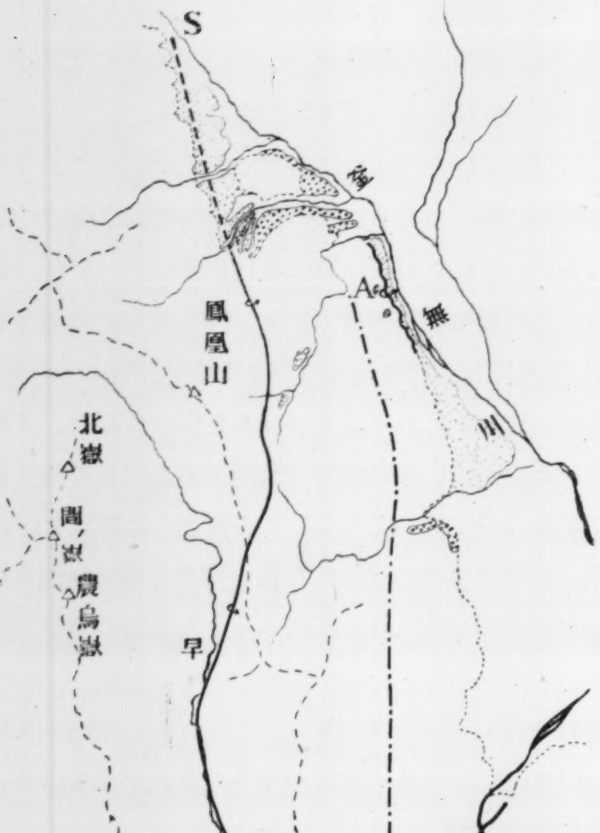

第 2 圖　鳳凰山附近の主要斷層分布圖

の東麓山地の東縁は前記境界線で代表されるが，西縁は巨摩山地との間の急斜面の麓と考へられ中山・鷹ノ田・椹池・穂見神社・向川・泊平・清水等の部落を結ぶ線がそれを代表してゐる．この西縁は第2圖ABに示す様に略ぼ南北の直線狀の境界をなし，斷層に起因した如き地形を想起させる．この地形は既に辻村先生によつて詳しく記載されたものである．

筆者等が大柳川溪谷に於いて地質調査をした限に於いてはこの境界部に近き位置に大きな斷層を認めることができた．併しこの急斜面の地質學的意義の
決には今後更に充分な調査を
す迄未決にして置きたい．

巨摩山地は 2000 m 前後
地からなり，御所山・
山・櫛形山・高谷山・丸
氏山等からなり，西縁は
呂川（早川の上流）の
く刻まれ 1 km² で比
に達する部分さへあ
地中を深く刻む大
から大武川・小
川・戸川・大柳川
れも下流は地質
横ぎる東西の
てゐるが上流は地質構造上の特長に従ひ南北の流路をとるものが多い．

第 3 圖　駒城村横手附近の地質圖．G は花…行線は桃ノ木層，V模樣は安山岩體，點模…段丘．

兩事實は一見互に相反し興味ある問題を提…する．

2. 新 第 三 系

本地域に發達する第三系は主として中新統…化石上鮮新世初期掛川時代に堆積したと考へ…統中には次に述べる圓井酸性深成岩體から由…ら圓井酸性深成岩體が地下深處に迸入して後隆…露出したものと推定できる．故に次に述べる圓…期と考ふることを得る．故に本地域に發達する…つた．

a. 圓井酸性深成岩體

この地方に發達する酸性深成岩類は之を時代的…る．こゝに述べる圓井深成岩體は 20 萬分の一地質圖…花崗岩とされたもので薄片を檢鏡した結果含紫蘇輝…つた．(第 14 圖はこの閃綠岩の薄片の顯微鏡寫眞で…

この深成岩體は略ぼ N 20°〜15° W の走向に約…幅さは約 2 km 以内の細長の形態をなして，第 2 地…この岩石體の北緣をなす圓野村上圓井附近で觀察し…石化作用を受けた石英閃綠岩で捕獲岩は比較的稀で…・御坂山地等にある石英閃綠岩と類似する)．

…の深成岩體の東緣は前に一寸述べた樣に一部は推し…に述べる玢岩體に貫入關係で接觸してゐる．鈴木…に變質を與へてゐるところの露出を觀察してゐ…

…御坂層及びそれを貫く玢岩體が固化した…して地表に露はされるに至つたものであ…閃綠岩體と略ぼ類似な地質時代に貫入した

…形山・桃ノ木兩層を岩脈或は岩床 (sheet) と…粒安山岩質の岩石から石英粗面岩その他玢岩

…體に貫かれ，明に後者より前に噴出したものと…圖地質圖に示すやうに西部では略ぼ南北に走り…に横はり，東部では東西に近い走向を有する岩脈…鐵鑛等を胚胎し，プロピライト化作用・曹長石化…石化作用を受けた玢岩を示す薄片．茂倉・湯島・御座石湯等には鑛床の露頭があり，之等の鑛床は…周緣の桃ノ木泥岩・砂岩中にも胚胎してゐる．之…玢岩の延長に平行分布してゐて，半深成岩體の各岩

…しやう．ただ本鑛床胚胎の成因に就いて次に述べん…によつて生じたものとされる學者もあるが，筆者等は…成したくない．

…されたものである．この地層の分布區域である中巨摩郡…をとつてかく名付けられたものである．櫛形山層は主と…前山山地を占めてゐる．主として綠色安山岩質集塊岩・…ゐる．その層理は不規則で，層位も一定してゐないが，…らしい．之も今後の研究に俟つところのものである．…は明でない．

…ものの内に櫛形山層の下位を占める地質系統として中山層と…地域の北部中山の山體を作る地質系統で斯く命名された譯で…は常磐炭田地方で既に使用されてゐて，而も略ぼ近い時代の…名稱の混亂を防ぐ意味で本地域の中山層を桃ノ木層と呼んだ．

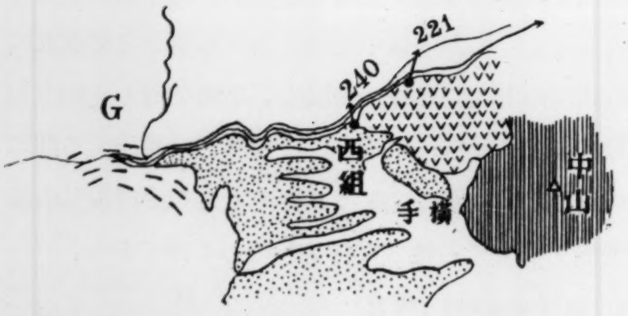

第 3 圖　駒城村横手附近の地質圖．G は花崗岩，平行線は桃ノ木層，V模様は安山岩體，點模様は低位段丘．

裾野の表面は同様 774 m 前後で，これらの高度の間に著しい差異のないことは注目すべきことである．この事實は中山山地と八ケ岳斜面との間に何等相對的な高度變化がなかつたかの如き觀を與へ，前に地形の項で言及した下圓井の第四紀推し被せ斷層の露出と共に考へ合はすと兩事實は一見互に相反し興味ある問題を提供してゐる．今後の調査研究に俟つこととする．

2. 新 第 三 系

本地域に發達する第三系は主として中新統及びそれ以下のものである．本地域には化石上鮮新世初期掛川時代に堆積したと考へられる靜川統の發達は見られない．靜川統中には次に述べる圓井酸性深成岩體から由來したと思はれる多數の圓礫をみた點から圓井酸性深成岩體が地下深處に迸入して後隆起し，著しき削剝作用を受けて地表に露出したものと推定できる．故に次に述べる圓井深成岩體の迸入は鮮新世以前の一時期と考ふることを得る．故に本地域に發達する第三系は中新統以下の諸層のみとなつた．

a. 圓井酸性深成岩體

この地方に發達する酸性深成岩類は之を時代的に 4 種に區別することが可能である．こゝに述べる圓井深成岩體は 20 萬分の一地質圖幅に於て角閃石を稀に含む黑雲母花崗岩とされたもので薄片を檢鏡した結果含紫蘇輝石石英閃綠岩であることが明となつた．（第 14 圖はこの閃綠岩の薄片の顯微鏡寫眞で多少曹長石化作用を受けてゐる．）

この深成岩體は略ぼ N 20°～15° W の走向に約 15 km の長さに延長し，東西の幅さは約 2 km 以内の細長の形態をなして，第 2 地形區中の東緣を劃してゐる．

この岩石體の北緣をなす圓野村上圓井附近で觀察した結果によればこの深成岩は曹長石化作用を受けた石英閃綠岩で捕獲岩は比較的稀である．（岩石相は甲府盆地の東北緣・御坂山地等にある石英閃綠岩と類似する）．

この深成岩體の東緣は前に一寸述べた様に一部は推し被せ斷層で境されてゐるが西緣は次に述べる玢岩體に貫入關係で接觸してゐる．鈴木博士は鹽の上附近で所謂御坂層の泥岩に變質を與へてゐるところの露出を觀察してゐる．

以上の點から察して，この深成岩體は所謂御坂層及びそれを貫く玢岩體が固化した後に貫入し，その後地殼變動のために變位して地表に露はされるに至つたものである．この深成岩體は恐らく丹澤山地の石英閃綠岩體と略ば類似な地質時代に貫入したものと思はれる．

b. 巨摩半深成岩體

巨摩半深成岩體は次に述べる第三系櫛形山・桃ノ木兩層を岩脈或は岩床（sheet）として貫くところのプロピライト化した粗粒安山岩質の岩石から石英粗面岩その他玢岩狀に至る諸種の半深成岩類を總稱する．

本火成岩體の一部は圓井酸性深成岩體に貫かれ，明に後者より前に噴出したものと考へられてゐる．その一般的分布は附圖地質圖に示すやうに西部では略ぼ南北に走り約五帶以上の岩脈又は貫入岩體として横はり，東部では東西に近い走向を有する岩脈が多い．特にその西緣部のものは黃鐵鑛等を胚胎し，プロピライト化作用・曹長石化作用を受けてゐる．第 13 圖は曹長石化作用を受けた玢岩を示す薄片．茂倉・湯島・奈良田・蘆安・金山澤・元靑木湯・御座石湯等には鑛床の露頭があり，之等の鑛床は何れもこの半深成岩體中に及びその周緣の桃ノ木泥岩・砂岩中にも胚胎してゐる．之等の鑛床露頭の分布をみると殆ど玢岩の延長に平行分布してゐて，半深成岩體の各岩石の迸入後の鑛化作用を思はせる．

詳細は更に研究を行つた上說明しやう．ただ本鑛床胚胎の成因に就いて次に述べんとする鳳凰山深成岩體の熱變成によつて生じたものとされる學者もあるが，筆者等は次に述べる理由からこの說に贊成したくない．

c. 櫛　形　山　層

櫛形山層は田中技師の命名されたものである．この地層の分布區域である中巨摩郡の櫛形山（2051·7 m）の名稱をとつてかく名付けられたものである．櫛形山層は主として巨摩山地の東半及び東麓前山山地を占めてゐる．主として綠色安山岩質集塊岩・凝灰岩・安山岩等からなつてゐる．その層理は不規則で，層位も一定してゐないが，大體南北の走向をとるものらしい．之も今後の研究に俟つところのものである．

この地層の上限は本域では明でない．

d. 桃　ノ　木　層

田中技師が命名されたものの內に櫛形山層の下位を占める地質系統として中山層と呼ぶものがある．之は本地域の北部中山の山體を作る地質系統で斯く命名された譯であるが，中山層なる名稱は常磐炭田地方で既に使用されてゐて，而も略ぼ近い時代の地質系統であるから，名稱の混亂を防ぐ意味で本地域の中山層を桃ノ木層と呼んだ．

桃ノ木層は主として暗灰色の泥岩層，細砂岩層からなり，1 mm 前後の大きさの角礫片を含んでゐる．又火成岩・黑色の頁岩又は泥岩の小礫を含んだ礫質砂岩及び礫岩を介在する．礫岩層は湯島仙城澤附近では比較的厚く分布してゐるが，北方へ至るに從ひ厚さは減少する．又礫岩層は一般に西部に多い．灰色砂岩は御座石湯北西の尾根から N 30° E : W 60° の層位で分布してゐるものが特に目立つ．

本層は從來地質時代を決定するに足る化石が發見されなかつたので，或は中生界，或は古第三系と考へられたが，今回筆者等は暗灰色砂質泥岩中の石灰質分の豐富な部分から次の様な化石有孔虫を採集した．(第 15・16・17 圖參照)

Lepidocyclina (*Amphilepidina*) *japonica* YABE, *Miogypsina ozawai* HANZAWA, *Cycloclypeus* sp.

上揭の化石有孔虫が群馬縣中小坂地方・宮城縣地方の *Lepidocyclina* を含む地層に略ぼ近い時代なことを確め得た．本層は極めて火山碎屑岩に乏しい地層で而も化石も乏しい．本地域の南方の本層から，中野治三學士は *Globigerina* のみを含む泥岩を採集された．之に依て本層は先に層序上の問題の項に於いて述べた如く，火山碎屑岩層である櫛形山層の下に横はり，且つ *Lepidocyclina japonica* を含み，幌內時代の暖流系の堆積物と考へて差支えないこととなつた．

本層の層位は玢岩・石英粗面岩・(プロピライト化した)安山岩等によつて後に貫かれてゐる他，その西緣に於いては大斷層が之を境してゐる等で未解決の部分も少くはない．特に斷層に接した約 1 km 程の間は泥岩も千枚岩狀に變質し，砂岩は珪岩又はホルンフエルス化してゐて，一見古期岩層の如き觀を呈してゐる．又この部分の地層の層理は殆ど西緣の大斷層に平行して壓し潰され南北上下にレンズ狀に延び連續してゐない．

本層と櫛形山層との境界は大柢の場合火成岩の迸入體で境されてゐるために明瞭を缺くが，桃ノ木層中には櫛形山層に見られる様な火成岩塊を含まないし，本層から櫛形山層へ向つて泥岩を matrix とした集塊岩質礫岩から徐々に集塊岩相に變化して行く狀態が觀察でき，櫛形山層中に桃ノ木層の泥岩が礫となつて含まれてゐる事等から桃ノ木層から櫛形山層へ向つて深い海の狀態から次第に淺くなつて火山活動の激しい狀態に移過して行つた様子がうかがはれる．

3. 新第三系以前

a. 鳳凰山深成岩體．附．賽ノ河原半深成岩體

鳳凰山深成岩體は甲斐駒ヶ岳・鳳凰山に主として露出する粗粒の閃雲花崗岩體で幅 10 km 以上長さ 50 km に達する南北に長い深成岩體である．この東緣はその北部

では急に高度を低めて第四系に被はれるが，大武川溪谷以南では前述した第三系桃ノ木層と斷層を隔てゝ接してゐる．

西南縁は御室澤附近から辻山の東の南御室小舍附近へ延び更に藥師ヶ岳の西斜面を縫つて地藏ヶ岳と高嶺との間の鞍部に出る．この高嶺鞍部では周縁の壁岩（wall rock）に Li-pa-Li 迸入をしてゐる．

北縁に就いては未だ調査を進めてゐないが大武川ヒョングリ瀧附近，尾白川不動瀧附近の觀察に依れば同樣閃雲花崗岩が露出してゐる．鈴木博士の說明書から判斷して恐らく甲斐駒ヶ岳もこの花崗岩からなるものと思はれる．（本花崗岩に類似な岩相を示すものとしてこゝに，山梨縣北部の昇仙峽及び金峯山の花崗岩をあげることができる．岩石相の類似を以て地質時代の對比を行ふことは避くべきことではあるが，之等の花崗岩類は野外の層位關係に於いて同一地質時代の貫入と見做すことができるので，筆者は大膽ではあつたが三者を同時代迸入と見做した）．

本花崗岩中には水成岩から由來したと考へられた捕獲岩（xenolith）が多く含まれてゐて，捕獲岩の一部は明にこの深成岩體の壁岩（wall rock）である古生界の雲母片岩と類似な見掛を呈してゐる．之等の捕獲岩は一つの露頭では何れもその長軸を平行におき流狀構造を暗示してゐる．故に筆者は之等の捕獲岩及び黑色斑晶，Schlieren 等により，この花崗岩の流狀構造を肉眼的に測定決定した．

第4圖はその測定結果を示してあるが，この花崗岩體は少くとも，その南部に於いては，その壁に對して調和した流狀構造をとり，Cloos 等の謂ふ所の "conformable structure" 卽ち調和流狀構造のもので，外側の地層の構造に對しては不整合流狀構造をとつてゐるものと言へる．

卽ちこの流狀構造は大體に於てこの花崗岩體の迸入凝固の際に生じた一次的流狀構造と見做せる．故に後に述べる樣に所謂古生界が略ぼ今日の構造をとつてから後に噴出・固結したものと見做せるのである．又その流狀構造は中心部に於いては流線・流層が水平に近く，その周縁部に於いてはその走向を周縁境界線に平行にし，傾斜を急にするので，一種のドーム狀流狀構造を作つてゐることを知ることができた．故にこの深成岩體は下方より上方へ迸入したものであらうと推定した．又この深成岩體中には何等著しい斷層構造を見なかつた．故にこの深成岩體が迸入固結してから後は著しい横轉運動や深成岩體を東西に横斷する樣な水平移動はなかつたかに見える．

この深成岩體の東縁に就いては，斷層であることを述べたが，この斷層に接近した部分の花崗岩の流狀構造はその東縁に平行な構造を示してゐるが，詳細に各鑛物の結晶をみると稍々變形を受けてゐる．併しこの變形は次に述べる如き燒地藏深成岩體の

構造程に壓碎 (mylonitize) されてゐない．故にこの花崗岩迸入時に既にその東緣に南北の走向を持つた直線的な地質構造上の境界があり，その影響により流狀構造が南北の走向を選んだかに見える．

又變形を受けたその斑晶（長石類・石英）は裂罅面に沿つて僅づゝづれ，その割れ目は壓碎粒狀構造となつてゐる．第 18 圖はその粒狀壓碎構造を示した．この迸入運動中にも斷層運動の影響があつたかに見える．

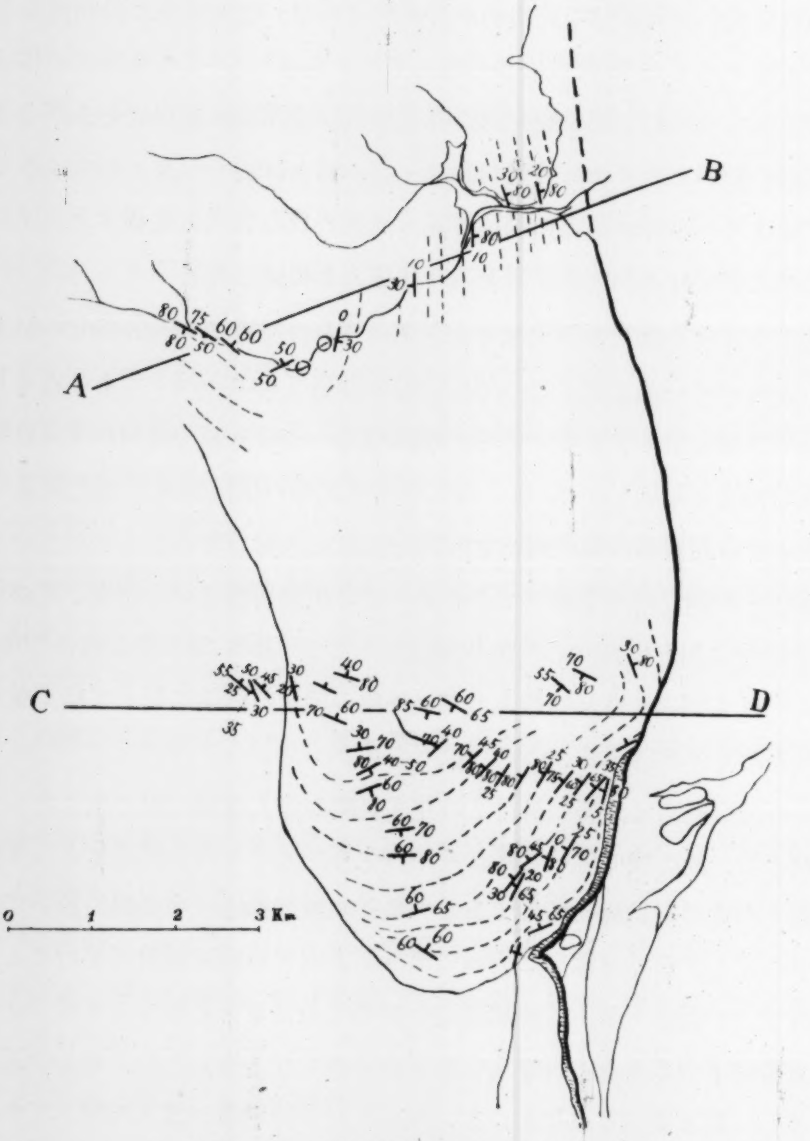

第 4 圖 A. 鳳凰山花崗岩體の流狀構造.

この花崗岩體の周圍への影響に就いてはこの壁岩である周圍の所謂古生界を接觸變成せしめて雲母片岩・石墨千枚岩等に變へてゐることを擧げることができる．

從來此の花崗岩東緣地區の桃ノ木層及び巨摩半深成岩體に胚胎してゐる鑛床をこの

花崗岩の變成作用として說明してゐた．この樣な鑛床は御座石・千丈瀧・青木・舊青木鑛泉等花崗岩體の東に接した區域の他，金山澤・ドノコヤ・西山・湯島・茂倉等花崗岩體の發達しない地方の新第三系中にも存在するので，筆者は之等の鑛床を花崗岩

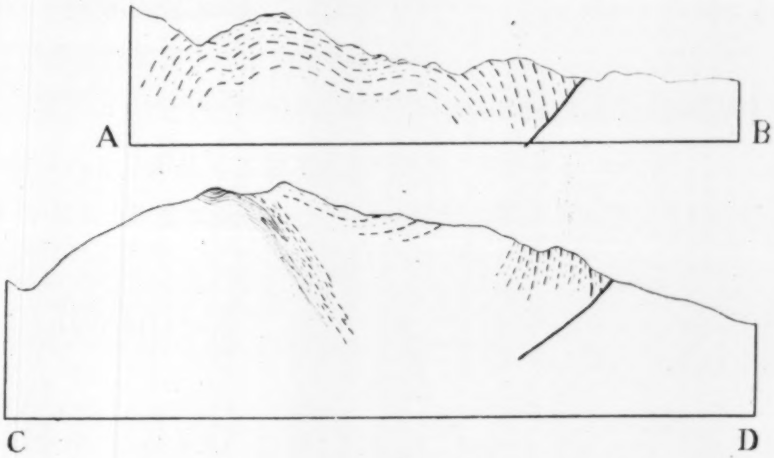

第 4 圖 B.

體の逆入の影響と見做さず，桃ノ木層・櫛形山層を貫いた巨摩半深成岩體成生後の鑛化作用の影響と見做したい．

賽ノ河原半深成岩體

この岩石は鳳凰山彙の地藏ヶ岳の頂上5丈5尺の岩中に厚さ約 1 m の岩脈として露出するもので次に述べる鳳凰山花崗岩より斑晶細密で，且つ鳳凰山花崗岩を貫いてゐる．この樣な岩脈岩は更に次の樣な狀態の岩脈として散見することができた．

白 絲 の 瀧	層向 N 30° E	傾斜 W 65°	厚さ 30 cm.
地藏ヶ岳頂上	層向 N 80° E	傾斜 S 50°	厚さ 100 cm.
賽ノ河原の西南 2740 m 標高の南	層向 N 30° E	傾斜 SE 55°	厚さ 100 cm.
觀音岳北方の突起	層向 N 45° E	傾斜 N 57°	厚さ 10 cm.
藥 師 ヶ 岳	層向 N 75° W	傾斜 N 30°	厚さ 5 cm.

この岩石は半花崗岩質で矢張黑雲母・稀に角閃石等を含んでゐる．之等の岩脈群の走向・傾斜等からは何等具體的な構造上の結論は得られなかつた．

b. 燒地藏深成岩體

この深成岩體は小武川の源流地方によく露出し，辻山の東麓を占め，略ぼ南北に長さ 4 km，東西に幅 1 km 程の小露出をなす深成岩體である．辻山の西北方 800 m の南御室小舍から東東北へ向ふ御室澤では，元青木湯（1543 m）附近から西へ向つて數 10 m の間桃ノ木層の礫岩が層向 N 10°～20° W 傾斜 W 20°～30° で橫はり，次に鑛脈の胚胎した玢岩を約 30 m の幅に橫へ，一斷層を經て層向 N 50° W，傾斜 WS

30° で整然と相重る桃ノ木層の黒色砂岩・頁岩が約500 m 程に露出してゐる．次に明瞭な斷層（走向 N 20° W 傾斜約 45° W）を境として白色のヘレフリンタ（hälle-flinta）狀岩石に變じ，之は 20 m 內外の厚さで終はり，燒地藏深成岩となり，見掛上桃ノ木層の上に横はつてゐる．ヘレフリンタ狀岩石と燒地藏深成岩體との境界は澤となり露出なく明でない．

この御室澤と藥師ヶ岳から東南へ向つて發する澤卽ち藥師澤との合流點附近（第 5 圖 Loc. 192）には鳳凰山花崗岩體と燒地藏花崗岩體とが接觸してゐる部分が露出してゐる．その境界面は稍々不規則な境界をなし，燒地藏深成岩中に第 6 圖の如き鳳

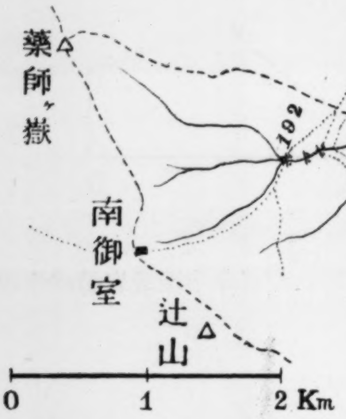

第 5 圖

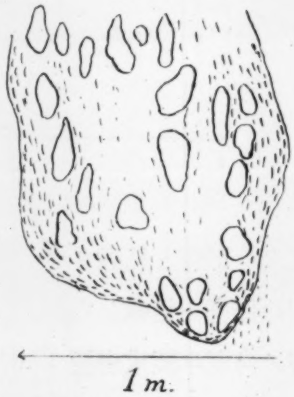

第 6 圖

凰山火成岩體の支脈と思はれるものが見られる．この支脈をみると多數の捕獲岩を含んでゐて，雲母・角閃石の配列はその外壁に對して調和した流狀構造を示してゐて，外部の燒地藏の流狀構造に對しては非調和の狀態にある．又捕獲岩は周緣に一つも接してゐず，必ず壁と捕獲岩との間には閃雲花崗岩體の一部が介在してゐる．故にこの露出から判斷すると鳳凰山火成岩體は燒地藏火成岩體より後成のものと考へることができる．

辻山から東北へと走る小武川では舊青木鑛泉の湯元附近（第7圖 Loc. 185）には黃鐵鑛等を含んだ綠色の曹長石化作用を受けた玢岩が横はるが，それより西へ向つて斷層數面を横へ，ヘレフリンタ狀の白色岩石が露出し，それより 0·5 m 程の厚さの斷層ネバからなる破碎された帶を經て燒地藏深成岩體となる．更に上流へ溯るとこの火成岩體は略ぼ N 30°～0° W の走向，70°～80° W の片理を持つた構造を示し最後に雲母片岩と接觸して，雲母片岩の片理に第7圖に示す樣に迸入してゐる．同樣の關係は青木から南小室への登山路の途中にも觀察できたしオホナジカ峠の西側のガレにもヘレフリンタ狀の岩石と共に轉石を見ることからその境界の存在を推定することができた．

辻山の東南約 1 km 餘の燒地藏附近にはこの岩石がよく露出してゐるのでこの火成岩體の名稱としたが，そこでは上述した樣な片理を示してゐない．

上の樣にこの火成岩は小さな細長い形をした迸入岩體である．

この火成岩は外見鳳凰山花崗岩體より稍々褐色を帶びヘイスチングスを含んだ角閃石花崗岩で鳳凰山花崗岩と明に肉眼的に區別できる．

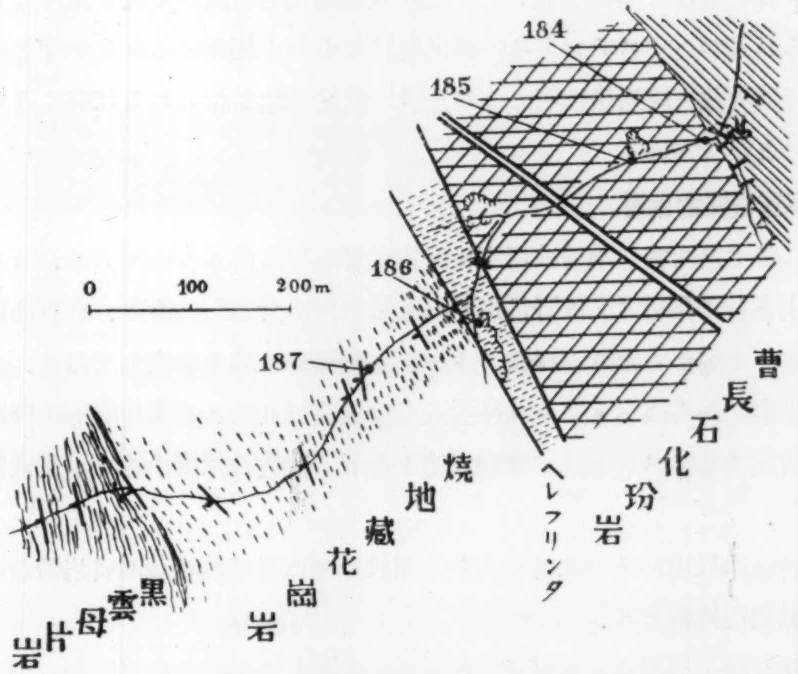

第 7 圖　御室澤地質調査圖

併しながらその東縁は肉眼的には流狀構造の如く見えるが實はさうでなく，顯微鏡でみると壓碎された mylonite 狀岩石で，ヘイスチングスは壓碎粒狀化した石英・斜長石の粒間を占め，殆ど壓碎化されてゐないので，恐らくこの苦鐵鑛物の結晶作用は壓碎化作用を起した造構運動（tectonic movement）の後の結晶作用と考へられる．

第 19 圖は壓碎化されない燒地藏附近の含黒雲母ヘイスチングス花崗岩で，第 20・21 圖は壓碎化された含黒雲母・ヘイスチングス花崗岩とそれを十字ニコルを通して寫したものとである．この mylonite 狀岩石の片理は略ぼ南北で，この火成岩體の東境の斷層に平行してゐる．又壓碎化の程度は東する程小さくなり，西する程原構造がよく保存されてゐる．之等の點から見て，この壓碎化作用はこの燒地藏火成岩體の東縁にあつた斷層構造に關係したものと考へられる．

ヘレフリンタ狀の白色岩石がこの東縁の斷層に接して分布してゐることは地質圖に示す通である．この岩石を顯微鏡下に觀察すると同樣に壓碎粒狀構造の岩石で mylo-

第四系
- 沖積統
- 段丘礫層 〔下圓井推し被せ斷層〕
- 中山輝石安山岩體（八ケ岳地方よりの噴出?）

圓井酸性深成岩體（石英閃綠岩）
巨摩牛深成岩（玢岩・石英粗面岩・安山岩）
櫛形山層（火山碎屑岩）

桃ノ木黑色泥岩層（*Lepidocyclina japonica* を含む）

鳳凰山深成岩體（閃雲花崗岩）
燒地藏深成岩體（黑雲母・ヘイスチングス花崗岩）
所謂秩父古生層

a. 表皮的な地層・岩石の構造

上表の岩石・地層の內中山輝石安山岩體までのものは最近地質時代の表成岩石で，殆ど皺曲構造を示してゐない．沖積統は現在の溪谷底に主として河礫として發達し，尙侵蝕を進めてゐる．而もそれらの河谷の沿岸には二段以上の河岸段丘が現河床上20～30 m・80 m 以上等の高度に發達し，之等は大部分礫層からなつてゐる．故にこの地方の侵蝕基準は甚しい速さで低下しつゝあるものと考へられるのである．

地形の項で述べた樣に下圓井推し被せ斷層に沿つて，圓井深成岩體はこの河岸段丘礫層の上に橫はる如き構造を示してゐるので，洪積世にも尙逆斷層運動がこの地方に行はれたことを知つた．

この逆斷層は地形の項でも述べた樣に巨摩山地東麓の前山山地と甲府盆地底の西部との境界部に該當し，前山山地の東緣の急斜面が推し被せ斷層に起因したものであることを暗示してゐる．又前山山地が根無地塊の疑さへ起る．

井尻理學士は北巨摩郡新富村山高の西南 300 m の地點に於いて段丘礫を低角度に截る斷層面を發見してゐるのでこの疑を更に深める．

中山輝石安山岩は前記の段丘より海拔高度高く段丘の下部から頭を出した火山碎屑岩で，八ケ岳泥流の表面の高度と略ぼその高度を一致させてゐる．併し兩者の間には前記の下圓井推し被せ斷層が走つてゐるものと考へられるので兩者には高度上の差異が豫想されるのに兩者が類似の高度をとることは假に兩者が八ケ岳系統の起源としても時代を異にするものと考へられる．

中山輝石安山岩體は第三系桃ノ木層からなる中山（海拔 887 m）の西北麓の海拔約700 m 以下を占め，殆ど皺曲してゐない．故に中山安山岩までを陸成の表皮的な岩石として，この地方の基盤地質構造の構成要素から除外することができる．今之等の表皮的な岩石の地質構造上の特長として，時代の古い岩石・地層程海拔高度の高い位置

にその分布があると言ふことで，この地方の侵蝕作用と地盤運動とが激しい爭をしてゐるのが理解できる．

b. 基盤岩石の地質構造

基盤岩石の地質構造は極めて複雑で一々こゝに記すのは困難な程であるし，未だ研究が漸く緒についた程度であるからその詳細は後日に譲ることとして大略を記して行く事とする．

先づ**第三系の發達區域**に就いて岩相上の問題から述べることとする．

この地方の第三系は前述した様に中新統のみであるが，桃ノ木層はその下部に礫岩を介在するが一般には泥質で角礫砂粒を含み，化石は極めて稀で，その上部に完外洋性高等有孔虫を含んでゐる他著しい化石類を含んでゐない點からみて，かなり深い海の泥帯の堆積物であつた疑がある．特に最近中野嶽三學士は桃ノ木層の南方延長の一地點から *Globigerina* 屬の有孔蟲のみを含む泥岩を採集されてゐる點から考へ併せて桃ノ木層は 2000 米以深の深い海の堆積物とさへ考へられる．

然るに櫛形山層は圓礫を含み，又集塊岩・凝灰岩等の火山砕屑岩を含み，その相は一見淺く，深い相とは考へられない．之等の點からみて櫛形山層堆積時代には桃ノ木層時代の様な靜穏な状態ではなく，かなり淺く火山活動の激しい状態であつたものと考へられるのである．

第9圖に示す如く構造的にみれば桃ノ木層の層向・傾斜は N 30°～0° E のものが極めて多く傾斜は東 60°～70° に急斜するものが多い．

然るに櫛形山層はその層向・傾斜は桃ノ木層程一定してゐない．之等の點からみて兩層堆積期間の間には著しい地殼變動があつたのではあるまいか．

巨摩火成岩體の迸入は兩層が略ぼ上掲の如き構造を選んでからの迸入と考へることができる．即ち岩床（sheet）狀に迸入して之が横轉して層向に略ぼ平行に露出してゐるのではないらしい．即ち之等の迸入岩體は一見桃ノ木層の走向に平行に迸入してゐるが，詳細に見ると桃ノ木層の層向に無關係に斜斷して連續して分布してゐるので，南北走向の地質構造上の特長が完成してからの迸入，即ち intrusion post tectonic disturbance と考へられる．この巨摩火成岩體は一種の岩脈で，その兩側の構造が異る場合があることからみて略ぼ南北に走る斷層線を利用した迸入體と考へられる．

然るに圓井酸性深成岩體は之等の岩石・地層を貫いて生じたものなので，この地方では少くとも次の様な地史が推定できる．即ち桃ノ木時代の深い海は地殼運動を經て櫛形山時代の火山活動時代に入り，兩者が南北の走向に變形した後，巨摩半深成岩體の迸入，圓井深成岩體の貫入があつた．之等は地殼運動で多少變形したが略ぼ現在の

nite と稱しても差支えない程であつた.

オホナジカ峠の西北のガレから採集したこのヘレフリンタ狀岩石も亦 mylonite と稱しても差支えないもので，顯微鏡でみるとこの粒狀構造は弱い片理狀の配列をなし，この片理狀の間隙に黑雲母が結晶してゐる. 第 22・23 圖參照.

上述した事により，燒地藏深成岩體は所謂古生界に迸入してから，その東緣部を斷層運動の影響を受けて壓碎され，その後に鳳凰山火成岩體の貫入を受けて，その北部延長を限られ且つヘイスチングスの晶出を見たものと解釋することができる. この解釋に從へば燒地藏火成岩體は明にその東緣の斷層構造が作られる以前に迸入したものと考へることができる.

c. 所謂秩父古生層

本地域に於て最も古い地層は所謂秩父古生層と呼ばれるものである. 筆者等の調査區域では主として早川（又は野呂川）の流域以西に分佈してゐる. 岩石は硬砂岩・千枚岩・スレート等からなり，稀にチャート，絹雲母片岩を介在してゐる. 之等の岩層は北方辻山附近から高嶺・アサヨ峰附近では黑雲母片岩・石墨片岩等に移過してゐるが南部では主としてスレート，硬砂岩等となり，變質の程度小さく，玄武岩岩脈等を挾んでゐる.

之等の變成の程度がその北部で大なる事は鳳凰山及び燒地藏深成岩體の影響による熱變成の結果と見做せる.

又一方井尻學士が農鳥岳東麓大門澤附近で採集した石墨千枚岩に就いて，杉山學士は壓碎された千枚岩，phyllonite とも稱すべきもの，であることを筆者に傳へられた. 若し上の如くであるならば，この地方の所謂古生界は既に上述した二深成岩體の影響から遠い產地でも壓碎されてゐる事實から，兩深成岩體迸入前に既に壓碎構造をとつたものと解釋しなければならなくなつた.

この地層は何等決定的な化石が發見されてゐないが，全般的に見て一先づ秩父古生層に對比しておいた.

この古生層は一般に層向南北のもの多く，複雜に皺曲してゐる. 例へば高嶺附近では黑雲母片岩で層向 N 10° W: 傾斜 W 45°; 層向 N 55° W: 傾斜 N 25° 等で緩であるが，夜叉神峠一鮎差間では主としてスレート・硬砂岩等で次表（第 1 表）の樣な層向・傾斜である(第8圖參照).

小武川の上流では層向 N 10° W: 傾斜 W 80° を示してゐる.

この樣な構造は所謂西南日本の帶狀構造の一部をなせるものと解釋でき，赤石山地では白堊系の瀨戸川統もこの帶狀構造を示してゐるので，少くともこの瀨戸川時代以

後に完成したものと言へやう．

この古生界の東緣は南部では斷層で桃ノ木層に接してゐる．この斷層に就いては後に述べよう．

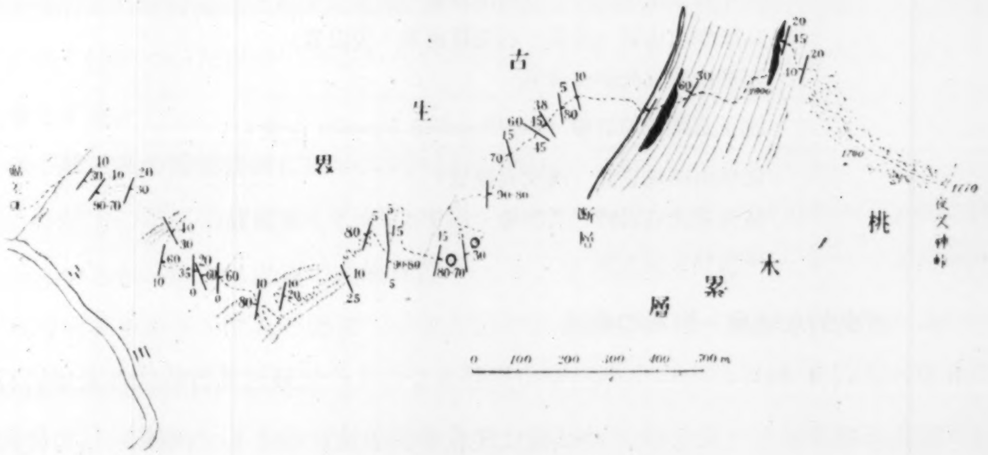

第 8 圖　夜叉神峠・鮎差間の地質調査圖

第 1 表　古生層の層向・傾斜

層　向	傾　斜	層　向	斜　傾
N 40° E	E 30°	N 15° E	E 80°
N 40° E	E 90°～70°	N 5° W	E 45°
N 20° E	E 30°	N 20° E	E 90°～80°
N 30° W	E 40°	N 15° E	E 80°～70°
N 10° E	E 60°	N 5° W	E 30°
NS	E 35°	NS	E 90°～80°
N 20° W	E 60°	N 15° W	W 70°
N 20° E	E 60°	N 60° W	S 45°
NS	E 60°	N 60° W	S 45°
N 10° E	W 80°	N 38° W	W 45°
N 10° E	E 20°	N 5° W	E 80°
N 25° W	E 10°	N 10° W	90°

地質構造

上に述べたやうに本地方に發達してゐる諸岩石を時代順序に並べると上部から下部へ次の様に配列できる．

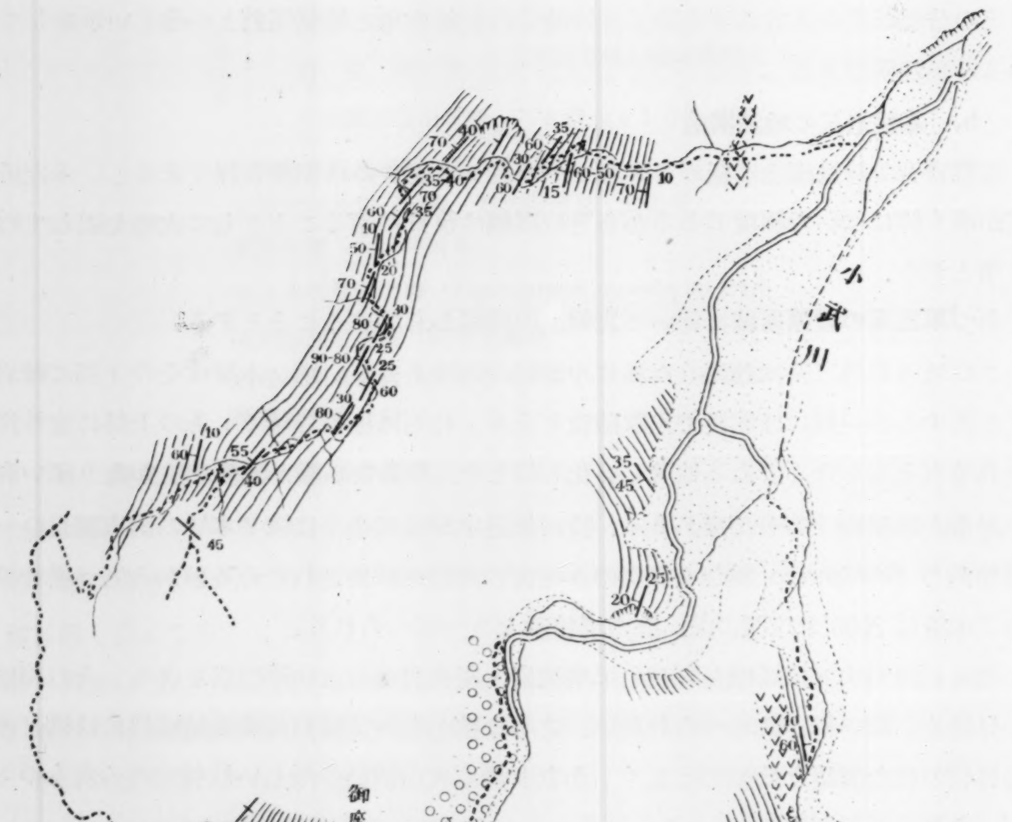

第 9 圖 小武川上流青木鑛泉附近地質圖. 平行線は桃ノ木層, 圓・點模樣は高位段丘, 點模樣は沖積統, ∨模樣は巨摩半深成岩體.

分布形態を取つた後に隆起し著しい削剝を受け深成岩體その他が地表に露出するに至つた．

この地史は第三系の發達地域のものであるが，次に古生界發達地域の地史を述べよう．

古生界發達區域の地史は先づ古生界の南北に走る所謂帶狀皺曲構造の形成運動から開始される．この帶狀皺曲構造の完成したのは千谷技師の靜岡圖幅中にある瀨戶川統と稱せられる中生代後期の地層堆積以後であるから中生代末から古第三紀へかけた地質時代のものと考へられる．

鳳凰山深成岩體はこの帶狀皺曲構造に無關係な迸入構造を示してゐるので，鳳凰山深成岩體は早くとも中生代末の迸入で，恐らく古第三紀前半の迸入ではあるまいか．

燒地藏深成岩體は之に反してこの帶狀構造に平行な構造組識を持つてゐるので，この構造形成時代に迸入したと解釋することも可能である．

之等の事實からみると古生界が白堊紀末――古第三紀前半間に帶狀皺曲構造を完成しつつある間に燒地藏が先づ迸入して次ぎに鳳凰山深成岩體が迸入した．そして燒地藏深成岩の迸入は恐らく漸新世後半より以前であつたと考へ得る．

鳳凰山深成岩體を假に昇仙峽・金峯山の花崗岩類と同時代に考へるならば兩露出地域の間に第三紀諸岩石が分布し，第三紀諸岩石分布地域には鳳凰山系の深成岩類が露出してゐないので，鳳凰山深成岩體も亦この地方の第三紀諸岩石の成生される以前に貫入固化したものと見做さぬ譯に行かない．

扨てこゝに第三系發達區域と古生界發達區域との地質構造上の特性を述べたから更に兩者の境界に就いて一應考察し樣．

c. 鹽尻――靜岡地質構造線

この地質構造線は極めて大規模な構造線で鹽尻峠附近から諏訪湖の西部を經て甲斐駒ヶ岳の東麓に延びてゐる．

甲斐駒ヶ岳の東麓では濁川・尾白川・大武川等の西から東へ展開する大きな扇狀地の堆積物の下に隱されて明でないが，藪ノ湯に至つて初めて地表にその露出を示し出す．藪ノ湯附近の斷層分布は第 24 圖地質圖に示す如くで，岡山學士によつて詳しく記載されてゐる．卽ち「藪の湯新湯の直前に，丸山と呼ばれる一小圓丘がある．この丸山の東側に於て，筆者は初めて所謂御坂層岩石（筆者註　桃ノ木泥岩層）の露頭を目擊した．丸山は形態的にはケルンバット狀をなし，ケルンコルの部分は，所謂御坂層（桃ノ木層）と花崗岩との境界にあたる．この兩者の境界は藪の湯元湯のほぼ N 35° W の小澤が表示するも，その接觸面は見ることができない．」（地形圖の溫泉

記號は新湯を示す).

又「藪の湯元湯の小澤を登り切つて反對側に下れば極めて小さい澤に出る．その兩岸は黑色片岩狀の所謂御坂層（桃ノ木層）岩石なるにも拘らず，谷底には花崗岩砂を認め，就いて登れば傾斜 40° に及ぶテーラスの上端に，甚しくもめた花崗岩の露出がある．併しこゝでも兩岩の接觸面は見出されない．

石空川が 740 m 及 760 m の曲線を切る中間に於て左岸より注ぐ小澤がある．便宜上今之を下わさび澤と呼ぶことにする．この澤の兩岸には黑色片岩狀の岩石を見，傾斜甚だ急であつて 80 度東或は垂直に達する．遡ることしばらくにして下わさび澤は三つ股に岐れる．但し北の股は澤と言ひ得るも，中及南の股はむしろ雨裂の狀をなしてゐる．而して花崗岩と所謂御坂層との接觸面は，南の股の谷頭，南の股，中の股中間の小山嘴上及び北の股右岸に比較的容易に見出し得る．それ等三ヶ所に於ける走向傾斜はほぼ近似の價を示し，第 2 表の如くである．卽ち接觸面は何れも西に傾き所謂御坂層上に花崗岩（鳳凰山）の乘り上げたる態を呈し，平均走向 N 21° W は，御座石湯西方及び石空川左岸に見るケルンコル狀のものを連ねる一線とほぼ近似である」.

第 2 表（岡山氏に依る.）

	走 向	傾 斜
南の股谷頭	N 30°W N 20°W	60°W 50°W
南の股・中の股中間の山嘴上	N 22°W N 22°W	48°W 52°W
北の股右岸	N 10°W N 20°W	38°W 60°W
平　均	N 21°W	51°W

御座石湯の西方で確められた斷層附近では鳳凰山深成岩體は直接に砂岩・泥岩からなる桃ノ木層に接してゐる．そして之等兩岩層の間には厚さ約 30 cm 内外に達する斷層ネバを挾んでゐる．この斷層に接した部分の鳳凰山花崗岩體は斷層に略ぼ平行した長軸面を持つレンズ狀に塊裂してゐて，各塊裂面の境は平滑で壓碎岩化し，且つその表面には條線を持つてゐる．

青木鑛泉元湯の西北に露出してゐる大きな崖は燕岩と呼ばれてゐるが，この燕岩に就いて觀察した結果は次の如きものである．卽ち青木鑛泉元湯附近に於いては鐵銹色に汚れた砂岩・泥岩であるが，斷層を境としてヘレフリンタ狀の白色岩石となり，之は更に N 35°～60° E : W 50° の斷層で鳳凰山花崗岩と接してゐる．この部分の鳳凰山花崗岩の流狀組織は斷層の走向に對して東へ偏してゐるが，それでも N 45° E : W 50° ; N 50° E : E 80° ; N 35°E : W 70 ° ; N 70° E : N 50° 等にして略ぼ平行してゐるとも言へる．

ドンドコ澤本流に於ける前記斷層の露頭に就いては岡山理學士の詳細な觀察があ

る．同氏によれば．

「ドンドコ澤本流が花崗岩と所謂御坂層との境界を過る地點は 1360 m 附近である．その接觸面は右岸に於て第3表の如く，下わさび澤の場合と等しく西に傾くも，走向は却つて東に偏し，花崗岩に接する岩石は蛇紋岩様の變質を蒙り，下わさび澤或は藪の湯附近に見たる如き片岩狀を呈さない．尙その少しく下流の谷底には小室大の花崗岩の塊横はり，それはドンドコ澤を通じてこの部分にのみ見られる現象である．卽ち流水により運搬せられたものではなく，明に所謂御坂層（桃ノ木層）に乘り上げた如き位置を占める花崗岩主體より轉落したものである．」と．

第 3 表（岡山氏に依る．）

	走向	傾斜
花崗岩と御坂層の接觸面	N 28° E	70° W
	N 25° E	60° W
平均	N 26° E	65° W

筆者がこゝに於いて觀察したところでは第11圖の如く Loc. 165 と Loc. 164 との間に白色のヘレフリンタ狀岩石が斷層を境としてその西側に横はり，Loc. 165 附近は厚さ 50 m 程の斷層ネバを露出し，その東方には層向 N 40°～25° E，傾斜 30° W の砂岩が露出してゐる．ヘレフリンタ狀岩石の帶は 300 m 以内の厚さを有し，その帶の中には前記の N 20°～23° E（之は前掲の第2表のものより 5° 許り東に偏してゐる．）の

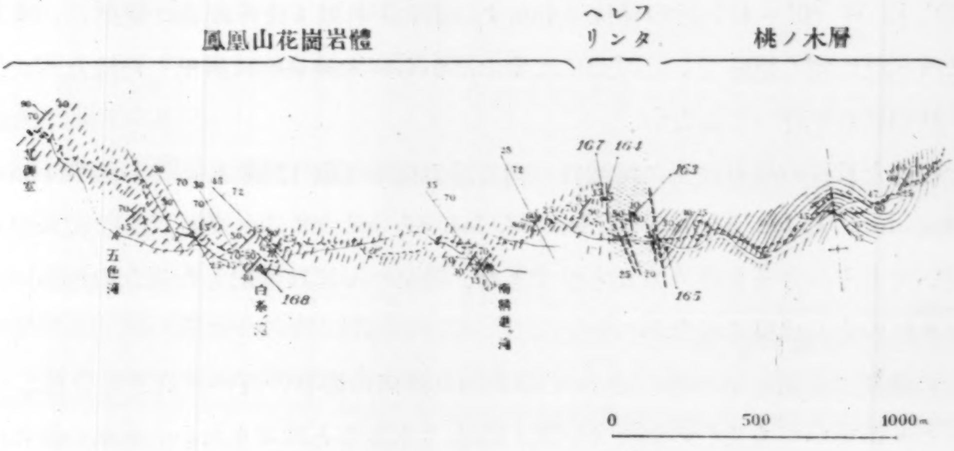

第 11 圖 ドンドコ澤本流に沿ふ地質圖．

走向の斷層に平行した多數の小斷層が混在してゐる．花崗岩とヘレフリンタ狀岩石との境界は不規則な境界を示し明瞭な斷層狀の境界は見られない．岡山氏が觀察した斷層はヘレフリンタ狀岩石の東緣を劃するものであつた．

この特長はドンドコ澤の支谷岩井澤でも兩者の間にヘレフリンタ狀岩石を介在して見られた．

小武川の上流御室澤では約 1760 m の御室の段瀧附近に燒地藏深成岩體と桃ノ木層

との間にヘレフリンタ狀の岩石を見，鳳凰山花崗岩體は 1850 m 附近の段瀧上部の三叉（第5圖 Loc. 192）で燒地藏火成岩體と不規則な境界で單なる接觸關係を示してゐる．

千頭星山の西方にある標高 1880m 餘の峠，オホナジカ峠，の西のガレに就いて調査した結果この地域にもヘレフリンタ狀の mylonite 岩が露出し，更にその南方の金山澤に就いても同樣にヘレフリンタ狀の mylonite 岩及び燒地藏深成岩の露出及び轉石を確めたので，今迄追跡して來た斷層がオホナジカ峠の西側の斜面の中腹を通過してゐることを確めることができた．

大崖頭山附近の觀察を次に記すと．夜叉神峠の尾根では桃ノ木層の砂岩・泥岩及び之を貫く玢岩が露出し，砂岩は珪質になつてゐるが層向 N 25° E, N 20° E, N 35° E, N 40° E 等を示し，傾斜は急である．玢岩は N 25° E の走向の岩脈として露出し，傾斜は急である．併し大崖頭山の西から西南へ走る溪谷を境として，桃ノ木層は消え，全く綠泥・石墨千枚岩と化し，之等の千枚岩の走向は N 10° E: W 60°～70°; N 15° E: 90°; N 10° E: W 80°; N 20° W: WN 60° 等で，この境界部は大崖頭山の三角點の東 300 m の位置を通つて，金山澤の上源へと延びてゐる．

夜叉神峠の西斜面に就いては，夜叉神峠から 1700 m 附近迄は珪化した砂岩層が N 20° E: W 40°～45° 程の層位で分布するが，それ以下は千枚岩に變化し，兩者の境は西へ急に傾く斷層で，この間には金山澤から青木鑛泉迄に露出した樣なヘレフリンタ狀の岩石を伴つてゐない．

この樣な性質の境界は更に樺澤口へ到る途の途中（第12圖 Loc. 63), 1744·8 m の西斜面 loc. 51, loc. 52, loc. 53, loc. 42, loc. 67, loc. 68, loc. 70（第12圖參照）等に於いてもその分布を確めることができた．併しこゝには前記した樣な白色のヘレフリンタ狀の岩石は見られなかつた．

この境界は次第に早川邊に沿つて奈良田部落西山溫泉の西の河底等に分布してゐる．こゝに於いても黑色の斷層ネバ狀の岩石をみることはできたが，前記の樣な白色のヘレフリンタ狀の岩石は見られなかつた．

この樣にこの斷層は諏訪湖附近より藪ノ湯・御座石湯の西，青木湯の西を經て，オホナジカ峠・大崖頭山を越して早川谷邊へと通ずる極めて大なる斷層である．

上述した樣に此の大きな斷層の兩側の岩石・地層の構造は極めてこの斷層と密接な關係を持つてゐる．

古生界の片岩化した岩石中にはこの斷層からかなり離れた位置の千枚岩でも壓碎化されてゐる．

先づ最初に迸入した燒地藏深成岩體はこの斷層に近づく程壓碎化してゐる．この深成岩體中のヘイスチングスは石英・斜長石等の壓碎化した粒狀間隙を占めて壓碎化を殆ど受けてゐないので，壓碎化後の成生と考へられる（第20・21圖參照）．

白色のヘレフリンタ狀岩石は燒地藏深成岩體の東縁にのみ分布し，他には見られなかつた．この岩石は粒狀の壓碎構造を有してゐる．オホナジカ峠の西側のものに就いても同樣な特長を持つてゐるが，之には片理の走向に平行に配列された壓碎化されてゐない黑雲母がある．

本岩と桃ノ木層及び之を貫く玢岩と燒地藏深成岩體とは互に斷層の關係にある．

鳳凰山深成岩體は斷層に接した部分に於いて壓碎化してゐる．この花崗岩と白色ヘレフリンタ樣岩石との境界は接觸的關係にある．

桃ノ木層を貫く玢岩類は現在見られる斷層分布と略ぼ平行してゐるが，玢岩は曹長石化作用を受けてゐる玢岩ではあるが，殆ど壓碎化されてゐない．

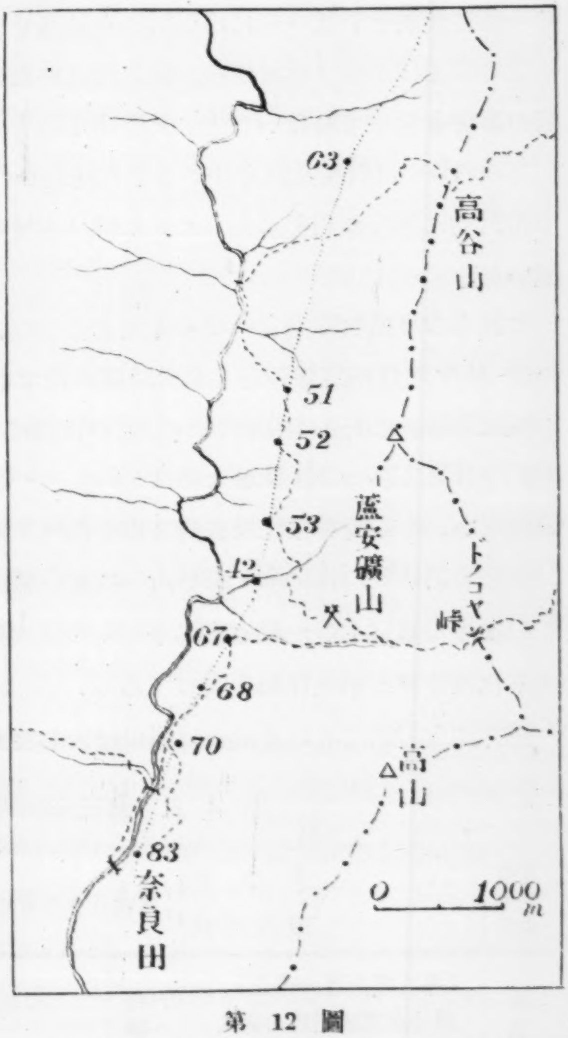

第 12 圖

上記の事實からみて筆者は次の如くこの大きな斷層とその兩側の構造との關係を解釋した．卽ち，

現在見られるこの斷層線（之を假に諏訪——鹽尻地質構造線又は SS 斷層と呼ぶ．）の成生される以前にこの SS 斷層の前身の斷層（之を鳳凰山——安倍川又は HA 地質構造線と呼ぶ．）が勁に存在してゐて，その成立時に古生界を壓碎變成させてゐた．（この斷層成生運動の時期は恐らく關東山地・赤石楔狀體が現在見られると略ぼ類似な構造上の配置を完成した時期と見做せる．）

燒地藏深成岩體はこの時期の後期に迸入し HA 構造線に接した部分は壓碎化された．斯して生じた斷層構造は更に活動をつゞけ，遂に白色ヘレフリンタ狀岩石をその

HA 地質構造線に沿つて生ずるに至つた.

鳳凰山花崗岩體はこのヘレフリンタ狀岩石の成生の後に貫入し，古生界を變成せしめ，燒地藏深成岩體の壓碎構造にヘイスチングスを結晶せしめ，ヘレフリンタ狀岩石の一部に接觸し，又一部には黑雲母を結晶せしめた.

之等の過程が桃ノ木層堆積以前に行はれたことは桃ノ木層以上の地層が之等の火成岩の影響を受けてゐないこと，又壓碎構造を殆ど持つてゐないことで判定した.

この HA 地質構造線を中心とした構造が作られた後この斷層の東側が西側に對して相對的に沈む傾向を示し，こゝに桃ノ木層の深い海，櫛形山層の火山活動の時代が續いた.

これらの堆積物は南北の皺曲構造をとつた．この南北の皺曲構造の作られた時期は勿論 HA 地質構造線の作られた時期の後であつて，この時にも恐らく HA 地質構造線は再活動したかも知れぬが，その位置に就いては HA 地質構造線と同樣その分布が今日見られる SS 斷層と略ぼ平行した一線であつたらうと考へるより他に推定の道はない．この時の推定地質構造線を後桃ノ木構造線と呼ばうと思ふ.

巨摩玢岩はこの桃ノ木・櫛形山の地層の皺曲構造が成生されてから後の迸入體で，この地方の構造上の一般走向に平行して長大な岩脈として分布し，大部分はプロピライト化及び曹長石化作用を受けてゐる.

圓井深成岩體はこの最後の時期に迸入したものである．斯して生じた構造に第三次

第 4 表 鹽尻-靜岡地質構造線成生史

古生代 中生代	古生界 瀨戸川統	〔西南日本外帶の帶狀に配列した構造の完成〕		
古第三紀	〔赤石楔狀體の獨立〕 燒地藏深成岩體の迸入 ヘレフリンタ狀壓碎岩成生 鳳凰山花崗岩體の迸入	HA地質構造線の成生	〔關東山地の基礎の成生〕 昇仙峽・金峯山花崗岩の迸入	
新第三紀			桃ノ木層堆積	〔關東山地の完成へ向ふ〕
		後桃木構造線	櫛形山火山碎屑岩層の堆積	
			巨摩玢岩の迸入	
			圓井石英閃綠岩の迸入	石英閃綠岩の迸入
		SS斷層の成生		

の斷層運動として HA 及び後桃ノ木地質構造線に略ぼ近い位置に沿うて SS 斷層の形成をみた．之によつて桃ノ木層及びそれ以後に生じた岩石・地層と基盤岩石との對照が今日みられる様に極めて明となつた．

この斷層は古い地質構造線の再活動的意義を有するため，桃ノ木層堆積以後の地層・岩石に對しては著しい熱變成も造構的（tectonic）變成作用をも與へずに濟み，之等の岩石中には壓碎構造も大規模に與へずに終つたと解釋できる．

以上の如く考察するとこの地方の SS 斷層の兩側の地質構造發達史は第 4 表の如く表示できる．

結　　語

斯してこゝに再び本論文の冒頭に述べた諸問題に就いて檢討を試みてみやう．先づ

1．地形上の問題である．岡山氏は切峯面の研究から甲斐駒ヶ岳東側の急斜面が韮崎町方面へ續く事を指摘したが，筆者は少くともその急斜面の麓の一部に麓の段丘を推し被せてゐる低角度の斷層が存在することを發見することができた．即ちこの急斜面は推し被せ斷層等の地質構造上の原因に基くもので單なる侵蝕崖でないことが明となつた．矢部博士の鹽尻――韮崎線の少くともその南半は斯の如き低角度の斷層に基く地形に據られたものではあるまいか．

又岡山氏の研究により明な如く藪の湯より千頭星山・辻山間を經て早川に沿う大地形上の一線は明に前記鹽尻―靜岡斷層線に沿う線と一致することが確められた．併しこの一致も南方に至れば地形上の線は地質上のこの斷層線から離れてゐる．

2．層序上の問題に就いては既に述べた通，*Lepidocyclina japonica* を含んだ黑色の泥岩が火山碎屑岩からなる櫛形山層の下に横つてゐる．之は筆者が *Lepidocyclina* を含む地層を幌內時代の堆積物とした推論に一つの資料を加へたこととなつた．

3．地質構造上の問題．糸魚川――駿東地質構造線の問題は別として，鹽尻――靜岡線の位置を決定し，鹽尻――韮崎の線から區別することができた．又鹽尻――靜岡線成立以前の地質構造線の存在を推定し，之を後桃ノ木及び鳳凰山――安倍川の兩構造線に分けて說明した．又之等の三構造線の兩側に於ける地質構造上の發達史を推定した．

4．深成火成岩は國井石英閃綠岩・鳳凰山花崗岩・燒地藏深成岩に分たれ，鳳凰山・燒地藏兩深成岩體は斷層線の西側の地域に屬することが明かとなつた．

本稿を草するに當つて種々の御批判を得た津屋弘逵博士，又地質學會講演會にて本稿を發表した時に熱心に御討議下さつた久野久助教授，小出博學士に深く謝意を表す．

久野・小出兩氏は燒地藏深成岩を一種の migmatite にして,之を貫く鳳凰山花崗岩の vein を aplitic vein にあらずやと述べられたが，小出氏は筆者の標本・薄片により親切な多くの教示を示されつゝ筆者の說に贊成された.

杉山學士は井尻學士を通じて，種々壓碎岩石に就いて教示され，燒地藏深成岩體は氏がよく研究されてゐる鹿鹽片麻岩と類似の條件の下に出來た岩石であらうと述べられた.

野外調査に協力された井尻學士は筆者と全く別な深成岩の構造發達史を考へてをられる．卽ち桃ノ木層堆積時代より古く鳳凰山花崗岩體の迸入を考へられ，次に桃ノ木層堆積後に巨摩玢岩の迸入があり，この玢岩からヘレフリンタが生じ，最後に燒地藏花崗岩の噴出があつたと解してをられる．之も亦極めて興味ある一解釋であるのでこゝに記して後の批判に待つことゝした．この說の重要な點は玢岩がヘレフリンタ狀岩石に變じたとする解釋に出發してゐる點で，その重要な露頭を筆者は遺憾ながら未だ見てゐない．筆者は玢岩類が凝固結晶作用の最後の狀態である熱水作用による曹長石化作用及びプロピライト化作用を受けてはゐても壓碎作用の證が殆どないこととヘレフリンタ狀岩石の分布・野外の觀察等上述した諸事實から本論に記載した如き結論に達したものであることをこゝに附記しておく．深く討議された諸氏に御禮をする.

本研究は文部省科學研究費及び日本學術振興會の援助に依りて行つたものであることを述べこゝに深く謝意を表する.

---

9. *Geology of Mt. Zizô and Hôô, Yamanasi Prefecture, Japan.*

By Yanosuke OTUKA,

Earthquake Research Institute.

In this paper, the writer describes the geology of Mt. Zizô and Hôô, in the western part of Yamanasi prefecture. Because the Omati-Sizuoka (formerly Itoigawa-Sizuoka) tectonic line, which transversely divides the island of Honsyû into two parts, runs along the eastern foot of these mountains, a study of the geologic structure of this district is of tectonical interest.

The strata and igneous rocks of this region in descending order are as follows:

1. The Quaternary.
   a. The Alluvium.
   b. The gravel beds of terraces.
   c. The Nakayama pyroxene andesite mass.

2. The Neogene.
   a. The Tuburai acidic plutonic mass (Quartz diorite).
   b. The Koma igneous mass (Porphyrite and other hypabyssal igneous rocks).

第 15 圖 *Miogypsina ozawai* HANZAWA.

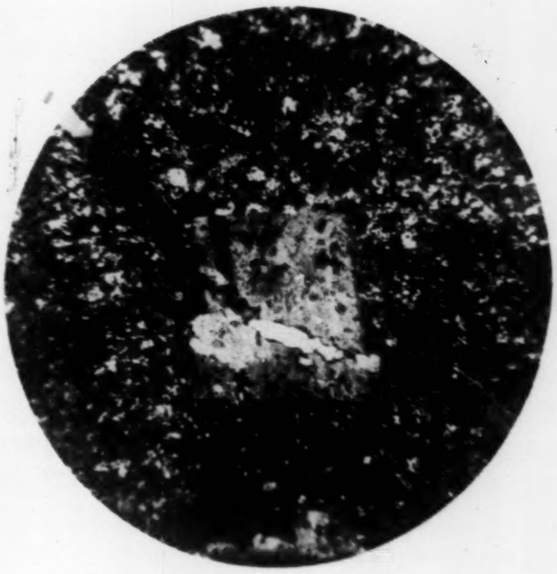

第 13 圖 曹長石化作用を受けた石英玢岩.
(薄片 c. 63. 第11圖 Loc. 165 の北 250 m.)

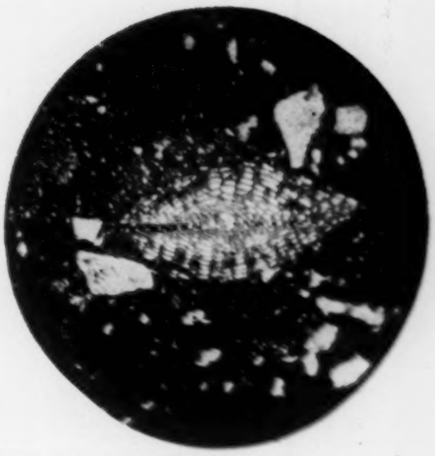

第 16 圖 *Lepidocyclina japonica* YABE.

第 14 圖 圓井石英閃緑岩、多少曹長石化作用
を受けてゐる.
(薄片 c. 48. 上圓井).

第 17 圖 *Cycloclypeus* sp.

(震研彙報 第十九號 圖版 大塚)

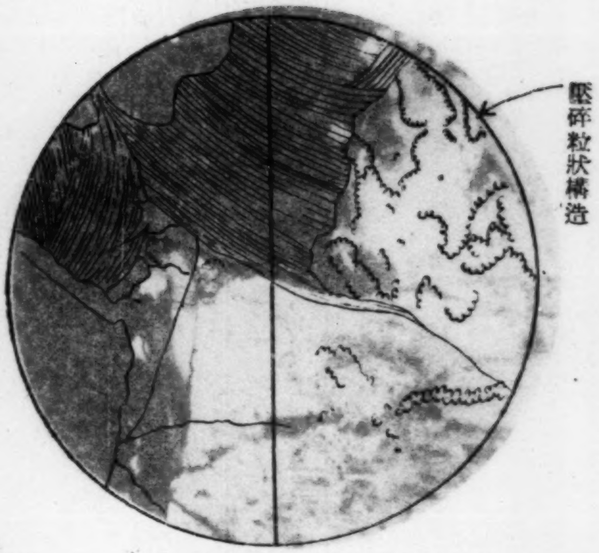

第 18 圖 鳳凰山花崗岩の壓碎化を示す.
(薄片 c. 66. 第 11 圖 Loc. 167, ドンドコ澤.)

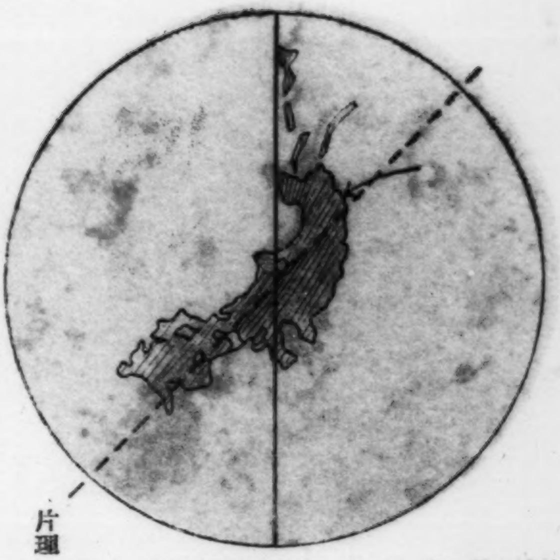

第 21 圖 第 19 圖に同じ. ヘイスチングスは
粒間を占め壓碎されてゐない.

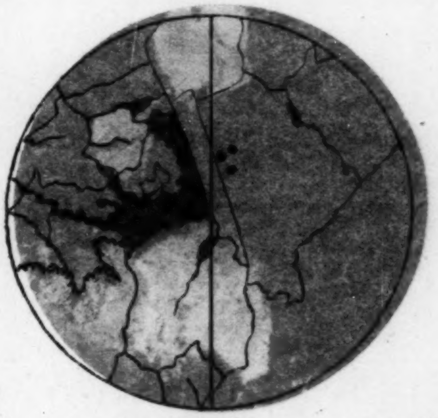

第 19 圖 含雲母ヘイスチングス花崗岩.
(薄片 c. 45. 辻山燒地藏附近.)

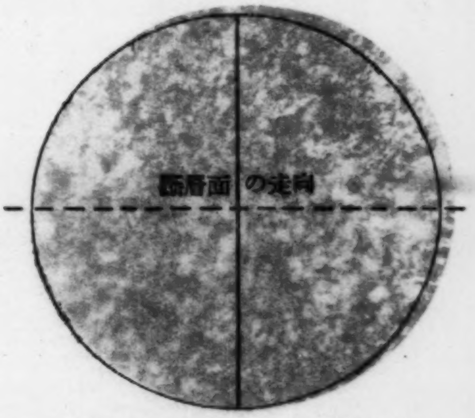

第 22 圖 ヘレフリンタ様壓碎岩.
(薄片 c. [illegible]. 第7圖 L.c. 186.)

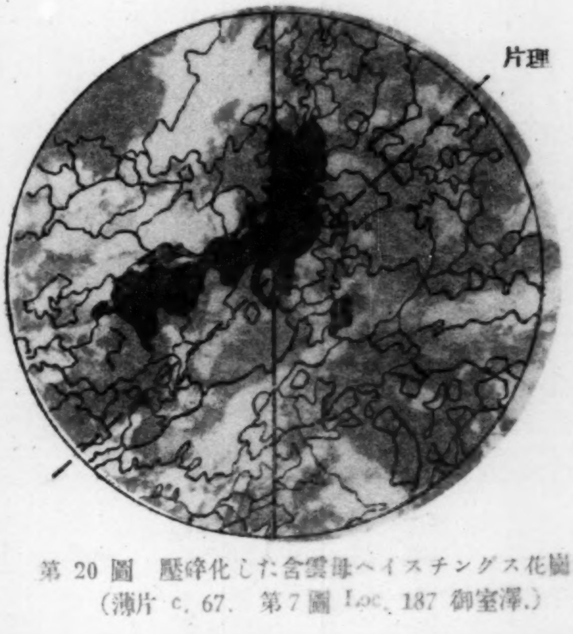

第 20 圖 壓碎化した含雲母ヘイスチングス花崗岩.
(薄片 c. 67. 第7圖 Loc. 187 御室澤.)

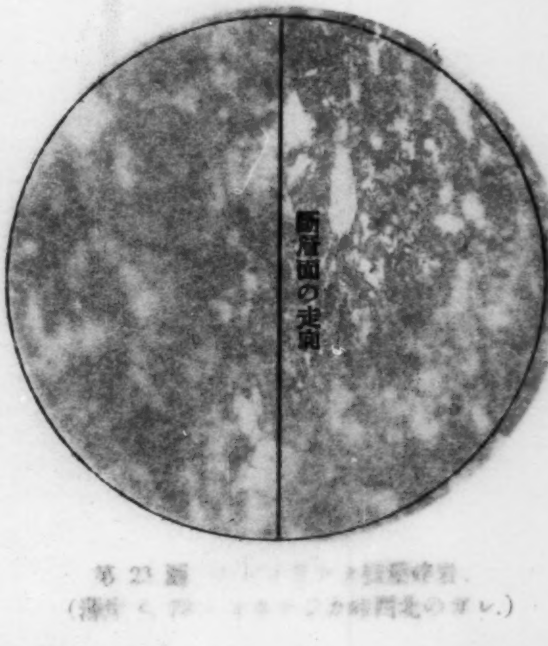

第 23 圖 ヘレフリンタ様壓碎岩.
(薄片 c. [illegible] [illegible]か崎岡北のズレ.)

震研彙報 第十九號 大塚

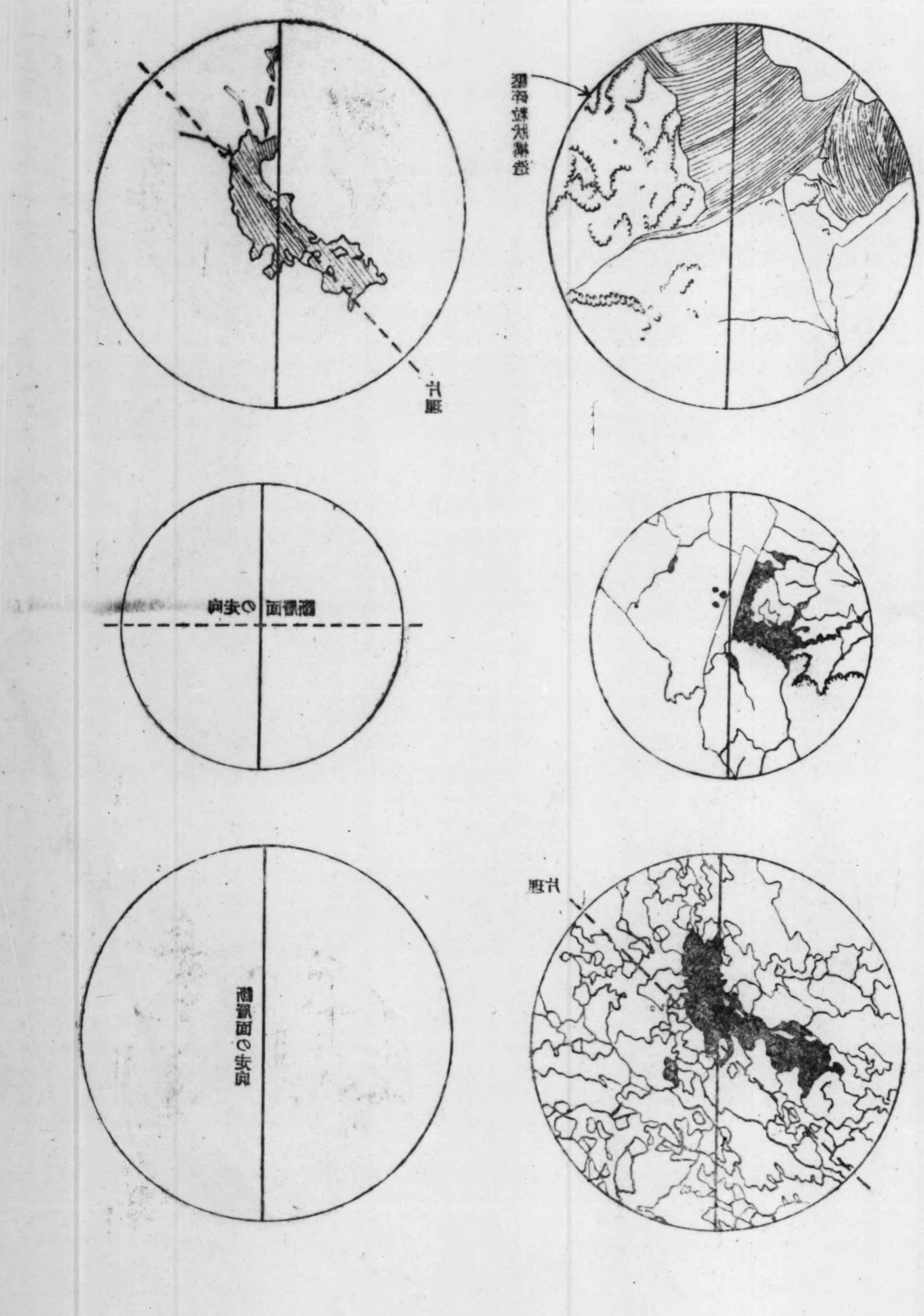

片理
斷層面の走向
斷層面の走向
片理

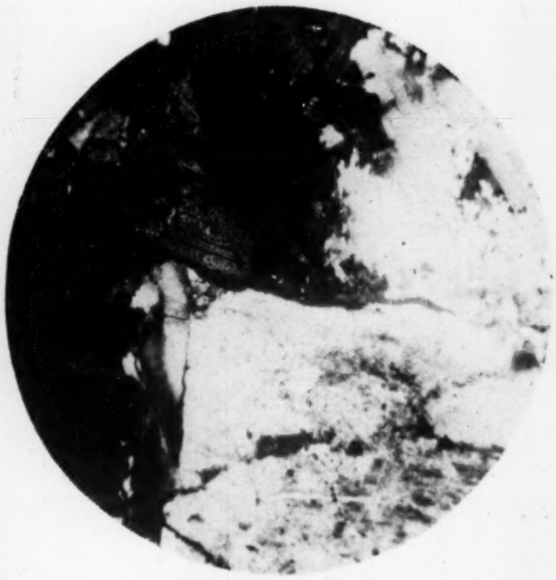

第 18 圖 鳳凰山花崗岩の壓碎化を示す.
(薄片 c. 66. 第 11 圖 Loc. 167, ドンドコ澤.)

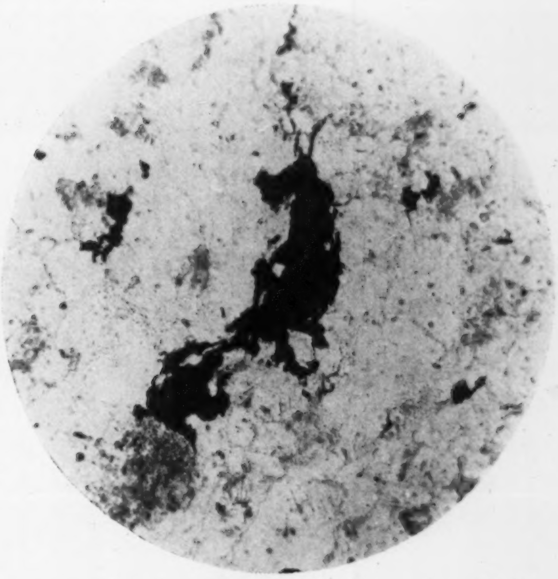

第 21 圖 第 19 圖に同じ. ヘイスチングスは
粒間を占め壓碎されてゐない.

第 19 圖 含雲母ヘイスチングス花崗岩.
(薄片 c. 45. 辻山燒地藏附近.)

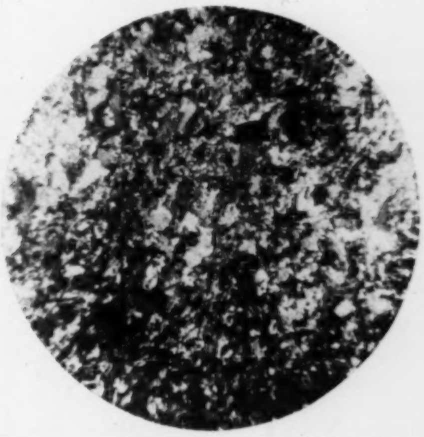

第 22 圖 ヘレフリンタ様壓碎岩.
(薄片 c. 67. 第 7 圖 Loc. 186.)

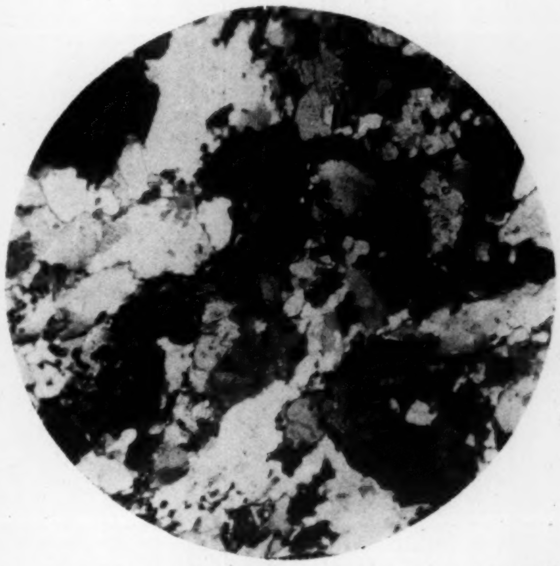

第 20 圖 壓碎化した含雲母ヘイスチングス花崗岩.
(薄片 c. 67. 第 7 圖 Loc. 187 御室澤.)

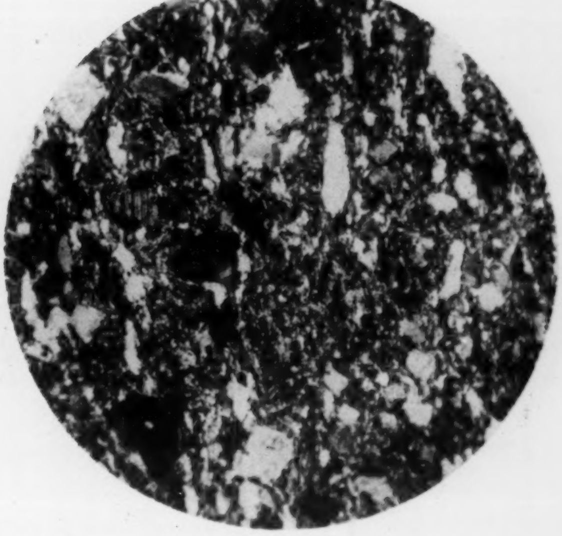

第 23 圖 ヘレフリンタ様壓碎岩.
(薄片 c. 78. オホナジカ峠西北のガレ.)

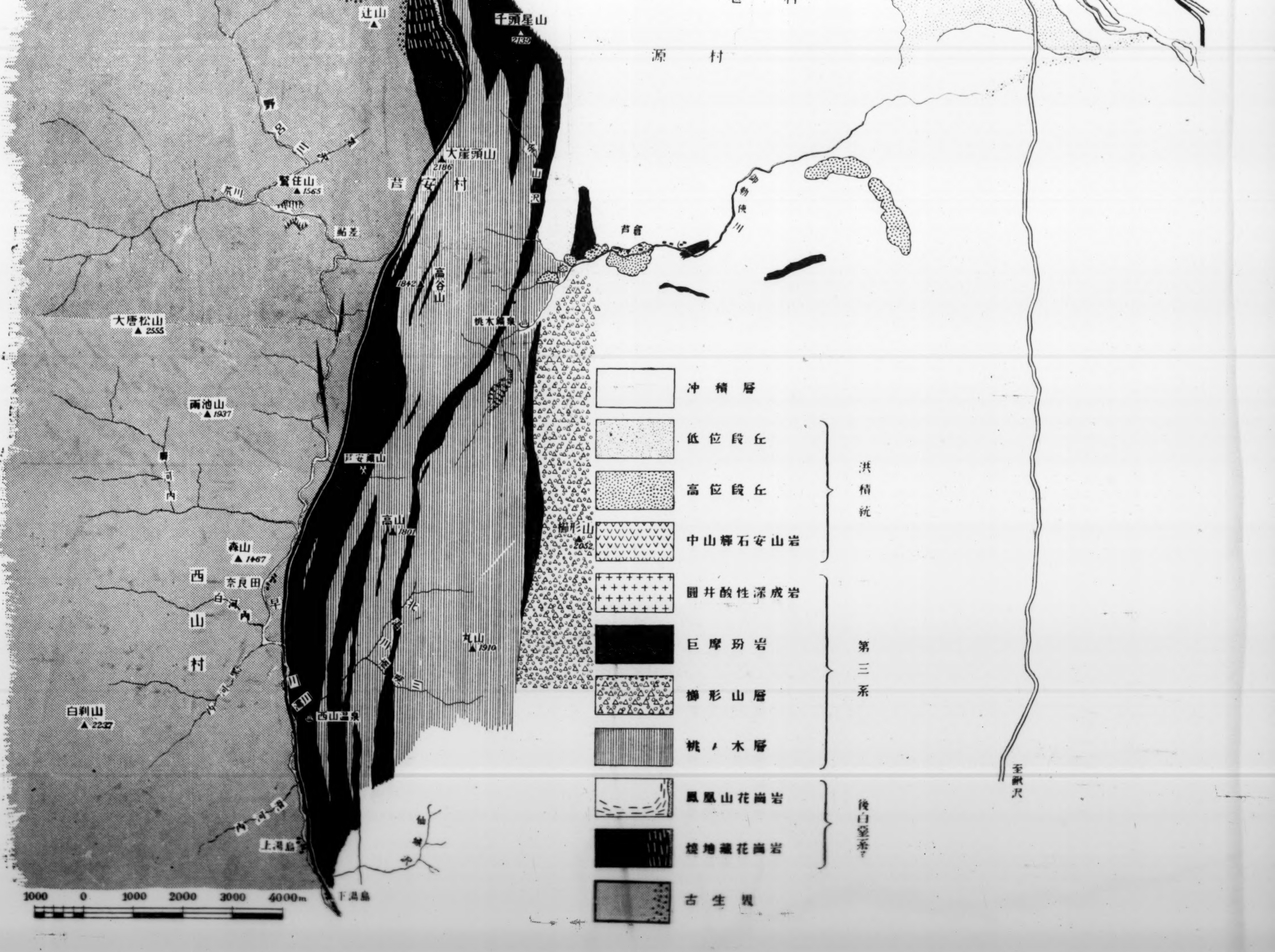

千頭星山 2139
辻山
源村
野呂川
大崖頭山 2186
芦安村
鷲住山 1565
荒川
鮎差
高谷山 1842
大唐松山 2555
桃木鑛泉
両池山 1937
芦安鑛山
河内
高山 1801
櫛形山 2052
森山 1467
奈良田
早川
西山村
白河内
丸山 1910
西山温泉
白剥山 2237
上湯島
下湯島
芦倉
至鰍沢
1000 0 1000 2000 3000 4000m
冲積層
低位段丘
高位段丘
中山釋石安山岩
洪積統
圓井酸性深成岩
巨摩玢岩
櫛形山層
桃ノ木層
第三系
鳳凰山花崗岩
燒地藏花崗岩
後白堊系?
古生層

[Bull. Earthq. Res. Inst., Vol. XIX, Pl. V.]

鳳凰山附近地質圖

第 24 圖

c. The Kusigatayama pyroclastic formation.
d. The Momonoki sandy mudstone formation (containing *Lepidocyclina japonica*).

3. Pre-Neogene (or Pre-Momonoki formations).

a. The Hôôzan plutonic mass (Hornblende biotite granite).
b. The Yakezizô plutonic mass (Biotite hastingsite granite).
c. The so-called Titibu Palaeozoic formations.

The conclusion is that there are, at least, three main tectonic activities along this Ômati-Sizuoka tectonic line.

The relations of these tectonic disturbances to the deformation of the strata and intrusion of the igneous rocks that are exposed on each side of this tectonic line are given below.

Recent tectonic division	Akaisi "Sphenoid"		"Fossa Magna"	Kantô mountainland
		Tertiary activities [Formation of SS tectonic line]		
Neogene			Intrusion of quartz diorite	Intrusion of quartz diorite
		Secondary activities [Formation of Post-Momonoki tectonic line]	Intrusion of Koma porphyrite etc.	
			Deposition of Kusigatayama formation	
			Deposition of Momonoki formation	
Palaeogene	Intrusion of Hôôzan plutonic mass	Primary activities [Formation of HA tectonic line]	Intrusion of Syôsenkyô and Kinpusan plutonic mass	
	Formation of "Hälleflinta"-like mylonite			
	Intrusion of Yakezizô plutonic mass			
	(Separation of Akaisi sphenoid)		(Completion of basal structure of Kanto mountainland)	
Mesozoic & Palaeozoic	Setogawa series (of Y. Chitani) Palaeozoic formation		(Completion of zonal arrangement of the Outer zone of S.W. Japan)	

*10. Characteristics of Deposits formed by Pumice Flows and Those by Ejected Pumice**.

By Hisashi KUNO,

Geological Institute, Tokyo Imperial University.

(Read March 14 th, 1940.—Received Dec. 20 th, 1940.)

Introduction.

The eruption of Komaga-take, Hokkaidô, in 1929, brought to light two different ways in which pumice is deposited, one as the result of pumice flows, and the other as the result of showers of ejected pumice. These two kinds of pumice deposits have each their own distinctive characters, as seen in their surface features and in their internal structure. The Recent and Pleistocene pumice beds of Hakone, Huzi, Asama, and Haruna, all in central Japan, exhibit the same features as those of Komaga-take. This paper is an attempt to describe the observed differences in the two kinds of pumice beds that are specially responsible to their modes of deposition.

The writer wishes to tender his cordial thanks to Professor Seitarô Tsuboi for his kindness in reviewing this manuscript. His thanks are also due to Assistant Professor Tosio Isikawa, of the Geological and Mineralogical Department, Hokkaidô Imperial University, for numerous courtesies extended to the writer in connexion with his trip to Komaga-take. He also acknowledges the grant from the Government Expenditure for Scientific Research, a part of which was used for the present study.

The Pumice Deposits of Komaga-take.

During the eruption of this volcano in 1929, large quantities of andesitic pumice were ejected from the summit crater. Some of the pumiceous ejecta that was thrown high above the crater, was wafted by the wind and rained on the southeastern and eastern slopes of the cone, where they accumulated and formed extensive beds, while some that fell near the crater rim, without accumulating there owing to the steepness of the slope, rolled down the flank as pumice flows. Three major flows were recognized, namely, the northern, western, and southwestern, all of which spread into fans of pumiceous debris, widening

* Dedicated to the late Professor Mishio ISHIMOTO.

out toward the foot of the volcano.

These phenomena have been already described by previous authors who studied the activity of this volcano.[1]

At the time of the writer's visit to the volcano in September 1939, these pumice deposits were traversed by the numerous gullies that had formed during a decade of erosion, along the bottoms of which could be seen the pre-1929 ejecta. These exposures enabled the writer to examine cross sections of the pumice deposits. He studied the pumice beds that cover the southeastern slope, and also the deposits of the western and the southwestern pumice flows (the Osidasi-zawa or Osiranai pumice flow, and the Goban-zawa or Akaigawa pumice flow respectively).

Distinctive Characters of the Deposits.

(I) The surface of the deposits formed by the ejected pumice is quite even throughout (Fig. 1), the minor undulations of the old topography having been smoothed out by accumulation of the pumice. In contrast to this, the surface of the debris of the pumice flows is greatly undulated;[2] a number of primary grooves and ridges being developed parallel to the direction of flow (Figs. 4, 5, and 6). The ridges, which usually stand from about 0·5 to 1 m above the bottom of the grooves, consist largely of coarse fragments (Figs. 4, 5, and 6),—a feature recalling the surface of the debris of some snow avalanches.

(II) The ejected pumice was accumulated so extensively that all traces of the pre-existing topography were erased, only the precipitous slopes escaping the mantle of the pumice. In the case of the pumice flows, however, the tendency to stream down along the lower parts of the pre-existing topography was so strong that even the small ridges and hills of the older lavas and ejecta stand above the surface of the flows. The pumice flows that came to cliffs simply cascaded down them.

(III) The variation in grain-size of the pumice fragments with distance from the crater is a feature that is not likely to be overlooked by any observer who traverses the devastated area of Komaga-take. In the deposits formed by the ejected pumice, the size of the pumice fragments increases as one approaches the crater. Thus, at Sin-ogawa, 6 km southeast of the crater, the average size of the grains is some-

1) H. TSUYA, *B. E. R. I.*, **8** (1930), 238~270.
S. KÔZU, *Tscherm. Min. Petr. Mitt.*, **45** (1934), 133~174.

2) On account of this feature, the areas covered by the debris of the pumice flows make walking difficult, in contrast to that covered by the ejected pumice, where the walking is easy.

what less than 10 cm (Fig. 2), near the triangulation point 244·8 m high, 4 km southeast of the crater, it is about 10 cm, and at an elevation of 500 m, 2 km eastsoutheast of the crater, it is about 30 cm. Moreover, within limited areas, the grain-size is fairly uniform, laterally and vertically. In the pumice flows, on the contrary, scarcely any regularity is to be noted in the variation in grain-size with distance from the crater, nor is there any uniformity in grain-size within limited areas. A distinct tendency is however noted for the coarser fragments to concentrate in the narrow ridges, as already mentioned, and also toward the end of each flow, where it often terminates in a steep front just as in the cases of certain block lavas and avalanche debris. Thus, at the end of the Osidasi-zawa pumice flow, 4 km northwest of the crater, pumice fragments 0·5∼0·3 m large were found almost to the exclusion of finer grains. Such contrast is best seen along the east-west trail in the southern flank of the cone, which crosses the boundary that separates the two different deposits 4 km distant from the crater.

(IV) The variation in thickness of the deposits with distance from the crater runs somewhat parallel to the variation in grain-size just mentioned. The thickness of the deposits formed by the ejected pumice gradually increases as one approaches the crater. Thus, at Sin-ogawa, the general thickness is about 0·3 m, while it becomes about 0·5 m near the triangulation point, 244·8 m high; and about 2 m at an elevation of 500 m. In the pumice flows, however, the maximum thickness is attained at a certain point near the end of each flow, and also just below the cliffs of the older rocks over which the pumice flows cascaded. The maximum thickness of the Goban-zawa pumice flow is at least 2 m, while that of the Osidasi-zawa flow is about 4 m.

(V) The virtual absence or paucity of the finer particles that cement the coarser fragments, is one of the characteristics of the deposits formed by the ejected pumice. The interstices between the fragments are usually empty spaces without any filling of foreign matter (Fig. 2). In the pumice flows, on the other hand, there are abundant fine particles that cement the coarser fragments, except at the tops of the flows (Figs. 3, 4, and 6), and also in some distinct zones, along which the coarser fragments are concentrated. The cement is always the finely divided particles of the pumice itself, usually of sand size. The proportion of this cement varies greatly in different layers within a flow (Fig. 6), some layers being made up almost exclusively of fine particles.

The most probable explanation of this contrast in feature is that, in the pumice flows, a large quantity of fine particles were formed by attrition of the pumice fragments as they rolled down the flank, while

in the ejected pumice, sorting of the grain by size was accomplished so completely during its flight through the air that the finer particles, if they were present, were transported for longer distances from the crater than the coarser fragments.

However, this distinctive character is not evident in the vicinity of the crater, because the ejected pumice that accumulated there was mixed wth a large proportion of fine particles.

(VI) The way in which the deposits are stratified differs markedly with their modes of origin. The deposits formed by the ejected pumice show regular stratification according to slight differences in size of the fragments in different layers. The strata continue fairly even as far as they are visible from any particular point. In great contrast to this is the irregular and indistinct stratification one sees in the deposits of the pumice flows. Generally speaking, they show a chaotic structure owing to the haphazard mixture of fragments varying widely in size (Fig. 6). Any particular layer is always interrupted when traced laterally for some distance. Again, some of the layers, consisting of more or less uniformly sized fragments, either thin out laterally or pass into an unstratified mass because of intermixture of fragments of different size (Fig. 7 a). However, some layers, which are chiefly made up of finely divided particles, contain somewhat coarser fragments arranged in ill-defined zones parallel to the general bedding (Fig. 7 b). It is not-

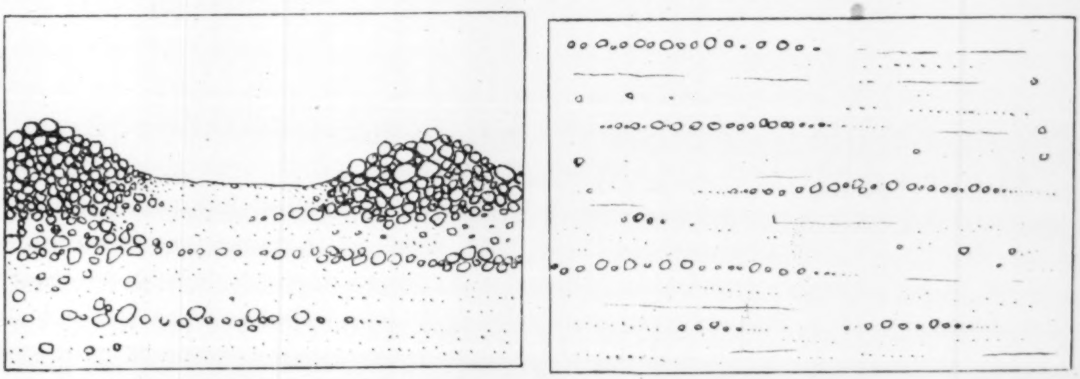

a b

Fig. 7. Cross sections of the deposits of the pumice flows of Komaga-take.

able that lenticular masses or bands, consisting largely of accessory fragments of compact andesite, are often intercalated between the deposits—a feature entirely lacking in the deposits of the ejected pumice.

The origin of the structures of these pumice flow deposits above described may be attributed to differential movements of a number of streams within each pumice flow, overlapping one another or merging the one into the other. Obviously, the differential movements are the

result of differences in the grain-size of the components that formed the pumice flows. The coarser fragments, which moved faster than the finer, were collected together to form narrow streams that deposited in the form of ridges (see p. 145). The accessory fragments, which form the lenticular masses already mentioned, were probably torn away from the bed-rocks that were exposed along the courses of the pumice flows.

Pumice Deposits of Hakone, Huzi, Asama, and Haruna.

In Hakone volcano, there are deposits which are believed to have been formed by pumice flows[3] (Fig. 8). These deposits, which are of Younger Pleistocene age, have much greater lateral and vertical extensions than those of Komaga-take. Deposits which are inferred as having been formed by ejected pumice are also found here.

In the adjacent Huzi volcano, lying northwest of Hakone, dacite pumice and basalt scoriae were ejected from the Hôei explosion crater in 1707,[4] a new crater that opened at the time on the southeastern flank of the cone. These ejecta rained on the eastern area. The regularly bedded deposits, consisting of dacite pumice at the base and basalt scoriae at the top, are extensively developed from the southern part of the Tanzawa Mountainland to the northern flank of Hakone.

Excellent examples of deposits formed by ejected pumice are also found in the Asama and Haruna volcanoes. In the former volcano, andesitic pumice that was ejected in 1783 from the summit crater,[5] accumulated on the mountainous land east of the cone. The deposits are well observed at various points to the north of the town of Karuisawa (Figs. 9 and 10). In the latter volcano, which lies about 30 km eastnortheast of the former, dacitic pumice was ejected from the crater that opened in the eastern part of the cone at a relatively younger period of its history[6] (probably Holocene). These deposits, which covered the eastern half of the volcano, are seen well developed around the town of Ikaho.

Although the surface features of the pumice deposits of these volcanoes are somewhat obliterated by weathering and vegetation, their internal structures can be studied from a number of exposed sections.

3) Inferred from the distribution of the deposits and their relation to the underlying topography. H. KUNO: *Jour. Geol. Soc. Japan*, **45** (1938), 493; *Proc. 6 th Pacific Science Congress*. (California), 1939, 875.

4) Oral communication by H. TSUYA.

5) H. TSUYA, *Geography* (Tirigaku), **2** (1934), 25.

6) S. TANEDA, a paper read before the 47 th annual meeting of the Geological Society of Japan, 1940.

Fig. 1. Cross section of a deposit of ejected pumice. The eastern flank of Komaga-take.

Fig. 2. Cross section of a deposit of ejected pumice. Near Sin-ogawa, the southeastern foot of Komaga-take.

Fig. 3. Cross section of a deposit of pumice flow. Goban-zawa, the southwestern flank of Komaga-take.

Fig. 4. The surface of a deposit of pumice flow. Goban-zawa, the southwestern flank of Komaga-take.

Fig. 5. The surface of a deposit of pumice flow. Goban-zawa, the southwestern flank of Komaga-take.

Fig. 6. Cross section of a deposit of pumice flow. Osidasi-zawa, the western flank of Komaga-take.

(震研彙報 第十九號 圖版 久野)

Fig. 8. Cross section of a deposit of pumice flow. South of Yamakita-mati, north-eastern foot of Hakone.

Fig. 9. Cross section of a deposit of ejected pumice (1783). Near Kose, east of Asama.

Fig. 10. Cross section of a deposit of ejected pumice (1783). Near Kose, east of Asama.

The structural similarity of the pumice flow deposits of Hakone to those of Komaga-take, and that of the deposits of the ejected pumice of Hakone, Huzi, Asama, and Haruna to those of Komaga-take are so marked that there is no need to describe the deposits of these central Japanese volcanoes.

Conclusion.

Based on observations of the Komaga-take volcano, the distinctive characters of the deposits of the pumice flows and those formed by the ejected pumice that rained on the ground are described ((I)～(VI), pp. 145～147). These distinctive characters are explained as the results of the particular ways in which they were deposited. The deposits formed by pumice flows and those by ejected pumice of some volcanoes in central Japan exhibit the same contrast in features that exists between the two different kinds of deposits of Komagatake. These characteristics form useful criteria for determining the mode of deposition of some pumice deposits. For deposits that are either only partly preserved or are somewhat disturbed, as may occur in those of Tertiary and still older ages, the characteristics described in (V) and (VI) appear to be especially useful in distinguishing their mode of deposition.

---

10. 輕石流堆積物と拋出輕石堆積物との差異に就いて

地質學教室 久野 久

昭和4年北海道駒ヶ岳火山噴火の際，拋出された輕石の一部は風で運ばれて，火山體の東南斜面に廣く堆積し，他の一部は北方・西方・西南方に斜面を流下して輕石流を形成し，火山體の麓に扇狀の堆積物を生じた．之等2種の堆積物の各々には，その表面の性質並びに內部構造に於いて明瞭な差異が認められる．之等の差異は其等堆積物の堆積機構の相異によつて生じたものと說明される．

箱根・富士・淺間・榛名等の諸火山の輕石堆積物も，駒ヶ岳に於けるものと全く同樣な性質を有する．此等の特徵に基けば，或種の輕石層の堆積機構を推定する事も可能である．

11. Transmission of Arbitrary Elastic Waves from a Spherical Source, Solved with Operational Calculus. I.

By Katsutada SEZAWA and Kiyoshi KANAI,

Earthquake Research Institute.

(Read Feb. 20, 1941.—Received March 20, 1941.)

1. *Introduction.*

The problem of transmission of arbitrary elastic waves generated from a spherical source, oscillating spheroidally, has been discussed by a number of investigators, for example, Kawasumi, Yosiyama, Nishimura, Sezawa, Kanai, and many others. Since the methods used by them were almost related to Fourier's double integrals, the calculations were rather complex, with the liklihood that the problems themselves would be limited to a few special cases. The recent development of the operational calculus, based on Laplace's transformation of integrals, enabled us to solve the problem in question more readily and to a much wider extent than here to fore. The relatively simple cases that have been solved will be shown in the present paper.

2. *General discussion of the problem.*

The equations of motion of elastic waves that radiate outward from a spherical source are

$$\left.\begin{aligned}\frac{\rho}{\lambda+2\mu}\frac{\partial^2\Delta}{\partial t^2}&=\frac{\partial^2\Delta}{\partial r^2}+\frac{2}{r}\frac{\partial\Delta}{\partial r}+\frac{1}{r^2}\frac{\partial^2\Delta}{\partial\theta^2}+\frac{1}{r^2}\frac{\partial\Delta}{\partial\theta}\cot\theta,\\ \frac{\rho}{\mu}\frac{\partial^2\varpi}{\partial t^2}&=\frac{\partial^2\varpi}{\partial r^2}+\frac{2}{r}\frac{\partial\varpi}{\partial r}+\frac{1}{r^2}\frac{\partial^2\varpi}{\partial\theta^2}+\frac{1}{r^2}\frac{\partial\varpi}{\partial\theta}\cot\theta-\frac{\varpi}{r^2}(1+\cot^2\theta),\end{aligned}\right\}\qquad(1)$$

for dilatational waves and distortional waves, respectively, Δ, ϖ being

$$\left.\begin{aligned}\Delta&=\frac{\partial u}{\partial r}+\frac{2u}{r}+\frac{1}{r}\frac{\partial v}{\partial\theta}+\frac{v}{r}\cot\theta,\\ 2\varpi&=\frac{\partial v}{\partial r}+\frac{v}{r}-\frac{1}{r}\frac{\partial u}{\partial\theta}.\end{aligned}\right\}\qquad(2)$$

For solving the problem operationally, we write

$$\Delta=\frac{1}{2\pi i}\int_{c-i\infty}^{c+i\infty}\frac{e^{zt}\phi}{z}dz,\quad 2\varpi=\frac{1}{2\pi i}\int_{c-i\infty}^{c+i\infty}\frac{e^{zt}\psi}{z}dz, \tag{3}$$

where ϕ, ψ are functions of z and the integral $\int_{c-i\infty}^{c+i\infty}$ indicates the Bromwich-Wagner's integral in the complex z-plane. Substituting (3) in (1), we get

$$\left.\begin{aligned}&\frac{\partial^2\phi}{\partial r^2}+\frac{2}{r}\frac{\partial\phi}{\partial r}+\frac{1}{r^2}\frac{\partial^2\phi}{\partial\theta^2}+\frac{1}{r^2}\frac{\partial\phi}{\partial\theta}\cot\theta-\frac{\rho}{\lambda+2\mu}z^2\phi=0,\\&\frac{\partial^2\psi}{\partial r^2}+\frac{2}{r}\frac{\partial\psi}{\partial r}+\frac{1}{r^2}\frac{\partial^2\psi}{\partial\theta^2}+\frac{1}{r^2}\frac{\partial\psi}{\partial\theta}\cot\theta-\frac{\psi}{r^2}(1+\cot^2\theta)-\frac{\rho}{\mu}z^2\psi=0,\end{aligned}\right\} \tag{4}$$

from which

$$\phi=A_n\frac{H^{(1)}_{n+1/2}(izrc_1)}{\sqrt{r}}P_n(\cos\theta),\quad \psi=B_n\frac{H^{(1)}_{n+1/2}(izrc_2)}{\sqrt{r}}\frac{dP_n(\cos\theta)}{d\theta}, \tag{5}$$

where $c_1=\sqrt{\rho/(\lambda+2\mu)}$, $c_2=\sqrt{\rho/\mu}$. The values of A_n, B_n are still arbitrary. Using the results in (3), it is possible to write

$$\left.\begin{aligned}u_1&=\frac{1}{2\pi i}\int_{c-i\infty}^{c+i\infty}\frac{e^{zt}dz}{z}\frac{A_n}{z^2c_1^2}\frac{d}{dr}\frac{H^{(1)}_{n+1/2}(izrc_1)}{\sqrt{r}}P_n(\cos\theta),\\v_1&=\frac{1}{2\pi i}\int_{c-i\infty}^{c+i\infty}\frac{e^{zt}dz}{z}\frac{A_n}{z^2c_1^2}\frac{H^{(1)}_{n+1/2}(izrc_1)}{r^{3/2}}\frac{dP_n(\cos\theta)}{d\theta},\\u_2&=\frac{1}{2\pi i}\int_{c-i\infty}^{c+i\infty}\frac{e^{zt}dz}{z}\frac{n(n+1)B_n}{z^2c_2^2}\frac{H^{(1)}_{n+1/2}(izrc_2)}{r^{3/2}}P_n(\cos\theta),\\v_2&=\frac{1}{2\pi i}\int_{c-i\infty}^{c+i\infty}\frac{e^{zt}dz}{z}\frac{B_n}{z^2c_2^2}\frac{1}{r}\frac{d}{dr}\left\{\sqrt{r}\,H^{(1)}_{n+1/2}(izrc_2)\right\}\frac{dP_n(\cos\theta)}{d\theta}.\end{aligned}\right\} \tag{6}$$

The values of A_n, B_n can be determined by using the conditions at the spherical source. Let the tangential stress at the spherical source, $r=a$, be zero and the normal stress there be distributed spheroidally, but changing with time in the form $f(t)$. It is then possible to write

$$\mu\left(\frac{\partial v}{\partial r}-\frac{v}{r}+\frac{1}{r}\frac{\partial u}{\partial\theta}\right)=0, \tag{7}$$

$$\lambda\Delta+2\mu\frac{\partial u}{\partial r}=P_n(\cos\theta)f(t), \tag{8}$$

at $r=a$, where $u=u_1+u_2$, $v=v_1+v_2$.

Since from Mellin's theorem, on the other hand, the function $f(t)$ may be expressed by

$$f(t)=\frac{1}{2\pi i}\int_{c-i\infty}^{c+i\infty}\frac{e^{zt}}{z}g(z)dz, \tag{9}$$

where $g(z)$ is the operational form of $f(t)$, that is to say,

$$g(z)=z\int_0^{\infty}e^{-zt}f(t)dt\ ^{1),2)}, \tag{10}$$

it is possible to write

$$\left(\lambda\Delta+2\mu\frac{\partial u}{\partial r}\right)_{r=a}=\frac{P_n(\cos\theta)}{2\pi i}\int_{c-i\infty}^{c+i\infty}\frac{e^{zt}}{z}g(z)dz. \tag{11}$$

Substituting (3), (6) in (7), (11), we get

$$B_n=\left(\frac{\lambda+2\mu}{\mu}\right)\frac{\Psi}{\Phi}A_n, \tag{12}$$

$$(\widehat{rr}_{r=a}=)\frac{P_n(\cos\theta)}{2\pi i}\int_{c-i\infty}^{c+i\infty}\frac{e^{zt}A_n}{z}\Omega dz=\frac{P_n(\cos\theta)}{2\pi i}\int_{c-i\infty}^{c+i\infty}\frac{e^{zt}}{z}g(z)dz, \tag{13}$$

where

$$\left.\begin{aligned}\Psi&=\frac{d}{da}\left\{\frac{H^{(1)}_{n+1/2}(izac_1)}{a^{3/2}}\right\}-\frac{H^{(1)}_{n+1/2}(izac_1)}{a^{5/2}}+\frac{1}{a}\frac{d}{da}\frac{H^{(1)}_{n+1/2}(izac_1)}{\sqrt{a}},\\ \Phi&=-\frac{d}{da}\left\{\frac{1}{a}\frac{d}{da}\left(\sqrt{a}\,H^{(1)}_{n+1/2}(izac_2)\right)\right\}+\frac{1}{a^2}\frac{d}{da}\left\{\sqrt{a}\,H^{(1)}_{n+1/2}(izac_2)\right\}\\ &\qquad-\frac{n(n+1)}{a}\frac{H^{(1)}_{n+1/2}(izac_2)}{a^{3/2}},\end{aligned}\right\} \tag{14}$$

$$\Omega=\frac{\lambda H^{(1)}_{n+1/2}(izrc_1)}{\sqrt{r}}+2\mu\frac{d}{dr}\left\{\frac{1}{z^2c_1^2}\frac{d}{dr}\frac{H^{(1)}_{n+1/2}(izrc_1)}{\sqrt{r}}\right.$$
$$\left.+\frac{n(n+1)}{z^2c_2^2}\frac{H^{(1)}_{n+1/2}(izrc_2)}{r^{3/2}}\left(\frac{\lambda+2\mu}{\mu}\right)\frac{\Psi}{\Phi}\right\}. \tag{15}$$

Thus, from (13) it is possible to write

$$A_n\doteq g(z)\frac{1}{\Omega}. \tag{16}$$

Substituting (16), (12) in (3), (6), we have

1) N. W. McLachlan, *Complex Variable and Operational Calculus* (Cambridge, 1939).

2) K. W. Wagner, *Operatorenrechnung* (Leipzig, 1940).

$$\Delta=\frac{1}{2\pi i}\int_{c-i\infty}^{c+i\infty}\frac{e^{zt}}{z}g(z)\frac{1}{\Omega}\frac{H^{(1)}_{n+1/2}(izrc_1)}{\sqrt{r}}P_n(\cos\theta)\,dz \tag{17}$$

for any value of r, and similar expressions for 2ϖ, u_1, v_1, u_2, v_2. Here, Δ corresponds to the interpretation of

$$g(z)\frac{1}{\Omega}\frac{H^{(1)}_{n+1/2}(izrc_1)}{\sqrt{r}}P_n(\cos\theta). \tag{18}$$

Since the forms of $g(z)$ for different forms of $f(t)$ have been calculated by various mathematicians[3),4)], the expressions of Δ, 2ϖ, u_1, v_1, u_2, v_2 in (17),......are known.

In the special case, $n=0$, $\widehat{rr}$, Δ, u may be expressed by

$$\left.\begin{aligned}
\widehat{rr}&=\frac{1}{2\pi i}\int_{c-i\infty}^{c+i\infty}\frac{e^{zt}}{z}g(z)\,dz,\\
\Delta&=\frac{1}{2\pi i}\int_{c-i\infty}^{c+i\infty}\frac{e^{zt}}{z}A_0\frac{H^{(1)}_{1/2}(izrc_1)}{\sqrt{r}}\,dz,\\
u&=\frac{1}{2\pi i}\int_{c-i\infty}^{c+i\infty}\frac{e^{zt}}{z}\frac{A_0}{z\,c_1^2}\frac{d}{dr}\left\{\frac{H^{(1)}_{1/2}(izrc_1)}{\sqrt{r}}\right\}dz,
\end{aligned}\right\} \tag{19}$$

where

$$A_0=\frac{g(z)}{\dfrac{\lambda H^{(1)}_{1/2}(izac_1)}{\sqrt{a}}+2\mu\dfrac{d}{da}\left\{\dfrac{1}{z^2c_1^2}\dfrac{d}{da}\dfrac{H^{(1)}_{1/2}(izac_1)}{\sqrt{a}}\right\}}. \tag{20}$$ [5)]

3. *The special case, $n=0$; $f(t)=p_0$ for $t>0$ and $f(t)=0$ for $t<0$.*

In this case, $g(z)=p_0$ for $t>0$, $g(z)=0$ for $t<0$. Thus, from (19), (20) we get

$$\left.\begin{aligned}
u&=\frac{-1}{2\pi i}\int_{c-i\infty}^{c+i\infty}\frac{a^3p_0(zrc_1+1)e^{z\{t-c_1(r-a)\}}dz}{2\mu r^2z\{z^2a^2c_1^2\,(1+\lambda/2\mu)+2zac_1+2\}}\\
&=\frac{ap_0}{2\mu(1+\lambda/2\mu)R^2\gamma_2}\left[-\frac{\gamma_2}{\gamma_1^2+\gamma_2^2}+\sqrt{\frac{(1-R\gamma_1)^2+(R\gamma_2)^2}{\gamma_1^2+\gamma_2^2}}e^{-\frac{\gamma_1 T}{ac_1}}\right.\\
&\qquad\left.\cdot\sin\left\{\frac{\gamma_2 T}{ac_1}+\tan^{-1}\frac{R\gamma_2}{1-R\gamma_1}+\tan^{-1}\frac{\gamma_2}{\gamma_1}\right\}\right],\quad (T>0)\\
u&=0,\qquad (T<0)
\end{aligned}\right\} \tag{21}$$

3), 4) *loc. cit.* 1), 2).

5) Results of calculation for $n=1, 2,$......will be shown in the second paper to appear in a forthcoming Bulletin.

where

$$R=r/a,\ T=t-c_1(r-a),\ \gamma_1=1/(1+\lambda/2\mu),\ \gamma_2=\sqrt{1+\lambda/\mu}/(1+\lambda/2\mu).$$

The first term within the bracket in (21) represents forced oscillation and the second term free oscillation. Using the above expressions, we calculated the vibrational form or wave form at $r=\infty$ and the vibrational form at $r=a$ for the case $\lambda=\mu$, the results of which are shown in Figs. 1, 2.

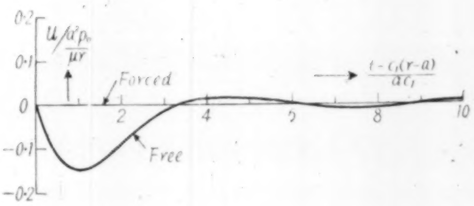

Fig. 1. Vibrational form or wave form at $r=\infty$. $f(t)=p_0$ for $t>0$, $f(t)=0$ for $t<0$.

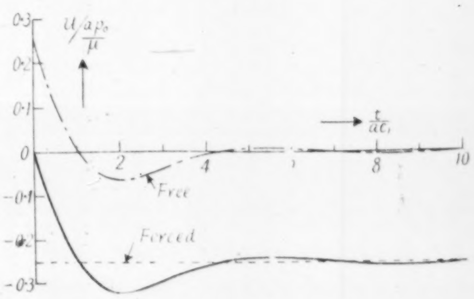

Fig. 2. Vibrational form at $r=a$. $f(t)=p_0$ for $t>0$, $f(t)=0$ for $t<0$.

From these figures it will be seen that although the vibration at $r=\infty$ is only of free oscillation, that at the origin consists of both free and forced oscillations. The displacement at the origin begins from zero owing to the forced oscillation cancelling out the free oscillation. The period of free oscillation corresponds to that of radial oscillation of the spherical cavity. Comparing Figs. 1, 2 it appears that the effect of permanent change of pressure in the spherical cavity is localized near the same cavity.

It is furthermore noted that in the present condition of the problem, the push and the pull of the medium near the origin as well as at infinity correspond to the pressure and traction at the origin, at least with respect to the first earthquake motion.

When the problem is extended to such a case as $f(t)=p_0$ for $0<t<\tau$, and $f(t)=0$ for $t<0$, and $t>\tau$, the solution can be obtained by merely superposing the case, $f(t)=p_0$ for $t>0$ and $f(t)=0$ for $t<0$, and the case $f(t)=-p_0$ for $t>\tau$, and $f(t)=0$ for $t<\tau$.

4. *The special case, $n=0$; $f(t)=p_0e^{-\alpha t}$ for $t>0$ and $f(t)=0$ for $t<0$.*

In this case, $g(z)=p_0z/(z+\alpha)$ for $t>0$ and $g(z)=0$ for $t<0$. From (19), (20), it follows

$$f(t)=\frac{p_0}{2\pi i}\int_{c-i\infty}^{c+i\infty}\frac{e^{zt}}{z}\frac{z}{z+\alpha}dz, \tag{22}$$

$$\left.\begin{aligned} u=&\frac{-\alpha p_0/\mu}{2(1+\lambda/2\mu)R^2}\left[\frac{(1-\xi R)e^{-\alpha T}}{(\gamma_1-\xi)^2+\gamma_2^2}\right.\\ &+\frac{1}{\gamma_2}\sqrt{\frac{(1-R\gamma_1)^2+(R\gamma_2)^2}{(\xi-\gamma_1)^2+\gamma_2^2}}\,e^{-\frac{\gamma_1\alpha T}{\xi}}\\ &\left.\cdot\sin\left\{\frac{\gamma_2\alpha T}{\xi}+\tan^{-1}\frac{R\gamma_2}{1-R\gamma_1}-\tan^{-1}\frac{\gamma_2}{\xi-\gamma_1}\right\}\right], \quad (T>0)\\ u=&0, \quad (T<0) \end{aligned}\right\} \tag{23}$$

where $\xi=\alpha c_1 a$, $R=r/a$, $T=t-c_1(r-a)$, $\gamma_1=1/(1+\lambda/2\mu)$, $\gamma_2=\sqrt{1+\lambda/\mu}/(1+\lambda/2\mu)$. The first term within brackets in (23) represents forced oscillation and the second term free oscillation. Using the above expressions we calculated either the vibrational form or wave form at $r=\infty$ and the vibrational form at $r=a$ for the case $\lambda=\mu$, $\alpha c_1 a=2$, with results as shown in Figs. 3, 4.

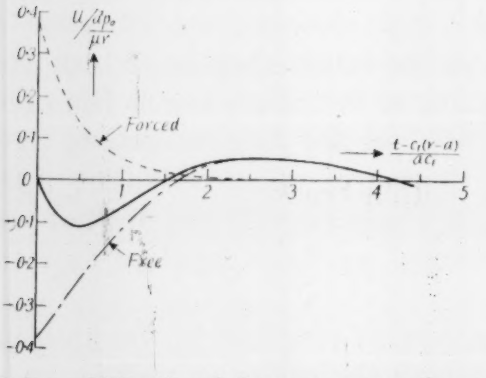

Fig. 3. Vibrational form or wave form, at $r=\infty$. $f(t)=p_0e^{-\alpha t}$ for $t>0$, $f(t)=0$ for $t<0$. $\alpha c_1 a=2$.

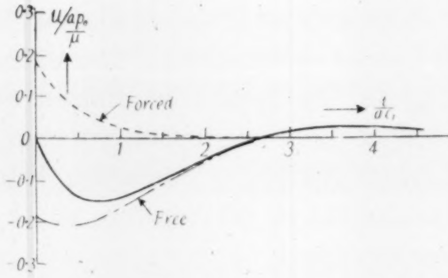

Fig. 4. Vibrational form at $r=a$. $f(t)=p_0e^{-\alpha t}$ for $t>0$, $f(t)=0$ for $t<0$. $\alpha c_1 a=2$.

These figures show that both the vibration at $r=\infty$ and that at $r=a$ consist of free as well as forced oscillations. In this case too the displacements at the origin and at $r=\infty$ begin from zero owing to the free oscillation cancelling the forced oscillation. When $\alpha c_1 a=0$, the displacement at $r=\infty$ would be merely of free oscillation.

The push and the pull of the medium, through which passes the first earthquake motion, near the origin as well as at infinity, correspond to the pressure and traction at the origin in the beginning of the pres-

sure change. Equation (23) show that damping of the free oscillation depends on the period of the same oscillation.

5. *The special case,* $n=0$; $f(t)=p_0 \sin \beta t$ *for* $t>0$ *and* $f(t)=0$ *for* $t<0$.

In this case $g(z)=p_0 z\beta/(z^2+\beta^2)$ for $t>0$ and $g(z)=0$ for $t<0$. From (19) and (20) it holds that

$$f(t)=\frac{p_0}{2\pi i}\int_{c-i\infty}^{c+i\infty}\frac{e^{zt}}{z}\frac{z\beta}{z^2+\beta^2}dz, \tag{24}$$

$$\left.\begin{aligned} u=&\frac{-ap_0/\mu}{2R^2(1+\lambda/2\mu)}\left[\sqrt{\frac{1+(\eta R)^2}{(\gamma_1^2+\gamma_2^2-\eta^2)^2+(2\eta\gamma_1)^2}}\right. \\ &\cdot\sin\left\{aT+\tan^{-1}\eta R-\tan^{-1}\frac{2\eta\gamma_1}{\gamma_1^2+\gamma_2^2-\eta^2}\right\} \\ &-\frac{\eta}{\gamma_2}\sqrt{\frac{(1-\gamma_1R)^2+(\gamma_2R)^2}{(\gamma_1^2-\gamma_2^2+\eta^2)^2+(2\gamma_1\gamma_2)^2}}\,e^{-\frac{\gamma_1 aT}{\eta}} \\ &\left.\cdot\sin\left\{\frac{\gamma_2 aT}{\eta}+\tan^{-1}\frac{\gamma_2R}{1-\gamma_1R}+\tan^{-1}\frac{2\gamma_1\gamma_2}{\gamma_1^2-\gamma_2^2+\eta^2}\right\}\right], \qquad (T>0) \\ u=&0, \qquad (T<0) \end{aligned}\right\} \tag{25}$$

where $\eta=\beta c_1 a$, $R=r/a$, $T=t-c_1(r-a)$, $\gamma_1=1/(1+\lambda/2\mu)$. $\gamma_2=\sqrt{1+\lambda/\mu}/(1+\lambda/2\mu)$. The first and second terms within brackets in (25) represent forced and free oscillations, respectively. The results of numerical calculations for the vibrational or wave form at $r=\infty$ and the vibrational form at $r=a$ for the case $\lambda=\mu$ and $\beta c_1 a=1/10$, 1, 10 are shown in Figs. 5~10.

The condition that $\beta c_1 a$ is small means that the length of the generated waves, namely, $2\pi/\beta$, is long compared with the radius of the spherical origin, whereas the condition that $\beta c_1 a$ is large signifies the reversed case. Figs. 5~10 show that in the case of long waves the component resulting from the free oscillation exists only at the very early stage of the disturbance, while in the case of short waves the same component does not vanish for a long time. Generally, in the present problem, the vibrations at infinity and at the spherical origin consist of both free and forced oscillations, particularly at the early stage of the vibration. Although the push and the pull of the medium through which passes the first earthquake motion, near the origin and at infinity, correspond

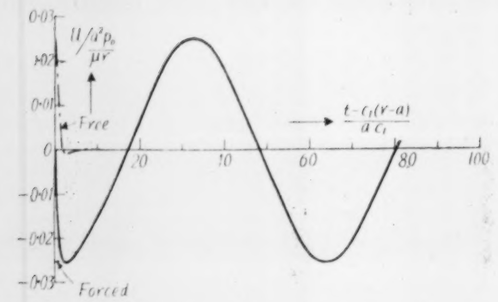

Fig. 5. Vibrational or wave form at $r=\infty$. $f(t)=p_0 \sin \beta t$ for $t>0$, $f(t)=0$ for $t<0$. $\beta c_1 a=1/10$.

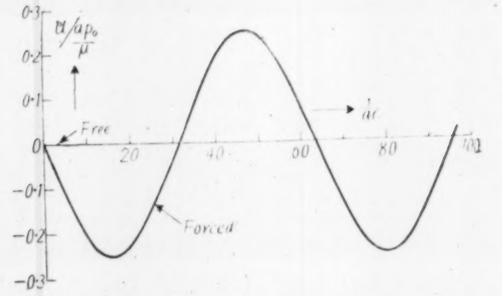

Fig. 6. Vibrational form at $r=a$. $f(t)=p_0 \sin \beta t$ for $t>0$, $f(t)=0$ for $t<0$. $\beta c_1 a=1/10$.

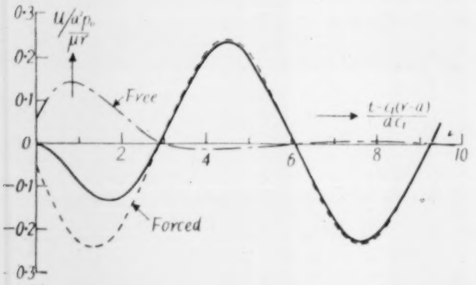

Fig. 7. Vibrational or wave form at $r=\infty$. $f(t)=p_0 \sin \beta t$ for $t>0$, $f(t)=0$ for $t<0$, $\beta c_1 a=1$.

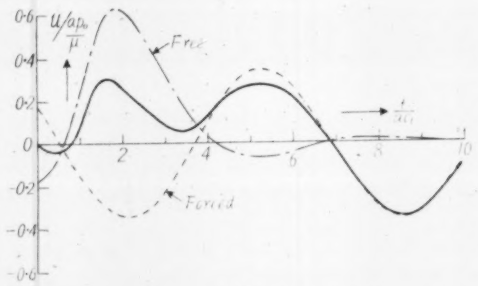

Fig. 8. Vibrational form at $r=a$. $f(t)=p_0 \sin \beta t$ for $t>0$, $f(t)=0$ for $t<0$. $\beta c_1 a=1$.

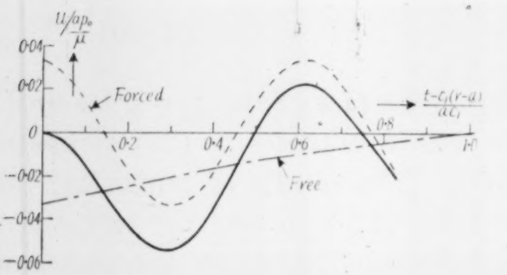

Fig. 9. Vibrational or wave form at $r=\infty$. $f(t)=p_0 \sin \beta t$ for $t>0$, $f(t)=0$ for $t<0$. $\beta c_1 a=10$.

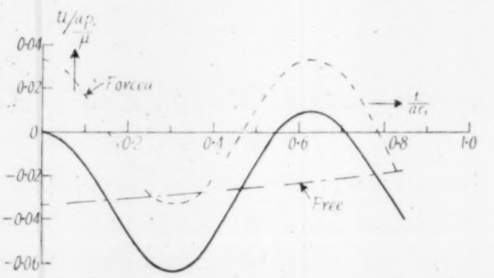

Fig. 10. Vibrational form at $r=a$. $f(t)=p_0 \sin \beta t$ for $t>0$, $f(t)=0$ for $t<0$. $\beta c_1 a=10$.

to the pressure and traction at that origin at the beginning of the pressure change, the duration of the same push and pull differing with difference in the length of the generated waves. For longer waves the duration is relatively short whereas for shorter waves the condition is reversed. Equation (25) shows that damping of the free oscillation depends merely on the frequency of the same oscillation.

In a more extended case of the present problem, say, $f(t)=p_0 \sin \beta t$ for $0<t<\tau$ and $f(t)=0$ for $t<0$ and $t>\tau$, the solution may be obtained by superposing the case $f(t)=p_0 \sin \beta t$ for $t>0$ and $f(t)=0$ for

$t<0$, and the case $f(t)=-p_0\sin\beta t$ for $t>\tau$ and $f(t)=0$ for $t<\tau$.

6. *The special case, $n=0$; $f(t)=p_0e^{-\alpha t}\sin\beta t$ for $t>0$, and $f(t)=0$ for $t<0$.*

In this case $g(z)=p_0z\beta/\{(z+\alpha)^2+\beta^2\}$ for $t>0$ and $g(z)=0$ for $t<0$. From (19) and (20) it holds that

$$f(t)=\frac{p_0}{2\pi i}\int_{c-i\infty}^{c+i\infty}\frac{e^{zt}}{z}\frac{z\beta}{(z+\alpha)^2+\beta^2}dz, \tag{26}$$

$$\left.\begin{aligned} u=&\frac{-a(p_0/\mu)\eta}{2R^2(1+\lambda/2\mu)}\left[\frac{1}{\eta}\sqrt{\frac{(1-\eta\kappa R)^2+(\eta R)^2}{\left\{(\gamma_1-\eta\kappa)^2+\gamma_2^2-\eta^2\right\}^2+\left\{2\eta(\gamma_1-\eta\kappa)\right\}^2}}e^{-\alpha T}\right.\\ &\cdot\sin\left\{\beta T+\tan^{-1}\frac{\eta R}{1-\eta\kappa R}-\tan^{-1}\frac{2\eta(\gamma_1-\eta\kappa)}{(\gamma_1-\eta\kappa)^2+\gamma_2^2-\eta^2}\right\}\\ &+\frac{1}{\gamma_2}\sqrt{\frac{(1-\gamma_1R)^2+(\gamma_2R)^2}{\left\{(\gamma_1-\eta\kappa)^2-\gamma_2^2+\eta^2\right\}^2+\left\{2\gamma_2(\gamma_1-\eta\kappa)\right\}^2}}e^{-\frac{\gamma_1\beta T}{\eta}}\\ &\left.\cdot\sin\left\{\frac{\gamma_2\beta T}{\eta}+\tan^{-1}\frac{\gamma_2R}{1-\gamma_1R}+\tan^{-1}\frac{2\gamma_2(\gamma_1-\eta\kappa)}{(\gamma_1-\eta\kappa)^2-\gamma_2^2+\eta^2}\right\}\right],\quad(T>0)\\ u=&0,\qquad\qquad(T<0)\end{aligned}\right\}\tag{27}$$

where $\kappa=\alpha/\beta$, $\eta=\beta c_1a$, $R=r/a$, $T=t-c_1(r-a)$, $\gamma_1=1/(1+\lambda/2\mu)$, $\gamma_2=\sqrt{1+\lambda/\mu}/(1+\lambda/2\mu)$.

In the present case the first and second terms within brackets in (27) correspond to the forced and free oscillations. The results of numerical calculation for two cases $\alpha/\beta=$ 10 and 1, are shown in Figs. 11∼13, from which it will be seen that the general feature of the

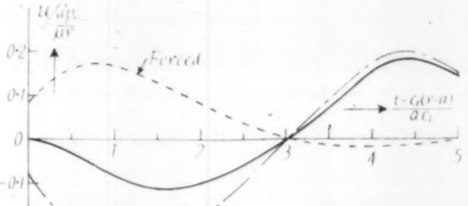

Fig. 11. Vibrational or wave form at $r=\infty$. $f(t)=p_0e^{-\alpha t}\sin\beta t$ for $t>0$, $f(t)=0$ for $t<0$. $\alpha/\beta=10$, $\beta c_1a=1/10$.

Fig. 12. Vibrational form at $r=a$. $f(t)=p_0e^{-\alpha t}\sin\beta t$ for $t>0$, $f(t)=0$ for $t<0$. $\alpha/\beta=10$, $\beta c_1a=1/10$.

problem closely resembles that for the case $f(t)=p_0 \sin \beta t$ for $t>0$ and $f(t)=0$ for $t<0$. The push and pull of the waves correspond to the traction pressure and at the spherical source. Equation (27) shows that, owing to the factor in the first term within brackets, the damping of the forced oscillation depends on the damping nature of the pressure in the spherical cavity, whereas that of free oscillation is a function of the free oscillation of that cavity.

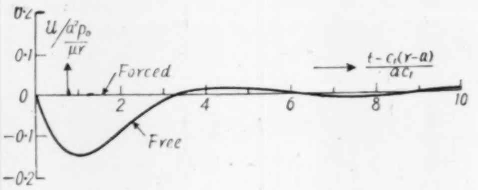

Fig. 13. Vibrational form at $r=a$. $f(t)=p_0 e^{-\alpha t} \sin \beta t$ for $t>0$, $f(t)=0$ for $t<0$. $\alpha/\beta=1$, $\beta c_1 a=1$.

7. *Concluding remarks.*

Using operational calculus, the problem of transmission of arbitrary elastic waves generated from a spherical source, oscillating spheroidally, was solved fairly simply. In the present investigation, the case of arbitrary disturbance occurring abruptly is discussed. In such a case, the solution consists of two parts, namely, the part of free oscillation and that of forced oscillation. The period and logarithmic decrement of free oscillation depend on the size of the spherical origin and the elastic nature of the surrounding medium.

Although the push and the pull of the medium of the first earthquake motion near the origin and at infinity correspond to the pressure and traction at that origin at the beginning of the pressure change, the duration of the same push or pull relative to the period of oscillatory part of the disturbance differs with difference in the length of the generated waves.

In conclusion, we wish to express our thanks to Mr. Watanabe, who assisted us greatly in our calculation. We also wish to thank the officials of the Division of Scientific Research, in the Ministry of Education, for financial aid (Funds for Scientific Research) granted us for a series of investigation, of which this study is a part.

11. 演算法を應用せる任意形彈性波の傳播の問題 (第1報)

地震研究所 {妹澤克惟
金井清}

演算法を用ひて球源から任意形彈性波が出る問題を可なり簡單に解く事ができた．殊に球源が不動狀態から急に動き始める場合は最も容易に取扱はれ得るのである．この樣な場合の數學的解は强制振動部分と自由振動部分とから成立ち，自由振動の波の繰返し振動周期と減衰係數とは球源の大きさと周圍の彈性的性質に關係する事がわかる．

球源附近と遠方での地震初動の押しと引きとは源點での壓力と張力に關係するけれども，その押し及び引きの繼續時間の割合は發生する波の波長により波長の範圍以上に渉つて可なり變化する．

12. *On the Initial Movement of a Seismograph subjected to an Arbitrary Earthquake Motion, Solved with Operational Calculus. I.*

By Katsutada SEZAWA and Kiyoshi KANAI,

Earthquake Research Institute.

(Read March 20, 1941.—Received March 20, 1941.)

1. *Introduction.*

The problem of the initial motion of a seismograph subjected to an arbitrary disturbance has been solved by a number of authors, mainly by means of Fourier's double integrals. On the other hand, Jeffreys[1] used Heaviside's operational calculus in solving the problem. We have recently found that the operational method, based on Mellin's inversion theorem, is more suitable in dealing with the problem.

If, in Mellin's theorem,

$$\phi(p)=p\int_0^\infty e^{-pt}f(t)\,dt, \tag{1}$$

then $f(t)$ is expressed by

$$f(t)=\frac{1}{2\pi i}\int_{c-i\infty}^{c+i\infty}\frac{e^{zt}\phi(z)}{z}dz, \tag{2}$$

where $\int_{c-i\infty}^{c+i\infty}$ constitutes the Bromwich-Wagner's integral in the complex z-plane. Thus, it is possible to say that $\phi(p)$ is an operational form of $f(t)$, and $f(t)$ an interpretation of $\phi(p)$.

2. *Expression of seismograph movements resulting from an arbitrary earthquake motion.*

Let ξ be the ground movement and x the displacement of the pendulum relative to the moving ground. Then, the equation of motion of the pendulum is expressed by

$$\ddot{x}+2k\dot{x}+n^2x=-\ddot{\xi}, \tag{3}$$

1) H. JEFFREYS, *Operational Method* (Cambridge Math. Tract, 1927).

Multiplying both sides of this equation by $pe^{-pt}dx$, and integrating, we get

$$p\int_0^\infty e^{-pt}dx' + 2kp\int_0^\infty e^{-pt}dx + n^2p\int_0^\infty e^{-pt}xdt = -p\int_0^\infty e^{-pt}d\xi', \qquad (4)$$

where x', ξ' mean dx/dt, $d\xi/dt$. Integrating (4) by parts, it becomes

$$(p^3+2kp^2+n^2p)\int_0^\infty e^{-pt}xdt = -p^3\int_0^\infty e^{-pt}\xi dt$$

$$+p^2(x_0+\xi_0)+p(x_0'+\xi_0'+2kx_0), \qquad (5)$$

where x_0, ξ_0, x_0', ξ_0' are the initial values of x, ξ, x', ξ'.

From (5) the operational form of x becomes

$$x \supset p\int_0^\infty e^{-pt}xdt = \frac{-p^3\int_0^\infty e^{-pt}\xi dt}{p^2+2kp+n^2} + \frac{p^2(x_0+\xi_0)+p(x_0'+\xi_0'+2kx_0)}{p^2+2kp+n^2}, \qquad (6)$$

from which the interpretation of the right-hand side of (6) becomes

$$x = \frac{1}{2\pi i}\int_{c-i\infty}^{c+i\infty}\frac{-z\phi(z)e^{zt}dz}{z^2+2kz+n^2} + \frac{1}{2\pi i}\int_{c-i\infty}^{c+i\infty}\frac{\{z(x_0+\xi_0)+(x_0'+\xi_0'+2kx_0)\}e^{zt}dz}{z^2+2kz+n^2}. \qquad (7)$$

The first term on the right-hand side of (7) represents the movement of the pendulum for zero displacements and zero velocities of the same pendulum and of the ground at $t=0$, while the second term gives the effect of their initial displacements and the initial velocities.

If, assuming temporarily that the second term does not exist, we calculate the first term, we have $x_0+\xi_0=0$, $x_0'+\xi_0'+2kx_0=0$, from which condition the second term in (7) should vanish. If the initial displacement and the initial velocity of the ground, namely, ξ_0, ξ_0', were zero, the initial displacement and the initial velocity of the pendulum, namely, x_0, x_0', would be zero. Although $x_0+\xi_0$ indicates zero displacement of the pendulum in space, $x_0'+\xi_0'+2kx_0$ is somewhat complex. However, if the damping of the seismograph were zero, we get the relations $x_0+\xi_0=0$, $x_0'+\xi_0'=0$, indicating that the displacement and the velocity of the pendulum relative to space are both zero.

3. *The special case, $\xi=1$ for $0<t<h$ and $\xi=0$ for $t<0$, $t>h$.*

Since, in this case,

$$\xi \supset 1 \quad \text{for } 0<t<h, \quad \xi \supset 1-e^{-ph} \quad \text{for } t>h, \tag{8}$$

we get

$$\left.\begin{aligned} x \supset p\int_0^\infty e^{-pt}x\,dt &= \frac{-p^2}{p^2+2kp+n^2}, \quad (0<t<h) \\ &= \frac{-p^2(1-e^{-ph})}{p^2+2kp+n^2}, \quad (t>h) \end{aligned}\right\} \tag{9}$$

from which

$$\left.\begin{aligned} x &= \frac{-1}{2\pi i}\int_{c-i\infty}^{c+i\infty} \frac{e^{zt}z\,dz}{z^2+2kz+n^2}, \quad (0<t<h) \\ x &= \frac{-1}{2\pi i}\int_{c-i\infty}^{c+i\infty} \frac{e^{zt}(1-e^{-zh})z\,dz}{z^2+2kz+n^2}. \quad (t>h) \end{aligned}\right\} \tag{10}$$

In the case of $k \neq n$ ($\alpha_2 \neq 0$), the integral (10) transforms to

$$\left.\begin{aligned} x &= \frac{-1}{2\pi i}\int_{c-i\infty}^{c+i\infty} \frac{e^{zt}z\,dz}{\left\{z+(k-i\alpha_2)\right\}\left\{z+(k+i\alpha_2)\right\}}, \quad (0<t<h) \\ x &= \frac{-1}{2\pi i}\int_{c-i\infty}^{c+i\infty} \frac{e^{zt}z(1-e^{-zh})\,dz}{\left\{z+(k-i\alpha_2)\right\}\left\{z+(k+i\alpha_2)\right\}}, \quad (t>h) \end{aligned}\right\} \tag{11}$$

where $\alpha_2=\sqrt{n^2-k^2}$, from which we get

$$\left.\begin{aligned} x &= \frac{n}{\sqrt{n^2-k^2}}\left[e^{-kt}\sin\left(t\alpha_2-\tan^{-1}\frac{\alpha_2}{k}\right)\right], \quad (0<t<h) \\ x &= \frac{n}{\sqrt{n^2-k^2}}\left[e^{-kt}\sin\left(t\alpha_2-\tan^{-1}\frac{\alpha_2}{k}\right)\right. \\ &\qquad \left. -e^{-k(t-h)}\sin\left\{\alpha_2(t-h)-\tan^{-1}\frac{\alpha_2}{k}\right\}\right]. \quad (t>h) \end{aligned}\right\} \tag{12}$$

In the case of $k=n$, the integral (10) becomes of the types

$$x=\frac{-1}{2\pi i}\int_{c-i\infty}^{c+i\infty}\frac{e^{zt}z\,dz}{(z+k)^2}, \quad x=\frac{-1}{2\pi i}\int_{c-i\infty}^{c+i\infty}\frac{e^{zt}z(1-e^{-zh})\,dz}{(z+k)^2}, \tag{13}$$

so that

$$\left.\begin{aligned} x &= -(1-kt)e^{-kt}, \quad (0<t<h) \\ x &= -(1-kt)e^{-kt}+\left\{1-k(t-h)\right\}e^{-k(t-h)}. \quad (t>h) \end{aligned}\right\} \tag{14}$$

From the results in (12), (14), it will be seen that in the present type of earth movement, there is apparently no term in the equations corresponding to forced vibration. The results of calculation for the two cases (i) $k/n=0$, $k/n=0{\cdot}6$, both for the same condition $nh=1$, are shown in Figs. 1, 2. The full lines represent the seismographic displacement

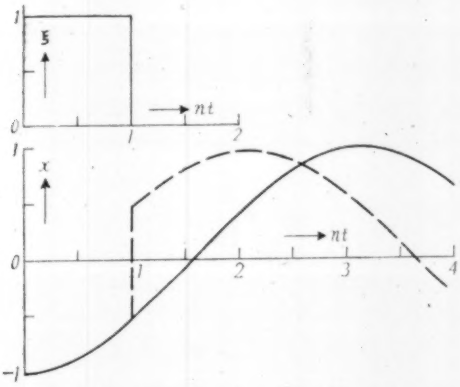

Fig. 1. $\xi=1$ for $0<t<h$, $\xi=0$ for $t<0$ and $t>h$. $nh=1$, $k/n=0$.

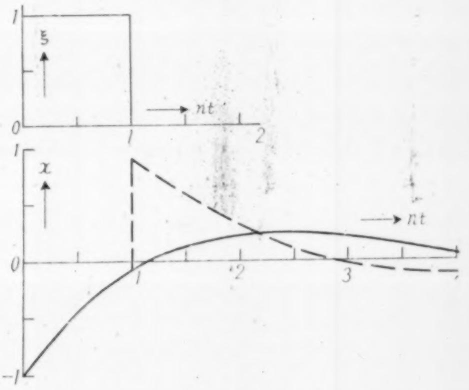

Fig. 2. $\xi=1$ for $0<t<h$, $\xi=0$ for $t<0$ and $t>h$. $nh=1$, $k/n=0{\cdot}6$.

for $0<t$ arising from the earth's displacement $\xi=1$ for $t>0$ and the broken lines that for $t>h$ arising from the displacement $\xi=1$ for $0<t<h$ and $\xi=0$ for $t>h$.

It will be seen that, as in common sense reasoning, the steepness of the damping curve for the seismographic movement increases with increase in logarithmic decrement, but the beginning of each damping curve corresponds to the forced vibration. The amount of initial movement of the pendulum is the same as that of the earth's displacement, but in the sense that is opposite to it for such a sudden movement. At all events, it is possible to say that the sense of the initial motion of the pendulum is opposite to that of the ground movement.

4. *The special case,* $\xi=e^{-at}$ *for* $t>0$ *and* $\xi=0$ *for* $t<0$.

In this case,

$$\xi \supset p\int_0^\infty e^{-pt}\xi dt=\frac{p}{p+a}, \tag{15}$$

so that

$$x \supset p\int_0^\infty e^{-pt}x dt=\frac{-p^3}{(p+a)(p^2+2kp+n^2)}, \tag{16}$$

from which

$$x=\frac{-1}{2\pi i}\int_{c-i\infty}^{c+i\infty}\frac{e^{zt}z^2dz}{(z+a)(z^2+2kz+n^2)}=\frac{-1}{2\pi i}\int_{c-i\infty}^{c+i\infty}\frac{e^{zt}z^2dz}{(z+a)(z+\alpha)(z+\beta)}, \tag{17}$$

where $\alpha=k-i\sqrt{n^2-k^2}, \qquad \beta=k+i\sqrt{n^2-k^2}.$ (18)

(i) If $\alpha \neq \beta \neq a \ (k \neq n)$,

$$x=\frac{-a^2e^{-at}}{(a-\alpha)(a-\beta)}-\frac{\alpha^2e^{-\alpha t}}{(\alpha-a)(\alpha-\beta)}-\frac{\beta^2e^{-\beta t}}{(\beta-a)(\beta-\alpha)}$$

$$=\frac{-e^{-at}}{1-\frac{2k}{a}+\frac{n^2}{a^2}}+\frac{\frac{n}{a}e^{-kt}}{\sqrt{\left(1-\frac{k^2}{n^2}\right)\left(1-\frac{2k^2}{n^2}+\frac{n^2}{a^2}\right)}}$$

$$\cdot\sin\left(nt\sqrt{1-\frac{k^2}{n^2}}\quad\tan^{-1}\frac{2\frac{k}{n}\sqrt{1-\frac{k^2}{n^2}}}{2\frac{k^2}{n^2}-1}+\tan^{-1}\frac{\frac{n}{a}\sqrt{1-\frac{k^2}{n^2}}}{-1+\frac{k}{a}}\right),$$

$$(\alpha \neq \beta \neq a,\ t>0)$$

$$x=0. \qquad (\alpha \neq \beta \neq a,\ t<0) \tag{19}$$

(ii) If $n=k$, $a \neq n$, then $\alpha=\beta$, $a \neq \alpha$, so that

$$x=\frac{-1}{2\pi i}\left[\int_{c-i\infty}^{c+i\infty}\frac{1}{(a+\alpha)^2}\frac{z^2e^{zt}}{(z-a)}dz-\int_{c-i\infty}^{c+i\infty}\frac{1}{(a+\alpha)^2}\frac{z^2e^{zt}\left\{z+(a+2\alpha)\right\}}{(z+\alpha)^2}dz\right],$$

$$=\frac{-a^2e^{-at}}{(a-n)^2}-\frac{n\left\{nt(a-n)-(2a-n)\right\}e^{-nt}}{(a-n)^2},$$

$$(\alpha=\beta,\ a \neq \alpha,\ t>0)$$

$$x=0. \qquad (\alpha=\beta,\ a \neq \alpha,\ t<0) \tag{20}$$

(iii) If $a=n=k$ $(a=\alpha=\beta)$,

$$x=\frac{-1}{2\pi i}\int_{c-i\infty}^{c+i\infty}\frac{z^2e^{zt}dz}{(z+\alpha)^3}=-\frac{n^2t^2}{2(1+nt)}-(1-2nt)e^{-nt}, \qquad (t>0)$$

$$x=0. \qquad (t<0) \tag{21}$$

The respective first terms in (19), (20), (21) represent forced oscillation and the respective second terms the free oscillation. The results of calculation for the two cases of k/n, a/n being unity, are shown in Figs. 3, 4. The thick lines correspond to the resultant displacements of the pendulum. With increase in damping coefficient the vibrations of the pendulum decays with increasing rapidity.

The results of calculation for different ratios of a/n and the various

values of k/n are given in Figs. 5~7. These figures show that although the damping of the pendulum vibration increases with increasing steep-

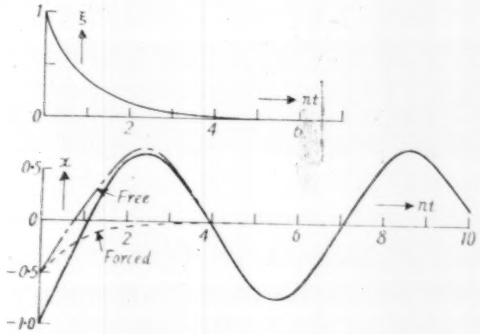

Fig. 3. $\xi=e^{-at}$ for $t>0$, $\xi=0$ for $t<0$. $a/n=1$, $k/n=0$.

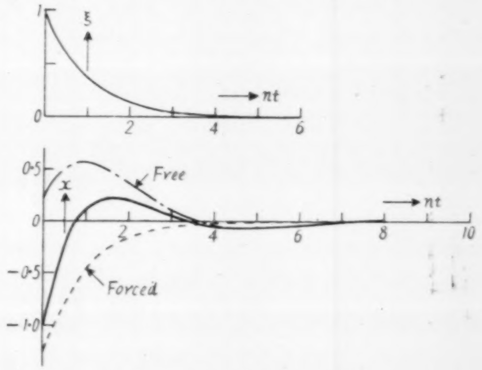

Fig. 4. $\xi=e^{-at}$ for $t>0$, $\xi=0$ for $t<0$. $a/n=1$, $k/n=1$.

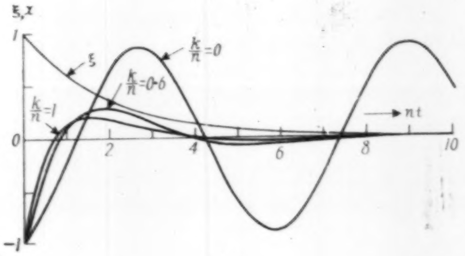

Fig. 5. $\xi=e^{-at}$ for $t>0$, $\xi=0$ for $t<0$. $a/n=0{\cdot}5$, $k/n=0$, $0{\cdot}6$, 1.

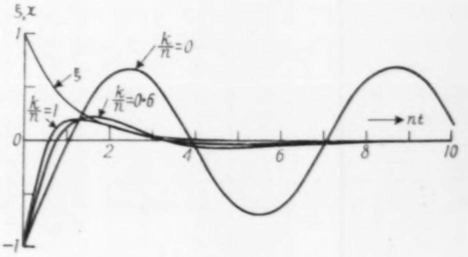

Fig. 6. $\xi=e^{-at}$ for $t>0$, $\xi=0$ for $t<0$. $a/n=1$, $k/n=0$, $0{\cdot}6$, 1.

ness of the damping curve of the forced vibration, the amplitude of the first motion of the same pendulum is the same as that of the initial motion of the ground, but in the sense opposite to it—a feature closely resembling the case of the preceding section. This feature results from the condition that the initial motion of the ground is quite instantaneous.

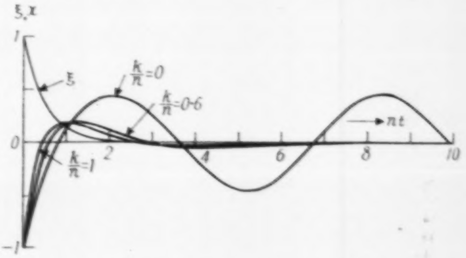

Fig. 7. $\xi=e^{-at}$ for $t>0$, $\xi=0$ for $t<0$. $a/n=2$, $k/n=0$, $0{\cdot}6$, 1.

5. *The special case,* $\xi=\sin bt$ *for* $t>0$, $\xi=0$ *for* $t<0$.[2)]

In this case,

2) This case was solved by S. T. NAKAMURA and also by C. TSUBOI by simple elementary methods. *Proc. Imp. Acad.* **3** (1927), 32; *Bull. Earthq. Res. Inst.*, **12** (1934), 426.

where $\alpha = k - i\sqrt{n^2-k^2}$, $\beta = k + i\sqrt{n^2-k^2}$. (18)

(i) If $\alpha \neq \beta \neq a$ $(k \neq n)$,

$$\left.\begin{aligned} x &= \frac{-a^2e^{-at}}{(a-\alpha)(a-\beta)} - \frac{\alpha^2e^{-\alpha t}}{(\alpha-a)(\alpha-\beta)} - \frac{\beta^2e^{-\beta t}}{(\beta-a)(\beta-\alpha)} \\ &= \frac{-e^{-at}}{1-\frac{2k}{a}+\frac{n^2}{a^2}} + \frac{\frac{n}{a}e^{-kt}}{\sqrt{\left(1-\frac{k^2}{n^2}\right)\left(1-\frac{2k^2}{n^2}+\frac{n^2}{a^2}\right)}} \\ &\quad \cdot \sin\left(nt\sqrt{1-\frac{k^2}{n^2}} \tan^{-1}\frac{2\frac{k}{n}\sqrt{1-\frac{k^2}{n^2}}}{2\frac{k^2}{n^2}-1} + \tan^{-1}\frac{\frac{n}{a}\sqrt{1-\frac{k^2}{n^2}}}{-1+\frac{k}{a}}\right), \\ & \qquad\qquad\qquad (\alpha \neq \beta \neq a,\ t>0) \\ x &= 0. \qquad\qquad\qquad (\alpha \neq \beta \neq a,\ t<0) \end{aligned}\right\} \quad (19)$$

(ii) If $n=k$, $a \neq n$, then $\alpha = \beta$, $a \neq \alpha$, so that

$$\left.\begin{aligned} x &= \frac{-1}{2\pi i}\left[\int_{c-i\infty}^{c+i\infty}\frac{1}{(a+\alpha)^2}\frac{z^2e^{zt}}{(z-a)}dz - \int_{c-i\infty}^{c+i\infty}\frac{1}{(a+\alpha)^2}\frac{z^2e^{zt}\left\{z+(a+2\alpha)\right\}}{(z+\alpha)^2}dz\right], \\ &= \frac{-a^2e^{-at}}{(a-n)^2} - \frac{n\left\{nt(a-n)-(2a-n)\right\}e^{-nt}}{(a-n)^2}, \\ & \qquad\qquad\qquad (\alpha=\beta,\ a \neq \alpha,\ t>0) \\ x &= 0. \qquad\qquad\qquad (\alpha=\beta,\ a \neq \alpha,\ t<0) \end{aligned}\right\} \quad (20)$$

(iii) If $a=n=k$ $(a=\alpha=\beta)$,

$$\left.\begin{aligned} x &= \frac{-1}{2\pi i}\int_{c-i\infty}^{c+i\infty}\frac{z^2e^{zt}dz}{(z+\alpha)^3} = -\frac{n^2t^2}{2(1+nt)} - (1-2nt)e^{-nt}, \qquad (t>0) \\ x &= 0. \qquad\qquad\qquad (t<0) \end{aligned}\right\} \quad (21)$$

The respective first terms in (19), (20), (21) represent forced oscillation and the respective second terms the free oscillation. The results of calculation for the two cases of k/n, a/n being unity, are shown in Figs. 3, 4. The thick lines correspond to the resultant displacements of the pendulum. With increase in damping coefficient the vibrations of the pendulum decays with increasing rapidity.

The results of calculation for different ratios of a/n and the various

values of k/n are given in Figs. 5~7. These figures sh
the damping of the pendulum vibration increases wit

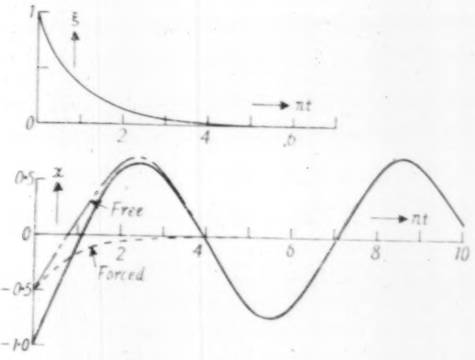

Fig. 3. $\xi = e^{-at}$ for $t > 0$, $\xi = 0$ for $t < 0$. $a/n = 1$, $k/n = 0$.

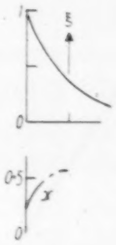

so

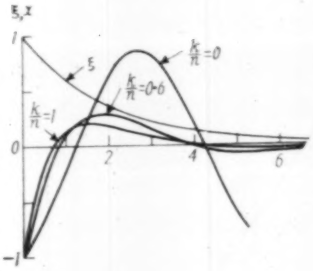

Fig. 5. $\xi = e^{-a}$
$t < 0$. a/n

where p^2

(27)

(i) If $a \neq$

.orced oscil-

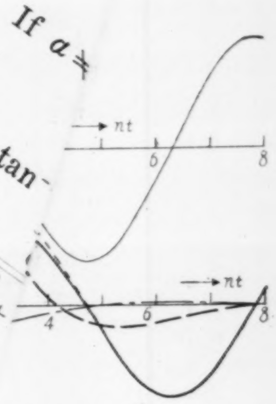

…sin bt for $t > 0$, $\xi = 0$ for
$=1$, $k/n = 0{\cdot}6$.

ness of th
forced v
the fir
dulur
init
t

$x = 0.$

(ii) If $a = \beta$ $(n = k)$, th

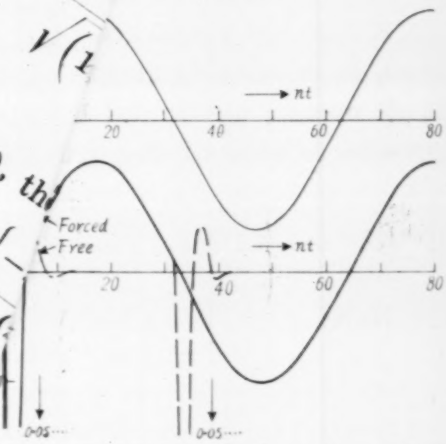

Fig. 10. $\xi = \sin bt$ for $t > 0$, $\xi = 0$ for $t < 0$. $n/b = 10$, $k/n = 0{\cdot}6$.

2)
elementa
426.

$$\left.\begin{aligned}\xi \supset p\int_0^\infty e^{-pt}\xi dt &= \frac{pb}{p^2+b^2}, \quad (t>0)\\ &= 0, \quad (t<0)\end{aligned}\right\} \tag{22}$$

so that

$$\left.\begin{aligned}x \supset p\int_0^\infty e^{-pt}x dt &= \frac{pb}{p^2+b^2}\,\frac{-p^2}{p^2+2kp+n^2}\\ &= \frac{-p^3 b}{(p+ib)(p-ib)(p+\alpha)(p+\beta)}, \quad (t>0)\\ &= 0, \quad (t<0)\end{aligned}\right\} \tag{23}$$

where $p^2+2kp+n^2=(p+\alpha)(p+\beta)$. Thus,

$$x=\frac{-b}{2\pi i}\int_{c-i\infty}^{c+i\infty}\frac{z^2 e^{zt}dz}{(z+ib)(z-ib)(z+\alpha)(z+\beta)}. \tag{24}$$

(i) If $\alpha \neq \beta$, from (24)

$$\left.\begin{aligned}x &= \frac{\sin\left(bt-\tan^{-1}\dfrac{\frac{2k}{b}}{\frac{n^2}{b^2}-1}\right)}{\sqrt{\left(\frac{n^2}{a^2}-1\right)^2+\frac{4k^2}{a^2}}}\\ &\quad -\frac{\frac{n}{b}e^{-kt}\sin\left\{nt\sqrt{1-\frac{k^2}{n^2}}-\tan^{-1}\dfrac{2\frac{k}{n}\sqrt{1-\frac{k^2}{n^2}}}{2\frac{k^2}{n^2}-1}+\tan^{-1}\dfrac{\frac{2k}{n}\sqrt{1-\frac{k^2}{n^2}}}{2\frac{k^2}{n^2}-1+\frac{b^2}{n^2}}\right\}}{\sqrt{\left(1-\frac{k^2}{n^2}\right)\left\{\left(\frac{n^2}{b^2}-1\right)^2+4\frac{k^2}{b^2}\right\}}} \quad (t>0)\\ x &= 0. \quad (t<0)\end{aligned}\right\} \tag{25}$$

(ii) If $\alpha=\beta$ $(n=k)$, then

$$x=\frac{-b}{(k^2+b^2)^2 2\pi i}\left[\int_{c-i\infty}^{c+i\infty}\frac{z^2\left\{-2kz+(k^2-b^2)\right\}e^{zt}dz}{(z+ib)(z-ib)}+\int_{c-i\infty}^{c+i\infty}\frac{z^2e^{zt}\left\{2kz+(3k^2+b^2)\right\}dz}{(z+k)^2}\right]$$

$$= \frac{1}{\left(\frac{n^2}{b^2}+1\right)}\left[\sin\left(bt-\tan^{-1}\frac{2\frac{n}{b}}{\frac{n^2}{b^2}-1}\right)+\frac{n}{b}\left\{\frac{2}{\left(\frac{n^2}{b^2}+1\right)}-nt\right\}e^{-nt}\right], \qquad (n=k,\ t>0)$$

$$x=0. \qquad (n=k,\ t<0) \tag{26}$$

(iii) If $k=0$, $n=b$, then

$$x=\frac{-b}{2\pi i}\left[\int_{c-i\infty}^{c+i\infty}\frac{z^2e^{zt}(iz-2b)dz}{4b^3(z+ib)^2}-\int_{c-i\infty}^{c+i\infty}\frac{z^2e^{zt}(iz+2b)dz}{4b^3(z-ib)^2}\right]$$

$$=-\tfrac{1}{2}(\sin bt+bt\cos bt), \qquad (k=0,\ n=b,\ t>0)$$

$$x=0. \qquad (k=0,\ n=b,\ t<0) \tag{27}$$

The respective first terms in (25), (26) represent forced oscil-

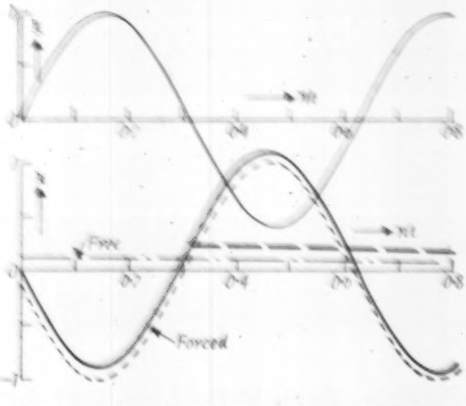

Fig. 8. $\xi=\sin bt$ for $t>0$, $\xi=0$ for $t<0$. $n/b=0{\cdot}1$, $k/n=0{\cdot}6$.

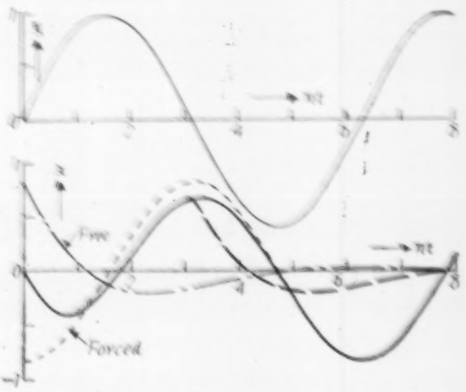

Fig. 9. $\xi=\sin bt$ for $t>0$, $\xi=0$ for $t<0$. $n/b=1$, $k/n=0{\cdot}6$.

lation and the respective second terms free oscillation. The results of calculation for the three cases of n/b, namely $n/b=0{\cdot}1$, 1, 10 for $k/n=0{\cdot}6$, are shown in Figs. 8, 9, 10. The full lines give the resultant vibrations for $t>0$ arising from $\xi=\sin bt$ for $t>0$ and $\xi=0$ for $t<0$, and the thick broken lines those for $t>\pi/2b$ arising from $\xi=\sin bt$ for $0<t<\pi/2b$ and $\xi=0$ for $t>\pi/2b$. The condition $n/b \ll 1$ corresponds to the state of the dis-

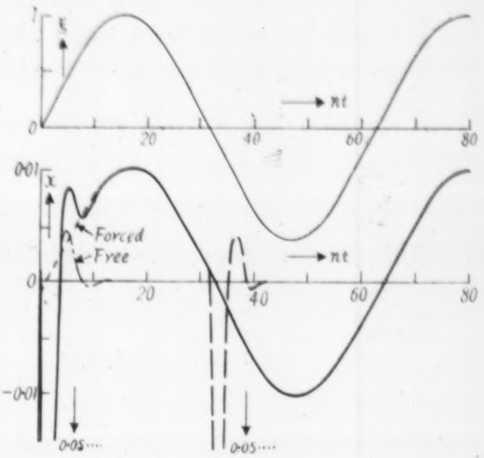

Fig. 10. $\xi=\sin bt$ for $t>0$, $\xi=0$ for $t<0$. $n/b=10$, $k/n=0{\cdot}6$.

placement seismometer, and that of $n/b \gg 1$ to that of the accelerometer. Comparing the results in Figs. 8~10, it will be seen that, for sinusoidal motion of the ground occurring at $t=0$, although the displacement seismometer can record the movement of the ground rather accurately, at least for the initial motion, it is not possible to do so with the acceleration seismometer, not at any rate, for the same initial motion. In the case of the acceleration seismometer, the duration of the initial motion of the pendulum is fairly small.

For ascertaining the effect of damping of the seismometer, we calculated two cases with respect to k/n for $n/b=1$, with results as shown in Figs. 11~12. Since the condition $n/b=1$ represents resonance, the vibration amplitude of the pendulum without damping increases without limit with time increase, whereas the vibration of the pendulum with critical damping fairly resembles the motion of the ground.

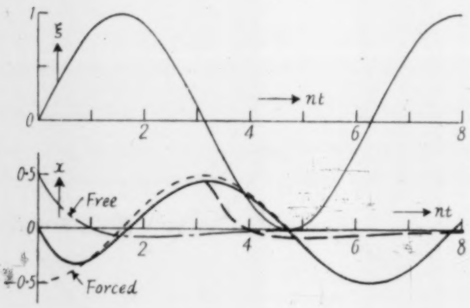

Fig. 11. $\xi=\sin bt$ for $t>0$, $\xi=0$ for $t<0$. $n/b=1$, $k/n=1$.

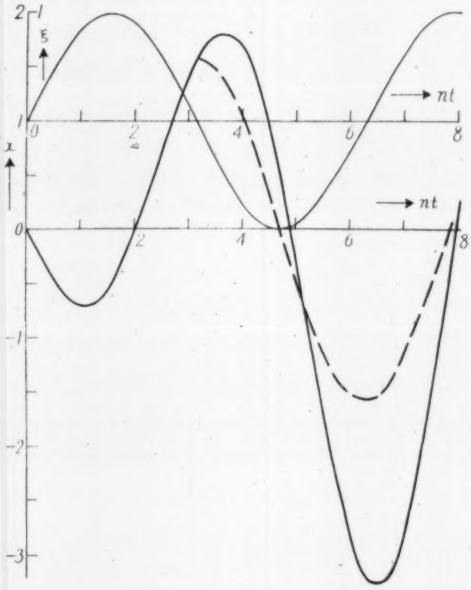

Fig. 12. $\xi=\sin bt$ for $t>0$, $\xi=0$ for $t<0$. $n/b=1$, $k/n=0$.

It may be remarked here that in the present problem, since $x_0=0$, $\xi_0=0$, it is possible from (7) for the initial conditions $x_0'=-\xi_0'$ to exist. At all events, the initial motion of the pendulum is always in the sense opposite to that of the ground motion.

6. *The special case,* $\xi=e^{-at}\sin bt$ *for* $t>0$, $\xi=0$ *for* $t<0$.

Here

$$\left.\begin{aligned} \bar{\xi} = p\int_0^\infty e^{-pt}\xi dt &= \frac{pb}{(p+a)^2+b^2}, \quad (t>0) \\ &=0, \qquad\qquad\qquad (t<0) \end{aligned}\right\} \tag{28}$$

from which

$$\left.\begin{aligned} x \supset p\int_0^\infty e^{-pt}x\,dt &= \frac{-p^3 b}{\left\{(p+a)^2+b^2\right\}(p^2+2kp+n^2)}, \quad (t>0) \\ &= 0. \quad (t<0) \end{aligned}\right\} \tag{29}$$

Thus,

$$\left.\begin{aligned} x &= \frac{-b}{2\pi i}\int_{c-i\infty}^{c+i\infty} \frac{z^2 e^{zt}dz}{\left\{z+(a-ib)\right\}\left\{z+(a+ib)\right\}\left\{z+(k-i\alpha_2)\right\}\left\{z+(k+i\alpha_2)\right\}}, \\ & \qquad\qquad (t>0) \\ x &= 0, \qquad\qquad (t<0) \end{aligned}\right\} \tag{30}$$

where $\alpha_2=\sqrt{n^2-k^2}$.

(i) If $a \neq k$, $b \neq \alpha_2$,

$$x = \frac{-\left(1+\frac{a^2}{b^2}\right)e^{-at}\sin\left\{bt-\tan^{-1}\dfrac{\frac{2a}{b}}{\frac{a^2}{b^2}-1}+\tan^{-1}\dfrac{2\left(\frac{a}{b}-\frac{k}{b}\right)}{\left(\frac{a}{b}-\frac{k}{b}\right)^2+\frac{n^2}{b^2}-\frac{k^2}{b^2}-1}\right.}{\sqrt{\left\{\left(\frac{a}{b}-\frac{k}{b}\right)^2+\frac{n^2}{b^2}-\frac{k^2}{b^2}-1\right\}^2+4\left(\frac{a}{b}-\frac{k}{b}\right)^2}}$$

$$-\frac{\frac{n^2}{b^2}e^{-kt}\sin\left\{nt\sqrt{1-\frac{k^2}{n^2}}-\tan^{-1}\dfrac{2\frac{k}{n}\sqrt{1-\frac{k^2}{n^2}}}{2\frac{k^2}{n^2}-1}-\tan^{-1}\dfrac{\frac{2n}{b}\sqrt{1-\frac{k^2}{n^2}}\left(\frac{a}{b}-\frac{k}{b}\right)}{\left(\frac{a}{b}-\frac{k}{b}\right)^2-\frac{n^2}{b^2}+\frac{k^2}{b^2}-1}\right\}}{\sqrt{\left(\frac{n^2}{b^2}-\frac{k^2}{b^2}\right)\left[\left\{\left(\frac{a}{b}-\frac{k}{b}\right)^2-\frac{n^2}{b^2}+\frac{k^2}{b^2}+1\right\}^2+4\left(\frac{n^2}{b^2}-\frac{k^2}{b^2}\right)\left(\frac{a}{b}-\frac{k}{b}\right)^2\right]}},$$

$$(t>0)$$

$$x=0, \qquad (t<0) \tag{31}$$

(ii) If $a=k$, $b=\alpha_2$,

$$\left.\begin{aligned} x &= \frac{-b}{2\pi i}\int_{c-i\infty}^{c+i\infty}\frac{z^2e^{zt}dz}{\left\{z+(k-i\alpha_2)\right\}^2\left\{z+(k+i\alpha_2)\right\}^2} \\ &= \frac{\sqrt{1-\frac{k^2}{n^2}}e^{-kt}\sqrt{P^2+Q^2}\sin nt\left(\sqrt{1-\frac{k^2}{n^2}}-\tan^{-1}\frac{Q}{P}\right)}{8\left(1-\frac{k^2}{n^2}\right)^{\frac{3}{2}}}, \quad (t>0) \\ x &= 0, \qquad (t<0) \end{aligned}\right\} \tag{32}$$

where $P=kt\left(7-8\frac{k^2}{n^2}\right)+\left(6\frac{k^2}{n^2}-5\right), \qquad Q=\sqrt{1-\frac{k^2}{n^2}}\left\{nt\left(3-8\frac{k^2}{n^2}\right)+6\frac{k}{n}\right\}.$

(iii) If $n=k$,

$$\left.\begin{aligned} x&=\frac{-b}{2\pi i}\int_{c-i\infty}^{c+i\infty}\frac{z^2e^{zt}dz}{\{z+(a-ib)\}\{z+(a+ib)\}\{z+k\}^2} \\ &=\frac{-(a^2+b^2)}{(a-k)^2+b^2}e^{-at}\sin\left\{bt-\tan^{-1}\frac{2ab}{a^2-b^2}+\tan^{-1}\frac{2b(a-k)}{(a-k)^2-b^2}\right\} \\ &\quad-\frac{bke^{-kt}}{\{(a-k)^2+b^2\}^2}\left[\{(a-k)^2+b^2\}(kt-2)+2k(k-a)\right], \\ &\qquad\qquad\qquad\qquad\qquad\qquad\qquad\qquad (t>0) \\ x&=0. \qquad\qquad\qquad\qquad\qquad\qquad\qquad (t<0) \end{aligned}\right\} \quad (33)$$

The respective first terms in (31), (33) represent forced oscillation and the respective second terms free oscillation. The results of calculation for the three cases of n/b (for $a/b=0{\cdot}1$ or 1) for $k/n=0{\cdot}6$ are shown in Figs. 13～15. Although, in these cases, the damping is relatively high, if n/b were not small, that is to say, if the condition were in that of the accelerometer, the movement of the seismograph would not necessarily agree with that of the ground motion. In such a condition, the duration of the initial motion of

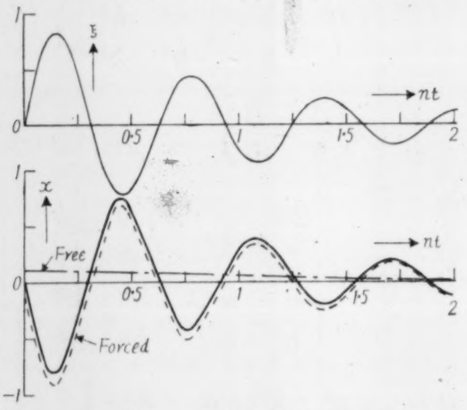

Fig. 13. $\xi=e^{-at}\sin bt$ for $t>0$, $\xi=0$ for $t<0$. $a/b=0{\cdot}1$, $n/b=0{\cdot}1$, $k/n=0{\cdot}6$.

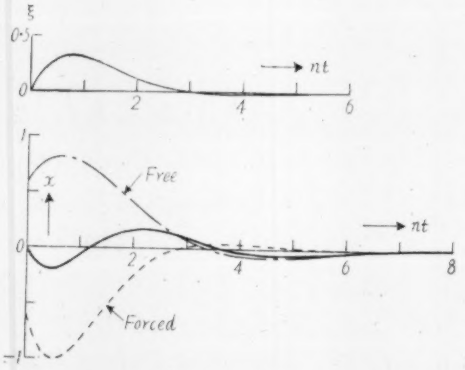

Fig. 14. $\xi=e^{-at}\sin bt$ for $t>0$, $\xi=0$ for $t<0$. $a/b=1$, $n/b=1$, $k/n=0{\cdot}6$.

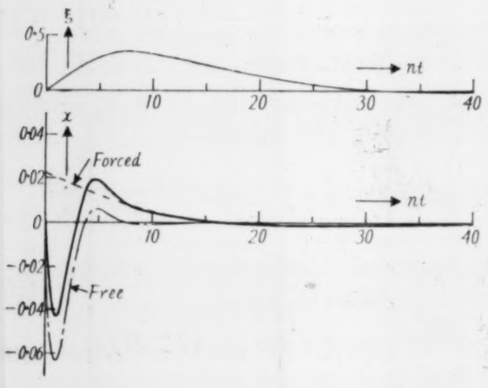

Fig. 15. $\xi=e^{-at}\sin bt$ for $t>0$, $\xi=0$ for $t<0$. $a/b=1$, $n/b=10$, $k/n=0{\cdot}6$.

the pendulum is unduly small and the amplitude of the same motion fairly large. It is however possible to say that the initial motion of the pendulum is in the sense opposite to that of the ground. Owing to the fact that $x_0=0$, $\xi_0=0$, it is also possible for condition $x_0'=-\xi_0'$ to exist.

7. *The special case of* $\xi=e^{-at}(2\sin bt-\sin 2bt)$ *for* $t>0$, $\xi=0$ *for* $t<0$.

In the examples shown in the foregoing sections, it was assumed that the ground motion begins suddenly with initial velocity. In such cases, the duration of the initial motion of the pendulum is unduly small and the amplitude of the same motion fairly large. If, on the other hand, the ground motion begins without initial velocity, the feature in the seismographic movements, particularly, that in the amplitude of the initial motion, is modified to a certain extent.

For the present purpose, we write

$$\left.\begin{aligned} &\xi=e^{-at}(2\sin bt-\sin 2bt), &&(t>0) \\ &\xi=0, &&(t<0) \end{aligned}\right\} \tag{34}$$

by means of which expressions it is possible for the initial displacement and velocity of the ground to be made zero.

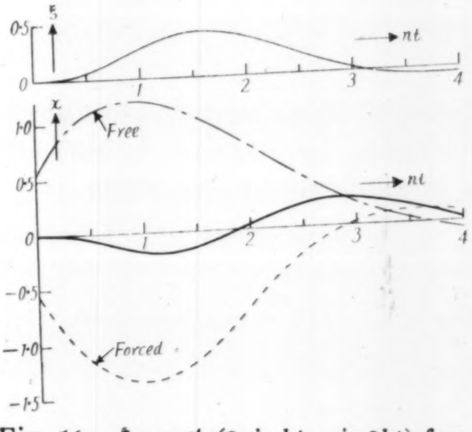

Fig. 16. $\xi=e^{-at}(2\sin bt-\sin 2bt)$ for $t>0$, $\xi=0$ for $t<0$. $a/b=1$, $n/b=1$, $k/b=0{\cdot}6$.

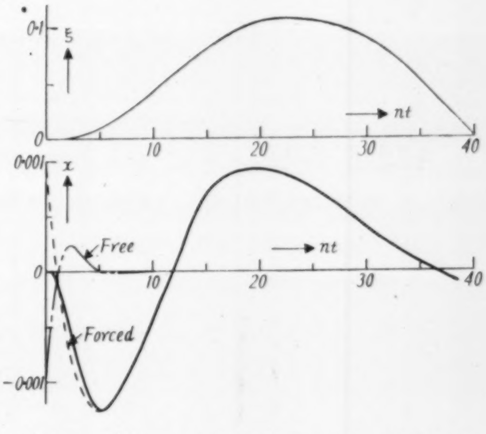

Fig. 17. $\xi=e^{-at}(2\sin bt-\sin 2bt)$ for $t>0$, $\xi=0$ for $t<0$. $a/b=2$, $n/b=20$, $k/n=0{\cdot}6$.

The results of calculation for two cases of n/b are shown in Figs. 16~17. It will be seen that although the duration of the initial motion of the pendulum becomes small for quick motion of the ground, the amplitude of the same initial motion is not abnormally large.

8. *Concluding remarks.*

Using the operational calculus, we calculated the type of movement of a seismograph subjected to arbitrary earthquake motion. Generally speaking, the motion of the pendulum consists of two parts, one of which corresponds to forced oscillation and the other to free oscillation. In any case, the initial motion of the pendulum is in the sense opposite to that of the ground motion. In the case of a displacement seismometer, the motion of the pendulum fairly agrees with that of the ground, whereas in the acceleration seismometer it does not. When the disturbance occurs suddenly, the amount of initial displacement of the seismometer is the same as that of the ground motion, but in opposite sense. If the ground motion of quick type begins with zero displacement and zero velocity, then, although the duration of the initial movement of the pendulum becomes very small, the amplitude of the same motion is not abnormally large.

In conclusion, we wish to express our thanks to Mr. Watanabe, who assisted us greatly in our calculations. We also wish to express our sincere thanks to the officials of the Division of Scientific Research, in the Ministry of Education, for financial aid (Funds for Scientific Research) granted us for a series of investigations, of which this study is a part.

Added notes—For getting, operationally, the earth's displacement from a seismographic record (without magnification), we write

$$\ddot{x} + 2k\dot{x} + n^2 x = -\ddot{\xi}. \qquad (1)$$

Using the sympol p of the operator for d/dt, (1) transforms to

$$\xi = -x - \frac{(2kp+n^2)}{p^2}x \equiv -x + \xi_1. \qquad (2)$$

Let $\phi(p)$ be the operational form of x. Then

$$\xi_1 \supset -\frac{(2kp+n^2)}{p^2}\phi(p), \qquad (3)$$

from which

$$\xi_1 = -\frac{1}{2\pi i}\int_{c-i\infty}^{c+i\infty} e^{zt}\frac{2kz+n^2}{z^3}\phi(z)dz. \tag{4}$$

If the pendulum movement were of the form $f(t)$, then, from Mellin's theorem, it would follow that

$$\phi(z) = z\int_0^{\infty} e^{-zt_1}f(t_1)dt_1. \tag{5}$$

Substituting (5) in (4), and changing the orders of the integrations,

$$\xi_1 = \frac{-1}{2\pi i}\int_0^{\infty} f(t_1)dt_1\int_{c-i\infty}^{c+i\infty} e^{z(t-t_1)}\frac{2kz+n^2}{z^2}dz. \tag{6}$$

Considering the nature of the contour of the integration,

$$\xi_1 = \frac{-1}{2\pi i}\int_0^{t} f(t_1)dt_1\int_{c-i\infty}^{c+i\infty} e^{z(t-t_1)}\frac{2kz+n^2}{z^2}dz = -\int_0^t f(t_1)dt_1\Big[2k+n^2(t-t_1)\Big]. \tag{7}$$

Integrating by parts,

$$\xi_1 = -2k\int_0^t f(t_1)dt_1 - n^2\int_0^t dt_2\int_0^{t_2} f(t_1)dt_1. \tag{8}$$

Putting this in (2), we naturally get

$$\xi = -x+\xi_1 = -f(t_1) - 2k\int_0^t f(t_1)dt_1 - n^2\int_0^t dt_2\int_0^{t_2} f(t_1)dt_1. \tag{9}$$

Although this formula can be obtained directly from (1), the foregoing calculation is specially to show the method of applying operational calculus to the present case. The case of Galitzin's pendulum can also be discussed in the same way.

12. 演算法によりて解いた地震計の初動問題について（第1報）

地震研究所 妹澤克惟
金井清

演算法を用ひる事によつて任意の地震動を受ける地震計の動きを計算した．一般的にいふと，振子の動きの表式は强制振動の部分と自己振動の部分とから成立つ．如何なる場合にも振子の動きは地動と反對方向になる．變位地震計の場合には振子の動きは地動と可成り一致するけれども，加速度地震計は必しも然らず．地動が極めて急激に起るときは地震計の動きは地動の動きと同じであつて地動とは反對方向になるといふ事も出るのである．尙，地動が最初に變位も速度も零から始まるときには，地震計の初動の繼續時間は短いが振幅は必しも大きくならぬ．之に反して地動の最初の速度が零でないときには地震計の初動の繼續時間も短いし，その振幅も非常に大きくなるのである．

13. *On the Problem of Instabilities of Higher Orders in a Seismometer. III. Experiments with a New Vertical Vibration Table.*

By Kiyoshi KANAI and Katsutada SEZAWA,

Earthquake Research Institute.

(Read Feb. 20, 1941.—Received March 20, 1941.)

1. *Introduction.*

In the previous paper,[1] the main point ascertained was the effect of vibration damping on the stability of a seismometer. In the same paper, the order of instability, particularly in experiments, was for such part as is near 1/2. In the present paper, the range of the instability condition has been extended to that of 3/2 as well as 4/2. Since our new vibration table of vertical type was only recently constructed, the instabilities under consideration were investigated by means of this table as well as by the horizontal vibration table in use since last year.

2. *A new vertical vibration table.*

Our new vertical vibration table is of the type shown in Fig. 1. The table T, 130 cm long and 40 cm wide, rotated about the axis AA. As the longer arm of the table was 100 cm long, if a seismometer or a structure model were placed near the end of the longer arm in question, it would be possible for the motion of that part to be virtually undergoing an up and down motion so long as the amplitude of that part exceeds a few milimeters. However, the amplitude during the experiments was always less than a milimeter. A steel plate weighing 50 kg was hung on the shorter arm, 30 cm long, in order to balance the static moment arising from the longer arm. The steel axle AA, 12 mm in dia. was mounted on ball bearings. The remaining part of the table, including the foundation of the ball bearings, was of cast aluminium and of framed construction. Wooden boards were placed on the top of the table.

The table was moved by a motor M of Leonald type through a steel

1) K. KANAI and K. SEZAWA, "On the Problem of Instabilities of Higher Orders in a Seismometer. II," *Bull. Earthq. Res. Inst.*, **19** (1941), 9∼13.

rod R of 19 mm dia., aluminium frame F, and steel springs S_1, S_2. The axle BB, a steel rod, 19 mm in dia., was also mounted on ball bearings. The crank pin end and the other end C of the rod R were both ball bearing.

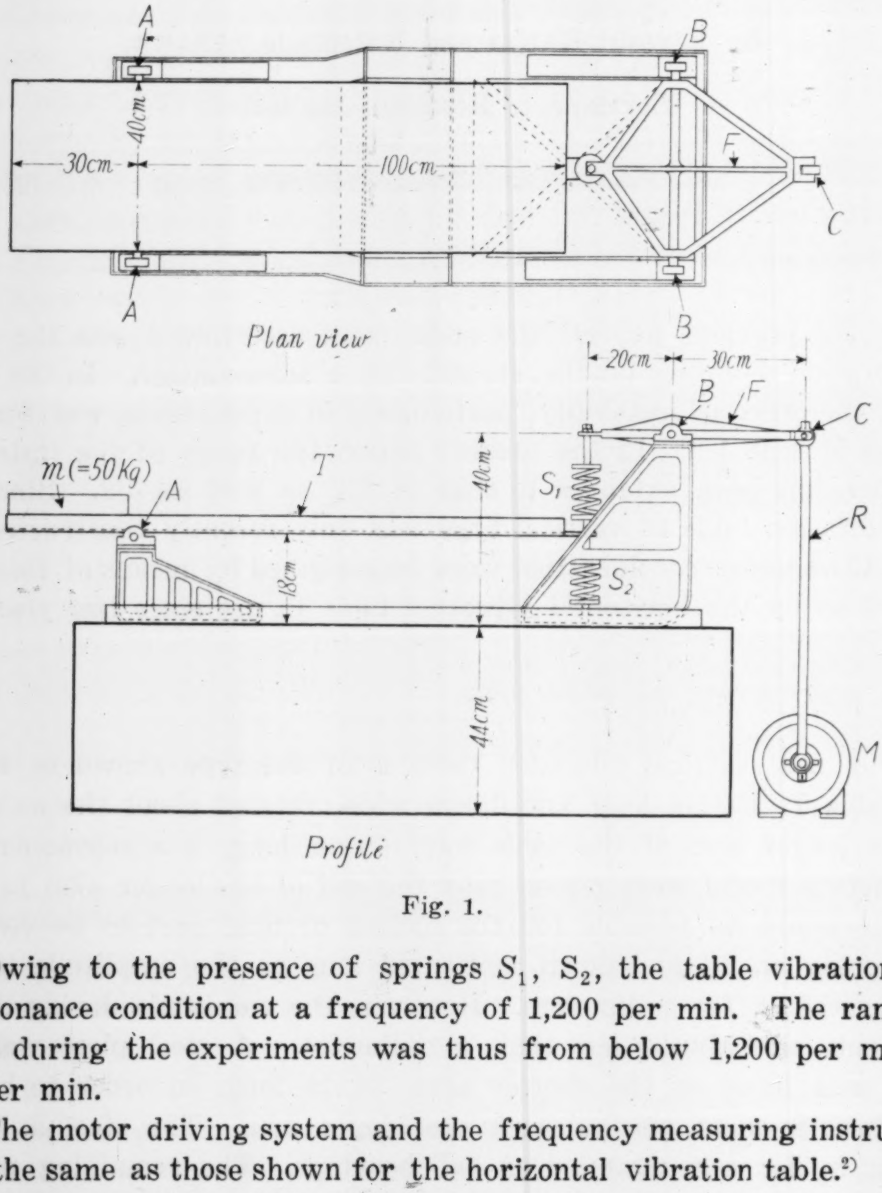

Fig. 1.

Owing to the presence of springs S_1, S_2, the table vibration was in resonance condition at a frequency of 1,200 per min. The range of cycles during the experiments was thus from below 1,200 per min. to 100 per min.

The motor driving system and the frequency measuring instrument were the same as those shown for the horizontal vibration table.[2] Since the vibratory motion of the table was about the pivot axis AA, oscillation in the present case was more satisfactory than in the case of the horizontal vibration table. Notwithstanding springs S_1, S_2, the vibration

2) K. KANAI and K. SEZAWA, "Effect of...and Model Experimental Confirmations of that Effect with a New Vibration Table," *Bull. Earthq. Res. Inst.*, 18 (1940), 370~383.

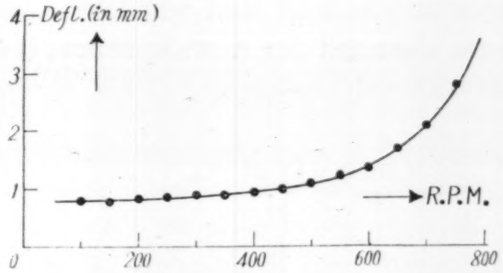

Fig. 2.

amplitude was always about 0·85 mm for such a wide range as that between 100 per min. and 400 per min. The amplitudes of the table observed for vibrational frequency between 100 per min. and 800 per min. are shown in Fig. 2, from which it will be seen that for frequencies less than 400 per min. the amplitudes were almost constant.

3. *Experiments with the vertical vibration table.*

Using the vertical vibration table shown in the previous section, the vertical stability of a horizontal seismometer was ascertained experimentally. The equivalent pendulum length, the natural period, and the mass of the seismometer used in this case were $L=11$ cm, $T=0{\cdot}133$ sec, $M=15$ kg, respectively. Because the pendulum was movable horizontally and at right angles to the direction of the pivot axis of the table, asymmetry of the pendulum motion resulting from small inclinations of the table was avoided. The movements of the pendulum were recorded optically, through a small mirror attached to the pendulum, on a bromide paper on a drum that lay at a certain height above the pendulum.

The vibration damping of the seismometer involved seven cases, the logarithmic decrements of which were $\kappa=0{\cdot}13$, $0{\cdot}23$, $0{\cdot}33$, $0{\cdot}90$, $1{\cdot}5$, 2, $2{\cdot}7$, in sec^{-1} unit. Since the value of κ for critical damping in the present condition of the pendulum was $\kappa=47\,\mathrm{sec}^{-1}$, the damping used in the experiments were much smaller than that in an actual seismometer. From the optical records for different vibrational frequencies of the table in these various cases, the actual displacements of the centre of percussion of the seismometer were calculated, with results as shown in Figs. 3~9

Since the natural period of the pendulum was 0·133 sec, frequencies of the 2/2, 3/2, and 4/2 orders of instability should have occurred at 451 per min., 300 per min., and 226 per min., respectively. From the experiments, it will be seen that the large amplitudes of the pendulum occurred close to such frequencies although there were some deviations. These deviations were the effects of vibration damping. It should be borne in mind that since resonance condition also participated in the 2/2 order of instability, amplitudes of the same order were not shown

in the results.

A special feature of all the experiments was that although the vibrational frequencies of the table were changed for a wide range, the seismometer oscillated always with its natural frequency. This is the

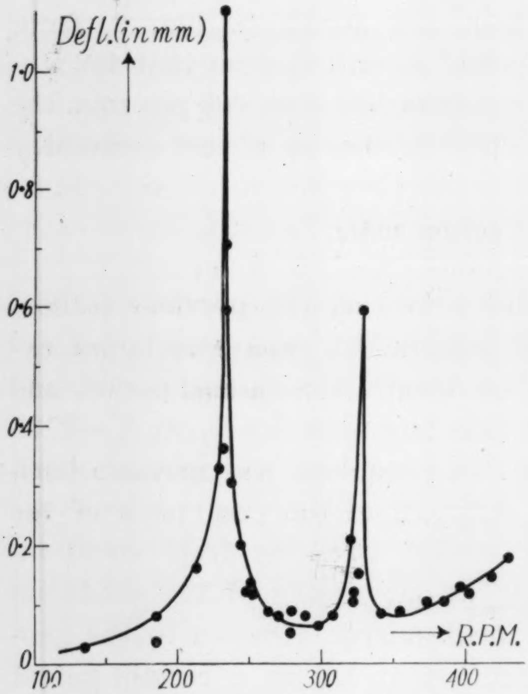

Fig. 3. Deflection of the centre of percussion in the case of $\kappa=0{\cdot}13$.

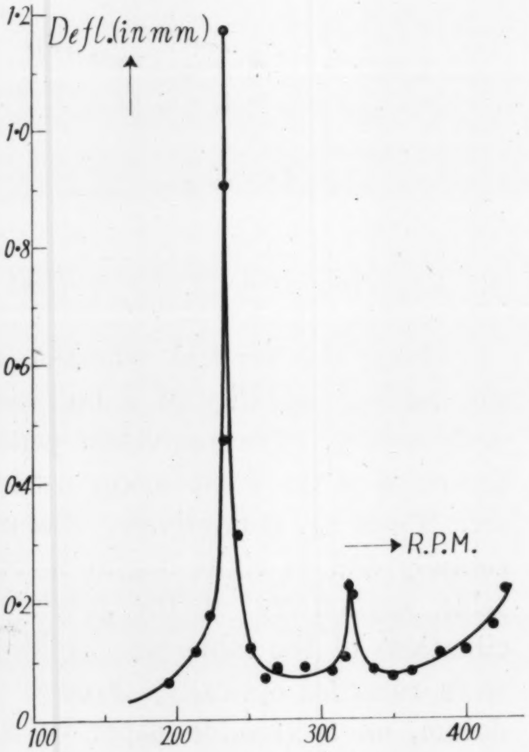

Fig. 4. Deflection of the centre of percussion in the case of $\kappa=0{\cdot}23$.

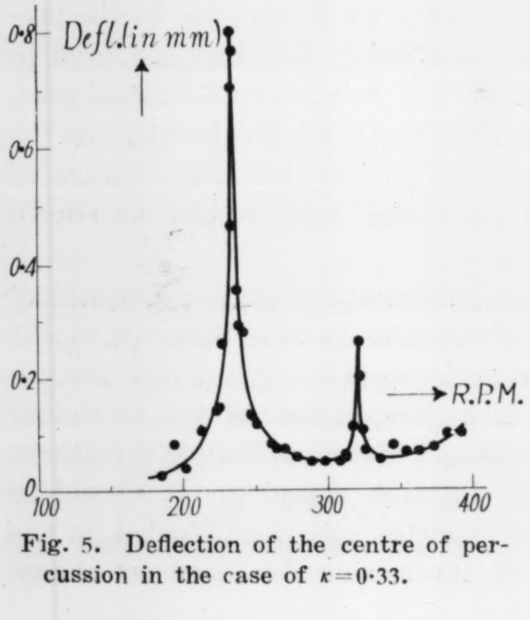

Fig. 5. Deflection of the centre of percussion in the case of $\kappa=0{\cdot}33$.

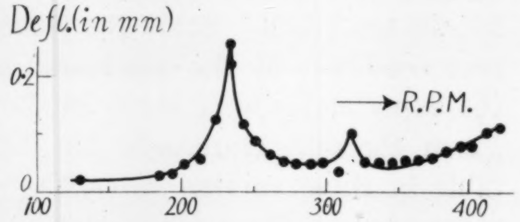

Fig. 6. Deflection of the centre of dercussion in the case of $\kappa=0{\cdot}90$.

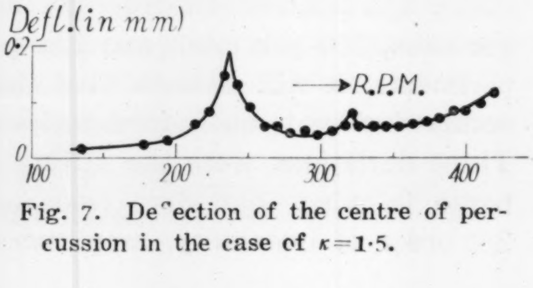

Fig. 7. De"ection of the centre of percussion in the case of $\kappa=1{\cdot}5$.

reason why the results in Figs. 3∼9 represent instability, and are not resonance curves. However, the instability shown in the present ex-

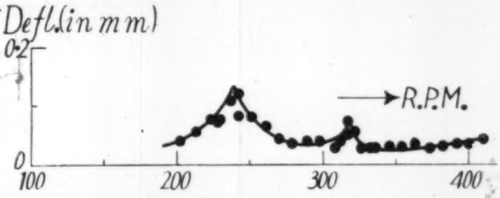

Fig. 8. Deflection of the centre of percussion in the case of $\kappa=2{\cdot}0$.

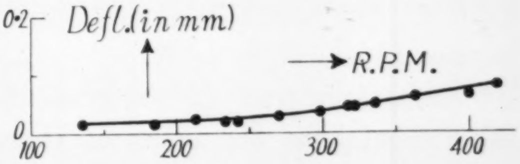

Fig. 9. Deflection of the centre of percussion in the case of $\kappa=2{\cdot}7$.

periments was not vibrational instability in the usual sense, not the vibration that augments without limit with time increase. As already mentioned in the previous paper, the seismometer becomes abnormally sensitive for certain frequencies of the table vibration, from which it is also assumed that some small amplitude at a frequency intermediate between those of the instability conditions in the present experiments, arose as the result of increase in the sensitivity of the seismometer with certain motions of the table.

Comparing Figs. 3∼9, it will be seen that the amplitudes of instability conditions diminished enormously with increase in the vibration damping of the pendulum. Even for such a value as $\kappa=2{\cdot}7$, there is no peak in the curve of the vibration amplitudes (see Fig. 9), whence it holds that for critical damping of the seismometer, that is to say, $\kappa=47\,\text{sec}^{-1}$ in the present case, it is not possible to consider any instability effect, at any rate, for the 4/2 and 3/2 orders of instability. For confirming the effect of change in κ on the instability condition, the am-

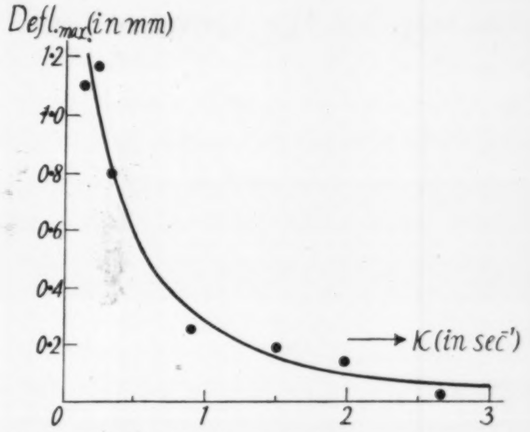

Fig. 10. Maximum deflection of the centre of percussion for different κ's.

plitudes at the frequency for the 4/2 order of instability for different values of κ were replotted in Fig. 10. The curve becomes nearly asymptotic to the abscissa at $\kappa=2{\cdot}7\,\text{sec}^{-1}$, that is, the abscissa much less than that corresponding to critical damping ($\kappa=47\,\text{sec}^{-1}$).

4. *Experiments with the horizontal vibration table.*

The main purpose of the present paper is to show the instability

condition of a horizontal seismometer for vertical vibration of the ground. Since however the problem was restricted to the 4/2 order and 3/2 order of instabilities (these instabilities had not yet been studied), the instabilities of these orders were also ascertained with the horizontal vibration table.

The table used in the present experiment was the same as that shown in the previous paper. The seismometer was so placed on the table that it could be moved horizontally about a vertical axis and at right angles to the direction of the oscillation of the table. Thus the axis of rotation of the pendulum in the present case differed 90 degree from that in the case of the vertical vibration table.

The natural period and the mass of the seismometric pendulum also differed from those in the previous case, but the equivalent pendulum length was the same as that for the vertical vibration table. The values under consideration were $L=11$ cm, $T_0=0{\cdot}0681$ sec, $M=1$ kg., respectively. Since there were no springs used in the horizontal vibration table, the amplitude of the same table was kept always at 2 mm for any

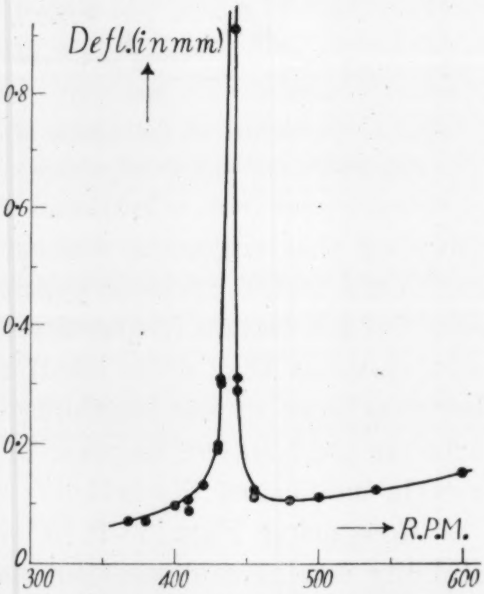

Fig. 11. Deflection of the centre of percussion in the case of $\kappa=0{\cdot}085$.

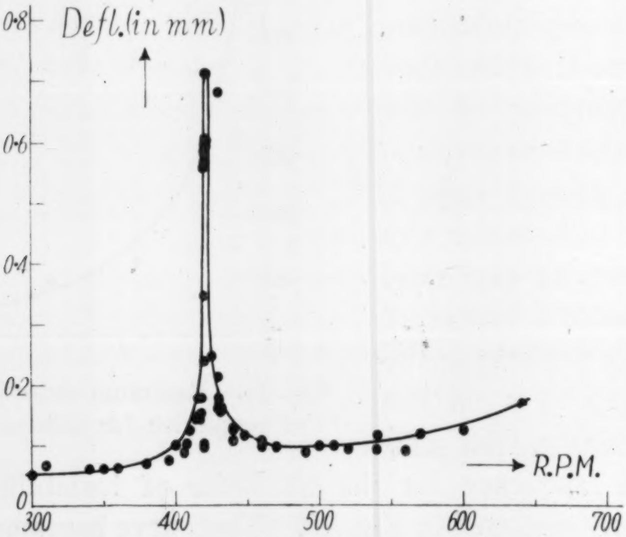

Fig. 12. Deflection of the centre of percussion in the case of $\kappa=0{\cdot}36$.

frequency. The vibration damping was of five kinds, namely, $\kappa = 0{\cdot}085$,

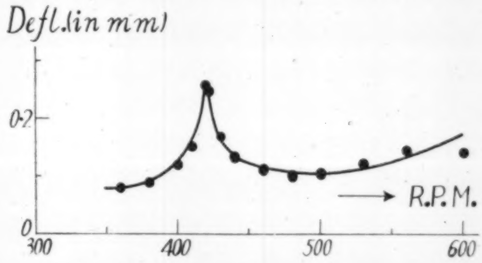

Fig. 13. Deflection of the centre of percussion in the case of $\kappa = 1{\cdot}03$.

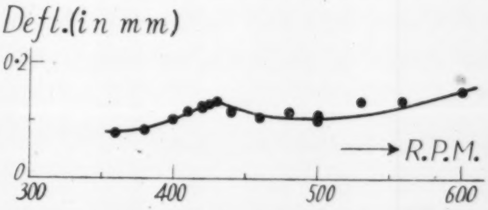

Fig. 14. Deflection of the centre of percussion in the case of $\kappa = 2{\cdot}95$.

0·36, 1·03, 2·95, and 5, in $\sec^{-1}$ units. In this case, too, the displacements of the centre of percussion were calculated from records observed optically, the results of which are shown in Figs. 11∼15. Although there is no appreciable peak for the 3/2 order of instability in the present case, the peaks corresponding to the 4/2 order of instability (frequency $=447$ per min.) are very marked, particularly, for smaller values of κ. When, however, $\kappa = 5$, the amplitude for the peak in question is almost indiscernible. The amplitudes of the 4/2 order of instability were replotted in Fig. 16. The reason that the

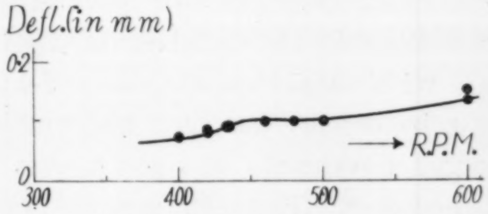

Fig. 15. Deflection of the centre of percussion in the case of $\kappa = 5{\cdot}0$.

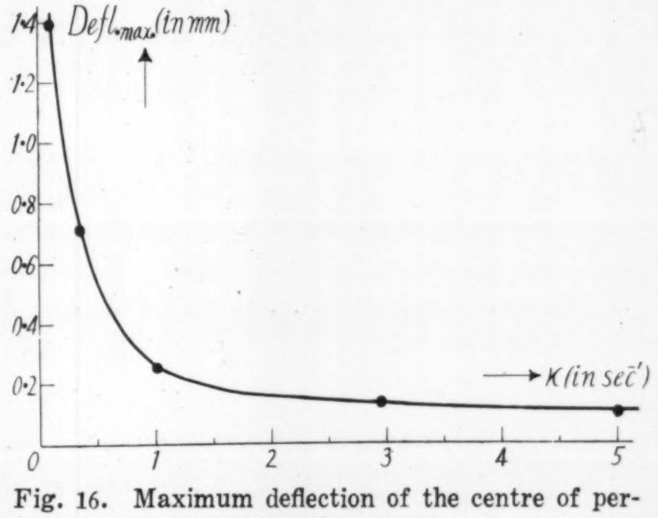

Fig. 16. Maximum deflection of the centre of percussion for different κ's.

amplitude in Fig. 16 does not touch the abscissa even at $\kappa = 5\ \sec^{-1}$, is rather that the general amplitude of the pendulum does not vanish for a large value of damping.

The important feature of the vibration in the present case is that, as in the vertical vibration table, the seismometric pendulum oscillated with its natural frequency for any frequency of table vibration, whence it follows that the nature of the instability for horizontal vibration was the same as that for vertical vibration.

5. *Concluding remarks.*

The instability conditions of the 4/2 and 3/2 orders in a horizontal seismometer were ascertained with the new vertical vibration table as well as with the horizontal vibration table shown previously. It was found that although the instabilities in question were not vibrational instabilities in the usual sense, that is, vibration that augments without limit with time increase, their features are such that the sensitivity of the seismometer becomes abnormally large for certain frequencies of ground movements at right angles to the movable direction of the same seismometer. The seismometric pendulum in such ground motion, should oscillate with its natural period for any frequency of the ground movement, including the frequencies that correspond to the instability condition of the pendulum.

In conclusion, we wish to express our thanks to Mr. Kodaira, who assisted us greatly in our experiments. We also wish to express our thanks to the officials of the Division of Scientific Research, in the Ministry of Education, for financial aid (Funds for Scientific Research) granted us for a series of investigations, of which this study is a part.

---

13. 地震計に於ける高次の不安定に就いて (第3報)
新しい上下動振動臺による實驗

地震研究所 {金井清
{妹澤克惟

水平動地震計の 4/2 次及 3/2 次の不安定を新しい上下動振動臺及びこの前からの水平動振動臺を用ひて確めた．このやうな不安定は普通の意味に於ける不安定即ち振幅が時間と共に際限なく増加する不安定ではないけれども，地震計の動く方向に直角をなす地動が特定の周期になるときに地震計の感度が異常によくなるやうな意味での不安定である．このやうな周期に於て地震計が振動する周期は地動のそれではなく，地震計の自己周期に當つてをる事もわかつたのである．

---

14. *Elastic Waves from a Point in an Isotropic Heterogeneous Sphere. Part 3.*

By Ryoiti YOSIYAMA,

Seismological Institute.

(Read Feb. 2, 1941.—Received March 24, 1941.)

1. As will become apparent by the following paragraph, in studying the propagation of waves through a medium, the heterogeneity of which in respect to its density and elastic constants is small, the problem eventually revolves itself into a mathematical treatment of a differential equation of the type

$$\frac{\partial^2\phi}{\partial T^2}=v^2\nabla^2\phi-\alpha^2\phi, \tag{117}$$

in which v stands for $\sqrt{\frac{\lambda+2\mu}{\rho}}$ or $\sqrt{\frac{\mu}{\rho}}$, and α^2 is some function of derivatives of ρ, λ, and μ. When the medium is homogeneous, these derivatives vanish, and the equation (117) reduces to the so-called "wave equation" in a homogeneous medium. In Parts 1 and 2,[1] the writer, dealing with a special heterogeneous medium, worked out equations of wave motion exactly similar to (117).

It is shown in this paper that, even through a more general heterogeneous medium, waves of a certain character are propagated in accordance with an equation of type (117), and it will be easily seen from the example in Part 2 that, in some cases, $\alpha^2=0$ or v is a constant, although the medium may be heterogeneous with respect to each of its elastic constants and density.

In certain branches of atomic physics, equations of the type (117) are studied, and some approximate solutions obtained. However, since the problems met with in seismology differ from those in atomic physics, it is not likely that those approximate solutions can be satisfactorily used for the former. Here, solutions of equation (117) are discussed, using the results obtained in Parts 1 and 2 of this paper.

2. After the notations in Part 1, equation (117) is written in the form

1) R. YOSIYAMA, *Bull. Earthq. Res. Inst.*, **11** (1933), 1~13., **18** (1940), 41~56.

$$\frac{\partial^2\phi}{\partial T^2}=\frac{h_2h_3}{h_1}\left\{\frac{\partial}{\partial t}\left(\frac{h_1}{h_2h_3}\frac{\partial\phi}{\partial t}\right)+\frac{\partial}{\partial\beta}\left(\frac{h_2}{h_3h_1}\frac{\partial\phi}{\partial\beta}\right)+\frac{\partial}{\partial\varphi}\left(\frac{h_3}{h_1h_2}\frac{\partial\phi}{\partial\varphi}\right)\right\}-\alpha^2\phi.$$

Putting (118)

$$\phi=\sqrt{\left|\frac{h_2h_3}{h_1}f(\beta)\right|}\ \ \phi_1\begin{matrix}\sin m\varphi\\ \cos m\varphi\end{matrix}\,e^{\pm ipT}, \tag{119}$$

the equation transforms to

$$\frac{1}{\phi_1}\frac{\partial^2\phi_1}{\partial t^2}+p^2-\alpha^2-\alpha'^2+\frac{h_2^2}{h_1^2}\left\{\frac{1}{\phi_1}\frac{\partial^2\phi_1}{\partial\beta^2}\right.$$

$$\left.+\frac{1}{\phi_1}\frac{\partial\phi_1}{\partial\beta}\frac{\partial}{\partial\beta}\log\frac{h_2^2}{h_1^2}f(\beta)-m^2\frac{h_3^2}{h_2^2}\right\}=0, \tag{120}$$

in which

$$-\alpha'^2=v^2\sqrt{\left|\frac{h_1}{h_2h_3f(\beta)}\right|}\ \ \nabla^2\sqrt{\left|\frac{h_2h_3}{h_1}f(\beta)\right|}\,. \tag{121}$$

The expression of $f(\beta)$, which is arbitrary as yet, had best be determined in such a way that ϕ_1 in equation (120) may be solved in the most convenient form possible to discuss the problem.

We see that $\frac{d\beta}{h_2}$ is equal to the length of a line-element, perpendicular to two wave rays in a plane $\varphi=$const., making an angle $d\beta$ with each other at the origin, and that, consequently, $\frac{1}{h_2}$ increases with t if, as in most conceivable cases, the wave-front spreads out as the wave motions are propagated, with the result that $\frac{h_1}{h_2}$, h_1 being equal to $\frac{1}{v}$, also tends generally to increase with t. The same conclusion also holds true with respect to $\frac{h_1}{h_3}$. Consequently, if m is small, we may put for sufficiently large values of t and p, neglecting the variations of α^2 and α'^2,

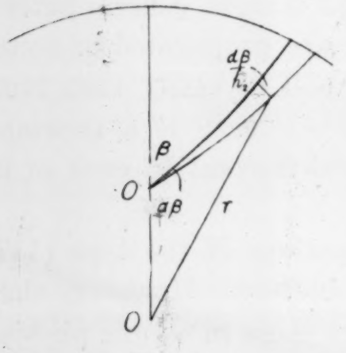

Fig. 1.

$$\phi_1=e^{\pm i\sqrt{p^2-\alpha^2-\alpha'^2}\,t} \tag{122}$$

in which $f(\beta)$ is required to be such that α'^2 is practically constant.

If we can get $f(\beta)$ for which $\alpha^2+\alpha'^2$ is a constant, then $\sqrt{\left|\frac{h_2 h_3}{h_1} f(\beta)\right|}$ $\cdot e^{\pm i\sqrt{p^2-\alpha^2-\alpha'^2}\,t}$ becomes one of the exact particular solutions of (117). This solution corresponds to that for a single source in a homogeneous medium, and from this solution it is possible to find a solution for the wave from a multiple source in a heterogeneous medium by the same method of procedure as that in the case of a homogeneous medium. Although the solution thus obtained must be equivalent to that obtained directly from (117) or (118), determination of such $f(\beta)$ is obviously equivalent to obtaining a particular solution of the original equation (117), which is none the less difficult. However, if we can get an approximate solution of $f(\beta)$, an approximate solution of (117) naturally follows. When v^2 and α^2 are both constant, we have $f(\beta)=\sin\beta$ and $\alpha'^2=0$, whence it may be assumed that generally $f(\beta)\doteqdot\sin\beta$. And if p is sufficiently large, $p^2-\alpha^2-\alpha'^2$ being considered practically constant, we can use (122) as a particular solution of ϕ_1.

In the case of a homogeneous medium, or such as that considered in Parts 1, 2, then ϕ_1 is expressible by a product of two functions, one of which is a function of t only, and the other a function of β only. Put, for example, X for the former and Y for the latter. In all the cases just given, $f(\beta)=\sin\beta$ and $Y=P_n^m(\cos\beta)$; $X=\sqrt{t}\,H_{n+\frac{1}{2}}(pt)$ in the case of a homogeneous medium, and $X=\left(\frac{\sinh 2\sqrt{ab}\,t}{2\sqrt{ab}}\right)^{\frac{1}{2}}U_n$ in the case considered in Parts 1, 2.

Now it is a debatable point whether or not ϕ_1 is in all cases expressed by a product of two functions. The answer to this question must be relevant to one of the theoretical bases of the method of procedure, by means of which we may discuss the mechanism of earthquake occurrence at the origin from observations of the amplitudes and the directions of initial motions on the earth surface.

Although a mathematical treatment of this problem without assuming the functional forms of v^2 and α^2 seems very difficult, there is no doubt, at any rate, that $Y=P_n^m(\cos\beta)$ holds true for only a few special cases. Even when $v=a-br^2$, α^2 being a function of r, the assumption $\phi_1=X\cdot Y$ is clearly inadmissible, even if Y is not restricted to $P_n^m(\cos\beta)$.

At all events, unsatisfactory conditions caused by putting

$$\phi_1=e^{\pm i\sqrt{p^2-\alpha^2-\alpha'^2}\,t}\,P_n^m(\cos\beta) \tag{123}$$

decrease as $\frac{h_2^2}{h_1^2}$, and $\frac{h_3^2}{h_1^2}$ decreases compared with p^2. This means that,

when the wave front duly spreads out, waves of sufficiently short period are propagated independently along each path, as determined by Fermat's principle, the wave form observed on each path not being affected by the phase difference between waves along contiguous paths.

The foregoing remarks refer to a stationary wave. Solitary waves, for example, the *P* wave and the *S* wave observed in seismograms, may be considered, from a knowledge of Fourier's series, as superpositions of stationary waves of various periods. Consequently it will be accepted that, at the beginning of the *P* phase, the *S* phase and other solitary phases, whose time of incidence are clearly identified in seismograms, waves of fairly short period predominate, with the result that, (123) being accepted, the effect of heterogeneity on the beginning of such phases, especially on the direction, push and pull, of the incidence, will generally be negligible. Moreover, by applying the results of the calculations in Part 2, the velocity of propagation of incidence of disturbances will be equal to v. The effect of heterogeneity of the medium becomes very marked in later observations, the most marked being a certain reduction in the maximum amplitude of the disturbance, besides the appearance of damped oscillation of a characteristic frequency, which we shall call the "tail." These conclusions above stated can be deduced from the results obtained in Part 2. Obviously, the oscillation just mentioned has a physical significance only when $\alpha^2+\alpha'^2>0$, as will be seen from (92) in Part 2. When $\alpha^2+\alpha'^2<0$, the effect increases exponentially with time, in which case we must take into consideration that, in building up the wave equation (117), we have neglected, as stated in Part 2, the terms of the product of any two of ϕ, $\frac{\partial \phi}{\partial t}$, and so on, and also that the stress-strain relation in the medium, in which there must be a very close connection between every molecule, will naturally be altered when the deformation increases. Therefore, when $\alpha^2+\alpha'^2<0$, the effect above stated loses its fitness for being interpreted physically, particularly in the case of an ordinary elastic medium. However, in a fluid medium, whose molecules are to a certain extent free and not closely bound to one another, such a state as $\alpha^2+\alpha'^2<0$ may be regarded as being unstable.

At any rate, referring here again to the results from (91) to (93), described in Part 2, we find that the terms expressing these effects are proportional to certain integral forms, such as $\int_0^{t_0}\psi_1(\omega)d\omega$ or $\int_{t-T}^{t_0}\psi_1(\omega)d\omega$. This clearly means that these effects, namely, the reduction of maximum amplitude or the amplitude of the "tail," decrease, so to speak, as the

apparent period of the disturbance decreases.

Although the solution of (117) will be expressed in various forms, we have attempted to find a solution that contains explicitly a factor of a harmonic function with regard to t, because if the results of observations are considered, such a solution would find wide application in the study of seismology.

From the foregoing discussions, we may use the expression $\sqrt{\left|\frac{h_2h_3}{h_1}\sin\beta\right|}$ as the attenuation factor due to the distance of the station from the origin in obtaining from the observations a more theoretically suitable magnitude of ϕ at the origin, while the area of the wave front, enclosed by wave rays, and spreading out from the origin in a certain solid angle, is equal to $\frac{d\beta d\varphi}{h_2h_3}$, from which last expression we may build up another formula for the attenuation factor.

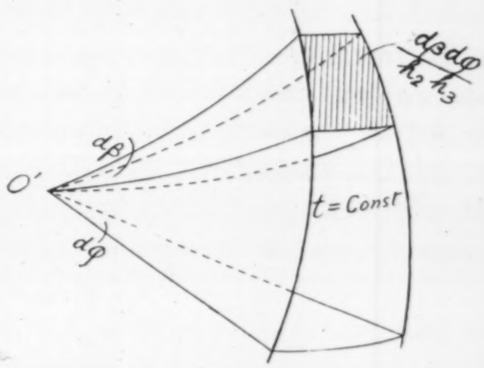

Fig. 2.

It will be seen that, in some cases, $\frac{1}{h_2}$ decreases as t increases, or vanishes at a certain value of t for a certain range of value of β, and that $\frac{1}{h_2}$ changes its sign, from positive to negative, for a smaller or a larger value than that of t, in which case, in the neighbourhood of that region where $\frac{1}{h_2}$ vanishes, $e^{\pm i\sqrt{p^2\alpha^2-\alpha'^2}\,t}$ is not admissible as an approximate solution even though t be large. Considering the significance of $\frac{d\beta d\varphi}{h_2h_3}$ above stated, $\frac{1}{h_2}=0$ means intersection of the wave rays. From (13) in Part 1, $\frac{1}{h_2}=0$ gives

$$\int^{r}\frac{g^2(r)dr}{r\left\{g^2(r)-\kappa^2\right\}^{\frac{3}{2}}}=0, \tag{124}$$

which is equivalent to the equation of the envelope of the wave rays. Although the solution in such a case may be applicable in explaining, say, the mirage, in optics, other mathematical technique will be necessary

in order to find a solution suitable for use in the neighbourhood of that region where $\frac{1}{h_2}=0$. This the writer hopes to treat on a future occasion.

In the following paragraph, we shall treat the problem more concretely and make clear the physical significances of ϕ and α^2 in connection with the elastic constants of the medium.

3. From the θ- and the φ-components of equation of motion (2), we get the following equation with respect to the r-component of rot $\boldsymbol{D}$, ϖ_r,

$$\rho\frac{\partial^2}{\partial T^2}\sqrt{\mu}\,r\varpi_r=\mu\nabla^2\sqrt{\mu}\,r\varpi_r-\left(\sqrt{\mu}\,\nabla^2\sqrt{\mu}+\frac{1}{r}\frac{d\mu}{dr}\right)\sqrt{\mu}\,r\varpi_r. \quad (125)$$

By performing divergence operations on both members of the equation (2), we get

$$\frac{d\rho}{dr}\frac{\partial^2 u_r}{\partial T^2}+\rho\frac{\partial^2\varDelta}{\partial T^2}=\nabla^2\left\{(\lambda+2\mu)\varDelta\right\}-\frac{2}{r^3}\frac{\partial}{\partial r}\left(r^3\frac{d\mu}{dr}\varDelta\right)$$

$$+\frac{2}{r}\frac{d\mu}{dr}\nabla^2 ru_r+2r\frac{d}{dr}\left(\frac{1}{r}\frac{d\mu}{dr}\right)\frac{\partial u_r}{\partial r}. \quad (126)$$

The r-component of equation (2) is modified to

$$\rho\frac{\partial^2 u_r}{\partial T^2}=\frac{\mu}{r}\nabla^2 ru_r+2\frac{d\mu}{dr}\frac{\partial u_r}{\partial r}+\frac{\partial}{\partial r}(\lambda\varDelta)+r^2\mu\frac{\partial}{\partial r}\left(\frac{\varDelta}{r^2}\right). \quad (127)$$

Since no one of the three equations, (125), (126), (127), is derived from the remaining two by mere mathematical operation, we can use these three equations instead of equation (2), consequently we can use the three quantities ϖ_r, $\varDelta$, and u_r instead of the three components of displacement, with the magnitudes of which three it is possible to discuss the deformation in the elastic medium. We find that ϖ_r appears only in equation (125), and also that equation (125) contains ϖ_r only. Consequently, the problem can be treated by considering that, in such a medium, the deformed state, generally, is a superposition of two kinds of waves, the one satisfying equation (125) and $u_r=\varDelta=0$, and the other equations (126), (127), and $\varpi_r=0$.

We know that two kinds of waves are propagated through a homogeneous medium. Although, in a heterogeneous medium, the propriety of assuming that it is possible to classify the waves is questionable, such assumption is clearly very convenient in solving the equations. And since, as a matter of fact, there are two distinct phases, such as

the P phase and the S phase, as observed in seismograms, solutions of problems on such assumption will also be of some use in seismological investigations.

Prof. K. Sezawa, for convenience in dealing with earthquake mechanism, classified the waves through a homogeneous medium into three kinds, namely, the irrotational dilatational wave and equivoluminal rotational waves of the first kind and of the second kind. In this paper, it is shown that it is convenient, in the case of a heterogeneous medium, to assort the waves according to their characteristic mode of propagation. Since waves of magnitude of ϖ_r, such that $u_r = \Delta = 0$, are propagated as a wave independent of other disturbance as already stated, we shall call it the "*transverse wave of type B.*" It will be easily understood that, generally speaking, if the elastic constants and density of the medium are some functions of one of the coordinates of a certain orthogonal curvilinear coordinate system, that component of rot $\boldsymbol{D}$ is propagated as a "*transverse wave of type B*" independently of other waves. In the case of a homogeneous medium, there are two other types of waves, one of which is the "*longitudinal wave,*" and the other the transverse wave, such that $\varpi_r = \Delta = 0$.

Neglecting the gradient terms of ρ, λ, and μ in (126) and (127), we get the following, as approximate equations in a heterogeneous medium,

$$\rho \frac{\partial^2 \Delta}{\partial T^2} = \nabla^2 \left\{ (\lambda + 2\mu) \Delta \right\}, \tag{128}$$

$$\rho \frac{\partial^2 u_r}{\partial T^2} = \frac{\mu}{r} \nabla^2 r u_r + \frac{\partial}{\partial r} (\lambda \Delta) + r^2 \mu \frac{\partial}{\partial r} \left(\frac{\Delta}{r^2} \right), \tag{129}$$

from which it will be seen that the magnitude of div $\boldsymbol{D}$ is propagated as a wave of velocity $\sqrt{\frac{\lambda + 2\mu}{\rho}}$, which we shall call the "*longitudinal wave.*" The solution of u_r consists of two parts, one of which is a particular solution corresponding to the magnitude of Δ, and the other a general solution obtained by putting $\Delta = 0$. The former is nothing but the magnitude of u_r due to the longitudinal wave, and is necessarily propagated with velocity $\sqrt{\frac{\lambda + 2\mu}{\rho}}$. The latter, however, represents another wave that is propagated with velocity $\sqrt{\frac{\mu}{\rho}}$, and in which $\Delta = 0$. To sum up, the wave that is propagated with velocity $\sqrt{\frac{\mu}{\rho}}$ consists of two types of waves, one of which we have called the "*transverse*

wave of type B" and the other which we shall call the "*transverse wave of type A.*" If we can construct an equation that contains Δ only, and no u_r, such as (128), div $\boldsymbol{D}$ will always vanish in the case of a transverse wave. However, the same is not the case in a heterogeneous medium, as may be seen from (126) and, according to the heterogeneity of the medium, there are some changes of volume necessarily associated with the "*transverse wave of type A.*"

4. *Transverse wave of type B.* For the transverse wave of type B,

$$u_r = \Delta = 0, \tag{130}$$

whence we may put

$$u_\theta = \frac{1}{\sin\theta}\frac{\partial F}{\partial\varphi}, \quad u_\varphi = -\frac{\partial F}{\partial\theta}, \tag{131}$$

where u_θ and u_φ are the θ- and φ-components of displacement $\boldsymbol{D}$. Substituting (131) into the original equation (2) we get, as would have been naturally expected, an equation of the same type as (125), namely,

$$\rho\frac{\partial^2}{\partial T^2}\sqrt{\mu}F = \mu\nabla^2\sqrt{\mu}F - \left(\sqrt{\mu}\nabla^2\sqrt{\mu} + \frac{1}{r}\frac{d\mu}{dr}\right)\sqrt{\mu}F. \tag{132}$$

Solving (132) or (125) in t, β, φ-coordinates, it is now possible to discuss the wave of type B having its source at any point. Putting $\sqrt{\mu}F = \phi$, $\frac{\mu}{\rho} = v^2$, and $\frac{1}{\rho}\left(\sqrt{\mu}\nabla^2\sqrt{\mu} + \frac{1}{r}\frac{d\mu}{dr}\right) = \alpha^2$, (132) transforms to an equation of exactly the same type as (117), so that the results of the discussion of ϕ apply equally well to that of $\sqrt{\mu}F$, and naturally, also, to that of $\sqrt{\mu}r\varpi_r$. Dispersion of the wave increases with α^2, and also with its wave length.

From the θ-, φ-components of displacement given above, the t-, β- and φ-components of displacement can be calculated geometrically as follows,

$$u_t = u_\theta \sin i, \quad u_\beta = u_\theta \cos i,$$

where $g(r)\sin i = g(h)\sin\beta = \kappa$, and $g(r) = \frac{r}{v}$. The magnitude of the transverse wave of the first kind and of the second kind, according to Sezawa's definition, were also calculated by similar formulae, and we have, as the relation between ϖ_r, ϖ_θ and ϖ_φ in the transverse wave of type B,

$$2\varpi_r = -\frac{1}{r\sin\theta}\left\{\frac{\partial}{\partial\theta}\left(\sin\theta\frac{\partial F}{\partial\theta}\right) + \frac{1}{\sin\theta}\frac{\partial^2 F}{\partial\varphi^2}\right\},$$

$$\left.\begin{aligned} 2\varpi_\theta &= \frac{1}{r}\frac{\partial}{\partial r}\left\{r\frac{\partial F}{\partial \theta}\right\}, \\ 2\varpi_\varphi &= \frac{1}{r\sin\theta}\frac{\partial}{\partial r}\left\{r\frac{\partial F}{\partial \varphi}\right\}. \end{aligned}\right\} \tag{133}$$

By putting

$$\frac{\mu}{\rho} = (a-br^2)^2,$$

$$\frac{1}{\rho}\left(\sqrt{\mu}\,\nabla^2\sqrt{\mu} + \frac{1}{r}\frac{d\mu}{dr}\right) = \alpha^2(\text{const}),$$

the wave will be discussed more concretely as done in Part 2.

If, for example, $\mu = \left(c + \frac{d}{r^3}\right)^2$, then

$$F = \frac{1}{\sqrt{\mu}\sqrt{a-br^2}}\sqrt{\frac{2\sqrt{ab}}{\sinh 2\sqrt{ab}\,t}}\,U_n^{(i)}(\sqrt{p^2-ab}\,t)P_n^m(\cos\beta)\frac{\sin m\varphi}{\cos m\varphi}e^{\pm ipT} \tag{134}$$

5. A special case of the wave problem mentioned above is the Love wave that is propagated over a spherical surface, which has already been discussed by the writer.[2]

6. *Transverse wave of type A and the longitudinal wave.* From the results obtained in Part 2, which, however, concerned a special medium, there is no doubt that so long as either its density or its rigidity is not constant, there are no longitudinal waves propagated through a heterogeneous medium in accordance with the usual conception, that is rot $\boldsymbol{D}=0$, which is established when the medium is homogeneous. A similar conclusion may be drawn for the transverse wave of type A, because div $\boldsymbol{D}$ does not vanish. We should conclude, as already suggested, that, through a heterogeneous medium, there is a wave such that $u_r=0$ and div $\boldsymbol{D}=0$, whose characteristics will be studied by equation (131) and (132), and which has been classified above as the transverse wave of type B, and that there is another type of waves, the law of propagation of which is given by equations (126), (127) and $\varpi_r=0$. When the medium is not very heterogeneous, the latter will be observed as a wave composed of two waves, one of which is that called the longitudinal wave, and the other that called in this paper the transverse wave of type A.

The two equation (126) and (127) suggest a coupled motion of two

2) R. YOSIYAMA, *Disin*, **10** (1938), 272~276.

systems in dynamics. The derivatives of ρ, λ, and μ may correspond to the coupling factor. When the two systems are tightly coupled, the characteristic mode of motion of each system will not be clearly observed. A similar argument could be used in the present problem, and we should expect theoretically that when the medium is heterogeneous to a certain degree, the phase of a longitudinal wave and that of a transverse wave of type A can be distinguished only with difficulty. Accordingly the observed fact that onsets of these waves, or time of incidence of these waves, in seismograms, are easily identified should be interpreted as suggesting that the inner part of the earth is only slightly heterogeneous.

In this paper, we are solving the equations approximately, assuming first the existence of waves of equivoluminal rotation and that of irrotational dilatation as in the case of a homogeneous medium, attempting to work out the magnitude of dilatation or that of rotation attached to each wave as a small correction.

7. *Transverse wave of type A, and change in volume.* As a first approximation, the transverse wave of type A is discussed with the aid of the following equation, obtained from (127). Putting $\Delta=0$ we get

$$\rho\frac{\partial^2}{\partial T^2}ru_r=\mu\nabla^2 ru_r+2r\frac{d\mu}{dr}\frac{\partial u_r}{\partial r}, \tag{135}$$

with $\Delta=\varpi_r=0$. Putting $\mu ru_r=\phi$, $\frac{\mu}{\rho}=v^2$ and $\frac{1}{\rho}\left(\nabla^2\mu+\frac{2}{r}\frac{d\mu}{dr}\right)=\alpha^2$, the equation transforms to (117), the results thus obtained being applicable to our case. The beginning of this wave is propagated with velocity $\sqrt{\frac{\mu}{\rho}}$. This wave, together with the transverse wave of type B, may form the S waves that are observed in seismograms. The amplitudes of these two waves which must be projected from the origin at the same time, are determined by the particular mechanism of earthquake occurrence. It is of some interest to know that the quantities which stand for α^2 may very likely differ in each case, so that a phase difference should be expected between these two waves, although the effect due to such phase difference, such for example, as the possibility of two peaks appearing in the S phase, or of a prolongation of the apparent period of the S phase, will be too feeble to be observed in practice because of the fact that the earth is only slightly heterogeneous.

We shall now try to find the change in volume in the S wave. Assuming that the period of the wave is $\frac{2\pi}{p}$, the time factor consequently

being e^{ipT} in common, and neglecting the second term in the right hand members in order to solve to a first approximation, we get from (126),

$$-\frac{d\rho}{dr}p^2u_r-\rho p^2\Delta=\nabla^2\left\{(\lambda+2\mu)\Delta\right\}+\frac{2}{r}\frac{d\mu}{dr}\nabla^2ru_r+2r\frac{d}{dr}\left(\frac{1}{r}\frac{d\mu}{dr}\right)\frac{\partial u_r}{\partial r}, \tag{136}$$

and from (135),

$$-\rho p^2ru_r=\mu\nabla^2ru_r. \tag{137}$$

Putting

$$(\lambda+2\mu)\Delta=\varepsilon ru_r+\delta r\frac{\partial}{\partial r}ru_r, \tag{138}$$

in which ε and δ are necessarily some functions of r. However, these, being assumed small, are treated as constant in the following calculation. Substituting (138) in (136), and using formula

$$\frac{\partial}{\partial r}r^2\nabla^2\phi=r\nabla^2r\frac{\partial\phi}{\partial r} \tag{139}$$

we get

$$-\frac{d\rho}{dr}p^2u_r-\frac{\rho p^2}{\lambda+2\mu}\left\{\varepsilon ru_r+\delta r\frac{\partial}{\partial r}ru_r\right\}=-\varepsilon\frac{\rho p^2}{\mu}ru_r+\frac{\delta}{r}\frac{\partial}{\partial r}r^2\nabla^2ru_r$$

$$-2\frac{d\mu}{dr}\frac{\rho p^2}{\mu}u_r+2r\frac{d}{dr}\left(\frac{1}{r}\frac{d\mu}{dr}\right)\frac{\partial u_r}{\partial r}. \tag{140}$$

Substituting (137) in the second term of the right hand members of the above equation, we get an equation which contains u_r and $\frac{\partial}{\partial r}ru_r$ only. Since each of the factors should then vanish, we have

$$-\frac{d\rho}{dr}p^2-\frac{\rho p^2}{\lambda+2\mu}\varepsilon r=-\varepsilon r\frac{\rho p^2}{\mu}-\delta p^2\frac{d}{dr}\frac{r^2\rho}{\mu}-2\frac{d\mu}{dr}\frac{\rho p^2}{\mu}-2\frac{d}{dr}\left(\frac{1}{r}\frac{d\mu}{dr}\right),$$

$$-\frac{\rho p^2}{\lambda+2\mu}\delta=-\frac{\rho p^2}{\mu}\delta+\frac{2}{r}\frac{d}{dr}\left(\frac{1}{r}\frac{d\mu}{dr}\right),$$

from which ε and δ are otained as follows:

$$\delta=\frac{2}{r}\frac{(\lambda+2\mu)\mu}{(\lambda+\mu)\rho p^2}\frac{d}{dr}\left(\frac{1}{r}\frac{d\mu}{dr}\right), \tag{141}$$

$$\frac{\lambda+\mu}{\lambda+2\mu}\frac{\rho p^2}{\mu}\varepsilon r=\rho p^2\left\{\frac{1}{\rho}\frac{d\rho}{dr}-\frac{2}{\mu}\frac{d\mu}{dr}\right\}-\frac{2(3\lambda+5\mu)}{\lambda+\mu}\frac{d}{dr}\left(\frac{1}{r}\frac{d\mu}{dr}\right)$$

$$-2r\frac{\lambda+2\mu}{\lambda+\mu}\frac{\mu}{\rho}\frac{d}{dr}\left(\frac{1}{r}\frac{d\mu}{dr}\right)\frac{d}{dr}\frac{\rho}{\mu}. \tag{142}$$

Substituting ε and δ thus obtained in (138), we get the expression for div $\boldsymbol{D}$, and substituting it into equation (127), we get the following equation for u_r to a second approximation,

$$-\rho p^2 \mu r u_r = \mu \nabla^2 \mu r u_r - a \mu r u_r - b \frac{\partial}{\partial r} \mu r u_r - c \frac{\partial^2}{\partial r^2} \mu r \varpi_r ,$$

where a, b, and c are some functions of p^2, ε, δ, and the derivatives of ρ, λ, μ. It will be seen from (141) that, when p tends to infinity, δ vanishes, and consequently c vanishes. Therefore, notwithstanding the presence of the term $\frac{\partial^2}{\partial r^2} \mu r u_r$ on the right hand side of the above equation, it will be seen that the velocity of propagation of a wave of unlimited short period, or, in consequence, the beginning of a disturbance (the S phase in seismograms), is not affected by the heterogeneity of the medium, being equal to $\sqrt{\frac{\mu}{\rho}}$. Since ε does not vanish even when $p \to \infty$, there is a change in volume at the beginning of the S phase.

Although we have put $\frac{1}{\rho}\left(\nabla^2 \mu + \frac{2}{r}\frac{d\mu}{dr}\right) = \alpha^2$ by way of estimating the order of magnitude of dispersion, it is clear from the results above obtained that $\frac{\partial}{\partial r}(\lambda \Delta)$ and $r^2 \mu \frac{\partial}{\partial r}\left(\frac{\Delta}{r^2}\right)$ are of the same order of magnitude as $\left(\nabla^2 \mu + \frac{2}{r}\frac{d\mu}{dr}\right) u_r$. Now, $\frac{1}{|r u_r|}\left|\frac{\partial(r u_r)}{\partial r}\right|$ is not greater than $\sqrt{\frac{\rho}{\mu}}\, p$, so that, for a large value of p, $\delta r \frac{\partial}{\partial r}(r u_r)$ is negligible compared with $\varepsilon r u_r$, and putting $(\lambda + 2\mu)\Delta = \varepsilon r u_r$, $\varepsilon r = \frac{\lambda + 2\mu}{\lambda + \mu} \mu \left\{ \frac{1}{\rho}\frac{d\rho}{dr} - \frac{2}{\mu}\frac{d\mu}{dr} \right\}$, we get from (127),

$$\rho \frac{\partial^2}{\partial T^2} r u_r = \mu \nabla^2 r u_r + \frac{\mu}{\rho}\frac{d\rho}{dr}\frac{\partial}{\partial r} r u_r - a'^2 r u_r ,$$

$$a'^2 = \frac{2}{r}\frac{d\mu}{dr} - r\frac{d}{dr}\frac{\lambda \varepsilon}{\lambda + 2\mu} - r^3 \mu \frac{d}{dr}\frac{\varepsilon}{r^2(\lambda + 2\mu)} ,$$

which is easily transformed to the type,

$$\rho \frac{\partial^2}{\partial T^2}\sqrt{\rho}\, r u_r = \mu \nabla^2 \sqrt{\rho}\, r u_r - a^2 \sqrt{\rho}\, r u_r , \tag{143}$$

$$a^2 = a'^2 + \frac{\mu}{\sqrt{\rho}} \nabla^2 \sqrt{\rho} :$$

8. *Longitudinal waves.* It is easier to discuss the longitudinal wave by the following method of mathematical treatment than to trouble with equations (126) and (127).

In the longitudinal wave, rot $\boldsymbol{D}=0$ to a first approximation, and strictly $(\text{rot } \boldsymbol{D})_r=0$, so that we may put

$$u_r=\frac{\partial P}{\partial r}+Q,\quad u_\theta=\frac{1}{r}\frac{\partial P}{\partial\theta},\quad u_\varphi=\frac{1}{r\sin\theta}\frac{\partial P}{\partial\varphi}, \tag{144}$$

when Q is treated as a small correction. The equation with respect to P and Q are

$$\rho\frac{\partial^2 P}{\partial T^2}=(\lambda+2\mu)\nabla^2 P+2r\frac{d\mu}{dr}\frac{\partial}{\partial r}\frac{P}{r}$$

$$+(\lambda+2\mu)\frac{1}{r^2}\frac{\partial}{\partial r}r^2 Q-\mu\frac{\partial Q}{\partial r}+\frac{d\mu}{dr}Q, \tag{145}$$

$$-\frac{d\rho}{dr}\frac{\partial^2}{\partial T^2}\frac{P}{r}+\rho\frac{\partial^2}{\partial T^2}\frac{Q}{r}=\mu\nabla^2\frac{Q}{r}-\left(\frac{d^2\mu}{dr^2}+\frac{4}{r}\frac{d\mu}{dr}\right)\frac{Q}{r}$$

$$-\frac{2}{r}\frac{d\mu}{dr}\left\{\nabla^2 P-\frac{\partial}{\partial r}\frac{P}{r}\right\}-2\frac{d^2\mu}{dr^2}\frac{\partial}{\partial r}\frac{P}{r} \tag{146}$$

Putting $Q=0$ in (145), and by a slight modification, we get the following equation, from which an approximate solution for the longitudinal wave can be obtained, namely,

$$\rho\frac{\partial^2}{\partial T^2}gP=(\lambda+2\mu)\nabla^2 gP-\left(\frac{2}{r}\frac{d\mu}{dr}+\frac{\lambda+2\mu}{g}\nabla^2 g\right)gP, \tag{147}$$

in which $\frac{1}{g}\frac{dg}{dr}=\frac{1}{\lambda+2\mu}\frac{d\mu}{dr}$. If $\lambda=n\mu$, n being constant, $g=\mu^{\frac{1}{2+n}}$, and in this case the wave path, determined with the aid of Fermat's principle, being common with that of transverse waves, the same t, β, φ-coordinates are available.

To get Q as a small correction, we approximate $-\rho p^2 P=(\lambda+2\mu)\nabla^2 P$, the time factor being assumed to be e^{ipT} as in the case of the transverse wave. Neglecting the second term on the right hand side of (146), and substituting the above approximate relation, we get

$$\frac{d\rho}{dr}p^2\frac{P}{r}-\rho p^2\frac{Q}{r}=\mu\nabla^2\frac{Q}{r}+\frac{2}{r}\frac{d\mu}{dr}\frac{\rho p^2}{\lambda+2\mu}P-2r\frac{d}{dr}\left(\frac{1}{r}\frac{d\mu}{dr}\right)\frac{\partial}{\partial r}\frac{P}{r}. \tag{148}$$

Putting,

$$\frac{Q}{r}=\varepsilon' P+\delta' r\frac{\partial P}{\partial r}, \tag{149}$$

into equation (148), we get an equation containing only P and $\frac{\partial P}{\partial r}$, from which, putting each factor zero, we have

$$\delta'=\frac{2}{\rho p^2}\frac{\lambda+2\mu}{\lambda+\mu}\frac{1}{r}\frac{d}{dr}\left(\frac{1}{r}\frac{d\mu}{dr}\right), \tag{150}$$

$$\frac{\lambda+\mu}{\lambda+2\mu}\rho p^2\varepsilon' r=\rho p^2\left\{\frac{1}{\rho}\frac{d\rho}{dr}-\frac{2}{\lambda+2\mu}\frac{d\mu}{dr}\right\}-\frac{2(\lambda-\mu)}{\lambda+\mu}\frac{d}{dr}\left(\frac{1}{r}\frac{d\mu}{dr}\right)$$
$$+\frac{2(\lambda+2\mu)\mu}{(\lambda+\mu)\rho}r\frac{d}{dr}\left(\frac{1}{r}\frac{d\mu}{dr}\right)\frac{d}{dr}\frac{\rho}{\lambda+2\mu}. \tag{151}$$

When p tends to infinity, δ' vanishes, so that the velocity of propagation of the beginning of the longitudinal wave, or the P phase of seismology, is, as would have been expected, $\sqrt{\frac{\lambda+2\mu}{\rho}}$.

We obtain the following equation for the longitudinal wave to a second approximation after a method of procedure similar to that used in getting (143),

$$\rho\frac{\partial^2}{\partial T^2}\sqrt{\rho}\,P=(\lambda+2\mu)\nabla^2\sqrt{\rho}\,P-\alpha^2\sqrt{\rho}\,P, \tag{152}$$

$$\alpha^2=\frac{2}{r}\frac{d\mu}{dr}-\varepsilon' r\frac{d\mu}{dr}+\mu\frac{d(\varepsilon' r)}{dr}-\frac{\lambda+2\mu}{r^2}\frac{d}{dr}(\varepsilon' r^3)+\frac{\lambda+2\mu}{\sqrt{\rho}}\nabla^2\sqrt{\rho}\,.$$

We get the r-, θ- and the φ-component of rot $\boldsymbol{D}$, associated with the longitudinal wave, and consequently propagated with velocity $\sqrt{\frac{\lambda+2\mu}{\rho}}$, as follows,

$$\left.\begin{aligned}
2\varpi_r&=0\\
2\varpi_\theta&=\frac{1}{r\sin\theta}\frac{\partial Q}{\partial\varphi}=\frac{1}{\sin\theta}\frac{\partial}{\partial\varphi}\left\{\varepsilon' P+\delta' r\frac{\partial P}{\partial r}\right\},\\
2\varpi_\varphi&=-\frac{1}{r}\frac{\partial Q}{\partial\theta}=-\frac{\partial}{\partial\theta}\left\{\varepsilon' P+\delta' r\frac{\partial P}{\partial r}\right\},
\end{aligned}\right\} \tag{153}$$

and we may also put, approximately,

$$\Delta \doteqdot \nabla^2 P \doteqdot -\frac{\rho p^2}{\lambda+2\mu} P. \tag{154}$$

These seem to be the essential points of the longitudinal wave through a heterogeneous medium.

If we put $\mu=0$,

$$a^2 = \frac{\lambda}{\sqrt{\rho}} \nabla^2 \sqrt{\rho} - \frac{\lambda}{r^2} \frac{d}{dr}\left(\frac{r^2}{\rho}\frac{d\rho}{dr}\right) = \lambda \sqrt{\rho}\, \nabla^2 \frac{1}{\sqrt{\rho}},$$

equation (152) then becomes

$$\rho \frac{\partial^2}{\partial T^2} \sqrt{\rho}\, P = \lambda \nabla^2 \sqrt{\rho}\, P - \left(\lambda \sqrt{\rho}\, \nabla^2 \frac{1}{\sqrt{\rho}}\right) \sqrt{\rho}\, P$$

and

$$(D_2)_r = \frac{\partial P}{\partial r} + \frac{1}{\rho}\frac{d\rho}{dr} P = \frac{1}{\rho}\frac{\partial}{\partial r}\rho P,$$

$$(D_2)_\theta = \frac{1}{r}\frac{\partial P}{\partial \theta} = \frac{1}{\rho}\frac{1}{r}\frac{\partial}{\partial \theta}\rho P.$$

These are exactly the results obtained in Part 2.

9. *Transverse waves of type A.* Although this wave has been dealt with in the previous paragraph, it will be considered again. Because of complexity of procedure, we have not yet given the magnitude of rot $\boldsymbol{D}$. It is clear that substitution (144) can be used, although neither P nor Q in this case is a small correction, and both of these, the magnitudes of which are obtained by the following calculation, are propagated with velocity $\sqrt{\frac{\mu}{\rho}}$, while those in the last paragraph are propagated with velocity $\sqrt{\frac{\lambda+2\mu}{\rho}}$. For convenience in discriminating P, Q, Δ and other quantites in the transverse wave of type A from those in the longitudinal wave, we shall affix the notation "$'$" to those in the transverse wave of type A, for example, P', Q', Δ' and so on.

To a first approximation, we can easily obtain from (145) and (146), neglecting the terms of the derivatives of ρ and μ, and putting

$$\Delta' = \nabla^2 P' + \frac{1}{r^2}\frac{\partial}{\partial r}(r^2 Q') = 0,$$

the equation

$$P' = \frac{\mu}{\rho p^2} \frac{\partial Q'}{\partial r} . \tag{155}$$

For the components of rot $\boldsymbol{D}$ we have

$$\left.\begin{aligned} 2\varpi_r &= 0, \\ 2\varpi_\theta &= \frac{1}{r\sin\theta} \frac{\partial Q'}{\partial \varphi}, \\ 2\varpi_\varphi &= -\frac{1}{r} \frac{\partial Q'}{\partial \theta} . \end{aligned}\right\} \tag{156}$$

10. *Recapitulation of the foregoing results, and remarks.* Through a heterogeneous medium, there are propagated two energy fronts of waves, one advancing with velocity $\sqrt{\frac{\lambda+2\mu}{\rho}}$ and the other with velocity $\sqrt{\frac{\mu}{\rho}}$, while we have three different phase fronts of waves. These three kinds of waves we call the "longitudinal wave," the "transverse wave of type A" and the "transverse wave of type B." The characteristics of dispersion of the transverse wave of type B are simple, while those of the other two are very complicated, with the result that all we got was a rough approximation. At any rate, owing to the characteristic dispersion of each of these waves, there are certain reductions of maximum amplitudes, the appearance of characteristic, damped oscillation, called the "tail"; and possibilities of the appearance of two peaks in the S phase in seismograms. If observations of these effects of dispersion are possible, they will be useful, with the aid of the results of investigations of earthquake mechanism, in studying the heterogeneity of ρ, λ, and μ respectively, whereas analyses of travel-time curves are of help only in the study of the heterogeneity of $\sqrt{\frac{\lambda+2\mu}{\rho}}$ or $\sqrt{\frac{\mu}{\rho}}$.

Displacement $\boldsymbol{D}$ due to the wave motion, generally speaking, may be expressed as a vector sum of those due to the three kinds of waves, namely,

$$\boldsymbol{D} = \boldsymbol{D}_1(\sqrt{p^2-a_1^2}\, t)e^{ipT} + \boldsymbol{D}_2(\sqrt{p^2-a_2^2}\, t)e^{ipT} + \boldsymbol{D}_3(\sqrt{p^2-a_3^2}\, t')e^{ipT} \tag{157}$$

in which t is calculated by putting $v=\sqrt{\frac{\mu}{\rho}}$, while t' is calculated by putting $v=\sqrt{\frac{\lambda+2\mu}{\rho}}$, and

$\boldsymbol{D}_1$ is due to the transverse wave of type B,

$\boldsymbol{D}_2$ 〃 〃 of type A,

$\boldsymbol{D}_3$ 〃 the longitudinal wave.

Obviously, the r-component of $\boldsymbol{D}_1$ is nil, and the beginning of the former two are propagated with velocity $\sqrt{\frac{\mu}{\rho}}$, while that of the last is propagated with velocity $\sqrt{\frac{\lambda+2\mu}{\rho}}$. These are affected by some dispersion characteristic of each of the three waves just mentioned.

We shall now consider some illustrative problems with the hope of throwing some fresh light on the investigation of earthquake mechanism, and consider the following two cases,

Case 1. $\text{div}\ \boldsymbol{D}=0$, $\text{rot}\ \boldsymbol{D}\neq 0$

Case 2. $\text{div}\ \boldsymbol{D}\neq 0$, $\text{rot}\ \boldsymbol{D}=0$.

on the surface, $t=t_0$.

When dealing with a homogeneous medium, we know that in case 1, transverse waves spread out from the surface with velocity $\sqrt{\frac{\mu}{\rho}}$, there being no (longitudinal) waves that are propagated with velocity $\sqrt{\frac{\lambda+2\mu}{\rho}}$, which is quite in contrast with case 2, in which only longitudinal waves of velocity $\sqrt{\frac{\lambda+2\mu}{\rho}}$ spread out, there being no (transverse) waves of velocity $\sqrt{\frac{\mu}{\rho}}$.

Owing to the property of the transverse wave of type B, as given by (130), $\text{div}\ \boldsymbol{D}_1=0$, and from (138) $\text{div}\ \boldsymbol{D}_2=\frac{1}{\lambda+2\mu}\left\{\varepsilon+\delta r\frac{\partial}{\partial r}\right\}(r\boldsymbol{D}_2)_r$, whence $\text{div}\ \boldsymbol{D}=0$ gives

$$\text{div}\ \boldsymbol{D}_3=-\frac{1}{\lambda+2\mu}\left\{\varepsilon+\delta r\frac{\partial}{\partial r}\right\}(r\boldsymbol{D}_2)_r \tag{158}$$

on the surface $t=t_0$, where $(\boldsymbol{D}_2)_r$ represents the r-component of $\boldsymbol{D}_2$, ε and δ being given by (141) and (142). Since, from (144) and (154), $\boldsymbol{D}_3=\text{grad}\ P$, approximately, where $P=-\frac{\lambda+2\mu}{\rho p^2}\text{div}\ \boldsymbol{D}_3$,

$$\boldsymbol{D}_3=\text{grad}\frac{1}{\rho p^2}\left\{\varepsilon+\delta r\frac{\partial}{\partial r}\right\}(r\boldsymbol{D}_2)_r \tag{159}$$

We shall suppose an earthquake mechanism such that a small rigid ball performs a rotational oscillation at the origin. When the axis of rotation coincides with the direction of $\boldsymbol{r}$, since there are no r-components of displacement and no change of volume, no waves other than transverse wave of type B, represented by $\boldsymbol{D}_1 e^{ipT}$ and such that $(\boldsymbol{D}_1)_r = \text{div}\, \boldsymbol{D}_1 = 0$, will be generated and propagated. However, when the axis does not coincide with the direction of $\boldsymbol{r}$, the r-component of displacement necessarily exists, so that, although there are no changes in volume, there will be longitudinal waves although their magnitudes may be small, as given by (158) and (159). Then if the medium is heterogenencous, but not otherwise, we shall observe waves of velocity $\sqrt{\frac{\lambda+2\mu}{\rho}}$ from a nondilatational origin.

Now, as to any function ϕ, representing a wave motion propagated with velocity v, approximately $\frac{1}{\phi}\,\text{grad}\,\phi = \frac{p}{v}\cos\omega$ for a large value of p, in which ω is an angle between the normal to the wave front and the direction to which the gradient of ϕ is taken. Therefore, for a wave of short period, we can put, neglecting the term of δ compared with that of ε,

$$\boldsymbol{D}_3 = \text{grad}\,\frac{(\lambda+2\mu)\mu}{(\lambda+\mu)\rho p^2}\left\{\frac{1}{\rho}\frac{d\rho}{dr} - \frac{2}{\mu}\frac{d\mu}{dr}\right\}(\boldsymbol{D}_2)_r, \tag{160}$$

or, further, we see that $\frac{\boldsymbol{D}_3}{\boldsymbol{D}_2}$ decreases, approximately inversely to p, as p increases. Consequently, considering again the above illustrative example, the amplitude of the longitudinal wave decreases as the frequency of the rotational oscillation of the rigid ball increases.

In order to study the case 2, we perform the calculation for the operation of rotation on both members of (157). We get easily, from (133), (153) and (156),

$$\left.\begin{aligned}
2\varpi_r &= -\frac{1}{r\sin\theta}\left\{\frac{\partial}{\partial\theta}\left(\sin\theta\frac{\partial F}{\partial\theta}\right) + \frac{1}{\sin\theta}\frac{\partial^2 F}{\partial\varphi^2}\right\},\\
2\varpi_\theta &= \frac{1}{r}\frac{\partial}{\partial r}\left(r\frac{\partial F}{\partial\theta}\right) + \frac{1}{r\sin\theta}\frac{\partial Q'}{\partial\varphi} + \frac{1}{\sin\theta}\frac{\partial}{\partial\varphi}\left\{\varepsilon' P + \delta' r\frac{\partial P}{\partial r}\right\},\\
2\varpi_\varphi &= \frac{1}{r\sin\theta}\frac{\partial}{\partial r}\left(r\frac{\partial F}{\partial\varphi}\right) - \frac{1}{r}\frac{\partial Q'}{\partial\theta} - \frac{\partial}{\partial\theta}\left\{\varepsilon' P + \delta' r\frac{\partial P}{\partial r}\right\}.
\end{aligned}\right\} \tag{161}$$

Consequently rot $\boldsymbol{D}=0$ gives,

$$F=0,$$

$$\frac{Q'}{r}=-\left\{\varepsilon' P+\delta' r\frac{\partial P}{\partial r}\right\}, \tag{162}$$

in which, from (144) and (154), approximately,

$$\boldsymbol{D}_3=\text{grad } P, \quad P=-\frac{\lambda+2\mu}{\rho p^2}\text{div } \boldsymbol{D}_3 \tag{163}$$

From (155) and (162),

$$P'=\frac{\mu}{\rho p^2}\frac{\partial Q'}{\partial r}=-\frac{\mu}{\rho p^2}\frac{\partial}{\partial r}r\left\{\varepsilon' P+\delta' r\frac{\partial P}{\partial r}\right\} \tag{164}$$

$F=0$ means that there are no transverse wave of type B. The displacement owing to the transverse wave of type A can be calculated from P' and Q' by a formula that is exactly the same as (144) as already stated. Thus it has been shown that in a heterogeneous medium, even from a pure dilatational or condensational origin, we should expect not only longitudinal waves, but also transverse waves of type A, which are propagated at the beginning with velocity $\sqrt{\frac{\mu}{\rho}}$, according to the following equation (approximate):

$$-\rho p^2\frac{Q'}{r}=\mu\nabla^2\frac{Q'}{r}. \tag{165}$$

From (162) and (164), we get, for example, the vertical and horizontal components of the amplitude of displacement due to such transverse wave, for large values of p, as follows;

$$\left.\begin{aligned}(\boldsymbol{D}_2)_r&=Q'+\frac{\mu}{\rho p^2}\frac{\partial^2 Q'}{\partial r^2}=-\left\{1+\frac{\mu}{\rho p^2}\frac{\partial^2}{\partial r^2}\right\}\\&\qquad\cdot\frac{\lambda+2\mu}{\lambda+\mu}\left(\frac{1}{\rho}\frac{d\rho}{dr}-\frac{2}{\lambda+2\mu}\frac{d\mu}{dr}\right)P\\(\boldsymbol{D}_2)_\theta&=(\text{grad } P')_\theta=-\frac{1}{r}\frac{\mu}{\rho p^2}\frac{\partial}{\partial r}\left\{\frac{\lambda+2\mu}{\lambda+\mu}\left(\frac{1}{\rho}\frac{d\rho}{dr}-\frac{2}{\lambda+2\mu}\frac{d\mu}{dr}\right)\frac{\partial P}{\partial \theta}\right\}\\&=-\frac{1}{r}\frac{\mu}{\rho p^2}\frac{\partial}{\partial r}r\frac{\lambda+2\mu}{\lambda+\mu}\left(\frac{1}{\rho}\frac{d\rho}{dr}-\frac{2}{\lambda+2\mu}\frac{d\mu}{dr}\right)(\boldsymbol{D}_3)_\theta,\end{aligned}\right\} \tag{166}$$

$$(D_2)_\varphi=(\text{grad } P')_\varphi=-\frac{1}{r}\frac{\mu}{\rho p^2}\frac{\partial}{\partial r}r\frac{\lambda+2\mu}{\lambda+\mu}\left(\frac{1}{\rho}\frac{d\rho}{dr}-\frac{2}{\lambda+2\mu}\frac{d\mu}{dr}\right)(D_3)_\varphi,$$

on the surface $t=t_0$. The operator of the "grad" is equivalent to the factor $\sqrt{\frac{\rho}{\mu}}p\cos\omega$, so that $\frac{D_2}{D_3}$ decreases inversely as p increases. When $\frac{\partial P}{\partial\theta}=\frac{\partial P}{\partial\varphi}=0$, and the wave is propagated in the direction of r, $-\rho p^2 Q'=\mu\frac{\partial^2 Q'}{\partial r^2}$ from (165), consequently no transverse wave is generated.

It was shown above that the amplitude of the longitudinal and the transverse wave, due to the heterogeneity of the medium, from the transverse and longitudinal wave respectively diminishes with shortening of the period. Needless to say, it should be remembered that so far as observations far from the surface $t=t_0$ are concerned, the attenuation factor of D_2 in (166), for example, differs from that of D_3.

The structure of the upper layer of the earth-crust is so complicated that application of the results of study outlined above to practical problems in seismology is clearly inadequate for their solution. However, in the case of a deep-seated earthquake, some application will be found in the interpretation of seismograms.

For several years past, the mechanism of earthquakes at the origin have been investigated by a number of workers from the amplitudes of the P phase or the S phase, and many reasonable conclusions have been drawn, especially for deepseated earthquakes. According to these investigations, if the earth is a homogeneous elastic medium, there ought to be "Nodal lines" of the P phase. There should also be "Nodal points" where only the P phase is observed, and no S phase. As a matter of fact, many seismograms have been recorded, clearly proving the existence of the "Nodal lines," and seismograms that virtually give the "Nodal points" are also recorded, although naturally less frequently.

However, upon closer investigations, owing to the heterogeneity of the earth, these conclusions regarding the necessity for Nodal lines and points, naturally seem to leave something to be desired.

From (159) and (152), we may calculate the amplitude of the P phase that will be observed on the "Nodal lines," and from (164), (165), and (166), we may calculate the amplitude of the S phase that is expected at the "Nodal points." From the foregoing discussion, the "Nodal lines" and the "Nodal points" should be clearly identifiable for a wave of short period, and, by close observations of waves of longer period, as also by observations of the effects of dispersion of the

P phase or the S phase, there are possibilities of estimating the order of heterogeneity of the earth at dephth with respect to ρ, λ and μ.

In conclusion, the author desires to express his sincere thanks to Professor T. Matuzawa and Dr. H. Kawasumi for their kind guidance in the course of this study.

---

14. 等方不均一球内の一點より起る彈性波（第３報）

地震學教室　吉　山　良　一

密度及び彈性常數の變り方が小さいとして彈性波の性質を調べて見た．波はその性質に從つて三種類に分類され，各々近似的に第２報で調べたと同樣な形の方程式を滿足する．三種類の波を假りに A 型の橫波，B 型の橫波，及び縱波と呼ぶことにする．不連續面に於ける反射屈折を調べる際橫波を SH 波と SV 波に分類して考へると便利であるのと同じ事である．B 型の橫波は全く獨立に一つの方程式を滿足する．他の二つの波は互に或る關聯を有つてゐるので地震の發震機構の問題に於いて云ふ所の節線或は節點は媒質が均質である場合と樣子が異つて來る．然し波の週期が短ければ短い程不均質性の影響は小さくなる．

---

15. 横濱港の埋立地及岸壁に於ける地震動

地震研究所　齋田時太郎

内務省土木試驗所　松尾春雄

(昭和14年9月21日發表 — 昭和16年3月20日受理)

本文にのせた地震動の觀測は，日本學術振興會第 14 小委員會に於ける，私の擔當の一事業として，昭和 13 年 12 月より昭和 15 年 3 月まで，横濱港外國貿易岸壁に於て，内務技師松尾春雄氏の助力に依りなされたものであるが，偶々私が昭和 14 年 4 月アメリカ合衆國及チリー國へ出張を命ぜられ不在であつたため，同技師が觀測を繼續し，その成果の一部分を土木試驗所報告第 53 號に「港灣の埋立地に於ける地震動の加速度及周期に關する調査」と題して發表された．こゝに同技師の調査に基き，私見をのべ責任を分擔する次第である．(齋田時太郎記す)

1. 緒　言

大正 12 年の關東大地震による横濱港岸壁の被害，及昭和 5 年 11 月の北伊豆地震，と昭和 10 年7月の靜岡地震による再度の清水港岸壁の震害は，港灣工作物に於ける災害の中で，最も著しいものであつた．これ等は我國在來の岸壁の設計に，地震動に對する處置が餘り考へられてゐなかつた事が，大きな原因であるが，岸壁は多く埋立地に設けられ，且つ 10 米乃至 15 米程度の高さに切立つてゐるので，地震動が一般に考へられてゐるものと著しく異なることに因るのではないかと言ふ疑がある．因て，この方面の調査研究を進め，地震動による埋立地及岸壁の振動の性質を解明することは，我が國の如き地震國に於ては重要なことである．

2. 地震動觀測の場所

地震計を設置した場所は，第1圖に示す通り横濱港の東北部に當り，省線東神奈川驛の東南に突出する，外國貿易用岸壁である．その幅員 150 米にして，一方は水深 10 米，他方は 3 米である．岸壁の構造は昭和 2 年に在來約 4 米の水深の場所に，岸壁構造物の基礎のところは 13.6 米まで浚渫し，そこに割栗石を厚さ約 3 米，幅 15 米を敷いた上に，底幅 9.15 米，上幅 6.00 米，高さ 13.20 米，1 個の重量約 1000 噸の鐵筋コンクリート潜函を据え，中詰後上部場所詰を施し岸壁とした．この重量 1 米當り約 220 噸（浮力を差引かない値）あり，潜函 1 個の長さ 18.75 米毎に目地を設け岸壁背後は浚渫から生じた土丹岩を以て裏込を施し，その背後の埋立地

は，ポンプ浚渫により生ずる土砂を多量に含んだ水を，波入れ沈澱せしめて出來たものである．物揚場は海面下4米に均し，厚さ1米の基礎割栗を施し，更にその上に底

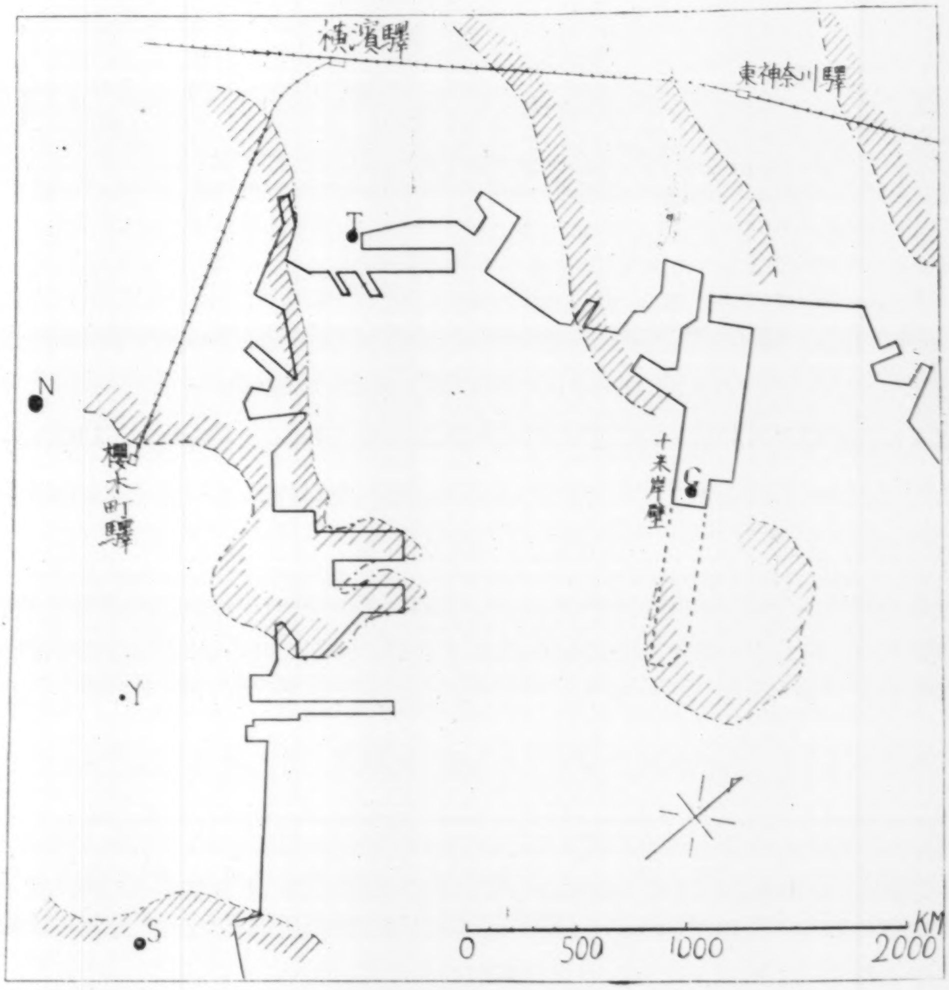

第1圖　地震計設置位置，N は野毛山震災紀念館，T は表高島町，G は今回調査のため新に設置した十米岸壁，Y は横濱公園（嘗て地震計が置かれた）S は横濱測候所，斜線を施した地域は第三紀層海面下 10 米以内を示す．

幅 3·5 米，高さ 5·05 米，長さ 4·90 米，1 個の重量約 46 噸の異型擁壁を置き，上部には場所結コンクリートを打ち，土丹岩の裏込を施した上に，斷面に於て延長約 10 米の斜路を設けた構造であつて，壁體延長1米當り重量は裏込共約 37 噸である．

岸壁及物揚場壁體は昭和3年頃の施工になり，埋立竣工は昭和5年であるが，其の後岸壁の耐震度を増すため，昭和 8 年に岸壁背後及前面に杭を打ち補强工事を行つた．

今回調査のため地震計を設置した場所は，第2圖に示す通り 4 箇所であるが，最初 No. 1, No. 2, No. 3 に於て同時に觀測を開始し，後に No. 3 のものを No. 4 に移

し No. 1, No. 2, No. 4 に於て同時觀測を行つた．それは No. 1 と No. 2 とで地震動に著しい差が認められたから，潜函より後方約 16 米に於て，直接潜函への土壓を

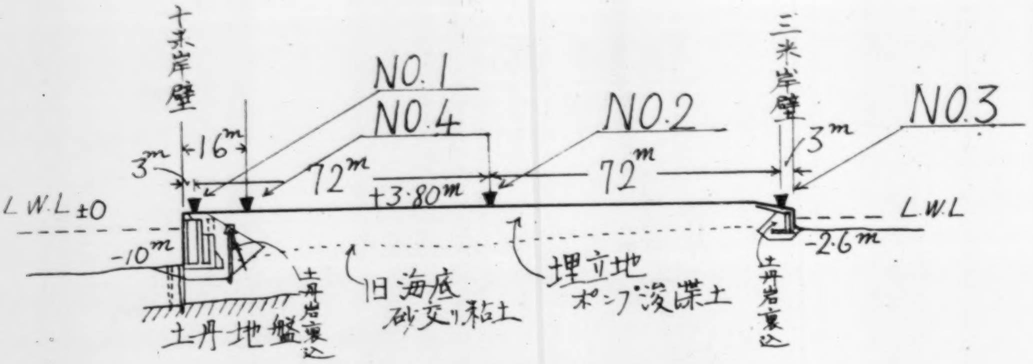

第2圖　十米及三米岸壁斷面及地震計設置位置．

支配すると思はれる位置の地震動の性質を知るためであつた．この外第1圖に示す表高島町の在來の觀測と，野毛山公園内震災記念館に据付けたものと合計 6 個所で觀測を行つた．

岸壁及物揚場附近の基盤の地質は，第三紀層の軟質砂岩である土丹盤が海面下 15 米位に在り，それと海底との間は粘土質砂である．表高島町の地震計は昭和6年頃埋立てられた，幅 20 米の狹い埋立地で明治年間の埋立地との境界線から 7 米の距離の所に設置してある．この附近の基盤である第三紀層は，深さ 40 米位に在り，その上の地表層は軟弱な粘土質砂である．野毛山公園の地質は第三紀層の基盤を覆ふ，洪積層の粘土砂互層のローム層であつて，表高島町附近の地盤より著しく硬い地盤である．なほ，後に引用する横濱測候所の地盤も亦野毛山と同様であるが，横濱公園は軟弱な沖積層の厚さ 30 米以上に及び表高島町附近と大差はない．

3. 地　震　計

今回觀測に使用した地震計は，石本式[1]水平加速度地震計で，岸壁に平行と直角との震動加速度成分を測定し得るやうに据付けた．在來の地動觀測は變位地震計を用ひてゐるのが常であるが，震動の最大加速度及びその週期が重要視される土木建築の工學に於ては，加速度地震計を用ふるのが適當である．なほ，この地震計の要素は下の通りであつた．

幾何倍率	213
振子の振動周期	0·1 秒
制振器	ピストン型空氣制振にして臨界制振狀態にある．

1) M. Ishimoto, *Bull. Eart'q. Res. Inst.*, **10** (1931), 171.

記象紙速さ	約1分間に6糎
感　　度	記象紙上1粍が 1·7 gal
記象紙回轉原動機	同調電動機

4. 觀測の結果

今回の觀測は昭和 13 年 12 月開始され，同 15 年 3 月末日に終了したが，その間頗る多數の有感無感の地震動を記錄することが出來た．その中第1表に示す 31 回の地震動について調査を進めて見た．これ等 31 回の震度を，岸壁觀測所の南方約 3 粁に在る橫濱測候所について見ると，弱震（震度 III）が 2 回，輕震（震度 II）が 3 回，他は皆微震と言ふ程度であつた．今回岸壁で觀測した最も强い震動である，上記の 2 回の弱震を加速度地震計の値と比較するため，橫濱測候所に於ける變位地震計より求めた，最大振幅とその周期とを示すならば，昭和 14 年 3 月 10 日 3 時 12 分頃の茨城縣下結城附近の地震は，關東地方の大部分から東北地方の南東部及び中部地方の一部に亘り有感であつて，橫濱測候所では弱震震度 III，その振幅及び周期は次の通りである．

最大動振幅 (μ)			周　期 (S)		
N	E	Z	N	E	Z
−1900	+1260	−263	1·2	0·7	0·8

次に昭和 14 年 12 月 31 日 15 時 53 分頃の銚子附近の地震は，震央は銚子の南西約 10 粁の沖合に當り，關東地方の大部分から福島，山梨及び靜岡等の諸縣にかけて有感であつて，橫濱測候所では弱震震度 III その振幅及び周期は次の通りである．

最大動振幅 (μ)			周　期 (S)		
N	E	Z	N	E	Z
−2400	−1400	−355	0·8	0·6	3·5

さて，これ等 31 回の地震動記象について工學的立場から最も重要な最大加速度，及その周期を讀みとつて見ると，第1表に示す通りである．それ等の數値から推定される事項を擧げるならば次の如くである．なほ，最後に二つの地震動の記象を添付しておいた．

（1） 岸壁に垂直な方向と，平行な方向とで最大加速度は著しく異る．例へば，No. 1 卽ち 10 米岸壁潛函上に於ては，垂直方向のものは平行な方向のものゝ 3·5 倍にも達することがある．この關係は No. 3 卽ち 3 米物揚場に於ても同じ數値を示した．なほ，これ等の比を No· 2 の地震の强さを標準として見ると，第3圖の (a) (b) の

第1表　各觀測點に於ける最大加速度

加速度の單位は gal, (　) 內の數字は最大加速度に於ける周期を秒にて示す．
加速度の方向にて表高島町，野毛山は EW, NS は自然の方向なるも，No. 1〜No. 4. にありては EW は岸壁面に直角，NS は岸壁面に平行の方向を示せり．震央，震央距離及震度は氣象要覽による．

地震番號	發震日時 年	月	日	時	分	加速度の方向	表高島町	野毛山	No. 1	No. 2	No. 3	No. 4	震央	震央距離 KM	横濱測候所に於ける震度
1	14	1	9	10	2	EW NS				1·96 1·61	0·94 1·36			65	
2		1	10	21	9	EW NS				2·21 1·91	0·98 0·94		伊豆神子元島沖	130	
3		1	24	13	2	EW NS	2·16 0·45			3·23 4·00	1·78 1·23		福島縣鹽屋崎東方沖	250	微震，I
4		1	25	3	8	EW NS	1·06			1·70 1·53	1·02 0·51		同上	200	
5		2	1	14	25	EW NS	1·06 0·90		0·17 1·28	5·28 4·50	 1·61		結城附近	90	微震，I
6		2	9	0	16	EW NS			1·28 0·51	0·94 1·10	0·60 0·17		鹿島灘	160	
7		3	10	3	12	EW NS	7·73(0·40) 3·60(0·25)		16·00(0·50) 6·46(0·50)	20·10(0·25) 16·60(0·25)	13·10(0·25) 7·40(0·37)		下結城附近	90	弱震，III
8		3	25	10	40	EW NS	3·29 0·45		3·10 1·70	9·17 7·56	6·63 3·31		八王子附近	32	
9		3	26	9	51	EW NS			 2·04	5·52 4·03	2·55 1·53		九十九里濱南部	80	微震，I
10		4	26	10	42	EW NS	1·62 0·45		1·87 0·72	4·69 4·08	2·12 1.45		勝浦南方沖	95	
11		5	1	14	58	EW NS	1·06 0·45		0·26 0·17	0·51 0·43	0·21 0·13		男鹿半島	510	
12		5	8	17	4	ES NW	2·70 0·90		3·14 0·85	2·38 3·06	1·53 0·85		犬吠岬東南東沖	130	
13		5	18	18	31	EW NS	3·02(0·32) 3·00(0·35)		8·68(0·40)	9·87(0·20) 13·60(0·25)	6·75(0·25) 4·50		東京灣北東部	40	微震，I
14		5	19	21	10	EW NS	2·92(0·35) 4·30(0·35)		3·40(0·40)	6·63(0·22) 5·27(0·32)	4·50(0·25) 2·30(0·21)		野島崎南東沖	135	微震，I

(次頁へ續く)

第 1 表 (續)

地震番號	發震日時 年	月	日	時	分	加速度ノ方向	表高島町	野毛山	No. 1	No. 2	No. 3	No. 4	震央	震央距離 KM	横濱測候所に於ける震度
15		6	14	20	9	E W N S			0·85	2·55 1·36	1·36		筑波山附近	110	
16		7	30	21	55	E W N S			 0·51	8·50 3·74	5·10 2·21		同上	100	
17		8	22	9	6	E W N S			2·89(0·62) 1·02(0·50)	2·04(0·23) 2·55(0·33)		2·21(0·38) 2·04(0·33)	福島縣東方沖	332	微震, I
18		9	12	14	5	E W N S	2·04 3·06	3·57 4·08		6·80 6·88		1·12 2·55	水海道附近	78	輕震, II
19		9	14	15	25	E W N S		3·31 2·21	 0·94(0·30)	5·45(0·20) 3·57(0·23)		0·43(0·20) 0·43(0·22)	千葉縣久留里附近	45	
20		9	30	23	37	E W N S	0·94(0·23) 1·45(0·33)	5·52(0·23) 3·57(0·25)	2·64(0·43) 0·43	3·74(0·20) 5·52(0·20)		2·04(0·23) 2·55(0·20)	勝浦南方沖	81	微震, I
21		10	2	6	50	E W N S	0·68 0·34	3·06 1·96	1·87 0·34	3·83 3·66		2·21(0·43) 1·53(0·25)	結城附近	88	
22		10	6	6	17	E W N S	2·87(0·38) 3·40(0·30)	7·65(0·25) 6·97(0·30)	9·35(0·50) 3·06(0·38)	19·80(0·23) 18·60(0·28)		8·68(0·45) 10·20(0·40)	成東附近	75	微震, I
23		10	6	15	21	E W N S	1·02(0·28) 1·19(0·33)	3·83 3·06	2·97 2·12	6·80 10·30		1·00 5·27	東京灣北東部	35	
24		12	31	15	53	E W N S	9·10 8-42	17·17(0·30) 26·52(0·33)	16·32(0·50) 2·89(0·53)	 9·86(0·38)		9·69(0·50) 5·78(0·50)	銚子附近	108	弱震, II
25	15	1	15	15	1	E W N S	1·17(0·23) 0·43(0·23)	12·15(0·23) 12·41(0·23	6·12 0·23) 0·94(0·20)	 14·96(0·25)		5·44(0·20) 9·69(0·18)	千葉市附近	50	微震, II
26		1	18	0	1	E W N S	2·04(0·15) 0·26(0·13)	5·95 6·29	4·59 0·34			6·55 5·95	野島崎沖	94	輕震, II
27		1	19	23	32	E W N S		5·78 5·78	6·80(0·35) 0·94			9·86 9·44	東京灣北部	33	輕震, II
28		2	25	3	50	E W N S		6·88(0·25) 5·10(0·23)	9·18(0·28) 1·53(0·38)	7·31(0·23) 6·97(0.30)		6·80(0·23) 5·44(0·25)	九十九里濱南部	67	
29		3	9	12	33	E W N S		1·19(0·30) 1·87(0·23)	1·62(0·43) 0·77(0·50)	3·74(0·20) 2·97(0.23)		1·70(0·28) 2·04(0·15)	埼玉縣杉戸附近	65	
30		3	9	19	48	E W N S		0·77 0·85	0·85 0·34	0·68 0·68		0·85 0·60	父島西北西沖	750	
31		3	15	21	34	E W N S			1·79 0·85			1·53 1·87	茨城縣南西部	71	

如くである．その圖表によれば，地震動が弱いときは No. 1 も No. 3 も，その比の

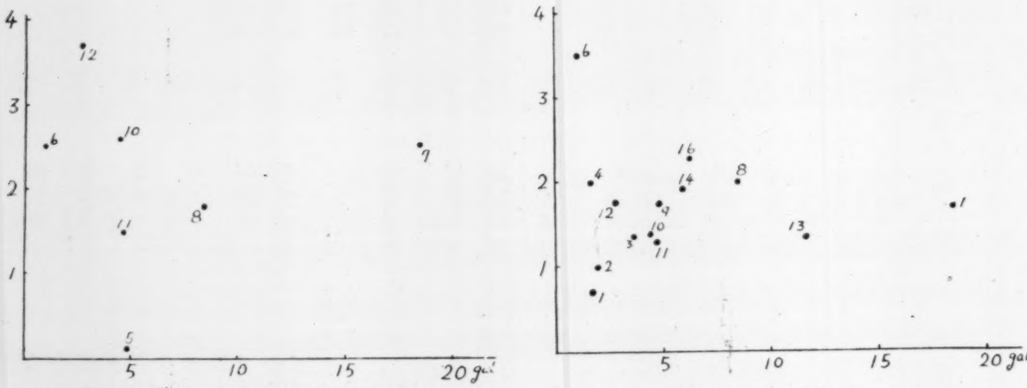

(a) No. 1 に於て岸壁面に垂直方向加速度に對する平行方向の比　(b) No. 3 に於て岸壁面に垂直方向加速度に對する平行方向の比

第 3 圖 地震の強さより見たる岸壁潜函上に於ける最大速度比
(横軸は No. 2 の平均最大加速度)

値が極大極小の間に著しく隔たつて散在するが，地震が強くなるに從ひ，大體 2 倍前後の値に接近するかの如き傾向が疑はれる．

（2） 埋立地の中央，No. 2, の最大加速度の値は方向に於て著しい相異がない，且つその周期も亦震央距離には殆ど關係なく，大體 0·2 乃至 0·3 秒の間に在るらしい．

（3） 岸壁に垂直方向の最大加速度を, No. 2 のものを標準として比較すると，第 4 圖 (b) に示す如く大部分の地震（震央距離 100 粁内外のもの）に於て No. 2 のものより小さく，少數のものが 1·4

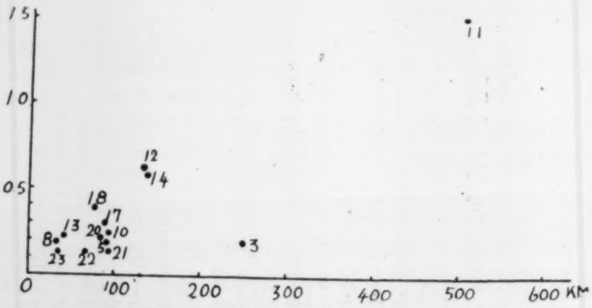

(a) 表高島町の平均最大加速度に對する No. 2 の平均最大加速度の比

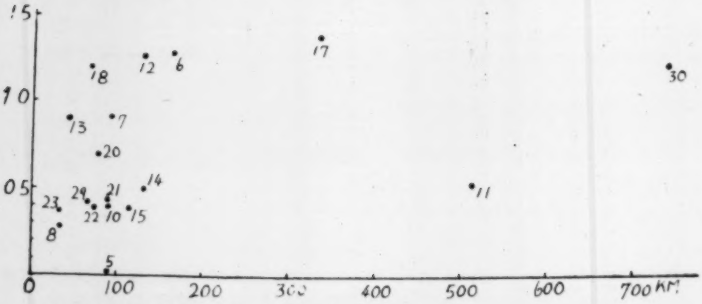

(b) 岸壁に垂直方向の最大加速度比，No. 1 對 No. 2.

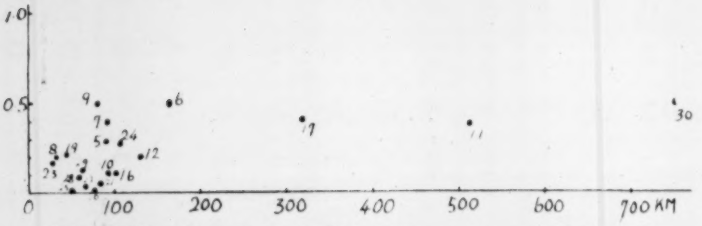

(c) 岸壁に平行方向の最大加速度比，No. 1 對 No. 2.

第 4 圖 各場所に於ける最大加速度比 (横軸は震央距離)

倍近くの値をとつた．震央距離小なるものには，概して短周期の波動が卓越し，震央距離大なるものは，長周期の波動が卓越すると言へるから，震央距離の大小より觀察することは，地震動周期の長短に基いて觀察することゝなる．No. 3 卽ち 3 米岸壁に於て，垂直方向の最大加速度を比較すると，第5圖（a）の如くで，この場合に於

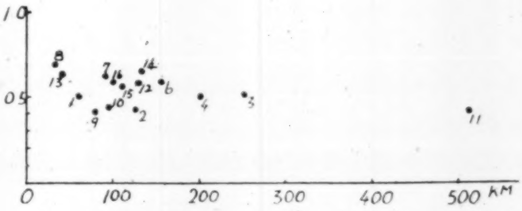

(a) 岸壁に垂直方向の最大加速度比，No. 3 對 No. 2.

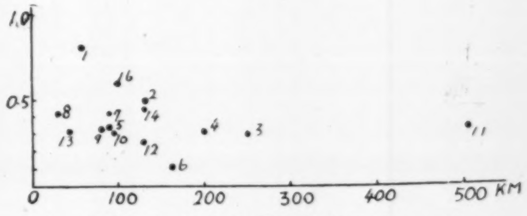

(b) 岸壁に平行方向の最大加速度比，No. 3 對 No. 2.

ては略 0·5 と言ふ一定の値をとり震央距離には無關係の傾向を示してゐる．

（4） 岸壁に平行方向の最大加速度を，No. 2 のものと比較すると，第 4 圖（c）及び第 5 圖（b）に示す如くである．No. 1 では常に No. 2 より小さく，震央距離に關係なく No. 2 の半分以下である．No. 3 に於ては平均して，No. 2 の半分であるが，震央距離 100 粁以下の地震で稍大なる値をとるも 1 倍に達するものはない．

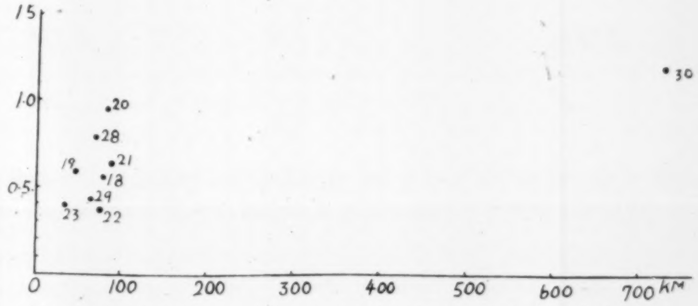

(c) 野毛山の平均最大加速度に對する No. 2 の平均最大加速度の比

第 5 圖　各場所に於ける最大加速度比（橫軸は震央距離）

（5） 岸壁埋立地の中央，No. 2 の平均最大加速度を表高島町及野毛山の平均最大加速度と比較すると，第4圖（a）第5圖（c）に示す通りである．卽ち震央距離 300 粁以內の地震に對して，表高島町は No. 2 の半分以下であつて，唯一つ昭和 14 年 5 月 1 日の男鹿半島の地震で 1·5 倍に達した．次に，野毛山で於ける値に就て比較すると，No. 2 は野毛山と同等か，或はそれ以下である．これを要するに，これ等 3 個所の最大平均加速度を比較すると，No. 2 が最も大きく次が野毛山で，表高島町が最も小なる値であつた．

（6） 10 米岸壁の背後の No. 4 に於て，岸壁に垂直及平行の二方向について，前記の如く比較すると，それ等の値は大體 No. 1 のものと大差なく，No. 2 のものより小さい値を示してゐるのを，第1表から窺はれる．

（7） 各場所に於ける地震動の卓越振動周期を見るために，二，三の地震動について，各波の周期を讀みとり，之を 0·025 秒毎の群に別け，各群の波數を圖表に示すと，第6圖～第10圖の如くである．それ等の圖表によると，各場所の卓越振動周期

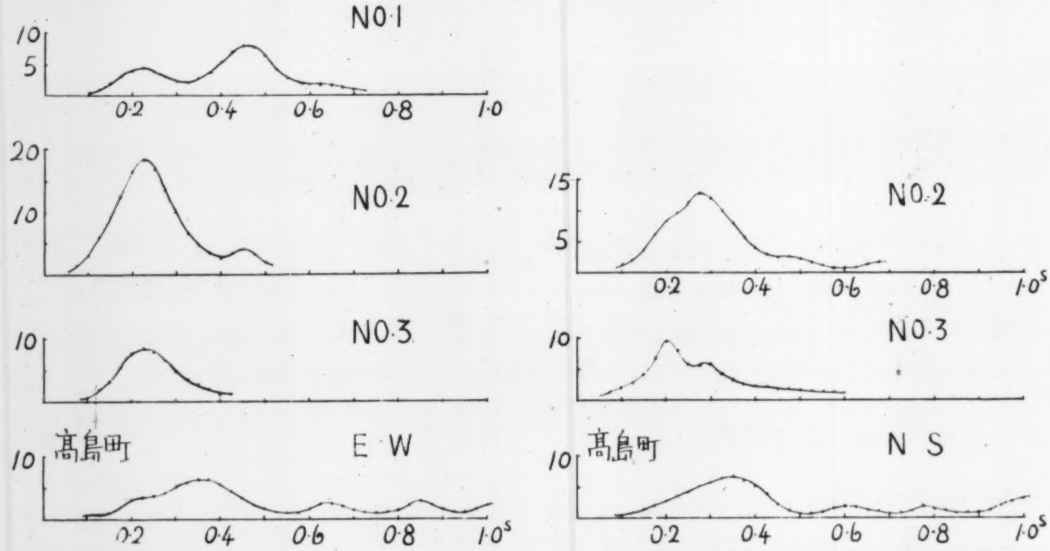

第 6 圖　昭和 14 年5月 19 日野島崎南東沖地震による各場所に於ける地震動中の卓越振動周期左方は岸壁面に垂直，右方は岸壁面に平行のものを示す（縱軸は波數）

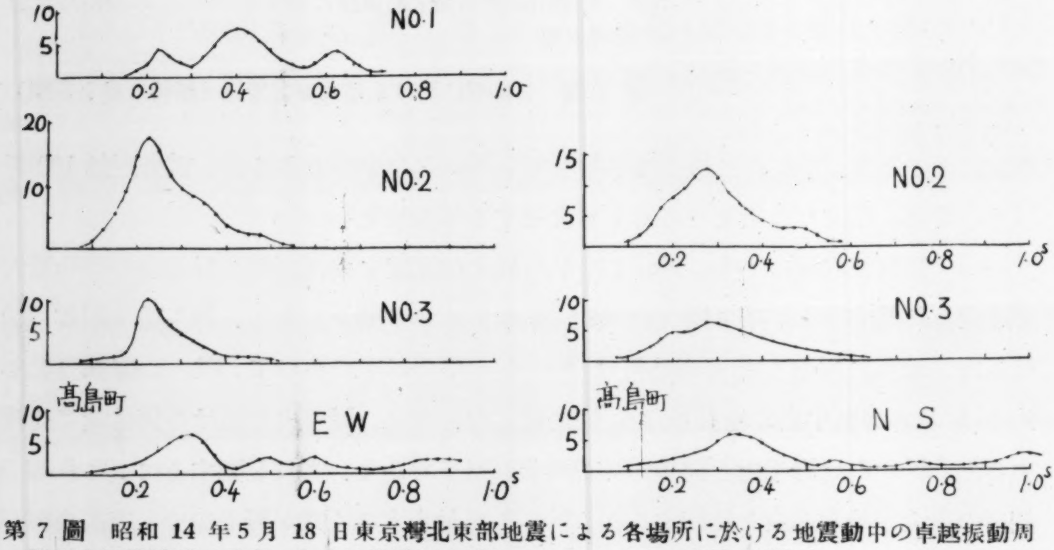

第 7 圖　昭和 14 年5月 18 日東京灣北東部地震による各場所に於ける地震動中の卓越振動周期左方は岸壁面に垂直，右方は岸壁面の平行のものを示す　縱軸は波數）

は第1表に示す最大加速度を與へる周期と，略同等であるのが觸る．圖表には示さなかつたが，No. 4 に於ける卓越振動周期は，震度が小さい地震に對しては No. 2 と略同等（0·25 秒内）外であるが，震度の大きい地震に對しては，No. 1 と略同等（0·5

秒內外）であるのが窺はれる．即ち 10 米岸壁の直背後の No. 4 は，小地震では埋立地中央部と大差ない運動をするが，少くして強い地震では岸壁潜函の運動に支配されるやうに考へられる．

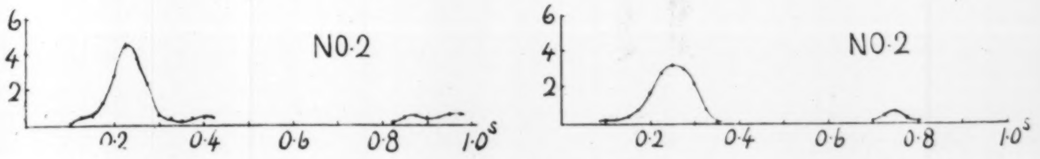

第 8 圖　附近海底に於て約 8 kg 爆薬 3 個の同時爆薬による No. の卓越振動周期

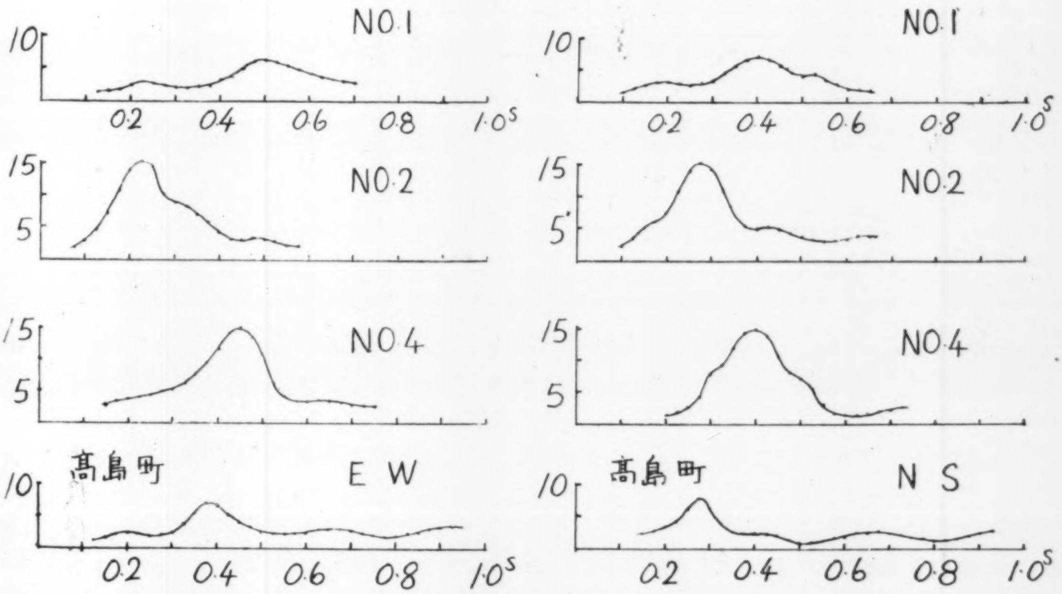

第 9 圖　昭和 14 年 10 月 6 日千葉縣成東附近地震による各場所に於ける地震動中の卓越振動周期左方は岸壁面に垂直，右方は岸壁面に平行のものを示す（縦軸は波數）

（8）　嘗て石本博士[2][3] が東京横濱の各所に於て，觀測したものによると，野毛山の平均最大加速度は常に横濱公園及び高島町より大きく，震央距離の遠近に無關係である．東京本郷と神田，丸の內と比較すると，震央距離 50 粁を境として近い場合は本郷の方が大きく，遠い場合には神田の方が大となつた．今回の觀測に於て，No. 2 のものが野毛山の値より常に大きく現はれたのは，所謂地盤の硬軟或は沖積層の厚薄から判斷すると，一見不可思議に思はれる，即ち洪積層ローム層の如き硬き地盤に於ては，近き地震で大なる加速度を與へるのに，No. 2 が前記の如く野毛山のものより常に大きいのである．多分，No. 2 は本郷と神田丸の內との關係に類似してゐるの

2)　石本巳四雄，地震研究所彙報 **12** (1934), 234.
3)　　〃　　　〃　　**13** (1935), 592.

ではないかと考へられる．それは既に述べた通り No. 2 の沖積層の厚さが，12〜15米で神田，丸の内と略同等であるによるらしい．東京市内での觀測によれば，向島・深川・赤羽の如き沖積層の厚さ 30〜40 米に及ぶ場所は，概して加速度が山手方面より大であつたのに，横濱公園・高島町の如く沖積層の厚さ，それ等と大差ない場所で

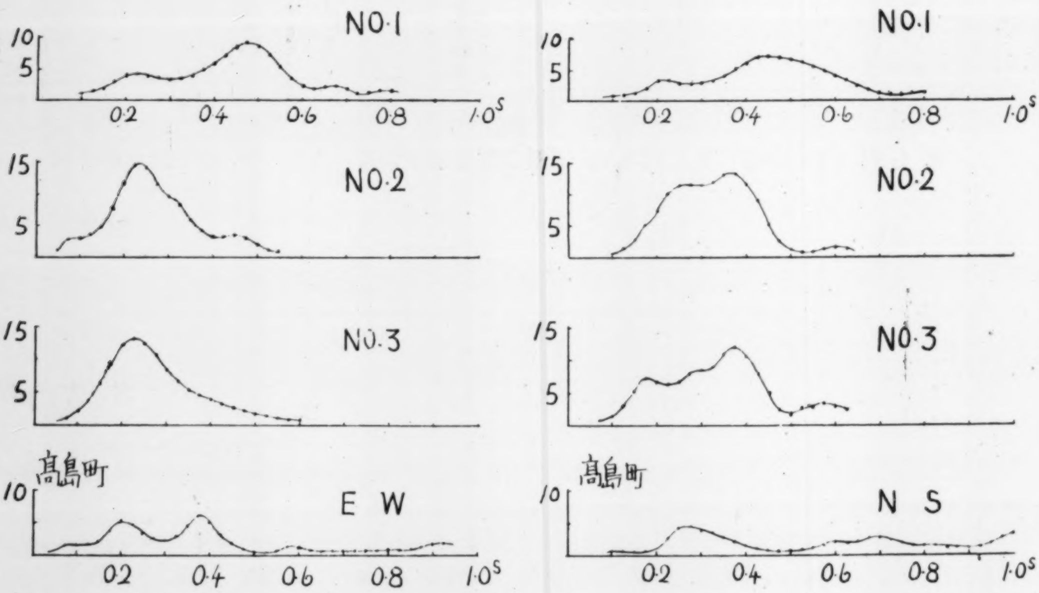

第10圖　昭和 14 年3月 10 日の下結域附近の地震による各場所に於ける地震動中の卓越振動周期，左方は岸壁面に垂直，右方は岸壁面に平行のものを示す（縱軸は波數）

ありながら，野毛山の如き堅い地盤のものより，常に小さい加速度であるのは，理解に苦しむことであるが，それは短周期の波動について比較した場合であつて，1 秒前後の長い周期の波動に於ける加速度を比較すれば，横濱公園及び高島町の方が野毛山の 10 倍にも達することがあるのは，厚い軟弱地層には基本振動の外に各種の倍振動が誘發されるのに依ると考へられる．

これを要するに，土地の卓越振動周期及び最大加速度は震央距離並に層の厚さ，地層を構成する土砂の性質或は埋立に使用せる材料の性質，その厚さ，埋立經過年月等によるのであらうと想像されるが，これ等の眞相の解明には，更に研究を進める必要がある．

No. 3

No. 2

No. 1

第 11 圖 昭和14年3月10日茨城縣下結城附近の地震
何れも岸壁面に平行方向の加速度記象を示す

No. 3

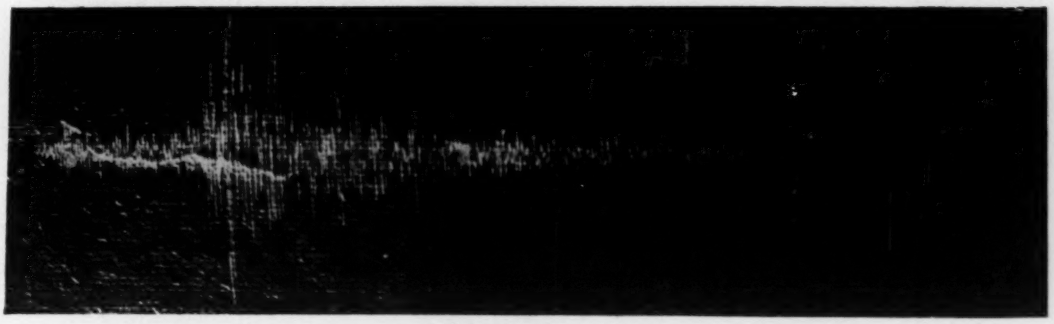

No. 2

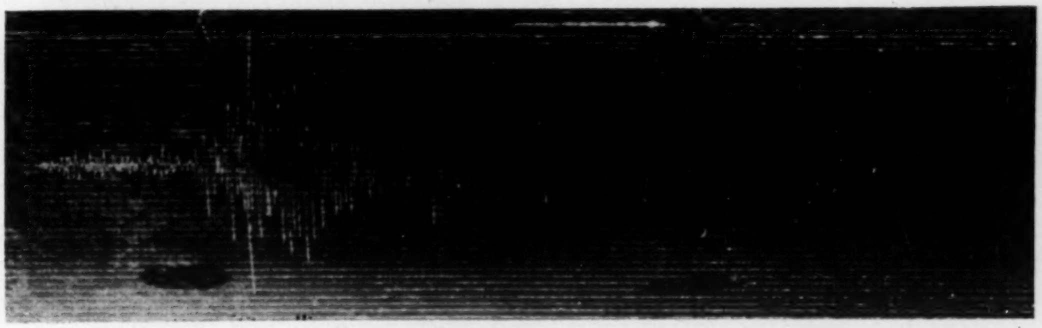

No. 1

第 12 圖　昭和14年3月10日茨城縣下結城附近の地震
何れも岸壁面に垂直方向の加速度記錄象を示す

No. 2

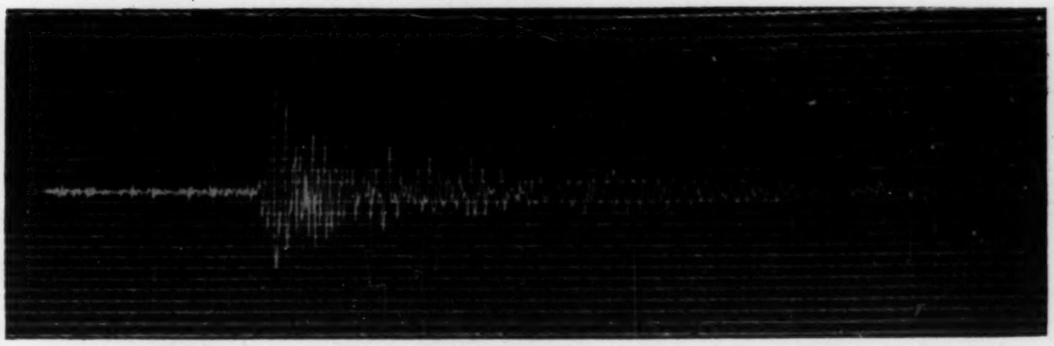

No. 4

No. 1

第13圖 昭和1年2月25日3時50分頃の九十九里濱南部地震
何れも岸壁面に垂直方向の加速度記錄象を示す

15. *Earthquake Vibrations on Quays and on Reclaimed Ground in the Harbour of Yokohama.*

By Tokitaro SAITA,

Earthquake Research Institute,

and

Haruo MATUO,

Research Office of Public Works, Department of Home Affaires.

Notwithstanding that the damage to quays in the harbour of Yokohama, after the great earthquake of 1923 and also in those of Simizu harbour, Sizuoka prefecture, after the violent earthquake of 1935, was extremely heavy, no marked progress has since been made in the study of earthquake damage to quays. The authors investigated the effects of a number of earthquakes on quays and on reclaimed ground in the harbour of Yokohama during the period from January 1939 to March 1940. with the following conclusion:

1. Earthquake acceleration in the case of quays are always smaller to that on reclaimed ground in their neighbourhood.

2. The earthquake accelerations of the perpendicular component in the case of quays are always greater than those of the parallel component in the case of quays.

3. The predominant periods of the ground due to earthquakes depend on the thickness of the ground that has been reclaimed over alluvium. etc.

16. *Observation of Changes in the Inclination of the Earth's Surface at Mt. Tukuba (Second Report).*

By Takahiro HAGIWARA,

Earthquake Research Institute.

(Read Feb. 20, 1941.—Received Mar. 20, 1941.)

The writer, in his previous paper[1], described the changes in inclination of the earth's surface that were observed at Mt. Tukuba with the all-silica clinographs during the period from 1935 to 1937. These observations were made in two rooms, one lying at the end of a gallery, 20 m long, that was bored hoirzontally through the partially weathered granite of the mountain side and the other at a place near the entrance of this gallery (for convenience these will be called rooms "A" and "B" respectively). Observations made in the intervals just mentioned showed that the changes in inclination in rooms "A" and "B" differ entirely. Although the main object of the observation was to ascertain whether or not the changes in inclination of the earth's surface are related to the earthquake activities in nearby regions, the foregoing result shows that measurement of changes in inclination of the earth's surface is a very difficult matter, seeing that they are greatly affected by irregular disturbances on the surface of the ground such, for example, as changes in air temperature, precipitation, sun-shine, etc., the effects of which are so complicated that it is not possible to eliminate them from the records of the clinograph. These disturbances, however, may diminish with increase in depth from the surface of the ground. As a matter of fact, the amount of the irregular changes in room "A" was usually only a fraction of that of room "B". Naturally, we have no evidence that all the changes observed in room "A" were due to geophysical causes, that is, to macroscopic changes, such as the deformation of the earth's crust, although it may be safely said that if a change in inclination with comparatively large amplitude were caused, accompanying an earthquake phenomenon, its detection on the record of room "A" ought to be possible. It was for this reason, that the observations were continued to the present day.

1) T. HAGIWARA, *Bull. Earthq. Res. Inst.*, **16** (1938), 366.

In this paper, the changes in inclination observed in room "A" during the period from Dec. 1937 to Oct. 1940 are shown by graphs (Fig. 3, a∼h), while certain meteorological elements, such as air pressure, air temperature, and precipitation, which we thought might be related in some way to the former, are also plotted in the figures. To ascertain the relations between the inclinations and the earthquake activities that occurred in the region near Mt. Tukuba, the number of daily earthquakes were plotted, those with comparatively large seismic intensity being marked by arrows.

The air temperatures that are plotted in the figures are the values for 14 h, and the precipitations are the net values for the preceding 24 hours observed at 10 h of the same day. The air pressures, which are the values at the summit of Mt. Tukuba for 6 h of the same day, were obtained from the weather charts of the Central Meteorological Observatory.

As will be seen from the figures, the changes in inclination are not correlated with either air pressure or air temperature, although they are closely related to precipitation, but the relation between them is very complicated. In some cases, the inclination is evidently affected by precipitation, whereas in others, fairly heavy precipitations do not affect the inclination. Although it may be said that precipitation does affect the inclination, it is difficult to say what particular part of the changes in the inclination depends on precipitation. This complicated phenomenon is probably the result of underground water, precipitation itself having no direct effect on the inclination. Consequently the most suitable days for studying the relation between changes in inclination and earthquake activity are those days when there was no marked precipitation.

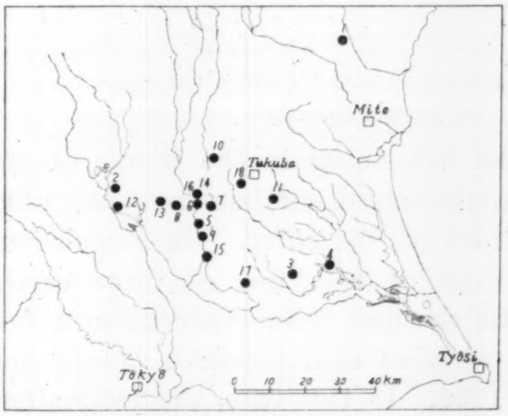

Fig. 1. Numerals are the earthquake numbers in Table I.

More earthquakes shake the neighbourhood of Mt. Tukuba than any other region, except only Formosa, in Japan. About one hundred sensible earthquakes, and a much larger number of non-sensible earthquakes occur in this region every year. These sensible and non-sensible earthquakes shown in the figure have their epicenters within a distance of about 40 km from Mt. Tukuba. The dates of the fairly severe earthquakes are shown in Table I and

marked with arrows in Fig. 3, their epicenters being shown in Fig. 1. The depths of these earthquakes are usually about 40～50 km. Recently none with origins shallower than 40 km have occurred in this region.

Table I. Fairly severe earthquakes that occurred near Mt. Tukuba.

No.	Date	Grade of seismic intensity		Remark
		Tukuba	Tôkyô	
	1938			
1	Mar. 23, 11h 21m	II	0	C
2	May 9, 19 46	II	I	C
3	June 6, 01 31	III	III	A
4	June 6, 04 53	I	I	C
5	Aug. 4, 19 48	II	II	C
6	Aug. 13, 15 58	III	I	C
	1939			
7	Feb. 1, 14 25	II	I	C
8	Mar. 10, 03 12	III	III	C
9	May 31, 19 01	II	I	C
10	June 14, 20 09	II	I	C
11	July 30, 21 55	III	I	C
12	Sept. 12, 14 05	III	II	C
13	Oct. 2, 06 50	II	I	C
	1940			
14	Feb. 24, 04 51	II	I	C
15	July 15, 00 31	VI	III	B
16	Aug. 15, 23 54	III	II	C
17	Aug. 25, 19 32	III	II	B
18	Sept. 17· 13 31	III	II	C

Remarks: Distances to which the earthquake was sensible from the epicenter:—
A. 100～200 km. B. 200～300 km. C. To beyond 300 km.

Although strong earthquakes did not occur in the course of the present study, there were eighteen well-marked earthquakes that were sensible at distance beyond 100 km from the epicenter. No conspicuous changes in the inclination were noticed at the time of these earthquakes, although certain characteristic changes were observed in a few cases; a typical example being the changes that occurred before and after the earthquake of March 10, 1939. In this case, the inclination, which turned gradually eastward at first, did so at an increased rate just before the earthquake, but later turned north-westward after the earthquake. Similar changes were recorded also in room "B" at this time

(See Fig. 2). One, or probably two, such characteristic examples were found in other earthquakes, but they were not so distinct as the foregoing examples.

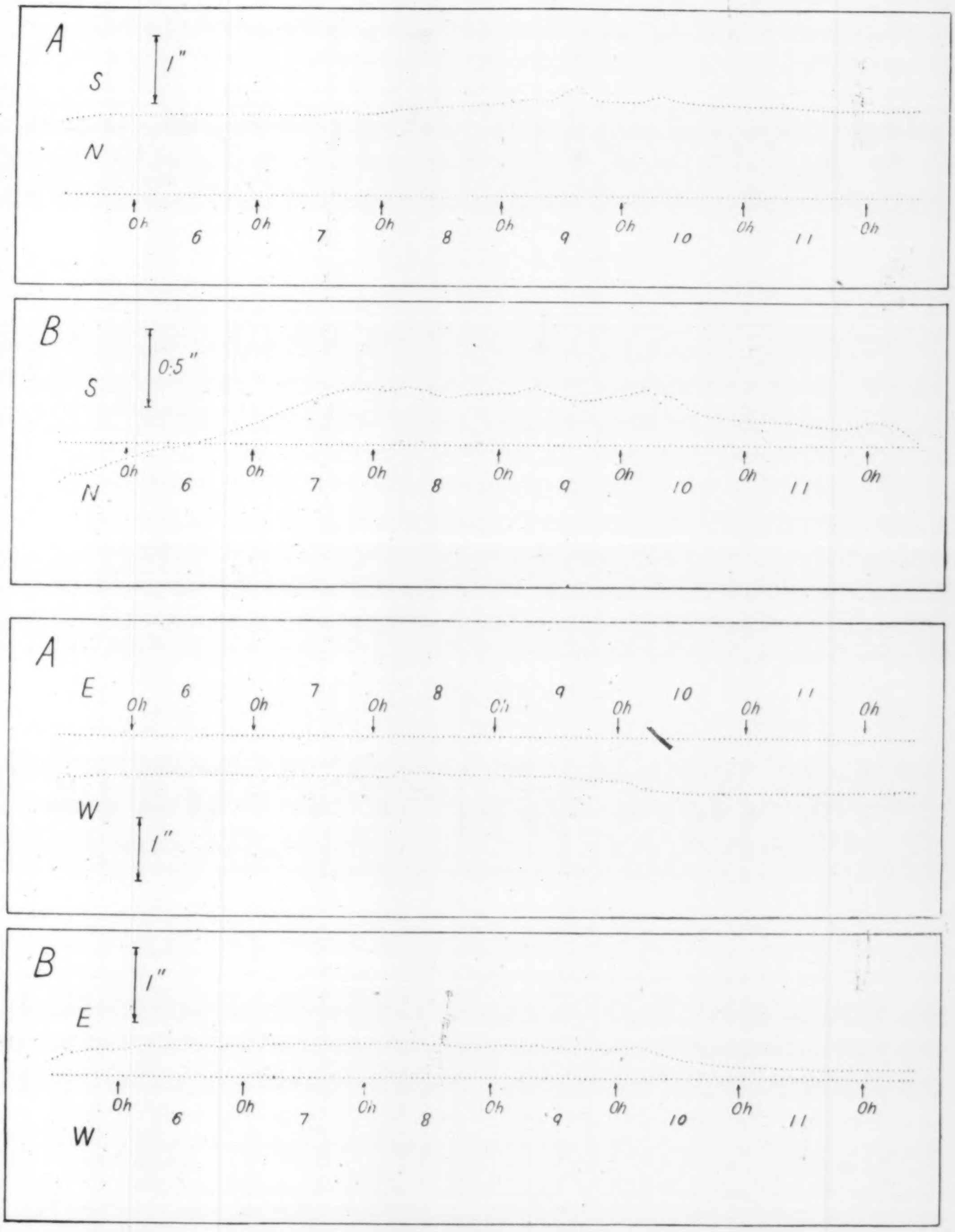

Fig. 2. The records of March 5~12, 1939.

The foregoing data are obviously inadequate for coming to any definite conclusion, the only course open being to make further observations. Plans are now being made for constructing an observation room

at a greater distance from the surface ground by boring still farther (horizontally) in order to be free from such disturbances as precipitation.

• Non-sensible earthquake, ● Sensible earthquake, ↑ Fairly severe earthquake.

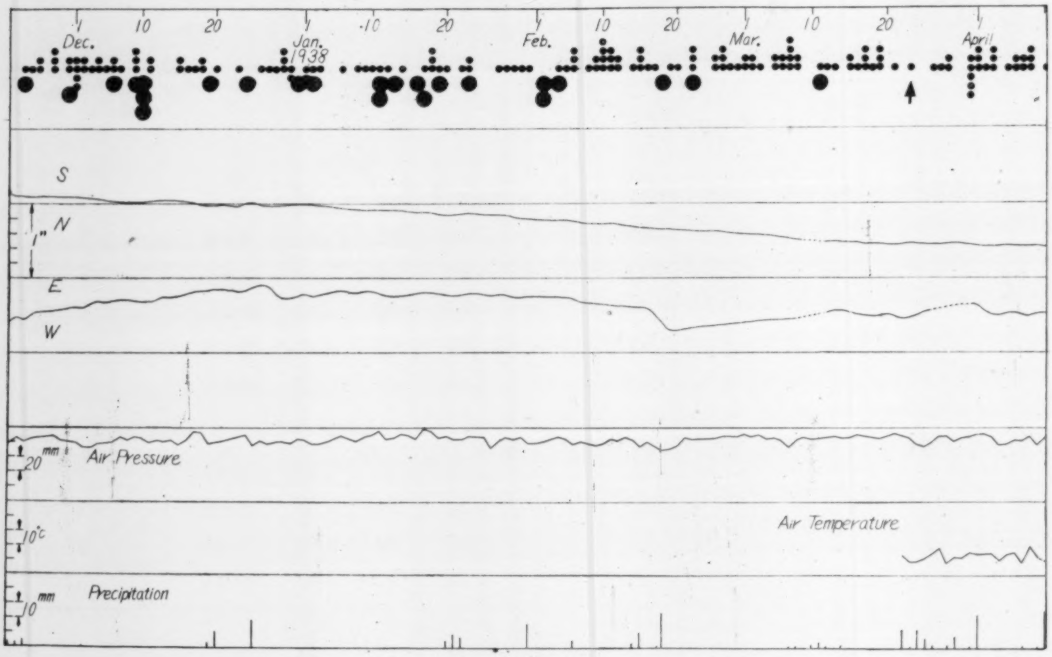

Fig. 3 a.

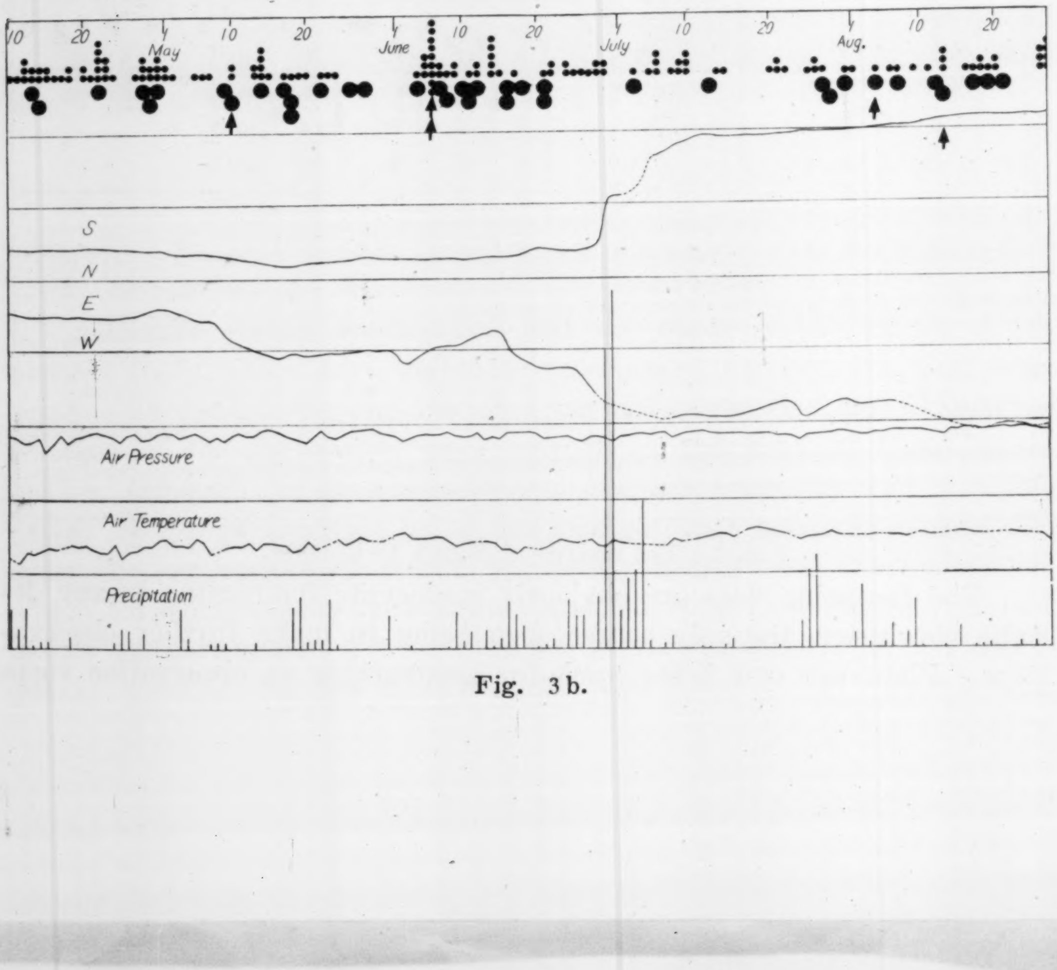

Fig. 3 b.

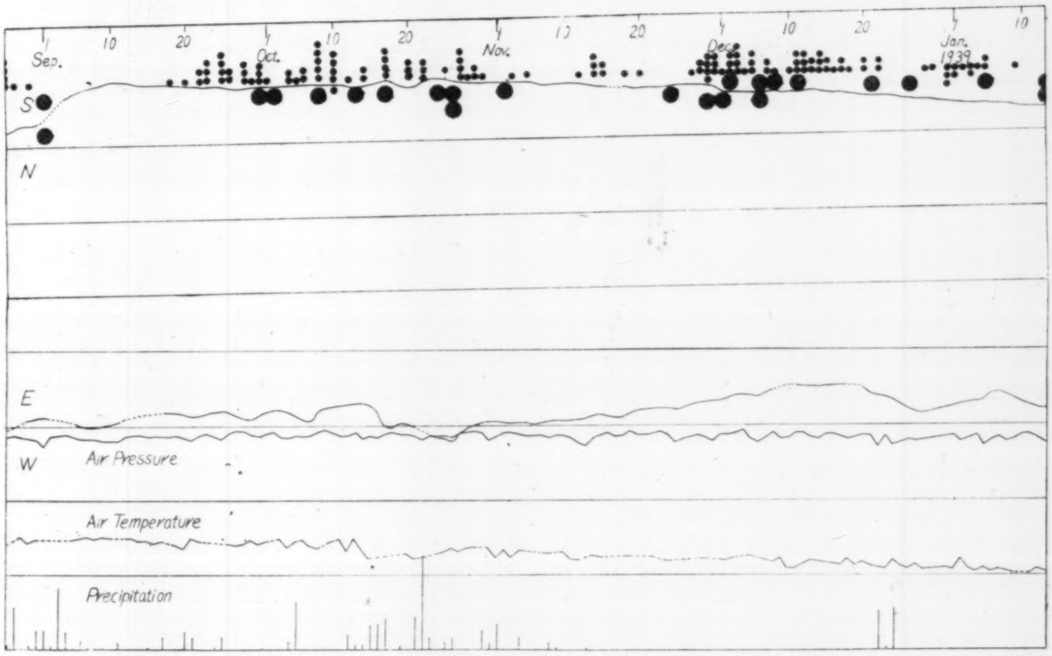
Sep.
Oct.
Nov.
Dec.
Jan.
1939
S
N
E
W
Air Pressure
Air Temperature
Precipitation

Fig. 3c.

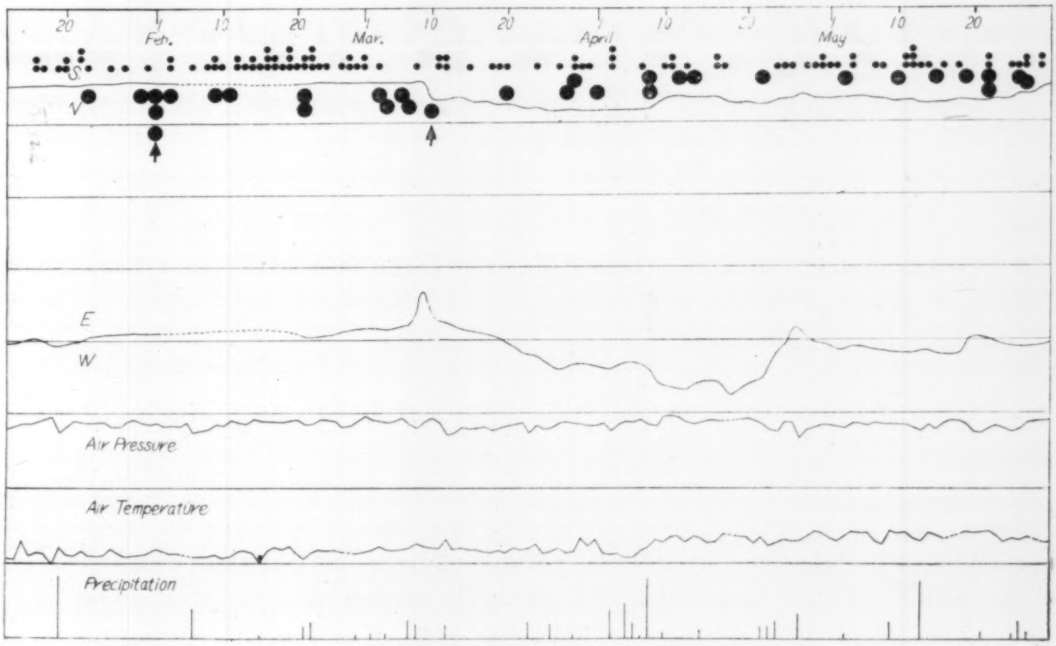
Feb.
Mar.
April
May
S
V
E
W
Air Pressure
Air Temperature
Precipitation

Fig. 3d.

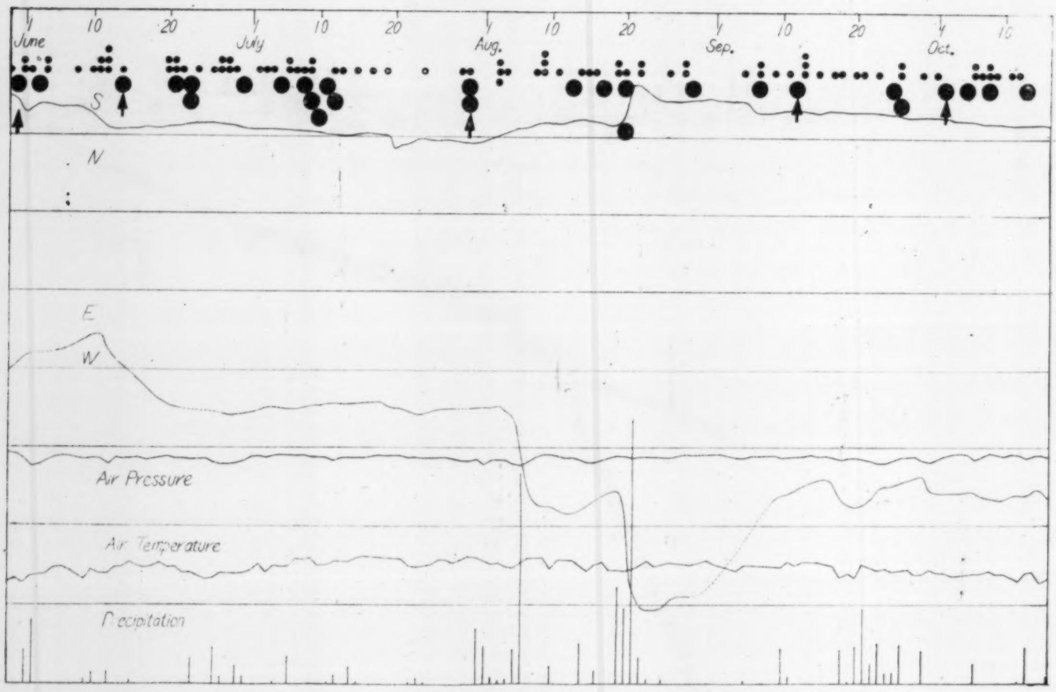
June
July
Aug.
Sep.
Oct.
S
N
E
W
Air Pressure
Air Temperature

Fig. 3e.

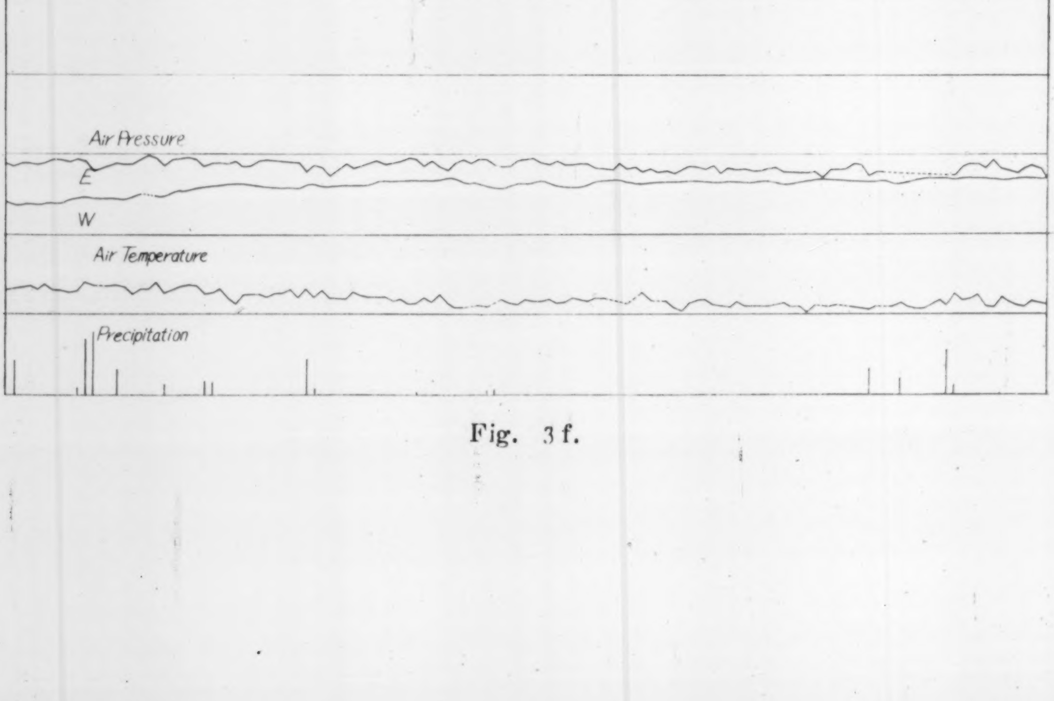
Nov.
Dec.
Jan.
1940
Feb.
S
N
Air Pressure
E
W
Air Temperature
Precipitation

Fig. 3f.

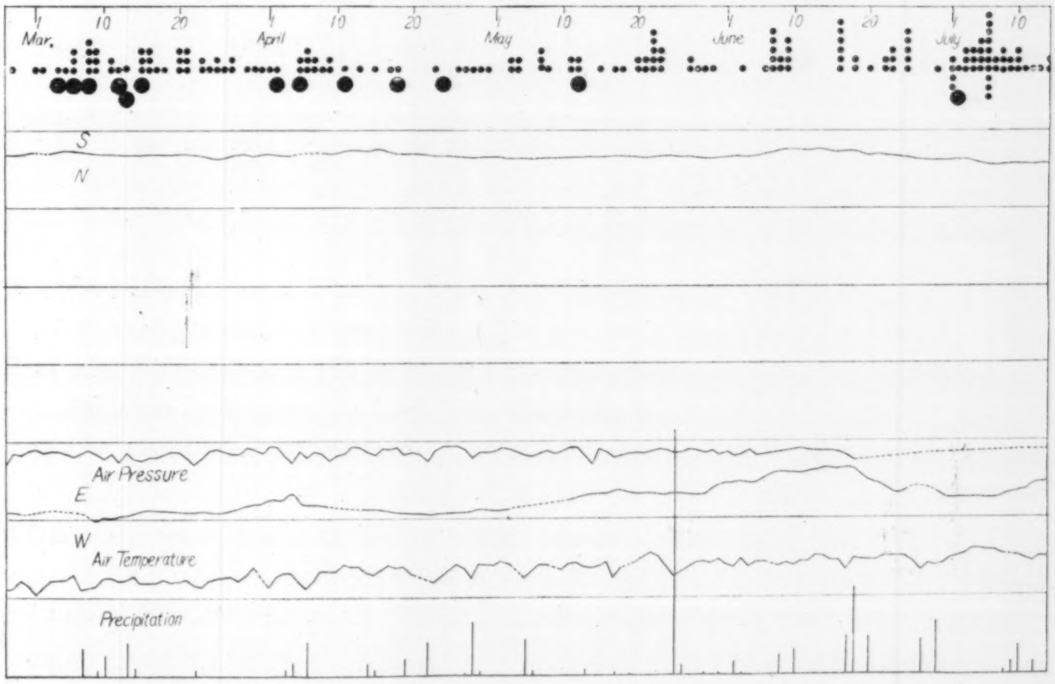

Fig. 3 g.

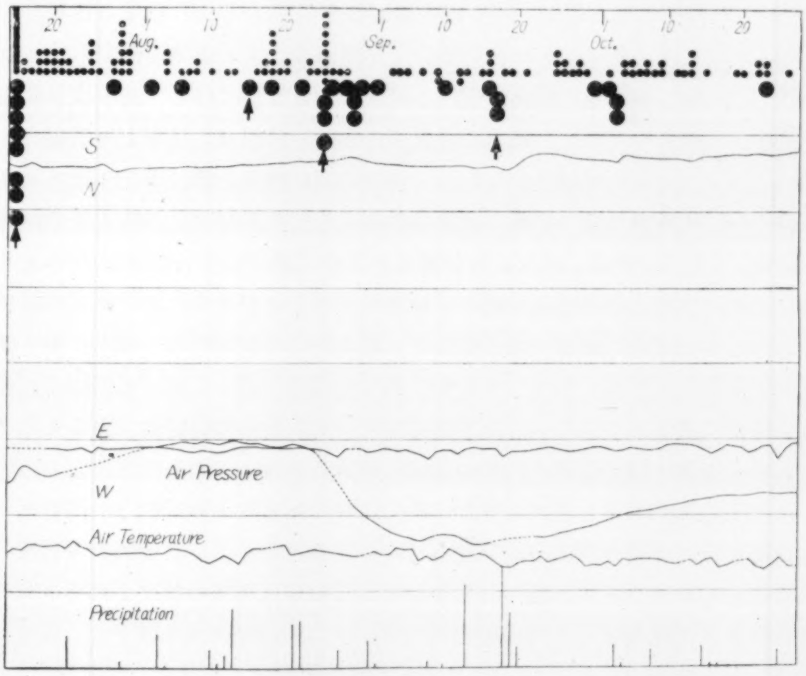

Fig. 3 h.

In conclusion, the writer wishes to express his sincere thanks to the officials of the Division of Scientific Research in the Ministry of Education for the Funds for Scientific Research, from which a part of expense necessary for this study was defrayed.

16. 筑波山に於ける土地傾斜變化の觀測 (其の二)

地震研究所 萩原尊禮

地表に於ける溫度變化の直接間接の影響から免れるために，筑波山支所附近の山腹に 20 米餘の橫坑を穿ち，其の最奧部に於て土地傾斜變化の觀測を行つてゐる．比較のため橫坑の入口に近い部分にも傾斜計を置き觀測を行つてゐるが，便宜上，橫坑の奧にある觀測室を A，入口に近いところの觀測室を B と名付けた．前回の報告（震研彙報第 16 號）に於ては，昭和 10 年 10 月より昭和 12 年 11 月に至る約 2 ケ年間の觀測結果に就て述べたが，其の結果は，傾斜日變化は A 室に於ては 0·01″ 程度，B 室に於ては 0·05″ 程度であり，不規則な變化や永久變化も亦 A 室の方が B 室のものよりも遙かに小であつた．而も是等の傾斜變化は，量のみならず其の方向に於ても全く，A 室と B 室とは趣きを異にしてゐた．觀測の第一の目的は，實は Macroscopic な地殼の傾斜變化，特に附近に發生する地震活動に伴ふ地殼傾斜變化を驗するにあつたのであるが，僅か 20 米を隔てた場所に於て全く異つた變化を與へると云ふことは，此の種の Macroscopic の變化を知ることが非常に困難な問題であることを示してゐる．然し乍ら，A 室に於ける變化は，降雨等による特別の影響を除いては，通常極めて小であり，時折現れる不規則變化も 1″ の分數程度であり，永久變化も年に 2″ 程度であるので，若し假に地震發生に伴つて 1″ 程度の特異な傾斜變化が地殼に生じたとするならば，我々はそれを記錄の上で認めることが出來る筈であり，而も其の樣な場合は A 室にも B 室にも共通な變化が現れる可きであると思はれる．此の樣な見地から，其の後も觀測を繼續して來たのである．此處に報告する分は，昭和 12 年末より昭和 15 年末に至る約 3 ケ年間に於ける A 室の傾斜變化である．此の期間の變化を圖に畫いて見ると第 3 圖の樣になる．比較のため，毎日の氣溫，氣壓，雨量等を記入してあるが，これによると傾斜變化は氣溫や氣壓とは關係はないが，降雨には大いに影響される樣に思はれる．昭和15年の 1 月前後には降雨が殆ど無いが此の期間の傾斜變化は極めて單調であることが見られる．然し降雨が傾斜變化に影響すると云つても，兩者の關係は頗る複雜で，或る時には比較的少い雨量に對し相當の傾斜變化が起されたと見做される時もあり，又反對に相當の雨量に對して殆ど傾斜變化が起つてゐない場合もある．降雨は地下水となり，之が觀測室附近の局部的の傾斜變化に與るものと考へられるから，此のために雨量と傾斜變化との間の關係が複雜となるのであらう．

地震は，上記の觀測期間中，筑波山附近に於て比較的顯著なものが約 10 回程起つてゐる．然し，是等の地震は何れも震央附近に於て震度 III の程度であつて，之を越える程度の大きさを持つた地震は發生しなかつた．第 3 圖には是等の比較的顯著な地震の發生した日を矢印を以て示してある．これによると地震發生と傾斜變化との間には，此の程度の地震では，餘り明瞭な關係はない樣である．只，昭和 14 年 3 月 10 日の茨城縣下妻附近（筑波山の西南西約 20 km）の地震の前後に稍々特異な傾斜變化が見られる．此の傾斜變化は A 室に於ても B 室に於ても略々同樣な變化が記錄されてゐる（第 2 圖參照）．是に似た傾斜變化は他の一，二の顯著な地震の場合にも起つてゐるやうに見えるが，前の例ほどに明瞭ではない．此の樣に，特異な傾斜變化が總ての地震の場合に起つてゐるわけではないのであるから，何等か他の（地震とは全く無關係な）事情のために傾斜變化が起され，これが偶然，地震と時を同じくしたと云ふ疑を一應は持つことが出來よう．此の問題は將來なほ觀測を續けた上でなければ正しい議論は出來ない．

今後は，更に横坑を深く掘進み，地下水等の影響を受けない場所に觀測室を設け，從來の觀測室に於けるものと比較して見たいと思つてゐる．永年に亘る緩慢な傾斜變化の問題，即ち其れが器械にあるものか，極めて局部的のものか，或は實在する地殼の變動であるか，の問題は尚將來に殘される．

17. *Upwarp Deformation of the Land in Tyūgoku.*

By Naomi MIYABE,

Earthquake Research Institute.

(Read March 20, 1941.—Received March 20, 1941.)

1. It has been pointed out that the results of revisions of precise levels, crossing Tyūgoku in a N—S direction, show an upwarping deformation of the land.[1]

This statement should however be discussed from various angles in order to ascertain whether or not the above mentioned mode of deformation is real.

Since, in the former survey, the results of which were compared with that of the later survey to deduce the vertical displacements, staves of Russian alder were used, while, for the later surveys, invar tapes[2] were used, the question arises whether or not the scale divisions on the former staves expanded at the time of the former survey at the same rate as the latter staves.

Revisions of precise levels show that bench-marks situated at altitudes rose compared with those situated in lower land. If this upwarping deformation is not real but only illusory, then the differences in expansion of the staves may be one of the causes of the apparent upwarp deformation. The apparent upwarp of the land may therefore be regarded as having resulted from the following causes:

(i) The length of the standard scales used for calibrating the scale of the Russian alder staves expanded, although only slightly, compared with those used for calibrating the scales of the invar tapes.

(ii) The lengths of the standard scales used for calibrating the scales of the Russian alder staves expanded uniformly only at the time of the first surveys. They have shrunk so much since then that the difference between the lengths of the standard scales for the old and the new staves can no longer be distinguished.

(iii) The integrated effect of the deviations due to atmospheric refraction.

In the case of precise levels, the effect of atmospheric refraction is generally considered negligible, because the distance between the

1) C. TSUBOI, *Jap. Journ. Astr. Geophys.*, **10** (1933), 94~248.
2) Invar tape stretched on a rong slender frame, used for staves in precise levels.

telescope and the staves is sufficiently small. Moreover, since field work is generally done under a variety of atmospheric conditions, there is automatic compensation of the deviations in measured heights due to atmospheric refraction, so that the effect of atmospheric refraction is usually negligible.

Besides, it is not possible to detect the effect of difference in the unit lengths of the standard scales used for calibrating the scales of the staves if the uniform expansion of the unit length of the scale used for calibrating the Russian alder staves was only a temporary phenomenon that existed only at the time of the former survey. Only case (i), mentioned above, admits of being investigated further. Studies in this direction will soon be made and the results reported.

In this paper, however, we deal with the actual data of vertical displacements of bench-marks on the lines of levels crossing Tyūgoku in order to show how the vertical earth movements are correlated with the actual heights.

2. The lines of levels from which the relation between the vertical displacements and the heights are studied in this paper by means of the positions of the bench-marks, are those linking Hirosima with Sinzi, Okayama with Yonago, and Okayama with Tottori. The geographical situation of these lines of levels are shown in Fig. 1.

Fig. 1. Geographical situations of lines of levels crossing Tyūgoku.

Although in the present study, the vertical displacements are com-

pared with the heights of the bench-marks, we take successive differences of the vertical displacements of contiguous bench-marks, (that

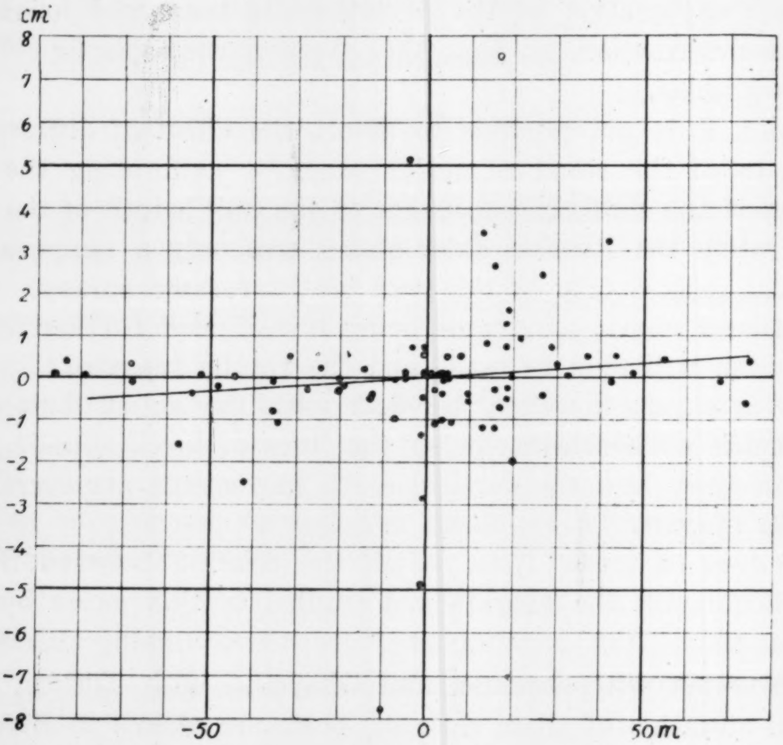

Fig. 2a. Relation between w (1891∼1921) and H for the line from Hirosima to Sinzi.

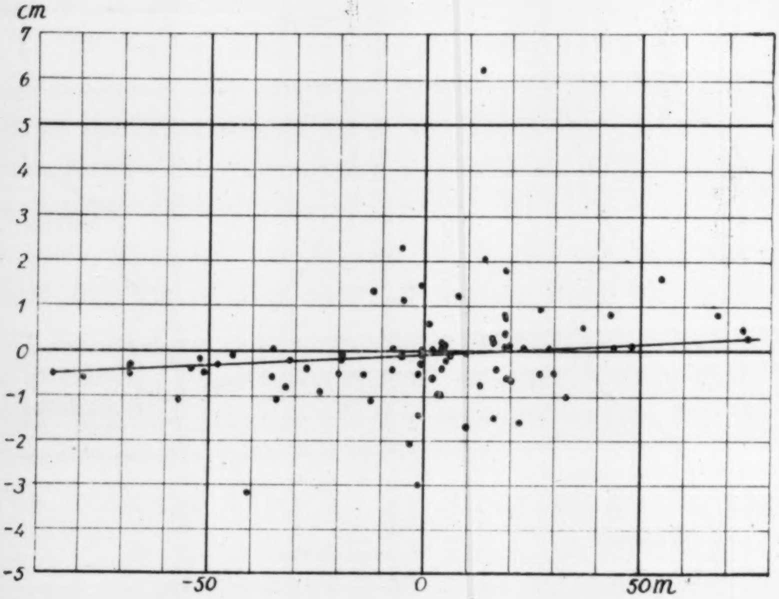

Fig. 2b. Relation between w (1921∼1935) and H for the line from Hirosima to Sinzi.

is, the differences between bench-marks A and B, B and C, C and D,

etc., deduced from changes in their heights above the sea-level since the last survey) for comparison with the differences in the present heights above sea-level of the corresponding bench-marks.

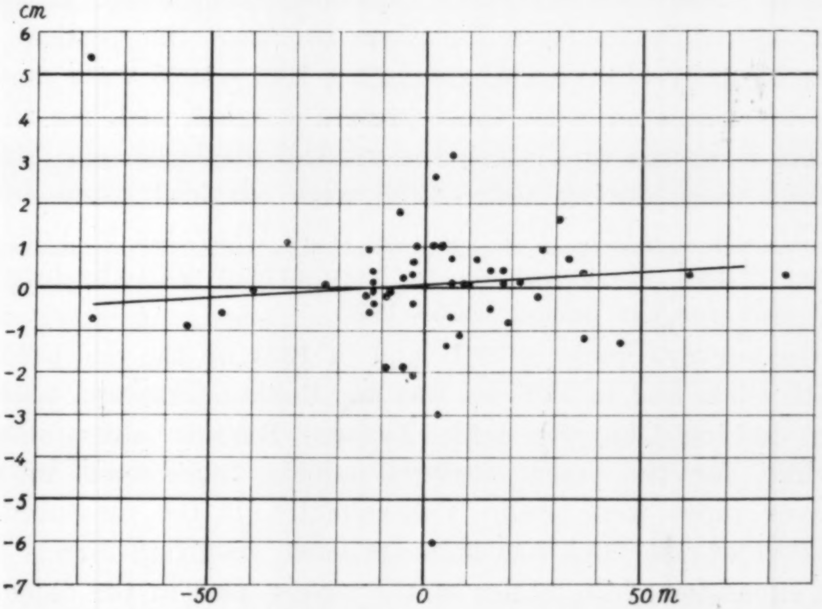

Fig. 3 a. Relation between w (1895∼1929) and H for the line from Okayama to Tottri.

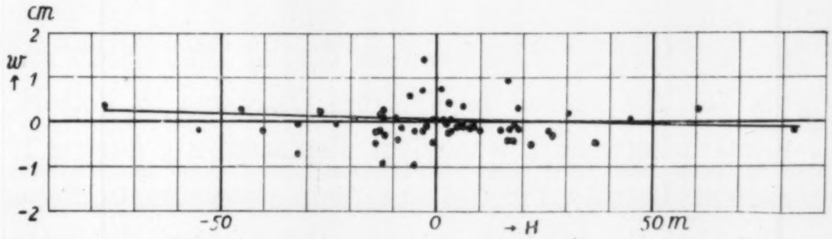

Fig. 3 b. Relation between w (1929∼1935) and H for the line from Okayama to Tottri.

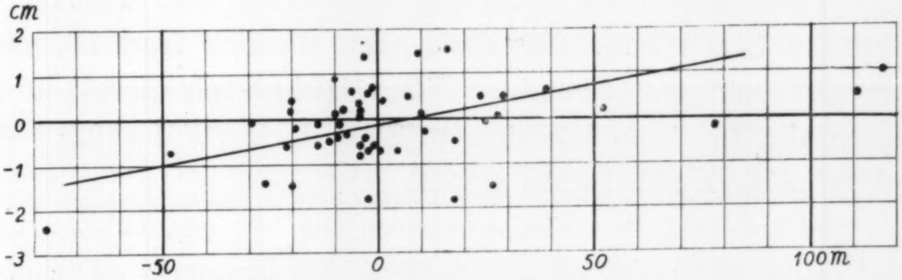

Fig. 4. Relation between w (1895∼1935) and H for the line from Okayama to Yonago.

In Figs. 2∼4, the successive difference between the vertical dispiacements of contiguous bench-marks are plotted against the successive difference between the heights of the corresponding bench-marks.

The line of levels from Hirosima to Sinzi was first run in 1891 and rerun in 1921 and also in 1935. The line from Okayama to Tottori was first run in 1895 and rerun in 1929 and 1935, while that from Okayama to Yonago was first run in 1895 and rerun in 1935. Consequently, for that line of levels from Hirosima to Sinzi, the vertical displacements during 1891~1921 and those during 1921~1935 were ascertained; these to be compared with their present heights, and, for the line of levels from Okayama to Tottori, the vertical displacements during 1895 ~1929 and those during 1929~1935 were obtained; these to be compared with the heights. For the line from Okayama to Yonago, however, the vertical displacements for comparison with the heights were obtained only for the period 1895~1935.

In the surveys made in 1891 and in 1921 on the line linking Hirosima with Sinzi and in 1895 on the line linking Okayama with Tottori and that linking Okayama with Yonago, Russian alder staves were used, while, for the recent surveys, namely, those made in 1929 and 1935, invar tapes were used. Consequently, if the measured upwarp deformation of the land was only apparent, resulting merely from the uniform expansion of the scales of the staves used in the older surveys, it will be found that the relation between the vertical displacements during the period 1921~1935 and the present heights for the line of levels from Hirosima to Sinzi is approximately the same as the relation between the vertical displacements during 1895~1929 and the present heights for the line of levels from Okayama to Tottori, and also with the relation between the vertical displacements during 1895~1935 and the present heights for the line from Okayama to Yonago. It is also probable that the relation between the vertical displacements and the presnt heights mentioned above differ entirely from the relations of the vertical displacements during 1891~1921 (for the line from Hirosima to Sinzi) and 1929~1935 (for the line from Okayama to Tottori) and their present heights. The vertical displacements of bench-marks on the line from Hirosima to Sinzi during 1891~1921 were measured by using Russian alder staves.

To find the average relation between the two quantities, namely, w the successive difference of the vertical displacements of contiguous bench-marks and H, the successive differences in the present heights of contiguous bench-marks, we calculated the value of the constants that connect w with H, in the form

$$w=\alpha H+\beta,$$

by the method of least squares.[3]

The values of α and β thus obtained are given in Table I, the average relations of $w=\alpha H+\beta$ being shown by straight lines drawn in the graphs of Figs. 2~4.

Table I.

Line of level	α		β	
	I	II	I	II
Hirosima-Sinzi	0·070	0·023	−0·11	−0·74
Okayama-Tottro	0·047	$-0{\cdot}003_3$	0·77	0·64
Okayama-Yonago	0·101		−1·23	

I: Values obtained with the data of w deduced as changes during the 1st and 2nd surveys.

II: Values obtained with the data of w deduced as changes during the 2nd and 3rd surveys.

In calculating the values of α and β, H was measured in metres and w in milimetres.

3. As already refered to, if the measured deformation, namely, the upwarp of the land of Tyūgoku, is nothing but an illusion caused by uniform expansion of the scales used in the 1891, 1895, and 1921 surveys, the values of the constants for the various lines of levels should turn out to be nearly equal. Actually however the values of the constant for various lines of levels differ more or less from one another.

It should also be noted that with regard to the line of levels linking Hirosima with Sinzi, the value of the constant α obtained by means of the vertical displacements during the time from 1891 to 1921 is about 3 times as large as the value of α obtained by means of the earth movements for the interval from 1921 to 1935, while, with regard to the line linking Okayama with Tottori, the value of α obtained by means of the earth movements during the interval from 1895 to 1929 and the value of α for the period from 1929 to 1935 have different signs, although the value α for the latter interval is very small.

The fact that the value of α, obtained in the line of levels that links Hirosima with Sinzi, are of the same sign even for different intervals of time, and that their amounts are approximately proportional

3) Values of α and β calculated by

$$\alpha=\frac{[wH]}{[HH]}\,\frac{1-\dfrac{[w][H]}{n[wH]}}{1-\dfrac{[H]^2}{n[HH]}},\quad \beta=\frac{1}{n}\,\frac{[w]-[H]\dfrac{[wH]}{[HH]}}{1-\dfrac{[H]^2}{n[HH]}}.$$

to the durations of the time intervals to which the vertical earth movements are due, may show that the measured upwarp movement of the land in Tyūgoku cannot be regarded as mere illusion resulting from using a scale that had expanded for calibrating the scales ot the Russian alder staves in the older surveys. The measured deformation of land in Tyūgoku contains, at any rate, a component of upwarp movements that really exist.

The following discussion on this point is from another point of view.

Since the bench-marks, which are imbedded in roads, are usually along valleys, when the road traverses mountaneous regions, the heights of the bench-marks do not show the general elevation of the profile in the region crossed by the line of levels. For this reason, contour lines of various altitudes are drawn with reference to the heights of the triangulation points only, thus smoothing the details in the actual topography. From the configuration of these contour lines, the heights of bench-marks are estimated.

The heights of bench-marks thus estimated and those measured by

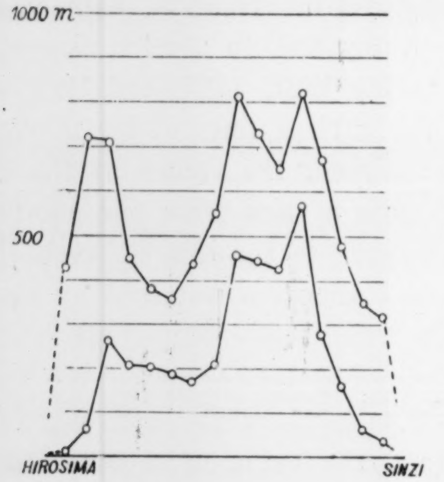

Fig. 5 a. Topographical profiles along the line of levels from Hirosima to Sinzi.

Upper curve: Referring to estimated heights of bench-marks.
Lower curve: Referring to true heights of bench-marks.

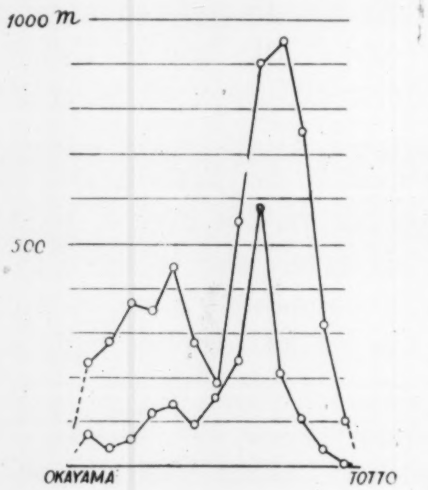

Fig. 5 b. Topographical profiles along the line of levels from Okayama to Tottori.

Upper curve: Referring to estimated heights of bench-marke.
Lower curve: Referring to true heights of bench-marks.

levellings, as designated by numerals on the odinary 1/50000 topographical maps, do not agree, as will be seen from the graphs compared in Fig. 5.

The differences in the heights of every tenth bench-mark was

then compared with the differences between the vertical displacements of the corresponding bench-marks. The graphs given in Figs. 6~8 show the relation between these two quantities.

The values of the constants α that connect the difference in the vertical displacements of every tenth bench-mark with the difference in the heights of the corresponding bench-mark are than calculated as before.

It may then be expected that, if the measured deformation of the land be a mere illusion, the value of the constant thus obtained would differ remarkably from those obtained from data of the true heights of the bench-marks.

The values of α and β thus obtained are shown in Table II.

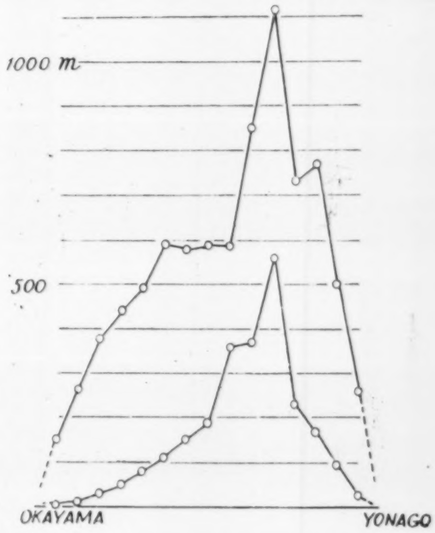

Fig. 5c. Topographical profiles along the line of levels from Okayama to Yonago.

Upper curve: Referring to estimated heights of bench-marks.
Lower curve: Referring to true heights of bench-marks.

Although it cannot be concluded from these results that the upwarp deformation, as revealed in the results of relevellings in the Tyūgoku region, is real, neither is there any reason for regarding the

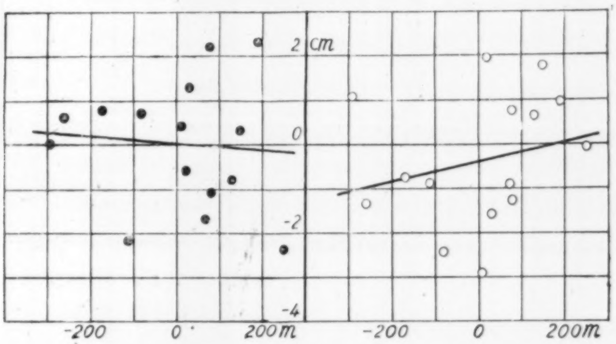

Fig. 6. Relation between w and H (estimated) for the line from Hirosima to Sinzi.

a. w (1891~1921) and H (estimated).

b. w (1921~1935) and H (estimated).

measured deformation as mere illusion, the result of the expanded standard scale used in calibrating the Russian alder staves used in the older surveys.

As to the lengths of the standard scales used for the old and recent levellings, the subject will be discussed in due course.

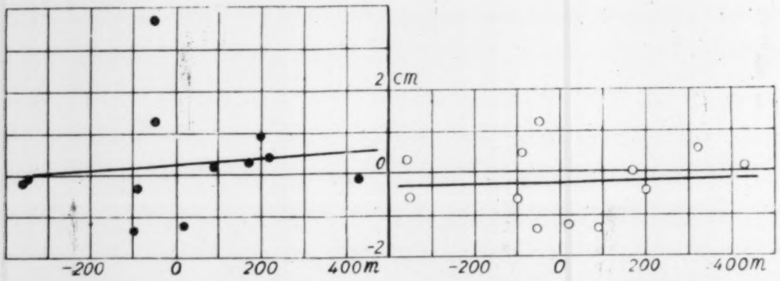

Fig. 7. Relation between w and H (estimated) for the line from Okayama to Tottori.

a. w (1895~1929) and H (estimated). b. w (1929~1935) and H (estimated).

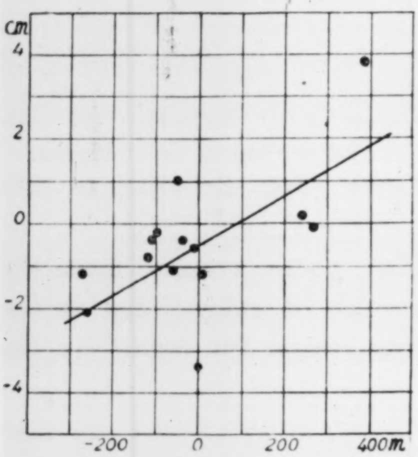

Fig. 8. Relation between w and H (estimated) for the line from Okayama to Yonago.

Table II.

Line of level	α	
	I	II
Hirosima-Sinzi	$-0{\cdot}009_6$	0·024
Okayama-Tottori	$0{\cdot}006_3$	0·0016
Okayama-Yonago	0·056	

Line of level	β	
	I	II
Hirosima-Sinzi	0·09	−4·17
Okayama-Tottori	2·76	−2·13
Okayama-Yonago	−4·97	

I: Values obtained with the data of w deduced as changes during the 1st and 2nd surveys.

II: Values obtained with the data of w deduced as changes during the 2nd and 3rd surveys.

In conculsion, the writer wishes to express his sincere thank to the Department of Education for the grant received for undertaking this study. His thanks are due also to Miss H. Maeda for her assistance in calculating the numerical data and preparing the figures.

17. 中國山地の隆起運動に就て

地震研究所 宮部直巳

中國を南北に連ねる水準線，廣島——宍道間，岡山——米子間，岡山——鳥取間の水準改測の結果によれば，それら各區間の中間部，換言すれば，比較的高い部分が兩端の低い部分に比して幾分隆起してゐる．この現象は，之を以て直にそのやうな地殼の變動があつたと見做すことも出來るが，若しも，前測量に用ゐられた標尺，乃至はその標尺の點檢に使用された標準尺が後の測量に用ひられた標尺，又は，その點檢に用ひられた標準尺に比して少しばかり長かつたとすればそれでも，その"高い場所が一層高まる傾向"を解釋することが出來る．

又，空氣層に於ける光の屈折の影響も考へられるが，普通の測量は，その影響の少ない時間にさうして，又，その影響の相殺される樣な方法で行はれるから，光の屈折の影響は先づ無視してもよからうと思はれる．

標尺の相異は，若しも以前の標準尺の長さが，今日まで變化してゐなければ，今尺の標準尺と比較して之を求めることも出來るが，若し，さうでなければ，標尺に相異のあつたことを今日確めることは不可能である．

實際の變動量について見れば，若し，それが，新舊の標尺の相異から生れたものとすれば，高さと變動量との關係が，場所や，新舊測量間の期間の長さなどには殆ど無關係であり，3 回測量の行はれた，廣島——宍道間，岡山——鳥取間等に就いては，前期の變動量と後期の變動量とが著しく異る場合も起り得ると思はれる．殊に，前期の變動量と後期の變動量とが，夫々，その變動を生じたと見られる期間の長さに略々比例するといふやうなことは，極めて稀にしか期待し得ないであらう．これらの點を確かめる爲に，各水準線につき，次々の水準點の高さの差 H と變動量の差 w との關係を調べてみた．

$$w=\alpha H+\beta$$

とおいて，常數 α を求めてみると，その値は，水準線により，又期間により，幾分かづゝ相異することが認められる．

又，H に水準點の眞高の差を採らず，附近の三角點の高さを平滑した値を用ひて描いた等高線に基いて推定した水準點の高さの差をとつて，w と比較しても略々同樣の結果を得る．

この結果により，標尺の相異による影響を否定することは不可能であるけれども，少くとも，敍上の如き地殼運動の實在することは，認めなければならないであらう．

18. *Secular Changes in the Heights of Yearly Mean Sea-Level at Japanese Stations.*

By Naomi MIYABE,

Earthquake Research Institute.

(Read Jan. 16, 1941.—Received March 20, 1941.)

1. Changes in the heights of sea-levels are caused by various disturbances, such as tidal forces, changes in atmospheric pressure, changes in direction and intensity of wind, fluctuations in sea-water temperature caused by ocean currents and local precipitations, etc. Of these disturbances, the dynamical effect of ocean current is believed to cause the irregular variations in the heights of sea-levels, but it is so small that it is negligible in discussing changes in heights of sea-level greater than a few centimetres.

The changes in height of sea-level caused by most of the other disturbances are regarded as periodic. The periods of the disturbances due to tidal forces are, as is well known, diurnal, semidiurnal, etc., while the period of disturbances due to meteorological disturbance is approximately annual. Hence, if we are dealing, as in the present study, with variations in the yearly mean heights of sea-level, then the effects of astronomical and meteorological disturbances may be disregarded in the first approximation.

For the yearly mean value of the height of sea-level[1], that of the heights of monthly mean sea-level for 12 or 13 lunar months was taken. Since the monthly mean heights of sea-level are given by the mean values of the daily mean heights of sea-level taken for the interval from the day of full moon to that of the next full moon, the yearly mean height of sea-level that was obtained as the mean value of daily mean heights of sea-level for 365 days i. e. from Jan. 1 to Dec. 31, may be regarded as differing, though only slightly, from the yearly mean height of the sea-level determined above. To serve as an example, these two kinds of mean values are compared in Table I, the data belonging to Kusimoto. As the table shows, it was found that the difference is very small, so that the yearly mean height deduced from the monthly mean values of 12 or 13 lunar months may well be substituted for the

1) Data taken from "*The Report of Tidal Observation,*" (Marine Mateorological Observation) Vols 1—13, and "*Tidal Record,*" (Military Land Survey).

yearly mean height for the interval from Jan. 1 to Dec. 31, within the limit of possible accuracy.

Table I.

Year	Mean height (From. Jan. 1 to Dec. 31.)	Mean height (12 or 13 Lunar Months.)	Difference.
	cm	cm	cm
1932	173·6	173·4	0·2
1933	177·2	178·2	−0·8
1934	170·4	170·2	0·2
1935	175·4	175·2	0·2

2. The changes in the heights of the yearly mean sea-level at various stations thus obtained may be regarded as showing the secular changes in the height of the land at the respective places; in certain cases, with an accurary of about ± 2 cm[2].

The changes in heights of the yearly mean sea-level at various stations thus obtained are shown by graphs in Fig. 1, the numerical data being given in Table II.

The station for which changes in the heights of the yearly mean sea-level are deduced and plotted in Fig. 1, are

HONTO in Karahuto, (Saghalin)
OSYORO, HANASAKI in Hokkaido,
MERA, ABURATUBO, TOBA, KATUURA, KUSIMOTO, SIMOTU on the Pacific side of Honsyū,
KOBE, in the Seto-naikai (Inland Sea).
WAZIMA, TONOURA (HAMADA) on the Japan Sea side of Honsyū,
SIMIZU, UWAZIMA in Sikoku, and HUKABORI, TOMIE, HOSOZIMA, ABURATU in Kyūsyū.

Mareograph observations were begun, in 1930, at Mera, Katuura, Tomie, Aburatu, and in 1931 at Simizu. At the other mereograph stations, the data were taken since, or considerably before, 1925 or 1926.

The geographical distribution of these mareograph stations may be seen from Fig. 2.

3. From the curves in Fig. 1, showing the secular variations in the yearly mean heights of sea-level, the following points outstand;

(i) The height of the sea-level at Hanasaki has dropped considerably since 1932;

(ii) The drop in sea-level at Toba in 1929 and 1930 is also con-

2) K. MUTO and N. MIYABE, *Bull. Earthq. Res. Inst.*, **16** (1938), 70~86.

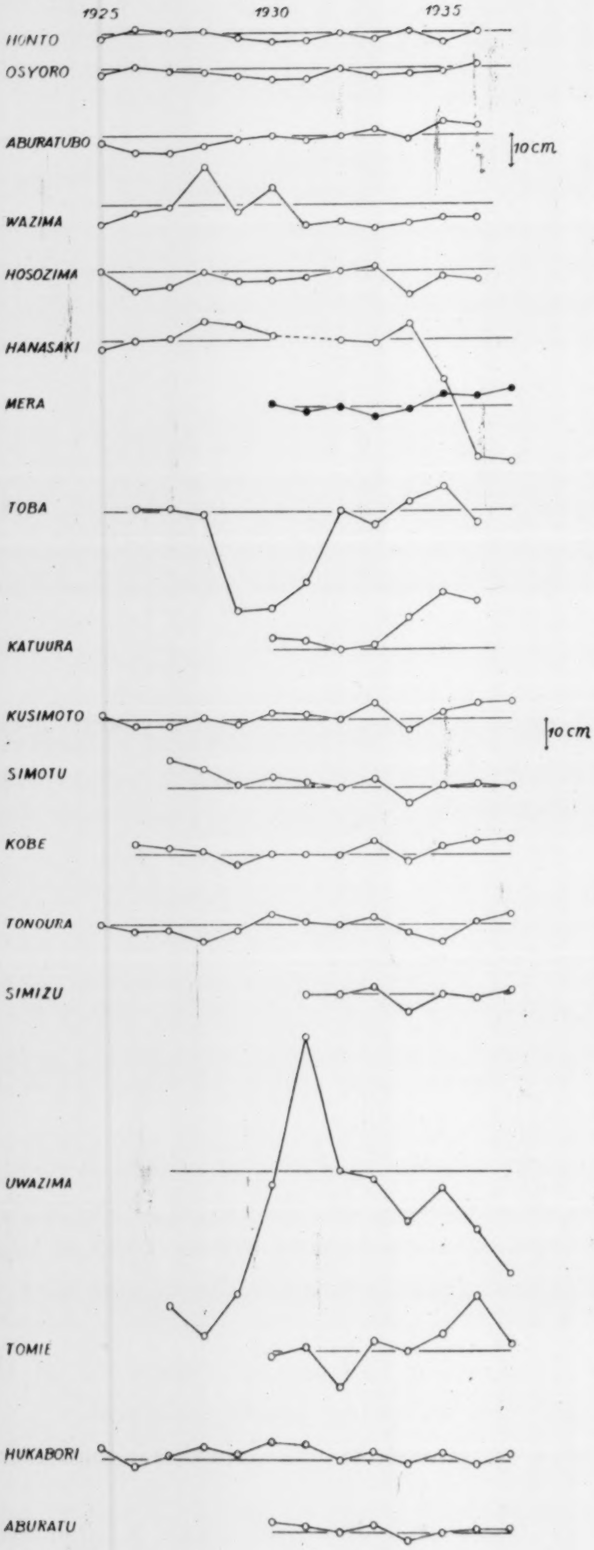

Fig. 1. Variations in the yearly mean heights of sea-level.

Fig. 2. Distribution of Mareograph Stations.

1 HONTO
2 OSYORO
3 ABURATUBO
4 WAZIMA
5 HOSOZIMA
6 HANASAKI
7 MERA
8 TOBA
9 KATUURA
10 KUSIMOTO
11 SIMOTU
12 KŌBE
13 TONOURA
14 SIMIZU
15 UWAZIMA
16 TOMIE
17 HUKABORI
18 ABURATU

Table II.

Group	Station \ Year	1925	1926	1927	1928	1929	1930	1931	1932	1933	1934	1935	1936	1937
		cm	cm	cm	cm	cm	cm	cm	cm	cm	cm	cm	cm	
I	1 HONTO	407·2	404·3	405·3	405·3	406·9	407·9	407·9	405·7	407·4	405·3	408·2	405·6	
I	2 OSYORO	203·5	201·5	202·4	202·8	204·0	205·0	204·6	201·8	204·0	203·4	202·6	200·7	
I	3 ABURATUBO	498·4	501·0	501·3	499·1	497·4	496·3	497·7	496·3	494·1	497·1	492·2	493·1	
I	4 WAZIMA	244·3	241·0	239·2	227·8	240·7	233·8	244·7	243·7	241·8	243·3	243·0	243·0	
I	5 HOSOZIMA	244·2	249·6	248·4	244·2	247·0	246·7	245·9	244·0	242·5	250·7	245·4	246·5	
II	6 HANASAKI	149·8	152·4	152·8	158·0	156·8	153·8	—	152·4	151·6	156·8	140·7	117·7	116·7
II	7 MERA						124·3	122·0	123·4	120·7	122·7	126·8	126·2	128·4
II	8 TOBA		216·0	216·0	214·8	185·8	187·4	195·1	215·5	211·7	217·9	222·7	212·0	
II	9 KATUURA						172·1	171·4	168·7	170·2	177·9	185·3	182·8	
II	10 KUSIMOTO	174·8	171·6	171·4	173·8	172·0	175·4	175·0	173·4	178·0	170·2	175·2	177·8	178·1
II	11 SIMOTU			174·2	172·0	167·3	169·3	168·1	166·5	169·0	162·0	167·1	167·5	166·8
II	12 KOBE		158·5	157·5	156·3	152·3	155·6	155·6	155·4	159·5	153·1	158·0	159·4	160·0
II	13 TONOURA	104·6	102·4	102·8	99·4	103·0	108·0	105·6	104·8	107·0	102·6	100·6	106·3	108·4
II	14 SIMIZU							167·7	167·8	169·7	163·1	167·9	166·7	168·6
II	15 UWAZIMA			165·8	157·6	169·0	199·6	241·5	203·5	201·0	189·8	199·0	187·6	175·1
II	16 TOMIE						189·1	191·8	180·5	193·4	190·2	194·9	205·7	192·6
II	17 HUKABORI	189·0	184·0	187·0	189·4	187·4	191·0	190·6	186.0	188·2	185·2	187·8	184·9	187·7
II	18 ABURATU						145·4	144·3	142·9	144·7	140·6	142·6	143·9	144·2

I: Military Land Survey. II: Meteorological Observatory.

siderable; since 1932 the sea-level at Toba and at Katuura rose at the same rate;
(iii) The rise and fall of sea-level at Uwazima since 1926 are very marked;
(iv) The heights of the yearly mean sea-level at six stations, i. e., Kusimoto, Simotu, Kōbe, Simizu, Hosozima, and Aburatu, have all changed in the same way, although the amount is not very large.

The remarkable fall in sea-level observed at Hanasaki is believed to be due to an artificial change in the height of the datum line and also to lack of observation data for a fairly long period of time.

The fluctuating curve in Fig. 3 suggests that the changes in the heights of the daily mean sea-level at Hanasaki were the result of frequent artificial changes in the height of the datum line.

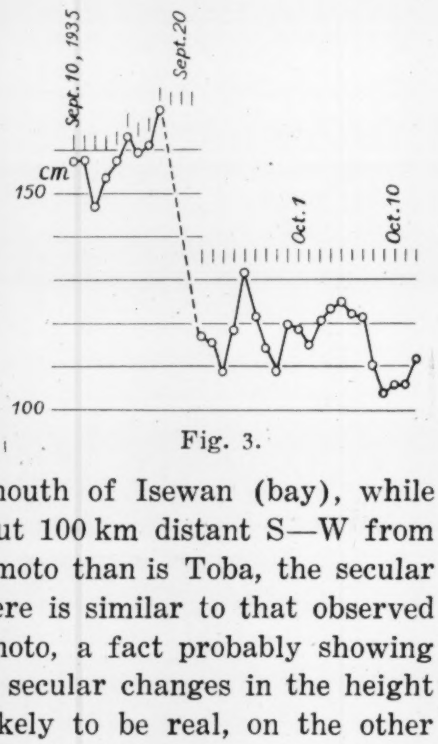

Fig. 3.

Similarly, the abnormal drop in sea-level at Toba in 1930 may be regarded as due to the fact that data for certain periods are lacking, and that the height of the datum line has been changed artificially.

It is also notable, as mentioned above, that the height of the yearly mean sea-level at Toba since 1932 varies approximately in the same way as that observed at Katuura. Toba lies at the mouth of Isewan (bay), while Katuura is situated near Kusimoto, about 100 km distant S—W from Toba. Although Katuura is nearer Kusimoto than is Toba, the secular variation in the height of the sea-level there is similar to that observed at Toba, not like that observed at Kusimoto, a fact probably showing that, while on the one hand, the observed secular changes in the height of the yearly mean sea-level are more likely to be real, on the other hand, the coast of Kumanonada, where Toba and Katuura are situated, has moved downwards these number of years at the rate of about 2∼4 cm/year. If this rate of downward movement was not a local subsidence of the land, it would be remarkable.

4. As shown in Fig. 1, the rise and fall of the yearly mean height of sea-level at Uwazima is remarkable. The yearly mean sea-level at this station gradually rose since 1927, until it reached about 90 cm in 1932, after which it began to drop, the subsidence in 1938, that is for 6 years, amounting to about 60 cm.

The rise of yearly mean sea-level at this station, however, seems

to be exaggerated, as the result of lack of observational data for the close of 1931. To verify this point, the changes in the monthly mean heights of sea-level are shown. In this case, the variations with approximate annual period, estimated as below, are substracted from the actual values of the monthly mean heights of sea-level.

The annual variation in the monthly mean heights of sea-level were estimated as follows. The deviations in the heights of the monthly mean sea-level from the yearly mean sea-level were deduced for the years 1933, 1934, 1935, 1936, and 1937, the results of which are given in Table III.

Table III.

Month \ Year	1933	1934	1935	1936	1937	Mean
	cm	cm	cm	cm	cm	cm
January	− 6·3	− 3·1	− 0·9	−15·4	− 7·2	− 6·6
February	−17·3	−16·2	− 9·8	−16·6	−16·4	−15·3
March	−13·1	−16·1	−10·2	− 8·3	−19·4	−13·4
April	− 5·7	−15·7	−10·9	−14·0	−15·1	−12·3
May	−11.3	−12·1	− 3·2	− 5·3	−16·2	− 9·6
June	2·6	− 5·3	8·2	3·0	7·9	3·3
July	3·3	7·6	11·7	6·8	15·2	8·9
August	10·7	11·5	13·4	3·8	18·2	10·8
September	17·8	10·9	17·5	3·9	14·8	13·0
October	12·2	9·5	20·4	20·3	13·4	15·2
November	7·6	0·9	1·8	19·1	8·4	7·6
December	4·9	− 2·4	− 5·4	3·0	− 5·7	− 1·1

The mean deviation for each month is then calculated as given in the last column of Table III, which is regarded as showing the mean annual variation of the monthly mean heights of the sea-level at Uwazima.

The curve in Fig. 4 shows the secular variation of the monthly mean height of sea-level, in which the terms of the mean annual variation are excluded. From this curve, we notice that the datum line for sea-level might have dropped toward the end of 1931 by about 20 cm. The datum line was raised again artificially by about 10 cm in the beginning of 1933. Taking into account these artificial changes in the height of the datum line, the rise in sea-level during 1927∼1932 amounts to about 70 cm, and that of the fall during the period 1932 ∼1938 to about 50 cm.

We have the data of vertical displacements of bench-marks distributed in this region for comparison with the secular change in the

height of sea-level. Precise levels in this region were rerun in 1932, with the result that the vertical displacements of the bench-marks near

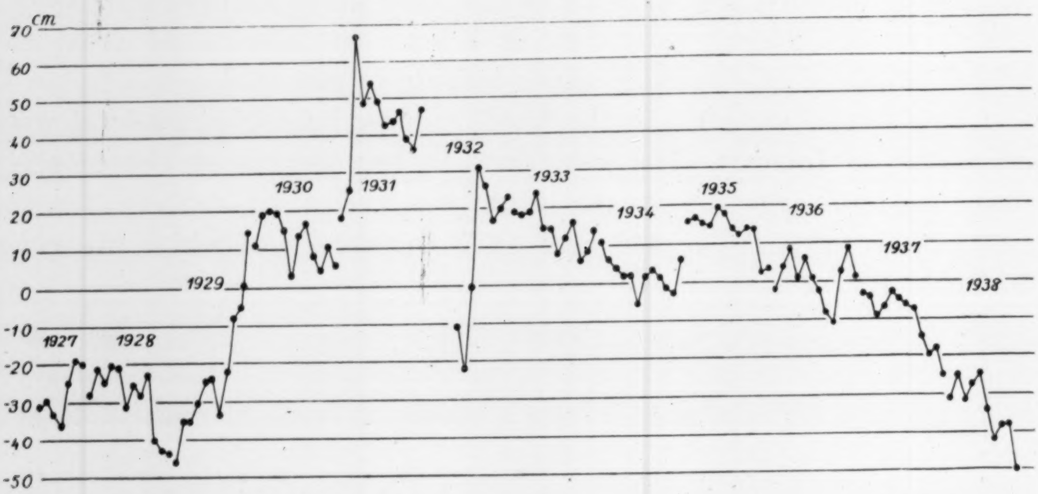

Fig. 4. Secular variation in monthly mean heights of sea-level at Uwazima.

Uwazima during the years 1898～1932 work out to –80 mm[3], relative to the bench-mark whose height was assumed to have remained unchanged. This subsidence of land is much less than the rise in sea-level during 1927～1932. This discordance in changes in the height of sea-level may be explained by assuming that the sea-level in 1898 was higher than that in 1927. It may be natural to assume that the land level which changes its height in an undulatory manner with time, reached minimum height in 1927, the integrated amount of the change in the height of the land level over the period from 1898 to 1932 being nearly –8 cm. Should, therefore, precise levels be rerun through this region and the rise of the land be found to be 50 cm and more, it will show that the secular change in height of the sea-level as deduced above gives the rise of the land.

It was supposed that if the land had risen about 50 cm it should be possible to confirm it by direct observations, resulting in the writer's visit to Uwazima to measure directly the amount of rise of the land through marks that may be found along the sea-shore. Marks of the old sea-level were found at several places more or less clearly. The heights of these marks above sea-level at the time of the measurement was made were recorded. The heights of the marks thus measured were reduced with the aid of predicted curves of the tides for Uwazima on the days the observations were made, to heights above the yearly

2) Rikuti Sokuryobu, (Military Land Survey) "Report on the results of precise levels in 1932".

mean sea-level. The distribution of heights of these marks thus measured and deduced are shown in Fig. 5.

Fig. 5. Distribution of the amounts of rise of the land in the neighbour-hood of Uwazima.

(Amounts of rise shown by numerals are in cm.)

The height of a bench-mark near the sea-shore, marked B 1 in Fig. 5. was measured and compared with the height given in the map. The comparison shows that the land rose about 58 cm.

Seeing that, with regard to the data of the yearly mean sea-level measured at Simizu, 70 km south of Uwazima, no marked change in the height of the sea-level, such as that found in Uwazima, was observed. The remarkable change in the height of the sea-level may be of a local character, confined to a certain area, including Uwazima.

Notwithstanding the marked fall and rise of the land level in the neighbourhood of Uwazima, no marked changes are seen in seismic activity, which may usually be regarded as having some relation to crustal deformation, such as those observed in this locality.

5. As already mentioned, the yeaaly mean sea-level at six mareograph stations, namely, Kusimoto, Simotu, Kobe, Simizu, Hosozima, and Aburatu, have moved in parallel, in that they rose in 1933 and fell in 1934, recovering their general level since 1935. The differences in the heights of the levels in 1933 and in 1934 range from 4 to 8 cm. These abnormal and ordinary changes in the heights of the sea-level may be connected with changes in sea-water temperature.

As already reported by Yamaguti[4], the fluctuations in the monthly mean heights of sea-level are affected by atmospherie pressure and sea-water temperature, as expressed by the formula

$$h = ap + bT.$$

As to the fluctuation in the heights of the yearly mean sea-level, a similar relation to the atmospheric pressures p and the sea-water temperatures T may hold. Since, however, the atmospheric pressure varies with the annual period, and since the yearly mean fluctuations atmospheric pressure are very small, the value of h is mainly affected by T, the sea-water temperature. The sea-water temperature in the neighbourhood of the mareograph station are probably affected by ocean currents, local precipitation, etc.

4) S. YAMAGUTI, *Bull. Earthq. Res. Inst.*, **19** (1941), 39~48.

To serve as an example, the relation between the yearly mean heights of sea-level and the yearly mean values of sea-water temperature at Hosozima was studied. In this case, the data of sea-water temperature from Yamaguti's paper were used, they being the values estimated from the configuration of isothermal curves drawn with reference to the data in "Kairyu Tūhō". The yearly mean heights of the sea-level were plotted against the yearly mean values of the sea-water temperature, as in Fig. 6.

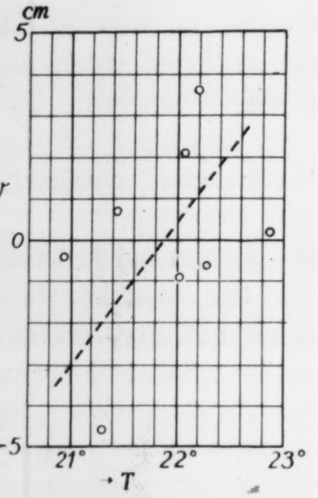

Fig. 6.

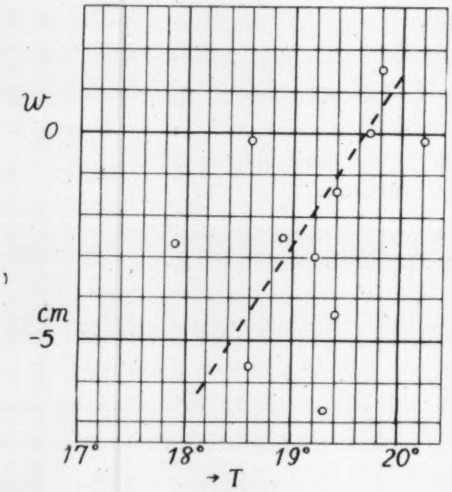

Fig. 7.

A similar relation between the yearly mean heights of the sea-level and the yearly mean values of the sea-water temperatures measured at Hosozima, is also shown graphically in Fig. 7[5].

From these curves in Figs. 6 and 7, the abnormal and ordinary-rise and fall of sea-level common to a number of stations may be regarded as due partly to secular changes in sea-water temperature. The abnormal rise and fall in 1933 and 1934 cannot be satisfactorily explained by assuming that they depend mainly on changes in sea-water temperature. This discordance may be due to the fact that the data of sea-water temperature used for the present discussion ought not to be compared with the changes in the heights of sea-levels.

Similar changes in the heights of yearly mean sea-level at other stations, namely, Kusimoto, Simotu, Kobe, Simizu, and Aburatu, may be due to a common reason, although their relation to sea-water temperature were not studied.

Thus the same rise and fall of the yearly mean heights of sea-

5) Data of sea-water tempertures taken from "*Tidal Record*", Rikuti Sokuryōbu, (Military Land Survey).

level observed in six mareograph stations may be regarded as having been caused by changes in the temperature of the sea-water.

In conclusion, the writer wishes to express his sincere thanks to the Department of Education, whose grant of a research fund enabled prosecution of the present study.

---

18. 年平均潮位の高さの變化

地震研究所　宮　部　直　巳

本邦各地に在る 18 個の驗潮場に於ける年平均潮位の最近の 10 餘年の間の變化を調べた．その結果，稍々異常的な變化をなして居るものが見出された．それらを擧げてみると

(i) 花咲に於いては昭和 10 年以後，水位が著しく，且つ急激に低下してゐる．これは，併し，主として人爲的に基準面を移動させた結果であると思はれる．

(ii) 鳥羽の，昭和 3—4—5 年における潮位も上述の花咲の場合に見られる樣な，人爲的の基準面移動の結果であると見られるが，昭和 7 年以後の變化は，勝浦のそれと稍々平行してゐる．

斯樣な變動が，鳥羽，勝浦を含む地域の全般的な沈下運動を示すか否かは甚だ疑はしい．ただ，勝浦の潮位變化が，場所的にはより近い串本に於ける潮位變化に似ず，遠い鳥羽のそれに似てゐるといふ點に注意をひかれる．

(iii) 宇和島における潮位の變化は極めて著しいものがあるが，色々の點から見て，陸地の隆起を示すもののやうである．併し，清水における潮位の變化には，斯樣な著しいものはないから，陸地の變形も局部的のものと思はれる．

(iv) 串本，下津，神戸，清水，宇和島，細島，油津等，西南部の太平洋岸の驗潮場における年平均潮位の變化には共通なものが認められる．それは，海水の温度によって支配される現象であらうと推察される．

19. 東京市内水準改測の成果

地震研究所　宮部直巳
東京市土木局　福西清治

(昭和15年11月21日發表—昭和16年3月20日受理)

1. 東京市内水準改測

東京市内に於ける多數水準點の眞高を知る爲に行ふ水準測量に際しては，地盤沈下の影響を無視することが出來ない．東京市内には既に屢々述べた様に約400個の水準點があり，之を含む水準線路の測量には延日數約1ヶ年を要するのである．

さうすると，若し，假りにある水準點が，年に 12 cm の割合で沈下してゐたとすると（實際その程度の沈下を示してゐる場所がある）毎月 10 mm，平均して毎日約 0·3 mm となる．斯の如き變動は明かに精密水準測量の精度の範圍を超えて居り，その爲に，測量の結果に表はれる，水準環線の閉塞誤差が，量的に大となるのみならず，單なる誤差として取扱ひ得ないことになる．この影響を出來るだけ小さくするには，一々の水準環線の閉塞を出來得る限り短時日の間に行ふのみならず，全體の測量をも出來るだけ短時日の間に完了せしめることが要求される．この要求に應ずる様な水準測量は，昭和13年3~4月にその第一回を行つた．所要日數は1個月餘であつた．併し，その結果についても，尙環線の閉塞誤差に，沈下の影響の多少含まれてゐるらしい形蹟を認め得たのであつた[1]

第2回の水準測量は昭和15年3~4月に行はれた．この時も，所要日數は約1個月であつた．この測量の結果は，前回の測量の結果と比較して，滿2個年間に生じた各地の高さの變化の分布を知ることが出來る．勿論，この場合に，高低變化の量といふのは，陸地測量部構內に在る水準原點の高さの變化を無いとした時のものである．だから，若し，原點に高さの變化があつたとすれば，それだけは全部の水準點の變動量に加算されるべき筈のものである．

とにかく，斯様にして求められた，2個年間の水準點の變動量は第1表に示す様なものである．又，その大體の分布は第1圖に示されてゐる．

次頁の圖又は表に於いて，水準點日~6號の變動量 +192·2 mm は疑問である．元

1) 永原茂，吉田貞博，地震，12 (1940)，145~153.

第 1 表

基標番號	所在地	變動量 15～13 (mm)
麴町區		
水準原點	永田町一丁目	0·0
陸 (甲)	同上	− 0·7
陸 (2)	紀尾井町	− 0·8
陸 (3)	富士見町三丁目	− 4·6
復 (1)	九段一丁目	− 5·8
復 (2)	千鳥ヶ淵公園	− 3·1
復 (3)	舊和田倉門	− 15·0
麴 (1)	大手町二丁目	＋ 4·2
麴 (2)	丸ノ内三丁目	＋ 2·1
麴 (3)	有樂町一丁目	− 33·4
麴 (4)	霞ヶ關一丁目	＋ 0·4
麴 (5)	隼町 1	＋ 0·6
麴 (6)	赤坂見附下	− 25·3
麴 (7)	麴町四丁目	＋ 0·8
麴 (8)	三番町	− 4·1
麴 (9)	富士見町三丁目	− 6·0
麴 (10)	代官町	− 4·8
神田區		
陸 (4)	駿河臺二丁目	− 2·2
復 (8)	同朋町	− 1·2
神 (1)	材木町	＋ 1·8
神 (2)	淡路町二丁目	＋ 2·4
神 (3)	一ツ橋町	− 50·1
神 (4)	三崎町二丁目	− 21·7
日本橋區		
陸交 (5)	馬喰町四丁目	＋ 0·9
陸 (6)	濱町三丁目	− 46·7
日 (1)	箱崎町四丁目	− 9·9
日 (2)	南茅場町	＋ 2·2
日 (3)	江戸橋三丁目	＋ 0·1
日 (4)	本石町一丁目	＋ 2·4
日 (5)	堀留二丁目	− 0·5
日 (6)	濱町一丁目	＋192·2
京橋區		
陸交無	越前堀一丁目	＋ 4·7
陸交 (7)	築地四丁目	− 2·8
復 (12)	寶町三丁目	＋ 1·9
復 (13)	月島八丁目	＋ 5·3
復 (15)	新佃島東町一丁目	− 2·9
京 (1)	銀座八丁目	＋ 2·8
京 (2)	銀座五丁目	＋ 2·1
京 (3)	銀座西一丁目	＋ 1·3
京 (4)	八丁堀三丁目	＋ 3·7
京 (5)	築地明石町	− 10·8
芝區		
陸 (8)	田町四丁目	＋ 0·8
陸交 (9)	高輪北町	＋ 4·0
復 (18)	新橋七丁目	− 44·9
復 (19)	今入町	− 20·2
芝 (1)	海岸通一丁目	不明（建物ノ下トナル）
芝 (2)	海岸通三丁目	− 7·8
芝 (3)	愛宕町一丁目	0·7
芝 (4)	芝公園	− 0·1
芝 (5)	片門前町二丁目	＋ 0·2
芝 (6)	金杉四丁目 8	＋ 0·3
芝 (7)	西芝浦三丁目	− 3·6
芝 (8)	西芝浦四丁目	− 5·2
芝 (9)	高濱町	− 10·1
芝 (10)	高輪南町	＋ 1·1
芝 (11)	高輪南町	＋ 3·0
芝 (12)	白金猿町	＋ 1·2
芝 (13)	白金臺町二丁目	＋ 0·6
芝 (14)	白金三光町	− 0·6
芝 (15)	白金臺町一丁目	− 1·2
芝 (16)	白金今里町	− 2·2
芝 (17)	車町	＋ 3·1
芝 (18)	三田綱町	− 1·8
芝 (19)	三田小山町	− 2·1
芝 (20)	舊第四臺場	− 0·5
麻布區		
麻 (1)	飯倉町二丁目	＋ 1·8
麻 (2)	宮下町	− 1·6

（次頁へ續く）

第 1 表 (續)

基標番號		所在地	變動量 15～13
			mm
麻	(3)	本村町	− 0·3
麻	(4)	新堀町	− 5·4
麻	(5)	本村町	+ 1·0
麻	(6)	富士見町	+ 0·9
麻	(7)	盛岡町	+ 0·6
麻	(8)	霞町	− 0·2
麻	(9)	新龍土町	+ 0·7
麻	(10)	三河臺町	+ 0·2
麻	(11)	簞笥町 38	− 3·3
赤坂區			
陸	(1)	葵町	− 39·1
赤	(1)	溜池町	− 63·4
赤	(2)	中ノ町	− 21·4
赤	(3)	表町三丁目	− 3·0
赤	(4)	元赤坂町	+ 2·7
赤	(5)	青山南町一丁目	− 1·3
赤	(6)	青山南町五丁目	− 0·2
赤	(7)	高樹町	+ 0·7
赤	(8)	青山南町六丁目	+ 1·5
四谷區			
陸	(16)	旭町	+ 2·6
四	(1)	本村町	− 0·8
四	(2)	赤坂離宮前記念公園	+ 1·4
四	(3)	西信濃町	+ 2·0
四	(4)	明治神宮外苑	+ 3·0
四	(7)	新宿町一丁目	+ 2·0
四	(8)	忍町	+ 0·9
四	(9)	片町	− 4·7
牛込區			
牛	(1)	新小川町二丁目	− 16·3
牛	(2)	肴町	− 1·7
牛	(3)	拂方町	− 1·2
牛	(4)	市ケ谷田町一丁目	− 1·4
牛	(5)	余丁町	− 1·0
牛	(6)	市ケ谷富久町	+ 1·2
牛	(7)	余丁町	− 1·1
牛	(8)	若松町	+ 1·9
牛	(9)	喜久井町	+ 0·9
牛	(10)	榎町	− 0·3
牛	(11)	矢來町	− 1·1
牛	(12)	市ケ谷柳町	− 0·9
小石川區			
小	(1)	江戸川町	− 10·4
小	(2)	西江戸川町	− 7·8
小	(3)	櫻木町	− 4·6
小	(4)	江戸川公園	+ 1·1
小	(5)	關口町	+ 2·0
小	(7)	高田豊川町	+ 1·1
小	(9)	大塚辻町	+ 1·9
小	(10)	丸山町	+ 3·3
小	(11)	西丸町	+ 3·0
小	(12)	原町	+ 0·4
小	(13)	指ケ谷町	− 2·5
小	(14)	柳町	− 14·5
小	(15)	表町	− 2·7
小	(16)	竹早町	− 2·1
小	(17)	音羽六丁目	+ 0·2
小	(18)	高田老松町	− 1·5
小	(19)	東青柳町	昭 14.6 改埋
小	(20)	大塚窪町	+ 1·0
小	(21)	白山御殿町	+ 1·6
本郷區			
復	(20)	本郷一丁目	− 4·5
鄉	(1)	湯島天神町一丁目	− 2·9
鄉	(2)	本富士町	− 4·9
鄉	(3)	森川町	− 3·2
鄉	(4)	蓬萊町	− 3·1
鄉	(5)	駒込片町	+ 1·5
鄉	(6)	駒込上富士前	+ 2·7
鄉	(9)	動坂町	+ 0·8
鄉	(10)	坂下町	− 1·6
鄉	(11)	駒込千駄木町	− 10·4
鄉	(12)	根津八重垣町	+ 1·4

(次頁へ續く)

第　1　表（續）

基標番號	所在地	變動量 15～13
下谷區		mm
復 (21)	上野公園	+ 0·7
復 (23)	三輪町	− 92·0
復 (27)	二長町	+ 0·5
下 (1)	御徒町一丁目	+ 1·4
下 (2)	下谷車坂町	+ 1·6
下 (3)	上野公園	+ 0·3
下 (4)	同上	− 4·7
下 (5)	櫻木町	+ 1·9
下 (6)	谷中初音町三丁目	− 1·5
下 (7)	中根岸町	− 3·2
下 (8)	下根岸町	− 80·0
下 (9)	龍泉寺町	− 48·8
下 (10)	小伏町	+ 1·4
淺草區		
陸 (26)	聖天町	− 34·9
復 (26)	森田町	− 4·2
淺 (1)	永住町	+ 1·5
淺 (2)	芝崎町三丁目	− 2·8
淺 (3)	日本堤二丁目	− 50·4
淺 (4)	山谷町四丁目	−100·8
淺 (5)	橋場町三丁目	− 86·0
淺 (6)	花川戸一丁目	− 17·8
淺 (7)	駒形一丁目	− 2·8
本所區		
陸 (3378)	江東橋三丁目	− 96·6
陸 (3379)	東兩國三丁目	− 56·3
陸無號	横網町	− 11·6
復 (32)	横網町	− 57·5
所 (1)	東駒形二丁目	− 5·5
所 (2)	吾妻橋一丁目	− 18·0
所 (3)	隅田公園	− 21·8
所 (4)	向島須崎町	− 89·5
所 (5)	向島請地町	−111·4
所 (6)	業平橋五丁目	−272·6
所 (7)	錦糸公園	− 95·9
所 (8)	業平橋一丁目	− 19.8

基標番號	所在地	變動量 15～13
		mm
所 (9)	太平町一丁目	− 90·9
所 (10)	西原町三丁目	− 26·5
所 (11)	綠町二丁目	− 17·5
所 (12)	竪川四丁目	− 66·8
所 (13)	菊川一丁目	− 40·8
所 (14)	竪川一丁目	− 50·2
所 (15)	千歲町一丁目	− 42·9
震研 (2)	江東橋三丁目	− 2·6
深川區		
陸 (9831)	富岡町(深川公園)	− 91·6
陸 (9832)	平井町三丁目	−257·8
復 (35)	門前仲町	− 70·5
深 (1)	永代一丁目	− 63·6
深 (2)	福住町一丁目	− 62·9
深 (3)	平野町一丁目	− 34·0
深 (4)	清澄町一丁目	− 32·6
深 (5)	新大橋二丁目	− 30·6
深 (6)	白川町三丁目	− 88·6
深 (7)	扇橋一丁目	−112·6
深 (8)	住吉町一丁目	−131·3
深 (9)	千田町	−196·8
深 (10)	平野町一丁目	−115·5
深 (11)	平井町一丁目	−143·4
深 (12)	東陽町三丁目	−161·6
深 (13)	木場三丁目	−102·2
深 (14)	洲崎辨天町一丁目	−126·7
深 (15)	古石場町	−118·3
深 (16)	濱園町	−104·6
深 (17)	越中島町	−116·8
深 (18)	越中島町	− 48·8
深 (19)	第三臺場	———
震研 (1)	富岡町一丁目	− 2·9
品川區		
陸 (9)	南品川三丁目	+ 4·2
陸 (10)	五反田町一丁目	− 2.9
陸 (27)	大井鈴ヶ森町	− 5·9
陸 (1)	西大崎二丁目	+ 3·3

（次頁へ續く）

第 1 表（續）

基標番號		所在地	變動量 15～13
		目黒區	
陸	(11)	鷹番町	mm + 1·4
		大森區	
陸	(271)	大森三丁目	− 7·6
		蒲田區	
陸	(28)	仲蒲田四丁目	− 3·4
陸	(281)	東六郷四丁目	− 46·4
		世田ケ谷區	
陸	(12)	上馬町一丁目	+ 6·7
陸	(13)	代田二丁目	+ 7·3
陸	(1221)	給田町	+ 19·3
		澁谷區	
陸	(15)	代々木初臺町	+ 0·7
東	(9)	穩田一丁目	+ 2·3
四	(5)	千駄ケ谷一丁目	+ 3·2
四	(6)	千駄ケ谷四丁目	+ 2·3
		淀橋區	
陸	(11)	柏木一丁目	+ 5·1
陸	(19)	下落合二丁目	+ 14·5
		中野區	
陸交	(17)	本町通四丁目	+ 8·8
陸	(18)	新井町	+ 11·9
		杉並區	
陸交	(14)	和泉町	+ 6·9
陸	(123)	上高井戸一丁目	+ 17·1
陸	(1231)	下高井戸一丁目	+ 12·6
		豐島區	
陸	(20)	千川町二丁目	+ 10·3
小	(8)	雜司ケ谷町一丁目	+ 1·5
郷	(7)	駒込四丁目	+ 6·0
郷	(8)	駒込六丁目	+ 4·3
		荒川區	
陸	(24)	日暮里九丁目	mm + 0·9
陸	(25)	南千住町八丁目	+112·4
荒	(1)	三河島五丁目	− 92·6
荒	(2)	尾久町三丁目	− 6·5
荒	(3)	尾久町八丁目	−103·9
荒	(4)	尾久町一丁目	− 86·4
荒	(5)	町屋一丁目	− 81·3
荒	(6)	南千住町十丁目	− 93·8
		王子區	
陸	(23)	王子町	+ 1·6
		板橋區	
陸	(III)	板橋五丁目	+ 11·1
陸	(21)	板橋九丁目	+ 12·0
陸交	(22)	板橋五丁目	+ 8·0
陸	(473)	志村清水町	+ 7·5
陸	(474)	志村町	+ 5·8
陸	(475)	志村蓮根町	——
		足立區	
陸	(3365)	千住仲町	− 79·6
陸	(IV)	千住八千代町	−103·6
陸	(2002)	梅田町	−151·4
陸	(2003)	保木間町	− 8·1
陸	(2004)	保木間町	− 6·7
葛	(1)	柳原町	−104·2
足	(1)	千住元町	− 89·1
足	(2)	本木町	−106·5
足	(3)	南宮城町	− 63·9
足	(4)	小臺大門町	− 92·0
足	(5)	新田下町	− 69·1
足	(6)	北鹿濱町	− 30·9
足	(7)	谷在家町	− 8·9
足	(8)	入谷町	− 11·4
足	(9)	舍人町	− 5·8
足	(10)	伊與前沼町	− 9·9

（次頁へ續く）

第　1　表（續）

基標番號	所在地	變動量 15～13
		mm
足 (11)	西新井町	− 74·3
足 (12)	六町	− 8·9
足 (13)	花畑町	− 9·4
足 (14)	內匠本町	− 25·5
足 (15)	大谷田町	− 87·9
足 (16)	五兵衞町	−120·0
向島區		
向 (1)	隅田町二丁目	——
向 (2)	吾嬬町西九丁目	− 98·8
向 (3)	吾嬬町西五丁目	−143·9
向 (4)	吾嬬町東八丁目	− 62·8
向 (5)	吾嬬町東二丁目	−270·4
向 (一)	隅田町二丁目	−104·7
向 (三)	寺島町六丁目	−127·0
向 (四)	寺島町四丁目	埋沒不明觀測セス
向 (五)	吾嬬町西八丁目	−139·6
向 (七)	吾嬬町東四丁目	−175·5
向 (八)	寺島町六丁目	−122·5
城東區		
陸 (3377)	角戶七丁目	−205·9
陸 (9833)	南砂町五丁目	−141·7
陸 (9834)	北砂町九丁目	−184·9
城 (1)	大島町七丁目	−179·4
城 (2)	北砂町四丁目	−224·9
葛飾區		
陸 (3366)	小菅町	−105·6
陸 (3367)	龜有一丁目	− 86·9
陸 (3368)	龜有二丁目	− 81·5
陸無號	新宿町一丁目	−100·1
陸 (3369)	金町二丁目	− 26·8
陸 (3370)	金町六丁目	− 23·3
葛 (2)	堀石町	−119·9

基標番號	所在地	變動量 15～13
		mm
葛 (3)	青戶町二丁目	− 73·1
葛 (4)	高砂町	− 19·8
葛 (5)	水元小合町	− 59·9
葛 (6)	水元猿町	− 36·7
葛 (7)	水元小合上町	− 18·0
葛 (8)	柴又二丁目	− 1·0
葛 (9)	奧戶新町	− 71·1
葛 (10)	下小松町	−115·1
葛 (11)	上平井町	−113·8
葛 (12)	四ツ木町	− 98·9
葛 (13)	本田立石町	− 84·5
江戶川區		
陸無號	小岩七丁目	− 0·4
陸 (3374)	小岩一丁目	+ 3·1
陸 (3375)	東小松川四丁目	−122·0
陸 (3376)	小松川一丁目	−124·8
陸 (9835)	東船堀町	−125·3
陸 (9836)	長島町	− 62·4
陸 (9837)	葛西一丁目	− 32·8
江 (1)	小松川一丁目	−148·2
江 (2)	平井町三丁目	−179·4
江 (3)	小岩町六丁目	− 2·6
江 (4)	北篠崎町	+ 4·7
江 (5)	鹿骨町	− 2·1
江 (6)	西一之江町	− 47·1
江 (7)	東小松川三丁目	−132·6
江 (8)	谷河內町	+ 0·3
江 (9)	下篠崎町	+ 2·4
江 (10)	前野町	− 9·9
江 (11)	一之江町	− 19·6
江 (12)	二之江町	− 50·2
江 (13)	長崎町	− 38·6
江 (14)	東宇喜田町	− 51·0
江 (15)	西宇喜田町	−164·2

來この水準點の所在地附近は何れかといへば沈下の地域であつて，變動量は（−）となつて然るべしと思はれるやうな場所である．然るに，斯くの如く上昇を示すのは，恐らく水準點そのものの移動で，附近の土地の水準變化を示したものではあるまいと思はれる．

尙，この改測の結果として注意される一事は，深川及び本所に於ける特種の水準點[2]，震1號及び震2號の變動夫々：−2·9 mm 及び −2·6 mm で何れも，その附近の

第1圖 變動量（昭和13年～15年）の分布

水準點の同一期間の變動量に比して遙かに小さいことである．

又，この測量の結果，向島區，葛飾區，城東區，江戸川區等には，平均潮位よりも低い水準點があることを知り得たのである．

例へば，次表（第2表）の如きものである．

これらの水準點によつて，その高さを代表される地域については，高潮に對して特別に考慮を拂はなければならないであらう．

2) これらの水準點は何れも 35 mm の長さを有する鐵管で，軟泥の層を貫いて下部の堅い岩盤に固定されてゐる．

第　2　表

水準點番號	昭和15年3～4月測定の高さ（東京灣中間海水面上）	水準點番號	昭和15年3～4月測定の高さ（東京灣中間海水面上）
	m		m
向 3	−0·2687	葛 2	−0·0719
向 4	−0·9413	葛 11	−0·2574
向七	−0·7879	3376	−0·2257
9834	−0·6131	江 2	−0·6731
城 1	−1·0339	江 7	−0·0860
城 2	−0·6864		

2. 日比谷附近の水準改測に就て

日比谷近附の數個の建築物に鐵製水準標を設けた事は旣に報告した[3]．これらの水準點及び，4個の普通水準點と，4個所の特種標識とを含む水準環線の測量は，昭和13年5月以來7回反復され，6個の期間に於ける各水準點の變動量が測定されてゐる．その結果は，第3表に示してある通りのものである．

第　3　表

水準點 ＼ 期間	I	II	III	IV	V	VI
	mm	mm	mm	mm	mm	mm
麹 4	− 0·3	− 2·9	2·0	− 2·1	2·9	− 4·3
復 3	−11·2	− 1·7	− 0·8	− 9·1	4·6	−14·8
麹 2	− 2·1	− 3·9	2·8	− 2·8	3·3	− 8·9
麹 3	−22·8	− 8·4	0·2	−12·9	5·4	−21·4
T	−36·9	−13·9	− 7·1	−27·9	− 2·3	−33·0
P′	−39·9	−14·5	− 8·1	−34·7	− 9·3	−33·9
P″	−27·2	− 9·8	− 6·8	−44·5	2·5	−31·6
K—W	− 1·9	− 0·4	1·1	− 2·5	4·8	− 6·2
K—E	− 1·2	− 1·2	1·7	− 2·9	4·6	− 5·8
M—E	− 3·7	− 5·1	2·4	− 6·7	1·5	−10·0
M—M	− 6·1	− 3·5	2·3	− 5·6	2·0	− 9·6
M—W	− 6·1	− 3·1	− 1·7	− 4·9	2·7	− 9·6
T—E	− 8·9	− 2·6	3·4	− 0·9	6·3	−12·3
T—W	− 8·8	− 2·6	3·8	− 1·1	6·7	−12·7
O—W	−13·1	− 1·4	1·0	−10·8	10·5	−17·8
O—M	−13·1	− 1·5	1·8	− 9·9	10·6	−17·2
O—E	− 9·3	− 2·3	1·3	− 7·6	11·0	−15·9
S—E	− 5·7	− 2·5	4·3	− 7·0	10·3	−11·9
S—W_U	− 3·1	− 3·8	4·5	− 6·9	9·5	−10·3
S—W_D	− 3·2	− 3·8	3·7	− 6·6	9·3	−10·6
A	−27·4	−11·9	− 0·3	−17·9	3·6	−24·6

3)　宮部直巳，地震，12 (1940)，59～64.

表に示してある期間は夫々次の通りである．

I　昭和13年5月～昭和13年11月　II　昭和13年11月～昭和14年12月
III　昭和14年2月～昭和14年6月　IV　昭和14年6月～昭和14年11月
V　昭和14年11月～昭和15年4月　VI　昭和15年4月～昭和15年10月

この表を見ると，ある期間における變動量は全體として（＋）になつてゐる場合がある．尙，水準點を設備した建物の中，少くともその一部は，基礎も堅く，下部の岩層に固定されたと見られるものであらうし，又普通水準點のあるものは，山の手地域に露出してゐるロームの層に直接設置されたものである．さうして，それらの水準點も僅少ではあるけれども，ある程度動いてゐると見られないこともないから，上述の如く，多數の水準點の變動量が（＋）符號を持つ，卽ち，原點に對して隆起してゐる期間もあるといふ事を，試みに“各期間の變動量として測定されたものは，上層の軟泥の收縮によるものと，地盤全體が傾斜した爲に生じたもののと2成分より成る”と考へてみる．さうしてこの2成分を分ける爲に“原點附近では上層の軟泥層はなく，從つて收縮はないこと，收縮と考へられる變動，量卽ち傾斜運動の影響を除いた殘餘の變動量はすべて（－）號を持つべきであること”といふことを假定する．さうして，原點と他の一つの水準點とを結ぶ線の方位と，その方向の傾斜との關係を表はす圖を作るのである．さうすると，その圖は第2圖に示すやうなものとなる．

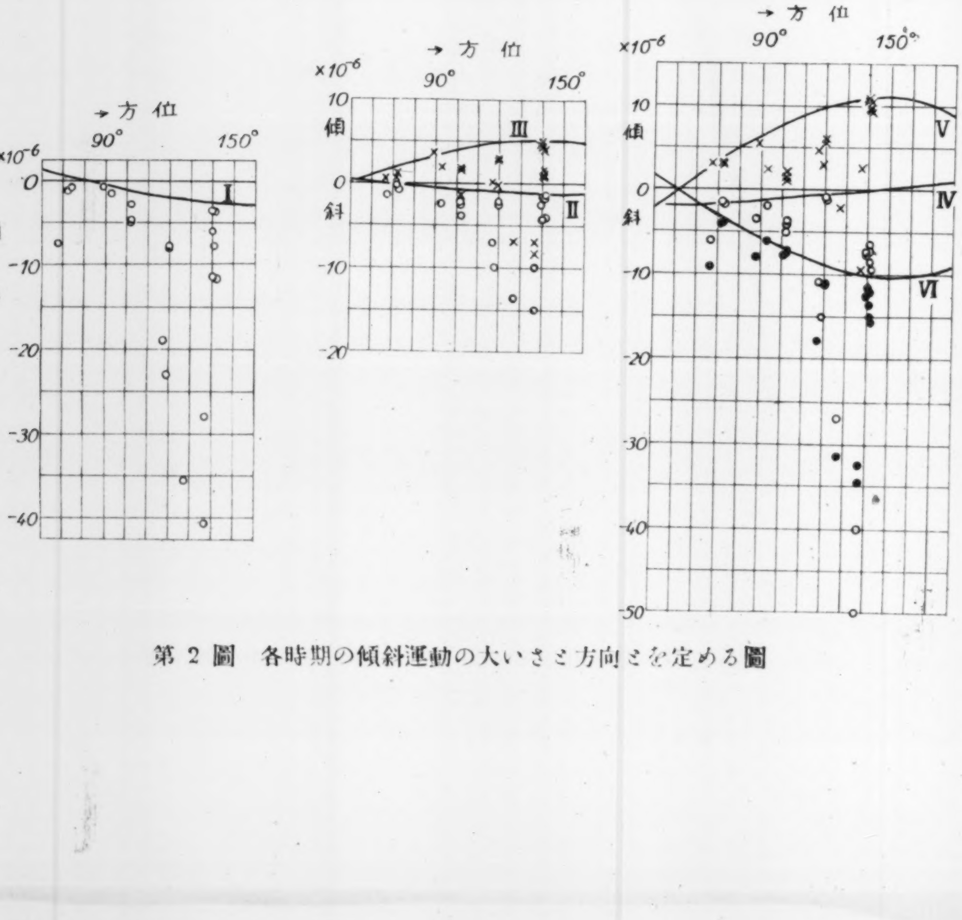

第2圖　各時期の傾斜運動の大いさと方向とを定める圖

若しも，上層の軟泥の收縮といふこともなく，而も，土地が全般的にある方向に傾斜運動をするものとすれば，第2圖に示した，傾斜 G と方位 θ との關係は

$$G=G_m\cos(\theta-\theta_m)$$

で示されるべく，G と θ との關係を示す點は，正弦型を示す筈であるから，その正弦曲線の振幅と，位相とにより（G_m と θ_m とは圖上に於いて求められる）傾斜の量と方向とが與へられる．併し，實際には軟泥層收縮の影響があるから，第2圖の如く，點は散布してしまふ．この第2圖に於ける點の散布する理由は假定の如く，軟泥層の收縮することにのみよるとして，この圖における點の散布區域の上線に沿うて正弦曲線を描き，その正弦曲線が岩盤の傾斜運動を示すものであるとする．斯樣にして求めた各期間の傾斜のヴエクトルを繫いでみると，それは，第 3 圖の如きものとなる．

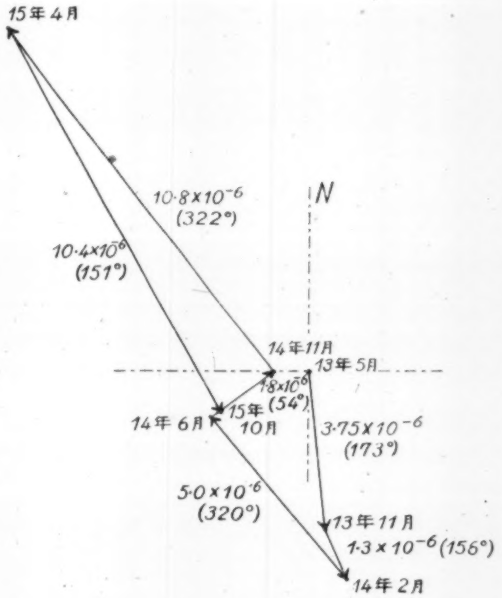

第 3 圖　傾斜變化

斯樣にして求められた傾斜運動の影響を

$$w-G_m s\cos(\theta-\theta_m)=w'$$

によつて取り去り，w' の値を求めてみる．G_m，θ_m はある期間の問題の地域における全般的な傾斜を示す量であり s は原點と w なる變動量を有する水準點との間の距離，θ はその方位である．斯樣にして求められた w' の値は第4表に示してある．

第　　4　　表

期間 / 水準點	I	II	III	IV	V	VI
	mm	mm	mm	mm	mm	mm
麴　4	− 0·1	− 2·6	0·3	− 1·3	− 0·6	− 1·7
復　3	−12·7	− 1·7	− 1·4	− 6·5	0·4	−13·6
麴　2	− 1·2	− 3·1	− 2·2	− 0·8	− 7·2	− 0·9
麴　3	−21·1	− 7·9	− 5·3	−12·0	− 6·3	−11·1
T	−35·8	−12·8	−12·2	−27·3	−13·2	−23·1
P′	−36·8	−13·2	−13·0	−34·5	−20·2	−24·0
P″	−24·2	− 8·5	−11·6	−44·2	− 8·0	−21·7

（次頁へ續く）

第 4 表（續）

期間 / 水準點	I	II	III	IV	V	VI
	mm	mm	mm	mm	mm	mm
K—W	−0·8	−0·4	−1·6	0·0	−0·7	−3·3
K—E	−0·2	−1·2	−1·3	−0·3	−1·3	−2·5
M—E	−2·0	−4·1	−2·9	−5·1	−9·6	−0·8
M—M	−4·5	−2·5	−2·9	−4·0	−8·9	−0·5
M—W	−4·5	−2·1	−5·5	−4·6	−8·1	−0·8
T—E	−6·4	−1·4	−1·9	−0·1	−5·0	−2·3
T—W	−6·2	−1·4	−2·0	−0·3	−4·7	−2·4
O—W	−9·4	0·0	−4·7	−10·7	−1·8	−6·1
O—M	−9·4	0·0	−4·0	−9·8	−1·7	−5·4
O—E	−5·5	−0·8	−4·7	−7·5	−1·6	−3·8
S—E	−2·7	−1·3	−0·4	−6·9	0·1	−2·2
S—W_U	−0·2	−2·7	0·0	−6·8	0·0	−1·2
S—W_D	−0·3	−2·7	−0·8	−6·5	−0·3	−1·4
A	−24·7	−10·7	−5·8	−16·8	−8·2	−14·3

この表に示してある數字を見れば，

（イ）大體期間の長い場合の變動量は大きく，

（ロ）夏一秋の期間を含む時期の變動量は，冬一春の期間を含む變動量よりも大きい．

（ハ）而して全體的に多少變動量の減衰しつゝあるかの如き

傾向を認めることが出來，w' が，軟泥層の收縮による沈下量に近いものではないかと思はせるものがある樣である．

若しも，この樣な推定が大して誤でなければ，次の樣なことが言へるであらう．

即ち，比較的長い期間における變動量として測定されたものの中には，地盤の全般的な傾斜運動も含まれるけれども，その影響は比較的小さく，これに對して，軟泥層の收縮は一方向きに增すのみであるから比較的大きいが，短期間の變動量の中には，地盤の全般的な傾斜運動が大きく影響する場合があり得るのみならず，軟泥層收縮の影響は期間の短かい爲めに，その大なることを豫期し得ない．

さういふ理由によつても，長期間の變動量では沈下する樣に見える地域に於いて，短期間の變動量に就いては却つて隆起するかに見える事實を理解することが出來る．

以上に述べた所の水準測量は，東京市土木局の委託により，陸地測量部に於いて實施されたものである．兹にこの資料を提供された兩當局に對し，深く謝意を表する次第である．

19. Results of Relevelling in Tokyo, in 1940.

By Naomi MIYABE,

Earthquake Research Institute,

and

Seizi HUKUNISI,

Bureau of Civil Engineering, Tokyo Municipality.

In order to measure the vertical displacements of bench-marks in a region, like Tokyo, which is sinking at the rapid rate of nearly 10 cm per year and more, the interral separating consecutive levellings should be made as short as possible.

In March-April 1938, a line of levels was run in Tokyo, involving about 400 bench-marks. This line was rerun in March-April 1940, and the vertical displacements of the bench-marks were deduced by comparing the results of the two levellings. The vertical displacements thus deduced are referred to the standard datum point, the height of which remained unchanged during the period between these two succesive surveys. The data of the vertical displacements are shown in Table I and Fig. 1 of this paper.

In connection with these surveys, a line of levels, involving 20 bench-marks, distributed in the neighbourhood of Hibiya, where the rapidity of the sinking of the earth's surface is rather marked, were relevelled seven times since May 1938. Analysis of the data, suggested that the vertical displacements measured as having occurred during the intervening months consist of two components, namely, the sinking due to the shrinkage of the soft soil composing the overlying layer and the displacement resulting from tilting of the underlying layer of hard rocks. Since the latter is quasi-periodic and the former is monotonically progressive, the vertical displacements measured for the shorter period of time aer fluctuate, while those for the longer period of time are steady, being approximately the same.

20. The Eruption of Miyake-sima, One of the Seven Izu Islands, in 1940.

About 8 p.m. on July 12, 1940, Volcano Miyake-sima began activities with a side crater eruption on its northeast flank. Although news of the eruption reached us that same night, it was not before the next evening, some twenty hours later, that we could leave for the island, owing to various preparations that had to be made for investigating the eruption. We reached the offing of Okubo-hama on the northern coast of Miyake-sima by the *Kiri-maru* in the early morning of July 14, when an enormous volume of black eruption clouds was seen rising through the thick clouds with which the upper half of the mountain was covered, and then to bend with the southwesterly wind that was blowing at the time, without being projected into the upper regions of the air. After landing from the bay of Igaya, we arrived toward the evening of the same day at Kamituki, where our main observing station was to be established, and began certain instrumental observations the same night.

By the time we arrived at the island, the eruption on the northeastern flank of the mountain had practically subsided, so that if the flank eruption were the only event of the present activity of the volcano, all that we could have observed would have been its after-effects. However, in the night of July 13, following the flank eruption, the central cone on the mountain began a summit eruption, which lasted well over three weeks, and which exhibited various phases of activity peculiar to eruptions of Strombolian type. Consequently, we had excellent opportunities of observing the summit eruption at close range as well as of recording various geophysical disturbances caused by the eruption.

After completing our alotted observations, the entire party left the island on August 5, when it was seen that the summit activities had practically ended. In the autumn of the same year, however, some of us revisited the island, individually, in order to add to previous field observations or to repeat certain temporary instrumental observations. The results of our observations are given in this joint report, consisting of the following parts.

Part I. Geological Observations of the Miyake-sima Eruption of 1940. (I)..............................Hiromichi TSUYA.

Part II. The Temperature of Lava. ....Takesi NAGATA.

Part III. Viscosity of the Akabakkyô Lava. .... Takahiro HAGIWARA.

Part IV. The Magnetic Properties of the New Ejecta. .... Takesi NAGATA.

Part V. The Earthquakes that accompanied the Eruption.. Takahiro HAGIWARA.

Part VI. Pulsations of the Ground that accompanied the Volcanic Activity. ....Takeshi MINAKAMI.

Part VII. Anomalous Change in Geomagnetism accompanying the Volcanic Activity. ....Takesi NAGATA.

Part VIII. A Magnetic Dip Survey of Miyake-sima... Takeshi MINAKAMI.

Part IX. Time Variations in Magnetic Dip, and their Topographical Distribution in Miyake-sima. .... Takeshi MINAKAMI.

Part X. Changes in Earth Potential after the Eruption... Takahiro HAGIWARA.

Part XI. Changes in the Vertical Intensity of Geomagnetism that accompanied the Eruption. ....Ryutaro TAKAHASI and Kintaro HIRANO.

Part XII. A Topographic Survey of the New Parasitic Cones and the New Lava Flow of Miyake-sima. .... Syun'itirô OMOTE.

Part XIII. Horizontal and Vertical Ground Displacements associated with the Eruption............Syun'itirô OMOTE.

Part XIV. A Graph for Comparing Changes in the Amplitude of Daily Pulsations, the Number of Daily Earthquakes, the Earth Potential, and the Magnetic Dip. .... Takahiro HAGIWARA, Takeshi MINAKAMI, and Takesi NAGATA.

We take this opportunity of expressing our sincere thanks to Professor K. Terazawa, Director of this Institute, for his interest throughout the course of the present investigations. We are also indebted to the officials of the Miyake-sima Branch of the Tokyo Prefectural Office and to those of the village offices in the island for the numerous facilities given us. Thanks are also due to Mr. Z. Asanuma, of Kamituki, for allowing us the use of his residence during our first visit to the

island. Lastly, we wish to acknowledge here with thanks that certain parts of the present investigations were accomplished with the aid of the Funds for Scientific Research granted by the Ministry of Education.

The Authors.

Part I. Geological Observations of the Miyake-sima Eruption of 1940. (I)

By Hiromichi TSUYA,

Earthquake Research Institute.

(Read Oct. 16 and Nov. 21, 1940.—Received March 20, 1940.)

CONTENTS.

I. Introductory Remarks.
Morphological and geological outlines.
Recorded history of past eruptions.
II. Sequence of Events.
Preliminary symptoms.
Flank eruption, July 12 to 13, 1940.
Summit eruption, July 14 to August 5, 1940.
III. Topographical Changes.
Zone of the flank eruption.
Zone of the summit eruption.
IV. Distribution and Volume of Solid Ejecta.
V. Damage Caused.
VI. Petrography of the Ejecta of 1940.
Lava-flows.
Akabakkyô lava.
Yoridai-sawa lava.
Hyotan-yama lava.
Oyama (central cone) lava.
Fragmentary ejecta.
VII. Summary and Conclusions.

I. Introductory Remarks.

Morphological and geological outlines. Miyake-sima, which is an insular volcano, easy of access, lying about 200 km SSW. of Tokyo (Figs. 1, 6), is well-known for its frequent eruptions in historic times as well as by the fact that it ejects anorthite crystal-lapilli. However, no detailed geological study of the island has been published, excepting Fukuchi's note on its geologic structure[1] and Tsujimura's observation on its morphology.[2] The writer, who made a geological study of the

1) N. FUKUCHI, *Jour. Geogr. Soc., Tokyo*, **16** (1904), 668.
2) T. TSUJIMURA, *Jour. Geol. Soc., Tokyo*, **24** (1916), 199; *ibid.*, **26** (1918), 497.

island in 1925, gave a short description of its structure and its petrography in an earlier paper,[3] without entering into details of its geology. It seems desirable however for the sake of convenience to summarise once more the structure of the volcano, and to take this opportunity of adding further data. Miyake-sima, which has a circular outline, measuring about 8 km in diameter, is a composite stratified volcano formed of basaltic ejecta, and consisting of a somma and a central cone, besides a number of parasitic knobs and flank vents.

Fig. 1. Index map showing the position of Miyake-sima volcano.

The somma is a conical mountain (Fig. 7) truncated at the top with a ring-wall whose northern segment is clearly seen as a semi-circular crestline around it. The caldera, whose northern part is preserved as a crescentic atrio (Hayono-tairo) encircled by the ring-wall (Fig. 8), must have originally been a circular depression, about 1·5 km in diameter, although its larger part is occupied at present by the central cone. The outer slopes of the somma have not developed uniformly in all directions. Thus the northwestern and southeastern flanks are older, morphologically as well as geologically, being characterized by steeper slopes and deeper radial valleys, compared with the other flanks where a number of younger parasitic volcanoes lie.

The central cone (Oyama), which is about 120 m above the floor of the atrio (Fig. 8), lies slightly south of the caldera. Before the eruption of 1940, it was truncated at the top, with walls surrounding a composite crater consisting of three bowls aligned in an east-west direction (Figs. 9, 10). Of these, the easternmost crater (the first crater), the principal one of the central cone, was the largest (about 400 m in diameter); the second crater (Oana), which was about 200 m

3) H. TSUYA, *Bull. Earthq. Res. Inst.*, **15** (1937), 290.

across, lying immediately west of the first, was the deepest (about 115 m below the highest rim of its walls); while the third crater lying immediately west of the second, was smaller and shallower than those just mentioned. Besides these, there was a pit-crater, about 20 m across, near the base of the inside western wall of the third crater. The western part of the central cone was greatly changed by the present eruption, resulting in the formation of a new central cone, which will be mentioned presently.

The somma has more than twenty parasitic knobs and flank vents, most of which lie on the northeast and southwest slopes (Fig. 2). The remarkable ones are: Kuwanoki-taira (cones and craters), Ana-hutatu, Simmyo, and Kosiki-ana of Ako, on the southwestern flank; Suwo-ana, Misodo-ana, Kosiki-ana, Oana, Aka-ana, Taka-yama, Hinoana, Misodo-ana, Daihannya-yama, and the crater-bay of Akabakkyô, on the northeastern flank; Kaze-ana, Huru-miyo, Yama-miyo, and Mizu-tamari, on the southern flank; Dono-yama and Miyaga-tairo on the northwestern flank; and Miike on the eastern foot. Besides these, there are a number of smaller, nameless rift-craters and crateriform pits. The central cone also has a parasitic knob on its southwest slope. The eruption of 1940 took place on the northeastern flank of the somma, besides, at the top of the central cone, resulting in the formation of a number of new flank vents and parasitic cones, as mentioned in later pages of this paper.

So far as judged from exposures on the sea-cliffs around the island and on the ring-wall surrounding the caldera, the somma is composed of many superposed lava-flows, most of them only a few meters thick, intercalated by layers of fragmentary ejecta. Although, petrographically, the lavas differ more or less, they are all basaltic in nature, and may be distinguished by the combinations of the phenocrystic minerals into four types: (1) olivine-basalt, (2) augite-olivine-basalt, (3) olivine-two-pyroxene-basalt, and (4) two-pyroxene-basalt. The fragmentary products consist of juvenile and accessory ejecta of the rocks enumerated above, besides anorthite lapilli, and micro-allivalite bombs. Some of the somma lavas, especially those (augite-basalt and augite-olivine basalt) exposed on the southwest shore between Ako and Higasiyama, must have come from the parasitic cones or from the vents on the flanks. On the northwestern shore of the bay of Akabakkyô, now buried under the ejecta of 1940, there were exposures of a lava-flow of augite-olivine-basalt containing large phenocrysts (1 cm dia.) of anorthite, which must have come from a crater in the bay. The lava is now exposed only locally on the former shore of Sitori and on the former sea-cliff of Akabakkyô-

saki. At the latter locality it occurs as a flow, about 5 m thick, sandwitched between reddish-brown layers of volcanic bombs, scoriaceous lapilli, and anorthite lapilli.

The central cone also is built up of lava-flows and fragmentary ejecta, as may be seen on exposures in the walls of the summit craters. Thus the inside northern wall of the second crater (Oana) exposes two sheets of lava intercalated by layers of fragmentary ejecta, of which the upper and lower ones are respectively hypersthene-bearing olivine-augite-basalt and augite-olivine-basalt. The inside southern wall of the same crater also exposes two sheets of lava, of which the upper one is augite-olivine-basalt. Furthermore, on the east wall of the same crater is exposed a columner lava, about 20 m thick, which must have once been a lava-lake that filled the first (easternmost) crater. The surface of the solidified lava-lake (the bottom of the first crater), before the

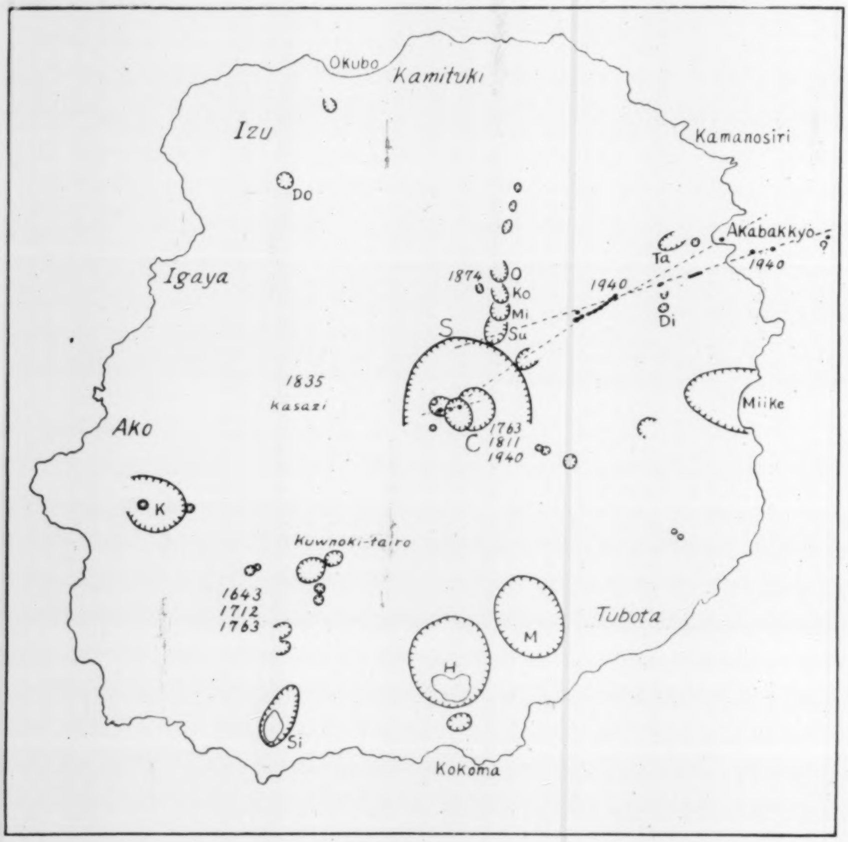

Fig. 2. Sketch-map of Miyake-sima showing location of the craters.

eruption of 1940, was covered with a thin bed of volcanic bombs, scoriaceous lapilli, and anorthite lapilli, although they are now buried beneath the material thrown out by the eruption.

Although Miyake-sima is a basaltic volcano as above outlined, it is noticeable that the island has locally a thin bed of liparitic pumice which was found by the writer for the first time during the course of the present investigation. Thus, so far as the writer's observations go, the bed occurs locally on the northern flank of the somma, in an area extending from the foot between Ano-saki and Igaya half way up the flank, about 200 m above the sea.

In the vicinity of Kamituki, the liparitic pumice bed lies about a meter beneath the surface of the mountain slope, occurring either as a more or less continuous bed, about 10 cm in thickness, or as lenticular masses, about 5～30 cm in thickness and 1～2 m in length, interbedded in a reddish-brown deposit of volcanic ash (Fig. 3). Accordingly, the pumice bed is exposed only in cuts, artificial as well as natural, on the mountain slope. So far as judged from exposures in several road-cuts as well as those in valleys, the pumice bed occurs, together with different beds of the basaltic material, in the following stratigraphic succession.

		(thickness)
1.	Black humus soil, a continuous surface-mantle of the slope, grading downward into a reddish-brown volcanc ash	1 m.
2.	White, sandy bed of liparitic pumice	10～30 cm.
3.	Reddish-brown volcanic ash	1 m.
4.	Black volcanic sand	10～20 m. (items 4–7)
5.	Light-grayish scoriaceous lapilli	
6.	Grayish volcanic sand and clayey volcanic ash[4] containing numerous prints of fossil leaves and ash-pisolites.	
7.	Volcanic breccia	
8.	Lava-flows (two-pyroxene-olivine-basalt) intercalated by layers of fragmentary ejecta.	

Outside the limited area of the slope near Kamituki, the liparitic pumice occurs neither as a distinct, continuous bed nor as lenticular masses. Thus, in the vicinity of Hodai and Ano-saki, about 3 km east of Kamituki, sand grains of the liparitic pumice, about 3～5 mm in diameter, are found in a humus soil, which lies about 1 m beneath the surface of the ground, and underlying the lapilli bed of the 1874 eruption and an older lapilli bed. The pumice-bearing humus soil overlies ash, sand, scoria, and volcanic breccia, which are underlain by sheets of lava-flows (olivine-basalt and augite-olivine-basalt). Likewise, in the

4) This bed is called "Kata" by the people of the island.

vicinity of Izu, about 2 km west of Kamituki, sand grains of the liparitic pumice are found in a humus soil near the surface of the ground, which grades downward into a bed of black scoria, about 1 m in thickness, overlying layers of clayey volcanic ash, sand, breccia, and sheets of lava-flows (augite-olivine-basalt).

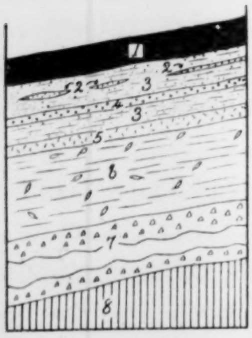

Fig. 3. Diagrammatic sketch showing the exposure of the liparitic tuff in a road-cut on the northern flank of the somma.

As mentioned above, the liparitic pumice bed rests on all the basaltic ejecta distributed on the northern, lower slope from Izu to Ano-saki, some local ejecta from younger parasitic vents excepted. Accordingly, the pumice bed must have been deposited some time after the lower part of the somma, at least, had already been formed.

The pumice bed, as observed in the vicinity of Kamituki, consists exclusively of finely-comminuted fragments of a pumiceous plagioliparite containing plagioclase (oligoclase, $Ab_{77\sim84}$), biotite, greenish-brown hornblende, magnetite, and colorless glass ($n=1{\cdot}497$).[5] Although the pumice bed consequently suggests the existence of a liparitic volcano that yielded it, on Miyake-sima itself there is no trace of a volcanic centre to which it can be traced. Thus neither the pumice bed nor other liparitic mass is found in the southern four-fifths of the island, including the central cone and the upper part of the somma.[6] Therefore, the material that constitutes the pumice bed must have come from a liparitic volcano on a neighbouring shore, or else from a submarine volcano in the adjoining ocean floor.

As possible sources of the liparitic material, we might mention a linearly-arranged group of three Quaternary liparitic islands, Kozu-sima, Sikine-sima, and Nii-sima, which are arranged in the order given, from SW to NE in the sea, about 30 km northwest of Miyake-sima. Although Sikine-sima is composed of a single lava of biotite-plagioliparite, both Kôzu-sima and the greater part of Nii-sima are composed of fragmen-

5) A specimen of the pumice sand collected on the mountain slope, about 2·5 km south of Kamituki, was chemically analysed by Nakajima, analyst of this Institute, with the following result: $SiO_2=71{\cdot}29$, $Al_2O_3=14{\cdot}38$, $Fe_2O_3=0{\cdot}55$, $FeO=1{\cdot}07$, $MgO=0{\cdot}69$, $CaO=1{\cdot}34$, $Na_2O=2{\cdot}70$, $K_2O=3{\cdot}14$, $H_2O(+)=3{\cdot}36$, $H_2O(-)=0{\cdot}71$, $TiO_2=0{\cdot}13$, P_2O_5 $0{\cdot}24$, $MnO=0{\cdot}03$.

6) Of several accidental rock-fragments found among the new ejecta of 1940 on the central cone, a white pumiceous block, which contains 75·98% SiO_2, may suggest the existence of an acidic volcanic rock at the base of the volcano. But even should the foundation of the volcano be of liparitic rocks, it is unlikely that the pumice bed came from this foundation.

ary ejecta and lava-flows of various liparites including hypersthene-plagioliparte, hornblende-plagioliparite, and biotite-plagioliparite. Since the liparitic pumice of Miyake-sima resembles in many respects some of these liparites, it is inferred that the source of the former may be located somewhere either in Kozu-sima or Nii-sima. Then, if this inference may be provisionally accepted, it follows that some of the pumiceous fragments ejected during the volcanism of either one of these islands were transported by the wind southeastward in the direction of Miyake-sima, accumulating locally on the northern flank of the somma, where the pumice bed is now found. At any rate, the presence of the liparitic pumice bed on the basaltic Miyake-sima volcano may be one of the positive evidences indicating that the Quaternary volcanism in the Seven Izu Islands has been alternately basaltic and liparitic.[7]

Fig. 4. The terrace gravel bed on the coast of Kamano-siri.

Along the shore of Kamano-siri, about 3 km east of Kamituki, is developed a terrace, about 15 m above the sea (Fig. 4). Although the lower part of this terrace is composed of a basaltic lava, it is overlain by a gravel bed, about 3 m in thickness, containing fossil shells. Accordingly, so far as this part is concerned, the island must have had a tendency to upheave, although there is at present no way of telling whether the upheaval is a local one caused by volcanism in the island or the result of regional crustal movement.

Recorded history of eruptions. Miyake-sima seems to have been active for untold ages, seeing that pieces of obsidan arrow-heads and other stone implements have been found buried together with certain earthen vessels underneath a pyroclastic bed that is exposed on the sea-cliff of Kokoma, an inlet in the southern coast of the island.[8] Of the activities of this island volcano all that history has recorded is the

7) H. Tsuya, *Bull. Earthq. Res. Inst.*, **16** (1938), 171.

8) According to Z. Asanuma, a village clerk of Kamituki, pieces of obsidian arrow-head were also found some years ago in the western part of the village, buried about half a meter deep under the volcanic ash.

elevens eruptions that occurred since 1085.[9] A short account of these recorded eruptions as compiled by Milne[10] and Omori,[11] follow.

(1) **1085.** An eruption took place in this year.

(2) **1154.** An eruption took place in November of this year.

(3) **1469.** An eruption took place on December 24, 1469. A legend says that the lava that is exposed on the coast of Igaya, a sea-port village on the west-northwest side of the island, is an outflow in this year.

(4) **1535.** An eruption took place in March of this year.

(5) **1595.** An eruption took place on November 22, 1595.

(6) **1643.** At 6 p.m. on March 31, 1643, earth-shocks were felt and loud reports like thunder were heard continually in the heavy rain. At 8 p.m. an eruption took place in the mountain. The village of Ako on the west coast of the island was entirely destroyed by fire. Lava flowed for a distance of about 1 km towards the coast near the village. Ash and lapilli, which fell in showers in the village of Tubota, on the leeward side of the island, laid waste the forests and farms thereabout. The activity lasted for about three weeks.

This activity was a flank eruption taat took place probably at Kuwa-noki-daira (or Togeno-o), a parasitic knob situated about 3 km south-east of Ako on the southwest slope of the somma, although it is uncertain which crater among the many found there represents the centre of the eruption at that time. The Ako lava which covers the area now occupied by the village of Ako is said to be an outflow by the eruption.

(7) **1712.** Shortly after 6 p.m. on February 4, 1712, earthquakes occurred repeatedly accompanied by thunder and lightning. At about 8 p.m. an eruption began at the foot (Yamabuki-zawa)[12] of the mountain. A lava flow which gushed out from Kuwanoki-daira reached the sea shore called Tatunega-hama. Lava from this crater reached about 200 m out to sea, besides spreading in the northwest direction for a distance of about 500 m. A majority of the houses in the village of Ako were buried in mud water which had gushed out at the moment of the eruption. In Kamakura, on the bay of Sagami, detonating sounds

9) In addition to these eruptions, Aomi mentions a record of the eruption in 372 B.C. K. AOMI, *Toyo Gakugei Zassi*, **32** (1915), 685. Asanuma also mentions this eruption with two others in 886 A.D. and 1777, although he does not give the sources for the records of these activities. E. ASANUMA, *Miyake-sima Rekisi-Nempyo.* 1938.

10) J. MILNE, *Transac. Seis. Soc., Japan, Part II*, **9** (1886), 86.

11) F. OMORI, *Report Earthq. Invest. Com.*, **86** (1918), 103.

12) This locality is not known.

like a distant thunder were heard and the sky was overcasted, accompanied by ash-fall. About 2 weeks later the eruption had died down to some extent, although the activity lasted for about three years afterwards.

This activity was evidently a flank eruption that took place in the vicinity of Kuwanoki-daira on the southwest slope of the somma, although the locality of the lava flow and the then active crater cannot be pointed out at the present time.

(8) **1763.** On August 16, 1763, rumblings were heard at night and ejection of incandescent stones from the summit of Oyama looked like flashes of lightning. From the next day on, rumblings and earthquakes occurred continually. In the meantime an eruption took place at Usuki in the village of Ako. Volcanic sand and lapilli fell in the villages of Ako and Tubota, and ash in the villages of Igaya, Izu, and Kamituki. By the eruption a deep crater with a pool of spouting water was formed at Usuki. The activity lasted for about seven years from 1763 to 1769.

This activity is characterized by its long duration as well as its compound nature as revealed by a successive occurrence of the summit eruption of Oyama and the flank eruption from Usuki at the southwestern foot of the somma. It is said that Sinmiyo, situated half way between Ako and Tubota, is a crater lake formed by the flank eruption at Usuki.

(9) **1811.** In the middle of the night of January 27, 1811, an eruption took place in company with continual rumblings and earthquakes at Hayono-tairo on the top of Oyama. By the eruption the night was light as day. Although the eruption died down at about 6 in the next morning, earthquakes occurred repeatedly for 6 days ending the evening of February 1, and roaring sounds like thunder continued after that day. Ash fell thickly in the village of Tubota. Two fissures, each having a width of about 30 cm, were formed on the northwest slope of the mountain. They run parallel with each other in a distance of about 2 m, extending in a southeast-northwest direction from near the top of the mountain to the shore of Daibono-hana through Nitanbara in the village of Izu. Two other fissures were also formed on the mountain slope extending from the summit called Yake-sinden to Anegakata on the northern shore.

This activity was a relatively small summit eruption that took place probably at the top of the central cone. No flank outflow of lava is mentioned, although remarkable fissures are recorded to have appeared on the northwestern slope of the somma.

(10) **1835**. On November 11, 1835, it rained heavily since the early morning. At noon or thereabouts several earthquakes took place followed by frequent rumblings. Dark volcanic clouds, fanned by a strong wind which was blowing at the time, were carried from the mountain toward the villages of Ako and Igaya. Shortly after a lava outflow took place near the cultivated ground Nagane, which lies between Ako and Igaya. A deep crater, from which the lava issued, was formed in the former site of the Nakayama Kan-on shrine of Kasazi-yama. Near the top of Hirabe-yama of Toga in the village of Ako, another eruption took place with an outflow of lava from thirteen craterlets. The lava reached the mountain path leading from Ako to Tubota. In the village of Igaya, earthquakes were severely felt. Although the eruption became less active at midnight of that day, earthquake and emission of volcanic cloud still continued. Thus, on November 14 a severe earthquake occurred, resulting in much damage at several places. Earthquake occurred repeatedly up to the night of November 20, when it died down at last. As a result of the eruption, a hotspring was created at Yuba in the village of Ako. Furthermore, in Igaya, landslides and rock-crumblings occurred, and fissures, less than 1 m in width, were formed at several places.

Although this activity was evidently a flank eruption that occurred near the villages of Igaya and Ako on the west slope of the somma, the craters as well as the lava flows of that day cannot be traced at the present time.

(11) **1874**. On July 3, 1874, earthquakes and rumblings began to occur repeatedly at noon. At the same time an eruption took place from the bottom of a pond, about 50 m deep, in the Ikeno-sawa valley on the north-northeast flank of the somma. A lava flow from the crater descended the mountain slope northward into the sea east of Kamituki, where it formed a new land, about 5000 m^2 in area. About forty five dwelling houses with a missing man of Higasigô, eastside of Kamituki, were buried under the lava flow. Ash and lapilli fell in quantity on the northeast side of the mountain. The eruption and rumblings declined after four days, although the activity lasted for about two weeks.

The areas covered by the lava flow and ejecta of 1874 can actually be traced for the most part, as indicated in Fig. 5. The source of the lava flow is situated about 550 m above the sea, outside the western wall of the Kosiki-ana paraitic crater on the north-northeast slope of the somma, where it is represented by a deep fissure-like opening. The lava flow which, near the source, has a width of about 200 m,

widens gradually northwards, attaining a maximum width of about 800 m in its down-stream at Yakeba, the east end of Kamituki. At the coast where the lava flowed into the sea, it forms a flat, about 800 m long by 200 m wide and about 5 m above the sea, fringing the former sea-cliffs. The lava has an average thickness of about 5 m. The volcanic ash and lapilli, which occupy a wide area adjoining the east margin of the lava field, are believed to have been ejected, mostly previous to the lava outpouring, from several openings which, together with a number of fissure-like depressions, are arranged almost linearly in a zone running from the crater of the lava north-northeast toward Bozu-yam. Thus the ejecta, which lie 30～50 cm deep on the ground near the northeast water-front between Yakeba and Hodai, increase in thickness of their deposit as well as in individual size southwestward to the direction of these craters; while there is no accumulation on the lava field.

Of the above-mentioned eruptions of Miyake-sima in historic times since 1085, four (1643, 1712, 1835, 1874) have been purely flank eruptions, one (1811) a purely summit activity, and one (1763) has been a flank eruption accompanied by summit activity, although the other five (1085, 1145, 1469, 1535, 1595) have been recorded briefly as eruptions. So far as the flank eruptions since 1643 are concerned, their centers have shifted in chronological order clockwise from the southwest slope to a point north-northeast of the somma. In accordance with this sequence, the centre of the flank activity of last year lies southeast of that of 1874, on the northeast slope of the somma. Furthermore, every flank activity in historic times was presumably a sort of fissure eruption accompanying an effluent lava flow. This is also true of the flank eruption of last year.

The average period of quiescence between eruptions since 1085 is about 60 years, with a minimum interval of 24 years between 1811 and 1835 and a maximum of 69 years between 1085 and 1154, except for the abnormally long interval of 315 years between 1145 and 1469. After a dormant period close to the average, the eruption of last year occurred in the 67th year from 1874.

The Osima volcanic zone, to which Miyake-sima belongs, shows a tendency that, in a particular period of its activity, the eruptions shift successively northward from a certain volcano in the southern part of the zone.[13] This tendency is clearly manifested by the activity of the

13) This tendency may be seen more clearly in the activity of the Ryukyu volcanic zone. H. TSUYA, *Bull. Earthq. Res. Inst.*, **18** (1940), 335.

zone in the latest period since 1939. Thus the latest eruption of Miyake-sima, to the description of which this paper is devoted, occurred subsequent to the eruption of Tori-sima of 1939, but prior to the eruption of Osima on August 19, 1940.[15]

II. Sequence of Events in the Eruption of 1940.

Although the eruption of Miyake-sima in 1874 seems to have been one of fairly striking activity, the island soon recovered from its effects and entered the dormant stage without any surface manifestations of activity. Thus none of the several authors who visited the island in the dormant stage between 1874 and 1939 have referred to any sign of volcanic activity, except that of the seaside hotspring near the village of Ako. In 1925, when the writer made a geological survey of the island, neither solfatara nor fumarole was found on the somma and the central cone. At that time, the Oana crater on the central cone was clothed for the most part with thick vegetation, although on its northern wall there were some marks of former fumaroles.

Preliminary symptoms of the eruption. After the dormant period that lasted for about sixty years since the end of the eruption of 1874, Miyake-sima was once more awakening into activity toward the end of 1939. Several unusual phenomena that might have been regarded as premonitory signs of volcanic activity occurred in the island during the seven months that preceded the last eruption, although even those islanders who had been previously aware of these phenomena never expected that the eruption was so close at hand. Of the unusual phenomena, attentions to which were called officially by the village masters of the island, or personally by those who experienced them, the following may be mentioned as premonitory symptoms of the eruption.

1. On December 20, or thereabouts, 1939, white smoke like water vapor was rising with whiffs of warm air from a damp spot in the vicinity of Hino-ana, a parasitic crater situated near the bay of Akabakkyô.

2. Toward the end of May, 1940, wisps of vapor like tobacco smoke were seen rising from the beach at the base of the sea-cliff

14) In Tori-sima (Mitugo-sima, or Ponafidin I.), in 30°28′ N. and 140°14′ E., there was a striking eruption, with lava outflows that lasted for about 4 months from August 18, 1939. H. TANAKADATE, *Jour. Geol. Soc., Japan*, **47** (1940), 387.

15) This eruption of Osima is the largest explosive activity we have had in recent years. T. NAGATA, *Zisin*, **12** (1940), 419.

facing the bay of Akabakkyô. Vapor was also issuing at the time from a point half way down the northeastern side of the somma, on the boundary between the villages of Kamituki and Tubota.

These incidents[16] indicated that, within about six months preceding the last eruption, the volcanic activity beneath Miyake-sima was drawing nearer to the surface, accompanied by precursory gas emissions from crevices on the northeast side of the volcano.

The following premonitory symptoms were observed during the few days that preceded the eruption.

3. For several days before the eruption of July 12, 1940, earthquake shocks were felt and subterraneous rumblings heard, occasionally, on the northeast side of the somma.

4. For two or three days before the eruption, unusual rumblings were heard at the bottom of the bay of Akabakkyô by some fisherwomen, who were engaged in collecting seaweed. About this time, the sea water of the bay of Akabakkyô was, locally, a few degrees higher in temperature than usual.

5. The day before the eruption, rumblings like thunder were heard at Mitoribata, a cultivated area situated about 1 km southwest of Akabakkyô.

6. On July 12, 1940, when the eruption had begun, the weather was both sultry and stormy, with a southwesterly wind, as in the few preceding days; it rained off and on. Subterranean rumblings were heard at Kamituki in the morning of that day. From 3 p.m., feeble intermittent earthquakes were felt at Kamituki till 6 p.m. About this time, houses at Mitoribata were shaken up and down, accompanied by whirring sounds, although nothing unusual was noticed outdoors. From 6 p.m., earth tremors were felt almost continuously at Kamituki, together with occasional upward shocks, till 7:30 p.m. of the same day, when the eruption burst out at last. The village of Tubota also was slightly shaken for a few hours before the eruption, while the villages of Ako and Igaya, where neither earthquakes nor rumblings were felt, was so quiet that people there were informed of the eruption by telephone from Kamituki a few hours after the eruption began.

The above-mentioned premonitory symptoms were indications that the volcanic activity beneath Miyake-sima was gradually approaching the surface of the island during the few days preceding the eruption of July 12. Thus the premonitory earthquakes and subterraneous rum-

16) Besides these, it is said that the levels of springs in Miyake-sima fell unusually during the few months that preceded the eruption.

blings, which were felt frequently, although locally, in the northeastern half of the island, are inferred to have occurred along with the intrusion of a lavic magma from which the volcanic activity originated, within a few kilometers below the surface in the vicinity of Akabakkyô.

The flank eruption. Subsequent to the above-mentioned premonitory earthquakes and rumblings on July 12, an eruption broke out on the northeast flank of the somma at about 7 : 30 p.m. Of the various reports relating to the intital state of this eruption, the following may be mentioned.

1. According to T. Kano,[17] subsequent to the continual earth's tremors that lasted for about an hour, thick dark smoke began to rise a few minutes before 8 p.m., but without detonation, from the valley ahead of his house. A little while later, when, with his family, he reached a place of safety, dense smoke began to rise also from the upper course of the valley, followed by showers of incandescent rock fragments, accompanied with detonations and lightning flashes.

2. According to K. Isikawa who lived in Mitoribata, the first eruption took place, following noises like the sighing of wind, a few minutes to 8 p.m. At that moment there rose a column of dense smoke, which glowed brightly near the base, accompanied by ejection of incandescent rock fragments half way up the mountain in a southwest direction from his house.

3. According to K. Ozawa, who observed the initial event at Simasita on the bay of Akabakkyô, the first eruption that occurred on the mountain side in a southwest direction from Simasita, was followed quickly by eruptions that started in succession for about two minutes from three places, one on the shore of Akabakkyô bay, and the other two from the bay itself. Almost concurrently with emission of pale bluish flashes in the dense clouds that rose up, came a cracking sound, followed by detonations, while at the same time pieces of incandescent lava shot up like sparks into the air.

4. M. Uematu observed at Miike-hama[18] that the first eruption broke out a few minutes to 8 p.m. on the mountain side in a N 50° W direction, and that it was followed quickly by eruptions in three places in the direction of Akabakkyô.

5. H. Murakami, a young cowherd who lived at the time of the

17) A charcoal burner who lived on the northern side (about 200 m above the sea) of the middle course of the valley that lies on the borders of Kamituki and Tubota.

18) An inlet situated about 3 km south of Akabakkyô.

eruption half-way up the western side of the somma, felt an earthquake in the twillight of the evening, but heard no detonation, and heard the news of the eruption only the next morning.

Although reports do not agree on the time that the eruption really began, it is inferred from the foregoing information and others not quoted here, that, beginning insensibly at about 7:30 p.m., the eruption was so violent about 7:50 p.m. that it was visible everywhere in the villages of Kamituki and Tubota. People in Ako and Igaya, however, scarcely took notice of the eruption, probably owing to the stormy weather at the time.

The following extract is taken from a report, dated July 16, 1940, addressed by Y. Kobayasi, Captain of the *Huzi-maru*,[19] to the police box at Kamituki.

> About 8 p.m., July 12, unusual rumblings were heard, and a column of flaming smoke was seen in the direction of Akabakkyô. Then the rumblings became more and more terrible; a column of flame shot skywards; volcanic sand rained continually from the clouds of dense black smoke that hung over our heads. About 8:45 p.m., when heavy rain came in torrents, the eruption increased in violence. Before long, lava flowed into the sea and approached us, forming white clouds at its front.

Some further details concerning the first phase of the eruption were given by E. Isii, Captain of the steamship *Hagi-maru*,[20] as told to a press representative. The following is an extract from his statement.[21]

> About 8 p.m., July 12, a soft sound like that when a bellows is worked, occurred, followed quickly by a loud sound that shook the hull of the ship. In the meantime, volcanic lapilli began to fall on her deck The lava stream that flowed into the sea looked like fishing flares. The eruption seemed to have occurred in three places, one on the bay of Akabakkyô, one on the mountain side close to the bay, and the other near the summit of the mountain.

From this time onward, according to information from various quaters,[22] the flank activity progressed as follows.

July 12.

9 p.m. The eruption was proceeding at a distance of about 2000 m southwest of Akabakkyô, on the boundary between Kamituki and Tubota. By this time, detonations like distant thunder were heard at Kamituki.

---

19) She was at anchor temporarily off Akabakkyô at the time the eruption began.

20) She was also at anchor about 500 m off Akabakkyô at that time.

21) The Tokyo Niti-Niti (newspaper), dated July 16.

22) Information, the sources of which are not given in parenthesis, were extracted from the village-office records of Kamituki.

9:20 p.m. From this time onward, earthquakes became more violent.

9:30 p.m. A violent explosion occurred, together with rumblings and frequent earthquakes. The weather was then cloudy, with occasional showers and lightning; the wind at Kamituki, about 5 m. per second, was blowing from the southwest.

9:52 p.m. From this time onward, the eruption increased in violence.

10 p.m. As viewed from Yakeba in Kamituki, the eruption was taking place on the highest point of the active zone on the mountain side. Explosions were heard almost continually. The weather was cloudy with light rain and a southerly wind of about 5 m.

10:15 p.m. The activity continued to be explosive.

10:25 p.m. Viewed through a rift in the clouds, eruptions were seen in two places in the direction of Kazahaya.

11 p.m. An eruption, severer than any of the preceding, was seen at Miike-hama in a N. 60° W. direction. (M. Uematu)

11:50 p.m. Explosions like distant thunder were heard at Kamituki.

12 p.m. Viewed from Yakeba, the centre of the eruption on the mountain side seemed to be shifting downward. (Z. Asanma)

July 13.

5 a.m. An aerial scout reported that until then, a 20 m (about) wind was blowing, together with heavy rain generally over Miyake-sima, and lava streams were seen, together with a dense eruption cloud spreading in a northeasterly direction toward Akabakkyô from the central part of the island. (The Tokyo Niti-Niti dated July 14)

6:30 a.m. According to T. Hiramatu and T. Asanuma, who visited the region about this time, eruptions were going on in three different places, one in the bay of Akabakkyô and the other two in the vicinity of Maruyama.

7 a.m. According to a telegram sent by Hiramatu, the postmaster of Miyake-sima, emission of black smoke, together with rumblings, still continued at this time with rather increasing intensity. The eruption area widened every moment, with lava streams invading the houses at Simasita on the bay of Akabakkyô. (The Tokyo Niti-Niti dated July 14)

7:15 a.m. According to R. Asanuma, at this time the eruption, as viewed from Ano-saki, near Akabakkyô, was taking place violently near the houses along the bay of Akabakkyô.

8 a.m. The activity increased in violence in the lower part of the

mountain side, where there were eruptions about every twenty minutes. (M. Uematu)

9 a.m. About this time a submarine eruption occurred off Akabakkyô, in a N 30° E direction from Miike-hama. (M. Uematu) About the same time, as viewed from Hodai, midway between Kamituki and Akabakkyô, volcanic bombs were falling in showers in the sea off Akabakkyô. A little while later, ascending Maru-yama, hot air was felt, along with a tremendous noise. Although it was raining heavily at the time, the eruption cloud was not very dense, so that the area underneath the eruption could be be seen clearly from the hill. In that area, besides lava streams and fire, there were eruptions from four separate points, each of which was sending out a continuous puffing sound. Incandescent bombs were being thrown up violently from one of these vents, situated near the foot of the cliff (Akabakkyô-hana) on the bay of Akabakkyô. (H. Morii)

10 a.m. About this time, when the weather was worsening, with occasional showers, the eruption was still going on. It was found that the ejecta had formed a new land, like a peninsula, in the bay of Akabakkyô, and that the coast-line in its vicinity had notably changed.

10 : 30 a.m. Up to this time, according to T. Asanuma, a lava flow had spread as far as Miyanosita (also called Kiarasiba) and a vast tract of the neighbouring sea had changed to land with a height of about 70 m above the sea. Volcanic bombs were being thrown up into the air to heights of about 100 m from a vent near the downstream of the river, on the boundary between Kamituki and Tubota.

1 p.m. The explosions became less violent for a while.

2 p.m. According to Y. Sato, Captain of the *Taihuku-maru*,[23] terrible rumblings were heard at sea in the direction of Miyake-sima, and a dense ash cloud was darkening the sky above the island. (The Tokyo Niti-Niti dated July 15)

4 p.m. There was a lull in the eruption.

4 : 30 p.m. After a temporary lull, activity resumed with increased violence, with continual explosions and rumblings. The weather continued overcast, with occasional showers and a southwesterly wind of about 10 m.

5 p.m. As viewed from Ano-saki, Hyôtan-yama[24] had now become almost the same size as that observed at the end of July. Three columns of dense ash cloud were rising from the surface of the lava that

23) At that time she was at anchor off the northwest coast of the island.

24) A new volcanic cone, which was named Hyôtan-yama, after its outward appearance which suggested a gourd, was formed in the bay of Akabakkyô.

had flowed into the bay of Akabakkyô. (Z. Asanuma) Earthquakes, which by this time became notably less frequent than hitherto, were felt only about once an hour.

6 p.m. From this time onward, according to a report from the "*Okino-sima*," a special service ship, the explosions diminished in frequency, although an ash cloud continued to rise. (The Tokyo Asahi dated July 15)

6:30 p.m. Explosions occurred several times, but later only a faint ash colud was rising.

7 p.m. Rumblings were hardly heard.

9 p.m. Neither explosion nor rumbling occurred. (M. Uematu)

9:30 p.m. Although several explosions took place in quick succession, quiet was soon restored.

July 14.

3:30 a.m. An explosion took place.

7 a.m. Neither explosion nor rumbling was heard, although an ash cloud continued to rise, and weak earthquakes were sporadically felt.

July 18.

About 4 p.m., a column of fire (?) rose from a crater situated in the uppermost part of the eruption zone on the mountain side. It was seen by a man who, coming from Kamituki, was present near the crater at that time.

July 20.

About 5 a.m., three columns of fire (?) were seen in the direction of the above-mentioned crater. They were seen by those who arrived at Kamituki on the *Huzi-maru*, at the time.

July 29.

At 4:30 p.m., small explosions took place near the shore of the east end of Hyôtan-yama. They were seen by passengers on the *Hagi-maru*, which at that time was steaming off the shore.

Judging from the foregoing reports, the flank eruption which began at 7:30 p.m. or slightly later, on July 12, were almost incessant, with occasional earthquakes and rumblings up to about 6 p.m. the next day. Following later intermittent explosions, activity had virtually subsided by early morning, July 14, whence it is inferred that the main events of the flank eruption had completed within about twenty-two hours up to 6 p.m. of July 13. Thus, during these hours, eruptions took place from several craters which, as will be mentioned presently, were newly formed both on the mountain side near the boundary between Kamituki and Tubota and in the bay of Akabakkyô (Figs. 5, 11, 12). Volcanic sand, lapilli, and bombs were not only scattered over a wide area sur-

rounding the craters (Figs. 15, 18), but also piled up on the craters, forming a number of new volcanic cones, of which Hyôtan-yama in the bay of Akabakkyô is the largest (Figs. 13, 17). A lava stream (Akabakkyô lava) had flowed down through the valley on the boundary between Kamituki and Tubota into the bay of Akabakkyô where, joining the northern side of Hyôtan-yama, it formed new land, covering the greater part of the bay (Figs. 11~14). Another lava stream that had flowed through the Yoridai-sawa[25] reached a point near the sea-cliff abutting the southern part of the same bay (Fig. 16).

So far as could be ascertained, no one had observed in detail from a close distance the sequence of events in the flank eruption. It was moreover said that the eruption could not be viewed fully from any quarter of the island, by reason of the stormy weather that prevailed at the time. Although the foregoing information, most of which are by random observers, have not served to give us a very clear picture of the actual activity, there is no doubt that the outburst first occurred half way up the mountain side, and later spread downward into the bay of Akabakkyô. It is certain that the craters on Hyôtan-yama, in the bay of Akabakkyô, were active for some time after the activity of the craters on the island had subsided, because, as will be mentioned presently, ejecta from the former were found accumulated on those from the latter.

Since July 14 inclusive, no marked activity occurred on the mountain side, the uncertain eruptions of July 18, 20, and 29 excepted, although white vapor clouds and thin bluish clouds of other volcanic gases continued to rise, together with the smoke of burning trees, from many places in the area devastated by the flank eruption (Fig. 19, 20).

The summit eruption. Following the flank eruption of July 12~13, the volcano began to get active at the summit. According to H. Murakami who, in the afternoon of July 13, visited, with other companions, the Oana crater on the central cone, the crater was seen to be the same as usual without any outward signs of activity. When he visited the crater again, the next morning, it was seen emitting vapor clouds. In the afternoon of July 15, when the same visitor arrived on the northeastern side of the central cone by way of the Hayono-tairo atrio, he was caught in the rain of volcanic ash that came falling from the direction of the Oana crater. From all this, it

25) A valley situated about 1 km south of the valley on the boundary between Kamituki and Tubota.

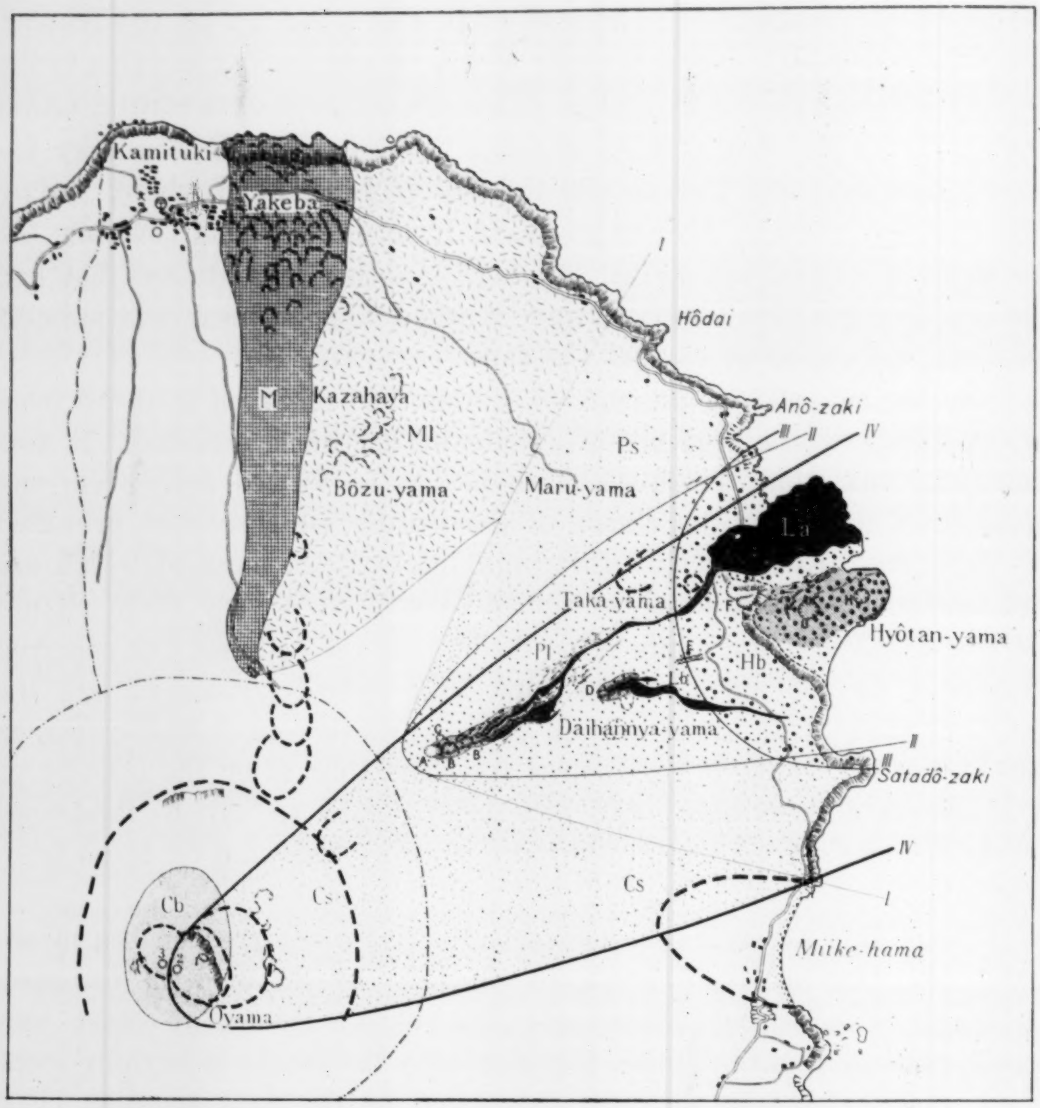

Fig. 5. Map of a portion of Vo'cano Miyake-sima showing the distribution of the ejecta of July, 1940.

The summit eruption of 1940:
- Cs, Volcanic ash and sand.
- Cb, Volcanic lapilli and b)mbs.
- 1, 2, 3, Active pits of July 25.

The flank eruption of 1940:
- Ps, Volcanic ash and sand.
- Pl, Volcanic lapilli and bombs.
- La, Akabakkyô lava-flow.
- Lb, Yoridai-sawa lava-flow.
- Hb, Hyôtan-yama ejecta.
- A, B, B′, C, D, E, F, G, H, Active pits of July 12 ~13.

The eruption of 1874:
- Ml, Volcanic lapilli and bombs.
- M, Lava-flow.

is inferred that the summit activity began at midnight between July 13 and 14, with the emission of vapor clouds from Oana.

Since the early morning of July 14, when we arrived at the island (Fig. 21), a tremendous column of black ash cloud kept rising from the mountain almost continually for several days, while ash fell at intervals over a zone extending from Akabakkyô to Miike-hama. But as the ash cloud on this day was rising through the cloud with which the upper part of the mountain was thickly veiled, its source could not be located from the foot of the mountain, but was ascertained for the first time on July 18, that the emission of ash cloud since July 14 was owing to an eruption of the central cone. The sequence of the summit eruption on and after July 18 follows.

July 18.

0 a.m. Lightning flashes were seen in the midst of the ash cloud above the mountain. (K. Isikawa)

6 a.m. It was fine with a southwesterly wind. A black ash cloud was rising from the mountain to an elevation of about 30° as observed at Kamituki.

8 : 40 a.m. The weather became so cloudy that the upper part of the mountain could not be seen. The writer left Kamituki for the mountain in company with Dr. Takahasi and others.

11 a.m. From this time, when we came near Bozu-yama on the way to the top of the monntain, rumblings were heard periodically at intervals of about 30~45 minutes. On approaching the summit the noises grew clearer and louder.

12 a.m. Upon reaching the top of the northeastern somma, a distance of about 1 km northeast of the summit of the central cone, the weather was stormy with occasional showers and the range of vision so limited that the central cone could not be seen, although the rumbling continued to be heard about every 30 minutes. A little later, at the eastern end of the Hayono-tairo light showers of ash came from the direction of the central cone. The ash lay a few centimeters deep on the ground, but neither newly-ejected bombs nor scoriaceous lapilli could be found.

1 p.m. The rainstorm grew worse. Making a wide detour by way of the Hayono-tairo atrio, we arrived at the northwestern foot of the central cone on the weather side. All that could be seen from here was the white vapor cloud which, together with a rain cloud, hung over the craters on the central cone. No new ejecta were found on the atrio adjoining the northern and northwestern sides of the central cone.

1:30 p.m. Braving the rainstorm, which at the time was still heavy, we started our descent to the bottom of the upper crater, and eventually reached a point half way down the western wall of the Oana crater.

The upper crater was quiet as usual without any sign of activity. Neither active vents nor recently ejected material were found on the crater floor, which was covered with grass.

The Oana crater was active, sending up an ash-laden cloud. On reaching half way down the western wall of the crater in order to watch the scene of the activity from the supposed safest distance, we saw a spiral column of ash-laden vapor rising continually from a new pit near the base of the northern crater wall, accompanied with fierce rumbling. The glowing vapor column, immediately above the orifice appeared to be several meters in diameter. Rumbling was heard at intervals of about 10 seconds. So far as could be seen, the interior of the Oana crater was still covered for the most part with vegetation, although a small part near the active pit was seen covered with a pile of new ejecta. Two cow-sheds that were on the crater floor midway between the active pit and the place where we stood, were still intact.

5 p.m. Upon returning to Kamituki, the rainstorm had cleared, exposing to view for the first time the top of the mountain which had been enveloped in a thick cloud since July 14. Black ash clouds, which were seen from Kamituki to rise continually from the summit, were bent in the direction of Akabakkyô by the wind from the southwest, without being projected high into the upper region of the air.

11:30 p.m. Black clouds shot up explosively from the summit about every 30 seconds, although these explosions were scarcely heard at Kamituki.

11:45 p.m. An earthquake was felt at Kamituki, but nothing unusual was noticed in the ash cloud that continued to rise from the summit at that instant.

July 19. This morning the size of the ash cloud from the summit was much the same as that of the previous evening, although its color had become less dark (Fig. 22).

9:50 a.m. When we came near Kazahaya on the way to the mountain, an explosion was heard in the direction of the summit, after which explosions accompanied by rattling noises, recalling rock-slides, were heard at intervals of from about 1 to 5 minutes.

0~2 p.m. During these two hours we stood watching the explosion of the central cone from the top of the northeastern somma. Although the central cone was covered with heavy fast drifting clouds, its top

came into view from time to time through rifts in the clouds. Thus we saw dense, dark whorls of ash-laden cloud shoot straight upward in rapid succession from the top of the cone. The explosions occurred with sharp staccato sounds like those of pistol shots in the open air, followed occasionally by rattling noises recalling rock-slides. Simultaneously with the explosions, non-incandescent rock-fragments were shot upwards to heights of at least 100 m above the top of the central cone. Among these rock-fragments were blocks so large that their flights through the clear air on the weather side were readily seen from our position on the top of the northeastern somma, a distance of about 1 km. Although they fell for the most part into the Oana crater whence they were originally ejected, some of them fell on the northern side of the central cone, as far as the central part of the Hayonotairo atrio.

The solid ejecta thrown out during these hours, namely, those collected at the Hayono-tairo atrio, were all angular rock-fragments, less than 50 cm in diameter, consisting of detritus, often coated with salts, besides angular fragments of a black, compact lava carrying abundant sandy detritus as xenoliths. When these ejecta were thrown out, their temperature must have remained at several hundreds degrees, seeing that the vegetation pinned under them were charred black. But neither scoria nor bombs, suggestive of incandescent molten lava, were found among them.

According to H. Murakami who, at about 10 a.m. of the same day, observed the interior of the Oana crater from the west margin of the upper crater, the active area appeared to have been enlarged to a point as far as the western wall of the Oana crater, where we reached the preceding day.

July 20. The morning was fine with a westerly wind. The eruption cloud became light grayish instead of the black of dark gray of the preceding days. At 7 a.m., its elevation was about 20°, as observed from Kamituki.

10: 10 a.m. An explosion was heard at Hodai in the direction of the mountain.

10: 40 a.m. Rumblings were heard at Akabakkyô in the direction of the mountain.

11: 5 a.m. Explosions were heard several times.

12: 10 p.m. A vertical shock was felt at the cliff-head of Akabakkyô, where ash was falling heavily.

12: 20 p.m. An explosion was heard at Yoridai in the direction of the mountain. About three minutes later, the explosion threw out a shower of ashes.

4 p.m. Four explosions were heard at Akabakkyô at intervals of about 5 minutes.

The volcanic ash and sand that fell this day in Akabakkyô and neighbourbood consisted entirely of detritus, containing not a few whitish rock-fragments that were either decolorized by fumarolic action or were coated with salts.

July 21. Fine with a westerly wind.

6 a.m. Explosions were heard at Kamituki at intervals of from about 3 to 5 seconds.

10 a.m. Ash, and scoriaceous lapilli, 5～10 mm in diameter, were falling in and around Akabakkyô. During the remaining hours of the day, explosions were frequently heard at Miike-hama and Tubota. In the night ash fell in Miike-hama.

According to S. Sakuta, who visited the summit of the mountain this day, activities increased all over the Oana crater (Fig. 27).

July 22. Fine with a southwesterly wind, but the upper half of the mountain was veiled with clouds.

9 a.m. Explosions were heard twice on the way from Tubota to Miike-hama.

10 a.m. Explosions were frequently heard at Miike-hama. They were incessant throughout the day, and ash rained over a zone extending from Miike-hama to Akabakkyô (Figs. 23～25, 28). In and around Yori dai, scoriaceous lapilli, 5 cm and less in diameter, were found scattered on the ground already covered with ash several centimeters deep.

10 p.m. The ash cloud continued to rise, although its volume was seen to have fallen off considerably.

July 23.

0 : 30 a.m. The ash cloud became smaller, but the rumblings were frequent.

5 : 30 a.m. Explosions like those of gun-fire were heard at intervals of from about 1 to 3 minutes, with at the same time frequent air-quakes. In addition to the explosions, long and monotonous sounds like those of surging waves were heard from time to time.

6 : 30 a.m. Air-quakes were felt about every 5 minutes.

10 a.m. The explosions died away, although the ash clouds increased.

11 a.m. When we arrived at the top of the northeastern somma (Figs. 29, 30), continuous noises were heard, while at the same time non-incandescent rock-fragments continued shooting straight upward from the rear of the northern summit of the central cone. The bulk of the ejecta seemed to fall back into the Oana crater.

11:13 a.m. Upon reaching the eastern part of the Hayono-tairo atrio, an explosion like that of heavy gun-fire was heard. The ground all round was filled with scoriaceous lapilli, up to 10 cm in diameter, besides being covered with ash about 5 cm deep.

12 a.m. When the northwestern part of the Hayono-tairo atrio was reached, explosions were heard, accompanied with air-quakes, but the central cone at the time was veiled so thickly with fog that we could not see what was happening at the scene of the explosions.

No volcanic bombs suggestive of juvenile molten lava had yet fallen on the ground in the central part of Hayono-tairo, all that could be found there being angular rock-fragments identical with the ejecta of July 19.

1 p.m. On our way back to Kamituki, the explosions that were going on from the central cone could be heard from the summit of the northeastern somma, accompanied with strong air-quakes. Fortunately the fog rapidly cleared, permitting an unobstructed view of the scene of the exposions. It was found that, although some explosions accompanied ejections of small masses of both black ash clouds and rock-fragments, there were many cases of explosions in connection with which nothing but emissions of a light bluish smoke could be seen. Regardless of the explosions, white vapor clouds were issuing without stop, and noises like those caused by working the bellows were heard, stopping suddenly for about 5 seconds at intervals of about 10 seconds. These sounds, which varied in loudness from time to time, resembled that of the beating of the sea against the shore. Besides, noises recalling rock-slides were occasionally heard.

10 p.m. From Kamituki the sky above the summit of the mountain was seen illuminated.

July 24.

1:50 a.m. An earthquake was felt at Kamituki. Detonations were heard about every 5 seconds.

2:30 a.m. Detonations heard once every ten seconds which, after a while, gradually became less frequent.

6 a.m. Noises like those caused by working the bellows were heard at Kamituki. Small masses of white vapor cloud and grayish ash were seen to rise intermittently from the summit of the mountain.

9 a.m. Noises like those caused by working the bellows were heard at intervals of from about 10 to 13 seconds.

1:30 p.m. Light bluish smoke, occasionally accompanied by a grayish ash cloud, rose from the summit.

In the night, detonations accompanied with air-quakes were of frequent occurrence.

July 25.

5:30 a.m. As in the preceding day, noises like those caused by working the bellows were heard at Kamituki at intervals of about 5~10 seconds. Detonations were also occasionally heard, but without air-quakes.

11~12 a.m. During this time, as we stood watching the activity of the central cone from the top of the northeastern somma, almost continual ejections of both black ash clouds and volcanic bombs could be seen (Figs. 31~34). The ash clouds appeared to rise from a pit in the Oana crater, while the bombs came from another pit behind the northern top of the central cone (Figs. 35, 36). The bulk of the bombs were thrown nearly straight upward to elevations of about 20°~25° and, after several seconds in the air, fell back into the crater whence they were ejected, while some of them, which were ejected obliquely northward, dropped on the northern slope of the central cone and on the adjoining flat of the Hayono-tairo atrio.

Besides the accessory rock-fragments that were being ejected for several days previously, on this day new volcanic bombs up to 1 m in diameter were found strewn on the Hayono-tairo atrio adjoining the northern side of the central cone (Figs. 37, 38), reaching, roughly as far as 600 m. About 3:30 p.m., on our way over this atrio, a bomb about 1 m across fell quite close to us. Although the surface of this bomb appeared to have rapidly acquired a black solid crust during its flight through the air, it was found, on breaking the bomb some time after it landed, that its interior beneath the crust, several centimeters thick, was still glowing with a temperature exceeding 700°C.

1~2 p.m. During this time, as we stood watching the summit activity from the safest distance (about 500 m northwest of the central cone) in the northwestern part of Hayono-tairo, we were fortunate in getting one of the best views of the summit eruption (Figs. 39~46). We could see three different phases of the eruptions that were taking place side by side from the three major centres of activity, as follows.

The first (easternmost) centre of activity which, being inside the Oana crater, and which seemed to correspond to the active pit of July 18, was sending up, continually, but very gently, only a small quantity of light-grayish ash cloud.

The second centre of activity, which was near the boundary between the Oana crater and the upper crater, in the southwestern direction of the first one, was ejecting, periodically, a black cloud densely

charged with ash upward to a height of about 100 m above the crater bottom. From time to time a number of non-incandescent black bombs were thrown out from the same place.

The third (westernmost) centre of activity, situated inside the upper crater, immediately west of the Oana crater, was erupting the most violently of the three. Thus, simultaneously with loud detonations that occurred at intervals of about 5 seconds, a light bluish smoke was thrown up with great force, while at the same time flashes like those of lightning appeared in the smoke, instantaneously followed by ejections of incandescent bombs. The explosions some times came at slightly longer intervals than 5 seconds. In these cases, the explosions were so loud that the resulting air-concussion forcibly struck our eardrums.

The flashes that appeared at the instant of explosion were seen to form more or less sinuous and even apparently forked arcs in the smoke just above the crater floor. With augumented explosions they increased in length as well as in width. Judging from their forms, the flashes may be due to rapid combustion in the air of certain oxidizable elements contained in the volcanic gases thrown out by the volcano at the time of the explosion.

The volcanic bombs appeared to have already acquired their characteristic forms when they were thrown off from the crater. Although they were incandescent, with a temperature presumably above 900°C. at the instant of ejection; in the air, their surfaces soon became black. In flying up into the air, some of the bombs appeared to wobble as they were bent into various shapes. Some of the long and slender shaped bombs were seen to revolve about their shorter axes at a rate of one or two revolutions a second.

According to the particular explosions, ejections of bombs occurred frequently at intervals of about 5 seconds; the number of bombs ejected with every explosion seeming to vary from scores to hundreds. But no collision of bombs in the air were noticed. Sometimes, a few bombs that were ejected without explosion, would fly through the air with high speed in meteor-like fashion.

The bombs ejected from the third centre of activity, in falling, scattered in and around the upper crater, reaching an extreme distance of about 500 m north-northeastward on the Hayono-tairo atrio. The maximum elevation of the bombs, as observed from a distance northwest of the crater, was about 500 m.

8:30 p.m. The sky above the summit of the mountain was illuminated. Ejections of incandescent bombs were seen from Tubota.

July 26.

1~2 a.m. The summit of the mountain was veiled with clouds. At Kamituki, slight explosions were heard about every 5 seconds, and heavy explosions with severe air-quakes at intervals of about 10 seconds.

2:30 a.m. Heavy explosions were heard about every 3 minutes.

5:30 a.m. Explosions like those of heavy gun-fire were heard at intervals of from 5 to 10 seconds. Air-quakes were also frequently felt. Sometimes noises like those caused by working the bellows were heard.

6 a.m. The explosions were no more, but the bellows-noise was audible about every 10 seconds.

8:30~9 a.m. Explosions were recurrent with air-quakes.

9:30 a.m. The upper part of the mountain was covered with clouds. Although there were no more explosions, the bellows-noise never ceased.

12 a.m. No explosion was heard at Akabakkyô.

5 p.m. A small mass of white cloud rose continually through the cloud that covered the summit of the mountain. A heavy explosion was heard at Kamituki, followed by occasional minor explosions.

9:50 p.m. Besides the bellows-noise that occurred at intervals of from 3 to 4 seconds, explosions accompanied by air-quakes were heard every few minutes. The illuminated sky above the summit flickered.

July 27.

7 a.m. Noises like those caused by working the bellows were heard every 10 seconds.

12 a m. Rumblings like distant thunder were heard at intervals of from about 10 to 20 seconds.

3 p.m. Small packs of black ash cloud rose intermittently from the summit. From this time on, the emission of black ash cloud increased in violence.

5:30 p.m. Black ash clouds rose at intervals of about 20 seconds. They were bent by the wind, which was blowing from the southwest, without being projected into the upper air regions. Besides the bellows-noises, which came nearly every 10~15 seconds, explosions were heard at intervals of a few minutes, but without any air-quakes.

11 p.m. Sky above the summit clear. Explosions accompanied by air-quakes occurred at intervals of from about 1 to 3 minutes, and noises like those heard in the preceding hours, at intervals of from about 5 to 10 seconds.

July 28.

6 a.m. Explosions accompanied with air-quakes occurred at intervals of from about 1 to 4 minutes. Noises like those caused by working the bellows were heard at intervals nearly every 10 seconds.

8:30 a.m. The eruption became slightly more violent this time, explosions accompanied with air-quakes occurring nearly every 10 seconds.

11:30 a.m. Explosions were heard at Akabakkyô, while at the same time, black ash clouds were seen through rifts in the clouds with which the summit of the mountain was covered.

3:45 p.m. With the explosions that occurred nearly every 10 seconds, black ash clouds rose from the summit.

6 p.m. Volcanic ash was falling in the village of Ako.

8 p.m. About this time, when we reached the top of the north-eastern somma for a night-view of the eruption, explosions and rumbling noises were heard nearly every 5 seconds, and simultaneously with these sounds, a number of incandescent bombs were seen shooting up like fireworks into the night air above the summit of the central cone.

July 29.

1 a.m. Explosions accompanied by air-quakes were heard nealy every 10 seconds. Since then, the summit eruption remained almost stationary the whole day and into the evening.

7 p.m. This time, when the writer stood watching the mountain on board the *Hagi-maru*, steaming off the coast of Igaya, bound for Tokyo, he saw a number of luminous bodies (incandescent bombs) shooting up continually through illuminated clouds into the night air above the summit of the mountain.

July 30～August 4. During these days, explosions were frequently heard at Kamituki, although they seemed to have declined in frequency as the days passed (Fig. 47). (T. Minakami)

August 5. Although no rumbling was heard, a small pack of ash clouds was rising from the summit. There were light showers of ash in the villages of Igaya and Izu. (Z. Asanuma)

August 6. A small quantity of ash fell in Akabakkyô and vicinity. At 1 : 30 p.m. an earthquake was felt at Kamituki. (Z. Asanuma)

August 7～8. The end of the summit eruption was practically complete. It was reported by one who had climbed the mountain, that a new mound (Fig. 48) had formed in the western part of the old crater on the summit of the central cone, and that a white vapor cloud had been rising gently from a crater on the newly-formed mound. (Z. Asanuma)

August 16. An earthquake was felt at Kamituki at 2:30 a.m.

August 18. An earthquake was felt at Kamituki at 0 a.m. (Z. Asanuma)

To summarize, the course of the summit eruption was as follows:

Following the flank eruption on the northeast side of the somma, which had virtually subsided about 6 p.m., July 13, the central cone, Oyama, began an eruption at midnight on the same day that lasted well over three weeks, exhibiting every phase of activity peculiar to the eruption of basaltic volcanoes.

During the four days ending July 18, ash clouds rose almost continuously with great energy from a new pit (the first centre of activity) in the Oana crater, and ash fell intermittently on the mountain side in the direction of Akabakkyô. It was on July 18, when a visit to the west wall of the Oana crater showed that active pit just mentioned had opened on the infallen talus at the base of the north wall of the same crater.

For the next two days (July 19 and 20) the activity continued to increase in violence. Thus on July 19, when we revisited the summit, it was found that the eruptions had spread to the west wall of the Oana crater (the second centre of activity), to which it was possible for us to descend the preceding day, and that rock-fragments were being ejected almost continually with staccato sounds, followed by noises recalling that of rock-slides. The same activity continued with rather increasing intensity till the next day. The rock-fragments ejected during these two days were exclusively angular detritus including fragments of the old cone material, besides those of a fresh, dense lava that was probably torn off by the explosions from the top of the solid lava plug that had risen near the crater floor from the interior of the volcano. It is inferred that the frequent staccato sounds were caused by the shattering of the solid crater floor during the explosions, while the noises recalling rock-slides were due to the falling of the shattered portions.

The next day (July 21), frequent explosions were audible at the foot of the mountain, and the crater began to throw out scoriaceous lapilli of a juvenile lava, besides ash. The same state of affairs continued the following day. The ejection of scoriaceous lapilli would seem to indicate that a more or less fluid, juvenile lava, from which the lapilli were formed, appeared in the crater floor where the old detritus and solid lava plug had been swept away by the explosions during the preceding days.

Since the middle of the night of July 22, the emission of ash clouds fell off markedly, while the explosions were becoming more frequent with noises like those caused by working the bellows—facts seem-

ing to indicate that the liquid lava, which by this time had became exposed in the crater, was being scattered about by the explosions in and around the crater, chiefly in the forms of bombs and coarser lava blocks, instead of in the form of finely comminuted ash. Thus on July 23, ejections of bombs were frequent, although on this day, none of them were able to reach so far northward as the Hayono-tairo atrio.

For the next three days (July 24~26) summit eruptions were most violent, with almost continual explosions and rumblings. Thus on July 25, when we observed the activity at close range in the northwestern part of Hayono-tairo, there were two major centres of eruption, in addition to the first centre of activity in the Oana crater, which was throwing up only light-grayish ash clouds—one (the second centre of activity) on the boundary between the upper crater and the Oana, the other (the third centre of activity) within the upper crater. The third centre of activity was throwing out incandescent bombs every few seconds, with flashes and explosions accompanying severe air-quakes, while the second centre of activity was throwing up black, dense, ash clouds, occasionally charged with non-incandescent bombs, at somewhat longer intervals. It was also found on this day that the accumulation of new ejecta in the Oana crater was growing into a conical mound (new central cone), whose top, however, was still far below the southern rim of the Oana crater.

On July 27, the summit eruptions appeared to decline somewhat with less frequent explosions, but with more active emissions of black ash clouds. After this temporary lull, the eruptions resumed toward the end of the month, with frequent explosions accompanying ejections of incandescent bombs. From July 31 and onward, explosions occurred frequently, but with decreasing intensity, until August 5, when activities practically ceased.

Judging from the events that have been followed thus far in their chronological sequence, the summit eruption that lasted for 24 days from July 13 to August 5, may be divided into three periods: (1) the activity from July 13 to July 23, during which its culmination was nearing with the shattering of the old crater floor and the rising of new fluid lava from below; (2) the culmination of the eruptions from July 24 to July 30, with continual explosions accompanying ejections of incandescent material;[26] (3) the slow subsidence of activities from July

26) It was possibly during this period of activity that a small mass of fluent lava flowed out, reaching a point immediately above the level of the western rim of the upper crater, although the exact time of its outflow could not be ascertained.

31 to August 5. In accordance with the sequence of activities, the micro-tremors recorded at Kamituki showed a gradual increase and decrease in number as well as in their amplitudes respectively in the earlier and later periods of the activity, with a maximum during the period from July 24 to July 30. In contrast to this, the earthquakes recorded at Kamituki and three other places in the island showed a rapid decrease in number from a maximum in July 14 to almost nothing in the period from July 24 to July 30, interrupted by a slight increase in July 18—facts indicating that the summit activity caused a number of micro-tremors, especially during its culmination, although its intensity was not sufficient to cause such a severe earthquake that could be recorded at the foot of the mountain. During the culmination of the summit activity, a great number of explosions occurred with ejection of incandescent material, but the ejected material were for the most part of comparatively small volume, and the intensity of the explosions low when compared with those of Asama, for example. It is inferred that the explosions in the culminating period took place near the surface of a lava pool that was probably formed in the summit crater. This inference is equally justified, whether it be based on the heights of the explosion clouds or on the range of scatter of the ejecta.

(To be continued).

圖版第十一乃至二十四 横須賀鎭守府檢閲濟

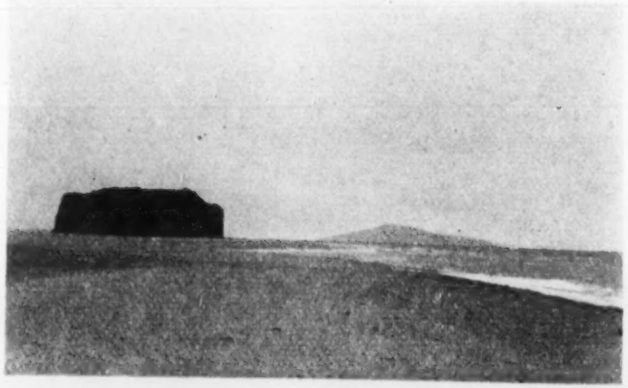

Fig. 6. Miyake-sima (right) as seen from the southeast coast of Nii-sima.
Photo Tsuya.

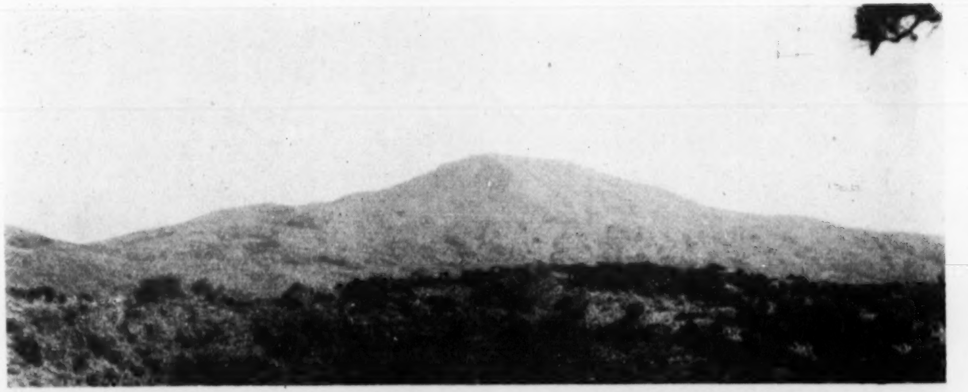

Fig. 7. The somma of the Miyake-sima volcano. View from Kamituki looking south. The lava-flow of 1874 is seen in the foreground.
Photo Minakami.

Fig. 8. The central cone, Oyama, viewed from the top of the northeastern somma looking southwest. Photo Tsuya.
S: Somma. *H*: Atrio (Hayono-tairo).

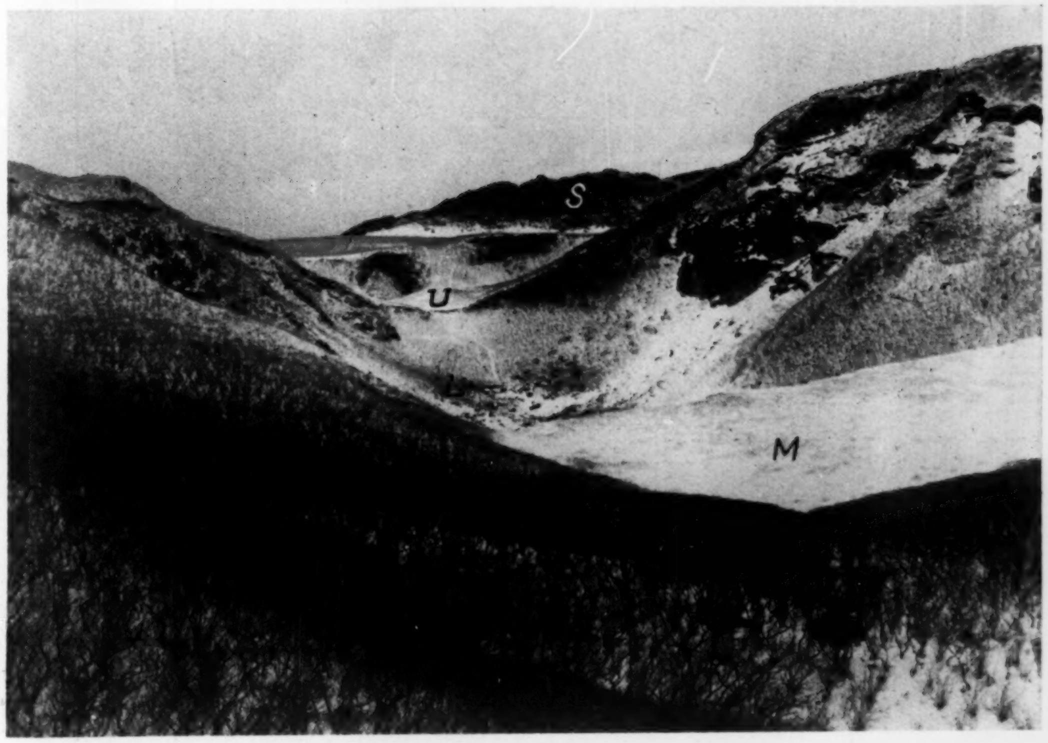

Fig. 9. March 7, 1936. Three old craters on the summit of the central cone, looking west from the rim of the easternmost crater (*M*).

Photo Sakuta.

(震研彙報 第十九號 圖版 津屋)

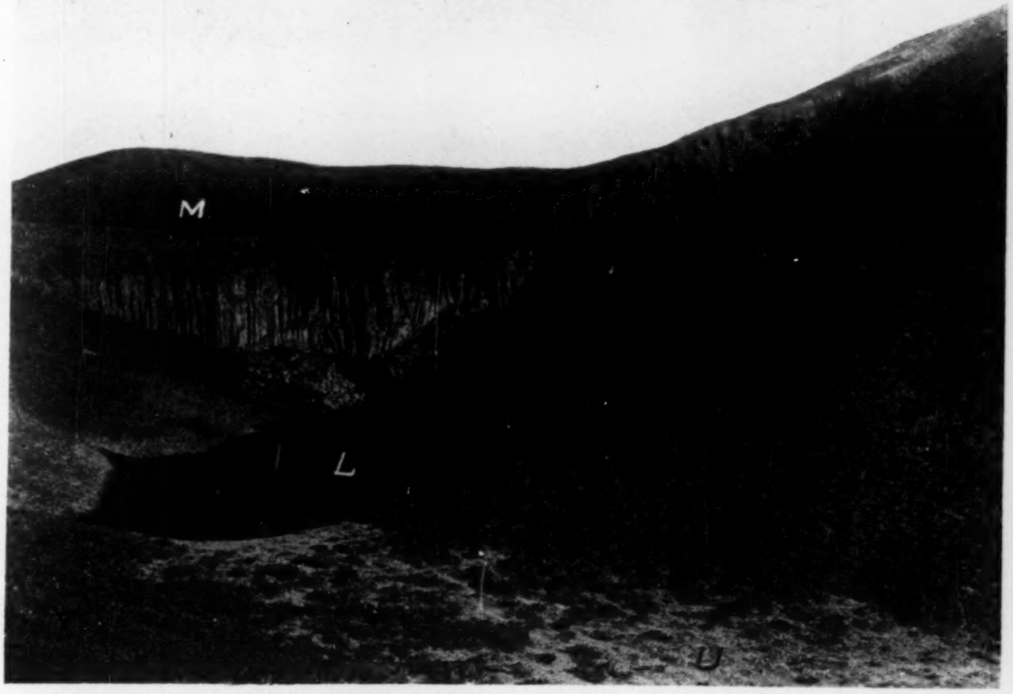

Fig. 10. Nov. 10, 1934. Three old craters on the summit of the central cone, looking east from the rim of the westernmost crater.

Photo Sakuta.

 [Bull. Earthq. Res. Inst., Vol, XIX, Pl. XIII.]

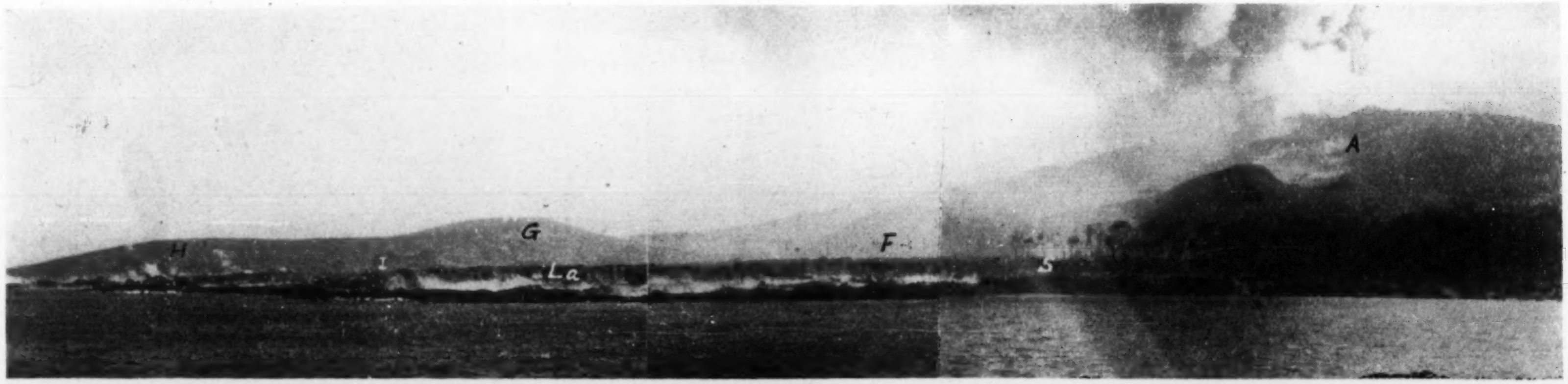

Fig. 11. July 21, 1940. The northeast flank of the somma, looking southwest, after the eruption of July 12~13, 1940.

A: The uppormost one of the new craters on the flank. *F*: Former sea-cliff of Akabakkyô. *G—H*: New parasitic volcano (Hyôtan-yama) formed by the eruption in Akabakkyô Bay. *La*: A new lava-flow (Akabakkyô lava). *S*: Village of Simasita, now buried beneath the Akabakkyô lava. *Ta*: Taka-yama, an old parasitic cone.

Photo Tsuya.

Fig. 12. July 21, 1940. The northeast flank of the somma, looking northwest, after the eruption of July 12~13, 1940.

D: One of the new craters on the flank. *Di*: Daihannya-yama, an old parasitic cone. *G—H*: Hyôtan-yama.

Photo Tsuya.

(震研彙報 第十九號 圖版 津屋)

Fig. 13. July 26, 1940. View of Hyôtan-yama, as seen southward from Anôsaki. Photo Tsuya.

Fig. 14. July 22, 1940. The Akabakkyô lava flow covering the village of Simasita. Photo Tsuya.

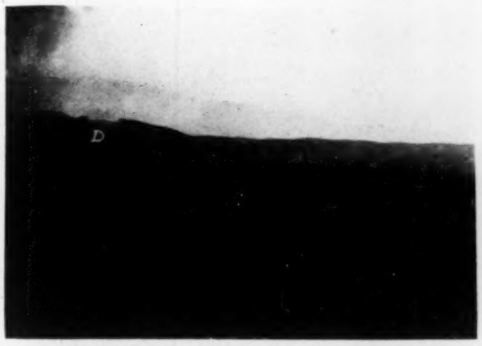

Fig. 15. July 17, 1940. A new parasitic crater (*D*) in the middle the left and the bomb-covered slope in foreground. Photo Tsuya.

Fig. 16. July 22, 1940. The Yoridaisawa lava-flow, looking upstream (west). Photo Tsuya.

Fig. 17. July 17, 1940. Hyôtan-yama, looking north. Photo Tsuya.

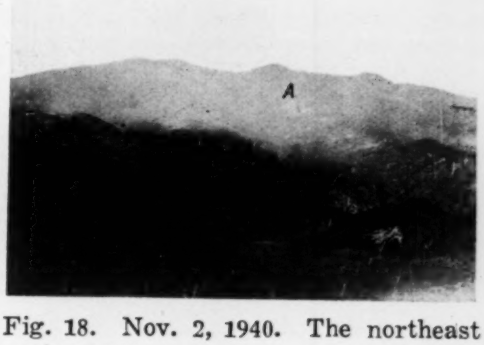

Fig. 18. Nov. 2, 1940. The northeast flank of the somma, as seen southwestward from Akabakkyô.

A: The uppermost of the new craters on the fank. *D*: Another new crater. *La*: Akabakkyô lava in the valley on the border between Kamituki and Tubota.

Photo Tsuya.

(震研彙報 第十九號 圖版 津屋)

Fig. 19. July 25, 1940. Fumarolic activity of the new parasitic volcano, Hyôtan-yama, after the eruption of July 12~13, 1940. Photo Sakuta.

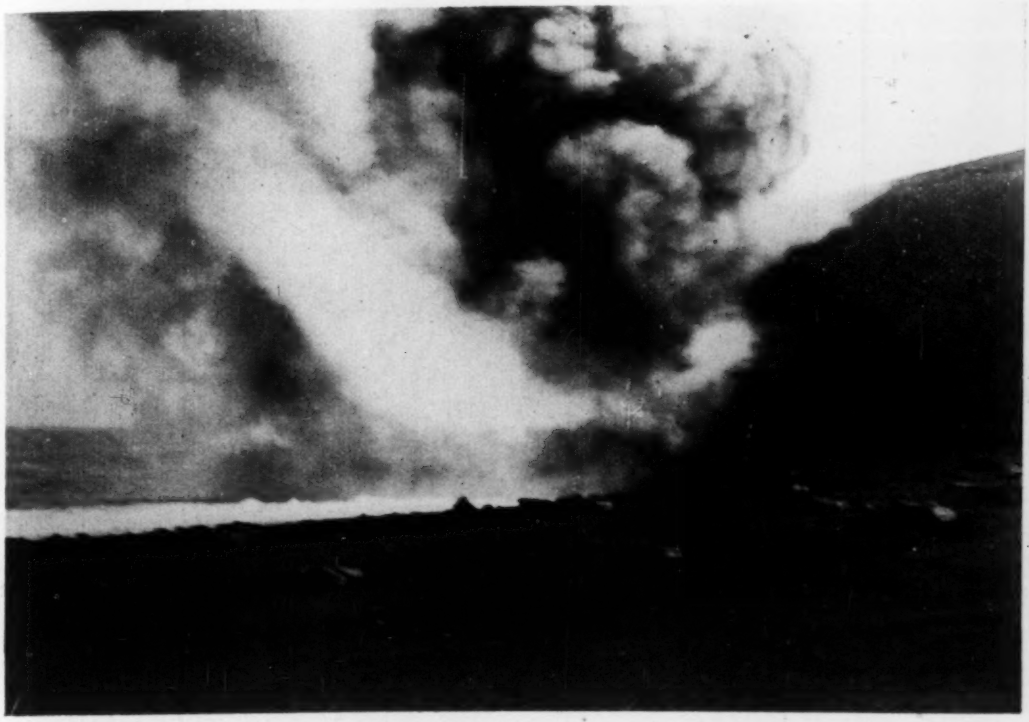

Fig. 20. Sept. 14, 1940. One of the minor explosions that occurred in Sept., 1940, on the eastern shore of Hyôtan-yama. Photo Sakuta.

Fig. 21. July 14, 1940. The summit eruption of Miyake-sima, looking south. Photo Suzuki.

Fig. 22. July 19, 1940. The summit eruption. View from near Maru-yama, looking southwest. Photo Tsuya.

Fig. 23. July 22, 1940. The summit eruption, looking west from Anô-saki. Photo Tsuya.

Fig. 24. July 22, 1940. Ash falling from the eruption cloud being bent toward Miike. Photo Tsuya.

Fig. 25. July 22, 1940. Ash cloud veering northeast toward the Pacific, as seen from Miike. Photo Tsuya.

Fig. 26. July 29, 1940. The summit eruption. View from Ako looking east. Photo Sakuta.

(震研彙報 第十九號 圖版 津屋)

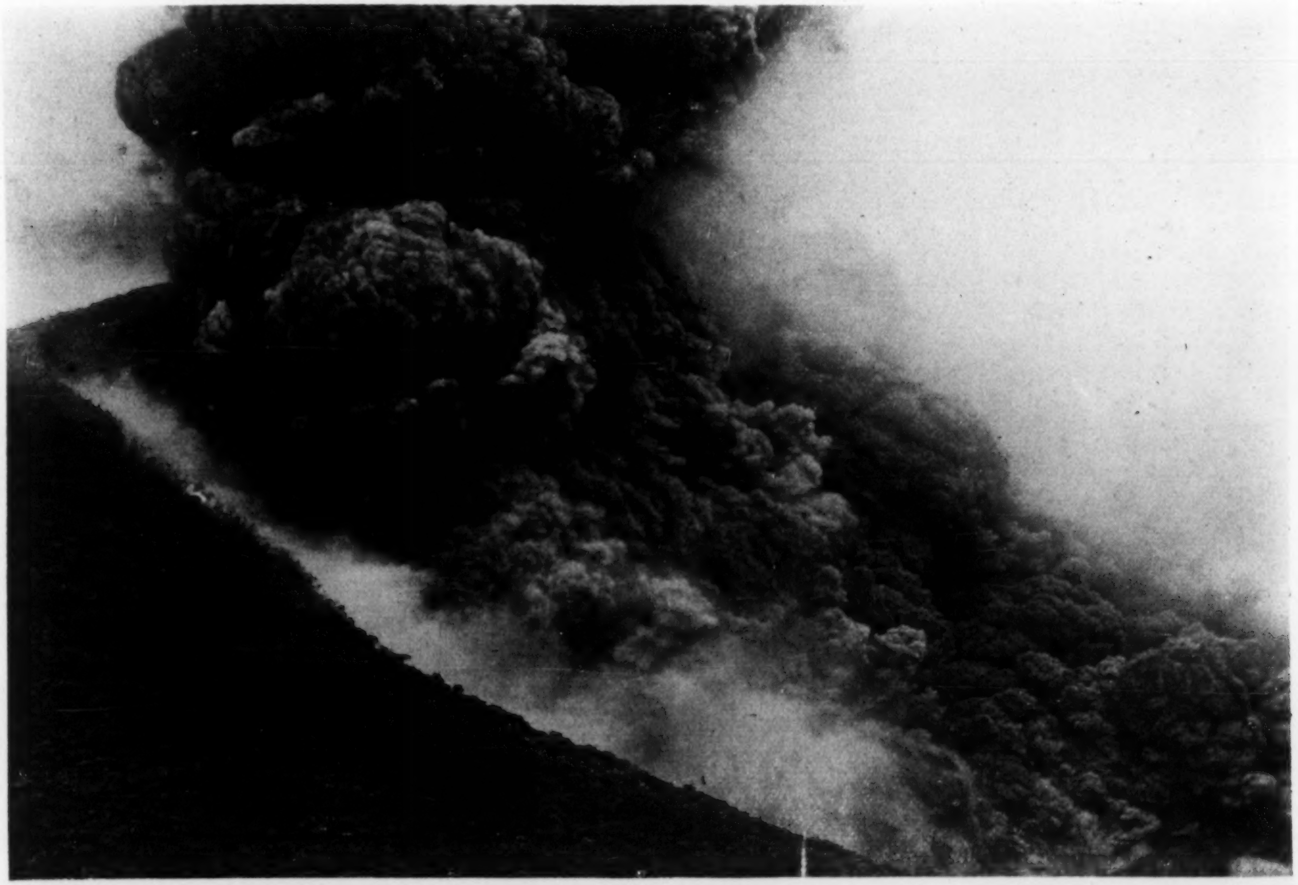

Fig. 27. July 21, 1940. Ash cloud rising from the northwestern part of the Oana crater. View from the southwestern rim of the upper crater looking northeast. Photo Sakuta.

(震研彙報 第十九號 圖版 津屋)

Fig. 28. July 22, 1940. Ash cloud rising from the summit crater and veering toward Akabakkyô.
Photo Tsuya.

Fig. 29.

Fig. 30.

Fig. 31.

Fig. 32.

Fig. 33.

Fig. 34.

Various phases of the summit eruption, as seen from the top of the northeastern somma. Figs. 28, 29. July 23, 1940. Figs. 30~34. July 25, 1940.

Photo Tsuya.

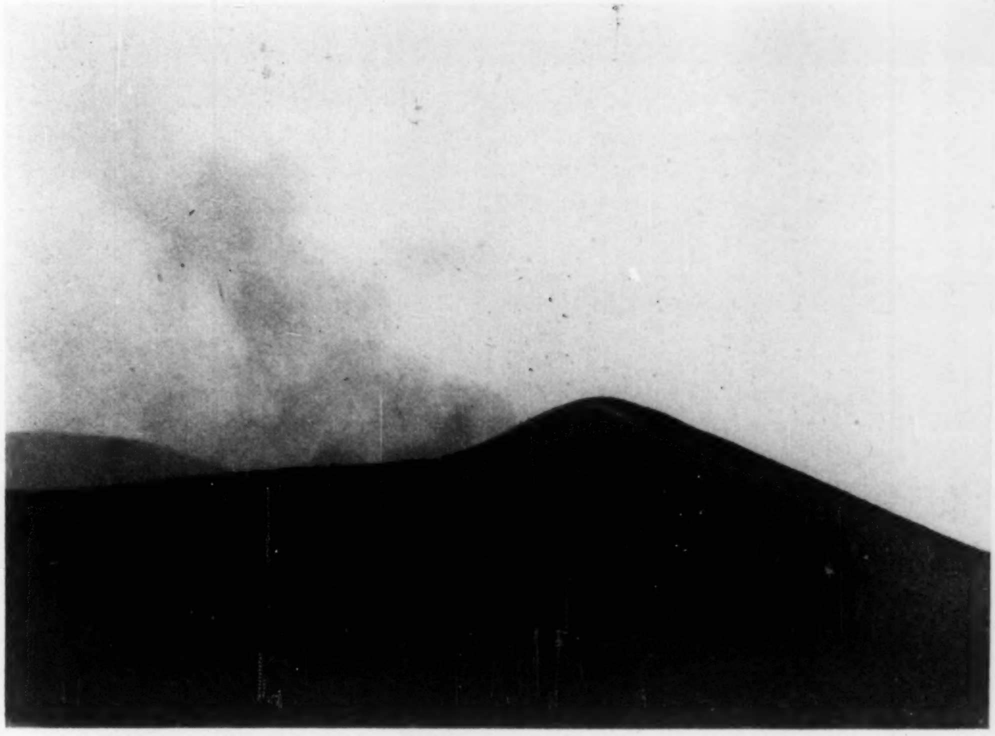

Fig. 35.

Figs. 35, 36. July 25, 1940. Ejection of volcanic bombs, as seen from the top of the northeastern somma. Photo Tsuya.

（震研彙報 第十九號 圖版 津屋）

Fig. 37.

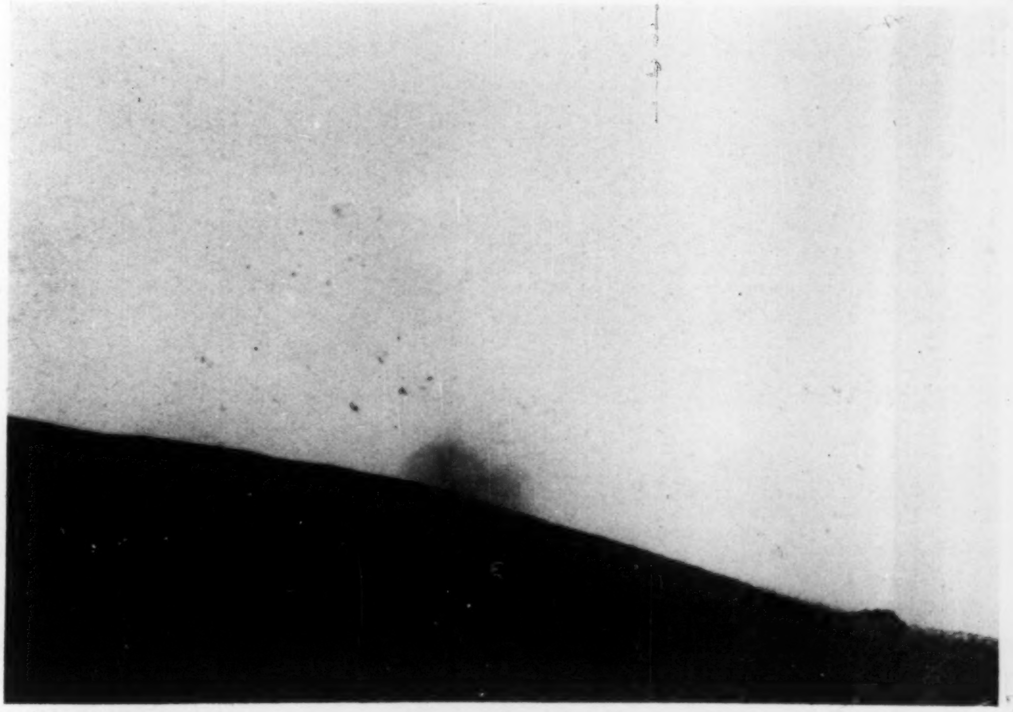

Figs. 37, 38. July 25, 1940. Ejection of volcanic bombs, as seen from the northern foot of the central cone. Photo Tsuya.

Fig. 39.

Fig. 40.

Fig. 41.

Fig. 42.

Fig. 43.

Fig. 44.

Figs. 39~44. July 25, 1940. Various phases of the summit eruption, as seen from the western part of Hayôno-tairo (atrio). Photo Tsuya.

(震研彙報 第十九號 圖版 津屋)

Fig. 45. July 25, 1940. Same view as Figs. 38～43.
Photo Suzuki.

Fig. 46. July 25, 1940. Ejection of volcanic bombs, looking east.
Photo Suzuki.

Fig. 47. Aug. 1, 1940. A declining phase of the summit eruption. Ash cloud rising from the new central cone. The north wall of the old Oana crater is seen in the left. Photo Sakuta.

Fig. 48. Oct. 25, 1940. Same view as Figs. 38~43, showing the new central cone. Photo Tsuya.

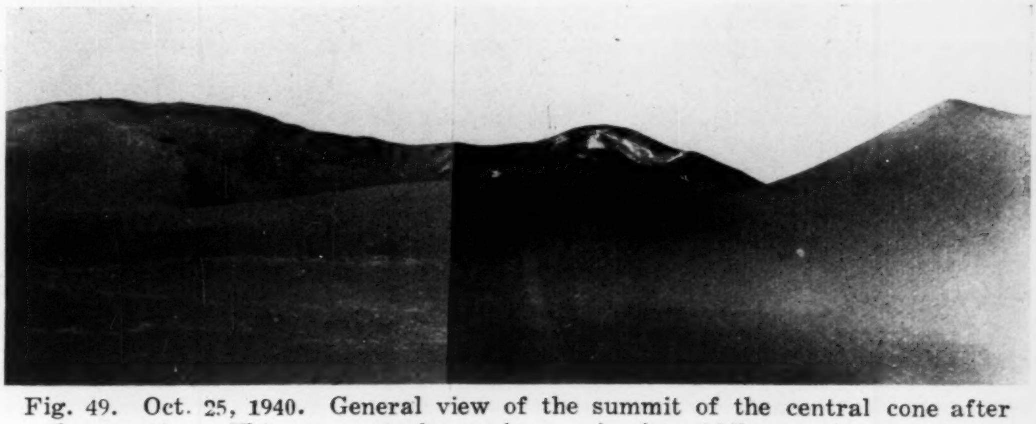

Fig. 49. Oct. 25, 1940. General view of the summit of the central cone after the eruption. The new central cone is seen in the middle. Photo Tsuya.

(震研彙報 第十九號 圖版 津屋)

Part II. The Temperature of Lava.

By Takesi NAGATA,

Earthquake Research Institute.

(Read Sept. 18, 1940.—Received Mar. 20, 1941.)

In the Akabakkyô lava, which flowed down probably during the night of July 12, 1940, there were several places that remained incandescent, or red hot, for some time after the flow, although the larger part of the surface of the lava had already solidified, showing on July 15 a temperature of less than 150°C. The temperature inside the lava, however, seemed to be fairly high, as we could see the incandescent lava through the fissures on the solidified surface of the lava flow. Through these openings, the temperature inside the lava flow was measured by means of an optical pyrometer. From calibrations of this instrument, the mean error in measuring temperatures of about 1000°C is less than 15°C. Observations made at ten points at four places in the lava flow will now be described.

(I) As shown in Fig. 1, the first observation was made at the northern end of the lava flow, the thickness of which, here, was about 3 meters. Through an opening one meter deep the temperatures at the bottom at two points A and B were observed, the results being shown in Table I.

Table I.
Place I. July 15, 15 h 30 m.

Observation Point	A(d=1·0 m)	B(d=1·0 m)
Temperature	935°C 938 940 929 926	962°C 968
Mean	934±5°C	965±3°C

It should be noted, however, that the temperature at these points declined so rapidly that on July 16 it was impossible to measure it with the pyrometer in the daytime. Estimating the temperature on that day from the colour, it was about 700°C. Seeing that a few large pine trees were knocked down in the neighbourhood of the observation point, and since the roots and the other lower parts of these trees were burnt off, there is the probability that the incandescent hot parts of the lava, where the temperature was observed, was due to burning of the roots of these trees inside the hot

lava flow. This presumption would explain the high velocity of cooling.

(II) The second observation point was in a fissure in the lava flow, about 2 m deep and 2 m wide, and about 30 m south of the first point, as shown in Fig. 1. Around this place, a large number of bombs and lapilli were piled on the surface of the lava. Through a number of gaps between the ejecta on the inside wall of the fissure, a few incandescent parts could be seen, namely, A, B, and C in Fig. 2. The temperature of the bottoms of these openings were measured on July 20, the results being shown in Table II, where d denotes the depth of the openings.

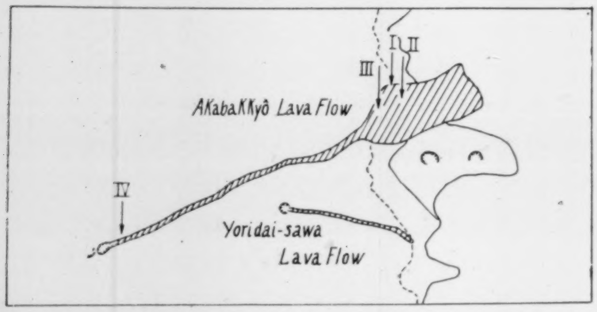

Fig. 1. Points where the temperature of lava was measured.

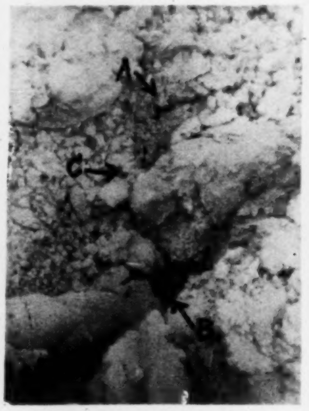

Fig. 2. The second observation point.

Table II. Place II. July 29, 14 h 20 m.

Observation Point	A(d=0·5 m)	B(d=1·0 m)	C(d=0·5 m)
Temperature	881°C	902°C	873°C
	870	910	887
	880	913	
Mean	877±5°C	908±4°C	880±7°C

(III) The third place was about 40 m west of the second, in the neighbourhood of which a number of red-hot parts could be seen through the cracks on the surface of the lava flow and through the gaps between large bombs. The results obtained on July 20 at their most incandescent part are given in Table III.

Table III. Place III. July 20, 14 h 45 m.

Observation Point	A(d=1·5 m)	B(d=0·8 m)	C(d=0·5 m)
Temperature	968°C	867°C	924°C
	952	878	913
	970	878	
Mean	963±7°C	874±5°C	919±6°C

On July 21, the temperatures of these points were re-observed, the results being shown in Table IV.

Table IV. Place III. July 21, 13 h 40 m.

Observation Point	A	B	C
Temperature	952°C	847°C	890°C
	942	852	890
Mean	947±5°C	850±3°C	890°C
Difference	−16°C	−24°C	−29°C

As given in these tables, the temperature inside these openings in the lava flow declined at the time at the rate of from 15° to 30°C a day. The larger the depth of the opening (d) the smaller was the cooling rate—a fact that may show that the rather rapid cooling observed was chiefly due to air convection on its touching the hot parts, and to radiation, and only very slightly to thermal conduction through the rock itself.

(IV) The fourth place was near the upper end of the lava flow, about 2 km south-west of the foregoing three places. In the northern slope of the eruption-fissure, we found a pit of elliptical shape, 2.5 m in its major axis, 1.5 m in its minor axis, and about 2 m deep. Near this point were piled a large number of giant bombs and lapilli, all covered with a layer of volcanic ash. On July 18, a part of the bottom of the pit, shaped like a crescent, was incandescently hot. The observed temperatures at two of the most incandescent points in the bottom are given in the annexed table.

Table V.
Place IV. July 18, 15 h 20 m

Observation Point	A(d=2·0 m)	B(d=2·0 m)
Temperature	968°C 960 951 942 949	930°C
Mean	954±8°C	

Putting together these results, we may conclude that the temperature of the lava flow or of the large mass of accumulated giant bombs at a point deeper than one meter from their upper surface during a period of from 3 to 9 days following their ejection, was at least about 850∼960°C. This temperature is less than that of the incandescent lava flow from Mt. Vesuvias[1] (about 1100°C) and those of the lava pools

1) A. MALLADRA, *Rep. Acad. Sci. Napoli*, **25** (1919), 1.

of various active volcanoes, i. e. Etna[2] (about 1100°C), Kilauea[3] (about 1200°C), Mihara[4] (1060°C), Asama[5] (more than 1000°C), and others. It is, however, nearly the same as the temperature (870°~965°C)[6] inside the cracks on the solidified surface of the lava covering the crater bottom of Volcano Mihara during its activity of 1911~1914.

Taking into consideration the circumstances of our observation and the time difference in that of our measurement and that of the ejection of the lava, we are confident of the reliability of these results. From this conclusion, it may be presumed that the temperature at a point immediately below the upper surface of the lava flow was more than 1000°C at the time it was just ejected, while the temperature of the inner part of the lava flow, with which the open air had no direct contact, would be still about 900°C or more about a week after its ejection. According to T. Hagiwara[7], as late as July 19 and for a few days following it, the Akabakkyô lava flow, on a gentle slope, was still moving down with fair velocity. This fact also shows that the interior of the lava flow had a fairly high temperature at that time.

2) G. PLATANIA, *Rep. Acad. Lincei*, (1912), 499.
3) T. A. JAGGAR, *Journ. Washington Acad. Sci.*, **7** (1917), 397.
4) R. TAKAHASI and T. NAGATA, *Bull. Earthq. Res. Inst.*, **15** (1937), 1047.
5) T. MINAKAMI, *Not Published.*
6) K. FUJI, *Proc. Phys. Math. Soc. Japan*, **7** (1914), 243.
7) T. HAGIWARA, *Zisin*, **12** (1940), 478. Part III of this report.

Part III. Viscosity of the Akabakkyô Lava.

By Takahiro HAGIWARA,

Earthquake Research Institute.

(Read Sept. 15, 1940—Received March 20, 1941.)

A remarkable phenomenon connected with the eruption of Miyake-sima, July 12, 1940, was the Akabakkyô lava flow.[1] The molten lava of andesitic basalt that welled out of the upper part of the fissure opened by the eruption on the mountain side, 400 or 500 m above sea level, flowed down the valley, buried several houses on the seashore, and filled the bay of Akabakkyô. The total volume of the lava that flowed out is estimated at 6×10^6 cubic meters.[2] This lava outflow occurred soon after the first eruption. The charcoal-burners ran down the sledge-way on the ridge on the left-hand side of the valley through which the lava flowed down. At that time, the lava was already flowing down the valley. These charcoal-burners, running down with all their might, saw the front of the lava flow moving at the same speed with which they were fleeing. If their statement may be trusted, it is possible to estimate the viscosity of the molten lava in order to flow with such velocity.

We shall consider a very simple one-dimensional case, in which an incompressible liquid of constant thickness h flows downward by its own gravity on a plane inclined at an angle α (Fig. 1). Since, in the steady state, the liquid is regarded as being in laminar motion, the equation of motion is written as follows, putting the origin at the surface of the liquid and taking the x-axis toward the bottom:

$$\mu\frac{d^2w}{dx^2}+\rho g\sin\alpha=0,$$

where w is the velocity of the liquid, μ the viscosity coefficient of the liquid, ρ the density of the liquid, and g the gravity acceleration. If we integrate this equation and put $\mu\frac{dw}{dx}=0$ at $x=0$ and $w=0$ at $x=h$, we get for w

1) A detailed description of this eruption was made by H. Tsuya. [H. TSUYA, *Bull. Earthq. Res. Inst.*, **19** (1941), 263.]

2) S. OMOTE, *Bull. Earthq. Res. Inst.*, **19** (1941), 382.

$$w=\frac{\rho g\sin\alpha\,(h^2-x^2)}{2\mu}, \quad \text{or} \quad w_{x=0}=\frac{\rho g\sin\alpha h^2}{2\mu}.$$

The mean inclination angle of the valley in which the lava flowed down is about 17°, so that $\sin\alpha$ may be put 0·3. Putting $w=4$ m/sec (100 m per 25 sec), $\rho=2$, and $h=10$ m, we get $\mu=7\times10^5$ c.g.s.. Actually, the bottom is not a plane, so that there is the effect of the side-face of the valley, while there must be a more complex motion at the front of the flow, whence the actual front velocity of the flow must differ from the foregoing calculation. However, since all these conditions operate to diminish the velocity, the calculated value of μ must exceed the real viscosity coefficient. From this standpoint, the actual viscosity coefficient of the lava, when it welled out, might have been of the order of 10^5 c.g.s.. The temperature of the lava when it welled out is believed to have been slightly higher than 1000°C, as estimated from optical pyrometer measurements of it made by Nagata[3] at Akabakkyô.

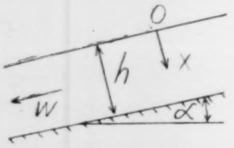

Fig. 1.

Nagata,[4] calculating from the damping motion of the lava generated by the gas explosion, obtained the value 5×10^4 c.g.s. (temperature 1060°C) for the viscosity coefficient of the molten lava of andesitic basalt in the central crater of Volcano Mihara, Oosima. Nichols[5] has calculated the viscosity coefficient of the basalt of the Alika flow (1919) of Mauna Loa and of the 1887 flow of the Kau district, Hawaii, assuming that the flow was in laminar motion, and that the density is 1·4. The temperature of these lavas when they flowed down is believed to have been between 1150° and 1200°C.

	Alika flow	1887 flow
Velocity of flow	11 mile/hour (5 m/sec)	0·7 mile/hour (0·3 m/sec)
Mean depth	6 m	2 m
Mean width	9 m	1 km
Mean inclination angle	7°	4°
Calculated viscosity coefficient	$4{\cdot}3\times10^4$ c.g.s.	$4{\cdot}8\times10^4$ c.g.s.

(After Nichols)

The value in the case of Miyake-sima is a few times larger than those of Oosima and Hawaii.

3) T. NAGATA, *Bull. Earthq. Res. Inst.*, **19** (1941), 295.
4) T. NAGATA and R. TAKAHASI, *Bull. Earthq. Res. Inst.*, **15** (1937), 1047.
5) R. L. NICHOLS, *Journ. Geol.*, **47** (1939), 290.

Fig. 2. Panoramic view of Akabakkyô, (photo. on July 24).

A—Parasitic cones created in the sea,
B—Lava flow that filled the bay of Akabakkyô,
C—Upper end of the fissure eruption,
D—Lava welled out of this place,
E—Sankakuten-Yama.

Fig. 3. The lava was still seen creeping along the entrance of the valley (July 19).

It was not until July 19, a week after the first eruption, that it was possible to walk over the solidified lava flow. Although the surface of the lava had solidified, the red hot lavas underneath could be seen from the cracks here and there. The lava was still seen creeping along at the entrance of the valley, which sloped at an angle of 10°. The full line in Fig. 4 shows the measured amount of displacement of the lava at the middle point of the valley. The broken line in the figure is the velocity as calculated from the displacement curve. The width of the flow was about 10 m, but the amount of displacement of its surface was uniform on a line vertical to the flow. The measurements were taken at

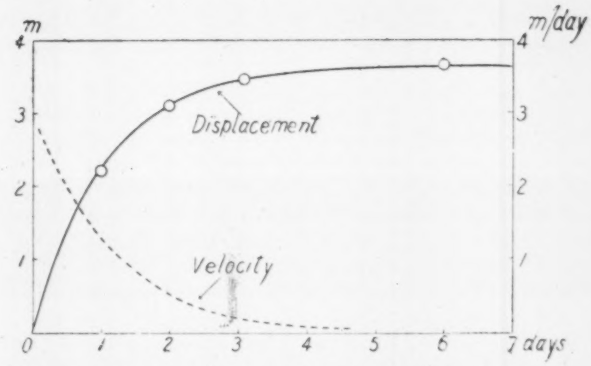

Fig. 4. Full line—measured amount of displacement of the lava. Broken line—velocity of the lava calculated from the displacement curve. The origin of the abscissa is taken at 12 h, July 19.

two separate points, distant 20 m along the flow, but the results obtained were the same. As will be seen from the figure, the velocity quickly decreased with lapse of time. When the measurement was begun, the surface of the lava was covered by blocks that had already solidified, but the interior was believed to be still red hot. Owing to the hot gases that issued from the crevices, it was not possible to stay on the blocks for any length of time. Nagata,[6] who measured the temperature of the red hot lava in the cracks, found it to be 900°C. Although the point where he measured it is about 100 m distant from the point where the velocity of flow was measured, the temperature may be regarded as being similar for the two points. The viscosity coefficient from the measurement of the velocity of the lava in the present case is expected to be very large, because in the foregoing the value 10^5 was obtained against the velocity 4 m/*sec*, while the value of the velocity in the present case is as small as 3 m/*day*. As a matter of fact, by the same calculation, we got 10^{10} as the viscosity coefficient of the lava a week after the outflow. In proportion to the drop in temperature, the rise in the viscosity coefficient is very large. Such an increase seems to be due largely to progressive crystallization of the rock minerals and to loss of the volatile substances that were held in the lava.

Finally, we shall refer to Kani's[7] laboratory experiment, in which he measured the viscosity coefficient of the dry melt of various samples of volcanic rocks. The following is a result obtained by him for the andesitic basalt from Motomura, Oosima, which is akin to the Akabakkyô lava.[8]

Temperature	Viscosity coefficient of dry melt of Motomura lava.	Temperature	Viscosity coefficient of dry melt of Motomura lava.
1400	138	1200	31200
1300	259	1150	79500
1250	542		

(After Kani)

The viscosity coefficient for temperatures lower than 1150°C could

6) T. NAGATA, *loc. cit.*.

7) K. KANI, *Proc. Imp. Acad., Japan*, **10** (1934), 82.

8) The chemical components of the two andesitic basalts, Akabakkyô lava and Motomura lava, are as follows.

	Motomura lava.	Akabakkyô lava.		Motomura lava.	Akabakkyô lava.
SiO_2	51·80	56·07	K_2O	0·32	0·82
Al_2O_3	15·00	15·26	H_2O	0·62	0·03
Fe_2O_3	3·68	4·48	TiO_2	0·60	0·36
FeO	10·14	10·34	P_2O_5	0·31	0·11
MgO	5·36	3·33	MnO	0·20	tr
CaO	9·77	7·22	Total	100·56	100·51
Na_2O	1·79	2·49		(After Kani)	(After Tsuya)

not be measured with his apparatus owing to the rapid increase of viscosity. Neither is it possible to compare briefly the viscosity of the Akabakkyô lava flow with that of Motomura lava, because the exact temperature of the former is not known, while in the latter the volatile stage was missed. However, by assuming that the viscosity of lava diminishes with increase of the volatile substances held in it, the foregoing conclusion that the Akabakkyô lava flow had a viscosity coefficient of 10^5 and a temperature slightly exceeding 1000°C may be regarded as rigorous compared with Kani's experiment.

Part IV. Magnetic Properties of New Volcanic Ejecta.

By Takesi NAGATA,

Earthquake Research Institute.

(Read Sept. 18, 1940 and Feb. 20, 1941.—Received March 20, 1941.)

1. Introduction.

It is scarcely necessary to stress the fact that the anomalous distribution of geomagnetism and its variation at any place is closely related to the magnetic properties of the rocks composing the earth's crust there and in its neighbourhood, as has been frequently pointed out by a number of investigators. In order to examine the reliability of the anomalous geomagnetic change observed at Miyake-sima after the severe volcanic activity it has displayed, a knowledge of the magnetic properties of the rocks composing this volcanic island as well as those of the new ejecta is also required. For this reason, the magnetic susceptibility in a weak magnetic field and its changes due to temperature variation, the intensity and direction of the natural remanent magnetization, and the characteristic quantities of the magnetization during cooling of several rock specimens from Miyake-sima were experimentally examined. The measuring apparatus and the method of observation will be dealt with in other papers, only the results of the experiments and their possible relations to the geomagnetic anomaly being considered here.

2. Rock specimens.

Three of the rock specimens examined in the present study were from the new lava flow, while there were besides five bombs ejected from the craters of Hyôtan-yama, two from the central cone, and two rocks from the old Meizi-lava flow. The localities of these rocks and their petrological characteristics[1] are as follows,

No. 1. (N–58) Akabakkyô lava flow
(olivine-hypersthene-pyroxene-basaltic-andesite),

1) See Part I of this report (By H. Tsuya).

No. 2. (N–59) Akabakkyô lava flow (in the sea) (olivine-hypersthene-pyroxene-basaltic-andesite),

No. 3. (N–60) Yoridai-sawa lava flow (olivine-hypersthene-pyroxene-basaltic-andesite),

No. 4. (N–57) Bomb from the central cone (O-yama) ejected July 25, 1940, (olivine-two-pyroxene-basaltic-andesite),

No. 5. (N–75) Bomb from the central cone ejected early August, 1940, (olivine-two-pyroxene-basaltic-andesite),

No. 6. (N–64) Bomb from the crater of Hyôtan-yama, (collected north of the Akabakkyô lava flow), (pyroxene-olivine-basalt),

No. 7. (N–65) Bomb from the crater of Hyôtan-yama, (collected at the same place as No. 6), (pyroxene-olivine-basalt),

No. 8. (N–63) Bomb from Hyôtan-yama, (collected south of the Akabakkyô lava flow), (pyroxene-olivine-basalt)

No. 9. (N–61) Bomb from one of the craters in the upper part of the eruption fissure,

No. 10. (N–62) }
No. 11. (N–66) } Meizi lava flow at the northern slope of the island (olivine-augute-basalt).

The chemical and normative compositions of two specimens from the rocks described above, as determined by H. Tsuya[2], are reproduced in Table I from his paper.

Table I. Chemical Composition of Ejecta from Miyake-sima.

	No. 1	No. 6	No. 11	Norms	No. 1	No. 6	No. 11
SiO_2	56·07	53·01	53·35	Q	14·59	12·67	9·61
Al_2O_3	15·24	14·83	15·62	Or	2·23	2·78	5·01
Fe_2O_3	4·48	5·35	4·21	Ab	20·97	14·68	18·35
FeO	10·05	9·98	8·12	An	29·48	31·15	30·32
MgO	2·57	3·82	4·44	Wo	4·99	6·85	7·48
CaO	8·34	9·97	9·18	En	6·42	9·54	11·05
Na_2O	2·45	1·76	2·68	Fs	14·25	12·79	9·50
K_2O	0·34	0·46	0·84	Mt	6·48	7·89	6·02
$H_2O(+)$	0·01	0·01	0·40	Il	0·68	1·21	2·28
$H_2O(-)$	0·02	0·01	*n·d*	Ap	t_r	0·66	—
TiO_2	0·36	0·61	1·18				
P_2O_5	0·03	0·32	—				
MnO	t_r	t_r	t_r				
Total	99·93	100·13	100·02				

2) H. TSUYA, Part I of this report. *Zisin.*, 12 (1940), 477.

From the foregoing description, the rocks newly ejected from Miyake-sima, associated with the volcanic activity of July 1940, are generally basic, namely, basalt or at least basaltic andesite, while according to Tsuya[3], the rocks composing this island and the old ejecta are also basalt, i. e. olivine-basalt, augite-olivine-basalt, olivine-two-pyroxene-basalt, two-pyroxene-basalt (the somma), and augite-olivine-basalt (central cone lava), these rocks containing from 4 % to 6 % by weight of normative-magnetite.

From these petrological and chemical data, we may expect the rocks from Miyake-sima to possess a fairly intensive magnetic character, like the usual basaltic rocks.

3. Magnetic Susceptibility.

The instrument for measuring the magnetic susceptibility of rocks in a weak magnetic field was already described in the writer's previous paper[4]. The observational error in measuring susceptibility by means of this instrument is always less than 0·1 percent. The observed values of the specific magnetic susceptibility of the rocks of Miyake-sima in various applied magnetic fields of from 0·6 Gauss are given in Fig. 1.

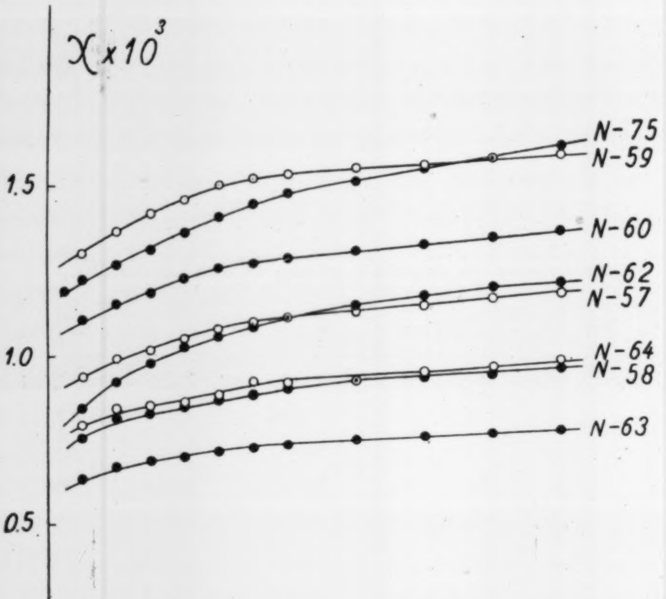

Fig. 1. Magnetic specific susceptibility of rocks from Miyake-sima.

Some typical examples of hysteresis phenomenon in the magnetization curve with the process 0→+19→0→−19→0→+19 Gauss are shown in Fig. 2. What is notable in these results is that the specific magnetic susceptibility of the new ejecta from Miyake-sima exceeds $0{\cdot}6\times10^{-3}$, and is less than $1{\cdot}3\times10^{-3}$ in the earth's

3) H. TSUYA, *Bull. Earthq. Res. Inst.*, **15** (1937), 295.
4) T. NAGATA, *Bull. Earthq. Res. Inst.*, **18** (1940), 102.

magnetic field of 0·45 Gauss. Seeing that the bulk density of the rocks is 1·27~2·57, (see Table II), we can estimate the magitude of susceptibility as $1{\cdot}0\times10^{-3}\sim3{\cdot}4\times10^{-3}$.

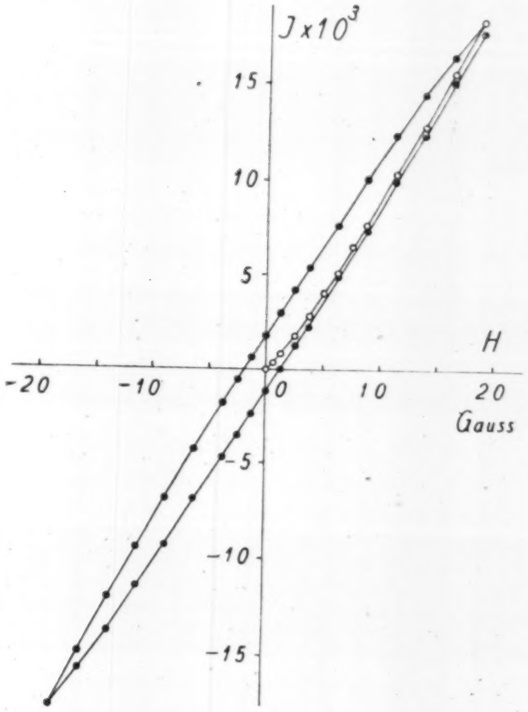

Fig. 2 a. Hysteresis loop of specimen No. 1 (N–58).

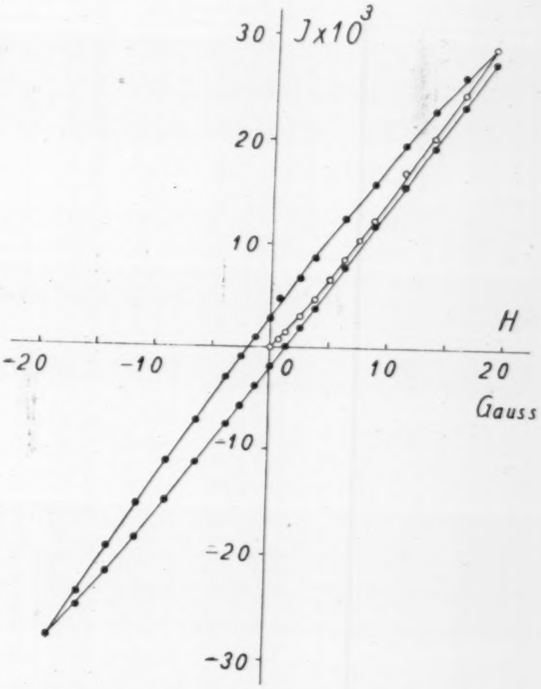

Fig. 2 b. Hysteresis loop of specimen No. 5 (N–75).

These magnetic susceptibilities, however, are considerably less than those expected from the chemical composition of the rocks. Dealing only with such rock specimens as those whose chemical composition, and therefore their normative compositions also, are given, the ratio of the susceptibility to the normative content of magnetite $\beta\equiv\chi/C_{Mt}$ works out as follows,

Sample	χ_0	C_{Mt}	β
No. 1	$0{\cdot}76\times10^{-3}$	6·48 %	$1{\cdot}17\times10^{-2}$
No. 6	0·85 〃	7·87	1·02 〃
No. 11	0·80 〃	6·02	1·41 〃

Comparing these values of β with its standard value that was obtained as the mean of 25 specimens of Japanese volcanic rocks[5], that is,

5) T. NAGATA, *Zisin*, **12** (1940), 111.

$$\beta = (2{\cdot}67 \pm 0{\cdot}17) \times 10^{-2}, \tag{1}$$

it will be found that the former are much smaller than the latter, while according to J. G. Koenigsberger[6], R. Chevallier[7], Y. Kato[8], and the writer[9], β is given by

$$\beta = \frac{\chi}{C_{Mt}} = \frac{K_0}{\rho_0[1+(\lambda - p\nu)K_0]} \doteq \frac{K_0}{\rho_0[1+\lambda K_0]}, \tag{2}$$

where ρ_0 and λ are respectively the density and the demagnetizing factor of a particle of the ferromagnetic minerals.

Consequently, the large deviation of β of Miyake-sima rocks from the standard value is either because K_0 of the ferromagnetic mineral is too small or because λ is too large compared with the standard value, assuming that the ferromagnetic minerals are composed chiefly of normative magnetite as calculated from the chemical composition. Since these phenomena are related to the amount of impurity in the ferromagnetic mineral and to the crystallinity of the rock, a more detailed study of this problem will be made at another opportunity. We shall merely say here that, so far as the writer's knowledge is concerned, the presence of such a small value of β in Miyake-sima rock is noteworthy, although rocks having nearly the same or a rather smaller β may sometimes be found in the ejecta from Volcano Mihara, Oosima island.

As to the hysteresis phenomenon in the magnetization curve of a rock specimen, it was not possible to get the true value of the residual magnetization nor that of the coercive force, since the intensity of the saturation magnetic field of igneous rocks far exceeds 1000 Gauss, which strength was beyond the writer's apparatus.

However, a quantity sufficient for showing the relative magnitude of the magnetic hardness of a rock specimen, obtainable from the hysteresis loop with respect to a given constant process of variation in the applied magnetic field, was proposed[10] for the sake of convenience, namely, the ratio of the residual magnetization J_r to the initial susceptibility χ_0. Generally speaking, it seems that the larger the J_r/χ_0, the harder magnetically the rock. We are concerned with the residual magnetization in the magnetization curve of $(0 \rightarrow +18{\cdot}8 \text{ Gauss} \rightarrow 0)$.

In Table II are given the quantity mentioned above of a few specimens, where $J_r/J_0 \equiv J_r/\chi_0 H$ ($H = 1{\cdot}26$ Gauss) is given for convenience

6) J. G. KNIGSBERGER, *Beitr. Angew. Geophys.* **4** (1932), 385.
7) R. CHEVALLIER, *C. R. Paris.*, **194** (1932), 1468.
8) Y. KATO, *Sci. Rep. T hoku Imp. Univ.*, **27** (1938), 97.
9) T. NAGATA, *loc. cit.*
10) T. NAGATA, *Bull. Earthq. Res. Inst.*, **18** (1940), 129.

Table II. Magnetic Properties of Rocks from Miyake-sima's*.

No. of Specimen	χ_0	R_χ	$J_r/J_{1.26}$	ρ	J_{rn}	$\Delta\delta$	θ	Q_n
No. 1 (N-58)	$0{\cdot}76\times10^{-3}$	0·276	1·64	2·29	$1{\cdot}40\times10^{-2}$	1°W	48°	42
No. 2 (N-59)	1·31 〃	0·213	1·14	2·57	2·24 〃			39
No. 3 (N-60)	1·11 〃	0·234	1·52	2·25				
No. 4 (N-57)	0·94 〃	0·265	1·74	1·53				
No. 5 (N-75)	1·19 〃	0·317	1·94	2·21				
No. 6 (N-64)	0·80 〃	0·237	1·41	1·38	0·71 〃	1° E	47°	20
No. 7 (N-65)	0·74 〃			1·38	0·51 〃	1°·5W	50°	16
No. 8 (N-63)	0·63 〃	0·235	1·54	1·50	0·47 〃	2° E	48°	17
No. 9 (N-61)	0·97 〃	0·083	0·60	1·27				
No. 10 (N-62)	0·85 〃	0·429	2·11	2·50				
No. 11 (N-66)	1·06 〃			2·50	1·08 〃	4° E	48°	24

* χ_0 J_{rn} and ρ denote respectively the specific initial magnetic susceptibility, the specific intensity of natural remanent magnetization, and the bulk density.

instead of J_r/χ_0. While, as already mentioned in connexion with the volcanic rocks of a few volcanoes in Japan, J_r/J_0 has a linear relation to the capacity for increase of the susceptibility with the magnetic field in the initial magnetization process, the coefficient of the correlation seeming unique for the various rocks ejected from one volcano, but differing from those of rocks from other volcanoes.

In order to examine this relation for the Miyake-sima rocks also, the amounts of J_r/J_0 were plotted against the values of the capacity for increase susceptibility R_χ as shown in Fig. 3, where $\frac{\chi_{18.8}-\chi_{1.26}}{\chi_{1.26}}$ was taken for R_χ. From these results, we get for the Miyake-sima rocks approximately

$$J_r/J_0=0{\cdot}22+5{\cdot}0R_\chi. \quad (3)$$

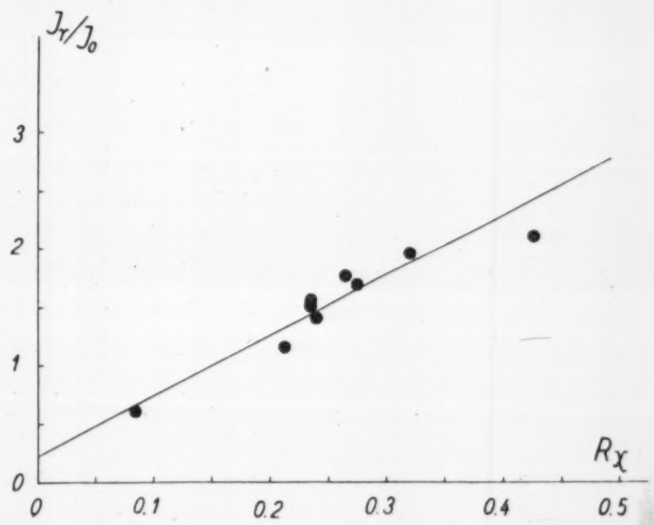

Fig. 3. Relation between J_r/J_0 and R_χ in Miyake-sima rocks.

The numerical values of the constant term and the correlation coefficient in eq. (1) clearly differ from those of the ejecta from volcanoes Asama, Huzi, and Amagi—a fact that may point to the

existence of magnetic property that is common to and unique with rocks from Miyake-sima.

4. Change in magnetic susceptibility with temperature.

The aspect of the change in magnetic susceptibility of a few specimens due to changes in their temperature was observed. The magnitude of magnetic susceptibility at a temperature fairly higher than that of the ordinary room, however, should be strictly defined, since rise or fall of temperature in igneous rock, even in a weak magnetic field, usually either extinguishes or sets up permanent "magnetization during cooling," which operation is irreversible with repect to temperature change, its intensity not being small. That is to say, the magnetization $\vec{J}$ of an igneous rock in magnetic field $\vec{H}$ at t^0 C is given[11] by

$$\vec{J}=\vec{H}\cdot\chi(t)+\vec{H}\cdot\int P(t)dt, \qquad (4)$$

where the integration of the second term should be performed along the entire range of temperature through which the rock has reached t from its initial state in $\vec{H}$. Then, so long as we define the initial susceptibility at a given temperature as the differential coefficient of the initial part of the magnetization curve with respect to the intensity of the magnetic field at the given temperature, the method of measuring the magnetic intensity of a specimen in a given constant magnetic field at various temperatures continuously by means of a magnetometer cannot be used for the present purpose. Therefore, in order to get the change in susceptibility with temperature, continuously, in a given weak magnetic field, the writer adopted the ballistic method. Since a description of this apparatus with a discussion of its sensitivity and accuracy will be made in a forthcoming paper, only a schematic

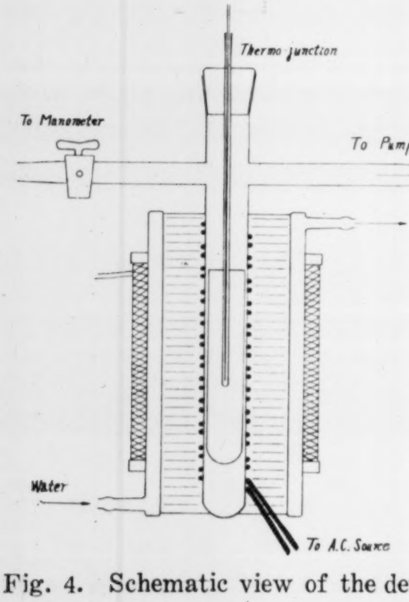

Fig. 4. Schematic view of the device for measuring magnetic susceptibility of rocks at various temperatures.

11) See § 6.

view of the most important part of the apparatus is shown in Fig. 4.

The susceptibilities of three typical specimens at temperature ranges of from 10°C to 750°C were measured, the heating and cooling of the specimens being made in air in the first case and *in vacuo** in the second case. The results for the first case are shown in Fig. 5 where (I) to (IV) give the initial heating, the initial cooling, the second heating, and the second cooling processes respectively.

In Fig. 6, the aspect of the change in susceptibility with temperature of the same specimens *in vacuo* is shown, where (I) and (II) denote the same processes as mentioned in the foregoing case. The intensity of the applied magnetic field was comparatively small, being 2·0 Gauss and 2·9 Gauss.

As will be seen from these figures, the susceptibility gradually increases with temperature from 0°C to a certin temperature, from which point it decreases abruptly with temperature.

The $\chi(t) \sim t$ curve of the rock specimen is not monotonic. Sometimes, the the susceptibility changes stepwise with temperature, as, for example, that shown in Fig. 5 a and c.

The rate of increase of susceptibility with temperature in a certin initial range from 0°C is 0·5 percent/degree in the largest

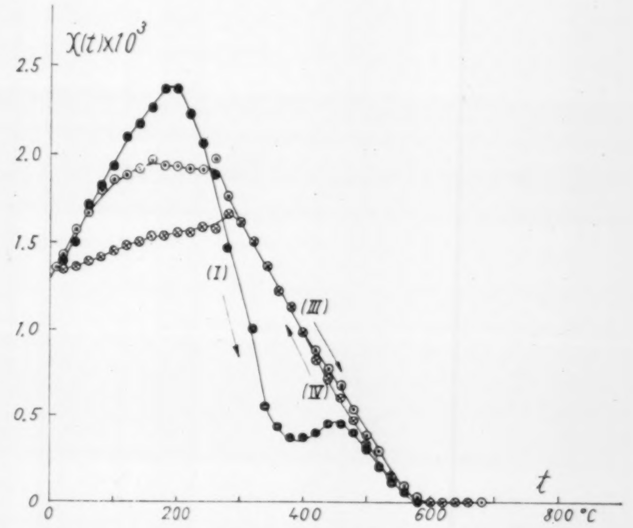

Fig. 5 a. Change in magnetic susceptibility with temperature in the open air. No. 2. (N-59), H = 2·06 Gauss.

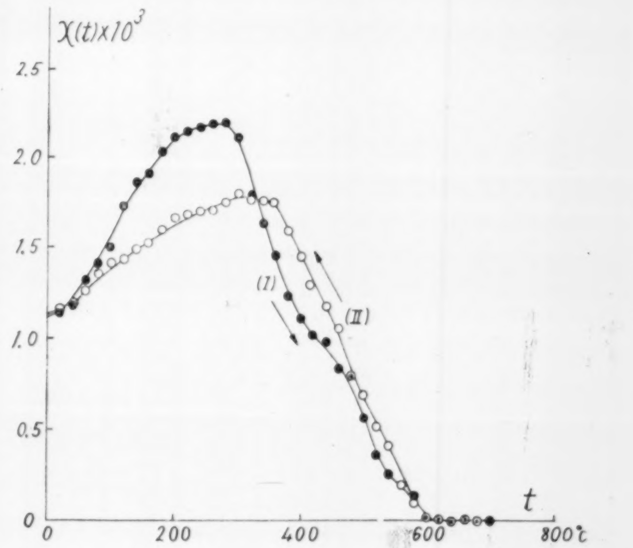

Fig. 5 b. Specimen No. 3. (N 60), H=2·21 Gauss.

* Actually, the air pressure in the instrument was 3~4 mm Hg.

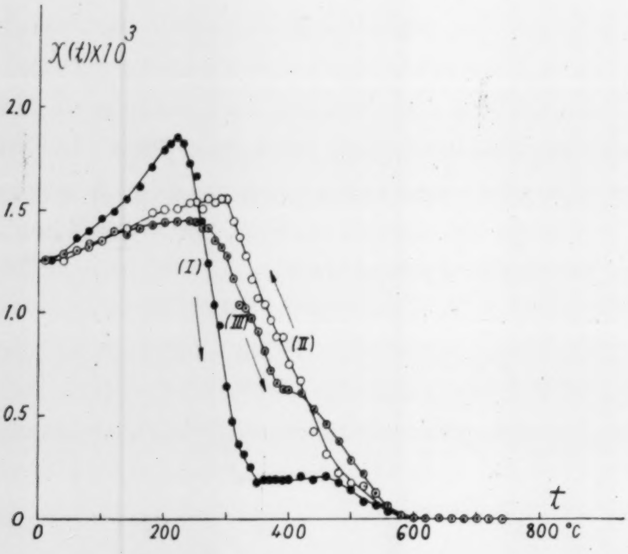

Fig. 5 c. Specimen No. 5. (N-75), $H=2{\cdot}19$ Gaus.s

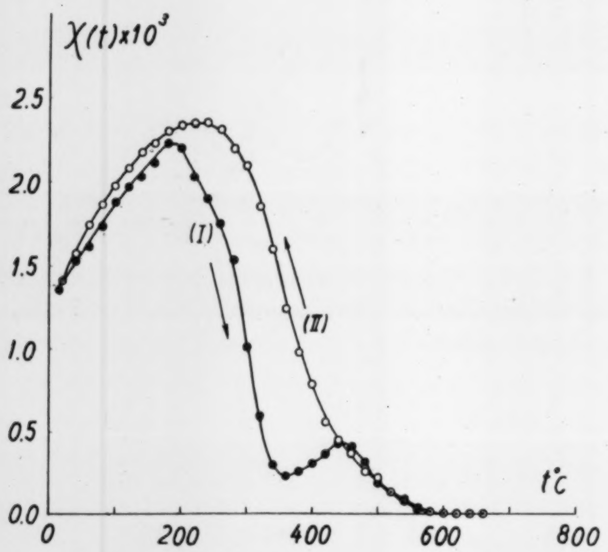

Fig. 6. Change in magnetic susceptibility with temperature in vacuo. (Air pressure = 4 mm Hg) No. 2. (N-59) $H=2{\cdot}20$ Gauss.

case. The amount of susceptibility at that temperature where it takes the largest value, however, does not exceed 1·8 times that at ordinary rcom temperature. In the case of a few volcanic rocks, this phenomenon of increase of magnetic susceptibility with temperature could not be seen in the $\chi(t)\sim t$ relations in a magnetic field of about 120 Gauss, as were obtained by R. Chevallier and J. Pierre[12]. It is believed that this phenomenon is peculiar to the rock in a weak magnetic field.

As the Curie temperature of a rock specimen, we shall take here the point on the axis of the temperature curve where the change of $\chi(t)$ with respect to temperature is maximum. Then the apparent Curie temperature θ in the heating and cooling processes are nearly the same when θ does not differ much from the curie-temperature of pure magnetie θ_M (580°C), while θ in process (II) takes a larger value than that in process (I), when θ in process (I) is much smaller than θ_M—a phenomenon probably due to change in the ferromagnetic minerals contained in the rocks. According to Chevallier's empirical formula[12], the Curie temperature θ of a ferromagnetic mineral composed of Fe_2O_3, FeO, and TiO_2 is given by

12) R. CHEVALLIER et J. PIERRE, *Ann. Phys. Paris*, **18** (1932), 353.

$$\left.\begin{aligned} \theta &= \frac{\theta_M}{0.69} S, \quad (^\circ K) \\ S &= \frac{C(Fe_2O_3)}{C(FeO)+C(Fe_2O_3)} \leq 0{\cdot}69, \end{aligned}\right\} \qquad (5)$$

where θ_M denotes the Curie temperature (in absolute temperature scale) of pure magnetite (853°K) and $C(Fe_2O_3)$ denotes the content of Fe_2O_3, etc. If eq. (5) holds in our case, the oxidation process of $FeO \rightarrow Fe_2O_3$ will be such that the magnitude of θ increases.

We see, however, comparing the $\chi(t) \sim t$ relations in Figs. 5 a, 6, that there is no difference in process (I) *in vacuo* and in the open air, the effect of oxidation in the temperature change in the air being marked only in the low temperature range in process (II), where $\chi(t)$ in *vacuo* is larger than that in air.

It must be noted also here that the temperature at which the ferromagnetic property of the three specimens examined here completely disappears is always about 580°C～600°C, regardless of the value of θ, showing probably that a part of the large number of ferromagnetic minerals in the rock specimen is almost pure magnetite, while the others consist of various percentages of Fe_2O_3, FeO, and TiO_2[15].

What strikes one most forcibly in connexion with the results mentioned in this paragraph is that some of the rocks newly ejected from Miyake-sima have their magnetic transcendental points at a rather low temperature (about 300°C), and that the susceptibility increases with temperature, sometimes amounting to nearly twice that at ordinary temperatures, after which it decreases abruptly at temperatures near the transcendental point.

5. Natural remanent magnetization.

The direction and intensity of the natural remanent magnetization of a number of specimens were measured by means of a magnetometric method (see previous paper for a rough description of this measuring instrument)[16]. In five of these specimens, the direction of the geomagnetic meridian and the horizontal plane that these rocks occupied in the field were measured and noted. This measurement was made

15) Details of the $\chi(t) \sim t$ relation in igneous rocks will be discussed in a paper to be published in the near future, particularly that relating to the mode of causation of thermo-remanent magnetism.

16) T. NAGATA, *Bull. Earthq. Res. Inst.*, **18** (1940), 281.

with a magnetic compass and level, the observational error being less than one degree, as already discussed. The lava flows and the large volcanic bombs from which these specimens were taken, appeared to be in the same position and direction that they occupied when the lava cooled and solidified, and when the bombs rained down on the earth's surface.

An example of distribution of magnetization on the surface of a rock specimen is shown in Fig. 7, while the specific intensity of the

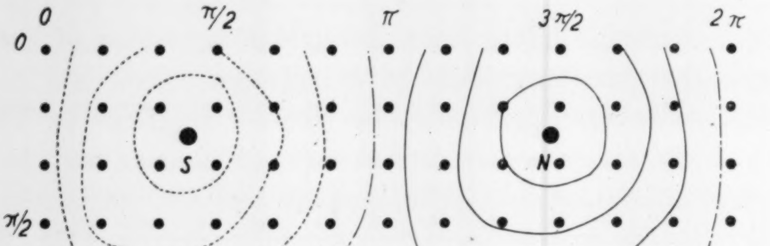

Fig. 7. Distribution of natural remanent magnetization on the surface of a rock specimen.

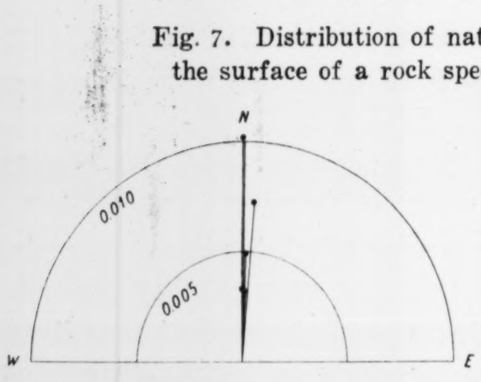

(a) Projection of the vectors of magnetization on a horizontal plane.

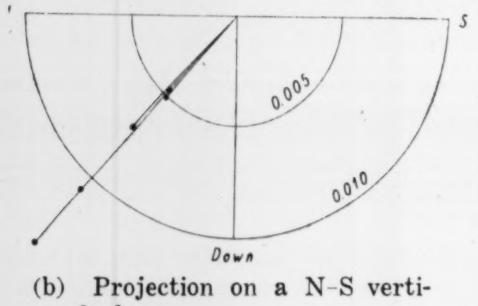

(b) Projection on a N-S vertical plane.

Fig. 8. Direction of the natural remanent magnetization of new ejecta from Miyake-sima.

natural remanent magnetization J_{rn} of every specimen measured and the direction of total magnetization of the five specimens are given in Table II and in Fig. 8, where $\Delta\delta$ and θ denote respectively the horizontal azimuth of the direction of magnetization from the geomagnetic meridian and the dip angle of the magnetization.

In Table II, the values of the coefficient of natural remanent magnetization ($Q_n \equiv J_{rn}/\chi_0 \times 0{\cdot}45$), that is, the ratio of the specific intensity of natural remanence to the specific intensity of induced magnetism in a magnetic field of 0·45 Gauss, are also shown. As will be seen from these results, the intensity of the natural remanent magnetization is much larger compared with that induced by the earth's

magnetic force, the specific intensity of the former amounting to $4{\cdot}7\,10^{-3}\sim2{\cdot}2\times10^{-2}$, while that of the latter at ordinary room temperature is only $0{\cdot}3\times10^{-3}\sim0.6\times10^{-3}$.

As to the direction of the natural remanent magnetization, it was found that the mean value of $\Delta\delta$ and θ of the four new ejecta were $0{\cdot}^{\circ}5\,\mathrm{E}\pm0{\cdot}^{\circ}7$ and $48{\cdot}^{\circ}3\pm0{\cdot}^{\circ}7$ respectively, while those of a specimen from the Meizi lava flow were 4°E and 48°, from which it may be concluded that the direction of natural remanence of the new ejecta well agrees with that of the geomagnetic field, so long as we neglect quantities smaller than the observational error.

It may be worthwhile mentioning here that not only a large mass of lava flow but also volcanic bombs that exceeded one meter in their mean diameters were also magnetized permanently coaxially with the direction of the geomagnetic field. From these facts, we know that we should take into full consideration the presence of natural remanent magnetization in dealing with the magnetism of volcanic rocks, at any rate of basaltic rocks.

6. Characteristics of magnetization during cooling in a weak magnetic field.

As is known from the studies of a number of investigators, natural remanent magnetization of igneous rocks is chiefly due to thermo-remanent magnetization, that is, the residual permanent magnetism caused during its cooling from a sufficiently high temperature in a weak magnetic field. According to experimental studies[17] on the mode of causation of thermo-remanent magnetization of igneous rock, the residual permanent magnetization during cooling from t to t' in the magnetic field of $\vec{H}$ is given by

$$\vec{J}=\vec{H}\cdot\int_{t'}^{t}P(t)dt, \qquad (6)$$

where $P(t)$ is a function of temperature, having the characteristics,

$$P(t\geq t_c)=0, \quad P(t_0)=\text{maximum},$$

and

$$\frac{\partial}{\partial\tau}P(t)=0,$$

where τ denotes the time required for cooling through unit temperature

17) T. NAGATA, *Bull. Earthq. Res. Inst.*, **19** (1941), 49.

range. The quantities giving the characteristics of the thermo-remanent magnetization of a rock are

transcendental temperature t_0,
critical temperature t_c,
intensity of saturated thermo-remanent magnetism J_{t_c},
coefficient of thermo-remanent magnetism $Q_t \equiv J_{t_c}/\chi$.

Therefore, provided we have the actual values of these quantities and the functional form of $P(t)$ of a rock specimen, it is possible with the aid of eq. (6), to estimate the intensity of magnetization during cooling of the rock at any temperature. In order to obtain an approximated form of $P(t)$ and the characteristic quantities, the intensity of "partial magnetization during cooling" ΔJ_{tH} through various partial temperature ranges were measured, these partial temperature ranges being included in the entire temperature range of from 0°C to 750°C. Thus, the relation between $\Delta J_{t_i H}$ and t_i was obtained, where $\Delta J_{t_i H}$ denotes partial magnetization during cooling through a temperature range of from $t_i + \Delta t$ to t_i.

Actually, the partial temperature range Δt and the intensity of the applied magnetic field were always taken as being 50° and 0·458 Gauss respectively. From the observed results mentioned above, it was possible to get the approximate relation between $P(t)$ and t with the aid of the relation

$$\frac{\Delta J_{t_i H}}{\Delta t} = P\left(t_i + \frac{1}{2}\Delta t\right) \cdot H.$$

The figures of the $P(t)$ curve of six specimens of new ejecta from Miyake-sima, Nos. 1, 2, 3, 5, 7, and 8 are given in Table III and in Figs. 9 to 14.

As will be clear from these figures, the transcendental temperature t_0 of the new ejecta from Miyake-sima is not a constant, each rock specimen having its own value of t_0. It should be said, moreover, that some of the specimens seem to have not only one but two, or sometimes three, transcendental points with respect to temperature.

Seeing that the fundamental figure of the $P(t)$ curve given by, for example, No. 3 and No. 5, has a single peak with respect to temperature, it may be assumed that the $P(t)$ curve of fairly complex shape given by Nos. 1 and 7 is the result of superposition of two or three fundamental curves of $P(t)$, each of which, as mentioned above, is of rather simple type. These complex figures of $P(t)$ have been analyzed into two or three simple type curves, as shown with dotted line in Figs. 9 to 14, a transcendental temperature corresponding to each of

Table III. Specific Intensity of Partial Magnetization during Cooling ($H=0{\cdot}46$ Gauss).

Specimen No. / Partial temperature range	No. 1 (N-58)	No. 2 (N-59)	No. 3 (N-60)	No. 7 (N-65)	No. 8 (N-63)	No. 5 (N-75)
100→ 50°C	$0{\cdot}07\times10^{-3}$	$0{\cdot}03\times10^{-3}$	$0{\cdot}05\times10^{-3}$	$0{\cdot}02\times10^{-3}$	$0{\cdot}02\times10^{-3}$	$0{\cdot}03\times10^{-3}$
150→100	0·02 ″	0·14 ″	0·14 ″	0·02 ″	0·03 ″	0·13 ″
200→150	0·07 ″	0·17 ″	0·21 ″	0·10 ″	0·06 ″	0·19 ″
250→200	0·71 ″	0·83 ″	0·21 ″	0·10 ″	0·09 ″	0·25 ″
300→250	2·87 ″	2·94 ″	0·26 ″	1·09 ″	1·16 ″	3·02 ″
350→300	2·30 ″	7·12 ″	0·32 ″	1·00 ″	1·14 ″	2·40 ″
400→350	1·59 ″	2·44 ″	0·43 ″	1·22 ″	1·04 ″	0·83 ″
450→400	1·04 ″	1·17 ″	0·44 ″	0·46 ″	0·83 ″	0·18 ″
500→450	2·00 ″	0·98 ″	2·20 ″	0·88 ″	1·14 ″	0·19 ″
550→500	1·72 ″	1·07 ″	11·40 ″	0·27 ″	0·43 ″	0·19 ″
600→550	0·96 ″	0·35 ″	6·86 ″	0·24 ″	0·31 ″	0·18 ″
650→600	0·20 ″	0·12 ″	0·14 ″	0·09 ″	0·14 ″	0·02 ″
700→650	0·10 ″	0·15 ″	0·14 ″	0·00 ″	0·10 ″	0·00 ″
750→700	0·07 ″	0·08 ″	0·08 ″	— ″	— ″	— ″

these separated curves. In the foregoing remarks, it is presumed that the fundamental form of $P(t)$ is composed of a large number of elemental transcendental states of magnetization during cooling, which are distributed along an axis of temperature following the law of probability, since the density of distribution should be maximum at t_0, although the range of distribution is restricted to one lower than t_c where the ferromagnetism of the rock vanishes. In the $P(t)$ curve of complex type, which consists of more than two fundamental curves of $P(t)$, the distribution of the elemental transcendental states group about more than two points on the temperature axis, where the density of distribution has maximum value. Putting it into formula, we get

$$\left.\begin{aligned} P(t) &= \sum_j P_j(t), \\ \vec{J}^{(c)}_{t't} &= \vec{H}\cdot\int_{t'}^{t} P(t)dt = \vec{H}\cdot\sum_j\int_{t'}^{t} P_j(t)dt, \end{aligned}\right\} \qquad (7)$$

In order to show the characteristic of each peak in the $P(t)$ curve quantitatively, we may take the height of the peak, that is, the magnitude of $P(t_0)$, and a quantity in order to give the sharpness of the peak. For the latter, we shall introduce the temperature range between

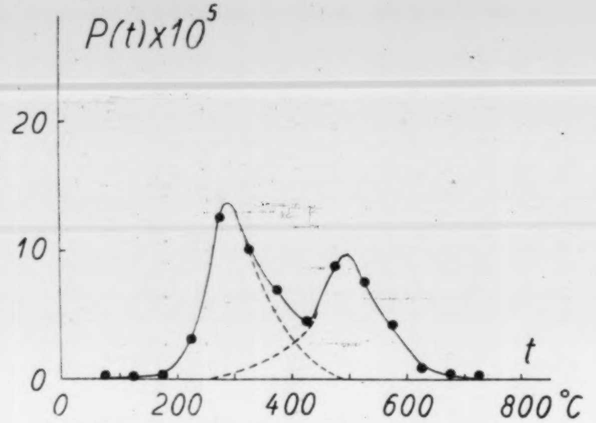

Fig. 9. Specimen No. 1 (N-58).

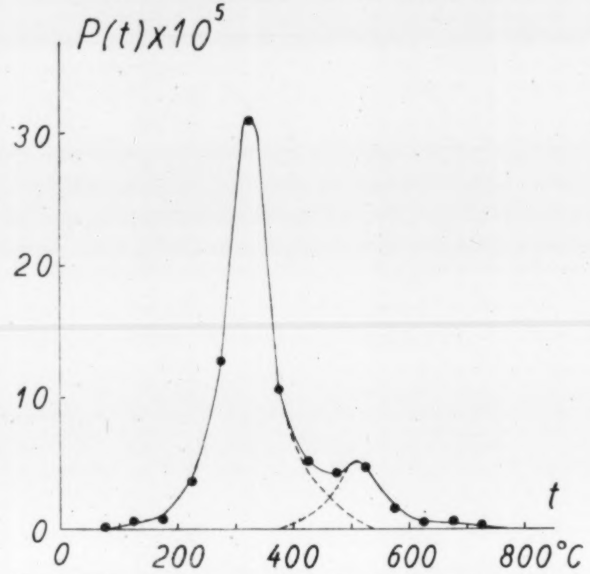

Fig. 10. Specimen No. 2 (N-59).

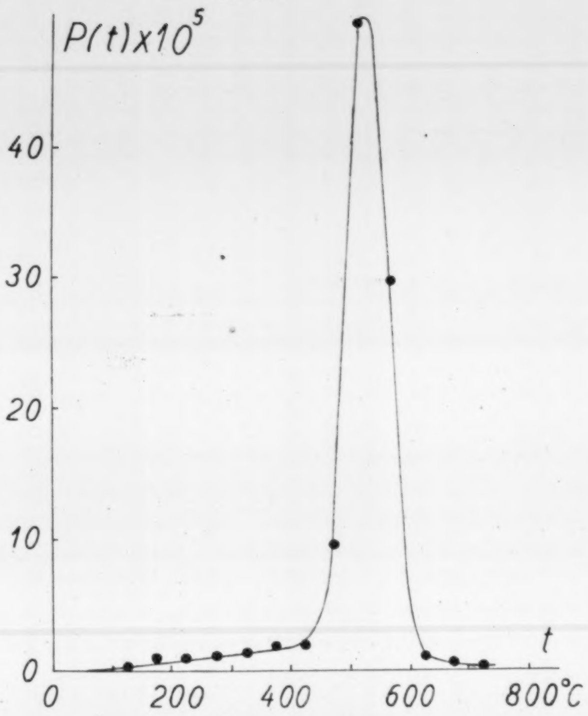

Fig. 11. Specimen No. 3 (N-60).

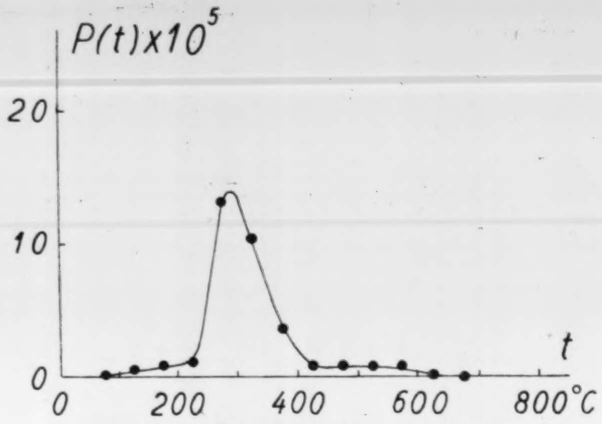

Fig. 12. Specimen No. 5 (N-75).

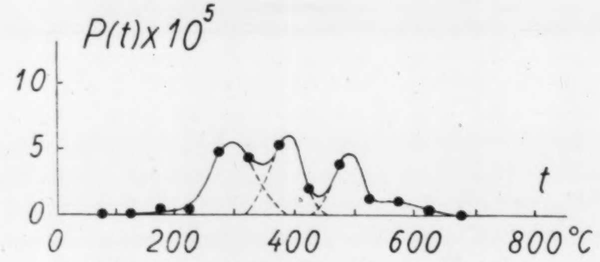

Fig. 13. Specimen No. 7 (N-65).

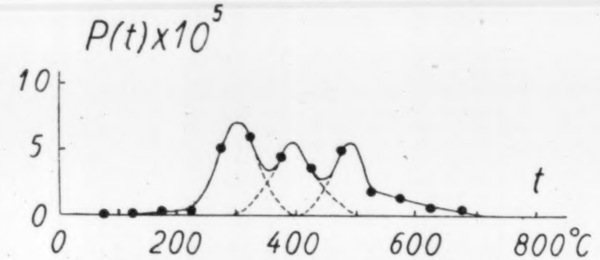

Fig. 14. Specimen No.8(N-63).

Fig. 9~14. Characteristic function of thermo-remanent magnetism $P(t)$ of rocks from Miyakesima.

the half-value-points of $P(t_0)$, a quantity denoted by 2ϑ, and defined by

$$2\vartheta = t_2 - t_1, \quad (t_2 > t_0 > t_1), \tag{8}$$

where

$$P(t_1) = P(t_2) = \frac{1}{2} P(t_0). \tag{8'}$$

The actual values of $P(t_0)$ and 2ϑ of the six specimens are given in Table IV, where t_0, J_{t_c}, and Q_t are also given.

Table IV. Characteristic Quantities of Thermo-remanent Magnetism of Rocks from Miyake-sima.

No. of Specimen	Rock	J_{t_c}	Q_t	t_0	$P_j(t_0)$	2ϑ
No. 1 (N-58)	Olivine-hypersthene-augite-basaltic-andesite.	$2\cdot98\times10^{-2}$	40	295°C	$5\cdot74\times10^{-5}$	105°
				495	4·00 〃	110
No. 2 (N-59)	〃	3·83 〃	29	320	14·24 〃	80
				520	2·14 〃	105
No. 3 (N-60)	〃	2·41 〃	46	525	22·80 〃	85
No. 8 (N-63)	Augite-olivine-basalt.	1·17 〃	19	300	2·35 〃	80
				395	2·30 〃	80
				495	2·30 〃	70
No. 7 (N-65)	〃	1·19 〃	17	300	2·20 〃	80
				395	2·45 〃	75
				495	1·80 〃	80
No. 5 (N-75)	Olivine-two-pyroxene-basaltic-andesite.	2·61 〃	28	295	6·04 〃	85

We shall here deal with these characteristic quantities of each specimen.

(i) Transcendental temperature.

The values of the transcendental temperature are graphically shown in Fig. 15, as the spectra with respect to temperature. Generally speaking, transcendental temperatures of nearly 300°C and 500°C seem to be common in rocks newly ejected from Miyake-sima, although specimens Nos. 3 and 5 have a unique transcendental temperature which is either the former or the latter. Although a t_0 of 400°C does not appear in the specimens from the lava flow nor in the ejecta from the central cone, it appears in the bombs ejected from Hyôtan-yama. Petrologically

also, the latter clearly differs from the former[18]. The height of $P(t)$ of the Hyôtan-yama bomb, however, is not so marked as that in the other rock specimens, whence we may say that, generally speaking, the characteristic transcendental temperatures that predominate in the new ejecta from Miyake-sima are about 300°C and 500°C.

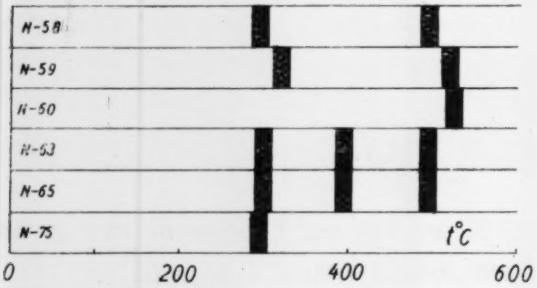

Fig. 15. Transcendental temperatures of new ejecta from Miyake-sima.

(ii) The sharpness of $P(t)$ around t_0.

The magnitude of 2ϑ of the fundamental $P(t)$ curve (simple peak type) is about 85°, while that of each peak separated from the other complex $P(t)$ curves is also much the same, from which it results that the larger part of the thermo-remanent magnetization in a rock having the character of the fundamental $P(t)$ curve should form during the cooling through a temperature of 85°. For example,

$$\int_{t_0-\vartheta}^{t_0+\vartheta} P(t)\,dt \Big/ \int_0^\infty P(t)\,dt = 0{\cdot}68 \text{ (in No. 5)}, \tag{9}$$

and $$= 0{\cdot}72 \text{ (in No. 3)}.$$

As for the complex type $P(t)$ curve, assuming that

$$P(t) = P_1(t) + P_2(t) + \ldots\ldots\ldots, \tag{10}$$

we get a similar quantity as that, for example, in No. 1,

$$\int_{_1t_0-\vartheta_1}^{_1t_0+\vartheta_1} P_1(t)\,dt \Big/ \int_0^\infty P_1(t)\,dt = 0{\cdot}76 \quad ({}_1t_0 = 295°\text{C}), \tag{11}$$

$$\int_{_2t_0-\vartheta_2}^{_2t_0+\vartheta_2} P_2(t)\,dt \Big/ \int_0^\infty P_2(t)\,dt = 0{\cdot}62 \quad ({}_2t_0 = 490°\text{C}), \tag{12}$$

while

$$\int_{_1t_0-\vartheta_1}^{_1t_0+\vartheta_1} P_1(t)\,dt \Big/ \int_0^\infty P(t)\,dt = 0{\cdot}41, \tag{13}$$

and

18) See Part I in this report, described by H. TSUYA.

$$\int_{2t_0-\vartheta_2}^{2t_0+\vartheta_1} P_1(t)dt \Big/ \int_0^{\infty} P(t)dt = 0{\cdot}29. \tag{14}$$

It will be seen from these examples that the largest part of the thermo-remanent magnetization (60～80%) is formed during the cooling through a narrow temperature range of from $t_0+\vartheta$ to $t_0-\vartheta$, if we consider only one of the component curves forming $P(t)$.

(iii) Magnitude of J_{t_c} and Q_t.

The specific intensity of the saturated thermo-remanent magnetization of new ejecta from Miyake-sima is always larger than 0·01 C. G. S. E. M. U., and we can see that the amount of $J_{t_c} \times 0.45$ of each rock specimen is nearly equal to its J_{rn}, although there is a discrepancy of of less than 10 percent between them. Especially, the fact that the amount of $J_{t_c} \times 0{\cdot}45$ of the bombs ejected from Hyôtan-yama nearly agrees with their J_{rn} may show that these bomb had a temperature higher than, or at least equal to, the highest transcendental temperature (495°C) of their thermo-remanent magnetism when they rained down on the earth's surface where they were found. It should be noted here that the coefficient of thermo-remanent magnetism Q_t always exceeds 16, amounting sometimes to 46 in the largest case, and that the Q_t of the lava flow is generally larger than that of the bombs. This tendency is also found in the J_{rn} values of the various rock specimens given in Table III. However, it may be rather an axiomatic result, since the natural remanent magnetism of rock is usually due to the causation of thermo-remanent magnetism in nature, that is, the former is the result of natural cooling from a fairly high temperature in the earth's magnetic field.

7. Possible relation of the magnetic properties of rock to the observed anomaly in geomagnetism and its changes.

It will be seen from § 3 that rocks newly ejected from Miyake-sima, associated with the severe volcanic activity, have magnetic susceptibility of fair magnitude, and from § 5 that these rocks have much more intense natural remanent magnetization than induced magnetization, the direction of which magnetization nearly agrees with that of the geomagnetic field. While on the other hand, according to the dip-survey by T. Minakami[19] and to the vertical intensity survey by R. Takahasi

19) T. MINAKAMI, Part VIII of this report.

and K. Hirano[20], the geomagnetic field on Miyake-sima seems to have been greatly disturbed, owing probably to the presence of the volcano itself, which is magnetized.

From the isoclinic chart which he has drawn, Minakami estimated the mean value of the magnetic susceptibility of the material composing Miyake-sima to be about 0·015~0·020; in other words, the mean intensity of magnetization of Miyake-sima is estimated as $0{\cdot}020 \times 0{\cdot}45 = 0{\cdot}009$.

By assuming that the whole of the magnetization of Miyake-sima is caused by its induced magnetization by the earth's magnetic field, we find that the magnetic susceptibility 0·020 required by this assumption is too large compared with the actual value of susceptibility of the Miyake-sima rocks obtained experimentally to be 0·0012~0·0025. In contrast to this the intensity as found by magnetic survey is too small compared with that of natural remanent magnetization. Hence, the most reasonable presumption is that Volcano Miyake-sima is composed of parts having natural remanence (lava) and parts having apparently no permanent magnetization (scoria and ash), although both parts have magnetization induced by earth's magnetic field, and that the total sum of these magnetizations causes the observed magnetic anomaly.

As to the direction of the natural remanent magnetization of the rocks underneath the surface of this volcanic island, although we have at present no corroborative knowledge, it does not seem to be very far from the truth to presume that the direction of magnetization of the largest part of lava deviates less than 20 degrees[21] from that of the present geomagnetic field. If so, the foregoing result of interpreting the magnetic anomaly should hold good as an approximation. Quantitative estimates of the structure of this volcano from geomagnetic studies, however, seems impossible at present.

It shoud be noted, however, that there are several possibilities that the magnetic susceptibility of rocks below the earth's surface are slightly

20) R. TAKAHASI and K. HIRANO, *Bull. Earthq. Res. Inst.*, **19** (1941), 82.

21) The $\Delta\delta$ and θ of the natural remanence of two specimens from the somma lava on the north-east coast of Miyake-sima are 10°E and 55° respectively. (Since accurate measurements of the geomagnetic meridian and the horizontal plane were not made with these specimens, an observational error of nearly 5° being expected, the data on these specimens are omitted from Table II.) For reference, the $\Delta\delta$ and θ of the somma lava of Volcano Mihara are shown to be $\Delta\delta = 7°\text{W}$, $\theta = 50°$. According to M. Matuyama's study on the directions of the natural remanent magnetization of basalts in Japan and Manchuria, almost all of them have directions either nearly equal to or nearly opposite to the direction of the present geomagnetic field, excluding deviations of magnitude less than 20 degrees. We may then presume that the old ejecta from Miyake-sima and Mihara belongs to the former case in Matuyama's results (See. M. MATUYAMA, *Proc. Imp. Acad. Japan*, **5** (1929), 202).

larger than the values given in § 3. This magnetic susceptibility may increase with depth, first because the temperature increases with depth, and second because the density also increases. The change in susceptibility with temperature given in § 4 shows, however, that the transcendental temperature of Miyake-sima rocks is rather low, sometimes about 300°C, the result of this fact being that the effective mean value of susceptibility of every part of this volcano, where the temperature gradient with respect to depth is probably very large, is rather smaller than that given in § 3.

That the change in susceptibility of a unit volume due to the increase in the density is not large, where the depth is less than a few kilometers, is expected from our knowledge of the compressibility of various rocks. The other possibility of larger susceptibility is in the case that the crystallinity of the rock underneath the earth's surface is sufficiently perfect, the largest part of the Fe_2O_3 in the rock consisting of phenocrysts of magnetite, a few tenths of a milimeter in their mean diameters.

According to the writer's study[22], the magnetic susceptibility of rock containing normative magnetite of C_{Mt} is

$$\chi_0 \leqq 0{\cdot}045 C_{Mt}, \tag{15}$$

where the upper limit of χ corresponds to that case in which the crystalization of magnetite is the most perfect from a large number of specimens of volcanic rocks in Japan. Taking the the amount C_{Mt} as 8 %, which is the largest value in the data of chemical analyses of Miyake-sima rocks, we get for the upper limit of magnetic susceptibility $\chi = 0{\cdot}0036$, so that even by assuming that the sum total of all the conditions mentioned above result in maximum susceptibility, it must be less than 0·009. It may thus be concluded that the largest part, or at least a part more than half, of the amount of the geomagnetic anomaly in Miyake-sima is due to the presence of natural remanent magnetization in the rocks composing this volcanic island.

Next, as to the anomalous change in geomagnetism observed after cessation of the severe volcanic activity, its possible relation to the change in the magnetic properties of the rocks is discussed in another part (Part VII of this report). Here, the following points alone will be noted.

If the observed changes in geomagnetism were the result of temperature changes in the subterranean rocks, the magnetic change should

22) T. NAGATA, *loc. cit.*

and K. Hirano[20], the geomagnetic field on Miyake-sima seems to have been greatly disturbed, owing probably to the presence of the volcano itself, which is magnetized.

From the isoclinic chart which he has drawn, Minakami estimated the mean value of the magnetic susceptibility of the material composing Miyake-sima to be about 0·015∼0·020; in other words, the mean intensity of magnetization of Miyake-sima is estimated as $0{\cdot}020 \times 0{\cdot}45 = 0{\cdot}009$.

By assuming that the whole of the magnetization of Miyake-sima is caused by its induced magnetization by the earth's magnetic field, we find that the magnetic susceptibility 0·020 required by this assumption is too large compared with the actual value of susceptibility of the Miyake-sima rocks obtained experimentally to be 0·0012∼0·0025. In contrast to this the intensity as found by magnetic survey is too small compared with that of natural remanent magnetization. Hence, the most reasonable presumption is that Volcano Miyake-sima is composed of parts having natural remanence (lava) and parts having apparently no permanent magnetization (scoria and ash), although both parts have magnetization induced by earth's magnetic field, and that the total sum of these magnetizations causes the observed magnetic anomaly.

As to the direction of the natural remanent magnetization of the rocks underneath the surface of this volcanic island, although we have at present no corroborative knowledge, it does not seem to be very far from the truth to presume that the direction of magnetization of the largest part of lava deviates less than 20 degrees[21] from that of the present geomagnetic field. If so, the foregoing result of interpreting the magnetic anomaly should hold good as an approximation. Quantitative estimates of the structure of this volcano from geomagnetic studies, however, seems impossible at present.

It shoud be noted, however, that there are several possibilities that the magnetic susceptibility of rocks below the earth's surface are slightly

20) R. TAKAHASI and K. HIRANO, *Bull. Earthq. Res. Inst.*, **19** (1941), 82.

21) The $\varDelta\delta$ and θ of the natural remanence of two specimens from the somma lava on the north-east coast of Miyake-sima are 10°E and 55° respectively. (Since accurate measurements of the geomagnetic meridian and the horizontal plane were not made with these specimens, an observational error of nearly 5° being expected, the data on these specimens are omitted from Table II.) For reference, the $\varDelta\delta$ and θ of the somma lava of Volcano Mihara are shown to be $\varDelta\delta=7°$W, $\theta=50°$. According to M. Matuyama's study on the directions of the natural remanent magnetization of basalts in Japan and Manchuria, almost all of them have directions either nearly equal to or nearly opposite to the direction of the present geomagnetic field, excluding deviations of magnitude less than 20 degrees. We may then presume that the old ejecta from Miyake-sima and Mihara belongs to the former case in Matuyama's results (See. M. MATUYAMA, *Proc. Imp. Acad. Japan*, **5** (1929), 202).

larger than the values given in § 3. This magnetic susceptibility may increase with depth, first because the temperature increases with depth, and second because the density also increases. The change in susceptibility with temperature given in § 4 shows, however, that the transcendental temperature of Miyake-sima rocks is rather low, sometimes about 300°C, the result of this fact being that the effective mean value of susceptibility of every part of this volcano, where the temperature gradient with respect to depth is probably very large, is rather smaller than that given in § 3.

That the change in susceptibility of a unit volume due to the increase in the density is not large, where the depth is less than a few kilometers, is expected from our knowledge of the compressibility of various rocks. The other possibility of larger susceptibility is in the case that the crystallinity of the rock underneath the earth's surface is sufficiently perfect, the largest part of the Fe_2O_3 in the rock consisting of phenocrysts of magnetite, a few tenths of a milimeter in their mean diameters.

According to the writer's study[22], the magnetic susceptibility of rock containing normative magnetite of C_{Mt} is

$$\chi_0 \leqq 0{\cdot}045 C_{Mt}, \tag{15}$$

where the upper limit of χ corresponds to that case in which the crystalization of magnetite is the most perfect from a large number of specimens of volcanic rocks in Japan. Taking the the amount C_{Mt} as 8 %, which is the largest value in the data of chemical analyses of Miyake-sima rocks, we get for the upper limit of magnetic susceptibility $\chi = 0{\cdot}0036$, so that even by assuming that the sum total of all the conditions mentioned above result in maximum susceptibility, it must be less than 0·009. It may thus be concluded that the largest part, or at least a part more than half, of the amount of the geomagnetic anomaly in Miyake-sima is due to the presence of natural remanent magnetization in the rocks composing this volcanic island.

Next, as to the anomalous change in geomagnetism observed after cessation of the severe volcanic activity, its possible relation to the change in the magnetic properties of the rocks is discussed in another part (Part VII of this report). Here, the following points alone will be noted.

If the observed changes in geomagnetism were the result of temperature changes in the subterranean rocks, the magnetic change should

22) T. NAGATA, *loc. cit.*

be due much more to changes in "thermo-remanent magnetization" than to changes in susceptibility. Then, since the transcendental temperature t_0 and the amount of $P(t_0)$ of the thermo-remanent magnetism have various values, a rock from a certain locality having its own characteristics, the distribution of geomagnetic change due to the variation in this permanent magnetization can be somewhat complex, even if the distribution of the subterranean temperature change were comparatively simple. This contingency must be taken into consideration in explaining the anomalous geomagnetic changes that accompany volcanic activities.

8. Summary and Conclusion.

In this part of the paper, the magnetic properties of rocks from Miyake-sima are described. Knowledge of the actual values of various characteristic quantities obtained in this study ought to be indispensable in explaining the geomagnetic anomaly and its changes, as observed by a number of workers in Miyake-sima.

In conclusion, the writer of this Part wishes to express his sincere thanks to Prof. H. Tsuya, chief investigator of the expedition party, and to the other members for their encouragement and helpful criticism in the course of this study. His hearty thanks are due also to the Hattori Hôkô Kai, with the aid of whose grant the measuring instruments were constructed.

Part V. The Earthquakes that accompanied the Eruption.

By Takahiro HAGIWARA,

Earthquake Research Institute.

(Read Sept. 15, 1940.—Received March 20, 1941.)

Following the volcanic eruption of Miyake-sima,[1] July 12, 1940, the writers carried four seismographs with them to the island. One of the instruments was first set up at Kamituki, a village in the northern part of the island, and observations begun at 20 h 30 m, July 14, succeeding which, the remaining three instruments were installed respectively at Kamanosiri, Miikehama, and Tubota. The observations were made with two seismographs set up on one side of the zone of volcanic activity and two on the opposite side (Fig. 1). The seismographs were all of the same type, of the following elements:

Mass	Component	Period	Damper	Magnification	Driving of drum
7 kg	Horizontal	sec 0·12	Air type	120	Clock work

It was found that the earthquakes were restricted to a small region in the neighbourhood of Kamituki. Many earthquakes that were felt by people at Kamituki were not felt at Miikehama and Tubota. The earthquakes recorded by the seismograph at Miikehama showed also a very small amplitude compared with that of Kamituki, while almost no records were obtained by the seismograph at Tubota during the period of observation. The reason for this is probably that the depth of the hypocenters is very shallow, for example, $0\sim1$ km, so that a small increase of the epicentral distance resulted in marked decrease in the seismic intensity.

The observations at Kamanosiri, Miikehama, and Tubota were continued to August 3, and that at Kamituki until November 15, 1940. Although there are no precise data covering earthquakes prior to the installation of the seismographs, certain conclusions are possible by putting together the various experiences of the residents of the is-

1) A detailed description of this eruption was made by H. Tsuya. [H. TSUYA, *Bull. Earthq. Res. Inst.*, **19** (1941), 263.]

land. The charcoal-burners who lived in the forest on the eastern mountain side of the island, about 250 m above sea level, where the present eruption opened a new crater, frequently heared faint earth-sounds coming from the east for several days before the eruption; and finally for several tens of minutes preceding the first eruption, felt a swarm of small earthquakes. The residents of Kamituki also felt these small earthquakes almost continuously during the four or five tens of minutes that preceded the eruption. After the first eruption occurred at 20 h, July 12, many earthquakes were felt at Kamituki, Akô, and Miikehama, but by July 14, they decreased in number. The seismic intensity of the strongest, however, did not exceed scale III. In Tubota, only a few earthquakes were felt by the people before and after the eruption.

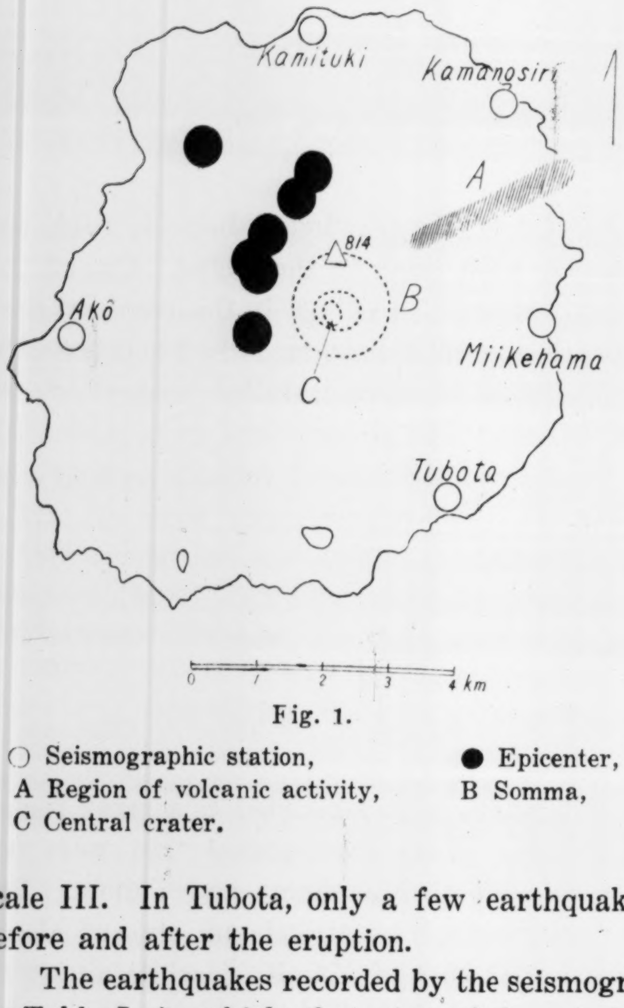

Fig. 1.

○ Seismographic station, ● Epicenter,
A Region of volcanic activity, B Somma,
C Central crater.

The earthquakes recorded by the seismograph at Kamituki are shown in Table I, in which that starred is a twin, or multiple, earthquake. Some reproductions of the records are shown in Fig. 5.

Table I. Earthquakes observed at Kamituki.

Date	Intensity	Preliminary tremors	Date	Intensity	Preliminary tremors
July d h m		sec	July d h m		
14 20 38	0	1·0	14 23 12	0	
20 41	II	1 0	23 21	0	
22 55	0		23 59	0	

(to be continued.)

Table I. (*continued.*)

Date	Intensity	Preliminary tremors	Date	Intensity	Preliminary tremors
July d h m		sec	July d h m		
15 0 38	III	*	21 22 22	I	
0 46	0		22 24	0	1·9
3 55	0		22 7 56	I	1·5
8 01	0		7 59	II	1·5
8 50	II	1·9	11 46	0	
8 51	0		11 47	0	
10 20	0		13 00	0	
10 54	0		17 01	0	
12 58	0	1·9	20 56	0	
13 02	0		22 53	I	2·0
15 17	0		22 58	I	1·8
15 28	0		23 11 25	0	
15 53	0		12 17	III	1·5
17 23	0		13 31	II	2·2
17 56	0		13 32	0	2·0
21 12	0		13 37	II	
16 3 21	0		22 14	I	1·7
3 48	0	1·0	22 49	I	2·5
4 34	0	1·0	23 18	0	
11 26	0	2·4	24 1 32	0	
16 04	0	2·4	1 48	II	1·2 *
16 34	0		19 32	0	
17 12 34	0	1·6	25 4 52	0	
18 22 44	III	2·1	11 03	0	
23 07	0	1·7	30 2 56	0	1·7
19 0 33	I	1·8	31 2 00	0	
0 58	I	1·8	August		
10 13	I	2·0	1 20 09	0	
13 56	II	1·7	2 1 26	0	
16 14	II	2·3	1 29	0	
20 0 59	I		1 34	0	
5 21	0		3 18	0	
7 56	0		3 51	0	
9 42	III	1·6	5 48	0	
9 43	I	1·5	6 17	0	
17 53	I	1·0	17 28	0	
21 6 44	I	1·8	3 9 57	0	

N.B. * Twin or multiple earthquake.

As already stated, the magnitude of the earthquake motion was very

small in all the stations except Kamituki, so that the earthquakes for which the duration time of the preliminary tremors could be read off at two or more stations numbered only seven, as shown in Table II.

Table II.

Date	Kamituki		Kamanosiri		Miikehama	
	Preliminary tremors	Maximum amplitude	Preliminary tremors	Maximum amplitude	Preliminary tremors	Maximum amplitude
July d h m	sec	μ	sec	μ	sec	μ
19 13 56	1·7	14	2·3	9		
20 17 53	1·0	7	1·5	4		
21 6 44	1·8	7	2·2	3		
23 12 17	1·5	25	2·0	8	2·2	3
23 13 31	2·2	13	2·5	8		
23 22 14	1·7	8	2·2	5		
24 1 48	1·2	12	1·7	8		

Usually, in order to determine the hypocenter of an earthquake, we need the time duration of the preliminary tremors of at least four stations. Since, in the present case, the data were obtained at only two stations, Kamituki and Kamanosiri, we have only two known quantities against four unknown quantities. Hence, in determining the hypocenter, at least two suitable assumptions have to be made. The first assumption that serves this purpose is that the depth of the hypocenter is almost zero. If the depth of the hypocenter were a few kilometers, the sudden decrease in the seismic intensity would not have been caused by the small increase in the epicentral distance. The second assumption is to make the value of k of the so-called Omori's formula ($D=kt$, where D is the hypocentral distance, t the duration of the preliminary tremors, and k a constant) to be equal to 2. The reason for this choice is based on the following fact. Takahasi and Nagata,[2] who studied the earthquakes that originated in Volcano Mihara, Oosima, a volcanic island about 80 km distant from Miyake-sima, obtained 2 as the mean value of k for the earthquakes that occurred in the shallow depth of the volcano. Since, geologically speaking, Oosima and Miyake-sima, which belong to the same volcanic zone, have many points in common, the same value of k may be used without any serious error. Next, the epicenter is determined by the graphical method, using the duration of the preliminary tremors of two stations under the assumption just mentioned. If, in Fig. 2, A and B are two seismographic stations, the intersection

2) R. TAKAHASI and T. NAGATA, *Zisin*, **11** (1939), 161 (in Japanese).

(E and F) of two circles of radius kt_A and kt_B is the required epicenter (in which t_A and t_B are the values of t at A and B respectively). The foregoing method gives two solutions (E and F), but, in the present case, of the two epicenters given by using the data of Kamituki and Kamanosiri, the one that lies in the island may reasonably be considered the required epicenter. Although the depth of the hypocenter was assumed to be zero in the foregoing case, it is not necessary for this to be exactly zero, so far as the epicentral position is concerned. If, in the figure, the depth of the hypocenter has a certain magnitude, then epicenter E would deflect to E', $E'H$ corresponding to the depth of the hypocenter. Since $E'E = E'H \tan \angle E'HE$ and $\angle E'HE \leqq 45°$, $EE' \leqq E'H$. Comparing the two cases, in which the depth of the hypocenter has a certain value h, and that is zero, then the difference of the epicentral position does not exceed h. In fact, by substituting the actual values for the present case, we find that whether the depth of the hypocenter be 1 km or zero, the epicenter does not deflect more than 300 m. The epicentral distributions thus determined are shown in Fig. 1. As will be seen from the figure, the earthquakes did not occur in the region of volcanic activity, but at a shallow depth on the north-western mountain side of the volcano island.

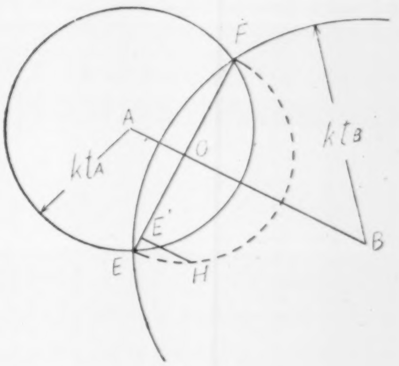

Fig. 2.

We shall next take the relation between the time distribution of the earthquakes and the volcanic activity. When seismographic observations were begun on July 14, the activity of the fissure eruption that occurred in the eastern mountain side had already ceased and large quantities of smoke were rising from the central crater of the summit. This crater emitted much smoke until July 17, after which (July 18) it showed sign of decrease. Thenceforward the detonations coming from the central crater could be heard at the village on the seashore, while at the same time the microseisms observed at Kamituki[3] gradually intensified. The earthquakes, which gradually decreased in number since July 14, increased again, beginning with that of increased severity, with seismic intensity III, that came at 22 h, July 18, followed by a number of sensible earthquakes every day until July 24. On this day, the smoke from the central crater greatly diminished, but, on the other hand, the sounds of the explosions increased in intensity. The loudness of the

3) T. MINAKAMI, *Bull. Earthq. Res. Inst.*, **19** (1941),

sounds, which reached maximum on July 25, did not abate until July 30. The detonations accompanied by air shocks shook the houses in the village, at intervals and sometimes almost incessantly. On July 31, the detonations diminished, and the microseisms recorded at Kamituki also decreased in amplitude. The number of earthquakes promptly decreased after the explosive activity reached maximum on July 25.

As already stated, the earthquakes were intimately related to the activity of the central crater. On the summit, we witnessed red hot lavas ejected upwards from the central crater accompanied by severe detonations. The origin of the microseisms observed at Kamituki must have been at the central crater, from which elastic waves were generated by the explosion. However, the origin of the earthquakes, as already stated, lay at a certain depth, away from the crater. The activity of the central crater began with the exhaustion of the gases that were accumlated in the upper part of the liquid lava, breaking through the solidified rocks, resulting in heavy smoke loaded with volcanic ash. The lava in the liquid state then gradually ascended until it reached the surface of the crater. The increase in the number of earthquakes since July 18 was simultaneous with the ascent of the lava from the depth of the crater. It may be explained that the increase of gaseous pressure in the lava forced the lava towards the central crater and, at the same time, resulted in destructive phenomenon under the ground, namely the earthquake. When the explosive activity of the crater began with free emission of gas from the crater, the earthquake activity came to an end.

In conclusion, the writer wishes to express his cordial thanks to Messrs. A. Zitukawa and M. Suzuki, who assited him greatly in the field work.

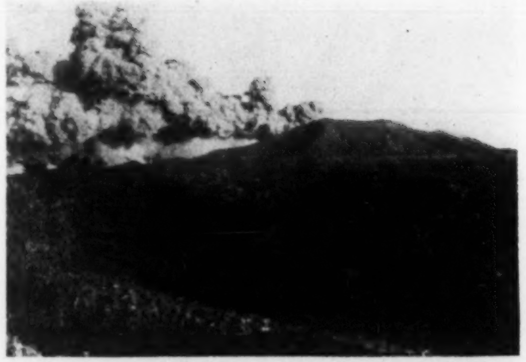

Fig. 3. Smoke rising from the central crater of the summit, seen from Kamituki (July 20).

Fig. 4. The smoke from the crater diminished, but, on the other hand, the sounds of the explosions increased (Kamituki, July 25).

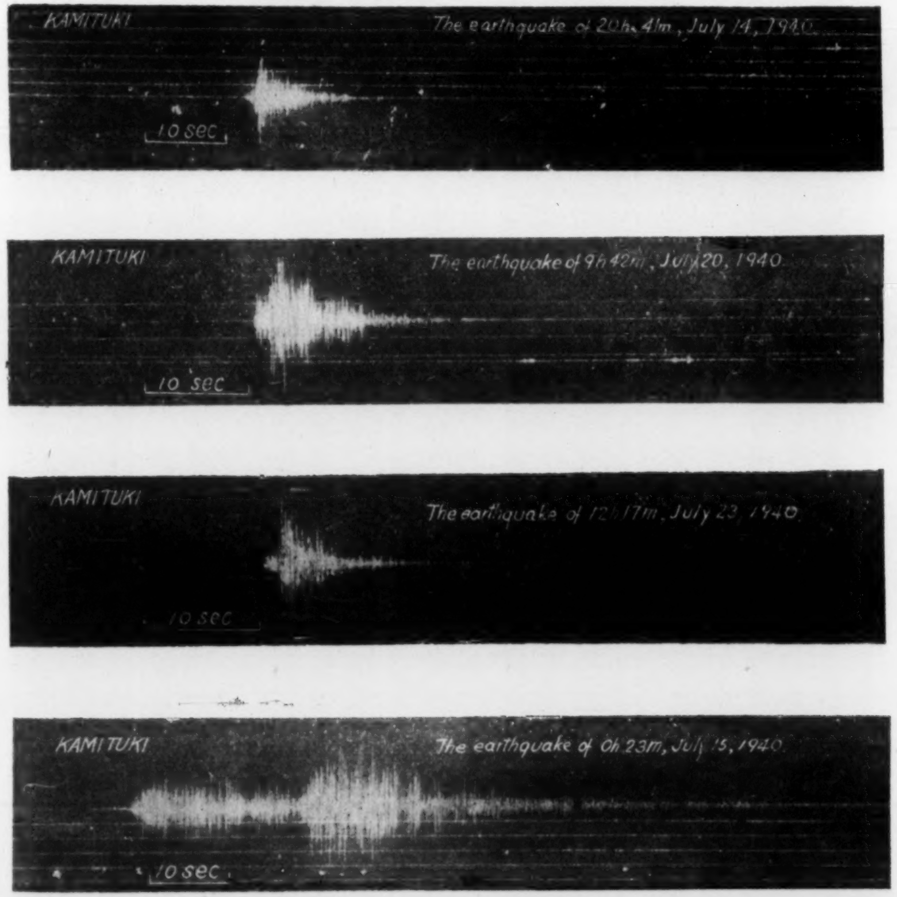

Fig. 5. Seismograms obtained at Kamituki (2·3 times the actual seismogram).

Part VI. Pulsations of the Ground that accompanied the Volcanic Activity of Miyakesima Island.

By Takeshi MINAKAMI,

Earthquake Research Institute.

(Read Sept. 15, 1940.—Received March 20, 1941.)

Observations with a microseismograph of one horizontal component was made at Kamituki, a village in the northern part of Miyakesima island, from 19 h 45 m, July 14, 1940, about 48 hours after the first eruption that occurred in the island. The constants of the microseismograph are

Geometrical magnification	330
Period	1·0 sec
Damping ratio	1/20

The recording drum was worked by a clock. When the observation was begun, the fissure eruptions that occurred on the mountain side and the activities of parasitic cones that were newly formed in the sea had already come to a standstill, although large volumes of smoke, loaded with ash, were rising from the central crater of the summit (Oyama).

Within four hours since the beginning, twenty earthquakes were recorded, fifteen of which were of very small amplitude, namely, less than 9·0 mm on the record, which corresponds to 27 μ actually. The amplitude of the volcanic pulsations at this time was $0{\cdot}9\,\mu \sim 2{\cdot}4\,\mu$, which was only one or two per cent of those that occurred later. From July 14 to 19, the wind and sea were so high that they excited pulsations of small amplitude, but these were easily distinguished on the record from those due to the volcano. These disturbances ceased after July 20. In this paper, we shall describe the volcanic pulsations and the micro-earthquakes that occurred during the period of about three weeks that we spent on the island.

In order to get a general aspect of the volcanic pulsations, we worked out a mean of the amplitudes of the ten largest pulsations that were recorded during the first five minutes of every hour. Using these mean values of amplitude, we worked out a mean for the period, that is, $0^h \sim 6^h$, $6^h \sim 12^h$, $12^h \sim 18^h$, and $18^h \sim 24^h$, as shown in Fig. 1. During the period since the beginning of observation to 18 h, July 18, the mean amplitude obtained in this way, which did not exceed 3 μ, then increased to

6 μ, and remained so until 6 h, July 19. Simultaneously with the larger volcanic pulsations, came the sounds of explosion from the summit at Kamituki. These sounds were not so loud as those that were heard later; they were not heard at Akô, lying about 10 km distant from

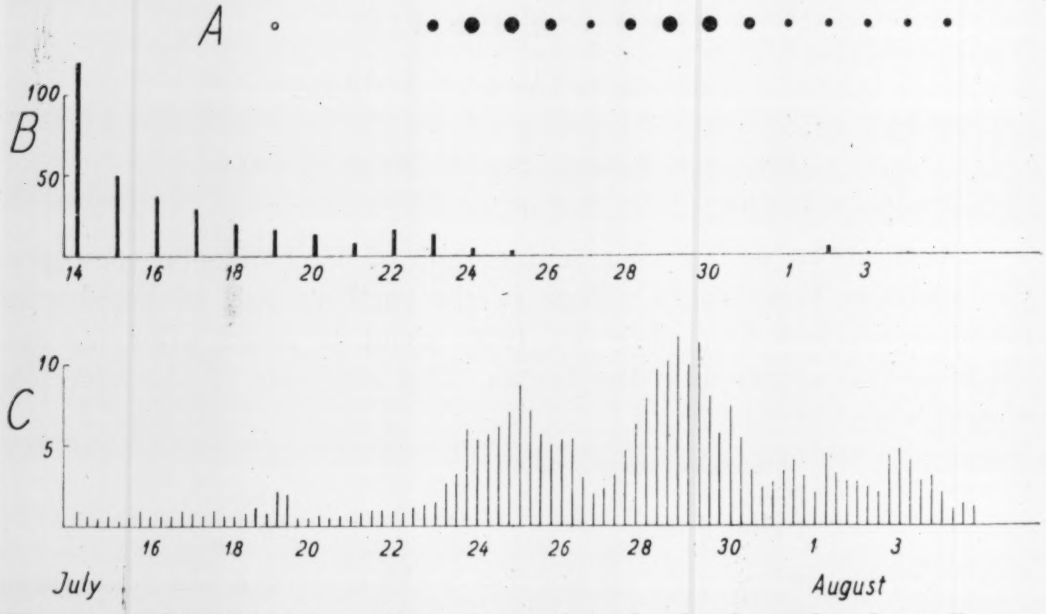

Fig. 1. A = detonation of eruption, B = number of volcanic earthquakes, C = amplitude of pulsation, unit = 3×10^{-3} mm.

Kamituki. During the period from July 20 to 23, the pulsations grew weaker and the amplitude decreased to 3 μ. But the amplitude gradually increased again from the morning of July 23 until it reached 9 μ at 8 h, July 24, and 18 μ at 12 h, the same day, and finally 25·5 μ in the evening of July 25. This time, the detonations were heard at Kamituki and severe air shocks shook the houses at intervals of 10 or 20 sec. The smoke, which issued in great volumes from the central crater since the beginning of the activities, diminished conspicuously since July 22, although the ejection of volcanic bombs from the crater continued with every explosion.

As already stated, the amplitude of the volcanic pulsations, which reached 25·5 μ in the afternoon of July 25, began then to decrease until on July 27, it was 5·4 μ, after which it again increased and remained at 33 μ during the period from the morning of July 29 to the night of July 30, on which last date it reached as much as 60 μ in some individual cases. The volcanic pulsations observed on these two days were the largest during the course of the present volcanic activity, the detonations coming from the central crater being also the loudest. After this activity, the pulsations promptly weakend, and the amplitude dropped to 3·6 μ on August 5, and the detonations which were now heard at

longer intervals became fainter.

A group of waves corresponding to the sounds of some explosion, was recognized on the pulsation records. The interval between two explosions was sometimes 10～30 sec. About ten seconds after the sounds were heard, a conspicuous group of waves was recorded. The distance between the seismograph and the central crater is about 4 km. The maximum amplitude of the pulsations in a group would run parallel with the loudness of the detonations. (Fig. 1).

As already stated, the volcanic pulsations were intimately related to the activity of the central crater. It is believed that volcanic pulsations are surface waves which expand from the surface of the crater as the result of the explosions. The same phenomenon was observed in the case of the activity of Volcano Kusatu-sirane,[1] during the years from 1938 to 1939, in which pulsations resembling those of the present case were observed about 500 m distant from the crater (Yukama) in which explosions occurred at intervals of 10 or 20 seconds.

According to K. Sassa,[2] who studied the volcanic pulsations that occurred in the case of the activity of Volcano Aso, which has many points in common with the central crater of Miyakesima, the volcanic pulsations that occurred incessantly for many hours had their origin in the intermittent explosions that occurred at intervals of several tens of seconds. Volcanic pulsations of this type are thought to be inseparable from eruptions of volcanoes of the *Stromboli* type, for example, Miyakesima, Oosima and Aso. These pulsations differ greatly from those that occur in connection with volcanoes of *Vulcano* type, for example, Volcano Asama.

The loudness of the detonations was divided into three classes, large, intermediate, and small, purely according to the writer's physical sensations, and plotted in Fig. 1, which gives a general idea of them.

The relation between the amplitude and the period of the volcanic pulsations is shown in Fig. 2. The period of the pulsations ranges from 0·45 sec to 0·68 sec, it being an almost constant value, 0·60 sec, when the amplitude exceeds 9 μ, which is shortened with decrease of amplitude when the latter is less than 9 μ.

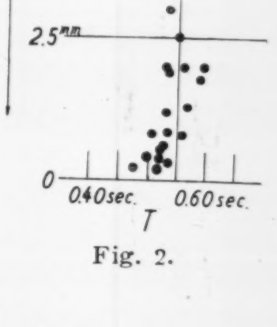

Fig. 2.

1) T. MINAKAMI, *Bull. Earthq. Res. Inst.*, **17** (1939), 590～623.
2) K. SASSA, *Memo, Coll. Sci. Kyoto Imp. Univ.* 18, **19** (1935, 1936).

The number of micro-earthquakes recorded by the same instrument is also shown in Fig. 1. Since the observation began from 20 h of July 14, the number that occurred on July 14 was estimated from the data for 4 hours from 20 h to 24 h, assuming that the hourly frequency of occurrence did not change throughout the day. This value may be somewhat small, because the number of earthquakes decreased with lapse of time. In other cases, as for example when observations were missed for a few hours, the gap was filled by estimates made by the same method. As will be seen from the figure, the number of volcanic earthquakes decreases with lapse of time in the same manner as in the after-shocks of a well-marked earthquake.

Comparing the time variation of the amplitude of the volcanic pulsations with the number of volcanic micro-earthquakes, it will be found that the number of micro-earthquakes decreased after the central crater began to eject molten lava by explosion, as the result of which the amplitude of the pulsations increased (on July 24). Although a number of earthquakes occurred on August 2, their amplitudes are very small compared with the one that occurred previously.

It may be concluded that the earthquakes were caused by the activity of the magma that lay at a certain depth under the ground, and that the origin of this activity ascended until there accumulated in the central crater the energy necessary for ejecting volcanic bombs and other fragments, consequently generating air sounds and causing pulsations.

Considering the mechanism of the occurrence of volcanic pulsations, it cannot be supposed that any volcanic pulsations were caused before the first eruption of Miyakesima, although many earthquakes had occurred. It is reported that earthsounds were heard near where the fissure eruption occurred which, however, differ, probably from the pulsations just mentioned.

Part VII. Anomalous Change in Geomagnetism Accompanying Volcanic Activity.

By Takesi NAGATA,

Earthquake Research Institute.

(Read Sept. 18, 1940.—Received Mar. 20, 1941.)

1. Introduction.

On July 12, 1940, a volcanic island, Miyake-sima, about 180 km south of Tokyô, erupted violently. Full details of the progress of the volcanic activity together with a description of the rocks will be found in a paper by H. Tsuya[1]. The expedition party to this volcano consisted of a geologist and some geophysicists. One of the interesting problems in recent volcano-physics is whether or not a local geomagnetic change of fair magnitude accompanies volcanic activity, and, if it does, what relation is there between the geomagnetic change and the internal physical conditions under the earth's surface. The question whether or not any marked geomagnetic change is caused by a change in the internal condition of the earth's crust, for example, volcanic activity or earthquake, has been put by a number of investigators, for example, A. Tanakadate and H. Nagaoka[2], S. Chapman[3], S. T. Nakamura and Y. Kato[4], J. P. Rothé, H. Nagaoka[6], T. Minakami[7], and the writer[8]. In answer to this question, a number are of the opinion that volcanic activity results in local geomagnetic changes, for example, S. T. Nakamura in the case of the Komagadake Volcano, H. Nagaoka and the writer in that of the Asama Volcano.

For a reliable answer, however, it is necessary to examine the geomagnetic field near the volcano with the aid of more certain methods than used heretofore and with the utmost care. Because Volcano Miyake-sima is, fortunately, a basaltic volcano, the rocks composing it having

---

1) H. TSUYA, Part I of this Report.
2) A. TANAKADATE and H. NAGAOKA, *Journ. Col. Sci. Tokyo Imp. Univ.*, **1** (1893), 149.
3) S. CHAPMAN, *Terr. Mag.*, **35** (1930), 81.
4) S. T. NAKAMURA, *Proc. Imp. Acad. Japan*, **11** (1935), 102.
5) J. P. ROTHÉ, *Ann. Inst. Phys. Globe*, **15** (1937), 1.
6) H. NAGAOKA and T. IKEBE, *Proc. Imp. Acad. Japan*, **13** (1937), 62, 251.
7) T. MINAKAMI, *Zisin*, **10** 1938), 430.
8) T. NAGATA, *Zisin*, **10** (1938), 221.

comparatively large magnetic susceptibility and a high intensity of thermo-remanent magnetization, the present activity was a unique opportunity for examining the above-mentioned problem. For this reason, the geophysicists, R. Takahasi and K. Hirano, measured the distribution of geomagnetic field in the island by means of a Z-field balance, and T. Minakami with a dip-circle, and obtained the difference in geomagnetic fields for different times, while the writer made continuous observations of changes in geomagnetism at a point near the volcano by means of a magnetograph. The results of all these observations showed that a local anomalous change in geomagnetism of fair magnitude accompanied the present activity. This report discusses the method and the results of observations with a magnetograph.

2. Instrument.

The magnetograph used in the present expedition was the dip-variometer designed by the writer, as already described[9]. Although, for studying local anomalous variation with a certain degrees of accuracy, observation by means of the three-component magnetograph is most desirable, it was possible to take only the dip-variometer with us, particularly as the volcanic eruption was quite unforeseen and unexpected, and the locality is a solitary island far from modern conveniences. However, as will easily be seen from the mechanic principle of this variometer, the temperature-coefficient is just as satisfactory as in the usual D-variometer, so long as it is carefully adjusted. This is the main reason that this variometer was chosen as the instrument for observation. The second reason for the choice was that absolute measurements with a magnetometer is very simple and easy in the dip compared with the other components.

Here, we shall deal only with the general characteristics of this instrument. In the portable dip-variometer used in the present expedition, the magnifying device by means of bifilar suspension of a mirror was done away with in order to ensure stability and to avoid unaccountable errors due to the particular device, although the sensitivity was reduced owing to lack of the device. This left, as the principal part of the instrument, only a bar magnet of M. K. steel, 10 cm in length and 1 cm in diameter, supported on agate plates by a knife edge, with which the centre of gravity of the magnet-system is brought in line. The deflection of the magnet was magnified solely with the aid of the usual optical lever.

9) T. NAGATA, *Bull. Earthq. Res. Inst.* **15** (1937), 185.

[Bull. Earthq. Res. Inst., Vol. XIX, Pl. XXVI.]

(震研彙報 第十九號 圖版 水上)

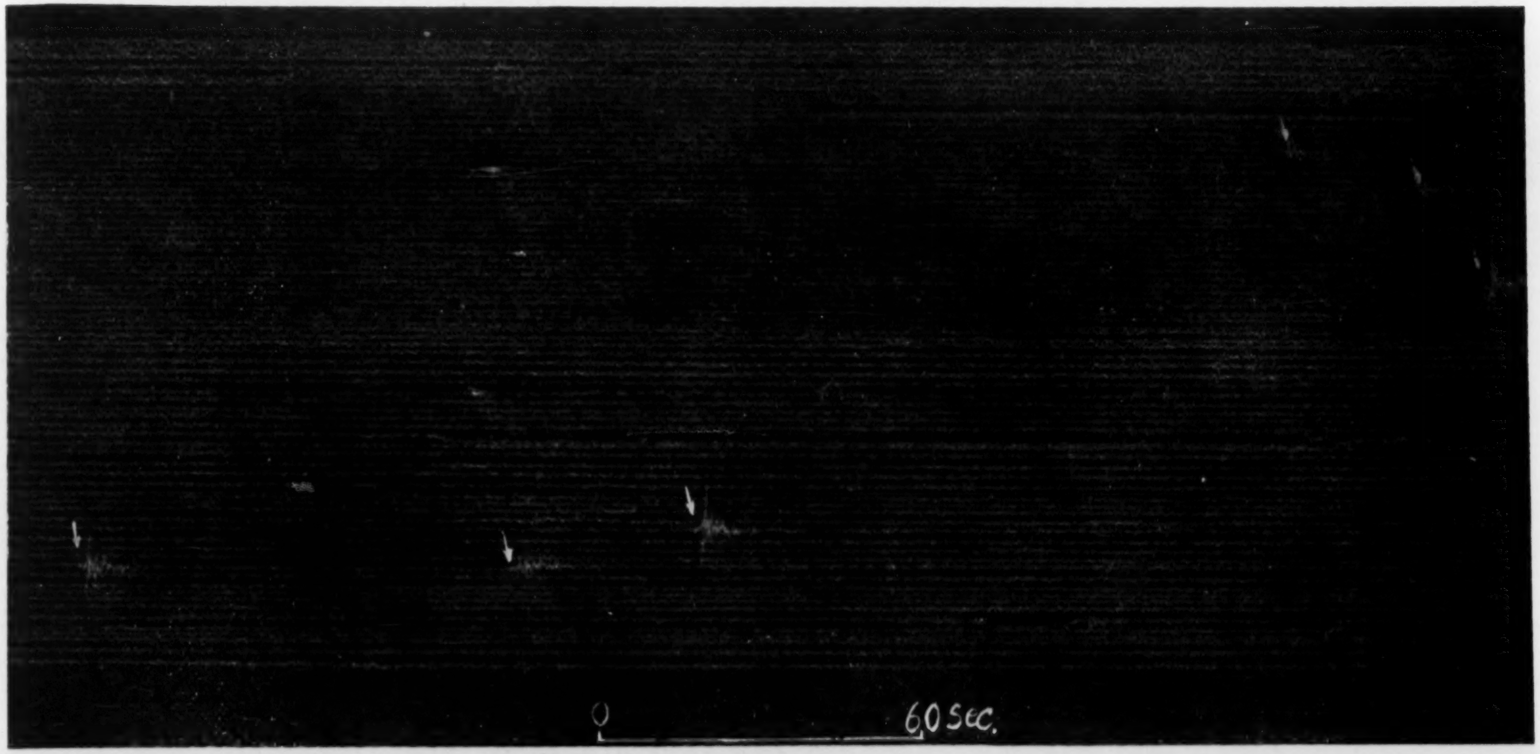

Fig. 3. Seismogram during July 22 and 23.

compar
thermo
tunity
geoph
geoma
Minak
fields
of ch
a ma
local
the p
of ol

met
stu
obs
rat
cul
an
ev
m
va
th
se
m
c

s
f

(震研彙報 第十九號 圖版 水上)

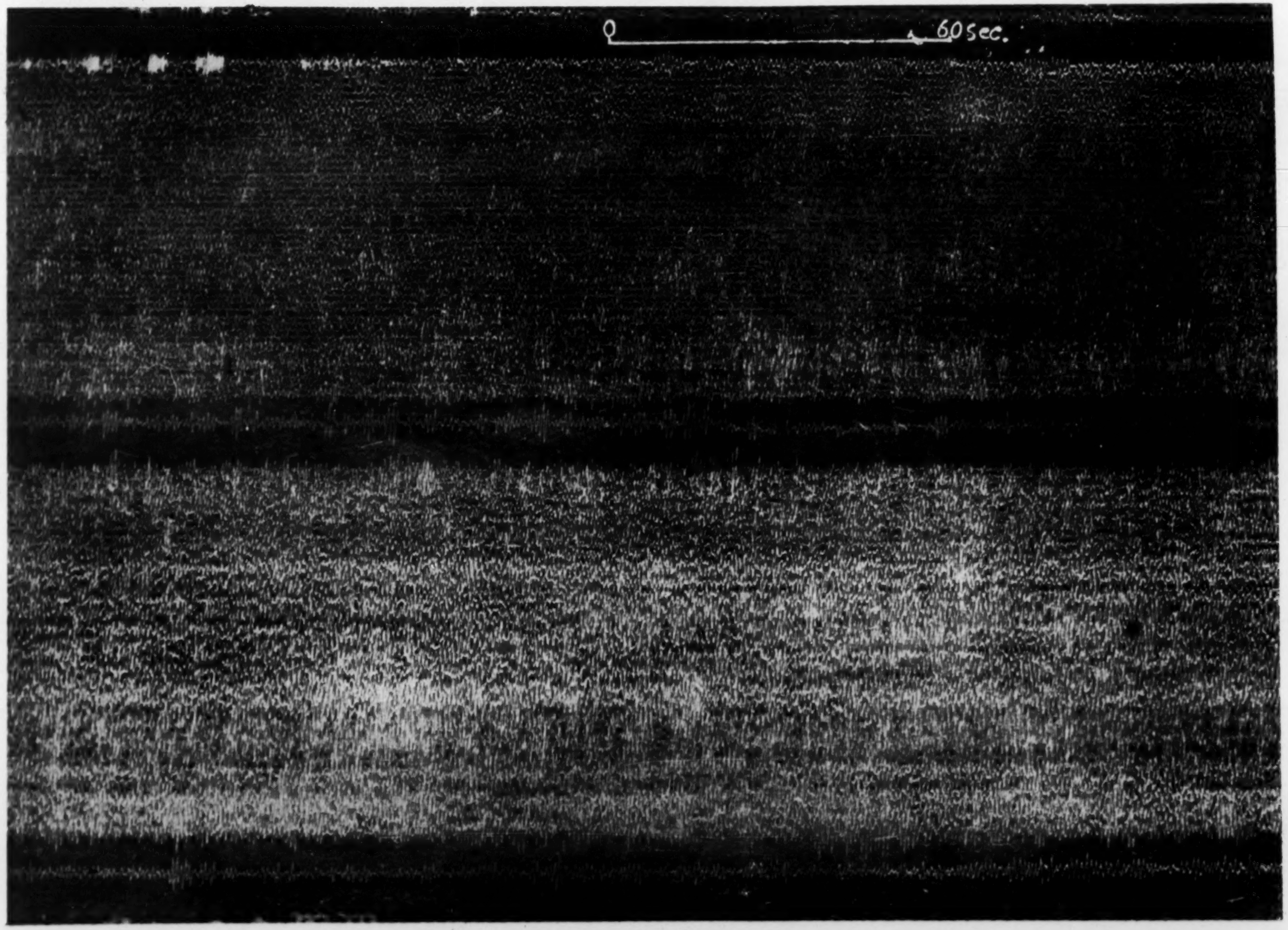

Fig. 4. Seismogram during July 26 and 27.

[Bull. Earthq. Res. Inst., Vol. XIX, Pl. XXVIII.]

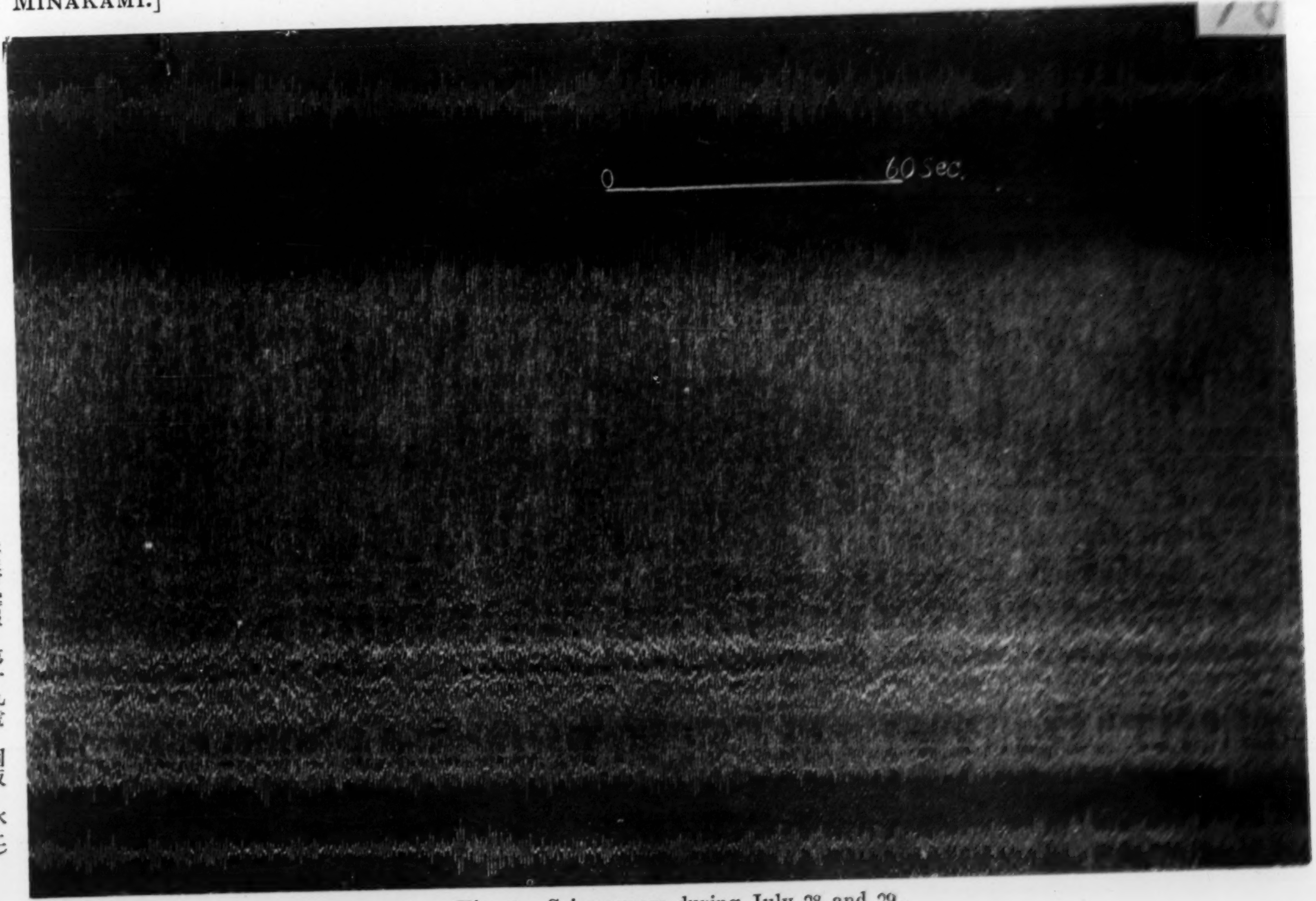

Fig. 5. Seismogram during July 28 and 29.

(震研彙報 第十九號 圖版 水上)

In such a case, the equation of equilibrium of the magnet system in its initial condition is

$$\left.\begin{aligned} M_0 H_0 \sin\theta_0 &= mgp_0 \sin\varphi \\ \theta_0 &= I_0 - \Theta_0, \end{aligned}\right\} \qquad (1)$$

where

M_0 = total magnetic moment of the magnet-system in standard temperature

m = total mass of the magnet-system

H_0 = initial value of total intensity of geomagnetism

I_0 = initial value of dip of the geomagnetic force

Θ_0 = initial value of dip of the bar magnet

p_0 = distance between the centre of gravity of the magnet system and the line of the knife edge

φ = angle between the vertical and the p-line

as shown in Fig. 1.

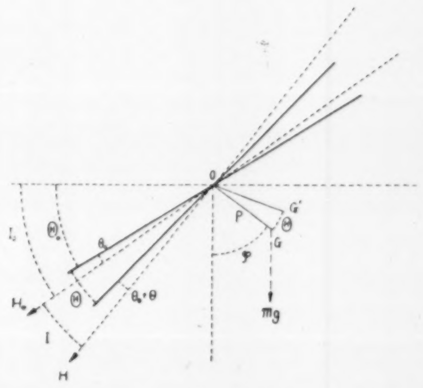

Fig. 1.

The equilibrium equation in the general case, in which the total geomagnetic force is $H = H_0 + \Delta H$ and the dip is $I_0 + I$, is

$$\left.\begin{aligned} MH\sin(\theta_0+\theta) &= mgp\sin(\varphi+\Theta), \\ I-\Theta &= \theta, \end{aligned}\right\} \qquad (2)$$

where I, Θ, and θ are respectively the angles given in Fig. 1. Eliminating θ from equation (2), we get

$$MH\sin(\theta_0 + I - \Theta) = mgp\sin(\varphi+\Theta). \qquad (3)$$

Then taking Θ, H, and t (temperature) as three independent variables, we get

$$\Delta I_1 = \int_{\Theta_0}^{\Theta_1} \frac{\partial}{\partial\Theta} I(\Theta, H_0, t_1)\,d\Theta + \int_{H_0}^{H_1} \frac{\partial}{\partial H}(\Theta_1, H, t_1)\,dH$$
$$+ \int_{t_0}^{t_1} \frac{\partial}{\partial t}(\Theta_0, H_0, t)\,dt^{10)},$$

10) Cf. H. H. HOWE, *Terr. Mag.*, **42** (1937), 29.

or approximately,

$$\Delta I=\left(\frac{\partial I}{\partial \Theta}\right)_0 \Delta\Theta+\left(\frac{\partial I}{\partial H}\right)_0 \Delta H+\left(\frac{\partial I}{\partial t}\right)_0 \Delta t, \tag{4}$$

where $(\ \ )_0$ denotes $(\ \ )_{\Theta_0, H_0, t_0}$.

While from eqs. (1) and (3), we obtain for the scale value

$$\left(\frac{\partial I}{\partial \Theta}\right)_0=1+\frac{mg\,p_0\cos\varphi}{M_0H_0\cos\theta_0}, \tag{5}$$

and for the spurious factor,

$$\left(\frac{\partial I}{\partial H}\right)_0=-\frac{1}{H_0}\tan\theta_0, \tag{6}$$

and for the temperature coefficient,

$$\left(\frac{\partial I}{\partial t}\right)_0=\left(\frac{\partial I}{\partial M}\right)_0\left(\frac{\partial M}{\partial t}\right)_0+\left(\frac{\partial I}{\partial p}\right)_0\left(\frac{\partial p}{\partial t}\right)_0+\left(\frac{\partial I}{\partial \varphi}\right)_0\left(\frac{\partial \varphi}{\partial t}\right)_0$$

$$=-\frac{1}{M_0}\tan\theta_0\left(\frac{\partial M}{\partial t}\right)_0+\frac{mg\sin\varphi}{M_0H_0\cos\theta_0}\left(\frac{\partial p}{\partial t}\right)_0+\frac{mg\,p_0\cos\varphi}{M_0H_0\cos\theta_0}\left(\frac{\partial \varphi}{\partial t}\right)_0. \tag{7}$$

In the temperature coefficient term, $\frac{1}{M_0}\left(\frac{\partial M}{\partial t}\right)_0$ is the temperature coefficient of the magetic moment of M. K. steel, $\frac{1}{p_0}\left(\frac{\partial p}{\partial t}\right)_0$, is the linear expansion coefficient of the entire magnet system, while $\left(\frac{\partial \varphi}{\partial t}\right)_0$ is the deflection of the p-line due to lack of uniformity in the thermal expansion of the material composing the magnet-system, namely, M. K. steel and brass. In the present instrument, however, it may be assumed that

$$\left(\frac{\partial \varphi}{\partial t}\right)_0 \ll \frac{1}{p_0}\left(\frac{\partial p}{\partial t}\right)_0, \quad \left(\frac{\partial \varphi}{\partial t}\right)_0 \ll \frac{1}{M_0}\left(\frac{\partial M}{\partial t}\right)_0,$$

seeing that the non-uniformity in thermal expansion appears to be small. Hence, putting

$$\frac{1}{M_0}\left(\frac{\partial M}{\partial t}\right)_0=\alpha, \quad \frac{1}{p_0}\left(\frac{\partial p}{\partial t}\right)_0=\beta,$$

we get

$$\left(\frac{\partial I}{\partial t}\right)_0 = -\alpha \tan\theta_0 + \beta \frac{mgp_0 \sin\varphi}{M_0 H_0 \cos\theta_0}. \tag{7'}$$

While on the other hand, we get from eq. (1)

$$\frac{mgp_0 \sin\varphi}{M_0 H_0 \cos\theta_0} = \tan\theta_0.$$

Substituting this relation in Eq. (7′), we obtain

$$\left(\frac{\partial I}{\partial t}\right)_0 = -(\alpha-\beta)\tan\theta_0. \tag{7}$$

Finally, from eqs. (3), (5), (6), (7), we get the general equation of the deflection of the dip variometer as

$$\Delta I = \left(1 + \frac{mgp_0 \cos\varphi}{M_0 H_0 \cos\theta_0}\right)\Delta\theta - \tan\theta_0 \frac{\Delta H}{H_0} - (\alpha-\beta)\tan\theta_0 \Delta t. \tag{8}$$

The values of the three terms in this general equation for the instrument actually used, and the method of the calibrations are as follows:

(i) Sensitivity. The balance of the magnet system was adjusted before the expedition started, that is, the centre of gravity of the magnet was brought in line with the knife edge. This operation was carried out in a non-magnetic space, which was attained by eliminating the geomagnetic field with the aid of a Helmholtz coil. The sensitivity calibrated by means of this coil in the laboratory, in Tokyo, was $\Delta\theta/\Delta I =$ 1.00, with an error of less than 0·005, namely,

$$\frac{mgp_0 \cos\varphi}{M_0 H_0 \cos\theta_0} < 0{\cdot}005.$$

Since, in the observing station on Miyake-sima such careful method of calibration was out of question, a different method was used. The equation for a small amplitude oscillation of the magnet system in a geomagnetic field H, in its total intensity, is given by

$$J\frac{d^2\theta}{dt^2} = -MH\sin(\theta_0+\theta) + mgp_0 \sin(\varphi-\theta), \tag{9}$$

where J is the moment of inertia around the line of the knife edge.

Since from eqs. (1) and (9) we get

$$J\frac{d^2\theta}{dt^2} = -(MH\cos\theta_0 + mgp_0\cos\varphi)\sin\theta, \tag{10}$$

if the amplitude of oscillation θ is sufficiently small, the period of oscillation T is given by

$$T=2\pi\sqrt{\frac{J}{MH\cos\theta_0+mgp_0\cos\varphi}}, \tag{11}$$

whereas if the centre of gravity of the magnet coincides exactly with the line of the knife edge, i. e. $p_0=0$, then the oscillation period is given by

$$T_0=2\pi\sqrt{\frac{J}{MH}}\ . \tag{12}$$

Hence, putting $\Delta T=T-T_0$, we get

$$\frac{\Delta T}{T_0}=-\frac{1}{2}\frac{mgp_0\cos\varphi}{MH\cos\theta_0},$$

and

$$\left(\frac{\partial I}{\partial\theta}\right)_0=1-2\frac{\Delta T}{T_0}\ . \tag{13}$$

Thus the scale value of the dip-variometer can be found by determining the period of free oscillation of the magnet, provided the total geomagnetic force in the localities concerned does not differ more than one percent. If there is a discrepancy of ΔH in the total geomagnetic intensities in the cases of eq. (11) and (12), then eq. (13) becomes

$$\left(\frac{\partial I}{\partial\theta}\right)_0=1-2\frac{\Delta T}{T_0}-\frac{\Delta H}{H_0}\ . \tag{13}$$

In the present case, T_0 was 5·50 sec. and $|\Delta T|$ was less than 0·04 sec., that is, $\left|\frac{\Delta T}{T_0}\right|<0{\cdot}01$, whereas, from the results of the magnetic survey by the Hydrographic Depertment, Imperial Japanese Navy[11], 1933, the value of $\left|\frac{\Delta H}{H_0}\right|$ is estimated to be less than two per cent. Hence, it may be concluded that the sensitivity of the dip-variometer was 1·00 ±0·005, assuming there was no change during its transportation from Tôkyô to Miyake-sima, but even if there was a change, it would be less than 4 percent.

The actual sensitivity on the record, magnified by means of the optical lever 120 cm long, was 0·698 mm per minute, with an error of less than 4 percent.

11) *Bull. Hydro. Dep. Imp. Jap. Navy*, **8** (1936).

(ii) The spurious factor.

The instrumental cause of the spurious factor is that due to the value of $\tan\theta_0$ alone. If the centre of gravity of the magnet has been properly adjusted, θ_0 must be zero. In the present case, where p_0 is sufficiently small, the amount of $\tan\theta_0$ would also be small. Since we get from eq. (1)

$$\tan\theta_0 \simeq \sin\theta_0 = \frac{mgp_0 \sin\varphi}{M_0 H_0} = \frac{mgp_0 \cos\varphi}{M_0 H_0 \cos\theta_0} \tan\varphi, \tag{14}$$

we may say that the value of $\tan\theta_0$ is of the same order of magnitude as that of $\frac{mgp_0\cos\varphi}{M_0H_0\cos\theta_0}$, provided $\tan\varphi$ does not greatly exceed unity.

For the purpose of estimating the amount of θ_0, the angle of dip of the magnet (θ) was measured with a graduater made of celluloid at the observing station. The measured angle was about 48°, with an error of $\pm 1°$, while the geomagnetic dip at a point about 20 m south of the station, determined with a dip-circle by Minakami[12], was 47°45′ ~48°10′, as mentioned in the next paragraph. It may therefore be assumed that $\theta_0 \lesssim 1°$, i. e. $\tan\theta_0 \lesssim 0{\cdot}02$, whence assuming that $H = 40{,}000\,\gamma$, we get

$$\left(\frac{\partial I}{\partial H}\right)_0 \lesssim 5\times 10^{-7} \quad \text{Rad.}/\gamma.$$

Since as will be seen from the above relation, a change of $600\,\gamma$ in total intensity corresponds to a spurious change in dip of one minute, the spurious factor my be neglected, seeing that the anomalous change in dip, the subject in consideration, amounted to 15′ and more, while the change in total intensity may not exceed $500\,\gamma$.

(iii) Temperature coefficient.

The temperature coefficient has the same mathematical form as that of the spurious factor, depending on the amount of $\tan\theta_0$. From a rough estimate of the magnitudes of α and β,

$$\alpha = 7\times 10^{-4}, \quad \beta = 2\times 10^{-5}.$$

Hence taking $\tan\theta_0 \lesssim 0{\cdot}02$, it is possible to estimate the value of the temperature coefficient, getting

$$\left|\left(\frac{\partial I}{\partial t}\right)_0\right| \lesssim 1{\cdot}4\times 10^{-5} \quad \text{Rad./degree.}$$

12) T. Minakami, Part IX of this Report.

This relation shows that a temperature change of 20°C causes the magnet to deflect one minute, whereas the temperature change of the magnet was three degrees at most during the period of the present observation, because the instrument was thickly covered with thermal insulating material, as mentioned in the next paragraph. Therefore, the temperature coefficient may also be neglected in the present problem in which only a large change in dip is discussed.

3. The observation and its results.

The dip-variometer was set up on the earthen floor in a wooden house at Hôdai, the north-eastern coast of Miyake-sima on July 15, and systematic observations was begun from the 17 th, five days after the violent eruption of this volcanic island. The observing station was situated about 4 km north-east of the central cone O-yama, and about 1·5 km north of the new fissure, as shown in Fig. 2. The dip-variometer, covered with a bell-jar made of thick glass, was shielded in a wooden box with sides 1 cm thick, around which many sheets of straw matting and a large quantity of dry grass were piled in heaps, 30 cm in total thickness, so that the seasonal and diurnal changes in temperature in the instrument would be much less than 5 degrees, the amount of total change in indoor temperature during the period of the present observation.

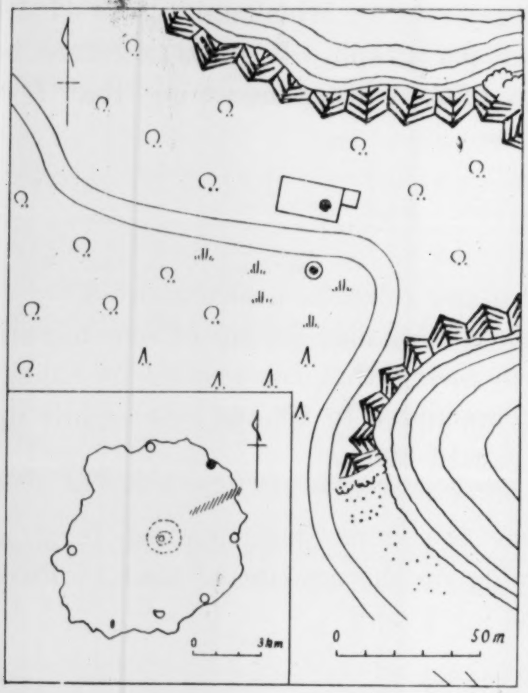

Fig. 2. The Magnetic station at Hôdai, Miyake-sima (Full Circle). Double circle shows the position where the absolute measurement was made.

The observations lasted 18 days, from July 17 to August 3, when the local anomalous change in geomagnetism seemed to have ceased. During the period of observation, absolute measurements of the dip by means of a dip circle were made five times by Minakami[12] at a point 20 m south of the observing station. On July 16, prior to beginning the geomagnetic observations with a magneto-

12) *loc. cit.*

Table I. Hourly Values (L. S. T.) of Dip at Hôdai. ($I=47°\pm$)

Date / hr	17	18	19	20	21	22	23	24	25	26	27	28	29	30	31	Aug. 1	2	3
	min	min	min	min	min	min	min	min	min	min	min	min	min	min	min	min	min	min
0		58·4	54·6	51·3	48·1	48·0	49·3	46·1	44·0	43·7	43·7	47·4	47·9	49·4	48·7	48·6	46·7	45·3
1		58·7	54·7	51·6	48·3	48·4	49·1	46·1	43·3	43·6	—	47·1	—	49·6	48·0	48·3	46·4	45·1
2		59·1	54·1	51·6	48·4	48·7	48·9	46·0	43·4	43·7	—	47·1	—	49·3	48·3	48·6	46·3	45·4
3		59·3	54·3	51·6	48·4	49·1	48·7	46·1	43·7	43·6	—	46·9	—	49·3	47·9	48·4	46·7	45·9
4		58·7	54·3	52·0	48·6	49·4	49·0	46·4	43·7	44·1	—	46·6	—	49·0	48·3	48·4	46·9	44·9
5		58·4	54·4	52·1	49·3	49·6	49·1	46·6	44·1	44·3	—	46·3	—	49·1	47·9	47·9	46·4	43·6
6		57·4	54·1	51·9	49·8	50·0	48·7	46·6	44·3	43·0	—	46·3	—	49·1	48 4	47·1	36·3	44·0
7		56·6	53·7	51·6	49·4	48·7	47·4	46·9	44·3	43·6	—	46·9	—	49·4	48·7	47·1	45·7	43·4
8		56·9	53·0	51·1	48·1	48·1	46·3	46·4	44·3	43·1	—	46·4	—	49·3	48·7	47·3	45·0	43·3
9		56·9	51·6	48·9	48·0	47·1	45·4	45·0	44·0	43·0	—	46·1	—	48·1	48·3	47·3	44·4	42·9
10		57·4	51·4	47·4	46·9	46·1	44·0	43·7	45·9	42·9	—	44·4	—	47·9	47·1	46·6	43·7	43·0
11	57·0	57·6	51·7	46·0	46·3	44·7	43·1	41·6	44·3	42·4	—	44·0	—	46·9	49·0	49·0	43·9	42·3
12	57·3	56·3	51·3	45·9	45·3	44·7	43·4	41·3	43·7	42·1	46·1	43·1	46·4	45·9	49·0	48·4	43·6	42·9
13	57·9	56·0	51·9	45·1	44·7	45·1	93·9	41·7	43·0	42·6	46·4	43·0	46·4	46·6	48·9	47·4	44·0	42·6
14	59·1	55·1	51·1	45·3	45·3	46·3	44·0	42·3	42·6	43·0	47·0	43·4	46·3	45·4	48·9	46·7	44·0	
15	59·9	54·7	51·0	44·9	45·9	47·9	44·4	42·3	43·4	43·6	47·1	44·4	47·1	45·0	49·4	46·3	44·0	
16	59·7	54·3	51·9	44·7	56·4	49·7	44·7	42·6	43·6	44·7	47·7	45·3	48·6	45·9	48·7	46·0	43·4	
17	58·9	54·1	51·9	46·1	46·7	48·9	45·3	43·0	45·0	44·6	47·9	46·6	49·3	45·7	48·4	45·9	43·4	
18	59·3	54·4	51·7	48·0	47·4	49·1	45·7	44·0	45·6	44·9	48·6	47·1	49·3	47·0	49·0	45·7	44·1	
19	59·4	55·0	51·6	48·1	48·1	49·3	46·0	45·1	45·4	44·7	48·6	47·4	49·1	48·7	48·6	46·0	44·6	
20	59·0	54·4	51·7	48·3	49·4	49·1	46·0	45·0	44·7	44·6	47·9	48·3	49·7	48·9	48·9	45·9	44·3	
21	59·0	54·1	51·3	48·3	49·7	49·3	46·3	44·4	44·9	44·4	47·9	47·9	49·9	48·3	49·0	46·0	44·4	
22	58·6	54·6	51·4	48·3	48·9	49·3	46·4	45·0	43·7	43·9	47·7	48·0	49·6	48·7	49·0	45·9	44·9	
23	58·4	54·9	51·1	48·1	48·6	49·1	46·0	44·1	43·9	43·6	47·6	48·3	49·3	48·6	48·7	46·1	45·0	

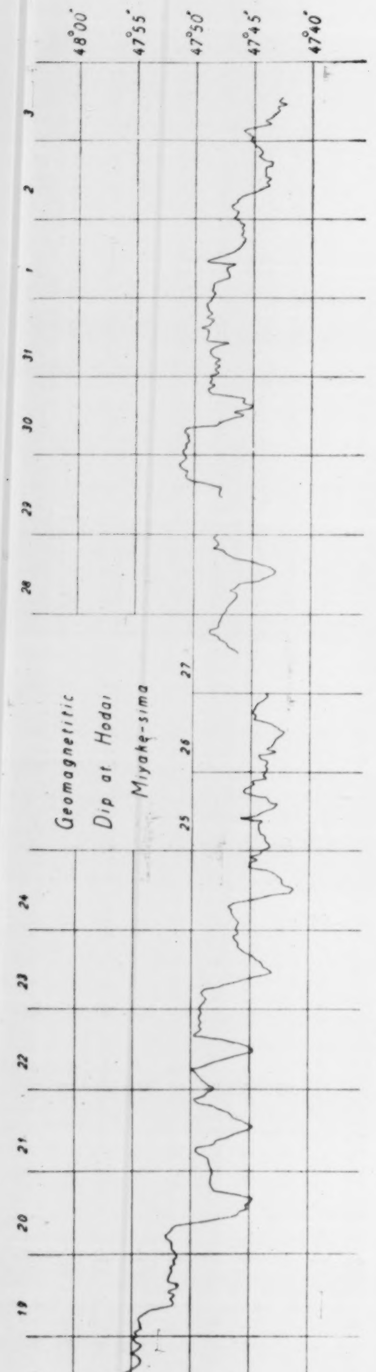

Fig. 3. Variation in dip at Hôdai, Miyake-sima.

graph, the dip value at the observing point was also measured. From these values, it was possible to determine the base-line value of the record obtained by the dip-variometer.

The hourly values of the dip thus determined are given in Table I, and plotted in Fig. 3.

As will be clear from this result, the dip at Hôdai gradually decreased from the time when the observation was begun until about July 25, although the diurnal variation was superposed on this gradual change. After the 25 th, the dip began to increase, reaching maximum about the 30th, after which it gradually declined again. The magnitude of the decrease in dip during the 9 days from the 17 th to the 25 th amounted to about 16 minutes.

In order to see the anomalous change more clearly, it is desirable to eliminate the diurnal variation from the observed result. For this purpose, we took the daily mean of these observed hourly values, where time is referred to G. M. T. These daily mean values are given in Table II, and shown in Fig. 4, where the anomalous change mentioned above can be seen more clearly. In Fig. 4, the daily mean values of dip, which are reduced from Minakami's absolute measurement by means of dip-circle, are also shown.

Before we deal with the extent of the anomalous change, it is necessary to examine the dip variation during the same period in other districts in order to see whether the anomalous change was merely local, regional, or general.

For this purpose we compared our

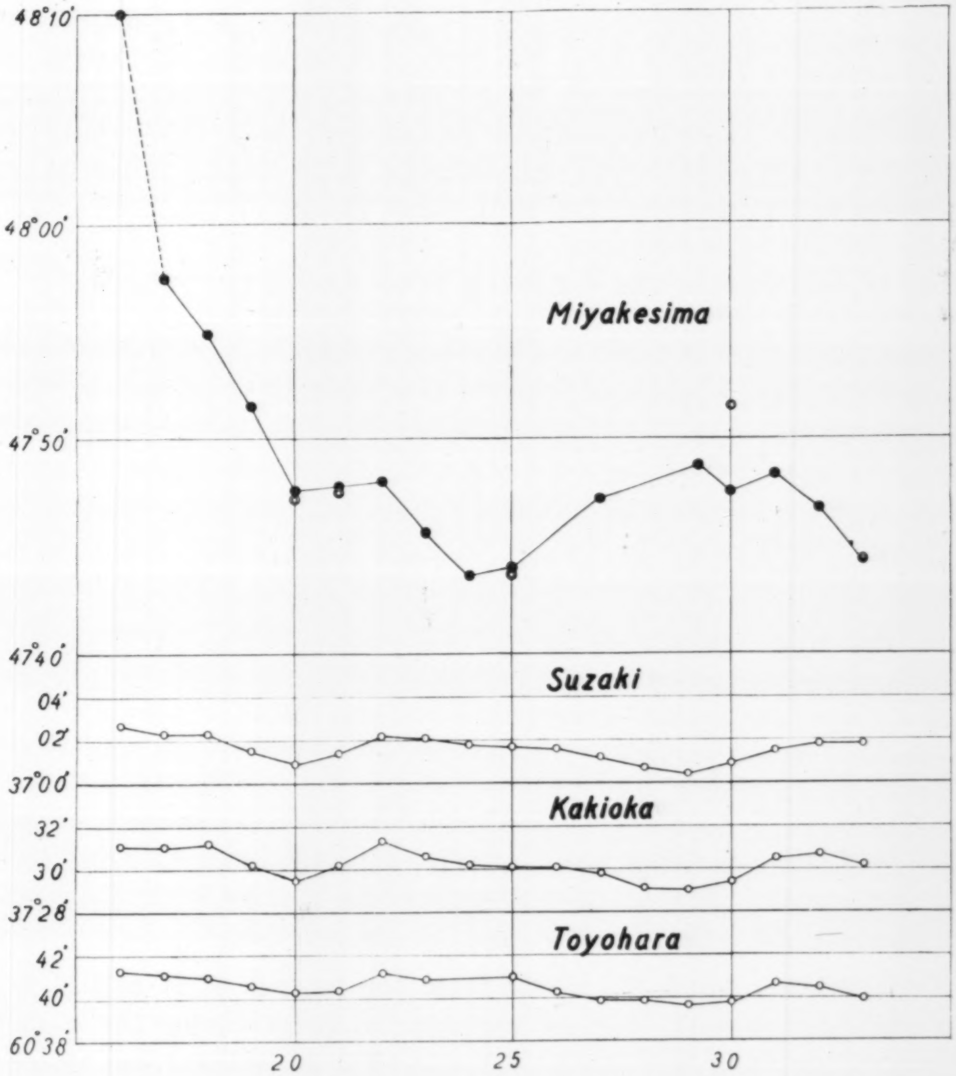

Fig. 4. The day-to-day variation in dip at Hôdai, Miyake-sima, and other stations. (Double circles give the corrected values of dip, which were absolutely measured by T. Minakami with the aid of dip-circle).

data with those obtained in three magnetic stations in Japan, namely, the Kakioka Magnetic Observatory, in the Kantô District (Lat. 36° 13′ 51″ N, Long. 140° 11′ 21″ E), the Tayohara Magnetic Observatory, in Karahuto (Lat. 46° 58′ N, Long. 142° 45′ E), and the magnetic station of the Mitui Geophysical Institute, at Suzaki, Izu Peninsula (Lat. 34° 40′ N, Long. 138° 59′). Of these three stations, that nearest Miyake-sima is the Mitui Institute, about 80 km distant, followed in proximity by Kakioka, 250 km distant, the farthest being Toyohara, 1500 km distant.

At these stations, the horizontal and vertical intensities and the

declination are continuously recorded, as in other geomagnetic observatories, but direct records of dip were not available. Moreover, since among the observed values of horizontal and vertical intensities at two of the stations, T. and K., up to the present only their daily mean values were reported[13], the approximate daily mean values of dip $\bar{I}$ have to be estimated from the daily mean values of the horizontal and vertical intensities, as follows.

As is well known, the following is an established relation :

$$\left.\begin{aligned} \tan I &= \frac{Z}{H} = \frac{\bar{Z}+\Delta Z}{\bar{H}+\Delta H} = \frac{\bar{Z}}{\bar{H}}\left[1+\left(\frac{\Delta Z}{\bar{Z}}-\frac{\Delta H}{\bar{H}}\right)+\left(\frac{\Delta Z\cdot\Delta H}{\bar{Z}\cdot\bar{H}}\right.\right. \\ &\qquad \left.\left.-\frac{(\Delta H)^2}{\bar{H}^2}\right)\right]+O\left[\left(\frac{\Delta Z}{\bar{Z}}\right)^3\right], \\ \text{and}\quad \overline{\Delta Z} &= \overline{\Delta H} = 0, \end{aligned}\right\} \qquad (14)$$

where the upper vinculum is the daily mean value of those hourly read quantities, whence, we get

$$\left.\begin{aligned} \overline{\tan I} &= \frac{\bar{Z}}{\bar{H}}\Big[1+\varepsilon\Big] \\ \varepsilon &= \frac{\overline{\Delta Z\cdot\Delta H}}{\bar{Z}\cdot\bar{H}} - \frac{\overline{(\Delta H)^2}}{\bar{H}^2} + O\left[\overline{\left(\frac{\Delta Z}{\bar{Z}}\right)^3}\right]. \end{aligned}\right\} \qquad (15)$$

On the other hand, we learnt from the records of H and Z in the Mitui Institute that the largest variation in them during the period of our expedition was less tnan $100\,\gamma$ in its deviation from the daily mean value ; that is,

$$\left|\frac{\Delta Z}{\bar{Z}}\right| < 3\times10^{-3}, \quad \left|\frac{\Delta H}{\bar{H}}\right| < 3\times10^{-3},$$

from which we get

$$|\varepsilon| < 2\times10^{-5}.$$

Similarly the relation between $\overline{\tan I}$ and $\tan\bar{I}$ is given by

$$\left.\begin{aligned} \overline{\tan I} &= \tan\bar{I}+\mu, \\ \mu &= \sec^2\bar{I}\cdot\sin\bar{I}\cdot\overline{(\Delta I)^2}+O\Big[\overline{(\Delta I)^3}\Big], \end{aligned}\right\} \qquad (16)$$

13) "Kisyôyô-ran" July and August, 1940.

where ΔI may be given by

$$\Delta I = \cos^2 I\left(\frac{\Delta Z}{Z} - \frac{\Delta H}{H}\right).$$

Provided the maximum values of ΔH and ΔZ are $100\,\gamma$, and I has a value of from 45° to 60°, we get $|\Delta I| < 3\times10^{-3}$, whence $|\mu| < 1\times10^{-5}$.

Finally from eqs. (15) and (16), we have

$$\left.\begin{aligned} \tan \bar{I} &= \frac{\bar{Z}}{\bar{H}} + \varepsilon - \mu, \\ \text{and} \quad |\varepsilon| + |\mu| &< 3\times10^{-5}. \end{aligned}\right\} \qquad (17)$$

Thus it is possible to estimate the daily mean values of the dip at three stations with the aid of the relation $\tan \bar{I} = \bar{Z}/\bar{H}$ with an error of less than 0·1′. This upper limit of the error is sufficiently small for the present purpose. The mean values obtained of the three stations are also given in Table II and Fig. 4.

Table II.

Date (in G.M.T.)		Geomagnetic Dip.				Mean Vlaue of ΔI of Kakioka and Suzuki*	Corrected Value of Dip at Hôdai
		Hôdai Miyake	Suzaki	Kakioka	Toyohara		
		min	min	min	min	min	min
July	16	47°	47° 02·7	49° 31·1	60° 41·3	+0·9	(48° 09·3)
	17	58·5	02·3	31·1	41·1	+0·7	47° 57·8
	18	54·9	02·3	31·2	41·0	+0 8	54·1
	19	51·5	01·5	30·2	40·6	+0·2	51·3
	20	47·6	00·9	29·5	40·3	−0·8	48·4
	21	47·8	01·4	30·2	40·3	−0·2	48·0
	22	48·0	02·2	31·3	41·2	+0·8	47·2
	23	45·6	02·1	30·6	40·9	+0·4	45·2
	24	43·6	01·8	30·2	—	0	43·6
	25	44·0	01·7	30·1	41·0	−0·1	44·1
	26	(43·9)	01 6	30·1	40·3	−0·2	(44·2)
	27	47·2	01·2	29·8	39·9	−0·5	47·7
	28	(46·0)	00·7	29·1	39·9	−1·1	(47·1)
	29	48·8	00·4	29·0	39·7	−1·3	50·1
	30	47·6	00·9	29·4	39·8	−0·9	48·5
	31	48·4	01·5	30·5	40·7	0	48·4
Aug.	1	46·7	01·8	30·7	40·5	+0·3	46·3
	2	44 3	01·8	30·2	40·0	0	44·3

* ΔI denotes the deviation of the daily mean value of dip from that on Aug. 2 (G.M.T).

As will be seen from Fig. 4, the day-to-day variation in dip at Hôdai, Miyake, was distinctly large compared with those at the other three stations, while those of the three stations were similar in their magnitudes as well as in their forms. It may then be assumed that the mean values of the day-to-day variation give the general variation for Japan and vicinity.

The true value of the local anomalous change at Hôdai, then, is given by the difference of the observed change and the general variation, the corrected values of the change being given in Table II and in Fig. 5, where the difference on Aug. 2 (G.M.T.) is assumed to be zero.

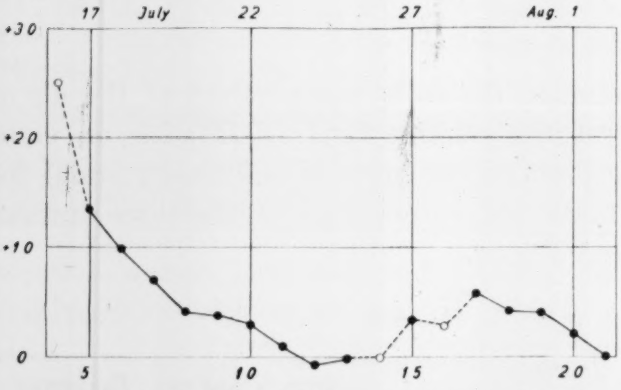

Fig. 5. Anomalous Change in Dip at Hôdai, Miyake-sima.

It is now possible to deal quantitatively with the amount of the local anomalous change, with possible, errors of less than 0′·5, even in this final corrected value. The general tendency of the day-to-day variation in the corrected values of the dip at Hôdai does not much differ from that in the directly observed values, that is, the dip decreased 14′·2 during the 7 days from the beginning of the observation until July 24, while it again increased from the 25 th to the 29 th, the magnitude of the increase being 6′·5, after which it decreased, the decrease during the period from July 29 to August 2 amounting to 5′·8.

But since, according to absolute measurements made by Minakami, the dip at Hôdai at 11 h 40 m July 16 (L. M. T.) amounted to 48° 09·′4, the difference of the value of the dip at about noon on the 16 th and that on the 17 th was 12′·7 at Hôdai. Since on July 16 and 17 there was no marked storm in the general geomagnetic field near Japan, the larger part of the difference of 12′·7 may be put down to the local anomalous change at Hôdai, provided we do not deal with quantities smaller than 3′. The decrease in dip during the period from July 16 to 24 then was about 26′. Although the final result obtained in the present study also may contain an observational error of about one minute, that, in the geomagnetic field near Miyake-sima, anomalous change occurred simultaneously with the present volcanic activity may be regarded as very probable. It is a remarkable fact that the geomagnetic field changed

in magnitude as much as 14′ in dip during such a short period as 7 days as also that it changed 26′ during 8 days.

4. Discussion.

In the figure of Part XIII of this report, the total number of volcanic earthquakes that occurred every day and the amplitudes of the volcanic tremors, both of which were observed at Kamituki by Hagiwara[14] and Minakami[15], are given. Comparing these variations with those of the geomagnetic dip, a correlation will be seen between the former and the latter. It may be presumed that the decrease of dip at Hôdai during the 8 days from July 16 was related to the after-effect of the great fissure eruptions on July 12 and 13, the after-activity being represented by the number of volcanic earthquakes. The larger part of the change in dip during the period from July 25 to August 3 might have been related to the volcanic activity of the central cone, O-yama, whose activity was shown by the volcanic earthquakes, the magnitudes of the tremors, and the magnitude of the detonation. Further quantitative discussions on this correlation, however, cannot be made with the present results alone.

Since we know nothing about the geomagnetic changes at Miyake-sima preceeding the beginning of our observations, it is not possible to say whether or not there was any remarkable anomalous change immediately preceeding or soon after the fissure eruption on July 12. For comparison, an example of geomagnetic changes that occurred simultaneously with the activity of other volcanoes, the secular variation in the daily mean values of dip (θ_A) at the Asama Volcano Observatory during the summer of 1937 (when Mt. Asama was comparatively calm), and in 1938 (when it was active), is shown in Fig. 6, where those at Kakioka (θ_K), and at Toyohara (θ_T), and the differences $\theta_A-\theta_K$, and $\theta_T-\theta_K$, are also given. As will be seen from Fig. 6, although there was no marked variation in the values of $\theta_A-\theta_K$ during the summer of 1937, the value of $\theta_A-\theta_K$, in 1938, once dereased before the beginning of the volcanic activity and then gradually increased, while there was no marked change in $\theta_T-\theta_K$ during the same periods in 1938 as well as in 1937. This tendency in dip-variation, which seems to accompany the volcanic activity of Mt. Asama, offers an interesting suggestion regarding the dip-variation prior to July 16, at Hôdai, Miyake-sima.

The general tendency of geomagnetic change accompanying volca-

14) Part V of this Report.

15) Part VI of this Report.

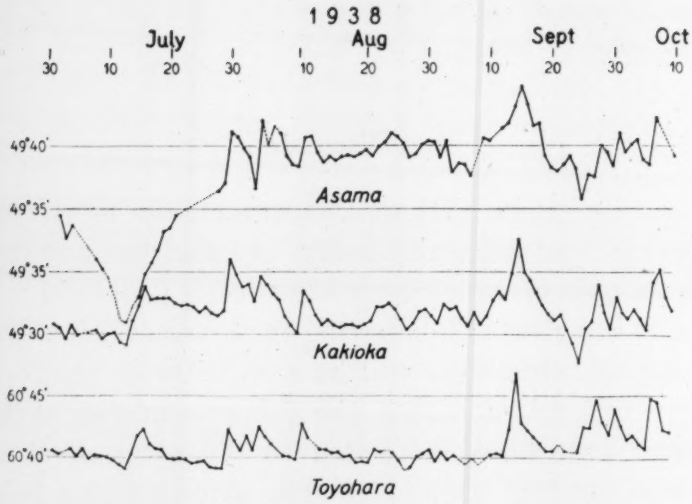

Fig. 6 a. The day-to-day variation in dip during the summer of 1938 at Volcano Asama.

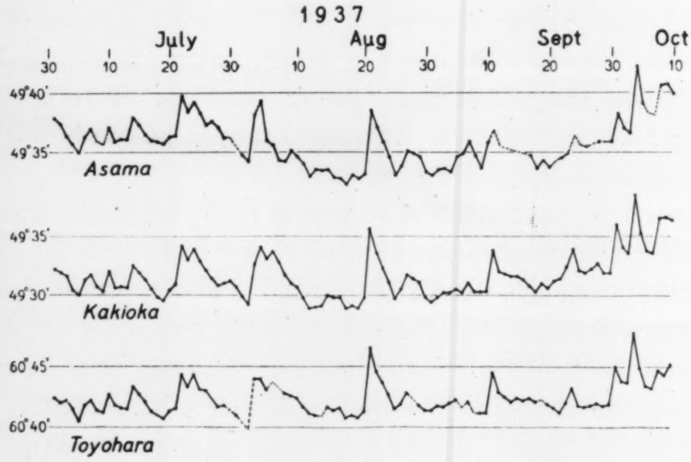

Fig. 6 b. The day-to-day variation in dip during the summer of 1937 at Volcano Asama.

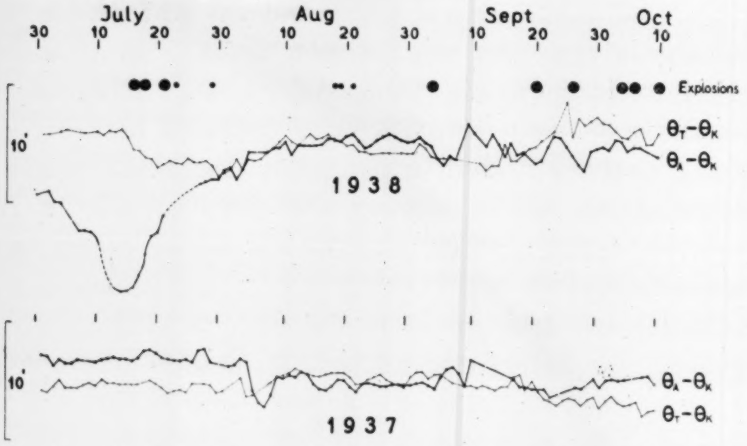

Fig. 6 c. Anomalous secular change in dip at Volcano Asama.

nic activity, however, will be dealt with after we have obtained a few more data on this problem.

Here, we shall merely compare the dip-variation obtained in the present study with the results of magnetic surveys in the island made by other investigators. According to the results of dip-measurement by Minakami[16], the values of the dip at seven stations distributed in the eastern and northern coast of the island decreased in magnitude from 15′ to 36′ during the period from the middle of July to the early part of August, although the tendencies of dip-variations at these stations were not always the same as that at H dai, except the observed result at a point 20 m south of our station. Some of these variations, observed at points near the lava flow may be explained as being due to change in magnetization of the lava flow itself, as the result of its cooling. The dip-variations at the other stations, for example, at Kamituki, showed the odd tendency that the dip decreased suddenly from July 29 although it seemed nearly constant during the period from July 15 to 29, so that by accepting these results as measured by the dip-circle, it may be concluded that the mode of geomagnetic changes at these various points assumed a variety of forms, although the general sense of the variation was always negative. Minakami presumed from this result that the origin of the geomagnetic change would consist of a wide area (not a small spot), at least probably embracing the whole area of Miyake-sima, under the earth's surface, since the changes at all the stations, so far as he has observed, were negative.

Takahasi and Hirano[17] measured the distribution of the vertical intensity (Z) of geomagnetism at various points on the island, and obtained the differences between those during the period from July 20 to 24 and those from July 26 to 29. The differences which they found as local change during the period are distributed fairly regularly, that is, the change in negative values was the largest near the centre of the island, while it was nearly zero or positive along the coast, so long as their measurements alone are concerned. They[18] also measured the magnitudes of Z at the same points in the early part of December, 1940, and found that the difference in the Z values in the last period and those of the second (July 26∼29) was nearly the opposite of the change in those for the second from those in the first. In order to explain

16) T. MINAKAMI, Part IX of this Report.
Zisin, **12** (1940), 507.

17) R. TAKAHASI and K. HIRANO, *Bull. Earthq. Res. Inst.*, **19** (1941), 82; *Zisin*, **12** (1940), 510.

18) R. TAKAHASI and K. HIRANO, Part XI of this Report.

these geomagnetic changes, they concluded that the magnetic field on the earth's surface, as the result of magnetization and demagnetization of a sphere or a spherical shell 3 km under the central cone of this volcano, nearly agreed with the distribution of the observed changes during the interval from the first to the second period and those during the interval from the second to the last respectively.

On the other hand, according to dip-surveys made at eight stations along the coast of this island by Y. Katô[19], the change in dip during the ten years from 1930 to July 1940 (at least till after July 19) was $-34'\cdot3$, the largest, at Miike in the eastern coast, and $-15'\cdot9$ at Minowa, about 300 m west of our magnetic station, while it was a negative change, smaller than $10'$, at the other stations, except at a point in the southern coast, where the change was $+4'\cdot9$. From these results, Katô assumed that the local dip-change was largest near the zone of the present fissure eruption, and that this change was due to the intrusion of a non-magnetic dyke of sufficiently high temperature (larger than the Curie-point of the rock) underneath the zone of volcanic activity.

It must be remembered here, however, that the geomagnetic dip in the seas surrounding Japan, especially in those south of the Japanese Islands, seem generally to have increased in recent years, according to the results of magnetic survey made by the Hydrographic Department, Imperial Japanese Navy[20]. From the empirical formula of the secular variation in dip in 1933, given in the result mentioned above, the magnitude of the annual change in dip at Miyake-sima is

$$+(0'\cdot847 \pm 0'\cdot54)[t-1933\cdot0] + (0'111 \pm 0'\cdot029)[t-1933\cdot0]^2,$$

whence the general secular variation in dip at Miyake-sima, which is here assumed to be independent of the present volcanic activity, during the period from 1930 to 1940, amounted to $+14'\cdot4 \pm 5'\cdot8$. It will therefore be in order to assume that the local changes in dip related to the present volcanic activity is given by the sum of the observed changes in dip during 1930∼1940, with a correction of $-14'\cdot4$ for the general secular variation, provided no remarkable local change is assumed for the period from 1930 until the present activity. The distribution of the change thus corrected seems almost to agree with Minakami's result.

The safest conclusion to be deduced from the studies of these three investigators and that of the writer is that a local anomalous geomagnetic change of fair magnitude accompanied the severe eruptions of

19) Y. Katô, *Proc. Imp. Acad. Japan*, **16** (1940), 440.
20) *loc. cit.*,

Miyake-sima in July 1940, and that the change in dip along the eastern and northern coasts of the island until about July 25 was negative, its magnitude probably being larger than 20′.

By assuming that the cause of the anomalous change lies in magnetization of the material underneath the volcanic island, the changes in their magnetic susceptibility and in their permanent magnetization, may be regarded as the most probable contributive cause. According to experiments made by the writer[21], the specific susceptibility of the rocks from Miyake-sima in a magnetic field of less than 1·5 Gauss are from about $0{\cdot}6 \times 10^{-3}$ to $1{\cdot}3 \times 10^{-3}$. The changes in susceptibility with temperature of a number of samples were also measured, with the result that the susceptibility increased with temperature in the range of a few hundred degrees above room temperature, reaching its largest value, a few tens percent larger than that at ordinary room temperature, at a point a hundred and more degrees lower than its Curie-point. Assuming therefore that the rock beneath Miyake-sima has the largest of the measured susceptibilities and that its bulk density is 2·3, a rock, one cubic cm, cooled in geomagnetic field of 0·45 Gauss from a temperature higher than its critical-point to the temperature of maximum susceptibility is estimated to acquire a magnetization of about $2{\cdot}0 \times 10^{-3}$ c. g. s. e. m. u.. This magnetization, however, is the largest obtained from the writer's experiments.

On the other hand, there must be considered the causation of permanent "magnetization during cooling" and its disappearance, corresponding to decrease and increase respectively of the temperature of the rock. From the writer's study[22], the amount of change in total magnetization of a rock of unit volume in a weak magnetic field of H during a temperature variation of from t_1 to t_2, is given by

$$\Delta\vec{J} = \vec{H}\Big[\kappa(t_2) - \kappa(t_1)\Big] + \rho \cdot \vec{H} \cdot \int_{t_2}^{t_1} P(t)\,dt. \tag{18}$$

Although the characteristic parameter t_0, $P(t_0)$ and ϑ of the Miyake-sima rocks cannot be given uniquely, since they vary with the origin of the rock, a magnitude of $0{\cdot}45 \times \rho \cdot \int_0^{t_c} P(t)\,dt$ amounts to 10×10^{-3} in the smallest case, and to 50×10^{-3} in the largest. These values are much larger than the upper limit of possible change of induced magnetization

21) T. NAGATA, Part IV of this Report; *Zisin*, **12** (1940), 523.

22) T. NAGATA, *Bull. Earthq. Res. Inst.*, **19** (1941), 49.

in 0·45 Gauss. Therefore the largest part of $\overrightarrow{\Delta J}$ is given by the second term of eq. (18).

Since the newly ejected lava and bombs of Miyake-sima possessed natural remanent magnetization[23], the coefficient of which (Q) was always larger than 16, and the intensity of the natural remanence agreed with that of the thermo-remanent magnetization obtained in the laboratory, it will be in order to presume that the causation and disappearance of permanent magnetism with changes in temperauture took place during the present volcanic activity. Then, so long as it is assumed that the temperature of the subterranean rock changed some one hundred degrees from t_0, the changes in its magnetization would amount to more than 10×10^{-3}.

For a local magnetic change larger than 20′ in dip to occur on the earth's surface, the dimensions of the source whence the intensity of magnetization changes, should be a few hundred meters, provided its centre is less than a few kilometers from the earth's surface, while if the source were a layer, it should be one of about one hundred meters thick and less than one kilometer from the points of observation. The dimensions of the thermaly disturbed space mentioned above should not differ much from our figures.

A point to be noted, however, is that the cooling down of such a subterranean space to the extent of about one hundred degrees during such a comparatively short period seems scarecely possible, so long as it is assumed that the cooling is due to thermal conduction through the rock, whereas heating of the rock through severe volcanicity, namely, instrusion of incandescent magma and hot gases, would seem rather possible. In these circumstances, therefore, the causation of thermo-remanent magnetization in the subterranean rock as the result of cooling can hardly be expected, except for that case in which the cooling is the result of processes other than thermal conduction; while the disappearance of thermo-remanence as the result of a rise in temperature will be considerable.

Although, in the foregoing discussion, we took only temperature as an element of the physical state of the substance, we could just as well have considered other elements, such for example, as hydrostatic pressure and stress, the latter being expected to fairly affect the causation of thermo-remanent magnetism. Besides, another possible phenomenon is that the stress within the volcanic island changed considerably at the the time of its severe activity.

23) T. NAGATA, *loc. cit.*,

But since, unfortunately, we have at present no experimental fact regarding the effect of stress on the mode of causation of thermo-remanent magnetism of rocks, it is not possible to estimate the amount of magnetic change due to this contingent phenomenon.

Within the limits of phenomena so far known with certainty from experiments, the writer is of opinion that there is no other possible reason for the local geomagnetic change observed in Miyake-sima except the causation and disappearance of thermo-remanent magnetization in the subterranean rock, although this presumption is not without certain drawbacks. This is a problem that needs to be carefully studied in the future by as many investigators as possible.

5. Conclusion.

An actual example of the fact that the geomagnetic field in the neighbourhood of a volcano is markedly disturbed simultaneously with its activity, was obtained from the results of geomagnetic studies on Miyake-sima's eruption by four investigators, with the result that we may expect the same phenomenon in the case of severe activities of such a basaltic volcano as Miyake. For the purpose of further developing the science of volcano-physics, the writer earnestly hopes that geomagnetic studies will be made in the future in connexion with basaltic volcanoes not only in Japan, but also in other countries, for example, with a number of volcanoes in Hawaii, with Stromboli, and Etna in Italy, and others.

In order to obtain more precise knowledge of the mode of local geomagnetic changes, it is desirable to make observations with a three component magnetograph at more than two points near the volcano, and to repeat the magnetic survey with more than two magneto-meters of different components at as many different points as possible.

In conclusion, the writer of this Part wishes to express his sincere thanks to Prof. C. Tsuboi, Prof. H. Tsuya, Dr. T. Hagiwara, and to Dr. T. Minakami for their helpful criticisms, and to Dr Y. Kosikawa for his kindness in placing the reprints of records of magnetic observations of the Mitui Institute at the writer's disposal.

Part. VIII. A Magnetic Dip Survey of Miyakesima Island.

By Takeshi MINAKAMI,

The Earthquake Research Institute.

(Read Sept. 15, 1940.—Received March 20, 1941.)

With the object of studying the magnetization of the body of the volcano itself and the variations in terrestrial magnetism that accompanied the volcanic activity, the writer made a magnetic survey of Miyakesima island, following the eruption of July 12, 1940.

The survey was done at 46 points during the period from July 14 to August 3, 1940. Since 27 of these points were only for the purpose of studying the magnetization of the mountain body, the measurements were not so full compared with those of the remaining 19 points in which time variations in the magnetic dip were detected. The errors expected in the measurement are as follows.

Errors in an observed value when a re-survey is required .... ±2.'0

Errors in the amount of variation obtained by re-survey .... ±3.'0

Errors in an observed value when a re-survey is not required... ±4.'0

The survey revealed large anomalies everywhere in this small island of only 8 km diameter. The magnetic dip observed on the somma, northeast of the central crater, which amounted to 58° 18.'5, was the maximum value found in the present survey, the minimum value, 44° 42.'1, was found at Akô, a village in the northwestern part of the island. The difference between the two, maximum and minimum, amounts to 13° 30′. Usually, in a magnetic survey, it is most important to select an observation point that is suitable for the work intended, especially when determing the magnetization of the body of the volcano itself that has large magnetic anomalies. In order to avoid the effect of very local anomalies, the observation point must be one that represents the mean topography of the volcano, that is, without any marked rise or fall of the ground. In determining the time variation by means of a re-survey, it is necessary to remember exactly the position, or location, of the observation point, and to see that the neighbourhood of that point has

Table I. Results of the survey.

Station No.	Date	θ	Δθ
	h m		
1	July, 14, 14 43	45° 39·′9	−1° 16·′7
2	〃 16 18	47° 2·′9	+ 6·′3
3	15, 10 29	47° 36·′8	+ 40·′2
4	〃 11 40	47° 9·′4	+ 12·′8
5	〃 12 20	48° 59·′5	+2° 2·′9
6	16, 11 40	48° 9·′4	+1° 12·′8
7	17, 9 40	47° 42·′1	+ 45·′5
8	〃 10 43	48° 55·′8	+1° 58·′7
9	〃 12 32	50° 45·′0	+3° 38·′4
10	〃 15 51	46° 2·′5	− 54·′1
11	18, 11 41	48° 7·′1	+1° 10·′5
12	〃 15 43	49° 1·′2	+2° 4·′6
13	〃 16 53	46° 43·′2	− 13·′4
14	19, 8 30	49° 10·′9	+2° 14·′2
15	〃 9 33	47° 25·′3	+ 28·′7
16	〃 10 53	46° 22·′5	− 34·′1
17	〃 12 17	47° 59·′3	+1° 2·′7
18	〃 13 53	49° 5·′4	+2° 9·′0
19	〃 15 3	45° 31·′6	−1° 25·′0
20	〃 16 45	45° 30·′0	−1° 26·′6
21	20, 11 55	46° 48·′6	− 8·′0
22	〃 16 50	45° 33·′6	−1° 23·′0
23	21. 10 55	47° 47·′0	+ 50·′4
24	22, 11 40	47° 38·′8	+ 42·′2
25	23, 11 13	46° 28·′3	− 28·′3
26	24, 11 20	52° 40·′0	+5° 43·′4
27	〃 12 15	46° 1·′0	− 55·′6
28	〃 13 25	51° 24·′9	+4° 25·′3
29	26, 11 30	48° 29·′9	+1° 33·′3
30	〃 12 15	53° 3·′2	+6° 6·6′
31	〃 13 30	58° 18·′5	+11° 21·′9
32	〃 16 45	54° 37·′6	+7° 41·′0
33	〃 18 15	46° 40·′2	− 16.′4
34	27, 10 48	44° 42·′1	−2° 14·′5
35	〃 12 10	49° 40·′4	+2° 43·′8
36	〃 13 15	49° 27·′7	+2° 31·′1
37	〃 13 55	53° 2·′9	+6° 6·′3
38	〃 15 25	47° 50·′8	+ 54·′2

(*to be continued.*)

Table I. (*continued.*)

Station No.	Date	θ	$\Delta\theta$
	h m		
39	July, 27, 16 22	49° 26·'0	+2° 29·'4
40	29, 15 00	45° 18·'8	−1° 37·'8
41	31, 11 20	46° 12·'6	− 44·'0
42	〃 12 30	45° 58·'6	− 58·'0
43	Aug, 3, 9 58	46° 28·'2	− 28·'4

θ = Magnetic dip.
$\Delta\theta = \theta - \theta_c$
θ_c = Value calculated from the experimental formula of the Hydrographic Department.

not been disturbed in any way by nature or by man, an example of the former being collapse of rocks. For this purpose, the topography of the place must be as flat as possible. Even if the position of the point

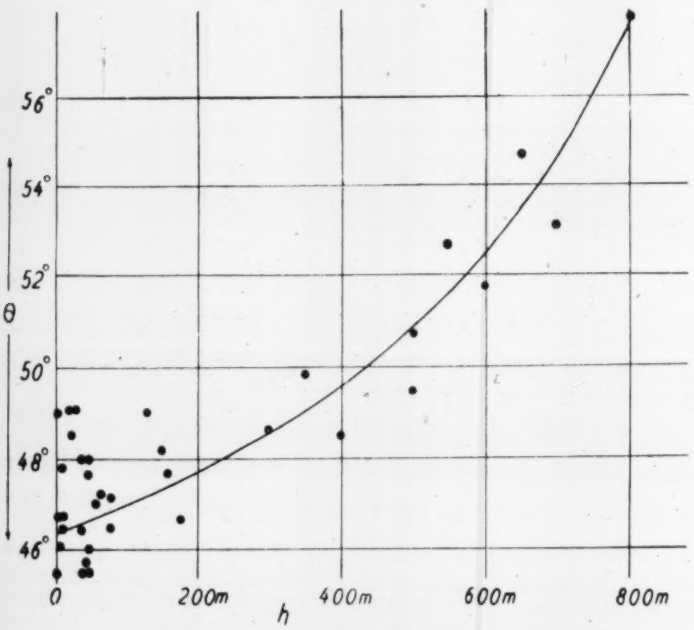

Fig. 1.
θ = magnetic dip, h = height above sea-level of the station.

were remembered exactly, it would be difficult to set the instrument so that there shall not be a deflection of even one centimeter from the previous position. Errors from this cause may be minimized by selecting an observation point in a flat topography, in which the gradient of the magnetic field is comparatively small. Since the object of the present survey was twofold, as already mentioned, a few of the points

from which the re-survey was done greatly affected by the topography.

We shall next take the relation between the magnetic dip and the altitude of the observation point. As will be seen from Fig. 1, the magnetic dip increases with increase of altitude. This fact has been already reported by the writer[1] with respects to certain volcanoes in Japan. Fig. 2~3 are the examples for Volcano Asama and Sakurasima island. These figures show that the magnetic dip increases gradually with increase of altitude, and does so abruptly near the summit. Although the plotted points in the figures are somewhat dispersed, the mean magnetization of the mountain body may be represented by simple curves. These curves depend not only on the intensity of the magnetization of the rocks that compose the mountain body, but also on the shape and volume of the mountain.

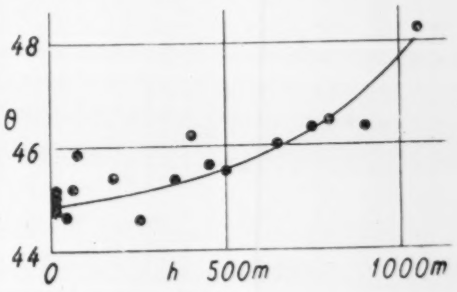

Fig. 2.

θ = magnetic dip of Sakurasima.
h = altitude of the station from the base of Sakurasima.

By means of the experimental formula that was supplied by the Hydrographic Department[2] for the purpose of calculating the geographical distribution of the standard magnetic dip in Japan, the standard magnetic dip in Miyakesima is given by

$$\theta_c = 46° \ 56.'6$$

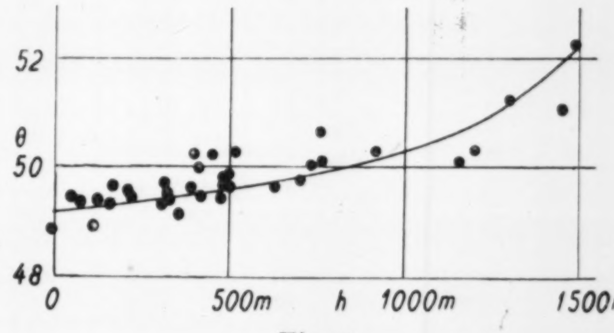

Fig. 3.

θ = magnetic dip of Asama.
h = altitude of the station from the base of Asama.

With this value as standard, the anomaly of the magnetic dip in Miyakesima is

$$\Delta\theta = \theta - \theta_c$$

Taking into consideration the relation between the magnenic dip and the altitude, just mentioned, we drew the lines of the anomalies as shown in Fig. 4. The difference between the magnetic dip on the

1) T. MINAKAMI, *Bull. Earthq. Res. Inst.* **16** (1938). 100; **18** (1940), 178.
2) Hydro. Depart. *Bull.Hydro. Depart.* **8**, (1936), 93.

summit and that of the seashore exceeds 10°, with local anomalies everywhere on the mountain. Since, in the present case, the number of observation points is too small to affect seriously the individual small anomalies, the general aspect of the magnetization of the mountain body is indicated by conformal lines with intervals of 2°. The negative anomalies are found in the neighbourhood of the seashore, where the altitude is less than 100 m, while the large positive anomalies are found in the remaining places. If we take the base of the volcanic island as being at a depth of 100∼150 m under sea level, these anomalies are explainable. Although it is difficult to determine the direction of the magnetization of the moutain body merely by a magnetic dip survey, if we consider the process of formation of the volcano and the results of similar survey that were made on other volcanoes, then the mountain body may be regarded, without any serions objections, as being magnetized almost in the direction of the present terrestrial magnetic field. Notwithstanding that the geological structure of the island is more or less complicated by many explosion craters and parasitic cones of the mountain side, the magnetization of the mountain body may be said to be simple, so far as the magnetic dip anomalies are concerned.

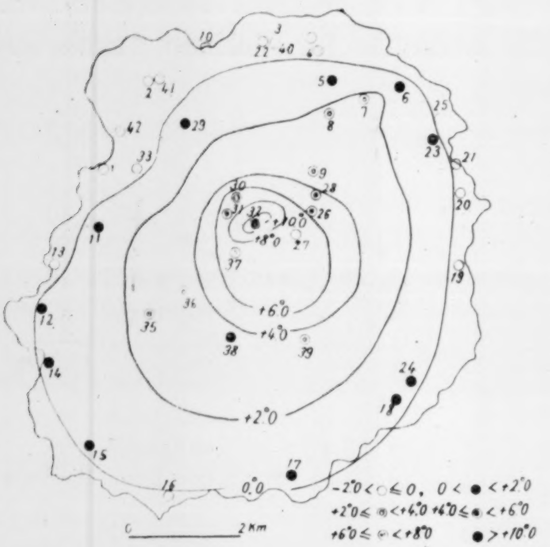

Fig. 4. Anomaly of dip in Miyakesima island.

Since the lave-flows that constitute the main part of the volcano at one time possessed a high temperature, for example, about 1000° C, it is probable that they are affected by magnetization due to terrestrial magnetism at the time of outflow. The lava-flows and other volcanic ejectaments as now seen near the surface of the mountain are believed to be the products of eruption that occurred at no distant age from the may present, so that the present direction of the magnetization in them be the nearly same as that of the present terrestrial magnetic field, whether it be induced magnetization or remanent magnetization. This conclusion is supported by T. Nagata's laboratory experiments[3]. The tem-

3) T. NAGATA, *Bull. Earthq. Res. Inst.* **18**, (1940), 102.

perature of rocks that constitute the interior of the volcano is believed to be around 1000° C. If the temperature is really high, for example, even 600°～700°C, the remanent magnetization that was brought about by the terrestrial magnetic field at the time the rocks came into existence, may have vanished, having been replaced by the induced magnetization due to the present magnetic field. Although the rocks near the surface of the mountain do not have such high temperature, since they have always been heated during the numerous occasions of volcanic activity, the remanent magnetization from old times must be replaced by new magnetization due to the present magnetic field.

The mean value of the magnetization of the rocks forming the mountain body of Miyakesima was calculated from the magnetic dip anomalies to be 0.015～0.020. This value is large, being four or five times those that were obtained by the same method at Volcano Asama and Sakurasima island. Since, as already stated, parts of the interior of the volcano have a high temperature, such as 1000°C, the induced magnetism there must be large compared with that case in which the rocks are only of ordinary temperature. For example[4], the magnetic susceptibility of hematite at a temperature of 500°～600°C is about ten times larger than that of ordinary temperature. In these circumstances, the mean magnetic susceptibility of the rocks in Miyakesima, namely 0.020, may be regarded as reasonable.

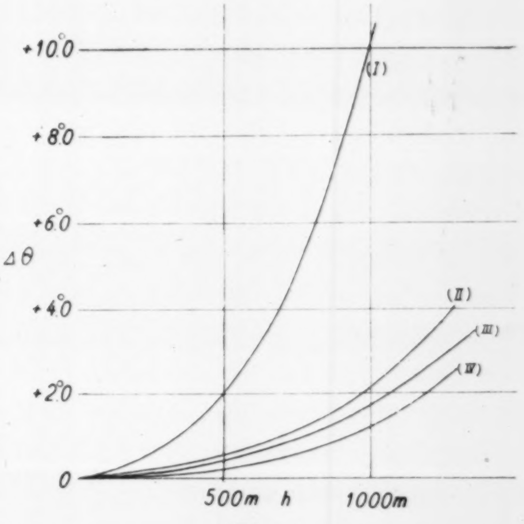

Fig. 5.
$\Delta\theta=\theta-\theta_0$, θ=magnetic dip, θ_0=magnetic dip at the foot of the volcano.
h=altitude of the station, measured from the base of volcano.
I=Miyakesima, II=Sakurasima,
III=Asama, IV=Kusatu-sirane.

Some marked anomalies were found on the comparatively fresh lava-flows at places showing no topographical singularity. For example, the magnetic dip observed in the grounds of the local primary school at Akô, which lies on a lava-flow, show, a large anomaly, amounting to 49° 1.'2, while the value observed at a place where the lava-flow is no more, and at a distance of 200 m from the former, was 46° 43.'2, which is almost the standard value for that

4) R. HAUL and TH. SCHOON, *Magnetismus und Chemie*, (1939), 71.

place. This marked local anomaly on lava-flow is believed to be due to the remanent magnetization of the lava.

To enable comparison of the magnetic dip anomalies of a few volcanoes, namely, Miyakesima island, Sakurazima island, Volcano Kusatu-Sirane, and Volcano Asama, the respective relations between the magnetic dip and the altitude are shown in Fig. 5. The shape of all these volcanoes is of *Conide* type; the volume of the mountain body of Miyakesima is to a certain extent smaller than the remaining three volcanoes. At all events, these four volcanoes resemble one another, both in shape and in volume, except that Miyakesima has very large magnetic anomalies compared with those of the remaining three volcanoes — a fact showing that the magnetic properties of the rocks in Miyakesima differ greatly from those of the other volcanoes. The rocks in Asama, Sakurasima, and Kusatu-Sirane are more acidic, whereas those of Miyakesima are basic. Since the magnetic properties of rocks depend much on the acidity of the chemical components in them, the difference in the magnetic property between Miyakesima and the remaining volcanoes can naturally be explained by the basic character of the rocks forming Miyakesima.

Part IX. Time Variations in the Magnetic Dip, and Their Topographical Distribution in Miyakesima Island. (preliminary note)

By Takeshi MINAKAMI,

Earthquake Research Institute.

(Read Sept. 15, 1940.—Received March 20, 1941.)

During the period from July 14 to August 3, 1940, following the eruption of Miyakesima, the magnetic dip was re-surveyed at 8 points on the island. These points lie all in the northern half of the island, at altitudes less than 100 m. Since the first survey was not begun until two days after the eruption, obviously the magnetic variations that might have occurred both before and soon after the first eruption are excluded. We shall therefore proceed with the magnetic dip variations that occurred during the period from July 14 to August 3.

The magnetic dip variation at Hôdai are shown in Fig. 1. Since T. Nagata made continuous observations with his magnetic dip variometer at a place about 20 m distant northward from our point, it is possible to compare the absolute measurements with the variometer records. During the period from July 17 to July 25, the magnetic dip here (Hôdai) decreased by 26′, almost linearly with respect to time, although an increase of 9·′4 was found on July 30, while a decrease of 9·′1 was measured on August 3. The net result was decrease of 25′6 for the total period of survey. The variation is too large to be put down to errors that may be expected in the measurement. Since no marked magnetic storms were recorded by the magnetic variometer installed at Komoro, at the foot of Volcano Asama, the variations obtained in the present survey may be regarded as real, within the limits of errors of measurement.

A point was taken at Akabakkyô, about 6 m north of the northern end of the new lava-flow. The surveys at this point were made for the purpose of detecting the variation in the magnetization of lava while in the process of cooling. As will be seen from Fig. 1 B, the magnetic dip here decreased by 7·′5 during the period from July 22 to 25, since which no marked variations occurred until July 30, when there was a decrease of 10·′3 on August 3. The net result for the period of the survey was a decrease of 15·′4.

Results of resurvey of magnetic dip.

Table I. Station No. 6. (Hôdai).

	Date and time (h m)	Magnetic dip	Variation of dip
1	July 16, 11 40	48° 9·'4	
2	21, 9 45	47° 52 '7	−16 '7
3	22, 17 35	47° 48 '4	− 4·'3
4	25, 14 25	47° 43·'5	− 4·'9
5	30, 11 0	47° 52·'9	+ 9 '4
6	3, 12 30	47° 43·'8	− 9·'1

Table II. Station No. 23. (Akabakkyo).

	Date and time (h m)	Magnetic dip	Variation of dip
1	July 21, 10 55	47° 47 '4	
2	22, 16 45	47° 50 '0	+ 3·'4
3	23, 10 20	47° 49 '1	− 1·'3
4	25, 12 25	47° 42·'5	− 6·'6
5	30, 12 30	47° 41·'6	− 0·'6
6	Aug. 3, 11 20	47° 31·'3	−10·'3

Table III. Station No. 25. (Sitori Zinsha).

	Date and time (h m)	Magnetic dip	Variation of dip
1	July 23, 11 13	46° 28·'3	
2	25, 12 55	46° 14·'5	−13·'8
3	30, 12 0	45° 49·'3	−25 '2
4	Aug. 3, 10 50	45° 49·'9	+ 0 '6

Table IV. Station No. 22. (Kamituki).

	Date and time (h m)	Magnetic dip	Variation of dip
1	July 20, 6 50	45° 33 '6	
2	29, 14 20	45° 33 '4	− 0·'2
3	30, 16 25	45° 26·'9	− 6 '5
4	31, 9 40	45° 26·'2	− 0·'7
5	Aug. 2, 13 5	44° 57·'0	−29·'2

The point at Sitori, which was selected for comparison with the point at Akabakkyô, was 150 m north of the northern end of the new lava-flow. Since it is believed that the variation at Sitori is not affected by magnetization of the new lava-flow, by assuming that variation which occurred at Sitori existed at Akabakkyô in the same way, the

difference between these two points (Akabakkyô and Sitori) may be the variation that was caused mainly by the cooling of the new lava-flow. Fig. 4 shows the variation obtained by this assumption. In contrast to this, the fact that the magnetic dip at Sitori (Fig. 2 C) decreased by 40′ during the period from July 23 to 30, indicates a large increase in magnetic dip at Akabakkyô, the magnetic horizontal intensity diminished as the result of decrease in the magnetization of the new lava, whereas the vertical intensity was not affected to such an extent by this case, so that the increase in magnetic dip at Akabakkyô means a decrease in the magnetic susceptibility of the new lava of high temperature. If the magnetic susceptibility (κ) of the lava had decreased much in the process of cooling from high temperature when the temperature may passe through the critical point then the large increase in the magnetic dip at Akabakkyô may be reasonablly explained. This problem will be discussed in detail at another opportunity. All that we shall do here is merely to point out that cooling of the lava caused a magnetic effect.

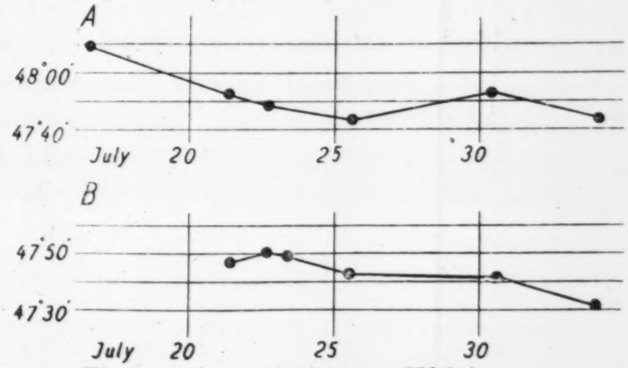

Fig. 1. A = variations at Hôdai. B = variations at Akabakkyô.

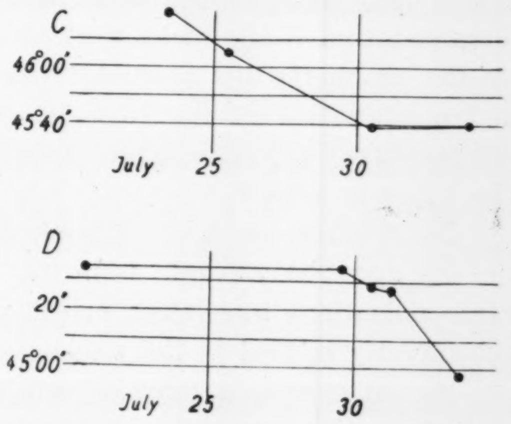

Fig. 2. C = variations at Sitori. D = variations at Kamituki.

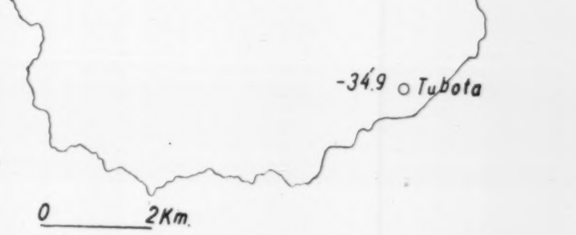

Fig. 3. Distribution of time variation.

Although the magnetic dip at Kamituki showed no marked variations during the period from July 20 to 29, it suddenly decreased on July 30. The net result

of the variation in the period of survey was a decrease of 36·6′.

Tubota, Sadadô, and Igaya showed decreases in magnetic dip amounting from 20′ to 40′ during the period of survey.

The foregoing results show that the same decrease in the magnetic dip affected the whole island. Although there are some local differences, a general tendency in the variations may be seen for all the observation points. Since the magnetic dip decreased everywhere on the island, its origin, may be supposed to have covered a large area, at any rate, covering the whole island. Such a change of dip may be explained qualitatively by the following facts: (1) The magnetization of the rocks that form this island is very large as proved by the magnetic dip anomaly which amounts to 10°; (2) The change in magnetization of the rocks is, generally speaking, very large at high temperature; (3) The large topographical deformations are caused by the volcanic activity.

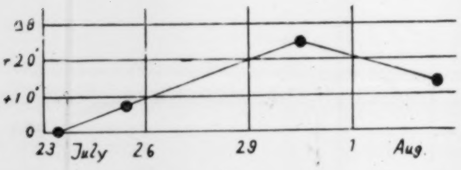

Fig. 4.

No relation could be established between the variation in the magnetic dip and the volcanic pulsations observed at Kamituki. Since volcanic pulsations have their origin at the surface of the crater, they are not directly related to the variations of dip that cover the whole island.

At all events, it may be said that considerable variation in terrestrial magnetism accompanied the volcanic activity of Miyakesima island.

Part X. Changes in Earth Potential after the Eruption.

By Takahiro HAGIWARA,

Earthquake Research Institute.

(Read Sept. 15, 1940.—Received March 20, 1941.)

After the eruption of Miyake-sima on July 12, 1940, the changes in the earth potential in one direction were observed at Kamituki, a village in the northern part of the island. The electrodes were embedded in the corners of the ground of the local primary school. For the electrode, a lead tube of 1 cm diameter and 3 m long, twisted into a spiral of 50 cm outer diameter was used. They were buried at a depth of 1 m, with the plane of the spiral horizontal. The distance between the two electrodes was 50 m, the line joining them being in the direction S14°W, pointing toward the summit of the volcano. The potential difference of the two electrodes was recorded on photographic paper by means of the deflection of a moving-coil-type galvanometer with a sensibility of 1×10^{-7} amp/mm when critically damped and with a period of 6·5 sec, in connection with which a high electric resistance was inserted in series. The inserted resistance, which was first 10 kΩ, was later reduced to 5 kΩ, and later still further to 2 kΩ. The observation, which was begun at 23 h on July 14, was continued to 16 h of August 3, of the same year.

All the records are reproduced in Fig. 1, in which the upward change means increase of potential on the upper side of the mountain. In order to show the gradual changes, the curve that was constructed by joining the hourly readings is shown in the figure of Part XIV[1]. For comparison, the time of occurrrence of the earthquakes as recorded by the seismograph at Kamituki is marked by an arrow in the figure.

There were no disturbances on account of the local atmospheric electricity in the interval from the beginning to August 2. From 0 h of August 2 to the end of the observation, the earth potential was greatly affected by thunderstorms that occurred in the island.

Some notable changes in earth potential, which seemed to be related to the volcanic activity, were seen at 7 h of July 22 and in the

1) See page 393.

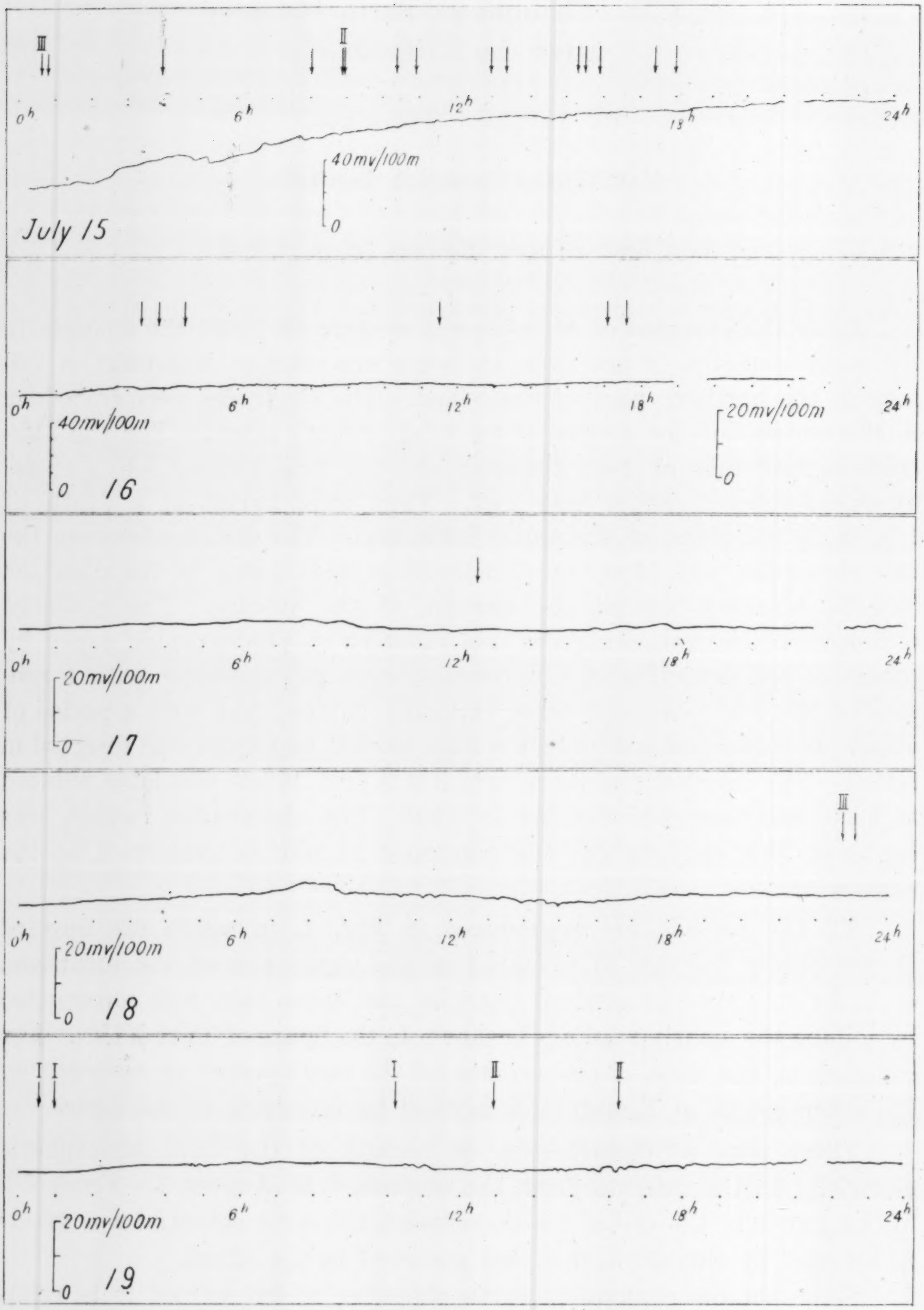

Fig. 1 a.

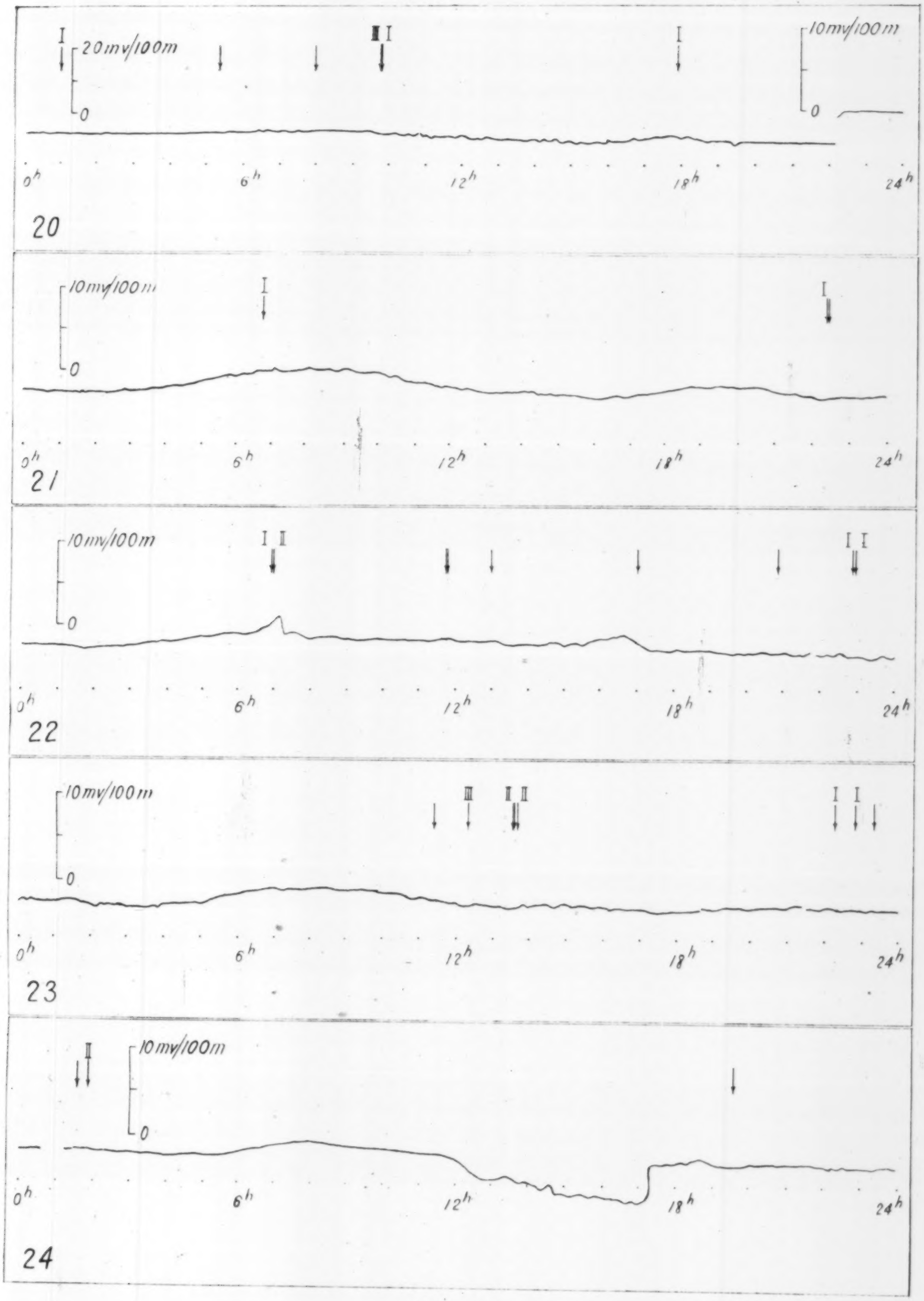

Fig. 1b.

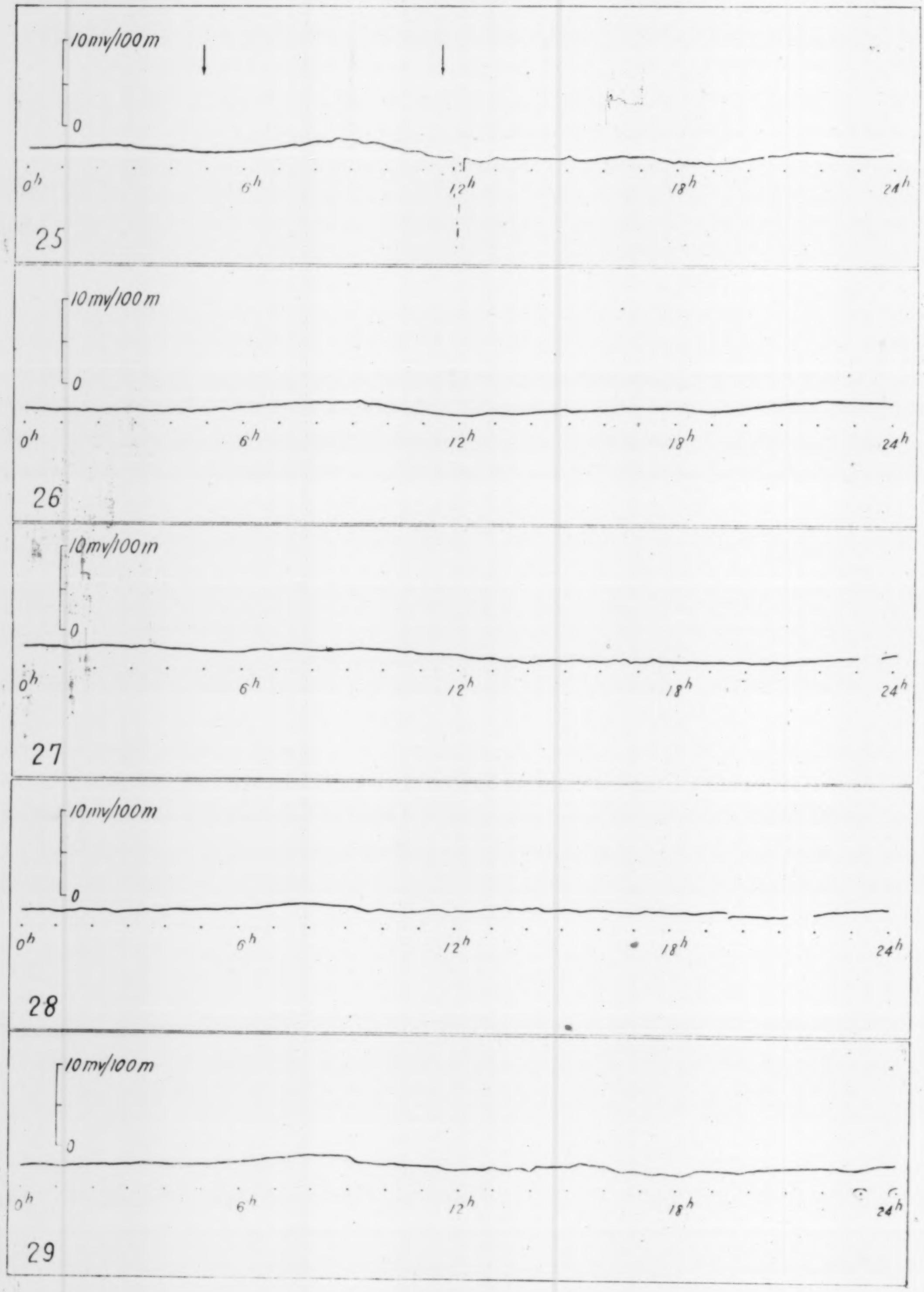

Fig. 1c.

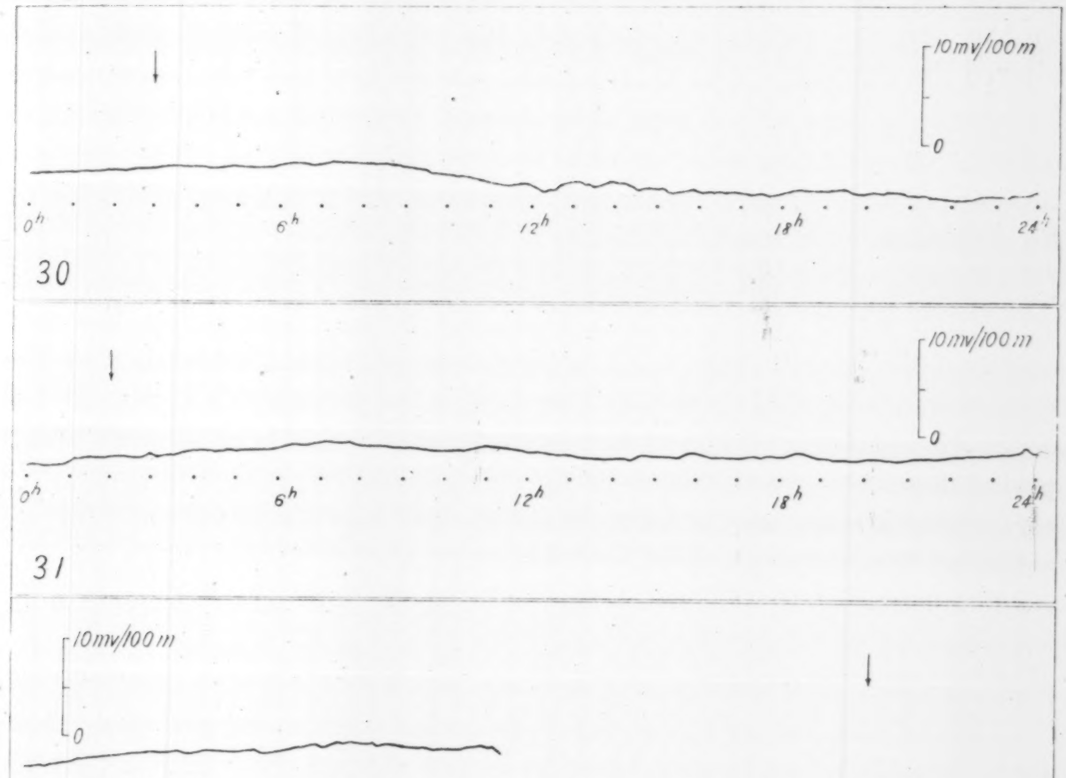

Fig. 1d.

interval between 12 h and 18 h of July 24. First the potential of one side of the mountain gradually increased and after some hours returned to the original state. On July 18, the activity of the central crater altered in manner. The intermittent explosions and the earthquakes increased in number. These intermittent explosion reached maximum activity on July 25, after which it gradually subsided. The changes in earth potential, just mentioned, preceded the maximum activities of the explosion in the central crater.

Nagata[1] observed continuously the changes in earth magnetic field at Hôdai, about 4 km distant from Kamituki. Comparing the two changes, the one in the earth potential at Kamituki and other in the magnetic dip at Hôdai, it was found that the changes in period of the order of 10 minutes in the two cases coincided. Changes of such small period however are believed to be the so-called magnetic storms that occur over a wide region and are not in any way related to the volcanic activity. The changes in earth potential with a larger time scale, already mentioned in the foregoing paragraphs, did not correspond with the changes in magnetic dip, which was probably because of the restricted space distribution of the earth curreut.

As to the variation in earth potential with a larger time scale (see page 393), the potential on the upper side of the mountain, which first increased considerably, decreased gradually since July 20, and again increased after July 25. Marked changes in electrode contact potential were noticed for one or two days after the electrode was buried, so that the observed values of the earth potential for the first one or two days are not reliable. The feeble changes recorded after July 17~18 may, however, be regarded as real changes in the earth potential. An interesting fact is that the sense of these gentle variations in the earth potential bear a striking resemblance to the variations in the vertical magnetic intensity measured at Kamituki by Takahasi and Hirano[2].

Since the present observation covered only a very short period of time, and was for only one direction, the data are obviously inadequate as basis for any detailed discussion.

In conclusion, the writer wishes to express his cordial thanks to Messrs. A. Zitukawa and M. Suzuki, who assisted him greatly in the field work.

---

1) T. NAGATA, *Bull. Earthq. Res. Inst.*, **19** (1941), 335.
2) R. TAKAHASI and K. HIRANO, *Bull. Earthq. Res. Inst.*, **19** (1941), 82.

Part XI. Changes in the Vertical Intensity of Geomagnetism that accompanied the Eruption.

By Ryûtarô TAKAHASI and Kintarô HIRANO,
Earthquake Research Institute.
(Read on Jan. 16, 1941.—Received Mar. 20, 1941.)

1. *Introduction.* In a previous paper[1], the writers gave the results of magnetic surveys that were executed in connection with the eruption of Miyakezima in 1940. These magnetic surveys were performed twice, in each of which the vertical intensity of geomagnetism were measured at 50 stations in the island by means of a magnetometer. The first survey was made during the period from July 20 to 24, and the second during that from July 25 to 29; that is, the first survey was made during the period in which the central cone eruption had been increasing its violence, whereas the second survey was executed when the central cone eruption had attained its maximum violence.

These two surveys showed that remarkable changes occurred in the distribution of the vertical intensity of geomagnetism during the interval between surveys. It was pointed out that these changes in the geomagnetism can well be explained by assuming a change in the intensity of magnetization of a part of a sphere, the centre of which is at a depth of 3 km beneath the summit of the volcano. This explanation seems to harmonize well with the results of other observations, such as those of the magnetic dip, the earth current, volcanic earthquakes, and volcanic tremors, executed respectively by Minakami[2], Nagata[3], and Hagiwara[4] concurrently with our surveys.

Recently a third magnetic survey was executed by the writers during the period from Dec. 2 to 7, 1940, the results of which form the subject of this paper, together with discussions.

2. *Instrument, Stations, and the Method of Survey.* The instrument used in the present survey was the magnetometer that was used in the two previous surveys. The sensitivity of the instrument, which, however, was adjusted this time to 79·0 gamma/div, was tested several

1) *Bull. Earthq. Res. Inst.*, **19** (1941), 82; *Zisin.*, **12** (1940), 26.
2) *Bull. Earthq. Res. Inst.*, **19** (1941), 363, 393; *Zisin.*, **12** (1940), 23.
3) *Ditto.* 335, 393 and *Zisin.*, **12** (1940), 12.
4) *Ditto.* 325, 367 and *Zisin.*, **12** (1940), 1.

times during the survey by means of a Helmholtz coil, but no appreciable changes were observed.

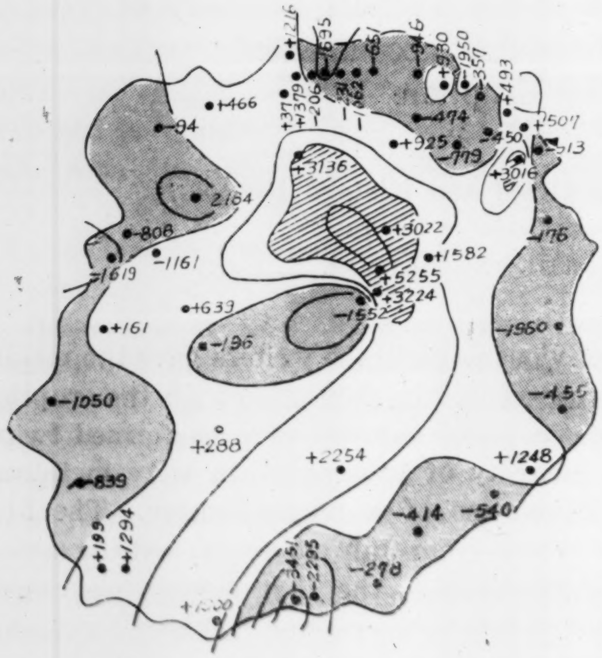

Fig. 1. Distribution of vertical intensity. Unit = γ.

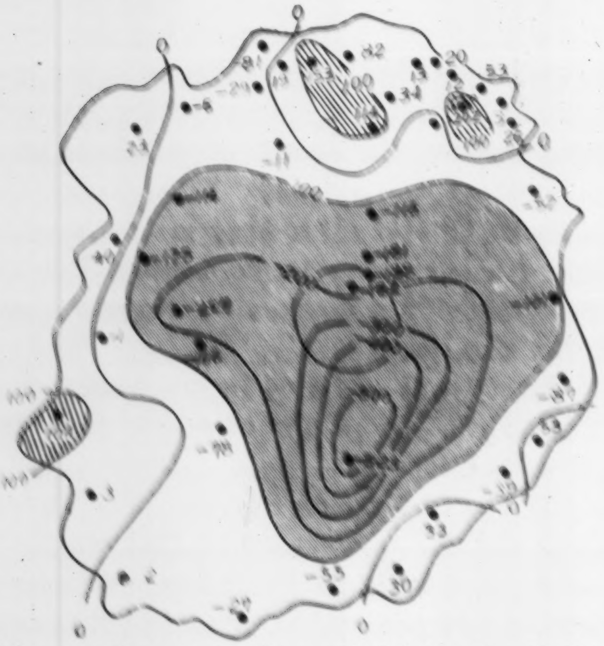

Fig. 2. Changes in the vertical intensity (II-I). Unit = γ.

The procedure of the survey was exactly the same as that described in the previous paper. Great care was taken in occupying the stations exactly. It was seen to that not only the horizontal position but that the height also of the instrument was the same as those in the case of the previous surveys. As in the previous surveys, the compensating magnet was unnecessary at all the stations, excepting No. 130. The temperature correction was made in the same manner as before.

In the results of the first and second surveys given in the previous paper, the corrections for diurnal variation of geomagnetism were made by distributing the differences of the morning and evening values at the reference station among the values measured on that day, in proportion to the time elapsed. By the courtesy of Mr. Y. Kosikawa, however, the records of the vertical intensity magnetograph installed at the Mitsui Biological Laboratory, at Simoda, a village situated at the head of the Idu peninsula, and about 80 km distant from Miyakezima, were recently placed at our

disposal, so that in the present paper, all the results, including those of the first and second surveys, were corrected for diurnal variation in accordance with the magnetograph records. The differences of the morning and evening values at the reference station, which sometimes remain even after all the corrections were made, although their amounts were very small, is due to shift of the zero-point of the magnetometer, and were distributed among the values measured that day. The results of the first and second surveys given in this paper consequently differ slightly from those given in the previous paper, but these differences are so small that the general tendency of the distribution in the vertical intensity (I and II) as well as the general trend of the change in geomagnetism (II–I, difference of survey II and I) suffer no serious changes, as shown in Figs. 1 and 2.

3. *Results of the Third Survey.* In Table I are given the results of the third survey (III), together with those of the first and second, as well as the differences II–I and III–II. The values III give the vertical intensity at each station relative to that at Station No. 1. The changes in the vertical intensity III–II during the interval separating the second survey from the third are also shown graphically in Fig. 3, in which the regions where the changes exceed +100 gammas are

Table I.

Nos. of Station	Locality		I	II	III	II–I	III–II
	(Kamitukimura)	(神着村)	γ	γ	γ	γ	γ
0	Mr. Asanuma's garden	浅沼方庭	+ 37	+ 8	—	− 29	—
1	Young Men's Hall	青年會館	+1379	—	—	—	—
2	Osyaku shrine	御笏神社	− 206	− 187	− 182	+ 19	+ 5
3	Mr. Inoue's garden	井上高蔵方庭	−1695	—	—	—	—
4	Yamanokami	山神碑前	− 231	− 78	− 98	+ 153	− 20
5	Ebine shrine	エビネ神社前	−1052	—	—	—	—
6	Mr. A. Inoue's garden	井上常次郎方前	− 651	− 569	− 635	+ 82	− 66
7	Nadaado	ナダアド	− 946	—	—	—	—
8	Minowa	三ノ輪入口	+ 930	+ 943	+1042	+ 13	+ 99
9	Hôdai	砲臺	− 357	− 345	− 358	+ 12	− 13
10	Kamanosiri	釜ノ尻	+ 493	+ 546	+ 533	+ 53	− 13
11	Cape of Nisiano	西アノー岬	+ 507	+ 510	—	+ 3	—
12	Siitori shrine	椎取神社前	− 913	− 887	− 882	+ 26	+ 5
13	Beside the new lava flow	新熔岩脇	+3061	—	—	—	—
14	Takenoo	竹ノ尾	− 450	− 248	—	+ 202	—
15	Uemiti	上道	− 779	− 825	− 867	− 46	− 42

(*to be continued.*)

Table I. (*continued.*)

Nos. of Station	Locality		I	II	III	II-I	III-II
			γ	γ	γ	γ	γ
	(Kamitukimura)						
16	Nadaado Ue	ナダアド眞上	− 474	− 440	− 558	+ 34	− 118
17	Sugiyama Hotel	杉山旅館	+1216	+1135	+1257	− 81	+ 122
101	Okubohama	大久保濱上	+ 466	+ 460	+ 508	− 6	+ 48
	(Idumura)	(伊豆村)					
102	Monument	伊豆村	− 94	− 71	− 30	+ 23	+ 41
	(Igayamura)	(伊ケ谷村)					
103	Igayamura	伊ケ谷へ下り口	− 808	− 768	− 824	+ 40	− 56
104	Public Office	伊ケ谷役場	−1619	—	—	—	—
105	Igayamura	伊ケ谷阿古間	+ 161	+ 160	+ 214	− 1	+ 54
	(Akomura)	(阿古村)					
106	Ako Primary School	阿古小學校	−1052	− 948	− 978	+ 104	− 30
107	Sabinohama	錆ノ濱	− 839	− 836	− 862	+ 3	− 26
108	Toga shrine	富賀神社	+ 199	+ 197	+ 159	− 2	− 38
109	Upward of Toga shrine	富賀神社上	+1294	—	—	—	—
110	Simmiyo	新ミヨ	+1900	+1873	+1941	− 27	+ 68
111	Boundary btw. Ako and Tubota	坪田，阿古境	−3451	—	—	—	—
111′	Do.	同上	−2295	−2350	−2399	− 55	− 49
	(Tubotamura)	(坪田村)					
112	Ninomiya	二ノ宮	− 278	− 248	− 275	+ 30	− 27
113	Tubotamura	坪田村	− 530	− 569	− 516	− 39	+ 53
114	Mitake shrine	御岳神社	+1248	+1301	+1335	+ 53	+ 34
115	Btw. 114 and 116	御岳，三池間	− 455	− 542	− 606	− 87	− 58
116	Miikehama	三池濱	−1960	−2061	−2062	− 101	− 1
117	Yoridaisawa	ヨリダイ澤	− 176	− 228	− 251	− 52	− 23
118	Entrance to Goyomiti	御用道入口	− 414	− 381	− 414	+ 33	− 33
119	Bato Kannon	馬頭觀音前	+2254	+1731	+2275	− 523	+ 544
120	Branch pt. of Ako and Tubota	坪田阿古分岐點	+ 288	+ 210	+ 256	− 78	+ 46
121	Kasadidaira	笠地平	− 196	− 362	− 318	− 166	+ 44
	(Igayamura)	(伊ケ谷村)					
122	Kamata	鎌田飼場	+ 639	+ 412	− 699	− 227	+ 287
123	Doromidu	泥水	+1161	+1036	+1068	− 125	+ 32
124	Huzikirazu	藤不切	−2183	−2297	−2351	− 114	− 54
	(Kamitukimura)	(神着村)					
125	Minowa	三ノ輪	−1950	−1930	−1938	+ 20	− 8
126	Kazahaya	風早	+ 925	+1039	+ 959	+ 114	− 80
127	Nango shrine	南郷祠	+3136	+3125	+3176	− 11	+ 51
128	Umamiti	雄山馬道	+3022	+2906	+3004	− 116	+ 98
129	Boundary of Kamituki and Tubota	坪田，神着境界	+1582	—	+1229	—	—
	(Tubotamura)	(坪田村)					
130	Ue no Zyo	上ノ錠	+5255	+5074	+5265	− 181	+ 191
131	Pass on Somma	外輪頂上	+3224	+3036	+3298	− 188	+ 262
132	Hayonotairo	八丁平	−1552	−1734	−1595	− 182	+ 139
	(Kamitukimura)	(神着村)					
133	Akkatayama	アツカタ山	—	+ 811	+ 957	—	+ 146

shaded by thick diagonal lines, and the regions where such changes are less than −100 gammas are shaded by a fine mesh.

It must however be borne in mind that, since our surveys measure relative vertical intensities of geomagnetism, not absolute intensities, the difference of the results of two surveys does not always represent the true changes in geomagnetism. To obtain the true values of the geomagnetic changes, a constant, which is the true change in the vertical intensity at the reference station, must be added, but, in contrast to case II–I, the constant is unknown in the case of III–II. Fig. 3 shows, therefore, only relative changes in geomagnetism.

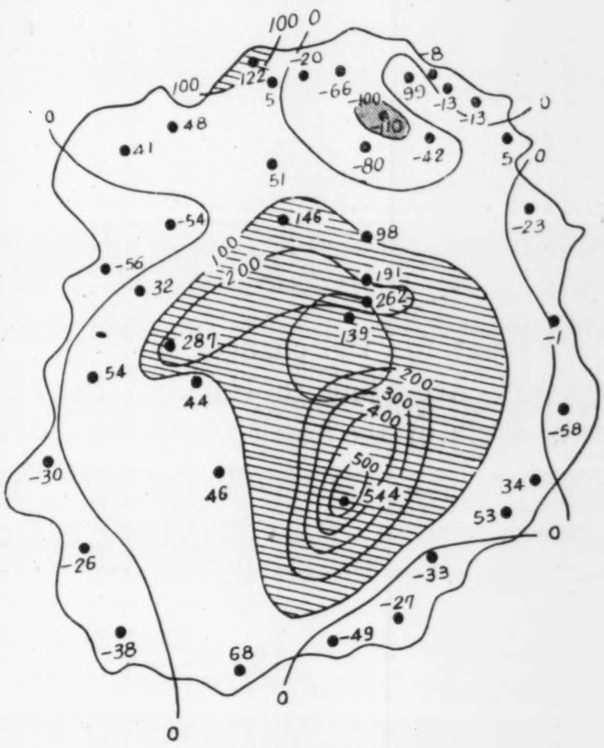

Fig. 3. Changes in the vertical intensity (III–II) Unit=γ.

Seeing, however, that only local and relative changes are necessary for elucidating phenomena that take place immediately underneath the volcano, a general shift of the measured changes, which means regional variation on a large scale with its cause operating at a great depth in the earth, may be left unknown.

4. *Interpretation of the Results, and Discussions.* Comparing Fig. 3 with Fig. 2, we find that they are very similar, except that the sense of the changes is reversed, whence it is clear that the changes in vertical intensity of geomagnetism that occurred during the interval from the second survey to the third may be explained by the same assumption as that made in the previous paper, the only difference being a gain of magnetic properties in the present case instead of loss in the former.

The explanation of the changes in geomagnetism found by the third survey is therefore that a sphere, which was heated owing to the eruption to a temperature exceeding the Curie point, had now cooled, under the earth's magnetic field, to a temperature below the Curie point, and thus acquired thermo-remanent magnetism. With this explanation, it

is more natural to consider that the cooled part is a spherical shell, rather than a sphere. It will easily be understood that the sphere in the former assumption may be replaced by a spherical shell of equal volume. Accordingly, it is better to replace the product kR^3 in equation (1) in the previous paper by $k\left\{R^3-(R-d)^3\right\}$, where d is the thickness of the shell. As before, the centre of the spherical shell is assumed as being at a depth of 3 km beneath the summit of the volcano. We must then have

$$k\left\{R^3-(R-d)^3\right\} \doteqdot 3R^2dk=4\times 10^{-2}$$

to account for the changes in vertical intensity found by the present survey. According to Nagata,[5] the intensity of the thermo-remanent magnetism of the basalt of Miyakezima is $5{\cdot}0\sim 1{\cdot}2\times 10^{-2}\Gamma$ per gramme, or $14\sim 3\times 10^{-2}\Gamma$ per cm^3. This is equivalent to $k=3{\cdot}3\sim 0{\cdot}8\times 10^{-2}$. If we assume for k the value 3×10^{-2} and $R=2{\cdot}7$ km, as obtained in the previous paper, we must have $d=0{\cdot}061$ or 61 m.

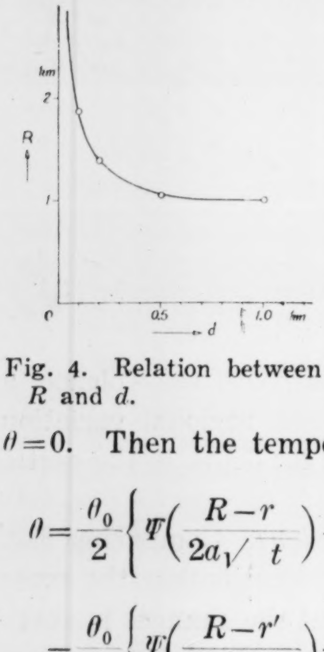

Fig. 4. Relation between R and d.

We shall now estimate the amount of d. We assume that a sphere of radius R, imbedded in a semi-infinite body at a depth of 3 km, is left to cool. At the instant $t=0$, the temperature is everywhere 0 excepting the sphere, the temperature of which is θ_0. The surface of the semi-infinite body is assumed to be kept at $\theta=0$. Then the temperature θ at a point P is given by the equation

$$\theta=\frac{\theta_0}{2}\left\{\Psi\left(\frac{R-r}{2a\sqrt{t}}\right)+\Psi\left(\frac{R+r}{2a\sqrt{t}}\right)\right\}+\frac{a\sqrt{t}\,\theta_0}{\sqrt{\pi}\,r}\left\{e^{-\left(\frac{R+r}{2a\sqrt{t}}\right)^2}-e^{-\left(\frac{R-r}{2a\sqrt{t}}\right)^2}\right\}$$
$$-\frac{\theta_0}{2}\left\{\Psi\left(\frac{R-r'}{2a\sqrt{t}}\right)+\Psi\left(\frac{R+r'}{2a\sqrt{t}}\right)\right\}-\frac{a\sqrt{t}\,\theta_0}{\sqrt{\pi}\,r'}\left\{e^{-\left(\frac{R+r'}{2a\sqrt{t}}\right)^2}-e^{-\left(\frac{R-r'}{2a\sqrt{t}}\right)^2}\right\},$$

where $\Psi(\xi)=\frac{2}{\sqrt{\pi}}\int_0^{\xi} e^{-\xi^2}d\xi$, r and r' being the distances of P respectively from the centre of the sphere and from the image of the centre of the sphere with respect to the surface of the semi-infinite body, and a is the square root of the diffusivity of the medium.

Since, according to the experimental results of Nagata, most of the

5) *Bull. Earthq. Res. Inst.*, **19** (1941), 304.

basalts of Miyakezima begin to acquire thermo-remanent magnetism at an average of about 600°C, we assume that the Curie point is at 600°C. Further, we assume $\theta_0=1000°C$, and that the diffusivity of basalt is 0·01. Then the thickness d of the spherical shell that acquires thermo-remanent magnetism, as computed by the above equation, becomes 1.3 m, when $t=130$ days—the interval from the second survey to the third. This is too small a value compared with that required to account for the observed magnetic changes.

Cooling of a magma pocket does not however occur through the conduction of heat to the surrounding rocks alone; heat consumption accompanying gas discharges may also play an important part. When volcanic gases, dissolved in magma under pressure p_0 and temperature θ_0, are brought to a lower pressure p, they expand and absorb heat from the surrounding magma. This heat quantity may be written $c_p\theta_0(p_0^{\gamma-1}-p^{\gamma-1})/p_0^{\gamma-1}$, where $\gamma=c_p/c_v$ and c_p, the specific heat of the gas under constant pressure.

Now in the case of the eruption of Miyakezima, lava fragments were observed shot up to heights of a few hundred metres. If we assume this height to be 500 m, the initial velocity of the ejecta becomes 100 m/sec. The velocity of the gases that leave the crater may therefore be assumed to be 100 m/sec, at the least. If we assume further that the diameter of this gas jet is 50 m, the gas volume that flows out from the crater is 2×10^5 m³/sec. Assuming further that the density of the gas is 0·6 g/litre, the mass of this gas flow is $1{\cdot}2\times10^8$ g/sec. If we take $p_0=$ 800 atm., corresponding to a depth of 3 km, $p=1$ atm., and $\gamma=1{\cdot}30$, the above equation gives as the heat consumption of the magma the value 4×10^{10} cal/sec., or $3{\cdot}4\times10^{15}$ cal/day. This is a heat quantity large enough to lower the temperature of a spherical shell of basalt, 2·7 km in radius and 100 m thick, by 0·8°C/day. Although the gas emmision from the crater did not last long with the violence assumed above, the total decrease in temperature through gas emmision cannot be small.

Seeing moreover that the gas concentration will be larger at the upper part of the magma pocket than at its deeper part, it may be supposed that the upper part of the lava pocket cools more quickly than that calculated above. Furthermore, seeing that the distribution of magnetic anomalies depends largely on the shape and the conditions of the upper part of a magnetic body, as the theory of magnetic prospecting shows, our opinion is that the magnetic changes revealed by the present survey can be explained to a certain extent by the cooling of the lava pocket underneath the volcano.

In short, it is possible to explain qualitatively the observed magnet-

ic changes III–II, either by heat conduction or by gas emmission, although we have failed to explain quantitatively the amount of the observed magnetic changes. According to Nagata, however, the basalts of Miyakezima have widely different magnetic properties, notwithstanding that they are very similar in appearance. In these circumstances, it is not altogether improbable that magma, when cooled slowly in the pocket under high pressure, acquires thermo-remanent magnetism far exceeding in strength those of effused basalts.

In support of this idea it may be pointed out that the lava which flowed out from the central cone crater in the last stage of the eruption is more magnetic than other lava flows and bombs. This central cone lava is more crystaline than the other lavas, whence it may be supposed to have come from deeper parts of the pocket and to have cooled slowly in the crater pipe under pressure.

In conclusion, the writers wish to express their cordial thanks to the officials of the Division of Scientific Research in the Ministry of Education for the financial aid granted them for the present series of investigations.

Part XII. A Topographic Survey of the New Parasitic Cones and the New Lava Flow of Miyake-sima Island.*

By Syun'itirô OMOTE,

Earthquake Research Institute.

(Read Sep. 15, 1940.—Received March 20, 1941.)

Introduction.

Eruption broke out from Miyake-sima, on June 7, 1940, pouring out enormous quantities of lave from the many newly formed craters. New craters were disposed along a fissure line that extended from the middle point of the eastern side of the mountain slope along a radial line from the summit down into Akabakkyô-Bay. Another small fissure extended from the north side of the Yoridaino-sawa valley, only a few tens of metres south of the main fissure, but the quantity of lava that flowed from the crater of this small fissure was much less. It seems that the first eruption occurred at the upper part of the main fissure, some 450 m above sea level, and large quantities of lava poured out from this crater and flowed down the border valley of the two villages, Kamituki and Tubota, eventually reaching the seashore at the northen part of Akabakkyô-Bay. The lava blocks filled the forshore, gradually extending the area of the new land seaward, covering at last an area of 30 acres.

On the other hand, in the midst of the side eruption, or soon after it ceased, two craters were formed in line in the southern part of Akabakkyô-Bay, at the lower extremity of the main fissure. These craters threw up large quantities of scoriaceous lava which piled up and formed new parasitic cones, the whole resembling a peninsula stretching some 700 m from the shore. These new parasitic cones and the lava flow, mentioned above, joined together and formed new land covering the old sea surface for a distance of 1000 m along along the seashore, and 700 m wide seaward. In order to determine the shape of this new land, topographical survey was resorted to twice, the first soon after the eruption and the second four months later.

The first survey.

At the time the first survey was being made, ten days or so after

* (横須賀鎮守府許可濟).

the eruption, the temperature of the surface of the parasitic cones and that of the lava flow were so high that it was impossible to set up the

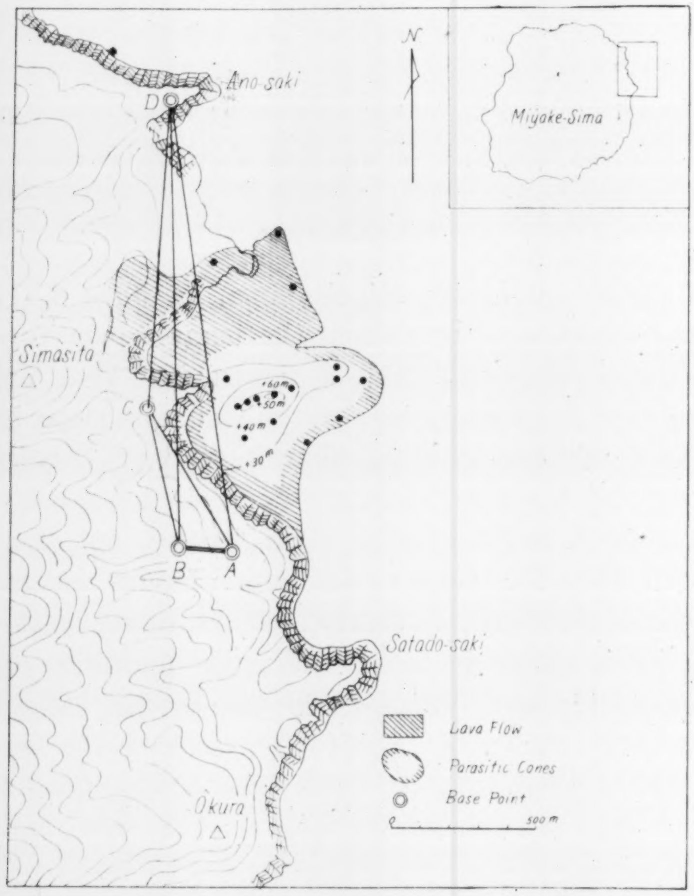

Fig. 1. Topographical map of new parasitic cones and Lava flow (first survey).

theodolite, with the result that measurements could be made only from base points taken on the old land.

In the survey, a Wild universal theodolite was used. As is well known, in order to construct topographical maps, triangulation points must be used as base points. As will be seen from the map, Fig. 1, two triangulation points of the third order, Ôkura and Simasita, were fabourably situated, but the latter was so close to the new fissure line, that the mark was buried under volcanic lapilli and ashes about 80 cm thick, so that when the writer visited the place for the first time it was not possible to find the Simasita triangulation point, for which reason it was necessary to establish a new base line as the standerd of length of the triangulations. Obviously, the site for a new base line should be on level ground, free from volcanic bombs and lava flow.

In the neighbourhood of the new land there was no site more suitable than *AB* (Fig. 1).

The length of the base line *AB* was measured with an ordinary hemp cloth tape. The horizontal distance beetwen *A* and *B*, which measured 184·78 m was taken as the base length. The position of the base line and it's expansion net is shown in Fig. 1. The form of the expansion net was not as the writer had desired, the topography preventing him from carrying out his plan. During the period of the first survey, the surface temperature of the parasitic cones and the lava flow were so high that it was almost impossible to fix the marks for the intersection points on them, with the result that natural objects, such as rocks, were used as marks showing the intersections, excepting the marks on the western flank of the parsitic cones. The western flank of the parasitic cones having a lower temperature, it was possible to drive wooden stakes into the ground for marks. These stakes were very useful for detecting the subsidence of the parasitic cones.

Measurements were made from base points established on the old land only by means of forward intersection throughout, as it was impossible to set the theodolite on the parasitic cones, owing to the high temperature of the last-named.

The result of the survey is shown in Fig 1. The map in this figure, however, was constructed on the assumption that the length of the base line *AB* is 184·097 m. Contour lines are drawn every 10 m, excepting the 10 and 20 metre contours, as the observed points were too few to enable these two contour lines being drawn.

The second survey.

Observations of heights of the new parasitic cones during the ten days of the first survey showed that these cones have a tendency to subside. In order to confirm this, a second survey was made in the Autumn of the same year. When the writer visited the island again four months after the eruption, the topographic features of the parasitic cones and the lava flow had greatly changed. The top part of the promontory formed by the parasitic cones had eroded away more than 100 m by the action of sea waves. The eroded frangments were carried by the tide and deposited on the northern shore of the lava flow, where it formed a new sand beach 500 m long, extending as far as the Anô-saki headland, as shown in Fig. 2.

In the second survey, the length of the base line was resurveyed using a one metre stadia bar and a Wild theodolite. The length of the

sub-base line, about 30 m long, was measured by the stadia bar, and expanding it to a quadrilateral, the length of line AB was calculated and found to be $184{\cdot}0972 \pm 0{\cdot}0061$ m, that is $0{\cdot}683$ m shorter than the first.

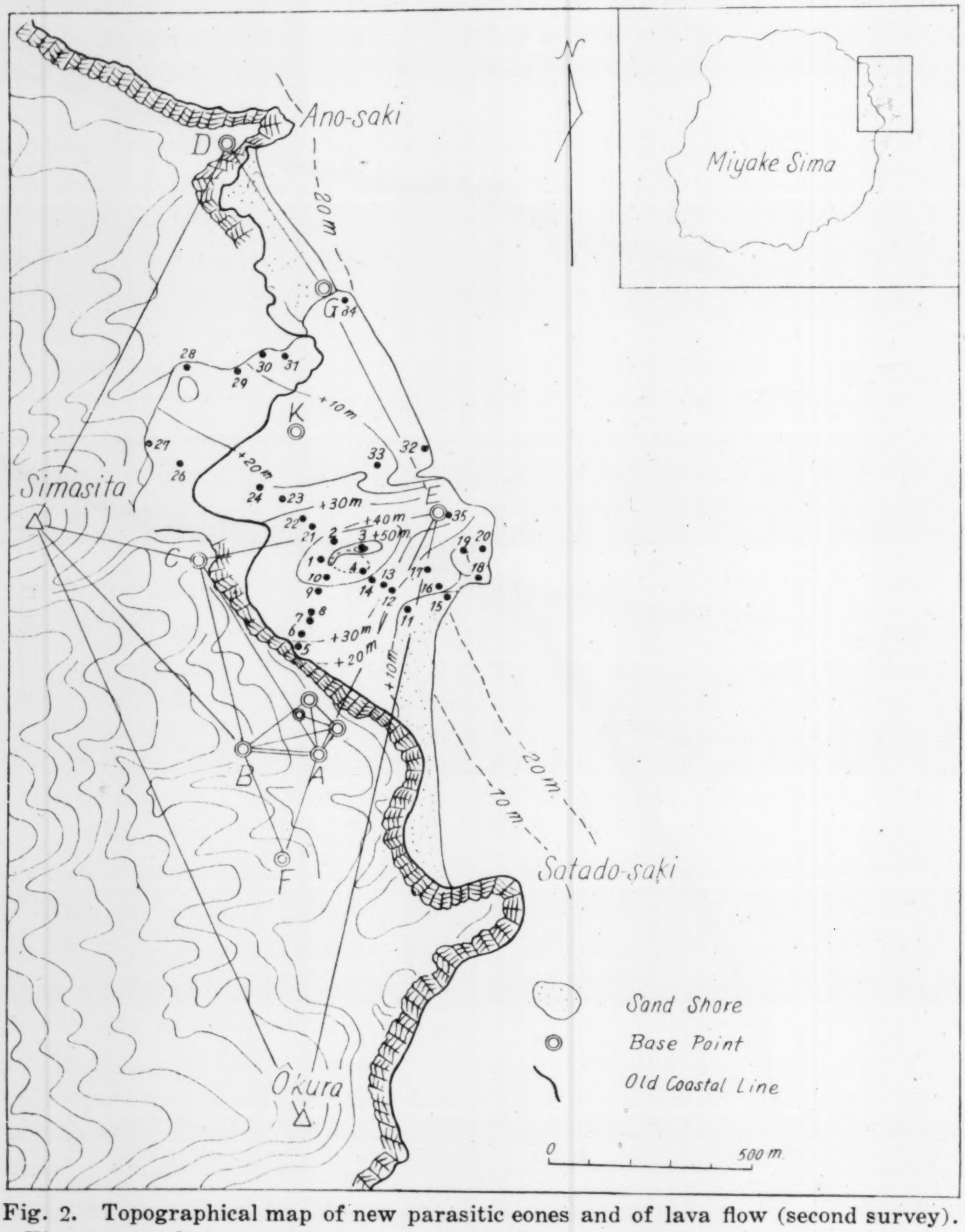

Fig. 2. Topographical map of new parasitic cones and of lava flow (second survey). Figures attached to each dot are mark numbers in Table I.

The triangulation points, Simasita and Ôkura, which could not be located at the time of the first survey, were traced about a month

after the writer made the first topographic survey, when a rough revison of the triangulation was carried out by the Millitary Land Survey with the aid of triangulation points distributed near the zone of eruption.

At the time of the second survey, the temperature of the parasitic cones had fallen considerablly, compared with what it was in the first survey, permitting the theodolite to be set up, so that the angles could be measured.

As will be seen from Fig. 2, there were eleven base points from which measurements of the intersections could be made. The triangulation net was expanded by means of these base points from base line *AB* to the two triangulation points, Simasita and Ôkura. The distance between Simasita and Ôkura was calculatred to be 1636·45 ± 0·12 m. According to triangulations made in 1912, the distance between Simasita and Ôkura was 1634·42 m. On comparing these two values it was found that the distance between these two points increased by 2·03 m. The topographical map of Fig. 2 is more full than the first one. In the figure, the height is calculated relative to triangulation point Simasita, the height of which was assumed to be 156·8 m above sea level.

The main topographical changes during the four months are

(1) Shortening by tidal erosion of the promontory formed by the parasitic cones.

(2) Formation of a sand beach between the lava flow and the Anô-saki headland.

(3) Formation of a sand beach south of the parasitic cones, extending to the Satadô-saki headland.

(4) Subsidence of the parasitic cones; marked change in the topography.

When surveyed for the first time, several points along the ridge of the parasitic cones, as shown in Fig. 3, were measured a number of times, from the base point D, namely, Anô-saki point. In the course of the second survey, two of these points were identified with points of the first survey. The horizontal displacements of these points during four months, which were very small, were of the same order as the observational errors. The vertical changes, however, were considerable, from which it would appear that the cones are still subsiding. The subsidence curves are shown in Fig. 4. Since the zero metre of the ordinate in the figure is arbitrary, the changes in heights of the first and the second survey are only relative. Mark P–1 was a wooden stake, all the other marks, D–1, D–3, etc. in the figure being natural objects. Judging from the same tendencies shown in the subsiding curves of P–1, D–1, D–2, D–3, D–4, the parasitic cones have sunk about 4 metres

in four months. The rate of subsidence of D–5, however, seems very much smaller than the others. D–5, which was the only point that was

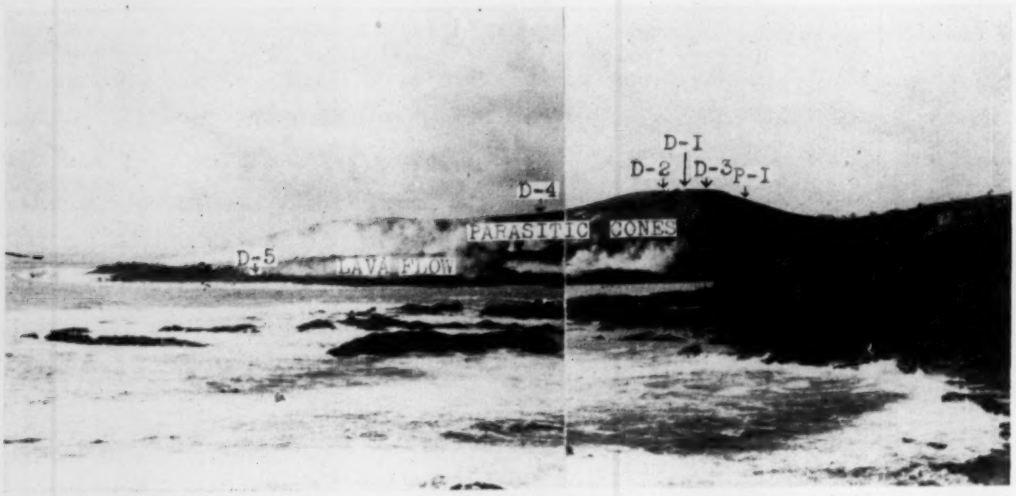

Fig. 3. Distribution of marks of subsidence curves. Photographed Aug. 5, 1940 from Anô-saki.

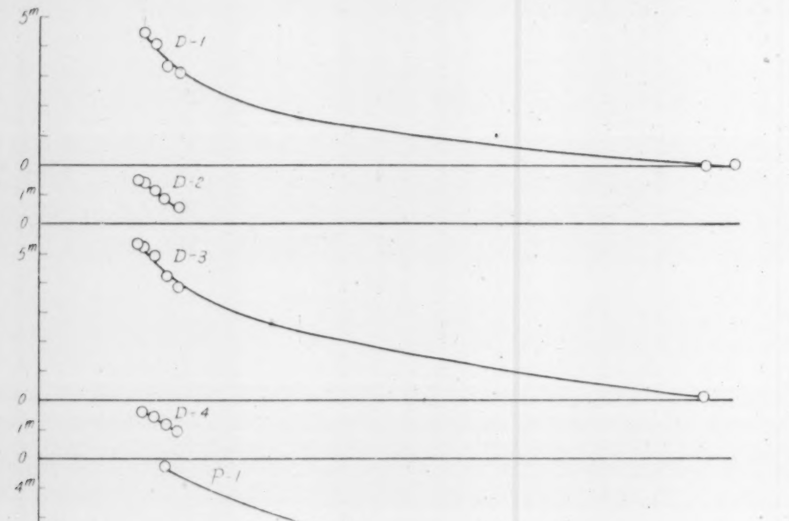

Fig. 4. Subsidence curves of parasitic cones and of the lava flow. The zero metre of the ordinate is arbitrary.

situated on the lava flow, was 7 m avove sea level while the heights of the other marks, P–1, D–1, D–2, D–3, and D–4 were respectively 52 m, 65 m, 65 m, 62 m, and 54 m. Unfortunately, mark P–5 had already eroded away when the second survey was made, so that the amount

of the vertical change of the lava flow is not known.

In order to facilitate detection of the subsidence of the parasitic cones, if any, new marks for the intersections were established in the course of the second survey, owing to possible difficulties in the future of identifing natural marks like D–1, and D–2. As new marks, a large number of wooden stakes were firmly driven into the ground all over the lava flow and the parasitic cones, except the upper parts of the cones. The surface temperature of the upper parts of the parasitic cones were still so high that the wooden stakes driven into the ground burned away in one or two days. In these cases, earthen pipes of about 10 cm in diameter were firmly embedded to serve as intersection marks. The co-ordinates and the heights of these marks are given in Table I. The origin of the co-ordinate axis is base point C.

Table I.

	x	y	h		x	y	h		x	y	h		x	y	h
	m	m	m		m	m	m		m	m	m		m	m	m
1	73·1	297·6	48·6	11	220·5	470·3	2·0	21	− 18·4	283·5	37·1	31	−457·3	323	4·8
2	31·6	330·6	44·9	12	178·3	440·3	25·3	22	− 41·6	271·3	32·1	32	−137·4	608·5	5·0
3	71·1	397·2	62·1	13	161·2	424·1	34·0	23	− 99 1	224·3	25·4	33	−139·5	493·8	26·0
4	126·4	384·2	44·8	14	146·5	409·8	38·5	24	−145·2	187·3	20·9	34	−554·3	492·5	2·5
5	262·7	182·4	24·3	15	227·3	569·3	1·7	25	− 51·7	350·5	32·3	35	35·8	610·7	41·3
6	234·4	205·1	30·2	16	198·5	544·0	13·2	26	−252·9	6·5	28·8	*E*	24·0	601·6	38·7
7	206·5	219·5	33·5	17	163·7	549·2	18·7	27	−323·7	−59·0	27·5	*K*	−262·4	311·3	17·2
8	192·8	248·4	35·8	18	219·2	664·6	2·7	28	−482	81	15·0	*G*	−589·2	453·7	3·5
9	143·3	274·3	36·8	19	129 0	644 0	19·5	29	−431	199	11·9				
10	115·1	293·9	42·2	20	138·1	684·3	17·4	30	−463	269	5·0				

In the course of the second survey, the position of the upper extremity of the craters of the side eruption was surveyed. The measured horizontal distances of this point from triangulation points, Ôkura and Simasita, were 1708 m, and 2103 m respectively, and the height of that point was 458 m above sea level. Assuming an error of as much as one minute in the angle reading the figures just mensioned will be true within a range of ± 2 m.

Quantity of lave erupted.

Besides the lava that flowed from the craters that opened on the main fissure, small quantities of lava flowed from the craters of the smaller fissures and ran down the Yoridai-no-sawa valley, while further small quantities of lava were thrown out from the summit craters of

Oyama, forming a central cone there. Compared with the quantity of lava that formed the Akabakkyô lava flow and the parasitic cones, the total quantity that flowed from these craters was not so large. As just mentioned, since the configurations of these new lands were surveyed, the amount of lava that formed this new land could be calculated. Although the shape of the seafloor buried by the eruptives was not known from the chart (scale 1 : 200000) it is assumed that the depth of the sea increased uniformly. From soundings of the neighbourhood of the coast of the new land, made by Mr. Y. Kosikawa about a month after the eruption, the old contour lines for a distance of several tens of metres from the coast of the new land, were not disturbed, leading to the conclusion that the lava never flowed out far seaward from the new coastal line. The area of the parasitic cones is $2{\cdot}7 \times 10^5\ m^2$ and that of the lava flow $2{\cdot}9 \times 10^5 m^2$, while the volumes of the parasitic cones and the lava flow are respectively $11{\cdot}6 \times 10^6$ and $7{\cdot}5 \times 10^6\ m^3$. The total volume of erupted lava amounts to $19{\cdot}1 \times 10^6\ m^3$, the same order of magnitude as that of lava erupted in the activities of 1874, as calculated by Dr. Tsuya.[1] Assuming the bulk density of the new ejecta to be $2{\cdot}0\ gr/cm^3$, the total weight of the new ejecta is estimated, without serious error, at 4×10^7 tons.

---

1) H. TSUYA, *Zisin.*, Vol. 12, No. 12.

Part XIII. Horizontal and Vertical Ground Displacements Associated with the Eruption of Miyake-sima Island.*

By Syun'itiro OMOTE,

Earthquake Research Institute.

(Read Oct. 16, 1940.—Received Mar. 16, 1941.)

Since the triangulation of Miyake-sima was first done in 1912, sixteen new triangulation points were established, four in the neighbourhood of the Oyama summit and the remaining twelve on the skirts of the mountain. Of the sexteen points, one was of the second order and the rest of the third order.

Fortunately, none of these triangulation points were destroyed by the eruption, the one or two points that were buried under lapilli or ashes were all traced. Two months after the eruption the Millitary Land Survey undertook rough revisions of several triangulation points near the zone of eruption, in order to ascertain whether or not the eruption caused any displacements of these points.

The results of these triangulation were placed at the writer's disposal by the courtesy of the Land Survey, to whom his hearty thanks are due.

The principal points of the first and second survey have been extracted as below:

Date of survey.	Instrument used.	Accuracy.	Method of calculation.
(Old) First year of Taishô (1912).	Theodolite for the third order triangulation.	—	Calculated the whole island as a net.
(New) 15th year of Shôwa (1940). from Sep. 3 to Sep. 14	Carl Zeiss theodolite I.	Inferior to theodolite for the third order.	The mean value adopted in calculating the co-ordinate and length of the trianguler side, forming the chain of triangles.

In computing the results of the observation, two assumptions were made:

(I) That triangulation point (11) and the azimuth and the length of the line from points (11) to (12) have not changed. The results of calculations of displacements of the other triangulation points with this

* (横須賀鎮守府許可濟).

Table I.

Triangular point	(11)	(12)	(14)	(13)	(9)	(8)
Δx	0	0	−0·90	−1·43	+0·28	−3·06
Δy	0	0	−0·06	+0·92	+0·70	+0·90
V	0	0	0·90	1·70	0·75	3·19
ΔH	0	+0·06	−0·29	−0·28	+0·29	+0·32

Δx: Northward Displacement.
Δy: Eastward Displacement.
V: Resultant Horizontal Displacement.
ΔH: Upward Displacement.

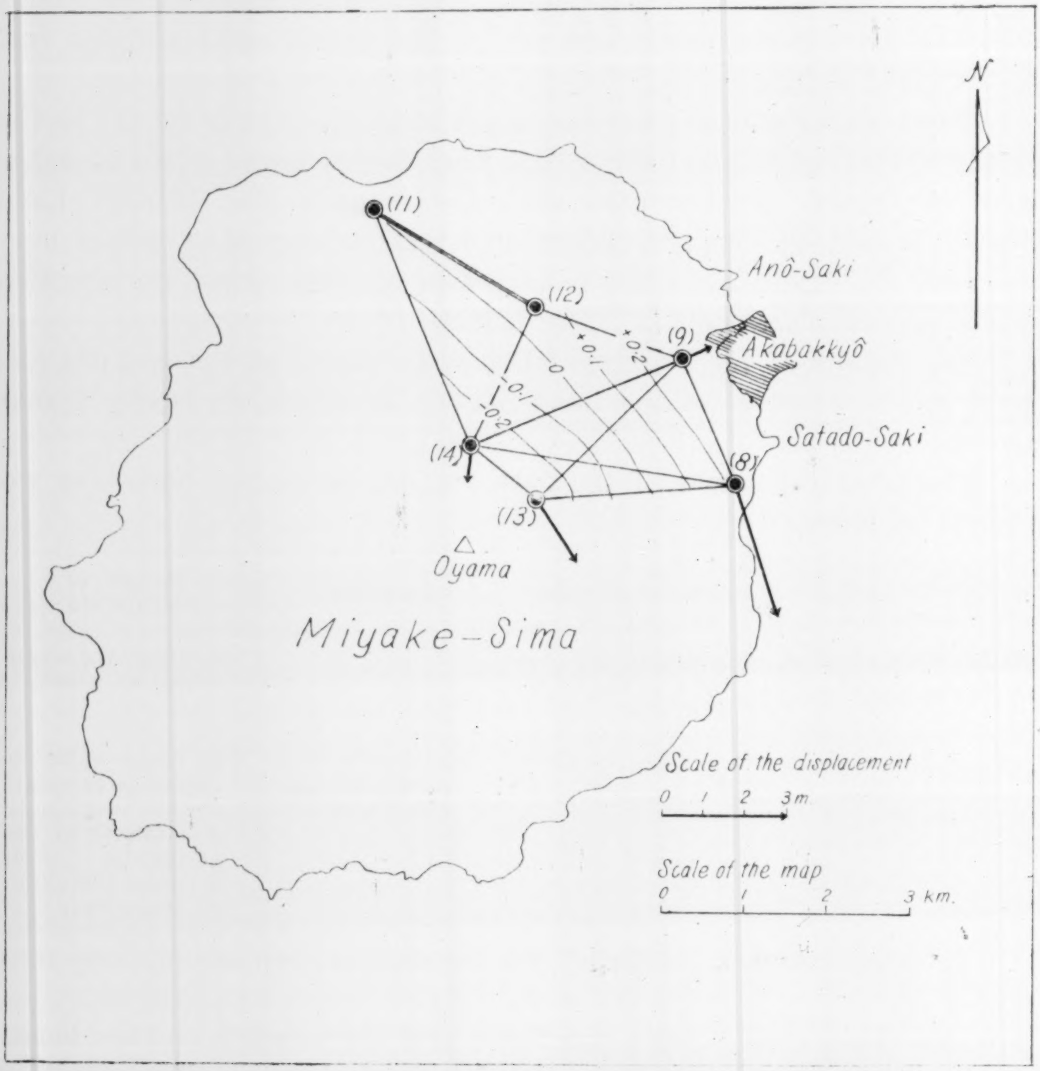

Fig. 1. Horizontal and Vertical displacements with the assumption that the point (11) and the azimuth and the length of the line from (11) to (12) have not changed. Contour lines indicate the vertical displacements for every 0·1 m.
Arrows represent the amounts and the directions of the horizontal displacements.

assumption are shown in Table I and Fig. 1. As point (12) lies not very distant from the upper end of the fissure that formed during the eruption of 1874, the 7th year of Meidi, it may rather unreasonable to assume that it had not moved since then. The contour lines in the figure indicate the vertical differences for every 0·1 m.

(II) That trianguler point (11) and the azimuth and the length of the line from (11) to (14) have not changed. Computations of the displaments of the other triangulation points whith this assumption are shown in Table II and Fig. 2. Point (14) lies about 600 m north of the summit of Oyama.

Table II.

Triangular point	(11)	(14)	(12)	(13)	(9)	(8)
Δx	0	0	+0·60	−0·15	+1·31	−1·63
Δy	0	0	−0·35	−0·30	−0·05	+0·15
V	0	0	0·70	0·34	1·31	1·64
ΔH	−0	−0·52	+0·01	−0·47	+0·26	+0·17

Δx: Northward Displacement.
Δy: Eastward Displacement.
V: Resultant Horizontal Displacement.
ΔH: Upward Displacement.

As just mentioned, it may not be reasonable to assume that triangulation point (12), has not moved, it being rather preferable, although each angle of the triangle (11)—(12)—(14) has changed more than 30 seconds, to assume that point (14) has not moved. Although all the displacements shown in Fig. 2 may contain the term of the seculer variations during the 30 years, the larger part of them is regarded as the result of the recent eruption. This eruption, of June 1940, caused a fissure from which large quantities of lava were poured out. This fissure lies between triangulation points (8) and (9). It will be seen from Fig. 2 that point (9) has been displaced 1·31 m northward and point (8) 1·64 m southward. It appears as if the lava intruded into this fissure in the form of a dyke, and pushed outward the crust of both sides of the fissure. The vertical displacements in Fig. 2 show that the lower part of the crust, distant some 700 or 800 m from the upper end of the fissure, has risen, while its upper part has sunk, but as no leveling survey was yet undertaken, and since the vertical changes were deduced from readings of the vertical angles of the theodolite, an error of 10 seconds in the angle reading would result in an error of about 10 cm in the difference of level, detailed discussions based on these data are impossible. The triangulation, however, was not con-

ducted for the entire island, so that it is not possible to say whether or not the vertical displacements shown in Fig. 2 indicate that the

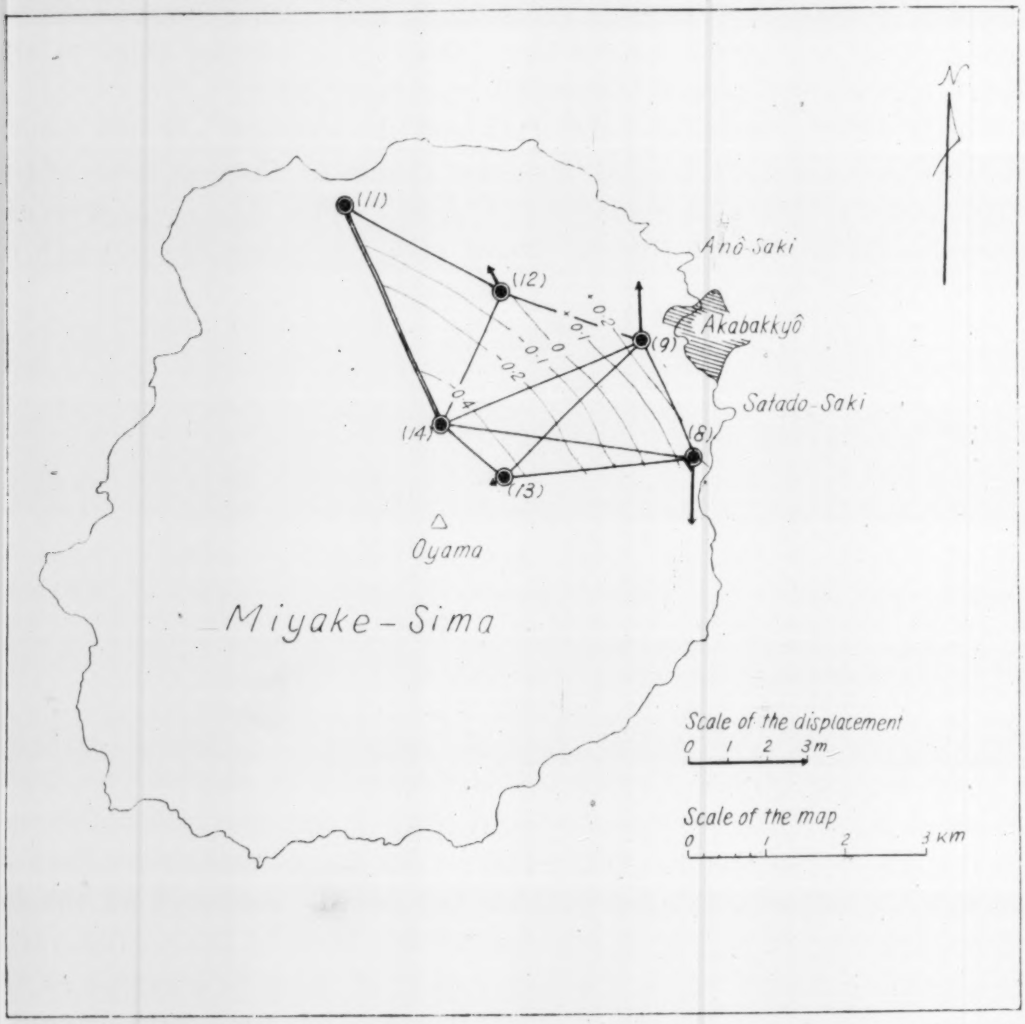

Fig. 2. Horizontal and Vertical displacements with the assumption that the point (11) and the azimuth and the length of the line from (11) to (14) have not changed. Contour lines indicate the vertical displacements for every 0.1 m. Arrows represent the amounts and the directions of the horizontal displacements.

island sank in the central part and rose in its margin, contrary to the case of Sakura-sima island,[1] which rose in the contral part and sank in its margin, or that the island as a whole had tilted. According to calculations based on the data of Fig. 2, assuming that the island tilted, the amount of tilt is estimated at 30 seconds.

Further details will be discussed later when the precise triangulations and the levelings have been completed with reference to all the triangulation points on the island.

1) T. TERADA and N. MIYABE, *Proc. Imp. Acad.*, **5** (1929), 325.

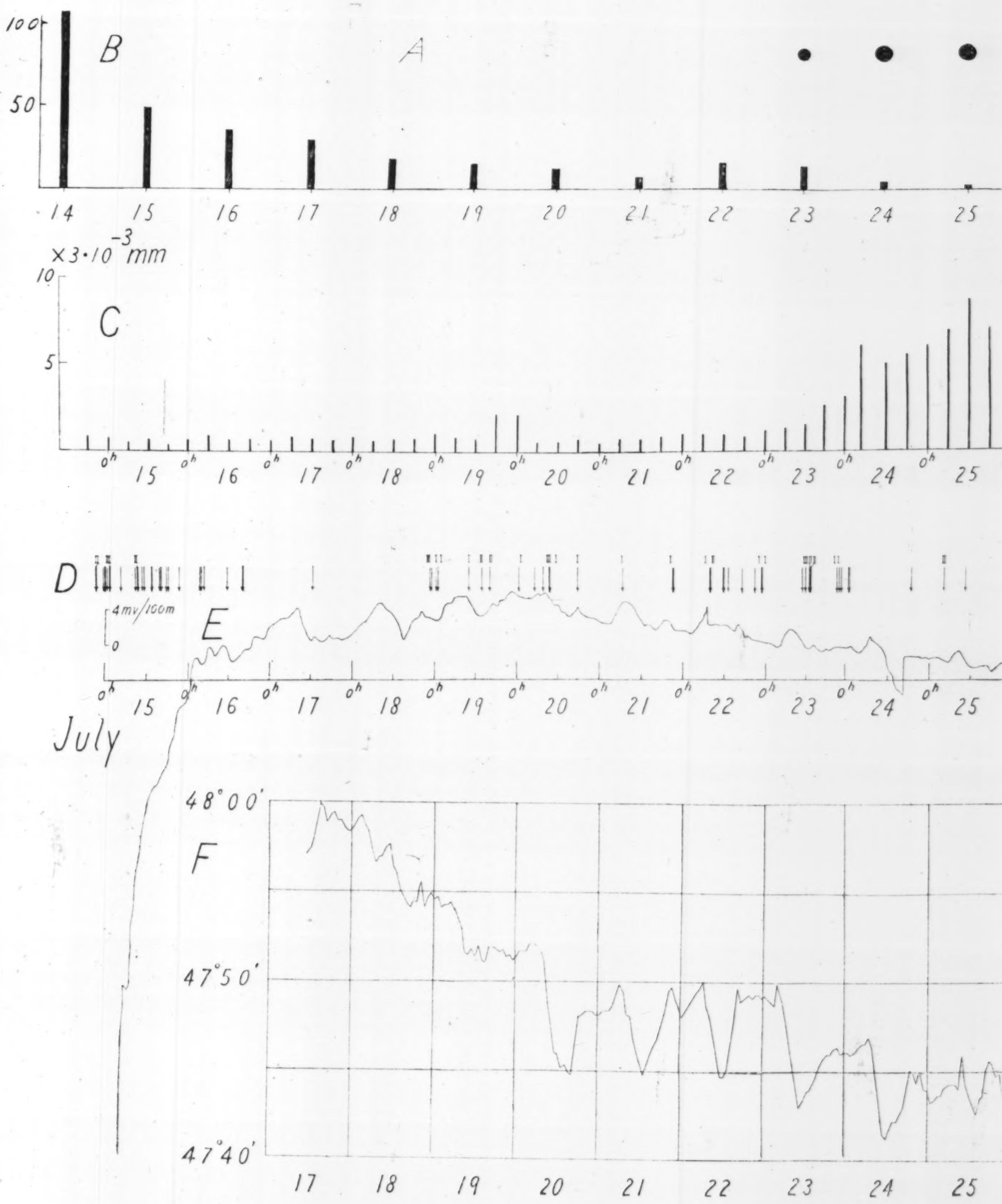

A—Radius of circles showing the loudness of the detonations, divided into three classes, larg
B—Number of daily occurrences of volcanic eathquakes observed at Kamituki with the seisn
C—Amplitude of daily volcanic pulsations observed at Kamituki.
D—Arrows indicate the volcanic earthquakes observed at Kamituki with the seismograph, m
E—Changes in the earth potential observed at Kamituki.
F—Magnetic dip observed at Hôdai.

（震研彙報　第十九號　圖版　萩原・水上・永田）

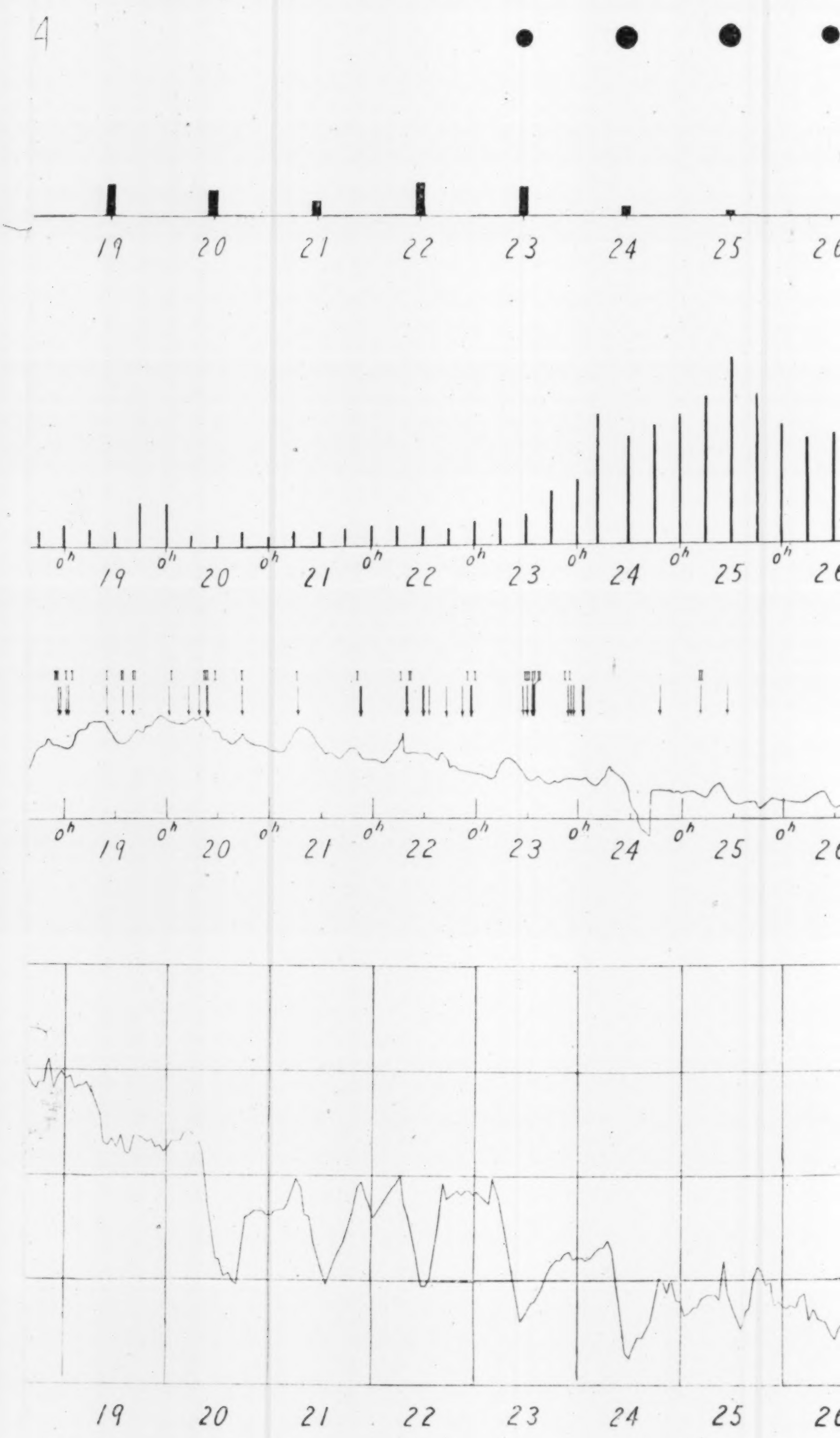

ıg the loudness of the detonations, divided into three classes, large, int
ences of volcanic eathquakes observed at Kamituki with the seismogra
anic pulsations observed at Kamituki.
canic earthquakes observed at Kamituki with the seismograph, magnifi
tential observed at Kamituki.
t Hôdai.

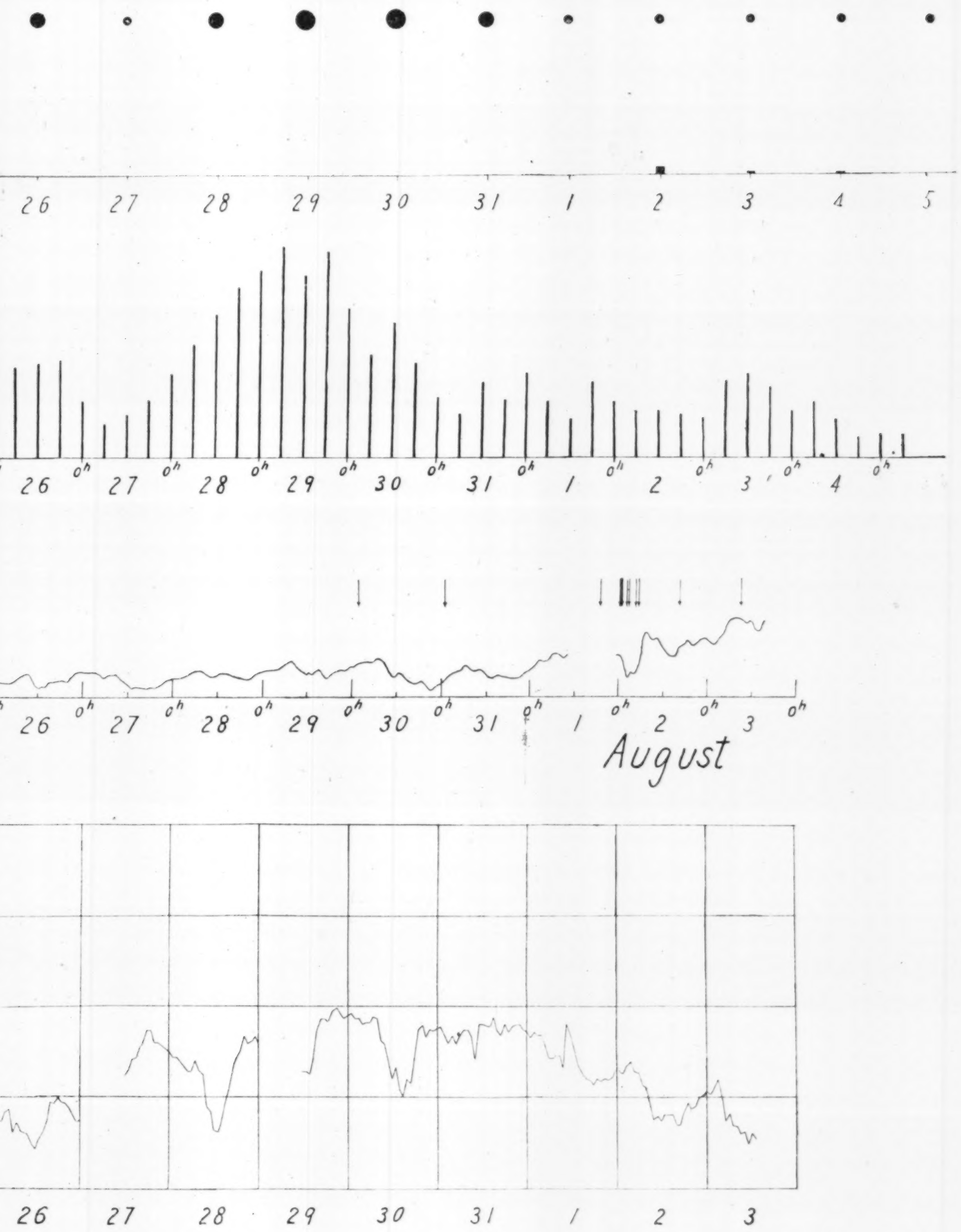

, intermediate, and small.
graph, magnification 330.

gnification 120, the Roman numbers showing the scale of seismic intensity.

Part XIV. A Graph for Comparing Changes in the Amplitude of Daily Pulsations, in the Number of Daily Occurrences of Earthquakes, in the Earth Potential, and in the Magnetic Dip.

By Takahiro HAGIWARA, Takeshi MINAKAMI, and Takesi NAGATA,

Earthquake Research Institute.

Following the eruption of July 12, various instrumental observations were made in Miyake-sima, the results of which have been reported in the foregoing papers by the respective observers concerned.[1] In order to facilitate comparison, these results are shown here in a single graph. When these observations were begun, the eruptions that occurred on the mountain side were already quiet, although the central crater of the summit had just begun to get active, so that the observed changes are intimately related to the activity of the central crater. Its activity began on July 14, when large quantities of smoke rose from the crater, but when the molten lava approached the surface of the crater, the smoke markedly diminished, while explosions began to take place intermittently, the detonations being heard in the villages on the seashore. Since the observed pulsations of the ground are waves that were caused by the explosions at the crater, the intensities of the explosions at various times may be expressed by changes in amplitude of the former. The severity of the explosions, which gradually increased, reached maximum on July 25, and then gradually declined. The volcanic earthquakes, which increased in number after July 18, stopped exactly when the severity of the explosions reached maximum on July 25. The gradual changes in the earth potential and in the magnetic dip also changed their directions on this day. The respective observers have discussed the reasons for these changes.

---

1) Parts V, VI, VII, and VIII.

20. 昭和15年7月三宅島の噴火

第I部 三宅島噴火の地質學的觀察 (I)

地震研究所 津屋弘逵

三宅島は所謂富士火山帶中の大島帶に屬し，數十の寄生丘及び側火口を有する外輪山と東西に連なる3火口を有する中央火口丘とから成る二重の成層圓錐火山である．同火山の噴出物は玄武岩質熔岩流と同質の火山砂礫層とであるが，少くとも外輪山の北及び北西山腹では，其他に厚さ10～30 cm の流紋岩質輕石灰砂層が玄武岩質火山灰層に挾まれて，地表下約 1 m の深さの所に存在する事實か今回の調査によつて見出された．此の流紋岩質火山灰砂層は三宅島自身の噴出物でなく，近隣の神津島或は新島の流紋岩火山の噴火に由來するものと推定されるから，伊豆七島に於ける玄武岩火山と流紋岩火山との火山活動の時代關係を明示する一つの重要な資料であらう．同層は有色鑛物として黑雲母及び角閃石を含んでゐて，之等を含む流紋岩は神津島及び新島では流紋岩火山發達の中期の噴出物である．從つて，三宅島の流紋岩灰砂層が神津島或は新島の流紋岩火山に由來するといふ推定が正しいとすれば，三宅島火山外輪山の大部分は神津島，新島等の流紋岩火山の活動の中期には既に形成されてゐたに相違ない．

三宅島神着の東方，釜ノ尻の海岸には海面上の高さ約 15 m の海岸段丘が發達し，その上部を構成する砂礫層は介殼化石を含んでゐる．また同島海岸には現在の海面上 2～3 m の高さの所に海蝕洞穴が見られる．從つて，同島は從來多少隆起する傾向に在るものと考へられる．然し上述の流紋岩灰砂層が隆起海底堆積層でなくて陸上堆積物である事は，同層が極めて純粹な流紋岩灰砂であり，海面上 200 m 以上の外輪山山腹にも見出される事，同層の直ぐ下に濶葉樹の葉の痕跡及び火山豆灰を多量に含む玄武岩質火山灰砂層（島で“堅”と呼ばれる土層の一部）が發達してゐる事等から明かである．

神着部落内及び坪田に近いコヽマの海崖では火山灰砂層の下から石器及び土器が見出されてゐる．從つて三宅島は先史時代から後に幾度も噴火して來たに相違ないが，有史時代では應德2年（皇紀 1745 年）以來明治 7 年（2534 年）までに 11 回の噴火記錄を有し，平均約 60 年に 1 回の割合で噴火した事を示してゐる．此の有史時代の噴火の中で，4 回（2303, 2371, 2495, 2534）は山腹噴火，1 回（2471）は山頂噴火，1 回（2423）は山腹及び山頂噴火であつた．而して，山腹噴火は 2303, 2371, 及び 2423 年には外輪山の南西側の桑木平から阿古及び東山に亘る地域内で起つたが，2495 年には外輪山西側の伊ヶ谷寄りの山腹に移り，2534 年には更に北東方に移つて外輪山北側に起つた．之等の山腹噴火の多くは何れも數個の小火孔或は噴火裂罅から起り，火山砂礫と熔岩流を噴出したものの樣である．明治 7 年（2534 年）の噴火地域及び噴出物は現在でも明かに認められる．即ち同噴火は同年 7 月 3 日曉から頻發した地震に次いで，正午頃外輪山北側の池ノ澤（山頂近くに在る一連の舊寄生火口列中の大孔西隣りの山腹）に主として始まつたのであるが，その噴出物の現在の分布狀況から考へると，同處から北東方のバウズ山に至る間に並ぶ數個の裂罅狀火孔から先づ火山砂礫を多量に噴出し，次いで大孔西隣りの火孔から熔岩を噴出したものの樣であつて，同熔岩は神着村東鄉の人家 45 戶を埋めて北方海中に迄流出した．

明治 7 年の噴火は 1 週間程で略鎭まり，噴煙も間もなく止まつて，其後昭和 15 年に至る迄三宅島は少くとも表面的の火山作用を全く休止してゐた．大正 14 年筆者が同島の地質を調査

した當時には，外輪山の山腹は勿論，中央火口丘の火口にも一つの噴氣孔すら認められなかつた．

今回の噴火は明治 7 年から 66 年を經て昭和 15 年 7 月 12 日に始まり，外輪山北東側と中央火口丘とに相次いで起つたのであるが，それより先に噴火の前徵と見られる二三の現象が氣付かれてゐた．即ち外輪山北東側の赤場曉に近い山腹では昭和 14 年 12 月頃既に噴氣孔が現れ，又赤場曉灣岸では昭和 15 年 5 月末頃同樣に噴氣孔が現れた．噴火開始の約 1 週間前頃から，外輪山北東側で地震及び地鳴りが感じられ，また二三日前から，赤場曉灣の海中で鳴動が聽かれ，海水の溫度が局部的に多少高まつてゐた樣である．

噴火開始の當日は數日來と同樣に南西風で，雨が降つたり止んだりする荒天であつた．神着では當日午前中に地鳴りが聽かれ，午後 3 時頃から地震が時々感じられ，6 時頃にはそれが殆ど連續的に成つた．かくして噴火は 7 時 30 分頃始まつたと推定されるが，神着では 7 時 50 分頃氣付かれるに至つた．同噴火は外輪山北東側上の山腹噴火で，その中腹に始まつた後に忽ち北東下方に擴がり，翌 13 日午後 6 時頃まで殆ど連續的に起り，其間に火山砂礫及び火山彈を飛ばし，熔岩を流出し，また赤場曉灣內には新山（瓢簞山）を形成した．

山腹噴火は 13 日午後 6 時頃までに事實上終り，その後同日午後 9 時及び 14 日午前 3 時頃小爆發を起したのみであるが，13 日夜から 14 日朝に至る間に中央火口丘の山頂噴火が始まつた．此の噴火は同丘上に在る 3 火口中の中央に位する大穴の北壁寄りの火口底に始まつたのであつて，7 月 18 日まではその一個から噴煙してゐたのみであつたが，翌 19 日には既に同火口の北西壁の下まで，その後更に同火口西隣の上段火口底にも擴がつた．而して 7 月 20 日までには，火口底及び火口壁の舊岩屑及び火口底に上昇して來てゐたと考へられる．新熔岩柱上部の既に固結した岩塊が拋出され，また之等の碎粉が火山灰砂として主として北東方向に散布されたのみであるが，21 日からは新熔岩の岩滓質砂礫及び火山灰が拋出され，更に 24 日からは噴煙の量が減少したのに反して空振を伴ふ爆音及び鳴響が一層頻繁となり，同時に赤熱の熔岩が火山彈として盛に拋出される樣になつた．此の活動は同日から 7 月 30 日頃まで最も盛で，その後次第に減衰し，8 月 5 日頃に至つて殆ど鎭まつた．此の山頂噴火に因つて，中央火口丘上には少量の新熔岩が流出し，また火山彈及び火山砂礫が大穴の一部及びその西隣の上段火口の全部を埋めて新火口丘を形成したのである．(未完)

第 II 部　熔岩の溫度

地震研究所　永　田　武

赤場曉熔岩流內 4 ケ所に於ける赤熱熔岩の溫度を光學高溫計を用ひて測定した．噴出後約 1 週間後に於いてそれ等の溫度は 850°C 乃至 965°C であつた．

第 III 部　赤場曉熔岩流の粘性係數の推定

地震研究所　萩　原　尊　禮

赤場曉熔岩流は，山腹に生じた裂罅噴火の上端に近い，海拔 400～500 米の箇所より流出したと推定され，其の流出は 7 月 12 日最初の噴火が起つて間もなくであつた．此の熔岩流は神着，坪田兩村の境にある澤を流下して赤場曉潟を埋めたが，當時の流下速度が略々 4 m/sec であつたことが目撃されてゐる．此の移動速度を基として，熔岩が所謂層狀運動にあつたとして計算を試みると流下當時の熔岩の粘性係數は 10^5 c.g.s. の程度であつたことが推定される．此の時の溫度は 1000°C を少しく越した程度であると思はれる．此の粘性係數 10^5 と云ふ値は，ハワイや三原山の熔岩に就き同じく計算から求められた値に比較すると，2～3 倍大きい．

第 IV 部　新噴出岩の磁氣的性質

地震研究所　永　田　武

三宅島噴火後觀測された顯著な地球磁場局部的異常變化の解釋に當つて，一つの重要な因子は新噴出岩の磁氣的諸性質である．新噴出岩及び明治熔岩から採集せる代表的岩石試料數種に就いてその磁氣的諸性質を吟味した結果は次の如くである．

(i)　帶　磁　率

比帶磁率は $0{\cdot}6\times10^{-3}$ 乃至 $1{\cdot}3\times10^{-3}$ の範圍であつて，火山岩の帶磁率としては比較的大きい部類に屬するが，岩石の化學成分から期待される標準値よりは著しく小さい．

(ii)　帶磁率の溫度變化

帶磁率は室溫からある溫度までは，溫度と共に增加し，最大値は 0°C に於ける値の 1·8 倍に達する事もある．それ以上の溫度では急激に減少する．見かけの磁氣的變態溫度の比較的低い (300°C 位) 試料では，溫度の變化に對して帶磁率の變化は非可逆的である．測定した範圍では強磁性を完全に消失する溫度は 580°C 乃至 600°C であつて，磁鐵鑛の Curie 溫度と一致してゐる事は注意するに足る．

(iii)　自然殘留磁氣

自然殘留磁氣係數は 16 乃至 46 に達し，磁化の方向は勿論地球磁場のそれと一致してゐる．

(iv)　熱殘留磁氣の諸性質

熱殘留磁氣の特性曲線 $P(t)$ の基本型を唯一つの遷移溫度 t_0 にて極大値を有し，その兩側では急激に減少する比較的簡單な曲線と考へる時，新噴出岩に於いては，この基本型の特性を有する物の他，$P(t)$ 曲線が異れる基本型曲線が 2 乃至 3 重疊してゐると思はれるものがある．後者に就いては，之を基本型に分離し，その各々の t_0, $P(t_0)$ 等を第 V 表に示した．卓越せる t_0 は300°C 及び 500°C であり，又 $P(t)$ の値は $t_0\pm50°$ で $P(t_0)$ の半分になつてしまふ事は注目すべきである．

之等の結果の中，自然殘留磁氣の强さ及び方向は水上氏によつて測定された地磁氣異常分布を說明するのに充分である．熱殘留磁氣の生成又は消滅，換言すれば自然狀態に於ける自然殘留磁氣の生成及び消滅はその帶磁の强さからして，水上氏，高橋，平野兩氏，及び永田によつてそれぞれ觀測された地球磁氣異常變化の原因の第一に擧げられる可きであるが，それでも猶且つ地下かなり廣範圍にわたる溫度變化を假定しなければ，現象を說明出來ない．又熱殘留磁氣遷移溫度 θ_0 が岩石によつて種々の値を採るといふ事實は，假令地下の溫度變化の分布が比較的單調であつても，磁氣分布の變化は，相當に複雜な形となり得る事を暗示する．本文には其の他，二三の附隨的議論を附加してある．猶ほこの章に述べた實驗裝置は服部報公會の援助によつて製作せられた．記して感謝の意を表する．

第 V 部　三宅島噴火に伴つた地震

地震研究所　萩原尊禮

昭和 15 年7月 12 日の三宅島噴火後，4 臺の地震計を同島に携帶して地震觀測に當つた．地震計設置前の地震發生の狀態は，島民の談を綜合すれば次の通りである．噴火地域の近くに住んでゐた人達は噴火の數日前から弱い地鳴を聞き，噴火の約 1 時間前からは噴火地域及び神着村及び坪田村三池に於て小地震を連續的に感じた．7 月 12 日午後 8 時，最初の噴火が山腹に起つてから後は，翌 13 日にかけて神着村方面に於て頻々と大小の地震を感じた（最大震度 III の程度）．

7 月 14 日以後地震觀測により判明したことは，地震は雄山の西北山麓に發生し，裂罅噴火の地帶に全く發生してゐないと云ふことであつた．地震觀測が開始された時は，山腹の裂罅噴火は既に活動を中止して，專ら中央火口の活動に移つた時であつたので，觀測された地震發生の狀態は中央火口の活動と密接な關係を持つた．中央火口は，最初盛に噴煙を行つたが，後次第に減少し，これと同時に間歇的に爆音を生じて赤熱熔岩を噴上げるに至つた．地震の發生の狀態を見るに，觀測開始後 2〜3 日を經てから地震發生の回數を增加したが，中央火口爆發が最高頂に達するに及んで，全く地震の發生を見なくなつた．即ち，地震發生回數の增加は，中央火口への熔岩の上昇期（即ち噴煙期）に起り，火口に熔岩が到達して自由に其の表面から瓦斯を放散する狀態に至つた時，地震の發生は中止したと考へられる．恐らく，熔岩內の瓦斯壓力の增加が火口への熔岩上昇を起すと同時に，地下に於て破壞現象を起して，これが地震發生となつたものと考へられる．

第 VI 部　三宅島の活動に伴つた火山性脈動

水　上　武

昭和 15 年 7 月 12 日 20 時の三宅島爆發の後約 48 時間を經過せる 14 日 19 時 45 分より同島神着村に微動計を設置して火山より發生せる微小地震並に火山脈動の觀測を行つた．本報告は筆者が同島に滯在せる約 3 週間に亘る間の結果である．微動計は引續き昭和 16 年 3 月現在に至る迄引續き同一場所に設置して觀測を行つてゐる．その結果は更めて報告する事にする．

第 VII 部　噴火に伴へる地球磁氣異常變化
(伏角變動計による觀測結果)

地震研究所　永　田　武

三宅島噴火後，島の東北部で伏角變動計による地球磁氣觀測を行つた．觀測誤差に對してあらゆる考慮をしても猶ほ 7 月 17 日以後 26 日迄の間に伏角に於いて約 16′ の減少を示した事を認めざるを得ない．變化の模樣は水上理學士による伏角の絕對測定の結果と良く一致する．地球磁氣變化の模樣とその機構に就いて若干の推測的議論を行つた．

第 VIII 部　三宅島の磁氣(伏角)測量

地震研究所　水　上　武

三宅島を一個のコニイデと考へた時の帶磁の概況を知るために略一樣に散在する樣に選ばれた 45 點に於いて伏角の測定を行つた．その結果第 1 圖に示せる如く標高の增加と共に伏角が增加を示してゐる．この事實は旣に淺間火山，櫻島，草津白根山の測量の結果指摘したところである．この現象は各火山の構成は各々複雜であつて個々の熔岩流，各々の岩石は勝手の帶磁方向を有してゐても，火山を全體として見る時は現在の磁場に近い方向に略一樣に帶磁せる事を示すものである．

然しながら三宅島ではその伏角と標高との關係より見られる樣に淺間山，櫻島等の酸性熔岩より成る火山に較べてその磁氣異常の量は略 10 倍に達して居る．

三宅島の伏角の測量はその後昭和15年10月に再測を行つた．

第 IX 部　三宅島の伏角の變化とその地理的分布（概報）

地震研究所　水　上　武

昭和 15 年 7 月 14 日より 8 月 3 日に至る期間に於いて數點の測定點に於いて 6 回乃至 2 回の再測を行つた結果その變動が判明した．之等の諸點に於いて何れも此の期間に於いて伏角の著しい減少を示し，その量 30′ に達してゐる．

その後昭和 15 年 10 月に再測を行つたが，詳細は更めて報告する事にする．

第 X 部　三宅島噴火後に於ける地電流變化の觀測

地震研究所　萩　原　尊　禮

三宅島噴火後，神着村に於て一方向の地電位差の觀測が行はれた．電極間の距離は 50 m，方向は S 14° W であつて略々其の場所から雄山を指す方向である．觀測は 20 日間に亘つて行はれたが，其の記錄全部を揭載してある．

比較的顯著な地電流變化としては，7 月 22 日の 7 時前後，及び 7 月 24 日の 12 時より 18 時の間に起つたものを擧げることが出來るが，何れも比較的緩慢に一方向に電位を增し，或る値に達して後急激に舊の値に復してゐる．火山活動の方から云へば，中央火口の活動は 7 月 18 日前後を境として，連續的に噴煙することから間歇的の爆發に代つて居り，同時に地震回數を增した．そして終に熔岩は火口表面に達し，火口の爆發は 25 日頃に最高頂に達したのであるが，前述の顯著な地電流變化は，丁度此の期間，即ち，熔岩が火口栓を破り次第に中央火口の表面まで上昇しつゝある期間に起つてゐる．數日に亘るやうな緩慢な地電流變化に就て言へば，7 月 25 日頃を境として，山側の電壓が徐々に低くなる變化からこれと反對の方向の變化へ移り代つてゐる．

今回の觀測は，一點に於ける一方向の，しかも短期間に行はれたものであるので，此處では單に一記載として止め，立入つた議論は差控へた．

第 XI 部　噴火に伴つた垂直磁力の變化（概要）

地震研究所 {高　橋　龍　太　郎
平　能　金　太　郎

昭和 15 年三宅島の噴火に際し，筆者等は島内 50 の測點に於て垂直磁力の測定を行つた．使用器械は筆者の一人の考案になる垂直磁力計である．第 1 回の測定は 7 月 20～24 日，即ち中央

火口丘の活動が擴大してゐる時季に，第2回測定は7月 26～29 日，即ち中央火口丘の活動が最盛に達してから行つた．此等測定の結果は此の兩回の測定の間に垂直磁力の分布が著しい變化を爲した事を示した．此の變化は中央火口丘下 3km の點を中心とする球狀部分の磁氣感應率が0になつたと考へれば甚だよく說明出來る．磁氣感應率が0になる原因は熔岩上昇の爲め，或は其れによる岩石の温度の上昇の爲めと考へられる．是等測定の結果並に其の解釋の詳細は旣に地震研究所彙報に發表してある．

昭和 15 年 12 月上旬，筆者等は第3回の磁氣測定を行つた．本論文に記載してあるのは此の第3回測定の結果並に其の解釋である．

第3回測定は前2回の測定と同一器械を用ひ，同一方法によつて測定した．其の結果は本文第1表に示した通りである．其の結果，第3圖に示した樣な垂直磁力の變化が第2回第3回の測定の間に起つてゐる事が判明した．此の垂直磁力の變化の有樣は第2圖に示した第1回，第2回測定間の變化と丁度反對になつてゐる．從つて今回の變化は山頂下 3km の地點を中心とする球狀部が，時の經過と共に冷却して，熱殘留磁氣を有する外殼を生じたと考へれば質的には說明される事になる．

冷却の原因としては周圍岩石への熱の傳導，瓦斯放出に際する熱の消耗等が考へられるが，何れも今回の變化を量的にまで說明する事は困難であつて，高温，高壓下に於ける岩漿が冷却する際には，地表に噴出固結した岩石に比して非常に大きな熱殘留磁氣を生ずるのではないかと思はれる．

尙此等測定の解釋について 2，3 の議論が行つてある．

第 XII 部　噴火に依つて生じた新寄生火山と熔岩流との地形測量

地震研究所　表　俊一郎

昭和15年7月12日の噴火により新らしく生じた寄生火山及熔岩流の地形測量を噴火直後及 4ケ月後の二回にわたつて行つた．測角には Wild の萬能經緯儀を用ひ，圖に示すごとき數個の基點から交會法により測量を行つた．基點間の距離は新らしく設定した Base line の長さを 1 米 Stadia を用ひて測定して，之を基準とした．Base line の長さは 184·0972 ± 0·0061 m，基線の角測量の誤差は ±15″ である．二つの三角點，島下及大倉間の距離は 1636·45±0·12 m となり之を大正元年に行はれた三角測量の結果 1634·42 m と比較すると 2·03 m 延びた事になる．第1回及び第2回の測量の結果は第1圖及び第2圖に示すごとくである．第1回及び第2回の測量の結果第4圖に示すごとく新寄生火山は 4～5 m 程沈下した事が分つた．

熔岩流及び寄生火山の形及び大きさを知り得たので，之から噴出した熔岩の量を算出する事が出來た．昭和 15 年の三宅島の活動により噴出した噴出物は地形測量を行つた場所以外に，ヨリ

ダイの澤を流れ下つたヨリダイの澤熔岩流と，山頂噴火により雄山の舊中央火口の中に新らたに形成された新中央火口丘及びそれの北西麓に新らたに流出した熔岩流とがあるが，それ等の量は少であるので計算から除く事にすれば噴出物の量は $1{\cdot}9\times10^7 m^3$ となる．熔岩流及寄生火山全體としての體積密度が大約 $2gr/cm^3$ であるとの假定が許されるならば噴出熔岩の全量を 4000 萬噸と推定しても大差ないであらう．

(横須賀鎭守府許可濟)

第 XIII 部　噴火に伴つた土地の水平及垂直移動

表　俊一郎

噴火の2ヶ月程後陸地測量部により噴火地帶に近い數個の三角點につき簡單な三角測量が行はれた．之を大正元年に行はれた三角測量と比較して三角點の移動を求めた結果は，第1圖及び第2圖に示してある．第1圖は三角點(11)は不動，(11)—(12)の方位及び長さ不動として計算した結果であり第2圖は(11)は同じく不同，(11)—(14)の方位及び長さ不動として計算した結果である．第2圖が實際の動きをあらはすに近いかと思はれる．等高線は10糎毎の高さの變化を示すものである．

(横須賀鎭守府許可濟)

第 XIV 部　器械觀測結果の總括

地震研究所　萩原尊禮　水上武　永田武

昭和15年7月20日の三宅島噴火後，同島に於て色々の器械觀測が行はれた．觀測の結果は，夫々の觀測擔當者により，個別的に報告されてゐるので，此處に一括した圖を揭げ，比較研究の便に供した．この觀測が開始されたのは，最初の噴火より約二日を經過した後であつて，山腹に於ける裂罅噴火は既に終止し，代つて山頂中央火口の活動が開始された時であるから，觀測結果は何れも中央火口の活動と密接な關聯を持つてゐる．

---

21. *A Geomagnetic Study of the Minor Activities of Volcano Mihara, Oosima Island, August 1940.*

By Takesi NAGATA,

Earthquake Research Institute.

(Read Oct. 16, 1940.—Received Mar. 20, 1941.)

1. Introduction.

Thirty-eight days after the beginning of the severe eruption of Miyake-sima, another Volcano, Mihara, in Oosima Island, about 80 km north of Miyake-sima and about 100 km south of Tôkyô, began to show activity. The geophysical aspect of this volcano has been the subject of frequent reports by R. Takahasi and the writer[1], while its geology and petrology have received the attentions of S. Tsuboi[2]. Although this volcano has been rather quiet since the end of the great eruption of 1911～1914, it has been growing active again since 1938, when, on August 11, there was a minor eruption, the bottom of the pit having turned into an incandescent lava pool, ejecting quantities of porous scoria that fell around the mouth of the pit. After this activity, comparative quiet reigned until eruptions started again in September, the following year. In this activity of 1939, the first eruption occurred on Sept. 2 and continued until the next day, the incandescent lava filling the crater bottom in a pool and throwing up quantities of bomb and scoria, although they did not reach the mouth of the pit; while the second eruption began on Sept. 16 and kept on all that day, the magnitude of the activity being nearly the same as that of the first.

During all these activities, owing to the accumulation of solidified lava masses on the floor of the pit, the depth of the pit became shallower. As measured from the edge of its mouth, the depth of the pit was 289·6 m in Nov. 1936, 298·7 m in Aug. 1937, 255 m in Aug. 1938, 250 m in Oct. 1938, 220 m on Sept. 3, 1939, and 218 m on Sept. 16, 1939, while according to H. Tsuya[3], it was about 400 m in 1933. This ten-

1) R. TAKAHASI and T. NAGATA, *Bull. Earthq. Res. Inst.*, **15** (1937), 441; 1047; **16** (1938), 87.

2) S. TSUBOI, *Journ. Col. Sci. Tokyo Imp. Univ.*, **53** (1920), 1.

3) H. TSUYA, "Volcano" (*Bôsai-Kagaku*) 1935, Tokyo.

dency to shallowing may be seen from a general view of the pit bottom as photographed from a position on the north-east edge of its mouth (Figs. 7, 8, 9). Thus, the bottom-floor of Mihara crater rose after August 1937, although intermittently. According to T. Minakami[4], there is a close relation between the activity of a volcano and the depth of its crater, in Mt. Asama; for example, the crater floor rises before a severe activity and falls after the eruption ends, for which reason, we may expect that Volcano Mihara has recently been getting active.

The geophysical phenomena leading to volcanicity, namely, volcanic earthquakes, volcanic microseisms, earth tilting, earth current, temperature in the fumaroles, volume of emitted gas, numbers and magnitude of rumblings, etc., have been continuously under observation for changes in them that may be related to the present activity. The results of studies of the present activity made from these standpoints will be reported by R. Takahasi in detail. To enable comparison with that in the case of the severe eruption of Miyake-sima volcano[5], we shall give here only an outline of the present activity and the results of our studies from the geomagnetic standpoint.

2. The eruption of August 19, 1940.

Volcano Mihara became active on the morning of Aug. 18. A large fissure opened in the solidified lava sheet that had formed the crater bottom, incandescent bombs being violently ejected from it to heights of more than 100 m from the bottom, along with rumblings and emission of gases, which lasted the whole of the 18th. From about 2h of Aug. 19, volcanic activities increased in violence. Numbers of incandescent bombs and lapilli were ejected accompanied with detonations and

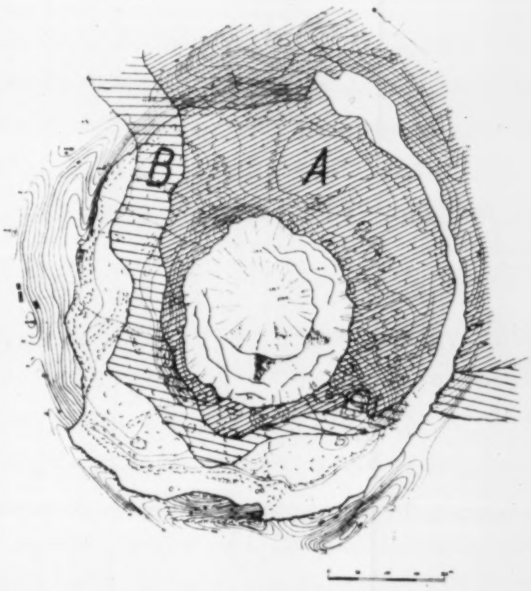

Fig. 1. Distribution of new ejecta (bombs and lapilli) from Volcano Mihara around its pit, August 19, 1940.
A. Covered with new ejecta. (See Fig. 11).
B. Bombs distributed intermittenly. (See Fig. 10).

4) T. Minakami, *Bull. Earthq. Res. Inst.*, **15** (1937), 49?.

5) H. Tsuya, T. Hagiwara, T. Minakami, T. Nagata S. Omote and R. Takahasi, *Bull. Earthq. Res. Inst* **19** (1941), 260.

rumblings, some of the lapilli reaching heights of more than 500 m from the summit of the central cone. The eruptions occurred continuously, until about 6 h of the same day. In the final stage of activity, after a lull from 6 h to 6 h 35 m, intermittent eruptions occurred at 6 h 35 m,–45 m,–55 m, and 56 m, and 7 h 04 m, two occurring at 7 h 22 m, three final eruptions at 7 h 40 m, when activities ceased.

Almost the entire bottom of the old crater was covered with newly ejected bombs and lapilli, the eastern side of the old crater especially being covered thickly with them, more than 2 m at the thickest part. The distribution of the ejecta is roughly shown in Fig. 1, from which it will be seen that the eastern side of the central cone was also covered with scoria more than 20 cm thick, these ejecta reaching distances as much as 2 km and more east of the crater. Owing to the present activity, the depth of the pit decreased to as little as 180 m from its mouth.

3. Geomagnetic variation following the eruption.

From August 20, the change in geomagnetic dip was observed by means of the dip-variometer at Gozinkatyaya, the north-western summit of the somma of this volcano. The constants and characteristics of this instrument were exactly the same as in the case of the Miyake-sima expedition. The probable error in the present observation was less than 0·2′.

Unfortunately, a typhoon which visited this island a week after observations were begun, disturbed the instrument, with the result that observations had to be suspended until September 3. The daily mean values of observed results are given in Table I and Fig. 2, in which the daily mean values of the dip at the magnetic observatory of the Mitsui Geophysical Institute, at Suzaki, Izu peninsula, are also given. By assuming that the dip-variation at Suzaki shows the general variation in geomagnetic dip in the neighbourhood of Oosima and Izu, the difference $\delta I = \Delta I_{\text{Mihara}} - \Delta I_{\text{Suzaki}}$ gives the amount of local anomalous change at our magnetic station. The values of δI are also shown in Table I and Fig. 2.

It will be seen from these results that the geomagnetic dip at our station gradually decreased about 6 minutes during the four days following the eruption of this Volcano, while that at Suzaki varied only 1·5 minutes from its largest value during the same period. The amount of change, however, is only one fifth of that observed at Miyake-sima after its great eruption. Although a change of 6 minutes in geomagnetic dip is not small compared with that which occurrs as the result

of changes in atmospheric conditions, itcan not be said that the observed anomalous changes were all due to the volcanic activity, because

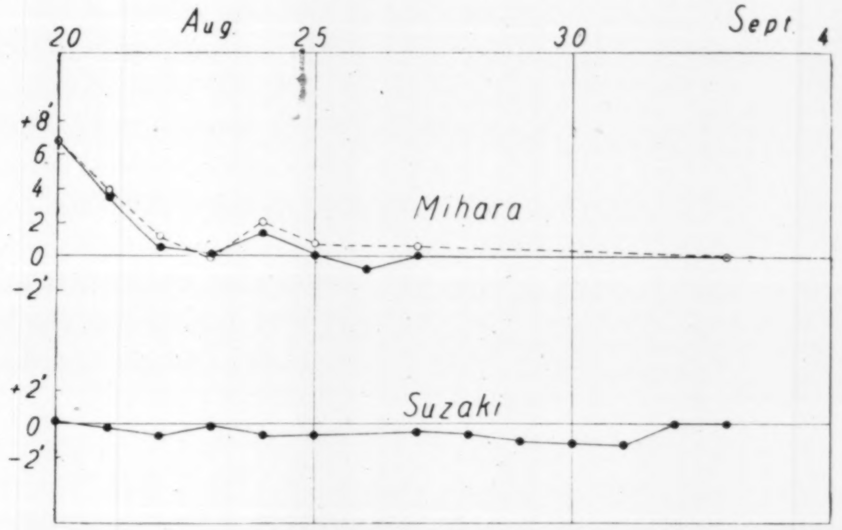

Fig. 2. Daily mean values of dip at Gozinkatyaya and Suzaki. Dotted line gives δI.

Table I. Daily Mean Values of Geomagnetic Dip at Mihara and Suzaki.

Date		ΔI_{Mihara}	ΔI_{Suzaki}	δI	Date		ΔI_{Mihara}	ΔI_{Suzaki}	δI
		min	min	min			min	min	min
Aug.	20	+6·7	+0·1	+6·6	Aug.	27	+0·2	−0·6	+0·8
	21	+3·5	−0·3	+3·8		28	—	−0·7	—
	22	+0·5	−0·7	+1·2		29	—	−1·1	—
	23	+0·2	−0·1	+0·3		30	—	−1·2	—
	24	+1 4	−0·7	+2·1		31	—	−1 3	—
	25	+0·1	−0·7	+0·8	Sept.	1	—	−0·1	—
	26	+0·7	—	—		2	0·0	0·0	0·0

there is always a difference of two or three minutes in dip in the magnetograph records obtained at two different stations, where no disturbance in the earth's crust, i. e. earthquake or volcanic activity, could be observed. Moreover, we should take into consideration that our magnetic station was situated on the summit of the somma, about 600 m above sea level, in a solitary volcanic island, while the other stations were in the open where the space gradient of geomagnetism as well as that of atmospheric electricity seem to be small. Hence, we shall not be far out in concluding that the geomagnetic field near volcano Mihara was not disturbed so much by the present volcanic activity as in the case of Miyake-sima's great eruption, and that if there were any local geo-

magnetic change, it was smaller than 6 minutes in dip at Gozinkatyaya.

4. Magnetic properties of the new ejecta.

Magnetic susceptibility, the intensity and direction of the natural remanent magnetization, and the characteristic quantities of the thermo-remanent magnetization of the newly ejected bombs from Volcano Mihara in the present activity were measured experimentally.

(i) Chemical composition.

A piece from a large bomb was chemically analyzed in Tsuya's laboratory at our Institute. The chemical and normative compositions are given in Table II, where those of the Meizi-Taisyô lava ejected at the time of the great eruption of this volcano during 1911~1914, analyzed by I. Iwasaki[6], are also given for comparison.

Table II. Chemical Composition of Rocks from Volcano Mihara.

	Bomb ejected Aug. 1940	Lava 1911~1914	Norms	Bomb ejected Aug. 1940	Lava 1911~1914
SiO_2	50·78	52·53	Q	4·63	7·87
Al_2O_3	17·05	15·25	Or	1·67	2·78
Fe_2O_3	3·65	2·69	Ab	13·35	15·73
FeO	8·76	10·57	An	35·38	31·99
MgO	4·55	4·54	Wo	7·67	7·78
CaO	11·08	10·76	En	11·34	11·34
Na_2O	2·20	1·89	Fs	12·13	16·36
K_2O	0·25	0·43	Mt	5·32	3·91
$H_2O(+)$	0·95	n d	Il	1·52	1·37
$H_2O(-)$	0·01		Ap	0·33	0·99
TiO_2	0·77	0·74			
P_2O_5	0·11	0·41			
MnO	0·21	0·24			
Total	100·39	100·16			

(ii) Magnetic susceptibility.

The magnetic susceptibility of the new ejecta was measured by the ballistic method[7] for various intensities of the applied magnetic field, from 0·6 Gauss to 19 Gauss. The specific intensity of susceptibility are given in Table III and Fig. 3. As will be seen from this result, the specific susceptibility of the newly ejected bombs is not fixed, varying

6) I. IWASAKI, *Journ. Chem. Soc. Japan*, **56** (1935), 1511.
7) T. NAGATA, *Bull. Earthq. Res. Inst.*, **18** (1940), 102.

from $0{\cdot}34\times10^{-3}$ to $1{\cdot}27\times10^{-3}$, probably the result of inequality in the structure and chemical composition of the ferromagnetic minerals in the rocks. In such basaltic rocks as the new ejecta from Mihara, the majority of the ferromagnetic minerals usually scattered in the groundmass as microcrystals, whence the magnetic susceptibility of the rock would have various values according to the fine differences in the impurities contained and the size of the microcrystals, even if the total chemical composition as a rock is almost definite. It is worth noting here, however, that the amount of $q=\chi_0/C_{M}$ of the rock specimen as chemically analyzed is 2·38—a value slightly differing from its standard value[8].

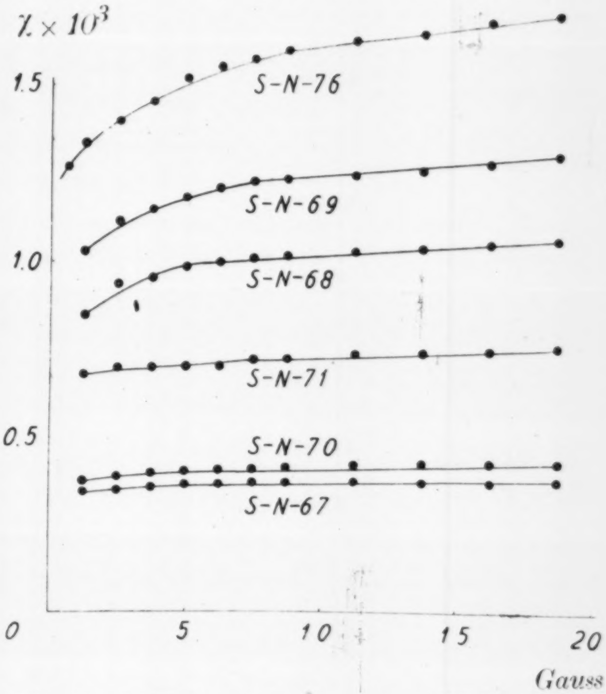

Fig. 3. Specific magnetic susceptibility of the ejecta from Mihara.

(iii) Natural remanent magnetization.

The bombs newly ejected have also intense natural remanent magnetization, exactly as those of the old ejecta from this volcano[9]. Five specimens were broken off by hammer from bombs that exceeded 50 cm in their mean diameters, and from bombs that were believed to be in the same position and direction that they occupied when they fell on the earth's surface.

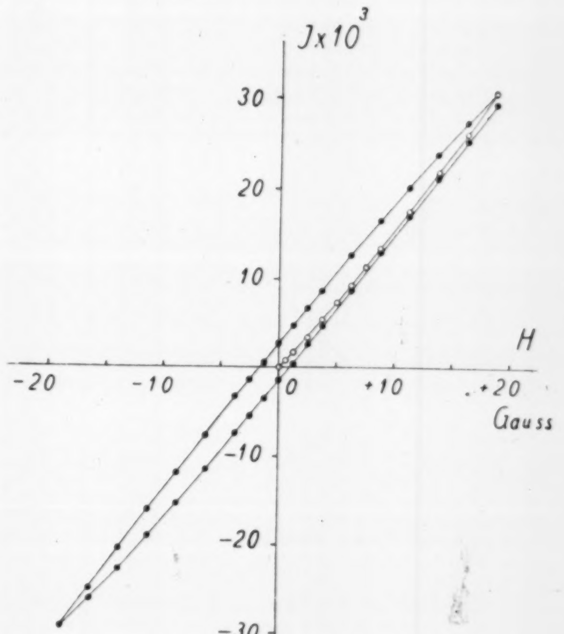

Fig. 4. Hysteresis loop in the magnetization of the new ejecta from Mihara. (Specimen No. 76.)

8) T. NAGATA, *Zisin*, **12** (1940), 111.
9) T. NAGATA, *Bull. Earthq. Res. Inst.*, **18** (1940), 281.

Table III. Magnetic Properties of New Ejecta from Volcano Mihara.

Specimen No.	χ_0	$\Delta\delta$	θ	J_{rn}	Q_n	$J_{tc}\times 0{\cdot}46$	t_0	Remark
67	$0{\cdot}34\times10^{-3}$	1°·5 W	52°·0	$1{\cdot}79\times10^{-2}$	115			
68	0·80 ″	3 ·0 W	48 ·0	1·44 ″	40	$1{\cdot}54\times10^{-2}$	410°C	
69	0·97 ″	2 ·0 E	47 ·5	1·17 ″	27			
70	0·37 ″	1 ·0 W	47 ·0	1·63 ″	99	2·23 ″	420	
71	0·68 ″	3 ·5 E	47 ·5	1·41 ″	46	2·84 ″	430	
76	1·27 ″	—	—			0·70 ″	330	Chemical Analysis

The orientation of these bombs was determined with reference to the vertical and the geomagnetic meridian at an imaginary point 100 cm distant along the normal line from the surface of the bomb at the very spots where they were found. The intensity and direction of the natural remanence of these specimens were measured by magnetometric method. The specific intensity of the natural remanence, its dip-angle, and the deviation of its horizontal component from the geomagnetic meridian, are tabulated in Table III and shown in Fig. 5, where the projection on the horizontal and N–S vertical planes are shown vectorially. The mean value of the specific intensity of these five specimens is $1{\cdot}49\times10^{-2}$, while the mean values of $\Delta\delta$ and θ are $0^\circ{\cdot}0\pm1^\circ{\cdot}2$ and $48^\circ{\cdot}4\pm 0^\circ{\cdot}9$ respectively. Exactly as in the case of bombs newly ejected from Miyake-sima[10], the new bombs from Mihara have also intense natural remanent magnetization, its direction agreeing with that of the geomagnetic field. The fact that the direction of natural remanence agrees

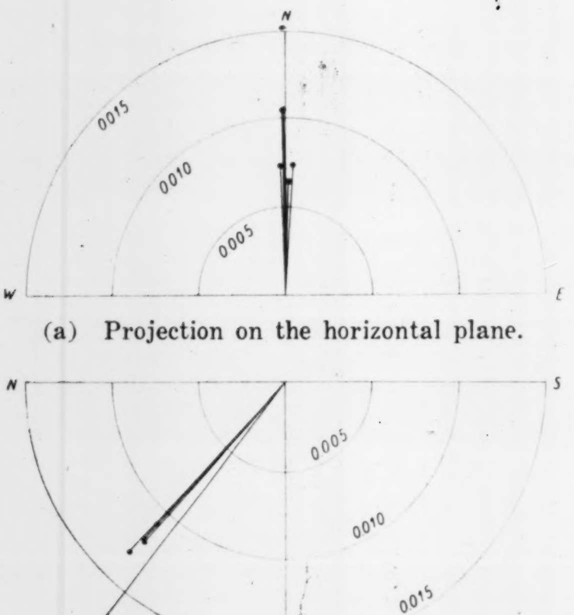

(a) Projection on the horizontal plane.

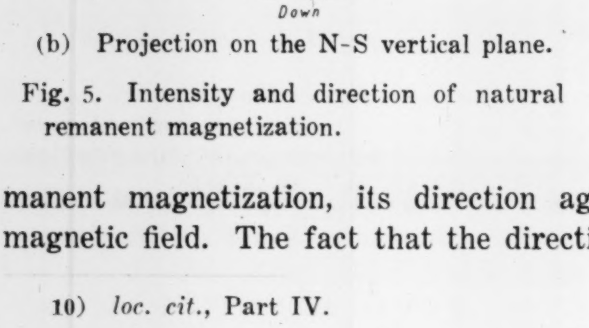

(b) Projection on the N-S vertical plane.

Fig. 5. Intensity and direction of natural remanent magnetization.

10) *loc. cit.*, Part IV.

with the geomagnetic direction shows that the bombs when they fell on the earth's surface, were at temperatures higher than the transcendental temperatures in the thermo-remanent magnetization.

(iv) Thermo-remanent magnetism.

The partial magnetization during cooling[11] of the specimens were also measured, some of the results being shown in Fig. 6.

The characteristic quantities of thermo-remanent magnetism are also given in Table III, where the t_0 of a specimen is about 300°C, while the others' are nearly 400°C. Since the amounts of $P(t_0)$ and J_{tc} are fairly large, the rock from Mihara volcano has also the potentiality of undergoing large anomalous geomagnetic changes, as in the case of the Miyake-sima eruption, provided the temperature change in the subterranean rock were fairly large, whence, it may be concluded that since the present volcanic activity was not severe, the subterranean rock was not so disturbed as to result in conspicuous changes in its magnetic intensity.

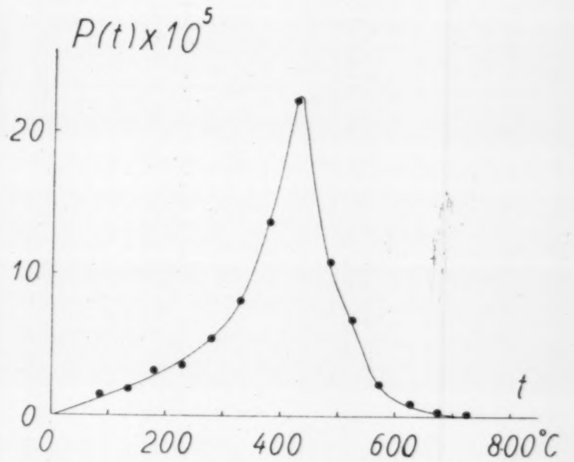

Fig. 6 a. $P(t)\sim t$ relation. (Specimen No. 70.)

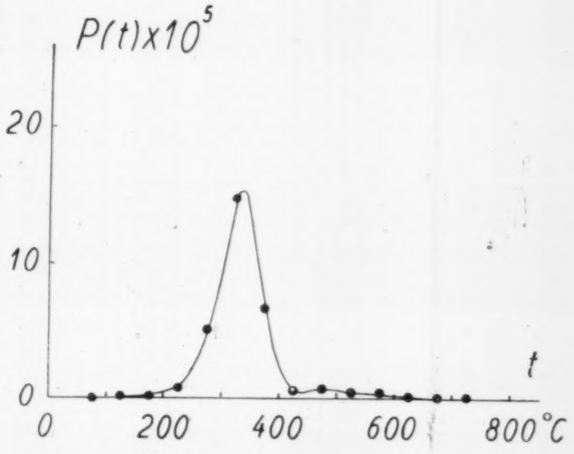

Fig. 6 b. $P(t)\sim t$ relation. (Specimen No. 76.)

5. Summary and Conclusion.

Although the rock specimens newly ejected from Volcano Mihara have fairly large magnetic intensity, nearly the same as those from Miyake-sima, the minor activity of Aug. 19, 1940, was not accompanied by any marked geomagnetic changes, the amount of the changes, after the eruption, if there were any, being smaller than 6 minutes at Gozinkatyaya. This is probably because the present minor activity affected rocks up to only

11) T. NAGATA, *Bull. Earthq. Res. Inst.*, **19** (1941), 49.

a slight area underneath this volcano. Hence, if severe activities again take place in this volcano in future, not an improbability by any means, we may expect that it will be accompanied with great disturbances in the geomagnetic field in its neighbourhood.

In conclusion, the writer wishes to express his sincere thanks to Prof. C. Tsuboi and Prof. H. Tsuya for their continued encouragement in his geomagnetic studies of the earth's crust. His hearty thanks are also due to the Hattori Hôkô Kai, with the aid of whose grant the studies of magnetic properties of the rock were made possible and to Dr. Y. Kosikawa who kindly placed the records of the magnetograph at Suzaki at the writer's disposal.

21. 昭和 15 年 8 月三原火山小活動に關する地球磁氣學的調査

地震研究所　永　田　　武

三宅島噴火開始後 38 日目に伊豆大島の三原火山が活動を開始した、噴火の規模としては明治—大正噴火以後に於いて最大のものであつたが、活動は 8 月 19 日 2 時頃から始まり、7 時には終熄してしまつたので，無數の火山彈，火山礫を抛出したに止り，熔岩は流出しなかつた、三宅島に於けると同樣な地球磁氣觀測を行ひ，且つ新噴出物の磁氣的諸性質を調べた、地球磁場はこの活動では著しい擾亂を生ぜず，若し生じたとしても，三原外輪山御神火茶屋附近の伏角に於いて 6′ 以内である、帶磁率，自然殘留磁氣，及び熱殘留磁氣の諸特性を測定した結果，新噴出岩は三宅島新噴出岩と同樣に著しい磁性を有してゐる事が分つた、從つて今後若し三原火山に大規模な火山活動が起れば，顯著な地球磁場擾亂の生ずる事が豫想される譯である、

この調査費の一部は服部報公會の援助による、記して同會に對し感謝の意を表す、

Fig. 7. Crater bottom of Volcano Mihara. (Aug. 11, 1938.)
(The incandescent lava pool is seen through the emitted gases.)

Fig. 8. Crater bottom of Volcano Mihara.
(Sept. 3, 1939.)

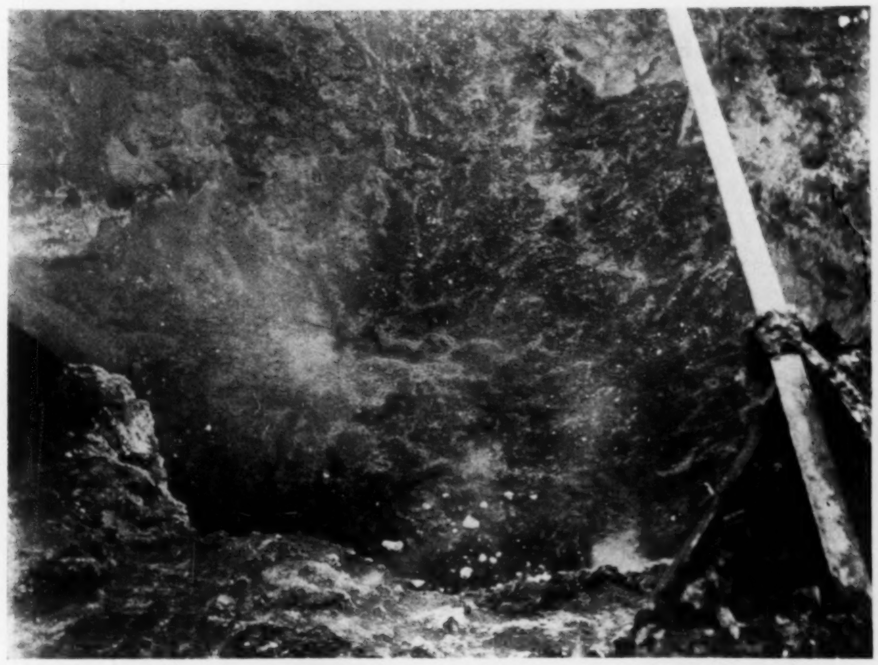

Fig. 9 a. Crater bottom of Volcano Mihara. (Aug. 20, 1940.)

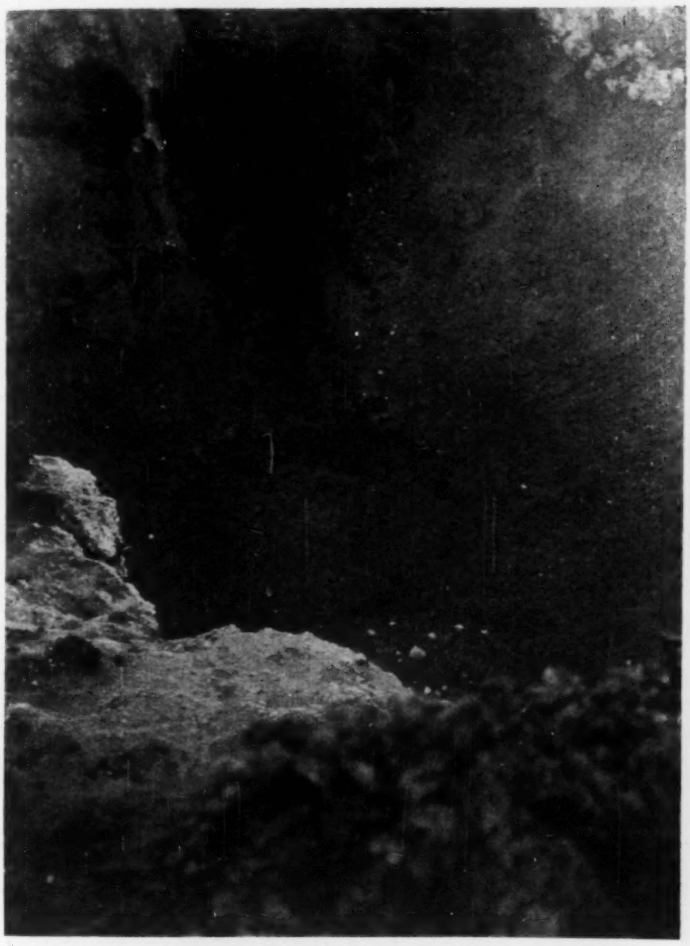

Fig. 9 b. Crater bottom of Volcano Mihara.
(Aug. 19, 1940.)

Fig. 10. Bomb newly ejected from Volcano Mihara. (Aug. 19, 1940.)

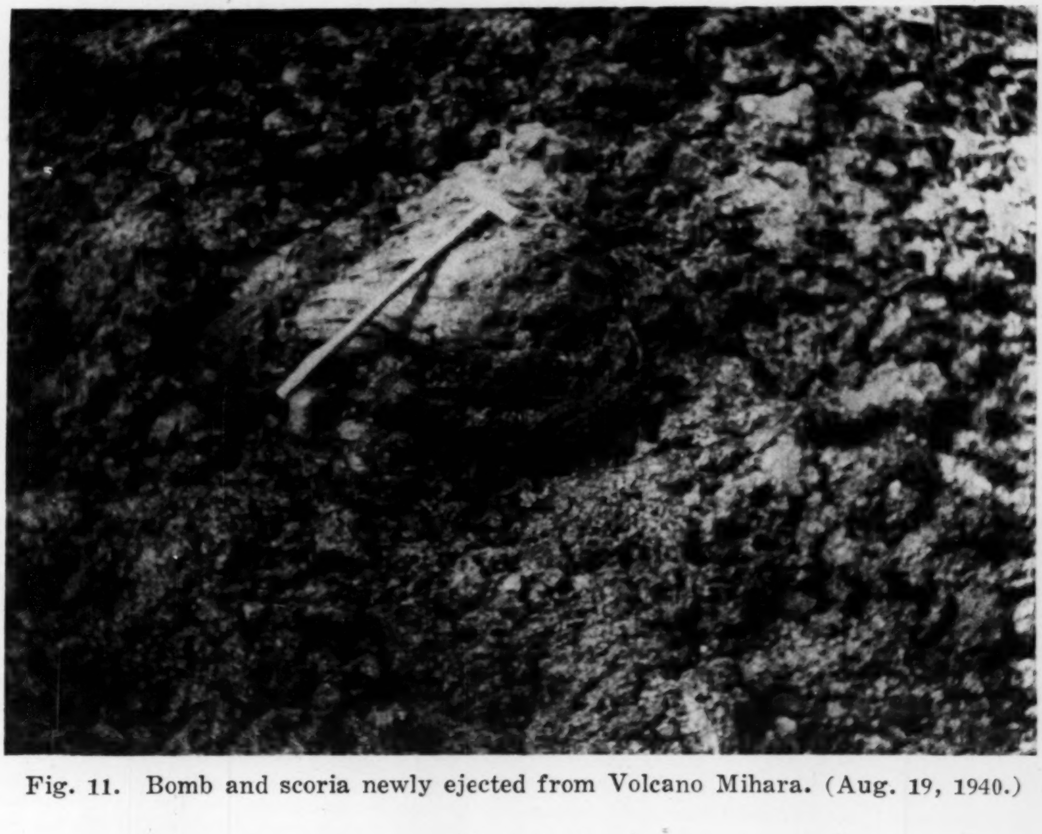

Fig. 11. Bomb and scoria newly ejected from Volcano Mihara. (Aug. 19, 1940.)

22. *Über die empirische Formel von Ishimoto und Iida $na^m = k$ zwischen der Bebenhäufigkeit n und der Amplitude a.*[1]

Von Takeo MATUZAWA,

Institut für Erdbebenforschung.

(Vorgelegt 20. März 1941.—Eingegangen 20. März 1941.)

Aus der Bebenbeobachtung für eine bestimmte Zeitdauer an einer betimmten Station z. B. Hongô oder Mitakamura, haben Ishimoto und Iida[2] eine empirische Formel zwischen der Bebenhäufigkeit und der Amplitude abgeleitet. Sie lautet nämlich

$$n(a)a^m = k, \tag{1}$$

wo a die beobachtete Maximal-Amplitude eines Erdbebens ist, und $n(a)\delta a$ die beobachtete Bebenzahl bedeutet, die zwischen a und $a+\delta a$ liegt.

In der Formel ist δa zu Einheit genommen. Daraus haben sie geschlossen, daß je kleiner das Erdbeben ist, desto häufiger kommt es vor. Hi r wird die Sache etwas näher betrachtet.

Es sei $f(A)$ die Verteilungsfunktion der Erdbeben in dem betrachteten Erdbebengebiet. Dann ist die Bebenzahl in dem Volumen-Element dV, dessen Maximal-Amplitude zwischen A und $A+\delta A$ liegt, wie folgt

$$Nf(A)\delta A dV, \tag{2}$$

wo N die Bebenzahl in der Volumeneinheit ist.

Die Amplitude A unterliegt gewißer Veränderung bei der Fortpflanzung von der Strecke r. Vorläufig wird vorausgesetzt

$$\left.\begin{aligned} a &= k^\lambda \frac{A}{r^\lambda}, \quad r \geq k, \\ a &= A, \quad 0 < r \leq k. \end{aligned}\right\} \tag{3}$$

Unter dieser Voraussetzung lautet die an einer Station beobachtete

1) Diese kleine Mitteilung ist dem seligen Herrn Prof. Dr. M. ISHIMOTO gewidmet.

2) M. ISHIMOTO et K. IIDA, *Bull. Earthq. Res. Inst.*, **17** (1939) 443~478; K. IIDA, ditto **18** (1940) 532~574; 575~674.

Bebenzahl, dessen Amplitude zwischen a und $a+\delta a$ liegt,

$$n(a)\delta a=\int^{V} Nf(A)\delta A dV. \tag{4}$$

Aus (3)

$$\delta A=\frac{r^{\lambda}}{k^{\lambda}}\delta a. \tag{5}$$

Also

$$n(a)=\int^{V} Nf(A)\frac{r^{\lambda}}{k^{\lambda}}dV. \tag{6}$$

Im Falle N und k überall konstant sind, ergibt sich in bezug auf die Polar-Koordinaten

$$n(a)=\frac{N}{k^{\lambda}}\int f\left(a\frac{r^{\lambda}}{k^{\lambda}}\right)r^{\lambda+2}dr\sin\theta\, d\theta\, d\varphi.$$

Durch die Transformation $y=a\frac{r^{\lambda}}{k^{\lambda}}$ bekommt man

$$n(a)=\frac{N}{\lambda}\frac{k^{3}}{a^{\frac{\lambda+3}{\lambda}}}\int f(y)y^{\frac{3}{\lambda}}dy\sin\theta\, d\theta\, d\varphi.$$

Wenn die Verteilungsfunktion überall zwischen r_1 und r_2 von der Station dasselbe ist, dann lautet

$$n(a)=2\pi\frac{N}{\lambda}\frac{k^{3}}{a^{\frac{\lambda+3}{\lambda}}}\int_{a\frac{r_1^{\lambda}}{k^{\lambda}}}^{a\frac{r_2^{\lambda}}{k^{\lambda}}} f(y)y^{\frac{3}{\lambda}}dy. \tag{7}$$

Im folgenden werden einige Sonderfälle betrachtet.

(i) Alle Beben haben dieselbe Maximal-Amplitude, nämlich

$$f(A)=\infty, \quad A=A_0,$$

$$f(A)=0, \quad A\neq A_0,$$

$$\lim_{\varepsilon\to 0}\int_{A_0-\varepsilon}^{A_0+\varepsilon} f(A)dA=1,$$

was formal ähnlich der δ-Funktion von Dirac[3] ist.

3) P. A. M. DIRAC, The Principles of Quantum Mechanics (1930) 63.

Aus (7) folgt

$$n(a) = 2\pi \frac{N}{\lambda} \frac{k^3}{a^{\frac{\lambda+3}{\lambda}}} A_0^{\frac{3}{\lambda}}.$$

Diese Gleichung ist formal gleich der Ishimoto-Iida'schen Formel, aber der Exponent von a hängt nur von λ ab. Diese Formel wird natürlich direkt abgeleitet wie folgt.

Aus (3)

$$a = k^\lambda \frac{A_0}{r^\lambda}, \quad \delta a = k^\lambda \lambda \frac{A_0}{r^{\lambda+1}} \delta r \ .$$

Also

$$n(a)\delta a = \int N r^2 dr \sin\theta \, d\theta \, d\varphi.$$

Nämlich

$$n(a) = 2\pi \frac{N}{\lambda} \frac{k^3 A_0^{\frac{3}{\lambda}}}{a^{\frac{\lambda+3}{\lambda}}}.$$

(ii) Keine Änderung der Amplitude bei der Fortpflanzung.

Durch die folgende Grenzübergang aus (7),

$$\lim_{\lambda \to 0} \frac{1}{\lambda a^{\frac{\lambda+3}{\lambda}}} \int_{a\left(\frac{r_1}{k}\right)^\lambda}^{a\left(\frac{r_2}{k}\right)^\lambda} f(y) y^{\frac{3}{\lambda}} dy,$$

bekommt man gleich

$$n(a) = \frac{2\pi}{3} N f(a) (r_2^3 - r_1^3).$$

Man kann diese Formel auch direkt ableiten wie folgt. Aus (3)

$$a = A, \quad \delta a = \delta A.$$

Darum bekommt man ohne weiteres

$$n(a) = \frac{2\pi}{3} N f(a) (r_2^3 - r_1^3).$$

In diesem Falle hat die Verteilungsfunktion $f(A)$ die gleiche Form wie $n(a)$ in Bezug auf A, was natürlich selbstklar ist.

Nun wollen wir wieder etwas allgemeiner betrachten. Aus (7) bekommt man

$$n(a)a^{\frac{\lambda+3}{\lambda}}=C\int_{ap_1}^{ap_2} f(y)y^{\frac{3}{\lambda}}dy, \tag{8}$$

wo

$$C=2\pi\frac{N}{\lambda}k^3,\quad p_1=\left(\frac{r_1}{k}\right)^{\lambda},\quad p_2=\left(\frac{r_1}{k}\right)^{\lambda}\quad \text{ist.}$$

Durch Differentiation von (8) nach a, ergibt sich

$$\frac{\lambda+3}{\lambda}n(a)+a\frac{dn(a)}{da}=2\pi\frac{N}{\lambda k^{\lambda}}\left\{r_2^{3+\lambda}f(ap_2)-r_1^{3+\lambda}f(ap_1)\right\}.$$

Wenn $n(a)=\dfrac{k}{a^{m}}$ ist dann .

$$\left(1+\frac{3}{\lambda}-m\right)\frac{K}{a^{m}}=2\pi\frac{N}{\lambda k^{\lambda}}\left\{r_2^{3+\lambda}f(ap_2)-r_1^{3+\lambda}f(ap_1)\right\}.$$

Als eine Lösung von $f(A)$, die dieser Gleichung genügt, kann man setzen

$$f(A)=\frac{Q}{A^{m}},$$

wo

$$Q=\frac{\lambda\left(1+\frac{3}{\lambda}-m\right)K}{2\pi Nk^{-\lambda+\lambda m}\left(r_2^{3-\lambda m+\lambda}-r_1^{3-\lambda m+\lambda}\right)}.$$

Q muss natürlich positiv sein, darum $\lambda\geq 0$.

Diese Lösung gilt natürlich, wenn die Erdbeben nur in einem beschränkten Raum außer Beobachtungsstation vorkommen und zwar die Verteilungsfunktion in dem betrachteten Bereich keine Unstetigkeit besitzt.

Streng genommen, kann man die Verteilungsfunktion $f(A)$ genau bestimmen, nur wenn man die Erdbeben aus ganz beschränktem Erdteil betrachtet.

22. *Zisin no Hindo to Sinpuku ni kwansuru Ishimoto-Iida no Zikken-siki* $na^m = k$ *ni tuite.*

Zisin Kenkyūsyo.

Matuzawa-TAKEO.

Aru hitotuno Kwansokuten (Hongô matawa Mitaka-mura) de aru Kikan tiisai Zisin wo kwansokusita toki ni, Zisin no Saidai-Sinpuku ga a to $a+\delta a$ tono Aida ni atta Zisin no Kazu wo $n(a)\delta a$ to suru toki

$$n(a)a^m = k,$$

to naru to iu noga Ishimoto-Iida no Kekka de ari, kore ni yotte tiisai Zisin hodo okoru Kazu ga ôi to iu Keturon wo dasite iru.

Koko dewa aru hitotu no Basyo de Sinpuku A to $A+\delta A$ tono Aida ni aru Zisin no okoru Bunpu-Kansû wo $f(A)$ to si, mata tutawaru Totyû de Sinpuku ga kawaru to site ue no Zikken-Siki wo sirabeta.

Atarimaeno koto dewa aruga kagirareta Han'i no Zisin ni Me wo tukereba $f(A)$ wa $n(a)$ to onazi Katati ni naruga, sô de nai Baai ya $f(A)$ no tokubetu na Baai niwa itumo sô naru towa iwarenai.

23. *Transmission of Arbitrary Elastic Waves from a Spherical Source, Solved with Operational Calculus. II.*

By Katsutada SEZAWA and Kiyoshi KANAI,

Earthquake Research Institute.

(Read June 19, 1941.—Received June 20, 1941.)

1. *Introduction.*

In the previous paper,[1] using operational calculus, the problem of transmission of arbitrary elastic waves generated from a spherical source, oscillating spheroidally, was solved. Since, however, the case discussed in that paper was restricted to the spheroidal vibration of order $n=0$, the feature of separation of distortional waves and dilatational waves, both generated from the spherical source, was not ascertained. In the present investigation, the case of spheroidal vibration of order $n=2$, particularly, is treated although the calculation is fairly complex. It will be shown that the dilatational waves and the distortional waves respectively consist of free waves and forced waves. Although, to a certain extent, the type of forced waves in each case agrees with the form of the exciting forces, that of free waves, particularly in vibrational period and damping, depends on the size of the spherical source. As a matter of fact, the vibrational period and damping in question have not yet been precisely ascertained. In the present investigation, these quantities are determined fairly accurately, say, to four decimal places. As to the type of exciting force, two cases, namely, that of rectangular type and that of sine type, both beginning from a quiescent state, will be treated in the present paper.

2. *General equations.*

The integral expressions of displacements of the waves for any n were given in equations (3), (6) in the previous paper. Rewriting these expressions, we get

1) K. SEZAWA and K. KANAI, "Transmission of Arbitrary Elastic Waves from a Spherical Source, Solved with Operational Calculus. I," *Bull. Earthq. Res. Inst.*, **18** (1941), 151~161.

$$\left.\begin{aligned} \Delta &= \frac{1}{2\pi i}\int_{c-i\infty}^{c+i\infty}\frac{e^{zt}dz}{z}\,\frac{A_n H^{(1)}_{n+1/2}(izrc_1)}{\sqrt{r}}P_n(\cos\theta), \\ 2\varpi &= \frac{1}{2\pi i}\int_{c-i\infty}^{c+i\infty}\frac{e^{zt}dz}{z}\,\frac{B_n H^{(1)}_{n+1/2}(izrc_2)}{\sqrt{r}}\,\frac{dP_n(\cos\theta)}{d\theta}, \end{aligned}\right\} \qquad (1)$$

$$\left.\begin{aligned} u_1 &= \frac{1}{2\pi i}\int_{c-i\infty}^{c+i\infty}\frac{e^{zt}dz}{z}\,\frac{A_n}{z^2c_1^2}\,\frac{d}{dr}\left\{\frac{H^{(1)}_{n+1/2}(izrc_1)}{\sqrt{r}}\right\}P_n(\cos\theta), \\ v_1 &= \frac{1}{2\pi i}\int_{c-i\infty}^{c+i\infty}\frac{e^{zt}dz}{z}\,\frac{A_n}{z^2c_1^2}\,\frac{H^{(1)}_{n+1/2}(izrc_1)}{r^{3/2}}\,\frac{dP_n(\cos\theta)}{d\theta}, \\ u_2 &= \frac{1}{2\pi i}\int_{c-i\infty}^{c+i\infty}\frac{e^{zt}dz}{z}\,\frac{n(n+1)B_n}{z^2c_2^2}\,\frac{H^{(1)}_{n+1/2}(izrc_2)}{r^{3/2}}P_n(\cos\theta), \\ v_2 &= \frac{1}{2\pi i}\int_{c-i\infty}^{c+i\infty}\frac{e^{zt}dz}{z}\,\frac{B_n}{z^2c_2^2}\,\frac{1}{r}\,\frac{d}{dr}\left\{\sqrt{r}\,H^{(1)}_{n+1/2}(izrc_2)\right\}\frac{dP_n(\cos\theta)}{d\theta}. \end{aligned}\right\} \qquad (2)$$

Using the same conditions at the spherical boundary as in the previous paper, we get

$$\widehat{r\theta} = \mu\left\{\frac{\partial(v_1+v_2)}{\partial r} - \frac{(v_1+v_2)}{r} + \frac{1}{r}\,\frac{\partial(u_1+u_2)}{\partial\theta}\right\} = 0, \qquad (3)$$

$$\widehat{rr} = \lambda\Delta + 2\mu\frac{\partial(u_1+u_2)}{\partial r} = f(t)P_n(\cos\theta). \qquad (4)$$

Since the function $f(t)$ is expressible in the form

$$f(t) = \frac{1}{2\pi i}\int_{c-i\infty}^{c+i\infty}\frac{e^{zt}}{z}g(z)dz \qquad \Big[R(t)>0\Big] \qquad (5)$$

when

$$g(z) = z\int_0^\infty e^{-zt}f(t)dt, \qquad (6)$$

it is now possible to write

$$\left\{\lambda\Delta + 2\mu\frac{\partial(u_1+u_2)}{\partial r}\right\}_{r=a} = \frac{P_n(\cos\theta)}{2\pi i}\int_{c-i\infty}^{c+i\infty}\frac{e^{zt}}{z}g(z)dz. \qquad (7)$$

Substituting (1), (2) in (3), (7), we get

$$B_n = \frac{2c_2^2}{c_1^2}\,\frac{Q}{S}A_n, \qquad (8)$$

$$(\widehat{rr}_{r=a}=)\ \frac{P_n(\cos\theta)}{2\pi i}\int_{c-i\infty}^{c+i\infty}\frac{e^{zt}A_n\Omega}{z}dz=\frac{P_n(\cos\theta)}{2\pi i}\int_{c-i\infty}^{c+i\infty}\frac{e^{zt}g(z)}{z}dz, \qquad (9)$$

where

$$\left.\begin{aligned}
\Omega&=\frac{2\mu}{Sz^2c_1^2a^{5/2}}\left\{RS+2n(n+1)PQ\right\},\\
R&=\left\{(\lambda/2\mu)(zac_1)^2+n(n-1)\right\}H^{(1)}_{n+1/2}(izac_1)\\
&\quad-izac_1(2n+1)H^{(1)}_{n+3/2}(izac_1)-(zac_1)^2H^{(1)}_{n+5/2}(izac_1),\\
S&=-2(n^2-1)H^{(1)}_{n+1/2}(izac_2)\\
&\quad+izac_2(2n+1)H^{(1)}_{n+3/2}(izac_2)+(zac_2)^2H^{(1)}_{n+5/2}(izac_2),\\
P&=(n-1)H^{(1)}_{n+1/2}(izac_2)-izac_2H^{(1)}_{n+3/2}(izac_2),\\
Q&=(n-1)H^{(1)}_{n+1/2}(izac_1)-izac_1H^{(1)}_{n+3/2}(izac_1).
\end{aligned}\right\} \qquad (10)$$

From (9) it is possible to write

$$A_n=\frac{g(z)}{\Omega}. \qquad (11)$$

Substituting (11) in (1), we get

$$\Delta=\frac{1}{2\pi i}\int_{c-i\infty}^{c+i\infty}\frac{e^{zt}g(z)}{z\Omega}\frac{H^{(1)}_{n+1/2}(izrc_1)}{\sqrt{r}}P_n(\cos\theta)dz. \qquad (12)$$

Thus Δ corresponds to the interpretation of

$$\frac{g(z)}{\Omega}\frac{H^{(1)}_{n+1/2}(izrc_1)}{\sqrt{r}}P_n(\cos\theta). \qquad (13)$$

3. *The expressions for $n=2$, $\lambda=\mu$.*

When $n=2$ and also $\lambda=\mu$; Ω, A_2, B_2, in (10), (11), (8) reduce to

$$\left.\begin{aligned}
\Omega&=\frac{i\mu e^{-zac_1}\sqrt{2/i\pi zac_1}\,\Omega_0}{z^2c_1^2a^{5/2}S_0},\\
A_2&=\frac{g(z)z^2c_1^2a^{5/2}S_0}{i\mu e^{-zac_1}\sqrt{2/i\pi zac_1}\,\Omega_0},\quad B_2=\frac{2g(z)z^2c_2^2a^{5/2}Q_0}{\sqrt{3}\,i\mu e^{-zac_2}\sqrt{2/i\pi zac_2}\,\Omega_0},
\end{aligned}\right\} \qquad (14)$$

where

$$\left.\begin{aligned}
S_0 &= (zac_2)^4+5(zac_2)^3+21(zac_2)^2+48(zac_2)+48, \\
Q_0 &= (zac_2)^3+5\sqrt{3}\,(zac_2)^2+36(zac_2)+36\sqrt{3}, \\
\Omega_0 &= (zac_2)^6+(5+13/\sqrt{3})(zac_2)^5+(58+41/\sqrt{3})(zac_2)^4 \\
&\quad +(113+123\sqrt{3})(zac_2)^3+(441+184\sqrt{3})(zac_2)^2 \\
&\quad +(552+184\sqrt{3})(zac_2)+552 \\
&\equiv \left\{zac_2+(p_1-iq_1)\right\}\left\{zac_2+(p_1+iq_1)\right\}\left\{zac_2+(p_2-iq_2)\right\} \\
&\quad \cdot\left\{zac_2+(p_2+iq_2)\right\}\left\{zac_2+(p_3-iq_3)\right\}\left\{zac_2+(p_3+iq_3)\right\}.
\end{aligned}\right\} \quad (15)$$

The roots of Ω_0, namely, $zac_2=-(p_1-iq_1)$, ..., $zac_3=-(p_3+iq_3)$, are calculated by the method of trial and error, the results of which are

$$\left.\begin{aligned}
p_1&=0{\cdot}8033, & q_1&=1{\cdot}0406, & p_2&=1{\cdot}8015, \\
q_2&=4{\cdot}1852, & p_3&=3{\cdot}648, & q_3&=1{\cdot}4410.
\end{aligned}\right\} \quad (16)$$

p_1/ac_2, p_2/ac_2, p_3/ac_2 are vibrational frequencies of the spherical source in the elastic medium and q_1/ac_2, q_2/ac_2, q_3/ac_2 the damping coefficients of vibrations of the same source.

In the present case, on the other hand, the expressions for displacements of the elastic medium become of the types

$$\left.\begin{aligned}
u_1 &= \frac{-a^3P_2(\cos\theta)}{\sqrt{3}\,\mu c_2^2 r^4 2\pi i}\int_{c-i\infty}^{c+i\infty}\frac{g(z)e^{z\{t-c_1(r-a)\}}F_1(z)\,dz}{z^3\Omega_0}, \\
u_2 &= \frac{4\sqrt{3}\,a^3P_2(\cos\theta)}{\mu c_2^2 r^4 2\pi i}\int_{c-i\infty}^{c+i\infty}\frac{g(z)e^{z\{t-c_2(r-a)\}}F_2(z)\,dz}{z^3\Omega_0}, \\
v_1 &= \frac{a^3}{\mu c_2^2 r^4 2\pi i}\frac{dP_2(\cos\theta)}{d\theta}\int_{c-i\infty}^{c+i\infty}\frac{g(z)e^{z\{t-c_1(r-a)\}}G_1(z)\,dz}{z^3\Omega_0}, \\
v_2 &= \frac{-2a^3}{\sqrt{3}\,\mu c_2^2 r^4 2\pi i}\frac{dP_2(\cos\theta)}{d\theta}\int_{c-i\infty}^{c+i\infty}\frac{g(z)e^{z\{t-c_2(r-a)\}}G_2(z)\,dz}{z^3\Omega_0},
\end{aligned}\right\} \quad (17)$$

where

$$\left.\begin{aligned}
F_1(z)&=\left\{(zac_2)^4+5(zac_2)^3+21(zac_2)^2+48(zac_2)+48\right\}\\
&\qquad\cdot\left\{(zrc_2)^3+4\sqrt{3}\,(zrc_2)^2+27(zrc_2)+27\sqrt{3}\right\},\\
F_2(z)&=\left\{(zac_2)^3+5\sqrt{3}\,(zac_2)^2+36(zac_2)+36\sqrt{3}\right\}\\
&\qquad\cdot\left\{(zrc_2)^2+3(zrc_2)+3\right\},\\
G_1(z)&=\left\{(zac_2)^4+5(zac_2)^3+21(zac_2)^2+48(zac_2)+48\right\}\\
&\qquad\cdot\left\{(zrc_2)^2+3\sqrt{3}\,(zrc_2)+9\right\},\\
G_2(z)&=\left\{(zac_2)^3+5\sqrt{3}\,(zac_2)^2+36(zac_2)+36\sqrt{3}\right\}\\
&\qquad\cdot\left\{(zrc_2)^3+3(zrc_2)^2+6(zrc_2)+6\right\}.
\end{aligned}\right\}\quad(18)$$

Substituting the form of $g(z)$, corresponding to a given $f(t)$, it is possible to evaluate the integrals in (17).

4. *The special case,* $n=2$; $f(t)=p_0$ *for* $t>0$ and $f(t)=0$ *for* $t<0$.

In this case, $g(z)=p_0$ for $t>0$, $g(z)=0$ for $t<0$. Thus from (17) we get

$$\left.\begin{aligned}
u_1&=\frac{-p_0a^3P_2(\cos\theta)}{\sqrt{3}\,\mu c_2^2r^4 2\pi i}\int_{c-i\infty}^{c+i\infty}\frac{e^{z\{t-c_1(r-a)\}}F_1(z)\,dz}{z^3\Omega_0},\\
u_2&=\frac{4\sqrt{3}\,p_0a^3P_2(\cos\theta)}{\mu c_2^2r^4 2\pi i}\int_{c-i\infty}^{c+i\infty}\frac{e^{z\{t-c_2(r-a)\}}F_2(z)\,dz}{z^3\Omega_0},\\
v_1&=\frac{p_0a^3}{\mu c_2^2r^4 2\pi i}\,\frac{dP_2(\cos\theta)}{d\theta}\int_{c-i\infty}^{c+i\infty}\frac{e^{z\{t-c_1(r-a)\}}G_1(z)\,dz}{z^3\Omega_0},\\
v_2&=\frac{-2p_0a^3}{\sqrt{3}\,\mu c_2^2r^4 2\pi i}\,\frac{dP_2(\cos\theta)}{d\theta}\int_{c-i\infty}^{c+i\infty}\frac{e^{z\{t-c_2(r-a)\}}G_2(z)\,dz}{z^3\Omega_0}.
\end{aligned}\right\}\quad(19)$$

The contour integrals will be evaluated as in Bromwich-Wagner's integral. The contributions from the poles for $\Omega_0=0$ represent that part which corresponds to free waves, while those from the remaining poles give the part that corresponds to forced waves.

Let u_{01}, u_{02}, v_{01}, v_{02} be the parts of u_1, u_2, v_1, v_2 that correspond

to forced waves and u_{f1}, u_{f2}, v_{f1}, v_{f2} the parts of u_1, u_2, v_1, v_2 that correspond to free waves, so that

$$u_{01}+u_{f1}=u_1,\quad u_{02}+u_{f2}=u_2,\quad v_{01}+v_{f1}=v_1,\quad v_{02}+v_{f2}=v_2. \tag{20}$$

The integration of (19) gives

$$\left.\begin{aligned}
u_{01}\Big/\frac{ap_0}{\mu}P_2(\cos\theta) &= \frac{-1}{184}\left(\frac{a}{r}\right)^4\Bigg[\left\{64\left(\frac{r}{a}\right)^2-144\left(\frac{r}{a}\right)\ \frac{279}{23}\right\} \\
&\quad +144\sqrt{3}\left(\frac{r}{a}-1\right)\left\{\frac{t-c_1(r-a)}{ac_2}\right\}+216\left\{\frac{t-c_1(r-a)}{ac_2}\right\}^2\Bigg], \\
&\qquad\qquad \Big[\{t-c_1(r-a)\}>0\Big] \\
&=0, \qquad \Big[\{t-c_1(r-a)\}<0\Big] \\
u_{02}\Big/\frac{ap_0}{\mu}P_2(\cos\theta) &= \frac{3}{46}\left(\frac{a}{r}\right)^4\Bigg[\left\{12\left(\frac{r}{a}\right)^2-36\left(\frac{r}{a}\right)+\frac{563}{46}\right\} \\
&\quad +36\left(\frac{r}{a}-1\right)\left\{\frac{t-c_2(r-a)}{ac_2}\right\}+18\left\{\frac{t-c_2(r-a)}{ac_2}\right\}^2\Bigg], \\
&\qquad\qquad \Big[\{t-c_2(r-a)\}>0\Big] \\
&=0, \qquad \Big[\{t-c_2(r-a)\}<0\Big] \\
v_{01}\Big/\frac{ap_0}{\mu}\frac{dP_2(\cos\theta)}{d\theta} &= \frac{1}{184}\left(\frac{a}{r}\right)^4\Bigg[\left\{16\left(\frac{r}{a}\right)^2-48\left(\frac{r}{a}\right)-\frac{93}{23}\right\} \\
&\quad +48\sqrt{3}\left(\frac{r}{a}-1\right)\left\{\frac{t-c_1(r-a)}{ac_2}\right\}+72\left\{\frac{t-c_1(r-a)}{ac_2}\right\}^2\Bigg], \\
&\qquad\qquad \Big[\{t-c_1(r-a)\}>0\Big] \\
&=0, \qquad \Big[\{t-c_1(r-a)\}<0\Big] \\
v_{02}\Big/\frac{ap_0}{\mu}\frac{dP_2(\cos\theta)}{d\theta} &= \frac{-1}{46}\left(\frac{a}{r}\right)^4\Bigg[\left\{18\left(\frac{r}{a}\right)^2-36\left(\frac{r}{a}\right)+\frac{563}{46}\right\} \\
&\quad +36\left(\frac{r}{a}-1\right)\left\{\frac{t-c_2(r-a)}{ac_2}\right\}+18\left\{\frac{t-c_2(r-a)}{ac_2}\right\}^2\Bigg], \\
&\qquad\qquad \Big[\{t-c_2(r-a)\}>0\Big] \\
&=0, \qquad \Big[\{t-c_2(r-a)\}<0\Big]
\end{aligned}\right\} \tag{21}$$

$$
\left.
\begin{aligned}
& u_{f1}\Big/\frac{ap_0}{\mu}P_2(\cos\theta)=\frac{-(a/r)^4}{\sqrt{3}}\sum_{s=1}^{3}\frac{1}{q_s}e^{-\{t-c_1(r-a)\}p_s/ac_2} \\
& \cdot\sqrt{\frac{Y_{s1}}{(A_{s1}^2+A_{s2}^2)\Gamma_s}}\sin\Big[\{t-c_1(r-a)\}q_s/ac_2+\eta_{s1}-\tan^{-1}(A_{s2}/A_{s1})-\gamma_s\Big], \\
& \qquad\qquad\qquad\qquad\qquad \Big[\{t-c_1(r-a)\}>0\Big] \\
& \qquad\qquad =0, \qquad\qquad\qquad \Big[\{t-c_1(r-a)\}<0\Big] \\
& u_{f2}\Big/\frac{ap_0}{\mu}P_2(\cos\theta)=4\sqrt{3}\,(a/r)^4\sum_{s=1}^{3}e^{-\{t-c_2(r-a)\}p_s/ac_2} \\
& \cdot\sqrt{\frac{Y_{s2}}{(A_{s1}^2+A_{s2}^2)\Gamma_s}}\sin\Big[\{t-c_2(r-a)\}q_s/ac_2+\eta_{s2}-\tan^{-1}(A_{s2}/A_{s1})-\gamma_s\Big], \\
& \qquad\qquad\qquad\qquad\qquad \Big[\{t-c_2(r-a)\}>0\Big] \\
& \qquad\qquad =0, \qquad\qquad\qquad \Big[\{t-c_2(r-a)\}<0\Big] \\
& v_{f1}\Big/\frac{ap_0}{\mu}\frac{dP_2(\cos\theta)}{d\theta}=(a/r)^4\sum_{s=1}^{3}\frac{1}{q_s}e^{-\{t-c_1(r-a)\}p_s/ac_2} \\
& \cdot\sqrt{\frac{Z_{s1}}{(A_{s1}^2+A_{s2}^2)\Gamma_s}}\sin\Big[\{t-c_1(r-a)\}q_s/ac_2+\zeta_{s1}-\tan^{-1}(A_{s2}/A_{s1})-\gamma_s\Big], \\
& \qquad\qquad\qquad\qquad\qquad \Big[\{t-c_1(r-a)\}>0\Big] \\
& \qquad\qquad =0, \qquad\qquad\qquad \Big[\{t-c_1(r-a)\}<0\Big] \\
& v_{f2}\Big/\frac{ap_0}{\mu}\frac{dP_2(\cos\theta)}{d\theta}=\frac{-2(a/r)^4}{\sqrt{3}}\sum_{s=1}^{3}\frac{1}{q_s}e^{-\{t-c_2(r-a)\}p_s/ac_2} \\
& \cdot\sqrt{\frac{Z_{s2}}{(A_{s1}^2+A_{s2}^2)\Gamma_s}}\sin\Big[\{t-c_2(r-a)\}q_s/ac_2+\zeta_{s2}-\tan^{-1}(A_{s2}/A_{s1})-\gamma_s\Big], \\
& \qquad\qquad\qquad\qquad\qquad \Big[\{t-c_2(r-a)\}>0\Big] \\
& \qquad\qquad =0, \qquad\qquad\qquad \Big[\{t-c_2(r-a)\}<0\Big]
\end{aligned}
\right\} \quad (22)
$$

where

$$\left.\begin{aligned}
Y_{s1}&=\left\{S_{s1}C_{s1}-(r/a)\,q_s^2S_{s2}C_{s2}\right\}^2+q_s^2\left\{(r/a)\,S_{s1}C_{s2}+S_{s2}C_{s1}\right\}^2,\\
Y_{s2}&=\left\{Q_{s1}D_{s1}-(r/a)\,q_s^2Q_{s2}D_{s2}\right\}^2+q_s^2\left\{(r/a)\,Q_{s1}D_{s2}+Q_{s2}D_{s1}\right\}^2,\\
Z_{s1}&=\left\{S_{s1}M_{s1}-(r/a)\,q_s^2S_{s2}M_{s2}\right\}^2+q_s^2\left\{(r/a)\,S_{s1}M_{s2}+S_{s2}M_{s1}\right\}^2,\\
Z_{s2}&=\left\{Q_{s1}N_{s1}-(r/a)\,q_s^2Q_{s2}N_{s2}\right\}^2+q_s^2\left\{(r/a)\,Q_{s1}N_{s2}+Q_{s2}N_{s1}\right\}^2,\\
\Gamma_s&=(A_{s3}^2+A_{s4}^2)\,(A_{s5}^2+A_{s6}^2),\quad \gamma_s=\tan^{-1}(A_{s4}/A_{s3})+\tan^{-1}(A_{s6}/A_{s5}),\\
\eta_{s1}&=\tan^{-1}q_s\left\{\frac{(r/a)\,S_{s1}C_{s2}+S_{s2}C_{s1}}{S_{s1}C_{s1}-(r/a)\,q_s^2S_{s2}C_{s2}}\right\},\\
\eta_{s2}&=\tan^{-1}q_s\left\{\frac{(r/a)\,Q_{s1}D_{s2}+Q_{s2}D_{s1}}{Q_{s1}D_{s1}-(r/a)\,q_s^2Q_{s2}D_{s2}}\right\},\\
\zeta_{s1}&=\tan^{-1}q_s\left\{\frac{(r/a)\,S_{s1}M_{s2}+S_{s2}M_{s1}}{S_{s1}M_{s1}-(r/a)\,q_s^2S_{s2}M_{s2}}\right\},\\
\zeta_{s2}&=\tan^{-1}q_s\left\{\frac{(r/a)\,Q_{s1}N_{s2}+Q_{s2}N_{s1}}{Q_{s1}N_{s1}-(r/a)\,q_s^2Q_{s2}N_{s2}}\right\},\\
A_{11}&=p_1(3q_1^2-p_1^2),\quad A_{21}=p_2(3q_2^2-p_2^2),\quad A_{31}=p_3(3q_3^2-p_3^2),\\
A_{12}&=q_1(3p_1^2-q_1^2),\quad A_{22}=q_2(3p_2^2-q_2^2),\quad A_{32}=q_3(3p_3^2-q_3^2),\\
A_{13}&=(p_2-p_1)^2-q_1^2+q_2^2,\quad A_{23}=(p_1-p_2)^2-q_2^2+q_1^2,\\
&\qquad\qquad A_{33}=(p_2-p_3)^2-q_3^2+q_2^2,\\
A_{14}&=2q_1(p_2-p_1),\quad A_{24}=2q_2(p_1-p_2),\quad A_{34}=2q_3(p_2-p_3),\\
A_{15}&=(p_3-p_1)^2-q_1^2+q_3^2,\quad A_{25}=(p_3-p_2)^2-q_2^2+q_3^2,\\
&\qquad\qquad A_{35}=(p_1-p_3)^2-q_3^2+q_1^2,\\
A_{16}&=2q_1(p_3-p_1),\quad A_{26}=2q_2(p_3-p_2),\quad A_{35}=2q_3(p_1-p_3),\\
S_{s1}&=(p_s^4-5p_s^3+21p_s^2-48p_s+48)-q_s^2(6p_s^2-15p_s+21)+q_s^4,\\
S_{s2}&=-(4p_s^3-15p_s^2+42p_s-48)+q_s^2(4p_s-5),\\
C_{s1}&=-\left\{p_s^3(r/a)^3-4\sqrt{3}\,p_s^2(r/a)^2+27p_s(r/a)-27\sqrt{3}\right\}\\
&\qquad+q_s^2(r/a)^2\left\{3p_s(r/a)-4\sqrt{3}\right\},\\
C_{s2}&=\left\{3p_s^2(r/a)^2-8\sqrt{3}\,p_s(r/a)+27\right\}-q_s^2(r/a)^2,
\end{aligned}\right\}\quad(23)$$

$$\left.\begin{aligned}
Q_{s1}&=-(p_s^3-5\sqrt{3}\,p_s^2+36p_s-36\sqrt{3})+q_s^2(3p_s-5\sqrt{3}),\\
Q_{s2}&=(3p_s^2-10\sqrt{3}\,p_s+36)-q_s^2,\\
D_{s1}&=\left\{p_s^2(r/a)^2-3p_s(r/a)+3\right\}-q_s^2(r/a)^2,\quad D_{s2}=-2p_s(r/a)+3,\\
M_{s1}&=\left\{p_s^2(r/a)^2-3\sqrt{3}\,p_s(r/a)+9\right\}-q_s^2(r/a)^2,\\
M_{s2}&=-2p_s(r/a)+3\sqrt{3},\\
N_{s1}&=-\left\{p_s^3(r/a)^3-3p_s^2(r/a)^2+6p_s(r/a)-6\right\}\\
&\qquad\qquad+3q_s^2(r/a)^2\left\{p_s(r/a)-1\right\},\\
N_{s2}&=3\left\{p_s^2(r/a)^2-2p_s(r/a)+2\right\}-q_s^2(r/a)^2.
\end{aligned}\right\}$$

Using (21), (22), it is possible to write the expressions for displacements at the spherical boundary of the origin and also at any radial distance.

The displacements at the spherical boundary $r=a$ are expressed by

$$\left.\begin{aligned}
u_{01}\Big/\frac{ap_0}{\mu}P_2(\cos\theta)&=\frac{2119}{4232}-\frac{27}{23}\left(\frac{t}{ac_2}\right)^2,\\
u_{02}\Big/\frac{ap_0}{\mu}P_2(\cos\theta)&=-\frac{1623}{2116}+\frac{27}{23}\left(\frac{t}{ac_2}\right)^2,\\
v_{01}\Big/\frac{ap_0}{\mu}\frac{dP_2(\cos\theta)}{d\theta}&=-\frac{829}{4232}+\frac{9}{23}\left(\frac{t}{ac_2}\right)^2,\\
v_{02}\Big/\frac{ap_0}{\mu}\frac{dP_2(\cos\theta)}{d\theta}&=\frac{265}{2116}-\frac{9}{23}\left(\frac{t}{ac_2}\right)^2,\\
&\qquad\qquad[t/(ac_2)>0]\\
u_{01}=u_{02}=v_{01}=v_{02}&=0. \qquad [t/(ac_2)<0]
\end{aligned}\right\}\quad(24)$$

$$\begin{aligned}
u_{f1}\Big/\frac{ap_0}{\mu}P_2(\cos\theta)&=\frac{-1}{\sqrt{3}}\sum_{s=1}^{3}\frac{1}{q_s}e^{-p_st/(ac_2)}\sqrt{\frac{Y_{s1,a}}{(A_{s1}^2+A_{s2}^2)\Gamma_s}}\\
&\quad\cdot\sin\left\{q_st/(ac_2)+\eta_{s1,a}-\tan^{-1}(A_{s2}/A_{s1})-\gamma_s\right\},\\
u_{f2}\Big/\frac{ap_0}{\mu}P_2(\cos\theta)&=4\sqrt{3}\sum_{s=1}^{3}\frac{1}{q_s}e^{-p_st/(ac_2)}\sqrt{\frac{Y_{s2,a}}{(A_{s1}^2+A_{s2}^2)\Gamma_s}}\\
&\quad\cdot\sin\left\{q_st/(ac_2)+\eta_{s2,a}-\tan^{-1}(A_{s2}/A_{s1})-\gamma_s\right\},
\end{aligned}$$

$$
\left.
\begin{aligned}
& v_{f1}\Big/\frac{ap_0}{\mu}\frac{dP_2(\cos\theta)}{d\theta}=\sum_{s=1}^{3}\frac{1}{q_s}e^{-p_st/(ac_2)}\sqrt{\frac{Z_{s1,a}}{(A_{s1}^2+A_{s2}^2)\Gamma_s}} \\
& \qquad\qquad .\sin\left\{q_st/(ac_2)+\zeta_{s1,a}-\tan^{-1}(A_{s2}/A_{s1})-\gamma_s\right\}, \\
& v_{f2}\Big/\frac{ap_0}{\mu}\frac{dP_2(\cos\theta)}{d\theta}=\frac{-2}{\sqrt{3}}\sum_{s=1}^{3}\frac{1}{q_s}e^{-p_st/(ac_2)}\sqrt{\frac{Z_{s2,a}}{(A_{s1}^2+A_{s2}^2)\Gamma_s}} \\
& \qquad\qquad .\sin\left\{q_st/(ac_2)+\zeta_{s2,a}-\tan^{-1}(A_{s2}/A_{s1})-\gamma_s\right\}, \\
& \qquad\qquad\qquad\qquad\qquad\qquad [t/(ac_2)>0] \\
& u_{f1}=u_{f2}=v_{f1}=v_{f2}=0, \qquad\qquad [t/(ac_2)<0]
\end{aligned}
\right\}
\tag{25}
$$

where

$$
\left.
\begin{aligned}
& Y_{s1,a}=(S_{s1}C_{s1,a}-q_s^2S_{s2}C_{s2,a})^2+q_s^2(S_{s1}C_{s2,a}+S_{s2}C_{s1,a})^2, \\
& Y_{s2,a}=(Q_{s1}D_{s1,a}-q_s^2Q_{s2}D_{s2,a})^2+q_s^2(Q_{s1}D_{s2,a}+Q_{s2}D_{s1,a})^2, \\
& Z_{s1,a}=(S_{s1}M_{s1,a}-q_s^2S_{s2}M_{s2,a})^2+q_s^2(S_{s2}M_{s2,a}+S_{s2}M_{s1,a})^2, \\
& Z_{s2,a}=(Q_{s1}N_{s1,a}-q_s^2Q_{s2}N_{s2,a})^2+q_s^2(Q_{s1}N_{s2,a}+Q_{s2}N_{s1,a})^2, \\
& \eta_{s1,a}=\tan^{-1}q_s\left(\frac{S_{s1}C_{s2,a}+S_{s2}C_{s1,a}}{S_{s1}C_{s1,a}-q_s^2S_{s2}C_{s2,a}}\right), \\
& \eta_{s2,a}=\tan^{-1}q_s\left(\frac{Q_{s1}D_{s2,a}+Q_{s2}D_{s1,a}}{Q_{s1}D_{s1,a}-q_s^2Q_{s2}D_{s2,a}}\right), \\
& \zeta_{s1,a}=\tan^{-1}q_s\left(\frac{S_{s1}M_{s2,a}+S_{s2}M_{s1,a}}{S_{s1}M_{s1,a}-q_s^2S_{s2}M_{s2,a}}\right), \\
& \zeta_{s2,a}=\tan^{-1}q_s\left(\frac{Q_{s1}N_{s2,a}+Q_{s2}N_{s1,a}}{Q_{s1}N_{s1,a}-q_s^2Q_{s2}N_{s2,a}}\right), \\
& C_{s1,a}=-(p_s^3-4\sqrt{3}\,p_s^2+27p_s-27\sqrt{3})+q_s^2(3p_s-4\sqrt{3}), \\
& C_{s2,a}=(3p_s^2-8\sqrt{3}\,p_s+27)-q_s^2, \\
& D_{s1,a}=(p_s^2-3p_s+3)-q_s^2, \quad D_{s2,a}=-2p_s+3, \\
& M_{s1,a}=(p_s^2-3\sqrt{3}\,p_s+9)-q_s^2, \quad M_{s2,a}=-2p_s+3\sqrt{3}, \\
& N_{s1,a}=-(p_s^3-3p_s^2+6p_s-6)+3q_s^2(p_s-1), \\
& N_{s2,a}=3(p_s^2-2p_s+2)-q_s^2.
\end{aligned}
\right\}
\tag{26}
$$

The expressions for displacements at a relatively large r can be

simplified by taking the term of the lowest order in $1/r$ in every case. We shall indicate such a condition by writing $r=\infty$. The results of calculation in that case give

$$\left.\begin{aligned}
u_{01}\Big/\frac{a^3p_0}{r^2\mu}P_2(\cos\theta) &= -\frac{8}{23}, && \Big[\{t-c_1(r-a)\}>0\Big] \\
&=0, && \Big[\{t-c_1(r-a)\}<0\Big] \\
u_{02}\Big/\frac{a^3p_0}{r^2\mu}P_2(\cos\theta) &= \frac{18}{23}, && \Big[\{t-c_2(r-a)\}>0\Big] \\
&=0, && \Big[\{t-c_2(r-a)\}<0\Big] \\
v_{01}\Big/\frac{a^3p_0}{r^2\mu}\frac{dP_2(\cos\theta)}{d\theta} &= \frac{2}{23}, && \Big[\{t-c_1(r-a)\}>0\Big] \\
&=0, && \Big[\{t-c_1(r-a)\}<0\Big] \\
v_{02}\Big/\frac{a^3p_0}{r^2\mu}\frac{dP_2(\cos\theta)}{d\theta} &= -\frac{9}{23}, && \Big[\{t-c_2(r-a)\}>0\Big] \\
&=0, && \Big[\{t-c_2(r-a)\}<0\Big]
\end{aligned}\right\}\left[\frac{t-c_1(r-a)}{ac_2}\ll\frac{r}{a}\right] \tag{27}$$

$$\left.\begin{aligned}
u_{f1}\Big/\frac{a^2p_0}{r\mu}P_2(\cos\theta) &= \frac{-1}{\sqrt{3}}\sum_{s=1}^{3}\frac{1}{q_s}e^{-\{t-c_1(r-a)\}p_s/ac_2} \\
&\cdot\sqrt{\frac{Y_{s1,\infty}}{(A_{s1}^2+A_{s2}^2)\Gamma_s}}\sin\Big[\{t-c_1(r-a)\}q_s/ac_2+\eta_{s1,\infty}-\tan^{-1}(A_{s2}/A_{s1})-\gamma_s\Big], \\
& \qquad \Big[\{t-c_1(r-a)\}>0\Big] \\
&=0, \qquad \Big[\{t-c_1(r-a)\}<0\Big] \\
u_{f2}\Big/\frac{a^3p_0}{r^2\mu}P_2(\cos\theta) &= 4\sqrt{3}\sum_{s=1}^{3}\frac{1}{q_s}e^{-\{t-c_2(r-a)\}p_s/ac_2} \\
&\cdot\sqrt{\frac{Y_{s2,\infty}}{(A_{s1}^2+A_{s2}^2)\Gamma_s}}\sin\Big[\{t-c_2(r-a)\}q_s/ac_2+\eta_{s2,\infty}-\tan^{-1}(A_{s2}/A_{s1})-\gamma_s\Big], \\
& \qquad \Big[\{t-c_2(r-a)\}>0\Big] \\
&=0, \qquad \Big[\{t-c_2(r-a)\}<0\Big]
\end{aligned}\right\} \tag{28}$$

$$v_{f1}\Big/\frac{a^3p_0}{r^2\mu}\frac{dP_2(\cos\theta)}{d\theta}=\sum_{s=1}^{3}\frac{1}{q_s}e^{-\{t-c_1(r-a)\}p_s/ac_2}$$
$$\cdot\sqrt{\frac{Z_{s1,\infty}}{(A_{s1}^2+A_{s2}^2)\Gamma_s}}\sin\Big[\{t-c_1(r-a)\}q_s/ac_2+\zeta_{s1,\infty}-\tan^{-1}(A_{s2}/A_{s1})-\gamma_s\Big],$$
$$\Big[\{t-c_1(r-a)\}>0\Big]$$
$$=0,\qquad \Big[\{t-c_1(r-a)\}<0\Big]$$
$$v_{f2}\Big/\frac{a^2p_0}{r\mu}\frac{dP_2(\cos\theta)}{d\theta}=\frac{-2}{\sqrt{3}}\sum_{s=1}^{3}\frac{1}{q_s}e^{-\{t-c_2(r-a)\}p_s/ac_2}$$
$$\cdot\sqrt{\frac{Z_{s2,\infty}}{(A_{s1}^2+A_{s2}^2)\Gamma_s}}\sin\Big[\{t-c_2(r-a)\}q_s/ac_2+\zeta_{s2,\infty}-\tan^{-1}(A_{s2}/A_{s1})-\gamma_s\Big],$$
$$\Big[\{t-c_2(r-a)\}>0\Big]$$
$$=0,\qquad \Big[\{t-c_2(r-a)\}<0\Big]$$

where

$$\left.\begin{aligned}
Y_{s1,\infty}&=(S_{s1}C_{s1,\infty}-q_s^2S_{s2}C_{s2,\infty})^2+q_s^2(S_{s1}C_{s2,\infty}+S_{s2}C_{s1,\infty})^2,\\
Y_{s2,\infty}&=(Q_{s1}D_{s1,\infty}-q_s^2Q_{s2}D_{s2,\infty})^2+q_s^2(Q_{s1}D_{s2,\infty}+Q_{s2}D_{s1,\infty})^2,\\
Z_{s1,\infty}&=(S_{s1}M_{s1,\infty}-q_s^2S_{s2}M_{s2,\infty})^2+q_s^2(S_{s1}M_{s2,\infty}+S_{s2}M_{s1,\infty})^2,\\
Z_{s2,\infty}&=(Q_{s1}N_{s1,\infty}-q_s^2Q_{s2}N_{s2,\infty})^2+q_s^2(Q_{s1}N_{s2,\infty}+Q_{s2}N_{s1,\infty})^2,\\
\eta_{s1,\infty}&=\tan^{-1}q_s\left(\frac{S_{s1}C_{s2,\infty}+S_{s2}C_{s1,\infty}}{S_{s1}C_{s1,\infty}-q_s^2S_{s2}C_{s2,\infty}}\right),\\
\eta_{s2,\infty}&=\tan^{-1}q_s\left(\frac{Q_{s1}D_{s2,\infty}+Q_{s2}D_{s1,\infty}}{Q_{s1}D_{s1,\infty}-q_s^2Q_{s2}D_{s2,\infty}}\right),\\
\zeta_{s1,\infty}&=\tan^{-1}q_s\left(\frac{S_{s1}M_{s2,\infty}+S_{s2}M_{s1,\infty}}{S_{s1}M_{s1,\infty}-q_s^2S_{s2}M_{s2,\infty}}\right),\\
\zeta_{s2,\infty}&=\tan^{-1}q_s\left(\frac{Q_{s1}N_{s2,\infty}+Q_{s2}N_{s1,\infty}}{Q_{s1}N_{s1,\infty}-q_s^2Q_{s2}N_{s2,\infty}}\right),\\
C_{s1,\infty}&=-p_s(p_s^2-3q_s^2),\quad C_{s2,\infty}=3p_s^2-q_s^2,\\
D_{s1,\infty}&=p_s^2-q_s^2,\quad D_{s2,\infty}=-2p_s,\quad M_{s1,\infty}=p_s^2-q_s^2,\quad M_{s2,\infty}=-2p_s,\\
N_{s1,\infty}&=-p_s(p_s^2-3q_s^2),\quad N_{s2,\infty}=3p_s^2-q_s^2.
\end{aligned}\right\}\qquad(29)$$

The results of numerical calculation for u_{01}, u_{02}, u_{f1}, u_{f2}, v_{01}, v_{02}, v_{f1}, v_{f2}, and also for $u_{01}+u_{f1}$, $u_{02}+u_{f2}$, $v_{01}+v_{f1}$, $v_{02}+v_{f2}$, all at $r=a$, are shown in Figs. 1, 2. It will be seen that with time increase the displacements of forced waves, whether in dilatational waves or in distortional waves, augment without limit, whereas the displacements of

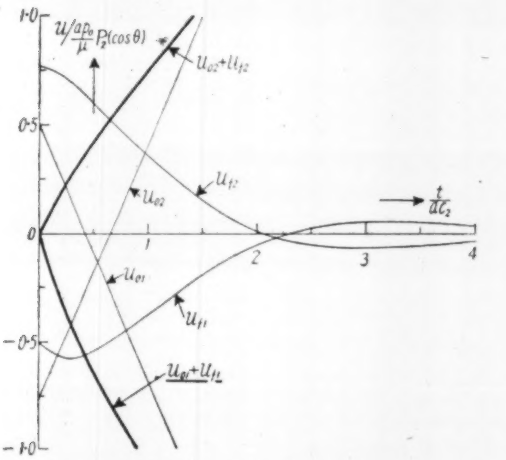

Fig. 1. Displacements for u's at $r=a$. $f(t)=p_0$ for $t>0$, $f(t)=0$ for $t<0$.

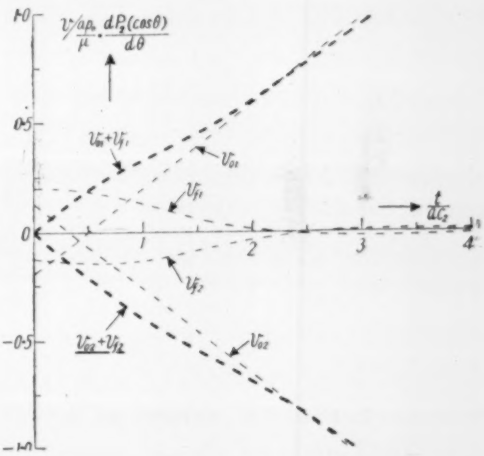

Fig. 2. Displacements for v's at $r=a$. $f(t)=p_0$ for $t>0$, $f(t)=0$ for $t<0$.

free waves decay. Thus, the resultant displacements, $u_{01}+u_{f1}$, $u_{02}+u_{f2}$, $v_{01}+v_{f1}$, $v_{02}+v_{f2}$ also diverge with time.

The diverging feature of the displacements just mentioned, as a matter of fact, arises from the condition that the dilatational waves and the distortional waves are considered separately. On the other hand, such resultant displacements of forced waves as $u_{01}+u_{02}$, $v_{01}+v_{02}$, never diverge. The values of $u_{01}+u_{02}$, $v_{01}+v_{02}$, together with $u_{f1}+u_{f2}$, $v_{f1}+v_{f2}$, $u_{01}+u_{02}+u_{f1}+u_{f2}$, $v_{01}+v_{02}+v_{f1}+v_{f2}$ are shown in Figs. 3, 4. It

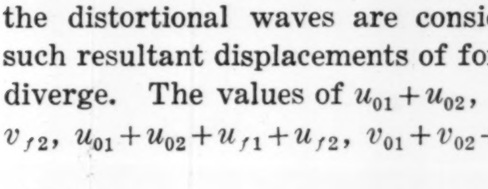

Fig. 3. Resultant displacements for u's at $r=a$. $f(t)=p_0$ for $t>0$, $f(t)=0$ for $t<0$.

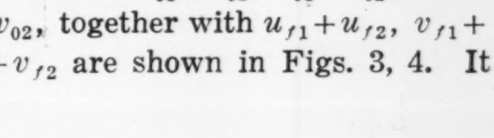

Fig. 4. Resultant displacements for v's at $r=a$. $f(t)=p_0$ for $t>0$, $f(t)=0$ for $t<0$.

will be seen that $u_{01}+u_{02}$, $v_{01}+v_{02}$ are constant for any t, and that $u_{01}+u_{02}+u_{f1}+u_{f2}$, $v_{01}+v_{02}+v_{f1}+v_{f2}$ tend to the constant values u_{01}

$+u_{02}$, $v_{01}+v_{02}$, in question, for $t\to\infty$. At all events, it is likely that the values of $u_{01}+u_{02}$, $v_{01}+v_{02}$ agree with the pressure change at the spherical boundary; this, however, is merely apparent, as will be seen in the next section.

The results of numerical calculation for u_{01}, v_{01}, u_{f1}, v_{f1}, $u_{01}+u_{f1}$, $v_{01}+v_{f1}$, and also for u_{02}, v_{02}, u_{f2}, v_{f2}, $u_{02}+u_{f2}$, $v_{02}+v_{f2}$, all at $r=\infty$, are shown in Figs. 5, 6. It should be borne in mind that although the order in $1/r$ for u_{01}, v_{01}, v_{f1}, u_{02}, u_{f2}, v_{02} is higher than that for u_{f1}, v_{f2}, all curves are plotted, for convenience, with the same scale for ordinate. Thus, the curves for $u_{01}+u_{f1}$, $v_{02}+v_{f2}$ are identical respectively with those for u_{f1}, v_{f2}. Although it may seem that the curves for u_{01}, v_{01}, u_{02}, v_{02} remain constant for any time and any radius, this condition is only apparent for such a range as $\{t-c_1(r-a)\}/ac_2$ or $\{t-c_2(r-a)\}/ac_2 \ll r/a$. Beyond such range, these displacements augment without limit, as in the case of forced waves at the spherical boundary. Since the front of the waves u_{01}, v_{01}, and that of the waves, u_{02}, v_{02}, are transmitted with velocities of longitudinal waves and transverse waves, respectively, divergence of the displacements in question would occur were the longitudinal waves and transverse waves separated greatly for an infinitely large epicentral distance. On the other hand, the mathematical solutions (21) show that if u_{01}, v_{01} were combined with u_{02}, v_{02}, respectively, the respective resultant displacements become constant and finite for $t-c_1(r-a)>0$, $t-c_2(r-a)>0$. This shows that the tail of the forced waves, accompanying the dilatational waves, that once tended to diverge before the arrival of the distortional waves, suddenly converges with the arrival of the latter waves.

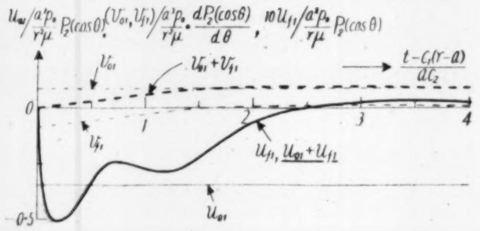

Fig. 5. Displacements for longitudinal waves at $r=\infty$. $f(t)=p_0$ for $t>0$, $f(t)=0$ for $t<0$.

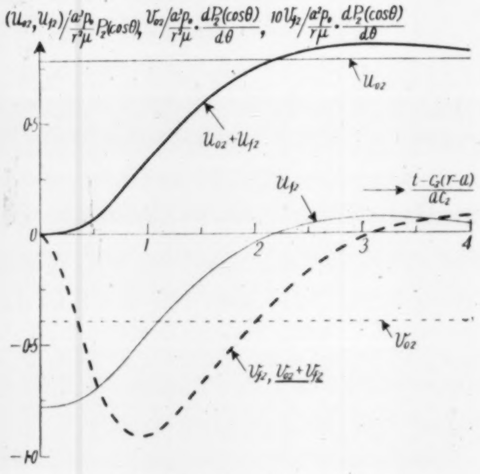

Fig. 6. Displacements for transverse waves at $r=\infty$. $f(t)=p_0$ for $t>0$, $f\ t)=0$ for $t<0$.

It may be questioned whether or not the initial motion of the waves at a large epicentral distance agrees with the resultant displace-

ment at the origin or with any component of displacement at the same origin. By comparing Figs. 1~6, we readily have the answer to this question. The initial motions at $r=\infty$ for $u_{01}+u_{f1}$, $v_{01}+v_{f1}$, $u_{02}+u_{f2}$, $v_{02}+v_{f2}$, are, respectively, in good accordance with those at $r=a$ for $u_{01}+u_{f1}$, $v_{01}+v_{f1}$, $u_{02}+u_{f2}$, $v_{02}+v_{f2}$. The motions corresponding to these curves begin from zero displacements. All these curves are indicated with thick lines (full lines for u's and broken lines for v's). As to the relation between the initial motions and the pressure change, it is likely that the initial motions of the displacements $u_{01}+u_{f1}$ and $v_{02}+v_{f2}$ at $r=a$ as well as at $r=\infty$ are invariably in the sense of pressure change at the spherical origin. The cases of such displacements are indicated with underlines.

Although it may seem that the displacements $u_{01}+u_{02}$, $v_{01}+v_{02}$ at $r=a$ obey the law of pressure change, not only for the initial motion but also for motion at any time, this contingency is restricted to the present problem. If we consider both the present case and that shown in the next section, it appears that the displacements represented by $u_{01}+u_{02}+u_{f1}+u_{f2}$, $v_{01}+v_{02}+v_{f1}+v_{f2}$ at $r=a$, agree with pressure change at the spherical origin, for initial motion as well as for motion at any time. The curves for these cases are also drawn with thick lines (full lines for u's and broken lines for v's) and furthermore indicated with broken underlines.

5. *The special case, $n=2$; $f(t)=p_0 \sin\beta t$ for $t>0$ and $f(t)=0$ for $t<0$.*

In this case $g(z)=z\beta/(z^2+\beta^2)$ for $t>0$, $g(z)=0$ for $t<0$. Thus, from (17) we get

$$\left.\begin{aligned}
u_1&=\frac{-a^3\beta p_0 P_2(\cos\theta)}{\sqrt{3}\,\mu c_2^2 r^4 2\pi i}\int_{c-i\infty}^{c+i\infty}\frac{F_1(z)e^{z\{t-c_1(r-a)\}}dz}{z^2(z^2+\beta^2)\Omega_0}, \\
u_2&=\frac{4\sqrt{3}\,a^3\beta p_0 P_2(\cos\theta)}{\mu c_2^2 r^4 2\pi i}\int_{c-i\infty}^{c+i\infty}\frac{F_2(z)e^{z\{t-c_2(r-a)\}}dz}{z^2(z^2+\beta^2)\Omega_0}, \\
v_1&=\frac{a^3\beta p_0}{\mu c_2^2 r^4 2\pi i}\,\frac{dP_2(\cos\theta)}{d\theta}\int_{c-i\infty}^{c+i\infty}\frac{G_1(z)e^{z\{t-c_1(r-a)\}}dz}{z^2(z^2+\beta^2)\Omega_0}, \\
v_2&=\frac{-2a^3\beta p_0}{\sqrt{3}\,\mu c_2^2 r^4 2\pi i}\,\frac{dP_2(\cos\theta)}{d\theta}\int_{c-i\infty}^{c+i\infty}\frac{G_2(z)e^{z\{t-c_2(r-a)\}}dz}{z^2(z^2+\beta^2)\Omega_0},
\end{aligned}\right\} \qquad (30)$$

$$\left.\begin{aligned}
&M_{\beta 2}=3\sqrt{3}\,, \quad N_{\beta 1}=-3\Big\{\zeta^2(r/a)^2-2\Big\},\\
&N_{\beta 2}=-\zeta^2(r/a)^2+6,\\
&P=-\zeta^6+81{\cdot}6714\zeta^4-759{\cdot}697\zeta^2+552,\\
&Q=\zeta(12{\cdot}50555\zeta^4-326{\cdot}042\zeta^2+870{\cdot}697), \quad \zeta=\beta a c_2,
\end{aligned}\right\} \tag{33}$$

The integration of (30) furthermore gives the free waves:

$$\left.\begin{aligned}
u_{f1}\Big/\frac{ap_0}{\mu}P_2(\cos\theta)&=\frac{-\zeta(a/r)^4}{\sqrt{3}}\sum_{s=1}^{3}\frac{1}{q_s}e^{-\{t-c_1(r-a)\}p_s/ac_2}\sqrt{\frac{Y_{s1}}{(B_{s1}^2+B_{s2}^2)\Gamma_s}}\\
&\quad\cdot\sin\Big[\Big\{t-c_1(r-a)\Big\}q_s/ac_2+\eta_{s1}-\tan^{-1}(B_{s2}/B_{s1})-\gamma_s\Big],\\
&\qquad\qquad\Big[\Big\{t-c_1(r-a)\Big\}>0\Big]\\
&=0, \qquad\qquad \Big[\Big\{t-c_1(r-a)\Big\}<0\Big]\\
u_{f2}\Big/\frac{ap_0}{\mu}P_2(\cos\theta)&=4\sqrt{3}\,\zeta(a/r)^4\sum_{s=1}^{3}\frac{1}{q_s}e^{-\{t-c_2(r-a)\}p_s/ac_2}\sqrt{\frac{Y_{s2}}{(B_{s1}^2+B_{s2}^2)\Gamma_s}}\\
&\quad\cdot\sin\Big[\Big\{t-c_2(r-a)\Big\}q_s/ac_2+\eta_{s2}-\tan^{-1}(B_{s2}/B_{s1})-\gamma_s\Big],\\
&\qquad\qquad\Big[\Big\{t-c_2(r-a)\Big\}>0\Big]\\
&=0, \qquad\qquad \Big[\Big\{t-c_2(r-a)\Big\}<0\Big]\\
v_{f1}\Big/\frac{ap_0}{\mu}\frac{dP_2(\cos\theta)}{d\theta}&=\zeta(a/r)^4\sum_{s=1}^{3}\frac{1}{q_s}e^{-\{t-c_1(r-a)\}p_s/ac_2}\sqrt{\frac{Z_{s1}}{(B_{s1}^2+B_{s2}^2)\Gamma_s}}\\
&\quad\cdot\sin\Big[\Big\{t-c_1(r-a)\Big\}q_s/ac_2+\zeta_{s1}-\tan^{-1}(B_{s2}/B_{s1})-\gamma_s\Big],\\
&\qquad\qquad\Big[\Big\{t-c_1(r-a)\Big\}>0\Big]\\
&=0, \qquad\qquad \Big[\Big\{t-c_1(r-a)\Big\}<0\Big]\\
v_{f2}\Big/\frac{ap_0}{\mu}\frac{dP_2(\cos\theta)}{d\theta}&=\frac{-2\zeta(a/r)^4}{\sqrt{3}}\sum_{s=1}^{3}\frac{1}{q_s}e^{-\{t-c_2(r-a)\}p_s/ac_2}\sqrt{\frac{Z_{s2}}{(B_{s1}^2+B_{s2}^2)\Gamma_s}}\\
&\quad\cdot\sin\Big[\Big\{t-c_2(r-a)\Big\}q_s/ac_2+\zeta_{s2}-\tan^{-1}(B_{s2}/B_{s1})-\gamma_s\Big],\\
&\qquad\qquad\Big[\Big\{t-c_2(r-a)\Big\}>0\Big]\\
&=0, \qquad\qquad \Big[\Big\{t-c_2(r-a)\Big\}<0\Big]
\end{aligned}\right\} \tag{34}$$

where

$$B_{s1}=(p_s^2-q_s^2)(p_s^2-q_s^2+\zeta^2)-4p_s^2q_s^2,\quad B_{s2}=-2p_sq_s\left\{2(p_s^2-q_s^2)+\zeta^2\right\}. \tag{35}$$

The displacements at the spherical boundary $r=a$ are expressed by

$$\left.\begin{aligned}
&(u_{01}+u'_{01})\Big/\frac{ap_0}{\mu}P_2(\cos\theta)=\frac{-1}{\sqrt{3}\,\zeta^2}\left\{\frac{54\sqrt{3}\,\zeta}{23}\left(\frac{t}{ac_2}\right)\right.\\
&\quad-\sqrt{\frac{(S_{\beta1}C_{\beta1,a}-\zeta^2S_{\beta2}C_{\beta2,a})^2+\zeta^2(S_{\beta1}C_{\beta2,a}+S_{\beta2}C_{\beta1,a})^2}{P^2+Q^2}}\\
&\quad\left.\cdot\sin\left[\beta t+\tan^{-1}\left\{\frac{\zeta(S_{\beta1}C_{\beta2,a}+S_{\beta2}C_{\beta1,a})}{S_{\beta1}C_{\beta1,a}-\zeta^2S_{\beta2}C_{\beta2,a}}\right\}-\tan^{-1}\frac{Q}{P}\right]\right\},\\
&(u_{02}+u'_{02})\Big/\frac{ap_0}{\mu}P_2(\cos\theta)=\frac{4\sqrt{3}}{\zeta^2}\left\{\frac{9\sqrt{3}\,\zeta}{46}\left(\frac{t}{ac_2}\right)\right.\\
&\quad-\sqrt{\frac{(Q_{\beta1}D_{\beta1,a}-\zeta^2Q_{\beta2}D_{\beta2,a})^2+\zeta^2(Q_{\beta1}D_{\beta2,a}+Q_{\beta2}D_{\beta1,a})^2}{P^2+Q^2}}\\
&\quad\left.\cdot\sin\left[\beta t+\tan^{-1}\left\{\frac{\zeta(Q_{\beta1}D_{\beta2,a}+Q_{\beta2}D_{\beta1,a})}{Q_{\beta1}D_{\beta1,a}-\zeta^2Q_{\beta2}D_{\beta2,a}}\right\}-\tan^{-1}\frac{Q}{P}\right]\right\},\\
&(v_{01}+v'_{01})\Big/\frac{ap_0}{\mu}\frac{dP_2(\cos\theta)}{d\theta}=\frac{1}{\zeta}\left\{\frac{18\zeta}{23}\left(\frac{t}{ac_2}\right)\right.\\
&\quad-\sqrt{\frac{(S_{\beta1}M_{\beta1,a}-\zeta^2S_{\beta2}M_{\beta2,a})^2+\zeta^2(S_{\beta1}M_{\beta2,a}+S_{\beta2}M_{\beta1,a})^2}{P^2+Q^2}}\\
&\quad\left.\cdot\sin\left[\beta t+\tan^{-1}\left\{\frac{\zeta(S_{\beta1}M_{\beta2,a}+S_{\beta2}M_{\beta1,a})}{S_{\beta1}M_{\beta1,a}-\zeta^2S_{\beta2}M_{\beta2,a}}\right\}-\tan^{-1}\frac{Q}{P}\right]\right\},\\
&(v_{02}+v'_{02})\Big/\frac{ap_0}{\mu}\frac{dP_2(\cos\theta)}{d\theta}=\frac{-2}{\sqrt{3}\,\zeta^2}\left\{\frac{9\sqrt{3}\,\zeta}{23}\left(\frac{t}{ac_2}\right)\right.\\
&\quad-\sqrt{\frac{(Q_{\beta1}N_{\beta1,a}-\zeta^2Q_{\beta2}N_{\beta2,a})^2+\zeta^2(Q_{\beta1}N_{\beta2,a}+Q_{\beta2}N_{\beta1,a})^2}{P^2+Q^2}}\\
&\quad\left.\cdot\sin\left[\beta t+\tan^{-1}\left\{\frac{\zeta(Q_{\beta1}N_{\beta2,a}+Q_{\beta2}N_{\beta1,a})}{Q_{\beta1}N_{\beta1,a}-\zeta^2Q_{\beta2}N_{\beta2,a}}\right\}-\tan^{-1}\frac{Q}{P}\right]\right\},\\
&\qquad\qquad\qquad\qquad\qquad\qquad\qquad\qquad\qquad[t/ac_2>0]\\
&u_{01}=u'_{01}=u_{02}=u'_{02}=v_{01}=v'_{01}=v_{02}=v'_{02}=0,\qquad[t/ac_2<0]
\end{aligned}\right\}\tag{36}$$

where

The contributions from the poles for $\Omega_0=0$ give the part that corresponds to free waves and those from the poles for $z(z^2+\beta^2)=0$ represent the part that corresponds to forced waves.

Let, again, $u_{01}+u'_{01}$, $u_{02}+u'_{02}$, $v_{01}+v'_{01}$, $v_{02}+v'_{02}$ be the parts of u_1, u_2, v_1, v_2 that correspond to forced waves and u_{f1}, u_{f2}, v_{f1}, v_{f2} the parts of u_1, u_2, v_1, v_2 that correspond to free waves, so that

$$\left.\begin{aligned} u_{01}+u'_{01}+u_{f1}=u_1, \quad u_{02}+u'_{02}+u_{f2}=u_2, \\ v_{01}+v'_{01}+v_{f1}=v_1, \quad v_{02}+v'_{02}+v_{f2}=v_2. \end{aligned}\right\} \tag{31}$$

Integration of (30) gives the forced waves:

$$\left.\begin{aligned}
(u_{01}+u'_{01})\Big/\frac{ap_0}{\mu}P_2(\cos\theta) &= \frac{-(a/r)^4}{\sqrt{3}\,\zeta^2} \\
&\cdot\left\{\frac{54\zeta}{23}\left\{\left(\frac{r}{a}-1\right)+\sqrt{3}\left(\frac{t-c_1(r-a)}{ac_2}\right)\right\}\right. \\
&-\sqrt{\frac{\left\{S_{\beta1}C_{\beta1}-(r/a)\zeta^2 S_{\beta2}C_{\beta2}\right\}^2+\zeta^2\left\{(r/a)S_{\beta1}C_{\beta2}+S_{\beta2}C_{\beta1}\right\}^2}{P^2+Q^2}} \\
&\left.\cdot\sin\left[\beta\{t-c_1(r-a)\}+\tan^{-1}\left\{\frac{\zeta\{(r/a)S_{\beta1}C_{\beta2}+S_{\beta2}C_{\beta1}\}}{S_{\beta1}C_{\beta1}-(r/a)\zeta^2 S_{\beta2}C_{\beta2}}\right\}-\tan^{-1}\frac{Q}{P}\right]\right\}, \\
&\qquad\qquad \left[\{t-c_1(r-a)\}>0\right] \\
&=0, \qquad\qquad \left[\{t-c_1(r-a)\}<0\right] \\
(u_{02}+u'_{02})\Big/\frac{ap_0}{\mu}P_2(\cos\theta) &= \frac{4\sqrt{3}\,(a/r)^4}{\zeta^2} \\
&\cdot\left\{\frac{9\zeta}{46}\left\{\sqrt{3}\left(\frac{r}{a}-1\right)+\sqrt{3}\left(\frac{t-c_2(r-a)}{ac_2}\right)\right\}\right. \\
&-\sqrt{\frac{\left\{Q_{\beta1}D_{\beta1}-(r/a)\zeta^2 Q_{\beta2}D_{\beta2}\right\}^2+\zeta^2\left\{(r/a)Q_{\beta1}D_{\beta2}+Q_{\beta2}D_{\beta1}\right\}^2}{P^2+Q^2}} \\
&\left.\cdot\sin\left[\beta\{t-c_2(r-a)\}+\tan^{-1}\left\{\frac{\zeta\{(r/a)Q_{\beta1}D_{\beta2}+Q_{\beta2}D_{\beta1}\}}{Q_{\beta1}D_{\beta1}-(r/a)\zeta^2 Q_{\beta2}D_{\beta2}}\right\}-\tan^{-1}\frac{Q}{P}\right]\right\}, \\
&\qquad\qquad \left[\{t-c_2(r-a)\}>0\right] \\
&=0, \qquad\qquad \left[\{t-c_2(r-a)\}<0\right]
\end{aligned}\right\}$$

$$(v_{01}+v'_{01})\Big/\frac{ap_0}{\mu}\frac{dP_2(\cos\theta)}{d\theta}=\frac{(a/r)^4}{\zeta^2}$$

$$\cdot\left\{\frac{18\zeta}{28}\left\{\frac{1}{\sqrt{3}}\left(\frac{r}{a}-1\right)+\left(\frac{t-c_1(r-a)}{ac_2}\right)\right\}\right.$$

$$-\sqrt{\frac{\left\{S_{\beta1}M_{\beta1}-(r/a)\zeta^2S_{\beta2}M_{\beta2}\right\}^2+\zeta^2\left\{(r/a)S_{\beta1}M_{\beta2}+S_{\beta2}M_{\beta1}\right\}^2}{P^2+Q^2}}$$

$$\left.\cdot\sin\left[\beta\left\{t-c_1(r-a)\right\}+\tan^{-1}\left\{\frac{\zeta\left\{(r/a)S_{\beta1}M_{\beta2}+S_{\beta2}M_{\beta1}\right\}}{S_{\beta1}M_{\beta1}-(r/a)\zeta^2S_{\beta2}M_{\beta2}}\right\}-\tan^{-1}\frac{Q}{P}\right]\right\},$$

$$\left[\left\{t-c_1(r-a)\right\}>0\right]$$

$$=0, \qquad \left[\left\{t-c_1(r-a)\right\}<0\right]$$

$$(v_{02}+v'_{02})\Big/\frac{ap_0}{\mu}\frac{dP_2(\cos\theta)}{d\theta}=\frac{-2(a/r)^4}{\sqrt{3}\zeta^2}$$

$$\cdot\left\{\frac{9\sqrt{3}\zeta}{23}\left\{\left(\frac{r}{a}-1\right)+\left(\frac{t-c_2(r-a)}{ac_2}\right)\right\}\right.$$

$$-\sqrt{\frac{\left\{Q_{\beta1}N_{\beta1}-(r/a)\zeta^2Q_{\beta2}N_{\beta2}\right\}^2+\zeta^2\left\{(r/a)Q_{\beta1}N_{\beta2}+Q_{\beta2}N_{\beta1}\right\}^2}{P^2+Q^2}}$$

$$\left.\cdot\sin\left[\beta\left\{t-c_2(r-a)\right\}+\tan^{-1}\left\{\frac{\zeta\left\{(r/a)Q_{\beta1}N_{\beta2}+Q_{\beta2}N_{\beta1}\right\}}{Q_{\beta1}N_{\beta1}-(r/a)\zeta^2Q_{\beta2}N_{\beta2}}\right\}-\tan^{-1}\frac{Q}{P}\right]\right\},$$

$$\left[\left\{t-c_2(r-a)\right\}>0\right]$$

$$=0, \qquad \left[\left\{t-c_2(r-a)\right\}<0\right] \qquad (32)$$

where u'_{01}, u'_{02}, v'_{01}, v'_{02} are oscillatory parts of forced waves and u_{01}, u_{02}, v_{01}, v_{02} the remaining parts of the same waves. We shall name u_{01}, u_{02}, v_{01}, v_{02} by forced waves of the first kind and u'_{01}, u'_{02}, v'_{01}, v'_{02} by forced waves of the second kind. In (32)

$$S_{\beta1}=\zeta^4-21\zeta^2+48, \quad S_{\beta2}=-5\zeta^2+48,$$

$$Q_{\beta1}=-\sqrt{3}\,(5\zeta^2-36), \quad Q_{\beta2}=-\zeta^2+36,$$

$$C_{\beta1}=-\sqrt{3}\left\{4\zeta^2(r/a)^2-27\right\}, \quad C_{\beta2}=-\zeta^2(r/a)^2+27,$$

$$D_{\beta1}=-\zeta^2(r/a)^2+3, \quad D_{\beta2}=3, \quad M_{\beta1}=-\zeta^2(r/a)^2+9,$$

$$\left.\begin{aligned}
&M_{\beta 2}=3\sqrt{3}, \quad N_{\beta 1}=-3\Big\{\zeta^2(r/a)^2-2\Big\},\\
&N_{\beta 2}=-\zeta^2(r/a)^2+6,\\
&P=-\zeta^6+81{\cdot}6714\zeta^4-759{\cdot}697\zeta^2+552,\\
&Q=\zeta(12{\cdot}50555\zeta^4-326{\cdot}042\zeta^2+870{\cdot}697), \quad \zeta=\beta a c_2,
\end{aligned}\right\} \tag{33}$$

The integration of (30) furthermore gives the free waves:

$$\left.\begin{aligned}
u_{f1}\Big/\frac{ap_0}{\mu}P_2(\cos\theta)&=\frac{-\zeta(a/r)^4}{\sqrt{3}}\sum_{s=1}^{3}\frac{1}{q_s}e^{-\{t-c_1(r-a)\}p_s/ac_2}\sqrt{\frac{Y_{s1}}{(B_{s1}^2+B_{s2}^2)\Gamma_s}}\\
&\cdot\sin\Big[\Big\{t-c_1(r-a)\Big\}q_s/ac_2+\eta_{s1}-\tan^{-1}(B_{s2}/B_{s1})-\gamma_s\Big],\\
&\qquad\qquad\Big[\Big\{t-c_1(r-a)\Big\}>0\Big]\\
&=0, \qquad\qquad \Big[\Big\{t-c_1(r-a)\Big\}<0\Big]\\
u_{f2}\Big/\frac{ap_0}{\mu}P_2(\cos\theta)&=4\sqrt{3}\,\zeta(a/r)^4\sum_{s=1}^{3}\frac{1}{q_s}e^{-\{t-c_2(r-a)\}p_s/ac_2}\sqrt{\frac{Y_{s2}}{(B_{s1}^2+B_{s2}^2)\Gamma_s}}\\
&\cdot\sin\Big[\Big\{t-c_2(r-a)\Big\}q_s/ac_2+\eta_{s2}-\tan^{-1}(B_{s2}/B_{s1})-\gamma_s\Big],\\
&\qquad\qquad\Big[\Big\{t-c_2(r-a)\Big\}>0\Big]\\
&=0, \qquad\qquad \Big[\Big\{t-c_2(r-a)\Big\}<0\Big]\\
v_{f1}\Big/\frac{ap_0}{\mu}\frac{dP_2(\cos\theta)}{d\theta}&=\zeta(a/r)^4\sum_{s=1}^{3}\frac{1}{q_s}e^{-\{t-c_1(r-a)\}p_s/ac_2}\sqrt{\frac{Z_{s1}}{(B_{s1}^2+B_{s2}^2)\Gamma_s}}\\
&\cdot\sin\Big[\Big\{t-c_1(r-a)\Big\}q_s/ac_2+\zeta_{s1}-\tan^{-1}(B_{s2}/B_{s1})-\gamma_s\Big],\\
&\qquad\qquad\Big[\Big\{t-c_1(r-a)\Big\}>0\Big]\\
&=0, \qquad\qquad \Big[\Big\{t-c_1(r-a)\Big\}<0\Big]\\
v_{f2}\Big/\frac{ap_0}{\mu}\frac{dP_2(\cos\theta)}{d\theta}&=\frac{-2\zeta(a/r)^4}{\sqrt{3}}\sum_{s=1}^{3}\frac{1}{q_s}e^{-\{t-c_2(r-a)\}p_s/ac_2}\sqrt{\frac{Z_{s2}}{(B_{s1}^2+B_{s2}^2)\Gamma_s}}\\
&\cdot\sin\Big[\Big\{t-c_2(r-a)\Big\}q_s/ac_2+\zeta_{s2}-\tan^{-1}(B_{s2}/B_{s1})-\gamma_s\Big],\\
&\qquad\qquad\Big[\Big\{t-c_2(r-a)\Big\}>0\Big]\\
&=0, \qquad\qquad \Big[\Big\{t-c_2(r-a)\Big\}<0\Big]
\end{aligned}\right\} \tag{34}$$

where

$$B_{s1}=(p_s^2-q_s^2)(p_s^2-q_s^2+\zeta^2)-4p_s^2q_s^2,\quad B_{s2}=-2p_sq_s\Big\{2(p_s^2-q_s^2)+\zeta^2\Big\}. \quad (35)$$

The displacements at the spherical boundary $r=a$ are expressed by

$$\left.\begin{aligned}
&(u_{01}+u'_{01})\Big/\frac{ap_0}{\mu}P_2(\cos\theta)=\frac{-1}{\sqrt{3}\,\zeta^2}\Bigg\{\frac{54\sqrt{3}\,\zeta}{23}\Big(\frac{t}{ac_2}\Big)\\
&\quad-\sqrt{\frac{(S_{\beta1}C_{\beta1,a}-\zeta^2S_{\beta2}C_{\beta2,a})^2+\zeta^2(S_{\beta1}C_{\beta2,a}+S_{\beta2}C_{\beta1,a})^2}{P^2+Q^2}}\\
&\qquad\cdot\sin\Big[\beta t+\tan^{-1}\Big\{\frac{\zeta(S_{\beta1}C_{\beta2,a}+S_{\beta2}C_{\beta1,a})}{S_{\beta1}C_{\beta1,a}-\zeta^2S_{\beta2}C_{\beta2,a}}\Big\}-\tan^{-1}\frac{Q}{P}\Big]\Bigg\},\\
&(u_{02}+u'_{02})\Big/\frac{ap_0}{\mu}P_2(\cos\theta)=\frac{4\sqrt{3}}{\zeta^2}\Bigg\{\frac{9\sqrt{3}\,\zeta}{46}\Big(\frac{t}{ac_2}\Big)\\
&\quad-\sqrt{\frac{(Q_{\beta1}D_{\beta1,a}-\zeta^2Q_{\beta2}D_{\beta2,a})^2+\zeta^2(Q_{\beta1}D_{\beta2,a}+Q_{\beta2}D_{\beta1,a})^2}{P^2+Q^2}}\\
&\qquad\cdot\sin\Big[\beta t+\tan^{-1}\Big\{\frac{\zeta(Q_{\beta1}D_{\beta2,a}+Q_{\beta2}D_{\beta1,a})}{Q_{\beta1}D_{\beta1,a}-\zeta^2Q_{\beta2}D_{\beta2,a}}\Big\}-\tan^{-1}\frac{Q}{P}\Big]\Bigg\},\\
&(v_{01}+v'_{01})\Big/\frac{ap_0}{\mu}\frac{dP_2(\cos\theta)}{d\theta}=\frac{1}{\zeta}\Bigg\{\frac{18\zeta}{23}\Big(\frac{t}{ac_2}\Big)\\
&\quad-\sqrt{\frac{(S_{\beta1}M_{\beta1,a}-\zeta^2S_{\beta2}M_{\beta2,a})^2+\zeta^2(S_{\beta1}M_{\beta2,a}+S_{\beta2}M_{\beta1,a})^2}{P^2+Q^2}}\\
&\qquad\cdot\sin\Big[\beta t+\tan^{-1}\Big\{\frac{\zeta(S_{\beta1}M_{\beta2,a}+S_{\beta2}M_{\beta1,a})}{S_{\beta1}M_{\beta1,a}-\zeta^2S_{\beta2}M_{\beta2,a}}\Big\}-\tan^{-1}\frac{Q}{P}\Big]\Bigg\},\\
&(v_{02}+v'_{02})\Big/\frac{ap_0}{\mu}\frac{dP_2(\cos\theta)}{d\theta}=\frac{-2}{\sqrt{3}\,\zeta^2}\Bigg\{\frac{9\sqrt{3}\,\zeta}{23}\Big(\frac{t}{ac_2}\Big)\\
&\quad-\sqrt{\frac{(Q_{\beta1}N_{\beta1,a}-\zeta^2Q_{\beta2}N_{\beta2,a})^2+\zeta^2(Q_{\beta1}N_{\beta2,a}+Q_{\beta2}N_{\beta1,a})^2}{P^2+Q^2}}\\
&\qquad\cdot\sin\Big[\beta t+\tan^{-1}\Big\{\frac{\zeta(Q_{\beta1}N_{\beta2,a}+Q_{\beta2}N_{\beta1,a})}{Q_{\beta1}N_{\beta1,a}-\zeta^2Q_{\beta2}N_{\beta2,a}}\Big\}-\tan^{-1}\frac{Q}{P}\Big]\Bigg\},\\
&\hspace{20em}[t/ac_2>0]\\
&u_{01}=u'_{01}=u_{02}=u'_{02}=v_{01}=v'_{01}=v_{02}=v'_{02}=0,\qquad [t/ac_2<0]
\end{aligned}\right\}\quad (36)$$

where

$$\left.\begin{aligned} &C_{\beta1,a}=-\sqrt{3}\,(4\zeta^2-27),\quad C_{\beta2,a}=-\zeta^2+27,\\ &D_{\beta1,a}=-\zeta^2+3,\quad D_{\beta2,a}=3,\\ &M_{\beta1,a}=-\zeta^2+9,\quad M_{\beta2,a}=3\sqrt{3},\\ &N_{\beta1,a}=-3(\zeta^2-2),\quad N_{\beta2,a}=-\zeta^2+6. \end{aligned}\right\} \tag{37}$$

$$\left.\begin{aligned} &u_{f1}\Big/\frac{ap_0}{\mu}P_2(\cos\theta)=\frac{-\zeta}{\sqrt{3}}\sum_{s=1}^{3}\frac{1}{q_s}e^{-tp_s/ac_2}\sqrt{\frac{Y_{s1,a}}{(B_{s1}^2+B_{s2}^2)\Gamma_s}}\\ &\qquad\cdot\sin\left\{tq_s/ac_2+\eta_{s1,a}-\tan^{-1}(B_{s2}/B_{s1})-\gamma_s\right\},\\ &u_{f2}\Big/\frac{ap_0}{\mu}P_2(\cos\theta)=4\sqrt{3}\,\zeta\sum_{s=1}^{3}\frac{1}{q_s}e^{-tp_s/ac_2}\sqrt{\frac{Y_{s2,a}}{(B_{s1}^2+B_{s2}^2)\Gamma_s}}\\ &\qquad\cdot\sin\left\{tq_s/ac_2+\eta_{s2,a}-\tan^{-1}(B_{s2}/B_{s1})-\gamma_s\right\},\\ &v_{f1}\Big/\frac{ap_0}{\mu}\frac{dP_2(\cos\theta)}{d\theta}=\zeta\sum_{s=1}^{3}\frac{1}{q_s}e^{-tp_s/ac_2}\sqrt{\frac{Z_{s1,a}}{(B_{s1}^2+B_{s2}^2)\Gamma_s}}\\ &\qquad\cdot\sin\left\{tq_s/ac_2+\zeta_{s1,a}-\tan^{-1}(B_{s2}/B_{s1})-\gamma_s\right\},\\ &v_{f2}\Big/\frac{ap_0}{\mu}\frac{dP_2(\cos\theta)}{d\theta}=\frac{-2\zeta}{\sqrt{3}}\sum_{s=1}^{3}\frac{1}{q_s}e^{-tp_s/ac_2}\sqrt{\frac{Z_{s2,a}}{(B_{s1}^2+B_{s2}^2)\Gamma_s}}\\ &\qquad\cdot\sin\left\{tq_s/ac_2+\zeta_{s2,a}-\tan^{-1}(B_{s2}/B_{s1})-\gamma_s\right\},\\ &\qquad\qquad\qquad\qquad\qquad\qquad[t/ac_2>0]\\ &u_{f1}=u_{f2}=v_{f1}=v_{f2}=0.\qquad\qquad[t/ac_2<0] \end{aligned}\right\} \tag{38}$$

The expressions for displacements at a relatively large r, that is, $r=\infty$, are of the forms

$$\begin{aligned} &(u_{01}+u'_{01})\Big/\frac{a^2p_0}{r\mu}P_2(\cos\theta)=\frac{-\zeta}{\sqrt{3}}\left\{\frac{54(a/r)}{23\zeta^2}-\sqrt{\frac{(\zeta S_{\beta2})^2+(-S_{\beta1})^2}{P^2+Q^2}}\right.\\ &\qquad\left.\cdot\sin\left[\beta\left\{t-c_1(r-a)\right\}+\tan^{-1}\left\{(-S_{\beta1})/\zeta S_{\beta2}\right\}-\tan^{-1}(Q/P)\right]\right\},\\ &\qquad\qquad\qquad\qquad\qquad\qquad\left[\left\{t-c_1(r-a)\right\}>0\right]\\ &\qquad=0,\qquad\qquad\qquad\qquad\quad\left[\left\{t-c_1(r-a)\right\}<0\right] \end{aligned}$$

$$
\left.
\begin{aligned}
&(u_{02}+u'_{02})\Big/\frac{a^3p_0}{r^2\mu}P_2(\cos\theta)=4\sqrt{3}\left\{\frac{9\sqrt{3}\,(a/r)}{46\zeta}-\sqrt{\frac{(-Q_{\beta1})^2+(-\zeta Q_{\beta2})^2}{P^2+Q^2}}\right. \\
&\qquad\cdot\sin\left[\beta\left\{t-c_2(r-a)\right\}+\tan^{-1}\left\{(-\zeta Q_{\beta2})/(-Q_{\beta1})\right\}-\tan^{-1}(Q/P)\right]\Big\}, \\
&\qquad\qquad\qquad\qquad\qquad\qquad\left[\left\{t-c_2(r-a)\right\}>0\right] \\
&\qquad\qquad\qquad=0, \qquad\qquad\qquad \left[\left\{t-c_2(r-a)\right\}<0\right] \\
&(v_{01}+v'_{01})\Big/\frac{a^3p_0}{r^2\mu}\frac{dP_2(\cos\theta)}{d\theta}=\left\{\frac{18(a/r)}{23\sqrt{3}\,\zeta}-\sqrt{\frac{(-S_{\beta1})^2+(-\zeta S_{\beta2})^2}{P^2+Q^2}}\right. \\
&\qquad\cdot\sin\left[\beta\left\{t-c_1(r-a)\right\}+\tan^{-1}\left\{(-\zeta S_{\beta2})/(-S_{\beta1})\right\}-\tan^{-1}(Q/P)\right]\Big\}, \\
&\qquad\qquad\qquad\qquad\qquad\qquad\left[\left\{t-c_1(r-a)\right\}>0\right] \\
&\qquad\qquad\qquad=0, \qquad\qquad\qquad \left[\left\{t-c_1(r-a)\right\}<0\right] \\
&(v_{02}+v'_{02})\Big/\frac{a^2p_0}{r\mu}\frac{dP_2(\cos\theta)}{d\theta}=\frac{-2\zeta}{\sqrt{3}}\left\{\frac{9\sqrt{3}\,(a/r)^2}{23\zeta^2}-\sqrt{\frac{(\zeta Q_{\beta2})^2+(-Q_{\beta1})^2}{P^2+Q^2}}\right. \\
&\qquad\cdot\sin\left[\beta\left\{t-c_2(r-a)\right\}+\tan^{-1}\left\{(-Q_{\beta1})/\zeta Q_{\beta2}\right\}-\tan^{-1}(Q/P)\right]\Big\}, \\
&\qquad\qquad\qquad\qquad\qquad\qquad\left[\left\{t-c_2(r-a)\right\}>0\right] \\
&\qquad\qquad\qquad=0, \qquad\qquad\qquad \left[\left\{t-c_2(r-a)\right\}<0\right]
\end{aligned}
\right\}
\tag{39}
$$

$$
\begin{aligned}
&u_{f1}\Big/\frac{a^2p_0}{r\mu}P_2(\cos\theta)=\frac{-\zeta}{\sqrt{3}}\sum_{s=1}^{3}\frac{1}{q_s}e^{-\{t-c_1(r-a)\}p_s/ac_2}\sqrt{\frac{Y_{s1,\infty}}{(B_{s1}^2+B_{s2}^2)\Gamma_s}} \\
&\qquad\cdot\sin\left[\left\{t-c_1(r-a)\right\}q_s/ac_2+\eta_{s1,\infty}-\tan^{-1}(B_{s2}/B_{s1})-\gamma_s\right], \\
&\qquad\qquad\qquad\qquad\qquad\left[\left\{t-c_1(r-a)\right\}>0\right] \\
&\qquad\qquad=0, \qquad\qquad\qquad \left[\left\{t-c_1(r-a)\right\}<0\right]
\end{aligned}
$$

$$\left.\begin{aligned}
&u_{f2}\Big/\frac{a^3p_0}{r^2\mu}P_2(\cos\theta)=4\sqrt{3}\,\zeta\sum_{s=1}^{3}\frac{1}{q_s}e^{-\{t-c_2(r-a)\}p_s/ac_2}\sqrt{\frac{Y_{s2,\infty}}{(B_{s1}^2+B_{s2}^2)\Gamma_s}}\\
&\qquad\cdot\sin\Big[\Big\{t-c_2(r-a)\Big\}q_s/ac_2+\eta_{s2,\infty}-\tan^{-1}(B_{s2}/B_{s1})-\gamma_s\Big],\\
&\qquad\qquad\qquad\qquad\qquad\qquad\Big[\Big\{t-c_2(r-a)\Big\}>0\Big]\\
&\qquad=0,\qquad\qquad\qquad\qquad\quad\Big[\Big\{t-c_2(r-a)\Big\}<0\Big]\\
&v_{f1}\Big/\frac{a^3p_0}{r^2\mu}\frac{dP_2(\cos\theta)}{d\theta}=\zeta\sum_{s=1}^{3}\frac{1}{q_s}e^{-\{t-c_1(r-a)\}p_s/ac_2}\sqrt{\frac{Z_{s1,\infty}}{(B_{s1}^2+B_{s2}^2)\Gamma_s}}\\
&\qquad\cdot\sin\Big[\Big\{t-c_1(r-a)\Big\}q_s/ac_2+\zeta_{s1,\infty}-\tan^{-1}(B_{s2}/B_{s1})-\gamma_s\Big],\\
&\qquad\qquad\qquad\qquad\qquad\qquad\Big[\Big\{t-c_1(r-a)\Big\}>0\Big]\\
&\qquad=0,\qquad\qquad\qquad\qquad\quad\Big[\Big\{t-c_1(r-a)\Big\}<0\Big]\\
&v_{f2}\Big/\frac{a^2p_0}{r\mu}\frac{dP_2(\cos\theta)}{d\theta}=\frac{-2\zeta}{\sqrt{3}}\sum_{s=1}^{3}\frac{1}{q_s}e^{-\{t-c_2(r-a)\}p_s/ac_2}\sqrt{\frac{Z_{s2,\infty}}{(B_{s1}^2+B_{s2}^2)\Gamma_s}}\\
&\qquad\cdot\sin\Big[\Big\{t-c_2(r-a)\Big\}q_s/ac_2+\zeta_{s2,\infty}-\tan^{-1}(B_{s2}/B_{s1})-\gamma_s\Big],\\
&\qquad\qquad\qquad\qquad\qquad\qquad\Big[\Big\{t-c_2(r-a)\Big\}>0\Big]\\
&\qquad=0,\qquad\qquad\qquad\qquad\quad\Big[\Big\{t-c_2(r-a)\Big\}<0\Big]
\end{aligned}\right\}\quad(40)$$

The results of numerical calculation for u_{01}, u'_{01}, u_{02}, u'_{02}, u_{f1}, u_{f2}, v_{01}, v'_{01}, v_{02}, v'_{02}, v_{f1}, v_{f2}, and also for $u_{01}+u'_{01}$, $u_{01}+u'_{01}+u_{f1}$, $u_{02}+u'_{02}$, $u_{02}+u'_{02}+u_{f2}$, $v_{01}+v'_{01}$, $v_{01}+v'_{01}+v_{f1}$, $v_{02}+v'_{02}$, $v_{02}+v'_{02}+v_{f2}$, all at $r=a$, are shown in Figs. 7, 8. The curves with full and broken lines and also with thick and thin lines, and the underlining of special cases of the curves follow the same rule as in the previous section. It will be seen that, with time increase, the displacements of forced waves of the first kind, namely, u_{01}, u_{02}, v_{01}, v_{02}, both in dilatational waves and distortional waves, augment without limit, while those of forced waves of the second kind, namely, u'_{01}, u'_{02}, v'_{01}, v'_{02} oscillate periodically with curves of sine form, tending to assume given amplitudes. The displacements of free waves, namely, u_{f1}, u_{f2}, v_{f1}, v_{f2}, on the other hand, diminish

with time increase. From these conditions, the resultants $u_{01}+u'_{01}$, $u_{02}+u'_{02}$, $v_{01}+v'_{01}$, $v_{02}+v'_{02}$, and also $u_{01}+u'_{01}+u_{f1}$, $u_{02}+u'_{02}+u_{f2}$, $v_{01}+v'_{01}+v_{f1}$,

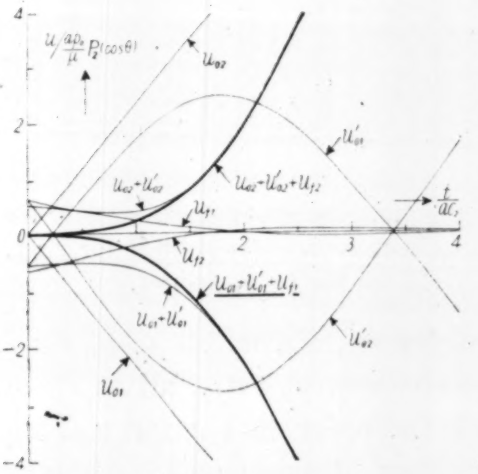

Fig. 7. Displacements for u's at $r=a$. $f(t)=p_0 \sin\beta t$ for $t>0$, $f(t)=0$ for $t<0$, $\beta ac_2=1$.

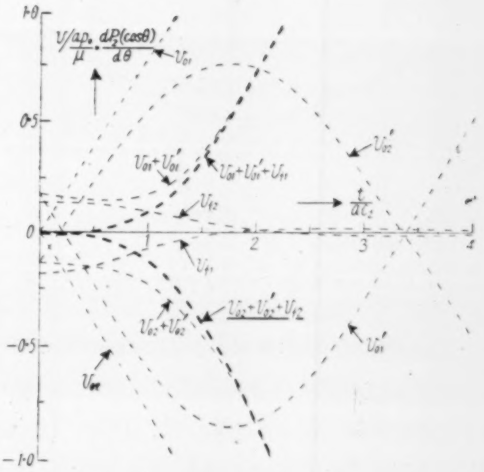

Fig. 8. Displacements for v's at $r=a$. $f(t)=p_0 \sin\beta t$ for $t>0$, $f(t)=0$ for $t<0$, $\beta ac_2=1$.

$v_{02}+v'_{02}+v_{f2}$, tend to diverge with time increase. It should be remembered that $u_{01}+u_{02}=0$, $v_{01}+v_{02}=0$ notwithstanding the diverging nature of each term in u_{01}, u_{02}, v_{01}, v_{02}.

The reason that the displacements last given have a diverging nature is the same as that given in the preceding section. In the present case, however, the displacements of forced waves of the second kind, that is, u'_{01}, u'_{02}, v'_{01}, v'_{02}, agree with the pressure change in the spherical origin, merely in periodic change, not in phase. Although the amplitudes of these waves are enormous, those of $u'_{01}+u'_{02}$, $v'_{01}+v'_{02}$ are not.

If we take the resultants of forced waves, say, $u_{01}+u_{02}$, $u'_{01}+u'_{02}$, $v_{01}+v_{02}$, $v'_{01}+v'_{02}$, $u_{01}+u_{02}+u'_{01}+u'_{02}$, $v_{01}+v_{02}+v'_{01}+v'_{02}$, the displacements never diverge. The values of $u_{01}+u'_{01}+u_{02}+u'_{02}$, $v_{01}+v'_{01}+v_{02}+v'_{02}$, together with $u_{f1}+u_{f2}$, $v_{f1}+v_{f2}$, $u_{01}+u'_{01}+u_{02}+u'_{02}+u_{f1}+u_{f2}$, $v_{01}+v'_{01}+v_{02}+v'_{02}+v_{f1}+v_{f2}$ are shown in Figs. 9, 10. It will be seen that the displacements of $u_{01}+u'_{01}+u_{02}+u'_{02}$, $v_{01}+v'_{01}+v_{02}+v'_{02}$ are of sine form, their amplitudes being much less than those of u'_{01}, u'_{02}, v'_{01}, v'_{02} shown in Figs. 7, 8. The resultant displacements for free waves, namely, $u_{f1}+u_{f2}$, $v_{f1}+v_{f2}$ are fairly small and, furthermore, tend to decay with time. In the present case, although $u_{01}+u'_{01}+u_{02}+u'_{02}$, $v_{01}+v'_{01}+v_{02}+v'_{02}$ do not agree with the pressure change at the spherical boundary, the resultant displacements of free waves and forced waves, namely, $u_{01}+u'_{01}+u_{02}+u'_{02}+u_{f1}+u_{f2}$, $v_{01}+v'_{01}+v_{02}+v'_{02}+v_{f1}+v_{f2}$ at $r=a$ are rather in the sense of

pressure change for initial motion as well as for motion at any time. The same conclusion applies to the case of the previous section.

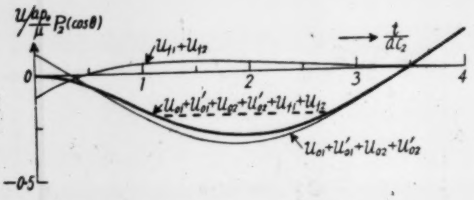

Fig. 9. Resultant displacements for u's at $r=a$. $f(t)=p_0 \sin\beta t$ for $t>0$, $f(t)=0$ for $t<0$, $\beta a c_2=1$.

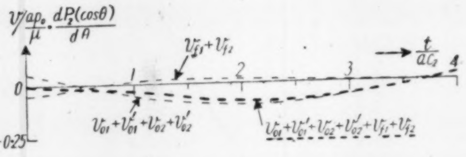

Fig. 10. Resultant displacements for v's at $r=a$. $f(t)=p_0 \sin\beta t$ for $t>0$, $f(t)=0$ for $t<0$, $\beta a c_2=1$.

The results of numerical calculation for u'_{01}, v'_{01}, u_{f1}, v_{f1}, $u'_{01}+u_{f1}$, $v'_{01}+v_{f1}$, and also for u'_{02}, v'_{02}, u_{f2}, v_{f2}, $u'_{02}+u_{f2}$, $v'_{02}+v_{f2}$, all at $r=\infty$, are shown in Figs. 11, 12. In this case the order in $1/r$ for u_{01}, v_{01}, u_{02}, v_{02} is twice as high as that for other displacements. Although

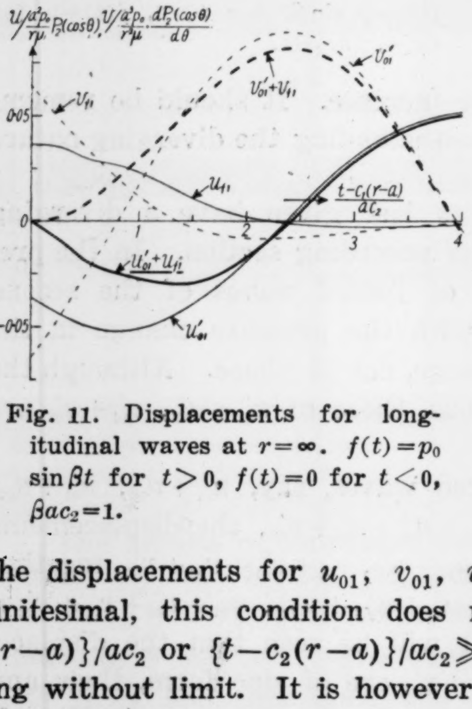

Fig. 11. Displacements for longitudinal waves at $r=\infty$. $f(t)=p_0 \sin\beta t$ for $t>0$, $f(t)=0$ for $t<0$, $\beta a c_2=1$.

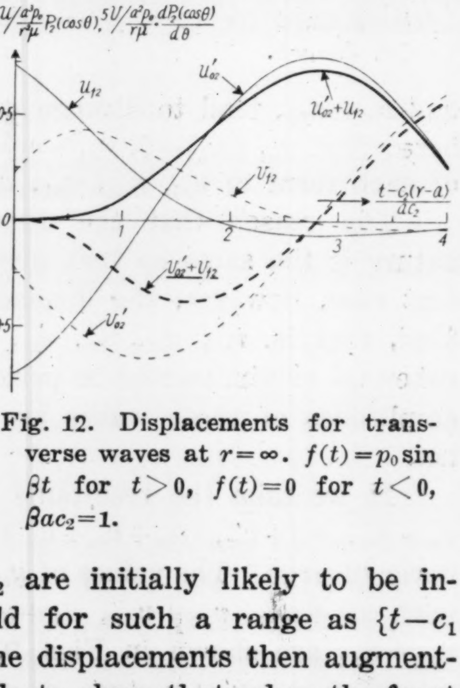

Fig. 12. Displacements for transverse waves at $r=\infty$. $f(t)=p_0 \sin \beta t$ for $t>0$, $f(t)=0$ for $t<0$, $\beta a c_2=1$.

the displacements for u_{01}, v_{01}, u_{02}, v_{02} are initially likely to be infinitesimal, this condition does not hold for such a range as $\{t-c_1(r-a)\}/ac_2$ or $\{t-c_2(r-a)\}/ac_2 \gg r/a$, the displacements then augmenting without limit. It is however possible to show that when the front of the distortional waves arrives at the diverging tail (u_{01}, v_{01}) of dilatational waves, the forced waves, u_{01}, v_{01}, cancel the forced waves, u_{02}, v_{02}. This results from the relations in (39) that $u_{01}+u_{02}=$ finite, $v_{01}+v_{02}=$ finite for $t-c_1(r-a)>0$, $t-c_2(r-a)>0$.

Upon comparing Figs. 7~12, it is possible to conclude that the initial motions at $r=\infty$ for $u_{01}+u'_{01}+u_{f1}$, $v_{01}+v'_{01}+v_{f1}$, $u_{02}+u'_{02}+u_{f2}$, $v_{02}+v'_{02}+v_{f2}$, respectively, accord with those at $r=a$ for the same components

of displacements. Of these initial motions, the components $u_{01}+u'_{01}+u_{f1}$, $v_{02}+v'_{02}+v_{f2}$ are also in the sense of pressure change at the spherical origin.

6. *Concluding remarks.*

Using operational calculus, the problem of transmission of arbitrary elastic waves generated from a spherical origin in the case of spheroidal vibration of the order $n=2$, is solved. Although the type of forced waves agrees with the form of the exciting forces to a certain extent, that of the free waves, particularly in vibrational period and damping, depends on the size of the origin. In the present investigation, such period and damping are ascertained fairly accurately, say, to four decimal places. As to the type of exciting forces, two cases, namely, that of rectangular type and that of sine type, both beginning from a quiescent state, have been examined.

Let u_{01}, v_{01}; u_{f1}, v_{f1}; u_{02}, v_{02}; u_{f2}, v_{f2} be forced waves and free waves, in dilatational waves and distortional waves, generated from the origin $r=a$. Although the initial motions of the displacements $u_{01}+u_{f1}$, $v_{01}+v_{f1}$, $u_{02}+u_{f2}$, $v_{02}+v_{f2}$ at $r=a$ conform with those of the same displacements at $r=\infty$, all these motions do not necessarily agree with pressure change at the spherical source. The initial motions of the displacements $u_{01}+u_{f1}$, $v_{02}+v_{f2}$ at $r=a$ and $r=\infty$ are only in the sense of pressure change at the origin $r=a$ in question. On the other hand, the resultant displacements consisting of free waves as well as forced waves, namely, $u_{01}+u_{f1}+u_{02}+u_{f2}$, $v_{01}+v_{f1}+v_{02}+v_{f2}$ at $r=a$, are always in the sense of pressure change at the origin, not only for initial motion but also for motion at any time.

The tails of forced waves, both in dilatational waves and distortional waves, tend to augment increasingly, although the amplitudes are infinitesimal. However, the tail of forced waves accompanying the dilatational waves, and which once tended to augment before the arrival of distortional waves, converges immediately with the arrival of the latter waves.

In conclusion, we wish to express our thanks to Mr. Watanabe, who assisted us greatly in our calculations. We also wish to thank the officials of the Division of Scientific Research, in the Ministry of Education, for financial aid (Scientific Research Expenditure) granted us for a series of investigation, of which this study is a part.

23. 演算法を應用せる任意形彈性波の傳播の問題 (第2報)

地震研究所 {妹澤克惟 / 金井清}

球形源に於て $n=2$ の球狀振動が行はれる場合の彈性波傳播の問題を取扱つた．强制波の型はある程度まで强制力のそれと一致するけれども自由波の型，特にその振動數と減衰係數とは球形源の大さに關係する．只今の問題ではこの振動數と減衰係數とを少數點以下4位まで確めた．强制力の型として矩形及び正弦形を用ひ，且つ何れも不動狀態から始まる場合を考へた．

u_{01}, v_{01}; u_{f1}, v_{f1}; u_{02}, v_{02}; u_{f2}, v_{f2} を夫々源點から出た縱波及橫波に於ける强制波と自由波とする．$r=a$ に於ける $u_{01}+u_{f1}$, $v_{01}+v_{f1}$, $u_{02}+u_{f2}$, $v_{02}+v_{f2}$ なる變位は $r=\infty$ に於けるそれ等の變位と一致するけれども，之等は $r=a$ に於ける壓力變化とは必しも一致しない．しかし $r=a$ に於ける合變位 $u_{01}+u_{f1}+u_{02}+u_{f2}$, $v_{01}+v_{f1}+v_{02}+v_{f2}$ は $r=a$ に於ける壓力變化と常に一致する．而も之等は初動のみでなく任意の時刻に於ても同方向を取る．又，初動のみを取つて考へると $r=a$ に於ける $u_{01}+u_{f1}$, $v_{02}+v_{f2}$ は $r=\infty$ に於ける夫等と共に $r=a$ に於ける壓力變化と常に一致する．

縱波に於ける强制波の尾部はその振動が無限小であるとはいへ少しづつ增大する．しかし橫波の初まりが來るとこの尾部は橫波の强制波と打消し合つて非常に小さくなる．

24. *On the Initial Movement of a Seismograph subjected to an Arbitrary Earthquake Motion, Solved with Operational Calculus. II.*

By Katsutada SEZAWA and Kiyoshi KANAI,

Earthquake Research Institute.

(Read June 19, 1941.—Received June 20, 1941.)

1. *Introduction.*

In the previous paper,[1] by using operational calculus, we calculated the type of movement of a seismograph subjected to an arbitrary earthquake motion. The result showed that the motion of the pendulum, generally, consists of two parts, one of which corresponds to forced oscillation and the other to free oscillation. In any case, the initial motion of the pendulum is in the sense opposite to that of the ground motion. In the case of a displacement seismometer, the motion of the pendulum fairly agrees with that of the ground, whereas in the acceleration seismometer it does not. Should the disturbance be sudden, the initial displacement of the seismometer will be the same as that of the ground, but in opposite sense.

In the previous paper, four cases of the ground movements were discussed, namely, (1) constant displacement, (2) sine motion, (3) exponential motion, and (4) damped sine motion, in all of which the motion begins from zero displacement and with zero velocity. In the present paper, we shall examine more complex cases such as that of constant displacement after passing through a certain transition period or a repetition of such constant displacement, in addition to which model experiments corresponding to some of the cases shown in the previous paper, will be investigated.

As shown in the previous paper, if $\phi(t)$ be the operational form of the ground motion ξ, the movement of the pendulum for zero initial displacement and zero initial velocity is expressed by

1) K. SEZAWA and K. KANAI, "On the Initial Movement of a Seismograph subjected to an Arbitrary Earthquake Motion, Solved with Operational Calculus. I," *Bull. Earthq. Res. Inst.*, **19** (1941), 162~176.

$$x=\frac{1}{2\pi i}\int_{c-i\infty}^{c+i\infty}\frac{-z\phi(z)e^{zt}dz}{z^2+2kz+n^2}. \qquad \text{(a)}$$

Using an equation of this type, the various cases will now be discussed.

2. *The special case,* $\xi=0$ *for* $t<0$, $\xi=t/h$ *for* $0<t<h$, *and* $\xi=\{t/h-(t-h)/h\}$ *for* $t>h$.

The ground motion in this case is of the type shown in Fig. 1. The operational forms (or Laplacian transforms) of the same motion are given by

Fig. 1.

$$\left.\begin{aligned}&\phi(t)=0 \text{ for } t<0,\\ &\phi(t)=\frac{1}{hz} \text{ for } 0<t<h,\\ &\phi(t)=\frac{1}{hz}-\frac{e^{-hz}}{hz} \text{ for } t>h.\end{aligned}\right\} \qquad (1)$$

The interpretation of the operational form for the pendulum motion is therefore

$$\left.\begin{aligned}&x=0, && (t<0)\\ &x=\frac{-1}{2\pi ih}\int_{c-i\infty}^{c+i\infty}\frac{e^{zt}dz}{\left\{z+(k-i\sqrt{n^2-k^2})\right\}\left\{z+(k+i\sqrt{n^2-k^2})\right\}}, && (0<t<h)\\ &x=\frac{-1}{2\pi ih}\int_{c-i\infty}^{c+i\infty}\frac{\{e^{zt}-e^{z(t-h)}\}dz}{\left\{z+(k-i\sqrt{n^2-k^2})\right\}\left\{z+(k+i\sqrt{n^2-k^2})\right\}}. && (t>h)\end{aligned}\right\} \qquad (2)$$

Evaluating these integrals, we get

$$\left.\begin{aligned}&x=0, && (t<0)\\ &x=\frac{-e^{-kt}\sin\sqrt{n^2-k^2}\,t}{h\sqrt{n^2-k^2}}, && (0<t<h)\\ &x=\frac{-e^{-kt}\sin\sqrt{n^2-k^2}\,t}{h\sqrt{n^2-k^2}}+\frac{e^{-k(t-h)}\sin\sqrt{n^2-k^2}\,(t-h)}{h\sqrt{n^2-k^2}}. && (t>h)\end{aligned}\right\} \qquad (3)$$

In the special case in which the damping is critical, namely, $k=n$, the contour integrals differ somewhat, the results being

$$\left.\begin{aligned} &x=0, && (t<0)\\ &x=\frac{-1}{2\pi ih}\int_{c-i\infty}^{c+i\infty}\frac{e^{zt}dz}{(z+n)^2}=\frac{-te^{-nt}}{h}, && (0<t<h)\\ &x=\frac{-1}{2\pi ih}\int_{c-i\infty}^{c+i\infty}\left\{\frac{e^{zt}}{(z+n)^2}-\frac{e^{z(t-h)}}{(z+n)^2}\right\}dz=\frac{-te^{-nt}}{h}+\frac{(t-h)e^{-n(t-h)}}{h}. && (t>h) \end{aligned}\right\} \quad (4)$$

If there is no damping resistance, the displacement for $t>h$ is expressed by $x=-(2/hn)\cos n(t-h/2)\sin nh/2$, so that the displacement for $t>h$ becomes maximum when $nh/2=\tan nh/2$. For a large value of $nh/2$, this condition is satisfied by $nh/2=(2m+1)\pi/2$. The displacement of the greatest maximum occurs for $nh=0$, the value of which maximum is unity. The results of numerical calculation for $nh/2\pi=1/4$, $1/2$, $2/4$, 1 are shown in Figs. 2~5. It will be seen that within the range of cal-

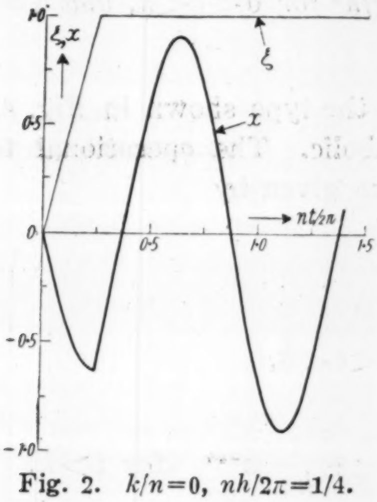

Fig. 2. $k/n=0$, $nh/2\pi=1/4$.

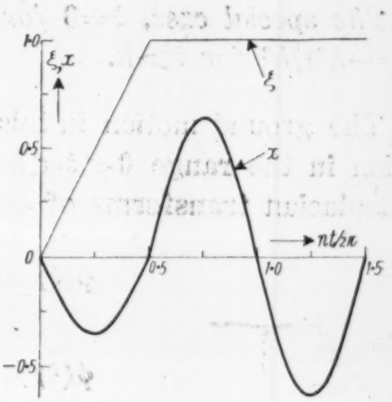

Fig. 3. $k/n=0$, $nh/2\pi=1/2$.

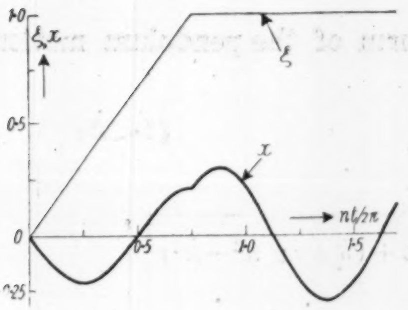

Fig. 4. $k/n=0$, $nh/2\pi=3/4$.

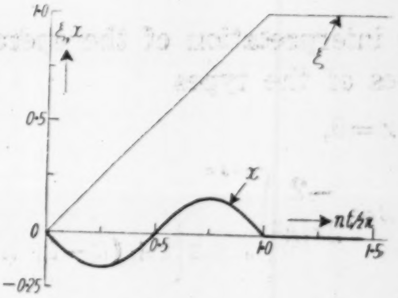

Fig. 5. $k/n=0$, $nh/2\pi=1$.

culation, the smaller the value of $nh/2$, the greater the displacement of the pendulum for $t>h$. When $nh/2\pi=1$, the displacement in question becomes zero.

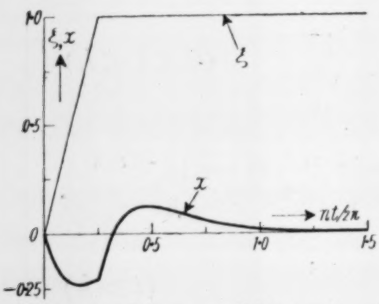

Fig. 6. $k/n=1$, $nh/2\pi=1/4$.

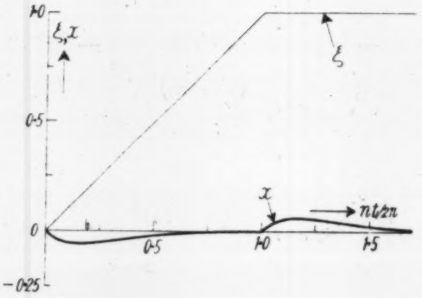

Fig. 7. $k/n=1$, $nh/2\pi=1$.

If there were damping resistance, the feature of the pendulum vibration would alter considerably. The results of calculation for $nh/2\pi=1/4$, $nh/2\pi=1$, both in the case of critical damping, are shown in Figs. 6, 7. In this case, even if $nh/2\pi=1$, the displacement for $t>h$ is not zero.

3. *The special case, $\xi=0$ for $t<0$, $\xi=t^2/h^2$ for $0<t<h$, and $\xi=t^2/h^2-(t^2-h^2)/h^2$ for $t>h$.*

The ground motion in this case is of the type shown in Fig. 8, the motion in the range $0<t<h$ being parabolic. The operational forms of Laplacian transforms of the motion are given by

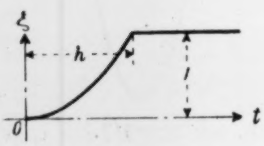

Fig. 8.

$$\left.\begin{aligned} &\phi(t)=0 \quad \text{for } t<0, \\ &\phi(t)=\frac{2}{h^2z^2} \quad \text{for } 0<t<h, \\ &\phi(t)=\frac{2}{h^2z^2}-2\left(\frac{1}{h^2z^2}+\frac{1}{hz}\right)e^{-zh} \quad \text{for } t>h. \end{aligned}\right\} \quad (5)$$

The interpretation of the operational form of the pendulum motion becomes of the types

$$\left.\begin{aligned} &x=0, && (t<0) \\ &x=\frac{-2}{2\pi ih^2}\int_{c-i\infty}^{c+i\infty}\frac{e^{zt}dz}{z\left\{z+(k-i\sqrt{n^2-k^2})\right\}\left\{z+(k+i\sqrt{n^2-k^2})\right\}}, && \\ & && (0<t<h) \end{aligned}\right\} \quad (6)$$

$$x=\frac{-2}{2\pi ih^2}\int_{c-i\infty}^{c+i\infty}\left\{\frac{e^{zt}}{z(z+\alpha)(z+\beta)}-\frac{(1/z+h)e^{z(t-h)}}{(z+\alpha)(z+\beta)}\right\}dz. \quad (t>h)$$
$$(\alpha=k-i\sqrt{n^2-k^2},\quad \beta=k+i\sqrt{n^2-k^2})$$

Evaluating these integrals, we get

$$\left.\begin{aligned}
&x=0, && (t<0)\\
&x=\frac{2}{h^2n^2\sqrt{n^2-k^2}}\Big[-\sqrt{n^2-k^2}\\
&\quad +ne^{-kt}\sin\left\{\sqrt{n^2-k^2}\,t+\tan^{-1}(\sqrt{n^2-k^2}/k)\right\}\Big], && (0<t<h)\\
&x=\frac{2}{h^2n\sqrt{n^2-k^2}}\Big[e^{-kt}\sin\left\{\sqrt{n^2-k^2}\,t+\tan^{-1}(\sqrt{n^2-k^2}/k)\right\}\\
&\quad -e^{-k(t-h)}\sin\left\{\sqrt{n^2-k^2}(t-h)+\tan^{-1}(\sqrt{n^2-k^2}/k)\right\}\\
&\quad +hne^{-k(t-h)}\sin\sqrt{n^2-k^2}(t-h)\Big]. && (t>h)
\end{aligned}\right\} \quad (7)$$

In the special case that the damping is critical, namely, $k=n$, the contour integrals assume such a variety of forms as

$$\left.\begin{aligned}
&x=0, && (t<0)\\
&x=\frac{-2}{2\pi ih^2n^2}\int_{c-i\infty}^{c+i\infty}\left\{\frac{e^{zt}}{z}-\frac{(z+2n)e^{zt}}{(z+n)^2}\right\}dz, && (0<t<h)\\
&x=\frac{-2}{2\pi ih^2n^2}\int_{c-i\infty}^{c+i\infty}\Big[\left\{\frac{e^{zt}}{z}-\frac{(z+2n)e^{zt}}{(z+n)^2}\right\}\\
&\quad -\left\{\frac{e^{z(t-h)}}{z}-\frac{(z+2n+n^2h)e^{z(t-h)}}{(z+n)^2}\right\}\Big]dz, && (t>h)
\end{aligned}\right\} \quad (8)$$

the results of which integration are

$$x=0, \quad (t<0)$$
$$x=(2/h^2n^2)\left\{-1+(1+nt)e^{-nt}\right\}, \quad (0<t<h)$$

$$x=(2/h^2n^2)\left[(1+nt)e^{-nt}+\left\{n(hn-1)(t-h)-1\right\}e^{-n(t-h)}\right]. \quad (t>h) \qquad (9)$$

When $k=0$, the displacement for $t>0$ is expressed by

$$\left.\begin{aligned} x=\frac{2}{n^2h^2}\sqrt{(1-\cos nh-nh\sin nh)^2+(\sin nh-nh\cos nh)^2} \\ \cdot\cos\left\{nt+\tan^{-1}\left(\frac{\sin nh-nh\cos nh}{1-\cos nh-nh\sin nh}\right)\right\}, \end{aligned}\right\} \qquad (10)$$

which is maximum when $nh/2=\tan(nh/2)$. For a large value of $nh/2$, this condition is satisfied by $nh/2=(2m+1)\pi/2$. The greatest maximum occurs when $nh=0$, the value of the maximum then being unity. The

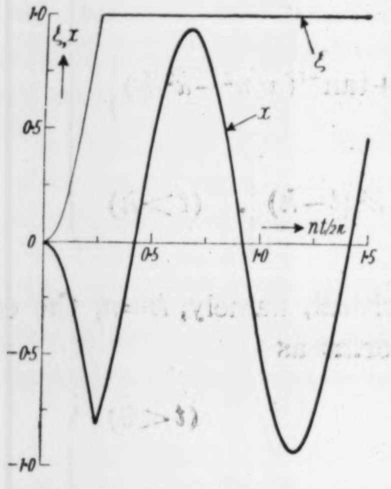

Fig. 9. $k/n=0$, $nh/2\pi=1/4$.

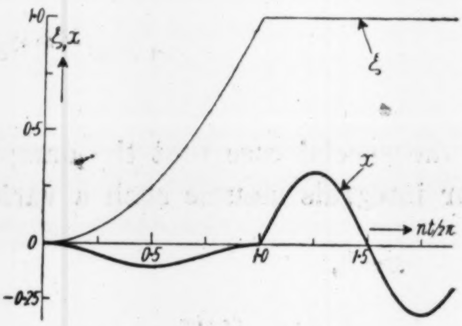

Fig. 10. $k/n=0$, $nh/2\pi=1$.

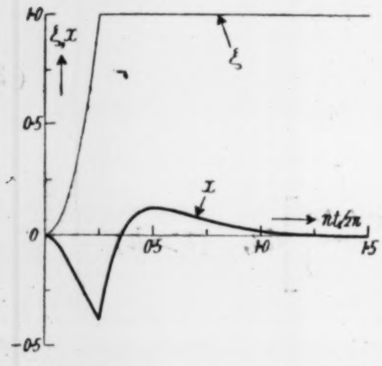

Fig. 11. $k/n=1$, $nh/2\pi=1/4$.

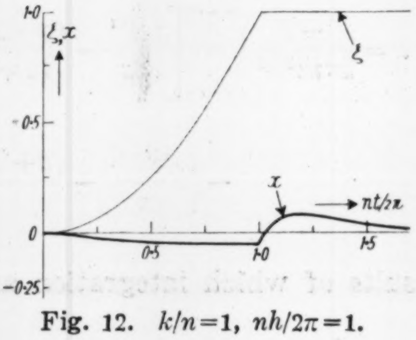

Fig. 12. $k/n=1$, $nh/2\pi=1$.

results of numerical calculation for four cases, (i) $k/n=0$, $nh/2\pi=1/4$, (ii) $k/n=0$, $nh/2\pi=1$, (iii) $k/n=1$, $nh/2\pi=1/4$, (iv) $k/n=1$, $nh/2\pi=1$, are shown in Figs. 9~12. It will be seen that although the vibrational

nature of the range $t>h$ does not differ much from that for the same range in that case treated in the previous section, the displacement for the range, $0<t<h$, in the present case is, generally, relatively small. This arises from the condition that the ground motion at $t=0$ begins from zero displacement and with zero velocity, although the motion in the range, $0<t<h$, is of uniform acceleration. In the case of the previous section, although the motion in the range, $0<t<h$, was of zero acceleration, that at $t=0$ did not begin with zero velocity.

4. *The special case,* $\xi=0$ *for* $t<0$, $\xi=1$ *for* $2mh<t<(2m+1)h$, $\xi=-1$ *for* $(2m+1)h<t<2(m+1)h$. $(m=0,\ 1,\ 2,\cdots,\ \infty)$.

The ground motion in this case is of the type shown in Fig. 13. The operational forms of the ground motion were shown in the previous paper. When the ground motion, as shown in the sketch, is repeated indefinitely, the pendulum motion for $t=\infty$ becomes

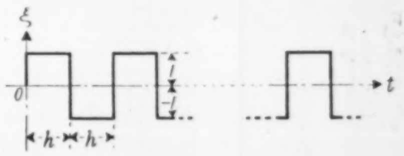

Fig. 13.

$$x=\frac{-1}{2\pi i}\int_{c-i\infty}^{c+i\infty}\frac{ze^{zt}\left\{1-2e^{-zh}+2e^{-2zh}\cdots\cdots+2(-1)^{s}e^{-szh}\cdots\cdots\right\}dz}{(z+k-ia)(z+k+ia)}$$

$$=\frac{-1}{2\pi i}\int_{c-i\infty}^{c+i\infty}\frac{ze^{zt}\sinh(zh/2)\,dz}{(z+k-ia)(z+k+ia)\cosh(zh/2)}.\quad (t=\infty)\qquad (11)$$

The poles of the integrand are obtained by equating the denominator of the same integrand to zero, the poles thus determined being

$$z=\pm\frac{i(2m+1)\pi}{h},\quad z=-k\pm ia.$$

Calculating the residues corresponding to all poles, we get

$$x=\sum_{m=0}^{\infty}\frac{4(2m+1)\pi}{\Psi}\sin\left[\frac{(2m+1)\pi t}{h}-\tan^{-1}\left\{\frac{(2m+1)\pi-ah}{kh}\right\}\right.$$

$$\left.-\tan^{-1}\left\{\frac{(2m+1)\pi+ah}{kh}\right\}\right]+\frac{ne^{-kt}}{\Phi}\left[\sinh(hk/2)\cosh(hk/2)\sin\left\{at\right.\right.$$

$$\left.\left.-\tan^{-1}(a/k)\right\}-\sin(ha/2)\cos(ha/2)\cos\left\{at-\tan^{-1}(a/k)\right\}\right],$$

$$\left[R(t-\infty)>0\right]\qquad (12)$$

where

$$\Psi=\sqrt{\left[(kh)^2+\left\{(2m+1)\pi-\alpha h\right\}^2\right]\left[(kh)^2+\left\{(2m+1)\pi+\alpha h\right\}^2\right]},$$

$$\Phi=\alpha\left\{\cosh^2(hk/2)\cos^2(h\alpha/2)+\sinh^2(hk/2)\sin^2(h\alpha/2)\right\},\quad \alpha=\sqrt{n^2-k^2}. \tag{13}$$

The first term in (12) represents the forced oscillation and the second gives the free oscillation.

When $k=0$, the value of x reduces to

$$x=-\sum_{m=0}^{\infty}\frac{4(2m+1)\pi\sin\left\{(2m+1)\pi t/h\right\}}{\left\{(2m+1)\pi-nh\right\}\left\{(2m+1)\pi+nh\right\}}-\tan(nh/2)\sin nt. \tag{14}$$

When $nh/2=\pi/2$, $3\pi/2$, ..., both terms in (14) tend to infinitely large values, the condition being then in resonance. It will be seen that the forced oscillation and free oscillation both contribute to the resonance condition. It should be remembered that such resonance condition occurs only when $t\to\infty$, whence for the amplitude to become very large for a small value of t, is improbable.

5. *The special case,* $\xi=0$ *for* $t<0$, $\xi=\left\{t-(4m-1)h\right\}/h-1$ *for* $(4m-1)h/2<t<(4m+1)h/2$, *and* $\xi=1-\left\{t-(4m+1)h\right\}/h$ *for* $(4m+1)h/2<t<(4m+3)h/2$.

The ground motion is of the type shown in Fig. 14, its expression for $t\to\infty$ being

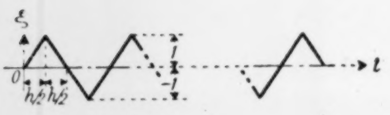

Fig. 14.

$$\xi=2\left\{\frac{t}{h}-\frac{2(t-h)}{h}+\frac{2(t-3h)}{h}-\frac{2(t-5h)}{h}+\cdots\cdots\right\}, \tag{15}$$

the operational form of which is

$$\xi\supset\frac{2}{h}\left\{\frac{1}{z}+\frac{2}{z}\sum_{m=1}^{\infty}(-1)^m e^{-(2m-1)zh/2}\right\}, \tag{16}$$

so that the pendulum motion becomes

$$x=\frac{-1}{2\pi i}\int_{c-i\infty}^{c+i\infty}\frac{2e^{zt}(1-2e^{-zh}+2e^{-3zh}-2e^{-5zh}+\cdots)dz}{h(z+k-ia)(z+k+ia)}$$

$$=\frac{-1}{2\pi i}\int_{c-i\infty}^{c+i\infty}\frac{2e^{zt}\left\{1-\dfrac{2}{\cosh(zh/2)}\right\}dz}{h(z+k-ia)(z+k+ia)}. \qquad (t=\infty) \qquad (17)$$

The contour integral will be evaluated in the same way as in the preceding section. The result of integration gives

$$x=16\sum_{m=0}^{\infty}$$

$$\cdot\frac{(-1)^m\cos\left[\dfrac{(2m+1)\pi t}{h}-\tan^{-1}\left\{\dfrac{(2m+1)\pi-ah}{kh}\right\}-\tan^{-1}\left\{\dfrac{(2m+1)\pi+ah}{kh}\right\}\right]}{\sqrt{\left[(kh)^2+\left\{(2m+1)\pi-ah\right\}^2\right]\left[(kh)^2+\left\{(2m+1)\pi+ah\right\}^2\right]}}$$

$$+\frac{2e^{-kt}}{ah}\left\{\sin at\right.$$

$$\left.-\frac{\cos at\sinh(kh/2)\sin(ah/2)+\sin at\cosh(kh/2)\cos(ah/2)}{\left\{\cosh(kh/2)\cos(ah/2)\right\}^2+\left\{\sinh(kh/2)\sin(ah/2)\right\}^2}\right\},$$

$$\left[R(t-\infty)>0\right] \qquad (18)$$

where $a=\sqrt{n^2-k^2}$. In this case, too, the first and second terms represent the forced and free oscillations, respectively.

When there is no damping, namely, $k=0$, the equation for x reduces to

$$x=-16\sum_{m=0}^{\infty}\frac{(-1)^m\cos\left\{(2m+1)\pi t/h\right\}}{\left\{(2m+1)\pi-nh\right\}\left\{(2m+1)\pi+nh\right\}}-\frac{4\sin^2(nh/4)\sin nt}{nh\cos(nh/2)}. \qquad (19)$$

Thus, the pendulum motion is in resonance when $nh/2=\pi/2,\ 3\pi/2,\cdots$. In this case there is also the restriction that $t\to\infty$.

6. *The special case,* $\xi=0$ *for* $t<0$, $\xi=(t-2mh)/2h$ *for* $2mh<t<2(m+1)h$.

The ground motion is of the type shown in Fig. 15. The operational form (or Laplacian transform) of the same motion for $t\to\infty$ is

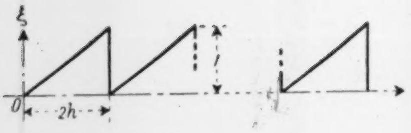

Fig. 15.

$$\xi \supset \frac{1}{2hz}-\sum_{m=1}^{\infty}e^{-2mhz}, \tag{20}$$

so that the pendulum motion becomes

$$x=\frac{-1}{2\pi i}\int_{c-i\infty}^{c+i\infty}\frac{e^{zt}\{1/2h-ze^{-2hz}-ze^{-4hz}-\cdots\cdots\}dz}{(z+k-ia)(z+k+ia)}$$

$$=\frac{-1}{2\pi i}\int_{c-i\infty}^{c+i\infty}\left\{\frac{1}{2h}-\frac{ze^{-hz}}{2\sinh hz}\right\}\frac{e^{zt}dz}{(z+k-ia)(z+k+ia)}. \quad (t=\infty) \tag{21}$$

In this case, we have the poles of $1/\sinh hz$ when

$$hz=0,\quad i\pi,\quad 2i\pi,\quad 3i\pi\cdots\cdots,$$

from which the integral for x becomes

$$x=-\sum_{m=0}^{\infty}\frac{(-1)^{m+1}(m+1)\pi}{\Psi}\sin\left[\frac{(m+1)\pi(t-h)}{h}-\tan^{-1}\left\{\frac{(m+1)\pi-ah}{kh}\right\}\right.$$

$$\left.-\tan^{-1}\left\{\frac{(m+1)\pi+ah}{kh}\right\}\right]+\frac{e^{-kt}}{2ha}\left\{-\sin at+he^{hk}\Phi^{-1}\Big[\sinh kh\cos ah\right.$$

$$\cdot\Big\{k\sin a(t-h)-a\cos a(t-h)\Big\}+\cosh kh\sin ah\Big\{k\cos a(t-h)$$

$$\left.+a\sin a(t-h)\Big\}\Big]\right\}. \qquad \Big[R(t-\infty)>0\Big] \tag{22}$$

where

$$\left.\begin{aligned}\Psi&=\sqrt{\Big[(kh)^2+\Big\{(m+1)\pi-ah\Big\}^2\Big]\Big[(kh)^2+\Big\{(m+1)\pi+ah\Big\}^2\Big]},\\ \Phi&=\sinh^2 kh\cos^2 ah+\cosh^2 kh\sin^2 ah, \qquad a=\sqrt{n^2-k^2}.\end{aligned}\right\} \tag{23}$$

The first and second terms correspond to the forced and free oscillations, respectively.

When $k=0$, the value of x reduces to

$$x=\sum_{m=0}^{\infty}\frac{(-1)^{m+1}(m+1)\pi\sin\Big\{(m+1)\pi(t-h)/h\Big\}}{\Big\{(m+1)\pi-nh\Big\}\Big\{(m+1)\pi+nh\Big\}}$$

$$+\frac{1}{2hn}\left\{-\sin nt+\frac{nh\sin n(t-h)}{\sin nh}\right\}. \tag{24}$$

Resonance condition occurs when $nh/2=\pi/2,\ 3\pi/2,\ \cdots\cdots (t\rightarrow\infty)$.

7. *The special case* $\xi=0$ *for* $t<0$, $\xi=\left\{-t+2h(m+1)\right\}/2h$ *for* $2mh<t<2(m+1)h$.

The ground motion in this case is of the type shown in Fig. 16. The operational form (or Laplacian transform) of ξ for $t\rightarrow\infty$ is

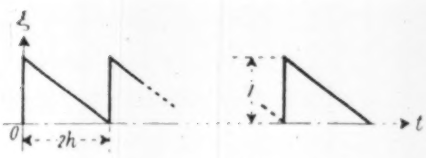

Fig. 16.

$$\xi \supset -\frac{1}{2hz}+1+\sum_{m=1}^{\infty}e^{-2mhz}. \tag{25}$$

The pendulum motion is expressed by

$$\begin{aligned} x&=\frac{-1}{2\pi i}\int_{c-i\infty}^{c+i\infty}\frac{e^{zt}z\{-1/2hz+1+e^{-2hz}+e^{-4hz}+\cdots\cdots\}dz}{(z+k-i\alpha)(z+k+i\alpha)} \\ &=\frac{-1}{2\pi i}\int_{c-i\infty}^{c+i\infty}z\left\{\frac{-1}{2hz}+\frac{e^{hz}}{2\sinh hz}\right\}\frac{e^{zt}dz}{(z+k-i\alpha)(z+k+i\alpha)},\quad (t=\infty) \end{aligned} \tag{26}$$

the integral of which is

$$\begin{aligned} x=&\sum_{m=0}^{\infty}\frac{(-1)^{m+1}(m+1)\pi}{\Psi}\sin\left[\frac{(m+1)\pi(t-h)}{h}-\tan^{-1}\left\{\frac{(m+1)\pi-\alpha h}{kh}\right\}\right. \\ &\left.-\tan^{-1}\left\{\frac{(m+1)\pi+\alpha h}{kh}\right\}\right]+\frac{e^{-kt}}{2h\alpha}\left[\sin\alpha t-h\Phi^{-1}e^{-kh}\left\{(k\cosh kh\sin\alpha h\right.\right. \\ &-\alpha\sinh kh\cos\alpha h)\cos\alpha(t+h)+(k\sinh kh\cos\alpha h \\ &\left.\left.+\alpha\cosh kh\sin\alpha h)\sin\alpha(t+h)\right\}\right],\quad \left[(R(t-\infty)>0\right] \end{aligned} \tag{27}$$

where

$$\left.\begin{aligned} &\Psi=\sqrt{\left[(kh)^2+\left\{(m+1)\pi-\alpha h\right\}^2\right]\left[(kh)^2+\left\{(m+1)\pi+\alpha h\right\}^2\right]} \\ &\Phi=\sinh^2 kh\cos^2\alpha h+\cosh^2 kh\sin^2\alpha h.\qquad \alpha=\sqrt{n^2-k^2}. \end{aligned}\right\} \tag{28}$$

When $k=0$, the value of x reduces to

$$\begin{aligned} x=&-\sum_{m=0}^{\infty}\frac{(-1)^{m+1}(m+1)\pi\sin\left\{(m+1)\pi(t+h)/h\right\}}{\left\{(m+1)\pi-nh\right\}\left\{(m+1)\pi+nh\right\}} \\ &+\frac{1}{2nh}\left\{\sin nt-\frac{hn\sin n(t+h)}{\sin nh}\right\}. \end{aligned} \tag{29}$$

Resonance condition occurs also when $nh/2=\pi/2,\ 3\pi/2,\ \cdots\cdots(t\to\infty)$.

8. *Resumé of the mathematical parts.*

Although in the case of constant displacement of the ground motion with transition period h, it is likely that maxima of the pendulum displacement occur, these maxima are not very large. Even should the movement of the ground in the transition period be linear or parabolic, the displacement of the pendulum after passing that transition period h, would be maximum when $nh/2=\tan(nh/2)$. Since the condition $nh/2=\tan(nh/2)$ applies to two different cases, the same condition would invariably hold for other motions in the transition period. For a large value of $nh/2$ this relation is satisfied by $nh/2=(2m+1)\pi/2$, —a condition quite similar to the resonance of a body with a natural period twice that of the transition period just mentioned. However, the greatest amplitude of the pendulum occurs when $nh=0$, from which it is possible to conclude that resonance conditions are not dynamic, but result from the superposed phases in the pendulum motion.

In the case of repeated displacements of the ground with initial zero displacement, the oscillation of the pendulum becomes of resonance type, the vibration being composed of free oscillation and forced oscillation even in such resonance type. This condition occurs when the ratio of the repetition period to the natural period is an odd integer. It is possible to obtain the same condition by using Fourier's analysis in the case of repetition of the ground oscillation for such time interval as $-\infty<t<\infty$. In the present case, the problem applies to the ground motion restricted to such range as $0<t<\infty$.

9. *Model experiments for confirming the mathematical results shown in the previous paper.*

Although there is no doubt of the consistency of the mathematical results shown in the previous paper, as a matter of interest, some model experiments were conducted, the vibration table being horizontal, the same as that shown in our papers[2), 3)] on the structural vibration and also on the stability of a seismometer. The driving motor with applied current, after having been kept in a quiescent state for a certain interval, was in sudden motion, which condition corresponded to the mathematically calculated case $\xi=\sin bt$ for $t>0$ and $\xi=0$ for $t<0$

2) K. KANAI and K. SEZAWA, *Bull. Earthq. Res. Inst.*, **18** (1940), 270~283.
3) *Ditto, Bull. Earthq. Res. Inst.*, **18** (1940), 483~496.

in the previous paper.[4]

The results of experiments covering four cases, (i) $k/n=0{\cdot}015$, $n/b=0{\cdot}6605$, (ii) $k/n=0{\cdot}015$, $n/b=1{\cdot}182$, (iii) $k/n=1$, $n/b=0{\cdot}714$, (iv) $k/n=1$, $n/b=2{\cdot}223$, are shown with dots in Figs. 17~20 (Plates XXXIII, XXXIV). At the same time, we calculated the same cases, mathematically, as shown in Figs. 21~24. The resultant vibrations consist-

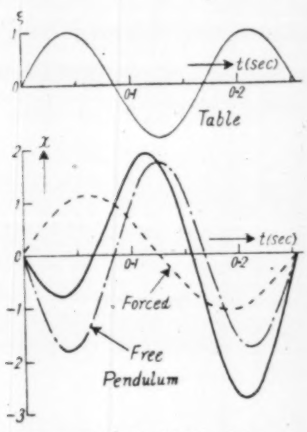

Fig. 21. $n/b=0{\cdot}6605$, $k/n=0{\cdot}015$.

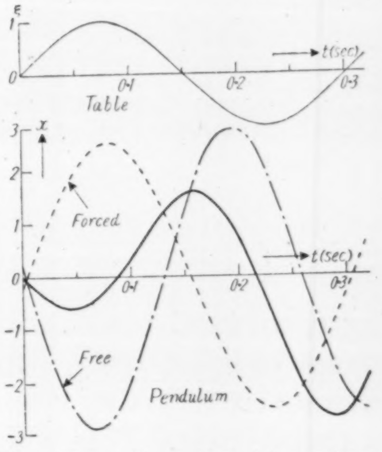

Fig. 22. $n/b=1{\cdot}182$, $k/n=0{\cdot}015$.

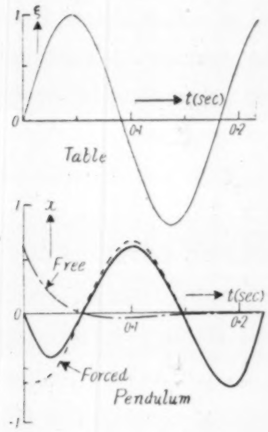

Fig. 23. $n/b=0{\cdot}714$, $k/n=1$.

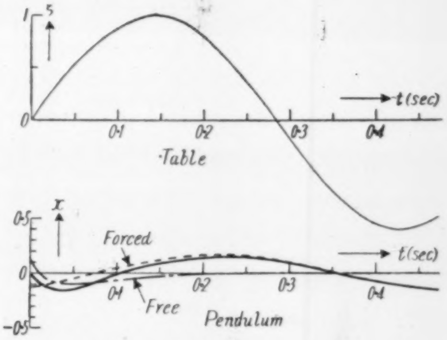

Fig. 24. $n/b=2{\cdot}223$, $k/n=1$.

ing of free and forced oscillations are shown with thick, full lines. The same resultant vibrations were replotted with full lines in Figs. 17~20. The table vibrations of pure sine form were also plotted in Figs. 17~20. It will be seen that the experimental result fairly agrees with the mathematical result. Any discordance between them is the result of the table vibration in the experiment disagreeing with that in the calculation. At all events, the greater the ratio of n/b, the better the agreement in the results of the two investigations.

4) K. SEZAWA and K. KANAI, *Bull. Earthq. Res. Inst.*, **19** (1941), 167.

Upon comparing Figs. 21∼24, it will be seen that free oscillation and forced oscillation both contributed to the motion of the pendulum. The feature of gradually increasing amplitudes of the pendulum in Figs. 17, 18 resulted from the two oscillations last given. That the amplitudes did not change much with time in cases in Figs. 19, 20, was due to the fact that forced oscillation formed the greater part of the oscillation.

As a matter of fact, although free oscillation and forced oscillation in the initial motion of the pendulum were generally of opposite senses, the resultant movement of that pendulum was always in the sense opposite to that of the ground motion.

10. *Concluding remarks.*

Using operational calculus, as shown in the previous paper, we calculated more complex cases, such as that of a constant displacement after passing through some transitional motion or repetition of such a constant displacement. It is shown that a constant displacement of the pendulum (of period $2\pi/n$) after passing a transition period h, is maximum when $nh/2=\tan nh/2$. It is likely that this condition holds for any form of the displacement in the transition period. The greatest amplitude of the pendulum, however, occurs for $nh=0$. It is possible to conclude that the resonance-like condition above given, is not dynamic, but results from the superposed phases in the pendulum motion. In the case of repeated displacements of the ground with zero initial displacement, the oscillation of the pendulum becomes of resonance type, the vibration being composed of free oscillation and forced oscillation even in such resonance condition. This condition occurs when the ratio of the repetition period to the natural period is an odd integer. Although the same condition can be obtained by using Fourier's analysis, that in the present case applies to such a case of ground motion as is restricted to the time interval $0<t<\infty$.

For confirming some of the mathematical results shown in the previous paper, merely as a matter of interest, we conducted certain model experiments, from which we found the manner in which free oscillation and forced oscillation contribute to the resultant vibration of the pendulum.

In conclusion, we wish to express our thanks to Mr. Kodaira, who assisted us greatly in our investigation, particularly in the experiments. We also wish to express our sincere thanks to the officials of the Division

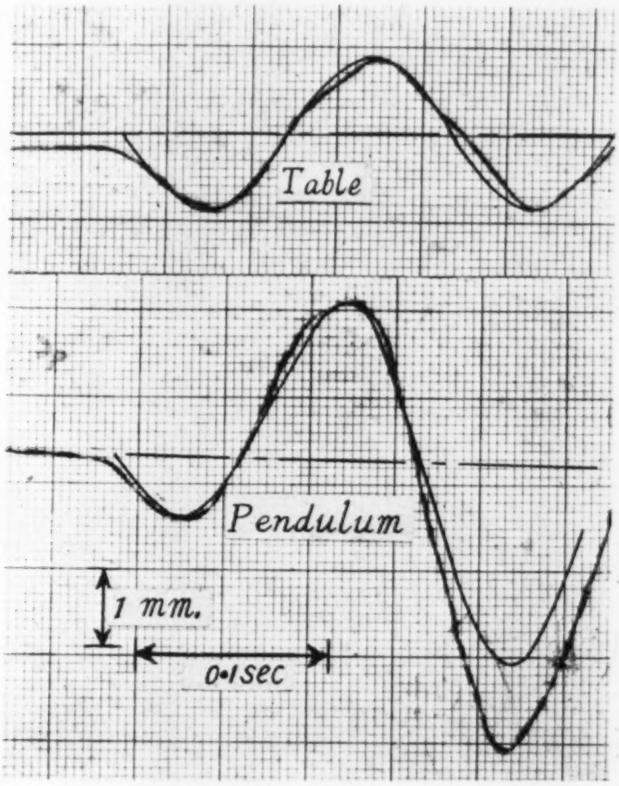

Fig. 17. $n=24{\cdot}57$, $b=37{\cdot}2$, $k=0{\cdot}3685$, $n/b=0{\cdot}6605$, $k/n=0{\cdot}015$.

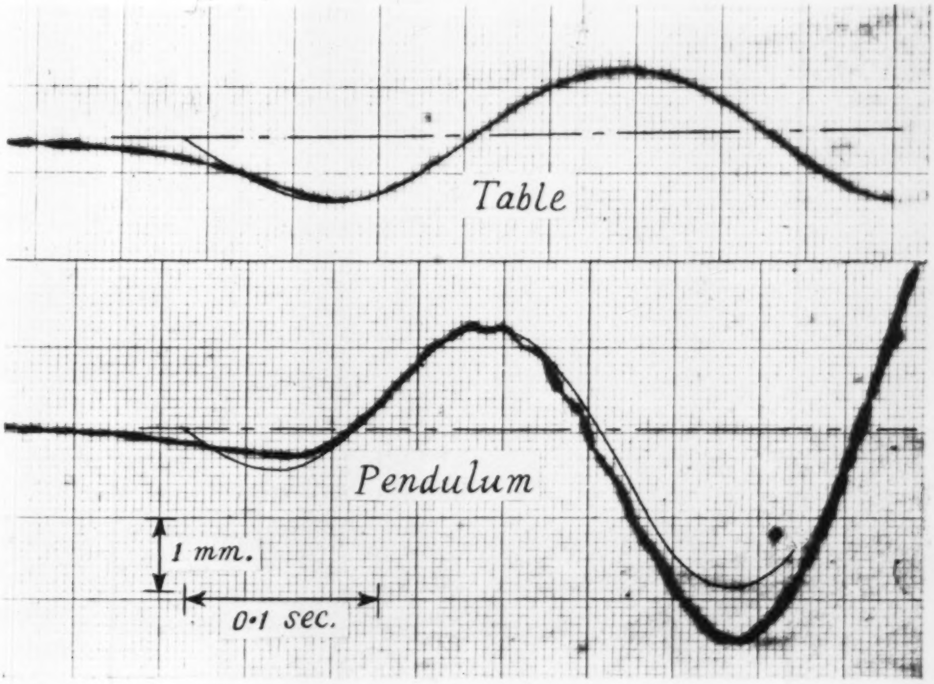

Fig. 18. $n=24{\cdot}57$, $b=20{\cdot}79$, $k=0{\cdot}3685$, $n/b=1{\cdot}182$, $k/n=0{\cdot}015$.

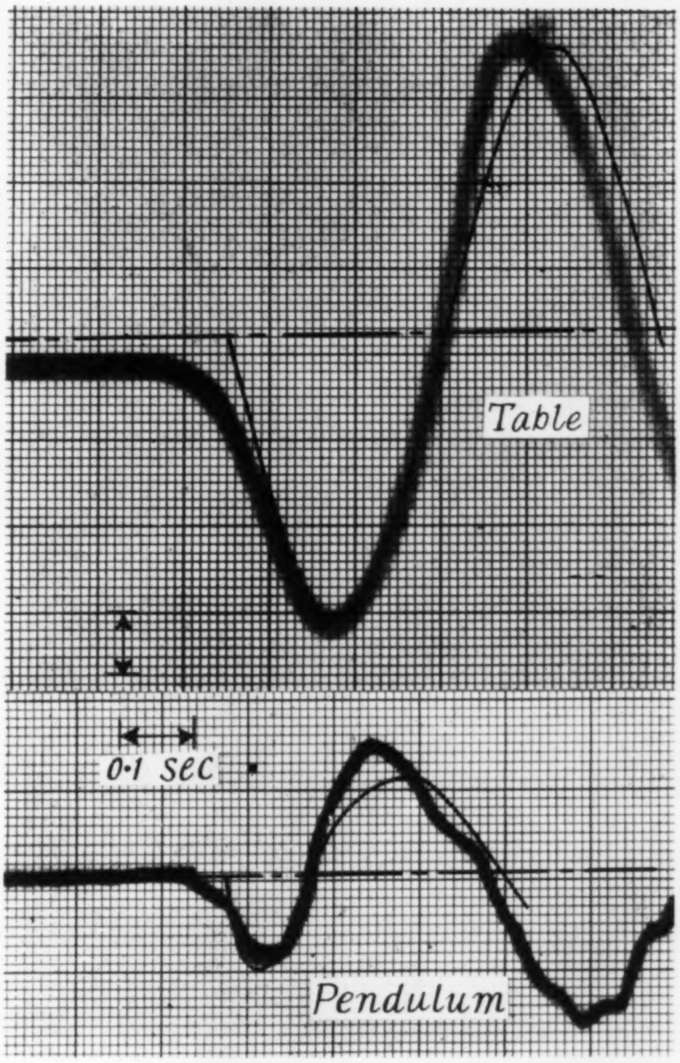

Fig. 19. $n=24{\cdot}57$, $b=11{\cdot}05$, $k=24{\cdot}6$, $n/b=2{\cdot}223$, $k/n=1$.

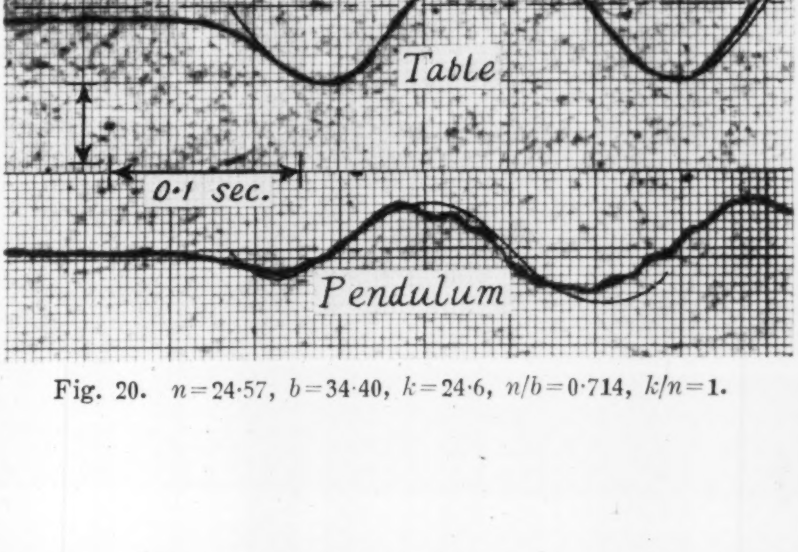

Fig. 20. $n=24{\cdot}57$, $b=34{\cdot}40$, $k=24{\cdot}6$, $n/b=0{\cdot}714$, $k/n=1$.

of Scientific Research, in the Ministry of Education, for financial aid (the Scientific Research Expenditure) granted us for a series of investigation, of which this study is a part.

---

24. 演算法によりて解いた地震計の初動問題について（第2報）

地震研究所 妹澤克惟
金井清

前報告の續きとして少しく複雜なる場合，卽ち地動が一定の過渡的運動の後に一定の變位狀態になる場合や，このやうな一定變位が繰返される場合を研究した．過渡的運動に要する時間を h とし地震計の週期を $2\pi/n$ とすれば，$nh/2=\tan nh/2$ なる關係のときに過渡的運動後の地震計の振幅が極大となるが，その最大振幅は $nh=0$ のときに起る．從てここに擧げた共振的の運動は力學上のそれでなく，單に振子の運動の位相の關係から起るものに過ぎない．最初不動狀態から始まつた地動の變位が繰返して行はれる場合には振子が遂に共振狀態に入る．而も之は强制振動と自由振動とから成立ち，何れも大振幅となるのである．强制振動のみの場合にはフーリエ分析でも出す事ができるけれども不動狀態から始まる場合には只今の方法の方が便利である．

前回の報告で出した數理的結果の一部分を單に興味上から模型實驗でためして見た，之によつて振子の自己振動と强制振動とが如何なる割合に與つてをるかを明瞭にする事ができた．

---

25. *A Problem of Weighted Mean.*

By Chuji TSUBOI,

Earthquake Research Institute.

(Read June 20, 1940.—Received June 20, 1941.)

In a number of natural as well as social phenomena, two quantities $\Psi(\xi)$ and $\psi(\xi)$ are connected in such a way that one of them, $\Psi(\xi)$, is a weighted overlapping mean of the other, $\psi(\xi)$, taken over a certain range, say, from a to b, of the independent variable ξ, which may be either time or a co-ordinate. Mathematically, the relation between two such quantities may generally be written

$$\Psi(\xi)=\int_a^b \psi(\xi+\alpha)p(\alpha)d\alpha, \tag{1}$$

where $p(\alpha)$ is the weight to be assigned to $\psi(\xi+\alpha)$ according to α. As examples of pairs of quantities that are connected in this way, we have the amount of water flowing in a river as Ψ and the precipitation in its basin as ψ; ground temperature and solar radiation; the reading on a hair hygrometer and the actual humidity; supply and demand in economical problems; and so on. In connection with these problems, it is often required to find that law by which $\Psi(\xi)$ is affected by $\psi(\xi)$, in other words, to determine the functional form of $p(\xi)$, starting from $\Psi(\xi)$ and $\psi(\xi)$ which are both known. The method hitherto resorted to for solving such a problem has mostly been that of trial and error, which method consists first in assuming a certain reasonable functional form for $p(\xi)$ and secondly in adjusting the numerical values of the constants contained in it until such a good agreement is obtained between the given $\Psi(\xi)$ and the calculated $\int_a^b \psi(\xi+\alpha)p(\alpha)d\alpha$ that the $p(\xi)$ assumed may well be regarded as a satisfactorily accurate solution. Owing to the considerable time required for doing so, especially when $p(\xi)$ contains two or more constants to be adjusted, it naturally behooves us to devise some other method that would enable the problem to be solved more simply.

In the method which the writer proposes in this paper, by using Fourier series, it is possible directly to find $p(\xi)$, starting from the given $\Psi(\xi)$ and $\psi(\xi)$. From the standpoint of mathematical rigorousness, it is admitted that there are some weak points in the method that are not

very satisfactory, but there can be no objection to applying the proposed method to actual problems.

Let $\Psi(\xi)$ and $\psi(\xi)$ be two functions that satisfy Dirichlet's conditions, hence expansible into Fourier series within the interval $a \leqq \xi \leqq b$. By means of transformation,

$$x = 2\pi \frac{\xi - a}{b - a},$$

the above assumption may be reduced to another, that $F(x)$ and $f(x)$ are both expansible into Fourier series within the interval $0 \leqq x \leqq 2\pi$, where

$$F(x) = \Psi\left(\frac{b-a}{2\pi}x + a\right),$$

and

$$f(x) = \psi\left(\frac{b-a}{2\pi}x + a\right).$$

Under this assumption, $F(x)$ and $f(x)$ may be written

$$F(x) = \sum_m A_m \cos mx + \sum_m B_m \sin mx \qquad (2)$$

$$f(x) = \sum_m a_m \cos mx + \sum_m b_m \sin mx \qquad (3)$$

where

$$A_m = \frac{1}{\varepsilon_m \pi} \int_0^{2\pi} F(\lambda) \cos m\lambda d\lambda$$

$$B_m = \frac{1}{\pi} \int_0^{2\pi} F(\lambda) \sin m\lambda d\lambda$$

$$a_m = \frac{1}{\varepsilon_m \pi} \int_0^{2\pi} f(\lambda) \cos m\lambda d\lambda$$

$$b_m = \frac{1}{\pi} \int_0^{2\pi} f(\lambda) \sin m\lambda d\lambda$$

and

$$\varepsilon_m = 2 \quad \text{for} \quad m = 0$$

$$\varepsilon_m = 1 \quad \text{for} \quad m \geqq 1.$$

Now if

$$F(x)=\int_0^{2\pi} f(x+\alpha)\varphi(\alpha)d\alpha \tag{4}$$

is the fundamental equation from which $\varphi(x)$ is to be determined, this is nothing but a Fredholm integral equation of the first kind which, in the present case, is solvable provided $\varphi(x)$ is also expansible into Fourier series. If now we assume this, and this is true in almost all practical problems, then $\varphi(x)$ may be written

$$\varphi(x)=\sum_m \alpha_m \cos mx+\sum_m \beta_m \sin mx \tag{5}$$

with

$$\alpha_m=\frac{1}{\varepsilon_m \pi}\int_0^{2\pi} \varphi(\lambda)\cos m\lambda d\lambda$$

and

$$\beta_m=\frac{1}{\pi}\int_0^{2\pi} \varphi(\lambda)\sin m\lambda d\lambda .$$

The equation (4) reduces then to

$$F(x)=\int_0^{2\pi} f(x+\alpha)\varphi(\alpha)d\alpha$$

$$=\int_0^{2\pi}\sum_m\left\{a_m \cos m(x+\alpha)+b_m \sin m(x+\alpha)\right\}\varphi(\alpha)\,d\alpha$$

$$=\sum_m a_m \cos mx\int_0^{2\pi}\varphi(\alpha)\cos m\alpha\, d\alpha$$

$$-\sum_m a_m \sin mx\int_0^{2\pi}\varphi(\alpha)\sin m\alpha\, d\alpha$$

$$+\sum_m b_m \sin mx\int_0^{2\pi}\varphi(\alpha)\cos m\alpha\, d\alpha$$

$$+\sum_m b_m \cos mx\int_0^{2\pi}\varphi(\alpha)\sin m\alpha\, d\alpha$$

$$=\pi\left\{\sum_m \varepsilon_m a_m \alpha_m \cos mx - \sum_m a_m \beta_m \sin mx\right.$$

$$\left.+\sum_m \varepsilon_m b_m \alpha_m \sin mx + \sum_m b_m \beta_m \cos mx\right\}. \qquad (6)$$

Comparing (6) with (2), we get

$$A_m = \pi(\varepsilon_m a_m \alpha_m + b_m \beta_m)$$

$$B_m = \pi(-a_m \beta_m + \varepsilon_m b_m \alpha_m)$$

and consequently

$$\left.\begin{aligned} \alpha_m &= \frac{1}{\varepsilon_m \pi}\,\frac{a_m A_m + b_m B_m}{a_m^2 + b_m^2} \\ \beta_m &= \frac{1}{\pi}\,\frac{b_m A_m - a_m B_m}{a_m^2 + b_m^2} \end{aligned}\right\}. \qquad (7)$$

In other words, the Fourier coefficients of the m-th order of the weight function $\varphi(x)$ are simple algebraic functions of those of $F(x)$ and $f(x)$ of the corresponding order, so that it is easy to determine the form of $\varphi(x)$, provided both $F(x)$ and $f(x)$ are known.

The point that is most unsatisfactory from the mathematical point of view in the theory developed above is that we have restricted the range of x to be between 0 and 2π. This makes it hardly possible to apply this method, should $\varphi(x)$ actually extend beyond this range. The range of 2π, in which $F(x)$ and $f(x)$ are to be developed in Fourier series, should be taken sufficiently wider than the range of x, in which $\varphi(x)$ is supposed to have sensible values.

In order to see at the outset what accurate results will practically be obtained by means of this method, the following test was made. $n(x)$ in Table I is a series of integers taken at random, $N(x)$ being constructed according to

$$N(x) = n(x-4) + 2n(x-3) + 3n(x-2) + 4n(x-1) + 5n(x)$$

$$+ 4n(x+1) + 3n(x+2) + 2n(x+3) + n(x+4).$$

The curves for $n(x)$ and $N(x)$ are both shown in Fig. 1. In this case, we know that the weight assigned to $n(x)$ has been linear with respect to x, so that the form of $\varphi(x)$ is

$$\varphi(x) = 5 \mp x,$$

the double sign before x being taken according as whether x is positive

or negative. What we shall do here is to determine $\varphi(x)$ anew, starting

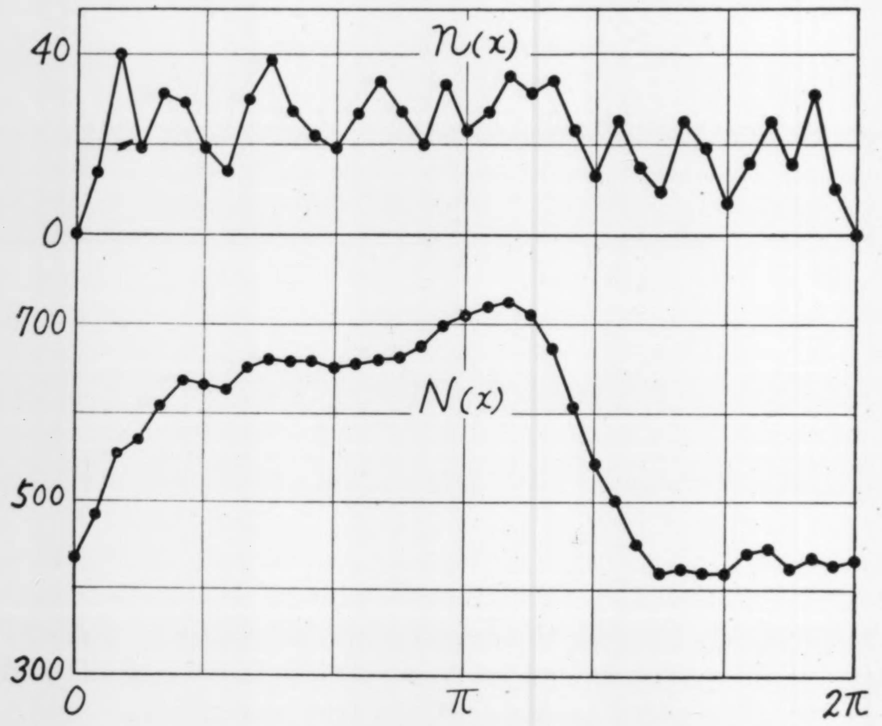

Fig. 1. $n(x)$........series of random numbers
$N(x)$........overlapping sum

from the given $n(x)$ and $N(x)$, acting as if the value of $\varphi(x)$ were not known beforehand. According to the method developed in the foregoing paragraphs, the Fourier coefficients for $n(x)$ and $N(x)$ were first calculated by means of ordinary harmonic analysis, with the results given in

Table I.

x	$n(x)$	$N(x)$	x	$n(x)$	$N(x)$	x	$n(x)$	$N(x)$	x	$n(x)$	$N(x)$
10°	14	485	100°	27	659	190°	27	720	280°	25	423
20	40	553	110	22	658	200	35	725	290	19	418
30	19	570	120	19	652	210	31	712	300	7	419
40	31	610	130	26	656	220	34	672	310	16	441
50	29	637	140	34	661	230	23	607	320	25	446
60	19	633	150	27	664	240	13	544	330	15	424
70	14	627	160	20	675	250	25	501	340	31	437
80	30	652	170	34	699	260	15	450	350	10	426
90	39	662	180	23	708	270	9	416	360	0	433

Table II. It may be pointed out here that the Fourier coefficients P_m and Q_m for $N(x)$ do not exactly correspond to the coefficients A_m and

Table II. Fourier Cofficients for $n(x)$, $N(x)$ and $\varphi(x)$.

m	$n(x)$		$N(x)$		$\varphi(x)$	
	a_m	b_m	P_m	Q_m	α_m	β_m
0	22·972	——	574·310	——	0·695	——
1	− 4·582	3·890	−107·743	92·463	1·330	0·007
2	1·176	2·090	22·889	41·736	1·103	− 0·012
3	− 1·442	− 1·540	− 20.083	−21·064	0·766	0·007
4	− 1·871	1·605	− 15·530	13·146	0·459	− 0·003
5	− 1·276	0·728	− 4·794	2·539	0·205	− 0·006
6	− 5·722	− 0·144	− 5·722	− 0·192	0·056	0·000
7	− 2·187	− 1·577	− 0·051	− 0·037	0·001	0·000
8	0·056	0·724	− 0·010	0·215	0·015	− 0·008
9	− 1·778	3·556	− 1·778	3·611	0·056	0·000
10	− 1·454	− 1·103	− 2·187	− 1·605	0·083	0·001
11	− 3·653	− 1·578	− 5·403	− 2·349	0·082	0·000
12	− 4·556	− 1·203	− 4·556	− 1·251	0·056	− 0·001
13	0·438	2·130	0·175	0.832	0·022	0·000
14	− 1·056	− 1·172	− 0·036	− 0·041	0·002	0·000
15	0·386	0·096	0·027	0·009	0·004	− 0·011
16	1·145	− 0 592	0·463	− 0·229	0·022	0·000
17	2·593	0·097	2·146	0·116	0·046	− 0·001
18	0·806	——	0·806	——	0·056	——

B_m of the function $F(x)$, because the values of $n(x)$ are given only at finite intervals of $\frac{2\pi}{360}\times 10$. Since

$$A_m = P_m \times \frac{2\pi}{360}\times 10$$

$$B_m = Q_m \times \frac{2\pi}{360}\times 10,$$

we have

$$\begin{aligned} a_m &= \frac{1}{\varepsilon_m \pi}\,\frac{a_m A_m + b_m B_m}{a_m^2 + b_m^2} \\ &= \frac{1}{\varepsilon_m \pi}\,\frac{a_m P_m + b_m Q_m}{a_m^2 + b_m^2}\,\frac{2\pi}{36} \\ &= \frac{1}{18\varepsilon_m}\,\frac{a_m P_m + b_m Q_m}{a_m^2 + b_m^2} \end{aligned}$$

and similarly,

$$\left.\beta_m = \frac{1}{18}\,\frac{b_m P_m - a_m Q_m}{a_m^2 + b_m^2}\right\} . \qquad (8)$$

The values of α_m and β_m calculated from (8) are also given in Table II. Since $\varphi(x)$ is an even function with respect to x, the Fourier coefficients β_m of all sine terms of $\varphi(x)$ ought to have vanished, but in Table II, we see that there are slight departures from this, which is the result of accumulations of errors in the actual numerical computations.

The function $\varphi(x)$ is then evaluated by summing up the series

$$\varphi(x) = \sum_m \alpha_m \cos mx + \sum_m \beta_m \sin mx,$$

with the results given in Table III. The values of $\varphi(x)$ calculated in this way agree well with what were first assumed, showing the feasibility of the proposed method.

Table III.

x	$\varphi(x)$	x	$\varphi(x)$	x	$\varphi(x)$	x	$\varphi(x)$
0°	5·08	100°	0·00	190°	− 0·04	280°	0·02
10	4·02	110	− 0·04	200	0·01	290	− 0·04
20	3·07	120	0·01	210	− 0·04	300	0·07
30	2·00	130	− 0·04	220	0·02	310	0·00
40	1·06	140	0·02	230	− 0·04	320	1·06
50	0·00	150	− 0·04	240	0·01	330	2·00
60	0·07	160	0·01	250	− 0·04	340	3·07
70	− 0·04	170	− 0·04	260	0·00	350	4·02
80	0·02	180	0·00	270	− 0·04	360	5·08
90	− 0·04						

Now in order to apply this method to a few actual problems, we shall consider first the relation between the amount of discharge from

Table IV.

	F (Discharge)	f (Prec.)	F'	$F-F'$		F	f	F'	$F-F'$
April	10·70 l/m	103·1 mm	3·34	7·36	Oct.	12·29	58·5	4·87	7.42
May	10·80	154·8	3·65	7·15	Nov.	11·86	69·5	4·68	7·18
June	11·57	220·5	3·98	7·59	Dec.	11·42	53·5	4·11	7·31
July	11·93	209·8	4·65	7·28	Jan.	11·01	43·9	3·93	7·08
Aug.	11·87	206·8	4·29	7·58	Feb.	10·76	78·0	3·44	7·32
Sept.	12·67	360·5	5·44	7·23	March	10·73	116·3	3·65	7·08

the Beppu hot springs and the precipitations in nearby regions, as reported by T. Nomitsu and others[1]. According to these investigators, the mean monthly discharge from the springs (per orifice) F and the mean monthly precipitation in nearby regions f are as given in Table IV. $F(x)$ and $f(x)$ are graphically shown in Fig. 2.

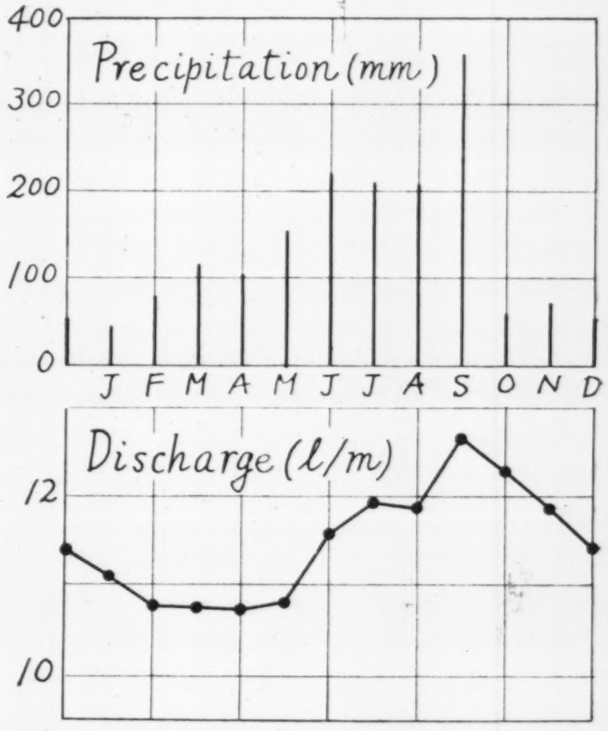

Fig. 2. Precipitation near Beppu and the discharge of the Beppu Hot Springs (per orifice).

Both these quantities were analysed into Fourier series with the results shown in Table V, in which are also given the Fourier coefficients for the function $\varphi(x)$, computed from those for the discharge and the precipitation, according to (7). With these coefficients, the Fourier series for $\varphi(x)$ was synthesised, with the results given in Table VI and shown graphically in Fig. 3. It is clear from Fig. 3 that the weight function $\varphi(x)$ is almost exactly linear with respect to time, that is to say, the discharge of the hot-spring water in a certain month is most strongly

Table V.

m	F (Discharge)		f (Prec.)		φ (Weight)	
	cos	sin	cos	sin	cos	sin
0	11·475	——	139·6	——	0·00685	——
1	− 0·563	− 0·380	− 59·6	78·5	64	−0 00115
2	0·095	0·052	31·2	− 22·0	21	− 43
3	− 0·008	− 0·068	− 27·3	1·1	3	− 43
4	0·112	0·128	48·1	− 13·5	25	− 51
5	− 0·120	− 0·023	− 35·3	6·0	53	− 20
6	0·077	——	19·5	——	66	——

1) T. Nomitsu and others, *Tikyubuturi*, **2** (1938), 97; *Mem. Coll. Sc., A*, **23** (1940), 41.

affected by the precipitation during that same month, and less and less by those in the preceding months.

Table VI.

x	$\varphi(x)$	x	$\varphi(x)$	x	$\varphi(x)$
0°	0·00917	150°	0·00579	270°	0·00715
30	435	180	677	300	857
60	707	210	637	330	817
90	531	240	761	360	917
120	581				

One point in this problem needs some amplifying remarks. It is generally believed that a considerable portion, say, J, out of the total discharge F of the hot-spring water comes from a deep origin, and that this portion is scarcely affected by precipitation and other meteorological elements. It might therefore have been better to assume that it is the difference $(F-J)$, not F itself, that is to be correlated with the precipitation, and to write the starting equation in the form

$$F(x)-J=\int f(x+\alpha)\varphi(\alpha)d\alpha.$$

Since J is taken as a constant, although unknown, the constant term in the Fourier expansion of $(F-J)$ differs from that in the expansion of F by that constant amount. The term a_0 in the series for $\varphi(x)$ is therefore indeterminate by another unknown constant amount. Now if $\varphi(x)$ is put zero at $x=2\pi$, that is, if it is assumed that after a year precipitation ceases to have any effect on the discharge of the hot-water, then the weight function $\varphi'(x)$ ought to be

$$\varphi'(x)=\varphi(x)-0{\cdot}00435.$$

Using these $\varphi'(x)$, the monthly discharges F', which were also given in Table IV, are calculated according to

$$F'(x)=\sum_{n=-12}^{0} f\left(x+\frac{2\pi}{12}n\right)\varphi'\left(\frac{2\pi}{12}n\right). \tag{9}$$

Between the observed monthly discharges and those calculated according to (9), we find almost constant differences of about $7\,l/m$, which may be identified with what we believed came from a deep origin.

It is interesting to compare the foregoing results with those of Nomitsu and others that were obtained in a quite different way.

They assumed from the outset that the effect of precipitation on

the discharge of hot-water diminishes exponentially with respect to time, and finally obtained

$$\varphi(x)=0{\cdot}00390\exp\left(-0{\cdot}11\times\frac{12}{360}x\right) \tag{10}$$

as the weight function. For comparison, the values of $\varphi(x)$ according to (10) were also plotted in Fig. 3. According to Nomitsu's expression, precipitation affects sensibly even after the lapse of a few years, but according to the results obtained in the present paper, it is not necessary to assume that the effect of precipitation lasts so long.

As to the value of J, Nomitsu and others found $6{\cdot}3\ l/m$, while our value is $7{\cdot}3\ l/m$.

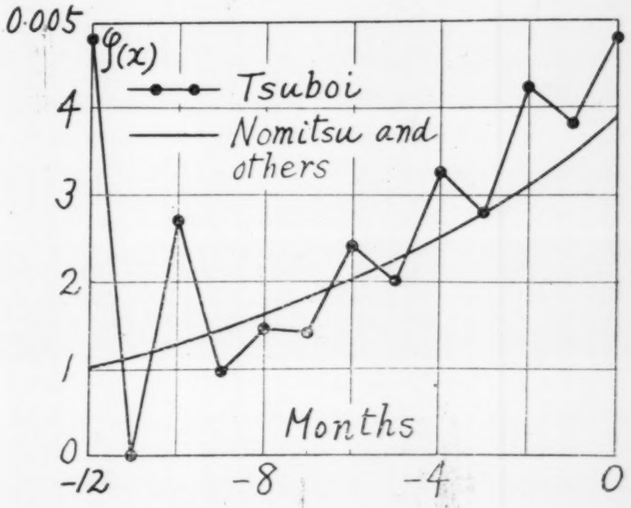

Fig. 3. Effect of precipitation on the discharge of the Ceppu Hot Spring.

The second example relates to the dependence of the daily height of the hot-water table in a certain hot-spring, at Rendaizi, on the daily precipitations in nearby regions. The daily readings of both these quantities from Sept. 6 to Oct. 11,

Table VII.

Date	Water Head	Prec.	Date	Water Head	Prec.	Date	Water Head	Prec.
Sept. 6	97 cm	0·2mm	Sept. 18	72 cm	15·7mm	Sept. 30	140	—mm
7	98	0·1	19	67	0·1	Oct. 1	136	—
8	98	—	20	64	—	2	132	37·7
9	97	—	21	63	15·8	3	130	8·3
10	96	11·5	22	66	38·8	4	128	26·8
11	93	11·6	23	70	42·7	5	126	—
12	84	—	24	75	2·8	6	125	—
13	83	—	25	84	105·2	7	125	0·4
14	82	1·2	26	116	10·2	8	118	—
15	78	8·5	27	128	—	9	95	—
16	74	0·1	28	135	—	10	113	—
17	73	—	29	137	—	11	112	6·1

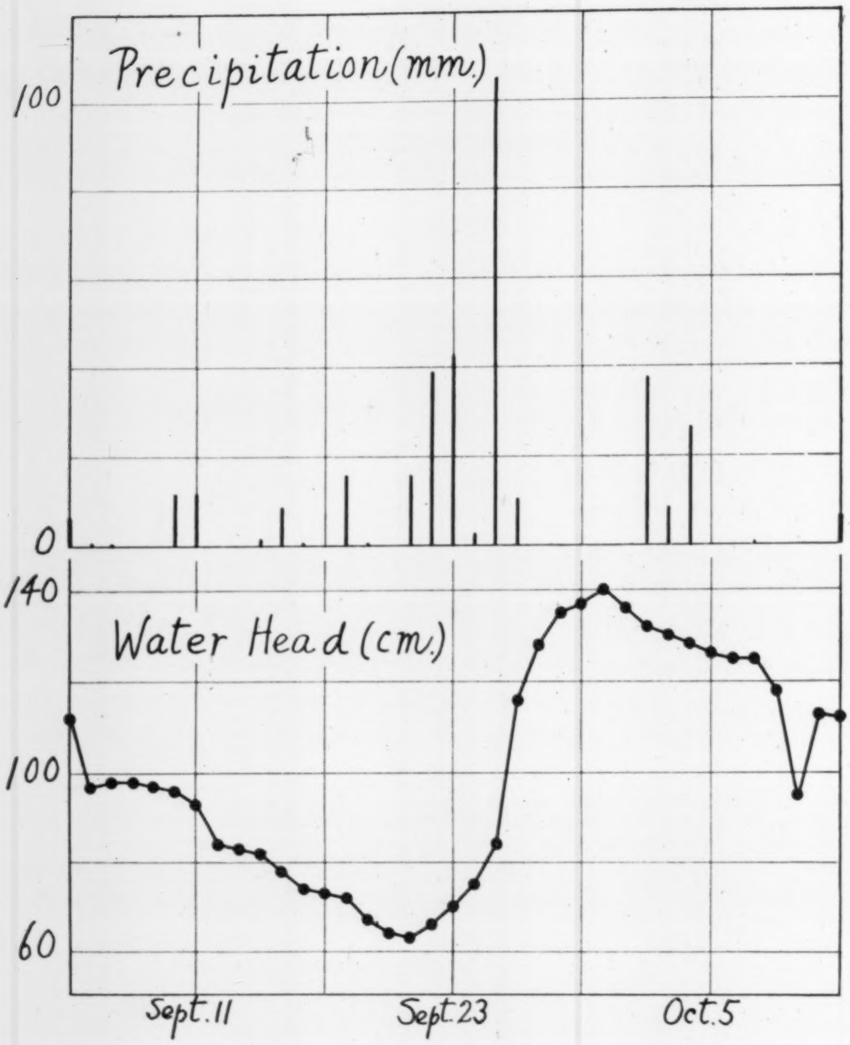

Fig. 4. Precipitation near Rendaizi and the head of the hot water table.

1935, as reported by T. Fukutomi[2], are given in Table VII, and shown graphically in Fig. 4.

The Fourier coefficients for the height of the water head and the precipitation are given in Table VIII, together with those for the weight functions that were calculated from them. Since the water head was measured from an arbitrary origin, no attention was paid to the constant term of the Fourier series for $\varphi(x)$. The values of $\varphi(x)$ computed from these coefficients are given in Table IX, and graphically shown in Fig. 5. In this case, the summation of the series for $\varphi(x)$ was carried out to various orders of harmonics. The rather large fluctuations of $\varphi(x)$ that result when the summation is made to highter orders, are due to slow convergence on the part of the Fourier coefficients for the preci-

2) T. Fukutomi, *Zisin*, **12** (1940), 195.

pitation. At any rate, it is clear from Fig. 5. that the water head on a certain day is most strongly affected, not by the precipitation on that identical day, but by the precipitation 4 or 5 days prior to it.

Table VIII.

m	Water Head		Precipitation		Weight function	
	cos	sin	cos	sin	cos	sin
0	——	——	9·558	——	——	——
1	12·192	−28·607	−10·384	− 3·333	−0·0146	−0·1577
2	−10·412	8·424	5·567	2·025	−0·0648	−0·1077
3	5·135	− 1·512	− 9·124	− 0·362	− 308	−0·0104
4	− 4·516	− 0·464	6·741	5·613	− 238	− 161
5	1·046	1·628	0·008	− 7·259	− 124	− 80
6	0·640	− 0·831	− 0·557	0·710	− 646	− 6
7	1·350	1·233	1·978	0·142	402	− 317
8	2·558	− 0·984	− 1·701	1·108	− 812	156
9	0·723	0·833	4·048	3·555	113	− 16
10	2·042	− 1·318	− 5·769	− 5·290	− 43	− 167
11	0·530	− 1·861	4·932	5·438	− 77	124
12	1·474	− 1·023	− 0·427	− 6·350	81	− 134
13	0·348	− 1·632	− 1·116	3·479	− 252	− 25
14	0·284	− 0·574	1·735	− 4·079	80	− 4
15	− 0·355	− 1·320	− 2·964	8·288	− 86	− 49
16	− 0·788	− 0·304	7·779	− 4·781	− 31	41
17	0·244	− 0·713	− 5·584	− 1·043	− 11	− 73
18	− 0·557	——	1·496	——	− 207	——

Table IX.

x	Up to 3 rd Harmonies.	Up to 6 th Harmonies.	Up to 12 th Harmonies.	Up to 18 th Harmonies.
0°	−0·1102	−0·2111	−0·2448	−0·2954
10	− 1714	− 2470	− 2804	− 2427
20	− 2109	− 2049	− 1623	− 1780
30	− 2276	− 1131	− 959	− 972
40	− 2234	− 1593	− 2009	− 1983
50	− 2034	− 1955	− 1985	− 1877
60	− 1742	− 2119	− 1664	− 1939
70	− 1409	− 1729	− 1599	− 1262
80	− 1003	− 1002	− 1434	− 1673
90	− 825	− 498	− 1009	− 962

(*to be continued.*)

Table IX. (*Continued.*)

x	Up to 3 rd Harmonies.	Up to 6 th Harmonies.	Up to 12 th Harmonies.	Up to 18 th Harmonies.
100°	− 615	− 529	− 173	− 76
110	− 460	− 841	132	53
120	− 346	− 879	− 1082	− 1131
130	− 261	− 444	− 1582	− 1251
140	− 200	306	200	− 239
150	− 159	579	1579	1921
160	− 143	202	816	722
170	− 157	− 534	− 684	− 806
180	− 193	− 953	− 1362	− 1171
190	− 239	− 712	− 706	− 705
200	− 266	− 92	1544	1223
210	− 236	323	1099	1701
220	− 111	242	− 1383	− 2062
230	140	− 16	− 1025	− 496
240	523	129	1249	983
250	1018	915	1923	1986
260	1575	1960	1610	1583
270	2121	2608	1742	1887
280	2568	2567	2236	1939
290	2836	2182	2801	3154
300	2857	2060	2721	2442
310	2607	2415	2685	2266
320	2094	2781	2143	2086
330	1374	2877	2806	2926
340	0534	1079	1619	1323
350	− 326	− 741	− 427	0039
360	− 1102	− 2111	− 2448	− 2952

Finally, the foregoing method may, with some modifications, be readily applied to many other problems that can be reduced to solving an equation of the form

$$F(x)=\int_{-s}^{+s} f(x+a)\,da,$$

where $F(x)$ is given and $f(x)$ is to be sought. Such a problem is encountered, for instance, as Mr. Z. Koana has noticed, when it is required to estimate the intensities of individual spectral lines that were taken on a photographic plate from the microphotometric curve of the plate obtained by a microphotometer, equipped with a slit of finite width. If the deflection of the photometer, when the photographic plate is run

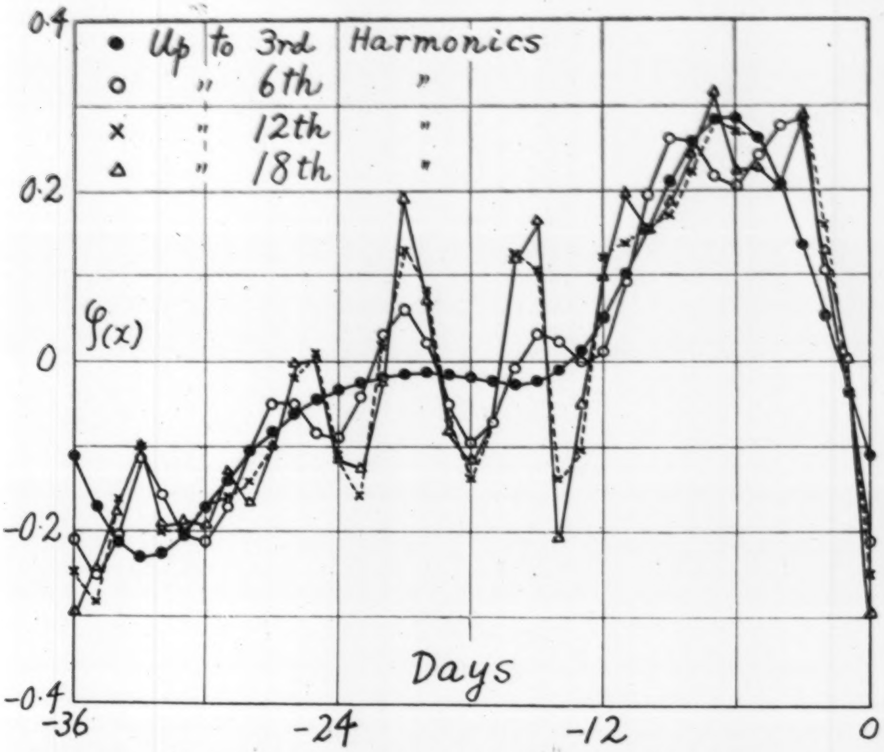

Fig. 5. Effect of precipitation on the head of the hot water table at Rendaizi.

under it, is $F(x)$, and the intensity distribution along the plate is $f(x)$, then the relation between $F(x)$ and $f(x)$ is exactly

$$F(x)=\int_{-s}^{+s} f(x+\alpha)d\alpha, \tag{11}$$

where s is half the width of the slit of the photometer. If, as before, we put

$$\left.\begin{aligned} F(x)&=\sum_m A_m \cos mx+\sum_m B_m \sin mx \\ f(x)&=\sum_m a_m \cos mx+\sum_m b_m \sin mx, \end{aligned}\right\}, \tag{12}$$

(11) reduces to

$$\begin{aligned} F(x)&=\int_{-s}^{+s} f(x+\alpha)d\alpha \\ &=\int_{-s}^{+s}\left\{\sum_m a_m \cos m(x+\alpha)+\sum_m b_m \sin m(x+\alpha)\right\}d\alpha \end{aligned}$$

$$=\int_{-s}^{+s}\left\{\sum_m a_m \cos mx \cos m\alpha - \sum_m a_m \sin mx \sin m\alpha\right.$$

$$\left.+\sum_m b_m \sin mx \cos m\alpha + \sum_m b_m \cos mx \sin m\alpha\right\} d\alpha$$

$$=\left[\sum_m \frac{a_m}{m}\cos mx \sin m\alpha + \sum_m \frac{a_m}{m}\sin mx \cos m\alpha\right.$$

$$\left.+\sum_m \frac{b_m}{m}\sin mx \sin m\alpha - \sum_m \frac{b_m}{m}\cos mx \cos m\alpha\right]_{-s}^{+s}$$

$$=\sum_m \frac{2a_m}{m}\cos mx \sin ms + \sum_m \frac{2b_m}{m}\sin mx \sin ms. \qquad (13)$$

Comparing (13) with (12), we get

$$\left.\begin{aligned} a_m &= \frac{mA_m}{2\sin ms} \\ \text{and} \qquad & \\ b_m &= \frac{mB_m}{2\sin ms} \end{aligned}\right\}. \qquad (14)$$

From these relations, the intensity distribution on a photographic plate can be evaluated from the microphotometric curve taken with a slit that may even be wider than the individual spectral lines to be measured.

In view of the fact that $\sin ms$ comes into the denominators, it is necessary to choose s so that $\sin ms$ for any m shall not vanish. In other words, s should be so chosen that it will not be an integral measure of π. For the case $m=0$,

$$a_0 = \frac{d}{dm}(mA_m) \bigg/ \frac{d}{dm}(2\sin ms)$$

$$= \frac{A_m}{2s}.$$

In order to demonstrate the usefulness of this procedure, it was applied to the following example. In Fig. 6, $f(x)$ represents two "spectral lines" that are two probability curves separated by $\frac{2\pi}{360}\times 80$ from peak to peak, while $F(x)$ in the same figure is the "microphotometric

curve" taken with a slit of half the width, namely, $\frac{2\pi}{360}\times 35$. The values of $F(x)$ and $f(x)$ are given in Table X. What is required here is to find $f(x)$ anew, knowing the form of $F(x)$, and that it was taken with a slit, half the width of which is $\frac{2\pi}{360}\times 35$. Using the Fourier coefficients for $F(x)$, those for $f(x)$ were calculated according to (14), the results being given in Table XI. The values of $f(x)$, which were obtained by synthesising the series

$$f(x)=\sum_m \frac{mA_m}{2\sin ms}\cos mx+\sum_m \frac{mB_m}{2\sin ms}\sin mx\,,$$

and which are also given in Table X, agree well with the given $f(x)$.

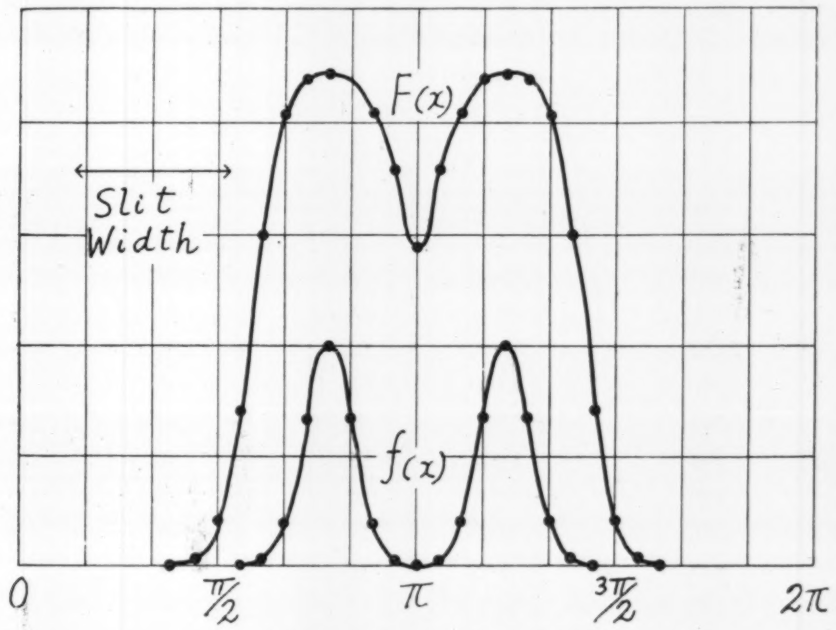

Fig. 6. $f(x)$........." Spectral Lines "
$F(x)$........." Photometric Curve " taken with a slit of finite width.

Table X.

x	f (assumed)	F	f (calc.)	x	f (assumed)	F	f (calc.)
0°	0·0	0·0	0·1	60°	0·0	0·0	− 0·9
10	0·0	0·0	− 0·2	70	0·0	17·0	0·8
20	0·0	0·0	− 0·7	80	0·0	263·0	− 1·1
30	0·0	0·0	0·9	90	0·0	1928·0	0·3
40	0·0	0·0	0·3	100	1·0	7205·0	1·5
50	0·0	0·0	− 0·3	110	25·0	14934·0	26·3

(to be continued.)

Table X. (*Continued.*)

x	f (assumed)	F	f (calc.)	x	f (assumed)	F	f (calc.)
120°	194·0	20215·0	192·7	250°	25·0	14934·0	26·3
130	664·0	21876·0	665·1	260	1·0	7205·0	1·5
140	1000·0	22105·0	1000·0	270	0·0	1928·0	0·3
150	664·0	21887·0	665·4	280	0·0	263·0	− 1·1
160	194·0	20473·0	192·1	290	0·0	17·0	0·8
170	25·0	16857·0	26·3	300	0·0	0·0	− 0·9
180	1·0	14404·0	2·3	310	0·0	0·0	− 0·3
190	25·0	16857·0	26·3	320	0·0	0·0	0·3
200	194·0	20473·0	192·1	330	0·0	0·0	0·9
210	644·0	21887·0	665·4	340	0·0	0·0	− 0·7
220	1000·0	22105·0	1000·0	350	0·0	0·0	− 0·2
230	664·0	21876·0	665·1	360	0·0	0·0	0·1
240	194·0	20215·0	192·7				

Table XI.

m	A_m	$a_m = mA_m/2\sin ms$	m	A_m	$a_m = mA_m/2\sin ms$
0	8609	15·4	10	− 59	3·7
1	−12156	−23·1	11	− 19	− 0·6
2	2133	5·0	12	− 70	− 1·6
3	3841	13·0	13	88	1·3
4	− 3163	−21·5	14	− 38	− 0·8
5	290	18·2	15	4	0·2
6	602	− 7·9	16	− 1	0·1
7	255	− 2·1	17	4	− 0·1
8	− 811	7·2	18	0	0
9	493	− 6·9			

It may be added, in conclusion, that the object of the present paper is merely to propose a method that will be useful in solving a certain class of problems related to weighted overlapping means.

The writer intends to use this method in a forthcoming paper discussing the mechanism of regional isostasy.

25. 重價平均に關する一問題

地震研究所 坪井忠二

$f(x)$ なる量と，それに $\varphi(x)$ なる重みを附して求めた平均

$$F(x)=\int_0^{2\pi} f(x+\alpha)\varphi(\alpha)d\alpha$$

とが與へられて居る時，$\varphi(x)$ を近似的に求める方法を述べた．即ち若し

$$f(x)=\sum a_m \cos mx+\sum b_m \sin mx$$

$$F(x)=\sum A_m \cos mx+\sum B_m \sin mx$$

であるならば

$$\varphi(x)=\sum\frac{1}{\varepsilon_m\pi}\,\frac{a_mA_m+b_mB_m}{a_m^2+b_m^2}\cos mx+\sum\frac{1}{\pi}\,\frac{b_mA_m-a_mB_m}{a_m^2+b_m^2}\sin mx$$

で與へられる．二三の實例に就いて其の應用例を示した．

26. *Recent Earthquakes of the Kwanto District.*

By Nobuji NASU and Chuji YASUDA,

Earthquake Research Institute.

(Read Dec. 21, 1939 and May 15, 1941.—Received June 20, 1941.)

It may be well before proceeding with this paper to point out that although earthquake activity in the southeastern part of Japan, i.e. the Kwanto district and its vicinity, declined during the more than ten years that followed the great earthquake of September 1, 1923, in recent years, no less than thirty shocks have been felt annually in Tokyo. These activities may be said to be quite ordinary compared with those in the years that preceded the great earthquake above-mentioned, in which period the activities did not differ from those in recent years.

Our observations of earthquakes of this district have been continued up to the present, the numerical data of earthquakes that were felt in Tokyo having already been published in the "Seismometrical Report" of our Institute. A number of papers relating to earthquakes of this district have also been published by various authors.[1), 2)]

Our earlier paper[3)] mainly dealt with the problem of the three dimensional distribution of the foci of earthquakes felt in Tokyo during the years from 1924 to 1936, showing that most of the shocks that occurred in this district originated from depths shallower than 70 km, excepting a few shocks of rather deep seated origins, to which we shall come back as we proceed in this paper.

Another problem that will be dealt with in this paper is migration of the seismically active centers in the Kwanto district. During the four years from 1936 to 1939, Tokyo had 185 sensible shocks which, for convenience, are here divided into eight groups according to the times of their occurrence, and the distribution of the epicenters of these earthquakes was considered for each semi-annual period, upon doing which, it was found that there had been considerable changes in the positions of the seismically active centers. Since they will be helpful

1) T. KODAIRA, "Earthquakes of the Kwanto District." *Bull. Earthq. Res. Inst.*, **11** (1933), 350~361.

2) T. NAGATA, "Space Distribution of Earthquake Hypocentres in the Kwanto District." *Bull. Earthq. Res. Inst.*, **14** (1936), 420~426.

3) N. NASU, T. HAGIWARA and S. OMOTE, "Studies on Earthquakes in the Kwanto District." *Bull. Earthq. Res. Inst.*, **14** (1936), 427~437.

in explaining these changes, brief notes on the earthquakes that occurred in each period are given in this paper.

As to the annual changes in the seismicity of the special regions, as will be shown later, statistics of the annual number of earthquakes from 1924 to 1939 were compiled, which showed that in regions that were once seriously affected by the great earthquake of 1923, the number of shocks that originated from them gradually diminished, whereas in other regions the number increased.

Network of Observations.

As already stated, our network of observations was expanded so that it would cover the whole region in which earthquakes were most active. Of this network, however, in the Sea off the coast of Iwaki and the sea to the south of the Boso Penninsula, for example, earthquakes were also frequent, as well as on land, but in the case of these earthquakes, the results obtained from the present network of seismological stations did not give very accurate values.

The seismological stations where records have been continuously obtained are shown in Table I.

Table I. The seismological stations.

Station	Position						Approximate distance from Hongo (km).
	Longitude (E)			Latitude (N)			
Hongo (Tokyo)	139°	45′	59″	35°	42′	40″	0
Komaba	139	41	01	35	39	18	10
Mitaka	139	32	32	35	40	21	20
Tukuba	140	06	36	36	12	39	64
Kamakura	139	32	39	35	18	32	48
Misaki	139	37	05	35	09	26	62
Kiyosumi	140	09	02	35	09	22	70
Titibu	139	04	54	35	58	56	69
Koyama	138	58	59	35	21	20	82
Yosiwara	138	41	07	35	09	35	116
Susaki	138	58	50	34	39	54	138

The last station, Susaki, is the Mitui Geophysical Institute, who supplied us with data for computing the positions of the seismic foci.

Determination of the Seismic Focus.

As usual, the positions of the seismic foci were determined graphically by means of the durations of the preliminary tremors at the respective stations.

Earthquakes during the years 1936 to 1939.

As already mentioned, 185 sensible earthquakes were experienced in Tokyo during the four years from 1936 to 1939, of which those whose epicenters and focal depths could be determined were 130, and those whose epicenters alone could be determined were 48, while for the remaining 7, these two data were undeterminable.

In studying the migration of seismically active centers, the following brief notes on the earthquakes for each year will be helpful.

Earthquakes in 1936.

In the earlier half of 1936, Tokyo had 13 sensible earthquakes, ten of which were distributed on the land side, including four that occurred in the Bay of Tokyo, while the remaining three were at sea, in the Pacific Ocean. Of these three shocks, in the one that occurred on April 26, the duration of the preliminary tremors was 51·2 sec in Tokyo and 46·0 sec at Susaki. The epicenter of this earthquake was at a point the coordinates of which were $\lambda=138{\cdot}86°$E, $\varphi=33{\cdot}48°$N, i.e., a distance of about 120 km due south of the cape of Idu Penninsula. This earthquake was one of the rare shocks that were sensible in Tokyo, notwithstanding its rather large epicentral distance.

Comparing the distribution of the eighteen earthquakes that were felt in the latter half of 1936 with those felt in the earlier half of the same year, a considerable change in the seismically active center will be noticed in that over half of the earthquakes that occurred in the latter half of that year, namely, eleven shocks, were on the sea side, and the remaining seven on the land side. Of these earthquakes, the one that occurred on November 3 was strongest at Tukuba, where its intensity was estimated at IV (rather strong), although, fortunately, there was no damage.

Near the southwestern extremity of our network of stations a shock was experienced on October 20, the duration of preliminary tremors of which was 6·9 sec at Yosiwara, its epicenter being the lower part of the River Huzi, and its focal depth 30 km.

Earthquakes in 1937.

In the earlier half of 1937, the sensible earthquakes in Tokyo numbered seventeen, the epicenters of sixteen of which could be determined, excepting the one that occurred on May 29. Seeing that the

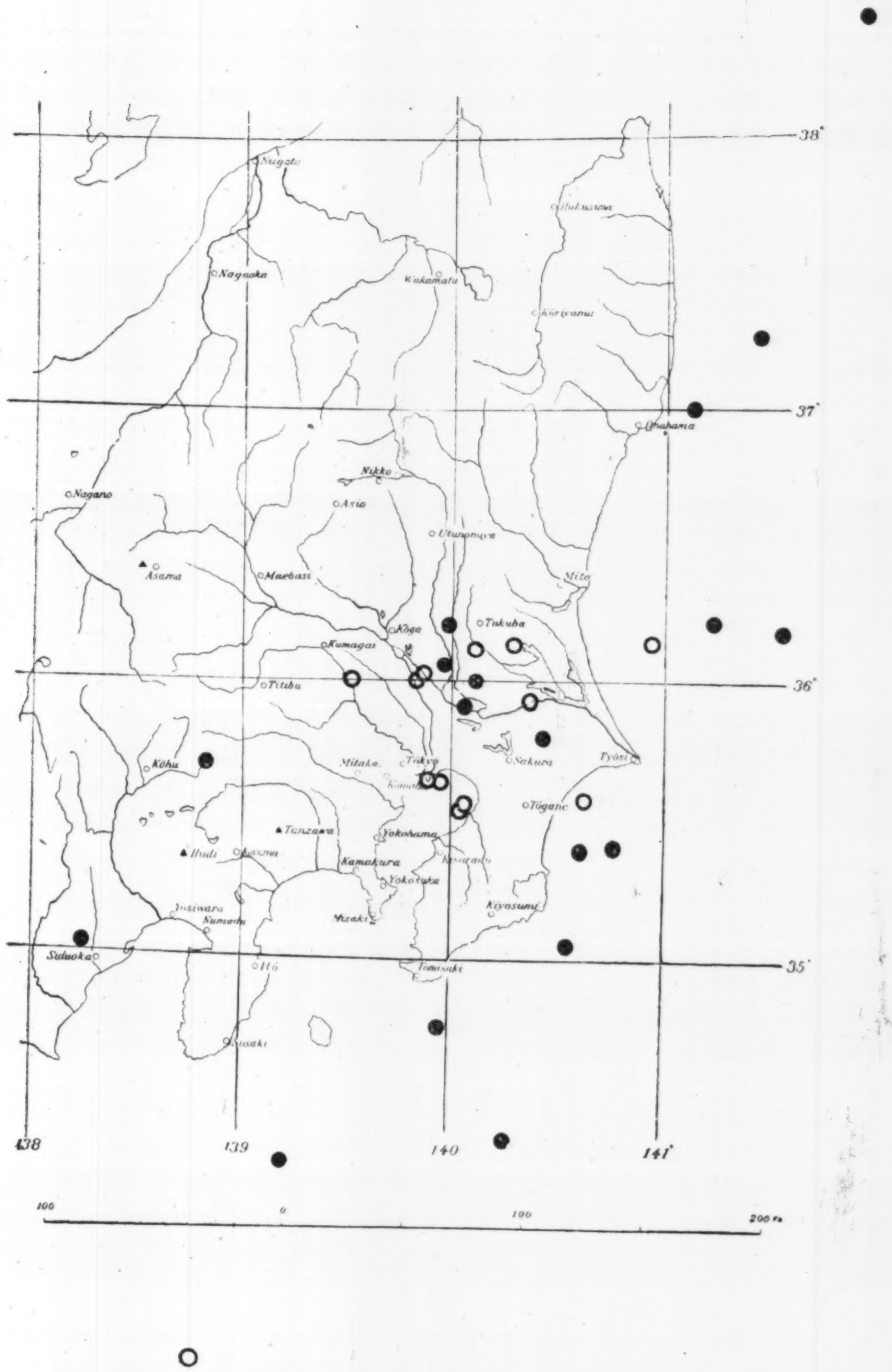

Fig. 1. Epicenters of the earthquakes that occurred in 1936.
Open circles are earthquakes of the first half of the year and closed circles earthquakes of the second half of the same year.

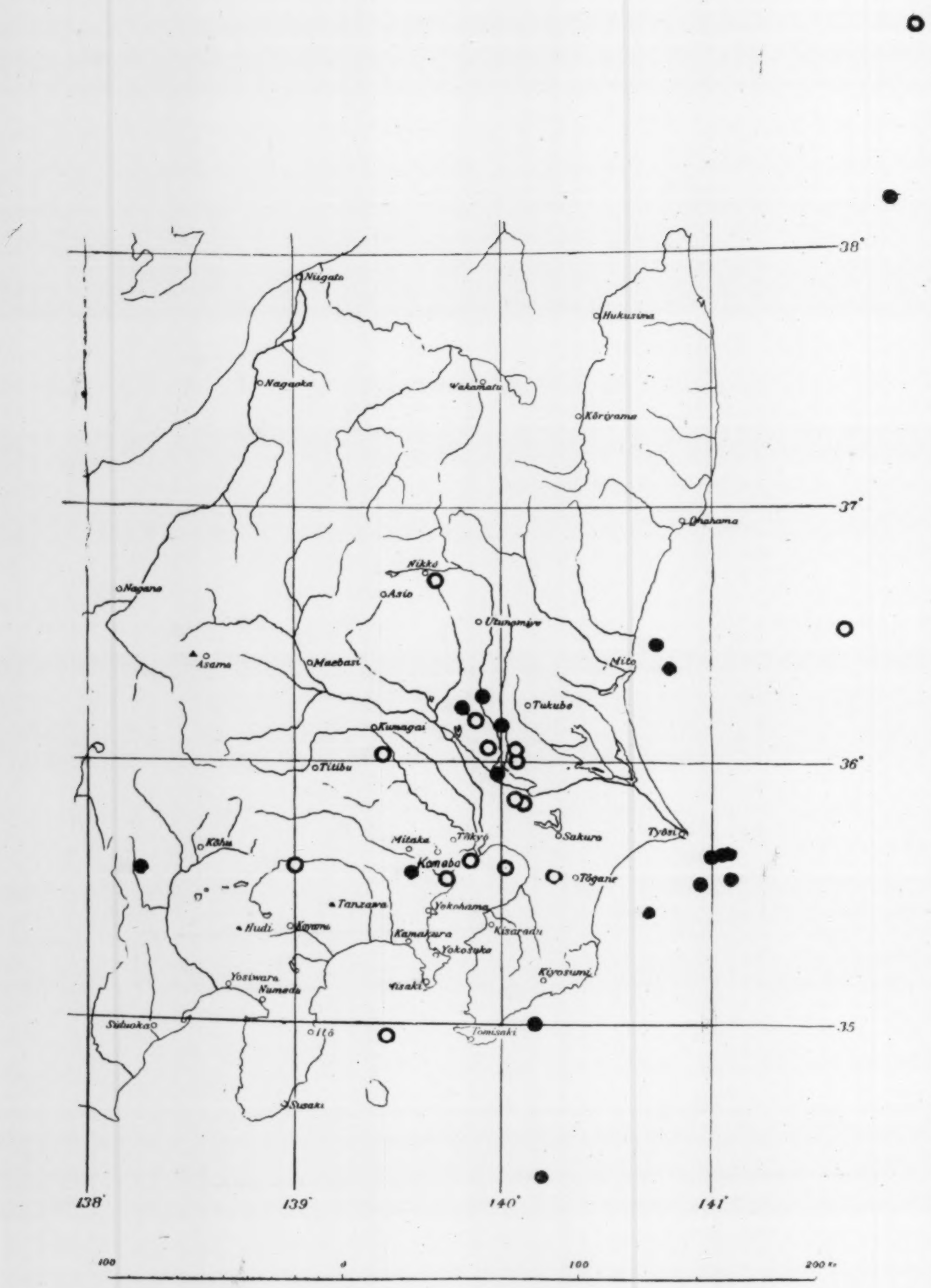

Fig. 2. Epicenters of earthquakes that occurred in 1937.

duration of its preliminary tremors exceeded 120 sec at all our stations, its origin was probably situated very far from the network of stations, so that the accurate position could not be determined by our network.

Of the sixteen shocks mentioned above, only two were in the Pacific Ocean, or to be more precise, in the sea off the northeastern coast of the Kwanto district.

In that region lying southwest of Mt. Tukuba, that is, on the river sides of Kinugawa and Tone, the earthquakes were always so active, that they were probably most densely distributed there. No marked change in the number of shocks could be seen; seven epicenters were distributed over this region.

During this period, three more shocks occurred in the Bay of Tokyo, the focal depths of which were 35, 40, and 50 km.

In the latter half of 1937, fourteen earthquakes were felt in Tokyo. What is remarkable is that six of them swarmed on the sea side near the cape of Inubozaki. The focal depths of these shocks were comparatively small, being estimated at between 30 and 40 km.

Two more shocks had their epicenters in the sea due east of Mito, where the earthquakes showed gradual increase in activity the following year, 1938.

Earthquakes in 1938.

In the period from January to June 1938, the earthquakes in the northeastern sea of the Kwanto district, that is, in the open sea of Kasima and the sea off the coast of Iwaki Province, suddenly increased in number, nine of them having been felt in Tokyo. Of these, the one that occurred on May 23 was so strong that, at Tukuba, its intensity exceeded IV. Acceleration seismographs there showed that the maximnm accelerations of the EW component and the vertical component were 27·0 gal and 29·0 gal respectively. Unfortunately, the NS component seismograph failed to give complete data.

The maximum displacements as observed in Tokyo were as follows; 60·3 mm in the NS component and 33·13 mm in the EW component. The periods of these waves were 8·8 and 9·9 sec respectively. The focal depth of this earthquake was worked out to be 80 km, being rather deep compared with the other shock that occurred in this region.

On the land side, one more remarkable earthquake occurred on Feb. 7. This earthquake had its epicenter northwest of Kumagai and a focal depth of 100 km. The intensity of the shock was estimated at IV in the City of Tokyo and its neighbourhood, for example, at Komaba and Mitaka. The maximum accelerations of the NS component, EW component, and the vertical component as measured at Hongo were 19·2, 27·6, and 6·8 gal respectively. The maximum displacements recorded at

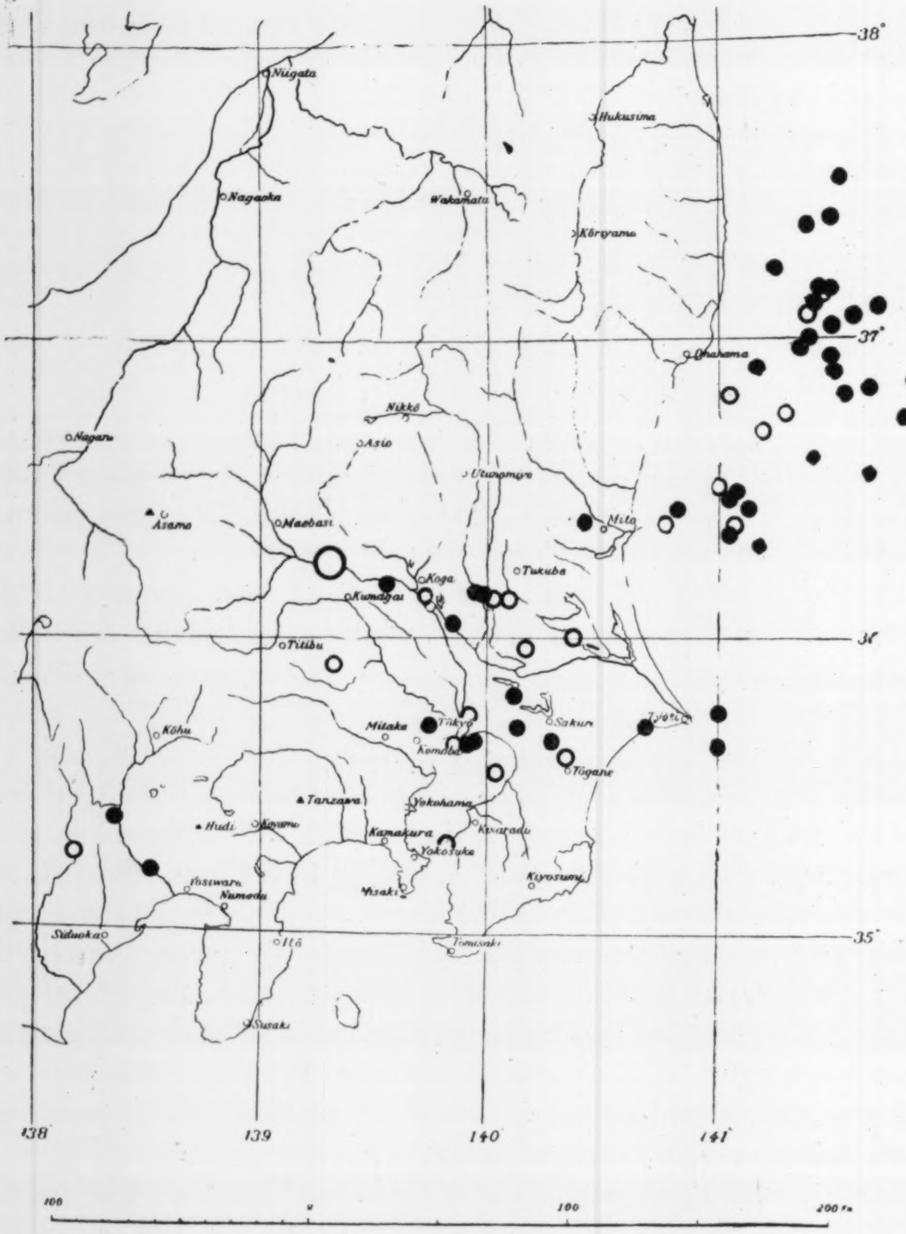

Fig. 3. Epicenters of earthquakes that occurred in 1938.

the same station were 25·6 mm in the NS component and 19·0 mm in the EW component. The initial motion of the earthquake registered by the displacement seismographs at Hongo were 1 μ southward, 2 μ eastward, and 14 μ upward. At Mitaka the vertical component of the initial motion predominated in magnitude, being 491 μ upward, while in the NS component it was 14 μ southward and 6 μ eastward respectively. This predominance in the vertical component motion might be caused by steepening in the angle of dip of the path of the rays along which the seismic waves proceed with increasing depth.

From our observations in the Kwanto district, the earthquakes that originated from depths, such as more than 100 km, were not so numerous. In our previous paper, we maintained the existence of such earthquakes as would either be restricted to comparatively small regions or arranged in a narrow zone, which was amply proved by the earthquake of February 7.

In the latter half of 1938, earthquakes were most active in November, the sensible earthquakes in this month totalling 25, followed by December, in which month 12 shocks were felt in Tokyo. The total number of earthquakes in the latter half of this year reached 54, of which the number of those whose epicenters could be determined were 48.

A remarkable feature about the distribution of epicenters was that on the sea side, earthquakes clustered in two groups, the region occupied by the first group having as its approximate center a point, the coordinates of which were $\lambda=141{\cdot}7°E$ $\varphi=37{\cdot}0°N$, while the area occupied by the second group was much smaller than the former, and lay south of it and east of Mito.

Besides the earthquakes mentioned above, there were two shocks on the seaside near the cape of Inubo, where shocks were active in the latter half of 1937.

Of earthquakes belonging to the first group, the severest was that which occurred on November 5, its intensity at Tokyo being estimated at IV. The acceleration seismograms obtained at Hongo showed that the maximum accelerations of the NS–, EW–, vertical components were 32·3, 32·3, and 11·7 gal respectively. The maximum displacements registered there were 99·4 mm, with a period of 14·0 sec in the NS component, and 69·25 mm, with a period of 13·8 sec, in the EW component.

Because the earthquakes belonging to this group extended far beyond our network of stations, most of their focal depths either showed errors or were indeterminable, but from computations of the initial motions at individual stations, such as Hongo and Kamakura, it could be said that most of them originated from depths not greater than 50 km or more.

On the other hand, the seven earthquakes belonging to the second group originated from depths between 40 and 60 km. In intensity, as felt in Tokyo, none of them exceeded II.

Two shocks were experienced west of Mt. Huzi. Their origins were comparatively shallow, their focal depths being 30 km.

A number of earthquakes had their epicenters near Tokyo and Tiba, the depths of most of which exceeded 50 km.

Earthquakes in 1939.

Tokyo felt 26 sensible earthquakes in the first half of this year, one of which was the strong earthquake of the Oga Peninsula, Akita Prefecture, that occurred on May 1. The intensity of this earthquake

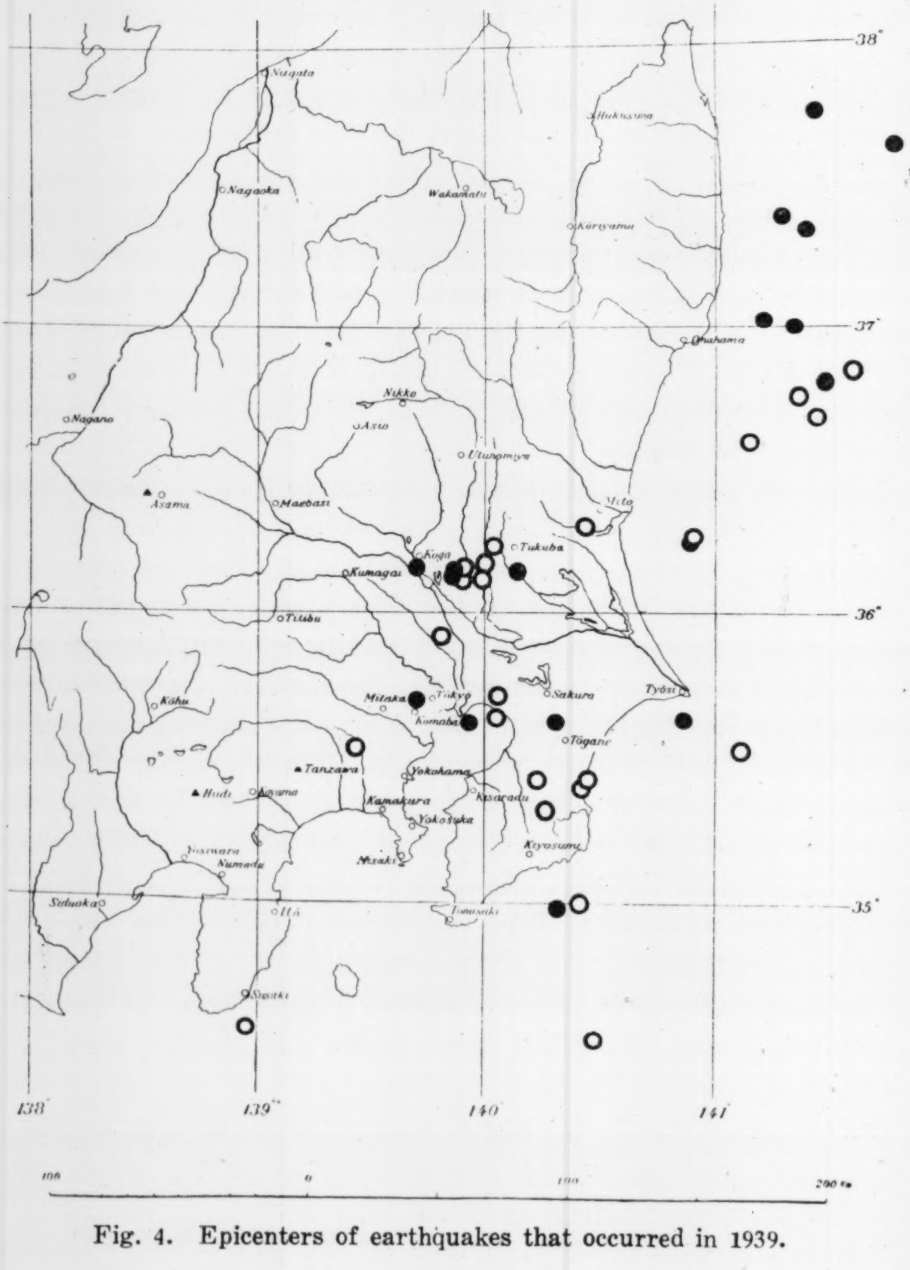

Fig. 4. Epicenters of earthquakes that occurred in 1939.

in Tokyo, however, did not exceed I (slight), the maximum accelerations of the NS component being 1·02 gal, the EW component 1·14 gal, and the vertical component 0·81 gal. The displacement seismograms gave

a maximum range of 20·00 mm, with a period of 7·28 sec in the NS component and that of 16·70 mm with a period of 8·0 sec in the EW component.

The following notes apply to seismic activities in the Kwanto district during this period.

The earthquakes were distributed in a region lying west of Mt. Tukuba and in the northeastern sea. As already mentioned, in the former region the earthquakes were constantly active, while in the latter region the activities were continuations of those in the previous year.

Another remarkable distribution in the epicenters was that four centers were found near the middle part of the Boso Peninsula, where it was found that these originated from comparatively shallow origins, their focal depths being less than 30 km.

In the latter half of 1939, eighteen earthquakes were felt. Upon comparing the distribution of the epicenters for this period with that for the earlier half of the same year, it was found that the seismically active center on the seaside migrated northward during the latter half of that year, because then the epicenters were mostly distributed north of latitude 37°, while in the earlier half they were distributed south of it.

Generally speaking, the recent earthquakes of the Kwanto district so far mentioned were mostly distributed east of the region just mentioned. By drawing a line corresponding to longitude 139·5° it will be found that the epicenters of the earthquakes are densely distributed east of it, whereas they are rare west of it.

Another noteworthy point is that, on the land side, the active region may be bordered by a line that passes through Mito in an E–W direction. Excepting the one that occurred near the Oga Peninsula on May 1, 1938, in that region lying north of this line, no sensible earthquake occurred during the period in question. This earthquake, which was especially severe, originated some distance away from the Kwanto district.

It must be remembered that the distribution, as mentioned above, was restricted to earthquakes of recent years, with the result that earthquakes of a different period will show different distribution. For example, the adjacent region lying west of the meridian line just drawn, namely, that covering the greater part of the two Prefectures of Kanagawa and Saitama, the Bay of Sagami, and the northeastern part of the Idu Peninsula, became very active during the ten years or so following the great earthquake of 1923. We may recall that numerous aftershocks of this great earthquake occurred, the countless shocks of the

so-called "Ito earthquake-swarms" of 1930, the destructive earthquake of the same year, and the strong earthquake of Saitama in 1932.

From these facts it may be concluded that, at present, seismic activity in the Kwanto district is limited to its eastern part, the active center in the last recent few years having migrated eastward or northeastward.

Annual changes in seismicity in various parts of the Kwanto District.

For the purpose of studying the annual changes in seismic activity in various parts of this district, the following eight regions were selected;

(1) Tokyo Bay
(2) Sagami Bay
(3) The provinces of Sagami and Kai
(4) The Boso Peninsula
(5) The sea off the coast of Kuzyukuri
(6) The sea south of Katuura
(7) The Kasima Sea
(8) The basin of the River Kinu.

The boundaries of these regions, as shown in Fig. 5, being merely for convenience, may have no definite meaning, either geologically or geographically. Table II contains a count of the annual number of earthquakes that originated in the respective regions between 1924 and 1939.

Table II. Annual numbers of earthquakes and their means for five years.

Region	1		2		3		4		5		6		7		8	
Year \ A, M	A	M	A	M	A	M	A	M	A	M	A	M	A	M	A	M
1924	11		2		12		5		1		0		0		5	
1925	6		2		1		4		1		0		2		8	
1926	7	8·6	2	1·6	2	5·6	9	6·2	1	1·0	1	0·4	2	3·0	10	11·4
1927	6	8·4	2	1·8	10	4·6	6	6·2	0	1·4	1	0·4	6	3·6	12	11·6
1928	13	8·4	0	2·2	3	4·8	7	6·2	2	2·4	0	0·4	5	4·8	22	11·4
1929	10	7·8	3	2·4	7	5·0	5	5·2	3	3·0	0	0·8	3	5·8	6	11·8
1930	6	7·8	4	2·0	2	4·0	4	5·2	6	3·8	0	0·6	8	5·4	7	13·0
1931	4	6·2	3	2·4	7	3·8	4	4·0	4	4·6	3	1·0	7	7·0	12	11·2
1932	6	5·2	0	2·2	1	2·8	6	4·2	4	4·4	0	1·8	4	7·8	18	12·4
1933	5	6·0	2	2·0	2	3·8	1	4·6	6	3·8	2	3·2	13	7·0	12	14·4
1934	5	6·0	2	1·4	2	1·6	6	3·8	2	3·6	4	3·2	7	6·2	13	13·4
1935	10	5·2	3	1·6	3	1·6	6	2·8	3	4·0	7	3·4	4	5·8	17	12·0
1936	4	5·2	0	1·2	0	1·2	0	3·2	3	3·2	3	3·0	3	8·4	7	11·2
1937	2	4·6	1	0·8	1	1·0	1	2·8	6	3·4	1	2·8	2	8·6	11	10·8
1938	5		0		0		3		2		0		26		8	
1939	2		0		1		4		3		3		8		11	

A = Annual number, M = Means for five years.

For our present purpose, however, it is better to take the overlapping means of these annual numbers. In doing so, the curves for the annual numbers may be smoothed, thus bringing out the general features of the seismic activity more clearly. In taking these overlapping means, care was taken to see that the divisions of years in which the means were taken did not extend to more than five, as otherwise the smoothed curves thus drawn might become too flat to show the actual tendencies. Thus the means of the annual numbers of five years were taken, this division being best suited to our present work.

By using these values of M, eight curves were drawn for the eight regions just mentioned, as in Fig. 6, in which three kinds of curves will be seen. The curves of the first kind descend, showing gradual decrease in activity with time, such as in the cases of Tokyo Bay, the Provinces of Sagami and Kai, and the Boso Peninsula all being regions affected by the great earthquake of September 1, 1923. According to Prof. A. Imamura[4] and Prof. Saem. Nakamura,[5] a number of conspicuous aftershocks followed this great earthquake. The epicenters of these aftershocks were distributed in the Bay and on the land of Sagami, densely, especially in the latter. On the other hand, a dense distribution of epicenters may be seen in the Boso Peninsula, where, however, the shocks were not so conspicuous as those in the former regions, although they were very numerous.

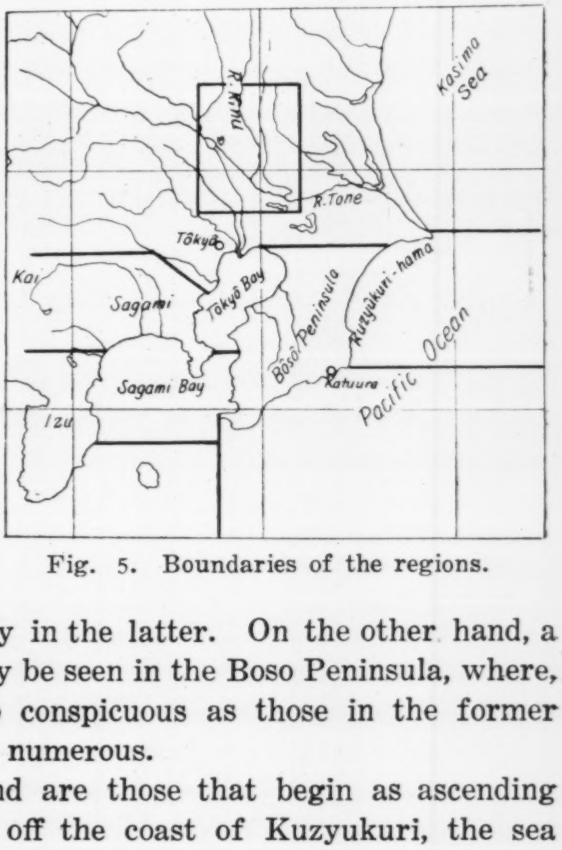

Fig. 5. Boundaries of the regions.

The curves of the second kind are those that begin as ascending curves, as in the case of the sea off the coast of Kuzyukuri, the sea to the south of Katuura and the Kasima Sea. The curves for the former two seas showed downward tendencies after they passed their maximum point, that is, they gradually declined in activity in recent years. In the case of the sea east of Kuzyukuri, the maximum was

4) A. IMAMURA, "The Great Kwanto (S. E. Japan) Earthquake on Sept. 1, 1923." *Report Imp. Earthq. Inv. Comm.*, No. 100, A. 1925.

5) Saemontaro NAKAMURA, "The Great Earthquake of S. E. Japan on Sept. 1, 1923," *ditto.*

in 1931, while in that of the sea south of Katuura, it was in 1935.

The curve for the Sea of Kasima, although somewhat undulatory, shows gradual increase in activity that lasted up to 1936, the year of its maximum.

Lastly, in curves of the third kind, no such clear tendencies as in the previous cases can be seen. These curves show that, notwithstanding the changes in seismic activity that may be seen from time to time, on the whole they are not marked. The typical curve was that for the region of the River Kinu. As often mentioned, earthquakes in this region were the most frequent in the Kwanto district. As shown in Table II, the annual number attained in 1928 a maximum of 22, whereas, in 1924, it was the minimum. The overlapping means, however, ranged between 14·40 and 10·80. The general tendency, as represented by using these overlapping means, suggests that the mean activity reached maximum in 1933, after which it slightly declined. Roughly speaking, the same degrees of activity were found at the beginning and the end of the period now under consideration.

Distribution of Earthquakes of rather deep origin.

Here, the words "rather deep" mean about 100 km below the surface of the earth.

During the period from 1924 to 1939, there were only nine earthquakes whose focal depths were deduced as being 100 km or more, the

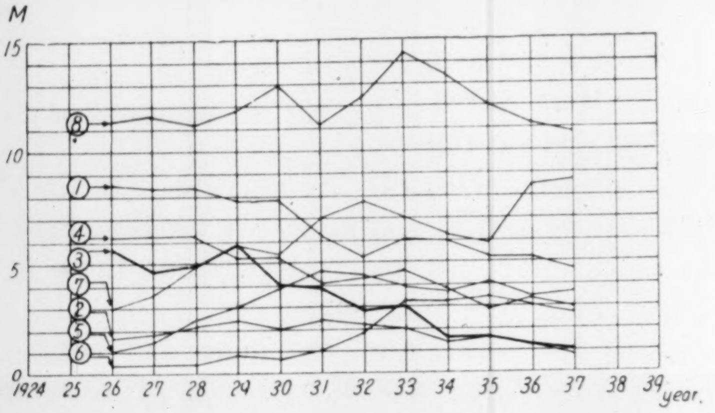

Fig. 6. Curves showing general tendencies of earthquake activity in various regions. (1=Tokyo Bay, 2=Sagami Bay, 3=The Provinces of Sagami and Kai, 4=Boso Peninsula, 5=The Sea off the coast of Kuzyukuri, 6=The Sea south of Katuura, 7=The Kasima Sea, 8=The Basin of the River Kinu.)

epicenters of which are indicated by crosses in Fig. 7. As will be seen from this figure, most of them are distributed in the western part of the Kwanto district, namely, three near Kumagai, one northwest of

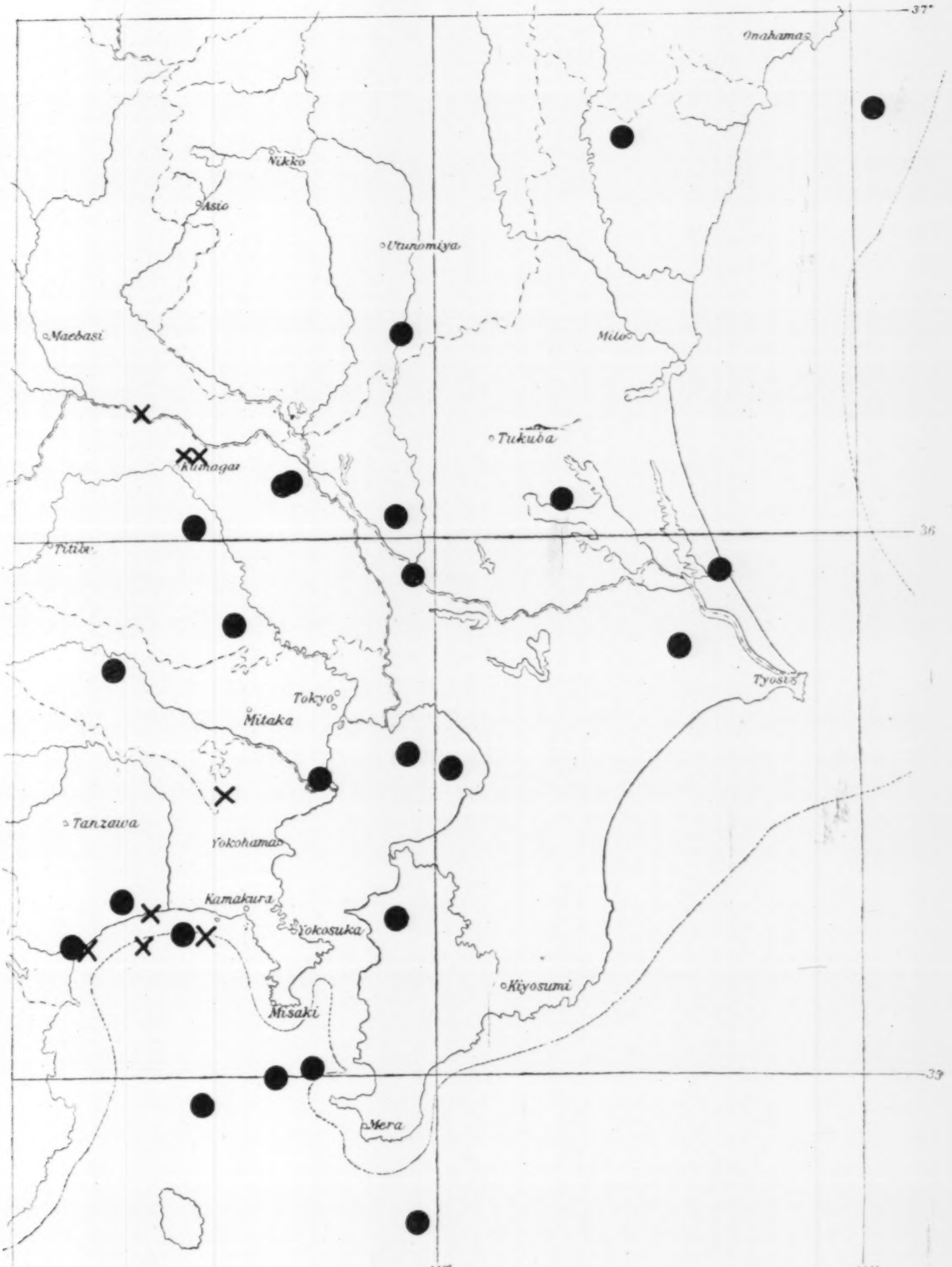

×

Fig. 7. Epicenters of earthquakes of rather deep origin.

Crosses are earthquakes whose focal depths exceeded 100 km, shaded circles shocks whose focal depths were 80∼100 km.

Yokohama, and four in the northern part of Sagami Bay. There is another one in the sea off the southern cape of the Boso Peninsula.

Although there were only a few epicenters of these shocks, there must be a zone or belt running in a N–S direction, or to be more precise, in a NNW–SSE direction, on which these epicenters ought to be distributed. As a matter of fact, the existence of such an earthquake belt can be deduced from the interesting studies of Dr. K. Wadati[6] and Dr. H. Honda,[7] which extended to the distribution of earthquakes in Japan as a whole, classifying the shocks according to their focal depths. The results show that besides the belt of deep seated earthquakes, there exist two other belts, from one of which originated earthquakes of rather deep origin, the focal depths ranging between 240 km and 100 km, and from the other, earthquakes of comparatively shallow origins less than 100 km. The former passes through the Kwanto district in the direction just mentioned, the epicenters of which, as indicated by crosses, being probably distributed in this belt. The other belt, which runs nearly parallel with the former, also passes through the eastern part of the same district.

In view of these facts, it may be concluded that earthquakes of rather deep origin occurred in the western part of the Kwanto district, while in the eastern part of it they were very rare.

For reference, the epicenters of shocks whose focal depths were deduced by computations to be 80∼100 km are shown in Fig. 7. As to their epicenters, it was also found that they are mostly distributed in the western part of the district now under consideration.

Acknowledgement. We wish to record here our great indebtedness to the various observers, whose arduous labours provided the valuable data for the present work.

6) K. WADATI, "On the Activity of Deep-focus Earthquakes observed in the Japan Islands and Neighbourhoods." *Geophys. Mag.*, 8 (1934∼1935), 305∼325.

7) H. HONDA, *Kensin-Ziho*, **11** (1940), No. 2, 183∼216.

26. 最近に於ける關東地方の地震に就いて

地震研究所 {那須信治 / 保田桂二}

此の論文には前年發表せる論文の續きとして主として昭和 11 年から同 14 年に至る期間に於いて起つた東京有感覺地震に就いて述べてある．これらの地震の分布を半年毎に區切つて考へ，その結果から地震活動區域の移動狀態を推察したのである．これの說明に供するため各期間に起つた地震に就いて略述しておいた．

關東地方の地震を更に區別し，或る定まつた區域內に於ける地震活動の消長を見ることにした．この目的のため東京灣，以下 8 區域を選び，大正 13 年から昭和 14 年に至る 16 年間の地震觀測結果を用ひて此區域に起つた地震回數の統計を取つた．

統計の方法としては移動平均法を用ひ地震活動の一般的狀勢を見ることにした．その結果，相模灣，相模甲斐地方，房總半島等關東大地震の餘震が比較的多かつた地方に於ては近年地震活動は順次減衰の傾向を示してゐるがこれと正反對の傾向を示してゐる地方もある．例へば鹿島灘の如きがそれである．尙ほ鬼怒川附近は地震の最も多い所であり，昭和 3 年には東京有感地震回數は 22 となり最大値に達した．

關東地方に發生する震原の稍深い地震（深さ 100 粁以上）の分布を見るに關東地方の西部に限られてゐる．此の種の地震が發生する地帶が本州を略南北の方向に橫斷して存在することは既に知られてゐることであるが尙ほこの研究に依つてその存在を確めることが出來た．

27. The Eruption of Miyake-sima, One of the Seven Izu Islands, in 1940.

Geological Observations of the Miyake-sima Eruption of 1940. (II)[1]

By Hiromichi TSUYA,

Earthquake Research Institute.

III. Topographical Changes.

THE ZONE OF FLANK ERUPTION.

As described in the preceding chapter, the present activity of Miyake-sima was a multiple eruption, consisting of a flank eruption and a summit eruption. It lasted for a period of 25 days from July 12 to August 5, 1940, during which interval a great number of explosions occurred, resulting in several topographical changes, mainly owing to accumulation of newly-ejected matter in the disturbed areas, although none of the explosions was sufficiently violent to alter radically the form of the mountain or to destroy any considerable part of it. The main topographical changes caused by the flank eruption of July 12～13 were the formation on the northeastern side of the somma, besides the fissures, of new parasitic craters (including the new parasitic cones) and new lava fields.

New parasitic craters and new parasitic cones.

1. Cinder cone A. This cone, situated at the highest level, about 430 m above the sea, and in the zone of the flank eruption, lies on a ridge sloping about 30° northeastward near the boundary between Kami-tuki and Tubota. It is not a perfect conical mound, but forms a shoulder on the steep slope of the former ridge, so that although its northeastern half is of conical shape, rising about 30 m above the ground of the former ridge, the other half constitutes the slope of this ridge itself (Fig. 51). The central part of the cone has an oval crater, about 50 m deep, the longer and shorter axes of which are about 150 m from north-west to southeast respectively. Except the northeast wall, which slopes about 40°, the inside walls of the crater are almost vertical. The crater-

---

1) Continued from page 294 of this Bulletin, **19**, (1941).
横須賀鎮守府検閲濟 (16. 8. 22)

floor, which is circular and flat, about 30 m across, is covered with detritus that fell from the surrounding walls.

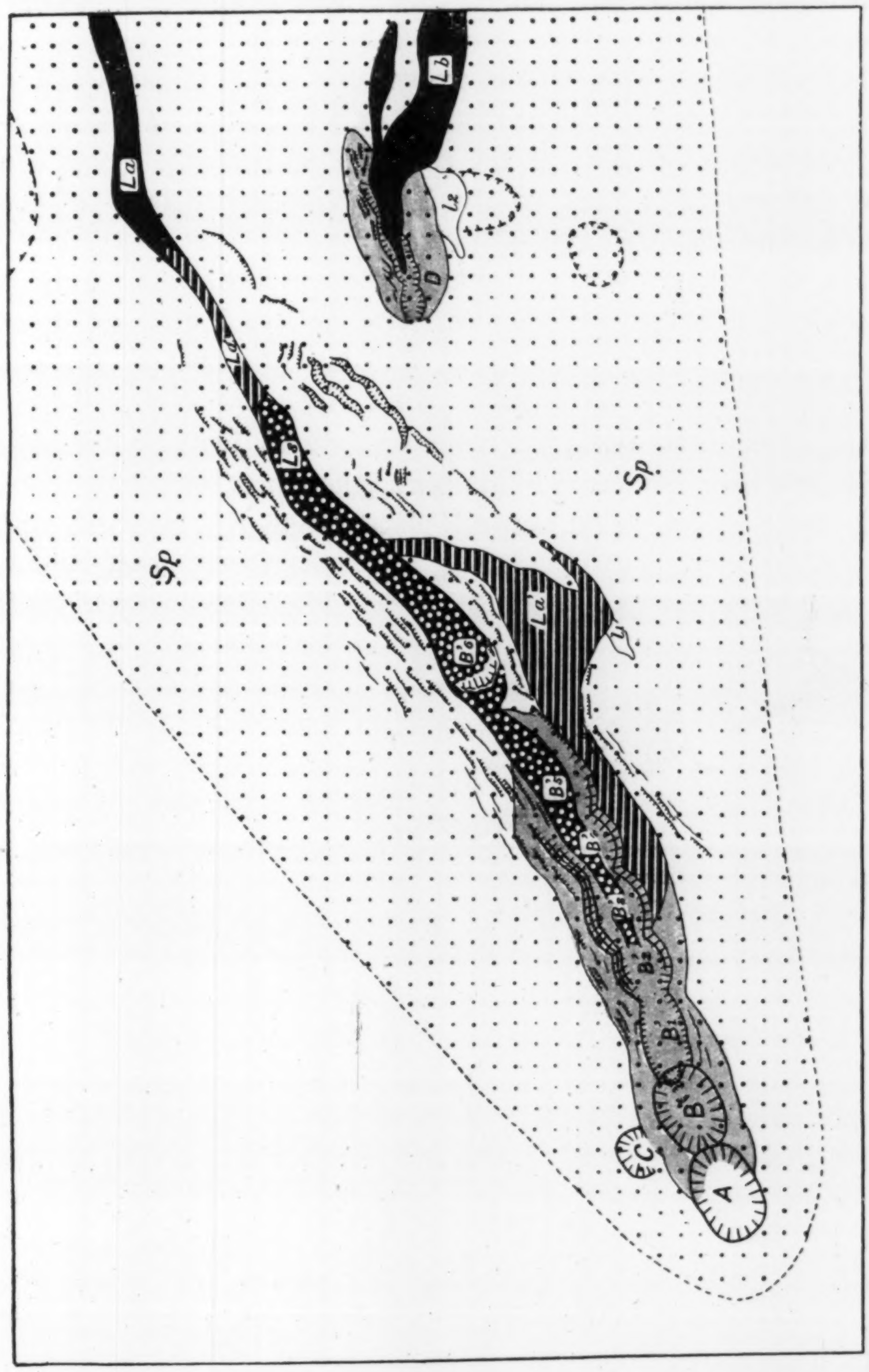

Fig. 50. Sketch-map showing the western part of the zone of flank eruption. *A*~*D*: New craters. *La*: Akabakkyô lava (fluent). *La'*: Akabakkyô lava (blocky). *Ls*: Debris flow (lapilli and bombs). *Lb*: Yoridaisawa lava. *Sp*: Volcanic sand, lapilli and bombs. l_1, l_2: Dammed ponds.

The southwestern inside wall of the crater, which is a vertical section of the ridge on which the crater opened, exposes three layers, 1~5 m thick, of old lava-flows (olivine-basalt) intercalated with layers of reddish-brown scoriaceous lapilli. The lower half of the inside north-

eastern wall also exposes the same old beds, while its upper half is formed of new ejecta.

The solid materials thrown out of this crater consist of accessory rock-fragments and juvenile ejecta (lava-blocks, bombs, and scoriaceous lapilli). The accessory ejecta, which are nothing but fragments of the old beds just referred to, are accumulated in a small area on the ridge adjoining the southwestern side of the crater. The juvenile ejecta are accumulated for the most part on the lower side (northeast) of the crater, forming the one-sided conical mound.

From the distribution of the ejecta, it is inferred that the eruptions at A first shattered one part of the old ridge, followed by ejection of the shattered portion as accessory ejecta and later by that of juvenile materials.

When the writer first visited the crater on July 19, 1940, no incandescent material was seen anywhere in or around the crater, although white vapor-clouds were rising from several places near the northern and shouthern crater-rims. When the writer made his second trip to the crater on Oct. 25, the same year, feeble fumaroles were still active at a number of places on the northeastern side of the crater.

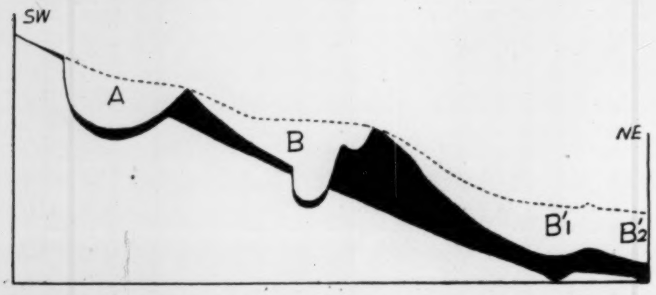

Fig. 51. Diagrammatic section of new parasitic cones *A* and *B*. New ejecta are shown in black.

2. *Cinder cone B.* Adjoining the northeastern side of *A*, and lying on the same old ridge, is another cinder cone *B* of somewhat smaller size, the central part of which has a circular crater of an average diameter of about 150 m. The inside southwestern wall of the crater, whose slope varies from 30° to 50°, deeply cuts the northeastern flank of cone *A*, the wall between the craters *A* and *B* consequently forming a sharp crest of such narrow surface as to be hardly passable. The northern and southern walls of this crater are nearly perpendicular, while the northeastern wall is terraced with a shallow side crater, about 30 m wide. The lower part of the main crater narrows, forming a cylindrical pit, about 30 m, the depth of which, on July 19, was beyond measure. Owing to infallen detritus, the bottom of the pit, on Oct. 25, was about 50 m from the upper rim of the crater. The surrounding wall of the pit exposes an old lava which may be the northeastern extension of one of the lavas that are exposed on the walls of crater A.

Cinder cone B consists largely of juvenile material (lava-blocks, bombs, and scoriaceous lapilli), although a few accessory rock-fragments are found among the juvenile ejecta. On July 19, vapor was issuing from a number of fumaroles in and around the crater-bowl, while on Oct. 25, vapors continued to rise from several places on the crater-wall and from the numerous fissures on the outer slope of the cone.

3. Craters $B'_1 \sim B'_6$. Adjoining the northeastern side of B, there is a trough-like depression, $50\sim150$ m wide and about 50 m deep, running northeast for a distance of about 700 m. This depression consists of six new craters, B'_1, B'_2,......B'_6, which are arranged in this order from southwest to northeast. Crater B'_1 thus lies at the southwestern end of the depression, next the northeastern side of cone B, the wall of the crater deeply cutting the flank of the latter. Crater B'_6, the most northeastern member of the crater group, lies about 180 m above the sea, in the valley on the boundary between Kamituki and Tubota, while the other craters are aligned between B'_1 and B'_6. Although the adjoining two of these craters open into each other, they are separated either by a low ridge between them or by a cliff, showing difference in level of their bottoms. Besides, the northern and southern walls of one crater join the respective walls of the adjoining crater, forming cusps that face each other at the boundary of the two craters.

The B' craters were opened by the recent eruption in the valley that lies on the border between Kamituki and Tubota. This valley had become wider as well as deeper downward from the end of the ridge on which stand cones A and B, with the result that the material exposed on the northern walls of these craters are exclusively new ejecta which, upon being thrown out of these craters, were piled thickly on the floor of the valley. The ejecta, as observed in the crater-walls, are mostly fragmentary material consisting of reddish-brown, scoriaceous lapilli, bombs, and lava-blocks, besides two sheets of a grayish compact lava, intercalated by layers of the fragmentary ejecta. On July 19, 1940, when the writer saw the craters for the first time at close range, the interior of some of the clefts here and there in the crater-walls was seen to be at red heat.

The B' craters are arranged, together with A and B, in a straight, SW–NE line, whose northeastern extension reaches the northern part of the bay of Akabakkyô, passing through the lower course of the valley at the boundary between Kamituki and Tubota, and whose southwestern extension lies almost in the direction of Oyama, the central cone. This distinct alignment of craters suggests the existence of a fracture-line in the said direction through the volcano. During the recent activity,

no eruption occurred anywhere on the supposed fracture-line, southwest of *A*, the central cone excepted; neither on the same line, northeast of B'_6, the bay of Akabakkyô excepted.

It is inferred that crater B'_6 lay where the flank eruption of 1940 originally started. Thus, as already mentioned in the preceding chapter, according to Kano, who lived on the northern side on the borders of Kamituki and Tubota, dark smoke began to rise a few minutes before 8 pm, July 12, from the valley ahead (southeast) of his house. Although he managed with difficulty to reach a place of safety, his neighbour, who lived in a house about 200 m southwest of B'_6, was missing, together with five members of his family.

4. Crater C. Adjoining the northern side of *B*, and lying on the southern slope of a ridge that runs parallel with the ridge on which lie *A* and *B*, there is a new horseshoe-shaped crater, about 50 m in diameter. This crater is surrounded on its northern side by an almost perpendicular wall exposing, besides layers of old reddish-brown lapilli, a sheet of old lava which is the northern continuation of the lava that is exposed in the middle of the southwestern crater-wall of *A*; while it is breached on its southern side, the crater-bottom communicating by means of a gap in the wall with the northern flank of *B*.

From the distribution of new ejecta in and around crater C, it is inferred that this is merely an explosion-crater, whose activity was of fairly short duration. Thus, although new ejecta (scoriaceous lapilli, bombs, and blocks of juvenile lava, and accessory rock-fragments) have accumulated thickly in and around crater C, they are mostly ejecta from the neighbouring craters *A* and *B*. Furthermore, the distribution of ejecta from *C*, *A*, and *B*, shows that the activity of these craters should have subsided in the order mentioned. On July 19, when the writer made his first visit to the crater, no steam vent was found either on the crater-floor or on the crater-walls.

5. Cinder cone D. At intervals of about 500 m east of B'_6 and on the gentle slope about 140 m above the sea, adjoining the southern side of the boundary valley between Kamituki and Tubota, there is a new mound *D*, about 30 m above the old ground, facing the old parasitic cone Daihannya-yama, lying beyond the Yoridai-sawa valley. Although, when viewed from a distance, east or west from it, the mound looks like a typical cone, it is a ridge-like mound,

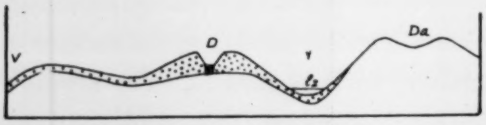

Fig. 52. Diagrammatic section of cone *D*. *Da*: Daihannya-yama, an old parasitic cone. *Y*: Yoridai-sawa. *V*: Boundary valley between Kamituki and Tsubota. l_2: Dammed pond.

about 50m wide and 200 m long, running in a ENE–WSW direction. The crater which, on this mound, is a trench-like stretch, is about 30m wide and 30~50m deep, running for a distance of 200m from the WSW end of the ridge ENE to the opposite end. The north and south walls of the crater form almost perpendicular cliffs, exposing a massive deposit of new ejecta. Judging from exposures in the crater-walls, the western part of the ridge is built up of reddish-brown, scoriaceous lapilli and bombs, while in its eastern part these ejecta are covered with a flow of block lava that descends eastward into the Yoridai-sawa, whence the inference that the eruption at *D* took place in a rift-crater that opened afresh on the gentle mountain slope, and that the successive ejections of scoriaceous lapilli and bombs from the crater were followed by an outflow of lava from the lower, eastern part of the same crater.

The old ground upon which the new mound *D* rests is composed of yellowish-gray ash-beds dipping less than 10°E, as observed in the south wall of the western end of the rift-crater, where the beds are exposed in the lower half of the crater-wall, and where they are overlain by a deposit of new ejecta (scoriaceous lapilli and bombs). Underneath the ash-beds, as observed in an exposure in the Yoridai-sawa between *D* and Daihannya-yama, lies a deposit of volcanic breccia, about 20m thick, followed by a lava-flow of augite-olivine-basalt. These old rocks are met with as accessory fragments, but sparsely in the ejecta from the crater of *D*.

At the end of July, the ground in the rift-crater, which contained numerous vents discharging steam and gases, was very hot, while three months later (end of October), it had everywhere cooled down with the exception of a few feeble fumaroles. But even at the latter time, there were numerous fumaroles on the ground outside the crater, particularly on the crest of the northern rim of the crater, where they were developed on fissures running parallel to the crater-rim as well as in a SW–NE direction. There were also some fissures discharging hot gases, the interiors of which former were red hot.

6. Rift-crater E. At a distance of about 500 m ENE of *D*, on the floor of a gully, called the Yomogiga-sawa, there formed a new rift-crater *E*, which is a trench-like stretch, about 100 m long, 10~15m wide, and 10m deep, consisting of seven small vents running ENE. Although two of the seven vents in the rift-crater communicate with each other without any distinct partition-wall, they are distinguished from each other by a step's difference in the depth of their floors.

The ejecta from the crater, which former are mostly black to grayish scoriaceous lapilli of juvenile and almost aphanitic lava, are relatively

Fig. 53. Sketch-map showing the eastern part of the zone of flank eruption. *EH*: New craters. *La*: Akabakkyô lava. *Lb*: Yoridai-sawa lava. *Lc*: Hyôtan-yama lava. *Sp*: Volcanic sand, lapilli, and bombs. *Sb*: Lapilli and bombs ejected from Hyôtan-yama craters *G* and *H*. *I*: Coast-line before the eruption of July 12~13, 1940. *II*: Coast-line immediately after the eruption. *III*: Coast-line in the middle of Sept., 1940. *ls*: Sitori lake.

small in amount; for, as observed in the exposure in the southern wall of the crater, they lie only about 2 m deep upon the former surface of the ground, which is composed of yellowish-brown lapilli beds, without forming a new mound around the crater.

At the end of July, the crater contained three feeble fumaroles. Three months later, they were still sending out small quantities of steam.

The craters just mentioned are all that were formed by the eruption on the subaerial part of the flank of the mountain. In addition to these, however, several craters were formed by the eruption on the floor of the bay of Akabakkyô, which may also be regarded as parasitic vents on the submarine extension of the same flank of the mountain. They are:

7. *Crater F.* According to accounts by eyewitnesses, an eruption occurred from a vent, denoted as crater *F*, in the innermost part of the former bay of Akabakkyô, and near the base of the former sea-cliff of Akabakkyô-hana (or Garaisino-hana). Although this vent, which has been buried beneath later ejecta from neighbouring vents (Hyôtan-yama craters *G* and *H*), does not present the form of a crater, its western inside wall is believed to have been the curved cliff newly cut in the former sea-cliff of Akabakkyô-hana. Thus, the cliff, which is in places both fissured and curved, forming a precipice with a talus conoid of fallen blocks at its base, runs from Akabakkyô-hana northwestward near to the mouth of the boundary valley of Kamituki and Tubota, surrounding the western side of the buried crater *F*, whereas formerly it was a sea-cliff facing the bay of Akabakkyô. At the end of July, vapor-clouds were issuing vigorously from numerous fissures on the ground of the buried crater *F* as well from fissures in the cliff, while at the end of October, vapor could be seen only in a few fumaroles at the base of the cliff.

At the above-mentioned cliff at Akabakkyô-hana are exposed beds of old ejecta which, from their structure, are regarded as products of a near-by crater that was probably situated in the former bay of Akabakkyô and near where the buried crater *F* is supposed to lie at present. The beds, which are composed of reddish-brown lapilli, bombs, and lava-blocks, are intercalated in the middle horizon of the cliff by a sheet of lava, about 3 m thick, dipping about 15°NW. The fragmentary ejecta are petrographically identical with the lava, both being an augite-olivine-basalt, containing large phenocrysts of anorthite more than 1 cm in diameter. Before the late eruption, the same lava was exposed on the northern shore of the former bay of Akabakkyô, forming

a costal platform, about 15 m above the sea, on which stood the fishing village of Simasita. At present most of it is buried beneath the new Akabakkyô lava-flow, although it is still exposed in a small area in the southern part of the former shore of Sitori.

Although the new ejecta from crater *F* cannot be recognized in the vicinity of the crater, owing to the latter being covered with ejecta from neighbouring vents, there is no doubt that they are fragmentary ejecta of an almost aphanitic lava. Thus the almost aphanitic bombs, which are scattered on the flat ground of Sitori, and among which those of more than 5 m in diameter are met with, must have been thrown out of crater *F*, seeing that the ground upon which they fell are bored in such a way that they show that the tracks of their flight were in the direction of the crater.

Crater *F* lies almost on the northeastern extension of a line connecting craterlets *A*, *B*, and *B′*, and which runs nearly along the boundary valley between Kamituki and Tubota. Judging from the accounts of eyewitnesses, in addition to *F*, there were probably two other vents active in the bay of Akabakkyô and on an extension of the same line, further northeast of *F*, although these vents cannot be found now.

8. *New cones G and H* (*Hyôtan-yama*). The submarine eruption that occurred at two places in the central part of the bay of Akabakkyô resulted in the formation of two new cones, *G* and *H*, which lie side by side on the northeastern extension of a line passing through craters *D* and *E*, and which have grown and joined into a mound named Hyôtan-yama, because its side view resembles a gourd.

The southwestern half of Hyôtan-yama is a flat cone, about 70 m above the sea, sloping $10\sim20°$ on all sides, except on the eastern side where it joins the western side of the other half of the mound. Thus the western slope of the cone extends to the former sea-cliff on the southern side of Akabakkyô-hana, where it joins the mainland of Miyake-sima. The base of the northern slope continues to the new lava-platform that occupies the northern part of the former bay of Akabakkyô; while the southern slope ends abruptly downward with a scarp, about 10 m high, which faces a new coastal flat that formed in the southern part of the former bay of Akabakkyô.

On the summit of the western cone, there is an oval crater *G*, the longer (EW) and the shorter (NS) axes of which are about 100 m and 80 m respectively. The upper rim of the crater gradually rises northward from its lowest point, about 50 m above the sea, on the southern side to its highest point on the northern side, the summit of the cone. The crater-bottom, which has an average diameter of about

20 m and lies about 50 m below the highest northern crater-rim, is covered with detritus that fell from the surrounding walls. The northern crater-wall has several vertical fissures, the larger ones of which form two vertical notches, about 5 m wide and 15 m deep, in the upper part of the wall.

The eastern half of Hyôtan-yama is occupied by another cone (eastern cone), which is both lower and smaller than the western cone, the two being joined together without forming any notable saddle or valley between them. Thus the eastern cone, which is about 40 m above the sea, and whose summit lies about 200 m ENE of the western cone, is joined to the latter by a ridge that runs ENE and gently descends in the same direction.

The eastern cone has a shallow, dish-shaped crater *H*, about 50 m in diameter, on the southern side of its summit. The bottom of the crater, which lies about 20 m below the summit of the cone, is flat ground, about 20 m across, covered with fragmentary ejecta (sand, lapilli, and bombs). The northern crater-wall is the highest, having a slope of about 25°, while the southern wall rises only a few meters from the crater-bottom. Thus the outer rim of the crater slopes steeply southward from the highest point on the northern side (top of the cone) to the lowest point, about 20 m above the sea, on the southern side.

The northern flank of the eastern cone extends with a slope of about 25° from the summit, near the upper rim of the northern wall of the dish-shaped crater, to the base, to which latter it is connected with a low, bomb-covered ground lying between Hyôtan-yama and the new lava-platform of Akabakkyô. The southern flank, which is but poorly developed, continues southward with a slope of less than 10° for a distance of about 50 m from the southern crater-rim, ending abruptly in a new sea-cliff, about 5 m high above sea level. The extensively developed eastern and northeastern flanks, which were still intact immediately after the eruption, gradually narrowed later, mainly owing to the erosive action of the sea until, at the end of October, as will be described in detail presently, the eastern half of the cone was found completely destroyed. Thus, at the end of July, these flanks showed a regular conical surface with a slope of about 20°, extending from the crater-rim downward to the foot, where they were fringed with a newly-formed sand-beach.

The conical part of Hyôtan-yama above the sea are composed of fragmentary ejecta (scoriaceous lapilli, bombs, and lava-blocks) containing large megascopic phenocrysts of anorthite, although they are underlain by a lava-flow containing the same phenocrysts. When the eastern

cone had been greatly worn down by the sea, a part of the lava-flow became exposed from beneath the overlying ejecta for the first time.

For several weeks following the eruption, the whole ground of Hyôtan-yama was so hot as to be almost unpassable, while at night the glow from the ejecta on the mound were visible quite a distance, so that although on July 24, the writer landed by a boat on the north-eastern shore of the eastern cone, he had to abandon all·hopes of ascending the mound on account of the heat and gases that charged every foot of ground. White vapor-clouds were issuing violently from fissures on the outer slopes near the crater of the western cone. Steam was also rising from the shore of the eastern cone, where the sea-water in contact with the hot ejecta had been heated locally to a temperature of as much as 60°C, killing a number of fish.

Three months later, at the end of October, the ground of Hyôtan-yama had cooled down to such an extent as to be freely passable, although some of the fissures near the summit were glowing inside and sending out hot gases. White vapors were issuing vigorously from fissures running ENE on the southern slope of the mound. So far as the summit of the western cone was then concerned, the mound had become a few meters lower than as observed in July.

9. Submarine crater. According to Uematu of Tubota, a submarine eruption occurred in the sea, east of Hyôtan-yama, in the direction N 20° E, as observed from Miike-hama. If his observation was fairly accurate, the crater whence the eruption occurred must have been situated in the sea, a few hundreds of meter off the eastern shore of Hyôtan-yama, almost on the eastern extension of the line connecting craters *D*, *E*, *G*, and *H*.

The above-mentioned craters, 1 to 9, with a total of more than twenty vents, were formed by the eruption almost simultaneously or in rapid succession within a few hours beginning at about 7:30 pm of July 12, 1940. Judging from the distribution of the ejecta, and also from the accounts of eyewitnesses, these craters must have erupted in the following order: B'_6 (and D ?) → (C, A, B, and $B'_{1\sim5}$) → (E and F) → (G, H, and the submarine crater No. 9), although the exact order in which they began or stopped activity can never be known. Roughly speaking, the eruption in craters $A \sim E$ on the mountain slope slightly preceded those from craters $F \sim H$ in the bay of Akabakkyô, both in beginning and ending, so that although the eruption of the former ended practically in the morning of July 13, that of the latter continued for several hours during the afternoon of the same day. The Hyôtan-yama craters (G and H) were no doubt the last to cease activity, seeing that

the ejecta from these craters overlie those from the remaining craters.

New lava-platform.

A lava-flow which, after descending the boundary valley of Kamituki and Tubota, poured into the northern part of Akabakkyô bay, formed a new platform which filled that part of the bay, covering also the old lava-platform of Simasita on the northern shore of the same bay. This new lava-platform occupies a rectangular area about 800 m long and 300 m wide in the EW and NS directions respectively. Although the surface of the platform is rough with small indentations peculiar to the surface of block lava, it forms as a whole a flat ground dropping imperceptibly eastward from a height of about 20 m above the sea in the western part to that of a few meters above the sea near its eastern margin. The northern margin in the western part of the platform forms a scarp about 5 m in height above the old ground, running east, while the southern margin of the platform is separated from the northern foot of Hyôtan-yama by a fissure-like channel, about 3 m both in width and depth, running east in a winding course on the boundary between them. At the end of July, the northeastern and eastern margins of the platform bordered the sea, although, as will be described in detail presently, they were fringed soon afterward with sand-beaches.

For several days following the eruption, the lava of the platform, which was moving very slowly, locally at least, in the direction of flow, was still red hot inside, as seen from crevices in the lava. During these days, the whole ground of the platform was so hot as to be hardly passable, discharging steam and other gases. Thus hot gases were issuing everywhere from the ground; steam was rising vigorously on the northeastern and eastern margins of the platform, where the lava came in contact with the sea; while smoke with the odour of burning trees rose from the northern part of the platform, where the lava buried every house in the village of Simasita. Three months later, at the end of October, the ground of the platform had cooled down sufficiently to permit passage over it, although local high temperatures ($80^\circ \sim 125^\circ C$) were observed at several places on the ground, where fumarolic activity was still going on. Steam was still rising from the eastern margin of the platform, although a sand-beach had walled off the latter from the sea.

Fissures.

On both sides of the boundary valley between Kamituki and Tubota, there are numerous fissures in the inside walls as well as on the crests

outside, running nearly parallel to the course of the valley. On the flat ground of the crests, the fissures often form trench-like depressions, a few meters in depth and width, while on the steep inner slopes of the valley, they form step-slips falling toward the valley-floor, causing occasional avalanches.

There are also numerous fissures on the ground of the newly-formed cones *A, B, D, G,* and *H*. Cones *G* and *H* of Hyôtan-yama have many fissures, of which those around the craters on the cones are mostly radial and concentric. The northwestern slope of cone *G* is crowded, particularly, with large fissures that run ENE, along which the ground of the slope slips down a step toward the northern foot of the cone. The bomb-covered, low ground adjoining the northern foot of Hyôtan-yama is also fissured, mostly in two directions, northwest to southeast and west to east.

Although most of the above-mentioned fissures were already present immediately after the eruption, they were seen at the end of October to have increased in number as well as in size. The majority of these fissures, which appear to have been confined to deposits of new ejecta without extending deeply into the underlying old ground, may be merely superficial as the result of settling and contraction of the deposits during cooling.

Besides these superficial fissures, there are two fissure-lines suggested by the linear arrangement of the newly-formed craters. One of these lines is the NE∼SW line obtained by joining craters *A*, *B*, and *B′*, and which may be regarded as a radial fissure-line extending the whole length of the northeastern slope of the volcano from the snmmit of Oyama downward to its foot near Akabakkyô. Thus the southwestern extension of the line reaches to the summit of Oyama, passing through an old parasitic crater near the northeastern rim of the caldera (Hayono-tairo); while the line extends from rift-crater *B′* northeastward to the site of crater *F* in the former bay of Akabakkyô, almost

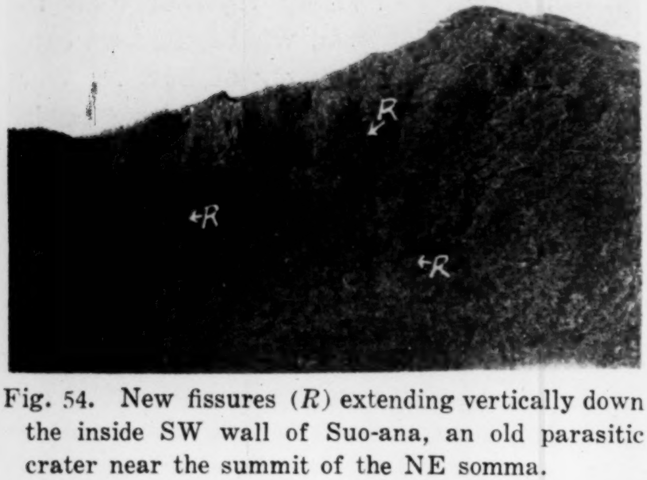

Fig. 54. New fissures (*R*) extending vertically down the inside SW wall of Suo-ana, an old parasitic crater near the summit of the NE somma.

following the lower course of the boundary valley between Kamituki and Tubota. The other fissure is an ENE～WSW line that connects craters *D*, *E*, *G*, and *H*. The western extension of this line which, however, is not in the direction of the summit of Oyama, appears to stretch to the somma, intersecting the above-mentioned line at crater *B*. Thus on the crest near the summit of the somma and in the western inside wall of Suo-ana, an old parasitic crater adjoining the east side of that summit, there are several new fissures lying on or near the western extension of this line (Fig. 54).

These two fissure-lines may be regarded as representing eruption-fissures that extend deep down from near the surface to the heart of the volcano, serving as an outlet for the underlying magma. According to a re-triangulation carried out immediately after the eruption by the Land Survey Department of the Imperial Army, the triangular points, Taka-yama (No. 9) near Akabakkyô and Okura-yama (No. 8) near Miike-hama, showed a northward displacement of 1·31 m and a southward displacement of 1·64 m respectively as compared with their former positions from the survey of 1912, suggesting a north-south dilatation of about 3 m of the land between them. These displacement may be well understood by assuming that the magma beneath the volcano intruded in the form of a dike along the eruption-fissures at the time of the late activity, and that the ground on both sides of the fissures was pushed aside by the intruded mass.

Change of coast-line.

The coast-line between Anô-saki and Satadô-saki shows a great change as the combined results of the formation of a new land reclaimed from the bay of Akabakkyô with the ejecta at the time of the late eruption and the marine action at work on the new land during subsequent days. Fig. 55 shows the coast-lines both before and after the eruption.

As will be seen from the figure, before the eruption, the coast-line between Anô-saki (*A*) and Satadô-saki (*G*) was deeply indented westward in the middle part from Mahana (*B*) to Yoridai-hana (*F*), bordering the bay of Akabakkyô, thus forming the best harbour in the island. The northern part of the coast (Sitori) between *A* and *B* was a gravel-beach dotted with exposures of old lava-flows, while its southern part near *B* was a vertical sea-cliff, 5～10 m above sea level, exposing a massive lava of augite-olivine-basalt containing large phenocrysts of anorthite. A sea-cliff of the same lava developed around the cape of *B* as far as the mouth of the boundary valley between Kamituki and Tubota (*C*). On this cliffy coast stood the fishing village

of Simasita. On the south side of C, there was a higher sea-cliff that rose gradually southward to the head of the cape of Akabakkyô-hana (D), where it attained a height of about 50 m. As already mentioned, this cliff was practically demolished by the eruption that lately occurred from crater F near its base. The coast between D and G was a sea-cliff, 20~30 m high above the sea, continuing for the whole length, the mouth of the Yomogiga-sawa (E) and that of the Yoridai-sawa (F) excepted, and exposing several superposed lava sheets. Being surrounded on its western side by sea-cliffs between B and F, Akabakkyô bay had an average depth of about 10 m.

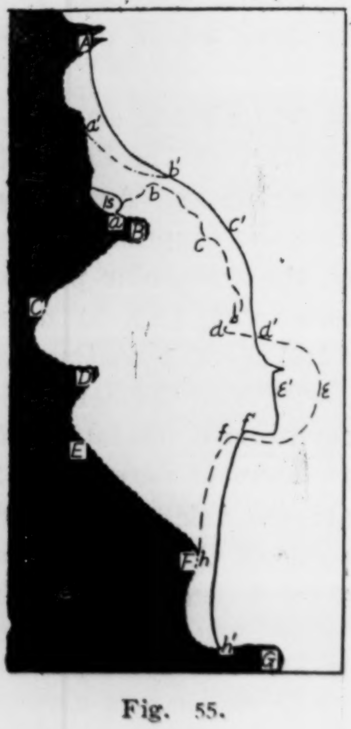

Fig. 55.

Immediately after the eruption, it was found that the bay, as a result of the activity, had been completely covered with new land, namely the Akabakkyô lava-platform and the Hyôtan-yama cones, and that the land had formed a new coast as shown by the line a–c–e–h in Fig. 55. At that time, coasts A–a and h–G were virtually as before. The new coast-line from a to c, which skirts the north-eastern margin of the Akabakkyô lava-platform, was greatly indented with small inlets that were the submerged ends of small depressions on the lava-flows of which the platform was formed. The farthest front of the lava-flows must have stopped on the sea-floor not far from the coast, seeing that, according to a provisional sounding executed by the officers of Kamituki, the sea near the shore between a and c had, as before, an average depth of about 10 m. The coast-line from c to d, which was the eastern margin of the bomb-covered, low ground between the Akabakkyô lava-platform and Hyôtan-yama cones, was also greatly indented with small inlets, although, a week after the eruption, it was seen already fringed locally by a narrow beach of sandy material brought from the sea by the incoming waves. The northeastern coast d–e of Hyôtan-yama was fringed with a long sand-beach, showing a smooth shore-line, while its south eastern coast e–f had already been cut with a sea-cliff, about 3~5 m above the sea. The coast between f and h was a sand-beach, fringing the eastern margin of the bomb-covered flat that had formed between the southern foot of Hyôtan-yama and the former sea-cliff E–F.

In the course of a few months following the eruption, the action

of the waves had completely changed the coast-line between *A* and *G*. In the middle of August, according to Honda[2] and his collaborators, the sand-beach between *f* and *h* had increased in width, and at the same time extended from *h* southward to the sea-cliff near *h'* on the northern side of Satado-saki. According to Miyamura[3], about the middle of the month following, it was found that much of the eastern part of Hyôtan-yama had been destroyed, and that the coast between *a* and *d* had been fringed with a continuous sand-beach extending from *a'* to *d'*. The inner part of the inlet (*a'–a–b*) of Sitori remained as a small lake (1s), about 150 m long and 50 m wide, embanked on its eastern side by a broad sand bar extending from *b'* to *a'*.

At the end of October, when the writer made his second visit to the island, the destruction of the eastern part of Hyôtan-yama and the growth of the sand-beaches on the neighbouring coast had advanced further, resulting in the formation of a coast-line, shown by the line *A–c'–e'–f'–h'*. Thus the eastern half of the eastern cone of Hyôtan-yama completely disappeared; a vertical sea-cliff was formed near the eastern crater-rim of the cone, giving rise to a north-south section that afforded a clear view of the internal structure of the cone; the sand-beach between *a'* and *b'* broadened and extended northward as far as Ano-saki, while the sand-beach between *f'* and *h'* increased in width as well as in the thickness of the deposit.

The newly-formed sea-cliff on the eastern side of Hyôtan-yama exposes massive lava, black scoria, and reddish-brown scoria, accumulating in succession from the base of the cliff upward. The lava, which is an olivine-basalt, sporadically containing large phenocrysts of anorthite, forms an almost horizontal bed, the visible part of which above the sea is about 3 m thick. The upper part near the surface of the lava bed is more or less scoriaceous, and contiguous (without any distinct boundary) to an agglutinate-like mass, 2～3 m thick, consisting of black scoria and bombs. The latter is overlain by an almost massive bed of reddish-brown scoria, the maximum thickness of which in the middle part of the cliff is about 20 m. Above this scoria-bed is a black lapilli-bed, less than 50 cm thick, sporadically containing bombs. Immediately after the eruption, this lapilli-bed was a continuous surface mantle of the eastern cone of Hyôtan-yama, although later it was covered by a thin bed of reddish-brown, scoriaceous sand that was scattered over the cone by the minor explosions that occurred several times on the eastern shore of Hyôtan-yama. The fragmentary ejecta exposed on the sea-cliff are, like

2) H. HONDA, *Kensin Ziho*, 11 (1940), 277.
3) Oral information.

the underlying massive lava, exclusively an olivine-basalt carrying large phenocrysts of anorthite.

The formation of the new sand-beaches, *A–d'* and *f'–h'*, is supposed by Honda and his collaborators to indicate a local upheaval of that part of the island, accompanied by local subsidence of the opposite coast near Ako. But, according to a levelling made after the eruption by the Land Survey Department of the Imperial Army, the island everywhere subsided more or less relative to the sea, excepting a small area near the coast around Satado-saki where a negligible upheaval of about 2 cm was measured. With this in view, and judging from the above-mentioned fact that the sand-beaches extended gradually from near the coast of Hyôtan-yama to a great distance in the course of a few months following the eruption, there is no doubt that they were virtually formed by the action of the waves. Thus, by wave action, the seaward side of Hyôtan-yama was washed away, its material distributed over the neighbouring sea bottom, and the material transported again, together with some ejecta that were scattered over the sea bottom by the eruption of July 12∼13, to accumulate on the adjoining coasts, resulting in the formation of the sand-beaches. The last-named consist of more or less water-worn fragments of new lava, isolated crystals of anorthite and olivine, and some accessory pumice. The lava fragments are almost exclusively, like the ejecta of Hyôtan-yama, an olivine-basalt carrying large phenocrysts of anorthite, although fragments of an aphanitic basalt, similar to the plateau-forming lava of Akabakkyô, are accumulated in a small area of the sand-beach that adjoins the eastern side of the new lake of Sitori. The isolated crystals of anorthite and olivine are not the primary ejecta (crystal-bombs or crystal-lapilli), but are regarded as pieces detached by wave action from lava fragments containing phenocrysts of these minerals.

The Zone of Summit Eruption.

As the result of the summit eruption of the central cone Oyama which, following the flank eruption of the somma on July 12∼13, lasted for 24 days from July 13 to August 5, the configuration of the area in and about the old craters on the central cone markedly changed. Sketch-map, Fig. 56, shows the feature of the top of the central cone when the writer visited it at the end of October, 1940.

New central cone. The most notable topographical change caused by the summit eruption was the formation of a new central cone extending over the northwestern half of the Oana crater and the whole of the upper (western) crater on the old central cone. The new central

cone has a composite structure consisting of three parts, the first, the second, and the third cones.

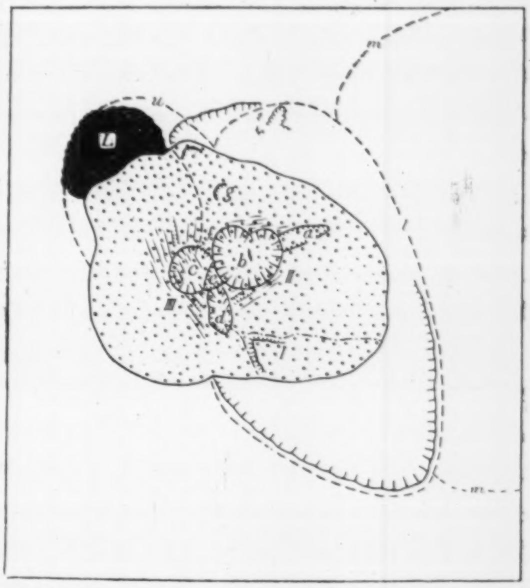

Fig. 56. Sketch-map showing the summit of Oyama.

I-II-III: New composite central cone. *a*∼*g*: Craters on the new central cone. *L*: New lava-coulee. *l*: Upper rim of Oana, the deepest crater on the old central cone. *m*: Upper rim of the eastern crater. *u*: Upper rim of the western (upper) crater.

The first cone. This cone, which had formed in an early phase of the summit eruption, was already seen at the time of our visit to the scene of the eruption on July 25, when, as viewed from the north-western part of the Hayono-tairo atrio, it appeared like a low homate formed around the second centre of activity, which was situated near the boundary between the Oana crater and the upper crater. After that, however, it was buried for the most part underneath the second and the third cones that were formed in the later phase of the summit eruption. Thus at present, only a small part of the first cone remains uncovered. forming a part of the southeastern side of the new composite cone.

Since the top of the remain of the first cone protrudes several meters from the slopes of the second and the third cones, the northern and western sides of the former adjoin the cliffs to the southern slope of the second cone and the southeastern slope of the third cone respectively. The southeastern side of the protrusion, which represents the original conical surface of the first cone, slopes about 35° southeast, widening from the top downward to the lowest part of the bottom of Oana, which lies about 60 m below the top. The top of the cone was dotted with feeble fumaroles at the time of the writer's visit.

The second cone. Although this cone, which rests on the first, occupying the greater part of the eastern half of the composite cone, is believed to have been formed by materials ejected largely from the second centre of activity, a slight change either in the centre of activity or in the direction of the ejecta must have occurred when the activity shifted from the first cone to the second, seeing that structurally they are slightly unconformable with each other.

Since the second cone, which has a diameter of about 300 m at the base, is slightly lower than the northern and southern walls of the Oana crater, its height is about 75 m above the lowest part of the pit of the bottom of Oana, or about 60 m above the flat ground in the north-western part of the Hayono-tairo atrio. Its outer slopes show a conical surface having a slope of about 30° on all sides except the west, where the cone joins the eastern side of the third cone, so that, although the southern slope of the cone is only imperfectly developed by protrusion of the first cone, the eastern and northern slopes are well developed, facing the inside eastern and northern walls of the Oana crater respectively.

The third cone. This cone, the result of materials ejected largely from the third centre of activity, forms the highest part of the composite cone, occupying the western half of the latter, and lying on the southeastern part of the old upper crater. It has a radius of about 250 m at the base, its height being about 90 m above the north-western atrio, or about 110 m above the lowest part of the crater-bottom of Oana, while its top is about 10 m lower than the head of the southern crater-wall of Oana.

The outer slopes of the third cone are regularly developed on all sides except the east, where the cone joins the western side of the second cone. The northwestern flank of the cone descends with a slope of about 35° from the top northwestward to the ground of a new lava-coulee which, as will be explained presently, fills up the northwestern part of the upper crater. The western and southern flanks of the cone, which form a slope of about 20°, stretch over the southwestern rim of the upper crater downward to the southwestern slope of the old central cone. The southeastern flank of the cone, which covers a part of the western crater-wall of Oana, descends abruptly with a slope of about 50° from the top to the base where it is contiguous to the western side of the remant of the first cone.

Craters on the new central cone. The new central cone has seven craters, as shown in Fig. 56, letters *a*, *b*.........and *g*. Of these, *a*, *b*, and *g* lie on the second cone, *c* on the third cone, and *d*, *e*, and *f* on the boundary of the two cones.

a. *Crater a*, which is a spoon-shaped hollow on the northeastern flank of the second cone, extends with a width of about 30 m from the top downward near to the base of the cone, forming a channel, about 5 m deep, in the ground of the cone surface. From its position, it is inferred that this crater corresponds to the first centre of activity, and consequently that, although the eruption at this point was not vigorous enough to form a conical mound, it lasted for some time after the vent

was buried beneath the materials (the second cone) ejected from a neighbouring vent (the second centre of activity), resulting in the formation of the crater in question. At the beginning of the summit eruption, as already mentioned, the first centre of activity was the only active vent that continually sent up a spiral column of ash-cloud, accompanied with fierce rumblings; while on July 25, when the eruption had culminated by ejecting bombs from the second and third centres of activity, it was sending up continually but very gently, only a small quantity of light-grayish ash-cloud. At the end of October, white vapors were rising from the ground in and about crater *a*, the successor to the first centre of activity.

b. *Crater b*, which is the largest of the craters on the new central cone, lying on the second cone, is a circular bowl, about 100 m in diameter, surrounded by almost perpendicular walls, exposing an unstratified pile of reddish-brown ejecta (volcanic sand, lapilli, bombs, and lava-blocks). The crater-bottom, which is also covered with these ejecta, is about 100 deep in its western part, and about 70 m deep in its eastern part.

Judging from its location, this crater corresponds to the second centre of activity. Thus, as viewed from the northwestern part of Hayono-tairo, the former is exactly in the direction of the latter which, on July 25, was seen from the same point sending up, periodically, a black ash-cloud densely charged with non-incandescent bombs. At the end of October, white vapors were issuing from many fissures on the ground outside the crater-bowl, the ejecta exposed in some of the fissures being still red-hot, although there was neither fumarole nor solfatara on the bottom of the crater.

c. *Crater c*, which represents the main vent of the third cone, lying on the eastern side of the highest point of the cone, is a circular dish-shaped hollow, about 80 m across. The crater-rim is highest on the western side, descending gradually eastwards. The crater-walls, that slope about 25° inward, are thus about 35 m and 20 m in height on the western side, and the northern and southern sides respectively, while the eastern crater-wall is almost non-existent. The eastern margin of of the crater-bottom, which is flat ground, about 30 m across, covered with sand, lapilli, and bombs, is delimited by the western rim of the adjoining deeper crater e.

This crater is succeeded to the third centre of activity which, as viewed on July 25 from the northwestern part of Hayono-tairo, was erupting in rapid succession with lightning-like flashes, accompanied by ejection of incandescent bombs. At the end of October, white vapors were issuing from many fissures on the ground in and about the crater.

d. Crater d lies about 25 m northwest of the top of the first cone and on a level several meters higher than the latter, on the boundary between the southwestern flank of the second cone and the southeastern flank of the third cone. It is an oval hollow about 50 m long and 30 m wide, becoming narrower toward the bottom, which has a diameter of about 5 m. The eastern and western crater-walls, sloping about 50° inward, cut deeply the southwestern flank of the second cone and the southeastern flank of the third cone respectively. The northern crater-wall is a narrow ridge, about 20 m high, which separates this crater from the adjoining crater *e*. The southern crater-wall forms a low, narrow ridge, sloping steeply toward the crater-bottom on one side and gently toward the top of the first cone on the other. At the end of October, neither fumarole nor solfatara was found on the crater-bottom, which was covered with detritus from the surrounding walls.

e. Crater e, which is a triangular-shaped hollow, about 20 m across and 10 m deep, occupying the interspace between *b*, *c*, and *d*, is separated by thin walls, probably less than 5 m thick, from *b* on the east as well as from *d* on the south. The western side of the crater forms a cliff falling almost perpendicularly from the eastern margin of the crater-bottom of *c*. At the end of October the crater contained several vents discharging white vapors.

f. Crater f, which is a shallow, dish-shaped hollow adjoining the northwestern and northeastern rims of *b* and *c* respectively, is separated from *c* by a low saddle, sloping very gently on both sides toward the crater-bottoms, while the former is cut on the eastern side by the rim of the inside northwestern wall of *c*. The crater-bottom is covered with lapilli and bombs. At the end of October, it was studded with numerous small vents sending up white vapors.

g. Crater g, a circular dish-shaped hollow, about 20 m across and 5 m deep, lies half-way down the northern flank of the second cone.

The foregoing seven craters are *b*, *c*, *d*, *e*, *a*, *f*, and *g* diminishing in size in the order given, while *a*, *b*, *g*, *d*, *e*, *f*, and *c* increase in the order of height of crater-bottom, as measured from the lowest part of the crater-bottom of Oana. Of these craters, *b* and *c*, which are the main vents of the new central cone, are arranged together with *a* on a ENE–WSW line, while the others, which may be regarded as subsidiary, rather epigenetic vents participating more or less in modifying the original form of the cone, are arranged on a NNW–SSE line running nearly along the boundary of the second and third cones. These two crater-lines intersect nearly at right angle in the vicinity of crater *e*.

Besides the foregoing craters, there is a small, shallow depression

on the northern foot of the second cone, and nearly on the northern extension of the NNW–SSE crater-line above referred to, which may be regarded as the remnant of a new crater, although most of it is buried in the talus of the cone.

New lava coulee. On the northwestern foot of the new central cone is a new lava coulee, about 130 m in length from northeast to southwest and about 85 m in maximum width from northwest to southeast, extending in a semi-circular area, approximately $2 \times 10^4 m^2$. The lava coulee is circumscribed by the rim of the old upper crater on all sides except on its southeast, where it is buried beneath the new central cone. Thus the northeastern and northern margins of the lava coulee come in contact with the inside northeastern and northern walls of the crater, while the western margin bulges out only a few meters westward over the rim of the western wall of the crater.

The surface of the lava coulee is generally flat with a veneer of fragmentary ejecta, which is less than 10 cm thick in the northwestern part, reaching an extreme thickness probably of more than 1 m in the southeastern part near the foot of the central cone. The northwestern margin of the lava coulee forms a cliff about 3～5 m high, exposing the lava which, although broken to angular blocks on the surface of the exposures we meet with a more or less ropy, fluidal structure, besides parallel scratches aligned in the direction of the flow.

New fissures. The new central cone is cut by numerous fissures as indicated by trench-like depressions, stepped slides, and by lines of fumaroles. Thus, in and around crater *c* on the third cone are numerous parallel fissures running in a NNW–SSE direction, while outside the northern and southern walls of crater *b* on the second cone are fissures running parallel in a ENE–WSW direction. These two fissure systems, NNE–SSE and ENE–WSW, which are nearly parallel to the crater-lines, *d–e–f–g* and *a–b–c*, respectively, indicate the lines of structural weakness not only of the new central cone but possibly also of the underlying ground. One of the fissures on the eastern side of the top of the third cone forms a trench-like depression, about 15 m wide and 5 m deep, cutting the southwestern wall of crater *c* in a NNW–SSE direction.

The southern inside wall of the Oana crater fissured and collapsed along its upper margin, probably owing to shocks received during the summit eruption, resulting in an almost perpendicular cliff with a talus conoid at the base, whereas formerly it was a slope clothed with vegetation. In the newly-formed cliff of the wall are exposed two sheets of lava, of which the upper one exposed at the brink of the cliff is an augite-olivine-basalt.

The western half of the northern inside wall of the Oana crater also fissured and broke down by explosions that probably occurred near the base of the wall early on July 19 and 20, so that the wall now forms an almost perpendicular cliff, about 30 m high, whereas formerly it was a slope of about 50°, clothed with vegetation. In the upper part of the cliff is exposed a sheet of massive lava (augite-olivine-basalt), about 1 m thick, intercalated in a thick bed of reddish-brown scoria. Under this bed, in the lower part of the cliff is exposed another lava (augite-olivine-basalt), more than 5 m thick which, near the surface of the cliff is white, probably due to decomposition by solfataric action. This rock may be the source of the whitish sand and lapilli that fell in quantity in the vicinity of Akabakkyô during the summit eruption of July 19 and 20.

The inside eastern wall of the Oana crater was not much altered by the summit eruption, remaining as before, a perpendicular lava-cliff, although the lower part of the cliff was deeply buried in new ejecta.

IV. Distribution and Volume of the Solid Ejecta.

The Zone of Flank Eruption.

The solid materials ejected by the flank eruption are volcanic ash, sand, lapilli, bombs, lava-blocks, and lava-flows. The distribution of these ejecta on the island will be seen from Fig. 5.

Volcanic ash. The volcanic ash are distributed in a fan-shaped area, widening northeastward from the uppermost crater A. Thus the northern limit of the ash-covered area is represented by a straight line connecting A and Hodai, and the southern limit by another straight line connecting A and the northern corner of Miike-hama. Very little ash accumulated in this area, their deposit being less than 1 m thick even in the central part near the boundary valley between Kamituki and Tubota. Although ash are accumulated about 5 cm deep in the southern part near Miike-hama, most of it is ejecta from the summit of the volcano.

Volcanic sand, lapilli, bombs, and lava-blocks. These cover a fan-shaped area, about 2 km long and 1 km wide, extending from the uppermost crater A northeastward to the former bay of Akabakkyô, besides having accumulated in the form of new parasitic cones about craters A, B, D, G, and H. Their thickest deposit is a zone, about 400 m wide, extending from crater A northeast toward Akabakkyô. The deposit, which reaches to about 3~5 m in thickness in this zone, thins out rapidly on both sides, while near the margin of the fan-shaped area, the ejecta

lie only sparsely on the surface of the old ground.

The quantities of volcanic sand and lapilli are, generally speaking, relatively small. Thus, so far as the visible parts are concerned, the above-mentioned fan-shaped area is covered for the most part with coarser ejecta—scoria, bombs, and lava-blocks—which usually exceed 5 cm in diameter. The only part where volcanic sand and lapilli are abundantly found was a small area, already washed away by the waves, in the eastern half of Hyôtan-yama. Although some volcanic sand and fine lapilli cover the gentle slope adjoining the southern side of the boundary valley between Kamituki and Tubota, most of them are materials that were ejected by the summit eruption.

The volcanic bombs have accumulated thickly on the ground around the craters. Judging from the distribution of these bombs, their ejection from a crater took place mainly at a later stage of the eruption of the crater. For example, Hyôtan-yama is thickly covered with volcanic bombs, while, as observed in the sea-cliff on its eastern side, its inner part is largely composed of scoriaceous lapilli and blocks.

The diameter of the volcanic bombs mostly exceed 10 cm, the largest one so far found being about 10 m, while those of less than 5 cm are rare. The bombs are divided into two kinds according to their internal appearance, compact bombs having relatively smooth surfaces and porous bombs having uneven surfaces. In their fall upon the ground, the compact bombs are either scarcely deformed or are broken into several angular fragments, whereas the porous bombs are either more or less flattend or are partly imbedded in the ground, their surface conformations indicating that they must have been plastic when they reached the ground. The ground on which the large-sized bombs are scattered is dotted in places with conical hollows formed by their fall. These hollows are nsually several times larger than the bombs found in them.

Along with the volcanic bombs, irregular-shaped lava-blocks are accumulated on the ground around the new craters, particularly so on the mountain slope adjoining the northern side of the *B′* rift-crater, where huge lava-blocks, about 10 m in diameter, are frequently met with.

The above-mentioned fragmentary ejecta are divided petrographically into two kinds, porphyritic olivine-basalt containing large phenocrysts of anorthite, and almost-aphanitic basaltic-andesite. The ejecta of porphyritic basalt, which were thrown out exclusively from craters G and H, are distributed in a circular area, about 600 m in radius, extending northward to Sitori and southwestward to Yoridai-sawa, with

Hyôtan-yama as the centre. The ejecta of the almost aphanitic basaltic-andesite, which were projected from all the new craters except G and H, are distributed over the greater part of the fan-shaped area just mentioned, widening out from crater A downward to an extreme width of about 2km. Although the products ejected from the various craters must have accumulated in various areas, each according to the source of ejection, owing to their uniform petrographic characters, they cannot be distinguished the one from the other. The northeastern part of the area that is covered with the almost-aphanitic ejecta falls on that of the porphyritic ejecta. Here, there are not a few instances in which a porphyritic bomb and an aphanitic bomb are piled one on top of the other, in which case the porphyritic bomb always rests on the aphanitic bomb, indicating that the outpouring of the porphyritic ejecta from Hyôtan-yama continued for some time after that of the aphanitic ejecta from a certain neighbouring crater had ceased.

The total volume of the fragmentary ejecta is approximately $85 \times 10^5 m^3$, inclusive of the subaerial part of Hyôtan-yama, which has a volume of about $72 \times 10^5 m^3$. Its greater part must be occupied by coarse scoria, bombs, and lava-blocks, seeing, as already mentioned, that the amount of the finer ejecta (ash and sand) is relatively small. This fact may be a characteristic of the flank eruption, suggesting that the eruption took place with a relatively week explosive force from the eruption-fissures that opened on the mountain slope as the result of interusion of magma underneath the volcano.

Lava-flows. In the zone of flank eruption are three new lava-flows, the Akabakkyô, the Yoridai-sawa lava-flow, and the Hyôtan-yama lava-flow. These lava-flows are distributed as follows:

The Akabakky) lava-flow. This flow, which is represented by the Akabakkyô lava-platform already referred to, can be traced from the mouth of the boundary valley between Kamituki and Tubota upstream to the B′ rift-crater, whence the lava is exposed in the northern and southern walls of the crater, while no more of it is found on the A and B cones, which are composed entirely of fragmentary ejecta. Besides, outside of the B′ crater are found a number of huge volcanic bombs and blocks, petrographically similar to the lava, so that it is inferred that the lava erupted from this crater.

Although most of the lava must have flowed directly into the boundary valley, part of it overflowed the southern wall of the crater, with the result that the lava is distributed on the mountain slope adjoining the southern side of the crater, where it forms a blocky lava-field extending about 250 m from WSW to ENE with a maximum width of

about 100 m. At the southeast corner of the field, the lava-flow branches off northeast across a small valley, while at the northeast corner it forms a lava-cascade, about 20 m wide, hanging over a steep southern wall of the boundary valley. The lava-field, which is composed of broken lava with some volcanic bombs and other fragmentary ejecta, is greatly indented with small ridges and furrows, most of them running E–W and N–S. At the end of October, 1940, white vapors were issuing from a number of fumaroles developed in the lava-field, and a small pond, about 20 m in diameter, was found at the southeastern corner of the field where the lava had dammed a small valley.

The lava-flow is scarcely exposed on the bottom of the B′ rift-crater nor on the space of about 600 m of the floor of the boundary valley into which the crater opened, where it is buried beneath the detritus (fragments of volcanic bombs and scoriaceous lapilli) that fell from the side wall (Fig. 57).

The lava-flow is exposed continuously on the floor of the boundary valley from the middle course of it, about 180 m above the sea, downstream to the mouth of the valley, although its margins near the valley walls are covered with detritus that slid down from the walls. Thus, on the southwestern foot of Taka-yama, where the valley floor is about 90m wide, the lava-flow is exposed for a width of about 35 m in the central part of the valley floor, while on the southeastern foot of the same hill, where the valley floor becomes less than 30 m wide, the flow not only covers the valley floor, but is thrown up like a lateral morain outside the valley. From the mouth of the boundary valley eastward, the lava-flow is distributed over an extensive area that covers the northern part of the former bay of Akabakkyô, forming the Akabakkyô

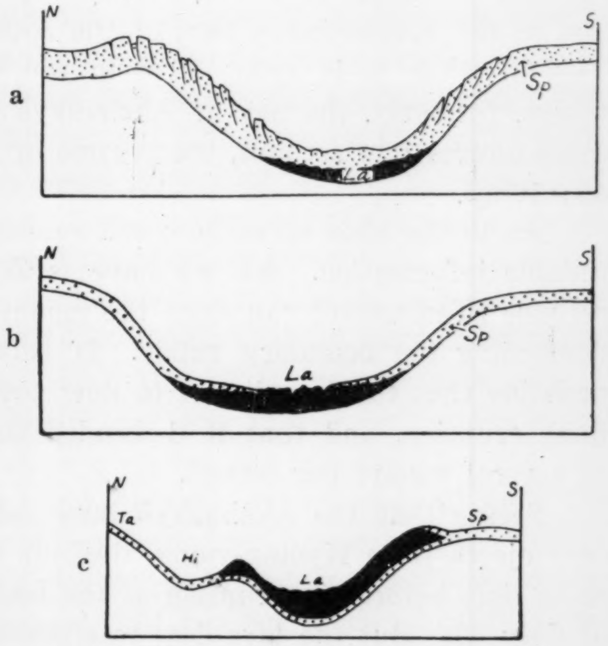

Fig. 57 a, b, c. Diagrammatic cross-sections of the boundary valley between Kamituki and Tubota. a. Upper course. b. Middle course. c. Lower course.

Sp: Volcanic sand, lapilli, and bombs. *La*: Akabakkyô lava. *Ta*: Taka-yama. *Hi*: Hino-ana.

Hyôtan-yama, where it lies almost horizontally, occupying the lower one-tenth of the cliff. On the southeastern coast of the mound, where the sea-cliff is about 3~5 m above sea level, the lava-flow forms almost the whole surface of the cliff, rising gently westward, while at the western end of the cliff, it gradually turns into an agglutinate-like mass of volcanic bombs and scoria. The same lava is also exposed patchwise on the sand-beach that adjoins the northern end of the eastern sea-cliff of Hyôtan-yama.

Judging from its distribution and its disposition as exposed in the sea-cliffs above referred to, the Hyôtan-yama lava-flow is believed to have erupted from crater G at an earlier date, when the crater was still below sea level. Although its bottom is not visible, it is possible that the lava-flow is about 13 m thick, assuming that the lava rests directly on the former bottom of the bay of Akabakkyô. The volume of this lava-flow is approximately $24 \times 10^5 m^3$.

The total volume of ejecta distributed over the zone of flank eruption is approximately $15{\cdot}7 \times 10^6 m^3$, and the entire mass $39{\cdot}2 \times 10^6$ tons, assuming that the average density of the ejecta is 2·5. This mass nearly equals the mass of the ejecta of 1874, while the former corresponds approximately to 1/75 of the whole of the ejecta of Sakura-sima in 1914.

The Zone of Summit Eruption.

New fragmentary ejecta. The fragmentary materials ejected by the summit eruption are volcanic ash, sand, lapilli bombs, and lava-blocks. These ejecta not only constitute the new central cone, but are also scattered around the cone.

The new central cone is composed wholly of fragmentary ejecta of various sizes. As to its remnants, the first cone is covered with relatively larger-sized bombs and lava-blocks. The second cone being composed of volcanic sand, lapilli, bombs, and lava-blocks, the sand, lapilli, and small-sized bombs are distributed on the top as well as on the northern slope of the cone, while relatively larger-sized bombs and lava-blocks are accumulated on the eastern and southern slopes. The third cone is also composed of volcanic sand, lapilli, bombs, and lava-blocks.

The new central cone, consisting of the foregoing three parts, has a volume of approximately $3 \times 10^6 m^3$.

Volcanic bombs and lava-blocks are distributed in an oval area measuring about 850 m from NNE to SSW and 650 m from WNW to ESE, with the new central cone as the centre. Thus they lie scattered in the central part of Hayono-tairo as well as on the ground outside the southern rim of the Oana crater. On the northern flank of the old central

cone are found not a few large bombs that reach an extreme diameter of about 3 m. Large bombs and lava-blocks are also found in the south-eastern foot of the new central cone, where they are accumulated possibly more than 10 m deep, together with smaller ejecta.

Volcanic ash, sand, and lapilli are distributed in a fan-shaped area that widens out from the point of eruption on the new central cone ENE to an extreme width of about 3 km. Thus their deposit is thickest in a zone running from the summit ENE toward Akabakkyô, where it reaches several centimeters in thickness, and thins out rapidly on both sides of that zone. Toward the summit, the thickness of the deposited ejecta as well as the sizes of the individual ejecta naturally increase, the volcanic sand and lapilli attaining a thickness of about 50 cm on the northeastern flank of the old central cone and about 1 m on the southern rim of the east crater, while they are accumulated possibly several meters deep on the bottom of the same crater, where formerly were found bombs, and anorthite lapilli of unknown age. A number of small bombs, about $0{\cdot}5 \sim 1{\cdot}0$ cm in diameter, are found on the bottom of the east crater, although neither Pele's hairs nor tears are found. In the later period of the summit eruption, ash fell on the mountain slopes in the directions of Tubota, Ako, and Igaya, according to change of wind, but their deposit on these slopes is negligible in amount, excepting within a distance of about 100 m from the foot of the new central cone, where ash are accumulated several scores of centimeter deep along with sand and lapilli. The total volume of the fragmentary ejecta distributed over the zone of summit eruption is approximately $7 \times 10^4 m^3$, exclusive of the new central cone.

New lava-flow. In the zone of summit eruption, as already mentioned, there is a new lava-flow on the northwestern foot of the new central cone. We have no information regarding the time of eruption and the centre of outflow of the lava, but, from field observations, the lava must have erupted either from the second or the third centre of activity some time between July 25 and 31, before the new central cone had grown into its present size. Consequently, although its bottom is not visible, it is possible that the lava extends for some distance underneath the central cone, with a thickness of possibly more than 5 m. So far as its visible part is concerned, the lava has a volume of $10^5 m^3$ approximately, assuming its average thickness to be 5 m.

V. Damage caused.

Since, in the late eruption of Miyake-sima, it was possible for the

lava-platform already referred to. The village of Simasita is buried completely by the lava, although a very small rocky hill of the village, called Nezumisama, is left uncovered.

Although the lava-flow is represented locally by a conglomeration of angular lava-blocks, it forms on the whole a continuous, massive lava-sheet, except for the surface crust which is broken into blocks. Thus, in the lower course of the boundary valley and on the Akabakkyô lava-platform, where the lava-flow is traversed by contraction-fissures in many directions, massive parts of the flow are exposed in the walls of the fissures. Furthermore, on the Akabakkyô lava-platform, the lava-flow consists locally of two or three massive lava-sheets intercalated by scoriaceous lapilli and blocks, accumulating one on top of the other.

The thickness of the lava-flow on the floor of the boundary valley and in the northwestern part of the Akabakkyô lava-platform is about $3\sim5$ m, while it is about 15 m in the southern part of the platform where, formerly, the bay of Akabakkyô was about 10 m deep. Taking these figures into account, the volume of the lava-flow is approximately $45\times10^5 m^3$.

As to the time of outflow and rate of flow of the lava, there is no reliable information. All we have is Z. Asanuma's statement that a refugee (Yamamoto) ran down the mountain slope, seeing the lava-front descending the boundary valley. If this information is correct, it is probable that the lava began to flow out shortly after the start of the flank eruption, and that it descended the boundary valley at the rate of several meters per second.

Seeing that the Akabakkyô lava-platform is dotted with fragmentary ejecta from Hyôtan-yama, the bulk of the former evidently formed some time before the eruption of the latter ceased during the afternoon of July 13. But the lava-flow was moving slowly, locally at least, for several days more. Thus, on the morning of July 13, some of the houses in Simasita were still uncovered, while the next morning, the

Fig. 58. Diagrammatic section of the new land reclaimed from the bay of Akabakkyô.
La: Akabakkyô lava-platform. *Lc*: Hyôtan-yama lava. *Sb*: Hyôtan-yama ejecta. *G*: crater on the western cone of Hyôtan-yama. *Ne*: Nezumisama. *Si*: Sitori. *SL*: Sea level.

ground adjoining the northern side of the small rocky hill (Nezumisama) in the village was still readily passable, whereas on the morning of July 15, when the writer visited Akabakkyô for the first time, the village had

been completely deluged with the lava-flow, exactly as we see it today Moreover, according to Hagiwara, the lava-flow at the mouth of the boundary valley, on July 19, was moving at the rate of about 3 m a day, and it was nearly five days later that the movement become almost imperceptibie.

The Yoridai-sawa lava-flow. This flow, which came from crater D, poured southwestward into the Yoridai-sawa valley, reaching Kurano-taira, about 1 km distant from the crater, in the lower course of the valley. Being dammed by the lava-flow, a gourd-shaped lake, about 100 m in maximum diameter, was formed on the valley floor adjoining the northern foot of Daihannya-yama. Besides this main flow, a smaller one, which overflowed the northern rim of the crater, descended the adjoining mountain slope eastward for a distance of about 150 m.

At a point about 500 m distant from the crater, the lava-flow in the Yoridai-sawa reaches a maximum width of about 100 m, while at the farthest front, it is only about 5 m wide. At a distance of about 300 m from the crater, where formerly a cliff stood on the valley floor, the lava-flow forms a lava-fall, about 15 m high and 20 m wide. The thickness of the lava-flow is about 5∼10 m throughout the whole course of the flow, its volume being approximately $3 \times 10^5 m^3$.

As to the time of outflow of the lava, although no reliable information is available, it may be said that the lava issued some time toward the end of the flank eruption, seeing that it is covered with only a small amount of fragmentary ejecta that was thrown out by the eruption. On July 17, when the writer observed the lava-flow for the first time, its end at Kurano-taira had already grown cold all over the surface except for a few spots where secondary fumaroles were issuing vapors. On the boundaries adjacent to the lava-flow, trees were down, but not burnt, pointing to comparatively low temperature of the lava at the time of flow. So far as the lava-flow in the lower course is concerned, its temperature at the time of eruption might not have been high enough to yield a stiff viscous flow. Thus the lava-flow, which is not traversed by gaping crevices due to thermal contraction, is broken into solid, angular fragments, suggesting in appearance nothing but boulders and debris.

The Hyôtan-yama lava-flow. Although, immediately after the eruption, Hyôtan-yama, from appearances was believed to have been built up with fragmentary ejecta alone, it was found later, when much of the eastern part of the mound was demolished by the action of the waves, that the fragmentary ejecta is underlain by a massive lava-flow, the last-named being exposed in the sea-cliff on the eastern side of

majority of those who lived in Simasita and on the mountain slope near Akabakkyô to escape the moment they saw the beginning of the activity, the casualities were fortunately small, although there was considerable damage to property. The following table, based on investigations made by the Miyake-sima Branch of the Tokyo Prefectural Office, gives the results of the eruption.

	Kamituki	Tubota
People killed (fate unknown)	9	2
People wounded	10	10
Cows killed	12	13
Houses burnt and buried under ejecta	47	20
Farms and forests devastated	$48\times10^4 m^2$	$90\times10^4 m^2$

(*to be continued.*)

---

27. 昭和 15 年 7 月三宅島の噴火

三宅島噴火の地質學的觀察 (II)

地震研究所　津屋弘逵

三宅島火山の今回の活動はその外輪山の北東側山腹と中央火口丘とに相次いで起つた複噴火で，昭和 15 年 7 月 12 日から翌月 5 日頃までの約 25 日間續き，同期間中に頻發した噴火は舊火山體を破壞し，その地形を著しく變化せしめる樣な激烈な爆發を起さなかつたが，噴火地帶内に新噴出物を堆積せしめ若干の新しい地形を形成した．即ち山腹地帶では，A 乃至 H の總計 22 に達する新噴出孔が生じ，何れも火山砂礫，火山彈等を拋出し，また B′，D，及び G 火口は夫々赤場曉，ヨリダイ澤，及瓢箪山熔岩流を流出せしめた．また山頂噴火地帶では，舊中央火口丘上に第一，第二，及び第三丘より成る新複合火口丘が生じ，少量の熔岩流が新熔岩臺地を形成した．本文では之等の噴火地帶に於ける新噴出孔の配列，新噴出物の分布及び量，地形變化等に就いて考察した．(未完)

Fig. 59. July 19, 1940. Cone *A*, looking south. Photo Tsuya.

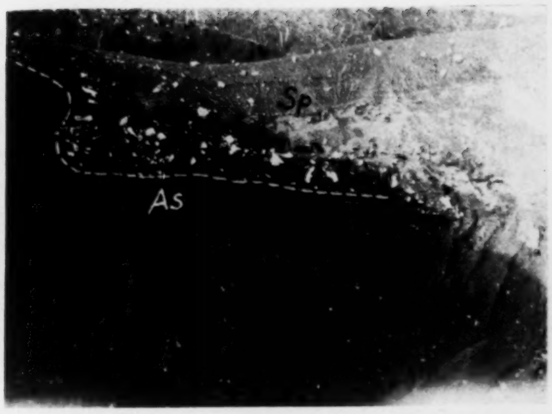

Fig. 60. Oct. 25, 1940. Northern inside wall of crater *A*. *Sp*: New ejecta. *As*: Old ground. Photo Tsuya.

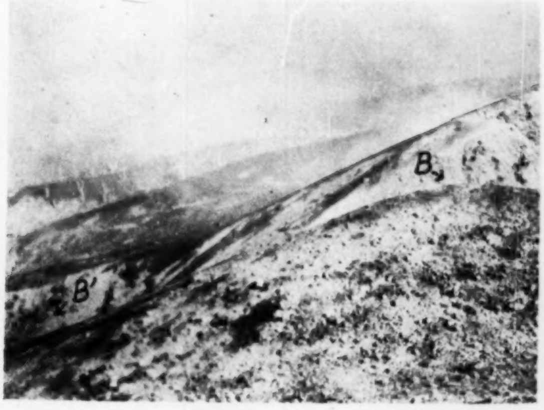

Fig. 61 a. July 19, 1940. Crater *B*, looking south. Photo Tsuya.

Fig. 61 b. July 19, 1940. Crater *B*, looking south. Photo Tsuya.

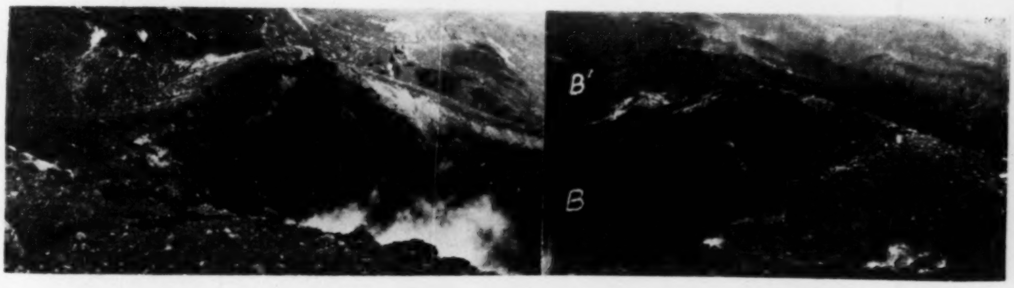

Fig. 61 c. Oct. 25, 1940. Crater *B*, looking east. Photo Tsuya.

(震研彙報 第十九號 圖版 津屋)

Fig. 69. July 27, 1940. Akabakkyô lava platform, looking south from Nezumisama. Hyôtan-yama in left background. Former sea-cliff of Akabakkyô-hana in right background. Photo Tsuya.

Fig. 70a. July 27, 1940. Southern margin of Akabakkyô lava-platform. *La*: Akabakkyô lava. *Hb*: Hyôtan-yama bombs. Photo Tsuya.

Fig. 70b. July 21, 1940. NE margin of Akabakkyô lava-platform. Hyôtan-yama in the background. Photo Tsuya.

Fig. 70c. July 26, 1940. Northern margin of Akabakkyô lava-platform. Hyôtan-yama in background. Photo Tsuya.

Fig. 68 a. Oct. 28, 1930. Western slope of Hyôtan-yama, looking north. Photo Tsuya.

Fig. 68 b. Oct. 28, 1940. Western cone (*G*) of Hyôtan-yama, looking north. Photo Tsuya.

Fig. 68 c. July 20, 1940. Northeastern flank of eastern cone of Hyôtan-yama. Photo Tsuya.

(震研彙報 第十九號 圖版 津屋)

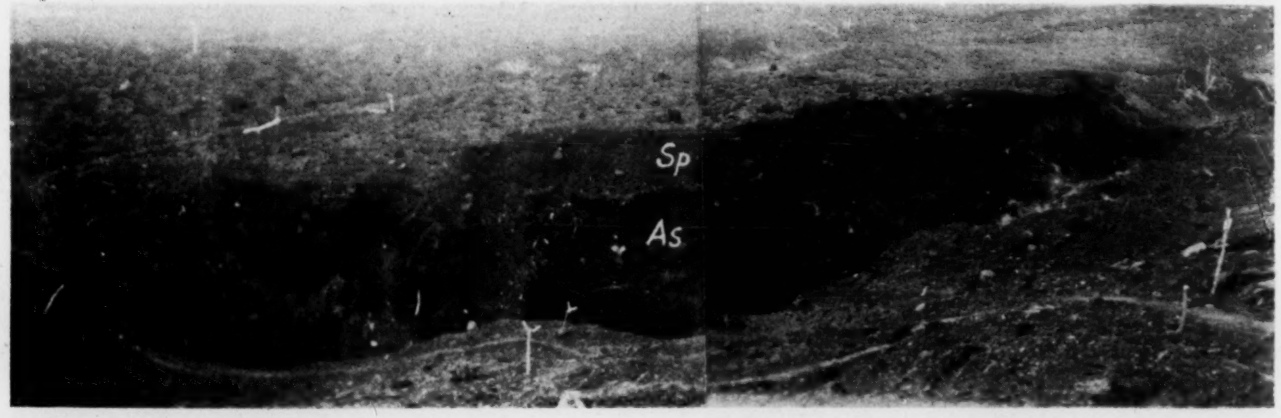

Fig. 66. Oct. 27, 1940. Craterlets *E*. *Sp*: New ejecta (volcanic sand and lapilli). *As*: Old ejecta (volcanic ash). Photo Tsuya.

Fig. 67 a. July 27, 1940. Crater *F*, now covered with volcanic bombs. Upper right, former sea-cliff of Akabakkyô-hana (point). Photo Tsuya.

Fig. 67 b. Nov. 2, 1940. Lower part of former sea-cliff of Akabakkyô-hana. Photo Tsuya.

（震研彙報 第十九號 圖版 津屋）

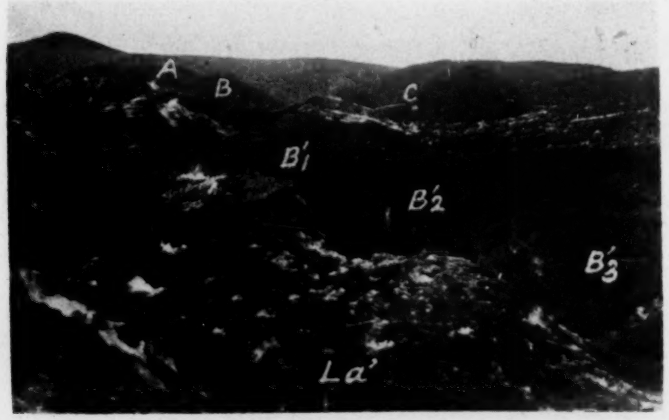

Fig. 62. Oct. 27, 1940. Craters $A \sim C$, looking west. La': Akabakkyô lava-flow. Photo Tsuya.

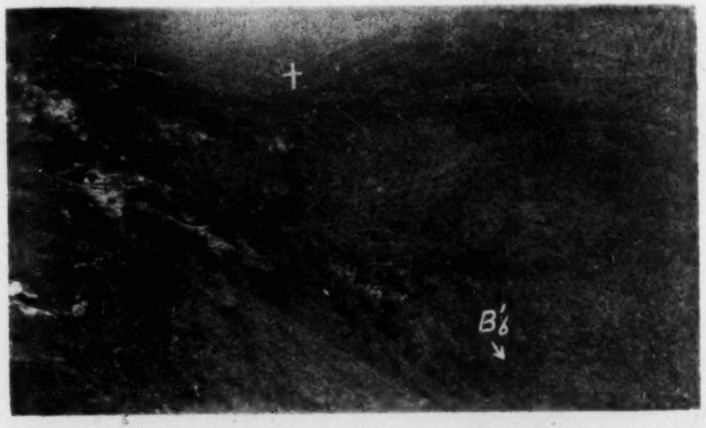

Fig. 63. Oct. 27, 1940. Crater B_6', looking north. Cross: The spot where a family consisting of 6 persons was buried beneath ejecta. Photo Tsuya.

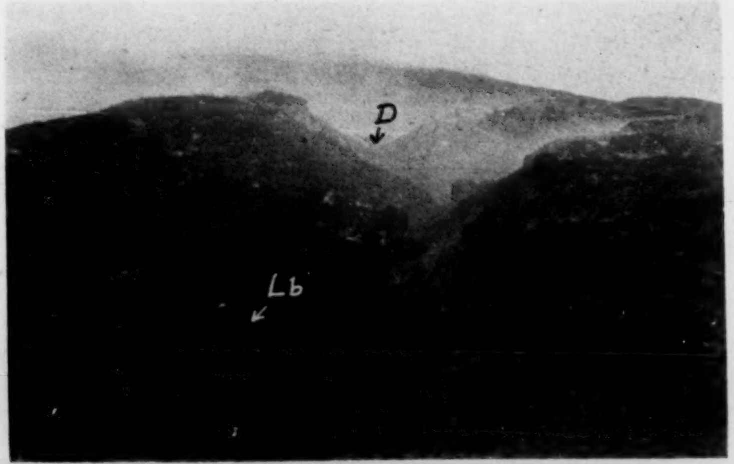

Fig. 64. Oct. 27, 1940. Crater D, looking west. Lb: Yoridai-sawa lava-flow. Photo Tsuya.

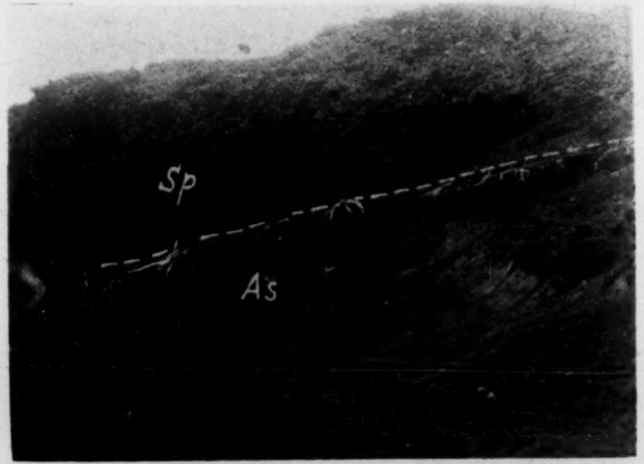

Fig. 65. Oct. 25, 1940. Southern inside wall of crater D. Sp: New ejecta. As: Old ejecta. Photo Tsuya.

(震研彙報 第十九號 圖版 津屋)

Fig. 71. Oct. 28, 1940. New sand-beach on eastern margin of Akabakkyô lava-platform, looking north. Photo Tsuya.

Fig. 72. Oct. 28, 1940. Lake Sitori (*ls*) embanked on its eastern side by sand-beach (*S*). *La*: Akabakkyô lava. *M*: Former sea-cliff. Photo Tsuya.

Fig. 73 a. Oct. 27, 1940. Sea-cliff on eastern side of Hyôtan-yama, looking south. Photo Tsuya.

Fig. 73 b. Oct. 28, 1940. Sea-cliff on SE side of Hyôtan-yama, looking north. Photo Tsuya.

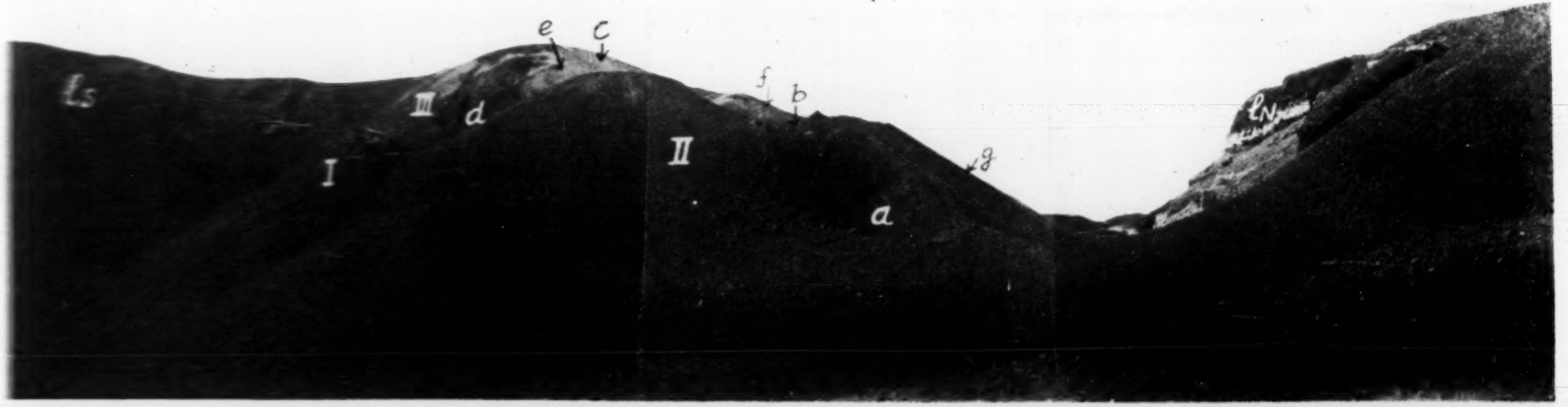

Fig. 74. Oct. 26, 1940. New central cone, looking west from floor of eastern crater. *I*: First cone. *II*: Second cone. *III*: Third cone. *a~g*: craters. *l*S: Inside S wall of Oana. *l*N: Inside N wall of Oana.

Photo Tsuya.

Fig. 75. Oct. 26, 1940. New central cone, looking northwest from S rim (*l*S) of Oana crater. *I*: First cone. *II*: Second cone. *III*: Third cone. *d*: Crater *d*. *l*N: Northern wall of Oana. *S*: Somma.

Photo Tsuya.

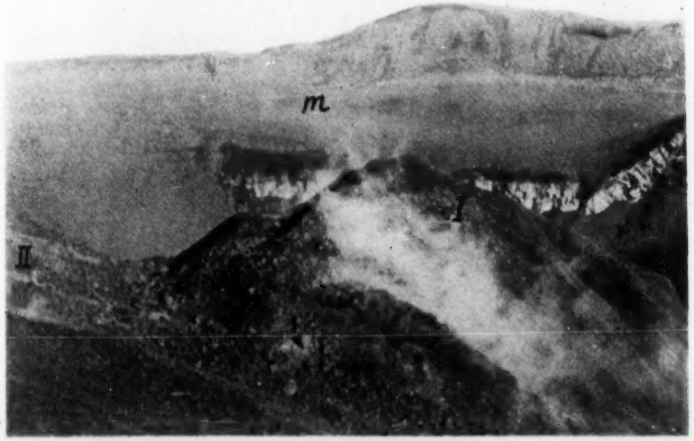

Fig. 76. Oct. 29, 1940. Top of first cone (*I*). *II*: S slope of second cone. *l*: Oana crater. *m*: Bottom of old eastern crater. Photo Tsuya.

Fig. 77. Oct. 29, 1940. Bottom of crater *a* on NE slope of second cone. Photo Tsuya.

Fig. 78. Oct. 26, 1940. Crater *b* on top of second cone. *c*: crater *c*. *e*: crater *e*. *f*: crater *f*. Photo Tsuya.

(震研彙報 第十九號 圖版 津屋)

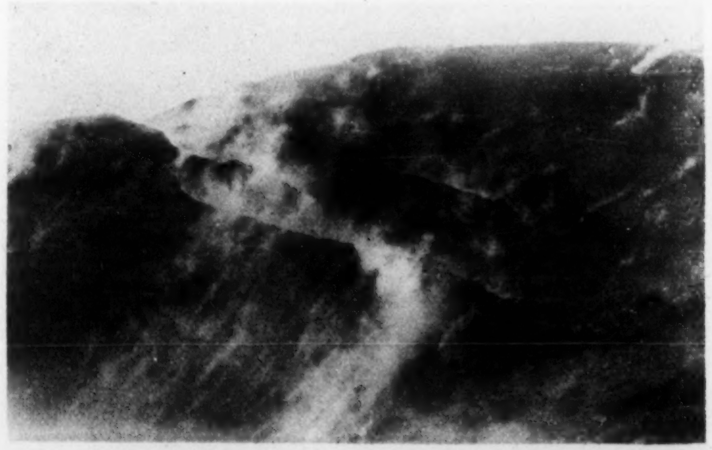

Fig. 79. Oct. 26, 1940. SW wall of crater *c* on third cone. Photo Tsuya.

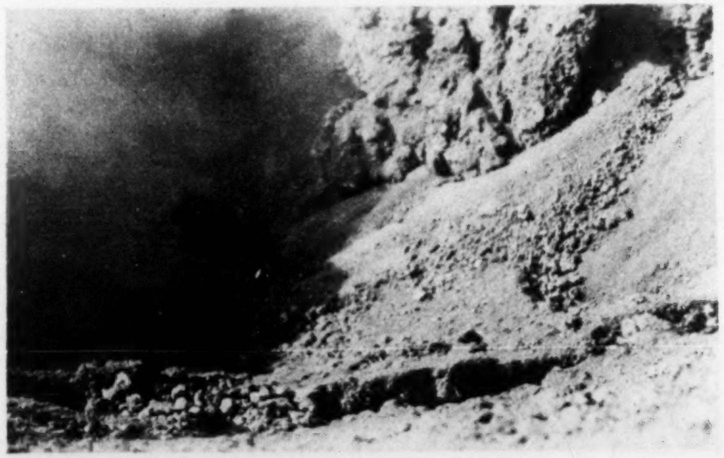

Fig. 80. Oct. 29, 1940. Bottom of crater *d* on border between second and third cones. Photo Tsuya.

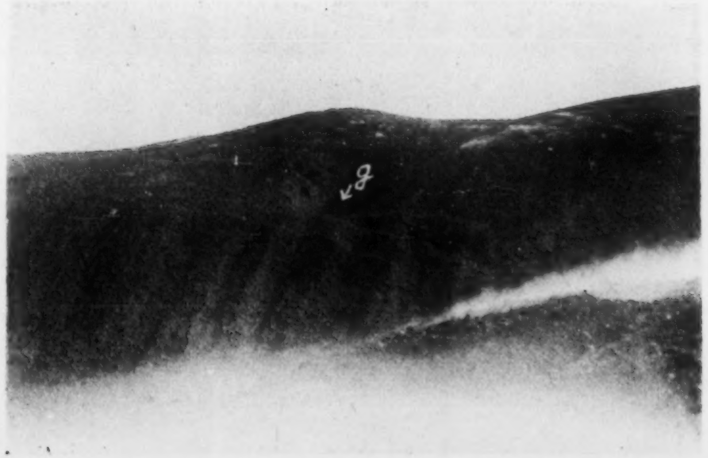

Fig. 81. Oct. 29, 1940. Crater *g* on northern flank of second cone. Photo Tsuya.

Fig. 82. Oct. 26, 1940. Lower part of inside N wall of Oana crater. Photo Tsuya.

(震研彙報 第十九號 圖版 津屋)

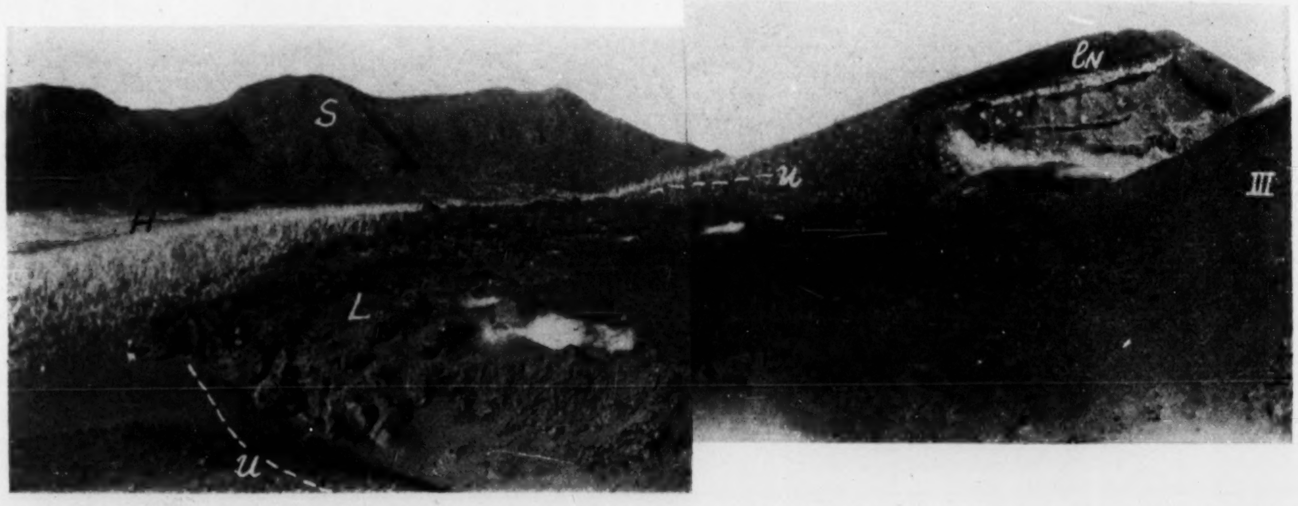

Fig. 83 a. Oct. 26, 1940. View of NW foot of new central cone, looking north. *III*: NW slope of third cone. L: New lava-coulee. *l*N: N wall of Oana crater. *u*: Upper rim of upper crater. *H*: Hayono-tairo atrio. *S*: N somma.
Photo Tsuya.

Fig. 83 b. Oct. 26, 1940. Front of lava-coulee.
Photo Tsuya.

Fig. 84. Oct. 26, 1940. Top of N wall of Oana crater (*l*N in Fig. 83 a), showing accumulation of juvenile and accessory ejecta (sand, lapilli, and bombs).
Photo Tsuya.

(震研彙報 第十九號 圖版 津屋)

Fig. 85. Oct. 26, 1940. Summit of new central cone, looking south. Upper right, fumaroles indicating fissure-lines. $b \sim g$: craters. ls: Southern rim of Oana crater. Photo Tsuya.

Fig. 86. Oct. 26, 1940. New central cone, looking southeast. Upper left, fumaroles indicating fissure-lines. Lower left, SW part of new lava-coulee. Lower right, SW rim of upper crater.

Photo Tsuya.

Fig. 87. July 27, 1940. Volcanic bombs at Sitori, piled one on top of the other. *a*: Porphyritic bomb, 7 m across. *b*: Aphanitic bomb, 2 m across. Photo Tsuya.

Fig. 88. July 17, 1940. Porous, aphanitic bomb partly imbedded in the ground. Photo Tsuya.

Fig. 89. July 27, 1940. Porous, aphanitic bomb (*B*) flattened by fall on the raised beach gravels. Photo Tsuya.

Fig. 90. Oct. 25, 1940. Bomb flattened by fall on a stump. Photo Tsuya.

Fig. 91. July 20, 1940. The NW foot of Hyôtan-yama, showing accumulation of volcanic bombs. Photo Tsuya.

Fig. 92. July 17, 1940. Mountain slope near Yoridai-hana, showing hollows formed by falls of volcanic bombs. Photo Tsuya.

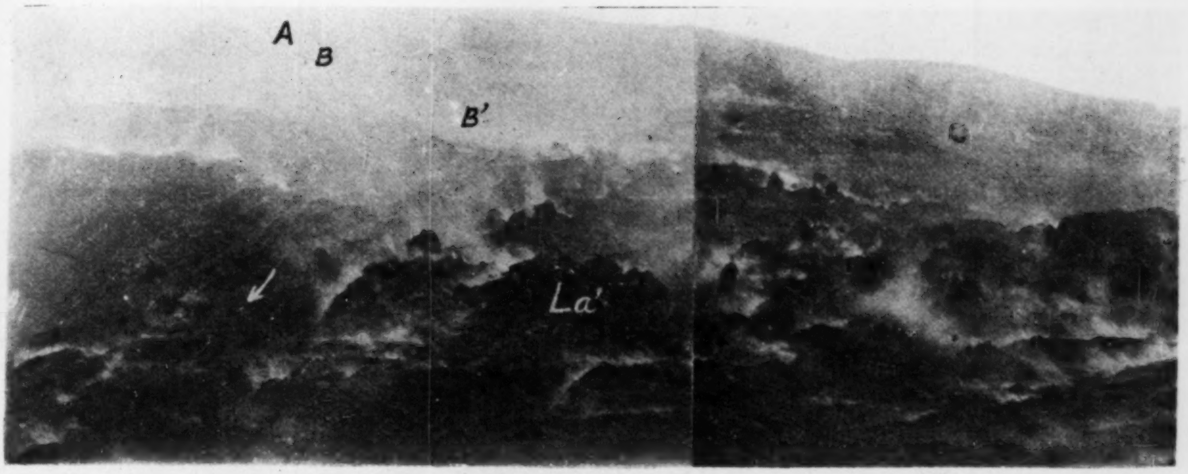

Fig. 93. Oct. 27, 1940. Akabakkyô lava-flow (*La'*) on the mountain slope adjoining the southern side of *B'* crater. *A*, *B*, *B'*: craters. l_1: Dammed pond. Photo Tsuya.

Fig. 94 a. Oct. 25, 1940. Dammed pond, l_1 in Fig. 93. *La'*: Akabakkyô lava. Photo Tsuya.

Fig. 94 b. Oct. 27, 1940. The southeastern branch of Akabakkyô lava-flow (*La'*). l_1: Dammed pond. Photo Tsuya.

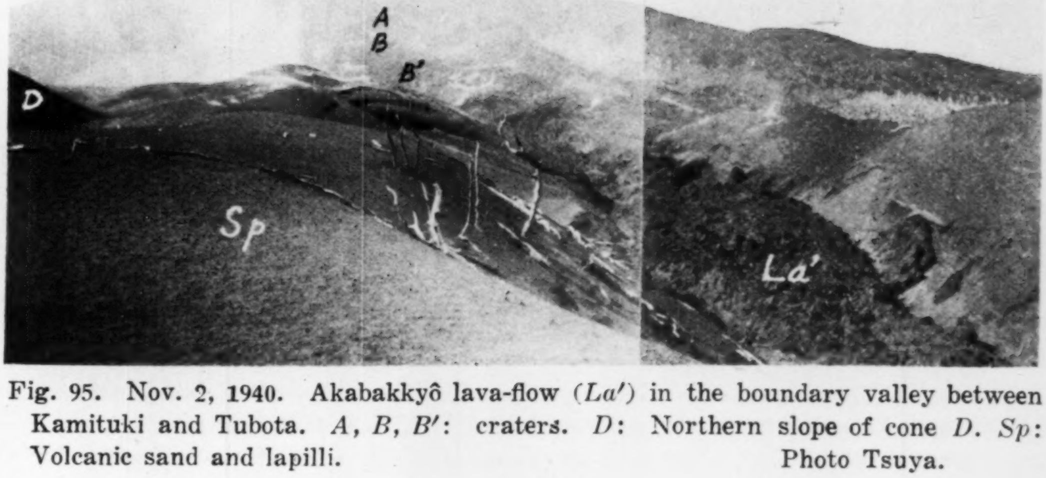

Fig. 95. Nov. 2, 1940. Akabakkyô lava-flow (*La'*) in the boundary valley between Kamituki and Tubota. *A*, *B*, *B'*: craters. *D*: Northern slope of cone *D*. *Sp*: Volcanic sand and lapilli. Photo Tsuya.

Fig. 96. Oct. 27, 1940. View across the boundary valley between Kamituki and Tubota, showing Akabakkyô lava (*La*) hanging over southern wall of valley.
Photo Tsuya.

Fig. 97. Nov. 2, 1940. Akabakkyô lava-flow on floor of boundary valley between Kamituki and Tubota.
Photo Tsuya.

Fig. 98. Nov. 2, 1940. Akabakkyô lava-flow near mouth of boundary valley between Kamituki and Tubota.
Photo Tsuya.

Fig. 99. July 26, 1940. Nezumisama, a small rocky hill in Simasita, left uncovered by the Akabakkyô lava (*La*). *H*: Hyôtan-yama. *D*: Former sea-cliff of Akabakkyô-hana.
Photo Tsuya.

Fig. 100 a. Nov. 2, 1940. Contraction fissures in Akabakkyô lava. Photo Tsuya.

Fig. 100 b. Nov. 2, 1940. Do. Photo Tsuya.

Fig. 101. July 15, 1940. Steep marginal slope of Akabakkyô lava-flow at Simasita. Photo Tsuya.

Fig. 102. July 26, 1940. A cliff at Sitori, showing compact part (*A*) of the Akabakkyô lava. *S*: An old lava exposed on the coast of Sitori. Photo Tsuya.

(震研彙報 第十九號 圖版 津屋)

Fig. 103. Oct. 27, 1940. Yoridai-sawa lava-flow near its source. *D*: Crater. *Lb*: Lava-flow.
Photo Tsuya.

Fig. 104. July 17, 1940. Farthest front of the Yoridai-sawa lava-flow.
Photo Tsuya.

Fig. 105. Oct. 27, 1940. Lava-flow in the middle course of the Yoridai-sawa, looking downstream from the lava-fall (left).
Photo Tsuya.

Fig. 106 a. Oct. 28, 1940. Lava-flow exposed in sea-cliff on SE coast of Hyôtan-yama.
Photo Tsuya.

Fig. 106 b. Oct. 28, 1940. Sea-cliff on eastern side of Hyôtan-yama, looking south. *Lc*: Hyôtan-yama, lava-flow. *Sb*: Volcanic sand, lapilli, and bombs.
Photo Tsuya.

Fig. 106 c. Oct. 28, 1940. Hyôtan-yama lava-flow exposed on sand-beach adjoining northern end of sea-cliff shown in Fig. 106 b.
Photo Tsuya.

（震研彙報 第十九號 圖版 津屋）

[Bull. Earthq. Res. Inst., Vol. XIX, Pl. LIII.]

Fig. 107. July 22, 1940. Trees bent and withered by ash-fall. Photo Tsuya.

Fig. 108. July 16, 1940. Tree trunks blasted by fall of lapilli. Photo Tsuya.

Fig. 109. July 19, 1940. Tree trunks blasted by fall of volcanic bombs and lava-blocks. Photo Tsuya.

Fig. 110. July 16, 1940. House in Mitoribata near Maru-yama burned by fall of incandescent volcanic bombs. Photo Tsuya.

(震研彙報 第十九號 圖版 津屋)

28. *A New Device for Remote Mechanical Recording of Slow Movements.*

By Takahiro HAGIWARA,

Earthquake Research Institute.*

(Read June 19, 1941.—Received June 20, 1941.)

By "slow movements" used in the title is to be understood the slow variations that occur in a quantity in the case of a large time scale such, for example, as the daily or secular variations in the inclination of the earth's surface, in the earth's magnetic field, etc.. Remote recordings of such changes are occasionally required in geophysical studies. The quantitiy that varies with the rapidity, such as earthquake motion, may be recorded at a distance from the source by means of an electric current in proportion to the amount of variation. Such an electrical method, however, is not suitable for continuous observations of the slow variations just mentioned, because of the difficulty of keeping the instrument to work constantly for any length of time.

The proposed method now to be described does not depend on the quantity of electric current, but on the time interval separating the electric signals. The principle is similar to that of photo-telegraphy. This method is applicable to measuring instruments that have a recording contrivance with optical lever, such as the clinograph, magnetograph, etc..

The apparatus shown in Fig. 1 is placed at a suitable distance from the mirror for the optical lever of the instrument (for example, the horizontal pendulum in the case of the clinograph). P is a lamp with a vertical filament. The light ray on leaving the light source is reflected by the mirror (lens mirror or plane mirror combined with a convex lens), and the image of the filament is formed on a vertical plane with a slit S, behind which a photo-tube is placed (in its cover C). If the image of the filament comes up to the slit, the light illuminates the cathod of the photo-tube and generates a photo-electric current. The lamp-house R moves horizontally on the cylinder D. A horizontal rotating spindle E has square screws of large pitch cut in its surface. These are right-handed and left-handed screws that cross and recross each other for the whole length of the spindle, meeting at the ends A,

* Dedicated to the memory of his late respected teacher, Professor Mishio Ishimoto.

B. A small piece of metal projecting from the bottom of the lamp-house fits into one of these screws and, with the rotation of the spindle, the lamp-house travels axially to the end of the spindle, where it fits into the opposite screw and travels to the opposite end of the spindle. Thus, the lamp-house (and, in the result, the image of the filament) repeats a horizontal to and fro motion. Fig. 2 is the mechanical recorder, of structure largely the same as the device just mentioned, except that the lamp-house is replaced by an electromagnet *F*. When an electric current is sent from the measuring device, it works the electromagnet and a dot is marked on recording paper *H* on the same principle of mechanism as that of the typewriter. The horizontal screws of the two devices, one containing the photo-tube and the other the recorder, are turned by means of a synchronous motor (*A. C.* 100 V, 6 Watt), so that both filament (*P*) and the dot-marker (*P'*) travel horizontally with equal speed along the lines *AB* and *A'B'* respectively. In the present case, the period of one complete repeating motion is 4 minutes when the *A. C.* is 50 cycle per sec.

For simplicity, we shall consider the matter abstractly. From Fig. 3, in which *P* represents the light source and *P'* the dot-marker of the recorder, *P* and *P'* move with uniform speed along the line *AB* and *A'B'* respectively. Both *P* and *P'* are assumed to be in the same phase, that is, $AP = A'P'$. The ray of light that leaves *P* is reflected by the mirror of the measuring instrument, and the image of *P* is formed on the line *TU*. When *P* reaches point *Q*, the image of *P* coincides with the slit *S*. At this instant, the photo-tube activates, sending the electric current to the electromagnet of the recorder, and the dot-marker *P'*, which is now at *Q'*, markes a dot there. Since $AQ = A'Q'$, it may be said that the quantity *AQ* was transferred to the recorder. Next, the relation between position *Q* and the rotating angle of the mirror will be considered. If we assume that a light source were placed at *S*, instead of at *P*, then the image of *S* should be *Q*, so that the position *Q*, which was transferred to the recorder, corresponds to the posi-

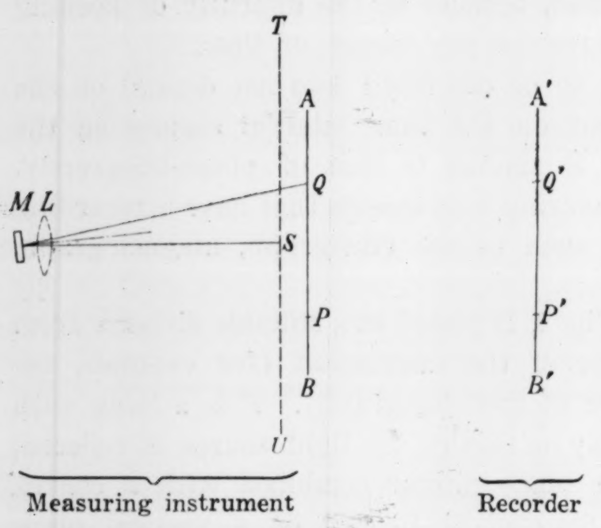

Fig. 3.

tion of the image of the light source that is placed at *S*. In other words, the record must be exactly the same as the one that would have been obtaind with a photographic paper placed at *AB*, with the light source placed at *S*.

Fig. 4 shows an example of the wiring diagram of the photo-tube

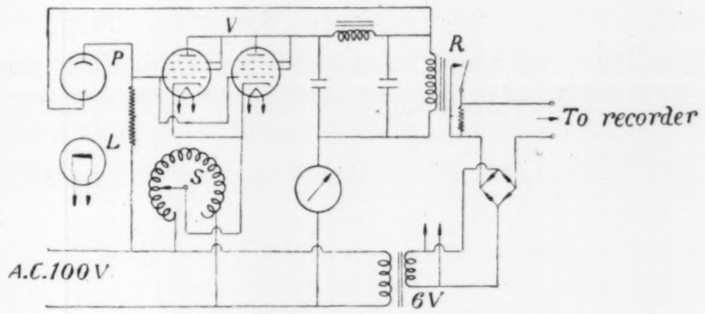

Fig. 4. Photo-tube circuit.

P—Photo-tube (PG50G), *V*—UZ6C6, *S*—Mazda Slidac (variable single winding transformer), *L*—Light source, *R*—Relay (2000 Ω, minimum working current 2·5 mA).

circuit, in which the electric source, *A. C.* 100 V, is obtained from the ordinary supply mains.

The record obtained by this method is not continuous, but consists of two dots marked every 4 minutes, but seeing that the object of this apparatus is only to record slow changes, no interruptions occur.

Exact maintainance of frequency of the electric source of the synchronous motors is not necessary when the two synchronous motors are driven by power from the same source; the apparatus is not disturbed by small variations in the frequency of the electric source, so long as the torque of the motors does not vanish.

As an experiment, recording from a distance was made in connection with the Ishimoto silica clinograph, see Fig. 5. The clinograph was set up on a concrete block in the basement of our Institute and the mechanical recorder placed in a chamber on the ground floor. A reproduction of the actual record is shown in Fig. 6 a. For comparison with it, an ordinary optical recording apparatus was placed side by side with the clinograph and its record was obtained simultaneously, see Fig. 6 b. As will be seen from the figure, the two records agree well. The two similar curves that are seen in the record of the new apparatus are due to small phase differences between the measuring instrument and the recorder; in this case, the interval between two consecutive dots is 4 minutes. The two dots, which are sometimes shown in the record of

the new apparatus, is due to vibration of the mirror from microseisms generated by street traffic.

A dark room is not required for this instrument, provided the light source is of sufficient intensity. This instrument easily records two or more different components on a single recording paper.

The expenses of this study were defrayed from the Scientific Research Expenditure of the Department of Education and also from a grant from the Hattori Hōkōkai.

---

28. 緩慢な變化の遠隔記錄法

地震研究所 萩原尊禮

地表傾斜變化や地磁氣變化等の場合に見られる，日變化乃至は永久變化の程度の，時間的に緩慢な變化を遠隔記錄させるこさは，地球物理學的の觀測に際して屢々必要を感じるこさである．地震動等のやうな時間的に比較的急な變化に對しては，適當な裝置により，變化の量（又は其れを時間につき1回微分した量）に比例した電流を生ぜしめ，遠隔記錄の目的を達するこさが出來るが，此の種の遠隔記錄法は，極めて緩慢な變化を長期に亘つて觀測しようさする場合は色々さ困難が伴ふものである．

本文に述べた方法は，變化の量を電流の變化に換へるこさを避けて，これを電氣的シグナルの時間的間隔の大小によつて傳達記錄するこさを試みたものである．此の方法は，傾斜計でも地磁氣變動計でも，要するに，鏡の廻轉を利用した所謂 Optical lever による記錄裝置を持つた測定器械には直ちに，應用するこさが出來る．變化の量を傳へるに際して，電流の變化に賴らないから，長期に亘る觀測に於て，器械の倍率或は感度が變化する恐れがない．變化の量を傳へるさころの電氣的シグナルの時間的間隔は，此の裝置のシンクロナスモートルを動かす交流のサイクルによつて決定されるのであるが，測定器側のモートルさ記錄器側のモートルさ同一電源を使用するさきは，サイクルが多少變動しても，モートルがトルクを失はない限り，その影響は現れない．

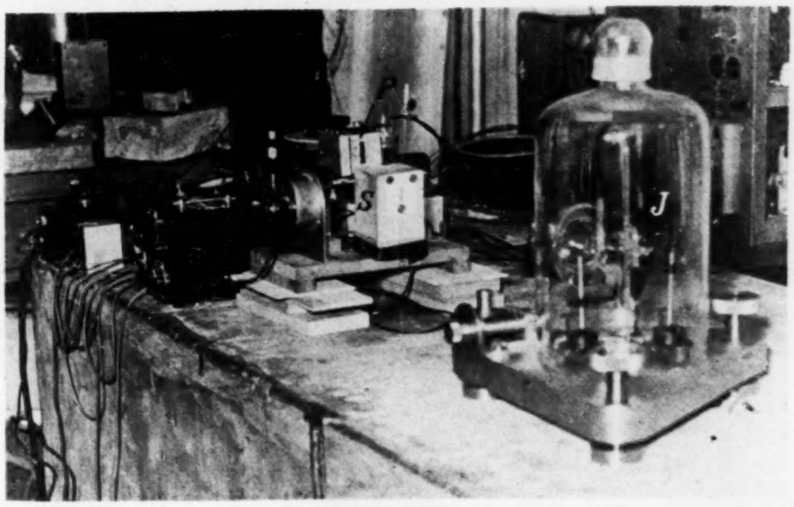

Fig. 5. Recording from a distance was made in connection with the Ishimoto silica clinograph.
P—Light source, *S*—Photo-tube, *J*—Clinograph (Silica pendulum).

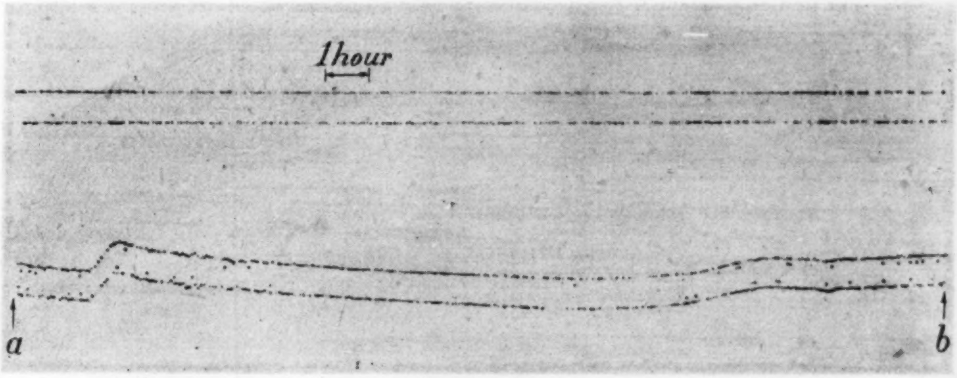

Fig. 6 a. Record obtained by the new device.
(*a*=17 h 15 m, May 29, 1941. *b*=15 h 57 m, May 30, 1941.)

Fig. 6 b. Record obtained by the old optical device.

(震研彙報 第十九號 圖版 萩原)

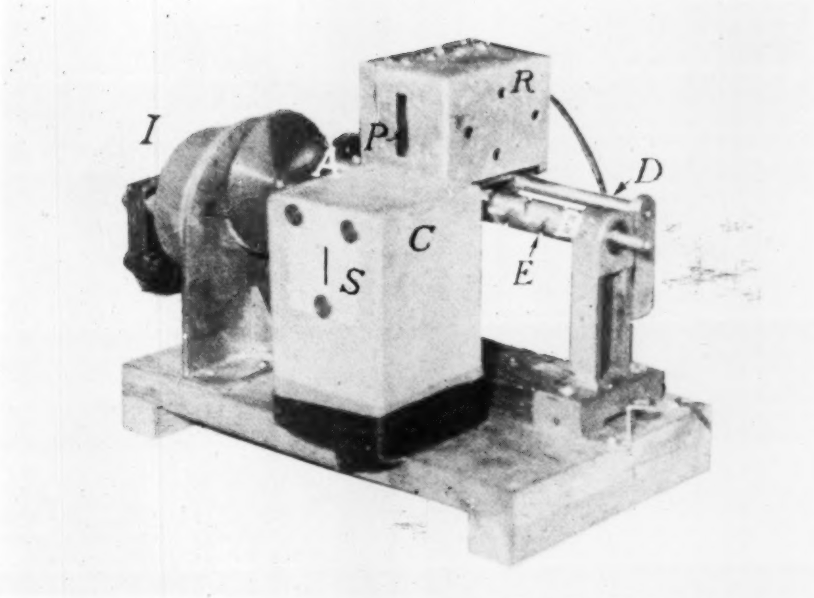

Fig. 1. *P*—Light source, *R*—Lamp-house, *S*—Slit, *C*—Cover for photo-tube, *I*—Synchronous motor, *D*—Cylinder, *E*—Spindle.

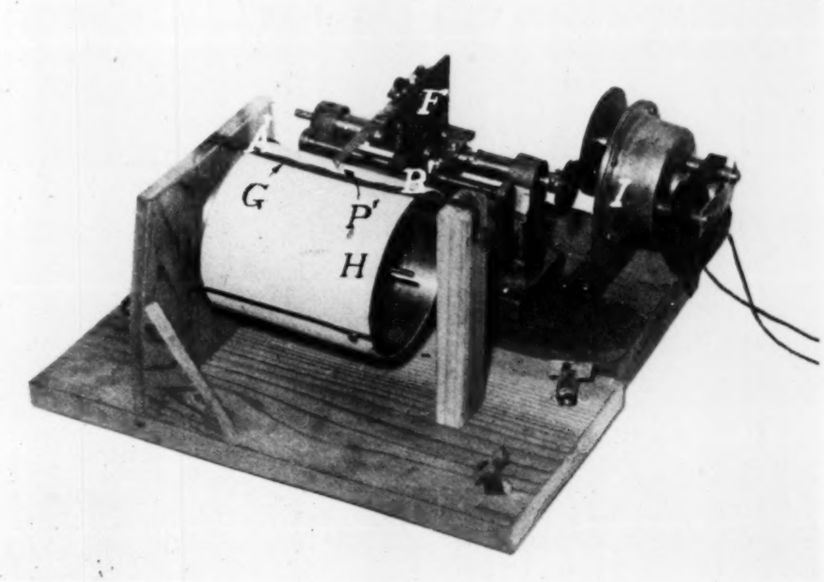

Fig. 2. *F*—Electromagnet, *P′*—Dot-marker, *H*—Recording paper, *G*—Typewriter ribbon, *I*—Synchronous motor.

29. 比較觀測を目的とする水平動變位計の製作

地震研究所 {高橋龍太郎
平能金太郎}

(昭和16年5月18日發表——昭和16年6月20日受理)

緒言 觀測所としての特別の設備を持たない場所に，數ケ月，或は十數ケ月の短期間地震計を設置して其處の地震動を臨時的に調査する必要は吾々の研究の途上に於て屢々感ぜられる處である．斯かる場合には共れが臨時的なものである同時に，移動，運搬等の便宜をも考へて，成る可く小型で簡單な地震計を用ひ，又觀測者も特に訓練を受けたのではない，其の土地の人に委囑される事が多い．地震計設置の場所としても，或時は物置の片隅が利用され，又或時は廊下の一端が用ひられる．

斯かる悪條件の下に於ては從來の地震計は屢々故障を起し，記錄不能に陷り，或は記錄不能とまで行かずとも，共の記象に信を置き難い狀態になるのが屢々經驗されるのである．特に變位地震計は其の固有振動周期長く，從つて復元力少なる關係上，擴大部に脆弱なる構造を含むので，最も故障の起り易いものである．

從來經驗された故障箇所の主なるものを發生回數の順に列記すれば次の樣である．(1)起動器の故障．此れは調製器軸の磨耗，塵埃の潛入等によるものであるが，近時小型同期電動機の使用により，記錄部分の故障は殆んど却かれてゐる．(2)連結針の逸脫．或る種の變位計に於ては擴大挺の結合方法として，挺端に附けた寶石受皿間に兩端に尖端を有する細針を介在せしめ，受皿同志，或は受皿と針とを弱い螺旋發條にて相索引せしめてゐるが，此の連結針は急激な地震動，或は振幅の大きな地震動によつて脫出し易く，或は一旦脫出後，不正の位置に復舊したまゝ氣附かれずに居る事がある．(3)空氣制振器の故障．空氣制振器は喞子と汽筒との間隙が小なる爲，防塵裝置があつても猶間隙に塵埃が潛入して地震計の運動を阻げる事がある．又氣溫の變化操返しによつて汽筒取附位置が匍匐し，汽筒と喞子とが接觸する事がある．(4)擴大裝置の挺軸は其の兩端を寶石受皿にて支へられるが，此の受皿は通常二重ナツトにより框に固定される捻子の先端につけられてゐる．然るに時の經過と共に二重ナツトが自然に緩み挺軸に遊びを生ずる樣になる事があるのを時々經驗した．框とナツトが熱膨脹係數を異にする場合に氣溫變化操返しによつて斯かる現象を生ずるのではな

いかと思はれる．（5）描針の脱落，反轉．此れは急激なる地震動，又は地震計の能力以上の大振幅の地震動によつて起る事は周知の事柄であるが，此の故障は氣附かれずに居る事なく觀測者自身によつて容易に修理し得るものであるから，今は問題にしない．

從つて委託觀測に用ふる地震計に於ては特に以上の如き故障の原因を除却する構造を持つてゐなければならぬ．

又從來臨時的に地震觀測を爲し或は其れを委託する樣な場合は，多くは主として地震の發震時，發生回數，初期微動繼續時間，最大振幅，其の周期位を目的としてゐたから，地震計に可成りの缺點があつても間に合つてゐたのである．然し若し數箇所の觀測に於て地震動の一々の波形の比較を爲したいといふ場合には，地震計の各々が皆眞正の地震動を其の儘に記錄するか，或は眞正の地震動を或る定まつた，既知の法則に從つて變形したものを描くのでなければならぬ．卽ち地震計は或る一箇所に並行に設置された場合には少なくとも，同一の地震については同一の記錄を與へるものであり，且つ据え換へによつて器械の調子の狂ふ事のないものでなければならぬ．

以上の如き要求を充す爲に，上に述べた如き意味に於て最も完全な，然も特別な訓練を受けた者でなくとも取扱へる樣な，輕便で，且つ故障の憂少なき變位地震計を目指して作られたのが，以下に述べる地震計である．此の地震計では運搬の便宜をも考へて成る可く小型に作る事を心掛けてある．

當面の目的たる地震動波形の比較觀測には有感以上の地震が記錄出來れば充分であり，又高倍率の地震計は擴大裝置が多く，從つて故障も起り易い．又同時に大きな重錘を要するから運搬に不便である等の點を考へ，倍率が 50 倍附近のものを設計した．勿論光學的記錄方法を用ひれば，以上の種々の問題の多くは忽ち解決するが，其れには感光紙の使用といふ委託觀測には不適な事柄があり，又費用の點からも我國では現在の煤紙の方法に劣るから，今回設計の器械でも煤紙の方法を用ゐる．

地震計の固有振動周期は出來得るかぎり長周期である事が希ましい．其れは圖式積分等の面倒な手數を經ずに眞正の地動を得る爲めである．然し徒らに長い周期のものは，又地表の傾斜や氣溫變化等によつて零點の移動甚だしく，又地震計の恆數も變化し易いから，委託觀測には不向である．

新水平動變位計　以上の如き種々の條件を考慮して製作された新水平動變位計は第1圖に示す如き，固有振動周期 8·0 秒，基本倍率 47·5 の逆立振子地震計である．新水平動變位計の特徴は次の諸點にある．擴大梃 ⑦ 及び ⑨ の軸の一端を受ける寶石受皿は框 ⑫，⑬ に固定されてゐるが，他の一端を受ける寶石受皿は框に固着された

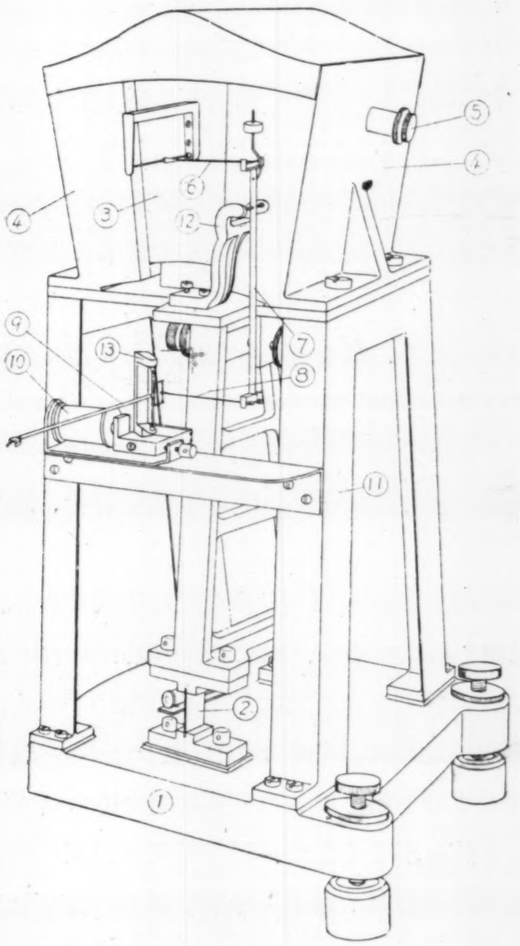

第 1 圖 a.

燐青銅平板バネに固着されてゐて，平板バネの彈力によつて梃軸を輕く壓迫し支へてゐる．此の壓力は運搬の爲，梃を着脱しても殆んど不變である．梃を連結する連結針 ⑥，⑧ は第2圖の

第 2 圖

如き構造にて其の兩端の小軸は梃端の彈力框につけた一對の寶石受皿間に挟まれ保持される．連結針の兩端には薄い平板バネが存在してゐて地震計の運動，或は組立の不正に因る部分品相互の位置の狂ひから來る應力を除く役目

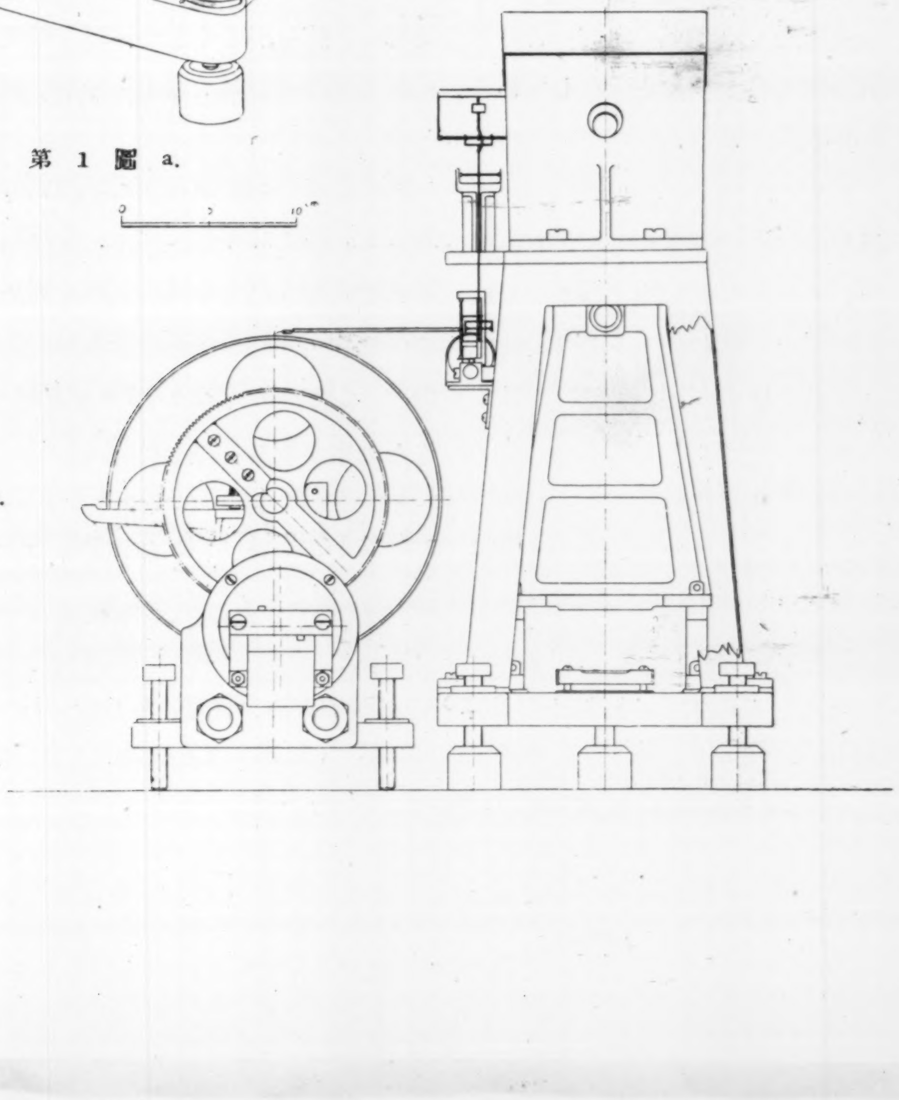

第 1 圖 b.

をする．以上の様にして凡ての回轉軸は彈力によつて支へられてゐるから軸に遊びを生ずる事が絶對にない．且つ急激又は過大な振動によつて軸の脱出する憂は殆んどない．重錘 ③ は其の上下面が重錘の回轉軸 ② を中心とする圓筒面を爲し其の兩端に空氣制振器 ④ がかぶさつてゐる．卽ち荻原簡單變位計[1] と同様に重錘を同時に喞子として用ゐてゐる．但し空氣制振器の箇數を多くし，底面積を大きくする事によつて制振器の間隙を 1.5 粍としてゐるから汽筒と喞子との接觸の憂なく，塵埃の潜入による被害がないのみならず，組立が非常に容易である．螺子 ⑤ の加減により容易に臨界減衰の狀態を得る事が出來る．

時刻標は枠 ⑪ に附けた小電磁石 ⑩ により第 2 擴大梃軸の框 ⑬ を僅か側方へ吸引して描針を横に移動させ記入する．電磁石の極片には一半に隅取線輪を附し，電源に 10 V の交流を用ゐてゐる．

記錄圓筒は 60 糎の周を有し，5 分に一回轉するから 2 粍/秒の記錄速度である．動力としては 6 watt の Warren 同期電動機を用ゐてゐる．現在では市販 50 cycle 交流を電源としてゐるが，近き將來に於て，音叉制御による交流を用ゐる豫定である．

記錄圓筒の軸は直徑 20 粍の引拔鋼管を用ひ此れに Pitch 1 粍の螺子と Key 道を刻した．回轉傳達齒車は直徑 12 糎の大徑のものを用ひ成る可く圓筒周に近い所で圓筒を驅動し，齒車の遊びによる圓筒回轉の脊隙を小さくした．圓筒軸受は相互に鋼管によつて結合する方式にしてある．此れは製作の容易，廉價と分解，運搬の容易なる點が長所である．

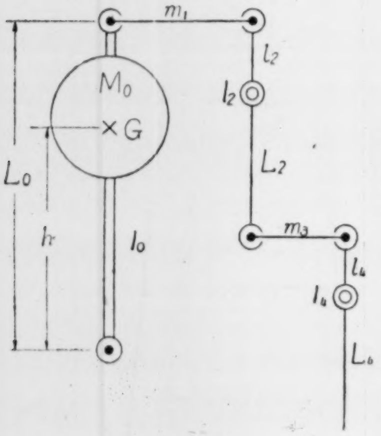

第 3 圖

次に以上の如き擴大装置が地震計の基本倍率に及ぼす影響を計算して見る．今地震計を圖形的に第 3 圖の如く表し各部の符號を圖示の如く定めると地震計の運動方程式は容易に

$$I\ddot{\theta} + 2\varepsilon\dot{\theta} + n^2\theta = -Mh\ddot{x}$$

となる事が判る．但し此處に

$$I = I_0 + \frac{L_0^2}{l_2^2} I_2 + \frac{L_0^2 L_2^2}{l_2^2 l_4^2} I_4 + L_0^2 m_1 + \frac{L_0^2 L_2^2}{l_2^2} m_3$$

$$M = M_0 + \frac{L_0}{h} m_1 - \frac{L_0 L_2}{h l_2} m_3$$

である．此の式は小野博士の計算[2] の擴張である．實際の地震計に於ては

1)　地震，6 (1934)，645
2)　氣象集誌，〔2〕，5 (1927)，39

振子の運動の取出し點高	L_0	=30	糎
振子の重心高	h	29·0	〃
第1擴大挺の劣腕長	l_2	1·8	〃
第1擴大挺の優腕長	l_2	9·0	〃
第2擴大挺の劣腕長	l_4	1·0	〃
第2擴大挺の優腕長	L_4	10·0	〃
振子の質量	M_0	$1{\cdot}27\times10^4$	瓦
第1連結針の質量	m_1	0·9	瓦
第2連結針の質量	m_3	4·5	瓦
振子の慣性能率	I_0	$1{\cdot}14\times10^7$	瓦糎^2
第1擴大挺の慣性能率	I_2	$9{\cdot}2\times10^2$	〃
第2擴大挺の慣性能率	I_4	11	〃

であるから，

$$M=1{\cdot}27\times10^4 \text{ 瓦}$$

$$I=1{\cdot}18\times10^7 \text{ 瓦糎}^2$$

となり等價單振子の長さは

$$\frac{I}{Mh}=31{\cdot}6 \text{ 糎}$$

となるから，

$$\text{基本倍率}=\frac{MhL_0}{I}\,\frac{L_2}{l_2}\,\frac{L_4}{l_2}=47{\cdot}5$$

となる．

試驗結果 以上の如き地震計を4臺製作したが，此等地震計の忠實さの試驗として地震研究所地下室に4臺平行に設置して，同一地震を同一に記錄するや否やを試驗した．其の結果は圖版第4圖，乃至第6圖に示す如く，頗る滿足すべき結果を得た．各圖は夫々近い地震，稍遠い地震及び脈動の例である．

此等の觀測期間中に，据附位置移動の爲め，或は時刻標記入裝置の改良の爲め，或は後に述べる物理教室と比較觀測の爲め，屢々器械を分解し，或は移動したが，何等特別の工夫をせずとも常に同一箇所に並置する時は同一の記錄を與へる事を經驗したから，分解，移動によつて一旦調節した器械の調子が狂ふ事はないものと考へられる．

地震研究所，物理教室に於ける地震動の比較 地震研究所地下室に No. 3, No. 4 地震計を，又物理教室地震計室に No. 1, No. 2 を，EW, NS に向けて設置し比較觀測をした結果の一例を圖版第7圖に示す．圖に於て明かなる如く，物理教室と地震研究所とは殆んど同樣の振動を爲すのである．只 EW 成分に於ては振動の有樣を稍異

にする所がある。殊に短周期の波に於て著しい．此れは第8圖に示すが如く，地震研究所の建物は南北に長く東西に短かい矩形なるに對し，物理教室の建物は略東西に長邊を有する L 形である事に原因があるものと思はれる．因に地震研究所地下室物理教室地震計室間の距離は約 70 米である．

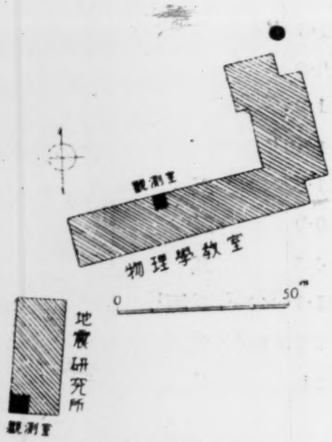

第 8 圖

地震研究所，忍岡國民學校，上野科學博物館の比較 次に地震研究所の地下室，下谷區七軒町忍岡國民學校並に上野公園内科學博物館に各1臺の上記地震計を設置して，各所に於ける地震動の比較觀測を爲た．地震計設置の方向は何れも北30度東—南30度西の方向である．地震研究所，忍岡國民學校間の距離は350米，忍岡國民學校，上野科學博物館間の距離は900米で三箇所は北 75° 度東の方向の一直線上にある．觀測結果の一例を第 9 圖（圖版）に示す．圖に見られる如く地震研究所と科學博物館とは略々同樣の振動を爲すにも不關，其の中間に存在する忍岡國民學校に於ては，初期微動並に主要動の初期に於ては他の二箇所とは著しく違つた振動を爲し，其の振動は比較的簡單な調和曲線であつて，周期0·6秒の振動が著しく卓越してゐて，甚だ大きな振幅を示してゐる．然し地震動の末期に近づき，振動の周期が大きくなると共に，三箇所共殆んど同樣な振動を爲し，地震動の波の一つ一つを相互に對應させる事が出來る樣になる．

以上は昭和 16 年3月8日房總半島沖合に起つた地震についての一例であるが，時には地震動の末期に於ける，周期の比較的長い波についてさへ上記三箇所共一々の波動を餘り對應出來ない地震が起つてゐる．其の一例として圖版第 10 圖に昭和 16 年 3 月 25 日の足柄山附近に震動を有する地震の記象を示した．此の事は主として震央の位置に關係するものと思はれるが詳細は今後の研究に俟たねばならぬ．

終に臨み此の研究は文部省科學研究費によつて行はれてゐるものである事を記し，深謝の意を表す．

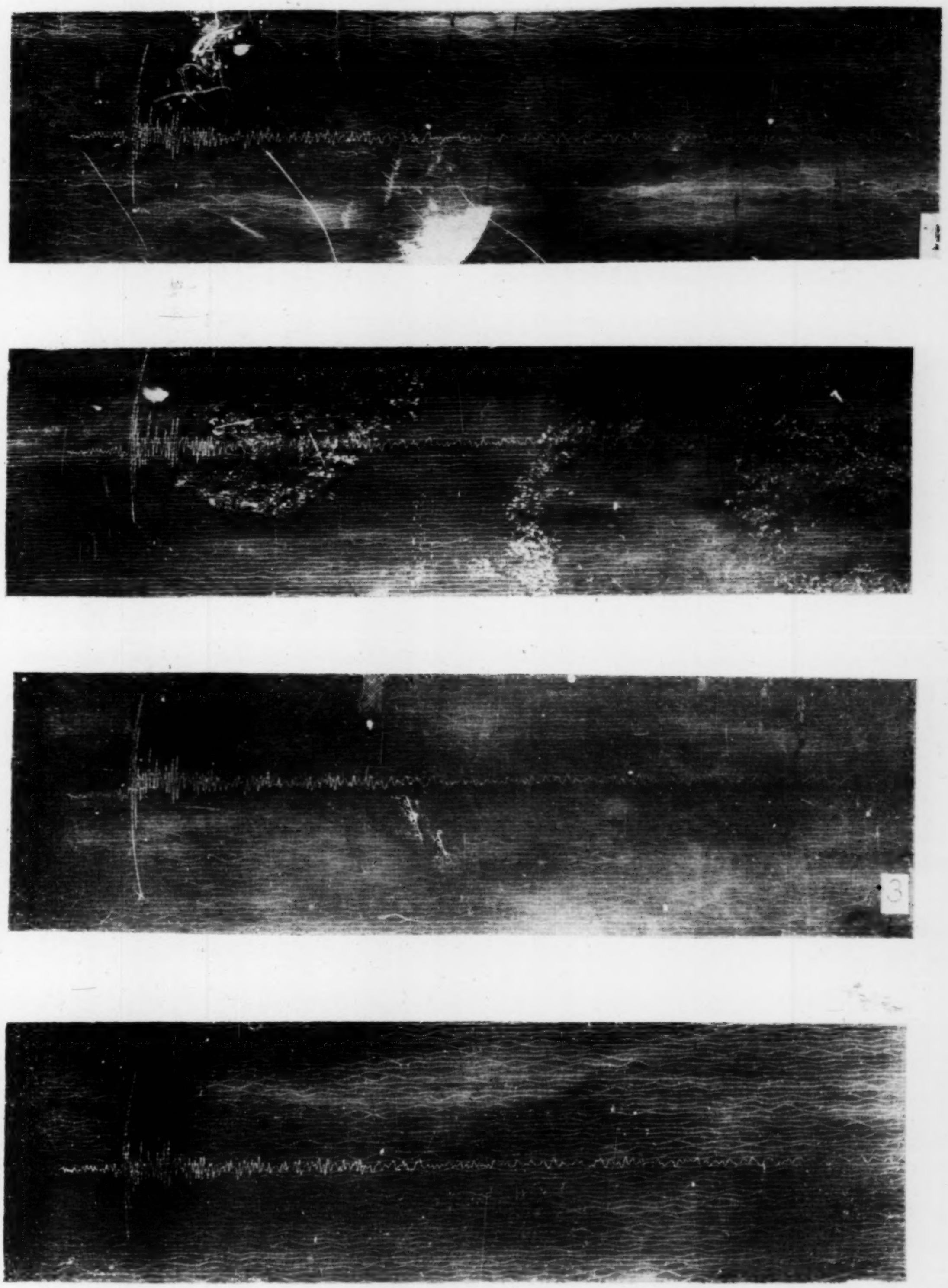

四臺並行觀測

第4圖　昭和15年1月19日23時32分　東京灣北部

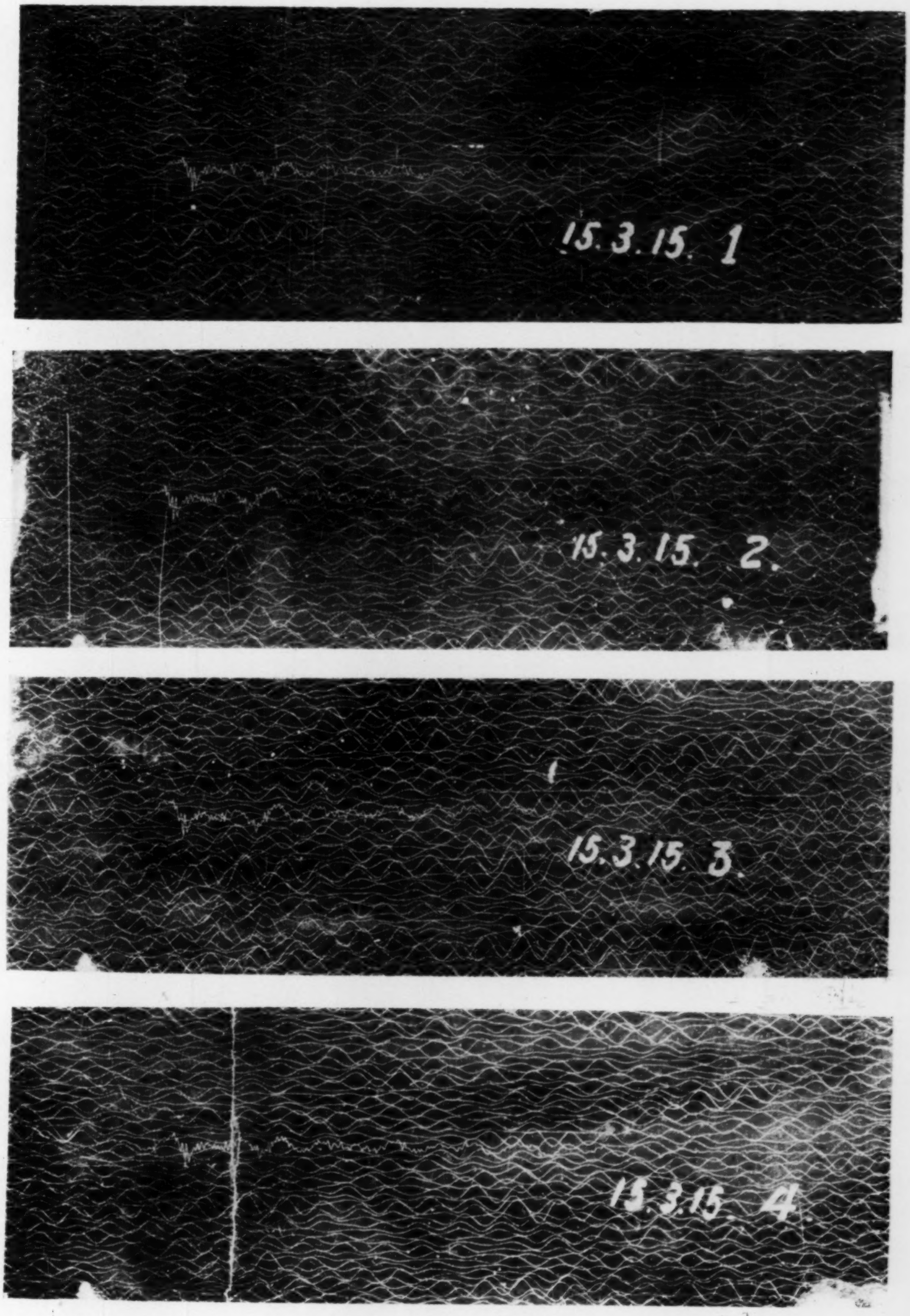

四臺並行觀測

第5圖 昭和15年3月15日21時34分 茨城縣南西部

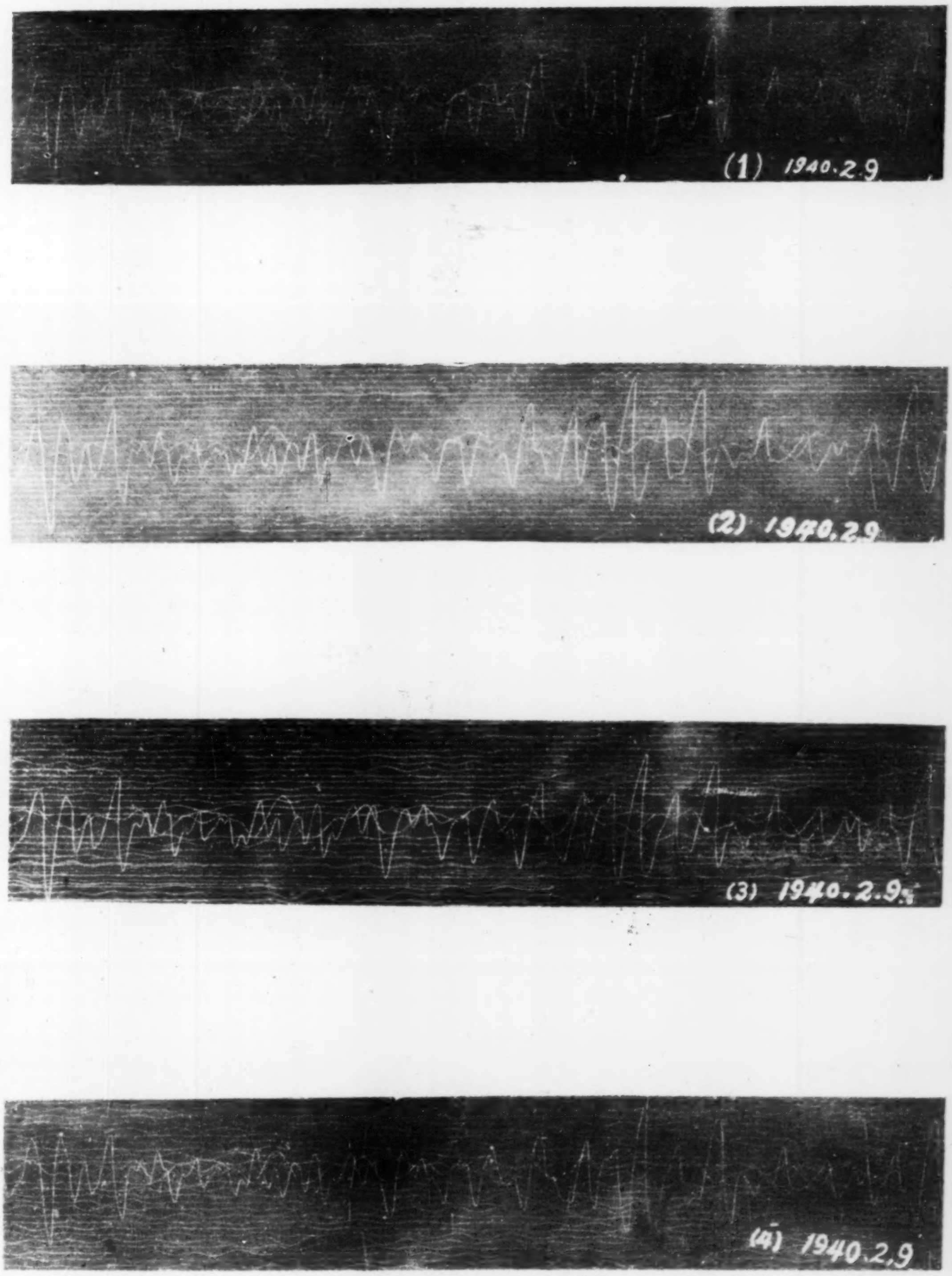

四 臺 並 行 觀 測

第 6 圖 昭和15年2月9日22時53分 岩手縣久慈東方沖（遠震の例）

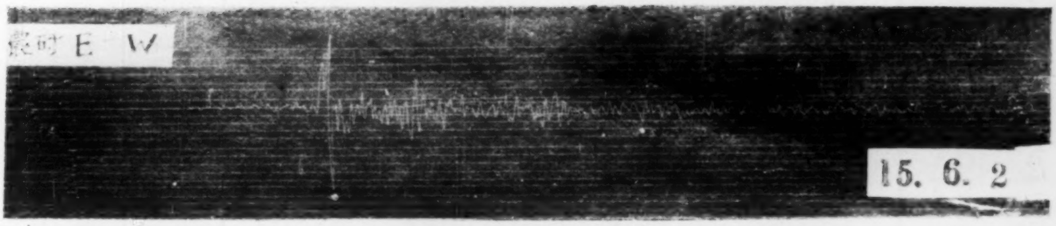

地震研究所地下室 E—W 成分

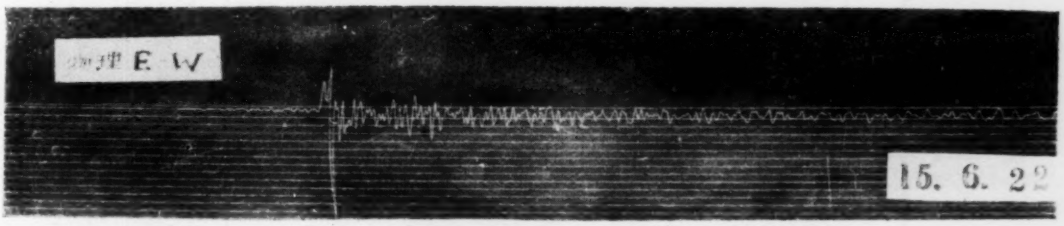

物理學教室 E—W 成分

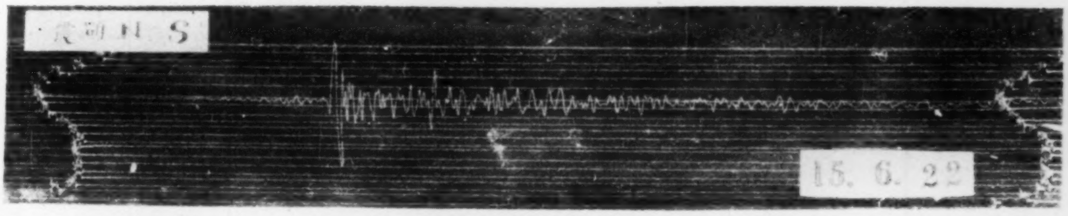

地震研究所地下室 N—S 成分

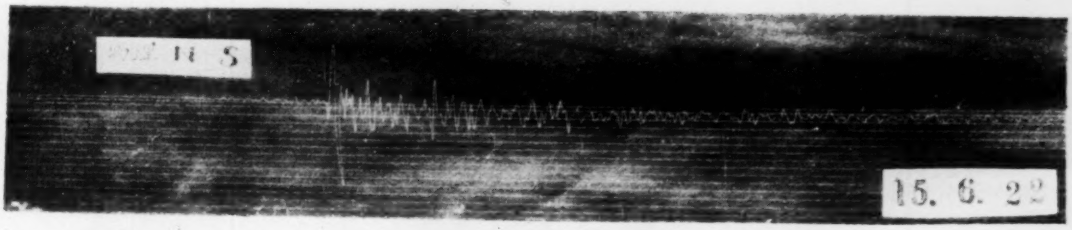

物理學教室 N—S 成分

第 7 圖 地震研究所と物理學教室との比較
(昭和15年6月22日9時24分 江戸川河口沖)

地 震 研 究 所

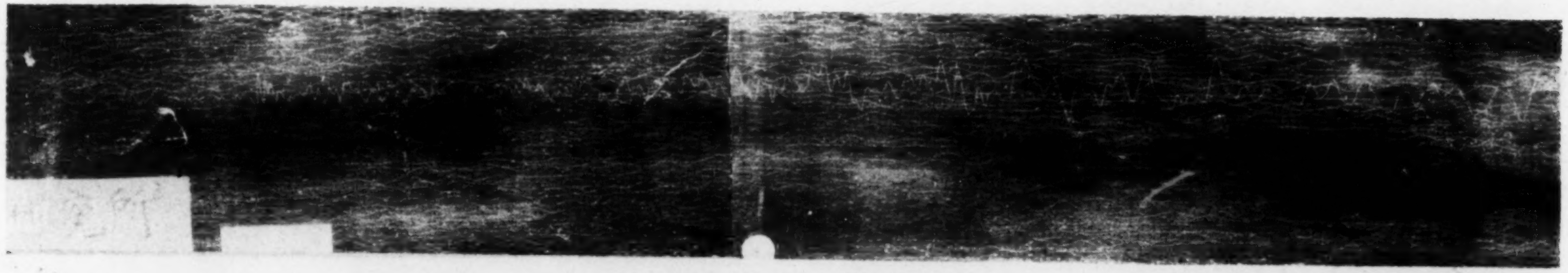

上 野 科 學 博 物 館

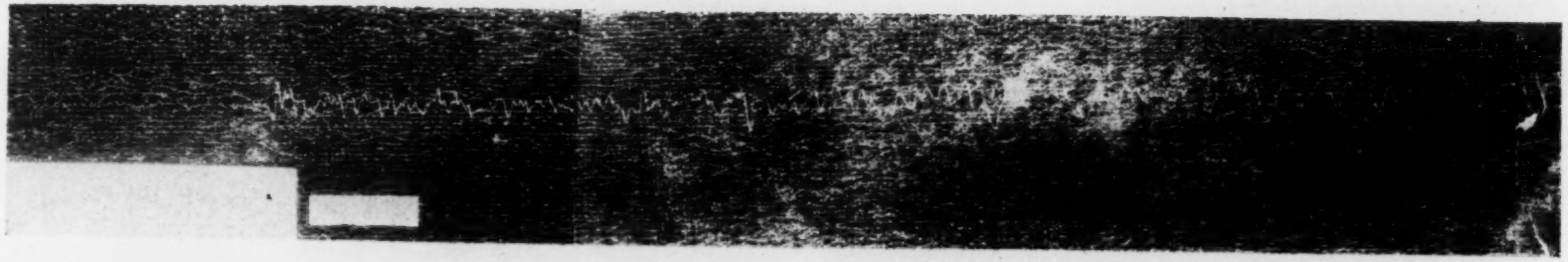

忍 岡 國 民 學 校

第 9 圖 昭和16年3月8日20時1分頃の地震 震央房總南沖合

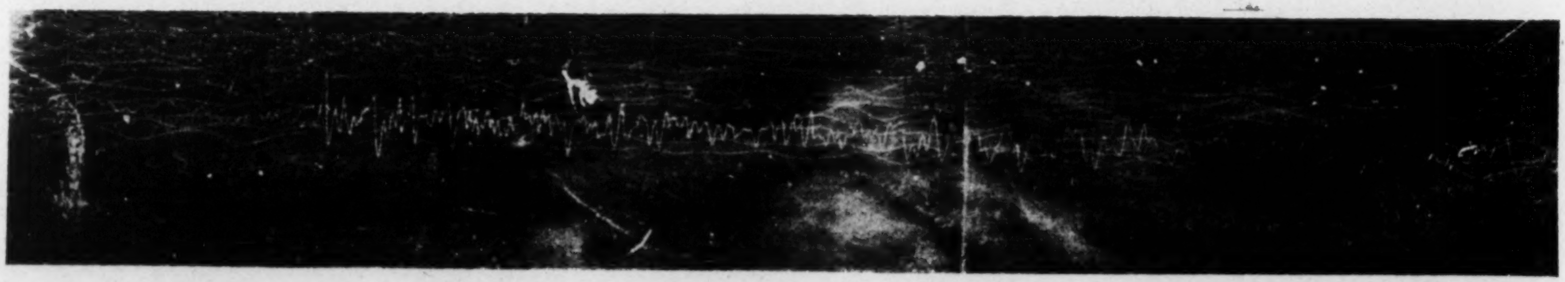

地　震　研　究　所

科　學　博　物　館

第 10 圖　昭和 16 年 3 月 25 日 10 時 32 分　神奈川縣足柄山附近地震

29. *A New Horizontal-Component Seismograph for Comparison Observations.*

By Ryûtarô TAKAHASI and Kintarô HIRANO,

Earthquake Research Institute.

A horizontal component seismograph of inverted pendulum type was newly designed. The main objects of this new design were ease of manipulation and great accuracy. To attain this object, all the jewels, by means of a flat spring, were made to press lightly against the pivots. This design was very effective in eliminating backlashes between the pivot and the jewels. As shown in Fig. 2, the helical spring and needle system that is so frequently used in connecting the magnifying levers was replaced in the new seismograph by a connecting rod, having pivots and plate springs at both ends. The air damper, which consists of a pendulum bob, which acts as the piston, and two cylinders covaring the both side of the bob, have a large functioing area, there being wide clearance between the piston and cylinder, making it easy to set up the instrument, and doing away with the contact of cylinder with the piston which is so liable to occur with rough manipulation, and bad observation conditions. The effective mass and the effective moment of inertia of the pendulum are 12·7 kg and $1{\cdot}18\times10^4$ kg cm^2 respectively. The geometrical magnification of the seismograph, that is, the magnification for an infinitely quick motion of the ground, is 47·5 and the period of free oscillation is 8·0 sec. The record is made on a sheet of smoked paper wound on a drum, 60 cm in circumference revolving once in 5 minutes. The drum is driven by a 6 watt Warren synchronous motor.

Four such seismographs were constructed and installed in parallel in the cellar of our Institute in order to test their accuracies, with satisfactory results, all the seismographs giving exactly the same records, as shown in Figs. 4~6. During these periods of test, the delicate parts of the seismograph, such as the magnifying levers, were removed and then reset several times in order to ascertain whether or not accuracy suffers by such treatment, since such last is inevitable when transportating the instrument. The result of this test was also very satisfactory, the seismographs being always very reliable.

After these tests were made, the seismographs were installed first at the Institute of Physics, Tokyo Imp. Univ. and at our Institute, and after that, at the Science Museum, Ueno Park, the Sinobugaoka Primary School and at our Institute. Examples of the records obtained by these comparison observations are shown in Figs. 7~10. The records obtained at the last three places are very similar to one another in some cases and totally different in others, owing probably to differences in the direction of the epicentres of earthquakes.

30. 軟弱地盤に於ける地震動*

地震研究所 {高橋龍太郎
平能金太郎

(昭和16年6月19日發表——昭和16年6月20日受理)

緒言 東京市内及び横濱市内の十數箇所に設置した加速度計の觀測によつて，石本教授[1)2)]は各地に於て大なる加速度を與へる地震動の周期は其の土地に固有な値を持つてゐる事を發見され，此れを其の土地の卓越振動周期と呼んだ．そして此の卓越振動周期は土地の表面層の固有振動周期と一致し，地震動に依つて表面層が共鳴の現象を起し，大なる振幅の加速度を與へるものと想像された．又妹澤教授[3)4)5)]は數學的方法によつて，土地が表面層を有する場合に，其れが地震動によつて如何に振動するかを考究されてゐる．

筆者等は最近，地震研究所地下室，下谷區七軒町忍岡國民學校の地階，並に上野公園内科學博物館の地階に筆者等の考案に成る地震計[6)]を設置して，各所の地震動の比較研究を行つてゐる．其の結果によると，或る地震の場合[7)]には科學博物館と地震研究所とは殆んど相似の記錄を與へるにもかゝはらず，其の中間に位する忍岡國民學校に於ては初期微動及び主要動の初期に於いては全然上記兩所とは違ふ振動を爲すが，主要動の末期に於て地震動の周期が長くなると共に次第に他の二箇所の記錄と似通つて來る事を認め，其の原因が忍岡國民學校の地盤にある事を實證し，更に軟弱地盤の地表に於ける地震動から，表面層の影響を取除く方法を考へた．

位置，地面，地形 科學博物館の在る上野臺地及び地震研究所の在る本郷臺地は表面に關東壚母，其の下に成田層，東京層等の洪積層を有する比較的堅剛なる地盤なのに對し，忍岡國民學校は上記兩臺地の間に狹まれる不忍池の谷の中に在り，此處では表面は有樂町層なる冲積層から成り，其の下は直ちに東京層である．復興局の試錐結

* 恩師故石本巳四雄先生に捧ぐ

1) *Bull. Earthq. Res. Inst.*, **10** (1932), 171.

2) *Bull. Earthq. Res. Inst.*, **13** (1935), 592; **12** (1934), 234.

3) *Bull. Earthq. Res. Inst.*, **8** (1930), 1.

4) *Bull. Earthq. Res. Inst.*, **10** (1932), 273.

5) *Bull. Earthq. Res. Inst.*, **8** (1930), 321.

6) *Bull. Earthq. Res. Inst.*, **19** (1941). 527.

7) 時には科學博物館と震研との記象が餘り波毎に相對出來ない場合も起る．震央の位置に關係あるものと思はれる．*Bull. Earthq. Res. Inst.* **19** (1914), 527.

果[8]に據れば七軒町に於ける沖積層の厚さは約 10 米である．地震計を設置した上記三箇所の相對的位置は第1圖に示すが如くで，三箇所は略一直線上にあり，其の方向は北 75° 度東である．因に地震計は何れも北 30° 度東の方向に据えてある．圖版第2圖には，昭和 16 年3月 8 日 20 時頃房總半島沖合に起つた地震の各所に於ける記錄の主要部分を示してある．

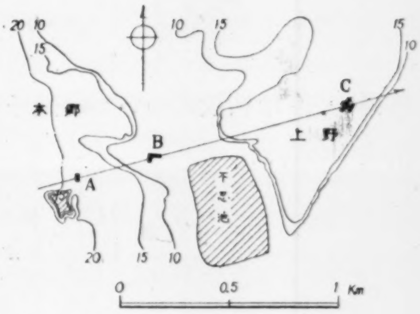

第1圖　A　地震研究所
　　　　B　忍岡國民學校
　　　　C　科學博物館
數字は標高（米）

軟弱地盤に於ける地震動　今座標の原點を地表に，x 軸を下方に取り，表面層の厚さを H, 表面層に於ける地震波（縱波或は橫波）の速度及び土の密度を夫々 V_1, ρ_1, 表面層下の地震波の速度及び土の密度を夫々 V_0, ρ_0 とする．而して地震波は平面波で垂直に傳播するものと考へる．然る時は各層に於ける波動の運動方程式は

$$\frac{\partial^2 u}{\partial t^2}=V^2\frac{\partial^2 u}{\partial x^2} \tag{1}$$

であり，u は

$$u=u\left(t\pm\frac{x}{V}\right) \tag{2}$$

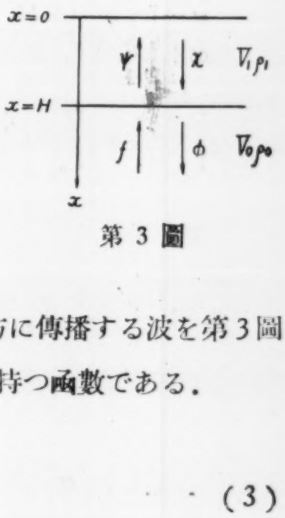

第 3 圖

なる形で與へられる．u なる函數は二度微分出來るものなら如何なるものでもよい．＋は上方に傳播する波を，－は下方に傳播する波を表す．今表面層及び基盤內を上方及び下方に傳播する波を第3圖に示す如く夫々 Ψ, χ, f, ϕ で表す．此等は夫々（2）の形を持つ函數である．

境界の條件として，下記 (3)，(4)，(5) の條件がある．

$$x=0 \text{ の時，}\quad \frac{\partial}{\partial x}(\Psi+\chi)=0 \tag{3}$$

$$x=H \text{ の時，}\quad f+\phi=\Psi+\chi \tag{4}$$

$$V_0^2\rho_0\frac{\partial}{\partial x}(f+\phi)=V_1^2\rho_1\frac{\partial}{\partial x}(\Psi+\chi). \tag{5}$$

從つて（2）の形を考慮して

$$\Psi'-\chi'=0 \tag{3'}$$

$$V_0\rho_0\left[f'\left(t+\frac{H}{V_0}\right)-\phi'\left(t-\frac{H}{V_0}\right)\right]=V_1\rho_1\left[\Psi'\left(t+\frac{H}{V_1}\right)-\chi'\left(t-\frac{H}{V_1}\right)\right] \tag{5'}$$

8) 復興局建築部，東京及橫濱地質調査報告，(昭和4年)．

を得る．又 (4) を t について微分して

$$f'\left(t+\frac{H}{V_0}\right)+\phi'\left(t-\frac{H}{V_0}\right)=\Psi'\left(t+\frac{H}{V_1}\right)+\chi'\left(t-\frac{H}{V_1}\right) \tag{4'}$$

を得る．$'$ は引數についての微分を表す．從つて $(3')$, $(4')$, $(5')$ から χ' 及び ϕ' を消去する時は

$$f'\left(t+\frac{H}{V_0}\right)=\frac{\alpha+1}{2}\Psi'\left(t+\frac{H}{V_1}\right)-\frac{\alpha-1}{2}\Psi'\left(t-\frac{H}{V_1}\right) \tag{6}$$

但し
$$\alpha=\frac{V_1\rho_1}{V_0\rho_0} \tag{7}$$

が得られる．α は振動に對するインピーダンスの比とも稱すべきものである．若し (6) 式に於て t の代りに夫々 $t-\frac{2H}{V_1}$, $t-\frac{4H}{V_1}$………, と書き，其の各式に夫々 $\frac{\alpha-1}{\alpha+1}$, $\left(\frac{\alpha-1}{\alpha+1}\right)^2$………, を乘ずれば

$$\left(\frac{\alpha-1}{\alpha+1}\right)f'\left(t+\frac{H}{V_0}-\frac{2H}{V_1}\right)=\frac{\alpha-1}{2}\Psi'\left(t-\frac{H}{V_1}\right)-\frac{\alpha-1}{2}\left(\frac{\alpha-1}{\alpha+1}\right)\Psi'\left(t-\frac{3H}{V_1}\right) \tag{6'}$$

$$\left(\frac{\alpha-1}{\alpha+1}\right)^2f'\left(t+\frac{H}{V_0}-\frac{4H}{V_1}\right)=\frac{\alpha-1}{2}\left(\frac{\alpha-1}{\alpha+1}\right)\Psi'\left(t-\frac{3H}{V_1}\right)-\frac{\alpha-1}{2}\left(\frac{\alpha-1}{\alpha+1}\right)^2\Psi'\left(t-\frac{5H}{V_1}\right)$$

$$\cdots\cdots\cdots\cdots \tag{6''}$$

$$\left(\frac{\alpha-1}{\alpha+1}\right)^nf'\left(t+\frac{H}{V_0}-\frac{2nH}{V_1}\right)=\frac{\alpha-1}{2}\left(\frac{\alpha-1}{\alpha+1}\right)^{n-1}\Psi'\left(t-\frac{2n-1}{V_1}H\right)$$
$$-\frac{\alpha-1}{2}\left(\frac{\alpha-1}{\alpha+1}\right)^n\Psi'\left(t-\frac{2n+1}{V_1}H\right) \tag{6'''}$$

を得る．然るに $\alpha\geqq 0$ で，若し $\alpha>0$ ならば

$$\left|\frac{\alpha-1}{\alpha+1}\right|<1$$

であるから，$(6''')$ の最後の項は次第に 0 に近づく．從つて (6), $(6')$ $(6'')$, $(6''')$ を相加する事により

$$\sum_{n=0}^{\infty}\left(\frac{\alpha-1}{\alpha+1}\right)^nf'\left(t+\frac{H}{V_0}-\frac{2nH}{V_1}\right)=\frac{\alpha+1}{2}\Psi'\left(t+\frac{H}{V_1}\right) \tag{7}$$

即ち

$$\Psi'(t)=\sum_{n=0}^{\infty}\frac{2}{\alpha+1}\left(\frac{\alpha-1}{\alpha+1}\right)^nf'\left(t+\frac{H}{V_0}-\frac{2n+1}{V_1}H\right) \tag{7'}$$

を得る. $\alpha=0$ の場合は表面層のない場合であるから問題にならない. ϕ' も, 從つて ϕ も同様にして求められるが, 後の議論に不要であるから略す. 今軟弱地盤の表面に於ける振動を $U_w(t)$ とし, Ψ, f 等は何れも t に關する積分恒數を含まぬと考ふべきであるから, (3′) を考慮し (7′) を t につき積分すれば

$$U_w(t)=\chi(t)+\Psi(t)=\sum_{n=0}^{\infty}\frac{4}{\alpha+1}\left(\frac{\alpha-1}{\alpha+1}\right)^n f\left(t+\frac{H}{V_0}-\frac{2n+1}{V_1}H\right) \tag{8}$$

となる.[9] 此式は U_w が, 最初の波の, 地表及び境界面での無限回反射の結果である事を示してゐる.

若し $V_1=V_0$, $\rho_1=\rho_0$, 即ち基盤が露出してゐる場合には $\alpha=1$ となる. 左様な堅剛な地盤の表面に於ける振動 $U_s(t)$ は (8) に於て $\alpha=1$ と置く事により

$$U_s(t)=2f(t) \tag{9}$$

となる.

(8), (9) 式より吾々は直ちに次の重要な關係を求められる.[10]

$$\frac{\alpha+1}{2}U_w\left(t+\frac{H}{V_1}\right)-\frac{\alpha-1}{2}U_w\left(t-\frac{H}{V_1}\right)=U_s\left(t+\frac{H}{V_0}\right) \tag{10}$$

即ち U_w に, 其れより $\dfrac{2H}{V_1}$ だけ前の U_w に $\dfrac{1-\alpha}{1+\alpha}$ を乗じたものを加へれば $t+\dfrac{H}{V_0}-\dfrac{H}{V_1}$ なる時刻に於ける V_s の $2/(1+\alpha)$ 倍を得る. 即ち軟弱地盤に於ける地震記象に或る係數を掛け, 少しくずらして原記象に加算すれば堅剛地盤に於ける地震記象と相似のものが得られる筈である.

問題は α 及び H/V_1 の値を推定する事にあるが其れは次の考察によつて求められる. 今 f が調和的振動で $f=e^{ip\left(t+\frac{x}{V_0}\right)}$ であるとすると

$$U_w=\sum_{n=0}^{\infty}\frac{4}{\alpha+1}\left(\frac{\alpha-1}{\alpha+1}\right)^n e^{-(2n+1)\frac{ipH}{V_1}}\cdot e^{ip\left(t+\frac{H}{V_0}\right)}$$

$$=\frac{2}{\cos p\dfrac{H}{V_1}+i\alpha\sin p\dfrac{H}{V_1}}e^{ip\left(t+\frac{H}{V_0}\right)} \tag{11}$$

從つて U_w の振幅, 即ち絶對値 $|U_w|$ は次の様になる.

---

9) 任意の x に對する f, ϕ, χ, Ψ は t の代りに $t\pm\dfrac{x}{V_{0,1}}$ さすればよい.

10) (10)式は常識により(3′), (9)及び(8)の前半を知つてゐれば (6) 式から直接求められる.

$$\frac{|U_w|}{2}=\frac{1}{\sqrt{\cos^2 p\frac{H}{V_1}+\alpha^2\sin^2 p\frac{H}{V_1}}}\qquad(12)$$

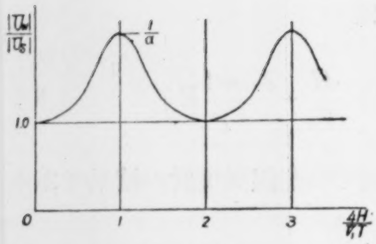

第 4 圖

此の値は第4圖に示す如き變化をする．圖に於て山の高さは $1/\alpha$ になり，山は $4H/VT=1, 3, 5$ の處に生ずる．從つて若し實際の地震記象について周期一振幅の圖を作る，卽ち周期分析をするならば其の山の高さから α が，又山を生ずる波の周期から H/V が判明するであらう．

然し此れは f の振幅が p に係らず，1の場合で，若し左樣でない場合には $U_s=2f$ である事に注意すれば上記の $\frac{|U_w|}{2}$ は $|U_w|/|U_s|$ とすべき事は明かである．

忍ケ岡國民學校の地震動 以上の方法を忍岡國民學校での地震記象に應用して見やう．其の結果は堅剛なる地盤にある地震研究所並に科學博物館に於ける地震動と同じものになる筈で，此れは又，忍岡國民學校のある冲積層の下に來り，冲積層を動かす振動である．

地震は前揭の昭和 16 年3月8日房總沖のものを用ゐる．忍岡國民學校での記象について波の周期と振幅とを畫くと第5圖に示した樣になる．此の分析に於ては初期微

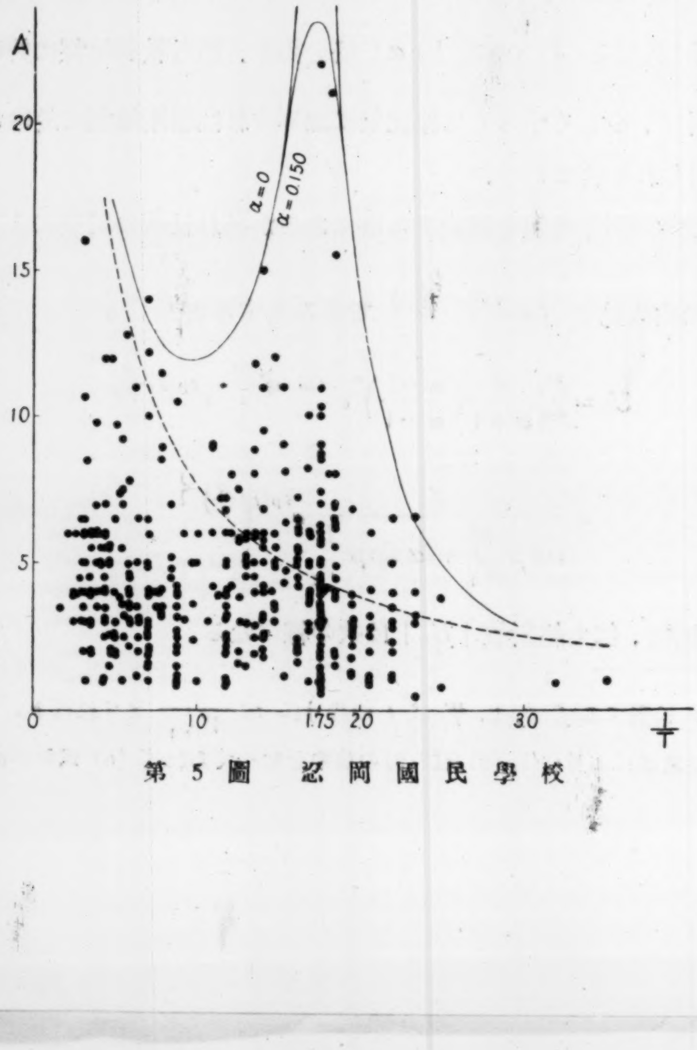

第 5 圖 忍岡國民學校

動以後の部分を用ゐた。卽ち $1/T=1{\cdot}75$ の所に山を生ずるが，其の形は第4圖の如くにはならない．此れは f が一様の振幅を持つてゐない事を示すものと思はれる．實際後に述べる地震研究所及び上野科學博物館の記象を周期分析した結果たる第6圖によつて明かである様に f の振幅(の上限)は周期に比例して增大する．此の事は地震波の勢力に等分割の法則が成立つてゐる事を示すものと考へられる．從つて逆に地震研究所及び科學博物館の記象の周期分析圖の點の大部分を限る雙曲線を書き，此れと同じ双曲線を第5圖にも書いて，此れに第4圖の變化を乘じたものを書くと第5圖の實線の如くになる．此れから $\alpha<0{\cdot}150$, $H/V_1=\ \ 0{\cdot}142$ sec を求め得た．

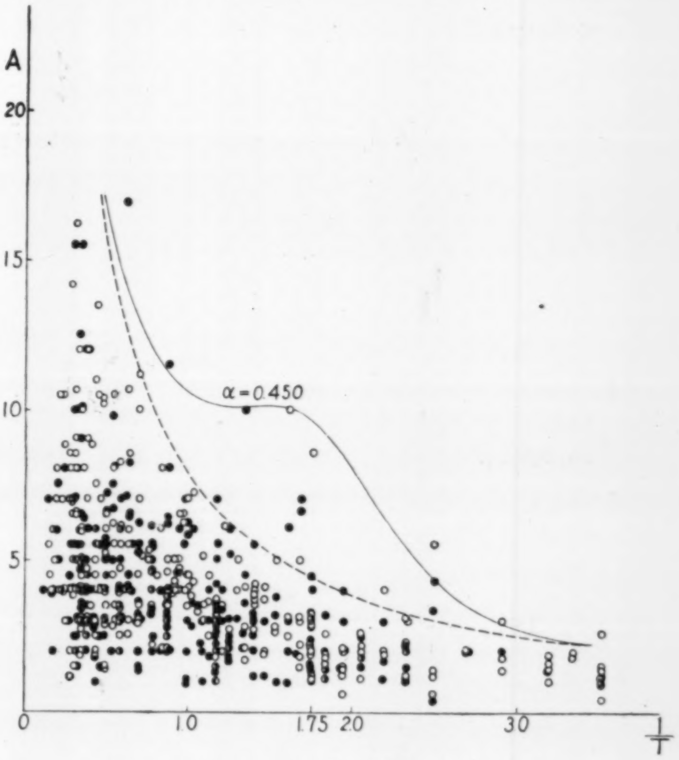

第 6 圖 ○ 地震研究所 ● 科學博物館

今試に $\alpha=0{\cdot}150$ 及び $\alpha=0{\cdot}0$ として U_r を求めた結果は第7圖に示せる如くで，科學博物館に於ける記象と酷似してゐる．同圖に於ては參考比較の爲め，忍岡國民學校及び科學博物館に於て得られた記象をも並記した．

然し乍ら第6圖に示した地震研究所及び上野科學博物館での記象の周期分析の結果からも判る通り，上野臺及び本鄕臺も完全に此處に言ふ堅剛な地盤なのではなく，矢張り小さい乍ら $1/T=1{\cdot}75$ の邊に山を有するものと思はれる．前述の如く本鄕臺，上野臺は忍岡國民學校の基盤である東京層の上に，成田層並に關東壚母が堆積して出來てゐる臺地であるから，此の二層が一つの表面層を形成してゐるものと見做されるのである．從つて比較の爲には科學博物館の記象に對しても上記の手段を應用して U_r を求め，其の結果を忍岡國民學校の記錄から出したものと較べる可きである．

科學博物館の記象に對しては第6圖から判る通り $\alpha=0{\cdot}45$ が適當である．此の値を用ゐて出した U_r は第7圖第3列に示した如くなる．卽ち第7圖の第1列又は第2列と其の形のみならず，振幅に於ても驚く可き相似を示してゐる．

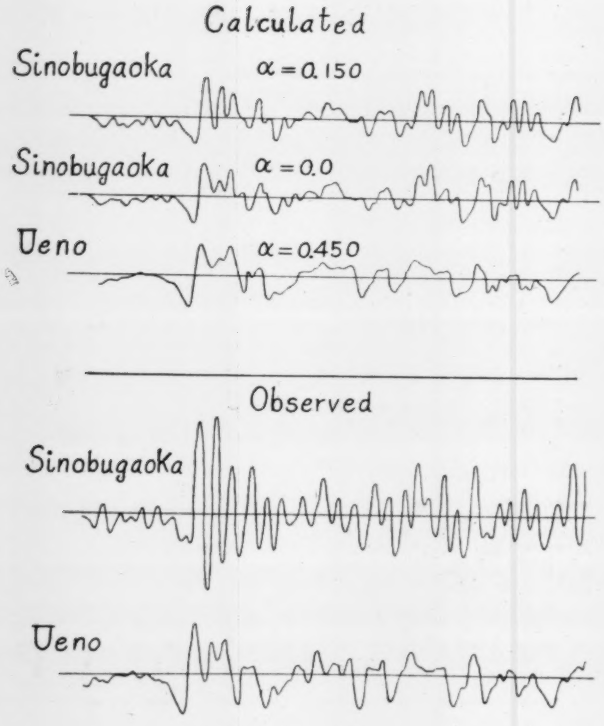

第 7 圖

結言　以上の結果から結論すれば，忍岡國民學校に於ける地震動の特異性は全く同校の存在する不忍池の谷を埋めてゐる沖積層の影響であつて，少なくとも沖積層の基盤たる東京層には，本郷，上野と同じ振動が到來してゐるものと考へられる．只し，基盤の振動共物も本郷，上野と同じであると言ふのではない．共れは東京層と共の上層との境界に於ける反射波の振幅が兩所に於て異るからである．

第 4 圖に示した山の位置は表面層の厚さが波長の 1/4，3/4 等に當る所で，即ち下面固定，上面自由の場合の表面層の固有振動周期と一致する．即ち此處に於ける振幅の增大は波動インピーダンスの少さいために振動勢力が蓄積されて起るものであつて，共鳴の現象に外ならない．共鳴の場合に振幅が無限大になると考へるのは數學的に單純化された模型に限るのであつて，凡ての物理的な共鳴の現象に於ては，何等かの連絡が勢力供給源との間にあるから，勢力の蓄積と共に勢力の逸散も大となつて，振幅は有限の大きさに止る事は妹澤教授[11] によつて既に屢々示された所である．

尤も上記計算に於ては地層は水平方向には一様の構造を有し，無限に擴がつてゐる事を假定し，地震波も直垂方向に傳播する平面波である事を假定してゐるが，表面層が横の境を有し，且つ地震波傳播の方向も，地表附近に於いては垂直に近づくとは言へ猶水平の成分をも有する現實に於ては，現象は上記の樣に簡單では無いかも知れぬ．然し乍ら上記の手段を忍岡國民學校の記象に應用し得た事は，表面層が或る程度の擴がりを有する場合には，共の表面層の或る一地點にのみ着目する限りに於て上記の假定は幾分の妥當性を有する事を示すものと考へられる．

尙ほ忍岡國民學校に於ける前記卓越振動周期 0·6 秒から，$H=10$ 米として有樂町

11)　例へば *Bull. Earthq. Res. Inst.* **14** (1936), 164, 189; **15** (1937), 385.

層中に於ける橫波の速度を概算すると約 70 米 / 秒となる．不忍池の谷に於ける様な含水量の非常に多い土に於ては縱波の速度は可成り大きいが，橫波の速度が非常に少さい事は既によく知られた事實である．石本教授，飯田波事理學士[12]の種々の土の彈性の實驗値から見ても，上記の値は尤も普通のものである．

猶上記の様な現象は只に表面層に於て起るのみでなく，其の下にも存在する種々の不連續面，例へば松澤教授，今村教授[13]によつて求められてゐる不連續面，或はモホロビチツク層と表面との間等にて於も起る筈であり，更に此等の不連續面の任意の二つを反射面としても起り得る筈である．又垂直方向の不連續面に考を限る理由はなく，水平方向の不連續面をも考へねばならない．地震動の總振動時間が震央距離と共に增大する事の一因は震央距離と共に不連續面の數が增加する事にあるとも考へられる．石本教授は夙に地震動と水槽內の水の振動との相似[14]について述べられ，又殘響現象或は擴散現象[15]との相似に氣附かれてゐたのである．

實際前述の昭和 16 年 3 月 8 日房總沖の地震の上野科學博物館に於ける記象[16]を詳細に點檢する時は，主要動の最初に於ける特種な形を持つた振動が，其の後の地震動中に少なくとも三度は出現してゐることを認め得るのである．只だ後のものになる程，段々と形も崩れ，振幅も少さくなつてゐる．此れは波動の分散減衰に因るものと思はれる．同じ形が數度，然も同じ向きに現れる事は，波動が傳播中の層よりも小さい振動インピーダンスを持つ層との境界面で反射されてゐる事を示すもので，反射波の大きさから見て其の境界面は地表ではないかと思はれる．

終りに臨み，本研究が文部省科學研究費によつて爲されたものである事を記し深謝の意を表する次第である．

---

12) *Bull. Earthq. Res. Inst.*, **7** (1936), 534; 632.
13) T. MATUSAWA, K. YAMADA and T. SUZUKI, *Bull. Earthq. Res. Inst.*, **7** (1929), 241.
A. IMAMURA, F. KISHINOUYE and K. KODAIRA, *Bull. Earthq. Res. Inst.*, **7** (1929), 471.
14) *Bull. Earthq. Res. Inst.*, **12** (1934), 706.
15) *Bull. Earthq. Res. Inst.*, **13** (1935), 130.
16) R. TAKAHASI and K. HIRANO, *loc. cit*, cf. Plate.

附錄 地震動の記象に於て變位の一つの極大（小）値を A_N，其の時刻を t_N，其れに續く變位の極小(大)値を A_{N+1}，其の時刻を t_{N+1}，とする時に，周期を $T=2(t_{N+1}-t_N)$，振幅を $A=\frac{1}{2}(A_N\sim A_{N+1})$として第5，6圖の點を畫いたのであるが，斯樣にして得られた點の分布の上限が，地震記象 $y(t)$ を調和解析した時の周期振幅スペクトルの上限卽ち

$$\frac{1}{\pi}\int_{-\infty}^{\infty} y(t)e^{-i\omega t}dt$$

の絕對値を表すかどうかは一つの問題である。差當つては此の證明を爲し得ないが，忍岡國民學校の記象により第2圖に示した範圍內の曲線につき 8～9 の周期について上記積分を行つた結果は第 8 圖に示す如く，第5圖の結果と相似してゐる．

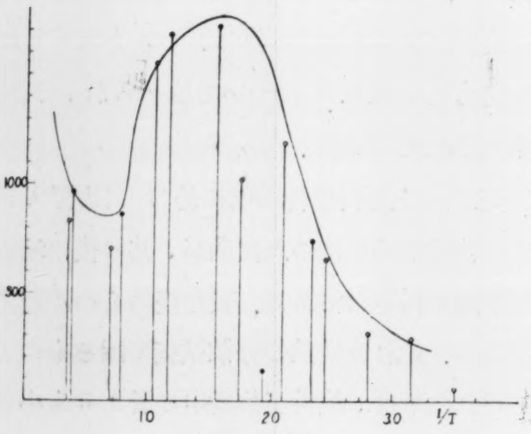

第 8 圖

忍岡國民學校の建物の振動については，平常時の微動を用ひて調査してある．此處にはたゞ建物が略々全體として剪斷振動を爲すが，一塊としてロッキングを爲すのではない事のみを記し，詳細は別の機會に記す事にしたい．

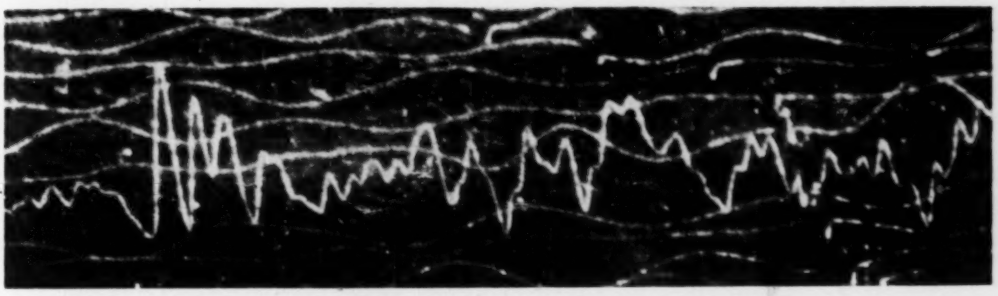

本郷，地震研究所．The Earthquake Research Institute, Hongo.

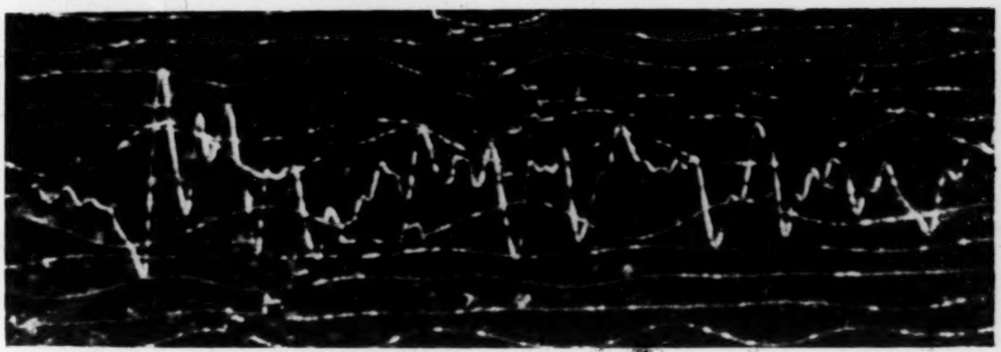

上野，科學博物館．The Science Museum, Ueno.

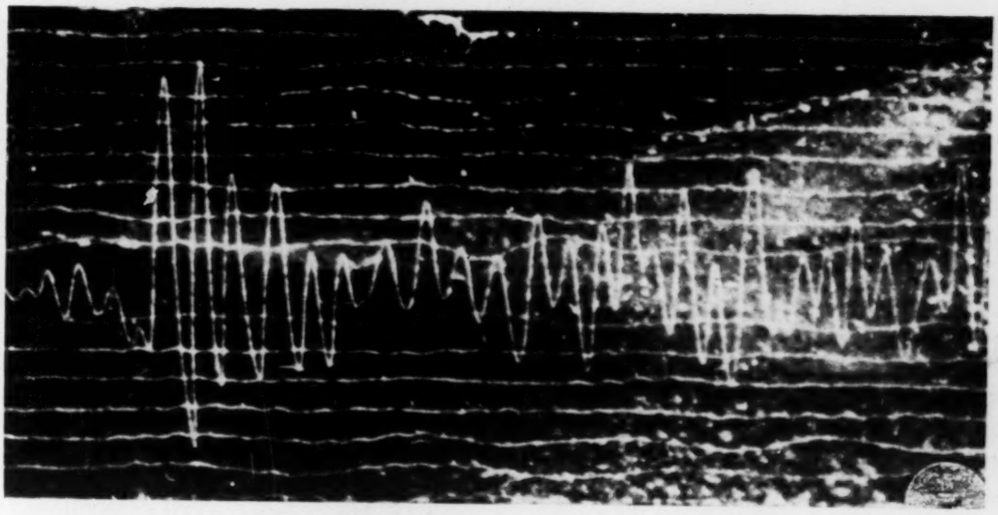

下谷區七軒町，忍岡國民學校．The Sinobugaoka Primary School, Sitaya.

第 2 圖　昭和 16 年 3 月 8 日房總沖の地震

30. *Seismic Vibrations of Soft Ground.*

By Ryûtarô TAKAHASI and Kintarô HIRANO,

Earthquake Research Institute.

Denoting by $U_w(t)$ the seismic vibrations of a ground with weak surface layer, and by $U_s(t)$ the seismic vibrations due to the same earthquake in ground without any surface layer, the writers obtained the formula

$$\frac{\alpha+1}{2}U_w\left(t+\frac{H}{V_1}\right)-\frac{\alpha-1}{2}U_w\left(t-\frac{H}{V_1}\right)=U_s\left(t+\frac{H}{V_0}\right),$$

where H is the thickness of the surface layer, V_1, V_0 the velocities of propagation of seismic waves respectively in the surface layer and in its base beds. α is the ratio of $V_1\,\rho_1$ to $V_0\,\rho_0$, where ρ_0 and ρ_1 denote the densities of the respective layers. α is, therefore, the impedance ratio for wave propagation. This formula enables us to deduce from seismograms obtained of shocks through soft ground, the seismogram that would have been obtained at a ground that has no surface layer. α and H/V_1 may be obtained from the amplitude period diagram of $U_w(t)$.

The foregoing method was used in connexion with seismograms obtained on March 8, 1941, at the Sinobugaoka Primary School and at the Science Museum, Ueno Park. The earthquake had its origin off the coast of the Boso Peninsula. The Sinobugaoka Primary School is situated at Sitikentyo, Sitayaku, between Ueno Park and Hongo, Tokyo. Sitayaku (a part of lower Tokyo) has a surface alluvial layer called the Yûrakutyô Beds, 10 m thick, under which lie the basement dilluvial beds called the Tokyo Beds, wheras both Ueno Park, and Hongo, are parts of upper Tokyo, the surface layer, overlying the Tokyo Beds, consisting of loam, 10 m thick, and the dilluvial Narita Beds, 10~15 m thick. The under-ground water level at Sitikentyô is 0·5~1 meter beneath the surface of the ground, so that the alluvial deposit there is very soft.

As will be seen from Fig. 2 (Plate), the seismograms obtained at the Science Museum and the Earthquake Research Institute, Hongo, closely resemble each other, whereas that obtained at the Sinobugaoka Primary School differs entirely from the other two.

The results after using the method mentioned above are shown in Fig. 7. The similarity in shape of the two curves obtained are surprising.

This shows that although the original seismic waves that pass through the Tokyo Beds at both Ueno and Sitikentyô are of the same shape, at the latter locality the seismic vibrations at the surface of the ground are modified by resonance oscillations of the surface layer.

The paper concludes with further discussions on the nature of seismic waves in general.

31.　三宅島における三角再測量の結果

昭和 15 年7月 12 日に三宅島に噴火があり，それに伴つて著しい地變が認められた．この地變を調べる爲に，三宅島において三角測量が施行され，その結果は前回の測量結果と比較されて同島內に在る 16 個の三角點の水平及び上下方向の移動量が測定された．

前測量は大正元年に行はれた．前測量に於いては島の西南隅に約 350 cm の假の基線を設けて，それを邊長の基礎とした．今回の測量に於いても全く同樣な基線に據り，水平移動量は，富賀山の位置と，富賀山から小松原への方位角とを不變なものとして算出された．富賀山，小松原の三角點は共に噴火地域からは最も遠く離れた島の西南部に在るので，噴火の影響は最も小さいであらうと想像され，從つて，移動量算出の基準點として撰ばれたものである．

三角點の高さは，坪田村で中等潮位の測定を行ひ，その結果を油壺における測定値と比較して適當な補正を加へたものを基準として觀測された．小手の倉，富賀山の 2 三角點の高さは，坪田村の中等潮位から直接水準によつて測り，他は間接水準によつた．その結果を，大正元年の結果と比較して，各三角點の上下方向の變動量が檢出された．

是等の野外作業は昭和 16 年1月 31 日から同年2月 26 日迄の間に行はれたものである．測定の結果知られた三角點の移動は，第1圖及び第 I～II 表に掲げてある．

第 I 表　水平移動量

Table I. Horizontal Displacements.

番號 Number	三角點 Triangulation Point		移動量 Displacement	方位角 Azimuth	
1	三宅島 II.	Miyakezima.	34 cm	247°	20′
2	富賀山 III.	Togayama.	00	0	0
3	二男山 〃	Hutaoyama.	23	257	10
4	小手ノ倉 〃	Kotenokura	18	211	0
5	伊ケ谷 〃	Igaya	26	252	20
6	長根山 〃	Naganeyama	28	220	40
7	坪田 〃	Tubota	32	214	40
8	賀良野 〃	Garano	64	193	40

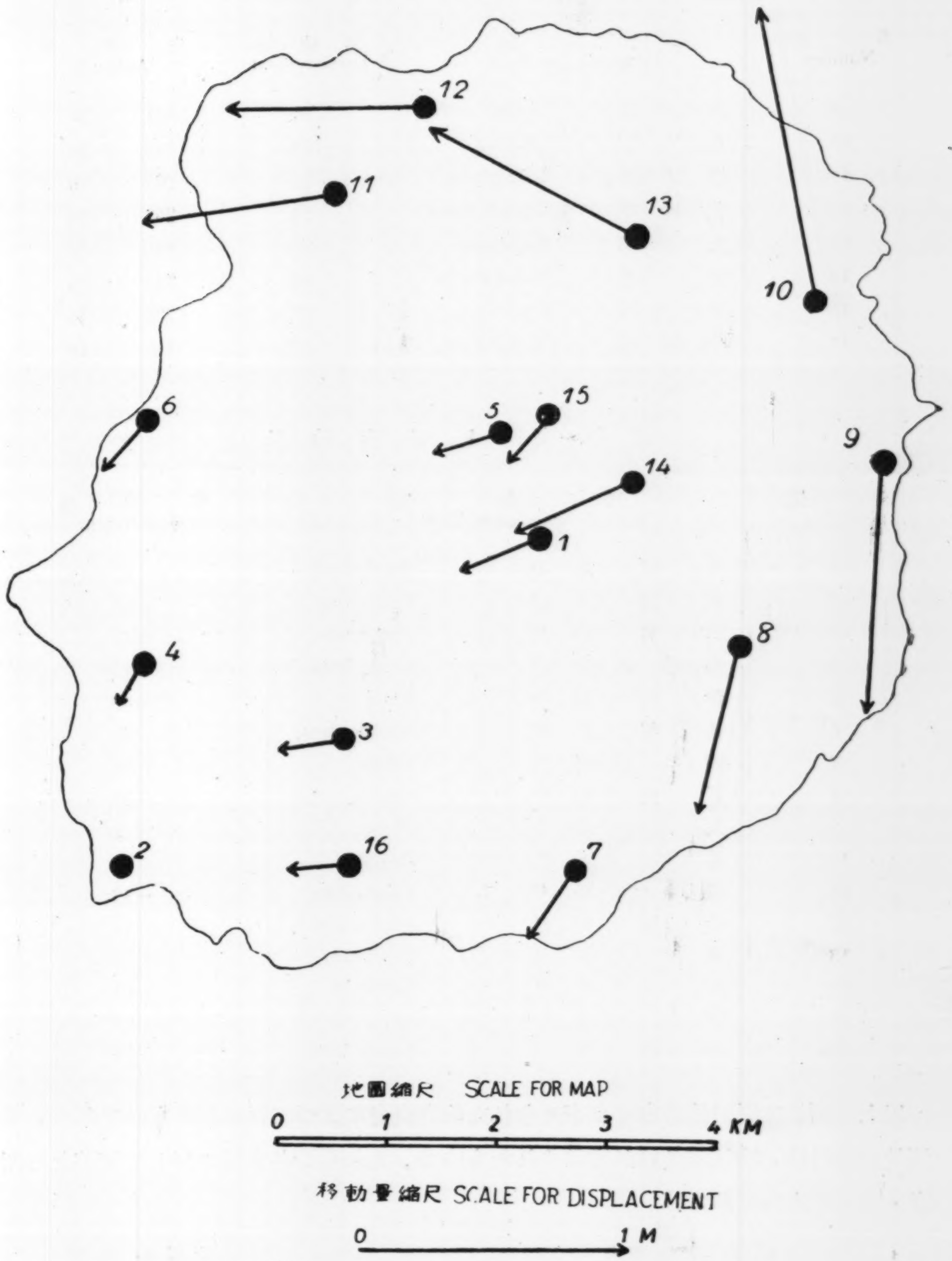

第1圖 三宅島に於ける三角點の分布と水平移動（數字は三角點の番號を示す）.

Fig. 1. Distribution of triangulation points and their horizontal displacements in Miyake-sima (numerals against points designate the number of triangulation points).

第 I 表 (續)

番號 Number	三角點 Triangulation Point		移動量 Displacement	方位角 Azimuth	
9	大倉 〃	Okura.	90	181	50
10	島下 〃	Simasita.	108	343	20
11	嶽ノ平 〃	Takenohira	63	260	50
12	北風平 〃	Kitakazetairo.	71	267	30
13	風早 〃	Kazahaya.	86	296	20
14	神着 〃	Kamituki.	44	245	50
15	伊豆 〃	Izu.	18	222	40
16	小松原 〃	Komatubara.	22	262	10

第 II 表 上下移動量

番號 Number	三角點 Triangulation Point		移動量 Displacement
1	三宅島 II.	Miyakezima.	−65 cm
2	富賀山 III.	Togayama.	−43
3	二男山 〃	Hutaoyama.	−47
4	小手ノ倉 〃	Kotenokura.	−43
5	伊ケ谷 〃	Igaya.	−63
6	長根山 〃	Naganeyama.	−47
7	坪田 〃	Tubota.	−54
8	賀良野 〃	Garano.	−35
9	大倉 〃	Okura.	2
10	島下 〃	Simasita.	−15
11	嶽ノ平 〃	Takenohira.	−35
12	北風平 〃	Kitakazetairo.	−31
13	風早 〃	Kazahaya.	−27
14	神着 〃	Kamituki.	−63
15	伊豆 〃	Izu.	−79
16	小松原 〃	Komatubara.	−59

以上の測量は原田積善會より寄せられた研究資金によつて行はれたものであり，又測量の遂行は，陸地測量部が擔當されたもので，これらの各當局に對して深甚なる謝意を表するものである．

昭和16年6月 地震研究所

31. *Results of Re-triangulation in Miyake-sima.*

The eruption of Volcano Miyake-sima, on July 12, 1940, was accompanied with marked crustal deformation, to measure which, its triangulation was revised. By comparing the new results with those of the last survey, the horizontal and vertical displacements of 16 triangulation points (including 1 secondary and 15 tertiary triangulation points) were deduced.

The former survey was done in 1912. A temporary base line 350 m long was established in the south-western corner of the island. The new survey was carried out in exactly the same way as last. The horizontal displacements of the triangulation points were deduced with reference to the Togayama triangulation point; and the azimuth from Togayama point to Komatubara point, which was assumed as not having been changed by the eruption. These points were selected because they are situated at the greatest possible distances from the centre of disturbance, so that the assumption is considered reasonable.

As to the heights of the triangulation points, the mean sea-level measured at Tubota-mura was chosen for the datum level. Taking into account the suitable correction, obtained by comparing the measurements at Tubota-mura with those obtained at Aburatubo, the heights of triangulation points measured recently were compared with those of former measurements, and the vertical displacements thus deduced.

The distribution of triangulation points is shown in Fig. 1, the numerical data of horizontal and vertical displacements being given in Table I and II respectively.

The present measurements of horizontal and vertical displacements of triangulation points in Miyake-sima were made possible by the aid of the research fund granted by the Harada Sekizenkwai, to the council of which we wish to express our sincere thanks. Our best thanks are also due to the Military Land Survey for their courtesy in carrying out the re-triangulation at our request.

June, 1941. The Earthquake Research Institute.

32. *On the Propagation of Rayleigh-waves in Dispersive Elastic Media.*

By Katsutada SEZAWA and Kiyoshi KANAI,

Earthquake Research Institute.

研究 17. 3. 2

(Read Sept. 18, 1941.—Received Sept. 20, 1941.)

Although attempts have been made to solve a number of problems relating to dispersive Rayleigh-waves, their dispersive nature as shown by the results of calculation is because stratified layers of elastic media were assumed and not because the media themselves are dispersive. In this paper we shall consider the case in which the waves are dispersed even though the layer through which the waves are transmitted is not stratified.

If we assume that the vibration of a point in the media is resisted by a force proportional to the displacement of the same point, in addition to the elastic force, it is possible for the equations of motion for longitudinal waves and transverse waves respectively to have the forms

$$\rho\frac{\partial^2 u}{\partial t^2}=(\lambda+2\mu)\frac{\partial^2 u}{\partial x^2}-au, \tag{1}$$

$$\rho\frac{\partial^2 u'}{\partial t^2}=\mu\frac{\partial^2 u'}{\partial x^2}-a'u'. \tag{2}$$

The solutions for the velocities of both these waves are of the types

$$V=\sqrt{\frac{\lambda+2\mu}{\rho}+\frac{a}{\rho f^2}},\quad V'=\sqrt{\frac{\mu}{\rho}+\frac{a'}{\rho f^2}}, \tag{3}$$

respectively, where $2\pi/f$ is wave length. It thus holds that if there is vibrational resistance proportional to the displacement, bodily waves are also dispersive.

We shall next consider the case of a semi-infinite body, the equations of motion of which are then expressed by

$$\left.\begin{aligned}\rho\frac{\partial^2 u}{\partial t^2}&=(\lambda+\mu)\frac{\partial \Delta}{\partial x}+\mu\nabla^2 u-au,\\ \rho\frac{\partial^2 v}{\partial t^2}&=(\lambda+\mu)\frac{\partial \Delta}{\partial y}+\mu\nabla^2 v-av.\end{aligned}\right\} \tag{4}$$

It is remembered that

$$\Delta=\frac{\partial u}{\partial x}+\frac{\partial v}{\partial y}, \quad 2\varpi=\frac{\partial v}{\partial x}-\frac{\partial u}{\partial y}. \tag{5}$$

From (4), (5), we get

$$\rho\frac{\partial^2\Delta}{\partial t^2}=(\lambda+2\mu)\nabla^2\Delta-a\Delta, \quad \rho\frac{\partial^2\varpi}{\partial t^2}=\mu\nabla^2\varpi-a\varpi, \tag{6}$$

the solutions of which are

$$\Delta=Ae^{i(pt-fx)+ry}, \quad 2\varpi=Be^{i(pt-fx)+sy}, \tag{7}$$

where

$$r^2=f^2-h^2, \quad s^2=f^2-k^2, \quad h^2=\frac{\rho p^2-a}{\lambda+2\mu}, \quad k^2=\frac{\rho p^2-a}{\mu}. \tag{8}$$

The displacements corresponding to (7) are

$$\left.\begin{aligned} u_1&=\frac{if}{h^2}Ae^{i(pt-fx)+ry}, \quad v_1=-\frac{r}{h^2}Ae^{i(pt-fx)+ry},\\ u_2&=\frac{s}{k^2}Be^{i(pt-fx)+sy}, \quad v_2=\frac{if}{k^2}Be^{i(pt-fx)+sy}. \end{aligned}\right\} \tag{9}$$

Substituting (7), (9) in the boundary conditions

$$\lambda\Delta+2\mu\frac{\partial}{\partial y}(v_1+v_2)=0, \quad \frac{\partial(v_1+v_2)}{\partial x}+\frac{\partial(u_1+u_2)}{\partial y}=0 \tag{10}$$

at $y=0$, we get

$$\left(2-\frac{k^2}{f^2}\right)^4=16\left(1-\frac{h^2}{f^2}\right)\left(1-\frac{k^2}{f^2}\right), \tag{11}$$

the form of which is the same as the characteristic equation for the usual Rayleigh-waves. Relation (11) shows that if $\lambda=\mu$,

$$V=\sqrt{0{\cdot}8453\mu/\rho+a/\rho f^2}, \tag{12}$$

and that if $\lambda/\mu=\infty$,

$$V=\sqrt{0{\cdot}9126\mu/\rho+a/\rho f^2}, \tag{13}$$

whence it follows that Rayleigh-waves in a semi-inifinite body would be dispersive, provided there is an additional resistance that is proportional to the displacement.

When elastic media composing stratified layers have a resistance that is proportional to the displacement, the dispersive nature of the surface waves alters considerably. The equations of motion in this case are expressed by

$$\left.\begin{aligned} \rho'\frac{\partial^2 u'}{\partial t^2} &= (\lambda'+\mu')\frac{\partial \Delta'}{\partial x}+\mu'\Gamma^2 u'-a'u', \\ \rho'\frac{\partial^2 v'}{\partial t^2} &= (\lambda'+\mu')\frac{\partial \Delta'}{\partial y}+\mu'\Gamma^2 v'-a'v', \end{aligned}\right\} \tag{14}$$

$$\left.\begin{aligned} \rho\frac{\partial^2 u}{\partial t^2} &= (\lambda+\mu)\frac{\partial \Delta}{\partial x}+\mu\Gamma^2 u-au, \\ \rho\frac{\partial^2 v}{\partial t^2} &= (\lambda+\mu)\frac{\partial \Delta}{\partial y}+\mu\Gamma^2 v-av, \end{aligned}\right\} \tag{15}$$

for the upper layer and the lower layer, respectively. The characteristic equation has the form

$$\begin{aligned} &\frac{4r's'}{f^2}\left(2-\frac{k'^2}{f^2}\right)\eta-\frac{r's'}{f^2}\left\{4\vartheta+\left(2-\frac{k'^2}{f^2}\right)^2\zeta\right\}\cosh r'H\cos s'H \\ &+\frac{r'}{f}\xi\left\{\frac{4rs'^2}{f^3}+\frac{s}{f}\left(2-\frac{k'^2}{f^2}\right)^2\right\}\cosh r'H\sin s'H \\ &+\frac{r'}{f}\xi\left\{-\frac{4sr'^2}{f^3}+\frac{r}{f}\left(2-\frac{k'^2}{f^2}\right)^2\right\}\sinh r'H\cos s'H \\ &+\left\{-\frac{4r'^2s'^2}{f^4}\zeta+\left(2-\frac{k'^2}{f^2}\right)^2\vartheta\right\}\sinh r'H\sin s'H=0, \end{aligned} \tag{16}$$

where H is the thickness of the surface layer and

$$\left.\begin{aligned} &4=\frac{\mu'k^2k'^2}{\mu f^4}, \quad \zeta=\frac{4rs}{f^2}\left(\frac{\mu'}{\mu}-1\right)^2-\alpha^2, \quad \eta=\frac{2rs}{f^2}\left(\frac{\mu'}{\mu}-1\right)\beta-\alpha\gamma, \\ &\vartheta=\frac{rs}{f^2}\beta^2-\gamma^2, \quad \alpha=\frac{2\mu'}{\mu}-\left(2-\frac{k^2}{f^2}\right), \quad \beta=\frac{\mu'}{\mu}\left(2-\frac{k'^2}{f^2}\right)-2, \\ &\gamma=\frac{\mu'}{\mu}\left(2-\frac{k'^2}{f^2}\right)-\left(2-\frac{k^2}{f^2}\right), \\ &r^2=f^2-h^2, \quad s^2=f^2-k^2, \quad r'^2=f^2-h'^2, \quad s'^2=k'^2-f^2, \\ &h^2=\frac{\rho p^2-a}{\lambda+2\mu}, \quad k^2=\frac{\rho p^2-a}{\mu}, \quad h'^2=\frac{\rho'p^2-a'}{\lambda'+2\mu'}, \quad k'^2=\frac{\rho'p^2-a'}{\mu'}. \end{aligned}\right\} \tag{17}$$

Using (16), (17), it is possible to calculate the relation between k'/f and fH. Since $k'^2/f^2=(\rho'p^2-a')/\mu'f^2$, by assuming the value of $a'/\mu'f^2$, we

get the velocity of transmission of Rayleigh-waves for different values of fH and $a'/\mu' f^2$. Since, however, the ratio of $a'/\mu' f^2$ is not a known quantity, the parameters will be so changed that the velocity of transmission of the waves is represented as functions of fH and aH^2/μ'. The results of calculation for the three cases, (i) $\lambda=\mu$, $\lambda'=\mu'$, $\mu/\mu'=5$, $\rho'/\rho=1$, $a'/a=1$, (ii) $\lambda=\mu$, $\lambda'=\mu'$, $\mu/\mu'=20$, $\rho'/\rho=1$, $a'/a=1$, (iii) $\lambda=\mu=\lambda'=\mu'$, $\rho'/\rho=1/2$, $a'/a=1/2$, are shown in Figs. 1, 2, 3. The numerical data for the present calculation are those that we obtained previously.[1),2),3)]

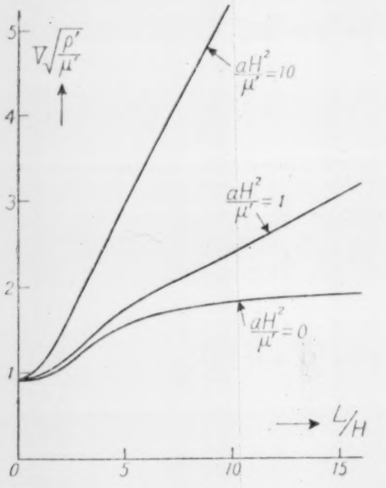

Fig. 1. $\lambda=\mu$, $\lambda'=\mu'$, $\mu/\mu'=5$, $\rho/\rho'=1$, $a/a'=1$.

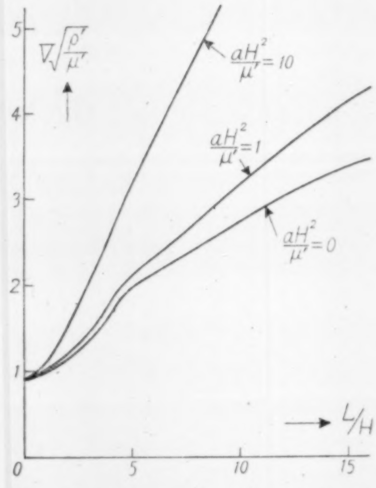

Fig. 2. $\lambda=\mu$, $\lambda'=\mu'$, $\mu/\mu'=20$, $\rho/\rho'=1$, $a/a'=1$.

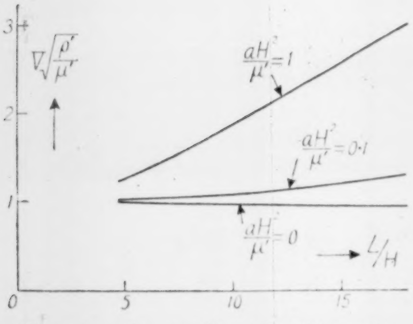

Fig. 3. $\lambda=\mu$, $\lambda'=\mu'$, $\rho'/\rho=1/2$, $a'/a=1/2$, $\mu'/\mu=1$.

From these figures it will be seen that the greater the value of a, the more the increase in the velocity of transmission of Rayleigh-waves. This feature is more pronounced with increase in the length of the waves. Although, in case (iii), the velocity of the waves in non-dispersive media diminishes with wave length, should the value of a exceed a certain limit, the velocity of the same waves would tend to increase with wave length.

1) K. SEZAWA, *Bull. Earthq. Res. Inst.*, **3** (1927), 1.

2) K. SEZAWA and K. KANAI, "Discontinuity in the Dispersion Curves of Rayleigh-waves," *Bull. Earthq. Res. Inst.*, **13** (1935), 237~244.

3) K. SEZAWA and K. KANAI, "Anomalous dispersion of Elastic Surface Waves," *Bull. Earthq. Res. Inst.*, **16** (1938), 225~237.

Finally, there remains to be seen whether or not it is possible for a resistance that is proportional to the displacement of the waves to exist in the actual crust. Although no elastic medium with such a property exists, if there were earth blocks having statistically the nature of the so-called oscillators, resistance such as that just mentioned would be conceivable.

---

32. 固體自體が分散性なる場合に於けるレーレー波の傳播

地震研究所 {妹澤克惟
金井清

今まで分散性のレーレー波について數多くの研究を試みたが，何れの場合にも地層の存在を假定する事によつてその分散性が現れ得たのである．玆に固體自體が分散性である場合を探して見たが，固體に彈性力の外に振動の變位に比例する抵抗が存在すると地層がなくても分散性がある事が確められた．勿論この分散性は表面波に限らず固體波にも存在する譯である．何れの波にしても上述のやうな分散性があると，波の傳播速度が波長とともに增加する．その速度の方則は本文中に示してある．地表層があるために旣に分散性を有するレーレー波は只今のやうな固體の性質によつて更に分散性が增加する．地表層によつて異常分散をなす場合例へば波長とともに速度が減ずる場合には只今の性質によつて速度が補はれ，波長とともに速度が增加する事もあり得るのである．實際問題として變位に比例する振動抵抗が地殼にあり得るかどうかといふ疑問が當然起るけれども，之は統計的に見て振動子と考へられるやうな地塊が存在すれば可能になるものと思はれる．

---

33. *The Seismic Vibration of a Saw-tooth Roof Structure.*

By K. KANAI,

Earthquake Research Institute.

(Read July 3, 1941.—Received Sept. 20, 1941.)

The problem of seismic resistance of a saw-tooth roof structure has not yet been attacked mathematically. Although Taniguchi[1] reported damage to such a structure in the Tango Earthquake of 1927, no analytical study of such damage has not yet been made. The present paper is an attempt to ascertain the free vibration of a saw-tooth roof structure, as shown Fig. 1. In order to simplify the problem, an infinite number of spans is assumed. Furthermore, it is assumed, for simplicity, that the masses are concentrated at the panel points, in consequence of which the mass for horizontal movement will differ from that for vertical movement, the respective masses in question then being m_1, m_1', m_2, m_2'. Let l_1, l_1', l_2, l_3, h be the length of lower column, length of upper column, beam span, length of roof member, and the total length of the vertical members, respectively; let also E_1I_1, E_2I_2, 0; E_1a_1, 0, E_3a_3 be the bending and longitudinal stiffnesses of the columns, beam, and roof member, respectively. The lateral movements y_1, y_1', y_2, 0 and the longitudinal displacements z_1, z_1', 0, z_3 of the respective members just mentioned satisfy differential equations of types

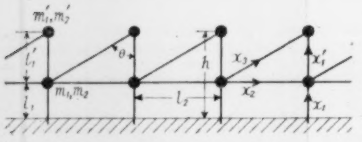

Fig. 1.

$$\frac{\partial^4 y}{\partial x^4}=0, \quad \frac{\partial^2 z}{\partial x^2}=0. \tag{1}$$

The solutions of these equations are

$$\left.\begin{aligned} y_1&=A_1+B_1x_1+C_1x_1^2+D_1x_1^3, & z_1&=\alpha_1+\beta_1x_1,\\ y_1'&=A_1'+B_1'x_1'+C_1'x_1'^2+D_1'x_1'^3, & z_1'&=\alpha_1'+\beta_1'x_1',\\ y_2&=A_2+B_2x_2+C_2x_2^2+D_2x_2^3, & z_3&=\alpha_3+\beta_3x_3. \end{aligned}\right\} \tag{2}$$

The boundary conditions are written

$$x_1=0; \qquad y_1=0, \quad z_1=0, \quad \frac{dy_1}{dx_1}=0, \qquad (3), (4), (5)$$

1) T. TANIGUCHI, *Bull. Earthq. Res. Inst.*, **3** (1927), 133.

$$x_1=l_1,\ x_1'=0,\ x_2=l_2,\ x_{22}=0,\ x_3=0;$$

$$y_1=y_1',\quad y_2=y_{22}=-z_1=-z_1',\quad z_3=z_1\cos\theta+y_1\sin\theta, \qquad (6),(7),(8),(9),(10)$$

$$\frac{dy_1}{dx_1}=\frac{dy_1'}{dx_1'}=\frac{dy_2}{dx_2}=\frac{dy_{22}}{dx_{22}}, \qquad (11),(12),(13)$$

$$E_1I_1\left(\frac{d^2y_1}{dx_1^2}-\frac{d^2y_1'}{dx_1'^2}\right)+E_2I_2\left(\frac{d^2y_2}{dx_2^2}-\frac{d^2y_{22}}{dx_{22}^2}\right)=0, \qquad (14)$$

$$E_1I_1\left(\frac{d^3y_1'}{dx_1'^3}-\frac{d^3y_1}{dx_1^3}\right)-E_3a_3\frac{dz_3}{dx_3}\sin\theta=m_1p^2y_1, \qquad (15)$$

$$E_2I_2\left(\frac{d^3y_{22}}{dx_{22}^3}-\frac{d^3y_2}{dx_2^3}\right)+E_1a_1\left(\frac{dz_1'}{dx_1'}-\frac{dz_1}{dx_1}\right)+E_3a_3\frac{dz_3}{dx_3}\cos\theta=m_2p^2y_2, \qquad (16)$$

$$x_1'=l_1',\ x_3=l_3;\quad z_3=y_1'\sin\theta+z_1'\cos\theta,\quad E_1I_1\frac{d^2y_1'}{dx_1'^2}=0, \qquad (17),(18)$$

$$-E_1I_1\frac{d^3y_1'}{dx_1'^3}+E_3a_3\frac{dz_3}{dx_3}\sin\theta=m_1'p^2y_1', \qquad (19)$$

$$E_1a_1\frac{dz_1'}{dx_1'}+E_3a_3\frac{dz_3}{dx_3}\cos\theta=m_2'p^2z_1'. \qquad (20)$$

Substituting (2) in (3) ~ (20), we get the frequency equation of free vibrations as follows:

$$MN+2\vartheta\xi\eta'^2\sin^2\theta RS=0, \qquad (21)$$

where

$$\left.\begin{aligned}
M&=\gamma_1\gamma_1'\eta^3\eta'^2\left\{12\zeta\eta\eta'+\phi(3+\eta')\right\}-12\gamma_1\eta^3(3\zeta\eta+\phi)\\
&\quad-12\gamma_1'\left\{3\zeta\eta(\eta^3+4\eta'^3)+\phi\right\}+36(12\zeta\eta+\phi),\\
N&=\gamma_2\gamma_2'\phi\eta\eta'-\gamma_2\xi\eta(\vartheta\eta'\cos^2\theta+\phi)-\gamma_2'\xi(\vartheta\eta\eta'\cos^2\theta+\phi)\\
&\quad+\xi^2(\vartheta\eta'\cos^2\theta+\phi),\\
R&=-2\gamma_1\eta^3\left\{3\zeta\eta\eta'+\phi(1+2\eta)\right\}-\gamma_1'\eta^2\left\{6\zeta\eta\eta'(1+5\eta')\right.\\
&\quad\left.+\phi(1+2\eta)(2+\eta')\right\}+6\left\{12\zeta\eta\eta'+\phi(1+2\eta)\right\},\\
S&=\gamma_2\gamma_2'\eta\eta'-\gamma_2\xi\eta-\gamma_2'\xi+\xi^2,\\
\gamma_1&=\frac{m_1h^3p^2}{E_1I_1},\ \gamma_1'=\frac{m_1'h^3p^2}{E_1I_1},\ \gamma_2=\frac{m_2h^3p^2}{E_1I_1},\ \gamma_2'=\frac{m_2'h^3p^2}{E_1I_1},\ \xi=\frac{a_1h^2}{I_1},\ \zeta=\frac{E_2I_2}{E_1I_1},
\end{aligned}\right\} \qquad (22)$$

$$\vartheta=\frac{E_3a_3}{E_1a_1},\quad \eta=\frac{l_1}{h},\quad \eta'=\frac{l'_1}{h},\quad \phi=\frac{l_2}{h},\quad \psi=\frac{l_3}{h}. \qquad (23)$$

Equation (21) gives four vibrational frequencies, two of them corresponding to motions of horizontal type and the others to those of vertical type.

If we assume, as is usually done, that the inertia masses of the movements in the vertical sense are the same as those in the horizontal sense, we may put $\gamma_1=\gamma_2\equiv\gamma\,(m_1=m_2\equiv m)$, $\gamma'_1=\gamma'_2\equiv\gamma'\,(m'_1=m'_2\equiv m')$.

With a view to ascertaining the quantitative nature of the seismic properties of the roof members, we selected certain cases with numerical conditions.

(i) First, let $\gamma=\gamma'$, $\xi(=a_1h^2/I_1)=8000$, $\vartheta(=E_3a_3/E_1a_1)=1$, $\phi(=l_2/h)=1$ be given. The numerical calculation of the vibrational frequencies for various inclinations θ of the roof members for two cases of ζ $(=E_2I_2/E_1I_1)$, i.e. $\zeta=0$, 1 are shown in Table I and plotted in Fig. 2.

Table I. The values of $p\sqrt{\dfrac{mh^3}{E_1I_1}}$ for various θ.

θ	45°	47°	50°	52°	60°	70°
$E_2I_2/E_1I_1=0$	43·95	—	8·459	6·205	3·13	2·257
	108·3	—	86·7	85·7	80·6	73·5
	∞	—	208	190·4	178·5	206·7
	∞	—	269	250	235·4	248
$E_2I_2/E_1I_1=1$	43·95	19·3	8·833	—	3·562	2·398
	108·3	90·6	87·2	—	80·56	73·50
	∞	—	230	—	182·2	197·6
	∞	—	291	—	240·8	242

θ	80°	85°	86°	88°	89°	90°
$E_2I_2/E_1I_1=0$	1·52	—	1·327	—	1·247	1·224
	67·8	—	65·0	—	63·6	63·3
	242	—	254	—	301	∞
	312	—	482	—	959	∞
$E_2I_2/E_1I_1=1$	1·780	1·564	—	1·666	—	2·208
	67·8	65·4	—	64·1	—	63·25
	217	244	—	284	—	∞
	311	429	—	680	—	∞

It will be seen that since there are four freedoms of vibration, there are four frequencies for every inclination of the roof members.

Since curves *I, I′* represent mainly vibrations of horizontal type and curves *II, II′* those of vertical type, frequencies of horizontal type are always fairly less than those of vertical type. Curves *I, II* are replot-

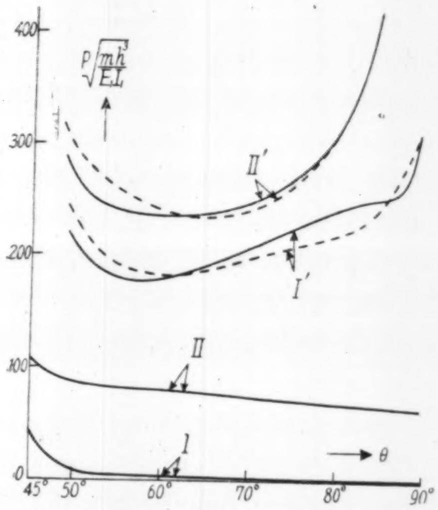

Fig. 2. Vibration frequencies of the case $\xi(=a_1h^2/I_1)=8000$, $\vartheta(=E_3a_3/E_1a_1)=1$, $\phi(=l_2/h)=1$. Full line: $\zeta(=E_2I_2/E_1I_1)=0$. Broken line: $\zeta(=E_2I_2/E_2I_1)=1$.

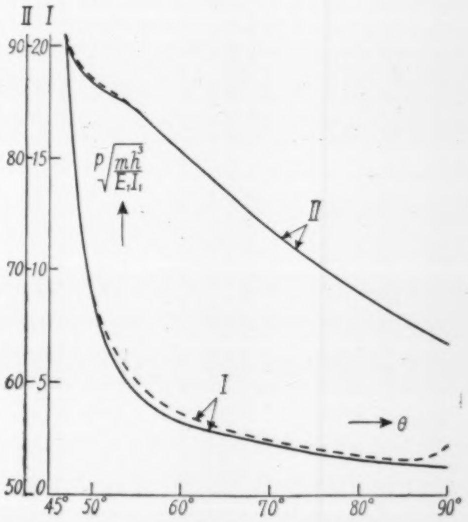

Fig. 3. Vibration frequencies of the case $\xi(=a_1h^2/I_1)=8000$, $\vartheta=(E_3a_3/E_1a_1)=1$, $\phi(=l_2/h)=1$. Full line: $\zeta(=E_2I_2/E_1I_1)=0$. Broken line: $\zeta(=E_2I_2/E_1I_1)=1$.

ted in Fig. 3 with different magnifying scales of ordinates. From Fig. 3, it will be seen that, beyond a certain inclination, namely, $\theta<80°$ in the present case, the change in E_2I_2/E_1I_1 is scarcely effective. It may be added that the vibrational frequencies of higher orders, namely, *I′*, *II′*, tend to be infinitely great at such angles as $\theta=0°$ and $90°$, which results from the condition that the masses are concentrated at the panel points.

(ii) We shall next assume that $\xi(=a_1h^2/I_1)=8000$, $\phi(=l_2/h)=1$, $\theta=60°$. The results of calculation for the vibrational frequencies for *I* (the lowest mode) for different ratios of $\vartheta(=E_3a_3/E_1a_1)$ are shown in

Table II. The values of $p\sqrt{\dfrac{mh^3}{E_1I_1}}$ for various $\vartheta(=E_3a_3/E_1a_1)$.

$\vartheta(=E_3a_3/E_1a_1)$	0	0·001	0·005	0·01	0·02	0·05	0·1	0·5	1·0	∞
$E_2I_2/E_1I_1=0$	1·688	—	2·676	2·858	2·981	3·071	3·101	3·129	3·131	3·133
$E_2I_2/E_1I_1=1$	2·519	2·749	—	3·288	—	3·494	—	3·550	3·564	3·564

Table II and plotted in Fig. 4. It will be seen that for such inclination of the roof as $\theta=60°$, a very slight stiffness of the roof member

relative to that of the column, say, $\vartheta(=E_3a_3/E_1a_1)=0{\cdot}03$, is just as effective as in the case of $\vartheta(=E_3a_3/E_1a_1)=\infty$. Besides, in such a condition, stiffness of the beam does not contribute much to the stiffness of the entire structure.

At all events, it has been ascertained that the roof members in a saw-tooth roof structure is much more effective in resisting the seismic vibration of a structure, than the horizontal members of a rectangular framed structure.

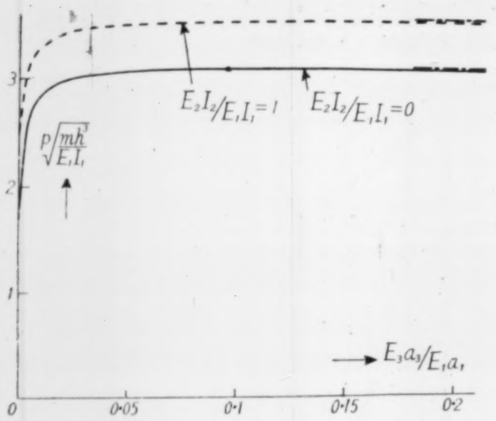

Fig. 4. Vibration frequencies for the lowest mode of the case $\xi(=a_1h^2/I_1)=8000$, $\phi(=l_2/h)=1$, $\theta=60°$.

In conclusion I wish to record my indebtedness to Professor Sezawa for many valuable suggestions in regard to this problem. I wish also to express my hearty thanks to Mr. Watanabe, for assistance in the numerical calculations.

---

33. 鋸歯狀小屋の耐震性

地震研究所　金　井　　清

鋸歯狀小屋は採光上最も有効な構造として工場建築に盛んに使用されて居るが，此の構造の耐震的效果に關する理論的研究は今迄誰によつても成されて居らぬやうである．

種々の意味から，この問題を一度理論的に研究しておく必要があると考へて手を附けた．

この論文では，計算を簡單にする爲に張間が無限にあり，質量は各屋根材と柱の結合點に集中してゐるものとした．又屋根材と柱は支持の狀態で，水平な梁がある場合と水平な梁がない場合の二通りに就いて計算を行つた．

計算の結果，屋根材の長さの方向の剛度の低い間はこの剛度を少しく增すと架構の振動數が著しく高くなり，屋根材の剛度が柱の長さの方向の剛度の 0·03 倍位になると，それ以上この剛度を增しても架構の振動數は一定以上高くはならぬ，又屋根材と柱の間の傾きが 80° 位以下になると梁の屈曲剛度は殆んど役に立たないことがわかつた．

要するに鋸歯狀小屋組が陸屋根，山形屋根等の小屋組よりも耐震的に效果のあることが理論的に確められた譯である．

尙，此の研究は妹澤先生の御指導によつて成されたもので，玆に深く感謝の意を表する．

---

34. *Secular Deformations of the Base Line Rhombus at Mitaka in Relation to Seismic Activities in its Vicinity.*[1]

By Chuji TSUBOI,

Earthquake Research Institute.

(Read Sept. 18, 1941.—Received Sept. 20, 1941.)

In 1916, the Japanese Geodetic Commission laid down a set of five geodetic base lines in the compound of the Tokyo Astronomical Observatory, at Mitaka, which are all very nearly 100 m in length and are so arranged as to form a rhombus consisting of two equal equilateral triangles (Fig. 1). Measurements of length of the base lines which, from 1916 up to 1939, inclusive, have been repeated 25 times with utmost care and precision by experts of the Military Land Survey under the auspices of the Geodetic Commission revealed that the lengths of the base lines do not remain unchanged, but are subject to secular variations.[2]

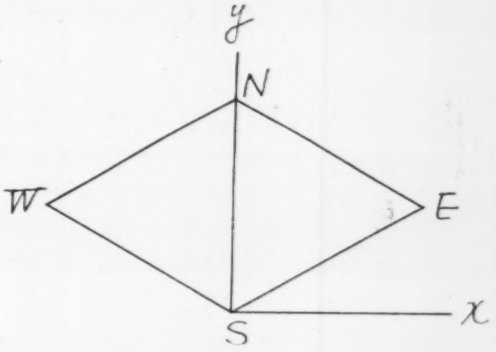

Fig. 1.

Although the variation in length of the base lines between any two successive measurements is usually no more than a few tenths of a millimeter, it occasionally amounts to a millimeter or even more. These large variations in length were observed where strong earthquakes have occurred near Mitaka. For example, at the times mentioned, the lengths of the base line NS were

	m mm
1922 Nov.	100 + 0·82
1923 Sept.	100 + 4·40,

the difference being as much as 3·58 mm. It is between these two times

1) A part of this paper was read on March 15, 1939, jointly by Dr. S. Yamaguti and the present writer.

2) MILITARY LAND SURVEY, Reports of Measurements of the Base Lines at Mitaka.

of measurement that the great Tokyo earthquake of Sept. 1, 1923, with its epicentre approximately 50 km SSW of Mitaka, occurred. Again, for the line WN, the lengths were

	m mm
1930 Feb.	100+1·12
1931 Oct.	100+1·86,

the difference being 0·74 mm. The Idu destructive earthquake of Nov. 26, 1930, with its epicentre 80 km SW of Mitaka, occurred just between these two measurements.

These outstanding facts call for a careful examination of the secular deformations of the triangles, NES and NSW, both of which are formed by the base lines, particularly in their relations to seismic activities within a reasonable distance from Mitaka, say 150 km.

The present writer, in 1930, calculated from the variations in length of the base lines, the variation in area of the triangles that are formed by the base lines and found a striking relation between the variation in area and the occurrence of strong earthquakes near Mitaka.[3] In 1932, T. Terada further found that the areas of the triangles are likely to vary in parallel rather more closely with the general seismic activity within a reasonable distance from Mitaka, than with the occurrence of any particular individual strong earthquake near that place.[4]

While, in these studies just mentioned, attention was concentrated on the variation in the area of the base line triangles, it recently occurred to the writer that from the variations in length of the base lines, not only are the variations in the area of the triangles calculable, but with a few reasonable assumptions, other strain components, such as shear and principal strains, as well as the relative displacements of the end points of the base lines are also calculable from the same data.

The object of the present paper is to show how these calculations were made, and to see if there is any correlation between deformations of the base line triangles and the general seismic activities near Mitaka.

First, Table I gives the dates and the results of the base line measurements as reported by the Military Land Survey. Since the variations in length between two successive measurements are mostly a few tenths of a millimeter, the relative variation $\Delta l/l$ is of an order not exceeding 10^{-6}. So small are these variations that one may be excused for conclud-

3) C. TSUBOI, *Proc. Imp. Acad.*, **6** (1930), 367; **7** (1931), 155. *Bull. Earthq. Res. Inst.*, **8** (1930), 384; **13** (1935), 558. *Erg. d. kos. Phys.*, IV. (1939), Leipzig.

4) T. TERADA, *Proc. Imp. Acad.*, **8** (1932), 8. *Bull. Earthq. Res. Inst.*, **10** (1932), 402.

Table I. Measured Lengths of the Base Lines and Their Variation. (in mm.)

Date of Measurement	Interval (m d)	NE (m 100+)	ΔNE	ΣΔNE	ES	ΔES	ΣΔES	SW	ΔSW	ΣΔSW	WN	ΔWN	ΣΔWN	NS	ΔNS	ΣΔNS
(1) 1916 VI 4~11		+0·92			+0·26			+0·72			+0·78			+0·59		
	8 9		0	0		−0·01	−0·01		−0·03	−0·03		0	0		−0·05	−0·05
(2) 1917 II 5~20		+0·92			+0·25			+0·69			+0·78			+0·54		
	7 27		+0·23	+0·23		+0·30	+0·29		+0·22	+0·19		+0·23	+0·23		+0·30	+0·25
(3) 〃 X 14~17		+1·15			+0·55			+0·91			+1·01			+0·84		
	3 23		−0·18	+0·05		−0·29	0		−0·05	+0·14		−0·12	+0·11		−0·37	−0·12
(4) 1918 II 8~10		+0·97			+0·26			+0·86			+0·89			+0·47		
	8 13		−0·16	−0·11		+0·03	+0·03		−0·17	−0·03		−0·13	−0·02		+0·04	−0·08
(5) 〃 X 20~23		+0·81			+0·29			+0·69			+0·76			+0·51		
	13 19		+0·22	+0·11		+0·23	+0·26		+0·25	+0·22		+0·10	+0·08		+0·12	+0·04
(6) 1919 XII 10~12		+1·03			+0·52			+0·94			+0·86			+0·63		
	11 12		+0·23	+0·34		+0·03	+0·29		+0·13	+0·35		+0·16	+0·24		+0·22	+0·26
(7) 1920 XI 20~24		+1·26			+0·55			+1·07			+1·02			+0·85		
	11 14		−0·01	+0·33		+0·01	+0·30		+0·04	+0·39		+0·09	+0·33		+0·08	+0·34
(8) 1921 XI 2~8		+1·25			+0·56			+1·11			+1·11			+0·93		
	12 0		−0·14	+0·19		−0·14	+0·16		−0·09	+0·30		−0·05	+0·28		−0·11	+0·23
(9) 1922 XI 6~8		+1·11			+0·42			+1·02			+1·06			+0·82		
	9 28		+0·62	+0·81		+0·11	+0·27		+0·82	+1·12		+0·06	+0·34		+3·58	+3·81
(10) 1923 IX 4~6		+1·73			+0·53			+1·84			+1·12			+4·40		
	1 18		−0·09	+0·72		−0·20	+0·07		−0·37	+0·75		−0·17	+0·17		−0·40	+3·41
(11) 〃 X 19~24		+1·64			+0·33			+1·47			+0·95			+4·00		
	3 5		+0·27	+0·99		−0·26	−0·19		−0·08	+0·67		−0·23	−0·06		−0·24	+3·17
(12) 1924 I 27~29		+1·91			+0·07			+1·39			+0·72			+3·76		
	6 16		−0·33	+0·66		−0·12	−0·31		+0·11	+0·78		−0·01	−0·07		−0·34	+2·83
(13) 〃 VIII 12~15		+1·58			−0·05			+1·50			+0·71			+3·42		
	16 2		+0·26	+0·92		+0·30	−0·01		−0·06	+0·72		+0·11	+0·04		+0·27	+3·10
(14) 1925 XII 15~17		+1·84			+0·25			+1·44			+0·82			+3·69		
	23 29		+0·54	+1·42		+0·55	+0·54		+0·72	+1·44		+0·56	+0·60		+0·22	+3·32
(15) 1927 XII 13~16		+2·38			+ ·080			+2·16			+1·38			+3·91		
	15 4		−0·17	+1·29		−0·08	+0·46		−0·14	+1·30		+0·06	+0·66		−0·13	+3·19
(16) 1929 III 17~20		+2·21			+0·72			+2·02			+1·44			+3·78		
	10 24		−0·24	+1·05		−0·19	+0·27		−0·29	+1·01		−0·32	+0·34		−0·19	+3·00
(17) 1930 II 8~14		+1·97			+0·53			+1·73			+1·12			+3·59		
	19 22		−0·20	+0·85		+0·04	+0·31		**+0·51**	+1·52		+0·74	**+1·08**		−0·01	+2·99
(18) 1931 X 1~6		+1·77			+0·57			+2·24			+1·86			+3·58		
	28 16		−0·01	+0·84		−0·04	+0·27		**−0·52**	+1·00		−0·53	**+0·55**		−0·29	+2·70
(19) 1934 II 8~22		+1·76			+0·53			+1·72			+1·33			+3·29		
	10 2		−0·17	+0·67		−0·38	−0·11		−0·09	+0·91		−0·27	+0·28		−0·17	+2·53
(20) 1934 XII 1~24		+1·59			+0·15			+1·63			+1·06			+3·12		
	11 29		−0·22	+0·45		−0·02	−0·13		−0·26	+0·65		−0·19	+0·09		−0·26	+2·27
(21) 1935 XI29~XII23		+1·37			+0·13			+1·37			+0·87			+2·86		
	11 29		+0·21	+0·66		0	−0·13		+0·07	+0·72		+0·05	+0·14		+0·03	+2·30
(22) 1936 XII 1~22		+1·58			+0·13			+1·44			+0·92			+2·89		
	11 6		−0·20	+0·46		+0·03	−0·10		+0·01	+0·73		−0·07	+0·07		−0·06	+2·24
(23) 1937 X22~XI28		+1·38			+0·16			+1·45			+0·85			+2·83		
	12 11		0·0	+0·46		−0·01	−0·11		−0·10	+0·63		+0·15	+0·22		+0·07	+2·31
(24) 1938 XI13~XII9		+1·38			+0·15			+1·35			+1·00			+2·90		
	12 3		+0·12	+0·58		+0·14	+0·03		+0·13	+0·76		+0·06	+0·28		+0·13	+2·44
(25) 1939 XI13~XII12		+1·50			+0·29			+1·48			+1·06			+3·03		

ing that they are due to errors in measurements, with doubts of their real significance, but the following examination of data will show that such is not the case.

Since the base lines NE and SW are parallel, the variations in their length, ⊿NE and ⊿SE, if any, must be equal, provided of course that the strain to which the ground at Mitaka is subjected is uniform. The extent to which the measured values of ⊿NE and ⊿SW are actually equal will therefore serve as basis for judging the accuracy of measurements and the uniformity in strain of the ground. The same test may equally be applied to the other pair of lines, NW and SE. Table II gives the residual values of (⊿NE–⊿SW) and (⊿NW–⊿SE), which ought to vanish if the measurements are accurate and the strain is perfectly uniform.

Since, with the few exceptions that are printed in Gothic type in the table, the residuals are mostly about 0·1 mm, the measured lengths of the base lines may be regarded accurate and the strain of the ground uniform with this accuracy.

Table II. Residuals of (⊿NE–⊿SW) and (⊿ES–⊿WN) (in mm).

	⊿NE-⊿SW	⊿ES-⊿WN		⊿NE-⊿SW	⊿ES-⊿WN
(1)~(2)	0·03	−0·01	(13)~(14)	0·32	0·19
(2)~(3)	0·01	0·07	(14)~(15)	−0·18	−0·01
(3)~(4)	−0·13	−0·17	(15)~(16)	−0·03	−0·14
(4)~(5)	0·01	0·16	(16)~(17)	0·05	0·13
(5)~(6)	−0·03	0·13	(17)~(18)	**−0·71**	**−0·70**
(6)~(7)	0·10	−0·13	(18)~(19)	**0·51**	**0·49**
(7)~(8)	−0·05	−0·08	(19)~(20)	−0·08	−0·11
(8)~(9)	−0·05	−0·09	(20)~(21)	0·04	0·17
(9)~(10)	−0·20	0·05	(21)~(22)	0·14	−0·05
(10)~(11)	0·28	−0·03	(22)~(23)	−0·21	0·10
(11)~(12)	0·35	−0·03	(23)~(24)	0·10	−0·16
(12)~(13)	−0·44	−0·11	(24)~(25)	−0·01	0·08

There is no question of the accuracy of the measured length of each line. As a matter of fact, the lengths were measured with the aid of as many as nearly thirty Jaderin wires, which were carefully calibrated before each measurement, the mean error in each measurement being reported to be as small as a few hundredths of a millimeter. Yet, such large residuals, as for instance, of 0·70 and 0·71 mm, appear both in (⊿NW–⊿SE) and (⊿NE–⊿SW) between the measurements (17) and (18), these exceeding the errors of measurement. This can only

indicate that either point E or point W made a real but accidental displacement of this amount unrelated to and quite apart from the general deformation of the ground. There is no theoretical basis on which to decide which of the points E or W made such a large residual displacement. Seeing however from Table I, that ΔSW and ΔWN are exceptionally large between measurements (17) and (18), it is very likely that the large residuals of (ΔNW–ΔSE) and (ΔNE–ΔSW) are the results of displacement of point W; and since this displacement of point W, although it may have really occurred, has nothing to do with the general deformation of the ground, so long as the uniformity in strain of the ground is going to be an assumption to be based upon in our subsequent calculations, the rational thing to do is to reject the reported values of ΔNW and ΔSW between (17) and (18). For the same reason, ΔNW and ΔSW between (18) and (19) will also be rejected.

Now in order to calculate the strain of the ground, we take the co-ordinate axes as shown in Fig. 1. The co-ordinates of point E are the solutions of the simultaneous equations

$$\begin{cases} x^2+y^2=\mathrm{SE}^2 & (1) \\ x^2+(y-\mathrm{NS})^2=\mathrm{NE}^2. & (2) \end{cases}$$

Taking the difference of the two equations, we get the y-co-ordinate of point E,

$$y=\frac{\mathrm{SE}^2-\mathrm{NE}^2+\mathrm{NS}^2}{2\mathrm{NS}}. \qquad (3)$$

The northward displacement of point E between any two measurements, which shall be denoted by v_E, is the differential of y, whence

$$\Delta y=v_E=\frac{1}{2\mathrm{NS}^2}\Big\{2(\mathrm{SE}\cdot\Delta\mathrm{SE}-\mathrm{NE}\cdot\Delta\mathrm{NE}+\mathrm{NS}\cdot\Delta\mathrm{NS})\mathrm{NS}$$
$$-(\mathrm{SE}^2-\mathrm{NE}^2+\mathrm{NS}^2)\Delta\mathrm{NS}\Big\}. \qquad (4)$$

But since

$$\mathrm{SE}=\mathrm{NE}=\mathrm{NS}=100\,\mathrm{m}=s,$$

v_E reduces to

$$v_E=\frac{1}{2}\left(2\Delta\mathrm{SE}-2\Delta\mathrm{NE}+\Delta\mathrm{NS}\right). \qquad (5)$$

Taking the differential of the equation (1), we get

$$u_E x+v_E y=\mathrm{SE}\cdot\Delta\mathrm{SE}, \qquad (6)$$

where u_E denotes the eastward displacement of point E. Since for point E,

$$x=\frac{\sqrt{3}}{2}s\,, \quad y=\frac{1}{2}s\,,$$

and

$$v_E=\frac{2\Delta SE-2\Delta NE+\Delta NS}{2}\,, \tag{7}$$

u_E is given by

$$u_E=\frac{2\Delta SE+2\Delta NE-\Delta NS}{2\sqrt{3}}\,. \tag{8}$$

Similarly for point W, we get

$$u_W=-\frac{2\Delta WS+2\Delta WN-\Delta NS}{2\sqrt{3}}\,, \tag{9}$$

$$v_W=\frac{2\Delta WS-2\Delta WN+\Delta NS}{2}\,. \tag{10}$$

By assumptions,

$$u_S=v_S=0, \quad u_N=0, \quad v_N=\Delta NS.$$

By means of these expresssions, the relative displacements of the end points of the base lines were calculated from the variations in their lengths, with results as in Table III.

Table III. Displacements of End Points of the Base-Lines (in mm).

	u_E	$\sum u_E$	v_E	$\sum v_E$	u_W	$\sum u_W$	v_W	$\sum v_W$	v_N	$\sum v_N$
(1)										
	+0·01	+0·01	−0·04	−0·04	0	0	−0·06	−0·06	−0·05	−0·05
(2)										
	+0·22	+0·23	+0·22	+0·19	−0·17	−0·17	+0·14	+0·09	+0·30	+0·25
(3)										
	−0·17	+0·06	−0·30	−0·11	−0·01	−0·18	−0·12	−0·03	−0·37	−0·12
(4)										
	−0·09	−0·02	+0·21	+0·10	+0·19	+0·01	−0·02	−0·05	+0·04	−0·08
(5)										
	+0·23	+0·20	+0·07	+0·17	−0·17	−0·16	+0·21	+0·16	+0·12	+0·04
(6)										
	+0·09	+0·29	−0·09	+0·08	−0·10	−0·27	+0·08	+0·24	+0·22	+0·26
(7)										
	−0·02	+0·27	+0·06	+0·14	−0·05	−0·32	−0·01	+0·23	+0·08	+0·34
(8)										
	−0·13	+0·14	−0·06	+0·09	+0·05	−0·27	−0·10	+0·14	−0·11	+0·23
(9)										
	−0·61	−0·48	+1·28	+1·37	+0·53	+0·26	+2·55	+2·69	+3·58	+3·81
(10)										
	−0·05	−0·53	−0·31	+1·06	+0·20	+0·45	−0·40	+2·29	−0·40	+3·41
(11)										
	+0·08	−0·45	−0·65	+0·41	+0·11	+0·56	+0·03	+2·32	−0·24	+3·17
(12)										
	−0·16	−0·62	+0·04	+0·45	−0·16	+0·41	−0·05	+2·27	−0·34	+2·83
(13)										
	+0·25	−0·37	+0·18	+0·62	+0·05	+0·46	−0·04	+2·23	+0·27	+3·10
(14)										
	+0·57	+0·20	+0·12	+0·74	−0·68	−0·22	+0·27	+2·50	+0·22	+3·32
(15)										

(*to be continued.*)

Table III. (*Continued.*)

	u_E	$\sum u_E$	v_E	$\sum v_E$	u_W	$\sum u_W$	v_W	$\sum v_W$	v_N	$\sum v_N$
(15)										
	−0·11	+0·09	+0·03	+0·77	+0·01	−0·21	−0·27	+2·24	−0·13	+3·19
(16)										
	−0·19	−0·11	−0·05	+0·72	+0·30	+0·09	−0·07	+2·17	−0·19	+3·00
(17)										
	−0·09	−0·19	+0·24	+0·96	−0·73	+0·64	−0·24	+1·94	−0·01	+2·99
(18)										
	+0·06	−0·14	−0·18	+0·78	+0·52	−0·12	−0·14	+1·80	−0·29	+2·70
(19)										
	−0·27	−0·41	−0·30	+0·49	+0·16	+0·04	+0·10	+1·90	−0·17	+2·53
(20)										
	−0·06	−0·47	+0·07	+0·56	+0·19	+0·23	−0·20	+1·70	−0·26	+2·27
(21)										
	+0·11	−0·36	−0·20	+0·36	−0·06	+0·17	+0·04	+1·73	+0·03	+2·30
(22)										
	−0·08	−0·44	+0·20	+0·56	+0·02	+0·18	+0·05	+1·78	−0·06	+2·24
(23)										
	−0·03	−0·47	+0·03	+0·59	−0·01	+0·18	−0·22	+1·57	+0·07	+2·31
(24)										
	+0·11	−0·35	+0·09	+0·67	−0·07	+0·10	+0·14	+1·70	+0·13	+2·44
(25)										

Now, if this part of the ground has been subjected to a uniform strain, then u_E and u_W must be equal and opposite in sign, since in the expressions (8) and (9),

$$\Delta SE = \Delta NW,$$

and

$$\Delta NE = \Delta SW.$$

The symmetrical relation of u_N and u_W is clearly shown in Fig. 2, in which they are compared as curves. Such symmetrical relation, however, does not exist between v_E and v_W, because the elongation of the ground in NS direction contributes the same amount to both of them, while the shear of the ground along the same direction contributes the displacements, equal in amount but opposite in sign.

Displacement of the ground at any point (xy) near the origin is given in the first approximation by

$$u(xy) = u_0 + \left(\frac{\partial u}{\partial x}\right)_0 x + \left(\frac{\partial u}{\partial y}\right)_0 y, \tag{11}$$

$$v(xy) = v_0 + \left(\frac{\partial v}{\partial x}\right)_0 x + \left(\frac{\partial v}{\partial y}\right)_0 y, \tag{12}$$

but since we have chosen the co-ordinate axes as in Fig. 1, (11) and (12) reduce to

$$u(xy) = \frac{\partial u}{\partial x} x + \frac{\partial u}{\partial y} y, \tag{13}$$

$$v(xy) = \frac{\partial u}{\partial x} x + \frac{\partial v}{\partial y} y. \tag{14}$$

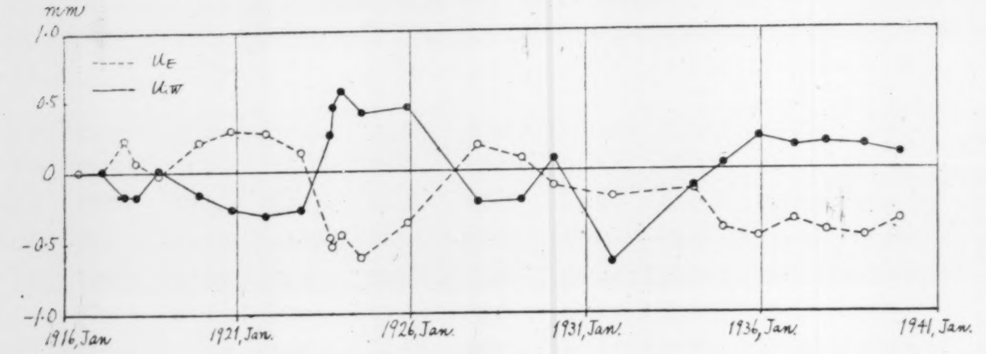

Fig. 2.

At the east and north vertices of triangle NES, we have then

$$u_E=\frac{\partial u}{\partial x}\frac{\sqrt{3}}{2}s+\frac{\partial u}{\partial y}\frac{s}{2}, \tag{15}$$

$$v_E=\frac{\partial v}{\partial x}\frac{\sqrt{3}}{2}s+\frac{\partial v}{\partial y}\frac{s}{2}, \tag{16}$$

$$u_N=\frac{\partial u}{\partial y}s=0, \tag{17}$$

$$v_N=\varDelta \mathrm{NS}=\frac{\partial v}{\partial y}s. \tag{18}$$

From these equations, we get

$$\frac{\partial u}{\partial x}=\frac{2}{\sqrt{3}\,s}u_E,$$

$$\frac{\partial v}{\partial x}=\left(v_E-\frac{v_N}{2}\right)\frac{2}{\sqrt{3}\,s},$$

$$\frac{\partial u}{\partial y}=0,$$

$$\frac{\partial v}{\partial y}=\frac{v_N}{s}.$$

These expressions enable us to calculate the strains of the ground from the variation in length of the base lines. Similar calculations can be made for the other triangle NSW also. But for the reason already given, it will be rational to take the mean of the strains within the two triangles NES and NSW as representing the general strain of the ground. They are given in Table IV.

Table IV. Simple Strains of the Ground. (in 10^{-5}).

	$\left(\frac{\partial u}{\partial x}\right)_E$	$\left(\frac{\partial u}{\partial x}\right)_W$	$\left(\frac{\partial u}{\partial x}\right)_{mean}$	$\left(\frac{\partial v}{\partial x}\right)_E$	$\left(\frac{\partial v}{\partial x}\right)_W$	$\left(\frac{\partial v}{\partial x}\right)_{mean}$	$\left(\frac{\partial v}{\partial y}\right)$	$\Sigma\frac{\partial u}{\partial x}$	$\Sigma\left(\frac{\partial v}{\partial x}\right)$	$\Sigma\left(\frac{\partial v}{\partial y}\right)$
(1)										
	+0·01	0	0	−0·01	+0·04	+0·01	−0·05	0	+0·01	−0·05
(2)										
	+0·25	+0·20	+0·23	+0·08	+0·01	+0·05	+0·30	+0·23	+0·05	+0·25
(3)										
	−0·19	+0·01	−0·09	−0·13	−0·08	−0·10	−0·37	+0·14	−0·05	−0·12
(4)										
	−0·10	−0·21	−0·16	+0·22	+0·05	+0·13	+0·04	−0·02	+0·08	−0·08
(5)										
	+0·26	+0·19	+0·23	+0·01	−0·17	−0·08	+0·12	+0·21	0	+0·04
(6)										
	+0·10	+0·12	+0·11	−0·23	+0·04	−0·10	+0·22	+0·32	−0·10	+0·26
(7)										
	−0·03	+0·06	+0·02	+0·02	+0·06	+0·04	+0·08	+0·33	−0·06	+0·34
(8)										
	−0·15	−0·06	−0·10	0	+0·05	+0·02	−0·11	+0·23	−0·04	+0·23
(9)										
	−0·71	−0·61	−0·66	−0·59	−0·88	−0·73	+3·58	−0·43	−0·77	+3·81
(10)										
	−0·06	−0·23	−0·14	−0·13	+0·23	+0·05	−0·40	−0·57	−0·72	+3·41
(11)										
	+0·09	−0·13	−0·02	−0·61	−0·17	−0·39	−0·24	−0·59	−1·11	+3·17
(12)										
	−0·19	+0·18	0	+0·24	−0·14	+0·05	−0·34	−0·59	−1·06	+2·83
(13)										
	+0·28	−0·06	+0·11	+0·05	+0·20	+0·12	+0·27	−0·48	−0·94	+3·10
(14)										
	+0·65	+0·78	+0·72	+0·01	−0·19	−0·09	+0·22	+0·24	−1·02	+3·32
(15)										
	−0·12	−0·01	−0·07	+0·10	+0·23	+0·17	−0·13	+0·17	−0·85	+3·19
(16)										
	−0·22	−0·34	−0·28	+0·06	−0·04	+0·01	−0·19	−0·11	−0·84	+3·00
(17)										
	−0·10	(**+0·84**)	−0·10	+0·28	(**+0·27**)	+0·28	−0·01	−0·22	−0·56	+2·99
(18)										
	+0·06	(**−0·60**)	+0·06	−0·04	(**−0·01**)	−0·04	−0·29	−0·15	−0·60	+2·70
(19)										
	−0·31	−0·18	−0·25	−0·24	−0·21	−0·23	−0·17	−0·40	−0·33	+2·53
(20)										
	−0·07	−0·21	−0·14	+0·23	+0·08	+0·16	−0·26	−0·54	−0·67	+2·27
(21)										
	+0·13	+0·07	+0·10	−0·24	−0·02	−0·13	+0·03	−0·44	−0·80	+2·30
(22)										
	−0·09	−0·02	−0·06	+0·27	−0·09	+0·09	−0·06	−0·50	−0·71	+2·24
(23)										
	−0·03	+0·01	−0·01	−0·01	+0·29	+0·14	+0·07	−0·51	−0·58	+2·31
(24)										
	+0·13	+0·08	+0·11	+0·02	−0·08	−0·03	+0·13	−0·49	−0·61	+2·44
(25)										

Once these simple strains are known, the other strain components, such as dilatation, maximum shear, magnitude and direction of the principal strains, pure shear and elongation along various directions, etc., are easily calculated by means of the well known formula in connection with the theory of plane strain.

Table V gives the strain between two successive measurements, and Table VI those as compared with the first measurement. Table VII gives the monthly rate of strain during the interval of two successive measurements, while Table VIII shows by plus or minus sign whether the rate during the interval between any two base line measurements has increased or decreased as compared with that during the preceding interval.

Now in order to see if there is any relation between the strain of the ground at Mitaka and the seismic activity within a reasonable dis-

Table V. Various Strains of the Ground. (in 10^{-5}).

	Dil.	Max. shear	γ_1	γ_2	θ	Elongation				Pure shear		
						E—W	E 45° N —S 45° W	N—S	N 45° W —S 45° E	N—S	N 45° W —S 45° E	N 45° E —S 45° W
(1)	−0·05	0·05	+0·01	−0·10	0	0	−0·02	−0·05	−0·03	+0·01	−0·02	+0·03
(2)	+0·53	0·09	+0·61	+0·44	+74°	+0·23	+0·29	+0·30	+0·24	+0·05	+0·06	−0·01
(3)	−0·46	0·30	−0·16	−0·76	−10	−0·09	−0·28	−0·37	−0·18	−0·10	−0·19	+0·09
(4)	−0·12	0·24	+0·12	−0·36	+73	−0·16	+0·01	+0·04	−0·13	+0·13	+0·17	−0·03
(5)	+0·35	0·13	+0·48	+0·21	−18	+0·23	+0·13	+0·12	+0·21	−0·08	−0·09	+0·01
(6)	+0·33	0·15	+0·43	+0·18	−69	+0·11	+0·12	+0·22	+0·21	−0·10	+0·01	−0·10
(7)	+0·10	0·08	+0·17	+0·02	+74	+0·02	+0·07	+0·08	+0·03	+0·04	+0·05	−0·01
(8)	−0·21	0·02	−0·19	−0·24	+37	−0·10	−0·10	−0·11	−0·12	+0·02	+0·01	+0·02
(9)	+2·92	4·30	+7·22	−1·38	−85	−0·66	+1·10	+3·58	+1·83	−0·73	+1·75	−2·49
(10)	−0·54	0·26	−0·28	−0·81	− 6	−0·14	−0·25	−0·40	−0·30	+0·05	−0·10	+0·16
(11)	−0·26	0·45	+0·19	−0·71	−31	−0·02	−0·33	−0·24	+0·07	−0·39	−0·31	−0·09
(12)	−0·34	0·34	0	−0·68	+ 4	0	−0·15	−0·34	−0·20	+0·05	−0·14	+0·20
(13)	+0·38	0·20	+0·58	+0·19	+71	+0·11	+0·25	+0·27	+0·13	+0·12	+0·14	−0·02
(14)	+0·94	0·51	+1·44	+0·43	− 5	+0·72	+0·43	+0·22	+0·51	−0·09	−0·29	+0·21
(15)	−0·20	0·18	−0·02	−0·38	+35	−0·07	−0·02	−0·13	−0·18	+0·17	+0·05	+0·12
(16)	−0·47	0·09	−0·38	−0·57	+86	−0·28	−0·23	−0·19	−0·24	+0·01	+0·05	−0·04
(17)	−0·11	0·29	+0·18	−0·41	+54	−0·10	+0·08	−0·01	−0·18	+0·28	+0·19	+0·10
(18)	−0·23	0·36	+0·13	−0·58	− 3	+0·06	−0·13	−0·29	−0·10	−0·04	−0·20	+0·16
(19)	−0·42	0·24	−0·18	−0·66	−55	−0·25	−0·32	−0·17	−0·10	−0·23	−0·07	−0·15
(20)	−0·40	0·20	−0·21	−0·60	+27	−0·14	−0·12	−0·26	−0·28	+0·16	+0·02	+0·14
(21)	+0·13	0·15	+0·28	−0·02	−31	+0·10	0	+0·03	+0·13	−0·13	−0·10	−0·03
(22)	−0·12	0·09	−0·03	−0·20	+44	−0·06	−0·02	−0·06	−0·10	+0·09	+0·04	+0·05
(23)	+0·06	0·16	+0·22	−0·10	+60	−0·01	+0·10	+0·07	−0·04	+0·14	+0·11	+0·03
(24)	+0·24	0·04	+0·27	+0·20	−65	+0·11	+0·10	+0·13	+0·13	−0·03	0	−0·03
(25)												

Table VI. Various Integrated Strains of the Ground. (in 10^{-5}).

	Dil.	Max. shear.	γ_1	γ_2	θ	Elongation				Pure shear.		
						E−W	E 45° N −S 45° W	N−S	N 45° W −S 45° E	N−S	N 45° W −S 45° E	N 45° E −S 45° W
(1)	−0·05	0·05	+0·01	−0·10	0	0	−0·02	−0·01	−0·03	+0·01	−0·02	+0·03
(2)	+0·48	0·06	+0·54	+0·42	56°	+0·23	+0·27	+0·25	+0·21	+0·05	+0·04	+0·02
(3)	+0·02	0·26	+0·28	−0·25	− 6	+0·14	−0·02	−0·12	+0·04	−0·05	−0·16	+0·10
(4)	−0·10	0·10	0	−0·20	+26	−0·02	−0·01	−0·08	−0·09	+0·08	+0·01	+0·07
(5)	+0·25	0·17	+0·42	+0·08	—	+0·21	+0·12	+0·04	+0·12	0	−0·09	+0·09
(6)	+0·58	0·11	+0·69	+0·46	−30	+0·32	+0·24	+0·26	+0·34	−0·10	−0·08	−0·02
(7)	+0·67	0·06	+0·73	+0·62	−48	+0·33	+0·31	+0·34	+0·37	−0·06	−0·03	−0·03
(8)	+0·46	0·04	+0·50	+0·43	−45	+0·23	+0·21	+0·23	+0·25	−0·04	−0·02	−0·02
(9)	+3·38	4·31	+7·69	−0·92	−85	−0·43	+1·31	+3·81	+2·08	−0·77	−1·73	−2·50
(10)	+2·84	4·04	+6·88	−1·20	−85	−0·57	+1·06	+3·41	+1·78	−0·72	+1·63	−2·35
(11)	+2·58	3·92	+6·50	−1·34	−82	−0·59	+0·74	+3·17	+1·85	−1·11	+1·32	−2·43
(12)	+2·24	3·58	+6·42	−0·74	−82	−0·59	+0·59	+2·83	+1·65	−1·06	+1·18	−2·24
(13)	+2·62	3·70	+6·32	−1·08	−83	−0·48	+0·84	+3·10	+1·78	−0·94	+1·32	−2·26
(14)	+3·56	3·25	+6·81	−0·31	−81	+0·24	+1·27	+3·32	+2·29	−1·02	+1·03	−2·05
(15)	+3·36	3·14	+6·50	+0·22	−82	+0·17	+1·25	+3·19	+2·11	−0·86	+1·08	−1·94
(16)	+2·89	3·22	+6·11	−0·34	−82	−0·11	+1·02	+3·00	+1·87	−0·84	+1·13	−1·98
(17)	+2·77	3·26	+6·03	−0·48	−85	−0·22	+1·10	+2·99	+1·67	−0·57	+1·32	−1·89
(18)	+2·55	2·92	+5·46	−0·37	−84	−0·15	+0·97	+2·70	+1·58	−0·60	+1·13	−1·73
(19)	+2·13	3·04	+5·18	−0·91	−82	−0·40	+0·65	+2·53	+1·48	−0·83	+1·05	−1·88
(20)	+1·73	2·89	+4·62	−1·16	−83	−0·54	+0·53	+2·27	+1·20	−0·67	+1·07	−1·74
(21)	+1·86	2·86	+4·72	−1·00	−81	−0·44	+0·53	+2·30	+1·33	−0·80	+0·97	−1·77
(22)	+1·74	2·83	+4·57	−1·09	−84	−0·50	+0·51	+2·24	+1·23	−0·72	+1·01	−1·73
(23)	+1·80	2·88	+4·68	−1·08	−84	−0·51	+0·61	+2·31	+1·19	−0·58	+1·12	−1·70
(24)	+2·04	2·91	+4·94	−0·87	−84	−0·40	+0·72	+2·44	+1·32	−0·61	+1·12	−1·73
(25)												

Table VII. Monthly Rate of Strain. (in 10^{-5}/Month).

	Dil.	Max. shear.	γ_1	γ_2	Elongation				Pure shear		
					E—W	N 45° E —S 45° W	N—S	N 45° W —S 45° E	N—S	N 45° W —S 45° E	N 45° E —S 45° W
(1)	−0·006	0·006	0·001	−0·012	0	−0·002	−0·006	−0·004	0·001	−0·002	0·004
(2)	0·067	0·011	0·077	0·057	0·029	0·037	0·038	0·030	0·006	0·008	−0·001
(3)	−0·122	0·080	−0·042	−0·202	−0·024	−0·074	−0·098	−0·048	−0·027	−0·050	0·024
(4)	−0·014	0·028	0·014	−0·043	−0·087	0·001	0·005	+0·015	0·015	0·020	−0·004
(5)	0·026	0·010	0·035	0·015	0·017	0·010	0·009	0·015	−0·006	−0·007	0·001
(6)	0·029	0·013	0·042	0·016	0·010	0·011	0·019	0·018	−0·009	0·001	−0·009
(7)	0·009	0·007	0·015	0·002	0·002	0·006	0·007	0·003	0·003	0·004	−0·001
(8)	−0·017	0·002	−0·016	−0·020	−0·008	−0·008	−0·009	−0·010	0·002	0·001	0·002
(9)	0·294	0·433	0·727	−0·139	−0·066	0·111	0·361	0·184	−0·074	0·176	−0·251
(10)	−0·338	0·163	−0·175	−0·506	−0·088	−0·156	−0·250	−0·188	0·031	−0·063	0·100
(11)	−0·082	0·142	0·060	−0·224	−0·006	−0·104	−0·076	0·022	−0·123	−0·098	−0·028
(12)	−0·052	0·052	0	−0·104	0	−0·023	−0·052	−0·031	0·008	−0·021	0·031
(13)	0·024	0·012	0·036	0·012	0·007	0·016	0·017	0·008	0·007	0·009	−0·001
(14)	0·039	0·021	0·060	0·018	0·030	0·018	0·009	0·021	−0·004	−0·012	0·009
(15)	−0·013	0·012	−0·001	−0·025	−0·005	−0·001	−0·009	−0·012	0·011	0·003	0·008
(16)	−0·044	0·008	−0·035	−0·053	−0·026	−0·021	−0·018	−0·022	0·001	0·005	−0·004
(17)	−0·006	0·015	0·009	−0·021	−0·005	0·004	−0·001	−0·009	0·014	0·010	0·005
(18)	−0·008	0·013	0·005	−0·020	0·002	−0·005	−0·010	−0·004	−0·001	−0·007	0·006
(19)	−0·042	0·024	−0·018	−0·066	−0·025	−0·032	−0·017	−0·010	−0·023	−0·007	−0·015
(20)	−0·033	0·017	−0·018	−0·050	−0·012	−0·010	−0·022	−0·023	0·013	0·002	0·012
(21)	0·011	0·013	0·023	−0·002	0·008	0	0·003	0·011	−0·011	−0·008	−0·003
(22)	−0·011	0·008	−0·003	−0·018	−0·005	−0·002	−0·005	−0·009	0·008	0·004	0·004
(23)	0·005	0·013	0·018	−0·008	−0·001	0·008	0·006	−0·003	0·011	0·009	0·002
(24)	0·020	0·003	0·022	0·017	0·009	0·008	0·011	0·011	−0·002	0	−0·002
(25)											

Table VIII. Increase or Decrease in the Rate of Strain and in the Monthly Seismic Activity.

			(1)(2)(3)(4)(5)(6)(7)(8)(9)(10)(11)(12)(13)(14)(15)(16)(17)(18)(19)(20)(21)(22)(23)(24)(25)																						
Strain		Dilatation	+	−	+	+	+	−	−	+	−	+	+	+	+	−	−	+	−	−	+	+	−	+	+
		Max. shear	+	+	−	−	+	−	−	+	−	−	−	−	+	−	−	+	−	+	−	−	−	+	−
		γ_1	+	−	+	+	+	−	−	+	−	+	−	+	+	−	−	+	−	−	0	+	−	+	+
		γ_2	+	−	+	+	+	−	−	−	−	+	+	+	+	−	−	+	+	−	+	+	−	+	+
	Elongation	E—W	+	−	−	+	−	−	−	−	−	+	+	+	+	−	−	+	+	−	+	+	−	+	+
		E 45° N—S 45° W	+	−	+	+	+	−	−	+	−	+	+	+	+	−	−	+	−	−	+	+	−	+	0
		N—S	+	−	+	+	+	−	−	+	−	+	+	+	−	−	−	+	−	−	−	+	−	+	+
		N 45° W—S 45° E	+	−	+	+	+	−	−	+	−	+	−	+	+	−	−	+	−	−	−	+	−	+	+
	Pure shear	N—S	+	−	+	−	−	+	−	−	+	−	+	−	−	+	−	+	−	−	+	−	+	+	−
		N 45° W—S 45° E	+	−	+	−	+	+	−	+	−	−	+	+	−	+	+	+	−	0	+	−	+	+	−
		N 45° E—S 45° W	−	+	−	+	−	+	+	−	+	−	+	−	+	−	−	+	+	−	+	−	+	−	−
Seismic Activity		N	−	+	−	−	0	0	+	−	+	−	−	+	−	+	−	0	0	0	0	0	0	0	0
		NE	+	−	−	+	−	+	+	−	+	+	−	−	−	+	−	−	+	−	−	+	+	−	−
		E	−	0	+	+	−	0	+	−	+	−	+	−	−	+	−	+	−	−	+	−	+	−	−
		SE	+	+	−	−	+	−	+	−	−	0	0	+	+	−	0	+	−	0	+	−	0	0	0
		S	0	0	0	+	+	−	−	+	−	+	−	+	−	0	0	+	−	−	−	+	+	−	0
		SW	+	−	+	−	0	+	−	0	+	+	−	0	0	0	+	+	−	0	+	−	−	0	0
		W	−	0	+	−	−	+	−	0	+	−	+	−	−	−	0	+	−	0	0	0	+	−	0
		NW	0	0	+	−	+	−	0	0	0	0	+	−	−	+	−	+	−	0	0	0	0	+	−
		Total	+	−	+	−	−	−	+	−	+	−	−	−	−	+	−	+	−	−	+	−	+	−	−
		NW+N+NE	+	−	−	+	−	−	+	−	+	+	−	+	−	+	−	+	−	−	−	+	+	+	−
		EN+E+ES	+	−	−	+	−	−	+	−	+	−	−	−	−	+	−	+	−	−	+	−	+	−	−
		SE+S+SW	+	−	−	−	+	−	+	−	+	+	−	+	+	−	+	+	−	−	+	0	+	−	0
		WN+W+WS	−	−	+	−	+	+	−	0	+	+	−	−	−	+	+	+	−	0	+	−	+	+	−
		N+NE	+	−	−	+	−	+	+	−	+	+	−	+	−	+	−	−	+	−	−	+	+	−	−
		NE+E	+	−	+	+	−	−	+	−	+	−	−	−	−	+	−	−	−	−	+	−	+	−	−
		E+ES	+	+	−	−	−	−	+	−	+	−	+	+	−	+	−	+	−	−	+	−	+	−	−
		SE+S	+	+	−	+	+	−	+	−	−	+	−	+	+	−	0	+	−	−	+	+	+	−	0
		S+SW	+	−	+	−	+	+	−	+	+	+	−	+	−	0	+	+	−	−	+	+	+	−	0
		SW+W	−	−	+	−	0	+	−	0	+	+	−	−	−	−	+	+	−	0	+	−	+	−	0
		W+WN	−	0	+	−	+	−	−	0	+	−	+	−	−	+	−	+	−	0	0	0	+	+	−
		WN+N	−	+	+	−	+	−	+	−	+	−	−	+	−	+	−	+	−	0	0	0	0	+	−

tance from this place, it is necessary to begin by arranging the earthquake data for this purpose. From the earthquake reports published monthly by the Central Meteorological Observatory, we selected 230 earthquakes that occurred within a radius of 150 km from Mitaka from the time of the first base line measurement to that of the last, and which were strong enough to be classed in the reports as "conspicuous" and "rather conspicuous".

In view of the anticipation that the closeness of the relation to be sought, if any at all, might eventually depend on the magnitude of the earthquake as well as on its distance from Mitaka, a suitable weight must be given to each earthquake in order to obtain a measure of the general seismic activity that suits the present purpose. Accordingly, weights 2 and 1 were given to "conspicuous" and "rather conspicuous" earthquakes respectively and weights 3, 2, and 1 were given to each of them according as it occurred within 50, 100, or 150 km from Mitaka. Thus a "conspicuous" earthquake that occurred within 50 km from Mitaka was given a weight 6, while a "rather conspicuous" earthquake that occurred between 100 and 150 km from the same place was given a weight 1. No attention was paid to the depths of the earthquakes. Table IX gives the seismic activities in various directions from Mitaka in terms of the measure just defined, while Table X gives the mean monthly seismic activities during various intervals. In Table VIII, the plus or minus sign indicates whether the mean monthly seismic activity during the interval between any two base line measurements has increased or decreased as compared with that during the one preceding it.

Since the relation between the strain of the ground at Mitaka and the seismic activity near that place, if it exists at all, is expected to be a qualitative one, comparison of the increase or decrease of these two quantities will be sufficient to show the essential feature of the suspected relation, a detailed quantitative study being scarcely necessary for the purpose.

If a certain quantity related to deformation of the ground varies in parallel with the seismic activity in a certain direction from Mitaka, then the plus and minus signs in the two corresponding rows of Table VIII must occur in like sequence. Thus, of the total number of pairs in which the algebraic signs in the rows can be compared, there will be more pairs with same signs than those with opposite signs. In the reverse case in which the two quantities that are compared vary in opposite sense, there are likely to be more pairs with opposite signs than those with same signs. The ratio

Table IX. Seismicity near Mitaka.

	Octant								Total	NW +N +NE	EN +E +ES	SE +S +SW	WN +W +WS	N+ NE	NE +E	E+ SE	SE +S	S+ SW	SW +W	W+ WN	WN +N
	N	NE	E	SE	S	SW	W	NW													
(1)																					
(2)	2	7	1				3		13	9	8	0	3	9	8	1	0	0	3	3	2
(3)		14		8		1			23	14	22	9	1	14	14	8	8	1	1	0	0
(4)	2	2		4					8	4	6	4	0	4	2	4	4	0	0	0	2
(5)	2	3	4	3		3	4	3	22	8	10	6	10	5	7	7	3	3	7	7	5
(6)		13	7	3	2		1		26	13	23	5	1	13	20	10	5	2	1	1	0
(7)		3	1	4	3			4	15	7	8	7	4	3	8	5	7	3	0	4	4
(8)		6			3	2	3		14	6	6	5	5	6	6	0	3	5	5	3	0
(9)	3	18	3	11					35	21	32	11	0	21	21	14	11	0	0	0	3
(10)	1	10	2	3	3				19	11	15	6	0	11	12	5	6	3	0	0	1
(11)	3	3	3			10	4		23	6	6	10	14	6	6	3	0	10	14	4	3
(12)	3	9			2	27	3		34	12	9	29	30	12	9	0	2	29	30	3	3
(13)		14	4				8	3	29	17	18	0	11	14	18	4	0	0	8	11	3
(14)	6	31	9	3	3		6	6	64	43	43	6	12	37	40	12	6	3	6	12	12
(15)		18	1	10			1	3	33	21	29	10	4	18	19	11	10	0	1	4	3
(16)	3	12	7					3	25	18	19	0	3	15	19	7	0	0	0	3	6
(17)		5				6			11	5	5	6	6	5	5	0	0	6	6	0	0
(18)		2	5	3	3	26	4	9	52	11	10	32	39	2	7	8	6	29	30	13	9
(19)		4	1		4				9	4	5	4	0	4	5	1	4	4	0	0	0
(20)		1			1				2	1	1	1	0	1	1	0	1	1	0	0	0
(21)			2	2		2			6	0	4	4	2	0	2	4	2	2	2	0	0
(22)		1			3	1			5	1	1	4	1	1	1	0	3	4	1	0	0
(23)		5	3		4		1		13	5	8	4	1	5	8	3	4	4	1	1	0
(24)		3	1					4	8	7	4	0	4	3	4	1	0	0	0	4	4
(25)									0	0	0	0	0	0	0	0	0	0	0	0	0

Table X. Monthly Rate of Seismic Activity near Mitaka.

	Octant								Total	NW +N +NE	EN +E +ES	SE +E +SW	WN +W +WS	N+ NE	NE +E	E+ SE	SE +S	S+ SW	SW +W	W+ WN	WN +N
	N	NE	E	SE	S	SW	W	NW													
(1)	0·24	0·84	0·12				0·36		1·56	1·08	0·96	0	0·36	1·08	0·96	0·12	0	0	0·36	0·36	0·24
(2)		1·77		1·01		0·12			2·91	1·77	2·78	1·13	0·12	1·77	1·77	1·01	1·01	0·12	0·12	0	0
(3)	0·53	0·53		1·06					2·12	1·06	1·59	1·06	0	1·06	0·53	1·06	1·06	0	0	0	0·53
(4)	0·23	0·35	0·47	0·35		0·35	0·47	0·35	2·61	0·94	1·18	0·71	1·18	0·59	0·83	0·83	0·35	0·35	0·83	0·83	0·59
(5)		0·95	0·51	0·22	0·14		0·07		1·90	0·95	1·68	0·36	0·07	0·95	1·46	0·73	0·36	0·14	0·07	0·07	0
(6)		0·26	0·08	0·35	0·26			0·35	1·31	0·61	0·70	0·61	0·35	0·26	0·70	0·43	0·61	0·26	0	0·35	0·35
(7)		0·52			0·26	0·17	0·26		1·22	0·52	0·52	0·43	0·43	0·52	0·52	0	0·26	0·43	0·43	0·26	0
(8)	0·25	1·50	0·25	0·91					2·91	1·75	2·66	0·91	0	1·75	1·75	1·16	0·91	0	0	0	0·25
(9)	0·10	1·00	0·20	0·30	0·30				1·91	1·10	1·51	0·60	0	1·10	1·20	0·50	0·60	0·30	0	0	0·10
(10)	1·87	1·87	1·87			6·25	2·50		14·37	3·75	3·75	6·25	8·75	3·75	3·75	1·87	0	6·25	8·75	2·50	1·87
(11)	0·94	2·83			0·63	8·51	0·94		10·72	3·78	2·83	9·14	9·46	3·78	2·83	0	0·63	9·14	9·46	0·94	0·94
(12)		2·14	0·61				1·22	0·45	4·44	2·60	2·75	0	1·68	2·14	2·75	0·61	0	0	1·22	1·68	0·45
(13)	0·37	1·92	0·56	0·18	0·18		0·37	0·37	3·98	2·67	2·67	0·37	0·74	2·30	2·48	0·74	0·37	0·18	0·37	0·74	0·74
(14)		0·75	0·04	0·41			0·04	0·12	1·37	0·87	1·21	0·41	0·16	0·75	0·79	0·45	0·41	0	0·04	0·16	0·12
(15)	0·19	0·79	0·46					0·19	1·65	1·19	1·25	0	0·19	0·99	1·25	0·46	0	0	0	0·19	0·39
(16)		0·46				0·55			1·01	0·46	0·46	0·55	0·55	0·46	0·46	0	0	0·55	0·55	0	0
(17)		0·10	0·25	0·15	0·15	1·31	0·20	0·45	2·63	0·55	0·50	1·62	1·97	0·10	0·35	0·40	0·30	1·47	1·52	0·65	0·45
(18)		0·14	0·03		0·14				0·31	0·14	0·17	0·14	0	0·14	0·17	0·03	0·14	0·14	0	0	0
(19)		0·09			0·09				0·19	0·09	0·09	0·09	0	0·09	0·09	0	0·09	0·09	0	0	0
(20)			0·16	0·16		0·16			0·50	0	0·33	0·33	0·16	0	0·16	0·33	0·16	0·16	0·16	0	0
(21)		0·08			0·25	0·08			0·41	0·08	0·08	0·33	0·08	0·08	0·08	0	0·25	0·33	0·08	0	0
(22)		0·44	0·26		0·35		0·08		1·16	0·44	0·71	0·35	0·08	0·44	0·71	0·26	0·35	0·35	0·08	0·08	0
(23)		0·24	0·08					0·32	0·64	0·56	0·32	0	0·32	0·24	0·32	0·08	0	0	0	0·32	0·32
(24)									0	0	0	0	0	0	0	0	0	0	0	0	0
(25)																					

$$r=\frac{\text{the number of pairs with same signs}}{\text{total number of pairs}}$$

may therefore be taken as a measure of the closeness of the suspected relation. If it is 1·0, the relation between the two quantities is closely positive, and if it is 0, then the relation is closely negative.

To illustrate, the increase and decrease in pure shear of the ground at Mitaka along a NS direction and those of seismic activity in the eastern octant are:

Pure Shear	+ − + − − + − − + − + − − + − + − − + − + + −
Seismic Activity	− 0 + + − 0 + − + − + − − + − + − − + − + − −.

There are altogether 21 pairs, of which 17 have same signs, giving the ratio $r=0{\cdot}81$.

Now if the plus and minus signs in any two rows that are compared occur with perfect haphazard, then the probability that out of the total m pairs, n will have same (or opposite) signs is

$$p=\frac{m!}{(m-n)!\,n!}\left(\frac{1}{2}\right)^m,$$

and the probability that more than n pairs will have same (or opposite) signs is

$$P=\sum_{n=0}^{n}\frac{m!}{(m-n)!\,n!}\left(\frac{1}{2}\right)^m.$$

In our present example, the probability that the total 21 pairs will be grouped into 17 and 4 with respect to sign, as is actually the case, is

$$p=0{\cdot}003,$$

while the probability that they will be grouped more unevenly than this is

$$P=0{\cdot}007.$$

Judging from the smallness of this probability, the relation between the simple shear along the NS direction and the seismic activity in the E octant is very likely real.

In Table XI will be found the probabilities P for various pairs of strains of the ground and the seismic activity. Judging from the smallness of the probabilities, the relation between the following pairs of quantities are too striking to be put aside as merely fortuitous:

(1) Pure shear along the NS direction and the seismic activity in directions east and west of Mitaka,

(2) Contraction of the ground along the NS direction and the

Table XI. Probability P. (in 10^{-3}).

		Dil.	Max. shear	γ_1	γ_2	Elongation				Pure shear		
						E—W	E 45° N —S 45° W	N—S	N 45° W —S 45° E	N—S	N 45° W —S 45° E	N 45° E —S 45° W
Octant	N	24	1·000	94	94	268	24	94	94	1·000	582	582
	NE	93	93	286	405	1·000	134	405	405	678	134	405
	E	383	189	115	383	383	503	383	78	7	824	7
	SE	804	77	607	454	454	454	1·000	804	804	804	804
	S	143	1·000	21	629	1·000	143	13	13	332	804	143
	SW	607	1·000	424	1·000	1·000	607	1·000	607	118	118	302
	W	454	804	210	210	210	454	804	210	21	454	210
	NW	582	268	1·000	1·000	582	388	268	1·000	24	94	582
Total		405	1·000	523	405	405	523	405	405	260	523	405
NW+N+NE		1·000	678	523	1·000	405	832	210	210	210	832	1·000
EN+E+ES		405	1·000	523	405	1·000	523	405	405	35	1·000	93
SE+S+SW		664	1·000	503	664	664	664	1·000	664	1·000	1·000	1·000
WN+W+WS		664	1·000	824	383	78	824	664	664	27	27	664
N+NE		210	35	523	678	1·000	286	678	678	1·000	286	678
NE+E		405	405	523	405	405	523	405	405	35	1·000	405
E+ES		405	1·000	134	405	1·000	523	405	93	35	523	93
ES+S		405	1·000	115	189	189	189	664	189	189	503	664
S+SW		383	383	263	1·000	664	383	383	383	383	41	189
SW+W		648	648	815	359	167	648	648	648	167	359	1·000
W+NW		1·000	481	815	815	238	359	815	815	8	96	1·000
NW+N		648	648	1·000	648	167	648	1·000	1·000	359	648	1·000

seismic activity in direction north of Mitaka,

(3) Elongation of the ground along the NS direction and the seismic activity in direction south of Mitaka.

These systematic correlations between the deformation of the ground and the seismic activity must at any rate be some indication of the geophysical characteristics of the earth's crust near Mitaka, or even more widely, that of the Kwanto district in which Mitaka is situated—characteristics that may have an important connection with the nature of occurrence of the earthquakes that originate in this district.

On the other hand, the geographical distribution of "push" and "pull" of the first impulsion of an earthquake has been known to serve as an important clue to the mechanism of its occurrence. Moreover, it is generally accepted that the earthquakes originating from one and the same region are mostly due to the same mechanism of occurrence. In fact, T. Fukutomi(5) and F. Kishinouye(6) were able to divide the Kwanto district into a few regions according to the particular ways in which most of the earthquakes originating in them differed the one from the other.

In connection with this problem, M. Ishimoto(7) suggested that the "push" and "pull" of the first impulsion of an earthquake and the permanent deformation of the ground that accompanies that earthquake show the same geographical distribution, the "push" corresponding to to the region of upheaval and the "pull" to that of sudsidence.

If the conclusions reached by these investigators are accepted, the relations that have been pointed out in the present paper to exist between the deformation of the ground and seismic activity seem only very natural consequences, although it does not follow from it that to draw a simple picture of the nature of occurrence of earthquakes in the Kwanto district that would square with all these facts and theories just mentioned will be anything like an easy task.

Leaving these discussions to a later opportunity, this paper is merely an attempt to describe the striking relations that obtain between the deformation of the ground at Mitaka and the general seismic activity near that place.

---

(5) T. Fukutomi, *Disin*, **3** (1931), 592. *Bull. Earthq. Res. Inst.*, **9** (1931), 510.
(6) F. Kishinouye, *Disin*, **4** (1932), 18.
(7) M. Ishimoto, *Bull. Earthq. Res. Inst.*, **11** (1933), 254.

34. 三鷹基線菱形の變形と其の附近に於ける地震活動

地震研究所　坪　井　忠　二

三鷹東京天文臺構内に於ける菱形基線の長さは大正5年以來昭和 14 年迄に 25 回測定されてゐる．まづ大等の邊長の變化から此の土地の變形を求めた．

次に同じ期間内に三鷹を中心として 150 km 以内の距離に起つた顯著及稍顯著地震を氣象要覽から拾ひ出し，顯著地震には 2，稍顯著地震には 1 といふ重みを，又 50 km 以内に起つた地震には 3, 100 km 以内のものには 2，150 km 以内のものには 1 と云ふ重みを附して，三鷹から見た各方向に於ける地震活動を求めた．

かくして求められた土地の變形と，地震活動の消長を較べて，次の如き關係があるを見出した．

(1)　東又は西に地震が多くなると，南北方向に沿つた土地の Shear の速度が大きくなる．

(2)　北に地震が多くなると，南北方向に於ける土地の短縮の速度が大きくなる．

(3)　南に地震が多くなると，南北方向に於ける土地の伸張の速度が大きくなる．

35. *Measurement of Changes in Magnetic Susceptibility of Igneous Rocks with Temperature in a Weak Magnetic Field.**

By Takesi NAGATA,

Earthquake Research Institute.

(Read July 4, 1940 and Sept. 18, 1941.—Received, Sept. 20, 1941.)

1. Introduction.

In his previous paper,[1] the writer described the magnetic properties of volcanic rocks ejected from a few of the volcanoes in Japan, dealing especially with their magnetization curve, initial susceptibility, natural remanent magnetism, and thermo-remanent magnetism. There is, however, another fundamental property of the rock's magnetism which it is necessary to examine before we can analyze the magnetic constitution of igneous rocks and ascertain its possible relation to local geomagnetic changes. This is the change in susceptibility of rock with temperature variation, especially in a weak magnetic field.

In the writer's opinion, the remarkable magnetization of natural effusive rocks is in most cases due to the presence of permanent magnetization, which is usually called "natural remanent magnetization." The intensity of this permanent magnetization is generally larger, relatively speaking, than that of magnetization induced by the geomagnetic field. Sometimes, the former is so large that, compared with it, the latter is negligible. Hence, so long as we are concerned only with the magnetization of effusive rocks from the standpoint of its relation to a conspicuous geomagnetic anomaly, the intensity of magnetization directly induced by the present geomagnetic field seems to be less important than that of the permanent component.

It has been proved,[2] on the other hand, that the natural remanent magnetization is chiefly due to the residual permanent magnetization that is produced during cooling in the geomagnetic field, the mode of its causation being given by

---

* Dedicated to the late Professor Mishio Ishimoto.

1) T. NAGATA, *Bull. Earthq. Res. Inst.*, **18** (1940), 102; 281; **19** (1941), 49; 304.

2) T. NAGATA, *Bull. Earthq. Res. Inst.*, **19** (1941), 49.

$$\vec{J}_{t_i, H}(t) = \vec{H} \cdot \int_t^{t_i} P(t)dt \quad (t_i > t). \tag{1}$$

Eq. (1) gives the thermo-remanent magnetization caused during cooling from t_i to t in a constant magnetic field of H, while $P(t)$ in the equation is its characteristic function of temperature, the form of which depends on the characteristics of the particular rock specimen. It is believed, however, that the form of $P(t)$ is closely related to or subject to the mode of change in magnetic susceptibility with temperature. Putting aside this close relation of form $P(t)$ to thermo-remanent magnetism, the mode of change in magnetic susceptibility with temperature also seems to show a fundamental characteristic of the magnetic property of rock, since the Curie-point temperature of a rock is directly related to the physical mechanism of causation of its magnetism.

The reason for the necessity of studying the thermal change in magnetic susceptibility of rocks will now be clear. A number of illuminating papers on the problem stated here have already been published by R. Chevallier,[3] and others.[4] Of these, Chevallier's work gives a fairly clear relation between the Curie-point temperature and the constitution of the rock, although his experiments were made by means of the magnetometric method in a rather strong magnetic field (about 150 Oersteds), which greatly exceeds the intensity of our geomagnetic field. Here, we shall study the mode of thermal change of magnetic susceptibility of various kinds of rock, especially in a weak magnetic field. Moreover, the writer's experiments were conducted under the conception that the total apparent magnetization of a rock specimen thermally agitated in a magnetic field is given by linear addition of the thermo-remanent magnetization to the induced magnetization, that is,

$$\vec{J}(t) = \vec{H} \cdot \chi(t) + \vec{J}_{t_i, H}(t), \tag{2}$$

where $\chi(t)$ denotes the magnetic susceptibility at temperature t. That relation (2) holds at ordinary room temperature was experimentally proved, while the contingency that it holds at any temperature was also examined by means of the magnetometric method, the result of the examination showing that it holds, at any rate, approximately.[5]

Hence, in the present study, the induced magnetization $\vec{H} \cdot \chi(t)$,

3) R. CHEVALLIER et J. PIERE, *Ann. de Phys.*, **18** (1932), 383.
4) Y. KATO, *Rep. Col. Sci. Tôhoku Imp. Univ.*, **27** (1938), 91.
5) T. NAGATA, *loc. cit.*

from which the susceptibility is derived, is rigidly separated from the permanent componet $\vec{J}_{t_i,n}(t)$, which depends on the history of the temperature change in the specimen in a magnetic field. Under these conditions, several typical specimens of Japanese volcanic rocks were examined. The method used and the results of the experiment will now be discussed.

2. Measuring Apparatus.

Since the intensity of thermo-remanent magnetization is usally larger than the induced magnetism in a weak magnetic field, it is difficult to determine accurately the intensity of the induced part alone by means of the usual magnetometric method, in which only the intensity of total magnetization is observable. This is because the induced magnetization, which is to be given as the residual after subtracting the permanent component from the observed total magnetization, so far as eq. (2) holds, is usually accompanied by large errors.

Hence, for the measuring apparatus in the present study we adopted the ballistic method, in which we measured the e. m. f. due to the electro-magnetic induction between two coils containing a rock specimen as a core. Since the magnetic susceptibility of rocks is usually small, (less than 3×10^{-3} in its specific value), several technical improvements were required in order to be able to determine the magnitude of susceptibility in a weak magnetic field with an error smaller than a few percent. The principle and details of the measuring apparatus now follow.

(i) *General electric circuit.*

The general electric circuit in the ballistic method is shown in Fig. 1, where M_1, M_2, and M_3 denote mutual inductance. In the axis line of M_1, which consists of two circular coils, the rock specimen to be examined is set as a core, while the compensating coils M_2 is exactly the same as M_1 in their forms. M_3 is the mutual inductance for calibrating sensitivity. The ballistic galvanometer G assumes its critical-damping condition with the aid of resistances r_1 and r_2. In measuring, the electric current I in the primary circuit is turned to $-I$ with the aid of a mercury switch C, when the induced charge Q in the secondery circuit is

$$Q=2k(M_1I\mu-M_2I\mu_0), \tag{3}$$

where k is a constant value depending on the characteristics of the

ballistic galvanometer and the resistance in the secondery electric circuit, while μ and μ_0 are permeabilities in M_1 and M_2 respectively, that is,

$$\mu=1+4\pi CS\kappa/A, \quad \mu_0=1, \tag{4}$$

where κ and S denote the magnetic susceptibility of the rock specimen inserted in M_1 and the area of its cross section respectively, while a constant, C, results from the condition that the rock specimen having κ had not sufficient length; that is, $CS\kappa/A$ gives the effective susceptibility of the whole space inside the secondary coil M_1. If M_2 is suitably adjusted to equal M_1, we get from eqs, (1) and (2),

$$Q=8\pi kM_1ICS\kappa/A. \tag{5}$$

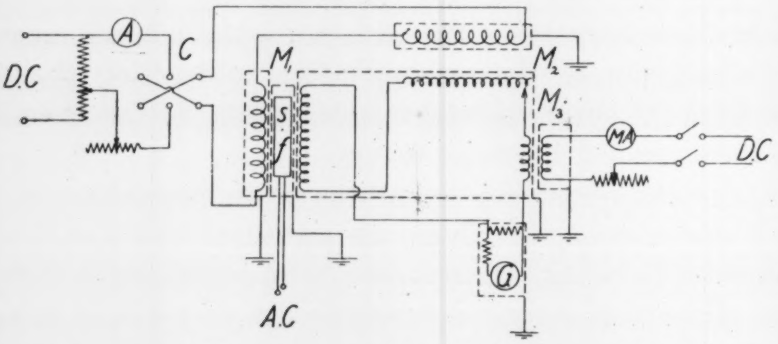

Fig. 1. Electric circuit in the apparatus for measuring susceptibility at high temperature.
M_1, M_2, mutual inductances,
M_3, mutual inductance for sensitivity test,
s, specimen,
f, non-inductive electric furnace.

Since the deflection of the ballistic galvanometer θ is proportional to Q, that is, $Q=c\theta$, we get.

$$\theta=K\kappa I, \tag{6}$$

where $K=8\pi kM_1CS/Ac$.

While, on the other hand, the intensity of magnetic field H, produced by the primary coil of M_1 and M_2, is proportional to I, i. e. $H=\frac{8}{5\sqrt{5}}\frac{N}{R}I=k'I$, we finally get

$$\kappa=\frac{\theta}{KI}=\frac{\theta}{K'H}, \tag{7}$$

where $K'=8\pi kM_1CS/Ack'$.

Thus magnetic susceptibility κ, corresponding to magnetic field H,

can be determined by the observable quantities θ and I, and by the given constants K and C.

(ii). *The M_1 and M_2 coils.*

The primary coil of mutual inductance M_1 is a Helmholtz's coil of 35 cm radius and 150 turns of wire, the intensity of magnetic field at the centre of the coil being 3·85 Oe./amp. corresponding to unit electric current through the coil. The magnetic field inside the co-axial cylindrical space, 25 cm long and 20 cm in diameter (± 10 cm along the the axis line and 10 cm in radial direction from the centre of the coil), is uniform with an error of less than 0·1 percent —an error sufficiently small for the present purpose of measurement. The secondary coil of M_1, which is a cylindrical solenoid, set coaxially with Helmholtz's coil, is 9·0 cm long and 6·7 cm in diameter, fine wire being wound on the outside of a double pyrex glass tube. The total number of turns and the electric resistance of the secondary coil are about 43000 and 45 KΩ respectively. Through the gap between the outer and inner glass tubes, water was always made to flow in order to absorb the heat from the furnace, as also to maintain the secondery solenoid at constant ordinary room temperature (10°C in winter and 25°C in summer).

As already mentioned, the primary and secondery coils of M_2 were constructed exactly like those of M_1. Since the turns of the secondery solenoid of M_2, however, can be varied from 40000 to 46000 with every two turns with the aid of four lever switches, mutual inductance M_2 can be equalized to M_1 with an error of only $2/43000 \simeq 5 \times 10^{-4}$. These two coil system M_1 and M_2 were set perpendicular to and 1·5 m apart from each other.

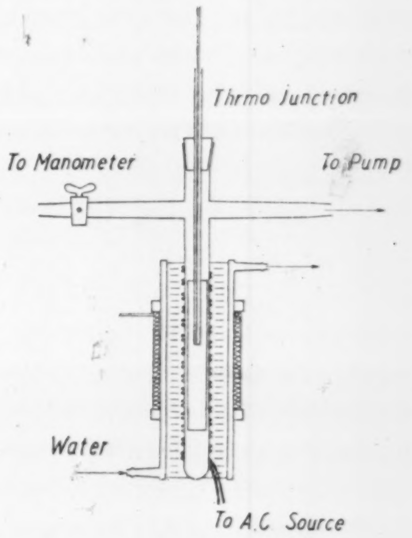

Fig. 2. Non-magnetic and non-inductive vacuum furnace in the apparatus.

(iii). *The rock specimen and the heater.*

The rock specimen to be examined was pulverized into small grains of 0·1 *mm*, mean diameter, and poured into a tube of fuzed silica, 1·62 *cm* in its inner diameter and 10·0 *cm* long. The temperature at the centre of the specimen was determined by means of a $P_t \sim P_t \cdot Rh$ thermo-junction, which was shielded in a thin silica tube, as shown in Fig. 2. A vacuum electric furnace was also made with a fuzed silica tube and platinum

wire, which last was wound non-inductively on the silica tube, while the air in the furnace was pumped out with the aid of a rotary pump, the air pressure being always kept at few *mm* of mercury. The furnace was held in the secondery coil, the gap between them being filled with pure asbestos. Needless to say, the materials inserted in the secondary coil of M_1 were almost non-magnetic ($\kappa < 10^{-5}$). The rotary pump was placed more than 2·5 m away from the coil systems M_1 and M_2 in order to avoid heterogeneity of and variations in the magnetic field in M_1 and M_2 due to the pump and the electric motor. The axes of the specimen, furnace, and secondary coil were set coaxially with that of the Helmholtz's coil, the magnetic field produced by which was sufficiently uniform in that space occupied by the secondary coil as well as by the specimen.

It may be worth noting here that all the parts mentioned above were sufficiently isolated, electrically, and that every part was shielded perfectly from the other by means of plates of conducters connected to earth.

(iv). *Sensitivity and its stability against temperature change.*

The sensitivity of the apparatus depends first on the dimensions of the specimen, that is, S and C in eq. (2), and next on the electric arrangement of the secondary circuit. Although it is desirable that the length of the specimen shall exceed three times that of the secondary solenoid, and that the diameter of the latter shall be the nearest possible to that of the former, for the purpose of determining absolutely the magnitude of the true susceptibility of the specimen, these conditions could hardly be satisfied in our apparatus, since the presence of the heater surrounding the specimen and the requirements in regard to uniformity of temperature in it prevented these conditions from being filled. In our case, moreover, a theoretical determination of the magnitudes of S and C seems to be difficult, and not accurate even if it could be done, seeing that the shapes of the specimens were rather irregular, for which reason the sensitivity of the whole measuring system was calibrated experimentally by testing the various specimens, the susceptibilities of which at ordinary room temperature have already been determined. The constants K and K' were thus determined experimentally. Strictly speaking, however, C is not a constant quantity, since it varies with various values of susceptibility κ of the inserted specimen, although the amount of change should be small, negligible in the present case, where the susceptibility itself is very small, usually of the order of 10^{-3} c. g. s. e. m. u., or less.

On the other hand, the sensitivity and stability of the secondary circuit, including the galvanometer, was checked by means of mutual inductance M_3. Since c/k usually varies slightly with weather conditions, especially with temperature and humidity, the check by means of M_3 was made both before and after every observation. The amount of variation, however, was always smaller than 0·5 percent throughout the the four seasons.

(v). *Errors in measurment.*

Uniformity in temperature of the specimen was examined at various temperatures. Actually, the distribution of temperature along the axis line was examined, an example of it being shown in Fig. 4, from which it may be said that the temperature of a specimen was uniform with

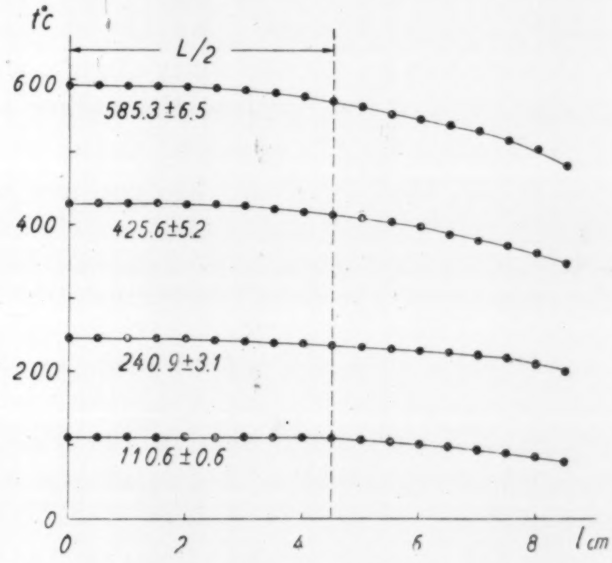

Fig. 4. Temperature distribution in the furnace. L denotes the length of specimen. (Heating velocity=2 degree/min.)

an error less than 10° in a temperature range of from 0°C to 650°C.

Since it was not possible to make M_1 exactly equal to M_2 in our apparatus, the former being adjustable only with a finite interval of 5×10^{-4} in $\Delta M_2/M_2$, equation (6) does not quite hold, but we have the relation

$$\theta = KI\kappa + \frac{2kI\rho_0 \Delta M_2}{c} = K\kappa I + \theta_0 ,$$

where, as will be seen from the above equation, θ_0 is a constant value, so long as I is constant, so that in the actual measurement, substituting $\theta-\theta_0$ for θ in eq. (6), it was possible to determine κ with the aid of the relation

$$\kappa=\frac{\theta-\theta_0}{KI}=\frac{\theta-\theta_0}{K'H}. \qquad (9)$$

Compared with θ, θ_0 was usually very small, the magnitude of the former corresponding to about 10^{-4} of the susceptibility of the inserted specimen. Although it would be very desirable to measure the change in susceptibility with temperature variation in a weak magnetic field nearly the same as the geomagnetic field, say 0·5 Oersteds, this was not possible in our case, seeing that we required an observational accuracy of 10^{-5} c. g. s. e. m. u. in the value of susceptibility, with the result that the intensity of the applied magnetic field, which is produced by the primary coils of M_1 and M_2, was always about 2 Oersteds, except the case in which the susceptibility of magnetite was examined.

While on the other hand, variation in θ usually fluctuated, probably due to a slight leakage current from the *A. C.* in the electric furnace, or from other sources, to the secondary circuit, which fluctuation depends on the temperature in the furnace, the higher the temperature the greater was the fluctuation. The observed values of $\theta-\theta_0$ at various temperatures, when $\mu=\mu_0$, that is, when the specimen vessel is empty, are as follows.

Temperature	$\Delta\kappa$	Temperature	$\Delta\kappa$
0~350°C	$(0{\cdot}0\pm1{\cdot}6)\times10^{-5}$	400~700°C	$(0{\cdot}0\pm2{\cdot}7)\times10^{-5}$

The quantities on the right-hand side in the Table are given in terms of magnitude of susceptibility of the specimen corresponding to the observed value of $\theta-\theta_0$.

Since this fluctuation was the largest source of observational errors, the error in our experiment throughout the whole temperature range from 0°C to 700°C in the term $\Delta\kappa$ was less than 3×10^{-5}. This observational error, however, is independent of the magnitude of the susceptibility of the inserted specimen, so that if the susceptibility of the specimen is larger, the error is relatively smaller. For example, an observed value of susceptibility of about 10^{-3} is expected to contain an error of 3 percent.

3. The results of experiment.

Several typical specimens of basaltic and andesitic rocks were examined with the aid of the present instrument, namely, six from the ejecta of Huzi (Fuji) Volcano, three from those of Miyake-sima Volcano,

and a magnetite from Manchuria. According to H. Tsuya, these rocks are[6]

No. 1 (S–N–17), Huzi, the lava of Hôei explosion crater, olivine-basalt,

No. 2 (S–N–20), Huzi, Makuiwa lava, olivine-basalt,

No. 3 (S–N–23), Huzi, Makuiwa lava, two-pyroxene-bearing olivine-basalt,

No. 4 (S–N–21), Huzi, Makuiwa lava, augite-bearing olivine-basalt,

No. 5 (S–N–18), Huzi, Makuiwa lava, hypersthene-augite-olivine-basalt,

No, 6 (S–N–22), Huzi, ejecta from Hôei crater, augite-bearing olivine-basalt,

No. 7 (S–N–59), Miyake-sima, Akabakkyo lava, olivine-hypersthene-pyroxene-basaltic-andesite,

No. 8 (S–N–60), Miyake-sima, Yoridaisawa lava, olivine-hypersthene-pyroxene-basaltic-andesite,

No. 9 (S–N–75), Miyake-sima, ejecta of the central cone, olivine-two-pyroxene-basaltic andesite,

No. 10 magnetite.

6) The chemical composition of specimens Nos. (1), (2), (3), (4), (5), and (6) are as shown in the following table. (Due to H. Tsuya, *Bull. Earthq. Res. Inst.*, **15** (1937), 307)

Chemical composition of Huzi ejecta.

	No. 1.	No. 2.	No. 3.	No. 4.	No. 5.	No. 6.
SiO	49·60	50·28	50·64	50·66	51·05	51·09
Al_2O_3	16·96	18·30	18·58	18·25	18·35	17·62
Fe_2O_3	5·40	4 50	3·04	4·78	2·76	2·64
FeO_3	6·65	6·89	7·29	5·72	7·72	8·42
MgO	5·92	3·80	5·58	4·94	4·63	5·09
CaO	10·03	9·76	10·00	9·98	9·90	9·68
Na_2O	2·48	2·87	2·64	2·78	2·81	2·80
K_2O	0·58	0·94	0·61	0·77	0·81	0·76
H_2O+	0·50	0·20	0·20	0·38	0·40	0·28
H_2O-	0·12	0·08	0·06	0·13	0·11	0·06
TiO_2	1·49	1·78	1·15	1·38	1·41	1·38
P_2O_5	0·20	0·34	0·16	0·25	0·24	0·26
MnO	0·21	0·20	0·17	0·17	0·18	0·21
Total	100·05	99·94	100·12	100·19	100·37	100·29
Q	3·78	3·96	1·98	4·14	2·34	2·04
Or	3·34	5·57	3·34	4·45	5·01	4·45
Ab	20·97	24·14	22·55	23·59	23·59	23·59
An	33·38	34·49	36·99	35·05	35·05	33·38
Wo	6·50	5·11	4·88	5·34	5·23	5·46
En	14·76	9·43	13·85	12·34	11·54	12·65
Fs	5·80	6·47	9.24	4·62	9·89	11·35
Mt	7·87	6·48	4·40	6·93	3·94	3·94
Il	2·73	3·34	2·12	2·58	2·73	2·58
Ap	0·33	0·65	0·33	0·65	0·65	0·65

Table I. Specific susceptibility of volcanic rocks at various temperatures.
(H, Heating process; C, Cooling process.)

Specimen / Temperature	(No. 1.) S−N 17 H=1·54 Oe.		(No. 2.) S−N 20 (1) H=1·93		(No. 2.) S−N 20 (2) H_2=1·93		(No. 3.) S−N 23 H=2·13		(No. 4.) S−N 21 H=2·14		(No. 5.) S−N 18 H=2·14		(No. 6.) S−N 22 H=2·19		(No. 7.) S−N 59 H=2·20	
	H	C	H_1	C_1	H_2	C_2	H	C	H	C	H	C	H	C	H	C
25°C	2·25	2·25	1·29	1·27	1·28	1·27	1·30	1·28	1·62	1·63	1·42	1·41	0·72	0·70	1·35	1·41
40	2·28	2·25	1·29		1·28		1·30	1·29	1·62	1·64	1·44	1·45	0·75	0·74	1·53	1·57
60	2·28	2·26	1·29		1·30	1·26	1·28	1·29	1·64	1·65	1·48	1·48	0·80	0·78	1·61	1·74
80	2·31	2·28	1·31		1·33		1·32	1·30	1·66	1·66	1·57	1·50	0·87	0·84	1·73	1·86
100	2·31	2·30	1·32		1·31		1·32	1·31	1·70	1·67	1·63	1·59	0·91	0·91	1·88	1·97
120	2·34	2·32	1·32		1·32	1·27	1·35	1·31	1·71	1·69	1·79	1·76	0·96	0·96	1·97	2·08
140	2·38	2·35	1·36		1·31		1·37	1·32	1·74	1·70	1·87	1·83	1·01	1·01	2·03	2·18
160	2·44	2·36	1·36		1·30		1·37	1·32	1·75	1·70	1·94	1·88	1·09	1·03	2·12	2·23
180	2·47	2·39	1·37		1·31	1·29	1·38	1·32	1·77	1·72	2·03	1·93	1·10	1·05	2·23	2·30
200	2·51	2·41	1·37		1·31		1·40	1·34	1·78	1·73	2·16	1·97	1·11	1·03	2·20	2·34
220	2·52	2·42	1·42	1·32	1·33		1·41	1·36	1·82	1·75	2·16	1·89	1·02	1·02	2·03	2·35
240	2·57	2·46	1·41		1·31	1·29	1·42	1·37	1·84	1·76	1·98	1·74	0·93	0·93	1·90	2·36
260	2·60	2·44	1·43		1·31		1·44	1·39	1·87	1·77	1·79	1·46	0·80	0·77	1·76	2·31
280	2·62	2·47	1·41		1·30		1·46	1·39	1·87	1·78	1·43	1·15	0·68	0·64	1·54	2·20
300	2·64	2·47	1·44	1·34	1·30	1·29	1·49	1·38	1·91	1·78	0·98	0·79	0·55	0·52	1·01	2·10
320	2·63	2·42	1·47	1·35	1·30	1·30	1·51	1·39	1·93	1·78	0·57	0·58	0·49	0·45	0·59	1·85
340	2·48	2·32	1·44	1·35	1·29	1·30	1·50	1·37	1·95	1·79	0·54	0·49	0·41	0·38	0·30	1·60
360	2·32	2·25	1·47	1·35	1·29	1·31	1·52	1·38	1·98	1·80	0·51	0·46	0·40	0·35	0·23	1·24
380	2·22	2·10	1·47	1·34	1·27	1·28	1·52	1·38	2·02	1·82	0·50	0·42	0·37	0·33	0·24	0·98
400	2·14	1·93	1·49	1·30	1·28	1·29	1·54	1·34	2·03	1·82	0·50	0·41	0·35	0·30	0·31	0·78
420	1·96	1·57	1·47	1·29	1·26	1·27	1·49	1·23	2·04	1·77	0·46	0·39	0·33	0·28	0·37	0·56
440	1·40	1·18	1·37	1·20	1·19	1·23	1·34	1·13	2·03	1·62	0·40	0·39	0·30	0·25	0·45	0·46
460	0·90	0·80	1·20	1·03	1·06	1·06	1·05	0·96	1·89	1·51	0·38	0·36	0·23	0·21	0·40	0·37
480	0·57	0·53	0·99	0·85	0·65	0·79	0·83	0·71	1·61	1·25	0·35	0·33	0·21	0·18	0·32	0·26
500	0·36	0·31	0·60	0·60	0·41	0·57	0·54	0·42	1·21	0·92	0·30	0·28	0·18	0·15	0·19	0·22
520	0·15	0·17	0·41	0·39	0·30	0·38	0·34	0·25	0·78	0·58	4·22	0·18	0·14	0·11	0·13	0·13
540	0·11	0·13	0·23	0·22	0·16	0·20	0·21	0·15	0·37	0·34	0·13	0·15	0·06	0·07	0·10	0·09
560	0·05	0·04	0·11	0·11	0·07	0·08	0·09	0·07	0·21	0·19	0·05	0·06	0·02	0·03	0·04	0·03
580	0·00	−0·01	0·00	0·01	0·01	0·01	0·03	0·03	0·05	0·07	−0·01	0·01	0·01	−0·01	0·00	0·00
600	0·00	0·00	0·01	0·02	−0·01	0·00	0·00	−0·01	0·00	0·02	0·00	0·00	0·00	0·01	−0·01	0·00
620	0·01	−0·01	0·00	0·00	0·00	0·00	0·00	0·00	0·00	0·00	0·00	−0·01	0·00	0·00	0·00	−0·02
640	0·00	0·00	−0·02	−0·01	−0·01	−0·01	0·00	−0·01	0·00	0·01	0·00	−0·01	−0·01	0·00	6·01	−0·02
660	0·00	0·00	−0·01	−0·01	−0·01	−0·01	−0·01	−0·01	0·00	0·00	−0·01	0·00	0·01	0·00	−0·01	0·00

Unit = 10^{-3} e.m.u.

Of the results of measuring susceptibility of these specimens, those of the ejecta from Miyake-sima were already described in the writer's previous paper,[7] so that we shall here deal with the other rock specimens. The observed values of magnetic susceptibility of these rocks at various temperatures from 20°C to 700°C are given in Table I and in Figs. 5 ~12. In these figures, the scale of the ordinate gives the specific value of magnetic susceptibility, (I) and (II) denote the heating and cooling processes respectively, while (III) and (IV) in Fig. 6 show the second heating and cooling processes respectively. As will be clearly seen from

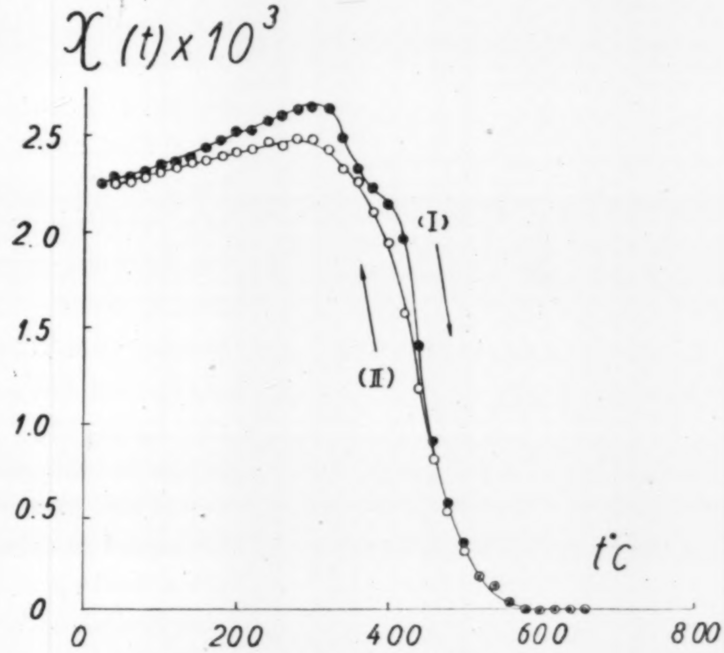

Fig. 5. Change in susceptibility with temperature, No. 1. (S—N 17) H=1·54 Oe.

these results, the $\chi(t) \sim t$ curves of the rock specimens are not always monotonic. Sometimes, the susceptibility changes stepwise with temperature, for example, those shown in Fig. 9~11. In some of the specimens, however, the thermal changes in magnetization have a fairly simple character, like those given in Fig. 6~8, in which the mode of change in susceptibility with temperature is nearly the same as those of ordinary ferromagnetic materials; that is, the susceptibility gradually decreases with temperature, the ferromagnetism disappearing at a critical temperature. Actually, the intensity of magnetization at temperature higher than the critical point could not be estimated by the present instrument, since its magnitude was much smaller than the observational error, with

7) T. NAGATA, *Bull. Earthq. Res. Inst.*, **19** (1941), 304.

the result that, practically speaking, the magnitude of susceptibility in the temperature range above the critical point is taken as zero.

It will be noticed that the susceptibility of these specimens slowly increases with temperature from 0°C, at any rate in the process of initial heating, to about 400°C in specimen No. 1, while it decreases rather abruptly from that point. Comparing the $\chi(t)\sim t$ relations in the heating (I) and cooling (II) processes, it will be said that they are nearly similar, excepting the slight difference that the susceptibility in the cooling process is usually slightly less than that in the heating process. While those in processes (III) and (IV) are nearly the same, they also nearly agree in process (II).

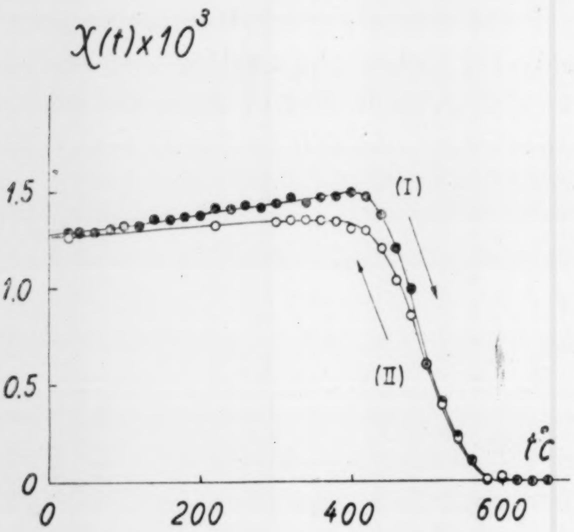

Fig. 6. (a) Change in susceptibility with temperature.
No. 2. (S—N 20) H=1·93 Oe.

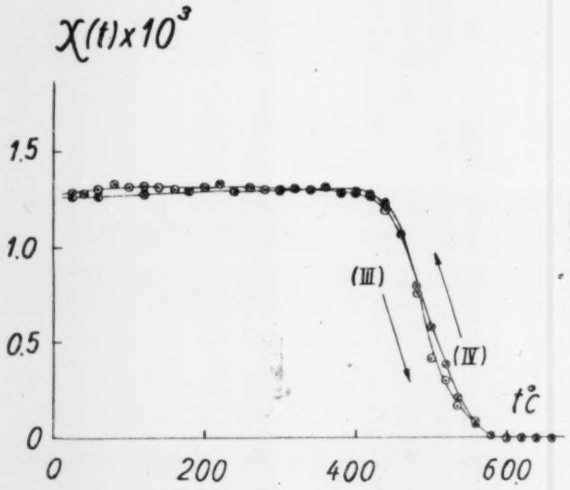

Fig. 6. (b) Change in susceptibility with temperature.
No. 2. (S—N 20) H=1·93 Oe.

This type of mode of change in susceptibility with temperature, as just mentioned, we shall call "the standard type" of rock. In the $\chi(t)\sim t$ relation of the standard type rock specimen, its susceptibility becomes approximately zero at critical temperature, at which the ferro magnetism of the rock specimen is believed to disappear. If we take this critical temperature as the apparent Curie-point of the rock specimen, the value of the standard type rock almost agrees with that of pure magnetite, namely, from 580°C to 600°C. However, since the temperature at which the rate of change in susceptibility with respect to temperature is maximum

does not agree with the citical point, the former usually being slightly lower than the latter, by taking into consideration that the ferromagnetic minerals in the rocks must be composed not of pure magnetite alone, but also of solid solutions of Fe_2O_3, FeO, TiO_2, and other elements in various phases, it may be presumed that the Curie-point temperature of the rock will not be given uniquely, but instead, as a band of finite width with respect to temperature. For these reasons, we take here the temperature at which $\partial\chi/\partial t$ is maximum as the mean Curie-point of a rock specimen, denoting it by θ. The critical temperature at which the ferromagnetism of a rock specimen disappears may then be interpreted as the upper limit of the band of Curie-point temperatures, which point will correspond to the Curie-point temperature of that part of the total ferromagnetic minerals in the rock that has the composition of pure magnetite, which point is denoted here by θ. The actual values of θ and θ are given in Table II.

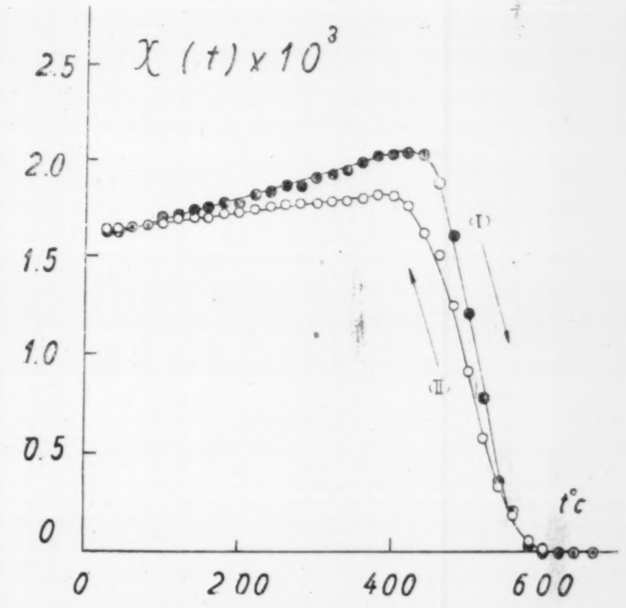

Fig. 7. Change in susceptibility with temperature.
No. 3. (S—N 23) H=2·13 Oe.

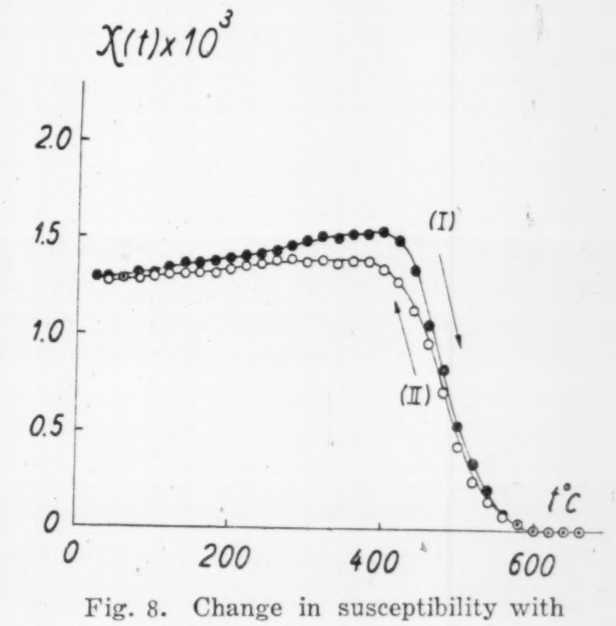

Fig. 8. Change in susceptibility with temperature.
No. 4. (S—N 21) H=2.14 Oe.

In contrast to this, those rock specimens of no standard type of character change in susceptibility with temperature in various ways. As to the curves of rock samples whose susceptibilities change stepwise with temperature,

they may be regarded as the result of superposition of two fundamental curves of $\chi(t)$, the mean Curie-point temperatures of which are θ_1 and θ_2, while the upper limits of the band of Curie-point temperatures of each of the two curves separated from $\chi(t)$ are θ_1 and θ_2 respectively. Here, the fundamental curve of $\chi(t)$ is defined as the curve, the mode of which is similar to the standard curve, that is, it changes monotonically with temperature, having only one mean Curie-point temperature, but its θ does not necessarily agree with the Curie-point of magnetite, namely, θ_M. The observed valuesof θ_1, θ_2, θ_1, and θ_2 are given in Table II, where it will be seen that their θ_2 agrees well with the θ of the standard type curve, as with θ_M. Hence, it may be said that one of the elemental curves composing the $\chi(t)$ curve of stepwise change type is of standard type.

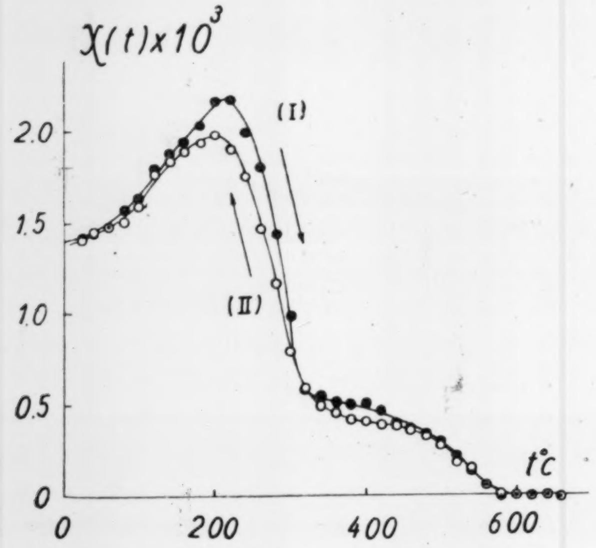

Fig. 9. Change in susceptibility with temperature.
No. 5. (S - N 18) H = 2·14 Oe.

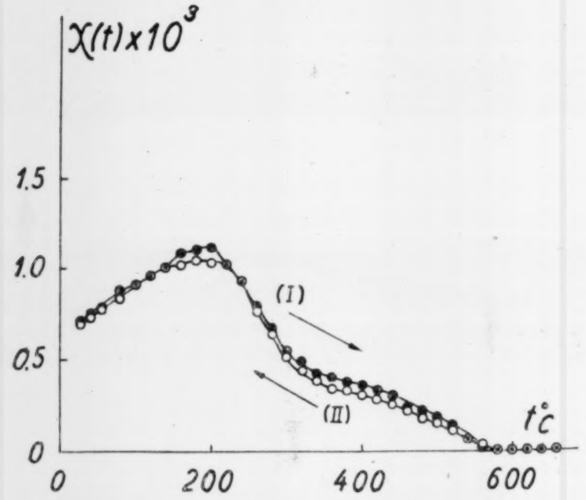

Fig. 10. Change in susceptibility with temperature.
No. 6. (S—N 22) H = 2·19 Oe.

Generally speaking, it may be possible that a $\chi(t)$ curve is composed of two or more fundamental curves, the mean Curie-point temperatures of which are not alike.[8] Thus, generally,

$$\chi(t) = \sum_j \chi_j(t).$$

In all these examples mentioned above, the susceptibility at any temperature in the process of heating and cooling is nearly the same, there

Table II.

Specimen	Locality	Rock	$(\chi_0)_{t=0}$	$\bar{\theta}$	θ	C_{Mt}
No. 1. (S—N 17)	Huzi	olivine-basalt	$2{\cdot}25\times10^{-3}$	460°C	575°	7·87 %
No. 2. (S—N 20)	Huzi	olivine-basalt	$1{\cdot}28\times10^{-3}$	500	580	6·48
No. 3. (S—N 23)	Huzi	two-pyroxene-bearing olivine-basalt	$1{\cdot}29\times10^{-3}$	495	590	4·40
No. 4. (S—N 21)	Huzi	augite-bearing olivine-basalt	$1{\cdot}55\times10^{-3}$	520	590	6·95
No. 5. (S—N 18)	Huzi	hypersthene-augite-olivine-basalt	$1{\cdot}31\times10^{-3}$	$\bar{\theta}_1=270$ $\bar{\theta}_2=520$	$\theta_1=320$ $\theta_2=580$	3·94
No. 6. (S—N 22)	Huzi	augite-bearing olivine-basalt	$0{\cdot}70\times10^{-3}$	$\bar{\theta}_1=280$ $\bar{\theta}_2=510$	$\theta_1=310$ $\theta_2=580$	3·94
No. 7. (S—N 59)	Miyake-sima	olivine-hypersthene-pyroxene-basaltic-andesite	$1{\cdot}31\times10^{-3}$	H $\bar{\theta}_1=320$ H $\bar{\theta}_2=520$ C $\bar{\theta}=360$	$\theta_1=380$ $\theta_2=580$ $\theta=580$	

being slight differences between them, as already described in the case of the standard type specimen. In other words, the susceptibilities of rock specimens, Nos. 1 to 6, are almost reversible with respect to temperature, regardless of whether it belongs to the standard type or not.

On the other hand, we have an example in which the change in susceptibility is irreversible with respect to temperature. It is shown in Fig. 11, where the susceptibility changes stepwise with temperature, $\bar{\theta}_1$, $\bar{\theta}_2$, θ_1, and θ_2 being 270°C, 500°C, 360°C, and 580° C respectively during heating, while in cooling it changes rather monotonically, $\bar{\theta}$ being 360°C, although θ is 580°C in this case also.

In all these examples, where the lower mean Curie-point temperature $\bar{\theta}_1$ is fairly smaller than that of pure magnetite, it is a common character that the rate of increase of susceptibility with temperature in a certain initial range from 0°C is much larger than that of the standard type rock, amounting to from 0·2 to 0·5 percent/degree. In such samples, the susceptibility at that temperature where it takes the largest value amounts to from 1·5 to 1·8 times that at oridinary room temperature. Since this phenomenon of increase of magnetic susceptibility with temperature could not be seen in the $\chi(t)\sim t$ relations in a magnetic field of from about 120 to 150 Oersteds, in the result of study

8) Specimen No. 1, (shown in Fig. 5) seems to be intermediate in type between standard and stepwise change.

by Chevallier and Piere, it is believed that this phenomenon is peculiar to the rock in a weak magnetic field.

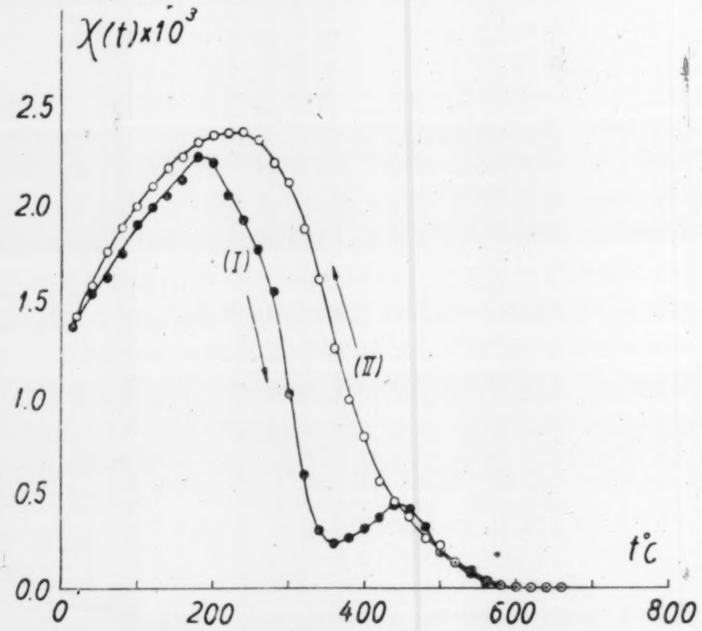

Fig. 11. Change in magnetic susceptibility with temperature (irreversible type). No. 7 (S—N 59) H=2·20 gauss.

Next, the fact that the susceptibilities of some rock specimens change stepwise with temperature shows that the ferromagnetic minerals contained in them consists of a few groups of different mineralogical characters, the number of these groups corresponding to that of θ_j.

For example, specimen No. 5, shown in Fig. 9, contains two different groups of forromagnetic minerals, one of which is nearly the same as pure magnetite, corresponding to the part of $\chi_2(t)$, (component of standard type), while the other differs greatly from pure magnetite, since θ_1, which corresponds to $\chi_1(t)$, is clearly much lower than θ_M. Further details of the relation between the mode of thermal change in the susceptibility of rocks and their petrological composition, as well as its relation to the mode of causation of thermo-remanent magnetism in a weak magnetic field, will be discussed in future papers. It may however be worth while to note here the fact that, according to microscopic observations of the Huzi ejecta by Tsuya, the groundmasses of specimens Nos. 1, 3, and 5 are clearly more crystalline than those of Nos. 2 and 4, which fact may correspond to our result in which the mode of change in susceptibility with temperature of the former specimens is of the standard type, while that of the latter is not.

Lastly, for comparison, the result of the same examination of a

specimen of magnetite is given in Fig. 12. That its mode of change differs slightly from that of pure magnetite must be chiefly because it contains impurities.

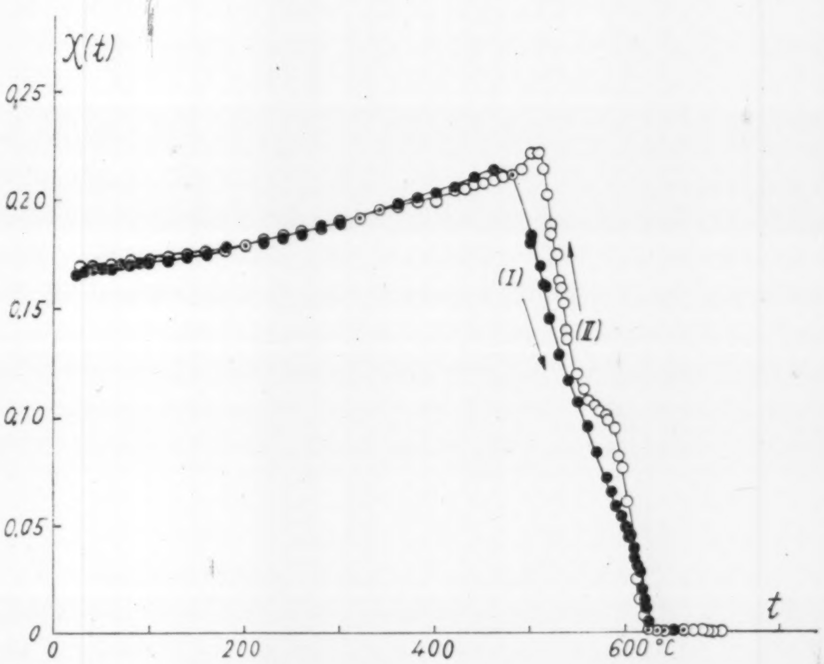

Fig. 12. Magnetite grains. H = 1·54 Oe.

4. Conclusion.

In this paper, the writer describes the method of measuring the change in magnetic susceptibility of rocks with temperature in a weak magnetic field, and gives several typical examples of the result alone, without any physical and petrological interpretation of these results. It is evident from the results of the present examination that the magnetization of these rocks, which is chiefly due to the ferromagnetic minerals present in them, changes markedly with temperature, exactly in the same manner as the usual ferromagnetic materials, although the mode of change in the former is usually much more complex than that of the latter. This phenomenon would be a contributive cause in the change in magnetization of the earth's crust, provided there were a a certain temperaturc change. There is, however, no such conspicuous increase of susceptibility in a weak magnetic field as that in the case of iron, usually known as "Hopkinson effect," so far as our experiment went. It is believed that the Hopkinson effect will not appear in a rock, even if the applied magnetic field were as small as 0·1 to 0·5 Oersteds, a field much weaker than that in the present case, since the

demagnetizing factor of the ferromagnetic minerals in the rock is usually very large, namely, 3 or 4, regardless of the smallness of the apparent demagnetizing factor of the whole specimen as a rock. Hence, the mode of change in susceptibility with temperature shown in Figs. 4 ~11 is believed to be general with all igneous rocks.

In conclusion, the writer wishes to express his sincere thanks to Prof. H. Tsuya for his interest and kind advices from the petrological point of view, and to Prof. C. Tsuboi for his continued encouragement in the writer's geomagnetic study of the earth's crust. His hearty thanks are also due, for grants received, to the Department of Education and to the Hattori Hôkô Kai.

---

35. 岩石の帶磁率の溫度に因る變化の測定

地震研究所　永　田　武

岩石の帶磁率の溫度による變化を知る事は地殼の磁性を論ずるには是非共必要な事である．岩石が磁場内で溫度變化を爲す時は一般に熱殘留磁氣の生成，消滅が起きるので，この影響をさける爲に磁場逆轉に依る彈動法を用ひて，帶磁率の溫度による變化の測定を爲した．種々の測定誤差が伴ふので，結局の測定誤差は比帶磁率の絕對値に於いて最高 3×10^{-5} である．從つて 10^{-3} の比帶磁率の測定には 3％の誤差を伴ふ．但し測定に用ひた磁場の強さは 1·5 乃至 2·2 Oersted である．然しこの樣な測定の結果に於いても，岩石の帶磁率の溫度による變化をかなり詳しく求める事が出來た．

測定した岩石試料のすべてに於いて，それ等の帶磁率は 580°C 乃至 600°C の溫度で 0 になる．この溫度は磁鐵鑛の磁氣變態點にほぼ一致する．然し帶磁率と溫度との關係は必ずしも單調でなく本文第 9 圖乃至第 11 圖に示す如く，300°C 附近で著しい變化を示す岩石もある．又溫度變化に對して帶磁率がほぼ可逆的に變化する場合と，著しい非可逆性を示す場合とがある．更に室溫からある溫度迄は溫度の增加と共に帶磁率は一般に若干增加する傾向（但し 1·5~2·2 Oersted の磁場に於いて）が明らかに見られる．この報告では主として測定裝置，及び測定結果の數例を報告するにとどめた．猶ほこの研究は文部省科學研究費，及び服部報公會の研究援助によつて遂行されたものである．兩當事者に對し厚く感謝の意を表する．

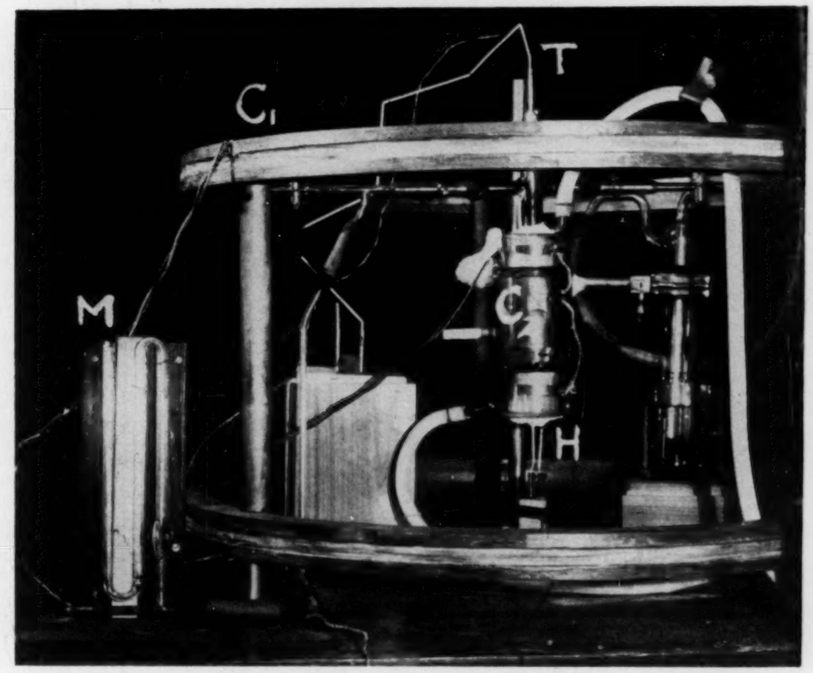

Fig. 3 a. Apparatus for measuring the magnetic susceptibility at high temperature.
C_1, primary coil, C_2, secondary coil,
H, plutinum heater, M, manometer,
T, thermo-junction.

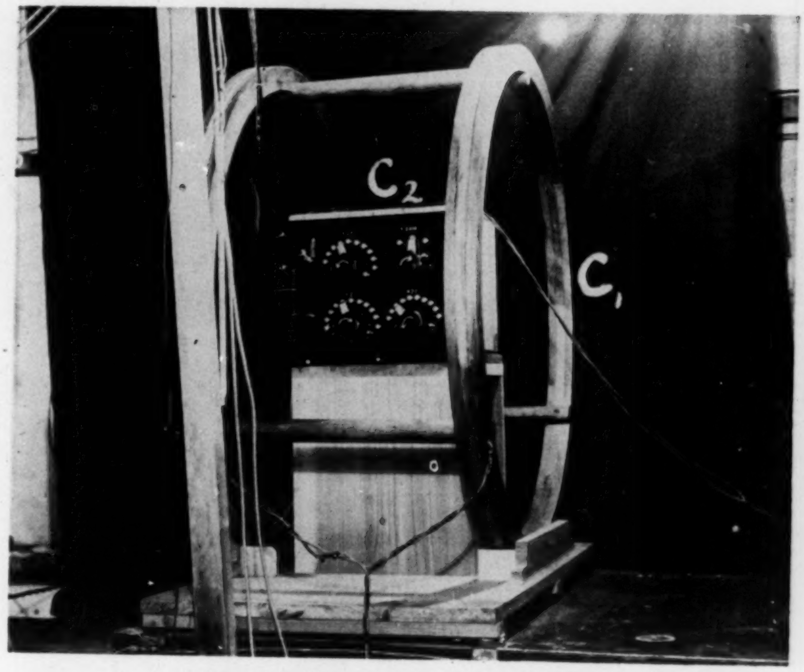

Fig. 3 b. Compensating equipment.
C_1, primary coil, C_2, variable secondary coil.

(震研彙報 第十九號 圖版 永田)

36. *On the Form and Structure of Volcanic Bombs from Volcano Miyake-sima.**

By Hiromichi TSUYA,

Earthquake Research Institute.

(Read Sept. 18, 1941.—Received Sept. 20, 1941.)

Introduction.

In a previous paper[1] dealing with the form and structure of volcanic bombs, with special reference to the origin of the basaltic bombs from Volcano Huzi, a volcanic bomb was defined as a piece of juvenile lava ejected in the air at the time of an eruption, and having (irrespective of size) certain characteristics peculier to one of a few distinct morphological and structural types. With this distinction, the basaltic bombs from Huzi were classified into fourteen types—(1) spindle-shaped, (2) conical, (3) spheroidal, (4) disk-shaped, (5) square, (6) dish-shaped, (7) twin, (8) cylindrical (long), (9) cylindrical (short), (10) leaf blade-shaped, (11) ribbon-shaped, (12) ellipsoidal, (13) goat's horn-shaped, and (14) hemispheroidal bombs. From a study of these bombs both in the field and in the laboratory, it was concluded that the characteristic shape and inner structure of the bombs could probably be traced to the "schlieren" (flow structure) that developed in the flowing lava within the crater from which they were ejected, although subjected to deformation later in their passage through the air.

The results of the writer's studies of volcanic bombs, both in the field and in the laboratory, on the occasion of the last eruption of Volcano Miyake-sima, in July 1940, amply confirm his views regarding their origin.

Mode of Occurrence of Volcanic Bombs.

Miyake-sima, one of the most distinguished basaltic volcanoes in Japan, together with Huzi, O-sima, Hatizyô-sima, etc., are rich in volcanic bombs. On the volcano, the bombs are frequently met with among old and new fragmentary ejecta, scattered about the craters on the

* Dedicated to the late Professor Mishio Ishimoto.

1) H. TSUYA, *Bull. Earthq. Res. Inst.*, 17 (1939), 809~825.

summit as well as on the flanks of the somma, their chief localities so far observed being Akabakkyô, Bôzu-yama, and Oyama, where they occur in the following manner:

Akabakkyô. As already mentioned in a previous paper,[2] in the northern part of the bay of Akabakkyô, near Simasita, on the northeastern foot of the volcano, a submerged crater of unknown age is now buried under the ejecta of 1940. On the cliff of Akabakkyô-hana (point), which before the late eruption (1940) was a sea-cliff facing the former bay, beds of old ejecta are exposed, which, from their structure, are regarded as products of a crater believed to be submerged now in the bay. These beds, which are composed of reddish-brown fragmentary ejecta, are intercalated in the middle horizon of the cliff by a lava-flow, about 3 m thick, dipping about 15° NW. The lava is an augite-olivine-basalt, containing large phenocrysts of anorthite, exceeding 1 cm in diameter. Before the late eruption, the same lava could be seen exposed on the northern shore of the former bay of Akabakkyô, forming a coastal platform, about 15 m above the sea, on which stood the fishing village of Simasita, most of which at present, however, is buried beneath the new Akabakkyô lava-flow of 1940. The fragmentary ejecta, which are petrographically identical with the lava, consist of scoriaceous lapilli, blocks, and bombs, of which, the bombs, 5~30 cm in diameter, occur more thickly in the upper horizon of the ejecta beds than in the lower. Before the late eruption, these bombs were found in great abundance on the lava-platform of Simasita.

The fairly large number of volcanic bombs that were ejected at the time of the eruption of 1940 came from about twenty new craters on the northeastern flank of of the somma, including those thrown up from the bay of Akabakkyô, and along with the other fragmentary ejecta, they have accumulated thickly on the ground around the new craters, particularly around the Hyôtan-yama craters (G and H), crater D, and on the mountain slope adjoining the northern side of the B′ rift-crater.[3] The diameter of most of the bombs exceed 10 cm, the largest one so far found being about 10 m, while those of less than 5 cm are rare. These bombs are divided, petrographically, into two kinds, porphyritic and almost-aphanitic bombs. The porphyritic bombs, which were ejected exclusively from the Hyôtan-yama craters, are augite-olivine-basalt, containing large megascopic phenocrysts of anorthite, while the aphanitic bombs, which were projected from all the new

2) H. TSUYA, *Bull. Earthq. Res. Inst.*, **19** (1941), 265.
3) H. TSUYA, *Bull. Earthq. Res. Inst.*, **19** (1941), 650.

craters, except those from Hyôtan-yama, are basaltic andesite. Judging from the distribution of these bombs, most of them were ejected from a crater at a late stage of its eruption. For example, although Hyôtan-yama is thickly covered with porphyritic bombs, its inner part as seen on the sea-cliff on its eastern side, is largely composed of beds of reddish-brown, scoriaceous lapilli and blocks, underlain by a lava-flow (Hyôtan-yama lava).

Bôzu-yama. Bôzu-yama, which is a parasitic knob, lying halfway up the north-northeastern flank of the somma, is thickly covered with fragmentary material ejected by the eruption of 1874. The fragmentary material occurs as black, scoriaceous lapilli, crystal-lapilli of anorthite, and volcanic bombs. Of these, the bombs are found in great numbers in a small area on and around the top of the mound, suggesting that they are products of a later stage of the eruption. Although ejection of the fragmentary material was followed by outpouring of lava, the latter occurred from a vent lying some distance away from the vents of the former. Thus, the lava-flow of 1874 outpoured from a deep fissure-like opening, situated about 550 m above the sea, outside the western wall of the Kosiki-ana parasitic crater on the north-northeast slope of the somma, and descended the mountain slope northward into the sea, east of the village of Kamituki, while the fragmentary ejecta, which occupy a wide area adjoining the eastern margin of the lava-flow, including Bôzu-yama, were ejected, mostly previous to the lava outpouring, from several openings, which, together with a number of fissure-like depressions, are arranged in a zone running from the vent of the lava NNE toward Bôzu-yama.

The volcanic bombs from Bôzu-yama are fairly small, their diameters being generally less than 5 cm. Petrographically, they are identical with the lava of 1874, which is an augite-olivine-basalt, containing large megascopic phenocrysts of anorthite.

Oyama (the central cone). Before the eruption of 1940, the central cone Oyama, situated slightly south of the caldera on the top of the somma, was truncated at the top, with walls surrounding a composite crater, consisting of three bowls aligned in an east-west direction—the first (the easternmost), the second (Oana), and the third (the westernmost) craters. Along with scoriaceous lapilli and anorthite crystal-lapilli, volcanic bombs were thickly scattered about the floor of of the first crater, being underlain by a lava more than 20 m thick which, as inferred from an exposure on the eastern wall of the second crater, must have once formed a lava-lake that filled the first crater. Similar bombs were also found on the slope outside the northeastern rim

of the first crater, as well as in the northeastern part of the Hayono-tairo atrio, although they are now buried beneath the material thrown out by the late eruption. The bombs, the largest of which have a diameter of about 2 m, differ petrographically from the rock of the solidified lava-lake in the first crater. The former is an augite-olivine-basalt, containing large megascopic phenocrysts of anorthite, while the latter is an almost aphyric augite-olivine-basalt, without any conspicuous megascopic phenocrysts, except a few very small olivine and plagioclase (anorthite-bytownite). Judging from their fresh appearance in the field as well as in the laboratory, the bombs must have been ejected, together with the other fragmentary material that accompanied them, from the second crater in the remote past.

During the summit eruption that lasted from July 13 to August 5, 1940, a large number of bombs were ejected together with other fragmentary ejecta, from the second and the third craters on the central cone, resulting in the formation of a new composite central cone in the craters. The bombs are scattered over an oval area, measuring about 850 m from WNW to ESE, with the new central cone as the centre. Thus they lie scattered in the central part of the Hayono-tairo atrio as well as on the ground outside the southern rim of the second crater (Oana). On the northern flank of the old central cone a considerable number of bombs are found that reach a maximum diameter of about 3 m. Similar large bombs are also found on the southeastern part of the crater bottom of Oana, adjacent to the southeastern foot of the new central cone, where they are accumulated perhaps more than 10 m deep, together with smaller ejecta. A number of smaller bombs, 1～5 cm in diameter, are accumulated, together with scoriaceous lapilli and sand, on the floor of the first crater, where formerly bombs, lava-blocks, and anorthite lapilli of unknown age were found.

Although the summit eruption of 1940 began in the night of July 12/13, the ejection of new volcanic bombs first became notable about a week later. Thus, during the four days that ended July 18, fragments of the old cone material alone were ejected in the form of ash and sand; during the next two days, angular blocks of the old cone material were ejected along with those of a fresh, dense lava that were probably torn off by the force of the explosions from the top of the lava plug that had risen near the crater floor from the interior of the volcano. The next day (July 21) in addition to ash, a juvenile lava began to pour out in the form of scoriaceous lapilli; and lastly, since the middle of the night of July 22, bombs were ejected every few seconds, together with ash,

lapilli, and lava-blocks, until Aug. 5, when the summit eruption practically ceased.

On the northwestern foot of the new central cone is a new lava coulee circumscribed on all sides by the rim of the third (westernmost) crater, except on its southeast, where it is buried beneath the new central cone. The western front of the coulee bulges out only a few meters westward over the rim of the western wall of the crater. Although we do not know when this lava extruded, it is inferred that it appeared in the form of a lava-pool in the crater where the eruption was going on, already before the new central cone had attained its present size, and that the level of the lava-pool had risen sometime, between July 25 and 31, as high as the western rim of the old third crater, where the lava was about to flow over the crater rim. The lava coulee is covered with fragmentary ejecta, including quite a number of volcanic bombs, which accumulated more than 1 m deep in the southeastern part near the foot of the new central cone. Petrographically, the new bombs are identical with the new lava, both being an almost-aphanitic olivine-two-pyroxene-basaltic andesite.

Form and Inner Structure of Volcanic Bombs.

So far as the specimens of more than a hundred volcanic bombs collected by the writer from Miyake-sima are concerned, they may be grouped, according to their external forms, into twelve types, as follows:

1) Spheroidal (Fig. 1)
2) Disk-shaped (Fig. 2)
3) Ellipsoidal (Fig. 3)
4) Conical (Fig. 4)
5) Square (Fig. 5)
6) Spindle-shaped (Figs. 6 a—d)
7) Cylindrical (short) (Fig. 7)
8) Cylindrical (long) (Fig. 8)
9) Leaf blade-shaped (Fig. 9)
10) Goat's horn-shaped (Fig. 10)
11) Ribbon-shaped (Fig. 11)
12) Twin bombs. (Figs. 12 a—d)

Morphologically, these types are almost identical with the respective types of bombs from Volcano Huzi, so that there is no need to describe their external forms once more. It is, however, notable that the twin bombs from Miyake-sima have a greater number of forms than bombs of similar type from Huzi. Thus, the twin bombs from Huzi have the

shape of a fiddle, only they are not flat, but consist of two lumps, joined together at the middle, with their longer axes in common, while the twin bombs from Miyake-sima consist of two bomb-shaped lumps which, besides being joined together in the shape of a gourd, as in Fig. 12 a, in contact with each other either in a parallel position, as in Fig. 12 c, or in an oblique position, as in Figs. 12 b, 12 d. Although the Huzi bombs include dish-shaped and hemispheroidal bombs, besides the twelve types mentioned above, neither of these two types is represented in the samples from Miyake-sima.

The bombs, except the spheroidal, disk-shaped, and square forms, frequently have either parallel grooves or ridges on their surfaces in the direction of their longer axes (Fig. 6 d). Regardless of these grooves or ridges, most of them have uneven surfaces, to which are sometimes attached irregularly shaped lumps of the same material as the bombs themselves. There are besides various transitional forms, ranging from the typical bombs to the irregularly shaped lava-blocks, as extreme examples of which are lava-blocks on the surface of which a bomb-like form is partially developed, as shown in Figs. 15 a—c.

The types just enumerated are most common in those of diameters ranging from about 5 cm to 10 cm, although a large proportion of them are also met with in smaller bombs, as shown in Figs. 13, 14. The larger bombs, having an extreme diameter of several meters, are usually spindle-shaped, disk-shaped, spheroidal, and ellipsoidal.

The inner structures of these bombs exhibit multifarious types according to their external forms. So far as have been observed in sections cut from several bombs of different morphological types, we have the following four principal structural types:

Type A.

Bombs of this type have solid inclusions in their cores. Petrographically the inclusions are divided into three kinds—juvenile, accessory, and accidental inclusions. The juvenile inclusions are represented by isolated crystals of anorthite (Fig. 16) and an allivalitic aggregate of anorthite and olivine (Fig. 17), besides lava-fragments which, petrographically, are identical with the bomb-forming lava with which they are coated. These crystal-inclusions are frequently met with in the bombs of 1874 (Bôzu-yama) and the Hyôtan-yama bombs of 1940. They are nothing but segregations in the bomb-forming lavas, seeing that both the lava of 1874 and the Hyôtan-yama lava of 1940 contain large megascopic phenocrysts of anorthite and olivine.

The accessory inclusions are represented by fragments of the old cone material, which differ only slightly in microscopic texture and

mineral composition from the bomb-forming lavas in which they are enclosed (Figs. 20, 21).

The accidental inclusions are fragments of foreign rocks which must have come from the wall of the volcano conduit at depth, and which are believed to represent the rocks that lie underneath the volcano. The writer collected two spheroidal bombs from the new central cone of 1940, in which accidental inclusions were found. One of them carries a block of tuff (Fig. 18), about 5 cm in diameter, and the other a block of an acid, porous rock (Fig. 19), about 10 cm in diameter.[4]

Bombs of the foregoing type are mostly spheroidal, disk-shaped, or spindle-shaped, although the inclusions that are found in their cores have various shapes. Microscopic examination of thin sections of these bombs shows that the lava-crust of such a bomb, which surrounds an inclusion, has a flow structure. Thus the lath-shaped crystals (plagioclase and pyroxene) that are found in the lava-crust show a parallel disposition in consequence of the flow of lava around the inclusion, their longer axes being roughly tangential to the outline of the inclusion (Figs. 21 b—c). The parallel arrangement of the crystals is seen more regularly in the outer part of the lava-crust than in the inner part near the surface of the inclusion. In the outermost part near the surface of the bomb, the flow-lines as revealed by the crystal-arrangement follow almost exactly the outline of the bomb.

Type B.

Bombs of this type have a zonal structure (or shell-structure), consisting of thin lava-layers which are alternately vesicular and compact, but which are exclusively of the same juvenile material. This structure is most frequently seen in the spindle-shaped and ellipsoidal bombs (Figs. 22~27).

The zonally-built bombs have a core which may be either vesicular or compact, in a variety of forms and sizes. Sometimes the core has the same form as the external form of the bomb in which it is found (Figs. 22, 27); and although the core is usually single, it occasionally occurs as a doublet (Figs. 24, 25). In some zonally-built bombs that belong also to type A, their cores may be the one of the two kinds of inclusions (juvenile and accessory) just mentioned.

---

4) The tuff contains a large amount of anhydrite, while the acid, porous rock consists wholly of colorless glass, except dust material and a few fragments of quartz and feldspar. These rocks are more or less thermally metamorphosed. Petrographic descriptions of them will be given in Part III of the paper on the eruption of Miyake-sima in 1940, Parts I and II of which have already appeared in this Bulletin, 19 (1941).

The outer shells of the zonally-built bombs surround the cores successively outward, conforming to the outlines of the latter. Thus in the longitudinal section of a flattened spindle-shaped bomb (Fig. 22), the shells show a lenticular flow-banding. In certain spindle-shaped and ellipsoidal bombs, the transverse sections of which are nearly circular, the shells are either concentric or there are spiral bandings surrounding the core. Not all the layers forming the shells of a bomb run the whole length around its core, some layers thinning out to half the size. Often, the two adjoining layers of the shells have gaps between them (Fig. 22). The shells of a bomb containing such gaps can be torn off one by one (Fig. 6 d).

Microscopically, the lath-shaped crystals in type B bombs, like those in type A, show a parallel disposition in consequence of flow according to the zonal banding (Figs. 27 b, c).

Type C.

Bombs of this type have a cavity in their cores (Fig. 28). They are frequently met with among bombs of the spheroidal, disk-shaped, ellipsoidal, and spindle-shaped types. Besides the cavity in the core, some large cavities are occasionally met with slightly below the surface of the bomb. In a spindle-shaped bomb, these cavities are drawn out in the direction of the longer axis of the bomb (Fig. 29).

Type D.

Bombs of this type have relatively smooth surfaces, and are compact inside. They are occasionally found among bombs of every morphological type (Figs. 30~33). Some of them are nothing but compact cores of bombs of type B that had been stripped of their shells at the time when they fell upon the ground.

Although these bombs are more or less compact fragments of a juvenile lava inside, good sections of the majority of them show either zonal structure or flow-pattern as recognized by differences in color of the various parts of the sections (Figs. 30, 31, 33). These structures are seen most clearly in thin sections of compact bombs (Figs. 32 a, 34~38, 39 a, 40 a). Thus thin sections show that these bombs consist of two parts, one darker in color than the other, which are arranged either zonally or in some complicated flow pattern. Microscopically, the groundmass of the darker part is thickly crowded with an opaque, black material, including a large proportion of magnetite granules, while the groundmass of the lighter part contains a light-brownish glass in place of the black material.

The lath-shaped crystals in bombs of this type also show a parallel arrangement following the outer form and the inner structure of the

bombs. This parallel arrangement is usually more regular in the lighter-colored part than in the darker part (Figs. 32 b, 39 b, 40 b, 40 c). The microscopic vesicular cavities with which bombs of the present type are often studded, also show banded arrangement conforming to the parallel arrangement of the crystals (Fig. 40 c).

Origin of Volcanic Bombs.

From his studies of the basaltic bombs from Huzi, the writer concludes that the characteristic shape and inner structure of the bombs originated from flow-banding ("Schlieren") that developed in the flowing lava within the crater from which they were ejected, subjected, however, to deformation in their passage through the air—a conclusion that applies also to the basaltic bombs from Miyake-sima, which, as mentioned above, show almost the same morphological and structural features as the Huzi bombs, besides some additional characteristics that further support the conclusion. The various inner structures of the Miyake-sima bombs are thus regarded as showing fluxion phenomena, including flow lines, parallel arrangement of crystals, banding, drawing out of vesicles, etc., that developed in the conduit lava from which they were ejected. The origin of these structures in the conduit lava is interpreted as due to segregation of phenocrystic minerals, capturing of xenoliths, irregular cooling, and local segregation of gas bubbles, forming vesicular parts in the lava at a shallow horizon near the top of the conduit, where the lava probably remains in a state of viscous, differential flow.

Although the outer forms of the bombs conform to their inner structures, it is unlikely that the latter were formed under the control of the former during the cooling of the bombs after they were thrown out from a crater. On the contrary, it is probable that the outer forms of the bombs were virtually determined by their inner structures, and consequently by the various structural heterogeneities just referred to in the lava from which they were torn off by volcanic explosions. Although the bombs might have deformed in their passage through the air as well as in striking the ground, it is not likely that the deformation was of such a nature as radically to change theis original shape and inner structure. For example, the origin of the shape and inner structure of the spindle-shaped bombs cannot be regarded as due to their rotatory motion in the air, seeing that, in the writer's experience, few bombs, if any at all, show in their flight upward into the air rotation of such high velocity as would explain some of the spindle-shaped bombs. For example, in July 25, 1940, when the writer was observing the summit

eruption of Miyake-sima at close range, some of the long and slender bombs were seen to revolve about their shorter axes in flying up into the air, but at a rate of only once or twice a second.

In short, most of the external forms and inner structures of basaltic bombs are believed to be virtually determined by the structural pattern of the lava from which they were detached by the force of the explosion. When the lava has an intricate flow-banding caused by local vesiculation, segregation of crystals, capturing of xenoliths, etc., it is liable to be broken by the force of the explosion into pieces along a boundary surface of least resistance between two adjoining layers in the banding, resulting in various kinds of bombs.

EXAPLANATION OF PLATES.

Volcanic Bombs from Miyake-sima.

Fig. 1. Spheroidal bomb (×2/3).
Fig. 2. Disk-shaped bomb (×2/3).
Fig. 3. Ellipsoidal bomb (×2/3).
Fig. 4. Conical bomb (×2/3).
} Ejecta of 1940. Locality: Oyama.

Fig. 5. Square bomb (×2/3). Ejecta of 1874. Locality: Bôzu-yama.

Figs. 6 a—d. Spindle-shaped bombs (×2/3).
Fig. 7. Cylindrical (short) bomb (×2/3).
Fig. 8. Cylindrical (long) bomb (×2/3).
Fig. 9. Leaf blade-shaped bomb (×2/3).
Fig. 10. Goat's horn-shaped bomb (×2/3).
Fig. 11. Ribbon-shaped bomb (×2/3).
} Ejecta of 1940. Locality: Oyama.

Figs. 12 a—d. Twin bombs (natural sizes). Ejecta of 1874. Locality: Bôzu-yama.

Figs. 13 a—f. Various forms of smaller bombs (natural sizes). Ejecta of 1940. Locality: Oyama.

Fig. 14. Various forms of smaller bombs (natural sizes). Ejecta of 1874. Locality: Bôzu-yama.

Figs. 15 a, b. Lava-blocks in which bomb-shaped parts are developed. (×1/2). Ejecta of 1940. Locality: Oyama.

Fig. 15 c. Do. Ejecta of 1874. Locality: Bôzu-yama.

Fig. 16. Section of a spheroidal bomb containing a large anorthite crystal in the core (natural size).
Fig. 17. Section of a spindle-shaped bomb containing an allivalitic segregation in the core.
} Ejecta of 1940. Locality: Hyôtan-yama.

Fig. 18. Section of a spheroidal bomb with an accidental xenolith (a white tuff containing anhydrite in the core (natural size).

Fig. 19. Piece of a spheroidal bomb with an accidental xenolith (an acid, glassy rock) in the core (natural size).

Fig. 20. Section of a spheroidal bomb with an accessory inclusion (porphyritic olivine-pyroxene-andesite) in the core (natural size).

Fig. 21 a. Section of a spheroidal bomb with an accessory inclusion (porphyritic augite-andesite) in the core (natural size).

Fig. 21 b. Thin section of the same bomb.

Fig. 21 c. Microphotograph of the part marked by a circle in the same thin section (×10).

Fig. 22. Section of a spindle-shaped bomb showing a zonal banding (natural size).

Fig. 23. Cross section of a cylindrical (short) bomb, showing a concentric zonal structure (×2/3).

Fig. 24. Section of a disk-shaped bomb, showing vesicular shells and compact lenticular cores (natural size).

Fig. 25. Cross section of a spindle-shaped bomb, showing two lenticular cores surrounded by scoriaceous shells (×2).

Fig. 26. Longitudinal section of a spindle-shaped bomb having a scoriaceous core (×1/2).

Fig. 27 a. Longitudinal section of a spindle-shaped bomb, show a lenticular compact core surrouuded by scoriaceous shells (natural size).

Fig. 27 b. Thin section of the same bomb.

Fig. 27 c. Microphotograph of the part marked by a circle in the same thin section (×10).

Fig. 28. Ellipsoidal bomb containing a lenticular cavity in the core (×2/3).

Fig. 29. Spindle-shaped bomb, containing cylindrical cavities, drawn in the direction of its longer axis (natural size).

[Figs. 18~29. Ejecta of 1940. Locality: Oyama.]

Fig. 30. Cross section of a spindle-shaped bomb, showing the compact inside (× 2/3). Ejecta of 1940. Locality: Hyôtan-yama.

Fig. 31. Cross section of a spindle-shaped bomb, showing the compact inside (natural size). A faint zonal structure is seen by difference in color of the core and the shells. Ejecta of 1940. Locality: Oyama.

Fig. 32 a. Longitudinal thin section of a spindle-shaped bomb (Fig. 6 a), showing flow-banding as recognized by differences in color of the various parts inside (×3/2).

Fig. 32 b. Microphotograph of the part marked by a circle in the same thin section (×10). Flow-structure is exihibited by a parallel disposition of the crystals. Ejecta of 1940. Locality: Oyama.

Fig. 33. Section of a square bomb (Fig. 5), showing a flow-structure as recognized by differences in color of its various parts (natural size).

Fig. 34. Cross section of a twin bomb (Fig. 12 c), showing a zonal structure as recognized by differences in color of the core and the crust. The left and right parts of the core correspond respectively to the two halves of the twin.

Fig. 35. Basal section of a compact, disk-shaped bomb, showing a zonal structure as recognized by differences in color of the core and the crust (×3/2).

Fig. 36 a. Basal section of a compact flat-ellipsoidal bomb, showing an intricate flow-structure as recognized by differences in color of its various parts (×3/2).

[Figs. 35, 36 a: Ejecta of 1874. Locality: Bôzu-yama.]

Fig. 36 b. Microphotograph of the part marked by a circle in the same thin section, showing flow-banding (×30).

Fig. 37. Longitudinal thin section of a long spindle-shaped bomb, showing flow-banding (×3/2).

Fig. 38. Thin cross section of a compact, spindle-shaped bomb, showing zonal structure as recognized by difference in color of the core and the shells (×3/2).

Fig. 39 a. Cross thin section of half of disk-shaped bomb, showing zonal structure as recognized by differences in color of the core and the shells (×3/2).

Fig. 39 b. Microphotograph of the part marked by a circle in the same thin section (×10).

} Ejecta of 1940. Locality: Oyama.

Fig. 40 a. Thin cross section of a spindle-shaped bomb, showing a zonal structure as recognized by linear arrangement of vesicles as well as by differences in color of the core and the shells (×3/2). Ejecta of 1940. Lacality: Oyama.

Fig. 40 b. Microphotograph of the part marked by a circle in the same thin section, showing flow-arrangement of the crystals (×10).

Fig. 40 c. Microphotograph of a part marked by a double circle in the same thin section, showing flow-arrangement of both crystals and vesicles (×25).

36. 三宅島産火山彈の形態及び構造に就いて

地震研究所 津 屋 弘 逵

筆者は先に富士火山産玄武岩火山彈の形態及び構造を研究し，それ等の本源が火山彈として拋出される前の噴火口内熔岩の流狀構造に求められることを推論した．本文では更に三宅島產火山彈の形態及び構造を觀察した結果を揭げ，此の場合にも同樣の推論を成し得る幾多の事實のあることを述べた．

三宅島は富士山，大島，八丈島等と共に玄武岩質火山彈を時に多量に產出する火山の一つであつて，特に同島山頂の中央火口丘（雄山）の火口附近，北東岸赤場曉附近，北腹坊主山等に多くの火山彈が見出され，また昭和15年噴火の際には，北東山腹に生じた新火口及び山頂に生じた新中央火口丘から多くの火山彈が拋出された．之等の火山彈は噴火口附近に特に多く，且つ他の同期噴出物の比較的上位に多く堆積し，一噴火の末期近くに噴火口附近に限つて多く拋出された事を示してゐる．例へば坊主山では，明治7年噴出の火山彈がその山頂附近に多量に見出され，同山の北東麓から北東海岸に亙つて堆積してゐる同年噴出の岩滓質砂礫層中には殆ど見出されない．之等の火山彈及び砂礫は同年噴出の熔岩流に先立つて拋出されたものであるが，兩者は噴出口を異にするのであつて，前者は坊主山頂上附近に形跡を留めてゐる裂罅狀火口から拋出されたのである．また昭和15年噴火の際に赤場曉灣內に生じた瓢簞山に於いても，その噴火口を中心として半徑約600 m の圓周地域內の地表に多くの火山彈が堆積してゐるが，同山東部の新海蝕崖で觀察される樣に，同山の內部を構成する物質卽ち比較的早期の噴出物は熔出流と岩滓質砂礫とであつて，火山彈を多く雜へてゐない．

三宅島で採集された100個餘の新舊火山彈は形態的特徵の上から次の12型に分類される．(1) 球形，(2) 圓盤形，(3) 楕圓體形，(4) 圓錐形，(5) 角盤形，(6) 紡錐形，(7) 柱形，(8) 棒形，(9) 葉片形，(10) 牛角形，(11) リボン形，及び (12) 双子形火山彈．之等の 12 型火山彈の形態的特徵は富士山火山彈に就いて分類された14型中の12型のそれに各々共通してゐる．たゞ後者中の2型卽ち皿型及び半球形火山彈に類するものは三宅島からの採集品中には見當らなかつた．また富士山に於いて見出された双子形火山彈は大小2個の火山彈が瓢簞形に連なつたかの如き形態を示す標品1個に過ぎなかつたが，三宅島火山彈中（特に坊主山產の明治7年火山彈）には双子形のものが屢々見出され，その中には，二つの個體が瓢簞形に連なるものゝ外に，兩個體か平列するもの，交叉するもの等がある．また不規則な形の熔岩塊の一部に火山彈の一面の形が發達してゐるものも見出される．

內部構造の上から見ると，三宅島火山彈は大體4種類に分かたれる．卽ち，その4種は (1) 核心に包裹物を有する火山彈，(2) 肉眼的の絮帶狀構造を示す火山彈，(3) 核心に空隙を有する火山彈，及び (4) 肉眼的に一樣に緻密質の火山彈である．

第一種火山彈の核心を成す包裹物としては，灰長石の單獨結晶，灰長石と橄欖石との集塊，舊熔岩片，火山の基盤岩の破片等が見出される．斯る包裹物を取圍む皮殼卽ち火山彈熔岩中の柱狀結晶（斜長石及び輝石）は包裹物を取巻いて流理構造を示す．而して，此の結晶の流狀配列は包裹物に接近する部分よりも火山彈の表面に近い部分に於いて一層整ひ，同表面の外郭線に略一致してゐる．

第二種火山彈はその表面から中心まで一續きの熔岩によつて構成されてゐるが，比較的緻密質の部分と多孔質の部分とが外形に應じて累帶構造を成してゐる．卽ちその核心部は緻密質又は多孔質で，それを取卷いて緻密質及び多孔質部が交互に相重なる．而して二つの累帶がその境の空隙によつて分離してゐる部分が屢々見られる．火山彈の皮殼は斯る部分に沿つて剝がれ易い．累帶構造を成す部分の各帶に含まれる柱狀結晶は累帶の方向に一致する流理構造を示し，また小氣泡は屢々同方向に連なり且つ引延ばされてゐる．

第三種火山彈の核心を成す空隙を取卷く熔岩も亦屢々累帶構造を示し，その中の柱狀結晶は流理構造を示す．長形の火山彈の或ものには中心以外にも比較的大きい空泡が在り，之等の空泡は火山彈の長軸方向に平行に引延ばされ夫々の圓筒を形成してゐることがある．然し核心部から外殼まで一樣に多數の氣孔が發達する樣な多孔質の火山彈は見出されない．

第四種火山彈には，緻密な核心を有する帶殼狀火山彈が地表に落下して後に皮殼を剝取られたものもある．一般に此の種の火山彈は肉眼的に一樣に略緻密であるが，その斷面は部分的に濃淡の色の差異に依つて累帶構造或は流理構造を示す事が多い．顯微鏡下では之等の構造が一層明瞭に認められる．卽ち斷面が肉眼的に略一樣に緻密で部分的の色の差異の認められない火山彈でも，その薄片は顯微鏡下では勿論，肉眼的にも黑色部と淡灰色部との累帶，層狀或は流理構造等を示す．顯微鏡下では，黑色部は石基中の斜長石及び輝石粒の間隙を鐵鑛粒を含む不透明物質に依つて塡められ，淡灰色部は石基結晶の間隙に比較的多量の褐色玻璃を殘してゐる．累帶構造を示す薄片では，その核心は黑色部によつて，その周圍の皮殼は一重の淡灰色部或は兩部の累帶によつて代表される．核心の黑色部には柱狀結晶の流理構造なく，周圍の皮殼部には同構造がよく發達してゐる．二つの個體が平行に連接する双子火山彈の橫斷面の薄片では，各個體の核心に當たる部分に夫々の黑色部が在り，相互にS字狀に連なる．また此の種の火山彈では，顯微鏡的の小氣孔が累帶或は流理構造に一致して數列に連なつてゐる事が少くない．

以上に述べた三宅島火山彈の產狀，形態，及び構造に就いて觀察し得た事實を綜合すると次の事が云はれる．

火山彈が噴火口の附近に限つて多く分布し，且つ他の噴出物に對して比較的上位に多い事實はその拋出が一噴火期の末期に於いて噴火勢力の減退しつゝある間に多く行はれることを示す．從つて火山彈の形成は熔岩片が空中に拋出されてから後の條件に左右されるのでなくて，主として火口內熔岩の活動狀體，卽ち內的條件に支配されるものと考へられる．若し火山彈が單に火口から熔岩片としての飛出し方や空中を飛行中の運動の仕方に支配されるものとすれば，噴火時期の前後を問はず形成されるはずであるが，噴火の最盛期に拋出されるものは主として岩滓狀砂礫であつて，一樣に岩滓狀多孔質の熔岩片は火山彈としては見出されない．卽ち火口內熔岩が比較的多量の火山瓦斯に飽和或は過飽和してゐる間の噴火では火山彈は形成され難いものと考へられる．

火山彈がその形態的特徵によつて種々の型に分たれ，普通一般に火山彈と呼ばれる紡錘形のそれが單にその中の特別の一型に過ぎない事實は火山彈の形成が空中飛行中に於ける或特定の運動に因つては行はれ難い事を示すものである．例へば，空中飛行中に於ける火山彈の廻轉が紡錘形火山彈の形成を說明し得る程著しいものでない事は昭和 15 年噴火の際に實見し得た所である．

火山彈の內部の緻密部と多孔部，或は結晶部と多玻璃部との累帶或は層狀構造，柱狀結晶の流理構造，一方向に長く引延された氣孔或は氣孔の列等が火山彈の空中飛行中或は地上落下後に生ずるものとしては到底說明されないであらう．之等の存在する事實は火山彈拋出當時の火口內熔岩が旣に斯る構造を有し，また氣孔を生ずる火山瓦斯に比較的乏しく且つ粘稠度を增してゐた事

Fig. 1.

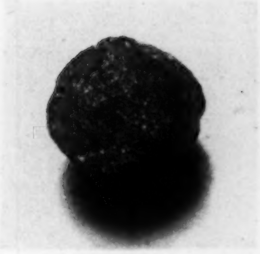

Fig. 2.

Fig. 3.

Fig. 4.

Fig. 5.

Fig. 6 a.

Fig. 6 b.

Fig. 6 c.

Fig. 6 d.

Volcanic Bombs from Miyake-sima.

（震研彙報 第十九號 圖版 津屋）

Fig. 7.

Fig. 8.

Fig. 9.

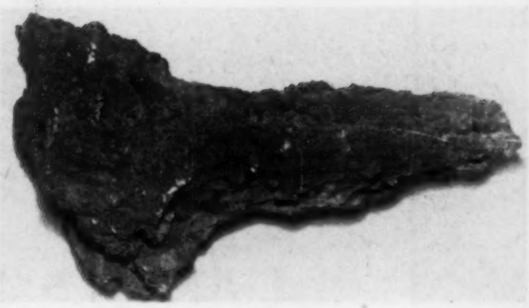

Fig. 10.

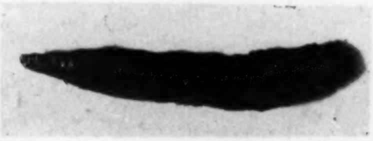

Fig. 11.

Fig. 12 a.

Fig. 12 b.

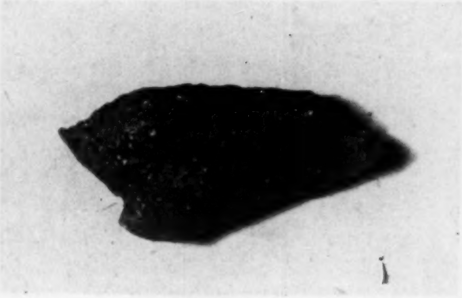

Fig. 12 c.

Fig. 12 d.

Volcanic Bombs from Miyake-sima.

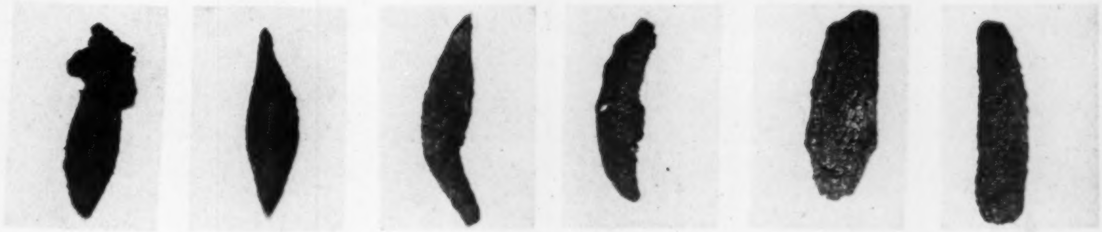

a b c d e f

Fig. 13.

Fig. 14.

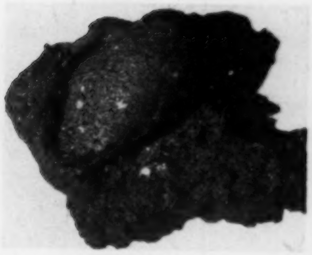

Fig. 15 a.

Fig. 15 b.

Fig. 15 c.

Volcanic Bombs from Miyake-sima.

Fig. 16.

Fig. 17.

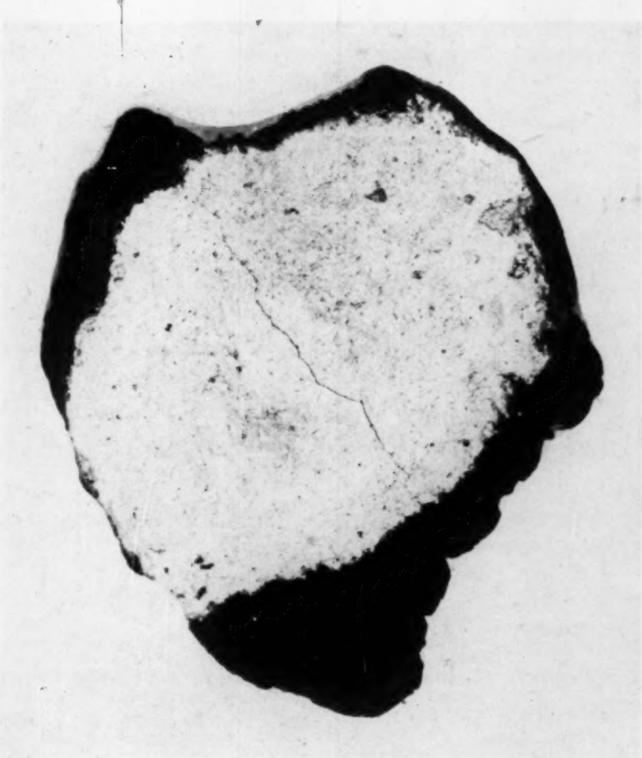
Fig. 18.

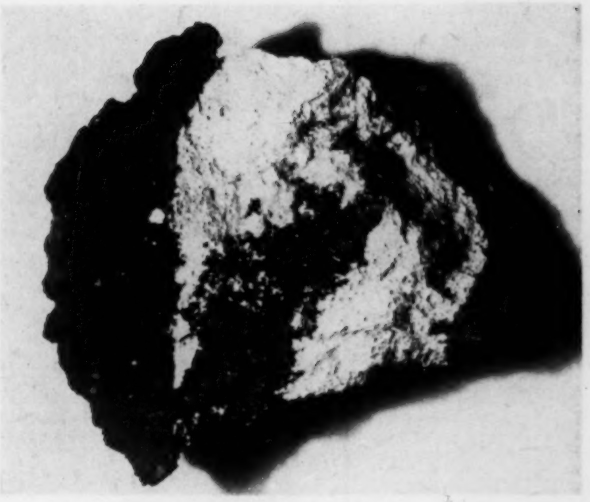
Fig. 19.

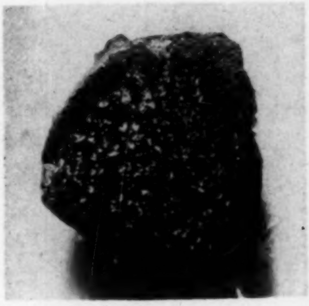
Fig. 20.

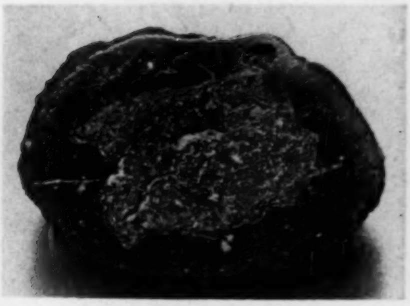
Fig. 21 a.

Volcanic Bombs from Miyake-sima.

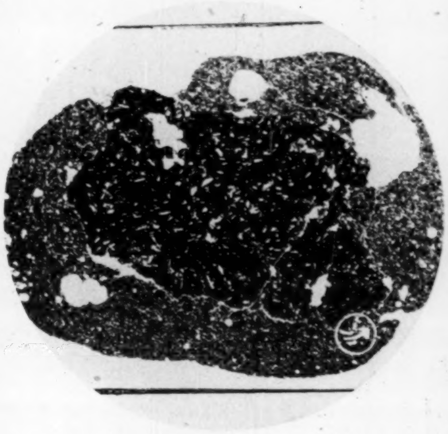

Fig. 21 b.

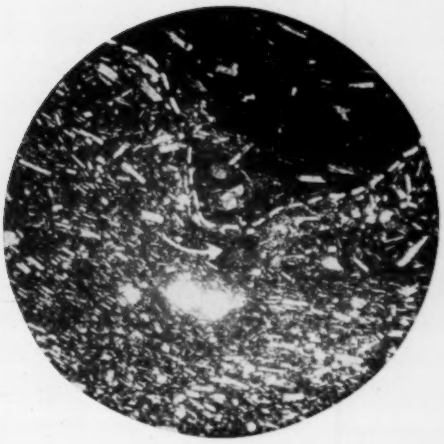

Fig. 21 c.

Fig. 22.

Fig. 23.

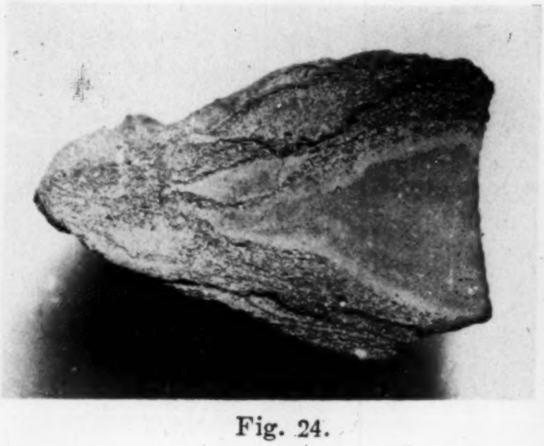

Fig. 24.

Fig. 25.

Volcanic Bombs from Miyake-sima.

(震研彙報 第十九號 圖版 津屋)

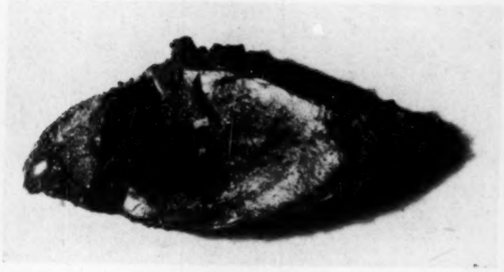

Fig. 26.

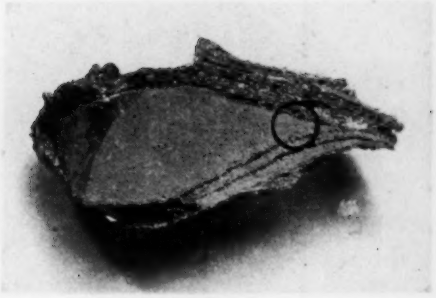

Fig. 27 a.

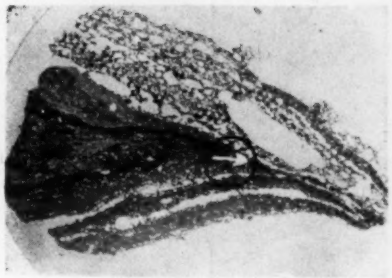

Fig. 27 b.

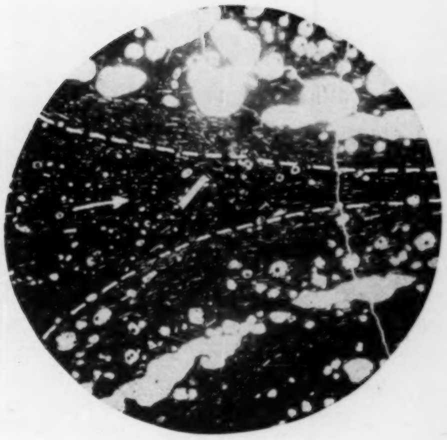

Fig. 27 c.

Fig. 28.

Fig. 29.

（震研彙報 第十九號 圖版 津屋）

Volcanic Bombs from Miyake-sima.

Fig. 30.

Fig. 31.

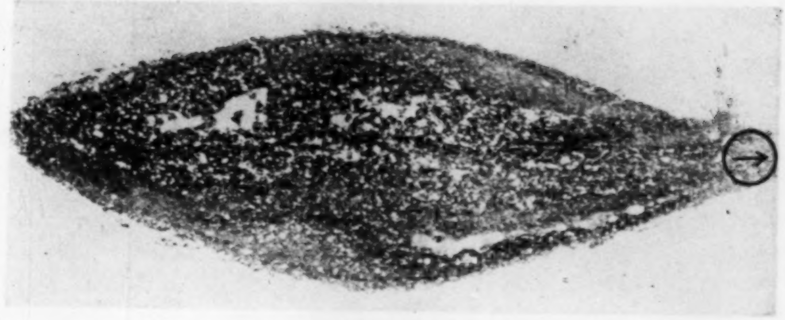

Fig. 32 a.

Fig. 33.

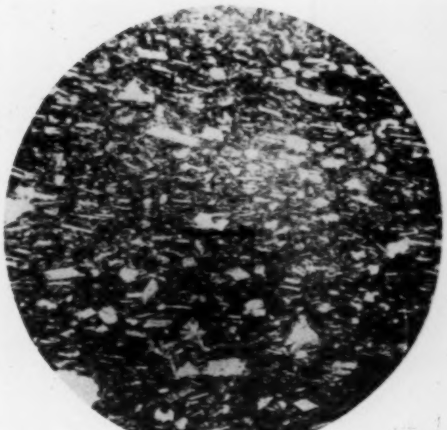

Fig. 32 b.

Volcanic Bombs from Miyake-sima.

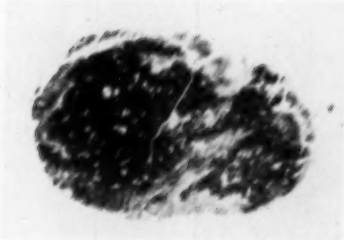

Fig. 34.

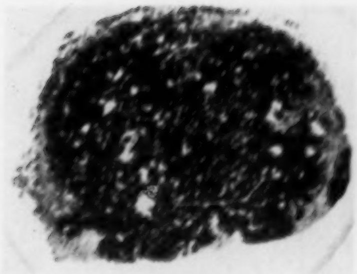

Fig. 35.

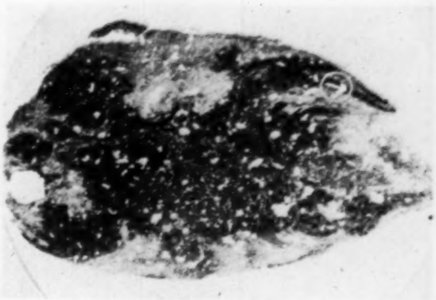

Fig. 36 a.

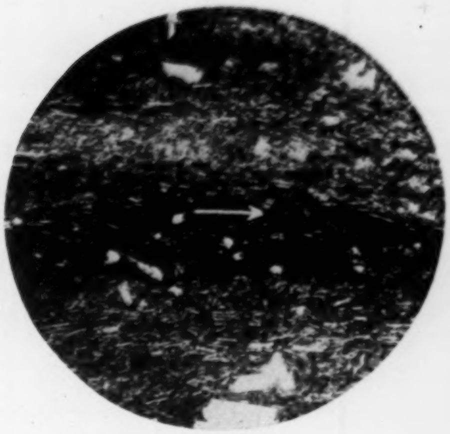

Fig. 36 b.

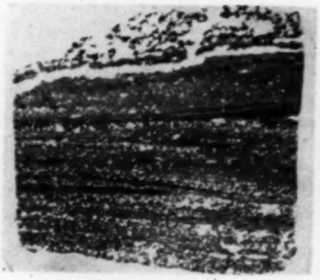

Fig. 37.

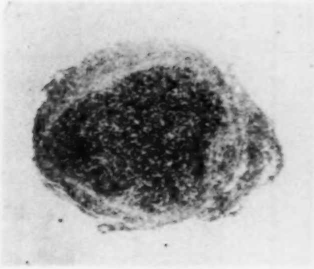

Fig. 38.

Volcanic Bombs from Miyake-sima.

(震研彙報 第十九號 圖版 津屋)

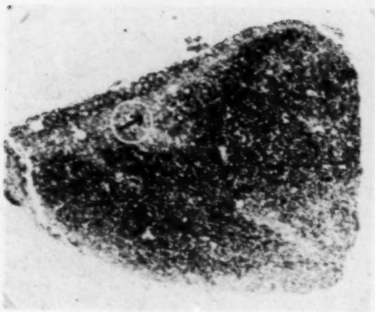

Fig. 39 a.

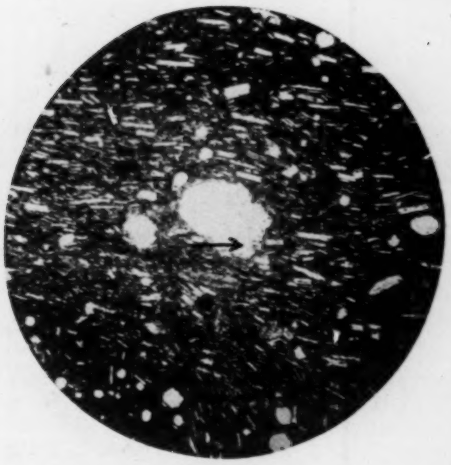

Fig. 39 b.

Fig. 40 a.

（震研彙報 第十九號 圖版 津屋）

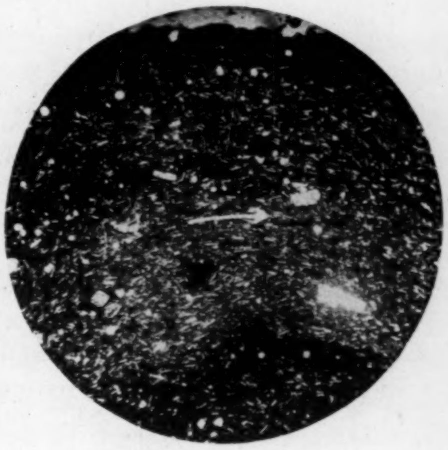

Fig. 40 b.

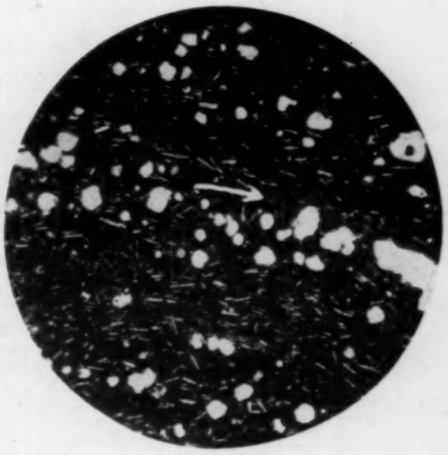

Fig. 40 c.

Volcanic Bombs from Miyake-sima.

を示すものと考へられる．從つてまた累帶構造や流理構造などが火山彈の外形に常に整合的である事實は火山彈の外形がその內部構造に全く無關係に生じたものでない事を示す．若し火山彈の外形が噴火に際して火口から熔岩片の飛出し方或はその後の空中飛行中の運動に支配されるとすれば，その內部構造と外形とが不整合的關係を示すものが存在するはずであるが斯る例は見出されない．故に火山彈の外形はその內部構造に支配されて生ずるものと考へられる．

熔岩內に緻密部と多孔部，或は多結晶部と多玻璃部との層狀或はレンズ狀構造，結晶の流理構造等の存在する事實は噴出の際比較的粘稠性が大であつたと思はれる熔岩流に於いて屢々見られる．火山彈が噴火口附近に多い事實は，勢力の比較的弱い噴火によつて火口內熔岩の極く地表に近い部分からそれが抛出された事を示すものであらう．地表近くの熔岩は深所のそれに比較すれば多少大なる粘稠性を有し，瓦斯泡の分量，結晶度等に關して多少不均質と成る．斯る熔岩は流動方向に從つて不均質な部分の層狀或はレンズ狀構造を生じ，包裹物を有すれば，それを取圍んで流線狀構造を生じ，何れの場合にもその中の柱狀結晶は同方向に流狀に配列され，また瓦斯泡は同方向に配列され且つ引延ばされ易いであらう．從つて斯る熔岩中に爆發が起れば，同熔岩は比較的分離し易い層狀或はレンズ狀構造の境界面或は瓦斯泡の配列面を境として片々に分たれ，その內部構造に相應する種々の形態の火山彈と成り，ただ火口內熔岩より分離する際及び空中を飛行中に多少引延ばされ，捻られ，或は曲げられる等の變形を受けるものと考へられる．

要するに火山彈の外形のみの起源の說明方法は色々あるにしても，その形態と內部構造との密接な關係を說明し得るものが一層事實に近いのであつて，その意味で上述の解釋は H. Reck (1915) や G. Ponte (1934) の考へに一致する點が少くない．

---

37. *Magnetization of the New Lava-Flows of Miyakesima Island.*

By Takeshi MINAKAMI,

Earthquake Research Institute.*

(Read Dec. 19, 1940.—Received Sept. 20, 1941.)

Regarding the severe eruptions that occurred in Miyakesima Island, on the evening of July 12, 1940, detailed reports of the various volcanic phenomena, together with the results of observations by the members[1] of the Institute, appeared in previous Bulletins of our Institute.

On that occasion, the writer made magnetic surveys at 40 stations in the island in July and October, 1940, and in May, 1941.

In the course of this outburst, new lava-flows appeared at four places, the first from inside the somma and which flowed out from the central crater, the second and third at Akabakyo and Yoridai-sawa, where the lava flowed down from the present active fissure on the eastern slope of the mountain, and the fourth from the base of a new parasitic cone, Hyotan-yama.

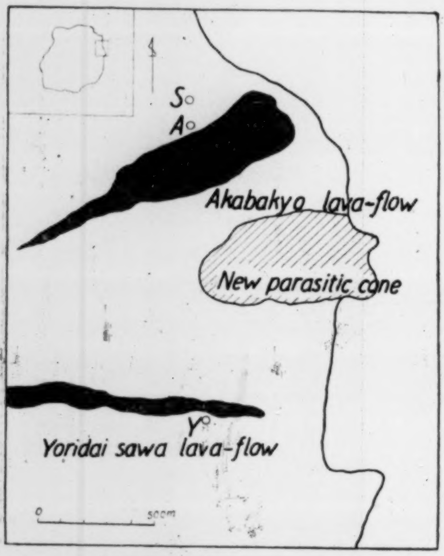

Fig. 1. Yoridai-sawa and Akabakyo lava-flows.
$Y, A, S,$ = stations.

This paper deals with the variations in the magnetic dip near the Yoridai-sawa and Akabakyo lava-flows, and the intensity of magnetization of these lava-flows.

The locations and shapes of the two lava-flows, together with the stations for these magnetic observations, will be seen from Fig. 1 and Table 1.

The stations just mentioned were at distances of 6 m and 100 m from the northern margin of the Akabakyo lava-flow and 2 m from the southern margin of the Yoridai lava-

* Dedicated to the memory of his late respected teacher, Professor Mishio Ishimoto.

1) H. TSUYA and others, *Bull. Earthq. Res. Inst.*, **19** (1941), 260.

flow. The results of observations are shown, with their dates and hours in Tables II∼IV and Figs. 2∼4, from which will be seen the very remar-

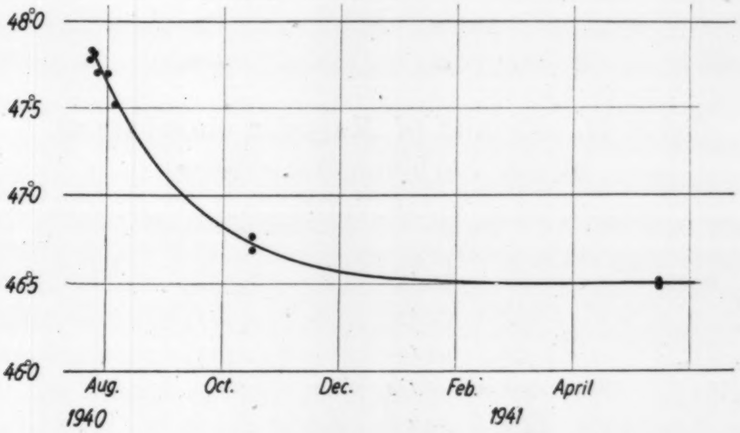

Fig. 2. Variations in dip at the Akabakyo station.

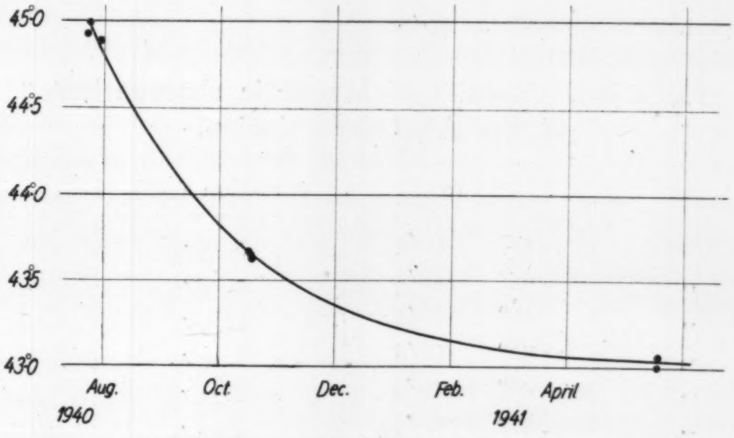

Fig. 3. Variations in dip at the Yoridai-sawa station.

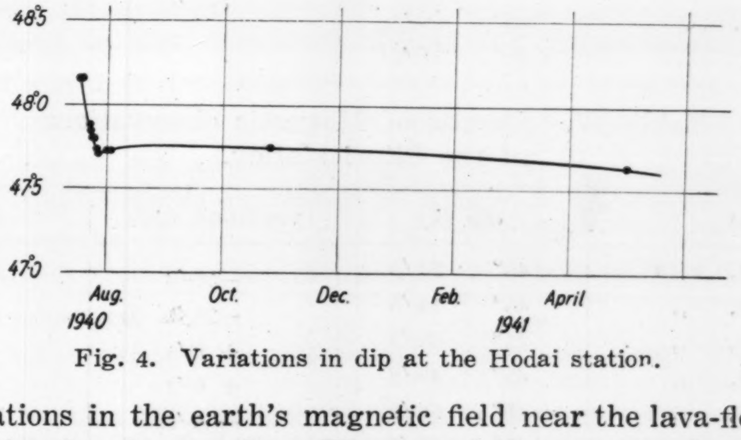

Fig. 4. Variations in dip at the Hodai station.

kable variations in the earth's magnetic field near the lava-flows during a period of only six months. These variations are a decrease of 1°

Table I.

lava-flow	mean width	mean depth	length
Akabakyo	200 m	7 m	500 m
Yoridai-sawa	20 m	6 m	1000 m

Table II. Results of Magnetic observations at the Yoridai-sawa station.

date	dip θ	variation $\Delta\theta$	$\Sigma\Delta\theta$
July 21, 1940	44° 56′.3	+4′.9	+4′.9
,, 22, ,,	45° 1′.2	−7′.0	−2′.1
,, 28, ,,	44° 54′.2	−1° 14′.8	−1° 16′.9
Oct. 25, ,,	43° 40′.8 }		
,, ,, ,,	43° 39′.7 }		
,, ,, ,,	43° 37′.9 }	−7′.9	−1° 24′.8
May 16, 1941	43° 31′.5 }		
,, ,, ,,	43° 32′.3 }		

Table III. Results of Magnetic observations at the Akabakyo station.

date	dip (θ)	variation ($\Delta\theta$)	$\Sigma\Delta\theta$
July 21, 1940	47° 47′.0	+ 3′.4	+ 3′.4
,, 22, ,,	47° 50′.4	− 1′.3	+ 2′.1
,, 23, ,,	47° 49′.1	− 6′.6	− 4′.5
,, 25, ,,	47° 42′.5	− 0′.9	− 5′.4
,, 30, ,,	47° 41′.6	−10′.3	−15′.7
Aug. 3, ,,	47° 31′.3	−47′.4	−1° 3′.1
Oct. 14, ,,	46° 41′.5 }		
,, ,, ,,	46° 46′.3 }		
May 16, ,,	46° 29′.3 }	−13′.5	−1° 16′.6
,, ,, ,,	46° 31′.6 }		

Table IV. Results of Magnetic observations at the Sitori station.

date	dip (θ)	variation ($\Delta\theta$)	($\Sigma\Delta\theta$)
July 23, 1940	46° 28′.3	−13′.8	−13′.8
,, 25, ,,	46° 14′.5	−25′.2	−39′.0
,, 30, ,,	45° 49′.3	+ 0′.6	−38′.4
Aug. 3, ,,	45° 49′.9	+ 0′.1	−38′.3
Oct. 25, ,,	45° 50′.0	− 6′.8	−43′.1
May 15, 1941	45° 43′.2		

24′.8 at the Yoridai station and the same of 1° 16′.6 and 43′.1 at the Akabakyo and Sitori stations respectively.

On the other hand, resurveys of the magnetic dip at stations other than the four in the island during the period from July 14 to August 3, 1940, showed a decrease of from 20′ to 30′ at almost all these stations. These decreases in dip at the last mentioned stations appeared only during the first survey (1940) just referred to. That is, the variations in dip during the first survey and those in the second survey on October are less than 10′ at all the stations except the former three stations, namely, Akabakyo, Yoridai-sawa, and Sitori. As an example of variations in dip at a station situated some distance away from the lava-flows and undisturbed by the lava-flow, we give the results at the Hôdai station as shown Fig. 4. On the other hand, the variations in dip at the former three stations continued to May, 1941, although the rate of variation gradually diminished after October, 1940.

From these results, it may be resonable to conclude that the main part of the magnetic disturbances that appeared throughout the island, came to on end in July. 1940, the remarkable variations that appeared after August, 1940, at the three stations near the lava-flows being due to magnetization of the new lava-flows.

According to Nagata,[2] the temperature near the surface of the lava-flow at Akabakyo in July was 900°~1000°. Since lava at such high temperature is scarcely magnetized, no magnetic desturbance from the lava-flow could appear even near it.

At the time of the third survey in May, 1941, the Akabakyo lava-flow cooled down to within 2 m of the surface, while in the Yoridai-sawa lava-flow the temperature of which was lower at the time of outflow than the former, cooled much more rapidly owing to the smaller quantity of lava-flow than the former.

Needless to say, therefore, before the temperature of the inner and outer parts of the lava-flow become equal, magnetization proceeds inward from the surface, as a consequence of which, magnetization of the lava-flow is not uniform, whence it may be reasonable to conclude that the characteristic variations in magnetic dip shown in Figs. 2 and 3 are the results of the condition just mentioned. It will be seen from Figs. 2 and 3 that the magnetization of the lava in May, 1941, remained almost unchanged.

Magnetic surveys of volcanoes[3] leave no room for doubt that

---

2) T. NAGATA, *Bull. Earthq. Res. Inst.*, **19** (1941), 295.

3) T. MINAKAMI, *Bull. Earthq. Res. Inst.*, **16** (1938), 100. 118; **18** (1940), 178; **19** (1941), 356.

magnetization of a comparatively new lava-flow is much more intense than other products of the volcano, such for example as the layer of scorie, pumice and ash. Moreover, Nagata's[4] laboratory work and the results of magnetic surveys of volcanoes showed that most lava-flows that have not been disturbed by the crustal deformation were magnetized in the direction of the earth's magnetic field at the time of ejection. It is probably only natural that a lava-flow that has cooled on the earth's surface from high temperature of about 1000°C should be magnetized in the direction of the earth's magnetic field. The writer's interpretation of the characteristics of the magnetic disturbance shown in Figs. 2 and 3, is based on this idea.

The Yoridai-sawa lava-flow runs from west to east, that is, the direction of flow is perpendicular to the magnetic meridian. Consequently in calculating the magnetization of the Yoridai-sawa, the lava-flow may be treated, without any serious objection, as a two dimensional problem. The origin of the co-ordinates is taken at the point where the observations were made, the x and z axes being taken in the magnetic north and downward. For convenience of computation, the lava-flow is divided into a large number of cylinders. The gravity potential of an infinite length of thin cylinder is

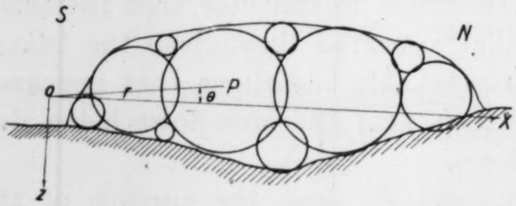

Fig. 5. Profile of the Yoridai-sawa lava-flow.

$$V=2\int_0^{\frac{\pi}{2}} \frac{k^2M\cos\varphi}{r}\,d\varphi=\frac{2Mk^2}{r}, \tag{1}$$

where $M=\rho\pi a^2$, $\rho=2{\cdot}0$ = mean density of lava-flow, a = radius of cylinder.

The second derivatives of the gravity potential of an infinite length of cylinder are

$$\left.\begin{aligned} \frac{\partial^2 V}{\partial x \partial z} &= 4k^2\frac{M}{r^3}\sin\theta\cos\theta, \\ \frac{\partial^2 V}{\partial x^2} &= 4k^2\frac{M}{r^3}\cos^2\theta, \\ \frac{\partial^2 V}{\partial z^2} &= 4k^2\frac{M}{r^3}\sin^2\theta, \end{aligned}\right\} \tag{2}$$

4) T. NAGATA, *Bull. Earthq. Res. Inst.*, 19 (1941), 304.

where k^2 = constant of gravitation.

The second derivatives of gravity potential of the lava-flow are

$$\left.\begin{aligned} W &= \sum V , \\ \frac{\partial^2 W}{\partial x \partial z} &= \sum \frac{\partial^2 V}{\partial x \partial z} , \\ \frac{\partial^2 W}{\partial x^2} &= \sum \frac{\partial^2 V}{\partial x^2} , \\ \frac{\partial^2 W}{\partial z^2} &= \sum \frac{\partial^2 W}{\partial z^2} , \end{aligned}\right\} \tag{3}$$

The variations in vertical and horizontal components of the dip due to magnetization of the lava-flow are given by the following equations:

$$\left.\begin{aligned} \Delta H &= \frac{1}{k^2 \rho}\left[a \frac{\partial^2 W}{\partial x^2} + \gamma \frac{\partial^2 W}{\partial z \partial x} \right], \\ \Delta Z &= \frac{1}{k^2 \rho}\left[a \frac{\partial^2 W}{\partial x \partial z} + \gamma \frac{\partial^2 W}{\partial z^2} \right], \\ \Delta \theta &= \sin \theta \cos \theta \left[\frac{\Delta Z}{Z} - \frac{\Delta H}{H} \right], \end{aligned}\right\} \tag{4}$$

where $$a = J \cos \theta, \quad \gamma = J \sin \theta ,$$

J = mean intensity of the magnetization of lava,

$\theta = \frac{\pi}{4}$ = magnetic dip near the lava-flow,

$H = Z = 0{\cdot}32$ (C.G.S.) = horizontal and vertical components of magnetic intensity near the lava-flow.

The calculation gives

$$\left.\begin{aligned} \Delta Z &= -0{\cdot}509 J, \\ \Delta H &= +1{\cdot}084 J, \\ \Delta \theta &= -2{\cdot}330 J. \end{aligned}\right\} \tag{5}$$

On the other hand, the variations in dip due to magnetization of the lava-flow is as given by the observations, is

$$\Delta \theta_0 = -1^\circ 40' = -0{\cdot}0291 \tag{6}$$

The mean intensity of the magnetization of the lava-flow is determined from (5), (6), from which the variations in the horizontal and vertical components of magnetic intensity at the station work out as follows.

$$J = 0{\cdot}0124, \quad \Delta Z = -631\,\gamma, \quad \Delta H = +1350\gamma.$$

As to the magnetic disturbance due to the lava-flow, the variations in the magnetic dip at points upward 1 m from the lava-flow are shown in Fig. 6.

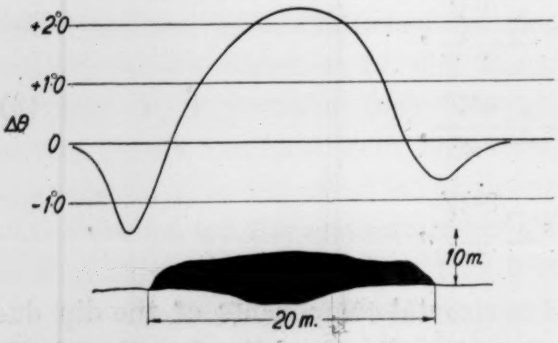

Fig. 6. Variations in dip on the Yoridai-sawa lava-flow obtained by calculation.

The mean intensity of magnetization of the Yoridai-sawa lava-flow as determined by the method above described agreed sufficiently well with that obtained by Nagata's laboratory experiments.

We may therefore conclude that the Yoridai-sawa lava-flow gradually cooled and was magnetized from the surface to the inner part of the lava-flow in the direction of the earth's magnetic field. The variations in dip at the Akabakyo and Sitori stations may reasonably be interpreted as the effects of the Akabakyo lava-flow. There is no doubt that the earth's surface near the stations tilted, owing to the weight of the lava-flow, but this effect on the variation of the magnetic field in the present case may be smaller than that due to magnetization of the lava.

In conclusion, the writer wishes to express his thanks to the Department of Education, with the aid of whose Scientific Research Encouragement Grant the present magnetic surveys were made possible.

---

37. 三宅島新熔岩流の帶磁

地震研究所　水上　武

昭和 15 年 7 月 12 日三宅島に著しい火山活動が起り，熔岩流の流出，寄生火山の成生等の火山現象が現はれた．その詳細は既に津屋博士其の他によつて報告されて居る．筆者は昭和 15 年 7 月，10 月，及び翌 16 年 5 月に同島に於いて磁氣伏角の測定を行つた．その際，ヨリダイ澤，赤場曉の新熔岩流の極めて近い點に於ける伏角の變動を測定し，熔岩の冷却さ共に熔岩の帶磁の進行する狀況を知る事が出來た．即ち熔岩流は地球磁氣の方向に帶磁し，その強さ約 0·012 (C.G.S.) である事が判つた．

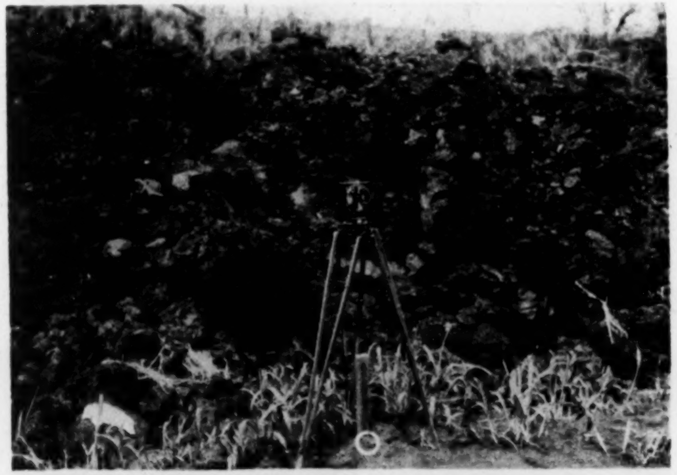
Yoridai-sawa lava-flow, and the station (○).

Akabakyo lava-flow, and the station (○).

Akabakyo lava-flow.

Akabakyo lava-flow.

(震研彙報 第十九號 圖版 水上)

Akabakyo lava-flow.

(横須賀鎮守府許可濟)

38. The Third Topographic Survey of the New Parasitic Cones and the New Lava Flow of Miyake-sima Island.

By Syun'itirô OMOTE,

Earthquake Research Institute.

(Read Sep. 18, 1941.—Received Sep. 21, 1941.)

Introduction.

Remarkable topographic changes accompanied the eruption of Miyake-sima island, in 1940. Parasitic cones were formed in the southern part of Akabakkyô Bay and lava flow buried the northern part of the same bay. A topographic survey of these newly formed lands was made soon after the eruption and repeated four months later, as the results of which their shapes were determined and the topographic changes during the interval made clear.

By permission of the Naval Department the writer was able to make a third topographic survey of this new land, the results of which will now be given.

In the third survey, the angle reading was done with a Wild Universal Theodolite, as in the first and second surveys.

Fortunately, when the writer visited the island for the third time the marks that were used as base points in the first and second surveys were found to be intact, so that revisions of the survey were easily made. The numerous wooden stakes that were established in the course of the second survey all over the parasitic cones were also intact, with the result that it was possible to ascertain the horizontal and vertical displacements of the parasitic cones and the lava flow.

These newly established marks, consisting of wooden stakes and earthen pipes, were firmly embedded in the ground, and the co-ordinates and the heights of those marks determined as stated in the previous report.[1] The origin of the co-ordinate was base point C, and its X axis the line CA in Fig. 1, and the Y axis a line perpendicular to the X-axis.

When the writer visited the island for the second time after a lapse

---

* 横須賀鎮守府許可濟

1) S. OMOTE, *Bull. Earthq. Res. Inst.*, **19** (1941), 387.

of four months from the end of the first survey, the topography of the parasitic cones had greatly changed. More than 100 m of the top of the

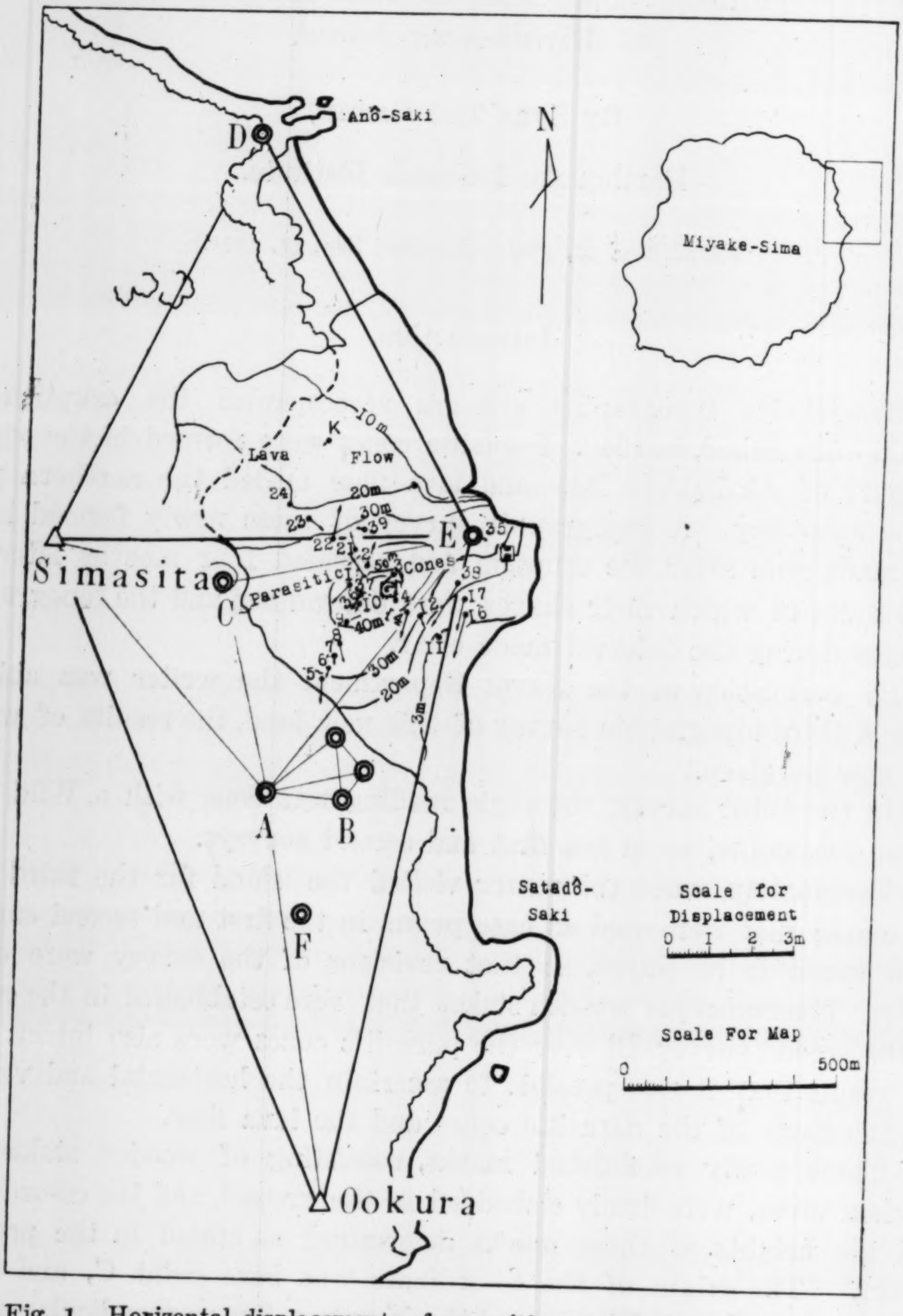

Fig. 1. Horizontal displacements of parasitic cones and lava flow. The numerals attached to the dots are the mark numbers in Table I.

promontory formed by the parasitic cones had eroded away by the action of sea waves, the eroded fragments being carried by the tide and deposited on the northern shore of the lava flow, where it formed

a new sand beach, extending as far as the Anô-saki headland.

The third survey.

On his third visit to the island six months after the second survey the changes noticed were not so marked as at the time of that survey. The top of the promontory of the parasitic cones had shortened only about 25 m compared with what it was in the autumn of last year.

The most notable changes were the numerous cracks all over the surface of the parasitic cones. Although these cracks were already there at the time of the second survey, this time they were very conspicuous, especially in the north-western flank of crater G (called by Dr. Tsuya[2]) and in the south-western flank of crater H of the cones, where many large cracks had formed.

Fig. 2 shows the cracks in the north-western flank of crater G. As will be seen from the figure, cracks run parallel to each other with their strikes perpendicular to the radial lines from the crater to the foot of the cone. Some of these cracks were more than 5 or 6 metres wide.

Fig. 2. Cracks on the north-western flank of cone G. Photographed May 15, 1941.

Horizontal displacement.

The horizontal displacements of the marks that were established in the second survey are shown in Table I and Fig. 1, from which Table it will be seen that the displacements of the marks are of the order of ten or several tens of centimetres, in contrast to which the horizontal displacements of the marks were very small, during the four months from the first survey to the second, when only a few cracks were seen. After that, with the development of the cracks, horizontal displacements of the marks began to be observed.

The lengths of the arrows in Fig. 1 represent the amounts of the

2) H. TSUYA, *Bull. Earthq. Res. Inst.*, **19** (1941), 282.

horizontal displacements of the respective marks. The enormous displacements of marks, M–2, –21, –36, –37 and M–16, –17, –38, are very notable. Of these the first five are in the north-western flank of crater G, and the remaining three are situated on the south-western flank of crater H.

Table I.

mark	Δx	Δy	v	Δh	mark	Δx	Δy	v	Δh
	m	m	m	m		m	m	m	m
1	+0·3	−0·5	0·6	−2·7	16	+0·9	−0·5	1·0	−0·6
2	−0·5	+0·3	0·6	−2·3	17	+0·6	−0·3	0·7	−0·9
3	+0·1	−0·1	0·1	−1·4	21	−0·3	−0·1	0·3	−0·1
4	0	0	0	−1·2	22	−0·8	+0·4	0·9	−0·6
5	+0·6	−0·2	0·6	−0·2	23	+0·4	+0·3	0·5	−0·5
6	+0·2	−0·1	0·2	−0·4	24	0	0	0	−0·3
7	+0·2	−0·1	0·2	−0·7	35	+0·1	+0·1	0·1	−0·9
8	+0·4	0	0·4	−1·6	36	+0·3	−0·3	0·4	−2·6
9	0	0	0	−1·3	37	−0·6	−0·2	0·6	−2·0
10	+0·1	−0·1	0·1	−2·0	38	+1·1	−1·0	1·5	−2·0
11	0	0	0	−0·1	39	−0·1	−0·2	0·2	−0·8
12	+0·2	+0·1	0·2	−0·4	K	+0·1	−0·2	0·2	−0·2
14	+0·5	−0·3	0·6	−0·2					

v: **Resultant Horizontal Displacement**
h: **Upward Displacement**

The sense of the arrows showing the direction of the horizontal displacements in Fig. 2 agrees with the radial lines from the respective craters to the foot of the cones, which seems to indicate that with the formation of cracks the surface layer of the cones slipped downward, so that the marks embedded in this surface layer also slipped down with it.

Table I shows that although the values of Δx of the mark are positive in the southern flanks of the cones, they are negative in the northern flanks. Since the Y axis almost coincides with the ridge of the parasitic cones, and looks eastward, by assuming that the surface layer slipped downward, we have a reasonable explanation of these changes.

Vertical displacement.

Observations of heights of the new parasitic cones during ten days of the first survey showed that these cones have a tendency to subside, which was confirmed by the second survey made four months after the eruption. As already reported,[3] in the first survey several points, D–1, D–2, D–3, D–4, P–1, and P–5 along the ridge of the parasitic cones and on the lava flow were measured a number of times from

3) S. OMOTE, *loc. cit.*

base point D, namely Anô-saki point. In the case of the second survey, only three points out of six that were distributed along the ridge of the cones were identified with the first ones.

Such marks as D–2, D–4, were not identified as they were natural object marks. In order to enable us to detect more easily the subsidence of the parasitic cones, new marks for the intersections were established in the second survey. These were wooden stakes or earthen pipes firmly embedded in the ground, and their co-ordinates and heights determined, as will be seen from the previous report.

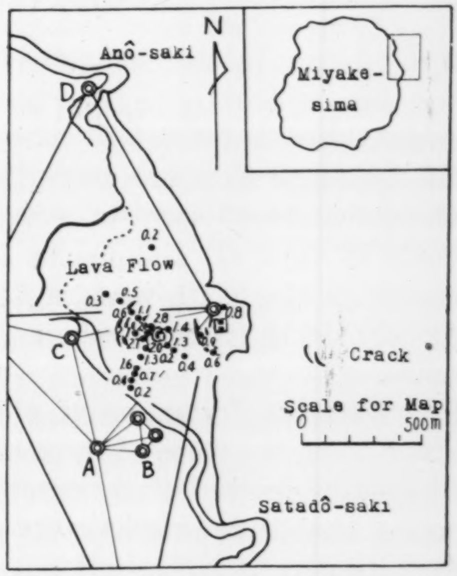

Fig. 3. Vertical displacements of parasitic cones and lava flow. The numerals attached to the dots are subsidences of the markes in metres.

In the third survey the heights of these marks were observed, and their vertical displacements determined, the results of which are shown in Fig. 3, in which the numerals affixed to each dot are the amounts of subsidence in metres. In this figure very rough sketches of the large cracks are also shown.

The relation between the amount of subsidence of each mark and

Fig. 4. Subsidence of marks in the interval between the 2nd and 3rd surveys.

its height from sea level are shown in Fig. 4, from which it seems that the heigher the position of the mark the larger its subsidence.

Excepting for a few marks, we are able to establish the following relation between the amount of subsidence and its height:

$$s = 0{\cdot}036 \times (h-12) \ldots\ldots\ldots (h > 12\ \mathrm{m}) \qquad (1)$$

where s = amount of subsidence of mark

h = height of mark above sea level.

Of the mark that are away from this straight line, M–1, M–2, M–10, M–36 and M–37 were in a region rich in cracks on the north-western flank of cone G, and marks M–16, M–17, also in the greatly cracked region on the south-western flank of cone H. Excepting these marks, namely, in the regions where the cracks are not numerous, equation (1) holds.

With the formation of cracks, surface layers several metres thick crept down the slope of the cones, so that the marks that were embedded in greatly cracked places crept downward along with the surface layers, seeing that these marks were driven into the ground no deeper than a metre.

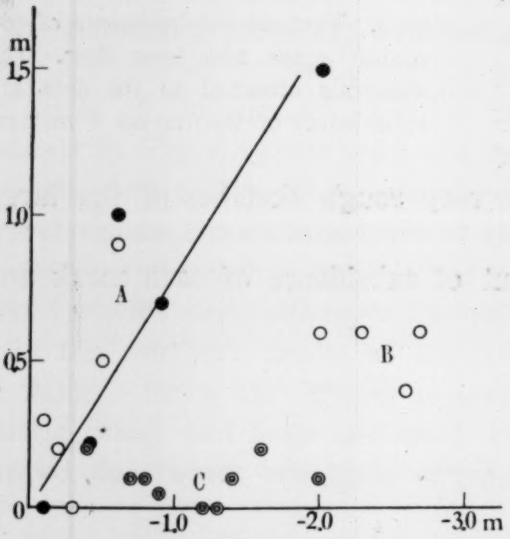

Fig. 5. Relation between the horizontal (ordinat) and the vertical (abscissa) displacements of marks.

● Marks erected on the south-western flank of cone H.

○ Marks erected on the north-western flank of cone G.

◎ Marks erected on the sparsely cracked region.

Naturally, this would show very large subsidences, as in Fig. 5. In this figure the abscissa represents the vertical and the ordinate the horizontal displacement. The shaded circles in Fig. 5 are the wooden stakes that were driven in on the south-western flank of cone H, and the open circles the marks on the northwestern flank of cone G. The double circles represent the marks established along the ridge of the parasitic cones. Since only very few cracks were formed in the last-named region, the double circles in Fig. 5 may be said to be the marks in the sparsely cracke region.

Refering to Fig. 5, we notice that these circles may be classified into three groups, A, B and C. To group A belong all the shaded circles and half the number of the open circles, the horizontal displace-

ments of marks of group A being in proportion to their respective vertical displacements. To group B belong the remaining half of the open circles. Although the ratio of displacements horizontal to vertical, of the marks of group B is not so large compared with the ratios of marks of group A, the horizontal displacements of markes of group B are considerable. In contrast to the marks of groups A and B, the horizontal displacements of marks of group C, denoted by double circles in Fig. 5, are very small compared with their vertical displacements, whence it may be concluded that the double circles represent the real subsidences of the parasitic cones.

The changes in height of the parasitic cones with time are shown in Fig. 6. The abscissa gives the number of days from the eruption and the ordinate the heights of the marks above sea level. It is evident from the figure that only two of the marks could be availed of in measuring the angles all through the three surveys.

As just mentioned, marks D are natural objects, P wooden stakes, and M earthen pipes, firmly embedded in the course of the second survey. It will be seen from Fig. 6 that although immediately following the

Table II.

marks \ days*	18	19	21	23	25	115	116	124	308	
	m	m	m	m	m	m	m	m	m	m
D-1	—	68·7	65·2	64·9	64·7	60·7	—	60·4	57·3	(58·8)
M-1	—	—	—	53·4	—	48·6	48·6	—	45·7	(47·1)
D-3	58·4	58·3	57·9	57·1	56·9	53·1	—	—	—	
M-37	—	—	—	—	—	—	—	60·3	56·3	
M-3	—	—	—	—	—	—	—	62·1	60·7	
M-4	—	—	—	—	—	—	—	44·8	43·6	
M-35	—	—	—	—	—	—	—	41·2	40·3	
D-5	2·6	2·5	2	2·4	—	—	—	—	—	

Change in Height of Marks.
* **Number of days since the Eruption.**

eruption the changes in height of these marks were very large, with lapse of time they rapidly decreased, so that these subsidence curves seem to be hyperbolae. The numerical values of the heights are tabulated in Table II.

The changes in height of marks D-1 and M-1 in six months, from the second to the third survey, are 2·9 m and 2·7 m respectively, while those of M-3, M-4, and M-35 are only 1·4 m, 1·2 m, and 1·1 m respectively.

The especially large subsidences of the former two marks were because they were in the middle of the greatly cracked region, in which these marks crept downward with the surface layer, with the result that the subsidence of marks D–1, M–1, in Table II, cannot be said to be values of subsidence of the parasitic cone itself. The subsidences of marks D–1 and M–1, under the assumption that they had never crept down as the result of crack formation, can be calculated from the above equation. The subsidences D–1 and M–1 are calculated to be 1·6 m and 1·2 m and the heights 58·8 m and 47·1 m respectively, as the bracketted figures in Table II show. In Fig. 6 these heights are plotted with shaded circles.

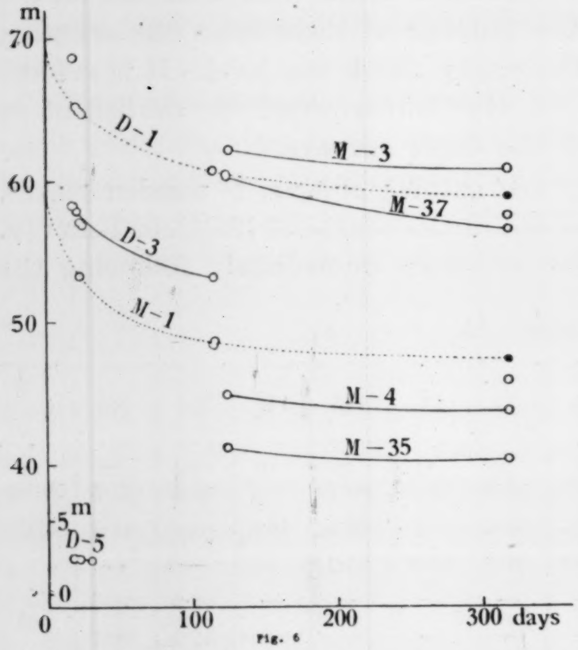

Fig. 6. Subsidence curves of parasitic cones and lava flow.

Using these values and assuming the subsidence curves in Fig. 6 are hyperbolae, we get the following relation between the height of the mark h above sea level and the number of days t from the eruption,

$$h-a=\frac{c}{b+t}$$

where a, b, and c are constants, a is the height of the assymptotic line parallel to the t axis, and a of the D–1 curve is 54·2 m and of the M–1 curve 46.0 m. These are the limiting values of marks D–1 and M–1 on the assumption that the surface layer did not move owing to the formation of cracks. By putting $t=o$, the height of the mark is given by h, by extrapolation, when the parasitic cones were formed. Those heights of the marks D–1, M–1, are 68 m and 59 m respectively, from which it is known that the top of the parasitic cones subsided 8 m during the first four months since they were formed and then subsided 2 m during the six months that followed. In short, the top subsided about ten metres during the ten months since the eruption. Mark D–1 subsided about 12 m during the same period.

The mode of subsidence of the lava flow cannot be known because mark D–5, the only mark that was established on the lava flow in the

first survey, had already eroded away when the second survey was made. The rate of subsidence of the D–5 curve in Fig. 6, however, is very much smaller than that of the other curves. Subsidence of marks M–24, M–23, and K (Fig. 1), established in lava flow in the second survey, as is shown in Table I, are very small. It therefore seems that the lava flow subsided much less than the parasitic cones.

---

38. 三宅島新寄生火山及び新熔岩流の第3回地形測量

地震研究所　表　俊一郎

昭和15年7月の三宅島の噴火により生じた新寄生火山及び新熔岩流の地形測量は，既に2回實施せられ，それらの形及び大いさが測量せられたのみでなく，それらの期間に於ける地形變化の有樣が明らかにせられた．今年5月許可を得て，第3回目の地形測量を行ふ事が出來たので其の結果を報告する．新寄生火山の山腹に第2回目の測量の際，新らたに設置せられた多數の杭を再測する事により其等の杭の水平並びに鉛直方向の移動量を知り得た．これらの移動量の中，G火口の北西側山腹にある杭と，H火口の南西側山腹にある杭とは數十糎から1米以上にも及ぶ著るしく大きい水平移動量を示すのであるが，其れ等の地域は丁度割目が著るしく發達して居る所にあたつて居る．之に反し割目がほとんど發達して居ない部分，即ち寄生火山の稜線に沿つた地域の杭の水平移動量は極めて少さく高々2〜30糎位にすぎない．從つて割目の多い地域に於ては表面層が下方へずり落ちる如き運動が行はれて居るものと思はれる．水平移動量の小さい覘點より寄生火山の沈下量を求めると，一番高い所の附近に於て第2回と第3回の測量の間の6ケ月間に1·4mとなる．第1回より第3回までの3回の測量に於て3回とも測量する事の出來た覘點は二點しかなかつたが，それらの覘點の沈下曲線が二次曲線であらはせると假定すれば，其等の覘點が割目のため表面層と共にずり落ちる事がないと假定したときの極限の高さはD–1には54·2m，H–1には46·0mとなる事となる．　(橫須賀鎭守府許可濟)

---

39. 昭和16年7月15日長野地震の統計的調査

地震研究所 岸上冬彦
永田武
宮村攝三

(昭和16年9月18日發表——昭和16年9月20日受理)

長野地方に弘化4年3月24日(西暦1847年5月8日),善光寺地震と稱へられてゐる大地震があつたことは改めて申す迄もなからう.昭和16年7月15日の地震は善光寺地震に比べては遙かに小さいもので,長野市の北東數個村が激震地域で死者5重傷者5を出し,全壊142戸,半壊538戸を數へた.

此の地震の前,明治30年1月17日に上高井郡及び上水内郡東部に地震があり,土藏の傾斜,墓石の顚倒,泥砂の噴出等を生じた.同年4月30日にも上高井郡及び下高井郡の一部に强震があり二度共多くの餘震が伴つた.又昭和16年3月7日に,下高井郡中野町附近に中震があり,穂波村及び夜間瀬村で岩石,土砂の崩壊があつた。7月15日21時45分に長野市に於て弱震を感じ,その2時間後23時45分に起つた强震が以上の災害を起したのであつた.東京市本郷の東京帝國大學内の記錄によれは,發震時は23時45分55·5秒であつた.

此の地震區域に最も近い地震研究所所屬の觀測所は,淺間山火山觀測所及び沓掛にある地震觀測所である.そこで長野地方の地震について觀測した結果は第I表の通りである.

第 I 表

	時刻	沓掛		峯の茶屋		時刻	沓掛		峯の茶屋
		東西	南北				東西	南北	
	d h m	sec	sec	sec		d h m	sec	sec	sec
前震	15 21 30	6·1	6·4	7·1	餘震	17 13 20	—	6·4	6·9
前震	15 22 30	6·2	6·3	7·3	餘震	18 1	—	不明	5·9
					餘震	19 2 10	6·1	6·2	6·5
餘震	16 3	—	(4回)	—	餘震	19 11 30	5·2	5·9	6·1
餘震	16 9 10	6·3	6·7	—	餘震	19 12 15	5·4	4·6	6·1
餘震	16 9 30	—	>6·0	6·8	餘震	25 22 30	—	不明	6·8
餘震	16 19 40	—	6·3	6·6	餘震	27 9 30	—	6·8	6·9
餘震	16 23	—	6·5	7·0	餘震	27 11 50	—	6·6	76·8

殆ど總ての大地震について，常時觀測の地震計が震原地に近くその周圍に適當に配置してゐることは無く，たとへ一．二個所あつても近くの最も震原位置を決定するに役立つ可き地震計は其の記錄針が外れ，餘震は地震計觀測が出來ても，本震については家屋の被害や墓石の顚倒から調査する外はない場合が多い．此の種の調査は方法として今日においても考究の餘地がある樣に考へられるので，家屋の被害に關する調査は他の研究に托すこととし，墓石の顚倒に就き從來とは變つた見方をした．

又地震調査表といふ名稱で調査用紙を印刷し，長野縣下の國民學校に配り，その回答を得，其についての結果も述べる．此の調査事項は(1)振子時計の止つたもの又は止らなかつたものの文字板の向き，(2) 井戶水の水量•色の變化，(3) 地鳴の音色及び聞えた方向，(4) 地震の際の光り物の形．色及び見えた時刻，(5) 地割れの生じた場所や水や砂の噴出の有無，(6) 家屋の傾斜方向又は屋根瓦の落ちた方向，(7) 水田の灌漑の地震前後による難易の差，(8) 其の他，地震に關した事といふ8項目に分けて回答を求めた．此の調査表を縣下各地の國民學校に分配し更に報告を集めるについて

第　II　表

郡	調査表數	調査戶數	光りものに關する報告數	地鳴に關する報告數
諏訪	59	1346	4	104
南佐久	29	89	1	34
北佐久	29	459	0	38
東筑摩	37	747	0	110
南安曇	14	83	0	32
北安曇	24	470	0	9
小縣	41	227	1	62
更級	206	3616	113	854
埴科	150	1299	65	285
長野	125	387	65	163
上水内	337	8139	574	1142
下水内	82	1058	38	72
上高井	163	1209	128	441
下高井	136	1359	90	206
計	1432	20488	1079	3552

は，長野縣學務部が援助され，第 II 表に示す樣に多くの報告を得たのは此の種の調査として先づ數量に於いて成功したといへよう．次に項を分けて記すこととする．

墓石の顚倒

墓石は我が國內では形も大さも類似してゐて，震度分布を調べるに都合がよいもので

ある．併しその据えてある所は多く住家とは離れた山麓等で，その爲に家屋の被害と多少事情を異にすることと，墓石の大さ形は略々一定してゐる爲に此によつて推定出來る震度の範圍が限定されることとは，此の方法の缺點である．

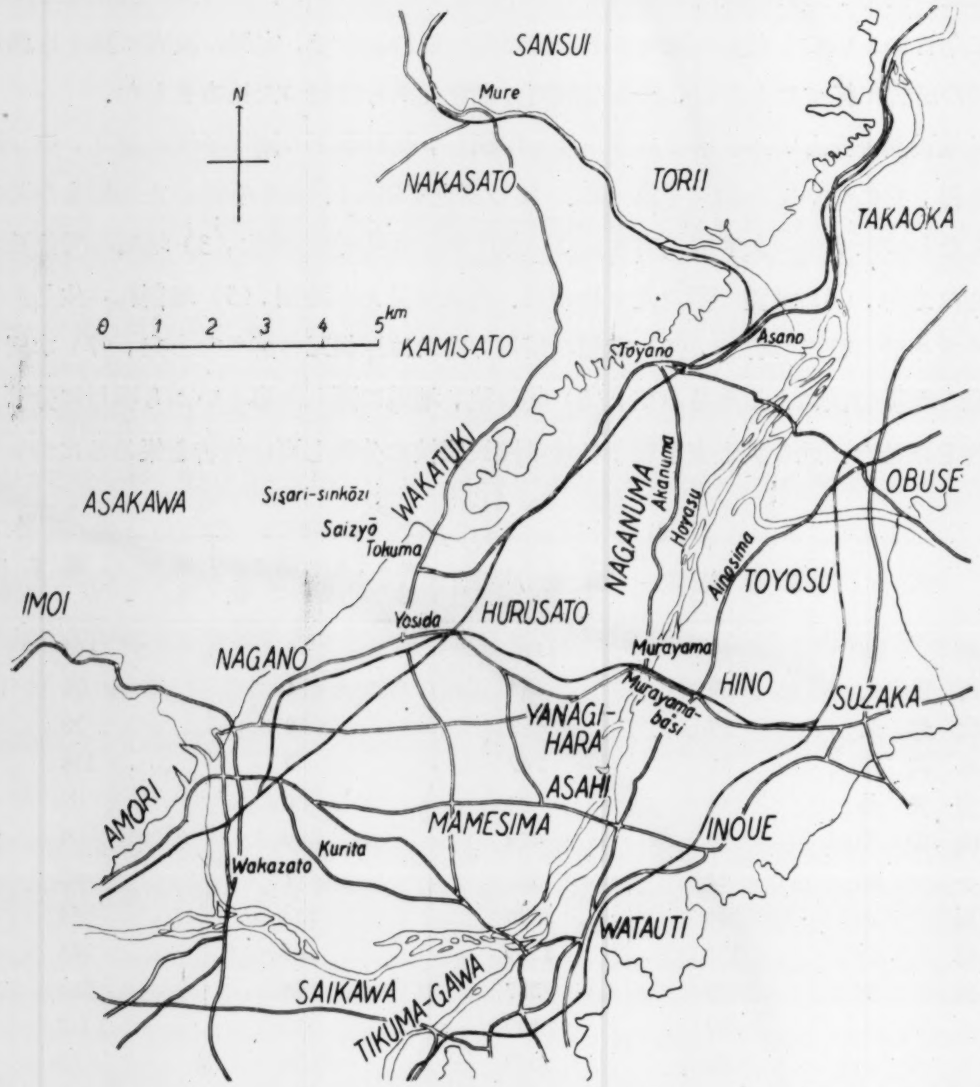

第１圖　震災地近傍略圖

従來は一個所の墓地の中，數個の代表的と思はれる墓石から震度を推定したが，同じ様な墓石が一つは倒れ他は倒れないといふ場合が多く，倒れたもので震度をきめることには疑問がある．そこで今回は，形や大さには無關係に墓地にあるもの總べてを同様に見做し，各々の墓石の倒れた方向を約 5° の精度内で測つた．そしてその倒れた數は 30° 宛の扇形に括めた．但し餘り數の多い墓地では一部分を限つて調べた．此の事については，朝陽(アサヒ)村石渡の長命寺に於て墓地の約 1/3 分について出した顚倒率

は，墓地全部について求めた顚倒率と等しかつたから，此の假定は餘り不合理でなはいであらう．その結果は第 3 表に示した通り測つた墓石の總數は 9462 であつた．

顚倒を百分率を以て表はしたものが第 2 圖である．此の圖によると千曲川沿岸と，その西の第三紀層と沖積層との境とに率の大きい所があらはれた．但し牟禮(第III表29)の墓地は崖の眞上にあり，地盤の影響によつて率が大きくなつたと考へた．そのことは此の墓地でも崖の端から少し離れた所では，全く倒れてゐなかつたことから推定した．震央は以上の率の大きい 2 個所の中間にあり，此の 2 個所を兩端とする直徑 4 ～ 5 km の地域を震央と考へるべきであらう．中央氣象臺發行の「長野强震調査概報」中地震計觀測の結果求められた震央位置も此の地域にはいる樣である．此をもし西の山麓にとれば山の方の率が餘り急激に減少し，又千曲川西岸長沼村にとれば，その東方の小布施・須坂の山麓が地質が違ふとはいへ西の山麓と大體顚倒率が似た値にならなければならないと考へられる．

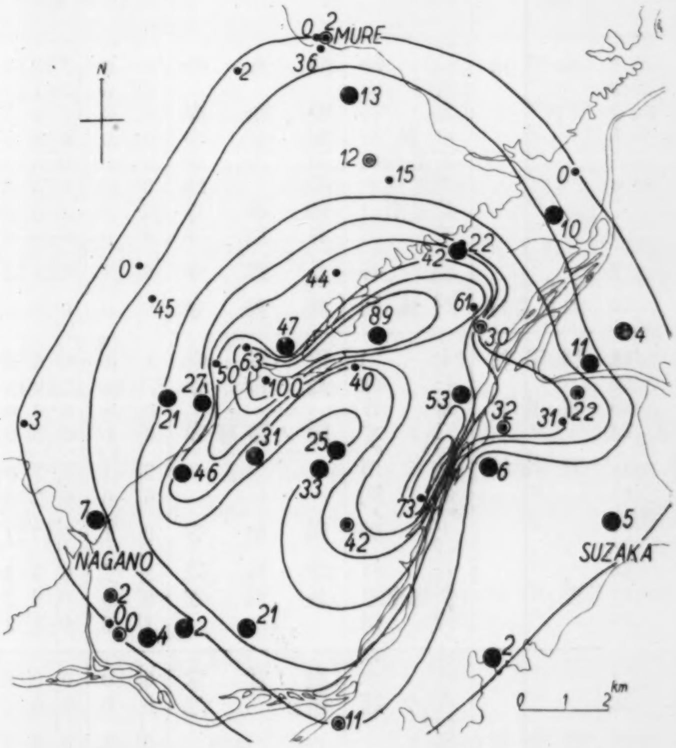

第 2 圖 墓石の顚倒率(大きい丸は墓石の數の多い所を示す)

地質に對する關係は，沖積層の方が顚倒率が他に比べて大きい様であるが，後で述べる振子時計に於ける關係程明瞭でない．

顚倒方向は 360° を 30° 宛に分けたが，その中で 1 方向に極大になるものは，急激な地震動によつて倒れたと考へ，180° の差を以て 2 方向に極大になるものは土地の往復運動によつて何れかの方向に倒れたと考へた．此の二つの倒れ方を分析しようとして，第 II 表の 12 方位の顚倒數を調和分析し，一つの極大を第 1 調和項で表はし，二つの極大を生ずる振動は第 2 項で示されるものと假定した．

その結果は第 3 圖に示した．圖中點線の圓は第 1 項の信用度を示さうと，分析した振幅卽ち矢の長さを統計學上の期待値と比べる爲に，期待値を示したもので，破線で圖示した第 2 項については第 1 項の場合の長さの單位を 2 分の 1 にしたから，破線の

第 III

番號	場所			倒れた墓石の數（北より東まはりで 30° づつ十二象限に分つ）												倒れた方向不明なるもの	倒れた墓石の總數
							E			S			W				
1	長野市	三輪	時丸寺	6	2	3	12	14	8	11	0	1	7	6	4	11	85
2	〃	吉田		2	6	7	61	11	4	6	0	6	24	3	1	16	147
3	〃	妻科	善松寺	5	3	2	4	2	3	5	0	0	1	0	3	3	31
4	〃	中御所	觀音寺	0	0	0	0	0	0	1	0	0	2	0	0	0	3
5	〃	若里九反	蓮心寺	0	0	0	0	0	0	0	0	0	0	0	0	0	0
6	〃	若里荒木	墓地	0	0	0	0	0	0	0	0	0	0	0	0	0	0
7	〃	若里南市	佛導寺	2	0	0	0	0	0	3	1	2	0	1	0	0	9
8	〃	千田	專福寺	0	0	0	0	0	0	0	0	0	0	0	0	2	2
9	〃	湯（ユ）ヶ谷	昌禪寺	5	10	4	23	13	8	8	12	6	13	7	7	0	116
10	大豆島（マメシマ）村	西風間	藤興寺	0	0	0	6	6	0	1	1	3	8	7	4	0	36
11	朝陽村	十二	常溫寺	1	1	0	6	5	2	0	0	2	2	0	1	6	26
12	〃	石渡	長命寺	37	15	12	19	15	15	24	5	6	13	7	11	9	203
13	古里村	富竹		0	4	0	4	4	1	5	2	3	2	2	2	2	31
14	〃	三才（ダ）	藤ノ淨專寺	0	0	0	0	2	5	0	1	0	2	0	0	0	10
15	若槻村	檀（マユミ）田		2	1	3	7	9	0	1	1	0	1	1	2	5	33
16	〃	徳間		0	0	0	2	5	0	0	1	0	0	0	0	0	8
17	〃	上（ウハ）ノ野	國胎寺	0	1	2	12	21	2	4	0	0	2	5	1	13	64
18	〃	吉（ヨシ）村	淨泉院	5	2	0	0	1	2	5	2	0	0	2	2	0	21
19	淺川村	西條東組	長福寺	0	0	0	0	3	2	5	0	0	0	0	0	2	12
20	〃	押田		1	0	0	1	1	1	1	0	0	0	0	0	0	5
21	〃	清（キヨ）水（ミズ）	觀音堂	0	0	0	0	0	1	3	0	0	0	0	1	1	6
22	〃	蟇ヶ窪	墓地	0	0	0	0	0	0	0	0	0	0	0	0	0	0
23	芋井村	鑪（タタラ）		0	0	0	0	1	0	0	0	0	0	0	0	0	1
24	中郷村	平出	高山寺	0	1	0	1	0	0	0	0	1	0	0	1	0	4
25	〃	平出	墓地	2	0	1	2	0	0	0	0	0	2	0	0	0	7
26	〃	四ツ屋	墓地	4	2	1	0	0	1	0	0	0	0	1	5	0	14
27	〃	牟禮	(石段の上の寺)	0	0	0	0	0	0	0	0	0	0	0	0	0	0
38	〃	牟禮	(石段の下の寺)	0	0	0	0	1(?)	0	0	0	0	0	0	0	0	1
29	〃	牟禮	(神社の傍の墓地)	6	9	0	9	8	6	13	5	5	7	12	6	2	88
30	高岡村	新井	墓地	0	0	0	0	1	0	0	0	0	0	0	0	0	1
31	鳥居村	淺野	寶藏院	0	0	0	3	4	1	0	1	3	1	7	3	0	23
32	〃	蟹澤	龍澤寺	0	0	0	0	0	0	0	0	0	0	0	0	0	0
33	小布施村	小布施	(驛近くの寺)	7	4	0	2	4	6	12	1	2	6	1	6	0	51
34	〃	大島	玄照寺	5	1	3	7	6	2	11	2	3	6	0	1	24	71
35	長沼村	赤沼	センケイ院	0	1	1	2	0	0	1	6	6	5	0	0	1	23
36	〃	赤沼	妙願寺	2	4	0	1	1	0	5	3	0	0	0	0	0	16
37	〃	穗保	(北の寺)	18	11	3	2	0	4	39	13	4	5	1	0	29	129
38	柳原村	村山	墓地	0	0	0	3	2	0	0	0	4	6	1	0	0	16
39	日野村	村山	墓地	0	2	0	0	0	0	3	1	0	0	0	0	0	6
40	豊洲村	相之島		4	1	1	0	0	1	4	5	0	1	1	2	1	21
41	〃	別府		0	1	1	1	1	0	1	0	0	1	5	2	2	15
42	〃	新田	墓地	2	0	0	2	1	1	2	1	0	0	0	0	8	17
43	神郷村	南郷	桃源院	4	4	4	5	8	16	28	50	16	9	7	6	82	239
44	〃	豊野	大日堂	1	0	0	0	0	3	2	0	1	0	1	1	0	9
45	〃	豊野	(大日堂の南下)	3	3	3	8	6	4	15	8	8	27	1	4	6	96
46	須坂町		常念寺	10	4	0	9	5	2	13	4	3	3	3	7	0	63
47	井上村		十運寺	3	1	0	0	1	0	0	0	0	0	0	0	1	6
48	川田村	牛島		0	0	0	1	0	0	0	0	1	0	0	0	4	6
49	柏原村	柏原		0	0	0	0	0	0	0	0	0	0	0	0	0	0
50	信濃尻村	野尻湖		0	0	0	0	0	0	0	0	0	0	0	0	0	0

表

墓石の總數	倒れた率(%)	震央距離(粁)	調和係數 a_1	b_1	$c_1=\sqrt{a_1^2+b_1^2}$	a_2	b_2	$c_2=\sqrt{a_2^2+b_2^2}$	c_1とc_2との間の角度	期待値 ε
187	46	7·1	−0·26	+0·45	0·52	−0·19	−0·61	0·64	3°	0·19
474	31	5 6	−0·08	+0·75	0·76	−1·29	±0·00	1·29	6°	0,15
459	7	9·4	+0·08	+0·34	0·38	+0·54	−0·18	0·57	72°	0·32
156	2	10·1	−0·68	−1·32	1·48	−0·68	±0·00	0·68	27°	1·02
43	0	10·5	—	—	—	—	—	—	—	—
50	0	10·5	—	—	—	—	—	—	—	—
244	4	10·2	−0·52	−0·69	0·86	+0·89	+0·39	0 97	41°	0·59
119	0	9·4	—	—	—	—	—	—	—	—
545	21	6·7	−0·17	+0·21	0·27	−0·34	−0·45	0·56	13°	·16
170	21	8·6	+0·03	−0·44	0·44	−1·03	−0·63	1·21	10°	0·30
62	42	5·6	−0·25	+0·76	0·80	−0·85	−0·43	0·95	5°	0·32
611	33	4·8	+0·19	+0·28	0·34	+0·46	−0 10	0·47	63°	0·12
124	25	4·2	−0·34	+0·11	0·36	−0·07	±0·00	0·07	(20°)	0·32
25	40	2·5	−1·25	+0·35	1·30	±0·00	−1·05	1·05	30°	0·56
121	27	6 0	+0·02	+1·04	1·04	−0·68	−0·43	1·80	19°	0·31
8	100	3·8	−0·84	+1·67	1·87	−1·00	−1·01	0·42	10°	0·63
137	47	4 4	−0·45	+0·62	0·77	−0·88	−0·85	1·22	12°	0·22
48	44	2·5	+0·05	−0 08	0·09	+1·19	−0·25	1·22	52°	0·39
19	63	4·6	−1·46	−0·72	1·62	+0·90	−0·87	1·25	0°	0·51
10	50	5·4	−0·55	+0·93	1·08	+0·41	−0·69	0·80	30°	0·79
11	55	6·6	−1·19	±0·00	1·19	+1·60	−0·69	1·74	23°	0·72
29	0	7·0	—	—	—	—	—	—	—	—
39	3	10·0	—	—	—	—	—	—	—	—
27	15	3·1	+1·12	+0·16	1·13	−0·24	+0·39	0·46	53°	0·89
60	12	3·7	+0·72	+0·24	0·76	−0·72	+0·24	1·76	61°	0·67
105	13	5·3	+1·45	−0·15	1·45	+1·00	−0·50	0·12	7°	0·47
11	0	6·8	—	—	—	—	—	—	—	—
57	2	6·8	—	—	—	—	—	—	—	—
243	36	6·5	+0·08	−0·05	0·09	+0·08	−0·26	0·27	36°	0·19
47	2	7·4	—	—	—	—	—	—	—	—
231	10	3·4	+0·07	−0·41	0·42	−0·74	−0·83	1·22	15°	0·37
37	0	4·2	—	—	—	—	—	—	—	—
1336	4	4·1	−0·19	−0·06	0·20	+0·63	−0·34	0·72	35	0·25
658	11	3·6	−0·46	+0·26	0·53	+0·00	±0·00	0·00	不定	0·21
38	61	0·7	−0·88	−0·90	1·26	−0·55	+1·10	1·23	12°	0·37
53	30	1·0	−0·33	+1·05	1·10	+1·13	+0·65	1·30	88°	0·32
242	53	2·2	−0·51	−0·07	0·52	+1·20	+0·45	1·28	0°	0·16
22	73	4·5	−0·32	−0·70	0·77	−1·56	+0·11	1·58	22°	0·44
109	6	3·9	−0·72	+0·16	0·74	+1·16	+0·86	1·44	31°	0·72
65	32	3·2	−1·59	−0·35	1·62	+1·05	+0·26	1·08	5°	0·39
48	31	3·9	+0·63	−0·48	0·79	−0·46	−0·81	0·93	22°	0·46
77	22	3·7	−0·49	+0·41	0·64	+0·56	−0·19	0·59	38°	0·43
267	89	1·7	−1·23	−0·40	1·2[illegible]	+0·49	+0·41	0·64	4°	0·11
41	22	1·4	−0·61	−0·16	0·63	+0·89	−0·77	1·18	35°	0·59
228	42	1·3	−0·48	−0·48	0·68	−0·37	+0·14	0·40	33°	0·18
1324	5	6·3	−0·04	+0·08	0·09	+0·44	−0·17	0·47	78°	0·22
359	2	8·0	+1·12	+0·46	1·21	+1·00	±0·00	1·00	22°	0·72
56	11	9·8	−0·47	+0·12	0·46	−1·47	+0·82	1·68	88°	0·72
—	0	13·0	—	—	—	—	—	—	—	—
30	0	15·5	—	—	—	—	—	—	—	—

全長を圓の半徑と比べて見なければならない．以後矢の端が圓の中にはいるものは偶然な場合とみなして，圓より外に矢が出てゐるものについてのみ考究を進める．第2圖の黑丸の大きいものが信用度も大きいことを示す．

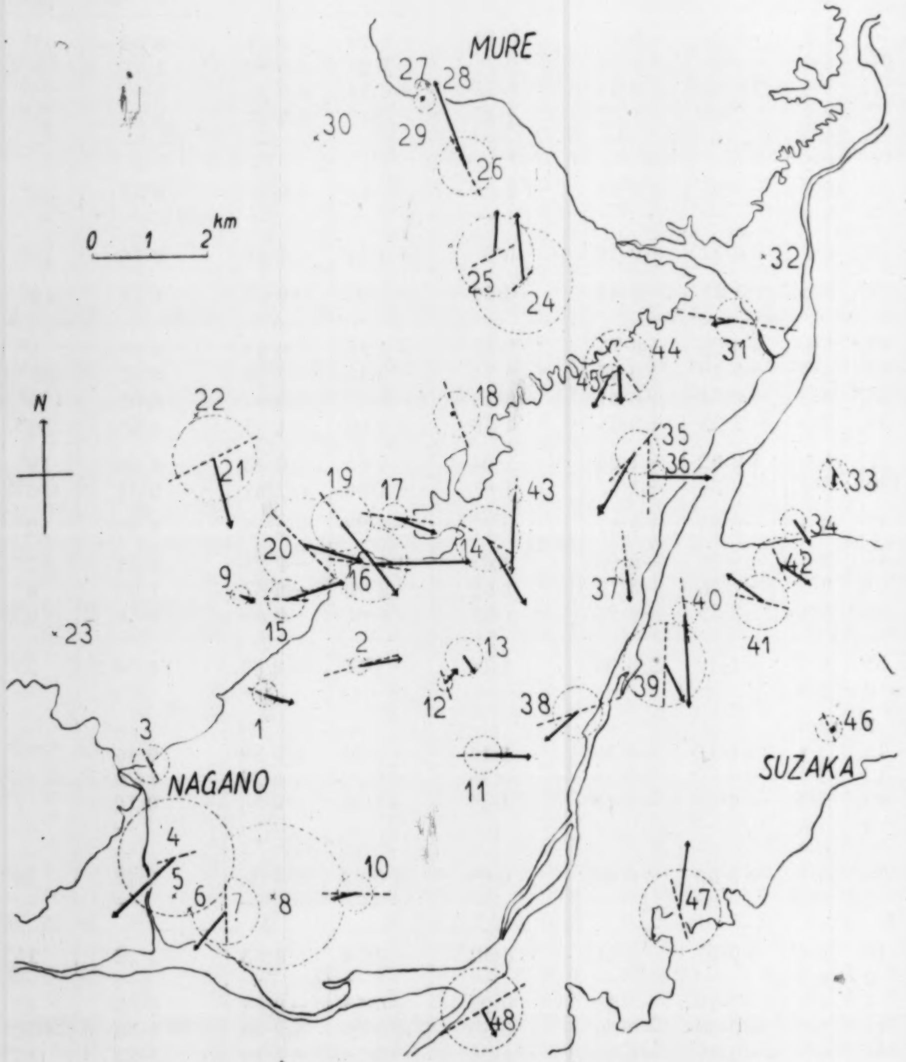

第3圖　墓石の顚倒方向(圓は第一調和項に對する期待値を示す)

第1項と第2項との間の角は 30° 以上になるものは大層少く，前述の樣に分析に用ひた材料が 30° を單位にしてゐることを考へれば其等の方向は等しいといつてもよい．此のことは從來明かでなかつた墓石の顚倒方向の地震動の進行方向に平行であることを示すものであらう．

その樣に考へると，第1項を示す矢をその方向に延長して，その交點の分布を調べれば，震央に於て交點の數が最も密になると推測される．そこで圖によつて交點をつくり，圖上で一邊 2·5 km に當る正方形内の交點數を數へた．その總數 155 となり，

正方形の網目の内の交點數の最も多い所は 27 となつて，その網目の位置は大體顚倒率からきめた震央と一致する．此の交點の總數を，矢が全く偶然な方向を向いた場合と比較して見る．

矢の數を m 個とすると，一つの交點は二つの矢によつてつくられるのであるから，交點の總數 N は m 個の中 2 個の組合せで求められる．卽ち

$$N=\binom{m}{2}=\frac{m(m-1)}{2}$$

併し矢は一方にのみ延長されるのであるから次の條件を要する．今第4圖の樣にA, B 二點からの矢の AB となす方向を夫々 φ,ψ とすれば，

$$\psi\leqq\pi-\varphi$$

でなければ矢は交はらない．此を ψ について平均すれば，交點をつくる確率 p は

$$p=\frac{\overline{\pi-\varphi}}{2\pi}=\frac{\pi-\pi/2}{2\pi}=\frac{1}{4}.$$

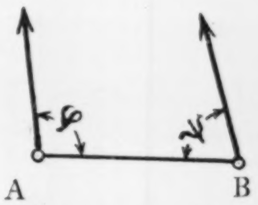

第　4　圖

交點の出來ない場合の確率 q は

$$q=1-p=\frac{3}{4}.$$

故に n 個の交點の出來る確率は

$$W(n)=\binom{N}{n}p^n q^{N-n}.$$

測定から求めた交點の數だけの交點の出來る確率卽ち期待値は

$$E=\int_{\delta_0}^{\infty}W(\delta)d\delta=\int_{\delta_0}^{\infty}\sqrt{\frac{\nu}{2\pi q}}e^{-\frac{\nu}{2q}\delta^2}d\delta$$

但し

$$\delta=\frac{n-\nu}{\nu}\quad,\quad\nu=pN.$$

となる．墓石について E を求めると，

$$m=23,\ n=155,\ N=253,$$

であるから

$$E\doteqdot O(10^{-10})$$

となる．故に測定して得た交點數は信用度の高いものである．

此の結果震央に近い所の矢は震央に向くことがわかり，數 km 離れた所では矢の外側を向くものもあつて，遠くの矢の分布は中央氣象臺發行の「昭和 16 年 7 月 15 日長野强震調査概報」中の P 波初動分布に一致するのは興味をひく．

地震調査表

我々のつくつた地震調査表は縣學務部が各地の國民學校へ記入依頼狀と共に配布するといふ便宜を與へられ，各町村の字毎に１枚宛の報告が書かれる様にした．記入者は多く高等科の二年生であつた．此の表によつて得られた結果は前の表に示した．

第５圖　光り物の見えた方向（３個の白丸は 33 KV の送電線の斷線個所）

此の表の中，調査戸數は主として振子時計の數から推定したもので戸數と時計の數とのわかつてゐる所で比較して見ると殆ど等しかつた．戸數が調査表の枚數より多いの

は1枚の中に統計的に調べた結果が括められたものが多かつた爲である.

光り物 大地震の時に起る光り物については武者金吉氏[1]の著書にそれまでの文獻と共によく調べられてゐるが，地震に伴つて必ずあるものではない様である．今回の地震には各地で多數の人々の見たことは第2表からもわかる通りである．見た人の數の多い村のみをとつて，各村に於いて光り物の見えた方向と見た人數とについてベクトル和を作り，その方向のみを圖示すれば第5圖の様になる．墓石の時とは違つて調和分析はしなかつたが，此の中觀測數の多いベクトルを延長して得た交點の數を 5 km 平方の網目の中にわけてかぞへ，前の通りに計算して見ると次の樣になる．

$$m=38,\quad n=292,\quad N=705$$

$$E\fallingdotseq O(10^{-6})$$

交點數は矢の向きが偶然の場合よりも遙かに多く，その結果は信用出來る．網目の隅にある交點數を更に4つ宛平均し，その値を正方形の網の中心に記した上で數の等しい線をひくと第5圖の通りで，楕圓形をなし，その中心は長野市の北東，吉田町に當る．光り物は如何にして生ずるかは寺田寅彦，清水武雄の二氏の說明されたものがある[2]が，今回のものは高壓線の斷線によるものではないかと思ふ．長野電氣株式會社の調査によると，淺川村伺去(シサリ)眞光寺・長野市吉田町に於て 33 KV の送電線が切斷され發光が見られたことは確かである．又同じ電壓の送電線の斷線が三水村字田中にもあつたが發光は確かでない．交點の數の方から求めた中心は前の二個所と大體一致するから，光り物は電光を見たとして說明がつく．三水村のは此の様にして說明は出來ないが，こゝに記載を略した字別の調査材料を見ると字田中で光を見た人の數が特に多いことは此處でも發光したと考へてもよいと思ふ．

尙調査表によつて光の色を見ると，色に關する報告數 1047 の中青白が 49%，赤 31%，黄 16% で，他に青，綠，橙以外に黄赤，黄茶，青赤，青黄といふ複雜な色が報告された．光の形について報告數 937 の中電光が 71 %，火柱 18 %，火の玉 9 %，他に火事，極光，星，花火等と記したものが少數であつた．時刻については地震後が最も多く 52·5%，同時か地震前に見た人の數は 19 % となる．長沼附近で直接聞いた話でも電光の様だつたといふのが多く，或ひは星が二つ見えたとも云ふ．光の目撃者の報告の代表として8月 22 日に長野市西長野の牛木辰一郎氏の報ぜられたものを掲げる．「……激震の止みたるを幸，家族と共に庭（南側）に避難したる時は電燈は消え手探りにて出でし所暗夜に善光寺（E 20° N）の方にあたり青白色の光芒 1 間位立

1) 武者金吉 地震に伴ふ發光現象の研究及び資料（昭和7年）
2) 前掲 1) を參照

上り，幅も 2 米を出ず，さてと思ひ居るうちに消えて間もなく 2 回目の光芒，不思議と思ひ居るうちに消えて最初の强烈なる餘震を受け家の甚しく動搖するを見受けました．月はなく電氣も消え，それでも變壓器の故障かと思ひました．地電氣の放電個所は震央地の方向なるも地形の方から震央地では遠過ぎるやうに思はれ，目擊個所よりはもつと近い所ではないかと思はれます．有樣は放電の際の遠くで見るものの如く，家並や庭園の木々の緣邊に幅 2 米位，高さは之より高いやうに見受けられました．色は放電の際の淡きもの，兎も角も地震に際して光現象を望みたるは最初の經驗，其後餘震はしきりにあるも光現象なく，小雨となり屋内に入る．右は參考までに御報告致します……」

當時雨模樣であつたが，近くに雷はなかつたので，吉田の送電線の斷線の際の電光と見ればよいのであらう．但し，雨模樣の雲の低い場合として觀測された距離が遠過ぎる樣にも思はれる．

尙普通の高壓線の斷線が吉田營業所管內で 2，柳原で 2，低壓線は吉田 3，長沼 18，柏原 1 であつた．

要する此の地震の際の光り物は高壓線の斷線によつて說明出來る樣である．

振子時計　地震調査表によつて振子時計が地震で止つたか否かを，文字盤の方向に關して調べた．1村につき 10 個以上の時計を調べた村の數が 124，20 個以上が 93 あつた．この 93 の村の結果（第 IV 表）から，止つた時計の百分率をとつてその値の等しい所を結んで見ると第 7 圖の樣になる．村落の分布が限られてゐることが影響してゐるかも知れないが，千曲川・犀川に沿うて時計を止めるに有効な地震動が强いと云へる．又野尻・諏訪の湖畔特に後者が異常であることは著しい事實である．

震央には假りに中央氣象臺の概報に記された位置を採り，震央距離△と時計の止つ

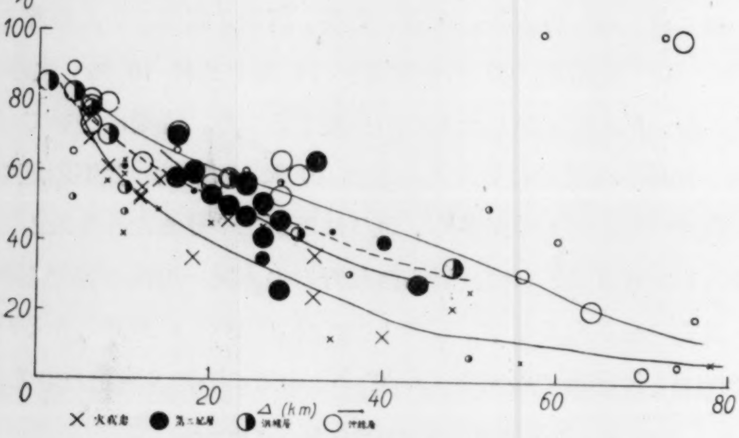

第 6 圖　振子時計の止つた率と距離及び地質との關係

第 IV 表

番號	郡	村	震央距離 (km)	止つた率 (%)	地質
1	諏訪郡	長地（オサチ）	70	3	沖積層
2		上諏訪	74	99	〃
3		川岸	78	6	火成岩
4		下諏訪	72	100	沖積層
5		四賀	76	19	〃
6		岡谷	74	5	〃
7	北佐久郡	三岡	48	33	洪積層
8		大里	44	26	〃
9		西長倉	52	50	〃
10		協和	50	29	火成岩
11		伍賀	50	7	洪積層
12		芦田	48	21	火成岩
13	東筑摩郡	島立	60	41	沖積層
14		芳川	64	21	〃
15		{松本市 城西町	58	100	〃
16	南曇安郡	豊科	56	31	〃
17	北曇安郡	八坂	40	40	第三紀層
18		社	44	28	〃
19	小縣郡	神川（カン）	36	31	洪積層
20		和田	56	6	火成岩
21	更級郡	鹽崎	22	58	沖積層
22		眞島	12	62	〃
23		村上	30	59	〃
24		信里	18	57	第三紀層
25		牧郷	32	63	〃
36		篠ノ井	16	58	沖積層
27		桑原	26	48	第三紀層
28		稲荷山	24	60	沖積層
29		大岡	34	43	第三紀層
30		力石	28	63	沖積層
31		上山田	28	26	第三紀層
32		共和	16	58	〃
33	埴科郡	坂城	28	53	沖積層
34		松代	16	70	〃
35		豊榮	18	35	火成岩
36		尾代	22	52	沖積層
37		五加	26	50	〃
38		埴生	24	60	〃
39		雨宮縣	20	56	〃
40		中ノ條	30	42	洪積層
41	長野市	吉田	6	77	〃
41		北石堂		38	〃
43		南石堂		60	〃
44		中御所		62	〃
45		岡田		55	〃
46	上水內郡	若槻	4	82	洪積層
47		信濃尻	16	66	沖積層
48		大豆島（マメシマ）	8	79	〃
49		三水（サンスイ）	6	69	火成岩
50		柏原	14	57	〃
51		中郷（ナカサト）	6	75	〃
52		南小川	26	41	第三紀層
53		北小川	26	35	〃
54		朝陽	6	78	沖積層
55		七二會	18	60	第三紀層
56		淺川	6	73	〃
57		柳原	6	80	沖積層
58		水內（ミノチ）	24	47	第三紀層
59		神郷（カミサト）	1	85	洪積層
60		富士里	10	59	火成岩
61		日里	22	50	第三紀層
62		柵（シガラミ）	18	54	〃
63		長沼	4	65	沖積層
64		小田切	16	70	第三紀層
65		古里	4	89	沖積層
66		芋井	10	61	第三紀層
67		古間	12	53	火成岩
68		鬼無里（キナサ）	26	51	第三紀層
69		津和	28	46	〃
70		榮	24	57	〃
71	下水內郡	柳原	20	53	〃
72		外様	24	56	〃
73		岡山	32	36	火成岩
74		太田	28	57	洪積層
75		水內	40	13	火成岩
76		常盤	22	58	洪積層
77	上高井郡	須坂	8	70	〃
78		綿內	8	61	火成岩
79		保科	12	53	〃
80		山田	14	49	〃
81		小布施	4	52	洪積層
82		豊丘	10	63	火成岩
83		川田	10	42	〃
84		井上	8	57	〃
85		都住	6	76	沖積層
86	下高井郡	瑞穗	26	44	火成岩
87		堺	34	12	〃
88		市川	32	24	〃
89		穗高	22	46	〃
90		穗波	12	55	〃
91		平野	10	55	洪積層
92		木島	20	45	火成岩
93		長丘	10	48	洪積層

た百分率との關係をみると，率の距離と共に減ることは明瞭である．更に此等の點を地質調査所の 40 萬分の 1 の地質圖によつて，火成岩・第三紀層・洪積層・沖積層

にわけ，更に率の信用度を區別する爲に報告された時計の數が 100 以上のもの，20 以上のもの，その中間のものとの三つに分けて印の大さで區別した圖（第 6 圖）を

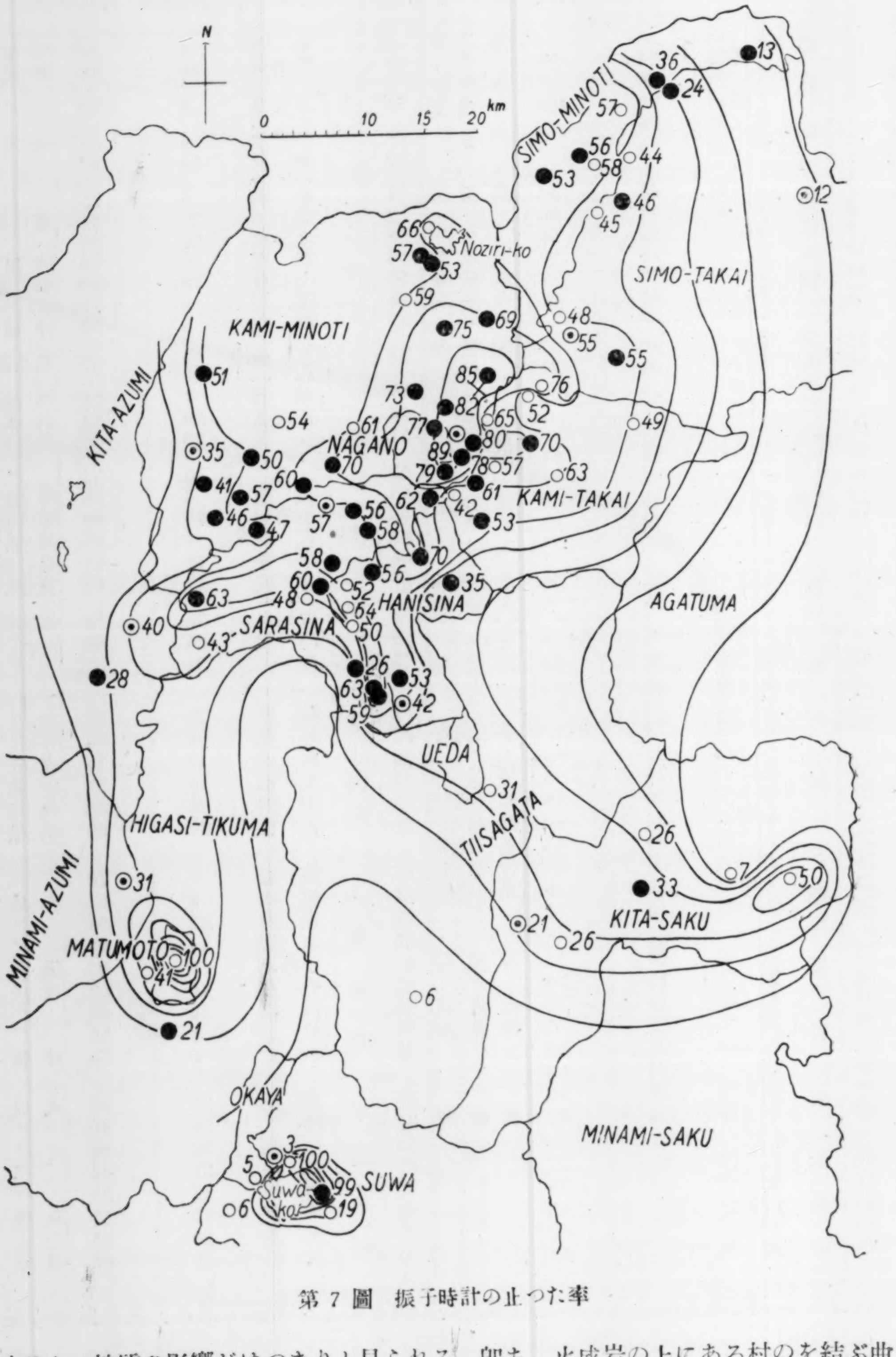

第 7 圖 振子時計の止つた率

つくると，地質の影響がはつきりと見られる．卽ち，火成岩の上にある村のを結ぶ曲

線は第三紀層及び洪積層の線の下に，沖積層のものはその上にある．第三紀層と洪積層とははつきり分れないが，結論として地質の差が時計に關する地震動に影響することが統計的に立證される．

止つた時計の文字盤の方向に關しては，長野市內各地では著しい結果であつたので，縣下一帶にまで調査を擴げたが，思つた程の結果は得られなかつた．東西南北の方向に分け，其の最大の率と最小の率との差を以て方向性の度合を示すものとしてこれと止つた率との關係をしらべたところ，30～40 % の率の所が最も方向性をもつてゐると言へる樣である．此以外は將來の調査にまつこととする．

地鳴　此の地震は音を伴つたので，我々の實地踏査以外の土地の狀況も知らうと，調査表に記入を依賴した．音は殆ど總べてドン又はゴーと形容された．方向性については，光り物と同樣にして調べ，矢の延長の交はる點の數から中心を求めると，墓石の顚倒方向から求めた震央に大體一致した．（第 8 圖）併し交點數を數へる網目が 6 km每であり．用ひた地圖も前者は 5 萬分の 1，後者は 20 萬分の 1 であるから餘り詳しいことは云へない．此の場合の統計の結果を次に記して此の問題は止める．

$$m=42,\quad n=267,\quad N=86,$$

$$N=O(10^{-4})$$

地割れ　i)　激震區域の各地で地割れが見られた．次に代表的のものを記す．千曲川兩岸の堤には小さい割れ目が無數にあり，堤の內側の數十年前から畑となつてゐる所にも 30～40 m の長さの割れ目を東岸では日野村村山，西岸では長沼村穗保．津野附近で見た．そして所々水と砂とを噴出した跡の砂が殘つてゐた．

ii)　朝陽村北長池の南外れ野菜畑の中に N 30° N の方向で 300 m 位小川を越して續いたものがあつた．（第 9 圖）割れ目の深さは 160 cm 以上の所があつた．此の割れ目の線は言傳へによる犀川の岸であつたといふ．

iii)　豐洲村相之島の道路は道に平行な割目が無數に出來て，方々から砂をまぜた水が噴出し足をぬらし，そのために地震を千曲川の氾濫と間違へた人さへあつたといふ．

iv)　此の地震で最も著しかつたのは長沼村赤沼東組のものであらう．無數の割れ目が道路にも家屋の下にも通つてゐた．その主なものをあげれば次の通りである．（第 10 圖）

a)　N 20 m の割れ目が北端から N 25° W に向きを變へて數 m 續いてゐるもの

b)　N 10° W から N 45° W に變り數十 m 續いたもの（第 22～23 圖）

c)　方向 N，長さ約 10 m のもの

かつた．それ故，この割れ目は引離されたもので捩れは無いと考へられる．そして此の變位は，割れ目に殆んど平行して北方に，以前は沼で現在は田になつてゐる低地があるので，その方に土地がずり落ちた結果地割れを生じたとすれば一應の説明はつく．

尚赤沼では地割れの多い土地より，南の部分の地割れの無い土地の方が家屋の震害は多かつたことが目についた．

鐵道の被害　省線では吉田驛の北 6 km の所では線路が左右に 70 mm，上下に 50 mm のずれがあり，そこから南 2.1 km 所に 2 個所少し變動があつたが別に測定はされなかつたといふ．長野電鐵では村山橋の東約 100 m の附近が 30 cm 程沈下したが，交通には支障りはなかつた．村山橋は電車と人や車の通路とがな並んだ鐵橋であるが中央を固定して兩端に橋桁のずれが增し，その量が對稱であつたことが見られた．

井戸　豐洲村では道路から水を噴出したことは前に述べたが，井戸水も噴出した所が多く水は濁つた．上水内郡若槻・朝陽・神郷の村々でも濁つたものが多かつた．

神郷村南郷村は家屋の被害の大きかつた所であるが，7 月 20 日に調査に行つたところ山麓の谷間に石油をとる目的で井戸を掘り，石油は出ないので鐵管を埋め殘してあつた所から 7 月 17 日の夜以來水が流れ出してゐた．

何の郡でも井水の濁を報じてゐるが本年は雨が多く，此の地方より南方の松本市では道路の眞中に割れ目が出來て水が涌き出した所があつたといふことであるから，以上は地震が一次的の作用をしたか否かは疑はしい．

溫泉については諏訪で溫泉調査數の 226 中 55 の溫度が騰つたと報告され，埴科郡寺尾の加賀井溫泉でも地震前水量が增し濁り，地震後に水量はへり色は澄んだといふ．上高井郡高井の山田溫泉では地震後量が增し溫度が上つたといふ．併し矢橋氏[2]の調査によると，今度の地震による溫泉の變化は確かとは云へない様である．

終りに臨み，此の調査は文部省科學研究費による所多く，地震調査表に就いては長野縣學務部の御援助によつて出來たものであつてこゝに御禮申上げる．其の他地震後の御多忙中種々調査に便宜を與へられた長野縣官民諸氏特に八木貞助氏には種々御力ぞへ下さり感謝に堪へない次第である．

---

2)　矢橋德太郎　地震 13（昭和 16），267—271．

39. *A Statistical Investigation of the Strong Earthquake of July 15, 1941, near Nagano.*

By Fuyuhiko KISHINOUYE, Takesi NAGATA, and Setumi MIYAMURA,

Earthquake Research Institute.

Detailed investigation of phenomena that accompany earthquakes is fundamental work in seismology. Unfortunately, however, we have not yet advanced to that stage where we could predict earthquakes, while the means at our disposal at present for studying them the instant they arrive are inadequate, particularly, in the case of destructive shocks near their epicentres, all that we can do being to study the aftershocks that are recorded on seismographs, which data are nevertheless very valuable. But there is much information besides that pertaining directly to the main shock, and it is this knowledge that the writers sought to obtain.

In the case of the recent earthquake in the neighbourhood of the City of Nagano, they tried to investigate the main shock from phenomena that accompanied it.

Overturning of gravestones have often been taken as a dynamical indicator of the seismic intensity. Although a few gravestones that were regarded hitherto as typical for this purpose were examined, it was found that they are not typical in every respects, to circumvent which drawback we set ourselves to study the earthquake statistically.

Fifty churchyards and cemetries were visited and the number of overturned gravestones counted, and the directions in which the stones fell were measured, ignoring the differences in their type, shape, and mode of setting. The results are shown in Table III and Figs. 2, 3. The rate of overturn was large in the village of Naganuma, lying the flood plain of the Tikuma-River, and on the hill side taluses in the villages of Kamisato and Wakatuki.

The total number of overturned gravestones was divided into twelve sectors, and the numbers in each of these sectors analysed in Fourier series, the first harmonics representing the number thrown down by the first shock and the second harmonics the number of those thrown down by the horizontal back and forth motions of the ground. The vectors of the first harmonics exceed the circles of their expectancy which, as shown by the dotted circles in Fig. 3, converge to Naganuma Village with a probability of 10^{-10}. The differences in the directions of the first and the second harmonics are small, as shown in Fig. 3.

We addressed questionnaires to the inhavitants of ten districts in Nagano Prefecture and received 1432 replies. Our questions concerned the effects of the earthquake motion on pendulum clocks; luminous phenomena and earthquake sounds that accompanied the earthquake, if any; earth fissures, and changes in the water of wells, as also in the ground level.

Isoseismal lines of the percentage of stopped clocks showed smaller values of seismic intensity than the isoseismal lines of the percentage of overturned gravestones (Fig. 6).

Luminous phenomena were seen. Many of the replies mentioned bluish white sparks having been seen immediately following the shock. The Electric Company informed us of three cases of of short-circuiting of 33 kV power cables. The vectors of the directions in which the spark was seen converge to the place where the cables were broken. So we concluded that the main cause of the luminosity was the electric sparks (Fig. 5) due to short-circuiting.

The vectors of the direction in which the earthquake sounds were heard also converged to the epicentral region (Fig. 8).

In addition to the foregoing phenomena, many fissures were met with in the macroseismic

d)　方向 N 30°E のもの

e)　割れ目 d の北のりんご畑にはいると，道を横切つて N に向つた小さな割れ目が無数にあつた．

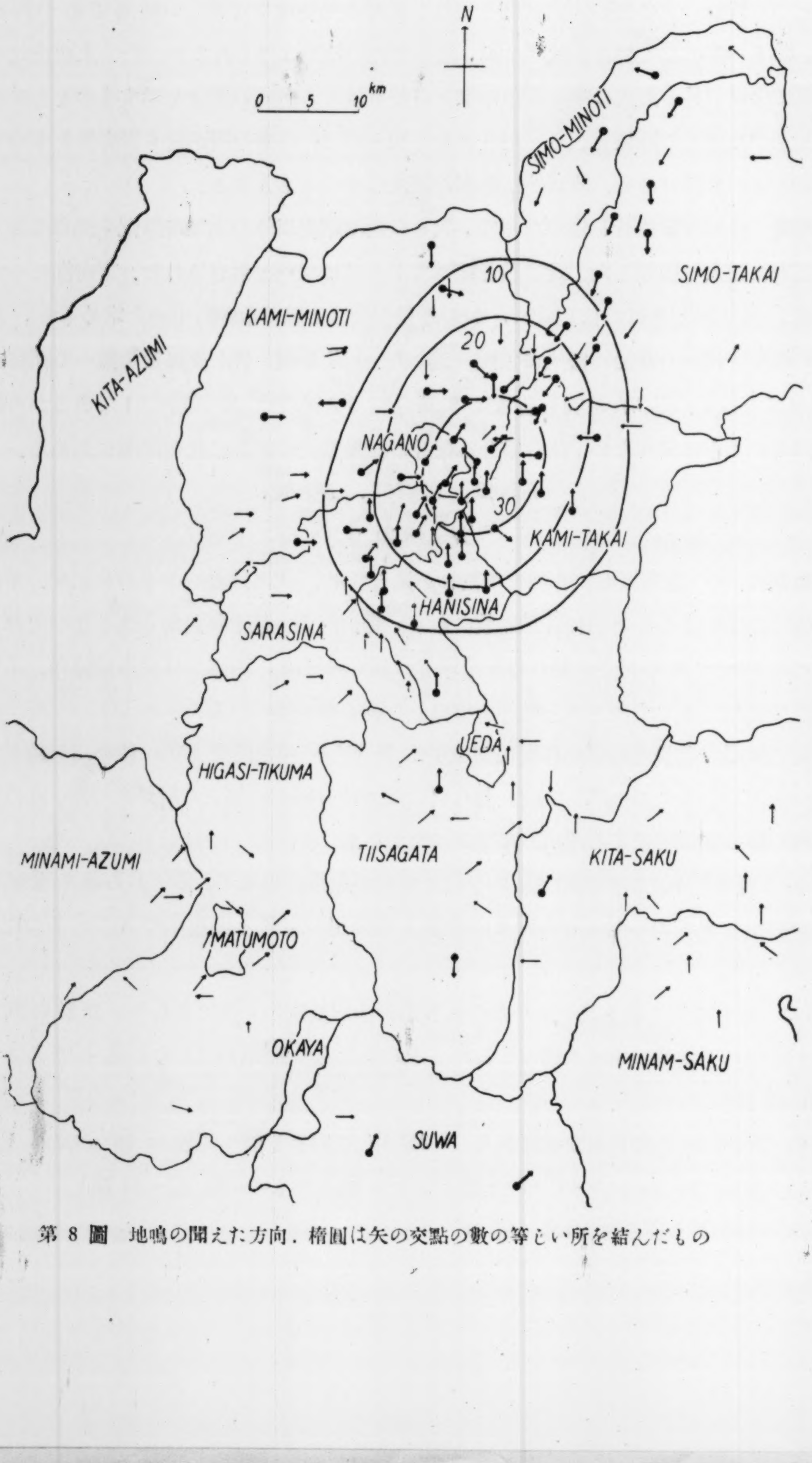

第 8 圖　地鳴の聞えた方向．楕圓は矢の交點の數の等しい所を結んだもの

V）赤沼東組の北，豊野から小布施に行く道の南約 500 m の所に今度の地震で生じた最も大きい割れ目が 7 月 18 日我々が此處に着いた少し前に見出された．全長約 250 m で第 11 圖の A と記した割目がその中でも大きく，地震斷層かと思はれる程であつた．簡單な測量を行つた結果は第 11 圖に示すとほりであつて兩端のかげをつけたところには水と砂とをふきだしたあとがあつた．(第 18～19 圖) A の附近に殆ど東西及び南北の畝がつくられ豆が植えられてゐたので，割目の兩側の變位が認められた．そこで一方の畝の上に紐を張り他方まで延長して横ずれを測定した．そして割れ目の兩端に横ずれがあるか否かを見ようと考へた．東西のずれを 6 個所南北 5 個所測つた結果，此の割れ目では

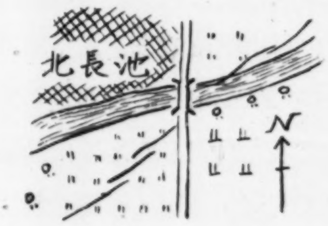

第　9　圖

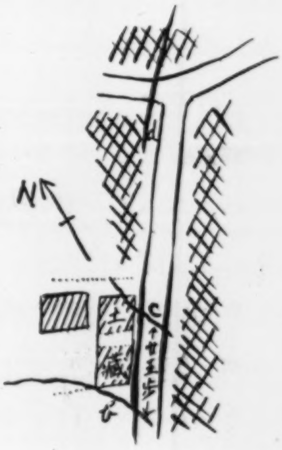

第　10　圖

東西のずれ	13.2 ± 1.9 cm
南北のずれ	15.0 ± 1.7 cm

となつて，此を合成すると割れ目の向きに垂直に 20 cm 程水平移動であつたことがわ

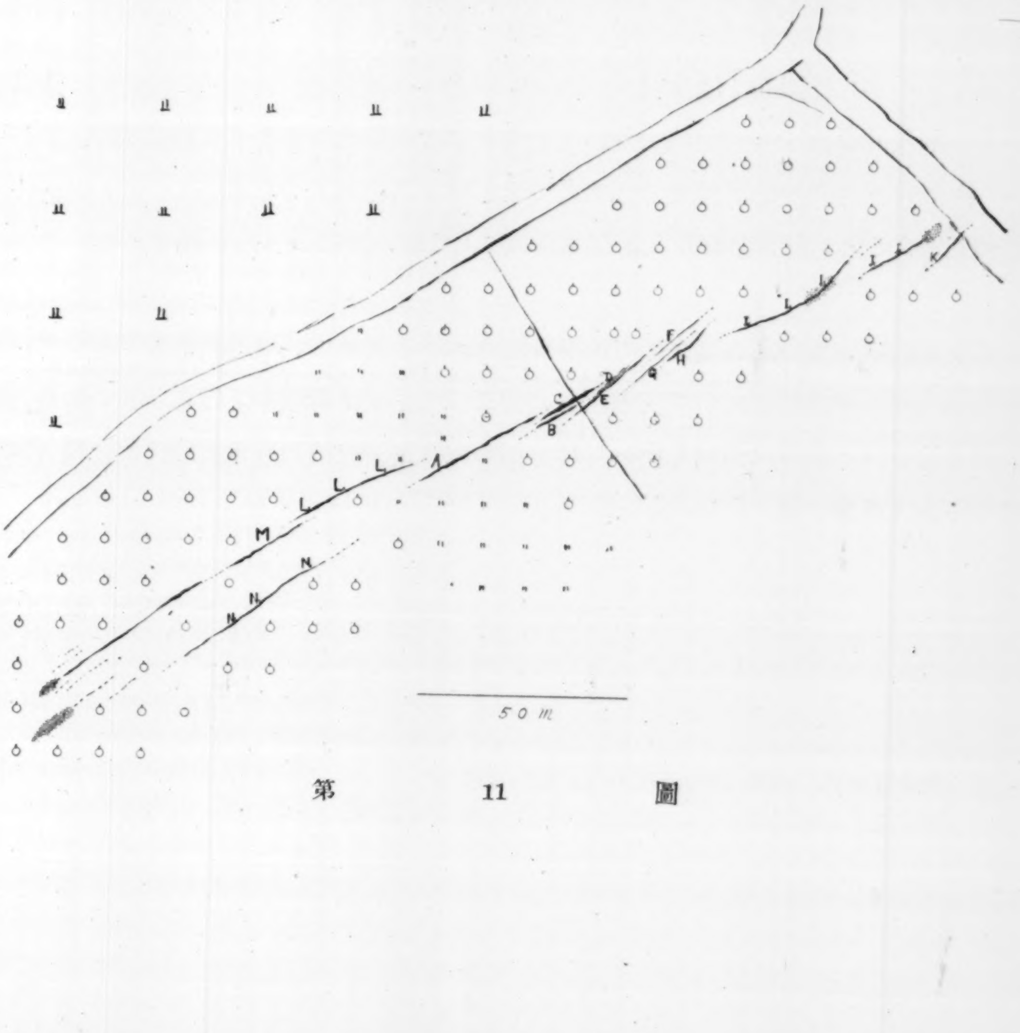

第　11　圖

region, crossing roads and fields, especially in the villages of Naganuma, Toyosu, and Hino, the largest being the one that occurred in the apple orchard at Akanuma-Higasigumi, Naganuma. Its total length was about 250 m, the maximum width of the opening being about 20 cm. These fissures were probably the result of local land-slides of the alluvial deposits of the Tikuma-River.

第 12 圖 豊洲村別府(No. 41)
顛倒率 31 % (15/48)

第 13 圖 神郷村南郷桃源院 (No. 43)
顛倒率 89 % (239/267)

第 14 圖 長野市吉田町(No. 2)
顛倒率 31% (147/474)

(矢橋德太郎氏撮)

第 15 圖 日野村村山 (No. 39)
顛倒率 6 % (6/190)

第 16 圖 中郷村四ツ屋(No. 26)
顛倒率 13 (14/105)

(矢橋德太郎氏撮)

第 17 圖 長沼村穗保(No. 37)
顛倒率 53 % (129/242)

0

第 18 圖　長沼村赤沼東組の地割れ

第 19 圖　赤沼東組の地割れの横ずれ測定

(永田康一氏撮)

第 20 圖　赤沼東組砂を噴出した地割れ

(永田康一氏撮)

第 21 圖　豊洲村相之島の地割れ

第 22 圖　赤沼東組の地割れ

第 23 圖　赤沼東組の地割れ第22圖の下の方

40. 昭和16年7月15日長野地震の家屋被害に就て

地震研究所 金 井 清

(昭和16年9月18日發表——昭和16年9月20日受理)

1. 緒 言

昭和16年7月15日23時45分長野市東北方10km附近に起つた地震は約100 km平方の地域に激甚な被害を生じ，全潰家屋總數259棟，半潰家屋總數319棟死者6人，重傷者11人に及んだ．

筆者は主として家屋の大黒柱及び筋違の耐震効果を被害家屋について調べる目的で踏査に向つたところ，被害區域にはこれ等を使用した家屋が極めて少く，その目的を十分に果すことができなかつた．然しながら，震害地に於ける數家屋の實例によつて大黒柱並びに筋違が理論[1),2),3)] と全く一致して家屋の耐震性に大きな効果を與へてゐることを確めることができた．

調査は古平秀數氏の非常な援助を得て，7月18日から7月22日に亘る5日間行つた．

玆に，家屋被害調査の結果を報告し，地震による家屋破壊に力學的解釋を若干附け加へて見ようと思ふ．

2. 家屋被害概況

各村役場の調査による部落別の被害統計を第I表に示す．

第I表 長野地震被害統計

		總戸數	總家屋數	全潰		半潰		計	住家倒潰率	死者	傷者	調査日
				住家	非住家	住家	非住家					
長沼村	大町	103		5	3	15	0	23	19			
	穂保	103		10	8	15	4	37	24			
	津野	52		10	1	6	1	18	31			
	赤沼	213		13	1	24	0	38	17	3	3	7月18日
	小計	471		38	13	60	5	116		3	3	

(次頁へ續く)

1) 筆者,"Aseismic Properties of a Daikoku-basira (Principal Column) or Similar Column in a Japanese Style Building," 地震研究所彙報 **16** (1938), 256～272.
2) 妹澤克惟，筆者，"Theory of the Aseismic Properties of the Brace Struts (Sudikai) in a Japanese-style Building. (Preliminary Notes)," 地震研究所彙報 **16** (1938), 702～713.
3) 筆者，地震研究所彙報**17** (1939), 233～252, 559～568, 569～578, 695～712, 713～722.

第 I 表 (續き)

		總戸數	總家屋數	全潰 住家	全潰 非住家	半潰 住家	半潰 非住家	計	住家倒潰率	死者	傷者	調査日
神郷村	豊野	535		0	0	5	3	8	1			7月19日
	石	215		10	7	15	5	37	12			
	南郷	144		39	12	50	17	118	62	3		
	小計	894		49	19	70	25	163		3	0	
淺川村 (部落 19)	伺去	135 概算	總戸數の約3倍	0	1	1	0	2	1			7月20日
	東條	90		3	1	0	0	4	3			
	西條	100		10	2	5	4	21	11	2	1	
	小計			13	4	6	4	27		2	1	
若槻村	稻田	170 概算	〃 2 〃	4	17	12	0	33	9			7月20日
	德間	120	〃 2 〃	10	4	8	3	25	15	2	3	
	東條	110	〃 1·5 〃	2	0	5	0	7	6			
	上野	100	〃 1·5 〃	0	0	3	0	3	3			
	田子	68	〃 1 〃	0	0	1	0	1	1			
	吉	115	〃 1·5 〃	0	1	3	0	4	3			
	小計			16	22	32	3	73		2	3	
古里村	金箱	51	84	0	4	7	1	12	14			7月21日
	上駒澤	87	168	1	1	3	1	6	5			
	下駒澤	60	131	2	1	8	5	16	17			
	三才	151	280	5	3	10	0	18	10			
	富竹	133	252	0	0	5	3	8	4			
	小計	482	915	8	9	33	10	60		0	0	
豊洲村	相之島	100 概算	總戸數の約3倍	10	16	29	11	66	39			7月23日
	小島	90		4	1	12	1	18	18			
	小河原	200		0	3	0	4	7	4			
	小計			14	20	41	16	91		0	0	
柳原村	北長池	117	總戸數の約2.5倍	0	5	3	1	9	2			7月23日
	北尾張部	75		1	3	1	1	6	3			
	石渡	74		0	6	2	2	10	3			
	南堀	78		1	3	1	1	6	3			
	北堀	48		0	0	5	3	8	10			
	小計	392		2	17	12	8	39		0	0	

(次頁へ續く)

第 I 表 (續き)

		總戸數	總家屋數	全潰		半潰		計	住家倒潰率	死者	傷者	調査日
				住家	非住家	住家	非住家					
柳原村	村山	70 概算	200 概算	1	4	0	5	10	2			7月23日
	小島	90	280	1	1	0	0	2	1			
	小計			2	5	0	5	12		0	0	
日野村	高梨	70	總戸數の約2倍	0	1	1	3	5	2			7月23日
	蘆川	115		0	1	4	7	12	3			
	沼目	62		0	0	5	0	5	8			
	八重森	35		0	0	1	2	3	9			
	五閑	10		0	0	1	0	1	10			
	村山	145		0	0	3	6	9	2			
	小計	437		0	2	15	18	35		0	0	
長野市				5		28		33				
高岡村				1		0		1				
總計				260		390		650		6	11	

本地震の家屋被害地域は長野市と上水内郡に限られ，長沼村，豐洲村相之島，神郷村南郷を包含する約 4 km 平方の千曲川流域の沖積層の地域が被害激甚にして家屋倒

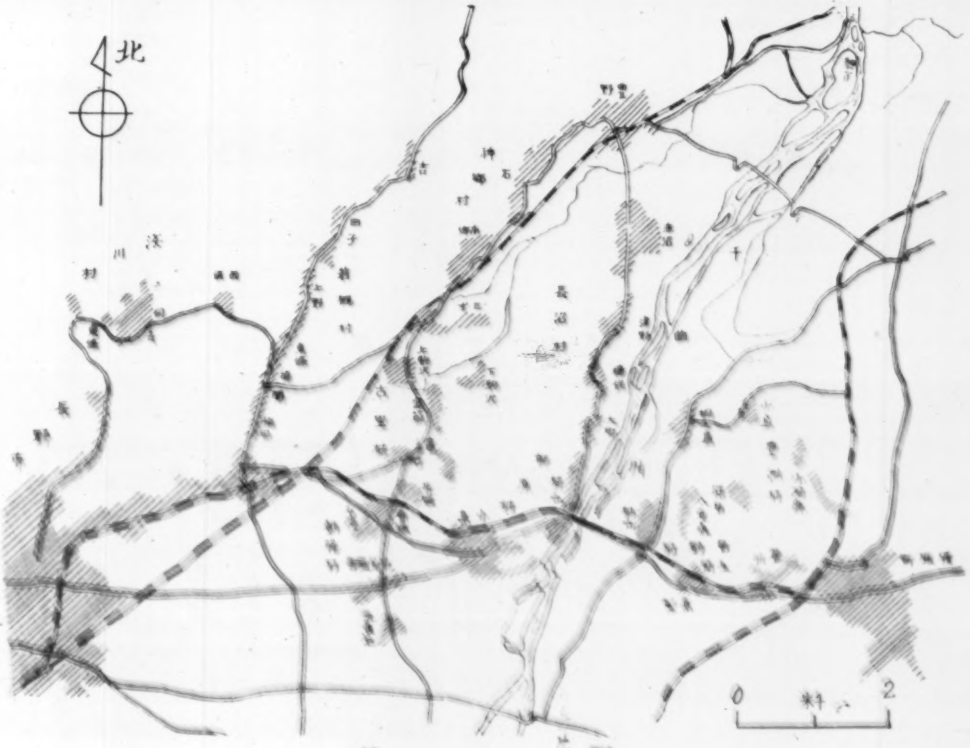

第 1 圖

潰率 15 %以上である．家屋被害の距離についての減少度は極めて大きく，被害激甚な地域の中心から 5 km 距ると棟瓦が僅かに落ちた程度の損傷しかない．

長沼村，豐洲村は屢大洪水に襲はれ，土臺，柱，壁等の腐蝕が多く，そのため地震の割合に家屋被害が大きかつたと考へられる．長沼村赤沼の道路脇田圃にある大洪水の地面よりの高さを示した木標の記録を参考のために記して置く． 明治 44 年 8 月 5 日，12 尺；明治 43 年 8 月 11 日，12·7 尺；弘化 4 年 4 月 12 日，14·6尺；明治 1 年 5 月，14·6 尺；明治 29 年 7 月 21 日，16·2 尺；寛保 2 年 8 月 2 日 20 尺以上．

土藏の損傷には倒潰と滑動があり，長沼村では特に倒潰が目立ち，淺川村，若槻村では滑動が目立つた．全被害地を通じて土藏の損傷は少く，倒潰した土藏の大部分は水害のために下部が腐蝕してゐた．

3. 震害地農家の住居構造

同地方の農村の住家構造は詳細にわたつては種々の差違があるが，本地震の被害の説明に必要な部分は大體第 2，3 圖に示す構造で代表できる．

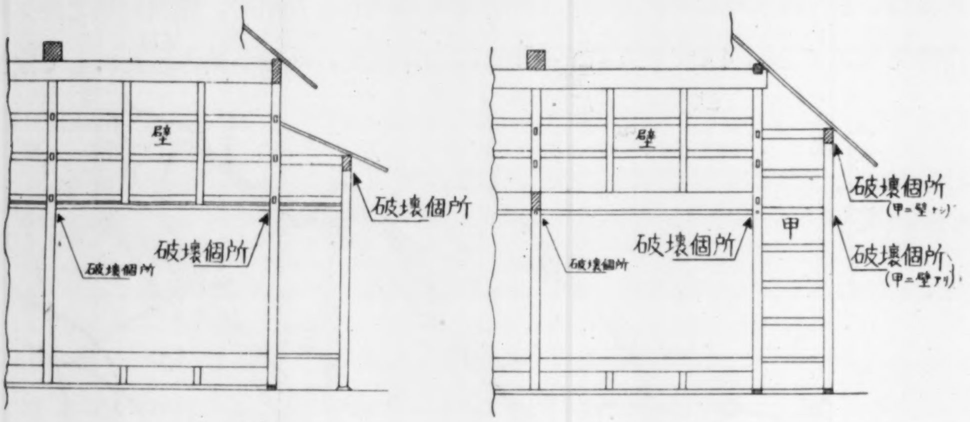

第 2 圖

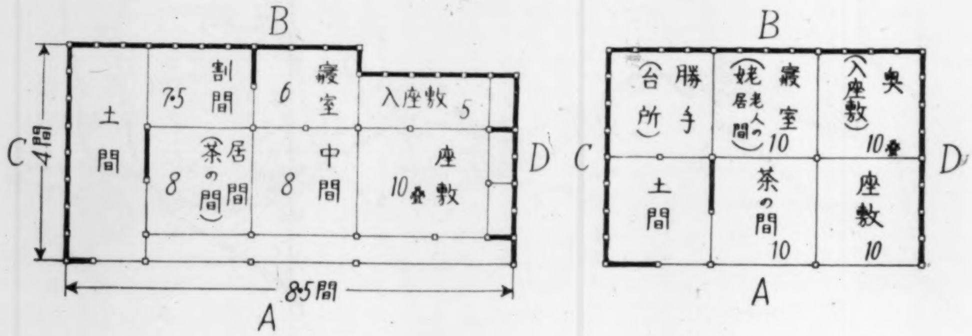

第 3 圖

力學的考察に關係のある構造部分を簡單に記すと，先づ外壁は表（A）には非常に少く，兩側（C，D）の全部と裏（B）の大部分にある．間仕切壁は疊敷の部分と土間との境に僅かにあるのみで，室と室との間は總べて襖で境されて居る．4尺以上の小壁が鴨居と天井の間にあり，天井裏は多くは窓のない壁體を廻らして物置として利用されて居る．此の物置の採光，換氣は天窓でなす．柱は4寸×4寸土臺は4寸×2寸，軒桁，胴差は4寸×10寸の松又は杉の角材の使用が多い．大黒柱，筋違を使用した家屋は稀である．下屋は第2圖の右圖の如く母家と共通の屋根のものと，左圖の如く外柱の中間と棰木受で連結して別に屋根を作つたものとがある．

4. 家屋倒潰方向

踏査に向つたのが地震2日後であつたため，既に損傷家屋の修理に着手され，長沼村以外は家屋倒潰方向の十分な統計的の調査ができなかつた．長沼村の踏査結果を第II表に示す．此表の右2列の相違の主原因は村道から遠隔な區域の踏査洩れである．

第II表　長沼村家屋倒潰統計

部落別	家屋の向	倒潰方向	住家 草葺	住家 瓦葺	土藏	納屋	小計	合計	村役場調査倒潰家屋總數
大町	南	南	2	2	0	0	4	15	23
		西	3	2	0	0	5		
	東	南	0	0	1	0	1		
		西	2	0	3	0	5		
穂保	南	南	3	5	0	0	8	26	37
		北	1	1	0	0	2		
		東	1	0	0	0	1		
		西	1	1	3	0	5		
	東	南	1	0	0	0	1		
		東	1	2	0	0	3		
		西	0	2	2	2	6		
津野	南	南	4	5	0	0	9	13	18
	東	東	1	1	0	0	2		
		西	0	0	1	1	2		
赤沼	南	南	6	4	1	1	12	28	38
		北	2	0	0	0	2		
		東	1	0	0	0	1		
		西	3	0	2	2	7		
	東	南	1	0	0	1	2		
		北	0	1	0	0	1		
		西	1	0	1	1	4		
合計			34	26	14	8	82		118

同地方の農家構造は第2圖に示す如く，表(A)には壁が非常に少く，裏(B)と兩側(C, D)は大部分壁體であるため，A面の剛度はB, C, D面に比して著しく弱い．又，A, B面はC, D面より長いのが普通であるから此の種の家屋に震力が作用すると先づ表(A)の柱が損傷して，家屋はその方向に倒潰する可能性が非常に多い．踏査の結果も果してその通りで，第II表に示す如く倒潰住家總數の50%以上は表(A)方向である．土藏，納屋は四面の剛度差違が少いため，各部落毎の倒潰方向は略一定して居り，住家の倒潰方向は見掛上は甚だ複雜であるが，表(A)方向の倒潰家屋を除くと，同部落の土藏，納屋の倒潰方向と殆んど一致する．又土藏の滑動，土塀の滑動，鳥居の横の方向への傾斜（寫眞第21, 22, 24, 32圖參照）その他特殊な構造物の倒潰方向は前の方法で決定した同地の家屋倒潰方向と略一致する．故に表(A)

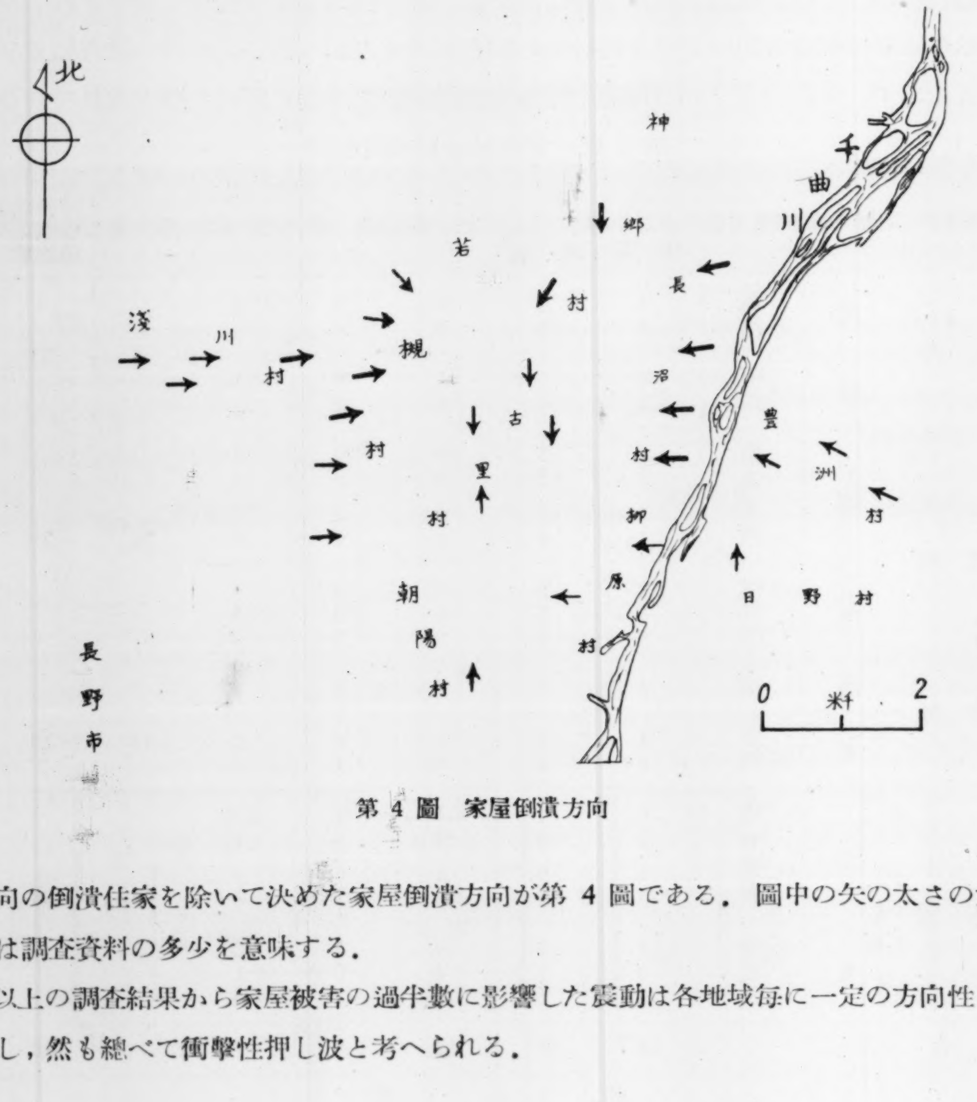

第4圖　家屋倒潰方向

方向の倒潰住家を除いて決めた家屋倒潰方向が第4圖である．圖中の矢の太さの大小は調査資料の多少を意味する．

以上の調査結果から家屋被害の過半數に影響した震動は各地域毎に一定の方向性を有し，然も總べて衝擊性押し波と考へられる．

5. 家屋倒潰率

土藏，納屋，蠶室その他の非住家總數は村役場でも容易に判明せず，又假令その總數が判つたとしても土藏と納屋では構造，剛度の差違が甚だしいから，非住家を除いて家屋倒潰率を作ることにした．即ち第Ⅰ表に示した家屋倒潰率は住家のみの全半潰總棟數と全戸數との比の百分率である．

尙，村役場の家屋被害統計は調査日が違ふし破壊の定義も一定してゐないから，そのまゝで數量的に比較はできない．それ故，實地踏査の結果を加味して等家屋倒潰率曲

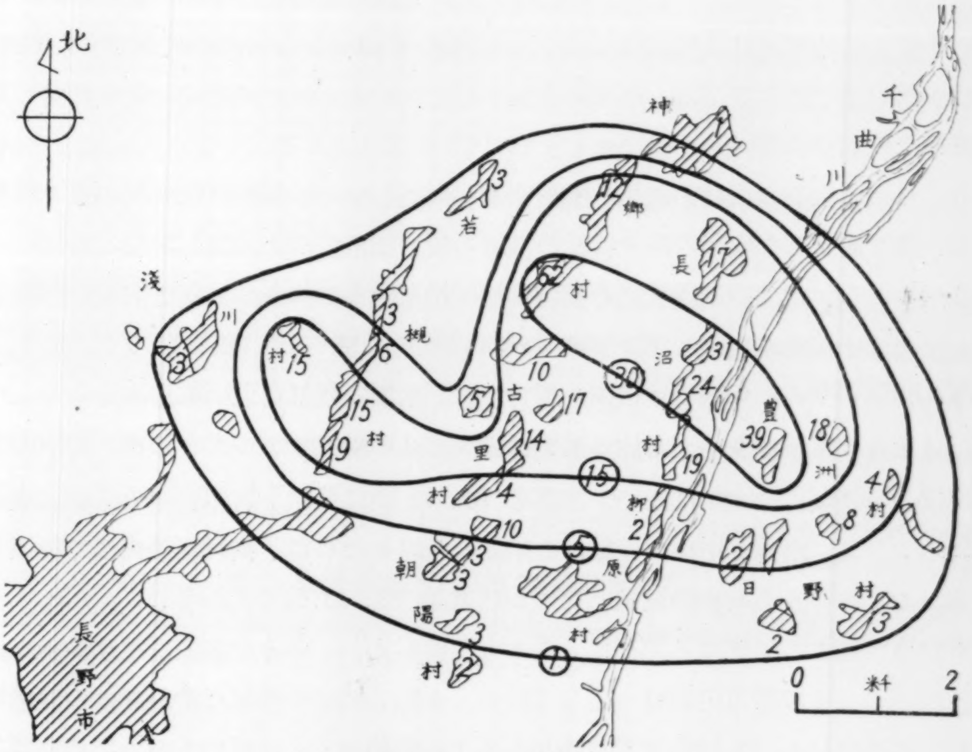

第5圖　倒潰家屋分布

線を作ると第5圖になる．圖中の各部落に附した數字は第Ⅰ表の家屋倒潰率を示す．

玆に，第4，5圖から家屋被害についての若干の考察をすると，先づ神郷村南郷の被害が特に著しいのは震動方向と住家の壁體のない方向（A）とが一致してゐたことで説明できる．淺川村西條，若槻村東條，德間，稻田が比較的堅い地盤であり，震央からの距離も割合に遠いのに被害が大きいのも亦同區域の住家に東向が多かつた爲であらう．

次に商店の構造は農家に比較して屋根が低くて，間仕切壁が多い剛構造であるが，

神鄕村豐野は商家又は事務所が全戸數 535 の中約 150 を占め，地盤の弱い南部に位置してゐるために特に被害が少かつたものであらう．又古里村富竹，上駒澤に被害の少いのは新しい様式のトタン葺の低い屋根が多い爲と考へられる．

6. 家屋構造と被害の關係

被害地踏査の結果，住家の倒潰狀態の最も多いのは，表柱が鴨居又は土臺の仕口で破損し，小壁を廻らした鴨居から上が小屋組共に一體となつて前方に押し出され，そのために中柱が次々に鴨居の仕口で破損して家屋全體が崩潰したか，或は傾斜したまゝ殘つた狀態である．故に此の場合には崩壞を免れて單に傾斜したのみの家屋は鴨居から上の小壁と小屋組には損傷は頗る少い．寫眞第 6 圖は此の有様を明かに示して居る．外柱が鴨居下で折れて下屋の壁部の中間を押し出し，そのため下屋の柱が鴨居の高さで裂けた狀態が寫眞 第 7 圖である．寫眞第 8 圖は此の様式で完全に崩壞した例で，後方に見える家屋は表柱が破損し家屋全體が傾斜したが小屋組は完全に破損を免れて居る．然も崩壞した家屋の向きは此の地域の家屋倒潰方向と一致し安全な家屋の向きは直角である．尙此の倒潰様式の特別な例で小屋組が特に弱い家屋は表柱，中柱が破壞したため小屋組が崩落し裏，兩側の壁體は安全に殘つた．(寫眞第 9 圖參照)．

次に間仕切壁のない細長い家屋の場合には，兩側の壁部に近い部分は安全で，中央部が破壞した家屋が多い．倉庫の被害は總べて此の狀態であつた．豐洲，赤沼兩國民學校校舍の損傷も此の例に近い．寫眞第 10，11 圖は住家，倉庫の中央部が崩壞したのを示す．又，兩側と中央部の軸部の剛度の差違のために，横材が中央部で破損した例も多く，そのうち軒桁の破損したのが寫眞第 12，13 圖でわかる．

前記の二通りの破壞型と異つて，表にも壁體があり，四方の剛度の差違が少い家屋は各地區により倒潰方向が略一定して居る．土藏，納屋の倒潰は殆んどこの狀態に屬した．寫眞第 14，15 圖の家屋は鴨居から上の壁體少く，小屋組も弱いため全體として破壞し，地震後に加へた斜材で辛じて崩壞を免れて居る．此の反對に鴨居上の小壁多く，小屋組も强固な爲，柱が鴨居下で損傷し壁體及び通柱も鴨居の高さで彎曲して壁體の下部は剝落したが，上部には殆んど損傷のない好例が寫眞第 16 圖である．

次に，筋違を使用した家屋は稀であるが，長沼村，神鄕村では，周圍の家屋が全部倒潰してゐるのに， 筋違を使用した家屋のみが安全に殘つたのが 2 棟宛あつた．1 階に僅か 4 分×4 寸の板を筋違として使用してゐた爲，1 階は安全であつたが，筋違のない 2 階が破壞した家屋が 2 棟あつた．全く理論の示す通りである．(寫眞第 17，18 圖參照) 大黑柱を使用した家屋も亦少いが，大黑柱は神鄕村の北國街道筋の商家

では 7 寸角の欅材を使用してゐたが，農家では皆 4.5 寸角の欅材である．大黒柱を使用した家屋は被害が極部的で全體の倒潰に至つたのは無い．卽ち大黒柱のみが鴨居下で裂けたり，大黒柱と接合する鴨居が破折した家屋が神郷村，若槻村で見受けられたが，家屋全體の破壞を大黒柱が負つた跡歴然たるものがあつた．

此度の激震地では土藏の倒潰は比較的に少く，長沼村の如く度々の水害で下部の腐蝕したものに限られてゐた．寫眞第 19 圖の土藏はその典型的な例で，水害の爲に腐蝕した下部のみが倒潰して上部は僅かに龜裂ができた程度である．土藏の滑動は淺川村，若槻村に最も多く，壁體の厚さ 24 cm 乃至 30 cm の土藏が 10 cm 乃至 40 cm 滑動してゐた．（寫眞第 20，21 圖參照）

特に關心を深くしたのは，下屋の葺下りが母家との接合部で分離して倒潰したものが極めて多いことと，豐洲，赤沼國民學校々舍の二階々段が連結部で拔け離れてゐたことである．何れも接合が頗る脆弱な爲である．此の接合部を强固にすることは，只に下屋又は階段の破壞を免れるのみならず，下屋及び階段が筋違の役目を果して建物全體の强度を增すに役立つのである．

尙，特殊な被害としては，裏に支柱のない土塀が長さの方向へ 9 cm 滑動し，瓦の剝落は 1 枚もなかつた．（寫眞第 22 圖參照．土塀の後に見える立派な家屋の柱は大部分破損した）此の事實は，此の地域の主要動が土塀の長さの方向であつて直角の方向の震力は極めて小さかつたことを示す．次に周圍を壁體で廻らした新築の剛構造の高い二階家屋が將に顚倒せんとする位傾斜したのがあつた．（寫眞第 23 圖參照）

7. 家屋被害の構造力學的吟味

今回の地震による家屋の破壞原因は力學的には次の種類に大別することができる．

（I）衝擊性震力による場合

（II）家屋全體の共振による場合

（III）家屋構造の一部材の共振による場合

次に，此の各場合に就いて簡單な吟味を試みることにする．

(I) 衝擊性震力による破壞

壁體のない表方向へ倒潰した住家を除くと，住家の倒潰は略震源に向ふ一定方向を示し，然も土藏の滑動及び倒潰は總べて此の方向と一致してゐる．卽ち此の破壞は衝擊性押し波によると推定されるといふことは旣に述べた．(I) の特徵は各軸部材が大體一樣に損傷し，その倒潰方向も一定である．從つて地盤の固有震動による共振では說明し難い．

今，加速度を推定する一つの目安として，古里村諏訪神社の石鳥居の破損に依つて簡單な計算を試みる．（寫眞第 24 圖及び第 25 圖參照）

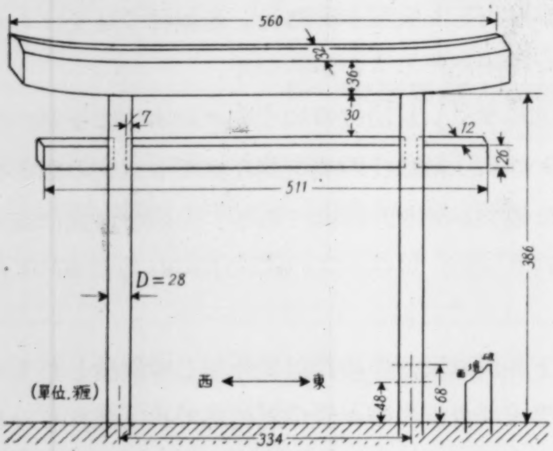

第 25 圖　破壞した石鳥居の構造

曲能率を受ける剛體の破壞を表す式は

$$kmlr/I > p_x \qquad (1)$$

にして，玆で

$$\left.\begin{array}{l} m=1400\ \mathrm{kg}\ (\text{柱 1 本と笠木，貫の半分の質量}) \\ l=2{\cdot}8\ \mathrm{m}\ (\text{地表から柱の重心までの高さ}) \\ r=14\ \mathrm{cm}\ (\text{柱の半徑}) \\ I=(\pi r^4/4)=3{\cdot}01.10^4\mathrm{cm}^4\ (\text{柱の慣性能率}) \end{array}\right\} \qquad (2)$$

である．石材の最高應張强度を $p_x=50\ \mathrm{kg/cm^2}$ とすると水平加速度 α と重力の加速度 g の比 k は

$$k > 0{\cdot}274 \qquad (3)$$

となる．次に，柱の 1 本が折れ，笠木，貫が落下した後の殘りの 1 本の柱について同様の計算を爲すと $k=1{\cdot}02$ となり，此の地震では考へられない大きな値である．尙此の場合には上下震動はあつても問題にならない．

次に將に轉覆せんとする狀態にあつた長沼村の剛構造の家屋（寫眞第 23 圖，第 26 圖參照）について計算を行ふと，轉覆の起る條件は

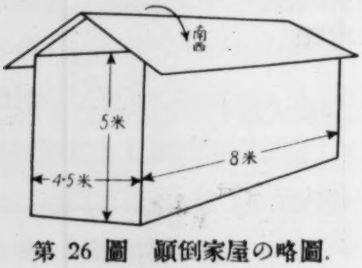

第 26 圖　顚倒家屋の略圖．矢は顚倒方向を示す

$$k/(1-k_1) > r/h \qquad (4)$$

であり，只今の場合

$$\left.\begin{array}{l} r=2{\cdot}25\ \mathrm{m}\ (\text{横の長さの半分}) \\ h=5{\cdot}1\ \mathrm{m}\ (\text{地面から重心までの高さ}) \end{array}\right\} \qquad (5)$$

であるから

$$k/(1-k_1) > 0{\cdot}44 \qquad (6)$$

となる．水平加速度を（3）から $0{\cdot}3\,g$ と假定すると上下加速度 α_1 と g の比 k_1 は

$$k_1 > 0{\cdot}318 \qquad (7)$$

となる．卽ち前記の鳥居の石材の破壞及び此の家屋の轉覆が限界に近いものと推定すると，水平上下兩加速度は各約 $0{\cdot}3\,g$ といふことになり，家屋倒潰率 10% 乃至20% の震害地としては肯ける値である．

尙，之等の値を吟味するために家屋の滑動を考へることにする．神郷村，淺川村に

は僅かに滑動した跡を残す住家があり，又淺川村，若槻村には 10cm 乃至 40cm 滑動した土藏が多かつた事實は，滑動を起す震力が，土，石並びに木，石の間の摩擦力に近いと考へられる．故に，之等の摩擦係數から推定される加速度の關係は

$$k/(1-k_1)=0{\cdot}4\sim0{\cdot}5 \tag{8}$$

となり，前記の計算と非常によく符合する．

即ち此の地震の衝擊性震動の加速度は水平，上下共に略 0·3 g と考へて間違いないと思ふ．

(II) 家屋全體の共振による破壞

共振で倒潰したと推察できる家屋も少くなかつたが，破壞狀態から特に明かに共振によると考へられる家屋が若槻村稻田にあつたから，その固有週期を算出して見る．同家屋の軸部の斷面圖は第 27 圖で，その中の第 14 號の柱を寫眞第 28 圖に示す．

第 27 圖に於て破壞した柱は第 1～10，18，彎曲した柱は第 11～14，17，安全な柱は第 15，16，19，20 であつた．鴨居から上は全部壁體で廻らされ，然も寫眞でわかる如く柱と梁の接合は相當に剛である．それ故柱は兩端固定，床は剛として計算を行ふことにする．

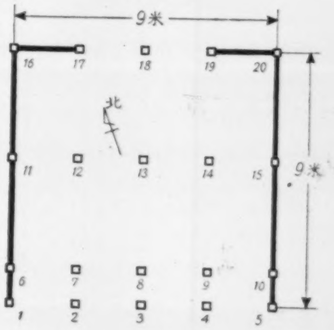

第 27 圖 共振による倒潰家屋の平面圖

柱の運動方程式は

$$EI\partial^4y/\partial x^4+\rho a\partial^2y/\partial t^2=0 \tag{9}$$

であるから，その解は

$$y=(A\cos nx+B\sin nx+C\cosh nx+D\sinh nx)\ \cos pt \tag{9}$$

である．茲で $n^4=\rho ap^2/EI$, E=柱のヤング率，I=慣性能率，ρ=密度，$a(=r^2)$=斷面積，$p=2\pi$/週期である．柱の兩端の條件は

$$x=0;\quad y=0,\qquad \partial y/\partial x=0, \tag{10),(11}$$

$$x=l;\quad \partial y/\partial x=0,\quad -EI\partial^3y/\partial x^3+m\partial^2y/\partial t^2=0, \tag{12),(13}$$

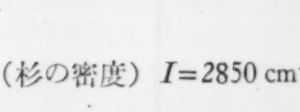

第 29 圖

と置けるから，(10)～(13) を (9) に代入すると次の振動數を決める式を得る．

$$\cos\alpha\sinh\alpha+\sin\alpha\cosh\alpha+\nu\alpha(\cos\alpha\cosh\alpha-1)=0 \tag{14}$$

但し $\alpha=nl$, $\nu=m/\rho al$ である．(14) 式から $\sqrt{\rho ap^2/EI}$ と $m/\rho al$ の關係を求めると第 30 圖の曲線になる．

只今の家屋に於て $r=6{\cdot}8$cm，$a=185\text{cm}^2$，$\rho=0{\cdot}4\text{gr/cm}^3$，(杉の密度) $I=2850\ \text{cm}^4$ である．$l=242$cm，$m=3{\cdot}5.10^5$gr と推定し，杉材のヤング率 $E=8.10^{10}$ C.G.S.と

して第 30 圖を使用して計算すると，自己振動週期は 0·265 秒 となる．此の値は l, m 及び E で多少變化するが，實際問題として大勢には影響はない．而して稻田の地盤は相當に發達した沖積層であるから，此の週期は稻田の地盤の固有週期に近いものと推定してよいであらう．

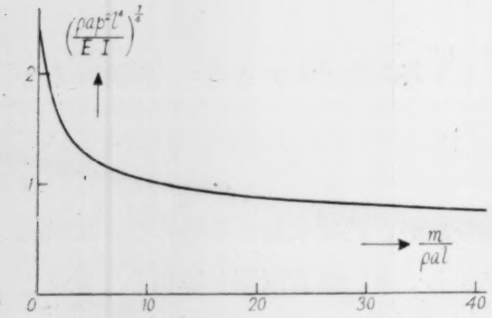

第 30 圖 床剛，柱の兩端固定の構造の固有振動數曲線

要するに，同地震は衝撃性震動による被害が最も多いが，次に地盤の固有週期と家屋のそれの一致による共振で說明できる被害も相當にあつたことがわかつた譯である．

(III) 家屋構造の一部材の共振による破壞

家屋の一部に破損を生じた原因は種々考へられるが，一部の柱の共振によつて破壞した家屋も少くないやうであつた．然も，梁，鴨居，胴卷，軒桁の連結點の通柱の破壞の場合には特に被害も大であつた．次に，このやうな破壞樣式が實際に起り得るものかどうかを力學的に檢討して見ることにする．

軸壓，固體粘性のある場合の棒の撓み振動の運動方程式は

$$\rho\frac{\partial^2 y}{\partial t^2}+Ek^2\frac{\partial^4 y}{\partial x^4}+\xi k^2\frac{\partial^5 y}{\partial t\partial x^4}+\frac{P}{A}\frac{\partial^3 y}{\partial x^3}=0 \tag{15}$$

であるが，此の式から壓縮力，粘性抵抗と振動週期の關係を出すのは棒の兩端の條件によつては極めて複雜である．幸ひ妹澤教授[4)] によつて計算された實驗公式があるから，その公式によつて數値計算を行ふ．卽ち (i) 棒の兩端が固定のとき，(ii) 一端固定他端支持のときの主要振動を表はす實驗公式，及び (iii) 兩端が支持のときの主要振動數の式は

$$\text{(i)}\quad p=\frac{501\,\xi k^2}{2\rho l^4}\pm\sqrt{\frac{12{\cdot}74}{\rho l^2}\left(\frac{39{\cdot}4Ek^2}{l^2}-\frac{P}{A}\right)-\frac{501^2\xi^2k^4}{4\rho^2l^8}} \tag{16}$$

$$\text{(ii)}\quad p=\frac{238\,\xi k^2 i}{2\rho l^4}\pm\sqrt{\frac{11{\cdot}8}{\rho l^2}\left(\frac{20{\cdot}2\,Ek^2}{l^2}-\frac{P}{A}\right)-\frac{238^2\xi^2k^4}{4\rho^2l^8}} \tag{17}$$

$$\text{(iii)}\quad p=\frac{i\pi^4\xi k^2}{2\rho l^4}\pm\sqrt{\frac{\pi^2}{\rho l^2}\left(\frac{\pi^2 Ek^2}{l^2}-\frac{P}{A}\right)-\frac{\pi^8\xi^2k^4}{4\rho^2l^8}} \tag{18}$$

である．玆に，$2\pi/p$＝振動週期，l＝棒の長さ，ρ＝棒の密度，E＝ヤング率，A＝斷面積，k＝斷面の慣性半徑，ξ＝粘性抵抗，P＝軸方向の壓縮力である．計算を簡單にするために粘性抵抗の項を除き，11·5 cm 角，長さ 420 cm，$E=6{\cdot}10^{10}$ C. G. S. の杉

4) 妹澤克惟，"Die Wirkung des Enddruckes auf die Beigungsschingung eines Stabes mit innerer Dämpfung," ZAMM **12**, (1932), 275〜279.

材がの1噸の荷重を受ける場合の柱の固有週期を(16)~(18)式を使つて出すと

(i)　$T=0{\cdot}038$ 秒，(ii)　$T=0{\cdot}059$ 秒，(iii)　$T=0{\cdot}1$ 秒

となり，柱の材質，受ける荷重の如何によつては震動週期と一致する柱の固有週期が存在し得ることがわかる.

8. 結　　論

震害地を踏査した結果によると，住家は壁體のない所謂"家の向き"の方向に倒潰したものが總倒潰住家の50%以上を占めてゐる.（このことは養蠶を業とする農村住家の倒潰に於ける一般の傾向ではないかと考へる）此の方向の倒潰住家を除いた住家の倒潰方向は各部落によつて殆んど一定し，然も同部落の土藏の滑動，倒潰と同一方向である. 然してこのやうな方法で決定した各部落の家屋倒潰方向が總べて集中性であることから，之等の損傷を起した震動は主として衝擊型の押し波であつたことが推定できる. 家屋倒潰は約100平方km の區域に限られてゐるが前記の方向と家屋の向きとが一致した部落に於ては特に家屋倒潰率が大きかつたやうである.

筋違を使用した家屋は稀であるが，その耐震効果は全く理論の示す通りであることを4棟の家屋が示してゐた. 大黒柱の使用も亦少いが，大黒柱の存在のために破壞を一部に止めて全體の損傷を免れたと考へられる家屋が多い.

家屋全體としては剛であるが，一部の弱い柱材の共振のために破損をしたと思はれる家屋が相當數あつたので力學的計算を試みたが，大きな荷重を受ける4寸角位の柱はその材質によつては，その固有週期が震動週期と一致して共振を起し得ることがわかつた. 何れにしても荷重を多く受ける場所及び横材の繼目の柱は特に强固にする必要があり，大黒柱，小黒柱を使用することは此の役目を果すものである.

本地震の被害の中，下屋の破壞が頗る多いことと，國民學校の二階々段が他の個所以上の破壞をしたことが特に眼についた. 何れも接續個所が脆弱の爲である. 之等の接續個所を强固にすることは，下屋，階段の破壞を免れるのみならず下屋，階段が筋違の役目をして構造全體の强度を高めるものである. その上國民學校の階段は人的損傷にも關係深いこと故十分の注意が必要と考へる.

最後に本調査に當り多大の御便宜を與へて下さつた岸上助教授並びに長野縣營繕課長野電氣，上水内郡各村役場，及び各村の有志の方々に厚く謝意を表する.

尙本報告をなすについて種々御教示，御指導を賜つた妹澤先生，並びに調査に非常なる御援助を與へられた古平秀數氏に深く感謝す.

40. *On the Damage to Buildings in the Nagano Earthquake of July 13, 1941.*

By Kiyoshi KANAI,

Earthquake Research Institute.

The present paper is a report of the damage to buildings in the Nagano earthquake that occurred on July 15, 1941, with a theoretical discussion. With the kind assistance of Mr. Kodaira, the writer examined the seismic region during the period from July 17 to July 23, which had an area of about 10 km in dia. consisting of nine villages, situated north-east of Nagano city, and quite close to it. The buildings in the seismic region are mostly farm houses together with granaries and sheds. The investigation in the field was made from the point of view of the dynamical theory of seismic vibration of a structure that we had developed recently.

Althougth only a few of the buildings had diagonal members, it seems possible to conclude that these members were fairly resistant to seismic vibrations. Generally speaking, the damage to buildings was of two kinds, one being of the type caused by seismic shocks or resonance of building vibration and the other of the type formed by resonance of column vibration. In the first type, every column in the building collapsed in the same manner, whereas in the second, certain columns failed in a particular way. Besides, in the latter type, the whole building was never in resonance condition; only the column themselves that were subjected to a vertical thrust were likely to be in resonance condition.

In the present investigation, the way in which a building overturned was also carefully examined. Since farm houses in Nagano district (and more generally in most parts of Japan) are built with one of its sides without wall, the house is liable to be overturned in the unwalled side, for which reason, in a statistical investigation of this kind, the writer omitted the houses that overturned in the direction of the unwalled side. Comparisons of all the overturned buildings, excepting the case just mentioned, showed that in almost every case the house overturned towards the seismic epicentre. The granaries and sheds that had on walls also overturned in the same sense. From the foregoing evidences it is possible to conclude that the seismic vibration that damaged the buildings was of the push type for every direction looking from the seismic epicentre.

第 6 圖　表柱破損小壁亀裂なし. 南向, 南へ(長沼村穗保)

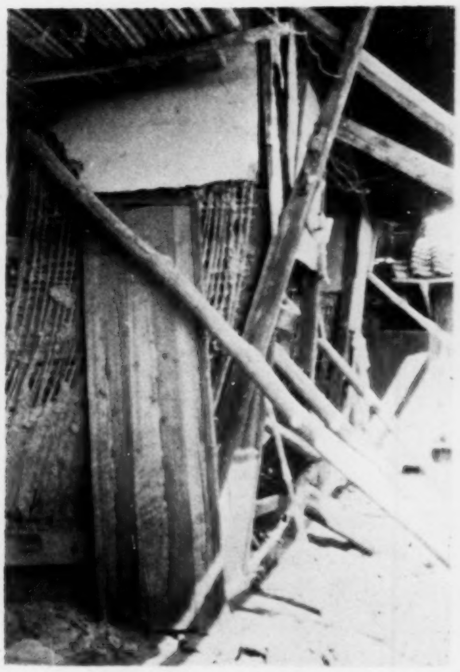

第 7 圖　下屋が鴨居の高さで破損. 南向, 南へ (長沼村穗保)

第 8 圖　崩壊家屋. 西向, 西へ (長沼村穗保)

第 9 圖　屋根崩落, 外壁安全. 南向, 南へ (長沼村津野)

第 10 圖 住家，兩側の壁部を殘し中央部倒潰. 南向，南へ(神鄕村石)

第 11 圖 倉庫，兩側壁部を殘し中央部倒潰. 南向，南へ(古里村三才)

第 12 圖 軒桁中央部で破損. 南向，南へ(長沼村赤沼)

第 13 圖 軒桁中央部で破損. 南向，南へ(神鄕村南鄕)

(震研彙報 第十九號 圖版 金井)

第 14 圖 柔構造住家倒壞. 南向, 北へ (長沼村大町)

號 15 圖 柔構造住家倒壞. 南向, 西へ (長沼村大町)

第 16 圖 鴨居より上部損傷なし. 南向, 東(淺川村東條)

第 17 圖 一階筋違使用, 二階倒壞. 南向, 南へ(長沼村津野)

第 18 圖　第 17 圖と同じ家屋

第 19 圖　下部腐蝕の土藏の破損．南向，西へ(長沼村穗保)

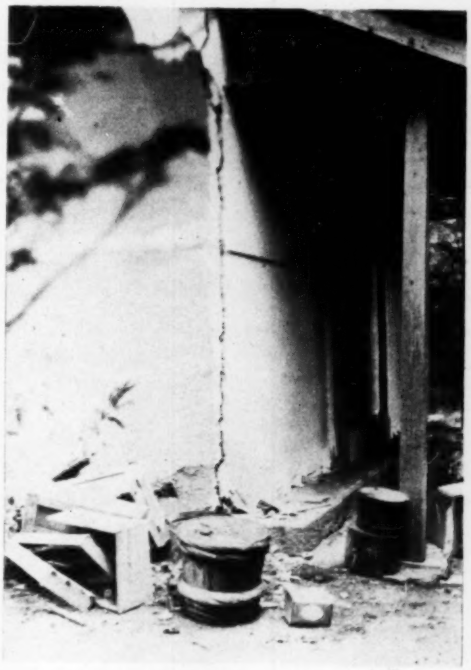

第 20 圖　土藏東方へ 40 cm 滑動
(淺川村西條)

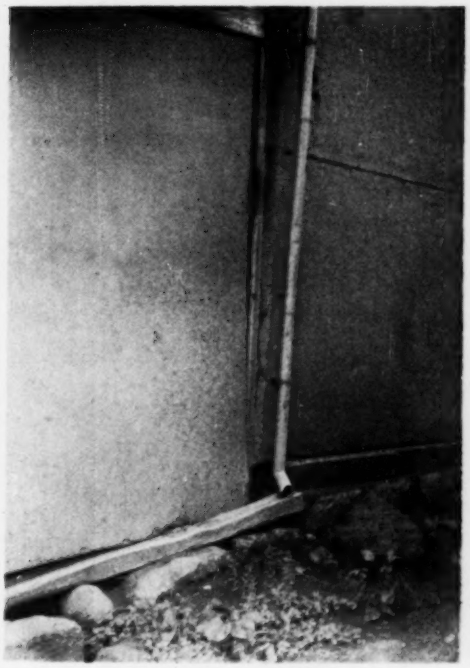

第 21 圖　土藏東北方へ 15 cm 滑動
(若槻村東條)

第 22 圖 土塀長さの方向(東北方)へ 9 cm 滑動(若槻村德間)

第 23 圖 新築剛構造の高い家屋南西へ顚倒(長沼村穗保)

第 24 圖 鳥居の倒潰(古里村諏訪神社)

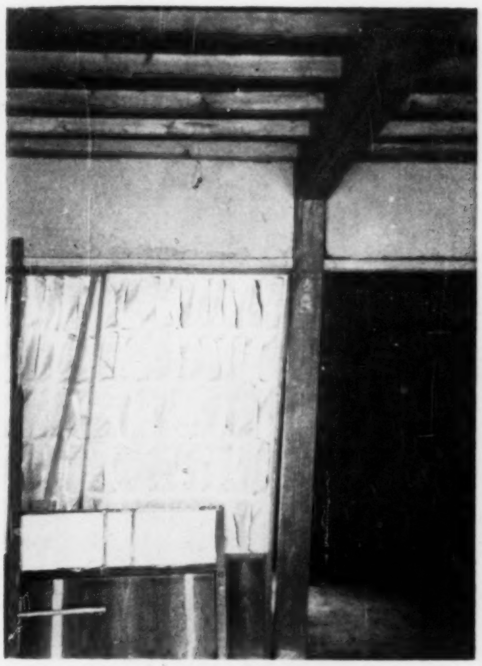

第 28 圖 柱彎曲(長野市吉田)

第 31 圖 鳥居横へ傾斜，貫破損（淺川村押田）

第 32 圖 土塀の轉覆（古里村）

41. 善光寺平に於ける民家構造の特異性と震害

地震研究所　齋田時太郎

(昭和16年9月18日發表——昭和16年9月20日受理)

長野市東北方地域が昭和16年7月15日夜半强烈な地震に襲はれ死者5，重輕傷19を出し住家の全壞29，半壞115，損害見積110萬餘圓と報導されてゐる．いまや我が國は空前の世界大動亂の間にあつて，未曾有の大業を完遂しなければならない秋であり，このやうな災厄が二度と國土に起らないやう祈らずにはをられない．

家屋震害調査のため，私は現地に出張したが震後數日を經過してゐたので，震害を蒙つた家屋の中には既に舊態に復したもの，或は取壞したものもあり，生々しい震害現象を觀ることが出來なかつた．しかし，既往數度の震害觀察の結果と比べて特に注意をひいた現象もなく，例の如く木造家屋が構造上の缺陷を暴露してゐるに過ぎないと言ふ印象を深めた．しかし觀點を，この地方特有の構造と震害との關係におくと興味あるものがあるので調査を進めてみた．

震害概況

今度の地震で被害が特にひどかつた地域は，信越本線吉田驛と豐野驛間で，千曲川左岸の沖積層地盤の，長徑約7粁短徑約4粁のせまい地域に限られてゐる．部落では吉田，稻田，德間，南鄕，石，赤沼，津野，穗保，大町，三才，下駒澤，上駒澤，金箱，富竹等が著しく被害のめだつた所である．

長野市は東北部の吉田附近の一部が著しく震害を蒙り，他の大部分は輕少な損傷を受けたに過ぎない．市中には土壁の龜裂，屋根瓦の滑落など至る所に見られたが，特に市の中央を東西に流れる鐘居川の北部地區卽ち善光寺附近に損傷が多く見られた．

被害地域に鐵筋コンクリート造になるものが數棟ある．その中，縣立圖書館と縣立農學校は共に三階建であるが，一階下部壁體に少龜裂を生じ且つ二階のスチールサツシユにはめ込まれた窓硝子が10枚近くも震動のため破損し，その上下層階の窓硝子には少しも破損したものが無かつた．これは高層建築が中間層で著しく震害を蒙るといふ現象を，輕少ながら現はしてゐるのではないかと思はれる．

國民學校で倒壞したといふのはないが，相當被害をうけ授業に差支へるといふ程度の

ものがあつた．その中で，著しい震害をうけた吉田國民學校の情況をのべると，そこで最も古い明治 35 年 7 月建築の二階建校舎は，土壁の龜裂剝落甚しく且つ東方へ少しく傾いた．この建物は近年，平板鐵物で柱と鴨居とを緊結しておいたので今度の地震に際し効力を發揮したらしく思はれた．なほ昭和 8 年建築の校舎は前者よりは幾分損傷が少いやうであるが，階段踊場框と齶桁とが離脱したのがあり，又東西に長い 8 間に 15 間の木造平家瓦葺の大講堂は，筋違方杖等を用ひてないものであるが，何等の傷損を受けてゐなかつた．かやうに間仕切のない大廣間の講堂が，全く無事であるといふのは意外に思はれる．この學校の近くに農學校があり，そこに同じやうに東西に長い 8 間に 12 間の木造平家瓦葺の大講堂があり，これは大きな頬杖を用ひ西洋風小屋組を露出したものであつたが，これも亦全く被害を受けてゐなかつた．

一般民家の被害は吉田，稻田，德間，南郷，石等の街道筋の商店と千曲川左岸に接する農家に多く現はれてゐる．特に興味のあるのは堅固に構築された土藏が地震動によつて滑動したことである．その滑動量は 20～30 糎に及ぶものがあり，特に南郷，石の部落の如く堅い豐野貝岩砂岩層[1] に接するところに大滑動をしたものがあり吉田稻田德間の如き階段堆積層に近接するところが前者についで滑動量が大きかつたことである．この現象は地震による構造物と地盤の振動性との關係によるのではないかと

昭和 16 年 7 月 19 日現在

市町村名	倒壞家屋					死傷者				損害見積
	住家		非住家		計	死者	重傷	輕傷	計	
	全壞	半壞	全壞	半壞						
長野市	2	22	3	6	33	—	—	1	1	200,000圓
長沼村	7	20	30	50	107	2	3	5	10	400,000
神郷村	3	30	—	13	46	—	—	2	2	150,000
若槻村	5	24	—	18	47	2	—	1	3	150,000
淺川村	4	9	6	6	25	1	—	2	3	48,150
柳原村	—	—	3	4	7	—	—	—	—	8,000
古里村	7	10	5	25	47	—	—	4	4	172,000
高岡村	1	—	—	—	1	—	—	—	—	60
豊洲村	—	—	1	—	1	—	—	—	—	50
日野村	—	—	1	—	1	—	—	—	—	800
高丘村	—	—	—	—	—	—	—	1	1	—
合計	29	115	49	122	315	5	3	16	24	1129,310

思はれる．これについては既に度々私見をのべてあるから，ここでは立ち入つて說

1) 長野油田地形及地質，二萬分ノ一，商工省地質調査所發行による

明をしない．なほ，長野縣警防課の發表した被害調査表があるから，それをここに示し震度及び被害の度合を推定していただくことゝする．

民家の構造

我が民家の間取は基本的に見れば，大して地方的差異はないと言へるが，その構造は氣候風土・風俗慣習・產業經濟等の關係で著しい相異がある．たとへば鹿兒島附近の木骨石造と秋田附近の小屋組及び差鴨居に過大と思はれる位木材を豐富に使用してゐる構造，或は關東地方の壯大な藁屋根と關西地方に見られる數段に庇を下ろしてゆく屋根の相異からくる軸部構造の違ひ，又仕口について言へば軒桁と梁とを京呂組にする地方と折置にする地方と言つたやうな異がある．

このやうに構造の地方的の異があるとしても，一縣內に限れば大體一様と言へるが，長野縣は一縣下でさへ地域的に異があり他の縣と著しく趣を異にしてゐる．たとへば善光寺平，佐久平の民家の間取は長方形の外廓の中におさまつて屋根は藁又は瓦葺で外壁は厚い土壁であり，松本平のものは方形に近いプランでしかも奥行の方向に 3 室もならぶものがあり，屋根は柿葺又は瓦葺である．諏訪伊那谷にかけて屋根は柿葺に玉石又は板狀鐵平石をのせたものが多く藁葺や瓦葺は少い．特に入口が切妻の方にあるのが變つてゐる．なほ面白いのは諏訪地方に土藏を中心とし，その周圍に部屋を配置した形式のものが見られることである．このやうな地域的に民家の形體や構造の異ふことは，その耐震性を考へる場合見のがすことの出來ない事柄であり且つ人文地理學の問題としても亦興味がある．

なほ，善光寺平には耐震性を考へる上に重要な事柄がある．この地域は今から 95 年前弘化 4 年，所謂善光寺地震の苦い經驗から家の高さを極めて低くしたこと，柱の數を增加したこと或は太いものを使用したこと等である．これ等の點は近年の建築になるものと比べて著しい異がある．かの大震直後には軒高を 11 尺を限度とし二階建を許さなかつたのに後にこれを15尺まで許し幸うじて低い二階建が建てられるやうになつた．しかるに年月の經過するに從ひ次第に高さを增してきた．このことは，現今，第 12 圖に示す通り長野市中に多數見出すことが出來る．また村落に於て特に養蠶を手廣くやるため天井を高くし且つ柱の細い仕口の粗略なものが多く見受けられる．

要するに善光寺平に於ける民家の構造と形態は第 1 圖に略示する通り，農家は平家建の藁葺で左右兩側には壁があるのみで前後の二側は大部分開放され，さうして土臺は周圍に廻してあるが內部には殆ど用ひてない．街道筋の商家には二階建で階上に厚い土壁をぬり柱を包み前後に圖の如く下屋を卸してゐるものが特に多く見られる．

土臺はこの形式のものも農家と同樣である．軒桁と梁との仕口は第5圖に示す兜蟻によるものが多く，下屋は母屋から梁を投げかけ折置組卽ち柱の上に梁を更にその上に桁をのせる仕口にしたものもある．

厚い土壁をつけてゐることは特に耐震上問題となるが，それに使用してゐる下げ繩卷き繩には腐蝕し易い藁繩を用ひてゐるのが多く，壁土も粘着力の大きい良質のものを用ひてゐるのは少いやうである．

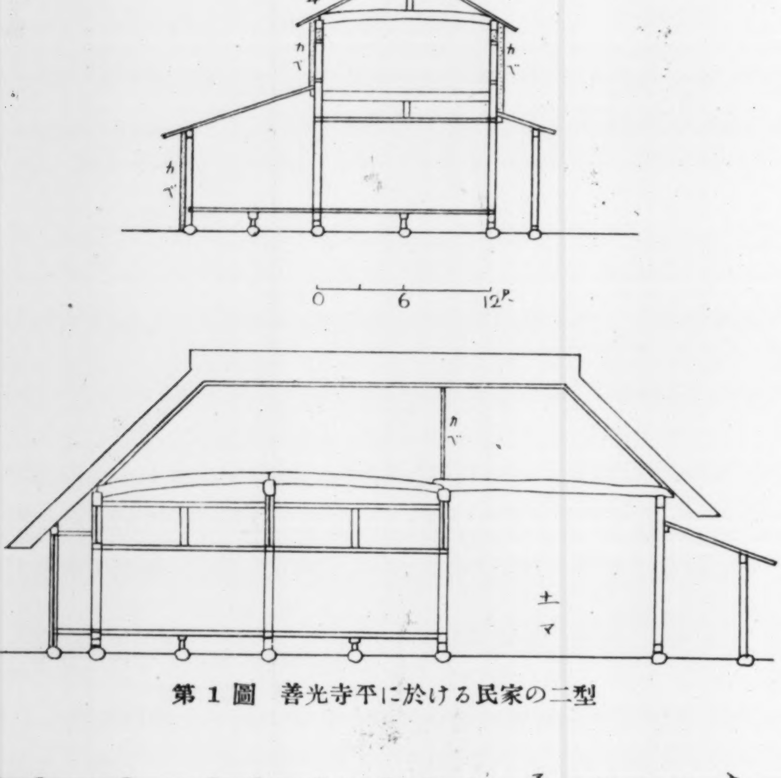

第 1 圖 善光寺平に於ける民家の二型

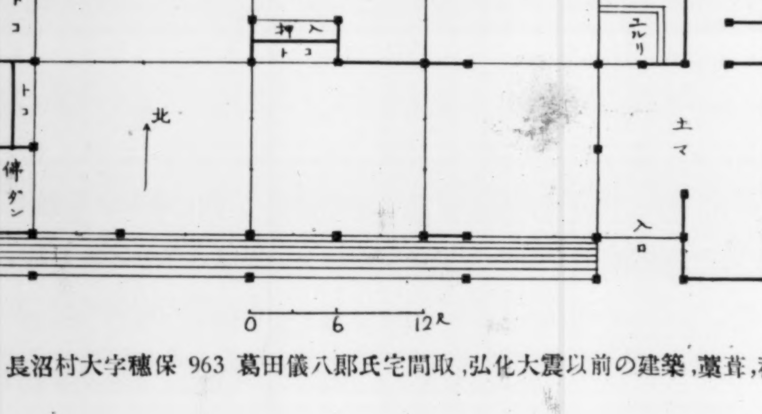

第 2 圖 長沼村大字穗保 963 葛田儀八郞氏宅間取，弘化大震以前の建築，藁葺，被害なし

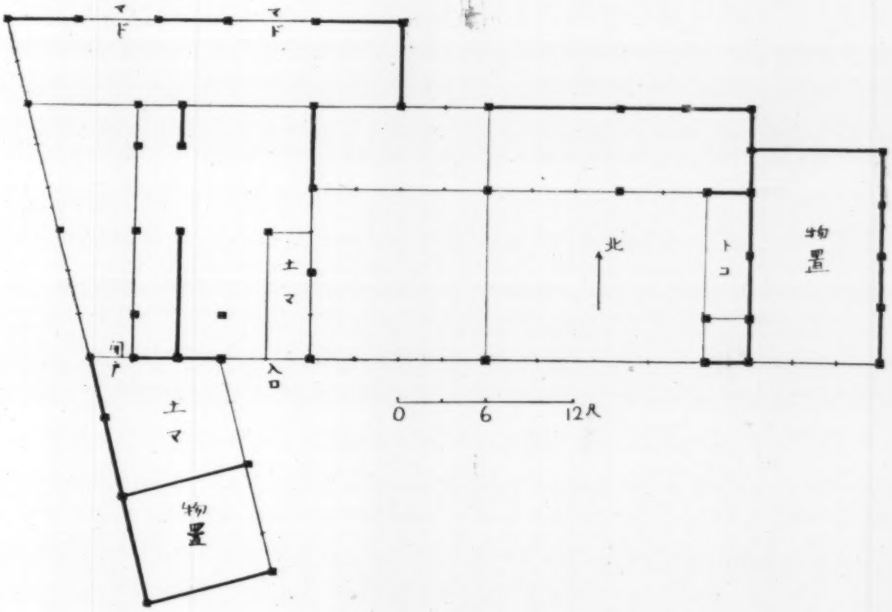

第 3 圖 長沼村字赤沼中村峯太郎氏宅間取
弘化大震直後の建築,三方の下屋は近年の増築,被害なし

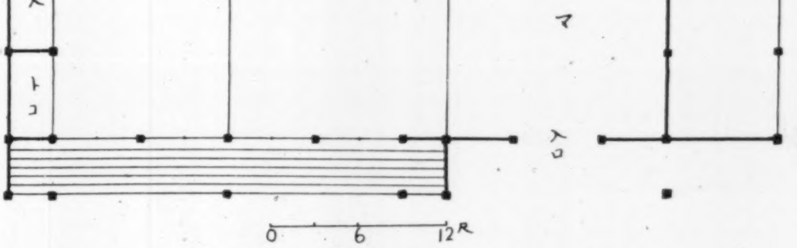

第 4 圖 長沼村村長森義忠氏宅間取,瓦葺,弘化大震直後の建築,被害輕少

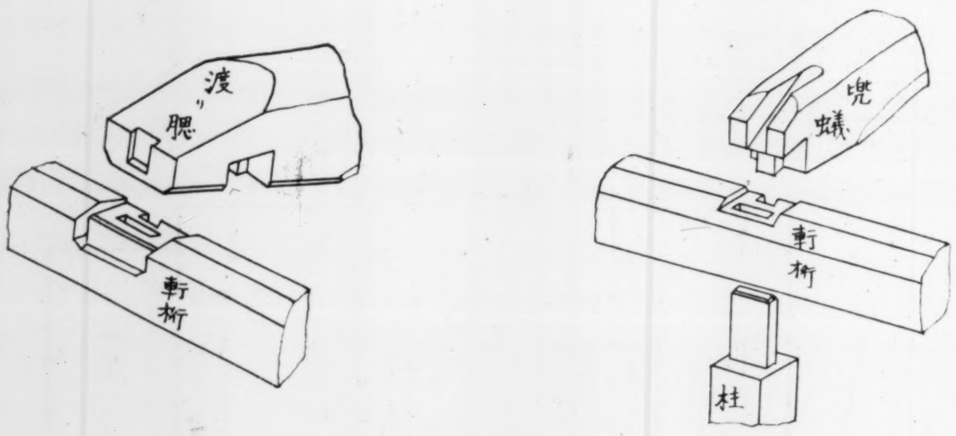

第 5 圖　京呂組の二法

震　　害

既往数多の震害調査の結果に徴すると，木造家屋の損傷の原因として，次の事項が擧げられてゐる卽ち

1. 屋根小屋組の重いもの
2. 間取及び形狀の正しくないもの
3. 老朽したもの或は施工粗惡なもの
4. 柱の細いもの
5. 土臺の使用不充分なもの
6. 軟弱地盤に建てられたもの
7. 高さの高いもの

これは主として軟弱地盤の震害から抽象されたものであつて，堅硬な地盤の震害はこれと稍趣を異にしてゐると言ふことが最近の研究[2]の結果明かになつてきたものもある．なほ，その他の事柄で諸家の間に意見の一致しないものもある．事實，震害の眞相を科學的に說明するものは容易なことでない．と言ふのは現象が動力學的で地震の性質家屋の構造仕口，形態，その他込み入つた事情からくる振動の複雜なため振力及び耐力について，とかく主觀的の解釋におち入り易いからであると思ふ．

震害を耐震構造設計の立場から見れば個々の被害の解釋が本來の目的ではなく，あくまでも設計の目安を探究するのにあるから，曖昧な假定の上に徒に論議するは愼しむべきことである．

既にのべた通り善光寺平の民家には，外壁に厚い土壁をめぐらしたものが多いので

2)　齊田時太郎「耐震及び耐風家屋」防災科學震災編，岩波書店

今度の地震で壁體の龜裂剝落が至るところに見られた．大正7年松本平の大町附近に起つた地震の被害も亦土壁の損傷が特記されてゐる．かの弘化の大震のときの落首に「この度は床を取りあへず潰れ家のもみあふ人は壁の間にまに」と言ふのがあるが，善光寺參道にあつた塗壁式の商店の倒潰して壁體間にはさまれて苦しんだのも當然である．輕くて堅固な壁體は耐震上有效であるが被害地で粗惡な土壁のあるのが多く見られた．特に千曲川に接する部落は明治 29，43，44 年の大洪水で鴨居までも浸水したと言ふことである．そのため壁を損じたもの多く修築の不充分なものもあつたそうである．街道の商店に於ては第 10 圖にて見らるゝ通り柱と鴨居又は二階梁との仕口で柱が折損してゐるのが多いが，これは下部には壁體がなく開放してゐるのに上部は壁體があつて剛度が上下の界で不連續であることに歸因すると思ふ．剛度の不連續のための被害と思はれるものに農家の土間と座敷との界の外側の柱に折損してゐるものの多く見受けられたことである．農家の土間には隨分大なものがありその軸部の剛性が座敷のそれと著しい差が認められる．第2圖は弘化大震にも今回の地震にも被害のなかつたもので，附近の農家の被害著しいものに比べて土間が小さく柱の配置が割合に均等で，しかも壁體が略中央にあるなどから考へて被害のないのは當然と思はれる．第3圖も被害のなかつた例で柱の配置の均等なことが注意される．近年養蠶を手廣くやるために柱を取りたるもの，壁體を除去したものがあり，これ等は何れも被害を蒙つてゐる．

柱の太く且つ坪當りの使用量の多いのは弘化大震直後の建築に特に目立つ，古里村で見た數棟の如きは戶障子のあるところは1間毎にその他には3尺間に4寸角以上の柱を立てゝゐるものがあり，中には2間を3等分して柱を立ててゐるものもあり，近年の建築になるもので，6 尺間に柱を立て其の間に 2 尺間に小さい間柱を立て土壁を支持せしめてゐるものとでは坪當りの柱數前者の 1.5 本乃至 1.7 本なるに對し後者は 1 本にも及ばないものがあつた．第8圖は最も柱の多く且つ形の整つた家で全く被害のなかつた例である．要するに柱を太く且つ均等に配置し數多く使用したものには被害はなかつたことが弘化大震直後に耐震を顧慮して建てたもので實證されてゐる．

筋違の使用は耐震上有效なものと考へられてゐるが，その使用上注意すべき點がある．既に壁體のところで述べたやうに剛度の不均一とならないやうに配置するのが望ましい．今度の地震で興味ある被害をうけた例に長沼村々長森義忠氏宅がある．この家屋の間取は第4圖に示す通りで，極めて一局部に偏して四寸角二割程度の筋違を一本大釘で打ちつけてあつたが，その取りつけた部分の近くの柱が 3~4 寸も移動し敷居が柱から離脫し柱の一部分を損じてしまつた．これは柱下に土臺がなかつたことと，

筋違を用ひたため，その部分に震力が集中したことによると考へられる．もしこの家屋に筋違が均等に配置されてあつたならば家屋全體として滑動し，このやうな部分的な滑動による損傷は生じなかつたと想像される．今回の强さの震動では寧ろこの家屋には筋違はなかつた方がよかつたのではないかと思はれる．しかしこの現象について，こう考へることも出來る卽ち，震力の大部分を筋違が負擔したので，この家屋はこの程度の輕少な被害ですんだのであると考へることである．この考へ方は一應尤に思はれるが，筋違を使用した場所が一側に偏し且つ數が少なさ過ぎることゝ，軸部構造が，この家屋のやうに從來の和風のものでは，筋違のある部分にその震力を傳達するほどの充分な剛性をもつてゐないから，この考へ方には同意しかねる．

こんな譯であるから筋違を用ひるならば均等に配置することが望ましい．しかし我が國の民家特に農村の民家には筋違や壁體を使用することが許されない事情がある，それは

1. 夏の暑さをしのぐために通風をよくすること
2. 養蠶の關係
3. 時に隣保の集會場として住家を使用すること

等のために間仕切を設けることは望まれない．因て耐震的に家屋を剛强にするためには，左右兩側の壁體にたより，そして中間軸部の剛性を增すために仕口を改良し柱を太くし，土臺を充分に用ひ軒桁上部で家屋を一體として緊結して，その部分の震力を左右兩側の壁體に傳達するやうに造るのがよい．こう考へると左右兩側の壁體は耐震上重要なもので，第1圖に示すやうな下屋構造として母屋の地廻材の下部のみに壁體のあるのは好ましくない．實際，今回の被害を蒙つた家屋をみると下屋構造のものに多くあつたのでも解る．既に說べた第8圖のやうな兩面切妻で壁體の整然とした軸部構造のもに震害のなかつたのも當然と思はれる．

軸部上部の緊結には燧材を軒桁と梁との仕口の箇所に全部設け，且つ梁を軒桁に渡り腮の仕口でかけるのがよいと思ふ．この地方の仕口を見ると殆ど全部が兜蟻の仕口であつて容易に離脫し易いものである．現在のやうな薄弱な軸部構造では到底上部の緊結が望まれないやうに思はれる．一方あの重々しい藁葺屋根は小屋組としては取るに足らぬ架構であるが，竹を縱横に組み合せ厚く葺き上げたものは，一種の殼構造と考へられるものとなつて，軸部の緊結に相當役立つてゐるのではないかと思はれる．實際瓦葺屋根が局部的の震害を蒙つてゐるのに，藁葺屋根にはそのやうなことは見られず．家屋の震動を一體的ならしめてゐると言ふ利益があるのではないかと思ふ．藁葺屋根はその重量の大なると，耐久的でないこと，及び防火的でないこと等の缺點が

あるから今後益々その數を減少するであらうが耐震的には今いふたやうな特色があるらしく思はれる．今回屋根職に依頼し萱葺6寸厚仕上のものゝ重量を測定したところ一平方米110粁で充分水分を含ましたとき，その3割の重量が増すことが解つた．葺土を用ふる瓦葺よりも重いものである．

既存農家の耐震力を增すには腐朽した材と仕口の修築と上にのべた剛度の不連續となつてゐる箇所の柱には更に添柱をつけることを望む．新築するならば剛度の不均一とならぬやうに間取と柱を配置し，止むを得ず柱の配置に均一を缺いた箇所には，その强度を考へて柱の大さを增すこと及び軒桁と梁とは渡り腮の京呂組とし，屋根は引掛棧瓦葺とし，土臺を縱横に通し柱下部を充分緊結すれば，今回の地震の强さの2倍位の震動にも致命的損傷を受けることはあるまいと思はれる．

終にのぞみ，この調査は文部省科學研究費にてなされたことを特記しておく．

なほ，附圖第 11，15 圖は長野縣農政課永田康一氏の，又第 13, 14, 16, 17, 18 圖は吉田國民學校の撮影されたものであることを附記し謝意を表す．

41. *The Peculiarities of Dwelling House Construction, and the Earthquake Damages in Zenkoji Plain, Nagano Prefecture.*

By Tokitaro SAITA,

Earthquake Research Institute.

At 11.45 p.m. on July 15th, a destructive earthquake occurred in the north-eastern district of Nagano city. According to the census of the Nagano Prefectural police office, the total damages was as follows:—

Number of dwelling houses, ware houses and Buddhist temples totally collapsed...78
Number of people killed... 5
Number of people wounded 19

The author visited the shaken district, a week after the shock and investigated the causes from which houses had collapsed, and the peculiarities of house construction. It was found that the majority of the houses in this district had remarkable weak points. The author describes his investigations under the following heads:—

1. Summary of earthquake damage.
2. Peculiarities of house construction.
3. Discussion on the earthquake damages to dwelling houses.

第 6 圖　吉田の壁の被害

第 7 圖　長沼村農家柱の破損

第 8 圖　古里村字富竹の住宅被害なし，七十年前の建築佐治木貞知氏宅柱四寸角

第 9 圖　長沼村太田神社の鳥居東へ 20 糎移動す，前方の家屋は第 3 圖に間取を示す.

第 10 圖　吉田に於ける塗壁式構造，柱の折損

第 11 圖 、若槻村稲田の震害 十六日午前十時半

第 12 圖 長野市の商店年代による高さの異

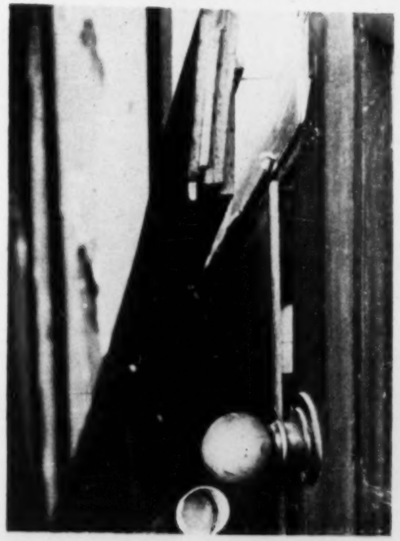

第 13 圖 新校舍の階段の破壞されたる一部（吉田國民學校）

第 14 圖 柱（五本）中折したる物置の壁の一部（同上）

第 15 圖 長野市刑務所西側土塀崩壞 七月十六日午前六時半

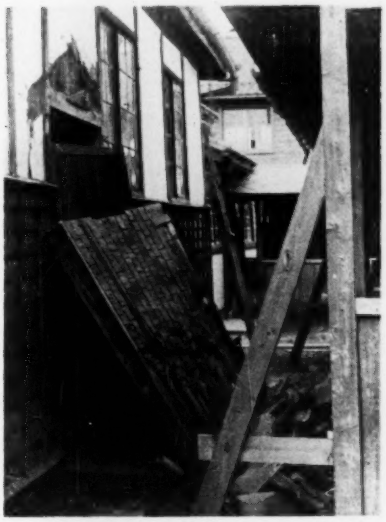

第 16 圖　廊下より物置への渡廊下の屋根の落ちたる所(吉田國民學校)

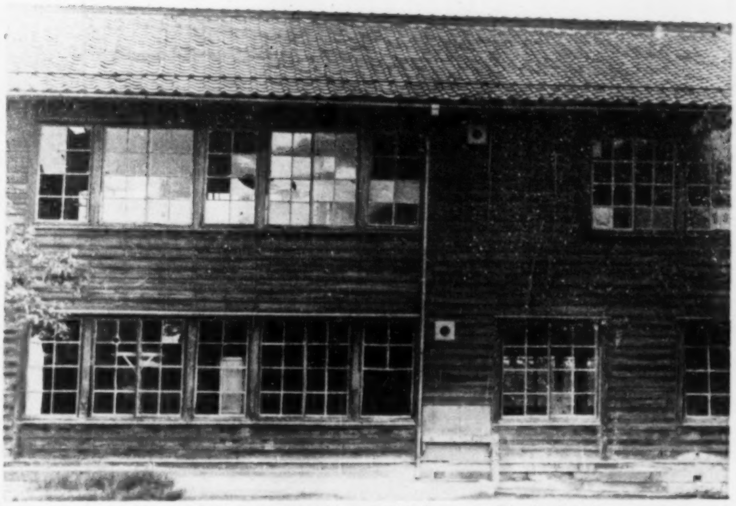

第 17 圖　東に傾きたる校舍の一部（同上）

第 18 圖　壞れたる便所の屋根及壁（同上）

42. 秋田縣男鹿半島附近震災地 三角點水準點復舊測量記事

陸 地 測 量 部

昭和 14 年 5 月 1 日男鹿島附近に發生せる地震に依る災害地の復舊作業成果を報告す.

抑も本地震は男鹿島及びその近傍に於て家屋の倒潰せるもの 600 余戸死者 29 名を出す等甚大なる震害を與へ且つ各所に顯著なる地變を生ぜしめたるを以て，震害地内の三角點及び水準點の復舊測量を實施せるものなり.

I. 一等三角測量

一等三角點は震災地を中心とする下記の 6 點を改測せり.（第 1 圖參照）

男鹿島，森山，赤山，太平山，姫ヶ岳，帹山，

但し，この中，太平山．帹山は一等本點なるも，總て一等補點の觀測を實施せり，一等三角測量の要項次の如し.

1 外業期間 舊觀測 明治 34 年 5 月乃至 10 月
新觀測 昭和 15 年 9 月乃至 11 月

2 觀測用機械 舊觀測［カールバンベルヒ」製 27 糎測微經緯儀
新觀測「ウィルド」製 14 糎經緯儀

3 計　算 新舊兩觀測値を用ひ，夫々同一規約の下に網平均を實施したる後，震央より遠く且比較的變動を受けざりしものと思惟せらるる帹山，姫ヶ岳の 2 點を不動と假定し，舊觀測値を以てする第一段及び新觀測値を以てする第二段の三角形，經緯度及び平面直角縱横線の計算を行ひ之を比較して各點の相對的水平移動量を算出せり，その結果は第 I，第 II，第 III，の各表に示すが如し.

4 新舊觀測の精度次の如し

新： $m=\sqrt{\frac{[\Delta\Delta]}{3n}}=\pm 0.''823$

舊： $m=\sqrt{\frac{[\Delta\Delta]}{3n}}=\pm 0.''682$

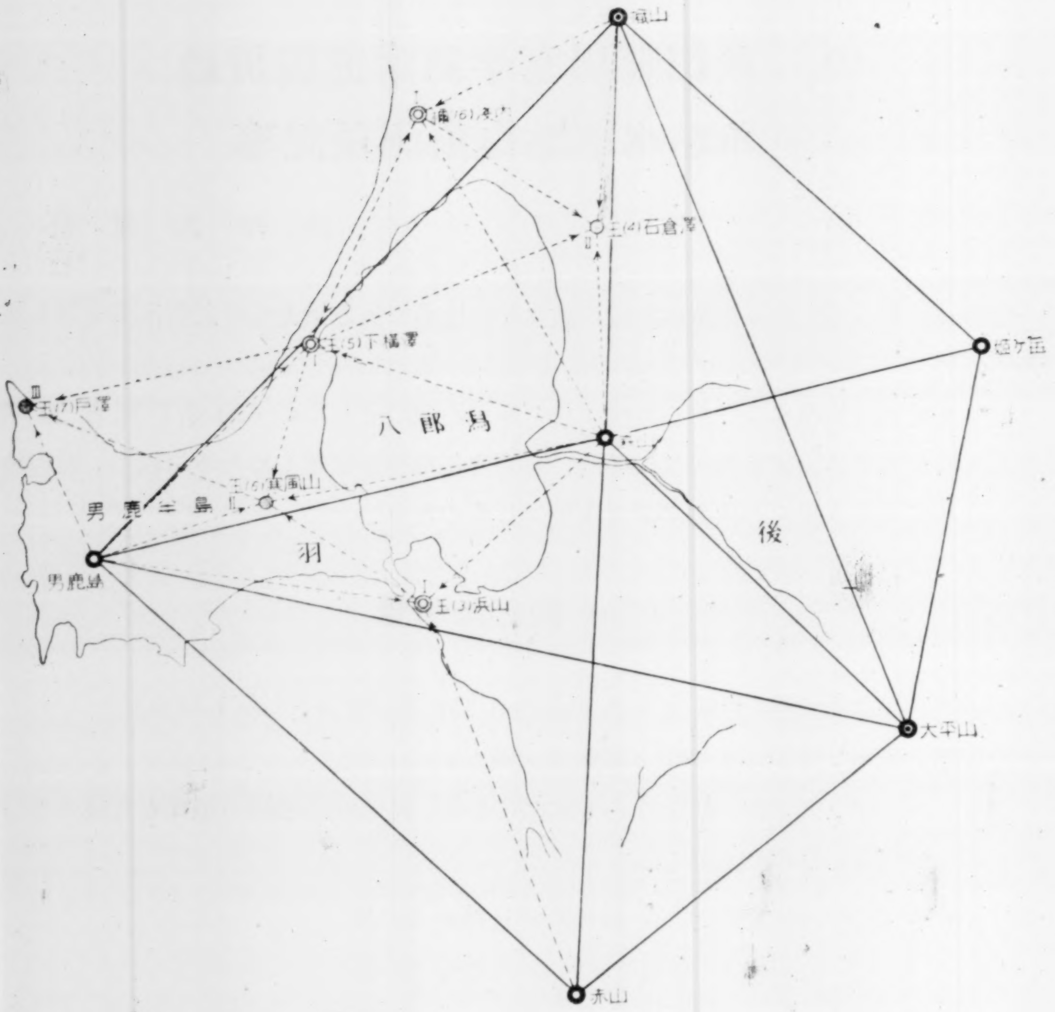

第 1 圖

第 I 表　男鹿半島附近震災地一二等三角點移動比較表

數號	測站名稱	新 觀測	新 平均	舊 觀測	舊 平均	新—舊 觀測角差	新—舊 平均角差	新 三角形閉鎖差	舊 三角形閉鎖差
		° ′ ″	″	″	″	″	″	″	″
1	幟　山	25 12 25,52	52·29	52·00	52·11	＋ 0·52	＋ 0·18	－ 1·52	－ 0·26
	太平山	32 35 29·50	30·26	29·95	29·84	－ 0·45	＋ 0·52		
	姫ケ岳	122 11 37·92	38·81	39·25	39·50	－ 1·33	－ 0·69		
2	幡　山	48 50 19·81	20·22	19·22	19·67	－ 0·08	＋ 0·55	＋ 0·09	－ 0·68
	森　山	74 41 36·24	35·65	35·65	35·47	＋ 1·07	＋ 0·18		
	姫ケ岳	56 28 5·46	5·56	5·56	6·28	－ 0·22	－ 0·32		
3	姫ケ岳	65 43 32·46	33·25	33·37	33·22	－ 1·2	＋ 0·03	－ 1·65	＋ 0·93
	森　山	37 43 12·38	12·97	14·61	13·67	－ 1·9	－ 0·70		
	太平山	55 33 14·74	15·00	14·18	14·32	＋ 0·5	＋ 0·68		

（次頁に續く）

第 I 表 (續き)

數號	測站名稱	新 觀測	新 平均	舊 觀測	舊 平均	新一舊 觀測角差	新一舊 平均角差	新 三角形閉塞差	舊 三角形閉塞差
		° ′ ″	″	″	″	″	″		
	幟　山	23 37 27·29	27·93	27·89	27·56	− 0·60	+ 0·37		
4	森　山	132 24 48·62	48·62	49·48	49·14	− 0·86	− 0·52	− 0·03	+ 0·42
	太平山	23 57 45·24	44·64	44·23	44·48	+ 1·01	+ 0·16		
	幟　山	42 0 43·27	43·72	42·30	42·91	+ 0·97	+ 1·81		
5	男鹿嶋	33 8 12·30	13·61	15·00	14·37	− 2·70	− 0·76	− 1·92	− 0·05
	森　山	104 51 4·43	4·58	4·57	4·65	− 0·14	− 0·07		
	森　山	122 44 6·95	6·80	5·95	6·21	+ 1·00	+ 0·59		
6	男鹿嶋	25 16 27·92	27·74	27·57	28·41	+ 5·35	− 0·67	− 1·03	− 0·42
	太平山	31 59 25·75	27·11	28·71	27·05	− 1·96	+ 0·06		
	森　山	48 57 45·86	45·05	44·29	45·15	+ 1·57	− 0·10		
7	赤　山	48 55 32·58	32·04	32·18	33·05	+ 0·40	− 1·01	+ 1·30	− 2·23
	太平山	82 6 44·43	44·48	72·87	43·38	+ 1·56	+ 1·10		
	太平山	50 7 18·68	17·37	15·16	16·33	+ 3·52	+ 1·04		
8	男鹿嶋	30 1 24·81	24·87	25·11	24·92	− 0·30	− 0·05	+ 1·23	− 1·77
	赤　山	99 51 20·23	20·17	20·36	21·14	− 0·13	− 0·97		
	森　山	73 46 21·09	21·75	21·66	21·06	− 0·57	+ 0·69		
9	男鹿嶋	55 17 22·73	52·61	52·68	53·33	+ 0·35	− 0·72	− 1·01	+ 0·04
	赤　山	50 95 47·55	48·13	48·18	48·09	− 0·13	+ 0·04		

第 II 表　男鹿半島附近震災地一二等三角點移動比較較表

點の名稱		邊長 新	邊長 舊	邊長の差 新 — 舊
		m	m	m
幟　山 —	姫ケ岳	29 285·03	29 285·07	− 0·00
	太平山	46 008·59	46 008·63	− 0·08
	森山	25 309·19	25 309·25	− 0·06
	男鹿嶋	44 752·16	44 752·62	+ 0·14
男鹿嶋 —	幟山	44 752·79	44 752·62	+ 0·14
	森山	30 987·51	30 981·30	+ 0·21
	太平山	49 201·93	49 201·30	+ 0·23
	赤山	38 312·95	38 322·64	+ 0·31
赤　山 —	男鹿嶋	38 322·95	38 323·64	+ 0·31
	森山	32 813·41	32 813·27	+ 0·14
	太平山	24 986·86	24 986·78	+ 0·08
太平山 —	赤山	24 986·86	24 986·78	+ 0·08
	男鹿嶋	49 201·53	49 001·30	+ 0·23
	森山	24 972·83	24 972·84	− 0·01
	幟山	46 008·59	46 008·67	− 0·08
	姫岳	23 160·98	23 161·03	− 0·05
姫　岳 —	太平山	23 160·98	23 161·03	− 0·05
	森山	22 858·44	22 858·39	+ 0·05
	幟ケ山	29 285·03	29 286·03	± 0·00

(次頁に續く)

第　II　表（續き）

點の名稱		邊長 新	邊長 舊	邊長の差 新——舊
森山——	幟山	25 309·19	25 309·25	− 0·06
	姫ケ岳	22 859·44	22 858·39	+ 0·05
	太平山	34 972·83	24 992·84	− 0·01
	赤山	32 813·41	32 883·27	+ 0·14
	男鹿嶋	30 987·51	30 997·30	+ 0·21

第 III 表　男鹿半島附近震災地一二等三角移動比較表

數號	等級	測點名稱	緯度 新	緯度 舊	經度 新	經度 舊	新——舊 dB″	新——舊 dL″
			″ ′ °	″	″ ′ °	′		
1	I	幟山						
2	〃	姫ケ岳						
3	〃	太平山	39 47 39·1931	39·1908	140 18 50·7960	50·7989	+ 0·0025	− 0·0029
4	〃	赤山	39 39 49·8418	46·8442	140 4 38·1838	38·1864	− 0·0024	− 0·0026
5	〃	森山	39 57 26·2420	26·2398	140 6 46·8478	46·3506	+ 0·0022	− 0·0028
6	〃	男鹿嶋	39 54 14·8741	14·8702	139 45 25·5388	25·5518	+ 0·0039	− 0·0130
7	II	石倉澤	40 4 19·6260	19·6240	140 6 44·0529	44·0556	+ 0·0020	− 0·0027
8	〃	下橫澤	40 0 58·6796	58·6755	139 54 45·9062	45·9142	+ 0·0041	− 0·0080
9	〃	濱山	39 52 21·5498	21·5462	139 58 58·0060	58·0090	+ 0·0036	− 0·0024
10	〃	寒風山	39 55 51·4546	51·4504	139 52 43·4788	43·4898	+ 0·0032	− 0·0110
11	〃	戸澤	39 59 14·8044	14·7918	139 42 51·5261	51·5292	+ 0·0126	− 0·0036

第　III　表（續き）

數號	等級	測點名稱	移動量 dB^m	移動量 dL^m	移動量 $\sqrt{dB^2+dL^2}$	移動量 方位角	眞高 新	眞高 舊	新——舊	備考
			m	m	m	° ″	m	m	m	
1	I	幟山								高度測量實施せず
2	〃	姫ケ岳								
3	〃	太平山	+ 0·07	− 0·07	0·10	315 0				
4	〃	赤山	− 0·07	− 0·06	0·09	220 40				
5	〃	森山	+ 0·07	− 0·07	0·10	315 0	325·36	325·26	+ 0·10	
6	〃	男鹿島	+ 0·12	− 0·13	0·33	291 10	716·33	716.10	+ 0·23	
7	II	石倉澤	+ 0·06	− 0·06	0·08	315 0	147·80	147·69	+ 0·11	
8	〃	下橫澤	+ 0·13	− 0·19	0·23	304 20	62·34	62·34	− 0·13	
9	〃	濱山	+ 0·11	− 0·06	0·13	331 20	22·04	22·04	− 0·02	
10	〃	寒風山	+ 0·13	− 0·26	0·29	296 30	354·75	354·98	− 0·07	
11	〃	戸澤	+ 0·39	− 0·09	0·40	347 0	103·70	103·54	+ 0·16	

第 IV 表　男鹿半島附近震災地三等三角點移動比較表

數號	等級	測點名稱	緯度 新	緯度 舊	緯度 新	度 舊	新—舊 dB''	新—舊 dL''
1	III	榮(1)大鼻崎	39 55 57·983	57·980	139 56 57·404	57·403	+ 0·003	+ 0·001
2	〃	〃(2)山崎	39 54 48·037	48·032	139 56 28·072	28·070	+ 0·005	+ 0·002
3	〃	〃(18)鹽口	39 54 10·612	10·605	139 58 19·669	19·070	+ 0·007	− 0·001
4	〃	〃(19)立木澤	39 54 13·216	13·218	139 53 30·852	36·860	− 0·002	− 0·008
5	〃	〃(20)屋布台	39 54 24·726	24·726	139 50 59·209	59·226	0·000	− 0·017
6	〃	〃(21)姫ケ澤	39 53 21·044	21·044	139 51 7·250	7·266	0·000	− 0·016
7	〃	〃(22)平澤	39 52 10·652	10·650	139 50 57·590	47·608	+ 0·002	− 0·018
8	〃	〃(24)三ツ森	39 54 47·110	47·088	139 48 33·426	33·428	+ 0·022	− 0 002
9	〃	〃(25)中ノ手	39 55 42·853	42·848	139 50 56·364	56·380	+ 0·005	− 0·016
10	〃	〃(26)中臺	39 52 0·584	0·584	139 48 35·294	35·312	0·000	− 0·018
11	〃	〃(27)椿山	39 53 6·678	6·678	139 46 48·910	48·922	0·000	− 0·012
12	〃	〃(28)馬場先	39 51 28·747	28·744	139 45 34·296	34·304	+ 0·003	− 0·008
13	〃	〃(31)小渫川	59 27 27·182	27·176	139 50 29·819	29·830	+ 0·006	− 0·011
14	〃	〃(3•)湯本山	59 57 23·474	23·450	139 44 37·360	37·365	+ 0·024	− 0·005
15	〃	〃(33)中山	39 55 46·175	46·152	139 43 23·712	23·715	+ 0·023	− 0·003
16	〃	〃(34)赤坂山	39 55 55·472	55·460	139 45 13·183	13·192	+ 0·012	− 0·009
17	〃	〃(35)長田	39 57 44·522	44·500	139 46 19·048	19·058	+ 0·022	− 0·010
18	〃	〃(36)大森	56 58 6·107	6.088	139 42 45·268	45·273	+ 0·019	− 0·005
19	〃	〃(38)高丘山	39 59 2·652	2·647	139 53 53·311	53·315	+ 0·005	− 0·004
20	〃	〃(39)大道	40 0 1·206	1·202	139 55 58·132	58·134	+ 0·004	− 0·002
21	〃	〃(40)十文字	49 57 23·384	83·378	139 53 55·144	55·146	+ 0·006	− 0.002
22	〃	〃(41)堂村	39 58 33·142	33·139	139 55 10·858	10·820	+ 0·003	− 0·002
23	〃	〃(42)白用	39 56 26·015	26·008	139 55 10·520	10·524	+ 0·007	− 0·004
24	〃	〃(44)鳥屋場	40 6 41·114	41·111	140 1 36·416	36·419	+ 0·003	− 0·003
25	〃	〃(49)森崎	40 4 54·549	54·547	140 3 20·844	20·850	+ 0·002	− 0·006
26	〃	〃(57)丸山	40 4 0·398	0·395	139 57 38·791	38·797	+ 0·003	− 0·006
27	〃	〃)61)吉崎	40 43 43·978	43·975	140 1 38·964	38·972	+ 0·003	− 0·008
28	〃	〃(62)野石	40 2 14·034	14·030	139 55 40·938	40·942	+ 0·004	− 0·004

第 IV 表 (續き)

數號	等級	測點名稱	移動量 dB^m	dL^m	$\sqrt{dB^2+dL^2}$	方位角	眞高 新	眞高 舊	新一舊	備考
						° ′	m	m	m	
1	III	榮(1)大鼻崎	+ 0·09	+ 0.02	0·09	12 30	1·53	1·19	+ 0·34	
2	〃	(2)山崎	+ 0·15	+ 0·05	0·16	18 30	10·16	10·20	− 0·04	
3	〃	〃(18)塩口	+ 0·22	− 0·02	0·22	350 50	1·53	1·56	+ 0·01	
4	〃	〃(19)立木澤	0·06	− 0·19	0·20	232 20	117·53	117·58	− 0.05	
5	〃	〃(20)屋布台	0·00	− 0·40	0·40	270 0	75·83	75·80	+ 0·03	
6	〃	〃(21)姫ケ澤	0·00	− 0·38	0·38	270 0	72·64	72·58	+ 0·06	
7	〃	〃(22)平澤	+ 0·06	− 0·43	0·43	278 0	39·67	39·68	− 0·01	
8	〃	〃(24)三ツ森	+ 0·68	− 0·05	0·68	355 50	140·97	141·48	− 0·51	
9	〃	〃(25)中ノ手	+ 0·15	− 0·38	0·41	291 30	83·68	83·90	+ 0·08	
10	〃	〃(26)中台	0·00	− 0·43	0·43	270 0	61·47	60·32	+ 0·15	

(次頁に續く)

第 IV 表 (續き)

數號	等級	測點名稱	移動量 dB m	移動量 dL m	移動量 $\sqrt{dB^2+dL^2}$	移動量 方位角 ° ′	眞高 新 m	眞高 舊 m	新一舊 m	備考
11	III	〃(27)椿 山	0·00	+ 0·26	0·29	270 0	399·39	399·40	+ 0·19	
12	〃	〃(28)馬場先	+ 0·09	+ 0·19	0·21	295 20	62·85	62·41	+ 0·44	
13	〃	〃(31)小渫川	+ 0·18	− 0·26	0·32	204 40	81·87	81·45	+ 0·02	
14	〃	〃(32)湯本山	+ 0·74	− 0·12	0·75	350 50	161·31	160·95	+ 0·36	
15	〃	〃(33)中 山	+ 0·71	− 0·07	0·71	354 20	291·06	190·62	+ 0·44	
16	〃	〃(34)赤坂山	+ 0·37	− 0·21	0·43	330 30	301·24	301·05	+ 0·19	
17	〃	〃(35)長 田	+ 0·68	− 0·24	0·72	240 30	29·69	29·57	+ 0·12	
18	〃	〃(36)大 森	+ 0·59	− 0·12	0·60	348 30	149·40	149·07	+ 0·33	
19	〃	〃(38)高丘山	+ 0·15	− 0·10	0·18	326 20	69·09	669·08	+ 0·01	
20	〃	〃(39)大 道	+ 0·12	− 0·05	0·13	337 20	20·38	20·27	+ 0·11	
21	〃	〃(40)十文字	+ 0·18	− 0·05	0·19	344 30	56·60	56·37	+ 0·03	
22	〃	〃(41)堂 村	+ 0·09	− 0·05	0·10	331 6	35·26	35·28	− 0·02	
23	〃	甚(42)百 川	+ 0·22	− 0·10	0·24	335 30	5·82	5·85	− 0·03	
24	〃	〃(44)鳥屋場	+ 0·09	− 0·07	0·11	322 10	45·24	45·25	− 0·01	
25	〃	〃(49)森 崎	+ 0·06	− 0·14	0·15	293 10	14·47	65·47	0·00	
26	〃	〃(57)丸 山	+ 0·09	− 0·14	0·17	302 40	65·21	65·14	+ 0·07	
27	〃	〃(61)吉 崎	+ 0.09	− 0·19	0·21	295 20	0·98	1·18	− 0·20	
28	〃	〃(62)野 石	+ 0·12	− 0·10	0·16	320 10	0·55	8·45	+ 0·10	

II. 二，三等三角測量

二，三等三角測量改測地域は一等三角點改測地區內に於いて震央に近き激震地帶を撰び，二等三角點 6 點三等三角點 35 點の改測を實施せり，(第 2 圖參照)

1 外業期間

(イ) 二等三角測量

舊觀測 明治 41 年 10 月〜11 月
新觀測 昭和 15 年 10 月〜11 月

(ロ) 三等三角測量

舊觀測 {南秋田郡地方 昭和 43 年 5 月〜 8 月 / 山本郡地方 明治 44 年 5 月〜 9 月}
新觀測 全 地 域 昭和 15 年 9 月〜11 月

2 觀測用機械

(イ) 二等三角測量

舊觀測 獨，カール・バンベルヒ製 21 糎測微經緯儀
新觀測 〃，ウィルド製 14 糎經緯儀

(ロ) 三等三角測量

舊觀測・新觀測} 獨，カール・バンベルヒ製 14 糎測微經緯儀

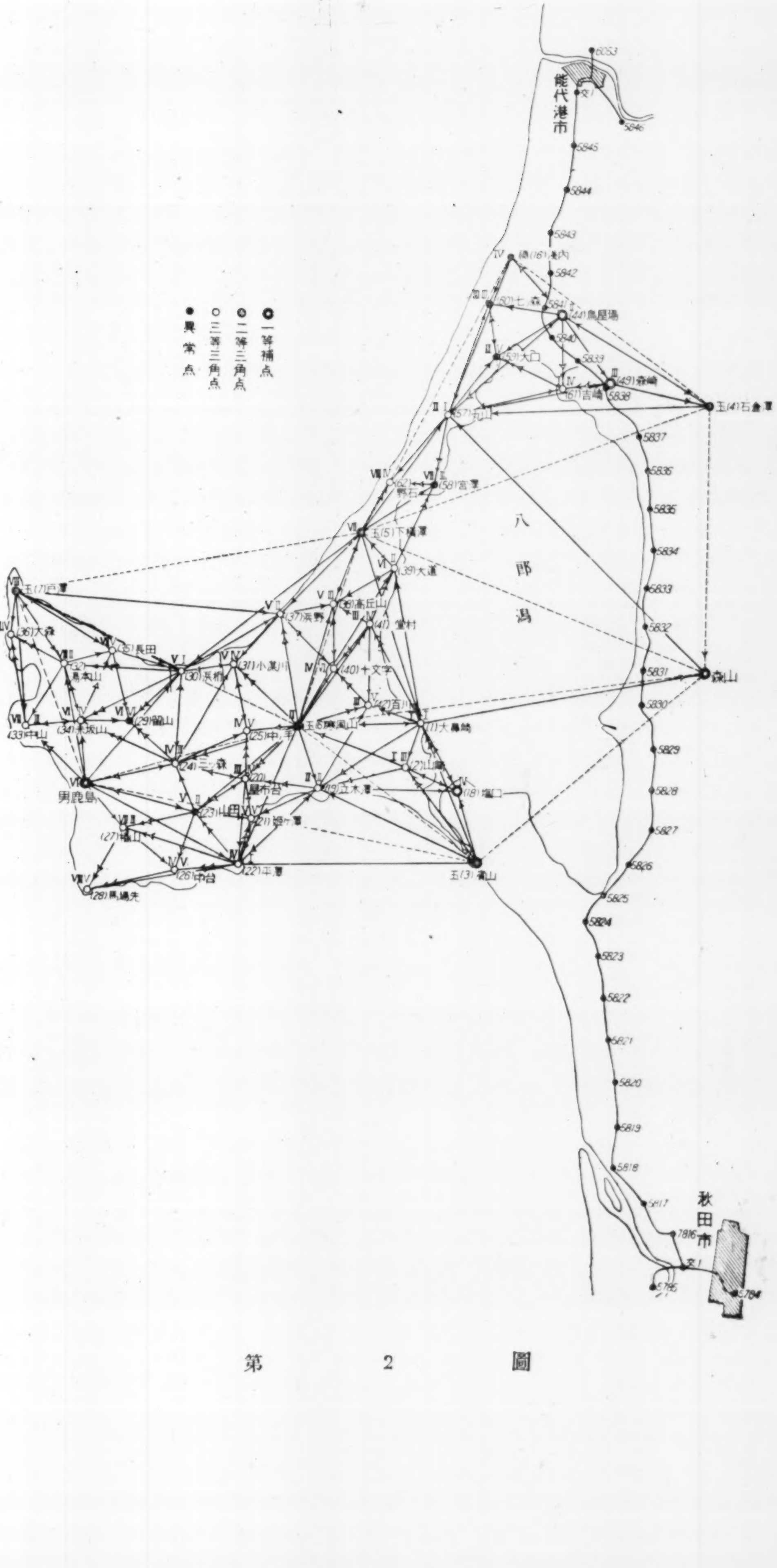
一等補点
二等三角点
三等三角点
異常点
能代港市
八郎潟
男鹿島
秋田市
森山
玉(4)石倉澤
玉(3)寒風山
玉(7)戸賀
(49)森崎
(44)鳥屋場
(39)大道
(37)浜野
(24)三ッ森
(28)馬過先

第 2 圖

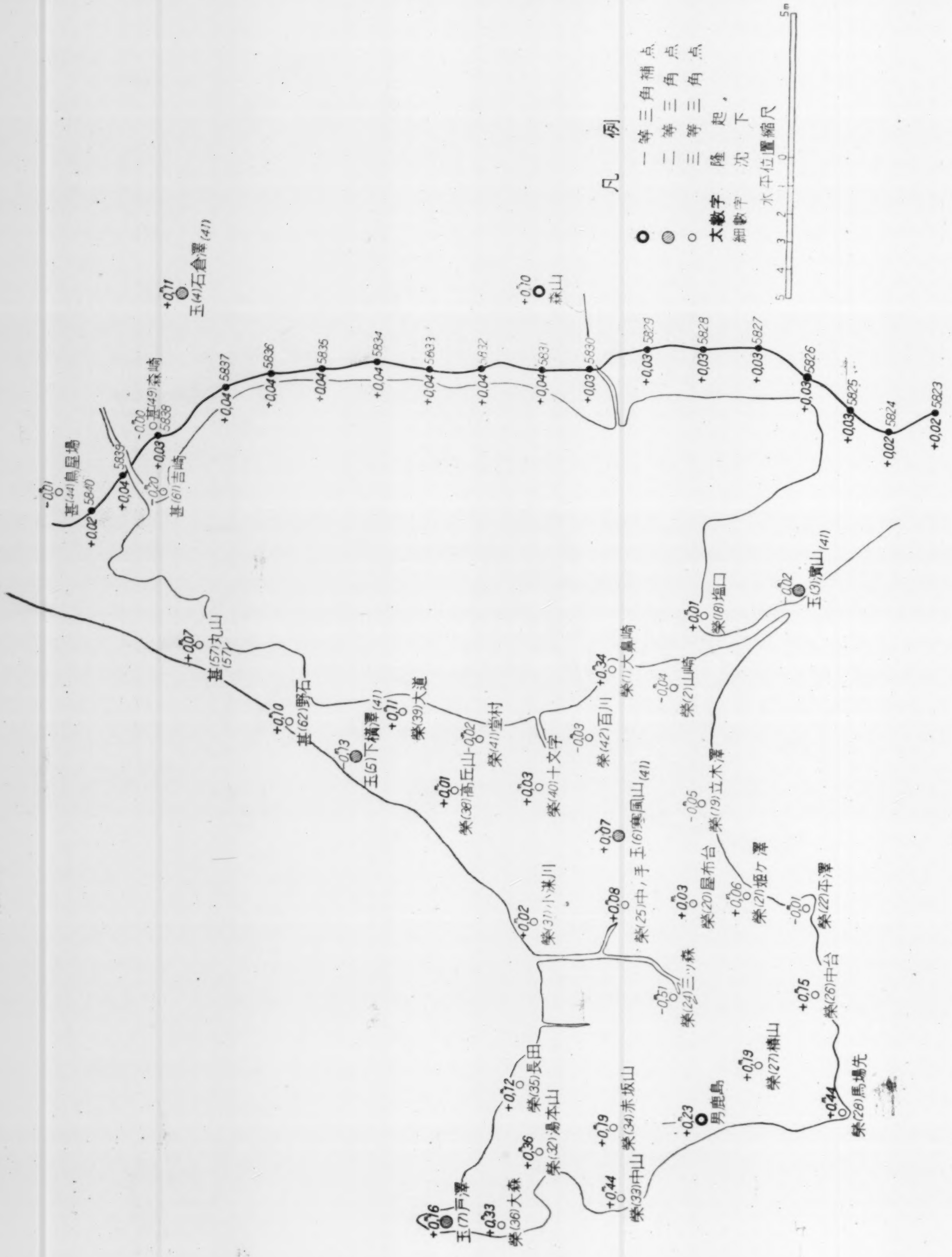

第 3 圖

3 計 算

二，三等三角點共舊觀測値を用ひ一等三角點第一段の結果を與件として第一段の平均計算及經緯度計算を行ひ，次に新觀測値を用ひ一等三角點第二段の結果を與件として第二段の平均計算及經緯度計算を行ひ，この兩結果を比較して各點の相對的水平移動量を算出せり，

但し，平均方向は新舊共全く同一ならしめたり，その結果は第 IV 表及第3圖に示すが如し.

4 新舊觀測精度次の如し

三角形の閉塞誤差より計算せる新舊觀測精度及縱橫線の平均計算に依る一方向の中等誤差 m，竝に平均位置に對する誤差 M は次の如し.

二等三角
$$\text{新}: \sqrt{\frac{[\Delta\Delta]}{3n}} = \pm 0.''98 \quad m = \pm .''143 \quad M = \pm 0.^{m}116$$
$$\text{舊}: \sqrt{\frac{[\Delta\Delta]}{3n}} = \pm 0.95 \quad m = \pm 0.90 \quad M = \pm 0.078$$

三等三角
$$\text{新}: \sqrt{\frac{[\Delta\Delta]}{3n}} = \pm 2.42 \quad m = \pm 2.28$$
$$\text{舊}: \sqrt{\frac{[\Delta\Delta]}{3n}} = \pm 1.73 \quad m = \pm 2.20$$

II. 高 程

一二三等三角點改測 47 點の中 4 點の直接水準點を撰び(舊觀測と一致) 附近改測一等水準測量の新結果を用ひて覘標水準測量を實施しそれを既知高として，逐次二方向よりする高程計算を行ひ各三角點の眞高を決定せり．其の新結果と舊結果とを比較して各三角點の垂直移動量を算出せり．

其の結果は第 III〜IV 表及第 4 圖に示すが如し.

精度：高程計算に當り二方向よりする結果の中數値に對する差異を誤差と看做して算出せる値は次の如し.

舊觀測	2·8 *cm*
新觀測	2.4 *cm*

IV. 一等水準測量

震災の影響比較的小なりし秋田市より起り能代市に至る延長 70 粁 (水準點 36 點の水準線を改測せり．(第 2 圖參照)

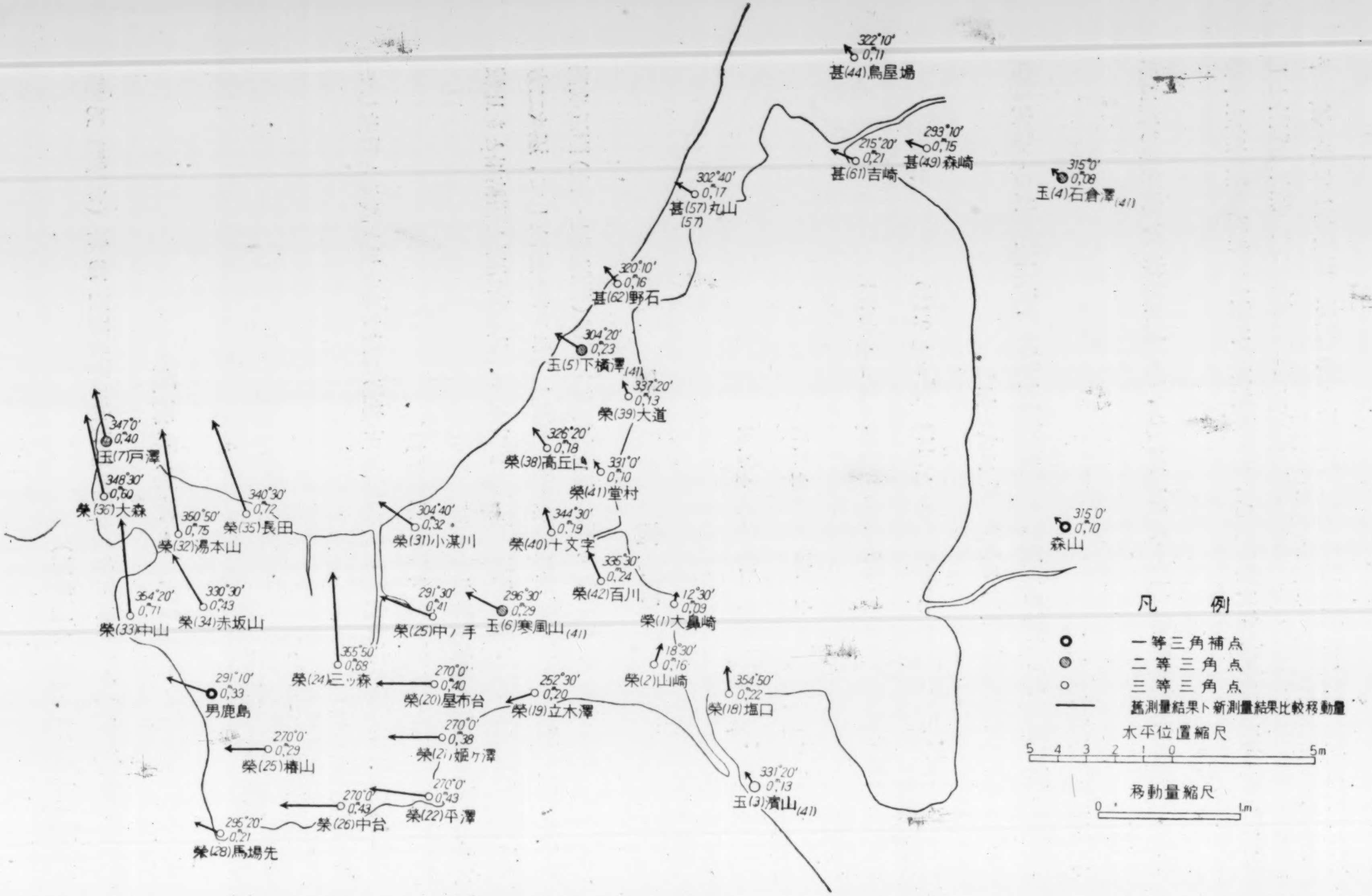
凡例
一等三角補点
二等三角点
三等三角点
舊測量結果ト新測量結果比較移動量
水平位置縮尺
5 4 3 2 1 0 5m
移動量縮尺
0 1m
甚(44)鳥屋場 322°10′ 0.11
甚(49)森崎 293°10′ 0.15
甚(61)吉崎 215°20′ 0.21
玉(4)石倉澤(41) 315°0′ 0.08
森山 315°0′ 0.10
甚(57)丸山 (57) 302°40′ 0.17
甚(62)野石 320°10′ 0.16
玉(5)下横澤(41) 304°20′ 0.23
榮(39)大道 337°20′ 0.13
榮(38)高丘山 326°20′ 0.18
榮(41)堂村 331°0′ 0.10
榮(40)十文字 344°30′ 0.19
榮(42)百川 335°30′ 0.24
榮(1)大鼻崎 12°30′ 0.09
榮(2)山崎 18°30′ 0.16
榮(18)塩口 354°50′ 0.22
玉(3)濱山(41) 331°20′ 0.13
榮(19)立木澤 252°30′ 0.20
榮(20)屋布台 270°0′ 0.40
榮(21)姫ヶ澤 270°0′ 0.38
榮(22)平澤 270°0′ 0.43
榮(26)中台 270°0′ 0.43
榮(25)椿山 270°0′ 0.29
榮(28)馬場先 295°20′ 0.21
男鹿島 291°10′ 0.33
榮(24)三ッ森 355°50′ 0.68
榮(25)中ノ手 291°30′ 0.41
玉(6)寒風山(41) 296°30′ 0.29
榮(31)小濱川 304°40′ 0.32
榮(33)中山 354°20′ 0.71
榮(34)赤坂山 330°30′ 0.43
榮(32)湯本山 350°50′ 0.75
榮(35)長田 340°30′ 0.72
榮(36)大森 348°30′ 0.60
玉(7)戸澤 347°0′ 0.40

第4圖

本水準線は帝國學士院の委託に基き昭和 10 年度改測を實施せるものなり．

1　外業期間

舊觀測　昭和 10 年 8 月 ～ 9 月

新觀測　昭和 15 年 9 月 ～ 12 月

2　觀測用機械

新舊共　獨，カールツァイス製三號型水準儀インバール製精密標尺

3　標高基準

秋田市に於ける水準點交 9 號を不動と假定せり．新舊兩觀測成果を用ひて計算せる水準點垂直變動量は第 V 表に示すが如し．

第　V　表

標石番號	所在地	新觀測年月日	最觀測年月日	變動量	
交 9	秋田市川尻町	昭和15年		mm 0·0	不動と假定す
5816	寺内町	10月 1日	昭和10年	− 7·9	
5817	〃	〃 2	8 月	−16·8	
5818	土崎港町	〃 3	|	− 3·3	
5819	〃	〃 4	9 月	5·9	
5820	飯島村	〃 5		7·5	
5821	下新城村	〃 6		13·8	
5822	天王村	〃 7		14·2	
5823	大久保町	〃 8		18·5	
5824	〃	〃 9		22·1	
5825	〃	〃 10		29·1	
5826	飯田川村	〃 11		37·3	
5827	〃	〃 12		27·8	
5828	下井川村	〃 13		34·5	
5829	大川村	〃 14		28·1	
5830	一日市町	〃 15		33·6	
5831	面潟村	〃 16		37·9	
5832	〃	〃 17		36·7	
5833	鹿渡町	〃 18		45·4	
5834	〃	〃 19		40·1	

標石番號	所在地	新觀測年月日	舊觀測年月日	變動量	
5825	鹿渡町	〃 20		42·7	不動ト假定ス
5836	〃	〃 22		35·1	
5837	〃	〃 23		36·3	
5838	鵜川村	〃 24		33·6	
5839	〃	〃 25		65·0	
5840	〃	〃 27		20·2	
5841	〃	〃 28		53·5	
5842	淺内村	〃 29		20·7	
5843	〃	〃 30		14·9	
5844	〃	〃 31		− 3·4	
5845	榊ノ村	10日 1日		− 3·0	
交 1	能代市			− 5·7	
5784	秋田市片島	9月29日		− 2·5	
交 9	〃 同川尻	〃 30			
5785	河邊郡新屋町	11月 2日		0·0	
5846	能代市能代町	〃 3		− 2·9	
交 1	〃			− 2·0	
6053	〃			− 6·4	

4 精　度

發起點	終點末	點數	距離	一鎖部往復差の平均	
				新	舊
秋田市	能代市				
交 9 號	交 1 號	36	70 km	1.3 mm	1.1 mm

IV. 結　　言

今回の作業の一部は帝國學士院の援助を受けられたる今村明恒博士の委託に基いて實施せるものなり．

尙改測三角點合計 47 點中異狀點として新舊兩成果を比較する能はざりしもの二等三角點 1 點三等三角點 7 點計 8 點の多きに達せりこの中震災の爲土地崩壞に依るもの 3 點を除き他は人爲的故障に基くものにして尙一層一般國民の測量標に對する理解竝に關心の徹底を切望する次第なり．

---

42. *Results of Revisions of Triangulation and Levelling in the Neighbourhood of Ogasima, Akita Prefecture.*

By the Military LAND SURVEY.

The region in the neighbourhood of Ogasima, Akita Prefecture, was remarkably deformed by the destructive earthquake of May 1, 1939. Triangulation was revised in this region in 1940, and the horizontal displacements of 39 triangulation points, including 6 primary points, 5 secondary points, and 28 tertiary points, were measured. At 8 points, marks were destroyed, and their displacements were not found.

The horizontal displacements thus measured are for the time interval from 1901～1908 to 1940, referring to two primary triangularion points, Noboriyama and Himegatake, situated east of the region, the displacements of which are assumed to be zero during the time interval mentioned above.

The vertical displacements of these triangulation points were measured, referring to 4 points, the heights of which were determined directly by levels from bench-marks.

The line of levels from Akita to Nosiro, including 36 bench-marks, was also rerun in 1940, and the vertical displacements of these bench-marks were measured relative to bench-mark J-9, in Akita. As this line was levelled in 1935, the displacements measured are regarded as due having occurred in the time interval 1935～1940.

The horizontal and vertical displacements of triangulation points obtained are designated by arrows and numerals against the points, as in Figs. 3～4, the vertical displacements of bench-marks being given in Table V.

——所　報——

○談話會記事

第165回談話會（昭和15年12月19日）

1.	三宅島の伏角の再測	水上武
2.	地盤沈下速度と地下水水位との關係	北澤五郎
3.	本邦附近に於ける地磁氣偏角日變化の振幅と位相差	永田武
4.	風の構造の研究（主として風力計に就て）	西村源六郎 鈴木正治
5.	風壓に對する構造物の抵抗に就て（豫報）	西村源六郎 鈴木正治
6.	地下70粁附近の深さの物理的狀態に就て	妹澤克惟 金井清
7.	鳳凰山下の斷層とその兩側の地質構造との關係	大塚彌之助

第166回談話會（昭和16年1月16日）

1.	湖水面を利用した富士五湖々畔水準測量	萩原尊禮 表俊一郎
2.	年平均潮位の變化	宮部直巳
3.	三宅島新寄生火山及熔岩流の地形再測量	表俊一郎
4.	太陽系の潮汐論的起原の問題（續報）	妹澤克惟
5.	任意の地震計の記錄から任意時間の地動を求める一方法	妹澤克惟
6.	昭和15年7月12日三宅島噴火に伴ひし垂直磁力の變化（第2報）	高橋龍太郎 平能金太郎

第167回談話會（昭和16年2月20日）

1.	宮城縣鳴子町金忠間歇泉に就て	野口喜三雄
2.	新潟縣瀨波温泉に就て	野口喜三雄
3.	兵庫縣養父郡地方の第三紀層	大塚彌之助
4.	三宅島新噴出岩の磁氣的性質（補遺）	永田武
5.	地殼の均衡に就て	坪井忠二
6.	兩面から壓力を受ける板の變形	坪井忠二 宮村攝三
7.	筑波山に於て觀測された地表傾斜變化（特に永久變化と二，三の特異な變化に就て）	萩原尊禮
8.	等方不均一球内の一點より起る彈性波（第2報）	吉山良一
9.	レーリー波の分散曲線に關する疑問	吉山良一
10.	昭和15年三宅島の活動に伴つた微動と地震との觀測 附，簡單地震計の製作	高橋龍太郎 平能金太郎
11.	地震波動の初動に就いて	妹澤克惟 金井清

12. 地震計に於ける高次の不安定に就いて（第 3 報）（新上下動振動臺によるその實驗）　妹澤克惟・金井清

第 168 回談話會（昭和 16 年 3 月 20 日）

1. 中國山地は隆起するか　宮部直巳
2. 砂層内の靜壓力に就て（序報）　宮部直巳・武井柳吉
3. 地震の頻度と振幅に關する石本，飯田の實驗式 $na^m = k$ に就て　松澤武雄
4. 地殼內の溫度變化と地表に於ける地球磁氣の變化　永田武
5. 演算法によりて解いた地震計の初動問題に就て　妹澤克惟・金井清

第 169 回談話會（昭和 16 年 4 月 17 日）

1. 地表の物理的性質（其の 1）　岸上冬彥
2. 初期微動中の諸相（北關東の深い地震に就て）　宮村攝三
3. 1897 年 6 月 12 日印度大地震の震央地方の地動に就て　松澤武雄
4. 淺間火山附近に於ける岩石及び土壤の浸出水の PH　野口喜三雄・川口正雄
5. 演算法によりて解いた地震計の初動問題（模型實驗との比較）　金井清・妹澤克惟
6. 三宅島三角再測量の結果　宮部直巳

——所　報——

○談話會記事

第 170 回談話會（昭和 16 年 5 月 15 日）

1.	關東地方に於ける地震觀測報告	那須信治 保田桂二
2.	地震動の比較觀測（其の 1）水平動變位計	高橋龍太郎 平能金太郎
3.	火山岩の初期帶磁率に就いて（補遺）	永田武
4.	岩石に於ける熱殘留磁氣及其の生成過程 (II)	永田武
5.	地殼の均衡に就いて（其の 2）	坪井忠二

第 171 回談話會（昭和 16 年 6 月 16 日）

1.	軟弱地盤に於ける地震動	高橋龍太郎
2.	津浪記錄用驗潮儀の製作	高橋龍太郎
3.	三宅島產酸性拋出岩に就て	津屋弘逵
4.	上諏訪に於ける水準測量の結果	宮部直巳
5.	靜岡縣興津町附近の地質構造	大塚彌之助
6.	緩慢な變化の遠隔記錄法	萩原尊禮
7.	演算法を應用せる任意形彈性波の傳播の問題（第 2 報）	妹澤克惟 金井清
8.	演算法によりて解いた地震計の初動問題に就て	妹澤克惟 金井清

第 172 回談話會（昭和 16 年 7 月 3 日）

1.	北滿綏化地方に起りたる地震に就て	河角廣
2.	弦の振動を利用せる時計裝置（第 2 報）	坪井忠二 川島正治
3.	鋸齒狀小屋の耐震性（序報） 附話　妹澤，金井の前回の報告の補遺	金井清
4.	淺間火山近傍の重力偏差と密度分布	水上武
5.	淺間火山近傍の重力偏差とゲオイドの凹凸	水上步
6.	軟弱地盤の卓越周期	鈴木正治
7.	風の構造	西村源六郎 鈴木正治
8.	風に依る家屋の動き	西村源六郎 鈴木正治

第 173 回談話會（昭和 16 年 9 月 18 日）

1.	新潟縣松之山溫泉に就て	野口喜三雄
2.	昭和 16 年 7 月 15 日長野地方の地震報告	岸上冬彥 永田武 宮村攝三

3. 昭和 16 年 7 月 15 日長野地震の家屋破害に就て　金井清
4. 喜光寺平に於ける民家構造の特異性と震害　齋田時太郎
5. 富士山產噴出岩の磁氣的性質（特に磁性と溫度との關係に就て）　永田武
6. 曲線で限られた平面盤の引力計算にポーセリエー，セル Paucelier Cell の應用　長岡半太郎
7. 三宅島新寄生火山及び熔岩流の第 3 回地形測量結果　表俊一郎
8. 三角測量より見たる三宅島の地形變化　表俊一郎
9. 三宅島火山彈の形態及構造　津屋弘逵
10. 三宅島產灰長石及橄欖石の化學成分　津屋弘逵
11. 伊豆大島の地震の發震時について　高橋龍太郎
12. 伊豆大島の水準再測量の結果　高橋龍太郎
13. 三鷹村基線菱形の變形と地震活動との關係　坪井忠二
14. 固體自體が分散性なる場合に於けるレーレー波の傳播　妹澤克惟・金井清

第 19 號 索 引

頁

萩原尊禮 (16) 筑波山に於ける土地傾斜變化の觀測 (其の二) (英文) ………… 218

萩原尊禮 (28) 緩慢な變化の遠隔記錄法 (英文) ………………………………… 523

萩原尊禮・津屋弘逵・高橋龍太郎・水上武・永田武・表俊一郎・平能金太郎
(20) 昭和 15 年 7 月三宅島の噴火 (英文) ………………………………… 260

平能金太郎・高橋龍太郎 (7) 三宅島の噴火に伴つた垂直磁力の變化 (概要)
(英文) ……………………………………………………………………… 82

平能金太郎・高橋龍太郎 (29) 比較觀測を目的とする水平動變位計の製作
(邦文) ……………………………………………………………………… 527

平能金太郎・高橋龍太郎 (30) 軟弱地盤に於ける地震動 (邦文) ………………… 534

平能金太郎・津屋弘逵・高橋龍太郎・萩原尊禮・水上武・永田武・表俊一郎
(20) 昭和 15 年 7 月三宅島の噴火 (英文) ………………………………… 260

福西清治・宮部直巳 (19) 東京市內水準改測の成果 (邦文) ………………… 248

金井清 (33) 鋸齒狀小屋の耐震性 (英文) …………………………………… 554

金井清 (40) 昭和 16 年 7 月 15 日長野地震の家屋被害に就て (邦文) ……… 647

金井清・妹澤克惟 (1) 地球核の熱力學的成因について (第 2 報) (英文) ……… 1

金井清・妹澤克惟 (2) 地震計に於ける高次の不安定について (第 2 報) (英文) … 9

金井清・妹澤克惟 (3) 地球の內部に於ける粘性の分布 (第 2 報) 地震波の
蔭になる地帶について (英文) ………………………………………………… 14

金井清・妹澤克惟 (11) 演算法を應用せる任意形彈性波の傳播の問題
(第 1 報) (英文) …………………………………………………………… 151

金井清・妹澤克惟 (12) 演算法によりて解いた地震計の初動問題について
(第 1 報) (英文) …………………………………………………………… 162

金井清・妹澤克惟 (13) 地震計に於ける高次の不安定に就いて (第 3 報)
新しい上下動振動臺による實驗 (英文) ……………………………………… 177

金井清・妹澤克惟 (23) 演算法を應用せる任意形彈性波の傳播の問題
(第 2 報) (英文) …………………………………………………………… 417

金井清・妹澤克惟 (24) 演算法によりて解いた地震計の初動問題について
(第 2 報) (英文) …………………………………………………………… 443

金井清・妹澤克惟 (32) 固體自體が分散性なる場合に於けるレーレー波の傳播
(英文) ……………………………………………………………………… 549

岸上冬彥・永田武・宮村攝三 (39) 昭和 16 年 7 月 15 日長野地震の統計的調
査 (邦文) …………………………………………………………………… 628

久野久 (10) 輕石流堆積物と拋出輕石堆積物との差異に就いて (英文) ……… 144

松尾春雄・齋田時太郎 (15) 横濱港の埋立地及岸壁に於ける地震動 (邦文)…… 206
松澤武雄 (22) 地震の頻度と振幅に關する石本・飯田の實驗式 $na^m=k$ に就いて (獨文) …… 411
陸地測量部 (42) 秋田縣男鹿半島附近震災地三角點水準點復舊測量記事 (邦文)…… 671
水上武 (37) 三宅島新熔岩流の帶磁 (英文)…… 612
水上武・津屋遼弘・高橋龍太郎・萩原尊禮・永田武・表俊一郎・平能金太郎 (20) 昭和 15 年 7 月三宅島の噴火 (英文) …… 260
宮部直巳 (8) 昭和 15 年 8 月 2 日日本海に起つた津波 (邦文) …… 104
宮部直巳 (17) 中國山地の隆起運動に就て (英文)…… 228
宮部直巳 (18) 年平均潮位の高さの變化 (英文)…… 238
宮部直巳・福西清治 (19) 東京市內水準改測の成果 (邦文) …… 248
宮村攝三・岸上冬彥・永田武 (39) 昭和 16 年 7 月 15 日長野地震の統計的調査 (邦文) …… 628
永田武 (6) 火成岩に於ける熱殘留磁氣生成の機構に就いて (序報) (英文)…… 49
永田武 (21) 昭和 15 年 8 月三原火山小活動に關する地球磁氣學的調査 (英文)…… 402
永田武 (35) 岩石の帶磁率の溫度に因る變化の測定 (英文)…… 579
永田武・岸上冬彥・宮村攝三 (39) 昭和 16 年 7 月 15 日長野地震の統計的調査 (邦文) …… 628
永田武・津屋弘遠・高橋龍太郎・萩原尊禮・水上武・表俊一郎・平能金太郎 (20) 昭和 15 年 7 月三宅島の噴火 (英文) …… 260
那須信治・保田柱二 (26) 最近に於ける關東地方の地震に就いて (英文)…… 476
表俊一郎 (38) 三宅島新寄生火山及び新熔岩流の第 3 回地形測量 (英文)…… 619
表俊一郎・津屋弘遠・高橋龍太郎・萩原尊禮・水上武・永田武・平能金太郎 (20) 昭和 15 年 7 月三宅島の噴火 (英文) …… 260
大塚彌之助 (9) 山梨縣鳳凰山・地藏ヶ岳附近の地質 (邦文) …… 115
齋田時太郎 (41) 善光寺平に於ける民家構造の特異性と震害 (邦文)…… 661
齋田時太郎・松尾春雄 (15) 橫濱港の埋立地及岸壁に於ける地震動 (邦文) …… 206
妹澤克惟・金井清 (1) 地球核の熱力學的成因について (第 2 報) (英文)…… 1
妹澤克惟・金井清 (2) 地震計に於ける高次の不安定について(第 2 報)(英文)… 9
妹澤克惟・金井清 (3) 地球の內部に於ける粘性の分布 (第 2 報) 地震波の蔭になる地帶について (英文) …… 14
妹澤克惟・金井清 (11) 演算法を應用せる任意形彈性波の傳播の問題 (第 1 報) (英文) …… 151
妹澤克惟・金井清 (12) 演算法によりて解いた地震計の初動問題について (第 1 報) (英文) …… 162

妹澤克惟・金井清 (13) 地震計に於ける高次の不安定に就いて (第3報) 新しい上下動振動臺による實驗 (英文) ……………………………… 177
妹澤克惟・金井清 (23) 演算法を應用せる任意形彈性波の傳播の問題 (第2報) (英文) ……………………………… 417
妹澤克惟・金井清 (24) 演算法によりて解いた地震計の初動問題について (第2報) (英文) ……………………………… 443
妹澤克惟・金井清 (32) 固體自體が分散性なる場合に於けるレーレー波の傳播 (英文) ……………………………… 549
高橋龍太郎・平能金太郎 (7) 三宅島の噴火に伴つた垂直磁力の變化 (概要) (英文) ……………………………… 82
高橋龍太郎・平能金太郎 (29) 比較觀測を目的とする水平動變位計の製作 (邦文) ……………………………… 527
高橋龍太郎・平能金太郎 (30) 軟弱地盤に於ける地震動 (邦文) ……………………………… 534
高橋龍太郎・津屋弘逵・萩原尊禮・水上武・永田武・表俊一郎・平能金太郎 (20) 昭和 15 年 7 月三宅島の噴火 (英文) ……………………………… 260
坪井忠二 (25) 重價平均に關する一問題 (英文) ……………………………… 458
坪井忠二 (34) 三鷹基線菱形の變形と其の附近に於ける地震活動 (英文) ……………………………… 559
坪井忠二・山口生知 (4) 重力異常と地下構造との關係 (VI.) (英文) ……………………………… 26
津屋弘逵 (27) 昭和 15 年 7 月三宅島の噴火 三宅島噴火の地質學的觀察 (II) (英文) ……………………………… 492
津屋弘逵 (36) 三宅島產火山彈の形態及び構造に就いて (英文) ……………………………… 597
津屋弘逵・高橋龍太郎・萩原尊禮・水上武・永田武・表俊一郎・平能金太郎 (20) 昭和 15 年 7 月三宅島の噴火 (英文) ……………………………… 260
山口生知 (5) 油壺及細島に於ける海水面變化に就て (英文) ……………………………… 39
山口生知・坪井忠二 (4) 重力異常と地下構造との關係 (VI.) (英文) ……………………………… 26
保田柱二・那須信治 (26) 最近に於ける關東地方の地震に就いて (英文) ……………………………… 476
吉山良一 (14) 等方不均一球內の一點より起る彈性波 (第3報) (英文) ……………………………… 185
(31) 三宅島における三角再測量の結果 (邦文) ……………………………… 544

Index to Vol. XIX.

Page

HAGIWARA, T. (16) Observation of Changes in the Inclination of the Earth's Surface at Mt. Tukuba (Second Report). (in English) 218

HAGIWARA, T. (28) A New Device for Remote Mechanical Recording of Slow Movements. (in English) 523

HAGIWARA, T.; TSUYA, H.; TAKAHASI, R.; MINAKAMI, T.; NAGATA, T.; OMOTE, S. and HIRANO, K. (20) The Eruption of Miyake-sima, One of the Seven Izu Islands, in 1940. (in English) 260

HIRANO, K. and TAKAHASI, R. (7) Changes in the Vertical Intensity of Geomagnetism that Accompanied the Eruption of Miyakezima, in 1940. (in English) 82

HIRANO, K. and TAKAHASI, R. (29) A New Horizontal-Component Seismograph for Comparison Observations. (in Japanese) 527

HIRANO, K. and TAKAHASI, R. (30) Seismic Vibrations of Soft Ground. (in Japanese) 534

HUKUNISI, S. and MIYABE, N. (19) Results of Relevelling in Tokyo, in 1940. (in Japanese) 248

HIRANO, K.; TSUYA, H.; TAKAHASI, R.; HAGIWARA. T.; MINAKAMI, T.; NAGATA, T. and OMOTE, S. (20) The Eruption of Miyake-sima, One of the Seven Izu Islands, in 1940. (in English) 260

HUKUNISI, S. and MIYABE, S. (19) Results of Relevelling in Tokyo, in 1940. (in Japanese) 248

KANAI, K. (33) The Seismic Vibration of a Saw-tooth Roof Structure. (in English) 554

KANAI, K. (40) On the Damage to Buildings in the Nagano Earthquake of July 13, 1941. (in Japanese) 647

KANAI, K. and SEZAWA, K. (1) Thermodynamical Origin of the Earth's Core. II. (in English) 1

KANAI, K. and SEZAWA, K. (2) On the Problem of Instabilities of Higher Orders in a Seismometer. II. (in English) 9

KANAI, K. and SEZAWA, K. (3) Viscosity Distribution within the

Earth. II. On the Shadow Zone for Seismic Waves. (in English) 14

KANAI, K. and SEZAWA, K. (11) Transmission of Arbitrary Elastic Waves from a Spherical Source, Solved with Operational Calculus. I. (in English) 151

KANAI, K. and SEZAWA, K. (12) On the Initial Movement of a Seismograph subjected to an Arbitrary Earthquake Motion, Solved with Operational Calculus. I. (in English) 162

KANAI, K. and SEZAWA, K. (13) On the Problem of Instabilities of Higher Orders in a Seismometer. III. Experiments with a New Vertical Vibration Table. (in English) 177

KANAI, K. and SEZAWA, K. (23) Transmission of Arbitrary Elastic Waves from a Spherical Source, Solved with Operational Calculus. II. (in English) 417

KANAI, K. and SEZAWA, K. (24) On the Initial Movement of a Seismograph subjected to an Arbitrary Earthquake Motion, Solved with Operational Calculus. II. (in English) 443

KANAI, K. and SEZAWA, K. (32) On the Propagation of Rayleigh-waves in Dispersive Elastic Media. (in English) 549

KISHINOUYE, F.; NAGATA, T. and MIYAMURA, S. (39) A Statistical Investigation of the Strong Earthquake of July 15, 1941, near Nagano. (in Japanese) 628

KUNO, H. (10) Characteristics of Deposits formed by Pumice Flows and Those by Ejected Pumice. (in English) 144

MATUO, H. and SAITA, T. (15) Earthquake Vibrations on Quays and on Reclaimed Ground in the Harbour of Yokohama. (in Japanese) 206

MATUZAWA, T. (22) Über die empirische Formel von Ishimoto und Iida $na^m=k$ zwischen der Bebenhäufigkeit n und der Amplitude a. (im Deutschen) 411

Military Land Survey. (42) Results of Revisions of Triangulation and Levelling in the Neighbourhood of Ogasima, Akita Prefecture. (in Japanese) 671

MINAKAMI, T. (37) Magnetization of the New Lava-Flows of Miyakesima Island. (in English) 612
MINAKAMI, T.; TSUYA, H.; TAKAHASI, R.; HAGIWARA, T.; NAGATA, T.; OMOTE, S. and HIRANO, K. (20) The Eruption of Miyake-sima, One of the Seven Izu Islands, in 1940. (in English) 260
MIYABE, N. (8) Tunami associated with the Earthquake of August 2, 1940. (in Japanese) 104
MIYABE, N. (17) Upwarp Deformation of the Land in Tyūgoku. (in English) 228
MIYABE, N. (18) Secular Changes in the Heights of Yearly Mean Sea-Level at Japanese Stations. (in Enhlish) 238
MIYABE, N. and HUKUNISI, S. (19) Results of Relevelling in Tokyo, in 1940. (in Japanese) 248
MIYAMURA, S.; KISHINOUYE, F. and NAGATA, T. (39) A Statistical Investigation of the Strong Earthquake of on July 15, 1941, near Nagano. (in Japanese) 628
NAGATA, T. (6) The Mode of Causation of Thermo-Remanent Magnetism in Igneous Rocks. Preliminary Note. (in English)... 49
NAGATA, T. (21) A Geomagnetic Study of the Minor Activities of Volcano Mihara, Oosima Island, August 1940. (in English)... 402
NAGATA, T. (35) Measurement of Changes in Magnetic Susceptibility of Igneous Rocks with Temperature in a Weak Magnetic Field. (in English) 579
NAGATA, T.; KISHINOUYE, F. and MIYAMURA, S. (39) A Statistical Investigation of the Strong Earthquake of July 15, 1941, near Nagano. (in Japanese) 628
NAGATA, T.; TSUYA, H.; TAKAHASI, R.; HAGIWARA, T,; MINAKAMI, T.; OMOTE, S. and HIRANO, K. (20) The Eruption of Miyake-sima, One of the Seven Izu Islands, in 1940. (in English) 260
NASU, N. and YASUDA, C. (26) Recent Earthqnakes of the Kwanto District. (in English) 476

OMOTE, S. (38) The Third Topographic Survey of the New Parasitic Cones and the New Lava Flow of Miyake-sima Island. (in English) 619

OMOTE, S.; TSUYA, H.; TAKAHASI, R.; HAGIWARA, T.; MINAKAMI, T.; NAGATA, T. and HIRANO, K. (20) The Eruption of Miyake-sima, One of the Seven Izu Island in 1940. (in English) 260

OTUKA, Y. (9) Geology of Mt. Zizô and Hôô, Yamanasi Prefecture, Japan. (in Japanese) 115

SAITA, T. (41) The Peculiarities of Dwelling House Construction and the Earthquake Damages in Zenkoji Plain, Nagano Prefecture. (in Japaneee) 661

SAITA, T. and MATUO, H. (15) Earthquake Vibrations on Quays and on Reclaimed Ground in the Harbour of Yokohama. (in Japanese) 206

SEZAWA, K. and KANAI, K. (1) Thermodynamical Origin of the Earth's Core. II. (in English) 1

SEZAWA, K. and KANAI, K. (2) On the Problem of Instabilites of Higher Orders in a Seismometer. II. (in English) 9

SEZAWA, K. and KANAI, K. (3) Viscosity Distribution within the Earth. II. On the Shadow Zone for Seismic Waves. (in English) 14

SEZAWA, K. and KANAI, K. (11) Transmission of Arbitrary Elastic Waves from a Spherical Source, Solved with Operational Calculus. I. (in English) 151

SEZAWA, K. and KANAI, K. (12) On the Initial Movement of a Seismograph subjected to an Arbitrary Earthquake Motion, Solved with Operational Calculus. I. (in English) 162

SEZAWA, K. and KANAI, K. (13) On the Problem of Instabilities of Higher Orders in a Seismometer. III. Experiments with a New Vertical Vibration Table. (in English) 177

SEZAWA, K. and KANAI, K. (23) Transmission of Arbitrary Elastic Waves from a Spherical Source, Solved with Operational Calculus. II. (in English) 417

SEZAWA, K. and KANAI, K. (24) On the Initial Movement of a Seismograph subjected to an Arbitrary Earthquake Motion, Solved with Operational Calculus. II. (in English) 443

SEZAWA, K. and KANAI, K, (32) On the Propagation of Rayleigh-waves in Dispersive Elastic Media. (in English) 549

TAKAHASI, R. and HIRANO, K. (7) Changes in the Vertical Intensity of Geomagnetism that Accompanied the Eruption of Miyakezima, in 1940. (in English) 82

TAKAHASI, R. and HIRANO, K. (29) A New Horizontal-Component Seismograph for Comparison Observations. (in Japanese) 527

TAKAHASI, R. and HIRANO, K, (30) Seismic Vibrations of Soft Ground. (in Japanese) 534

TAKAHASI, R.; TSUYA, H,; HAGIWARA, T.; MINAKAMI, T.; NAGATA, T.; OMOTE, S. and HIRANO, K. (20) The Eruption of Miyake-sima, One of the Seven Izu Islands, in 1940. (in English) 260

TSUBOI, C. (25) A Problem of Weighted Mean. (in English)......... 458

TSUBOI, C. (34) Secular Deformations of the Base Line Rhombus at Mitaka in Relation to Seismic Activities in its Vicinity. (in English) 559

TSUBOI, C. and YAMAGUTI, S. (4) Relation between the Gravity Anomalies and the Corresponding Subterranean Mass Distribution. (VI.) (in English).. 26

TSUYA, H. (27) The Eruption of Miyake-sima, One of the Seven Izu Island, in 1940. Geological Observations of the Miyake-sima Eruption of 1940 (II) (in English) 492

TSUYA, H. (36) On the Form and Structure of Volcanic Bombs from Volcano Miyake-sima. (in English)................................ 597

TSUYA, H.; TAKAHASI, R.; HAGIWARA, T.; MINAKAMI, T.; NAGATA, T.; OMOTE, S. and HIRANO, K. (20) The Eruption of Miyake-sima, One of the Seven Izu Island, in 1940. (in English) 260

YAMAGUTI, S. (5) On the Change in the Heights of the Monthly

Mean Sea-level at Aburatubo and Hosozima. (in English) 39
YAMAGUTI, S. and TSUBOI, C. (4) Relation between the Gravity Anomalies and the Corresponding Subterranean Mass Distribution. (VI.) (in English) 26
YASUDA, C. and NASU, N. (26) Recent Earthquakes of the Kwanto District. (in English) 476
YOSIYAMA, R. (14) Elastic Waves from a Point in an Isotropic Heterogeneous Sphere. Part 3. (in English) 185
(31) Results of Re-triangulation in Miyake-sima. (in Japanese) 544